

Konferenzbeiträge / Atti / Proceedings

Building Simulation Applications BSA 2017

3rd IBPSA Italy conference

Bozen-Bolzano, 8th – 10th February 2017

Edited by

**Giovanni Pernigotto, Francesco Patuzzi, Alessandro Prada,
Vincenzo Corrado, Andrea Gasparella**

bu,press

bozen
bolzano
university
press

unibz
—
Freie Universität Bozen
Libera Università di Bolzano
—
Università Lìdia de Bulsan

Konferenzbeiträge / Atti / Proceedings

Building Simulation Applications BSA 2017

3rd IBPSA-Italy conference

Bozen-Bolzano, 8th–10th February 2017

Edited by

**Giovanni Pernigotto, Francesco Patuzzi, Alessandro Prada,
Vincenzo Corrado, Andrea Gasparella**

bu,press

bozen
bolzano
university
press

Scientific committee

Ian Beausoleil-Morrison, Carleton University, Canada
Jan L.M. Hensen, Technische Universiteit Eindhoven, The Netherlands
Gregor P. Henze, University of Colorado Boulder, USA
Ardeshir Mahdavi, Technische Universität Wien, Austria
Athanasios Tzempelikos, Purdue University, USA
Reinhard Radermacher, University of Maryland, USA
Francesco Asdrubali, Università degli Studi Roma Tre, Italy
Paolo Baggio, Università degli Studi di Trento, Italy
Maurizio Cellura, Università degli Studi di Palermo, Italy
Vincenzo Corrado, Politecnico di Torino, Italy
Andrea Gasparella, Free University of Bozen-Bolzano, Italy
Livio Mazzarella, Politecnico di Milano, Italy
Adolfo Palombo, Università degli Studi di Napoli Federico II, Italy

Students Tutoring Scientific Committee

Daniel Cóstola, University of Strathclyde, Scotland, UK
Pieter-Jan Hoes, Technische Universiteit Eindhoven, The Netherlands
Bruno Lee, Concordia University, Canada
Fabian Ochs, Universität Innsbruck, Austria
Matthias Schuss, Technische Universität Wien, Austria
Fabrizio Ascione, Università degli Studi di Napoli Federico II, Italy
Francesca Cappelletti, Università IUAV di Venezia, Italy
Gianpiero Evola, Università degli Studi di Catania, Italy
Francesco Patuzzi, Free University of Bozen-Bolzano, Italy
Giovanni Pernigotto, Free University of Bozen-Bolzano, Italy
Alessandro Prada, Università degli Studi di Trento, Italy

Organizing committee

Paolo Baggio, Università degli Studi di Trento, Italy
Marco Baratieri, Free University of Bozen-Bolzano, Italy
Francesca Cappelletti, Università IUAV di Venezia, Italy
Vincenzo Corrado, Politecnico di Torino, Italy
Andrea Gasparella, Free University of Bozen-Bolzano, Italy
Norbert Klammsteiner, Energytech G.m.b.H./S.r.l -Bozen, Italy
Fabian Ochs, Universität Innsbruck, Austria
Francesco Patuzzi, Free University of Bozen-Bolzano, Italy
Giovanni Pernigotto, Free University of Bozen-Bolzano, Italy
Alessandro Prada, Università degli Studi di Trento, Italy
Fabio Viero, Manens – Tifs, Italy

bu,press

Bozen-Bolzano University Press
Free University of Bozen-Bolzano
www.unibz.it/universitypress
2018

Cover design: DOC.bz

ISSN 2531-6702
ISBN 978-88-6046-136-0



This work—excluding the cover and the quotations—is licensed under the Creative Commons Attribution-ShareAlike 4.0 International License.

Table of Contents

Preface.....	1
Urban Energy Computing: An Hourglass Model <i>Ardeshi Mahdavi, Neda Ghiassi</i>	3
The Viability of Using Different Types of Recycled Plastic as Glazing in Windows <i>Islam A. Mashaly, Yussra Rashed, Salah El-Haggar, Khaled Nassar</i>	13
Implications of Increasing Daylighting in Deep Energy Retrofitting in Norwegian Shopping Centres <i>Matthias Haase, Andreas Ampenberger</i>	19
PV-PCM Integration in Glazed Buildings. Numerical Study Through MATLAB/TRNSYS Linked Model <i>Hagar Elarga, Francesco Goia, Ernesto Benini</i>	27
Dynamic Simulation as a Tool for the Analysis of the Interactions Among the Controllers of HVAC Systems <i>Mara Magni, Jean Pierre Campana, Gian Luca Morini</i>	37
The Benchmark of a New SIMULINK Library for Thermal Dynamic Simulation of Buildings <i>Jean Pierre Campana, Mara Magni, Matteo Dongellini, Luca Morini</i>	45
A New Methodological Approach for Estimating Energy Savings due to Air Movement in Mixed-Mode Buildings <i>Francesco Babich, Malcolm Cook, Dennis Loveday, Rajan Rawal, Yash Shukla</i>	53
On the Indoor Thermal Behavior of a Building with Cool Envelope Components <i>Anna Laura Pisello, Veronica Lucia Castaldo, Claudia Fabiani, Franco Cotana</i>	61
How Microclimate Mitigation Affects Building Thermal-Energy Performance in Residential Zero Energy Italian Settlements <i>Anna Laura Pisello, Veronica Lucia Castaldo, Claudia Fabiani, Cristina Piselli, Franco Cotana, Mattheos Santamouris</i>	69
Thermal Performance of Innovative Building Envelope Systems in Mediterranean Climate <i>Maurizio Detommaso, Gianpiero Evola, Antonio Gagliano, Luigi Marletta, Francesco Nocera</i>	77
Pitfalls in Weather Data Management Strategies of Building Performance Simulation Tools <i>Livio Mazzarella, Martina Pasini</i>	87
Comparison Among Different Green Buildings Assessment Tools: Application to a Case Study <i>Benedetta Mattoni, Francesco Asdrubali, Giorgio Baldinelli, Francesco Bianchi, Fabio Bisegna, Luca Evangelisti, Paola Gori, Gianluca Grazieschi, Claudia Guattari</i>	97
Integrated Numerical Analysis and Building Information Modeling for Cultural Heritage <i>Elena Gigliarelli, Filippo Calcerano, Michele Calvano, Francesco Ruperto, Mario Sacco, Luciano Cessari</i>	105
Weather Scenario Generation for Stochastic Model Predictive Control Using Vector Autoregressive Prediction <i>Samuel R. Currie, Gregor P. Henze</i>	113
Historical Buildings in Protected Areas in Italy: A Re-Design Study of a Rural Building <i>Maurizio Cellura, Giuseppina Ciulla, Francesco Guarino, Sonia Longo</i>	119
On the Cost-Optimal Design: Comparison of Quasi-Steady-State and Dynamic Simplified Methods of Calculation of H/C Energy Needs <i>Ilaria Ballarini, Andrea Costantino, Domenico Dirutigliano, Enrico Fabrizio, Simona Paduos, Vincenzo Corrado</i>	129
Static and Dynamic Strategies for Improving Daylight Use in Side-Lit Classrooms: A Case Study <i>Vincenzo Costanzo, Gianpiero Evola, Luigi Marletta, Dario Panarelli</i>	137
RC Building Modelling for Control Purposes: A Case Study <i>Erica Zavaglio, Mario Motta</i>	145
Architectural Integration of Photovoltaics: Performance Evaluation of Curved Modules <i>Marco Lovati, Laura Maturi, David Moser</i>	153

Validation of a PCM Simulation Tool in IDA ICE Dynamic Building Simulation Software Using Experimental Data from Solar Test Boxes <i>Cristina Cornaro, Marco Pierro, Daniele Roncarati, Valerio Puggioni</i>	159
Analysis of the Influence of Thermal Losses of the Recirculation Flow Loop in a Residential Hot Water Solar System <i>Paolo Valdiserri</i>	167
Calibration of the Energy Simulation Models using Tikhonov-Type Regularization: Application to a Residential Building Apartment <i>Maja Miletić, Chiara Dipasquale, Roberto Fedrizzi</i>	175
On-Site Measurements and Whole-Building Thermal Dynamic Simulation of a Semi-Confined Prefabricated Building for Heritage Conservation <i>Francesca Frasca, Anna Maria Siani, Cristina Cornaro,</i>	185
Comparison Between Simplified and Detailed Methods for the Calculation of Heating and Cooling Energy Needs of Livestock Housing: A Case Study <i>Andrea Costantino, Ilaria Ballarini, Enrico Fabrizio</i>	193
Effect of Blind Control Strategies on Energy Demand of Office Buildings and Melanopic Effect for Occupants <i>Daniel Plörer, Matthias Werner, Martin Hauer, David Geisler-Moroder</i>	201
Introducing a Hybrid Energy-Use Model at the Urban Scale: The Case Study of Turin (Italy) <i>Marta Carozza, Guglielmina Mutani, Silvia Coccolo, Jérôme Kaempf</i>	209
OpenBPS: A New Building Performance Simulation Tool <i>Livio Mazzarella, Martina Pasini</i>	217
A Comparative Study of Computational Algorithms Used in the Automatic Generation of Reduced-Order Models from CFD Simulations <i>Thibault Marzullo, Sajjad Yousefian, Marcus M. Keane, Marco Geron, Rory F.D. Monaghan</i>	225
Comparison of Direct Radiation Split Algorithms for Energy Simulation of Buildings <i>Giorgio Lupato, Marco Manzan, Stefano Cirilli</i>	233
Introduction of a New Dynamic Simulation Screening Tool to Support Early-Stage Building Design <i>Marco Picco, Giorgio Ghisalberti, Gaetano Fabio Graziano, Marco Marengo</i>	241
On the Influence of Storage Size and Management on the Consumption of Air Source Heat Pumps in High Performance Buildings <i>Elena Bee, Alessandro Prada, Paolo Baggio</i>	249
Energy Refurbishment of Social Housing Stock in Italy: Analysis of Some Scenarios from the Impact of Climate Change to Occupant Behaviour <i>Leone Pierangoli, Cristina Carletti, Gianfranco Cellai, Fabio Sciurpi</i>	257
Analysis of Simplified Lumped-Capacitance Models to Simulate Thermal Behaviour of Buildings <i>Jacopo Vivian, Angelo Zarrella, Giuseppe Emmi, Michele De Carli</i>	265
Measurement of the Impact of Buildings on Meteorological Variables <i>Dasaraden Mauree, Laurent Deschamps, Paul Bequelin, Pierre Loesch, Jean-Louis Scartezzini</i>	273
Improving Local Wind Estimation for the Automated Control of Blinds <i>Dasaraden Mauree, Ali Motamed, Laurent Deschamps, Jean-Louis Scartezzini</i>	279
Modelling of Complex Fenestration Systems – Validation Results by Long-Term Measured Data <i>Martin Hauer, Michael Grobbauer, Stefan Holper, Daniel Plörer</i>	285
Cooling Energy Needs in Non-Residential Buildings Located in Mediterranean Area: A Revision of the Quasi-Steady Procedure <i>Roberto Bruno, Natale Arcuri, Cristina Carpino</i>	293
Steady-State and Transient Simulation of a Radiant Heating System <i>Fabian Ochs, Mara Magni, Michele Bianchi Janetti, Dietmar Siegele</i>	301
Comparison Between Energy-Optimized and Cost-Optimized Design of Multi-Family Buildings Through Automated Optimization <i>Maria Ferrara, Elisa Sirobo, Enrico Fabrizio</i>	309
Effective Building Modelling for Energy Performance Contracting <i>Alberto Giretti, Massimo Lemma, Miquel Casals, Marcel Macarulla, Alba Fuertes, Rory Jones</i>	317
Integrated Energy Modelling to Support District Cooling Optimisation: Methodological Approach <i>Francesco Passerini, Andrea Bassani, Pietro De Cinque, Raymond Sterling, Jesus Febres, Anna Magrini, Andrea Costa, Marcus M. Keane</i>	325

The Development and Verification of a Computational Tool for the Evaluation of the Visual Accessibility of Architectural Spaces <i>Dawid Wolosiuk, Harald Hofstätter, Ardeshir Mahdavi</i>	333
The Diversity Challenge in Models of Occupants' Presence in Buildings <i>Ardeshir Mahdavi, Farhang Tahmasebi, William O'Brien, H. Burak Gunay</i>	339
Accounting for the Diversity of Use Patterns in Representations of Office Plug Loads in Building Performance Simulation <i>Ardeshir Mahdavi, Farhang Tahmasebi</i>	345
A Comparison Between Numerical Methods for Evaluating Ground-Coupled Heat Pump Systems Performance <i>Angelo Zarrella, Roberto Zecchin, Diego Guzzon, Michele De Carli, Giuseppe Emmi, Michele Quaggia</i>	351
Data Transfer from BIM to Building Performance Simulation Tools: A Case Study <i>Mirjana Bucevac, Ulrich Pont, Sigrun Swoboda, Ardeshir Mahdavi</i>	359
A Comparison of the Performance of Two- and Three-Dimensional Thermal Bridge Assessment for Typical Construction Joints <i>Ulrich Pont, Ardeshir Mahdavi</i>	367
Comparison Between Simulated and In-Situ Measured Speech Intelligibility in the Multilingual Context of the Free University of Bozen-Bolzano <i>Simone Torresin, Chiara Visentin, Nicola Prodi, Francesca Cappelletti, Andrea Gasparella</i>	375
Simulation-Assisted Monitoring-Based Performance Evaluation of a Historically Relevant Architectural Design <i>Matthias Schuss, Ulrich Pont, Mahnameh Taheri, Christoph Lindner, Ardeshir Mahdavi</i>	385
Bio-Based and Recycled-Waste Materials in Buildings: A Study of Energy Performance of Hemp-Lime Concrete and Recycled-PET Façades for Office Facilities in France and Italy <i>Chadi Maalouf, Carlo Ingrao, Flavio Scrucca, Tala Moussa, Caterina Tricase, Francesco Asdrubali</i>	393
Case Study for Energy Efficiency Measures of Buildings on an Urban Scale <i>Domenico Dirutigliano, Mark-Alexander Brüntjen, Christian Fliegner, Jérôme Frisch, Vincenzo Corrado, Christoph van Treeck</i>	403
Investigating the Suitability of the WRF Model for Improving Prediction of Urban Climate Boundary Conditions <i>Kristopher Hammerberg, Oscar Brousse, Ardeshir Mahdavi</i>	411
On the Global Performance of Offices with Different Complex Fenestration Systems <i>Anna Maria Atzeri, Francesca Cappelletti, Athanasios Tzempelikos, Andrea Gasparella</i>	421
Sensitivity of WRF/Urban Simulations to Urban Morphology Parameters: A Case Study in the City of Bolzano <i>Gianluca Pappaccogli, Lorenzo Giovannini, Francesca Cappelletti, Dino Zardi</i>	433
Numerical Analysis of Thermal Bridges in Dynamic Conditions <i>Alessandra Romagnoli, Costanzo Di Perna, Davide Barbaresi, Elisa Di Giuseppe</i>	441
Building Integrated Photovoltaics/Thermal (BIPV/T) System: A New Dynamic Simulation Model and a Case Study <i>Andreas Athienitis, Giovanni Barone, Annamaria Buonomano, Adolfo Palombo</i>	449
Buildings Integrated Phase Change Materials: Modelling and Validation of a Novel Tool for the Energy Performance Analysis <i>Giovanni Avagliano, Annamaria Buonomano, Maurizio Cellura, Vasken Dermardiros, Francesco Guarino, Adolfo Palombo</i>	459
From Energy Signature to Cluster Analysis: Comparison Between Different Clustering Algorithms <i>Lorenza Pistore, Giovanni Pernigotto, Francesca Cappelletti, Piercarlo Romagnoni, Andrea Gasparella</i>	469
The Building Information Model and the IFC Standard: Analysis of the Characteristics Necessary for the Acoustic and Energy Simulation of Buildings <i>Costantino Carlo Mastino, Roberto Baccoli, Andrea Frattolillo, Martino Marini, Antonino Di Bella, Valerio Da Pos</i>	479
Mapping Savings in Energy Demand by Heat Recovery for European Countries Under Consideration of Humidity Control <i>Stefanie Tafelmeier, Giovanni Pernigotto, Andrea Gasparella</i>	487

Calibrated Simulation Models for Indoor Comfort Assessment: The Case of a Healthcare Facility in Vienna <i>Luca Zaniboni, Giovanni Pernigotto, Matthias Schuß, Kristina Kiesel, Andrea Gasparella, Ardeshir Mahdavi</i>	497
Temporal and Spatial Predictability of Occupants' Presences in a Library Building <i>Ki Uhn Ahn, Won Jun Suh, Cheol Soo Park</i>	505
Stochastic Multi-Criteria Decision Making of Energy Recovery Ventilation Systems using Cumulative Prospect Theory <i>Young Jin Kim</i>	513
Proposing a Life Cycle Energy Efficiency Index for Comparative Assessment of Insulation Materials' Performance <i>Hashem Amini Toosi, Ali Vakili-Ardebili, Nasim Hasheminejad</i>	521
Development of a Design Numerical Model of a Hybrid Cooler <i>Matteo D'Antoni, Roberto Fedrizzi</i>	529
Selecting Roller Shades Properties Based on Glare Mitigation, Energy Performance and Connection to the Outdoors <i>Iason Konstantzos, Athanasios Tzempelikos</i>	539
Dynamic Simulation of the Influence of Fenestration on Buildings Energy Consumption. A Comparison Between Northern and Southern Europe <i>Angelo Spena, Viola Iaria, Carlo Mazzenga</i>	547
A New Control Strategy for Variable Refrigerant Flow Systems <i>Xiaojie Lin, Yunho Hwang, Reinhard Radermacher, Byungsoon Kim</i>	557
Development of an Energy Performance Benchmark Using Quantitative Analysis of Energy Consumption of Office Buildings <i>HyeGi Kim, SunSook Kim</i>	565
Parametric Technical and Economic Analysis of Thermal Comfort and Productivity in Industrial Buildings <i>Mariantonietta Tarantini, Giovanni Pernigotto, Fabian Ochs, Andrea Gasparella</i>	573

Preface

The third edition of Building Simulation Applications BSA 2017, the biannual conference of IBPSA Italy hosted by the Free University of Bozen-Bolzano, proved to be at least as successful as the previous events. From February 8th to 10th 2017, it featured more than 100 participants and more than 75 presentations, about 40 % of which from abroad – Austria, US, South Korea, Ireland, Switzerland and the UK, among the first contributors. In addition, besides researchers, it also hosted a half-day special roundtable discussion about the potential and limitations of a set of simulation tools, attended by about 80 practitioners, to discuss the opportunities opened up to professionals by the use of building simulation, as well as the main barriers preventing its broader diffusion.

This was one of the reasons for presenting awards to some distinguished examples of use of building simulation in practice with the second edition of the IBPSA Italy Project Award, and, since the student of today will be the practitioner and the designer of tomorrow, for starting the first edition of a simulation introductory school for students.

Regarding the topics, some clear trends were documented in BSA 2017, as highlighted by the four keynotes.

If parametric simulation has increased the possibility of investigating a broader range of configurations, the adoption of optimization techniques allows the identification of the best design or operative configuration. Real time optimization, in particular, enables model-predictive control strategies in which the building model is used to identify and update the best control actions based on short-term weather and occupancy forecasts. Gregor Henze (University of Colorado Boulder, USA – Department of Civil, Environmental and Architectural Engineering) addressed those aspects in his keynote “Exploration of Building Model Complexity for Residential and Commercial Model Predictive Control”.

Multi-domain simulation is at the base/bottom of an integrated analysis of building performance, allowing the occupant to effectively become the aim of the design and operation activities. Energy

efficiency, global cost and environmental sustainability in this perspective are only constraints, which need to be considered in the light of the quality of the indoor environment. Humans are at the very core of the project, and buildings have to be designed to interpret their needs and to facilitate their interactions in order to achieve high performance levels, as Panagiota Karava (Purdue University, USA – School of Civil Engineering) clarified in her speech about “Cyber-Physical-Human Systems for High Performance Buildings”.

Reinhard Radermacher (University of Maryland, USA – Center for Environmental Energy Engineering) reminded the audience about a long-lasting trend in building simulation dealing with the constant increase in the simulation detail and complexity and the co-simulation of building and technical systems. Design of high-performance buildings requires careful use of natural resources, from solar gains to renewable energy sources, using new technologies whose potentialities need to be explored and evaluated by means of coupled simulation of building and HVAC systems, as emerged from the keynote “Thoughts on Emerging Technologies and Simulation Aspects for HVAC in Buildings”.

Finally, in the keynote “Urban Energy Computing: an Hourglass Model”, Ardeshir Mahdavi (Technische Universität Wien, Austria – Department of Building Physics and Building Ecology) reported about an additional tendency, related to multi-scale simulation. Buildings interact with each other and with the external environment, especially in urban contexts, and such an intertwined performance needs to be studied simultaneously. The capability of predicting the behavioral whole of urban areas is then of crucial importance but, nonetheless, still challenging and requiring innovative approaches.

Andrea Gasparella, Free University of Bozen-Bolzano

Urban Energy Computing: An Hourglass Model

Ardeshir Mahdavi – TU Wien – bpi@tuwien.ac.at

Neda Ghiassi – TU Wien - neda.ghiassi@tuwien.ac.at

Abstract

This contribution describes an urban energy modelling method that enables the use of dynamic performance simulation for urban-scale energy inquiries. The associated framework involves two components. The first component is tasked with the systematic reduction of the computation domain through clustering based sampling of the urban building stock. The second component recovers part of the lost diversity (due to the reductive procedure) via stochastic variation of selected model parameters such as thermal properties of building components and occupancy-related factors.

1. Introduction

The development of energy performance improvement strategies for the built environment requires reliable data on the spatial and temporal distribution of energy demand and supply. This implies the need for modelling environments that can facilitate energy-related district-level inquiries (pertaining, for example, to candidate intervention scenarios) beyond the scope of individual buildings. The bottom-up modelling approach (Swan and Ugursal, 2009) has the potential to support the impact investigation of energy-relevant change and intervention scenarios (Kavgic et al., 2010). Thereby, results from thermal models of a number of sample buildings are up-scaled to the neighbourhood or even whole-city level. The effectiveness of this approach depends not only on the underlying performance assessment routines, but also on the nature of the reductive procedure adopted to reduce computational loads.

Past efforts have frequently adopted simplified and reduced order algorithms in order to meet massive data requirements and extensive computational loads. This may yield a broad urban-scale energy view, but is unlikely to capture the temporal

dynamics of building thermal states given transient internal and external (occupants and climate). On the other hand, most current reductive procedures follow stock segmentation methods that ignore a number of relevant morphological aspects of the urban stock such as adjacency relations and the effect of mutual shading. In our implementation of the reductive method, such issues were addressed in the adopted classification criteria, together with measures to include the building operational properties beyond function-related assumptions (Ghiassi et al., 2015).

In this context, we have developed a reductive bottom-up urban stock heating demand model, which relies on a Building Performance Simulation (BPS) tool to assess the performance of the buildings, such that scenario modelling capabilities and resolution are enhanced. To enable the large-scale adoption of BPS tools a two-module framework (an hourglass model) was conceived. The first (reductive) module uses data-mining methods to reduce the computational load via representative sampling. As this inadvertently results in some loss of diversity, a second module was designed to partially recover lost diversity. The resulting urban energy decision support environment has thus the potential to comparatively analyse and evaluate various change and intervention scenarios pertaining to macro and micro-climate conditions, inhabitants' demography and behaviour, physical and technical aspects of the buildings, and urban morphology.

2. Approach

The framework architecture is depicted in Fig. 1. To accommodate the high informational and computational requirements of BPS as the framework's computational engine, the first module involves the

selection of a sample of buildings representative of the energy diversity of the stock. The second module aims to recover part of the building diversity lost through the reductive process. The initial reduction and subsequent re-diversification steps explain the authors' choice of the "hourglass model" to characterise their approach.

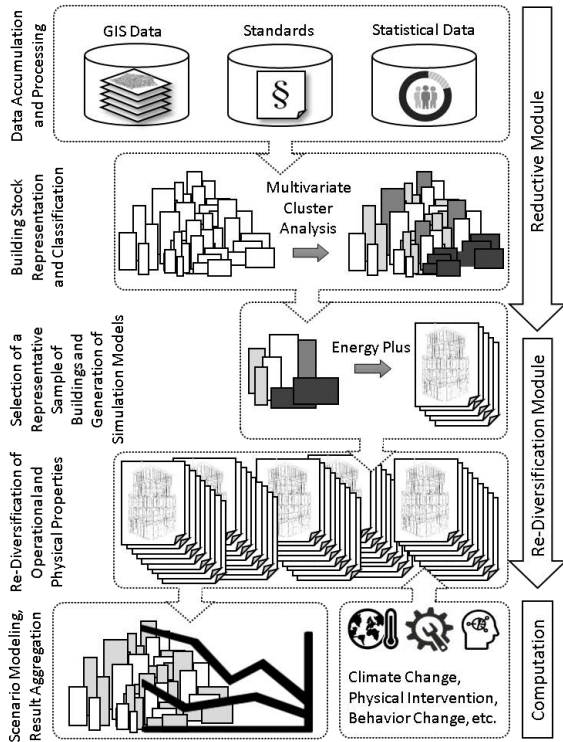


Fig. 1 – The proposed urban energy computing framework

3. The Reductive Module

The reductive module is designed and implemented as a plug-in for the open source GIS environment QGIS (2015). The plug-in, written in Python programming language (2016), uses the available GIS data of an urban area, as well as relevant standards and statistical data to reach an energy-relevant sample of buildings. The prerequisite urban stock representation includes the geometry and adjacency status of the building enclosures; area, orientation and shading condition of transparent building components; various usages present in each building, and relevant standard operational parameters; age-dependent thermal properties of building components; floor area, etc. (for more details, Ghiassi et al.,

2015; Ghiassi and Mahdavi, 2016a; 2016b, 2016c).

Once the representation is created, key energy-relevant features of the buildings are aggregated into descriptive indicators (Table 1) that constitute the criteria adopted for the segmentation of the building stock. The resulting matrix of indicator values for all buildings is subjected to Multivariate Cluster Analysis, MCA (Hair et al., 2010), to identify groups of buildings with similar properties. Three different MCA techniques, K-means (MacQueen, 1967), model-based (Fraley and Raftery, 2002), and hierarchical agglomerative (Hair et al., 2010) were examined towards their efficiency for the segmentation of building stock. Preliminary performance tests, carried out using the results of steady state heating demand calculations on the neighbourhood based on the previously derived stock representation, suggest that the representatives emerging from the application of the k-means method on the presented set of classification criteria, performs best in predicting the monthly heating energy demand of the neighbourhood (according to ÖNORM, 2014).

4. The Re-Diversification Module

The re-diversification module was developed to reintroduce part of the diversity lost due to the reductive step and to obtain more realistic representations of energy demand's spatial and temporal distribution. Once the reductive module selects the representative buildings, reference simulation models are developed using EnergyPlus (2016) and detailed building plans. In reference models, operational parameters are represented through standard schedules.

Constructions are specified according to available plans or the common practice of the construction period of the buildings. Ventilation is modelled as dependent on the occupants' presence. The re-diversification module, also developed in Python programming language, requires these reference models as an input.

Given the extensive time and effort required for the acquisition of building information and generation of the geometric building models (Mahdavi and El-Bellahy, 2005), the reductive module limits the modelling domain to a manageable (user-defined)

number of buildings. The re-diversification module readjusts a number of non-geometric parameters of the reference simulation models. For this purpose, for all buildings within the study domain, permutations of the relevant reference simulation models are created with the modified parameters. Building parameters subjected to diversification include:

- Schedules of the occupants' presence and activity, lighting, and equipment use;
- Thermal properties of building envelope;

- Internal loads (inhabitants, equipment and lighting power);
- Ventilation (air change) rates.

This diversification process is guided by the information contained in the initially generated building stock representation. The reference simulation model is modified based on descriptive indicators defined in Table 2. Simulation models generated by the re-diversification module are subjected to computations with hourly resolution.

Table 1 – Descriptive energy-related indicators of buildings' characteristics as the classification criteria by the reductive module

	Abbr.	Variable Description	Formula	Parameters
Geometry	V_n	Net Volume [m ³] An indicator of the size of the building	$V_n = \sum (A_{feat,i} \cdot h_{feat,i}) \cdot f_n$	$A_{feat,i}$ Area of footprint feature [m] $h_{feat,i}$ Height of foot print feature [m] f_n Net to gross volume ratio
	h_e	Effective floor height [m] Ratio of the building volume to the floor area	$h_e = V_n / (A_{t,i} \cdot n_f)$	$A_{t,i}$ Total floor area [m] n_f Number of floors
	C_t	Thermal compactness [m] Ratio of the net building volume to the thermally effective envelope area	$C_t = V_n / A_e$ $A_e = \sum (A_i \cdot f_{t,i})$	A_e Thermally effective envelope area [m] Area of element [m] A_i Corresponding temperature correction factor $f_{t,i}$
Solar Gains	GR_e	Effective glazing ratio Average glazing to wall ratio weighted by orientation and corrected for the shading effect of the surroundings Weights associated with orientations were based on reference climate data	$GR_e = WWR \cdot GWR \cdot g \cdot SVF_i$ $\sum (A_{ow,i} \cdot f_{o,i} \cdot SVF_i) / \sum A_{ow,i}$	WWR Window to wall ratio GWR Glass to window ratio $A_{ow,i}$ Area of outside wall [m] $f_{o,i}$ Corresponding orientation correction factor g Solar factor of glazing SVF_i Sky View Factor near the wall
	U_e	Effective average envelope U-value [W.m ⁻² .K ⁻¹] Average u-value of the envelope corrected for adjacency relations and weighted by the corresponding areas	$U_e = \sum (U_i \cdot A_i \cdot f_{t,i}) / A_e$	U_i U-value of element [W.m ⁻² .K ⁻¹]
Operation Parameters	O_u	Fraction of time the building is used annually	$O_u = t_{use,a} / t_a$	$t_{use,a}$ Annual use hours [h] t_a Total hours in a year[h]
	Ig_d	Daily area related internal gains [Wh.m ⁻² .d ⁻¹]	$Ig_d = \sum (q_{i,h} \cdot t_{use,d} \cdot f_i)$	$q_{i,h}$ Usage-based internal gains rate [W.m ⁻²] Daily use hours [h] $t_{use,d}$ Share of the usage in the overall building volume f_i
	Ac_d	Daily air-change rate [d ⁻¹]	$Ac_d = \sum (n_v \cdot t_{use,d} \cdot f_i)$	n_v Usage-based hourly air-change rate [h ⁻¹]

4.1 Diversification of schedules

Reference schedules suggested by standards (e.g. ASHRAE, 2013), represent the temporal distribution of internal gains in aggregate terms. Use of these average profiles for detailed demand assessments

on a large scale, however, will result in unrealistically monotonous internal load profiles and identical peak hours across the computation domain. To achieve a more realistic representation

of occupancy-related factors, for each building, a set of randomized schedule files are created, based on the reference schedules for various days of the week. To diversify each schedule, for every time step, the value provided by the reference schedule is considered as the mean of a Gaussian probability

distribution. A default Coefficient of Variance (CV) is used along with the mean value to generate this distribution (Mahdavi and Tahmasebi, 2015). Based on the generated distribution for each time step, a value is randomly selected for the schedule.

Table 2 – Descriptive indicators for the re-diversification process

Abbr.	Variable Description	Formula	Parameters
$U_{e,r}$	Effective roof/ceiling value [$W.m^{-2}.K^{-1}$]	$U_{e,r} = \Sigma(U_{i,r} \cdot A_{i,r} \cdot f_{i,r}) / A_e$	$U_{i,r}$ U-value of roof/ceiling element [$W.m^{-2}.K^{-1}$] $A_{i,r}$ Area of roof/ceiling element [m] $f_{i,r}$ Corresponding temperature correction factor A_e Effective envelope area [m] (Table 1)
$U_{e,f}$	Effective floor U-value [$W.m^{-2}.K^{-1}$]	$U_{e,f} = \Sigma(U_{i,f} \cdot A_{i,f} \cdot f_{i,f}) / A_e$	$U_{i,f}$ U-value of floor element [$W.m^{-2}.K^{-1}$] $A_{i,f}$ Area of floor element [m] $f_{i,f}$ Corresponding temperature correction factor
$U_{e,w}$	Effective wall U-value [$W.m^{-2}.K^{-1}$]	$U_{e,w} = \Sigma(U_{i,w} \cdot A_{i,w} \cdot f_{i,w}) / A_e$	$U_{i,w}$ U-value of wall element [$W.m^{-2}.K^{-1}$] $A_{i,w}$ Area of wall element [m] $f_{i,w}$ Corresponding temperature correction factor
I_{gd}	Daily area related internal gains [$Wh.m^{-2}.d^{-1}$]		See Table 1
A_{cd}	Daily air-change rate [d^{-1}]		

4.2 Readjustment of internal loads and ventilation rates

The diversified operational parameters (i.e. reference values for equipment and lighting power, number of occupants, and air change rate) are computed for each building such that the aggregated internal gains and ventilation rates, match the values of the daily area-related internal gains and daily air change rate computed for the building.

For this purpose, annual area-related internal gains are computed based on the average daily values and the number of annual use days provided by standards (e.g. ÖNORM, 2011). Similarly, the average hourly air change rate across the year is calculated. The annual value of internal gains is disaggregated into occupants, lighting and equipment gains, based on the share of these items in contributing to the internal gains according to literature (e.g. Kemna and Moreno Acedo, 2014).

4.3 Readjustment of thermal properties

The readjustment of the thermal properties of the main building elements is informed by the respective effective element U-values. The buildings that belong to the same construction period, with different geometries and adjacency situations, have different effective component U-values.

This diversification step modifies each simulation model, so that the resulting effective U-values of the major envelope components match the expected values calculated for every building. Since the geometry of the simulation model associated with every building is identical to that of the corresponding reference model, any deviations from the effective U-values of the reference building must be accounted for by modifying the U-values of the constructions in the new model. For this purpose, the differences between the effective U-values of the elements of the reference building and

the building undergoing diversification are calculated. Subsequently, the thermal properties of the main constructions in the new model (external walls, uppermost and lowermost enclosures) are determined so that they reflect the deviation in effective U-values from those of the reference model. Since a modification of the thermal mass of the building was not intended, only the thermal conductivity of the main layer (massive load bearing element or insulating element) is readjusted.

5. Illustrative Example

5.1 Case Study

The utility of the developed computational framework was tested via a case study in the city of Vienna, Austria (located in the centre of the city, featuring over 740 buildings of various usages and construction periods). Following data was incorporated:

- Land Use Plan (ViennaGIS, 2015)
- Digital Elevation Model (ViennaGIS, 2015)
- Building Inventory (ViennaGIS, 2015)
- Building Usage (Open Street Map, 2015)
- Sky View Factor map generated by DEMTools plug-in for QGIS (Hammerberg, 2014)
- Austrian standard: Model of climate and user profiles (ÖNORM, 2011)
- Austrian standard: Principles and verification methods, heating demand and cooling demand (ÖNORM, 2014)
- Guidelines: Energy-technical behaviour of buildings (OIB, 2015)

5.2 Modelled Scenarios

To assess the impact of the diversification process, predictions of the non-diversified model were compared with the predictions resulting from models with two levels of diversification. The non-diversified model is based on the reference simulation files. The first level of diversification involves only operational schedules. The second level includes all diversification steps introduced in the method (Table 3).

Table 3 –Overview of the investigated models with various levels of diversification. (D: Diversified, ND: Not Diversified)

Abbr.	Schedules	Thermal properties	Internal gains	Number of simulations
NDM	ND	ND	ND	7
DM-1	D	ND	ND	744
DM-2	D	D	D	744

Three simple illustrative scenarios pertaining to changes in the operational parameters of buildings (occupant behaviour) were designed. The first scenario follows the standard assumptions for internal temperature and HVAC availability hours. The second scenario assumes a setback heating setpoint for the vacant hours in non-residential spaces, which is closer to the actual building operation tendencies. The third scenario, emulating the behaviour of a more energy-aware population, maintains the setback threshold, and modifies the internal heating setpoint temperatures in proportion to the occupancy rate of the building in every time step. These scenarios were simulated with the NDS and DS-2 models. Table 4 provides an overview of the modelled scenarios.

6. Results and Discussion

6.1 Reductive Module

The implementation of the reductive method for the case study area resulted in 7 clusters. The buildings representing these clusters include three residential buildings, two office buildings, as well as two mixed use residential and gastronomy building (Fig. 2).

As mentioned before, the representational performance of the reductive module was tested using the results of simplified steady state demand calculations (ÖNORM, 2014). The volume related heating demand of the buildings in every cluster as well as that of the representing building is shown in Fig. 3. Buildings grouped together in each cluster, feature similar performances. The most representative building performance is close to the cluster mean, however, the representatives of Clusters 3 and 6 underestimate their respective categories demand. To investigate the representativeness of the selected sample, the volume-related demand of the representative buildings along with the volume of

buildings in every cluster were used to predict the heating demand of the represented buildings. These predictions were compared to the standard-based

values (Fig. 4), suggesting an acceptable building-level predictive performance.

Table 4 – An overview of the modelled behaviour change scenarios

		Residential		Non-Residential	
S0	Setpoint assumptions [°C]	20		20	
	HVAC Availability	24 hours a day		14 hours on weekdays	
S1	Set point assumptions [°C]	20		20 during work hours 14 other times	
	HVAC Availability	24 hours a day		24 hours a day	
S2	Set point assumptions [°C]	16	Night hours	14	Not working hours
		16	Occupancy rate <25 %	16	Occupancy rate <25 %
		20	Occupancy rate >55 %	20	Occupancy rate >75 %
		Interpolate	Other times	Interpolate	Other times
	HVAC Availability	24 hours a day		24 ours a day	

6.2 Re-Diversification Module

The impact of the diversification process is illustrated for an office building in Fig. 5, where reference schedules are compared to a one-week data generated for one building. The generated schedules maintain the overall tendencies of the reference schedules, but provide, due to their probabilistic nature, unique profiles for various buildings. The diversification of the schedules results in minor modifications in the annual peak load (+1 %) and the aggregated annual demand of the neighbourhood (-1 %). The additional readjustment of the building thermal properties, internal loads, and ventilation rates causes more significant changes in model predictions (-3.4 %).

The impact of the diversification process is magnified when the observation scale is reduced. At a building level, the annual volume-related heating demand of the buildings computed by DM-2 can deviate by as much as 30 % from reference buildings, but the values predicted by DM-1 do not vary

significantly from the reference values. If the observation scale is further reduced to a single time step, both DM-1 and DM-2 result in noticeable deviations from the non-diversified hourly predictions (Fig. 6). Although unnoticeable at aggregate scale, such variations can have significant implications (e.g. for the design of small scale distributed generation schemes).

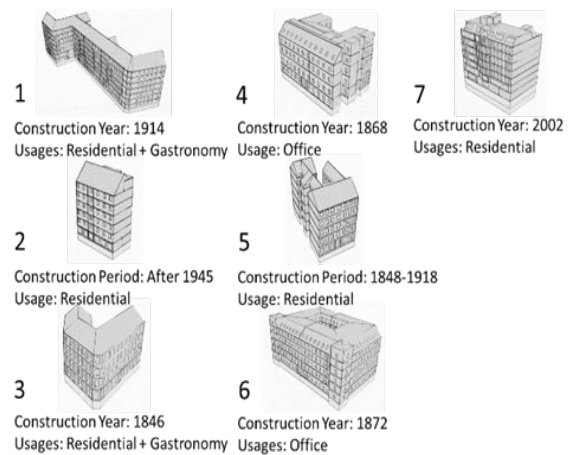


Fig. 2 – Buildings representing the clusters emerged from applying the reductive module to the case study

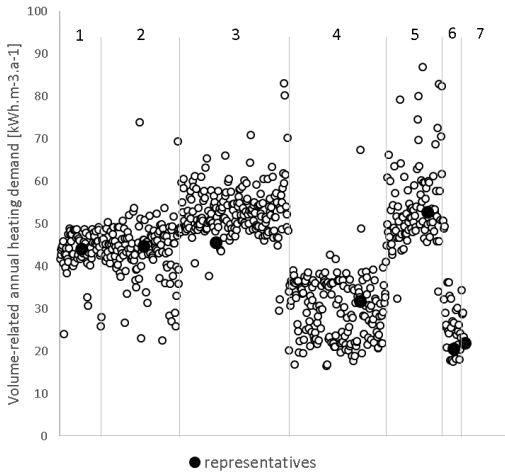


Fig. 3 – Volume related heating demand of buildings in each cluster and the cluster representative

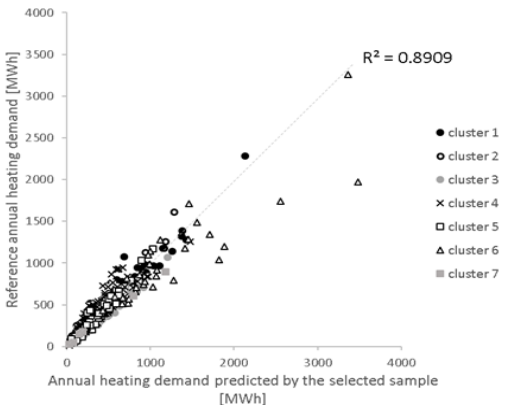


Fig. 4 – Sample-based prediction of heating demand compared to the computed heating demand

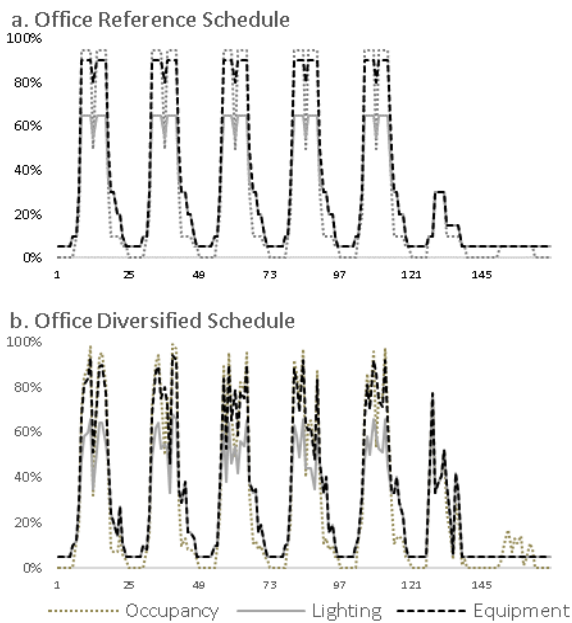


Fig. 5 – a. Office reference schedules according to ASHRAE
 b. One-week data of the diversified schedules generated for an office building

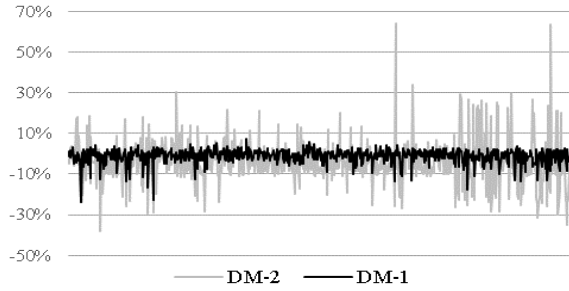


Fig. 6 – Relative deviation of hourly demand results of all buildings as predicted by the DM-1 and DM-2 from NDM predictions for a single time step in heating period

6.3 Scenario Modelling Results

The results of modelled scenarios are summarised in Table 5. At the aggregated level, peak, mean, and total heating demand simulated for the base case assumptions (S0) change little due to the inclusion of a re-diversification in the modelling procedure. The application of the first behaviour change scenario does not result in the divergence of the tendencies of non-diversified and the diversified model. This is to be expected, as the modifications applied in this scenario are somewhat independent from the occupancy-related aspects (they apply only to non-residential spaces in non-occupied hours).

Table 5 – Results of the behaviour change scenarios as simulated by the diversified and non-diversified computational models

Scenarios		Annual Peak load [MWh]	Relative deviation from NDM-S0 [%]	Total annual space heating load [GWh]	Relative deviation from NDM-S0 [%]
Non-Diversified Model (NDM)	S0	153.1	0	198.35	0
	S1	128.2	-16.3	200.70	1.2
	S2	122.6	-19.9	169.14	-14.7
Diversified Model (DM-2)	S0	151.4	-1.1	191.66	-3.4
	S1	124.5	-18.7	195.22	-1.6
	S2	111.7	-27.0	170.30	-14.1

The differences become more visible in case of the second scenario. The comparison of the second scenario predictions of both models (NDM-S2, DM-2-S2) shows significant deviations in peak and total heating demand.

DM-2-S2) with the respective base case predictions of the same models (NDM-S0, DM-2-S0) shows that in the non-diversified model, the application of the occupant-sensitive HVAC control scenario has led to a much larger decrease in demand than in the diversified model (14.7 % compared to 11.1 %). Moreover, the peak load predicted by the non-diversified model is much higher than the predictions of the diversified model, which provides a more realistic representation of the people's presence and actions. The non-diversified model appears to overestimate annual demand reduction due to occupant behaviour change, while failing to realistically predict the impact of these improvements on the peak loads. This can have major implications for the design of energy infrastructure and sizing of distributed generation systems.

7. Conclusion

This contribution described an urban energy-computing environment for urban-level change and intervention scenario modelling. The proposed "hourglass" framework entails a reductive module toward a sampling-based reduction of the computational domain via cluster analysis. Thus, detailed transient numeric simulation can be deployed to analyse the building thermal behaviour. Thereby, to more systematically capture the dynamic nature of the urban building stock and its transformations through retrofitting and densification, as well as operative changes, an original set of energetically relevant indicators was assembled for stock segmentation. The computational framework involves a second (re-diversification) module to partially reintroduce to the model diversity lost through the reductive procedure as well as the adoption of standard-based reference schedules. The utility of the diversification was illustrated via simple behaviour change scenarios. The non-diversified model appears to overestimate the urban-level consequences of occupancy-related changes in the system control settings, due to its unrealistic representation of the occupants' presence and behaviour. Re-diversification has the potential to ameliorate this circumstance, supporting thus, amongst other things, a more effective approach to the design and

deployment process of urban-scale distributed energy networks.

References

- ASHRAE. 2013. *ASHRAE Standard 90.1. 2013. Energy Standard for Buildings Except Low-Rise Residential Buildings*. Atlanta, U.S.A.: American Society of Heating, Refrigerating and Air-Conditioning Engineers, Inc.
- EnergyPlus. 2016. www.energyplus.net (cit. 11.18.2016)
- Fraley, C., E. Raftery. 2002. "Model-based clustering, discriminant analysis, and density estimation". *Journal of the American statistical association* 97(458): 281-297.
- Ghiassi, N., A. Mahdavi. 2016a. "Utilization of GIS data for urban-scale energy inquiries: a sampling approach". In: *Proceedings of the 11th European Conference on Product and Process Modelling*. Limassol, Cyprus.
- Ghiassi, N., A. Mahdavi. 2016b. "A GIS-based framework for semi-automated urban-scale energy simulation". In: *Proceedings of the Central Europe towards Sustainable Building 2016*. Prague, Czech Republic
- Ghiassi, N., A. Mahdavi. 2016c. "Urban energy modelling using multivariate cluster analysis". In: *Proceedings of BAUSIM 2016*. Dresden, Germany.
- Ghiassi, N., K. Hammerberg, M. Taheri, U. Pont, O. Sunanta, A. Mahdavi. 2015. "An enhanced sampling-based approach to urban energy modelling". In: *Proceedings of BS2015, the 14th Conference of International Building Performance Simulation Association*. Hyderabad, India: IBPSA.
- Hair, J.F., W.C. Black, B.J. Babin, R.E. Anderson. 2010. *Multivariate Data Analysis – a Global Perspective*. New Jersey, U.S.A.: Pearson Global Editions.
- Hammerberg, K. 2014. DEMTools. QGIS plugins repository. <https://plugins.qgis.org/plugins/DEMTools>
- Kavgic, M., A. Mavrogianni, D. Mumovic, A. Summerfield, Z. Stevanovic, M. Djurovic-Petrovic. 2010. "A review of bottom-up building stock models for energy consumption in the

- residential sector". *Building and Environment* 45(7): 1683–1697. doi: 10.1016/j.buildenv.2010.01.021.
- Kemna, R., J. Moreno Acedo. 2014. *Average EU building heat load for HVAC equipment*. Delft, Netherlands: VHK.
- MacQueen, J. 1967. "Some methods for classification and analysis of multivariate observations". In: *Proceedings of the 5th Berkeley symposium on mathematical statistics and probability*. Berkeley, U.S.A.: University of California Press.
- Mahdavi, A., F. Tahmasebi. 2015. "The inter-individual variance of the defining markers of occupancy patterns in office buildings: a case study". In: *Proceedings of BS2015, the 14th Conference of International Building Performance Simulation Association*. Hyderabad, India: IBPSA.
- Mahdavi, A., S. El-Bellahy. 2005. "Effort and effectiveness considerations in computational design evaluation: a case study". *Building and Environment* 40: 1651–1664. doi: 10.1016/j.buildenv.2004.11.014.
- OIB. 2015. *RL-6: Energy behavior of buildings*. Vienna, Austria: Austrian Institute of Construction Technology.
- ÖNORM. 2011. *B 8110-5 Thermal insulation in building construction, Part5: Model of climate and user profiles*. Vienna, Austria: Austrian Standards Institute.
- ÖNORM. 2014. *B 8110-6 Thermal insulation in building construction, Part6: Principles of verification methods – Heating demand and cooling demand – National application, national specifications and national supplements to ÖNORM EN ISO 13790*. Vienna, Austria: Austrian Standards Institute.
- Open Street Map. 2016. www.openstreetmap.org (cit. 11.18.2016)
- Python. 2016. www.python.org (cit. 11.18.2016)
- QGIS. 2016. www.qgis.org (cit. 10.03.2016).
- R Project for Statistical Computing. 2015. www.r-project.org (cit. 11.18.2015).
- Swan, L.G., V.I. Ugursal. 2009. "Modeling of end-use energy consumption in the residential sector: A review of modelling techniques". *Renewable and Sustainable Energy Reviews* 13 (8): 1819–1835. doi: 10.1016/j.rser.2008.09.033.
- Vienna GIS. 2015. www.wien.gv.at (cit. 11.18.2015)

The Viability of Using Different Types of Recycled Plastic as Glazing in Windows

Islam A. Mashaly – American University in Cairo – imashaly@aucegypt.edu

Yusra Rashed – American University in Cairo – yusra.mer@aucegypt.edu

Salah El-Haggar – American University in Cairo – elhaggar@aucegypt.edu

Khaled Nassar – American University in Cairo – knassar@aucegypt.edu

Abstract

Plastic waste is a growing issue that needs to be addressed, multiple solutions are established to reduce its impact on the environment. The aim of this research is to make use of the plastic waste piling up and, at the same time, to create a convenient daylighting solution. The research proposes a sustainable fenestration system to be used in hot-arid climates, particularly in Egypt, where it is common to use tinted glass to lower the heat gain. First, a recycling process was carried out to create samples, the samples were then tested to obtain their optical properties and lastly Radiance, a daylighting simulation tool, was used to test the performance of recycled plastics as a window glazing material. In the recycling process, three plastic types were used to create the samples: polypropylene PP (number 5), polystyrene PS (number 6), and polycarbonate PC (number 7). It was concluded that the use of recycled plastics as a glazing material is indeed possible. Polycarbonate ranked as the most transparent, yet its impurities were the most visible. Polystyrene was also observed to be quite transparent, however its transparency was inversely related to its thickness. Polypropylene was the least transparent under the selected settings. Nonetheless, further research is required regarding the recycling process settings, to determine the possibility of obtaining more transparent results.

1. Introduction

Daylighting is one of the major indoor environmental aspects that has a major influence on the behaviour and attitude of the occupants (Cuttle, 1983). Daylighting is used as one of the effective passive strategies to uniform illumination within living spaces, where high energy savings can be achieved (Lim et al., 2012). It is a major factor in human health

and productivity that has a positive effect on the psychological comfort more than artificial lighting (Cheung and Chung, 2008; Cuttle, 1983). Nevertheless, daylighting is hard to fully exploit due to the challenges that accompany it, like excessive heat gain or the need for complex expensive strategies to introduce it adequately into the space. Consequently, daylighting benefits are often overlooked in Egypt as most common practices favor the small fenestration area, which hardly allows an adequate daylighting distribution. For instance, according to the Egyptian Energy Code 306-2005 (2006) a window-to-wall ratio that exceeds 30 % is unacceptable, a rather insufficient value for deep spaces. Moreover, very few daylighting techniques utilize passive strategies that don't require the use of virgin materials.

Egypt produces around 980,000 tons of plastic waste annually (2005/2006) while only 30 % gets recycled and 5 % is reused. The remaining 65 % is either burnt or buried unused (Plastic Technology Center, 2008).

This paper proposes a sustainable Fenestration System with a translucent glazing that makes use of the accumulating plastic waste and serves as a convenient means to utilize daylighting as well. The translucent layer will be made of recycled plastics, such as polypropylene PP (number 5), polystyrene PS (number 6), and polycarbonate PC (number 7). PC is considerably used in construction projects for semi-transparent roof tiles, therefore, considered fairly expensive compared to other types of plastics. PP is the main kind of plastic for food containers that comes in different colours, transparencies, and optical properties. PS is also used in the food sector, however, more disposable than PP and less cheap.

Polystyrene products consist of a very high percentage of air gaps in between their structure, therefore they are considered light. The recycled plastic layer will diffuse the light transmitted into the room in order to prevent bright spots near the window. At the same time, this will ensure privacy to users inside the space as well as adequate daylighting.

2. Literature Review

2.1 Recycle Plastic Usage

Recycled plastics have numerous uses in the building industry. Aminudin et al. (2011) reviewed the potential use of recycled expanded polystyrene (EPS) as a thermally insulating material in buildings. Aminudin et al. also stated that EPS has high compressive stress, which makes it suitable for integrating with building materials.

In an extensive literature review Lei Gu and Togay (2016) stated that plastics such as Polyethylene terephthalate (PET), EPS, high-density polyethylene (HDPE) and low-density polyethylene (LDPE) can be recycled and used as plastic aggregates, while PP and PET fibres can be used as plastic fibres, and both Polyamide (PA) and Phenol formaldehyde (PF) are used in concrete in different ratios and weights, since they give different properties to the concrete mix.

Recently, Dalhat and Al-Abdul Wahab (2016) formulated a cement-less and asphalt-less concrete mix using recycled plastic such as recycled PP and recycled HDPE.

Yet, no cited research mentioned the use of recycled plastic as a glazing in a fenestration system, and a few researchers mentioned the optical properties of recycled plastics to be used for glazing.

2.2 Glazing Technologies

Glazing systems went through several improvements since the beginning of the 20th century, from the introduction of the double and triple pane glass to the creation of tinted and Low-E glass. In his paper entitled "Solar Radiation Glazing Factors for Window panes, Glass Structures and Electrochromic Windows in Buildings—Measurement and Calculation" Bjørn Petter Jelle (2013) summarized

the state of the art technologies in glazing systems. He specifically focused on Electro Chromatic Windows (ECW), which are dynamic window structures that vary in voltage according to the solar radiation, thus changing the window's color and tint. In "The Role of Window Glazing on Daylighting and Energy Saving in Buildings" Hee et al. (2015) compared the performance of single, double, and triple glazing windows thermally and visually.

2.3 Glass Properties and Use in CFS

One of the windows' main design parameters, with regard to visual properties, is the visible transmittance (T_{vis}), which ranges from 0 to 1.0. When it approaches 1.0 it means that the material transfers more light energy when light passes through (Lawrence Berkley National Laboratories, 2015). Another main property is the transparency of the material, defined as the amount of perception of an object within or at the other side of any material. When light is transmitted without the clarity of the image this is called "translucency" (Tripathi, 2002). Last but not least, the refraction index is a vital optical property of any material which controls the refraction angle of any incident light on a material, furthermore the total internal reflection of the material (TIR) is determined by the value of the refraction index. As the refractive index value is higher, a higher refraction angle occurs as light propagates through the material.

3. Methodology

The process of manufacturing and selecting the suitable recycled plastic included several steps which are categorized as experimental physical work and simulation and validation work. The experimental work involves recycling plastic products and testing the optical properties of the final recycling output. While the simulation work engages with the optical properties and incorporates them in a Radiance-based simulation to test the daylight performance of the materials.

3.1 Recycling Plastic Material Manufacturing Process and Optical Property Testing

A suitable plastic material was selected by testing different alternatives, and visually observe the optical properties of the products. The plastic types included Polycarbonate PC, Polypropylene PP and Polystyrene PS in this paper. The 3 materials were bought as post-consumer products and a recycling process was carried out. First the materials were cleaned then shredded using a shredding machine. The shredded plastic underwent another refined shredding process in order to reach fine pellets of the material.

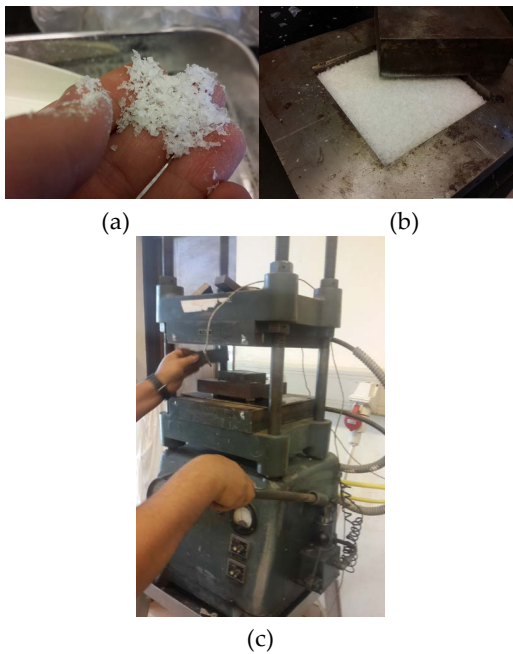


Fig. 1 – (a) Fine pellets of PS shredded (b) Pellets inserted between two plates (c) Hydraulic press machine with heaters

The fine pellets were inserted between two plates as shown in Fig. 1. Afterward, the dyes were placed on a hydraulic press with heaters installed on the upper and lower plates. Different pressures and temperatures were tested for each material, in order to reach an acceptable range of optimum settings as shown in Table 1. The final product dimensions were 10 cm x 10 cm, and 4 mm thickness.

The successful products were optically tested using a UV/VIS spectrometer to measure the optical properties of the material such as the transmission and reflectance.

Table 1 – Settings for recycling different types of plastics

Material	Temperature (°C)	Pressure (psi)
PC	150-170	2000
PS	105-110	1500
PP	120-140	2000

3.2 Daylight Simulation Software: Radiance

After manufacturing and testing different recycled plastics, they were simulated on Radiance, a light simulation software to ensure viability before manufacturing an actual prototype.

Radiance simulates prismatic designs with variable outputs, dependent on the input angle, using the BSDF. The BSDF is generated by creating an accurate geometrical 3-dimensional model, also the material is modelled on Radiance using flexible material definitions. To model a translucent plastic material on Radiance the *trans* definition is used. However, it is highly probable that the recycling process would not be 100 % pure homogenous plastic. Any type of impurities will affect the optical properties of the final product. The impurities are randomly present within the medium of the panel. Therefore, to represent those impurities during the simulation the prismatic panel material should contain a *Function File* replicating those impurities. The most suitable function file done in radiance for the previous circumstances is the *Noise.cal*. In order to use the *Noise.cal* function file, another material definition should be used. The *transfunc* is a unique material definition script that is used for arbitrary Bidirectional Reflection Distribution Function (BRDF). The arguments to this material are the data file, in this case, the *Noise.cal*, and coordinate index functions in addition to specular transmission and reflectance. The only modifier that is not available in this material definition is roughness, which is not required since the BRDF data is dominant. The *transfunc* parameters is defined as follows:

<i>modifier</i>	<i>transfunc</i>	<i>identifier</i>
2+	<i>brtd</i>	<i>funcfile</i>
0		
6	<i>R</i>	<i>G</i> <i>B</i> ◀(Colour)
	<i>rspec</i>	◀(specularity)
	<i>trans</i>	◀(transmission & transmitted specularity)
	<i>tspec</i>	

The BSDF is created using genBSDF and afterwards tested using Radiance’s latest 5-phase method. The 5-phase method is considered an effective method for performing annual simulations of complex fenestration systems (CFS) and dynamic fenestration systems. The flux transfer is categorized into 3 independent simulation stages as the following:

1. Sky dome to the exterior of fenestration
2. Transmission by BSDF through fenestration
3. Interior of fenestration into the simulated room

The space design used to test the proposed design is a standard office room by Reinhart et al. (2013) used for daylighting and illumination. The test was conducted in Cairo, Egypt, a hot arid area, with clear sky conditions throughout the year.

Table 2 – Simulation settings for Radiance

Interior Room Surface	Parameter	Value
Interior Walls	Reflectance (%)	0.50
Floor		0.50
Ceiling		0.80
Window Frame		0.50
Window/wall ratio	Ratio (%)	0.20
Windows Dimensions	Length x Width (m)	2.0 x 1.8
Shading Device	Y/N	No
Illuminance sensor point	Height (m)	0.75
	Distance in-between (m)	0.50
	Number of points	45
	Distribution (L x W)	8 x 5
Sky Condition	Clear/Overcast/uniform	Clear Sky

To obtain accurate and comparable results for an annual simulation, it is recommended to use the state-of-the-art measurement method. The Spatial Daylight Autonomy (sDA) and Annual Sunlight Exposure (ASE) are 2 factors lately published by the US Illuminating Engineering Society in the LM-83-12 document “Approved Method: IES Spatial Daylight Autonomy (sDA) and Annual Sunlight Exposure (ASE)” (IES, 2013). The sDA describes “the percentage of floor area that receives at least 300 lx for at

least 50 % of the annual occupied hours”. Specifically, ASE measures “the percentage of floor area that receives at least 1000 lx for at least 250 occupied hours per year”. Combining both measurements gives an indication of daylighting adequacy and visual comfort (IES, 2013).

4. Results and Discussion

4.1 Optical Properties and Visual Observations of Different Recycled Plastic Materials

Visual Observation of the different recycled materials: First, the samples were visually observed. All 3 materials are translucent but with different grades. The polycarbonate is the most transparent, visually, while the polypropylene is hardly transparent. Yet, it can transmit some light. Both polycarbonate and polystyrene developed a brownish colour; however, polypropylene developed a white colour.

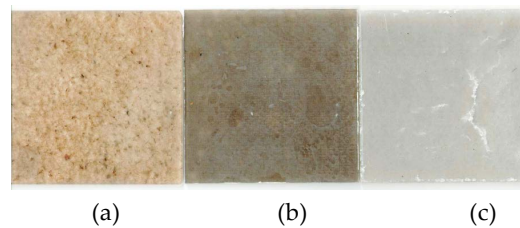


Fig. 2 – The recycled plastic samples (a) PC (b) PS (c) PP

The polycarbonate visual texture indicates the presence of high impurities and incomplete mixing of the polycarbonate pellets. However, polystyrene had a clearer texture with little impurities to see. On the other hand, polypropylene showed some vine-like impurities which resulted from “un-cooked” PP particles.

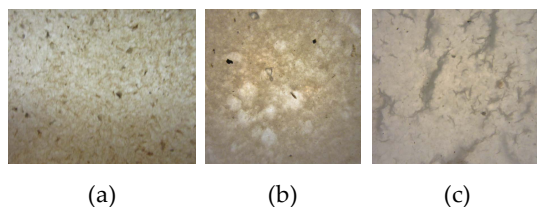


Fig. 3 – Close-up of the 3 materials (a) PC (b) PS (c) PP

Diffused Transmission Measurements:

The spectrophotometer results at 550 nm are shown as follows:

Table 3 – Diffused and specular transmittance and reflectance of the different plastics

Material	Transmittance		Reflectance	
	Diffused	Specular	Diffused	Specular
RPC	8.6 %	20.0 %	34.0 %	37.4 %
RPS	2.5 %	2.8 %	45.1 %	49.6 %
RPP	2.2 %	2.4 %	45.5 %	50.0 %

The previous findings resulted from the average values of the material along different points on the surface since recycled plastic is impure and contains different foreign particles within the medium of the material. Those impurities would affect the overall light transmission of the material.

4.2 Radiance Simulation Results of the Different Recycled Plastic Materials

The readings from the spectrophotometer were used in the material definition in Radiance in order to accurately model the behaviour of the materials selected along the whole year using the five-phase method. The rPC material was chosen for comparison and was modelled with *trans* where the diffused and specular transmission and reflection were converted to Radiance’s *trans* material definitions.

```
void      transfunc      FlatGlass
2        brtd      noise.cal
0
6        0.672  0.672  0.672
         0.370
         0.286  0.20
```

As for the Radiance simulation, the recycled PC samples resulted in decreasing the direct illumination in front of the window in comparison with the ordinary tinted glass of the same transparency; however, the illumination also decreased in the whole room due to the decrease in total transmission of the sample.

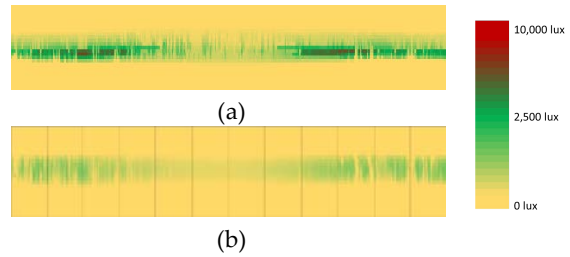


Fig. 4 – Total hourly illuminance in lux for 1 year at the node near the window (a) Tinted glass (b) Recycled Polycarbonate

As for the sDA and ASE, there was a decrease in the total values of both measurements, which means that less direct daylighting has entered the space. The sDA decreased from 40 % to 22 % whereas the ASE decreased from 33 % to 18 %.

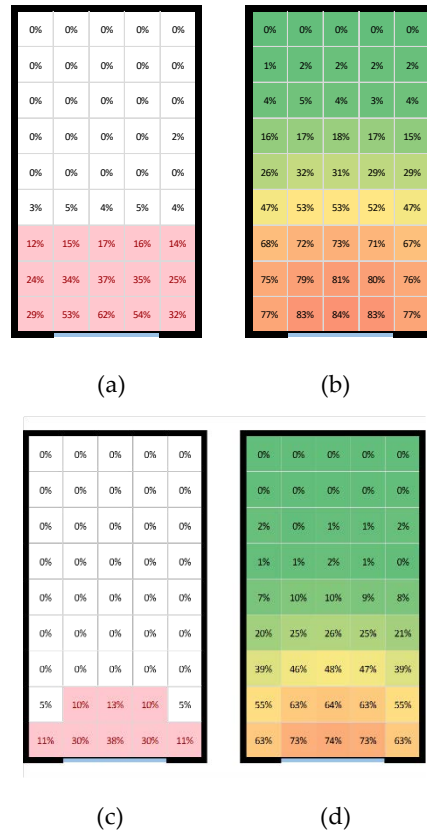


Fig. 5 – ASE (left) and sDA (right) for both Tinted glass (a,b) and recycled PC (c,d)

5. Conclusions

The idea of using recycled plastic as a glazing part in the window is feasible, and its texture and visual appearance could serve as a tinted glazing material. However, further modifications in the recycling

process and proper treatments are needed. Polycarbonate has the highest transparency yet its impurities are the most visible. While polystyrene might have greater potential in achieving greater transparency either by decreasing the thickness or enhancing the recycling process. As for polypropylene, further research has to be done on the right settings and smaller thicknesses should be tested since it has the potential of creating white and translucent glazing. On the other hand, further tests should take place to analyze the material's thermal properties, such as the U-value, and physical properties to ensure that the recycle plastic will withstand internal and external changes in the environment. A wider variety of plastics should be tested, as well as different mixtures of plastics.

References

- Aminudin, E., M.F. Md Din, Z. Mohamad, Z.Z. Noor, K. Iwao. 2011. "A review on recycled expanded polystyrene waste as potential thermal reduction in building material." In: *Proceedings of the International Conference on Environment and Industrial Innovation IPCBEE*, Singapore: IACSIT Press.
- Bjørn, P. 2013. "Solar radiation glazing factors for window panes, glass structures and Electro chromic windows in buildings—Measurement and calculation", *Solar Energy Materials and Solar Cells* 116: 291-323. doi: 10.1016/j.solmat.2013.04.032.
- Cuttle, C. 1983. "People and windows in workplaces." In: *Proceedings of the people and physical environment research conference*. Wellington, New Zealand: Ministry of Works and Development.
- Cheung, H.D., T.M. Chung. 2007. "A study on subjective preference to daylit residential indoor environment using conjoint analysis." *Building and Environment* 43 (12): 2101-2111. doi: 10.1016/j.buildenv.2007.12.011.
- Dalhat, M.A., H.I. Al-Abdul Wahhab. 2016. "Cement-less and asphalt-less concrete bounded by recycled plastic", *Construction and Building Materials* 119: 206-214. doi: 10.1016/j.conbuildmat.2016.05.010.
- ECP 306-2005. 2006. *Egyptian Code for building energy conservation*.
- Hee, W.J., M.A. Alghoul, B. Bakhtyar, OmKalthum Elayeb, M.A. Shameri, M.S. Alrubaih, K. Sopian. 2015. "The role of window glazing on daylighting and energy saving in buildings", *Renewable and Sustainable Energy Reviews* 42: 323–343. doi: 10.1016/j.rser.2014.09.020.
- IES. 2013. *LM-83–12. Approved Method: IES sDA and annual sunlight exposure (ASE)*.
- Lawrence Berkeley National Laboratory. 2015. "Visible Transmittance (VT or Tvis)" <http://www.commercialwindows.org/vt>, Accessed: 22nd April 2016.
- Lei, G., O. Togay. 2016. "Use of recycled plastics in concrete: A critical review", *Waste Management* 51: 19–42. doi: 10.1016/j.wasman.2016.03.005.
- Lim, Y.W., M.Z. Kandar, M.H. Ahmad, D.R. Ossen and A.M. Abdullah. 2012. "Building façade design for daylighting quality in typical government office building." *Building and Environment* 57: 94–204. doi: 10.1016/j.buildenv.2012.04.015.
- Plastic Technology Center. 2008. *Plastic Recycling Development Strategy*, Egypt.
- Reinhart, C., F.J. Alstan Jakubiec, D. Ibarra. 2013. "Definition of a reference office for standardized evaluations of dynamic façade and lighting technologies", In: *Proceedings of the 13th Conference of International Building Performance Simulation Association*. Chambéry, France.
- Tripathi, D. 2002. *Practical Guide to Polypropylene*, Smithers Rapra.

Implications of Increasing Daylighting in Deep Energy Retrofitting in Norwegian Shopping Centres

Matthias Haase – SINTEF Building and Infrastructure – matthias.haase@sintef.no

Andreas Ampenberger – BLL – andreas.ampenberger@bartenbach.com

Abstract

The analysis of 11 shopping centres in Europe reveals a lack of availability of indoor natural daylight, especially in shops and sales areas. The aim of this paper is to investigate the consequences on energy consumption and electricity use for lighting that novel retrofitting measures have when applied to Norwegian shopping centres (Haase et al., 2015a).

Internal daylight and internal illuminance levels were measured in two shopping centre buildings in Trondheim and Modena together with detailed monitoring of energy use and indoor air quality.

Scenarios were modelled to simulate the artificial lighting use patterns and control strategies in the shopping centres by considering occupancy hours and type of activity (illuminance levels), in order to cover different possible combinations used in the energy and daylight simulations.

Existing conditions of shopping centres (pre-retrofitting) in Trondheim, Norway were modelled based on drawings and validated with energy use measurements. Energy and daylighting simulations were performed and combinations of use pattern scenarios and facade variables were used to evaluate the influence on the electricity use for lighting and energy use for heating and cooling of the different scenario combinations. There is a trade-off, which is quantified in terms of reduction in electricity use and cooling demand as well as an increase in heating demand. The implications of lighting retrofitting on heating and cooling (aside from the end energy use savings) make the application complicated in shopping centres. Modelling and simulation of a shopping centre can help us understand the holistic consequences of single energy retrofitting measures.

1. Introduction

The paper is part of activities performed in the ComONEnergy project, where the aim is to transform

shopping centres into lighthouses of energy efficiency. It is a project with 23 partners that studies comprehensive retrofit solution sets to save energy and promote high IEQ in shopping centres, as well as the optimal environmental conditions for display and sale of merchandise. In a comparison with the pre-retrofit conditions, the project aimed to achieve a 75 % reduction of energy demand, power peak shaving, a 50 % increased share of energy used from Renewable Energy Sources (RES) compared to a base-case (renewables share so far), and an improved Indoor Environmental Quality (IEQ). The research was based on the demand for a comprehensive approach for the development of a retrofitting package for shopping centres, taking into account the specific needs of the building, such as indoor conditions, complex energy flows and the lack of standard energy intensity performance indicators (Bointner et al., 2014; Haase et al., 2015a; Haase et al., 2015b; Haase et al., 2015c).

Shopping centres are not interchangeable with other kinds of complex buildings, such as office blocks, hospitals or schools (ICSC, 2008; Stensson, 2014; Coleman, 2006). Their form, function, usage, and users give shopping centres a particular character with special implications for energy use (Coleman, 2006; Stensson, 2014; Woods et al., 2015; Woods et al., 2017). To support the understanding of what causes the main inefficiencies in energy usage and to enable the development of the best solution-sets, Bointner et al. (2014) developed a definition of shopping centres which describes shopping centres as "a formation of one or more retail buildings comprising units and 'communal' areas which are planned and managed as a single entity related in its location, size and type of shops to the trade area that it serves". The definition gives an indication of the

main form and function of shopping centres. In addition, location, type of development, the size and GLA, the type of anchor stores and the trip purpose are all aspects that have been used to indicate the needs that a shopping centre serves within a social and physical context (Woods et al., 2015; Woods et al., 2017).

In the CommONEnergy project a number of solution-sets were developed starting from 11 real reference buildings located in different climatic, environmental, social and economic contexts, representative of the whole EU shopping centre building stock. Such solution-sets are tailored on architectural, constructive and technological features of this very special kind of building. Both energy load profiles and final uses are not comparable with other building categories, needing specific tools and dedicated approaches to achieve the best benefits/costs ratio. The analysis of 11 shopping centres in Europe (Fig. 1) reveals a lack of availability of indoor natural daylight, especially in shops and sales areas (Woods et al., 2015; Haase et al., 2015b).



Fig. 1 – The 11 different reference buildings

2. Objectives

The aim of this paper is to investigate the consequences on energy consumption and electricity use for lighting that novel retrofitting measures have, when applied to a Norwegian shopping centre.

3. Methodology

Together with detailed monitoring of energy use and indoor air quality, internal daylight and internal illuminance levels were measured in a shopping centre in Trondheim.

Scenarios were modelled to simulate the use patterns and control strategies of artificial lighting in the shopping centres considering occupancy hours and type of activity (illuminance levels), in order to cover different possible combinations used in the energy and daylight simulations.

The building was modelled in TRNSYS according to the plans and architectural drawings. A sketchup model (Fig.2) was developed and the functional units in the shopping mall were divided into common areas, shops, and others (Haase et al., 2015d). Existing conditions of the Norwegian shopping centre (pre-retrofitting) were modelled in TRNSYS based on the energy use measurements and energy and daylighting simulation were performed. Combinations of use pattern scenarios and facade variables were used for daylight and energy simulations in the retrofitted shopping centres to evaluate the influence on the electricity use of lighting and energy use of the combinations of the scenarios. Radiance was used for the lighting buildings analysis (Ward, 1989).

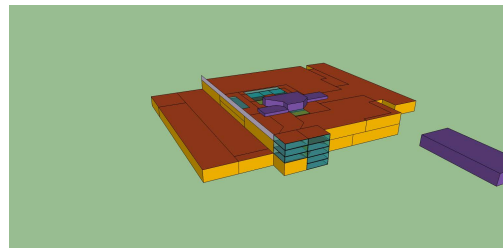


Fig. 2 – Sketchup model of the shopping centre from Haase et al. (2015d)

3.1 Energy Audit

The shopping centres that were analysed vary in size and energy use. Fig. 3 shows the share of gross leasable areas in the different reference buildings.

Fig. 3 shows that common areas cover 13 % of the gross leasable area (GLA) in all the shopping centres. Retrofitting measures will have an accordingly minor effect on the total energy use in shopping centres.

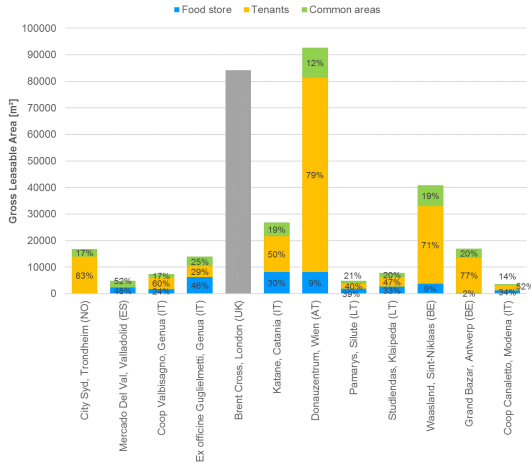


Fig. 3 – Gross leasable areas (GLA) of the different reference buildings

An identification and analysis of the current building energy behaviour was done in order to define the power peaks and the energetic balance in different time frames (from day to year). Technological active-installation check-ups were done in order to get a clear and detailed understanding of where and how the different facilities operate to match the building loads. An evaluation of the gathered data provided valuable input for the dynamic simulation platform, through a reverse engineering process, to compare generation and consumption profiles, highlighting overloads, overproductions, inefficiencies, lack of coordination, possible gaps and overlapping, necessities of shifting and storing among others, based and verified through the monitored data.

Fig. 4 shows that the simulated and measured electricity use in the Norwegian shopping centre match well.

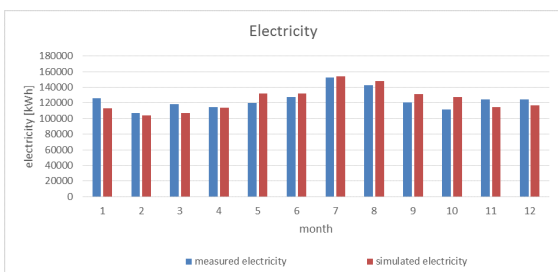


Fig. 4 – Validation of model with measured data

Finally, a definition of the energy retrofitting process – through the implementation in dynamic software of the novel developed and proposed concepts – was developed in order to verify the viability of the selected technologies and to assess foreseen results. The output of this analysis was used to define the baseline for the development of the control strategy for the improvement of existing technologies and the implementation of new ones.

3.2 Climatic Influence and Schedules

Sky conditions, especially the amount of sunny skies is different. Trondheim has few hours of clear blue sky. Opening hours are from 09:00 to 21:00, preparation hours are from 07:00 to 09:00 and night milieu hours are from 17:00 to 21:00 (see also Tab. 1 for further explanations of the lighting concept. Cases (3) and (4) introduce preparation periods.).

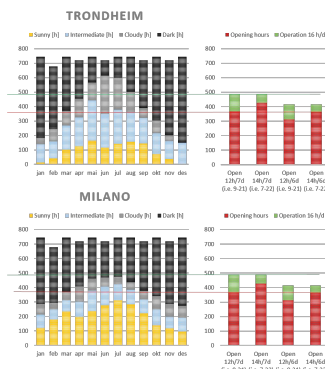


Fig. 5 – Sky conditions in Trondheim and opening hours of the shopping centre

Fig. 5 shows that almost during the whole year sunrise takes place before the opening hours. Bear in mind that even before sunrise and after sunset, it is not completely dark either. Preparation hours (re-stocking, cleaning, etc.) are often before sunrise/ after sunset. Cloudy and intermediate sky have brighter diffuse light levels than a blue sky.

3.3 LED Lighting

Description of the LED lighting strategy:

- Case (0)
- Case (1) New luminaires
- Case (2) constant light output (CLO)
- Case (3) zoning
- Case (4) night milieu with reduced intensity
- Case (5) light pipes

Each case is described in more detail in Tables 1 and 2. It can be seen that the resulting power per luminaire is reduced for Cases (1) to (5) compared to Case (0).

Table 1 – Lighting control strategy

Case	No. of luminaires	Control strategy	Power per luminaire [W]
(0)	43	constantly on during op. hours	70
(1)	57	constantly on during op. hours	37.72
(2)	57	constantly on during op. hours	33.86
(3)	57	+ PREP hours	27.02
(4)	57	+ PREP hours + day/night milieu	27.02
(5)	31		32.26
Not daylit zone			
(5)	26	+ light tubes	21.15
Daylit zone			

By installing three light tubes it was possible to reduce the lighting according to daylight illuminance. Table 2 shows the results of the nominal power for the demonstration shop area in the Trondheim shopping centre. Cases (1) to (3) reduce nominal power during opening hours. Cases (3) to (5) introduce additional preparation periods with reduced nominal power. Cases (4) and (5) introduce in addition a night milieu period with again reduced nominal power.

Table 2 – Lighting power installed in demonstration shop area

Case	Power per lum. (PREP) [W]	Nominal power		
		during opening hours [kW]	during prep hours [kW]	during night milieu [kW]
(0)	-	3.39	-	-
(1)	-	2.15	-	-
(2)	-	1.93	-	-
(3)	18.95	1.54	1.08	-
(4)	18.95	1.54	1.08	1.08
(5)	22.58	1	0.7	0.7
not daylit zone				
(5)	14.628	0.55	0.38	0.38
daylit zone				

3.4 Light Tube Solutions

In one demonstration shop on the first floor of the shopping centre in Trondheim, a retrofitting to enhance daylight was conducted with three light tubes (see Fig. 6 for details).

The demonstration shop area was 100 m² (including 15 m² storage). Fig. 6 shows the plan and a section, Fig. 7 a photo. The diameter of each light tube is 1000 mm. Rooftop domes were placed on top of each light tube to provide air and water tightness.

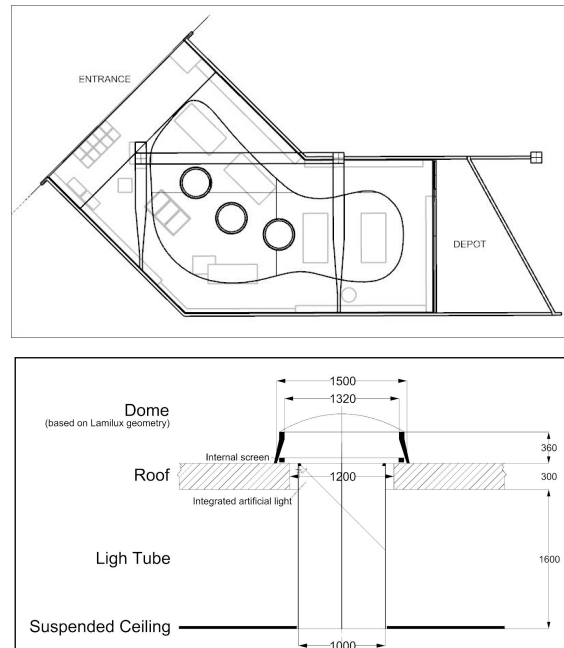


Fig. 6 – Plans of light tube solution in demonstration area



Fig. 7 – Photo of the light tube solution in demonstration area

4. Results

The implications of the installed power reductions of the cases (1) to (5) compared to case (0) are shown in Table 3. The mean specific power demand per area is reduced from 39.8 (case (0) to 16.5 W/m² (case (4)) and to 15.2 W/m² (case (5)) with luminous flux. The implications of the different lighting retrofitting measures were then applied to the whole shopping centre. Two strategies were tested. First, the lighting retrofitting cases (1) to (5) were applied to the common areas (cma). Electricity savings were determined in primary energy (PE). Heating and cooling implications were determined. Secondly, the lighting retrofitting cases (1) to (5) were applied to the shop areas. Electricity savings were determined in primary energy (PE). Heating and cooling implications were determined.

The results from energy the simulations can be divided into electricity use, heating and cooling needs. Here, a focus was put on the lighting retrofitting measures, not on appliances nor on ventilation.

Table 3 – Results of the lighting strategy

Case	Specific yearly energy demand [kWh/m ² a]	Mean specific power demand per area [W/m ²]	Specific luminous flux per area [klm/m ²]
(0)	178.2	39.8	2.06
(1)	113	25.3	1.69
(2)	102	22.8	1.69
(3)	77	17.2	1.28
(4)	74	16.5	1.23
(5)	68	15.2	1.23

4.1 Final Energy Use

Table 4 shows the heating and cooling implications. Cooling decreases from 20.1 kWh/(m² a) (case (0) to 4 kWh/(m² a)) in cases (4) and (5). The need for heating increases from 49.5 kWh/(m² a) (case (0)) to 70.4 kWh/(m² a) for case (4) and 84.3 kWh/(m² a) for case (5). Together with the electricity reduction from lighting the total also decreases from 206.8 kWh/(m² a) (case (0)) to 124.4 kWh/(m² a) for case (4) and 119.5 kWh/(m² a) for case (5).

The changes are small when looking at the results for the common areas. Energy use for cooling decreases insignificantly from 20.1 kWh/(m² a) (case (0) to 19.4 kWh/(m² a) in case (4). Energy use for heating increases from 49.5 kWh/(m² a) (case (0) to 58.1 kWh/(m² a) in case (4).

Table 4 – Final energy use of lighting strategy in [kWh/(m² a)]

Case	area	Lighting	Heating	Cooling	Total
(0)	-	137.3	49.5	20.1	206.8
(1)	cma	121.6	57.2	19.5	198.3
	cma+shp	109.3	58.2	16.2	183.7
(2)	cma	120.9	57.5	19.5	197.9
	cma+shp	80.1	59.9	7.0	147.0
(3)	cma	120.1	57.8	19.4	197.3
	cma+shp	55	67.5	4.0	126.5
(4)	cma	119.4	58.1	19.4	196.9
	cma+shp	50	70.4	4.0	124.4
(5)	shops on first floor	31.2	84.3	4.0	119.5

4.2 Primary Energy Use

Fig. 8 shows the energy implications in Trondheim with cases (1) to (5) applied to different parts of the shopping centre.

Primary energy (PE) use for the whole shopping centre is 712 kWh_{PE}/(m² a). Primary energy (PE) use for case (0) for lighting is 343 kWh_{PE}/(m² a), for appliances 141 kWh_{PE}/(m² a), for ventilation 110 kWh_{PE}/(m² a), for heating 67.2 kWh_{PE}/(m² a), and for cooling 50 kWh_{PE}/(m² a).

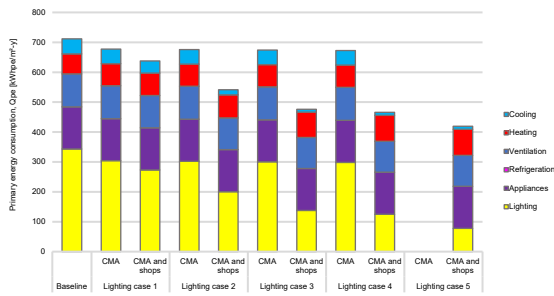


Fig. 8 – Primary energy use in Trondheim

Primary energy (PE) use for lighting can be reduced to 34 kWh_{PE}/(m² a) (4.8 % for case (1)) to 39 kWh_{PE}/(m² a) (5.5 % for case (4)) if applied to the common areas (cma). These are the typical areas, which are managed and maintained by the centre managers directly.

The application of lighting retrofitting cases (1) to (4) to all areas (cma and shops) results in PE savings of 74 kWh_{PE}/(m² a) (10.4 % for case (1)) to 246 kWh_{PE}/(m² a) (34.6 % for case (4)).

PE savings of 282 kWh_{PE}/(m² a) (39.6 % for case (5)) could be reached, if case (5) was applied to all suitable shops (all shops on the first floor).

5. Discussion

Existing conditions of the Norwegian shopping centres (pre-retrofitting) were modelled based on the energy use measurements and energy and daylighting simulations were performed. Combinations of use pattern scenarios and facade variables were used for the daylight and energy simulations in the retrofitted shopping centres to evaluate the influence on the electricity use of lighting and energy use of the combinations of the scenarios.

Together with the reduction of electricity employed for lighting, the total used for lighting, heating and cooling also decreases. However, the final energy use for heating increases.

PE savings of 35 % were possible with lighting retrofitting (case (4)) in common areas and shop areas. However, lighting retrofitting of shop areas is the responsibility of the shop owner/manager. It requires further engagement of these stakeholders to effectively implement lighting retrofitting solutions. These solutions save electricity (end energy use) but

also influence heating and cooling end energy use. The highest heating energy use is for case (5) (up to 84 kWh/(m² a)). Even if the total energy use is minimized, an increase in heating demand requires additional investment in a heating system upgrade. In the next step, further measures should be applied to reduce energy use for heating to complement the lighting retrofitting strategy.

6. Conclusions

The work that formed the basis for this paper investigated the consequences on energy consumption and electricity use for lighting that novel retrofitting measures have when applied to a typical shopping centre. Lighting retrofitting results in a PE reduction of up to 40 %. The end energy use for lighting, heating and cooling also decreases. However, while end energy use for lighting and cooling decreases, the end energy use for heating increases.

There is a trade-off, which can be quantified in terms of reduction in electricity use and cooling demand as well as an increase in heating demand. As a consequence, existing window and roof structures needs to be further developed in order to give centre and shop managers a basis for decision making on refurbishment investments.

Shopping centre managers are usually responsible for providing heating (and often cooling, or at least cooling energy) to the shops. Lighting is usually in the responsibility of (each) shop owner/manager. The implications of lighting retrofitting on heating and cooling, aside from the end energy use savings, make the application complicated in shopping centres. The modelling and simulation of a shopping centre can help to understand the holistic consequences of single energy retrofitting measures. Aside from the straight forward end energy use savings (electricity), lighting retrofitting has implications for heating and cooling end energy use and primary energy savings. Shopping centre managers need to collaborate closely with shop owners/managers on energy retrofitting measures if the full potential is to be applied.

Acknowledgement

The research leading to these results has received funding from the European Community Seventh Framework Programme (FP7/2007-2013) under grant agreement no. 608678.

Nomenclature

Symbols

cma	Common areas
shp	Shop areas
PE	Primary energy
PREP	Preparation period

References

- Bointner, R., A. Toleikyte, R. Woods, B. Atanasiu, A. De Ferrari, C. Farinea, F. Noris. 2014. *Deliverable 2.1 report - Shopping malls features in EU-28 + Norway, EU FP7 project CommONEnergy – Reconceptualizing Shopping Malls*, access date: April 2015: <http://www.commonenergyproject.eu/>
- Coleman, P. 2006. *Shopping environments: Evolution, planning and design*. Oxford, UK: Elsevier.
- Haase, M., K.S. Skeie, R. Woods, S. Mellegård, R.D. Schlanbusch, S. Homolka, J. Gantner, S. Schneider, F. Lam-Nang. 2015a. *Deliverable 2.3 report - Typical functional patterns and socio-cultural context, EU FP7 project CommONEnergy – Reconceptualizing shopping malls*, access date: April 2015: <http://www.commonenergyproject.eu/>
- Haase, M., R. Woods, S. Mellegård, K.S. Skeie, R. Lollini, F. Noris, J. Antolín. 2015b. *Deliverable 2.5 report - Main drivers for the deep retrofitting of shopping centres, EU FP7 project CommONEnergy – Reconceptualizing shopping malls*, access date: April 2015: <http://www.commonenergyproject.eu/>
- Haase, M., R. Woods, K.S. Skeie. 2015c. "The key drivers for energy retrofitting of European shopping centres". *Energy Procedia* 78: 2298–2303. doi:10.1016/j.egypro.2015.11.368.
- Haase, M., A. Belleri, C. Dipasquale, K.S. Skeie. 2015d. "Modelling of a complex building in Norway". In: *Proceedings of Building Simulation conference (BS2015)*. Hyderabad, India: IBPSA.
- ICSC. 2008, *The Importance of Shopping Centres to the European Economy*. Access date Oct 2015: (http://sigs.icsc.org/srch/rsrch/wp/FINAL_Mar08_Complete%20WITH%20new%20cover%20and%20charts%20and%20tables.pdf)
- Stensson, S. 2014. *Energy efficiency in shopping malls - some aspects based on a case study*. Göteborg, Sweden: Chalmers University of Technology.
- TRNSYS, URL: <http://www.trnsys.com/>.
- Ward, G. 1989. "The RADIANCE lighting simulation and rendering system". In: *Proceedings of the 21st annual conference on computer graphics and interactive techniques*. New York, U.S.A: ACM.
- Woods, R., S. Mellegård, R.D. Schlanbusch, M. Haase, K.S. Skeie, A. De Ferrari, M.V. Cambronero Vazquez, A. Ampenberger, R. Bointner. 2015. *Deliverable 2.2 report – Shopping mall inefficiencies, EU FP7 project CommONEnergy – Reconceptualizing shopping malls*, access date: April 2015: <http://www.commonenergyproject.eu/>
- Woods, R., K.S. Skeie, M. Haase. 2017. "The influence of user behaviour on energy use in European shopping centres." *Sustainable Development* 25: 11–24. doi: 10.1002/sd.1638.

PV-PCM Integration in Glazed Buildings. Numerical Study Through MATLAB/TRNSYS Linked Model

Hagar Elarga – University of Padova – hagar.elarga@dii.unipd.it

Francesco Goia – Norwegian University of Science and Technology – francesco.goia@ntnu.no

Ernesto Benini – University of Padova – ernesto.benini@unipd.it

Abstract

The paper describes the implementation of a 1-dimensional transient model based on the enthalpy method to analyse the thermal behaviour of a Phase Change Material (PCM) layer integrated in a window. The model and algorithm have been validated by comparison with experimental data. The model has then been expanded to couple a PV layer with the PCM layer. The complete model is implemented in MATLAB and linked to TRNSYS in order to estimate the dynamic thermal energy demand of a building equipped with a double skin façade with a PV-PCM layer in a ventilated cavity.

A parametric study was carried out, investigating three different cavity ventilation strategies for two European cities (Venice and Helsinki). The results show that, when the PCM layer is coupled with the PV layer, in Venice the cooling energy demand is 60 % lower, while in Helsinki the heating demand during the winter season is 36 % lower.

1. Introduction

PV modules conversion efficiency depends on the temperature of the panel, and an increment in PV surface temperature reduces the solar to electrical energy conversion efficiency by 0.4–0.5 %/K (Batagiannis et al., 2001). Therefore, the thermal control of PV modules (Machniewicz et al., 2015) is an important aspect to ensure effective solar energy conversion. According to the literature, six basic techniques for PV thermal management are possible: natural or forced air circulation, hydraulic or thermoelectric cooling, heat pipes, and the implementation of PCM. As far as the latter strategy is concerned, quite a few studies have appeared in the literature. A numerical PV/PCM model was

presented and validated through comparison with experiments for three different configurations. This model provided a detailed insight into the thermal performance of a solid–liquid transition PCM when employed in a PV.

Ciulla et al. (2012) presented a one-dimensional thermal analysis of an isothermal PV-PCM model by using an explicit finite-difference approach. The numerical model was validated against experimental data given by a test facility in Palermo, Italy. Then, it can be used to determine the thermal behaviour of a multilayer (opaque) wall where PCM is coupled with a PV module. A simplified thermal network model to build integrated photovoltaic with PCM (BIPV-PCM) was analysed by Aelenei et al. (2014), it was developed in MATLAB/SIMULINK and validated with experimental results during the heating period. The comparison showed a good agreement, with most discrepancies occurring when airflow begins to flow into the gap. The maximum electrical efficiency of the PV system reached 10 %. The economic consequences of applying PCM to a PV system in two different climates, were investigated by Hasan et al. (2014). They concluded that such a system is financially viable in higher temperature and higher solar radiation environments. The implementation of PCM in combination with PV seems a very promising technique but it requires a good design under many aspects (Machniewicz et al., 2015).

The aim of the study presented in this paper is to develop one-dimensional fixed nodal grid model for PV-PCM in double skin facades. The model is capable of describing, with a sufficient degree of accuracy, the optical and thermal performance of such a façade system, which is particularly

challenging in terms of modelling because of the cavity's airflow, and of the dynamic thermal and optical properties of the PCM.

The present work is a continuation of an activity presented by Elarga et al. (2016). It improves the simulation of the phase change of the PCM through the use of the enthalpy method, and couples the PV-PCM double skin façade to a building (modelled in TRNSYS) in order to calculate heating and cooling demands. The innovations presented in this paper are:

1. A validated one dimensional heat transfer model for the PCM layer based on the enthalpy linearization method; and
2. The coupling (co-simulation) of the PV-PCM double skin facade model, developed in MATLAB, with the model of a building in TRNSYS, in order to evaluate in detail the annual thermal energy demand of a building equipped with such a façade system.

A numerical study is also presented to highlight the importance of PCM cooling time related to external and internal building loads.

2. Methods

Different elements control the efficient implementation of the PCM in building components, especially the melting/solidification temperature range, specific heat capacity value, and the charging/discharging synchronization with thermal loads. Accordingly, accurate and effective modelling and simulation tools are required to ensure the proper selection of PCM type. Different methods have been proposed to track the phase transient behaviour of the material. In the present article, the numerical modelling is divided into three sections:

- Enthalpy method and validation.
- PV-PCM model implemented in MATLAB.
- MATLAB-TRNSYS coupling for annual simulations.

2.1 Enthalpy Method

The enthalpy method was proposed by Swaminathan and Voller (1992) in order to model the thermal

behaviour of the materials undergoing a phase change, under the assumption that a phase change occurs over an arbitrarily narrow temperature range. In this way, enthalpy can relate to the temperature by a piecewise continuous function. Enthalpy can be approximated with three temperature possibility ranges by assuming constant specific heat capacity in each phase, as in Equation 1.

$$H = \begin{cases} c_s T & T \leq T_{m-\epsilon} \\ c_s(T_m - \epsilon) + \left[\frac{c_s + c_l}{2} + \frac{L}{2\epsilon} \right] (T - T_m + \epsilon) & T_{m+\epsilon} < T < T_{m-\epsilon} \\ c_l T + (c_s - c_l)T_m + L & T \geq T_{m+\epsilon} \end{cases} \quad (1)$$

where ϵ is an arbitrarily small value representing half the phase change temperature interval. The approximate definition $H(t)$ can be differentiated into Equation 2 with respect to temperature:

$$C^A = \frac{dH}{dT} = \begin{cases} c_s & T \leq T_{m-\epsilon} \\ \left[\frac{c_s + c_l}{2} + \frac{L}{2\epsilon} \right] & T_{m+\epsilon} < T < T_{m-\epsilon} \\ c_l & T \geq T_{m+\epsilon} \end{cases} \quad (2)$$

The definitions of $H(T)$ and C^A can be used to linearize the discretized enthalpy equation in iterative form as in Equation 3:

$$\sum a_{nb} T_{nb} - (a_p + \rho C^A) T_p^n = a_p \rho C^A T_p^{n-1} - \rho \cdot \frac{v}{\Delta\tau} [H_p^\circ - H_p^{n-1}] \quad (3)$$

Where:

H_p° : Enthalpy node value of the previous time step

H_p^{n-1} : Enthalpy node value of iteration $n-1$

a : Nodal coefficients

τ : Time Step

The solution domain is defined where the derived linear equations form a matrix system and is solved instantaneously by inverting the matrix to obtain the temperature values according to an iterative scheme.

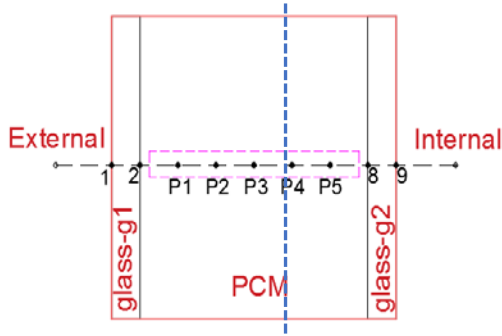
At the start of the time step the initial iterative fields are set to the previous time step values. From the known temperature field and enthalpy at iteration $n-1$ the temperature nodes are achieved. In order to ensure solution consistency, a correction and iterative loop has to be followed by saving the solution of the matrix in the previous iteration, and

then re-solving the system after having corrected the nodal temperature T_p^n by Equation 4 with three possibilities of enthalpy ranges until convergence is reached. The code thus saves the calculated temperature field, and starts a new time step.

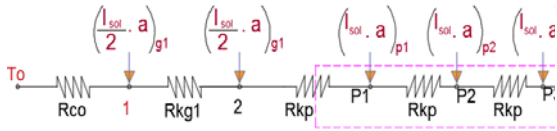
$$T_p^n = \begin{cases} \frac{H_p^n}{c_s}; & H_p^n \leq c_s(T_m - \epsilon) \\ \frac{H_p^n + \left[\frac{c_s + c_l}{2} + \frac{L}{2\epsilon}\right](T_m - \epsilon)}{\frac{c_s + c_l}{2} + \frac{L}{2\epsilon}}; & H_p^n > c_s(T_m - \epsilon) \\ & H_p^n < c_l(T_m + \epsilon) + L \\ \frac{H_p^n - (c_s - c_l)T_m - L}{c_l}; & H_p^n \geq c_l(T_m + \epsilon) + L \end{cases} \quad (4)$$

2.1.1 Mathematical model description

A nodal scheme was developed to describe the double glazed layered window integrated with PCM (Goia et al., 2012; Elarga et al., 2016). The PCM window is schematized in nine-temperature nodes (Fig. 1-a) and the code solves instantaneously the nine linear equations. The validation of the model was carried out by comparing the numerical simulations with the data measured by Goia et al. (2015). For the sake of brevity, only half of the RC model is illustrated in Fig. 1-b since the scheme is symmetric.



(a)



(b)

Fig. 1 – PCM glazing scheme (a), (b) symmetric scheme of RC model

Nodes (1) and (9):

$$\left(\frac{-k_{g1}}{x_{g1}} - h_o\right) T_1 + \left(\frac{k_{g1}}{x_{g1}}\right) T_2 = -I_s \left(\frac{a_{g1}}{2}\right) - (T_o h_o) \quad (5)$$

$$\left(\frac{k_{g2}}{x_{g2}}\right) T_8 + \left(-h_i - \frac{k_{g2}}{x_{g2}}\right) T_9 = -I_s \left(\frac{a_{g2}}{2}\right) - (T_i h_i) \quad (6)$$

Nodes (2) and (8):

$$\left(\frac{k_{g1}}{x_{g1}}\right) T_1 + \left(-\frac{k_{g1}}{x_{g1}} - \frac{k_{p1}}{x_{p1}}\right) T_2 + \left(\frac{k_{p1}}{x_p}\right) T_{p1} = -I_s \left(a_{g1}/2\right) \quad (7)$$

$$\left(\frac{k_{g2}}{x_{g2}}\right) T_9 + \left(-\frac{k_{g2}}{x_{g2}} - \frac{k_{p5}}{x_{p5}}\right) T_8 + \left(\frac{k_{p5}}{x_p}\right) T_{p5} = -I_s \left(a_{g2}/2\right) \quad (8)$$

PCM nodes (3:7); each homogenous sub-layer (from the five nodes comprising PCM layers) is represented by a conductive resistance and the enthalpy term. The resulting thermal balance Equation 9 is shown for one node only (P2).

$$\begin{aligned} & \left(\frac{k_p}{x_p}\right) T_{p1} + \left(-2\frac{k_p}{x_p} - \frac{(\rho \cdot x_p \cdot (c^A))_{p2}}{\Delta\tau}\right) T_{p2} + \\ & \left(\frac{k_p}{x_p}\right) T_{p3} = -I_s \cdot \left(\frac{a_{p2}}{2}\right) + \\ & \left(\frac{(\rho \cdot x_p \cdot (c^A))_{p2}}{\Delta\tau}\right)^{n-1} T_{p2}^{n-1} - \rho \frac{x_p}{\Delta\tau} [H_p^\circ - \\ & H_p^{n-1}] \end{aligned} \quad (9)$$

2.1.2 Short-wave radiation

Within the PCM layer, the analysis of the optical performance, and accordingly the short wave radiation, is not simple because the PCM has variable optical characteristics that depend on the current physical status of the material. When the PCM is in solid state, the dominant transmission mode is (direct to diffuse), and the scattering effect is prominent. While in the liquid phase the transparency increases and (direct to direct) transmission takes place. Accordingly, the optical properties such as absorption, scattering, and transmission, which control the radiation propagation within the PCM, were evaluated based on auxiliary equations that compute the nodal optical properties as a function in the liquid fraction β . The

liquid fraction value is the relative amount of liquid phase present in the PCM. This approach has been explained thoroughly in Gowreesunkera et al. (2013) and Elarga et al. (2016). The code is then able to identify the solar radiation energy balance for each time step of the entire glazing-PCM assembly. The final resultant solar radiation transmitted to the façade cavity (i.e. the solar gain), is then provided to the TRNSYS model as input, as explained in Section (2.3), to calculate the hourly profile of the thermal loads.

2.1.3 Enthalpy linearization method validation

Experimental data available in the literature (Goia et al., 2012) for a PCM glazing made of two panels of clear glass and a layer of paraffin wax (15 mm thickness) was used for validation purpose. A comparison between the measured and calculated surface temperature values of the inner and outer glass layers as illustrated in Figs. 2a and 2b respectively for a week during the summer, has shown a good agreement. The RMSE for the inner glass reached 1.6 °C and within the outer glass 2 °C.

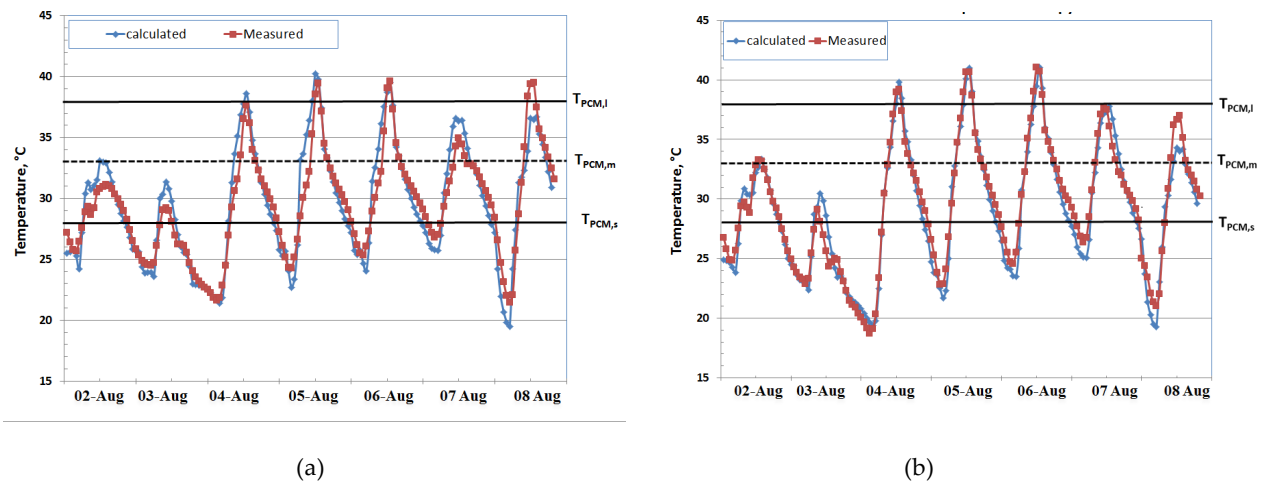


Fig. 2 – Numerical Model validation, calculated vs measured, (a) inner glass surface, (b) outer glass

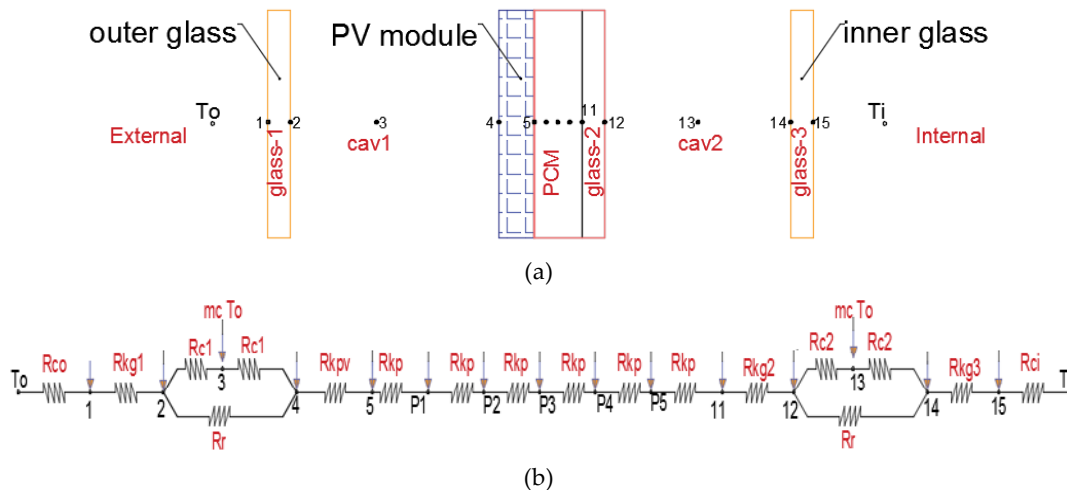


Fig. 3 – Numerical Model validation, calculated vs measured, (a) inner glass surface, (b) outer glass

2.2 PV-PCM Resistance Model in MATLAB

The second model developed is that of a PCM layer integrated with a PV module, and installed inside a façade cavity composed of two glass layers (the inner and outer) as shown in Fig. 3a. The entire 1-D numerical model of the glazed façade was developed. Thermal nodes of each element are illustrated in Fig. 3b. PCM were divided into 5 homogenous layers.

2.2.1 Mathematical model description

For the sake of brevity, the energy balance equations for Nodes 3 and 13 that describe the cavity ventilation from outside air (out-out technique), are presented below. The rest of the nodes are similar to Equations 5 to 9, previously mentioned. More information on this model can be found in Elarga et al. (2016).

$$\begin{aligned} (h_{c1}) T_2 + (-2 h_{c1} - m \cdot c) T_3 + \\ (h_{c1}) T_4 = -(m \cdot c) T_o \end{aligned} \quad (10)$$

$$\begin{aligned} (h_{c2}) T_{12} + (-2 h_{c2} - m \cdot c) T_{13} \\ + (h_{c2}) T_{14} = -(m \cdot c) T_o \end{aligned} \quad (11)$$

2.2.2 PCM Technical specifications

It is important to highlight that PCM physical specifications ($T_m, h_{PCM}, L, c_s, c_l$) are those of a real, commercially available product (Rubitherm RT35), and summarised in Table 1.

Table 1 – PCM Table of properties

Name	RT35- Organic
Solid temperature	29°C
Nominal melt. temperature	33°C
Liquid temperature	36°C
Specific heat Capacity	2 kJ kg ⁻¹ K ⁻¹
Latent heat of fusion	160 kJ kg ⁻¹

2.3 MATLAB-TRNSYS Coupling

In order to obtain a reliable simulation of the impact of a PV-PCM double skin façade on the building energy demand it is necessary to link the previously presented PV-PCM 1-D model developed in MATLAB to TRNSYS (Klein et al., 2009). TRNSYS is a dynamic thermal model that takes into account the

external, internal loads and the stored heat in the building components. The interaction between MATLAB and TRNSYS simulation studio was carried out using TYPE 155 from TRNSYS library. This type is dedicated to read external codes executed by MATLAB. The numerical algorithm starts by linking the required weather condition from TYPE 16 to both the MATLAB and the zone built in TRNbld (TYPE 56). Generally, it is mandatory to link the weather file to (TYPE 56) in order to operate the simulation model. On the other hand, for each listed inner zone on (TYPE 56), there is the availability to set its input data and boundary conditions as a user defined option. The PV-PCM - 1D numerical code estimates the temperature and transmitted solar radiation for each of the fixed grid nodes, including the last node that represents the inner surface layer temperature Node 15 (see Fig. 3a). However, the transient interface between TRNSYS and MATLAB models happens in air node B (see Fig. 4), i.e. Node 13 (Fig. 3a). The estimated transmitted solar radiation and air temperature with a five-minute time step are read as a user defined value for the inner layer zone on (TYPE 56). The reason behind considering the coincident interface between the two models in node B is that the complete room structure and the correspondent radiative/convective heat exchange (which include thermal storage of the room components) are computed by the MATLAB code alone. These heat transfer components have an influence on the energy balance of the inner glass layer and its final surface temperature. The inner glass layer was identified in the TRNbld (TYPE 56) library with the specifications as in Table 2. The considered facade is west oriented.

Table 2 – Glazed layer specifications

Density (kg/m ³)	2500
Heat capacity kJ/(kg K)	0.84
Conductivity kJ/(h m K)	0.27

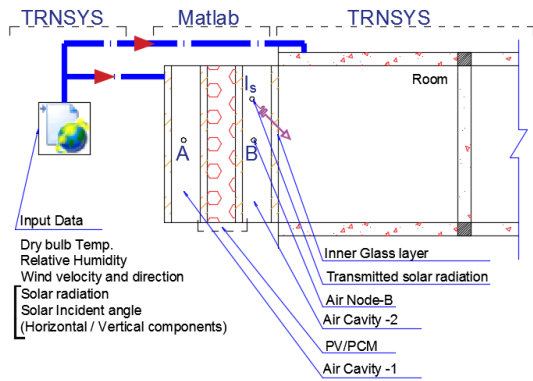


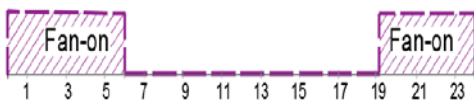
Fig. 4 – MATLAB/TRNSYS link scheme

2.4 PV.PCM Module Cavity Ventilation

The influence of the façade cavity ventilation schedule on the building energy performance is very relevant in general, and especially after PCM integration given the ventilation, strategy resides in controlling the pattern of phase changing. A compromise evaluation through three strategies was analysed, shown in Fig. 5. Strategy 1 assumed ventilation all year at day-time, Strategy 2 during the winter season the ventilation stopped entirely while in the summer season it was on during night hours, Strategy 3 assumed ventilation off all year. The ventilation volume flow rate was assumed 5 l/s per façade meter and the ventilation technique was (out-out), i.e. air flows from the outside passing through the cavity and then expelled from the top to the outside again.



(a) The ventilation system of the façade cavity was on all year during working hours only.



(b) This strategy investigates the ventilation influence throughout the summer season only during night hours from 8 pm to 7 am of the following morning.



(c) No active or passive ventilation system was considered in this strategy in order to investigate the PCM charge/discharge phase.

Fig. 5 – Different ventilation strategies during summer season, (a) Strategy 1, (b)-Strategy 2, (c)-Strategy 3

3. Results of the Parametric Analysis

The parametric study includes the comparison between the three ventilation strategies and a case of PV-PCM double skin façade, and a baseline case where the façade is without PCM. An open office area of 80 m² was considered in TRNBld (Klein et al., 2009) to estimate the yearly thermal loads. The internal loads were 70 W/person, 10 W/m² for lighting, and 130 W for the equipment. The following results were presented:

- Yearly thermal loads for each ventilation strategy and also a case study without the PCM (considered as a baseline reference).
- Inside operating temperature for each of the investigated cases (to highlight the PCM influence on the stability of the indoor temperature, and how that will support the peak load shaving).

3.1 Thermal Loads

Yearly thermal loads were calculated for two European cities with different climate classifications. Venice (Italy) with a fully humid, warm summer climate, and Helsinki (Finland) with a cool summer climate (Kottek et al., 2006). As shown in Fig. 6, the thermal performance varies according to the different investigated ventilation strategies. In Venice (Fig. 6a), during winter months, the highest consumption was recorded for Strategy 1 followed by the case without PCM. Strategies 2 and 3 came next with an almost similar pattern. The illustrated energy profiles were influenced by the PCM, and ventilating the cavity during daytime kept the PCM in its solid state. Under these conditions, the solar radiation transmission and the cavity temperature were reduced (Goia et al., 2015). Accordingly, the required thermal loads for Strategy 1 had the highest values. On the other extreme, the ventilation of the cavity during the night (Strategy 2) and the lack of ventilation (Strategy 3) allowed the PCM during daytime to be charged and melt, thus inducing a higher transmission and solar gains to the room. However, during the summer season, the highest energy consumption was recorded for the case without PCM (a predictable result), followed by Strategy 3 and finally, a similar pattern for Strategies 1 and 2.

In Strategy 3, the lack of cavity ventilation combined with higher solar radiation intensity and external temperature values caused the PCM to reach the melting phase without having a chance to be cooled and re-solidified (Turnpenny et al., 2000). Conversely, using the Strategies 1 and 2, ventilation allowed the PCM to be cooled either during the day or night-time to efficiently fulfill the purpose of integrating phase changing substances. In Helsinki (Fig. 6b), during summer season thermal energy demand (Strategy 3) with no ventilation shows the highest value compared to other cases, with the case without PCM being the next in line. Strategies 2 and 1 determine the minimum energy demand, with almost zero demand during all summer months in the latter strategy. This shows that a proper integration of PCM in building elements, combined with a right synchronization between PCM's charging/discharging phase and thermal loads can support the nearly zero energy-building concept (Zalba et al., 2004). During the winter season, the case without PCM and ventilation (Strategy 1) showed the highest energy demand, followed by Strategies 2 and 3, with the same thermal energy demand – as in both cases there was no ventilation of the cavity during the winter season.

3.2 Inner Zone Operating Temperatures

The impact of the PCM layer on the thermal comfort was investigated by analysing the inner zone operating temperatures for each strategy. In Fig. 7a; the daily profiles of the inner zone operating temperature are shown for July 16 (the design day for summer load). As shown, the closest profiles to the design temperature during working hours are those in case of ventilation (Strategies 1 and 2), followed by (Strategy 3) and the case without PCM. This can be explained by considering the PCM melting/solidification influence: the ventilation of the PCM during working hours or during the night improves the zone operating temperature and makes it closer to the desired setpoint temperature. Conversely, the lack of ventilation prevents the PCM from an efficient discharge phase, which leads to a performance similar to that of the reference case without PCM. In Helsinki, Fig. 7-b, the ventilation of the PV-PCM during working hours leads to indoor operating temperatures below the design set temperature by about 3 °C. Starting from midday, the difference decreased and the profiles were almost identical with the design temperature. This increment was due to the facade's west orientation and the solar intensity propagation. The temperature profiles for the (Strategy 3) and for the case without PCM were almost the same within the working hours. The difference reached 1.5 °C higher than the design set temperature.

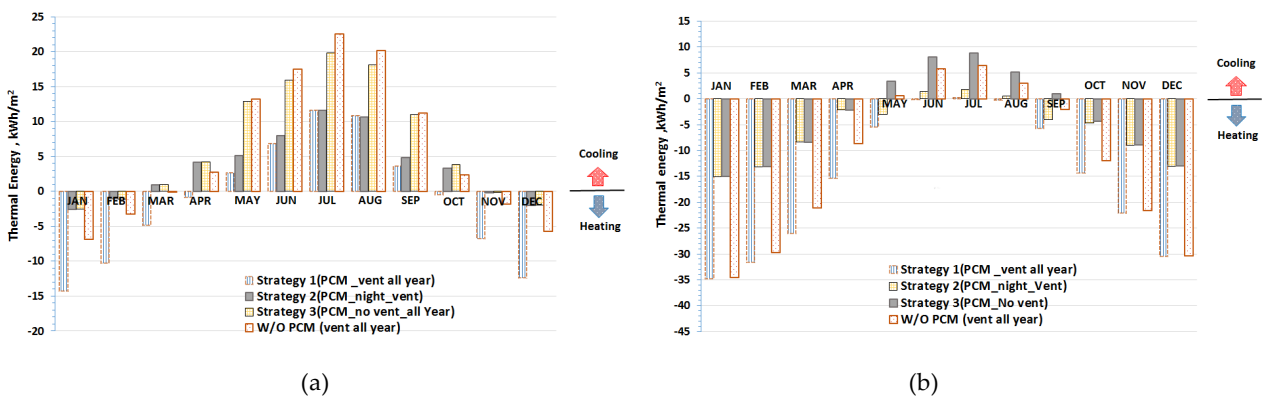
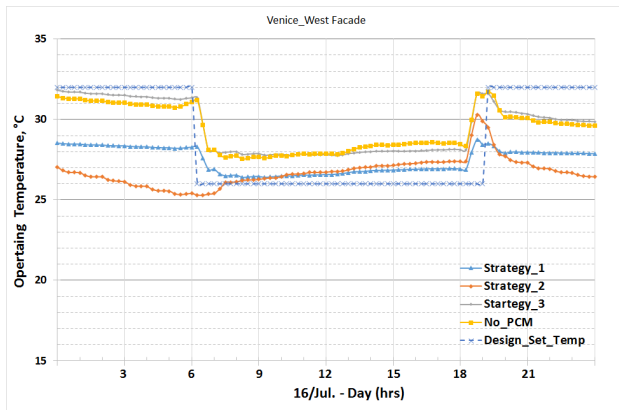
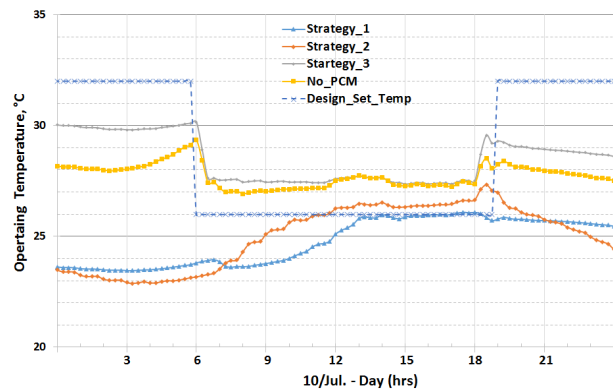


Fig. 6 – Yearly thermal energy profiles, (a) Venice city, (b) Helsinki city



(a)



(b)

Fig.7 – Operating daily temperature profiles (a) Venice city, (b) Helsinki city

4. Conclusions

The article presents a validated numerical model that adopts the enthalpy method to describe a PCM glazing thermal performance. The model based on the enthalpy method was implemented in MATLAB to simulate an integrated PV-PCM system in a ventilated transparent façade. Then, this model was linked to an office building in TRNSYS environment, to estimate the dynamic thermal performance of the system (PV/PCM ventilated transparent façade and office building). Simulations were then carried out through a combination of software tools/models and the impact of three ventilation strategies on the performance of the system estimated for two European cities. The results show that the energy savings obtained through this façade system are significant and that PV-PCM can be a promising solution especially in Nordic countries, considering the thermal properties of the PCM as adopted in the simulation. In fact, it is important to stress that the PCM performance has to match transmission losses due to external temperature, solar radiation intensity, and internal loads, to be optimal. Further studies will focus on optimizing the features of the PCM in relation to different climates and ventilation strategies.

Acknowledgement

This work was partially developed in the framework of COST Action TU1403 – Adaptive Facades Network.

References

- Aelenei, L., R. Pereira, H. Gonçalves, A. Athienitis. 2014. "Thermal Performance of a Hybrid BIPV-PCM: Modeling, Design and Experimental Investigation". *Energy Procedia* 48: 474-483. doi:10.1016/j.egypro.2014.02.056.
- Batagiannis, P., C. Gibbons. 2001. "Thermal assessment of silicon based composite materials used in photovoltaics." In: *Proceedings of Renewable Energy in Maritime Island Climates Conference*. Belfast, UK: UK-ISES.
- Ciulla, G., V. L. Brano, M. Cellura, V. Franzitta, and D. Milone. 2012. "A finite difference model of a PV-PCM system." *Energy Procedia* 30: 198-206. doi:10.1016/j.egypro.2012.11.024.
- Elarga, H., F. Goia, A. Zarrella, A.D. Monte, E. Benini. 2016. "Thermal and electrical performance of an integrated PV-PCM system in double skin façades: a numerical study". *Solar Energy* 136: 112-124. doi:10.1016/j.solener.2016.06.074.
- Goia, F., M. Perino, M. Haase. 2012. "A numerical model to evaluate the thermal behavior of PCM

- glazing system configurations". *Energy and Buildings* 54: 141–153. doi:10.1016/j.enbuild.2012.07.036.
- Goia, F., M. Zinzi, E. Carnielo, V. Serra. 2015. "Spectral and angular solar properties of a PCM-filled double glazing unit". *Energy and Buildings* 87: 302–312. doi:10.1016/j.enbuild.2014.11.019.
- Gowreesunkera, B.L., S. Stankovic, S. Tassou, P.A. Kyriacou. 2013. "Experimental and numerical investigations of the optical and thermal aspects of a PCM-glazed unit". *Energy and Buildings* 61: 239–249. doi:10.1016/j.enbuild.2013.02.032.
- Hasan, A., S.J. McCormack, M.J. Huang, B. Norton. 2014. "Energy and Cost Saving of a Photovoltaic-Phase Change Materials (PV-PCM) System through Temperature Regulation and Performance Enhancement of Photovoltaics". *Energies* 7: 1318-1331. doi:10.3390/en7031318.
- Klein, S., W. Beckman, J. Mitchell, J. Duffie, N. Duffie, T. Freeman. "TRNSYS 16 - A transient system simulation program, User manual". Madison, U.S.A.: University of Wisconsin-Madison.
- Kottek, M., J. Grieser, C. Beck, B. Rudolf, F. Rubel. 2006. World Map of the Köppen-Geiger climate classification updated, *Meteorologische Zeitschrift* 15: 259-263. doi:10.1127/0941-2948/2006/0130.
- Machniewicz, A., D. Knera, D. Heim. 2015. "Effect of Transition Temperature on Efficiency of PV/PCM Panels". *Energy Procedia* 78: 1684–1689. doi:10.1016/j.egypro.2015.11.257.
- MATLAB 6.1, The MathWorks Inc., Natick, MA, 2000.
- Rubitherm. 2016. [HTTP://www.rubitherm.com](http://www.rubitherm.com). (Accessed: 12/2016).
- Swaminathan, C.R., V.R. Voller. 1992. "A general enthalpy method for modeling solidification processes." *Metallurgical and Materials Transactions* 23: 651-664. doi:10.1007/BF02649725.
- Turnpenny, J., D. Etheridge, D. Reay. 2000. "Noval ventilation cooling system for reducing air conditioning in buildings, Part I: Testing and theoretical modeling", *Applied Thermal Engineering* 20: 1019–1037. doi:10.1016/S1359-4311(99)00068-X.
- Zalba, B., J. Marin, L. Cabeza, M. Harald. 2004. "Free cooling of buildings with phase change materials". *International Journal of Refrigeration* 27: 839–849. doi:10.1016/j.ijrefrig.2004.03.0.

Dynamic Simulation as a Tool for the Analysis of the Interactions Among the Controllers of HVAC Systems

Mara Magni – University of Bologna – mara.magni2@unibo.it

Jean Pierre Campana – University of Bologna - jeanpierre.campana2@unibo.it

Gian Luca Morini – University of Bologna – gianluca.morini3@unibo.it

Abstract

During the last decade, the application of electronics to the different components of HVAC systems has offered new and sophisticated control systems capable of adapting the behaviour of each single device and of the whole plant to design specifications. These sophisticated finely-tuned control systems are, in principle, able to play an important role in reducing energy consumption and in improving thermal comfort. At the same time, there has been a marked increase in the complexity of the HVAC plant layout. By combining the complexity of the plants with that of the control systems and by taking into account the possibility of equipping each component of the plant with its own control system, the result is a new generation of energy systems with many possible interactions between controllers. Hence, it becomes impossible for a designer to evaluate, in an easy way, the effects of such interactions. As a consequence, it is difficult to know, at the design-stage, how the overall control system will operate. Nowadays, the dynamic simulation of the complete HVAC system makes it possible to emulate the system in which the controllers operate. In this paper, the dynamic model of a basic HVAC system involving a condensing boiler, radiators with thermostatic valves and an inverter driven hydraulic pump is presented. Each element of the circuit is equipped with its own control. The model of the system was built by using a custom-made library of Simulink blocks specifically created for the dynamic simulation of controlled HVAC systems. The dynamic model will be used in order to underline the strong influence of the control system on the HVAC energy efficiency and thermal comfort conditions. Specific design rules limiting the negative interaction among the activated control systems are inferred by the results shown in this paper.

1. Introduction

Dynamic simulation is an important tool for designers of hydronic systems. Satyavada and Baldi (2016) highlighted the importance of an effective control strategy for HVAC system in order to reduce energy consumption and to avoid instabilities. As shown by Morini and Piva (2007; 2008), SIMULINK is a suitable framework for the analysis of the behaviour of a controlled HVAC system. CARNOT (Conventional And Renewable eNergy Optimization Toolbox) is one of the most popular SIMULINK block sets for dynamic modelling of heating equipment (Wemhöner et al., 2000), developed with the financial support of Viessmann GmbH. One of the main advantages in adopting a MATLAB/SIMULINK framework is that this platform is widely used both in academic and professional environments, and it becomes easy for users to model new HVAC devices and control logic. In this way, each user can easily add new components to the library either by designing directly new graphical Simulink models or by using C-, Fortran- or MATLAB M-scripting languages. Since the authors are convinced of the potential of this approach, for this study a SIMULINK library named ALMAHVAC, fully compatible with the CARNOT block set, was used for modelling of heating plants coupled with ALMABuild library for the description of the building thermal characteristics. A description of ALMABuild can be found in Campana et al. (2017). In this paper, ALMAHVAC was used in order to analyse the impact on the energy and indoor comfort performance of some design choices regarding the supply temperature setpoint, the continuous or intermittent operating mode of the heating plant, as well as the pump sizing and its control mode, and the valve sizing.

2. Description of the Model

ALMAHVAC is used in order to model the heating plant of a building (modelled with ALMABuild) by using a series of blocks able to simulate boilers, thermostatic valves, pumps, and radiators. The hydraulic loops are built in SIMULINK by simply connecting the blocks to thermal bus lines (defined in CARNOT), able to exchange data among the blocks. The building is a one floor detached house located in Bologna and composed of four thermal zones (kitchen, living room, bathroom, bedroom). A description of the envelope components of the building is given in Campana et al. (2017). A room temperature equal to 24 °C is set for the bathroom, and 20 °C for the other rooms.

Winter simulations were carried out considering the typical winter period of Northern Italian sites from September 15 to April 30 (5448 hours). The complete set of METEONORM climatic hourly data for Bologna was considered in the simulations. The heating system was based on a condensing boiler; radiators were used as terminals and each radiator was controlled by means of a thermostatic valve according to the operative temperature. Fig. 1 shows the layout of the hydraulic loop. Different types of circulation pumps were considered in this work (i.e. constant or variable speed circulators). The performances of the variable speed circulators were calculated following the method presented in Ahonen et al. (2010). The condensing boiler used in the heating plant is a VITODENS 222-W B2LB, with a nominal thermal power equal to 19 kW and a large power modulation ratio (1:10).

A SIMULINK model was created on the main technical data of this boiler. The model needed as inputs only the values which are available from the boiler technical sheet.

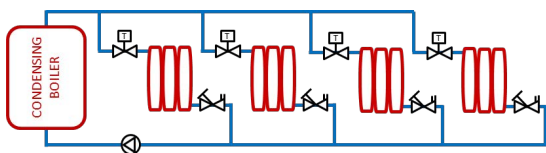


Fig. 1 – Hydraulic system scheme

Starting from a first guess, exhaust gas temperature, the chimney and envelope losses were calculated on the knowledge of both the exhaust gas and water return temperature. Then, the power released to the water was calculated. Finally, the exhaust gas temperature was recalculated by means of a thermal power balance between the exhaust gas and water. The condensing boiler was controlled by a PI controller on the supply water temperature; its parameters were determined by the Ziegler-Nichols loop tuning method for open loop test. The PI control implements a back calculation for anti-windup. The condensing boiler control implements two additional logics based on the water mass flow rate and on the minimum switch off time. When the water mass flow rate across the boiler is lower than 1/12 of its nominal value, the control switches off the boiler. This kind of control is mandatory especially for boilers having low water content in order to avoid boiling conditions within the device. In addition, in order to reduce the on-off cycles, it is generally imposed that a minimum time interval equal to $\Delta\tau$ (i.e. 15 minutes) must be guaranteed between two consecutive boiler switches. The radiator was modelled by using an RC scheme with 7 thermal resistances and 7 capacities (7R7C). The whole radiator was divided into 7 nodes with the same thermal capacity. The power exchanged with the room air and with the water was calculated in each radiator node. The total thermal power delivered from the radiator to the room was divided between the radiative node and the convective node of the thermal zone on the basis of the radiator characteristics. In this case, 30 % of the heat exchanged with the room was charged on the convective node (low temperature radiators). The thermostatic valve block calculated the pressure drop over the valve body by considering the valve flow coefficient K_v as a function of the valve position, both for linear and equal percentage valves. In this work, only equal percentage valves were considered. Reference thermostatic valves with a rangeability of 40, and the appropriate flow coefficient values for each room ($K_{v,0\text{ Kitchen}} = 0.64$, $K_{v,0\text{ Livingroom}} = 0.72$, $K_{v,0\text{ WC}} = 0.48$ and $K_{v,0\text{ Bedroom}} = 0.47$), were considered in the simulations. In order to simulate oversized valves, in some cases the reference $K_{v,0}$ values were increased by a C_{Kv} factor (as indicated in Table 1) larger than 1.

Table 1 – A summary of the different cases simulated (A: fixed speed pump, B: variable speed pump with controlled constant pressure head, C: variable speed pump with controlled decreasing pressure head)

Case	Valve sizing (C _{Kv})	Pump type	Pump sizing (C _H)	ϑ _{supply,set} [°C]
(1)	1	A	1	60
(2)	1	A	1	70
(3)	1	A	1	80
(4)	1	B	1	70
(5)	1	B	1.2	70
(6)	1	B	1.5	70
(7)	1	B	2	70
(8)	1	B	3	70
(9)	1	C	1	70
(10)	1.2	B	1	70
(11)	1.5	B	1	70
(12)	2	B	1	70
(13)	3	B	1	70
(14)	1	B	1	70

The reference pump had a hydraulic head of 18 kPa for a volume flow rate of 0.6 m³/h. In order to simulate oversized pumps, in some cases the pump hydraulic head was increased by a C_H factor (as reported in Table 1) larger than 1. A complete overview of the different scenarios analysed in this paper is given in Table 1; for each case the values of C_H and C_{Kv}, the pump type and the water supply temperature setpoint used in each simulation are indicated. Fourteen cases were simulated to gain information about the role played by the pump type and sizing, valve sizing, and water temperature supply on the seasonal performance of the heating plant.

3. Influence of Supply Temperature

The interaction between the imposed boiler setpoint temperature (water supply temperature) and the thermostatic valves was analysed first, by considering the layout of the heating system analysed in this paper. The thermostatic valve controls the water mass flow rate across the radiators with the goal to maintain a constant room temperature. Since the power exchanged between the radiators and the room depends on the mean radiator temperature, if

the room load is fixed the mean radiator temperature is also fixed. If the water supply temperature increases, the thermostatic valve reduces the water mass flow rate and, as a consequence, the water temperature at the radiator outlet, is also reduced. The lower the water return temperature, the higher the condensing boiler efficiency is. However, by increasing the water supply temperature, the water mass flow rate is progressively reduced, and lower mass flow rates can become a problem for the boiler and the system stability.

In fact, boilers with low water content cannot operate with low water mass flow rates in order to avoid the risk of localized water boiling. For this reason, the interaction between the water supply temperature setpoint and the thermostatic valves becomes so important for variable mass flow rate hydraulic loops, as demonstrated by Lazzarin (2012 and 2014). The results of Cases (1), (2) and (3) are now analysed (see Table 1). Fig. 2 shows the trend of the yearly distribution of the total water mass flow rate ($m_{w,tot}$), of the water supply temperature (ϑ_{supply}), of the water return temperature (ϑ_{ret}) and of the load factor (ϕ). By comparing the different charts, it is possible to highlight the percentage of winter time in which the heating system works under defined operating conditions. It becomes evident how, when reducing the water supply temperature, the time during which the boiler is switched on and the thermostatic valves are opened, increases; at the same time, the water return temperature is larger when the water supply is reduced.

Table 2 summarizes the most important results carried out from the yearly simulations by varying the water supply temperature setpoint. Table 2 shows that by adopting a supply temperature of 80 °C (Case (3)) the boiler works in condensing regime and the amount of condensate per hour is 142 % higher when compared to Case (1) and 81 % higher than Case (2).

This is due to the lower water return temperature obtained through a larger water supply temperature.

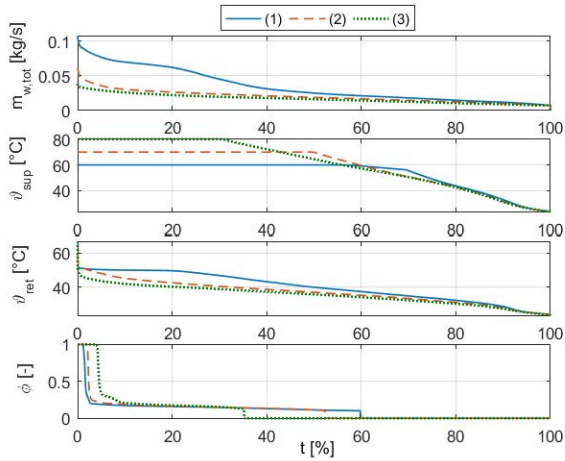


Fig. 2 – Yearly simulation results with different supply water temperature setpoints at full load: ((1) $\theta_{\text{supply}} = 60^\circ\text{C}$, (2) $\theta_{\text{supply}} = 70^\circ\text{C}$, (3) $\theta_{\text{supply}} = 80^\circ\text{C}$)

However, more condensation doesn't always correspond to higher boiler seasonal efficiency. In fact, it can be noticed that the seasonal efficiency of the boiler, by neglecting all the losses ($\eta_{g,\text{no losses}}$), increases when the supply temperature is increased; on the contrary, the boiler seasonal efficiency η_g (which takes into account the losses) decreases when the supply temperature goes from 70°C (Case(2)) to 80°C (Case(3)). The opposite trend of $\eta_{g,\text{no losses}}$ and η_g highlights that from Case (2) and Case (3) the boiler losses are increased. This is due to the increase of the boiler on-off cycles from Case (2) to Case (3). In fact, Case (3) is characterized by a higher number of on-off cycles because when the supply temperature is increased, the water mass flow rate becomes lower and its value, especially during the warmest months, can become lower than the value in correspondence of which the boiler with a low water content, must be switched off. In Case (1) the water mass flow is higher than in the other cases because of the low supply temperature; in this case the condensing boiler operation is rarely stopped due to the large value of the mass flow rate. This means that during the warmer periods when the building thermal loads are lower and the condensing boiler works with low load factors (close to the minimum of its modulation range) in Case (1), the boiler on-off cycles have a frequency limited only by the minimum time interval between two consecutive switches (i.e. 15 min). The net energy delivered to the water increases with the supply temperature setpoint, but it is necessary to notice that also the comfort level increases. In fact, the number of hours

in which the rooms are under their setpoint temperature decreases when the supply temperature increases; this means that the radiators were designed to work with a supply temperature higher than 70°C and in the colder periods a supply temperature of 60°C is not enough to cover the building demands. However, the heating plant is not able to satisfy the bathroom setup temperature during the entire colder season, even in Case (3). The energy demand of the pump decreases if the supply temperature increases because the water flow rate is reduced.

Table 2 – Seasonal results reached by varying the water supply temperatures setpoint

	(1)	(2)	(3)
E_{fuel} [kWh/y]	9785	9907	10040
E_w [kWh/y]	9705	9826	9898
η_g	99.18	99.18	98.59
$\eta_{g,\text{no losses}}$	100.66	101.06	101.79
t_{on} [h/y]	3258	2854	1919
% t_{cond}	98	98	100.0
Cond [kg H_2O /h]	0.12	0.16	0.29
Nr. on/off cycles	1355	668	1016
E_{pump} [kWh/y]	17	13	12
$\vartheta_{\text{kitchen}} < 19.9^\circ\text{C}$ [h]	335	0	0
$\vartheta_{\text{living}} < 19.9^\circ\text{C}$ [h]	0	0	0
$\vartheta_{\text{wc}} < 23.9^\circ\text{C}$ [h]	3144	1300	873
$\vartheta_{\text{bedroom}} < 19.9^\circ\text{C}$ [h]	0	0	0

4. Influence of Pump Type and Size

4.1 Pump size

In this section, the effects generated by the adoption of an oversized circulation pump are analysed. The interactions between circulation pump and thermostatic valves have an influence on the correct behaviour of the whole circuit. The pump must be chosen in order to avoid that thermostatic valves operate at the limits of their operative field. Since the thermostatic valves are not able to close their cross section area (A) completely, a minimum mass flow rate is always present, and its amount depends on the pressure drop over the valve for a fixed value of the valve rangeability (R) and K_v , as indicated by the following relationship:

$$\dot{V} = \sqrt{\frac{DP_{valve}}{10^5}} K_{v,0} [R^{(A\%-1)}] \quad (1)$$

By selecting a more powerful pump, the mass flow rate increases and the thermostatic valves tend to operate closer to the final part of their stroke (small values of A). In this way, they lose their modulating capacity completely and become on-off controls. The thermal indoor comfort can be affected by this behaviour. In order to investigate this effect, different simulations by adopting different variable speed pump sizes were carried out. Five different cases (Cases (4), (5), (6), (7) and (8)) were considered (see Table 1).

Table 3 – Seasonal results obtained by adopting pumps of different sizes

	(4)	(5)	(6)	(7)	(8)
E_{fuel} [kWh/y]	9857	9905	9975	10081	10300
E_w [kWh/y]	9773	9824	9902	10019	10274
η_g	99.14	99.19	99.27	99.38	99.74
$\eta_{g,no\ losses}$	101.1	101.1	101.1	101.1	101.1
t_{on} [h/y]	2853	2863	2906	2993	3279
$\%t_{cond}$	98.4	98.4	98.1	97.9	97.8
E_{pump} [kWh/y]	10.1	12.2	15.3	20.6	31.0
On Off/h [n/h]	0.23	0.23	0.22	0.20	0.14
Cond [kg _{H2O} /h]	0.16	0.16	0.16	0.16	0.15
$\vartheta_{kitchen} > 20.8$ °C [h]	1206	1304	1416	1645	2234
$\vartheta_{living} > 20.8$ °C [h]	2313	2469	2881	3498	4358
$\vartheta_{wc} > 24.8$ °C [h]	7	5	7	14	21
$\vartheta_{bedroom} > 20.8$ °C [h]	1865	2181	2421	2857	3616

Table 3 shows that when the pump hydraulic head is increased, the thermostatic valves are no longer able to control the ambient temperature and the overheated periods are longer.

The bathroom is the room where overheating is less important, due to the higher thermal loads which allow the thermostatic valve to work in its whole operative range.

Along with the indoor comfort issue, also energy consumption supports the conclusion that the adoption of an oversized pump is always a bad design choice. Table 3 shows that with an oversized pump the heating system delivers more energy to the building, but unfortunately, this additional heat is mainly used to overheat the rooms. The condensing boiler efficiency is not influenced by the pump size, but the pump energy consumption increases proportionally to the pump hydraulic head.

4.2 Pump Type

In this section, three different pump types are compared (i.e. Cases (2), (4) and (9), see Table 1). Variable speed circulation pumps are generally coupled to thermostatic valves in order to minimize the pressure drop across the valve when the load factor goes down. In this way noise problems due to high-pressure drops across the valve can be overcome and the pump energy consumptions can be reduced.

In Table 4 the main results obtained by adopting constant speed and variable speed pumps are reported. It is evident that the condensing boiler efficiency and its operating time are not influenced by the pump type. It can be noticed that adopting a variable speed pump with a decreasing pressure head (Case (9)) less energy is delivered to the water, and this is underlined by longer periods in which the rooms are underheated. The overheating period is strongly reduced in Case (9) because the pump reduces its hydraulic head when the valves are closing. Therefore, the water mass flow rate along the hydraulic loop is lower than in the other cases. On the other hand, the underheating periods are longer in Case (9) with respect to the other cases because the mass flow rate moved by the pump is slightly lower than in Cases (2) and (4). The minimum operative temperature guaranteed in the rooms is similar in the three cases; it can thus be assessed that the indoor comfort level is quite good, independently from the adopted pump type. The results reported in Table 4, put into evidence that the pump energy consumptions are considerably reduced in Case (9) (-51 % with respect to Case (4), -62 % when compared to Case (2)). In large hydraulic networks important energy savings are expected by the use of

variable speed pumps with a decreasing pressure head coupled to thermostatic valves.

Table 4 – Seasonal results obtained by using different pump types

	(2)	(4)	(9)
E_{fuel} [kWh/y]	9907	9857	9723
E_w [kWh/y]	9826	9773	9630
η_g	99.18	99.14	99.04
$\eta_{g,no\ losses}$	101.06	101.06	101.06
E_{pump} [kWh/y]	13	10	5
t_{on} [h/y]	2854	2853	2805
$\vartheta_{kitchen < 19.9\ ^\circ C}$ [h]	0	2	45
$\vartheta_{living < 19.9\ ^\circ C}$ [h]	0	0	0
$\vartheta_{wc < 23.9\ ^\circ C}$ [h]	1300	1665	3000
$\vartheta_{bedroom < 19.9\ ^\circ C}$ [h]	0	0	0
$\vartheta_{min,kitchen}$ [$^\circ C$]	19.93	19.90	19.84
$\vartheta_{min,livingroom}$ [$^\circ C$]	20.22	20.19	20.14
$\vartheta_{min,wc}$ [$^\circ C$]	23.61	23.57	23.50
$\vartheta_{min,bedroom}$ [$^\circ C$]	20.18	20.15	20.09
$\vartheta_{kitchen > 20.8\ ^\circ C}$ [h]	1300	1206	1020
$\vartheta_{living > 20.8\ ^\circ C}$ [h]	2479	2313	1668
$\vartheta_{wc > 24.8\ ^\circ C}$ [h]	5	7	4
$\vartheta_{bedroom > 20.8\ ^\circ C}$ [h]	2190	1865	1526

5. Valve Sizes

Thermostatic valve sizing is important because it is correlated to its authority. The authority is the ratio between the pressure drop over the open valve to the total pressure drop over the controlled branch of the hydraulic circuit in which the valve is inserted. A rule of thumb for the valve sizing is to select the valve size in order to obtain a valve authority of around 0.5. In fact, if the valve is oversized its authority is low and the valve is no longer able to reduce the mass flow rate in the controlled branch, if needed. In order to show the effects of the adoption of oversized valves on the performances of the heating plant five yearly simulations were carried out in order to compare the seasonal results obtained with different valve sizing (Cases (4),(10),(11),(12),(13)), by changing the C_{kv} factor as described in Table 1. Table 5 summarizes the main results. By increasing the valve size, the water mass flow rate increases because the valves are characterized by lower authority; this means that, even in the warm period, the

radiators receive larger water flow rates with high temperatures that contribute to the room overheating. Since the minimum mass flow rate increases with the valves size, the boiler is switched on for longer periods when larger valves are adopted. The water return temperature increases and the flow rate of condensed water decreases. The number of the boiler on-off cycles per hour is lower in the Cases (4), (10), and (11) because in the warm periods due to the low mass flow rates the boiler remains switched off. This parameter is 0 in Case (13) because the mass flow rate is always large enough to avoid the boiler switch off, and it has a peak in Case (12).

Table 5 – Seasonal results obtained by using different valve sizes

	(4)	(10)	(11)	(12)	(13)
E_{fuel} [kWh/y]	9857	9957	10129	12004	13553
E_w [kWh/y]	9773	9883	10075	12069	13567
η_g	99.1	99.3	99.5	100.5	100.1
$\eta_{g,no\ losses}$	101.1	101.1	101.1	101.6	100.1
t_{on} [h/y]	2853	2899	3049	4417	5448
On Off/h	0.23	0.22	0.19	0.47	0.00
Cond [kg _{H2O} /h]	0.16	0.16	0.16	0.16	0.08
E_{pump} [kWh/y]	10.1	10.2	10.3	9.8	11.0
$\vartheta_{kitchen > 20.8\ ^\circ C}$ [h]	1206	1390	1787	3225	4306
$\vartheta_{living > 20.8\ ^\circ C}$ [h]	2313	2822	3624	5088	5448
$\vartheta_{wc > 24.8\ ^\circ C}$ [h]	7	7	17	2089	2912
$\vartheta_{bedroom > 20.8\ ^\circ C}$ [h]	1865	2380	3040	4268	5437

In Case (12), the water mass flow rate is always larger than the minimum value needed in order to keep the boiler switched on but the load factor is often close to the boiler minimum modulation level. This leads the boiler to work in on-off cycles with a frequency imposed by the minimum switch off time of the boiler (i.e. 15 min). The energy required by the pump is almost constant because when the water mass flow rate increases, the pressure drop over the valves decreases if larger valves are adopted. The most important aspect linked to the adoption of valves having different sizes, is related to the room

comfort. From Table 5 it is evident that oversized valves can have problems in controlling the room temperature: important overheating periods are present especially in Cases (12) and (13). This leads to an increase of energy consumptions (see E_{fuel} in Table 5), too.

6. Intermittent Operation Mode

It often happens that, during the nighttime, the users decide to reduce the setup value of the room temperature or to switch the heating plant off with the aim to reduce energy consumption. If the heating plant is switched off, room temperature can decrease 2-4 K during the nighttime, depending on the building thermal insulation level. This leads the thermostatic valves to be open completely when the heating system restarts in the morning.

Table 6 – Seasonal results obtained under continuous (case (4)) or intermittent (Case (14)) operation mode

	(4)	(14)
E_{fuel} [kWh/y]	9857	9664
E_w [kWh/y]	9773	9524
η_g	99.14	98.56
$\eta_{g,\text{no losses}}$	101.06	100.41
t_{on} [h/y]	2853	2358
% t_{cond}	98	55
Cond [kg _{H2O} /h]	0.16	0.14
E_{pump} [kWh/y]	10.1	15.6
$\vartheta_{\text{kitchen}} < 19.9$ °C [h]	0	1185
$\vartheta_{\text{living}} < 19.9$ °C [h]	0	480
$\vartheta_{\text{wc}} < 23.9$ °C [h]	1665	3544
$\vartheta_{\text{bedroom}} < 19.9$ °C [h]	0	521

The boiler will work at the maximum load factor and also the water mass flow rate will be at its maximum.

This makes the system work with larger water return temperature, which can reduce the boiler seasonal efficiency. In Table 6 the main results of the simulations in continuous operation mode (Case (4)) and intermittent regime (Case (14)) are reported: the same input parameters of Case (4) but the boiler is switched off every day from 11pm to 6 am during the whole winter). From Table 6, it becomes evident how the adoption of an intermittent regime reduces the boiler seasonal efficiency. Since the boiler has

good performance even when it works without condensation, the seasonal efficiency is always quite large.

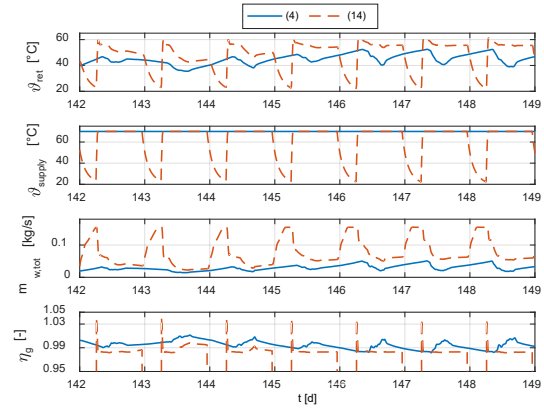


Fig. 3 – Supply temperature, return temperature, water mass flow rate and boiler efficiency under continuous (Case (4)) and intermittent (Case (14)) operation mode

The energy saving is only 1.95 % in Case (14) with respect to Case (4) even if the average room temperatures are much lower. This result can be explained if one considers that the number of hours in which the boiler works in condensation regime is reduced to 50 % by adopting an intermittent regime. Fig. 3 shows a period of seven days in wintertime starting from December 19. The trends of the water mass flow rate, of the water return temperature and of the boiler efficiency confirm that the intermittent regime is characterised by lower efficiency due to larger water flow rates and higher return temperatures.

7. Conclusion

In this work the capability of a new Simulink block set named ALMAHVAC (coupled with ALMA-Build) as tools for the dynamic simulations of hydronic systems was tested. The Simulink blocks used to model pumps, boilers, radiators and thermostatic valves are fully compatible with the CARNOT library. A series of numerical results are shown, analysing the influence of the pump sizing rules, the pump control type, the valves sizing and user behaviour (by varying the water supply temperature setpoint and by selecting the intermittent use of the heating system) on the seasonal efficiency,

and on the thermal indoor comfort. A higher supply temperature leads to a lower return temperature, which is a good condition for the condensing boiler, and to a lower water mass flow rate which can increase the number of on-off cycles especially during the warmest winter periods. This means that a trade-off supply temperature value exists in order to maximize the seasonal efficiency of the system. Oversized valves and pumps make the system less efficient in terms of capacity, to guarantee both ideal indoor thermal conditions and low energy consumption. It is also proven that the adoption of an intermittent regime for the heating plant can reduce significantly the indoor comfort and the boiler efficiency.

Nomenclature

Symbols

η	Efficiency [-]
ϕ	Load factor [-]
ϑ	Temperature (°C)
E	Energy [kWh]
T	Time [h]
A	Valve position [%]
K	Flow coefficient [$\text{h}^{-1} \text{m}^3 \text{bar}^{-1/2}$]
R	Rangeability [-]
DP	Pressure difference [Pa]
\dot{V}	Volume flow [m^3/h]
Cond	Condensation
m	Mass flow rate [kg/s]
C	Multiplication factor

Subscripts/Superscripts

g	Generation
g,no losses	Generation without the boiler losses
g,ist	Instantaneous generation
ret	Return
w	Water

References

- Ahonen, T., J. Tamminen, J. Ahola, J. Viholainen, N. Aranto, J. Kestilä. 2010. "Estimation of pump operational state with model based methods". *Energy conversion and management* 51: 1319-1325. doi: 10.1016/j.enconman.2010.01.009.
- Campana, J.P., M. Magni, M. Dongellini and G.L. Morini, 2017. "The benchmark of a new SIMULINK library for thermal dynamic simulation of buildings". In: *Proceedings of BSA 2017*. Bolzano, Italy: BUPRESS.
- Lazzarin, R.M. 2012. "Condensing boilers in buildings and plants refurbishment". *Energy and Buildings* 47: 61-67. doi: 10.1016/j.enbuild.2011.11.029.
- Lazzarin, R.M. 2014. "The importance of the modulation ratio in the boiler installed in refurbished buildings". *Energy and Buildings* 75: 43-50. doi: 10.1016/j.enbuild.2014.01.043.
- Morini, G.L., S. Piva. 2007. "The simulation of transients in thermal plant. Part I: Mathematical model". *Applied thermal engineering* 27: 2138-2144. doi: 10.1016/j.applthermaleng.2006.05.030.
- Morini, G.L., S. Piva. 2008. "The simulation of transients in thermal plant. Part II: Applications". *Applied thermal engineering* 28: 244-251. doi: 10.1016/j.applthermaleng.2006.05.035.
- Satyavada, H., S. Baldi. 2016. "An integrated control-oriented modeling for HVAC performance benchmarking". *Journal of Building Engineering* 6: 262-273. doi: 10.1016/j.job.2016.04.005.
- Wemhöner, C., B. Hafner, K. Schwarzer. 2000. "Simulation of solar thermal systems with CARNOT blockset in the environment MATLAB-Simulink". In: *Proceedings of Eurosun 2000*. Copenhagen, Denmark: ISES.

The Benchmark of a New SIMULINK Library for Thermal Dynamic Simulation of Buildings

Jean Pierre Campana – University of Bologna - jeanpierre.campana2@unibo.it

Mara Magni – University of Bologna – mara.magni2@unibo.it

Matteo Dongellini – University of Bologna – matteo.dongellini@unibo.it

Gian Luca Morini – University of Bologna – gianluca.morini3@unibo.it

Abstract

Nowadays, the complexity of the interactions between thermal plants and buildings for NZEB buildings is increasing. The decrease in primary energy consumption by NZEB is generally pursued by maximizing the use of renewable energy which gives a discontinuous contribution during the season; it becomes important to study in detail the dynamic interactions between the building and the adopted HVAC systems, by taking into account unsteady state behaviour of walls, roofs, windows, and so on. This kind of analysis can be carried out with conventional dynamic simulation software (i.e. TRNSYS, ESP-r, Energy Plus, DesignBuilder). It has been demonstrated that a detailed analysis of controlled HVAC systems can also be carried out by using SIMULINK, and in the past open block libraries made in SIMULINK were proposed for HVAC system analysis, like in the case of the CARNOT blockset. However, besides its completeness, the building modelling is still considered a weak point of CARNOT due to its limited flexibility. For this reason, a new specific library named ALMABuild based on SIMULINK blocks for the dynamic modelling of a building is presented in this paper with the aim to integrate and improve the blocks already available in CARNOT.

In ALMABuild, the modelling of a building with SIMULINK is driven by means of a series of Graphical User Interfaces (GUI). In this paper a benchmark of ALMABuild is shown by using TRNSYS as a reference. The comparison evidenced a good agreement between the two methods. However, differences were present each time that the procedure indicated by the European Standard EN ISO 13790:2008 (and integrally followed by ALMABuild) was not in agreement with the procedure followed by TRNSYS (based on American standards).

1. Introduction

During the last two decades, the awareness of the public opinion on the environmental costs of the overall energy consumption has strongly increased. Since the building sector represents one of the most important energy consumers (up to 40 % of the European Union final energy demand), the European Commission issued a series of Directives to improve building energy efficiency and the exploitation of renewable energy sources (European Commission, 2010). As a consequence, the current legislation of most Member States imposes upper limits to the annual energy consumption of HVAC systems coupled to buildings. During the design phase, the evaluation of the predicted building energy needs is carried out by means of simulation models, according to various techniques: some of them are based on the knowledge and resolution of the thermal balance equations of the building, while others are based on the monitoring of data inside the thermal zones (Fouquier et al., 2013).

SIMULINK has been demonstrated in the past decade, to be an efficient framework to develop Lumped Parameters Whole Room models (LPWR), which evaluate the behaviour of a thermal zone by lumping the whole zone, and Lumped Parameter Construction Element models (LPCE) that simulate each building high mass element (i.e. walls, roofs, and so on) by means of RC models (Oliveira Pano et al., 2016; Morini and Piva, 2007 and 2008). More specifically, Fraisse et al. (2002) and Hudson et al. (1999) developed RC models of high mass elements in SIMULINK in order to study the minimum number of capacities needed for the accurate evaluation of the surface temperature of both sides of a wall,

whilst Riederer et al. (2000) and de Wit (1988) showed how a room and a multi-zone building model can be obtained in SIMULINK.

In 2000, the Solar Institute Juelich (Wemhöner et al., 2000) proposed an open library of SIMULINK blocks for the modelling of solar plants. This library is commercially available since 1999 with the name of CARNOT blockset (Conventional And Renewable eNergy Optimization Toolbox). The development of CARNOT was started with the financial support of Viessmann GmbH, a German manufacturer and market leader for house heating equipment, who needed models of conventional and renewable components of house heating systems to accelerate the design process of the control systems. However, the success of CARNOT has been scarce, as proved by the actual limited diffusion of this library (limited to German countries). Nowadays, under the impulse of Viessmann, CARNOT contains a set of blocks representative of the most important HVAC devices but only simplified blocks for the building modelling are available, this aspect is still an open problem for the diffusion of the CARNOT blockset. One of the main advantages to operate in a MATLAB/SIMULINK framework is that this platform is very well known and spread both in academic and professional environments and it becomes easy for the users to approach it in order to model new HVAC devices and building elements. In this way each user can easily add new components to the library both by designing directly new graphical Simulink models and by using C-, Fortran- or MATLAB M-scripting languages.

Since the authors are convinced of the huge potential of this approach and are aware that the improvement of the building modelling is one of the most important constraints to be removed in order to enhance the spreading of CARNOT, in this paper a SIMULINK library named ALMABuild, useful for the realization of LPCE models, is presented. ALMABuild allows to describe and to evaluate the heat transfer mechanisms in a thermal zone by coupling a 3R4C model to each massive building element.

Each elementary building element is modelled through customized SIMULINK blocks, by means of which the energy conservation equation is solved according to a lumped formulation procedure. Since

this approach is the same proposed by CARNOT, the complete compatibility of the new ALMABuild library blockset with CARNOT has been guaranteed by adopting the same structure of the bus connection among blocks. In this way ALMABuild can be used as an integration of CARNOT blockset in a similar way in which TRNBuild is used in TRNSYS in order to improve the native building modelling.

2. The ALMABuild Library

ALMABuild contains all the elementary blocks needed for a complete description of the heat transfer mechanisms in a building. The ALMABuild blockset is composed by three different kinds of blocks: (i) Building Massive Element blocks (BME) that contain the physical model of each massive opaque building component (walls, floors, roofs, etc.); (ii) Building Clear Components (BCC) that contain the physical model of low mass clear components of the building envelope (windows, etc.) and (iii) Building Thermal Balance (BTB) blocks that enable to couple BME and BCC blocks in order to solve the thermal balance of the thermal zone.

The BME blocks are based on a fourth order RC model in which three thermal resistances and four capacities (3R4C) are used to calculate the dynamic trend of temperature and heat flux across the building element.

On the contrary, BCC blocks contain a 1R2C model for the dynamic analysis of light and clear building elements. BTB blocks are based on a two-star model for the calculation of the air and the radiative temperature associated to a single thermal zone defined by a series of BME and BCC blocks. One BTB block is used for each thermal zone in order to put together all the BME and BCC blocks related to the zone. Since each building element (i.e. walls, roofs, floors, ceilings, windows) differ in exposition (internal, external, or on the ground), slope (vertical, inclined, or horizontal) and optical behaviour (clear or opaque), in order to facilitate the creation of a complete model for each element, ALMABuild uses a series of Graphical User Interfaces (GUIs) by means of which all the properties of each building element and each thermal zone can be defined. In this way a

complete set of BME, BCC, and BTB are created automatically without the use of the SIMULINK graphical desktop. GUIs facilitate the use of ALMABuild also for users without experience in the use of SIMULINK.

Once all the data requested by the GUIs are set, each thermal zone will be associated to a BTB block and the connections between the different BTB blocks are automatically created in SIMULINK.

In this way, the creation of a building model in ALMABuild is faster than in CARNOT and, most importantly, the risk of making a mistake during the creation of the building model in SIMULINK is strongly reduced.

3. ALMABuild vs TRNSYS

With the aim to demonstrate the accuracy of the numerical results by using ALMABuild for the dynamic modelling of a building, a comparison between ALMABuild and TRNSYS was carried out. In order to test each single heat transfer mechanism, a series of numerical runs have been done to decouple a single mechanism from the other ones. The first test considers a single thermal zone delimited by opaque components only. In this way, it is possible to test how ALMABuild is able to reproduce the expected dynamic behaviour of the opaque walls linked to: (i) the heat transfer due to the inner and outdoor temperature difference (ii) the external radiative heat transfer with the sky, (iii) the heat transfer linked to the absorption of solar radiation on the wall external surface. The second test is related to the thermal zone behaviour in the presence of a clear component (vertical window). In this way it is possible to check if ALMABuild is capable of predicting accurately the effect on the zone's thermal balance due to the entrance of solar radiation into the room. In all the numerical runs shown in this paper, the external conditions, are evaluated using METEONORM climatic data of Bologna (Italy). No internal gains or HVAC systems are considered.

3.1 Room with Opaque Walls Only

3.1.1 Heat transfer due to inner and outlet temperature difference

In this first numerical run a thermal zone delimited by opaque walls only is considered. The internal volume of the room is 210 m³, the room has a rectangular shape and is closed with 4 external vertical walls, two of them of 21 m² (East and West) and the other two of 30 m² (North and South), an adiabatic floor and a horizontal roof of 70 m². The main characteristics of the layers of the external walls and roof are described in Table 1 and Table 2.

Table 1 – Thermophysical characteristics of the main wall layers (from the internal to the external side)

Layer	s [cm]	λ [W m ⁻¹ K ⁻¹]	ρ [kg m ⁻³]	cp [J kg ⁻¹ K ⁻¹]
Plaster	1.5	0.9	1800	910
Bricks	25	0.287	800	840
Insulation	6	0.039	30	1200
Plaster	1.5	0.9	1800	910

Table 2 – Thermophysical characteristics of the main roof layers (from the internal to the external side)

Layer	s [cm]	λ [W m ⁻¹ K ⁻¹]	ρ [kg m ⁻³]	cp [J kg ⁻¹ K ⁻¹]
Ceiling	24	0.65	800	840
Screed	4	1.35	2000	1000
Insulation	3	0.039	30	1200

Solar absorbance and infrared emissivity of all components are set to zero. In this way, the only heat flux considered across the opaque walls is due to the temperature difference between the inside and the outside. The numerical simulation period started on January 1 and lasted for the full month of January. In order to have more readable figures, only the result of the last two simulated days were plotted. It is important to highlight that for each opaque element ALMABuild uses an RC-model (3R4C); on the contrary TRNSYS uses the Mitalas transfer function

method (Mitalas et al., 1972) for the modelling of the dynamic heat transfer across opaque walls.

Fig. 1 shows a comparison between the room air temperature calculated for the room described before by ALMABuild and TRNSYS models.

It can be noticed that both ALMABuild and TRNSYS give the same value of the room air temperature with an average difference less than 0.01°C ; in addition, the phase lag between internal air temperature and the external one is the same, be it with TRNSYS or ALMABuild. However, Fig. 1 evidences a slight average time delay of the order of 20 minutes, between the two temperature trends. However, these results show that the 3R4C model and Mitalas transfer function method are in good agreement, and that the total thermal inertia of the room is correctly accounted for by ALMABuild.

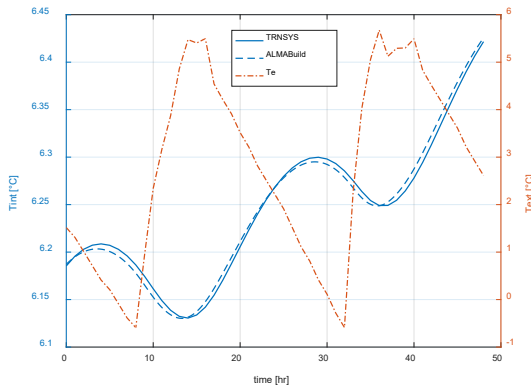


Fig. 1 – Comparison of the room air temperature (T_{int}) obtained with ALMABuild (dashed line) and TRNSYS (solid line)

3.1.2 Radiative heat exchange with the sky

The infrared emissivity coefficient of all the opaque walls was set to 0.9, in order to verify the effect of the radiative heat exchange between the external surface of the opaque walls and the sky.

ALMABuild calculates the radiative heat transfer in agreement with UNI EN 13790: 2008 and UNI TS 11300-1: 2014; the sky temperature is obtained as a function of the external vapour pressure following the method proposed by UNI TS 11300-1. On the contrary, TRNSYS uses as sky temperature with hourly values as given by the METEONORM database.

The comparison of the radiative heat transfer (Q_{sky}) calculated by ALMABuild and TRNSYS is shown in Fig. 2. It is evident that the values of Q_{sky} calculated by ALMABuild and TRNSYS are of the same order

of magnitude but their trend is very different. This is mainly due to the fact that the effective sky temperature, T_{sky} , used in the two models, is not the same, as evidenced in Fig. 2.

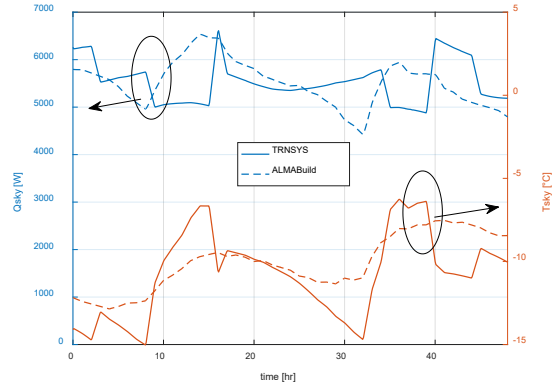


Fig. 2 – Comparison of the radiative heat exchange with the sky (left side, upper lines) and effective temperature of sky (right side, lower lines) obtained with ALMABuild (dashed line) and TRNSYS (solid line)

In order to check if the difference in terms of Q_{sky} is mainly due to the different way to calculate T_{sky} , the same evaluation has been repeated by imposing in both ALMABuild and TRNSYS, the same trend of T_{sky} . The values of Q_{sky} , obtained by assuming the same value of T_{sky} are shown in Fig. 3. It is evident that a systematic difference between the predictions of ALMABuild and TRNSYS still remains; however, the maximum deviation in the evaluation of Q_{sky} is reduced from 19 %, using different T_{sky} values, down to 5 %, using the same trend of T_{sky} .

The 5 % difference evidenced in Fig. 3 is due to the use of a different Q_{sky} formulation in TRNSYS and in ALMABuild. In fact, TRNSYS takes into account that the radiative heat transfer between the external surface of a building and the sky is in reality a three-body radiative problem in which also the presence of the ground surface must be taken into account. On the contrary, ALMABuild, according to the European Standard UNI EN 13790: 2008 ignores the presence of the ground.

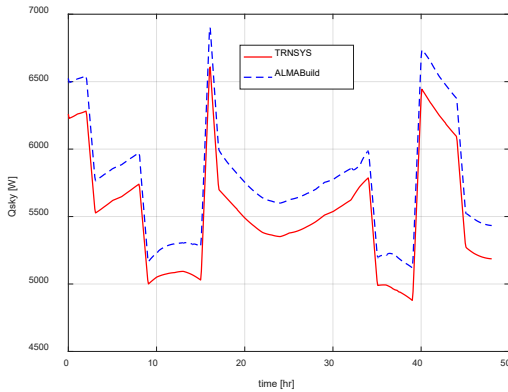


Fig. 3 – Comparison of the radiative heat exchange with the sky obtained with ALMABuild and TRNSYS, using the same T_{sky}

Fig. 4 puts in evidence the effect of the difference evidenced by Q_{sky} on the room air temperature. In this specific case, the different values of T_{sky} lead to a different evaluation of the room air temperature of 0.5 °C. This difference goes down to 0.2 °C if the value of T_{sky} is the same.

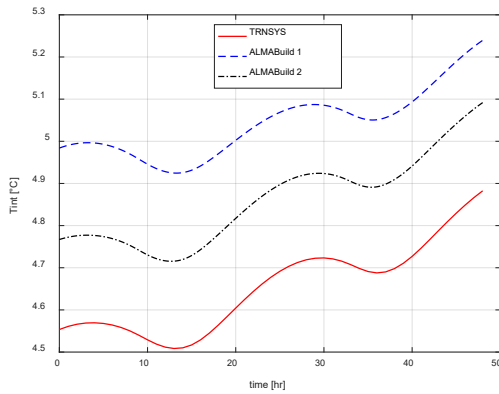


Fig. 4 – Comparison of the room air temperature considering radiative heat exchange, with the same T_{sky} used in TRNSYS, (ALMABuild 2) and with a different T_{sky} , ALMABuild 1

3.1.3 Solar heat gain

In this section, the radiative heat exchange with the sky of the external walls is once again disabled (by setting the infrared emissivity coefficient to zero), whilst solar heat gain of the opaque walls is enabled by setting the solar absorbance coefficient to 0.3. In this way, starting from the same climatic data, it is possible to compare the calculation of the solar radiation that strikes a surface with a defined orientation and slope made by TRNSYS and ALMABuild, and its effect on the room air temperature.

Fig. 5 shows the solar radiation that strikes a vertical surface exposed to South. From Fig. 5, it is clear that

the two models give the same results since the calculation of the solar radiation is based on the same solar model due to Perez (Perez et al., 1990).

Fig. 6 shows the difference in terms of room air temperature between the values obtained with TRNSYS and ALMABuild. It is evident that the trend is similar to the trend shown in Fig. 1; this means that TRNSYS and ALMABuild count the contribution of the solar gains exactly in the same way.

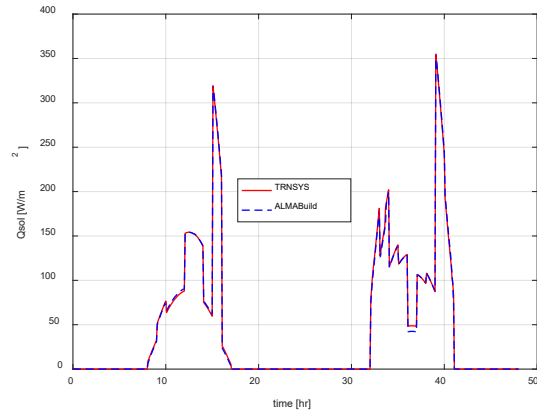


Fig. 5 – Comparison of the incident solar radiation, per surface unit, on a vertical South wall, obtained with TRNSYS and ALMABuild

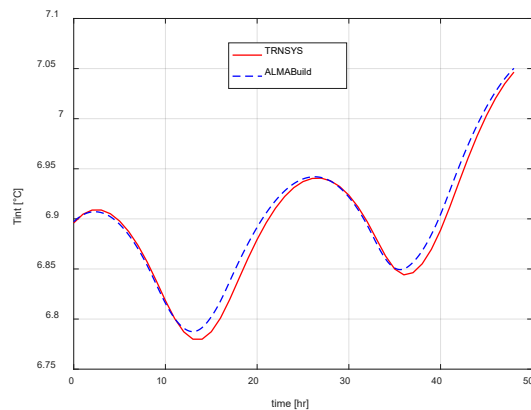


Fig. 6 – Comparison of the room air temperature, considering solar heat gains, with TRNSYS and ALMABuild

3.1.4 The overall simulation

After analysing the differences between TRNSYS and ALMABuild in terms of each single thermal flux, all the main heat transfer mechanisms are simultaneously taken into consideration. The infrared emissivity and solar absorbance coefficient of all the external opaque surfaces are set to 0.9 and 0.3 respectively.

In this way, it is possible to see if there is any interference between the different mechanisms and

which is the overall effect on the room air temperature.

Fig. 7 shows the room air temperature trend obtained by using TRNSYS and ALMABuild. In this comparison the evaluation of T_{sky} in ALMABuild is done according to UNI TS 11300-1.

It is evident from Fig. 7 that the trends of the room air temperature obtained with TRNSYS and ALMABuild have the same phase lag but a systematic shift of 0.3 °C which is less than the greatest deviation noticed when only radiative heat exchange, with a different evaluation of T_{sky} , was considered (see Fig. 4).

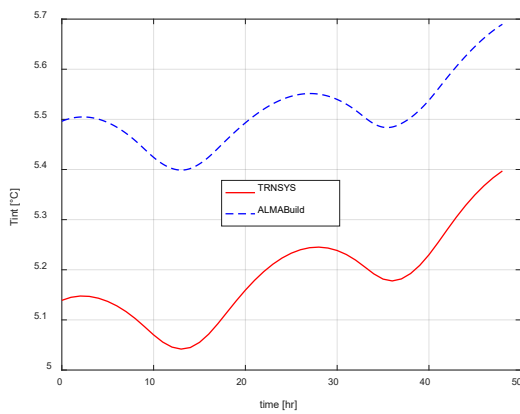


Fig. 7 – Comparison of the room air temperature, considering all the thermal fluxes on the opaque component, with TRNSYS and ALMABuild

This means that the combination of different heat fluxes across the building elements leads to a compensation of the single deviation between the two considered models.

In summary the results shown in Figs. 1–7 can be considered a positive benchmark for ALMABuild when only opaque building elements are present in a thermal zone.

3.2 Room with a Window

In this section a clear component (windows) is added to the previous thermal zone.

The room is the same of the previous simulations but there is a window inserted in the South wall, the properties of which are shown in Table 3. The goal of the following simulation is to compare the clear building component model used by TRNSYS with the BCC block of ALMABuild. Incident solar radiation in a window surface can be absorbed or reflected by the frame or by the glass, and transmitted

through the glass. In order to define a window, reflection, transmission, and absorbance coefficient have to be known, since they are functions of the angle of incidence of the solar radiation. Moreover, not only the window model is more complex than the model for an opaque component, but also the introduction of a clear component in a thermal zone makes the thermal balance model of the zone more complex. In fact the incoming solar radiation transmitted by the window, has to be distributed among the internal surfaces of the opaque components that bind the thermal zone.

The TRNSYS model calculates the global heat flux through the window glazing, evaluating the pane temperature distribution with an iterative procedure. The distribution of the incoming solar radiation is carried out evaluating the short wave radiation distribution factor (Klein et al., 2010) defined by the user.

Table 3 – Window properties

Property	Value	Unit
Surface	2	m ²
Frame Fraction	20	%
Number of glass	2	-
Thermal Transmittance	1.4	W m ⁻² K ⁻¹
Solar Transmittance	0.589	-

On the contrary, in ALMABuild windows are described using a 1R2C model, so that the temperature of the internal and external side of the window is calculated, whilst the short wave radiation distribution factor is automatically evaluated as a function of the thermal zone geometry.

The external conditions considered are the same for ALMABuild and TRNSYS models, but with a different evaluation of T_{sky} .

Fig. 8 shows the global solar radiation incoming in the thermal zone, that is the solar radiation transmitted by the window, evaluated by using TRNSYS and ALMABuild. It can be noticed that the two profiles are very similar with a maximum absolute deviation of about 10 W/m². The room temperature

evaluated by TRNSYS and ALMABuild are compared in Fig. 9.

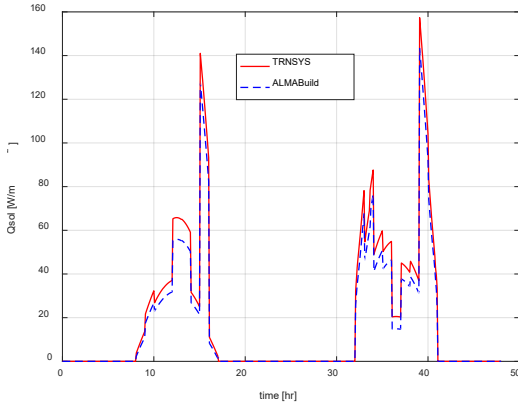


Fig.8 – Comparison of the solar radiation entering the thermal area from the window, with ALMABuild and TRNSYS

From Fig. 9, we can notice that the maximum deviation between these two profiles is around 0.3 °C, which is the same value reached by considering a room with only opaque elements.

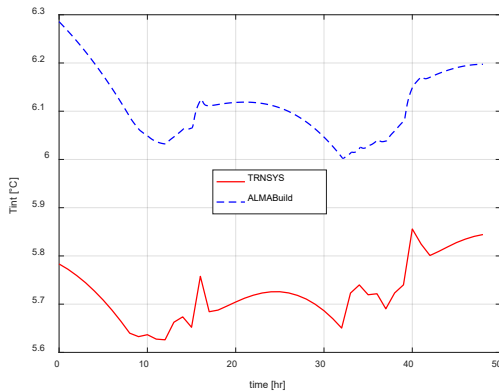


Fig.9 – Comparison of the room air temperature, considering the thermal zone with a window, obtained with TRNSYS and ALMABuild

3.3 Annual Simulations

Annual simulations by considering the room with a window have been made in order to compare TRNSYS with ALMABuild. For this comparison the BESTEST methodology was followed, even if the geometry of the room is different from the cases proposed by the BESTEST procedure (Judkoff et al., 1995). In Table 4 the maximum, minimum, and average annual hourly-integrated internal room temperature values are shown. The annual incident solar radiation is not reported because the results are identical, since the two codes use the same solar model.

Table 4 – Comparison of the annual result obtained using TRNSYS, ALMABuild 1 (considering different T_{sky}) and ALMABuild 2 (considering the same T_{sky})

Internal Temperature	TRN Build	ALMA Build 1	ALMA Build 2
Max (°C)	26.47	25.85	26.33
Min (°C)	2.81	3.01	2.86
Mean (°C)	15.66	15.63	15.71

The results reported in Table 4 show a good agreement between TRNSYS and ALMABuild in terms of internal temperature, both considering equal and different T_{sky} values. Moreover, the hours at which minimum and maximum temperature values were observed with ALMABuild are shifted by 2 and 6 hours with respect to TRNSYS, for both equal and different T_{sky} values. The results quoted in Table 1 confirm that ALMABuild is in good agreement with TRNSYS. However, the validation process of ALMABuild is at its early stage, that is why new validation cases, following the BESTEST procedure, are scheduled in the future.

4. Conclusion

In this work the benchmark of a new SIMULINK library for building modelling named ALMABuild is presented. This library is composed by Building Massive Element (BME) blocks based on 3R4C models, by Building Clear Components (BCC) blocks based on 1R2C models and by Building Thermal Balance (BTB) blocks based on a two-star thermal balance model of a thermal zone.

Comparing the main results, in terms of heat fluxes and room air temperature profiles, with the results obtained using TRNSYS, the benchmark of ALMABuild has been set. The results shown in this paper highlight that differences are present each time that the procedure indicated by the European Standard EN ISO 13790:2008 (and integrally followed by ALMABuild) is not in agreement with the procedure followed by TRNSYS (based on American standards), like in the case of the evaluation of radiative heat transfer between the building external

surface and the sky. Even if further validations are planned, it is possible to conclude that ALMABuild library can be considered a good tool for dynamic simulation; its strengths are its full coherence with European Standards and its full compatibility with the CARNOT blockset.

Nomenclature

Symbols

cp	Specific heat capacity (J/(kg K))
Q	Heat flux (W)
s	Thickness (cm)
T	Temperature (°C)
λ	Thermal conductivity (W/(m K))
ρ	Density (kg/m ³)

Subscripts/Superscripts

ext	Referred to the external air
int	Referred to internal room air
sky	Referred to the sky
sol	Referred to the solar radiation

References

- de Wit, M.H. 1988. "ELAN - a multizone simplified thermal simulation model". In: *Proceedings of the sixth international PLEA Conference*. Porto, Portugal: PLEA.
- European Commission. 2010. *Directive 2010/31/EU of the European Parliament and of the Council of 19 May 2010 on the Energy Performance of Buildings*. Brussels, Belgium: European Commission.
- Fouquier, A., S. Robert, F. Suard, L. Stéphan, A. Jay. 2013. "State of the art in building modeling and energy performances prediction: a review". *Renewable and Sustainable Energy Reviews* 23: 272-288. doi: 10.1016/j.rser.2013.03.004.
- Fraisse, G., C. Viardot, O. Lafabrie, G. Achard. 2002. "Development of a simplified and accurate building model based on electrical analogy". *Energy and Buildings* 34: 1017-1031. doi: 10.1016/S0378-7788(02)00019-1.
- Hudson, G., C. Underwood. 1999. "A simple modeling procedure for Matlab/Simulink". In: *Proceedings of the IBPSA Building Simulation 1999*. Kyoto, Japan: IBPSA.
- Judkoff, R., J. Neymark. 1995. *International Energy Agency Building Energy Simulation Test (BESTEST) and Diagnostic Method*. NREL/TP-472-6231. Golden, U.S.A.: National Renewable Energy Laboratory.
- Klein, S., W. Beckman, J. Mitchell, J. Duffie, N. Duffie, T. Freeman. "TRNSYS 16 - A transient system simulation program, User manual". Madison, U.S.A.: University of Wisconsin-Madison.
- Mitalas, G.P., J.G. Arseneault, 1972. *Fortran IV program to calculate Z-transfer functions for the calculation of transient heat transfer through walls and roofs*. Ottawa, Canada: National Research Council Canada, Division of Building Research.
- Morini, G.L., S. Piva. 2007. "The simulation of transients in thermal plant. Part I: Mathematical model". *Applied Thermal Engineering* 27: 2138-2144. doi: 10.1016/j.applthermaleng.2006.05.030.
- Morini, G.L., S. Piva. 2008. "The simulation of transients in thermal plant. Part II: Applications". *Applied Thermal Engineering* 28: 244-251. doi: 10.1016/j.applthermaleng.2006.05.035.
- Oliveira Panoa, M.J.N., C.A.P. Santos, N.M. Mateus, G. Carrilho da Graça. 2016. "Validation of a lumped RC model for thermal simulation of a double skin natural and mechanical ventilated test cell". *Energy and Buildings* 121: 92-103. doi: 10.1016/j.enbuild.2016.03.054.
- Perez, R., P. Ineichen, R. Seals, J. Michalsky, R. Stewart. 1990. "Modeling daylight availability and irradiance components from direct and global irradiance". *Solar energy*, 44(5): 271-289. doi: 10.1016/0038-092X(90)90055-H.
- Riederer, P., D. Marchio, P. Gruber, J. C. Visier, R. Lahrech, A. Husaunndee. 2000. "Building zone modelling adapted to the study of temperature control systems". In: *Proceedings of ASHRAE/CIBSE Conference 2000*. Dublin, Ireland.
- Wemhöner, C., B. Hafner, K. Schwarzer. 2000. "Simulation of solar thermal systems with CARNOT blockset in the environment MATLAB-Simulink". In: *Proceedings of Eurosun 2000*. Copenhagen, Denmark: ISES.

A New Methodological Approach for Estimating Energy Savings due to Air Movement in Mixed-Mode Buildings

Francesco Babich - Loughborough University - f.babich@lboro.ac.uk

Malcolm Cook - Loughborough University - malcolm.cook@lboro.ac.uk

Dennis Loveday - Loughborough University - d.l.loveday@lboro.ac.uk

Rajan Rawal - CEPT University - rajanrawal@cept.ac.in

Yash Shukla - CEPT University - yash.shukla@cept.ac.in

Abstract

In recent years, there has been a proliferation of air-conditioning in both residential and commercial buildings in India. Mixed-mode buildings are buildings in which a combination of air-conditioning and natural ventilation is used to provide comfortable indoor environments. These buildings are likely to be less energy consuming than fully air-conditioned buildings, and further energy savings can be achieved by using air movement to increase the cooling setpoint temperature without jeopardizing the occupants' thermal comfort. The aim of this research was to develop and test on a typical Indian apartment a methodology to quantify these energy savings using dynamic thermal simulations. The core of this method is the definition of the cooling setpoint, which varies monthly according to the ASHRAE 55-2013 adaptive model. The results show that the annual energy demand for space cooling can be reduced by as much as up to 70 percent by using air motion devices. Moreover, the indoor thermal conditions during the occupied periods predicted by the model are closer to the values measured in field studies in India.

1. Introduction

In recent years, there has been a proliferation of air-conditioning in both residential and commercial buildings, and, due to the warming climate and the growing disposable income in several densely populated developing countries, energy demand for space cooling is dramatically increasing. The additional electricity demand generated by new in-room air conditioners purchased between 2010 and 2020 is projected to grow to more than 600 billion kilowatt-hours globally by 2020, and four countries, namely China, India, Brazil, Japan, together with

the EU, are expected to represent 90 per cent of this market in 2014 (Shah et al., 2013).

Mixed-mode buildings are buildings in which a combination of air-conditioning and natural ventilation is used to provide comfortable indoor environments (Brager, 2006). There are three possible types of mixed-mode buildings based on operation strategy: concurrent, changeover, and zoned. In the first case, mechanical and natural ventilation are simultaneously used in the same space; with the second case, only one ventilation type is used in the entire building for a certain amount of time such as one day or one month; in the third case, 'zoned' means that both modalities are used at the same time, but in different parts of the building.

Mixed-mode buildings are likely to be less energy consuming than fully air-conditioned buildings, but predicting their performance is a more complex task. An approach has been proposed (Spindler and Norford, 2009a and 2009b), but its authors stated that this model cannot be used in domestic buildings because the occupants have direct control over the system. Moreover, research showed that the choice of the comfort criteria significantly affects the analysis of mixed-mode buildings (Borgeson and Brager, 2011), but the international standards (ISO 7730-2005, EN 15251-2007 and ASHRAE 55-2013) offer too little support for this choice.

Further energy savings can be achieved by using air movement devices, such as ceiling fans. Previous research (Schiavon and Melikov, 2008) estimated these savings in fully air-conditioned buildings, varying the cooling setpoint temperature based on category (EN 15251-2007) and air speed. In that study, and also in a more recent one (Hoyt et al, 2015), the cooling setpoint temperature did not vary

across the year, and both studies considered office buildings.

However, research on Indian apartments (Indraganti, 2010) highlighted that the use of air conditioners highly correlates with both outdoor and indoor temperatures. Moreover, previous work on the Indian commercial building sector (Manu et al., 2011) recognized the potential impact of using a floating setpoint temperature based on external environmental indicators such as air temperature and behavioural and psychological adaptations by the occupants in energy consumption estimates.

These studies and also recent work (Manu et al., 2016) on the Indian Model of Adaptive Comfort (IMAC) support the idea that the adaptive modelling approach is to some extent applicable also to mixed mode residential buildings.

Thus, the aim of this research was to develop and test a new methodology based on the adaptive theory to quantify the energy savings achievable in mixed-mode buildings due to air movement.

2. Methods

In this study, computer simulations have been used to test the new methodology, and the analysis focused on the energy demand for space cooling and the indoor environmental conditions predicted using this methodology. The core of this methodological approach is the way by which the cooling setpoint is defined. The proposed method was applied to an apartment in Ahmedabad, India, which is a typical example of a mixed-mode building with ceiling fans.

2.1 Cooling Setpoint Definition

IMAC was specifically developed from Indian data, but its equations implicitly incorporate the effect of

air speed. Thus, it is not possible to use this model to estimate the energy savings due to the use of fans. The ASHRAE adaptive model was therefore used in this study.

According to ASHRAE 55-2013 (point 5.4.1), the adaptive model is applicable when all the following conditions are met:

- a) There is no mechanical cooling system installed. No heating system is in operation
- b) Metabolic rates range from 1.0 to 1.3 met
- c) Occupants are free to adapt their clothing to the indoor and/or outdoor thermal conditions within a range at least as wide as 0.5-1.0 clo
- d) The prevailing mean outdoor temperature is greater than 10 °C and less than 33.5 °C

Considering the Ahmedabad climate and the Indian typical domestic environment, all conditions are met, with the partial exception of the first condition for the case of a mixed-mode building. However, based on recent previous works (Indraganti, 2010; Manu et al., 2016), in this study we assumed the ASHRAE adaptive model is applicable also if air conditioning is available.

Moreover, the acceptable operative temperature limit in occupant-controlled spaces can be increased by 1.2 °C, 1.8 °C, and 2.2 °C due air speed equal to 0.6 m/s, 0.9 m/s, and 1.2 m/s, respectively (ASHRAE 55-2013, table 5.4.2.4). In warm and hot conditions, an elevated air speed can improve the thermal sensation of the occupants, rather than being the cause of an undesired draught.

In this research, a dynamic thermal model was created for a chosen mixed-mode building in which there are also fans. In the initial simulation, the cooling setpoint for temperature was varied monthly according to the ASHRAE 55-2013 adaptive model, considering the 90 per cent acceptability upper limits. In the subsequent three simulations, these

Table 1 – Dynamic cooling setpoint

	JAN	FEB	MAR	APR	MAY	JUN	JUL	AUG	SEP	OCT	NOV	DEC
T_m	20.0	22.0	27.0	31.0	33.0	32.0	29.0	28.0	29.0	28.0	25.0	20.0
T_{comf}	24.0	24.6	26.2	27.4	28.0	27.7	26.8	26.5	26.8	26.5	25.6	24.0
$T_{max(90\%)}$	26.5	27.1	28.7	29.9	30.5	30.2	29.3	29.0	29.3	29.0	28.1	26.5
$T_{maxAirSpeed(1.2\ m/s)}$	28.7	29.3	30.9	32.1	32.7	32.4	31.5	31.2	31.5	31.2	30.3	28.7
$T_{maxAirSpeed(0.9\ m/s)}$	28.3	28.9	30.5	31.7	32.3	32.0	31.1	30.8	31.1	30.8	29.9	28.3
$T_{maxAirSpeed(0.6\ m/s)}$	27.7	28.3	29.9	31.1	31.7	31.4	30.5	30.2	30.5	30.2	29.3	27.7

monthly setpoints were increased according to ASHRAE 55-2013 for air speeds up to 1.2 m/s. The Ahmedabad weather file used in this study to calculate the monthly cooling setpoint (see Table 1) was created by ISHRAE in TMY2 format for use with building energy performance simulation programs (EnergyPlus weatherdata, 2016). T_{comf} comfort temperature, that is neutral operative temperature at which the lowest total percentage of people are expected to be either too hot or too cold (Borgheson and Brager, 2011), and $T_{\text{max}(90\%)}$ 90 per cent temperature upper limit, are calculated based on T_m monthly arithmetic mean of the daily average outdoor dry bulb temperatures:

$$T_{\text{comf}} = 17.88 \text{ }^\circ\text{C} + 0.31 \times T_m \quad (1)$$

$$T_{\text{max}(90\%)} = T_{\text{comf}} + 2.5 \text{ }^\circ\text{C} \quad (2)$$

2.2 Dynamic Cooling Setpoint Implementation

Once the four sets of monthly cooling setpoints were calculated (see Table 1), they were implemented in DesignBuilder/EnergyPlus using an advanced feature called Energy Management System (EMS), available in DesignBuilder from the recently realised version 5 (EMS, 2016b).

In EMS, a simple programming language called EnergyPlus Runtime Language (Erl) is used to describe the control algorithms. EnergyPlus interprets and executes the Erl program as the model is being run (EMS, 2016a).

In this study, an Erl script has been written to specify a different cooling setpoint per month using an IF and ELSEIF structure. Erl currently supports up to 199 ELSEIF statements, which means that by using Erl the cooling setpoint could not be changed every day of the year as would be required by the IMAC or EN15251 adaptive model. This is the technical reason why the ASHRAE adaptive model was chosen in this study rather than IMAC.

Four scripts have been developed, one for each simulation. These were used only to specify the setpoint value, while the ON/OFF control strategy has been defined in DesignBuilder.

2.3 The Case Study Building

The dynamic cooling setpoint method was tested on a typical Indian apartment, this being one of the

apartments in an on-going international project on thermal comfort and air movement in residential buildings (Loveday et al., 2016). The project involves Loughborough University and De Montfort University in the UK, CEPT University in India, and University of California Berkeley in the USA.

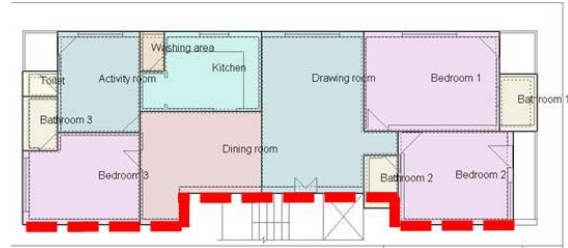


Fig. 1 – Floor plan (the red dashed line indicates an adiabatic party-wall)

Table 2 – Characteristics of construction elements

Element	Layers	U-value [W/m ² K]
Internal partitions	12mm cement plaster 115mm brick 12mm cement plaster	1.98
External walls	From inside: 12mm cement plaster 230mm brick 18mm cement plaster From the top: 10mm vitrified tile	1.59
Ceiling and floor	50mm cement – sand mix 150mm reinforced cement concrete slab 12mm cement plaster	2.17

This apartment (see Fig. 1) has a floor surface area of 145 m², internal height 3.2 m, and is surrounded by other apartments above, below, and to the side. Thus, ceiling, floor and party-wall have been assumed to be adiabatic. Typical construction elements of the Ahmedabad region were used (see Table 2). Due to the hot climate, there are no insulation layers, all windows have single glazing, and there is no heating system installed. The balconies were added in DesignBuilder to simulate shading effect, and the internal doors were assumed to be open 50 per cent of the time.

Physical partitions were used to create a zone for each room of the apartment, and an additional virtual partition was placed between the dining room and the drawing room. Although this is a unique open space, the former is used for having meals,

while the latter is a living room. Therefore, their use is significantly different.

Since the aim of this work was to model a typical house, the occupancy schedule and relative internal heat gains were chosen from the available standard templates based on the type of each room.

Within DesignBuilder, the chosen method for natural ventilation is “calculated”, which uses the EnergyPlus airflow network (AIRNET) method to calculate the ventilation rates using wind and buoyancy-driven pressure, opening size and operation, and crack sizes. This option slows the simulation down, but it is preferable if a reasonable estimate of the natural ventilation rates and infiltration rates in the building are not available (EnergyPlus documentation, 2016). The “medium” crack template was used. The “mixed-mode” option was selected, and, for any given cooling setpoint temperature, the air conditioning system was ON if:

- a) The space was occupied
- b) The indoor air temperature was above set point temperature
- c) The outdoor air temperature was above indoor air temperature

Moreover, the air-conditioning was installed only in two rooms, namely “bedroom 1” and “bedroom 2”. In an on-going field study, the authors observed that in Indian apartments there is often air conditioning only in a few rooms, not everywhere in the house. Within DesignBuilder, the modelled system

is a typical residential mini-split system, with a coefficient of performance of 4.5. This type of air conditioners dominates air conditioner sales in most parts of the world including Asia and Europe (Shah et al., 2013).

In order to compare E_{nofan} energy demand for space cooling of the first simulation and the values of the subsequent three $E_{withfan}$, the energy used by the fan must also be taken into account. Considering that a higher setpoint could have been chosen due to the use of a fan, n total number of hours in which this was ON in the subsequent three simulations must be equal to the total number of cooling hours in the first simulation. The fan energy consumption E_{fan} is obtained by multiplying n for the average power of the fan, which for a typical Indian ceiling fan is 50 W (BEE, 2016):

$$E_{fan} = n \times 50W / 1000 \tag{3}$$

Since the air conditioning is available in two rooms, in a real scenario two fans may be operating at the same time, doubling E_{fan} . Therefore, this second possible scenario was also considered.

This value is then added to E_{AC} energy used by the air conditioning system:

$$E_{withfan} = E_{AC} + E_{fan} \tag{4}$$

The energy savings achievable using ceiling fans are therefore:

$$E_{savings} = E_{nofan} - E_{withfan} \tag{5}$$

Both T_A air temperature and T_O operative temperature setpoints were simulated to assess savings benefits using both approaches.

Table 3 – Energy saving without including energy used by the fan

Simulation	Cooling hours h]	Energy for space cooling [kWh]	Energy for space cooling [kWh/m²]	Savings without including the fan energy consumption [kWh]	Savings without including the fan energy consumption [%]
Control type: T_A					
no fan	1482	1381	9.52	0	0
with fan - 0.6 m/s	873	691	4.76	690	50
with fan - 0.9 m/s	654	469	3.23	912	66
with fan - 1.2 m/s	526	359	2.47	1022	74
Control type: T_O					
no fan	2527	2827	19.49	0	0
with fan - 0.6 m/s	1843	1655	11.41	1172	41
with fan - 0.9 m/s	1524	1235	8.52	1592	56
with fan - 1.2 m/s	1327	1011	6.98	1815	64

Table 4 – Energy saving including the energy used by the fan

Simulation	n [h]	Fan average power [W]	E_{fan} [kWh]	$E_{savings}$ kWh]	$E_{savings}$ [%]	Fan only hours [h]
Control type: T_A						
no fan	0	0	0	0	0	0
with fan - 0.6 m/s	1482	50	74	616	45	609
with fan - 0.9 m/s	1482	50	74	838	61	828
with fan - 1.2 m/s	1482	50	74	948	69	956
Control type: T_O						
no fan	0	0	0	0	0	0
with fan - 0.6 m/s	2527	50	126	1046	34	684
with fan - 0.9 m/s	2527	50	126	1466	52	1003
with fan - 1.2 m/s	2527	50	126	1689	60	1200

3. Results and Discussion

This section initially focuses on the effect that the choice between T_A and T_O as control parameter has on the energy predictions. It then analyses the demand for space cooling, and the energy savings that can be achieved in a typical Indian residential mixed-mode building using ceiling fans when a dynamic cooling set point is used.

3.1 Effect of Using Air Temperature or Operative Temperature

There is a noticeable difference in the energy consumption depending on whether T_A or T_O was chosen as the control parameter. In the initial case where no fan was used, the total number of cooling hours (see Table 3) is 1482 when T_A is used, but it reaches 2527 with the other control type, which is a 70 per cent increase due only to a change in this setting within the simulation program. As the fan speed goes up to 0.6 m/s, 0.9 m/s, and 1.2 m/s, this percentage grows to 111 per cent, and 133 per cent and 152 per cent, respectively. The respective energy consumption expressed in kWh is relatively low when using both T_A or T_O , but should these predictions be used to scale up the energy saving estimates to a regional scale, then these differences would make a bigger impact.

In general, T_O is a function of T_A and T_{MR} mean radiant temperature. For low air speed, smaller than 0.2 m/s, T_O is the arithmetic mean of T_A and T_{MR} . Then, as the air speed increases, the relative weight of T_{MR} decreases (Niu and Burnett, 1998).

International standards on thermal comfort usually refer to T_O when a certain temperature limit is given, and this is the case also for the ASHRAE adaptive model on which the cooling setpoints used in this study are based (ASHRAE 55-2013). Indeed, T_O gives a better indication of the temperature that a person feels in a certain environment.

On the other hand, real-world room air-conditioners are controlled by a simple thermostat, which is likely to be sensing the air temperature nearby its location, but far less influenced by the radiant component. In a real scenario, this means that a user would simply decrease the setpoint if uncomfortably warm. However, if the model uses T_A as a control, this behaviour is not captured.

It is important to highlight that in the two conditioned bedrooms, T_A and T_O are almost identical when no air conditioning is used. As the air conditioning is turned on, T_A decreases faster, with the difference ($T_O - T_A$) being within 1.6°C in over 85 per cent of the hours in which the air conditioning is used.

Previous research on Indian offices (Jain et al., 2011) also noticed that the energy demand for space cooling obtained using T_A is significantly lower than when T_O is used in EnergyPlus simulations. The difference was found to go up to 29 per cent, which at first sight might look a lot smaller than the figures mentioned earlier in this paper. However, in that case the chosen setpoint temperature was 24 °C, which means that the cooling load in kWh was very high using either T_A or T_O . Therefore the relative dif-

ference was smaller. Similarly, in this study, the percentage difference grows as the setpoint is increased due to the higher air speed.

Therefore, whenever in a given space T_A and T_{MR} are different, the energy load for space cooling is more realistic if calculated using T_O when the users have total direct control over the setpoint, and using T_A when they do not. When air conditioning is used in bedrooms overnight, it is likely to be in between these two extreme conditions.

For all these reasons, in this study both control types have been used and the respective results reported.

3.2 Energy Savings

Despite the choice between T_O and T_A , a significant reduction in energy consumption is achievable if ceiling fans are used to increase the setpoint temperature (see Table 4). The figures go up to 69 and 60 per cent or 948 and 1689 kWh using T_A and T_O as a control temperature, respectively.

The simultaneous use of a second ceiling fan only slightly reduces the energy savings (see Table 5). For both T_O and T_A based estimates, the energy savings would be negligible only if 9 ceiling fans were to be operating at the same time, which is not a realistic scenario. This significant margin has also another positive consequence. In an average Indian apartment, there are small fluctuations in the electricity supply, and also different speed settings lead to slightly different power usage. Both variations depend on the specific house and fan, but having such a big margin ensures that ceiling fans are clearly an effective way to improve thermal comfort while saving energy.

These energy predictions are calculated using the new approach based on the dynamic cooling setpoint that varies each month. If the methods used in previous research on office buildings (Schiavon and Melikov, 2008) had been applied, then the setpoints would have been constant throughout the year. Considering category II (EN 15251-2007), in which case 10 per cent of people are considered to be dissatisfied, the temperature thresholds would have been 26.0 °C, 27.7 °C, and 28.5 °C for 0.2 m/s or less, 0.5 m/s, and 0.8 m/s, respectively. These values are lower than those used in this study (see Table 1), both for the cases without and with air movement,

and therefore the annual energy consumption calculated with these setpoints would be higher. However, research showed that the comfort band in Indian residential buildings can be extended up 32.5°C (Indraganti, 2010), which is much closer to the highest setpoint used in this work, that is 32.7 °C in May with air speed equal to 1.2 m/s, than the values used in previous research. Moreover, the same study highlighted how complex the domestic environment is, that users are heavily influenced by the outdoor conditions, and that the different adaptive solutions such as ceiling fans and air conditioners are widely used and combined. Therefore, energy savings predictions calculated with the proposed methodology are lower than those calculated with traditional methods for fully air-conditioned buildings, but they are likely to be more realistic for the situation of Indian residential mixed-mode buildings.

Table 5 – Energy saving including the energy used by two fans

Simulation	$E_{savings}$ [kWh]	$E_{savings}$ [%]
Control type: T_A		
no fan	0	0
with fan - 0.6 m/s	542	39
with fan - 0.9 m/s	764	55
with fan - 1.2 m/s	874	63
Control type: T_O		
no fan		
with fan - 0.6 m/s	919	33
with fan - 0.9 m/s	1339	47
with fan - 1.2 m/s	1563	55

4. Conclusions

The research presented in this paper aims to develop and test a new methodological approach for estimating the energy savings achievable due to air movement in mixed model buildings.

The key findings are:

- The dynamic cooling setpoint led to more realistic simulation scenarios since it captures the existing connection between the users of mixed-mode buildings and the outdoor temperature
- The energy demand for space cooling can be reduced by as much as 70 percent by using ceiling

fans, without jeopardising the occupants' thermal comfort.

- The simultaneous use of two fans slightly reduces the energy savings.
- Using the operative or air temperature as control parameters in EnergyPlus significantly affects the results. Since the air temperature decreases faster when the air conditioning is turned on, estimates based on it may be excessively low.

4.1 Limitations and Future Work

The currently available field-based research on mixed-mode buildings supports the idea that the users of these buildings are affected by the outdoor conditions, and therefore a method based on the adaptive model is likely to be closer to real-world scenarios.

However, these studies also show two other important things. Firstly, when air conditioning is available, even if only in certain rooms or at a certain time, then the occupants of a building tend to be a little less tolerant than people in fully naturally ventilated buildings. The second point is that in mixed-mode buildings the use of air-conditioners depends on a range of factors that are not related to the outdoor temperature, such as noise, pollution, and disposable income, and the situation is even more complex in domestic buildings.

Thus, more studies based on real field data are needed to properly address mixed-mode buildings. The economies of developing countries such as India are growing fast, and represent the main market for air conditioners, and mixed-mode buildings are extremely common. Therefore over- or underestimating their energy requirements for space cooling would heavily affect the global figures for energy demand.

It will then be possible to say whether the most suitable method for estimating energy savings due to air movement in mixed-mode buildings is the one proposed in this paper and based on ASHRAE adaptive model, one based on IMAC, or a different one that has not been developed yet.

Acknowledgement

This research was financially supported by the Engineering and Physical Sciences Research Council (EPSRC) via the London-Loughborough Centre for Doctoral Research in Energy Demand (LoLo), and by the British Council under the Global Innovation Initiative, the latter involving an international research collaboration between UC Berkeley (USA), CEPT University (India), Loughborough University and De Montfort University (UK). The authors express their gratitude for this support.

References

- ASHRAE Standard 55. 2013. *Thermal Environmental Conditions for Human Occupancy*. Atlanta, U.S.A.: American Society of Heating, Refrigerating and Air-Conditioning Engineers, Inc.
- BEE. 2016. Last access: 10.10.2016. <https://www.bijlibachao.com/top-ten-appliances/best-ceiling-fan-khaitan-havells-usha-crompton-greaves-orient-in-india-electricity-consumption.html>
- Borgeson, S., G. Brager. 2011. "Comfort standards and variations in exceedance for mixed-mode buildings". *Building Research & Information*. 39: 118-133. doi: 10.1080/09613218.2011.556345.
- Brager, G. 2006. "Mixed-mode cooling". *ASHRAE Journal*. 48: 30-37.
- CEN. 2007. EN 15251. 2007. *Indoor environmental input parameters for design and assessment of energy performance of buildings addressing indoor air quality, thermal environment, lighting and acoustics*. Brussels, Belgium: European Committee for Standardization.
- EMS. 2016a. Last access: 05.10.2016. https://energyplus.net/sites/all/modules/custom/nrel_custom/pdfs/pdfs_v8.6.0/EMSApplicationGuide.pdf
- EMS. 2016b. Last access: 05.10.2016. https://designbuilder.co.uk/helpv5.0/Content/Energy_Management_System_-_EMS.htm
- EnergyPlus documentation. 2016. <https://energyplus.net/documentation>

- EnergyPlus weather data. 2016. Last access: 01.10.2016. https://energyplus.net/weather-region/asia_wmo_region_2/IND%20%20
- Hoyt, T., E. Arens, H. Zhang. 2015. "Extending air temperature setpoints: Simulated energy savings and design considerations for new and retrofit buildings". *Building and Environment*. 88: 89-96. doi: 10.1016/j.buildenv.2014.09.010.
- Indraganti, M. 2010. "Behavioral adaptation and the use of environmental controls in summer for thermal comfort in apartments in India". *Energy and buildings*. 42(7): 1019-1025. doi: 10.1016/j.enbuild.2010.01.014.
- ISO. 2005. ISO 7730. 2005. *Ergonomics of the thermal environment - Analytical determination and interpretation of thermal comfort using calculation of the PMV and PPD indices and local thermal comfort criteria*. Geneva, Switzerland: International Organization for Standardization.
- Jain, V., V. Garg, J. Mathur, S. Dhaka. 2011. "Effect of operative temperature based thermostat control as compared to air temperature based control on energy consumption in highly glazed buildings". In: *Proceedings of Building Simulation 2011: 12th Conference of International Building Performance Simulation Association*. Sydney, Australia: IBPSA.
- Loveday, D.L., L.H. Webb et al. 2016. "The role of air motion for providing thermal comfort in residential/mixed mode buildings: a multi-partner global innovation initiative (GII) project". In: *Proceedings of 9th Windsor Conference Making Comfort Relevant NCEUB*. Windsor, UK: NCEUB.
- Manu, S., Y. Shukla, R. Rawal, L.E. Thomas, R. de Dear. 2016. "Field studies of thermal comfort across multiple climate zones for the subcontinent: India Model for Adaptive Comfort (IMAC)". *Building and Environment*. 98, 55-70. doi: 10.1016/j.buildenv.2015.12.019.
- Manu, S., J. Wong, R. Rawal, P. Thomas, S. Kumar, A. Deshmukh. 2011. "An initial parametric evaluation of the impact of the energy conservation building code of India on commercial building sector". In: *Proceedings of Building Simulation 2011: 12th Conference of International Building Performance Simulation Association*. Sydney, Australia: IBPSA.
- Niu, J., J. Burnett. 1998. "Integrating Radiant/Operative Temperature Controls into Building Energy Simulations". *ASHRAE Transactions* 104(2) 210. Atlanta, U.S.A.: American Society of Heating, Refrigerating and Air-Conditioning Engineers, Inc.
- Schiavon, S., A.K. Melikov. 2008. "Energy saving and improved comfort by increased air movement". *Energy and buildings*. 40(10): 1954-1960. doi: 10.1016/j.enbuild.2008.05.001.
- Shah, N., A. Phadke, P. Waide. 2013. *Cooling the Planet: Opportunities for Deployment of Superefficient Room Air conditioners*. Berkeley, U.S.A.: Lawrence Berkeley National Laboratory and Navigant consulting, Inc.
- Spindler, H.C., L.K. Norford. 2009a. "Naturally ventilated and mixed-mode buildings - Part I: thermal modelling". *Building and Environment*. 44(4): 736-749. doi: 10.1016/j.buildenv.2008.05.019.
- Spindler, H.C., L.K. Norford. 2009b. "Naturally ventilated and mixed-mode buildings - Part II: Optimal control". *Building and Environment*. 44(4): 750-761. doi: 10.1016/j.buildenv.2008.05.018.

On the Indoor Thermal Behavior of a Building with Cool Envelope Components

Anna Laura Pisello – University of Perugia – anna.pisello@unipg.it

Veronica Lucia Castaldo – University of Perugia – castaldo@crbnet.it

Claudia Fabiani – University of Perugia – fabiani@crbnet.it

Franco Cotana – University of Perugia – cotana@crbnet.it

Abstract

During the last decade, computational fluid dynamic simulation tools have been widely applied for accurately modelling outdoor airflows and local microclimate conditions. In fact, a complete understanding of heat transfer phenomena occurring within the built urban environment is needed to properly predict the energy balance, both on a single-building and on an inter-building scale. In this scenario, several research studies have been carried out to evaluate the impact of local passive solutions on buildings indoor environment, especially by means of dynamic simulation tools. However, only a few investigations were performed by considering the local distribution and spatial variability of the indoor building physics generated by the application of passive cooling strategies.

The present research is aimed at bridging this gap by modelling the indoor thermal environment of a case study prototype building, i.e. square cavity, located in central Italy, by considering indoor heat transfer phenomena. A calibrated and experimentally validated CFD model of the building was elaborated to predict the indoor temperature distribution and profile generated by the application of an innovative highly-reflective cool façade painting and cool roofing membrane on the building envelope, compared to a more traditional “non-cool” envelope finishing. So far, the authors have produced only one work about cool roofs in buildings that concerned sloped roofs in a non-insulated building envelope. Here, we deal with insulated architectures, designed according to the recent energy efficiency regulation, and a combined cool roof and cool façade indoor effect. The experimental validation of the model is carried out by means of experimental data that are continuously monitored both inside and outside the case study building by means of dedicated microclimate and weather stations.

Simulation results were therefore post-processed in terms of (i) indoor temperature and (ii) indoor airflows. Main

findings confirmed the huge potentiality of the model in realistically reproducing the indoor behavior of the case study building and therefore the urgent need for a CFD-based approach in investigating thermal-comfort conditions. In fact, a non-negligible and positive impact of the cool building envelope on the local indoor thermal comfort conditions is detected with respect to the more traditional non-reflective component.

1. Introduction

The passive cooling capability of highly reflective building envelope materials and solutions, i.e. roofs, walls, and pavements, has been largely acknowledged over the course of the years (Georgakis et al., 2014).

Such high-albedo solutions characterized also by high thermal emittance have been demonstrated to be very effective, not only in reducing buildings cooling energy requirements and improving the indoor thermal comfort conditions by avoiding summer overheating, but also in mitigating local microclimate events such as urban heat island and heat waves phenomena (Wong et al., 2016; Gracik et al., 2015).

The use of cool envelope solutions like cool roofs can lead up to 125 kWh/year of annual electricity saving and up to an 80 % seasonal energy reduction in temperate climates, with little penalties in winter (Akbari 2003; Akbari et al., 1997). Moreover, indoor air temperature reductions up to 3-4 K in peak summer conditions were detected by applying cool coatings on the roof of residential buildings with a consequent considerable reduction of the discomfort

hours within different climate boundary conditions (Synnefa et al., 2007).

Nowadays, many different tools and approaches are available to analyze the impact of the application of cool solutions on both the buildings thermal-energy performance and the urban environment (Corrado et al., 2016; Atzeri et al., 2016), i.e. experimental, analytical, and numerical methods (Pisello et al., 2015; Synnefa et al., 2011; Crawley et al., 2001).

Among such approaches, computational fluid dynamic tools represent a suitable and multifunctional approach to predict the indoor effect generated by the modification of the thermal-optical properties of the building envelopes and urban surfaces in terms of (i) airflow distribution, (ii) air quality, and (iii) temperature field (Yang et al., 2013). More in detail, many research studies focus on the CFD evaluation of the impact of the roof inclination, roof-covering materials, and the geometry of the environment on the internal flow (i.e. laminar or turbulent regimes) and temperature distribution in enclosed spaces (Saha et al. 2010; Basak et al., 2008). Moreover, a huge effort in the use of CFD tools to predict the flow and thermal field in enclosed cavities with different geometrical characteristics, such as attic spaces, is registered (Hasani et al., 1998; Asan et al., 2000; Kamiyo et al., 2010; Pisello et al., 2016), by considering $10^9 \leq Ra \leq 10^{11}$ when turbulence occurs.

2. Motivation

Even if many studies were performed to investigate both numerically and experimentally the impact of passive cool solutions applied to building envelope components, still a few studies, focusing on the combination of different cool technologies, can be found in the literature. Therefore, building upon previous research efforts about (i) cool roof application for improving indoor thermal comfort conditions and (ii) the use of CFD tools to properly describe the indoor airflow and thermal environment of buildings, the present work concerns the CFD numerical analysis of the indoor thermal field and airflow inside a case study prototype building, i.e. test-room. The final aim is to assess the combined effect of the application of two cool envelope solutions, i.e. cool roofing membrane and cool

façade painting, when applied on the building envelope. In particular, the CFD was used in order to determine the indoor air temperature spatial distribution profile inside the cavity, by investigating at which height the passive cooling effect of the cool membrane is extinguished. To this aim, a preliminary continuous monitoring of the main indoor-outdoor microclimate parameters was carried out to support the validation and calibration of the numerical CFD model of the building. Therefore, two scenarios were simulated and compared: (i) a more traditional building envelope (standard non-cool surfaces) and (ii) a cool building envelope (characterized by the application of the cool roofing membrane and cool façade painting on the envelope).

3. Description of the Case Study

The case study building consists of a fully instrumented test-room ($3.78 \times 3.78 \times 2.85$ m) located in Perugia (Italy), and designed according to the recent construction techniques (Pisello et al., 2014a).

Fig. 1 reports the pictures of the roof and the façades of the case study building before (Fig. 1a) and after the application of the cool membrane and reflective painting (Fig. 1b).



Fig. 1 – (a) Cool and (b) standard configuration of the case study building

The reference building is characterized by a rectangular double shutter window with wood frames in the South façade and a rectangular armored door in the North façade, for a global fenestration ratio of about 0.041.

The opaque envelope of the case study building was developed by using an innovative construction stratigraphy in order to be consistent with the Italian regulations in terms of walls' thermal stationary

properties, and representative of a common residential building in Italy. The specific characteristics of the test-room envelope components are specified in Table 1.

Table 1 – Building characteristics in terms of materials and main thermal properties of the envelope

	Material	Thickn. [m]	Th. Cond. [W/mK]	Th. Transm. [W/m ² K]
Walls	plaster	0.02	0.50	0.49
	EPS	0.09	0.04	
	brickwork	0.30	0.27	
	plaster	0.02	0.40	
Roof	waterproof membrane	0.01	0.23	0.25
	mineral wool	0.10	0.04	
	concrete slab	0.20	0.16	
	plaster	0.015	0.40	
	cast concrete	0.2	1.13	
Floor	stone wool	0.08	0.04	0.38
	linoleum	0.015	0.17	

All the real thermal properties and characteristics of the building envelope components were used as input data in both models of the building.

More in detail, a simplified building geometry was implemented, by assuming a single solid layer for each building envelope component.

Therefore, the thermal properties of the one-layer simulated configuration were accurately calculated by considering the realistic multi-layer components connected in series.

4. Methodology

The methodology applied consists of the following main steps:

- selection of the proper case study, i.e. prototype test-room;
- continuous monitoring of the main indoor-outdoor microclimate parameters;
- CFD simulation of the summer indoor thermal profile and velocity field generated inside by

the application of (i) traditional non-cool materials and (ii) cool highly-reflective envelope materials;

- validation of the model by means of the experimental continuously monitored data;
 - post-processing and discussion of the achieved results.
- Therefore, two building scenarios were assessed:
- *Standard configuration*: building envelope covered by traditional non-cool materials;
 - *Cool configuration*: building envelope covered by innovative high albedo materials, i.e. cool roofing membrane and wall painting.

The more traditional envelope materials are characterized by an albedo of 19 %, while the innovative cool envelope materials are characterized by a higher albedo i.e. 77 %. In both the building configurations, the building envelope materials present a thermal emissivity of 88 %, as previously experimentally measured (Pisello et al, 2014a; Pisello et al., 2014b).

4.1 Experimental Monitoring Campaign

The purpose of the study is to (i) compare the thermal behavior of the two innovative cool envelope solutions, i.e. cool roof membrane and cool façade painting and (ii) validate the numerical model elaborated. To this aim, the two envelope solutions were applied on the roof and on the differently oriented walls of a prototype case study building, i.e. test-room, located inside the university campus in Perugia, in central Italy. The in-situ continuous monitoring of the thermal performance of the proposed solutions was carried out under real dynamic boundary conditions during the summers of 2014 and 2015. Both the main indoor/outdoor thermal parameters and the roof albedo were monitored.

Firstly, the case study building with non-cool envelope materials, i.e. bitumen membrane and red-colored painting, was monitored as a base case scenario. Secondly, the cool membrane was applied on the test-room roof, in order to assess the specific contribution of the cool roof to the thermal performance of the test-room in summer conditions. Thereafter, the cool painting was applied to the differently oriented façades, i.e. South, North, East,

and West facing façades of the same case study prototype building.

In this way, the performance of the coupled solutions was analysed in terms of passive cooling effect. The monitored data were subsequently post-processed to compare the thermal effect of the two cool solutions.

In detail, the following different scenarios for the case study building envelope were identified:

- *Standard scenario (S)*: The materials implemented in the building envelope were representative of the solutions commonly used in new buildings in Italy. In particular, the roof is covered with a bituminous black membrane and the walls with a red-colored traditional painting;
- *Cool Envelope scenario (CE)*: The innovative cool façade painting is applied on all the façades of the case study building.

In detail, the cool roofing membrane consists of a polyurethane-based waterproof liquid white membrane with high elasticity. The cooling potential of such membrane was optimized through iterative laboratory and in field tests by increasing specific components such as the titanium dioxide (TiO₂) and hollow ceramic microspheres percentage. The final optimized membrane presented almost 12 % of TiO₂ and 4 % of hollow ceramic microspheres.

The proposed cool painting for building façade applications consists of an almost white non-organic painting, mainly composed by potassium silicate with a small percentage of resin. It is characterized by high vapor permeability.

Also the painting was optimized through an iterative procedure by increasing TiO₂ and the hollow ceramic microspheres' percentage.

The most performing combination was found to be again with 12 % of TiO₂ and 4 % of hollow ceramic microspheres.

4.2 Elaboration of the Model

In order to compare the effect of cool envelope materials on (i) the indoor air temperature distribution and (ii) indoor airflow of the case study prototype building, a two-dimensional finite element CFD analysis was performed. Two different 2-d models were elaborated and compared, i.e. referring to the

standard and cool configuration of the case study building, respectively. The simulations were performed in transient conditions by considering one representative summer day selected from the experimental monitoring campaign previously described. Moreover, the simulation was reiterated by using each time, as input values, the final outputs from the previous simulation in order to achieve stability. A simplified scheme of the prototype case study building, i.e. North-South oriented square cavity, was simulated in order to predict the thermal behavior of the building (Fig. 2).

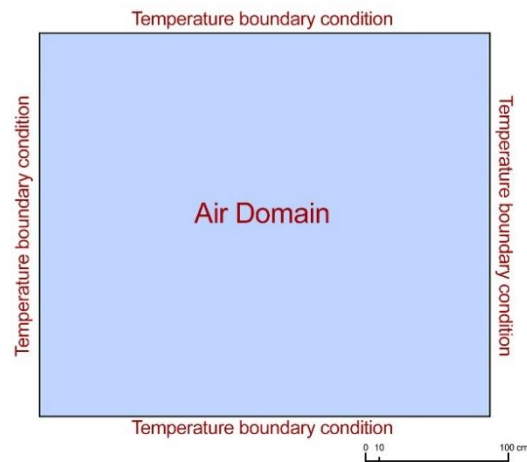


Fig. 2 – Cross section and main dimensions [cm] of the simplified square cavity representing the test-room case study building

The boundary conditions in terms of surface temperatures were set by using experimental measurements monitored in the field, and collected (averaged) every 10 minutes. Such measurements were imposed both on (i) the vertical wall and (ii) the horizontal roof. As for the bottom boundary, i.e. pavement surface, a stationary thermal profile, i.e. 294.15 K, was imposed according to spot measurements performed on site indicating an almost constant temperature of the paving slab. Simulations were carried out by considering the average indoor air temperature experimentally measured within the cavity. A triangular mesh with refinements at the boundaries was implemented. The implemented models fully solve the Navier-Stokes equations, since no Boussinesq approximation was considered. Moreover, the K-epsilon Low-Reynolds model was applied to solve the turbulent flow regime inside the square cavity. After the numerical analysis, a validation of the simulation outputs was carried out for each scenario, assessed by comparing

the results with the monitored data in terms of indoor temperature. The transient simulation was carried out with a 600-second time-step by using a two-variable group segregated solver and by considering an acceptable relative error of 10^{-5} .

5. Results and Discussion

5.1 Validation of the Model

After the implementation of the CFD model, preliminary validation was performed by using the experimental data available from continuous monitoring. Therefore, the simulation output and the collected data were compared in terms of air temperature. In particular, the air temperature values for the validation were extracted at a height of 1.4 m and almost at the center of the square cavity, in correspondence with the position of the temperature sensor. Fig. 3 shows the results of the validation procedure by highlighting the gap between the simulation output and the measurements. Globally, the elaborated model is shown to be sufficiently representative of the realistic thermal behavior of the prototype test-room case study building, since the simulated and experimental air temperature profiles are consistent with each other. However, a negligible and almost constant discrepancy of about 0.5 K on average between the simulated and measured indoor air temperature can be detected on a typical summer day. This indicates that the model slightly underestimates the indoor air temperature value, yet it is still valid and useful in relative terms for comparing the impact of cool envelope solutions applied over the case study building with the traditional one, which is the main objective of the present work.

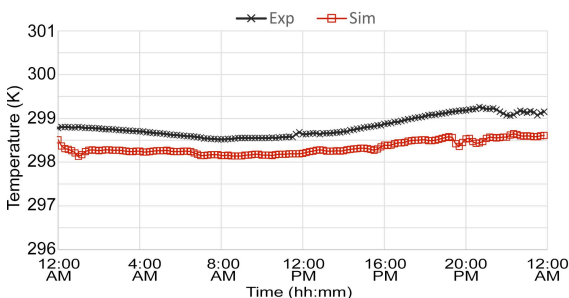


Fig. 3 – Validation of the CFD model against the experimental data available from the continuous monitoring of the main indoor/outdoor microclimate parameters of the case study building

5.2 Indoor Thermal Environment

After the validation of the CFD model, the simulation of the indoor thermal field inside the square cavity was carried out, for both the standard and cool configuration of the case study building envelope. The results of the simulations are shown in Fig. 4.

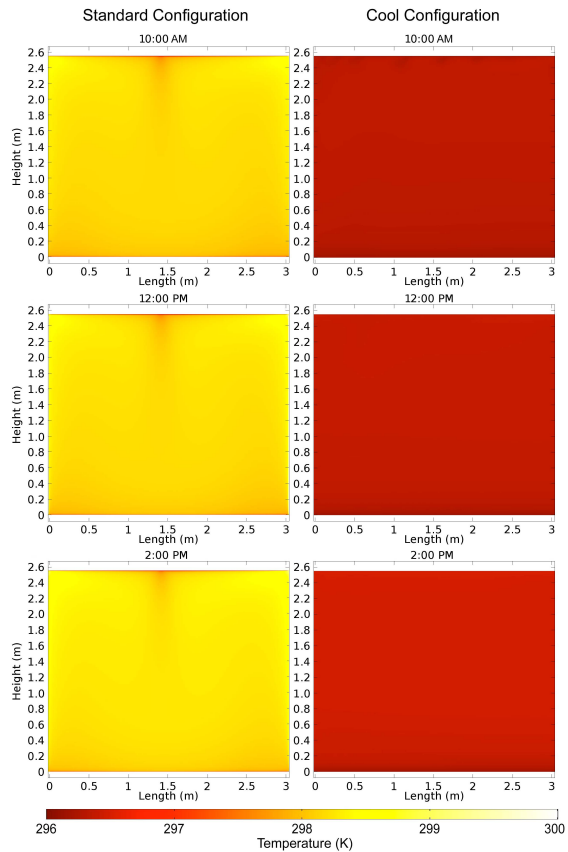


Fig. 4 – Indoor temperature distribution inside the square cavity in the standard and cool configurations at different times during the day, i.e. 10:00 am, 12:00 am, and 2:00 pm

In general, the temperature distribution inside the square cavity is almost always homogenous and fairly uniform in both the evaluated scenarios, i.e. standard and cool building envelope materials. More in detail, when the standard configuration is considered, a quasi-defined thermal stratification can be detected, with a thermal-instability at the middle-top part of the cavity due to the effect of developing convective cells generated by the colder pavement. Therefore, the detected thermal gradient in the cavity is not completely defined due to the lower temperature of the North-facing wall and of the slab that causes a partially developed convective

flow generating thermal instability. When the cool configuration is considered, on the other hand, the lower temperature difference between the different surface temperature profiles of the case study building causes a more stable temperature distribution. The square cavity is characterized by a well-established thermal stratification, causing a more uniform temperature distribution. By comparing the standard and cool scenarios, an almost constant temperature difference of about 2 K is always registered. Therefore, according to the simulations results, which are consistent with the experimental measurements performed, the application of highly-reflective materials on the building envelope is able to lower the indoor air temperature inside the square cavity compared to more traditional non-cool surface covering materials, by consequently improving the indoor thermal comfort inside the building.

5.3 Indoor Airflow Distribution

In this section, the results of the simulations of the indoor airflow conditions inside the case study square cavity are reported, for both the standard and cool configuration of the building envelope. Fig. 5 shows the indoor airflow distribution in the standard and cool scenarios at different hours during the day. From the results of the numerical analysis, a different indoor airflow distribution can be detected in the two configurations. In particular, in the standard scenario, two non-completely developed macro-convective cells can be identified, as a consequence of the huge temperature difference between the roof, the North and South wall surface temperatures. In the cool configuration, on the other hand, the reduced surface overheating caused by the highly reflective materials produces a reduced temperature difference between the considered temperature boundary conditions, and consequently a more stable airflow distribution.

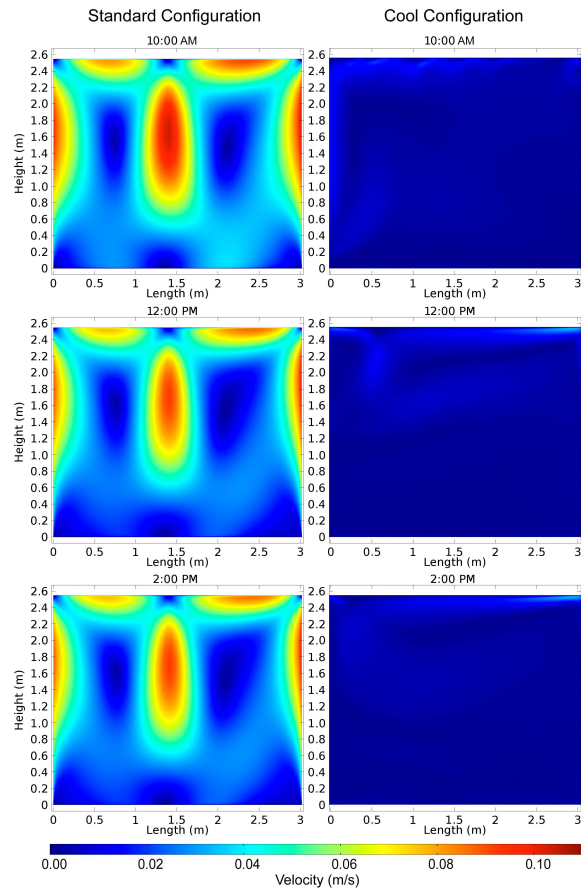


Fig. 5 – Indoor airflow distribution inside the square cavity in the standard and cool configurations at different times during the day, i.e. 10:00 am, 12:00 am, and 2:00 pm

6. Conclusion and Future Developments

The purpose of the present paper was to numerically predict the building indoor thermal environment and airflow distribution. To this aim, the calibrated CFD model of a case study prototype building, i.e. test-room, situated in central Italy, was elaborated, by considering the indoor heat transfer phenomena. In particular, the indoor thermal effect of the application of an innovative highly-reflective cool façade painting and cool roofing membrane compared to a more traditional “non-cool” envelope finishing is assessed. The results show that the implemented CFD model is able to accurately predict the realistic thermal behavior of the case study building. Therefore, the numerical analysis is detected to represent a suitable tool for predicting buildings thermal performance based on a few experimental data. According to the experimental

campaign previously carried out, the results demonstrate that the application of cool envelope materials can significantly lower the indoor air temperature by consequently avoiding overheating risk, especially during extreme summer conditions. In particular, an average indoor air temperature reduction of 1.8 K is found in the cool scenario with respect to the standard one. Finally, the numerical analysis of the indoor airflow distribution shows that in the cool configuration a more stable airflow is generated compared to the standard scenario, where macro convective cells appear. This is motivated by the reduced temperature difference between the considered temperature boundary conditions generated by the highly reflective covering materials, that are able to maintain a lower surface temperature of the envelope components in the cool configuration of the square cavity. Future developments of the study will concern the numerical analysis of the indoor thermal field and airflow distribution in winter conditions.

Acknowledgement

This project has received funding from the *European Union's Horizon 2020 research and innovation programme* under grant agreement No 657466 (INPATH-TEs) and from the *European Union's Horizon 2020 research and innovation programme* under grant agreement No 678407 (ZERO-PLUS).

References

- Akbari, H., S. Bretz, D.M. Kurn, J. Hanford. 1997. "Peak power and cooling energy savings of high-albedo roofs". *Energy and Buildings* 25(2): 117-126. doi: 10.1016/S0378-7788(96)01001-8.
- Akbari, H. 2003. "Measured energy savings from the application of reflective roofs in two small non-residential buildings". *Energy* 28(9): 953-967. doi: 10.1016/S0360-5442(03)00032-X.
- Asan, H., L. Namli. 2000. "Laminar natural convection in a pitched roof of triangular cross-section: summer day boundary conditions". *Energy and Buildings* 33(1): 69-73. doi: 10.1016/S0378-7788(00)00066-9.
- Atzeri, A.M., F. Cappelletti, A. Tzempelikos, A. Gasparella. 2016. "Comfort metrics for an integrated evaluation of buildings performance". *Energy and Buildings* 127(1): 411-424. doi: 10.1016/j.enbuild.2016.06.007.
- Basak, T., S. Roy, S.K. Babu, A.R. Balakrishnan. 2008. "Finite element analysis of natural convection flow in a isosceles triangular enclosure due to uniform and non-uniform heating at the side walls". *Heat and Mass Transfer* 51(17-18): 4496-4505. doi: 10.1016/j.ijheatmasstransfer.2007.12.018.
- Corrado, V., I. Ballarini. 2016. "Refurbishment trends of the residential building stock: Analysis of a regional pilot case in Italy". *Energy and Buildings* 132: 91-106. doi: 10.1016/j.enbuild.2016.06.022.
- Crawley, D.B., L.K. Lawrie, F.C. Winkelmann, W.F. Buhl, Y.J. Huang, C.O. Pedersen, R.K. Strand, R.J. Liesen, D.E. Fisher, M.J. Witte, J. Glazer. 2001. "EnergyPlus: creating a new generation building energy simulation program". *Energy and Buildings* 33: 319-331. doi: 10.1016/S0378-7788(00)00114-6.
- Georgakis, C., S. Zoras, M. Santamouris. 2014. "Studying the effect of "cool" coatings in street urban canyons and its potential as a heat island mitigation technique". *Sustainable Cities and Society* 13: 20-31. doi: 10.1016/j.scs.2014.04.002.
- Gracik, S., M. Heidarinejad, J. Liu, J. Srebric. 2015. "Effect of urban neighborhoods on the performance of building cooling systems". *Building and Environment* 90:15-29. doi: 10.1016/j.buildenv.2015.02.037.
- Hasani, S.M.F., B.T.F. Chung. 1998. "Combined Natural Convection and Radiation in a Triangular Enclosure". In: *Proceedings of the 7th AIAA/ASME Joint ThermoPhysics & Heat Transfer Conference* 357-1:63-72. doi: 10.2514/MJTHT98.
- Kamiyo, O.M., D. Angeli, G.S. Barozzi, M.W. Collins, V.O.S. Onunloyo, S.O. Talabi. 2010. "A comprehensive review of natural convection in triangular enclosures". *Applied Mechanics Reviews* 63(6). doi:10.1115/1.4004290.
- Pisello, A.L., V.L. Castaldo, C. Fabiani, F. Cotana. 2016. "Investigation on the effect of innovative cool tiles on local indoor thermal conditions:

- Finite element modeling and continuous monitoring". *Building and Environment*. 97(5): 55-68. doi: 10.1016/j.buildenv.2015.11.038.
- Pisello, A.L., V.L. Castaldo, G. Pignatta, F. Cotana, M. Santamouris. 2015. "Experimental in-lab and in-field analysis of waterproof membranes for cool roof application and urban heat island mitigation". *Energy and Buildings* 114: 180-190. doi:10.1016/j.enbuild.2015.05.026.
- Pisello, A.L., F. Cotana, A. Nicolini, C. Buratti. 2014a. "Effect of dynamic characteristics of building envelope on thermal-energy performance in winter conditions: in field experiment". *Energy and Buildings* 80:218-230. doi:10.1016/j.enbuild.2014.05.017.
- Pisello, A.L., F. Rossi, F. Cotana. 2014b, "Summer and Winter Effect of Innovative Cool Roof Tiles on the Dynamic Thermal Behavior of Buildings". *Energies* 7:2343-2361. doi: 10.3390/en7042343.
- Saha, S.C., J.C. Patterson, C. Lei. 2010. "Natural convection and heat transfer in attics subject to periodic thermal forcing". *International Journal of Thermal Sciences* 49(10):1899-1910. doi: 10.1016/j.ijthermalsci.2010.05.010.
- Synnefa, A., M. Santamouris, H. Akbari. 2007. "Estimating the effect of using cool coatings on energy loads and thermal comfort in residential buildings in various climatic conditions". *Energy and Buildings* 39(11): 1167-1174. doi: 10.1016/j.enbuild.2007.01.004.
- Synnefa, A., T. Karlessi, N. Gaitani, M. Santamouris, D.N. Assimakopoulos, C. Papakatsikas. 2011 "Experimental testing of cool colored thin layer asphalt and estimation of its potential to improve the urban microclimate". *Building and Environment* 46 (1): 38-44. doi: 10.1016/j.buildenv.2010.06.014.
- Wong, P.P.Y., P.C. Lai, C.T. Low, S. Chen, M. Hart. 2016. "The impact of environmental and human factors on urban heat and microclimate variability". *Building and Environment* 95 (4262): 199-208. doi: 10.1016/j.buildenv.2015.09.024.
- Yang, L., M. Ye, B.J. He. 2013. "CFD simulation research on residential indoor air quality". *Science of the Total Environment* 472: 1137-1144. doi: 10.1016/j.scitotenv.2013.11.118.

How Microclimate Mitigation Affects Building Thermal-Energy Performance in Residential Zero Energy Italian Settlements

Anna Laura Pisello – University of Perugia – anna.pisello@unipg.it

Veronica Lucia Castaldo – University of Perugia – castaldo@crbnet.it

Claudia Fabiani – University of Perugia – fabiani@crbnet.it

Cristina Piselli – University of Perugia – piselli@crbnet.it

Franco Cotana – University of Perugia – cotana@crbnet.it

Mattheos Santamouris – University of New South Wales – m.santamouris@unsw.edu.au

Abstract

A key research effort has been dedicated toward zero energy buildings in the last decades. Recent interest is currently switching its focus from single-building scale to the inter-building scale, by enlarging the thermal-energy balance up to the settlement level, with the purpose to optimize the whole district energy efficiency and its environmental sustainability. This scale enlargement up to the district size leads to further optimization opportunities that must be considered when performing building thermal-energy dynamic simulations. In this view, buildings within net Zero-Energy Settlements (nZES) can improve their performance thanks to outdoor microclimate improvement techniques that could succeed in mitigating both winter thermal losses and summer overheating risks. In this work, microclimate modeling and building dynamic simulation tools are integrated to assess the impact of varying microclimate conditions on the building energy performance at a settlement level. The case study is performed on a residential district in Italy. In particular, microclimate simulations are carried out to predict the mitigation potential of specific strategies applied at settlement scale, i.e. cool materials, greenery, and their combination. Therefore, starting from the results of the microclimate optimization, new microclimate boundary conditions are generated to be used within the dynamic simulation environment. The final aim is to quantify the impact of such optimized microclimate boundary conditions on the buildings energy performance.

The results from the microclimate simulations, supported by the European funded Horizon 2020 project ZERO-PLUS, highlighted how microclimate can play a key role in affecting outdoor thermal comfort conditions. Moreover, the dynamic simulations carried out by using the results from a microclimate optimization as input weather

files, always show a decrease on the final energy needs of the building in the nZES. The highest and non-negligible reduction is reached in the final cooling need of the optimized scenario by coupling both cool and green optimization strategies, i.e. about 12 % of the initial value.

1. Introduction

The local urban microclimate has recently become a fundamental issue for designers and urban planners (Corrado et al., 2015). This is due to the fact that local microclimate phenomena have a strong impact on buildings performance at urban scale, therefore climatic considerations must be necessarily taken into account in urban design (Grobman et al., 2016). Different approaches are currently available to estimate the local microclimate and evaluate its effect on the built environment, i.e. numerical simulations and experimental monitoring campaigns (Carlon et al., 2016; Salata et al., 2016; Atzeri et al., 2016). In fact, local different boundary conditions, i.e. streets geometry (Jihad et al., 2016), vegetation (Dimoudi et al., 2003), and building materials (Kaloniti et al., 2016), can considerably modify the local microclimate in terms of air temperature, relative humidity, ventilation, and air quality (Maiheu et al., 2010) by affecting indoor and outdoor thermal comfort conditions at an inter-building scale, in addition to energy consumption (Ballarini et al., 2014). In (Nicol et al., 2015) the microclimate in Hong Kong was mapped to estimate the influence of urban morphology. In fact, it has become very urgent to develop

reliable modeling approaches to couple the microclimate evaluation with dynamic building simulation tools for predicting buildings thermal-energy behavior. Nakaohkubo et al. (2007) implemented a tool combining a heat balance simulation for urban surfaces by using GIS for input data, and a simple simulation algorithm to predict the surface temperature distribution of urban blocks. Such a tool was able to predict the impact of building shape, materials, and tree shade on the local thermal environment. Moreover, in Peng et al. (2012) the combination of outdoor and indoor environmental simulation was performed to support the design of sustainable urban dwellings, by bridging three simulation platforms, i.e. Envi-met for urban settlement simulations, Ecotect for building simulation, and U-Campus for combined indoor-outdoor 3D visualization modeling of urban precincts. Many approaches have been used to determine how local urban microclimate can influence the building performance. Sanchez de la Flor et al. (2006) implemented an analytical methodology to assess building performance under modified outdoor conditions. They proved that building energy consumption is strongly correlated to climate factors, and therefore improvements in urban microclimate have direct and indirect consequences on energy savings. Moreover, De la Flor et al. (2004) proposed a computational model able to quantify the modification of the climatic variables in an urban context and to assess how they affect the thermal performance of urban buildings. They highlighted the evident interaction between such two systems, able to modify their mutual energy balances. This proved that the coupling of urban models and building thermal performance simulations is useful to understand the consequences on heating/cooling requirements and even on outdoor thermal comfort. Similarly, Liu et al. (2016) investigated the effects of outdoor air temperature, air humidity, global temperature and wind speed on outdoor thermal sensation. The results revealed that outdoor microclimate parameters play important roles on outdoor thermal sensation. Gros et al. (2016) coupled building energy simulations and microclimate simulations to assess the impact of urban morphology and density, urban landscaping, and buildings and soil thermal properties on so-

lar irradiance, wind flows, air temperature, and energy demand. Solar irradiance reduction up to 7 % and of wind speed reduction up to 80 % were detected in different districts. This work deals with the simulation of the microclimate of a case study residential net Zero-Energy Settlement (nZES), which includes four nearly Zero-Energy houses (EPISCOPE, 2012). The aim of such simulation was to evaluate the mitigation capability of different strategies applied at settlement-scale, represented by (i) the implementation of cool coatings on building roofs and outdoor pavements, (ii) the conscious greenery design and optimization, and (iii) the combination of both these solutions. Microclimate simulation outputs were used as input of building dynamic thermal-energy simulation in the form of .epw weather files. Therefore, the optimized microclimate weather files were used as boundary conditions of the case study nZES. Finally, the impact of mitigated microclimate conditions on buildings energy performance was evaluated.

2. Materials and Methods

Firstly, the microclimate simulation was carried out. Four different scenarios were elaborated, i.e. the "Reference (Ref)" scenario, corresponding to the realistic configuration of the settlement according to the architectural design, and three "mitigation" scenarios, where innovative optimization solutions were applied at district scale to counteract local climate phenomena. Such three mitigation scenarios consist of:

- "Green" scenario: increase of vegetation percentage;
- "Cool" scenario: increase of solar reflectance (R_{solar}) of built surfaces, i.e. roof and pavement;
- "Combined (Comb)" scenario: combination of both the above-described solutions.

The aim of the microclimate simulations was to (i) optimize the local microclimate of the settlement and (ii) produce new weather files to be used in the dynamic simulations to see the impact of the improved local microclimate on the buildings' energy performance.

Secondly, the microclimate simulation outputs were used to generate new optimized weather files to be

used in the dynamic simulation of the energy performance of the buildings of the nZES.

Therefore, the applied methodology globally consisted of the following steps:

- Microclimate simulation and analysis of the (i) reference and (ii) mitigation scenarios;
- Generation of new optimized weather files;
- Dynamic energy simulation of the case study buildings with the (i) original TMY weather file and (ii) different mitigated microclimate boundary conditions deriving from the microclimate simulations previously fulfilled.

2.1 Description of the Case Study

The case study district (nZES) is situated in Rimini (Italy) and is constituted by four single-family houses. Such villas, referred to in the text as nZES buildings (i.e. buildings in the net Zero-Energy settlement), are nearly Zero-Energy buildings. In fact, single buildings present high-energy performance (EPISCOPE, 2012), while in the district a net zero energy balance is achieved thanks to the inclusion of energy efficient technologies at settlement level. In the “Reference” settlement microclimate model (Ambrosini et al., 2014), the following inputs were defined:

- Ground: the “Loamy soil” was selected to represent natural ground, while “asphalt road” was used to represent the street cover. The “pavement concrete” was used for the surrounding built surfaces.
- Buildings: traditional building technologies from the current regulation were used.
- Vegetation: it was modelled consistently with the vegetation percentage and position of the real site.

Fig. 1 shows the geographical location of buildings. The thermo-physical properties of the materials are summarized in Table 1 (Ref).

the nZES buildings dynamic energy model was elaborated in order to evaluate the energy benefits deriving from the microclimate mitigation strategies by using (i) the original TMY weather file and (ii) the optimized weather boundary conditions derived by the microclimate simulation output.

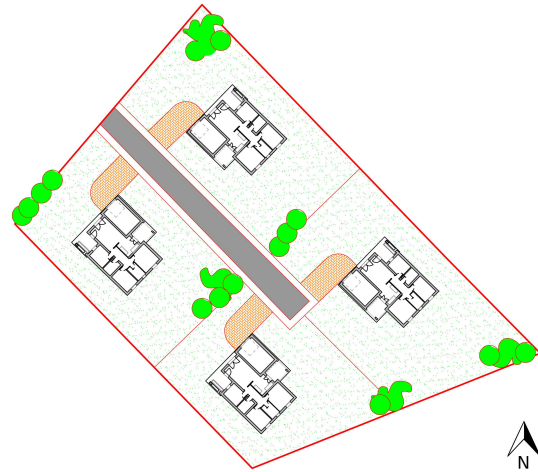


Fig. 1 – Plan view of the Italian case study settlement

2.2 Microclimate Simulation of the “Reference” Scenario

The simulations of the outdoor microclimate conditions were carried out by using ENVI-met. The input climate data used for the simulations were provided by Meteoblue (2016) which enables the inclusion of detailed topography, ground cover (e.g. forest, fields, rock, and water) and surface cover (e.g. snow and water). The model was implemented by considering a 1-m unit grid dimension.

2.3 Microclimate Simulation of the Optimization Scenarios

Additional optimization scenarios were simulated for the settlement to (i) improve the local microclimate conditions, (ii) evaluate the most performing mitigation solution, and (iii) provide new weather files able to consider the microclimate improvement to be used in the dynamic energy simulation for assessing the role of microclimate mitigation on buildings energy performance. Three mitigation configurations were proposed. The first mitigation strategy consisted in the increase of the vegetation percentage according to the different landscape constraints of the settlement. In particular, deciduous trees (South-West) and hedges (North-East) were introduced in addition to the draining pavement for the asphalt road. The introduction of such elements was aimed at (i) protecting the buildings from direct sun irradiation in summer and let it seep out in winter, and (ii) protecting them from the Northern cold winds while keeping an external boundary which could easily be over crossed by the wind in summer.

The second mitigation strategy consisted of (i) the increase of the solar reflectance of roof tiles and external walls, and (ii) the implementation of cool paving materials, e.g. with natural cool gravels (Castaldo et al., 2015). Moreover, highly reflective asphalt was used for the roads. Table 1 shows the solar reflectance values of all the surface materials, before and after the implementation of the mitigation strategies. The last mitigation strategy consisted in the simultaneous combination of the two above-mentioned solutions.

Table 1 – Solar reflectance values [%] for each material in the different modeled scenarios

Material	Ref	Cool	Green	Comb
Asphalt road	20	60	20	60
Concrete paving	40	40	-	40
Gravel paving	-	80	-	80
Flat tiles	15	58	15	58
Pitched clay tiles	30	77	30	77
External walls plaster	40	71	-	71

2.4 Dynamic Energy Simulation

The simulation of the case study nZES (net Zero-Energy Settlement) was carried out using the DesignBuilder-EnergyPlus tool in thermostatically controlled conditions (EERE, 2014). All four buildings within the settlement, characterized by similar characteristics in terms of construction technologies, HVAC systems, occupancy schedule, etc., were modelled together and their energy performance was separately simulated. In particular, the following technologies are implemented in the buildings: XPS insulation, cool materials as roof and wall external coating, low-e double glazing PVC windows, LED lighting system, high efficiency air-to-water heat pump as HVAC system, mechanical ventilation with heat recovery, photovoltaic panels with storage, building integrated wind turbine system, and smart energy systems control. The nZES building components main technical characteristics are reported in Table 2. Since the results from the dynamic simulations showed a maximum 3 % energy performance difference among buildings, the simulation outputs related to one single building (referred in the text as nZES standard building) are

here reported. The comparative energy performance analysis between the reference nZES building scenario, characterized by original typical weather dataset (TMY), and the optimized scenarios, i.e. considering the optimized microclimates generated by means of the previous numerical analyses, was carried out in terms of annual energy consumption. The considered set-point temperatures were equal to 20 °C and 26 °C for heating and cooling, respectively.

Table 2 – General technical characteristics of the case study building

nZES building characteristics	
Flat roof U-value [W/m ² K]	0.15
Flat roof R _{solar} [%]	58
Pitched roof U-value [W/m ² K]	0.16
Pitched roof R _{solar} [%]	77
External wall U-value [W/m ² K]	0.18
External wall R _{solar} [%]	71
Ground floor U-value [W/m ² K]	0.22
Windows U-value [W/m ² K]	1.50
Heating system COP	4.1
Cooling system EER	3.8

3. Results and Discussion

3.1 Microclimate Simulations of the “Reference” Scenario

This section shows the results of the “Reference” scenario microclimate simulations both in summer and winter conditions. Such simulations are aimed at evaluating the optimization potential of the selected mitigation strategies in terms of outdoor thermal comfort, and consequently their impact on the building energy performance.

The data were extracted at pedestrian height (0.9 m above the ground). The results were post-processed in terms of dry bulb temperature (°C), relative humidity (%), mean radiant temperature (°C), and wind speed (m/s). The air temperature ranged between 21 °C and 36 °C. Moreover, a maximum temperature of 35.4 °C and a minimum temperature of 32.5 °C were detected. As for the relative humidity, this varied between a 27.6 % and 33.2 %. The mean radiant temperature fluctuated between 49 °C

and 73.6 °C. Finally, the wind speed ranged between zero and 1.57 m/s. Fig. 2–3 show the spatial distribution of the air temperature in different hours of the day, in summer and winter conditions, respectively. As for the wind speed in the Green scenario, the presence of the hedge does not allow the air circulation at 0.9 m and has the effect of reducing the wind velocity in the proximity of the buildings. This generates a reduction of the convective mixing in the whole settlement. In winter, a globally lower mitigation effect is registered, with no penalties.

3.2 Microclimate Simulations of the Optimized Scenarios

This section describes the results of the 24 h simulations of the optimized mitigation scenarios in summer (Fig. 4).

In summer conditions, a good mitigation of the outdoor air temperatures (i.e. up to -1.5 °C) was detected by comparing the Green and Ref scenario. A lower mitigation effect but more effective at night was registered by implementing the cool strategies. Finally, a non-negligible air temperature reduction was found out by comparing the Comb and Ref configuration, especially around the two buildings in the northern part of the settlement. The increase in relative humidity is more significant in the Green and Comb scenarios compared to the Cool one. This is motivated by the presence of the 5 m high trees. On the contrary, no microclimate mitigation effect is registered in close proximity of the 2-m high hedge.

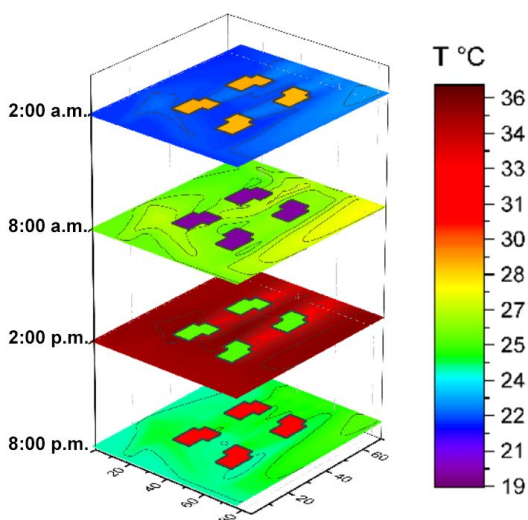


Fig. 2 – Summer air temperature map at different times of the day

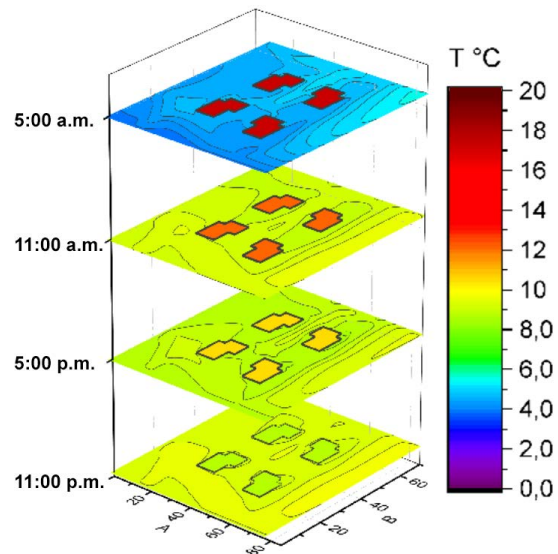


Fig. 3 – Winter air temperature map at different times of the day

As for the mean radiant temperature, a reduction of about 20 °C is detected in the Green configuration due to the shading effect of vegetation to the incoming solar radiation. On the contrary, the mean radiant temperature slightly increases due to the presence of the reflective gravel on the paving surfaces. Additionally, there is a slight mean radiant temperature increase and reduction up to 10 m of height in the Cool and Combined configuration, respectively.

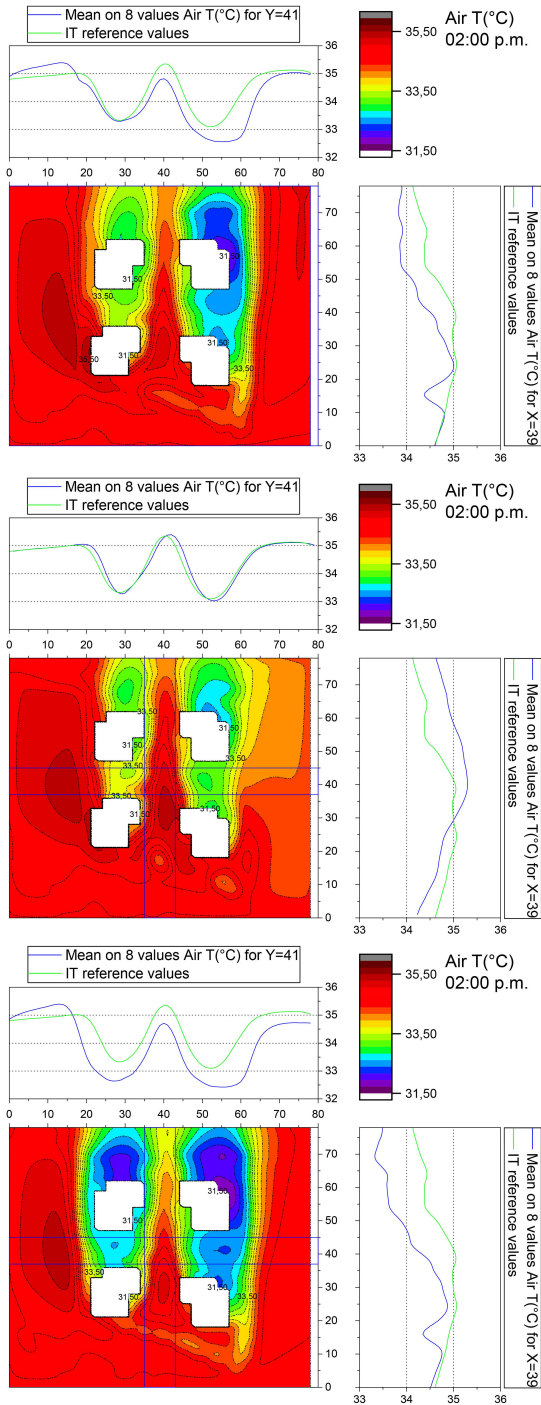


Fig. 4 – Summer air temperature distribution in the Green, Cool, and Combined scenarios

3.3 Assessment of the nZES Building Energy Performance

This section shows the results of the annual energy dynamic simulation of the nZES standard building in the four different scenarios considered, i.e. reference (nZES), mitigated Green, Cool, and Comb. Buildings were simulated under thermostatically

controlled conditions to assess the achievable energy saving corresponding to local microclimate boundary conditions variation.

Table 3 – Annual energy consumption, production, and Primary Energy requirement (E_P) for nZES standard building

Building in the nZES	Energy [kWh/m ² /y]	E_P [kWh/m ² /y]
Heating	45.0	108.9
Cooling	0.8	1.9
DHW	3.8	9.2
Regulatory Energy	49.6	120.0
Lighting	12.5	30.3
Equipment	15.4	37.3
Total Energy	77.5	187.6
Wind Generated Energy	23.7	-
Solar Generated Energy	46.2	-
Total Generated Energy	69.9	-

Table 3 reports the results of the analysis under thermostatically controlled conditions, in terms of final annual energy consumption of the nZES standard building. The final energy consumption is defined as the sum of regulatory energy, i.e. heating, cooling, and domestic hot water (DHW), and the additional energy consumption for appliances, i.e. lighting and equipment. Such two energy contributions are separated since the regulatory energy is the only one affected by the microclimate mitigation strategies applied to the nZES. Moreover, Table 4 shows the difference in terms of building regulatory, heating, and cooling energy among the three optimized scenarios and the nZES reference scenario. As expected, the results show that the greater effect of the implementation of both cool materials and greenery in the outdoor areas of the settlement is detected in summer. In fact, all the optimized scenarios present a lower cooling energy need compared to the reference nZES scenario, which is maximized in the Combined scenario with a final 11.8 % cooling need reduction. Therefore, the combination of the application of cool materials and greenery in the outdoor areas of the settlement optimizes both outdoor microclimate conditions and building energy performance in summer. Moreover, in the optimized scenarios the energy need for heating is reduced though slightly, i.e. up to 2.5 %. Therefore, the optimized scenarios present a lower total energy

need with respect to the reference nZES scenario, with up to a 4 % regulatory energy consumption reduction in the Comb scenario.

Table 4 – Energy requirements variation in the three optimized scenarios with respect to the reference nZES scenario

		Cool	Green	Comb
Heating	ΔE	-0.37	-0.24	-0.18
	[kWh/m ² /y]			
	% decrease	-2.48	-1.62	-1.21
Cooling	ΔE	-0.09	-0.34	-0.90
	[kWh/m ² /y]			
	% decrease	-1.22	-4.42	-11.83
Regulatory	ΔE	-0.46	-0.58	-1.08
	[kWh/m ² /y]			
	% decrease	-1.76	-2.20	-4.09

4. Conclusions and Future Developments

In the present work, 3D Computational Fluid Dynamics and building energy simulation tools were coupled in order to investigate the mitigation potential of specific strategies applied at settlement level, and to quantify their effect on buildings' energy need. The purpose was to develop outdoor mitigation strategies to improve the outdoor microclimate conditions perceived by pedestrians, and to reduce the buildings' energy needs. To this aim, preliminary microclimate simulations stressing the effect of selected mitigation strategies, i.e. implementation of cool coatings on buildings roofs and outdoor pavements, greenery, and their combination were carried out. Therefore, building upon the results of such microclimate simulations, new optimized weather files were generated and used as boundary conditions for the dynamic simulation of the nZES buildings energy performance. Finally, the comparison between the energy performance of the nZES standard building carried out by using (i) the original typical weather dataset (TMY) and (ii) different optimized weather files was performed. Microclimate analysis allowed a preliminary assessment of the outdoor thermal comfort conditions at settlement scale. Results showed how the different proposed mitigation strategies lead to an improvement of the outdoor thermal comfort. The selected

mitigation strategies also produce non-negligible reductions on the final energy need of the nZES building, mostly affecting regulatory energy consumption. A maximum of 4 % energy saving was reached in the Combined scenario.

In conclusion, this work demonstrated that properly selected microclimate mitigation strategies applied at district scale, aside from improving the local outdoor thermal comfort, can also produce non-negligible effects on the thermal energy performance of buildings. Future developments of this work will concern the comparison between the effect of the microclimate mitigation strategies and the occupants' behavior on the final energy consumption and indoor comfort of the nZES buildings.

Acknowledgement

The authors' acknowledgements go to the European Union's Horizon 2020 program under grant agreement No 678407 (ZERO-PLUS). The authors would like to thank Dr. Marco Colleluori for his precious collaboration during the computational phase of the research.

References

- Ambrosini, D., G. Galli, B. Mancini, I. Nardi, S. Sfarra. 2014. "Evaluating Mitigation Effects of Urban Heat Islands in a Historical Small Center with the ENVI-Met Climate Model". *Sustainability* 6(10): 7013-7029. doi:10.3390/su6107013.
- Atzeri, A.M., F. Cappelletti, A. Tzempelikos, A. Gasparella. 2016. "Comfort metrics for an integrated evaluation of buildings performance". *Energy and Buildings* 127(1): 411-424. doi: 10.1016/j.enbuild.2016.06.007.
- Ballarini, I., S.P. Corgnati, V. Corrado. 2014. "Use of reference buildings to assess the energy saving potentials of the residential building stock: The experience of TABULA project". *Energy Policy* 68: 273-284. doi: 10.1016/j.enpol.2014.01.027.
- Carlson, E., M. Schwarz, A. Prada, L. Golicza, V.K. Verma, M. Baratieri, A. Gasparella, W. Haslinger, C. Schmidl. 2016. "On-site monitoring and dynamic simulation of a low energy house

- heated by a pellet boiler". *Energy and Buildings* 116: 296-306. doi: 10.1016/j.enbuild.2016.01.001.
- Castaldo, V.L., V. Coccia, F. Cotana, F., G. Pignatta, A.L. Pisello, F. Rossi. 2015. "Thermal-energy analysis of natural "cool" stone aggregates as passive cooling and global warming mitigation technique". *Urban Climate* 14: 301-314. doi: 10.1016/j.uclim.2015.05.006.
- Corrado, V., I. Ballarini, L. Madrazo, G. Nemirovskij. 2015. "Data structuring for the ontological modelling of urban energy systems: The experience of the SEMANCO project". *Sustainable Cities and Society* 14: 223-235. doi: 10.1016/j.scs.2014.09.006.
- De la Flor, F.S., S.A. Dominguez. 2004. "Modelling microclimate in urban environments and assessing its influence on the performance of surrounding buildings". *Energy and Buildings* 36: 403-413. doi:10.1016/j.enbuild.2004.01.050.
- Dimoudi, A., M. Nikolopoulou. 2003. "Vegetation in the urban environment: microclimatic analysis and benefits". *Energy and Buildings* 35: 69-76. doi: 10.1016/S0378-7788(02)00081-6.
- EPISCOPE. 2012. "EE Project TABULA: Typology Approach for Building Stock Energy Assessment, 2009-2012." Accessed November 17. <http://episcopes.eu/iee-project/tabula/>
- Grobman, Y.J., Y. Elimelech. 2016. "Microclimate on building envelopes: Testing geometry manipulations as an approach for increasing building envelopes' thermal performance". *Architectural Science Review* 59: 269-278. doi: 10.1080/00038628.2015.1025688.
- Gros, A., E. Bozonnet, C. Inard, M. Musy. 2016. "Simulation tools to assess microclimate and building energy-a case study on the design of a new district". *Energy and Buildings* 114: 112-122. doi: 10.1016/j.enbuild.2015.06.032.
- Meteoblue. 2016. "Meteoblue." Accessed November 21. <http://www.meteoblue.com/>
- Jihad, A.S., M. Tahiri. 2016. "Modelling the urban geometry influence on outdoor thermal comfort in the case of Moroccan microclimate". *Urban climate* 16: 25-42. doi: 10.1016/j.uclim.2016.02.002.
- Kaloniti, A., G. Georgiou, K. Marakos, P. Kumar, M.K.A. Neophytou. 2016. "The role of materials selection in the urban heat island effect in dry mid-latitude climates". *Environmental fluid mechanics*, 16 (2): 347-371. doi: 10.1007/s10652-015-9426-z.
- Liu, W., Y. Zhang, Q. Deng. 2016. "The effects of urban microclimate on outdoor thermal sensation and neutral temperature in hot-summer and cold-winter climate". *Energy and Buildings* 128: 190-197. doi: 10.1016/j.enbuild.2016.06.086.
- Maiheu, B., B. De Maerschalck, J. Vankerkom, S. Janssen. 2010. "Local air quality and its interaction with vegetation in the urban environment, a numerical simulation using Envi-met". In: *HARMO-13th International Conference on Harmonisation within Atmospheric Dispersion Modelling for Regulatory Purposes*.
- Nicol, F., M. Wilson, Y. Shi, C. Ren, Y. Zheng, E. Ng. 2015. "Mapping the urban microclimatic spatial distribution in a sub-tropical high-density urban environment". *Architectural Science Review* 59 (5): 370-384. doi: 10.1080/00038628.2015.1105195.
- Nakaohkubo, K., A. Hoyano, T. Asawa. 2007. "Development of support tool for outdoor thermal environmental design of urban/building using numerical analysis". In: *Proceedings of Building Simulation 2007*. Beijing, China: IBPSA.
- Peng, C., A.F.A. Elwan. 2012. "Bridging outdoor and indoor environmental simulation for assessing and aiding sustainable urban neighborhood design". *Archnet-IJAR* 6 (3): 72-90.
- Salata, F., I. Golasi, R. De Lieto Vollaro, A. De Lieto Vollaro. 2016. "Urban microclimate and outdoor thermal comfort. A proper procedure to fit ENVI-met simulation outputs to experimental data". *Sustainable Cities and Society*, 26: 318-343. doi:10.1016/j.scs.2016.07.005.
- Sanchez de la Flor, F.J., J.M. Salmeron Lissen, S.A. Dominguez. 2006. "A new methodology towards determining building performance under modified outdoor conditions". *Building and Environment* 41: 1231-1238. doi:10.1016/j.buildenv.2005.05.035.
- U.S. Department of Energy, Energy Efficiency and Renewable Energy (EERE). 2014. Building Technologies Program: EnergyPlus.

Thermal Performance of Innovative Building Envelope Systems in Mediterranean Climate

Maurizio Detommaso – Freelance engineer, Italy – mauriziodet105@tiscali.it

Gianpiero Evola – University of Catania – gevola@unict.it

Antonio Gagliano - University of Catania – agagliano@dii.unict.it

Luigi Marletta – University of Catania – luigi.marletta@dieei.unict.it

Francesco Nocera –University of Catania – fnocera@unict.it

Abstract

Energy efficient buildings, besides saving energy, should provide adequate indoor thermal comfort. Hence, to maximize advantages, a balance between different energy efficient technologies and solutions must be found. In this sense, the European directives on the energy performance of buildings have defined a high standard of thermal insulation for buildings in order to comply with strict energy performance limits. However, several studies have highlighted that such an approach can have negative effects in summer, especially in the Mediterranean area, thus inducing an increase in the energy needs for cooling and a remarkable overheating.

In this context, the main objective of this study is to investigate the thermal performance of Vacuum Insulation Panels (VIPs) and Phase Change Materials (PCMs) when applied to the building envelope, and their ability to improve the building thermal behavior in the Mediterranean area. To this aim, a numerical model of a test room with standard construction technologies was implemented on Design Builder. This model was validated against experimental measurements available in the literature. Once the model was calibrated, a further series of simulations was performed by applying to the same test room the above-mentioned innovative building envelope systems. The simulations were run both in free-running conditions, in order to assess thermal comfort and thermal inertia of walls, and by assuming the presence of an HVAC system, to calculate the energy needs for space heating and cooling on a yearly basis.

The results highlight that, in summer, thermal discomfort and remarkable increases in the energy needs for cooling may occur when the building is retrofitted with VIPs, whereas better conditions are achieved with PCMs.

1. Introduction

The energy demand of buildings accounts for a remarkable part of the world energy consumption (Seong et al., 2013). Hence, improving the energy efficiency, while also providing indoor thermal comfort in buildings through high performance thermal insulation and sustainable materials, has a strategic role (Gagliano et al., 2016a).

In recent years, many developed countries have introduced programs directed at decreasing energy consumption and improving the carbon performance of buildings. Some researchers (Alotaibi et al., 2014; Alam et al., 2011; Thorsell, 2011) suggest the use of VIPs for highly energy efficient buildings. Indeed, VIPs can reduce the energy needs for the heating of a building from 158.7 to 127.5 kWh m⁻². A decrease of about 24 % can be achieved after retrofitting, due to a reduction in the transmission losses through the walls by 23 % (Johansson, 2014).

On the other hand, PCMs are innovative materials capable of storing or releasing thermal energy as latent heat. Since the amount of latent heat absorbed or released is much larger than the sensible heat, the application of PCMs in buildings has a significant potential to reduce both the peak heating and cooling loads, and the energy consumption (Seong et al., 2013; Bejan et al., 2016). The results of dynamic thermal simulations conducted on an office equipped with honeycomb PCM wallboards have shown a reduction in the peak operative temperature of about 1 °C during the summer period. Moreover, in the same study the peak surface temperature of the east wall decreases from 29.7 °C to 28 °C (Evola et

al., 2013; 2014). An experimental investigation carried out during two days in summer on a test room where PCM panels were superimposed on three walls, has highlighted that the indoor air temperature is about 1 °C lower when compared to the values measured before installing the panels (Kuznik et al., 2008; Kuznik et al., 2009). Simulations have shown a potential reduction by 2 °C in the peak indoor air temperature in a test room where micro-encapsulated paraffin was added to a 30 mm gypsum plaster during a week (Voelker et al., 2008).

In this framework, the present study aims at assessing the effectiveness of VIPs and PCMs in reducing the energy needs of a virtual office test room located in Southern Italy. Dynamic thermal simulations have been conducted both in free-running conditions, to assess the thermal comfort and thermal inertia of the walls, and by assuming the presence of an HVAC system to calculate the energy needs for space heating and cooling on a yearly basis.

2. Methodology

In order to investigate the thermal performance of these innovative materials, the software used for dynamic thermal simulations is DesignBuilder (Design Builder, 2014). The model of the virtual test room was first validated against the experimental results of the survey conducted on a real prototype of the same test room located in Milan (Rossi, 2009), with an average error below 1 %. After the validation, the virtual test room was simulated in a different location, namely Cozzo Spadaro, near Syracuse (Southern Italy)

As well known, in summer the energy needs and the thermal behavior of buildings strongly depend on the thermal inertia of their envelope. Generally, traditional constructive systems based on double brick walls do not have adequate thermal inertia to maintain good indoor thermal conditions and to guarantee low energy needs for space cooling. In particular, the facades facing east and west receive, in summer, a high solar irradiance that is comparable to that received on the south-facing façade. Consequently, one way to increase their performance may consist in the adoption of materials operating as a barrier against the outer external forcing conditions,

and capable of absorbing heat from the indoor spaces. Hence, VIPs and PCMs are proposed as potential solutions. Moreover, different ways to install these materials on the walls are considered in order to analyze the possible effects of their position in the walls.

Therefore, five scenarios are analyzed in the paper:

- the base case, with double brick walls;
- two cases with VIPs and PCMs placed on the inner side of the baseline wall;
- two cases with VIPs and PCMs placed on the outer side of the baseline wall.

The base case and all VIPs scenarios are simulated by using the Conduction Transfer Function (CTF) method, whereas for the PCMs scenario the finite difference method is adopted (EnergyPlus, 2011). The simulations of the test room are carried out with a frequency of 12 timesteps per hour.

The indoor thermal comfort conditions and the thermal inertia of the walls facing east and west are studied through free-running simulations (without HVACs) from July 24th to 31st, which is the warmest week in summer. In particular, the results of the simulations are analyzed in terms of indoor operative temperature, inner and outer surface temperature, Time Lag (TL) and Decrement Factor (DF) of the walls. It is useful to remember that TL is the time shift between the maximum outer and inner surface temperatures occurrence, while the DF can be defined as the ratio of the amplitude of the inner surface temperature fluctuations to the amplitude of the outer surface temperature fluctuations (Gagliano et al., 2016b).

On the other hand, to measure the indoor thermal comfort in summer the *Intensity of Thermal Discomfort* (ITD) is adopted. The ITD is defined by the integral, over a certain period P , of the positive difference between the current indoor operative temperature (T_{op}) and the threshold value $T_{lim} = 26$ °C, needed to have comfortable indoor conditions (Sicurella et al., 2012). Moreover, the energy needs for heating and cooling are calculated through a second series of simulations where a thermostat control is set for the entire heating (20 °C) and cooling (26 °C) season.

2.1 Properties of VIPs

VIPs are innovative insulating solutions consisting in an evacuated, open-pore core material surrounded by thin laminates, used to maintain a high level of vacuum (Alam et al., 2011).

Their insulating capability is approximately seven times better than conventional insulating materials, such as mineral wool or EPS. Indeed, according to Johansson (2014), their thermal conductivity can be even below $5 \text{ mW}\cdot\text{m}^{-1}\cdot\text{K}^{-1}$. Consequently, a mineral wool board with a thickness of 185 mm is equivalent to a 20-mm thick VIP (Alotaibi et al., 2014). In this study, the authors used the following values to describe the VIPs performance: $\lambda = 7 \text{ mW}\cdot\text{m}^{-1}\cdot\text{K}^{-1}$, $\rho = 160 \text{ kg}\cdot\text{m}^{-3}$ and $c_p = 800 \text{ J}\cdot\text{kg}^{-1}\cdot\text{K}^{-1}$

2.2 Modeling the PCMs

The thermal behavior of a PCM undergoing phase change can be described by means of the relation between temperature and enthalpy:

$$dh(T) = C_{eq}(T) \cdot dT \quad (1)$$

Here, the enthalpy is set as $h = 0 \text{ kJ kg}^{-1}$ at $T = 0 \text{ }^\circ\text{C}$, while C_{eq} is determined experimentally. The melting process occurs through a temperature range; the maximum equivalent heat capacity is measured at the so-called *peak melting temperature*.

The PCMs adopted in this study consist of wallboards developed at CSTB (Centre Scientifique and Technique du Batiment), the performance of which is described in Evola et al. (2011). They are included in an aluminium honeycomb matrix, which contains 60 % of micro-encapsulated paraffin with a diameter of approximately $5 \mu\text{m}$ (Micronal T23 produced by BASF). Two thin aluminium sheets close the panel, the overall thickness of which is 2 cm (Hasse et al., 2011). According to the experimental measurements, the peak melting temperature is $27.6 \text{ }^\circ\text{C}$ for these PCM wallboards. However, since this temperature is quite low when compared to the thermal conditions expected in the case study, the real wallboards may not operate appropriately. Hence, the authors decided to consider a fictitious PCM wallboard in the simulations: they are exactly the same as the real honeycomb panels, but their melting curve is shifted in order to obtain a peak temperature of $30 \text{ }^\circ\text{C}$.

The corresponding curve for Eq. (1) is depicted in Fig. 1. The melting process corresponds to the segments with the highest gradient: It begins at $27 \text{ }^\circ\text{C}$ and ends at $33 \text{ }^\circ\text{C}$.

The honeycomb PCM panel has $\rho = 545 \text{ kg}\cdot\text{m}^{-3}$ and $\lambda = 2.7 \text{ W}\cdot\text{m}^{-1}\cdot\text{K}^{-1}$, which is imputable to the aluminium honeycomb matrix. Thanks to the aluminium honeycomb, the heat flux easily transfers through the panel, thus allowing the PCM included in the structure to work effectively.

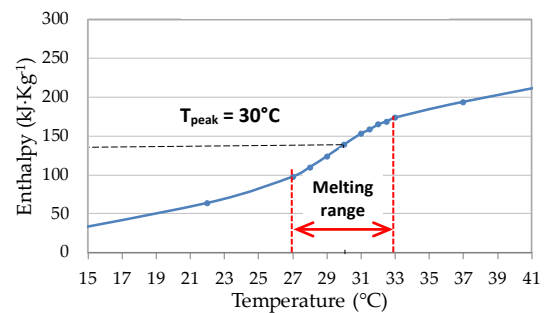


Fig. 1 – Enthalpy per unit mass for the PCM wallboards

3. Test Room

The test room (Fig. 2) has a gross surface area of $5.00 \times 5.00 \text{ m}$ and a height of 3.00 m . There are no obstructions and shields on all the outer sides. The façade facing south has a window measuring $3.00 \times 1.35 \text{ m}$, that is to say 30 % of the external surface of the wall. The main geometric features of the building are reported in Table 1. In the simulations, the test room is located near Syracuse (lat. 36.7° N , long. 15.1° E , alt. 51 m). This area has a mild climate with hot dry summers and moderately cool winters.

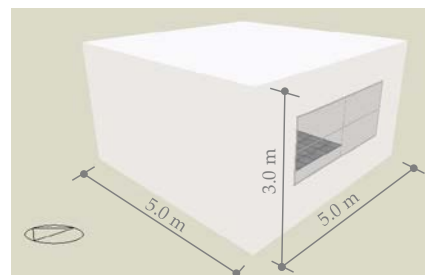


Fig. 2 – 3D model of the test room

Table 1 – Geometric features of the building

Geometric features			
Heated gross volume	V	58	m ³
Total external surface	S	85	m ²
Shape factor	S/V	1.70	m ⁻¹
Net floor area	S _n	19.40	m ²

In summer, the average outdoor temperature ranges from 22 °C to 33 °C. In winter, the outdoor temperature varies from 5 °C to 15 °C, while in spring and autumn the climate is mild and the temperature fluctuates from 10 °C to 26 °C.

The test room was with an office program from Monday to Friday from 9:00 to 18:00. The internal loads are characterized by occupants, computers and lighting systems for a total of 380 W with a density of 15 W·m⁻². The occupancy density is 0.08 people·m⁻²; lighting and office equipment power density is 8 W·m⁻². The air change rate is 0.5 vol·h⁻¹, without mechanical ventilation systems. The test room is equipped with a heating system represented by a natural gas boiler ($\eta = 0.85$), and a chiller for cooling purposes with COP = 2.50 in order to keep the indoor air temperature equal to 20 °C in winter and 26 °C in summer, respectively. The heating system is switched on during the occupancy period from December 1st to March 31st, whereas the air conditioning system operates from June 1st to September 30th.

3.1 Building Components

The building envelope of the test room in the base case is characterized by opaque vertical closures made by double brick walls with internal air gap and an overall thickness of 30 cm. The outer layer of the wall is in plaster with solar absorbance $\alpha = 0.60$ and thermal emissivity $\varepsilon = 0.90$. The properties of the double brick walls are reported in Table 2; the air gap has a thermal resistance of 0.18 m²·K·W⁻¹. A traditional slab with concrete and brick (thickness 20 cm) characterizes the flat roof and the floor.

Table 2 – Thermal properties of double brick walls

Layers	s m	λ W·m ⁻¹ ·K ⁻¹	ρ kg·m ⁻³	C _p J·kg ⁻¹ ·K ⁻¹
Outer Plaster	0.015	0.25	900	1000
Hollow brick	0.12	0.39	716	840
Mortar	0.01	1.00	1800	1000
Air gap	0.06	-	-	-
Hollow brick	0.08	0.40	775	840
Plasterboard	0.015	0.25	900	1000

The window has an aluminum frame without thermal break ($U_f = 5.9$ W·m⁻²·K⁻¹), and two glasses ($s = 6$ mm) separated by an air gap ($s = 12$ mm); the glazing has $U_g = 2.78$ W·m⁻²·K⁻¹ and SHGC = 0.70.

The U-value and the surface mass (SM) of the building components are reported in Table 3.

We validated the results of the simulation conducted on the base case with the measured data (24th–31st July) coming from an actual test room located in Milan (Rossi, 2009).

Table 3 – U-values and SM of the building components

	U (W·m ⁻² ·K ⁻¹)	SM (kg·m ⁻²)
Wall	1.02	160
Roof	1.84	332
Ground floor	1.98	332
Window	3.25	-

3.2 Solutions for Wall Insulation

We considered four configurations in the application of VIPs and PCMs respectively, to the inner and the outer surface of the standard wall in the test room (Fig. 3). The application of a 2 cm continuous layer of VIPs, either on the inner or the outer surface of the wall, allowed for the reduction of the U-value by 74 %.

Therefore, the U-value of the wall after retrofitting is 0.26 W·m⁻²·K⁻¹. On the contrary, PCMs do not significantly reduce the U-value of the wall compared to the base case; indeed, the new value is 1.00 W·m⁻²·K⁻¹.

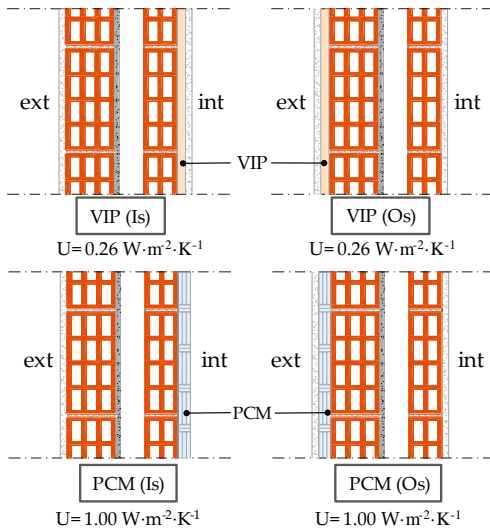


Fig. 3 – Wall configurations with VIPs and PCM on the inner surface (Is) and outer surface (Os)

4. Results

4.1 Energy Comparison

The energy needs for space heating and cooling in the different scenarios are shown in Fig. 4. Here, the energy savings in the heating period (ES_H) and in the cooling period (ES_C), compared with the base case, are also reported.

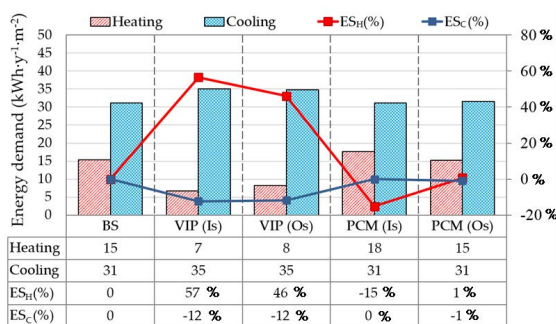


Fig. 4 – Energy needs for space heating and space cooling

The results highlight that the application of VIPs allows for a significant reduction in the energy needs in the heating period. This is certainly due to the remarkable insulating capacity of the VIPs if compared to traditional insulating materials.

In particular, VIPs placed on the inner surface produce $ES_H = 57\%$, which is higher than the case where VIPs are placed on the outer surface ($ES_H = 46\%$). On the contrary, VIPs involve an increase in the energy needs during the cooling period in both sce-

narios ($ES_C = -12\%$). In fact, a highly insulated envelope does not promote heat dissipation, and determines overheating into the building in hot summer days.

Overall, the use of PCMs does not change the energy needs significantly. The only exception occurs in winter when the PCM is placed on the inner side ($ES_H = -15\%$). Indeed, the HVAC system imposes a constant value of indoor temperature ($20\text{ }^\circ\text{C}$ and $26\text{ }^\circ\text{C}$ in the heating and cooling period), which is well below the melting temperature of the PCM. Therefore, the PCM remains in its solid phase almost the entire day. The exception that has been pointed out is probably due to the high thermal conductivity of the PCM, which also reduces the indoor surface temperatures, as shown in the following section.

4.2 Evaluation of Indoor Thermal Comfort

The operative temperature (T_{op}) within the test room was through simulations in free running conditions from July 1st to 31st. The main results are reported in Table 4.

As shown in Table 4, the operative temperature in the base case ranges from a minimum value of $28\text{ }^\circ\text{C}$ to a maximum value of $34.1\text{ }^\circ\text{C}$. On the other hand, VIPs are generally responsible for an increase in both the minimum and the maximum values. In particular, when the VIPs are placed on the inner surface, the maximum operative temperature increases from $34.1\text{ }^\circ\text{C}$ to $35.2\text{ }^\circ\text{C}$; when the VIPs are placed on the outer surface, the maximum operative temperature keeps almost the same as in the base case, but the minimum value increases by $1\text{ }^\circ\text{C}$. These results can be explained by considering that VIPs act as a barrier to the heat flux transferred from the inside to the outside, thus causing overheating. The overheating effect is also shown by the ITD value that increases by 17% if compared to the base case. Hence, VIPs seem not to be suitable in hot climates. Furthermore, the PCM panels placed on the inner surface reduce the maximum operative temperature from $34.1\text{ }^\circ\text{C}$ to $32.9\text{ }^\circ\text{C}$, with a decrease of $1.2\text{ }^\circ\text{C}$. This result is achieved thanks to the heat storage capacity of the PCM. In fact, in this case without thermostat controls, the PCM can reach the melting

temperature range, thus it can be effectively exploited. If we look at ITD, this reduces by 2 %. Instead, the PCM placed on the outer surfaces does not offer significant improvement compared to the base case, as it cannot interact with the indoor environment. In this case, the ITD slightly increases.

Table 4 – Main results in terms of indoor thermal comfort.

		T_i (°C)	T_{op} (°C)	ITD (°C·h)
Base case (Bs)	Max	34.8	34.1	2631
	Min	27.9	28.0	
VIP (Is)	Max	35.8	35.2	3183
	Min	28.3	28.4	
VIP (Os)	Max	34.8	34.1	3137
	Min	28.8	29.0	
PCM (Is)	Max	33.6	32.9	2590
	Min	28.7	28.9	
PCM (Os)	Max	34.6	33.9	2669
	Min	28.3	28.1	

Overall, the proposed solutions for the retrofitting of the walls provide worse conditions in terms of summer thermal comfort, with the only exception of the PCM placed on the inner side.

4.3 Dynamic Thermal Behaviour

Time Lag and Decrement Factor were in relation to the inner (T_{si}) and the outer (T_{so}) surface temperatures, based on hourly simulations in free running conditions during the period from 1st to 31st July. Fig. 5 and Fig. 6 illustrate the hourly profiles of T_{si} and T_{so} for the walls facing east during three summer days (July 27th–30th). The results, also including the walls facing west, are shown in Table 5. As reported in Fig. 5, in the base case the east wall has a maximum outer temperature $T_{so,max} = 44.4$ °C, which occurs at 10:00 am; the peak temperature on the inner surface ($T_{si,max} = 33.8$ °C) is attained at 17:00. Thereby, in this case the TL is about 7 hours, while $DF = 0.22$ (see Table 5). The minimum values of T_{so} and T_{si} occur at 6:00 am and 9:00 am, and are about 23°C and 28 °C respectively.

When the VIP is placed on the inner side, the T_{so} assumes the same trend as in the base case, but the peak of T_{si} increases by 1.1 °C. The maximum T_{si} value is $T_{si,max} = 34.9$ °C and occurs at 16:00; as reported in Table 5, TL = 6 h and $DF = 0.26$. Instead, the scenario with the VIP on the outer side provides

a significant increase in the maximum outer temperature, compared to the base case. Indeed, $T_{so,max}$ increases from 44.4 °C to 47.9 °C.

The profile of T_{si} remains almost the same, with the only exception of the minimum value, which increases by 1.6 °C compared to the base case. It has to be highlighted that this scenario is able to attenuate the peak of the heat wave better than a standard wall ($DF = 0.13$). According to these results, the placement of the VIP layer on the outer side offers better performance in terms of dynamic behaviour. The performance of PCMs is reported in Table 5. When the PCMs are placed on the inner side, the peak inner surface temperature decreases by about 1.4 °C, irrespective of the exposure, and the outer surface temperature is quite similar to that of the standard wall.

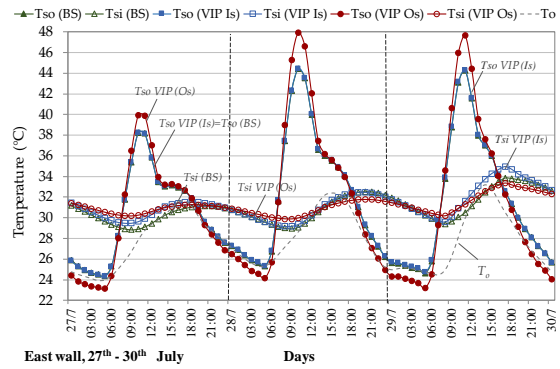


Fig. 5 – Inner and outer surface temperature of east wall (VIP)

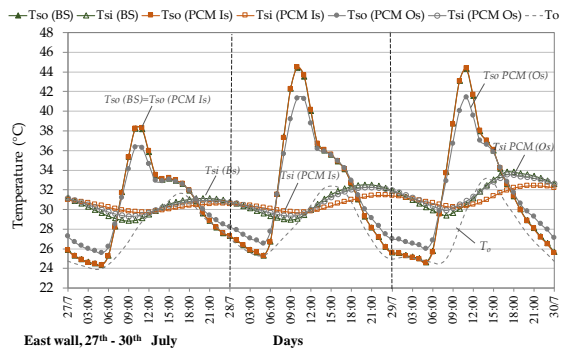


Fig. 6 – Inner and outer surface temperature of east wall (PCMs)

Table 5 – Surface temperatures and dynamic thermal parameters

		$T_{so,max}$ (°C)	$T_{si,max}$ (°C)	TL (h)	DF (-)
Base case (Bs)	East	44.4	33.8	7	0.22
	West	44.8	33.7	4	0.20
VIP (Is)	East	44.4	34.9	6	0.26
	West	44.8	34.8	2	0.24
VIP (Os)	East	47.9	33.4	7	0.13
	West	47.4	33.3	2	0.12
PCM (Is)	East	44.5	32.4	10	0.09
	West	44.9	32.4	7	0.08
PCM (Os)	East	41.4	33.5	7	0.24
	West	42.9	33.2	3	0.19

In fact, the PCM is able to delay and attenuate the heat wave better than the other solutions thanks to its ability to store heat and release it afterwards.

Hence, with reference to the east wall (Fig. 6), $T_{so,max}$ occurs at 10:00 am and $T_{si,max}$ occurs at 20:00, so TL = 10 hours while DF = 0.09.

On the other hand, the PCMs placed on the outer side provide a significant reduction in the peak outer surface temperature. Indeed, in the east wall $T_{so,max}$ decreases from 44.4 °C (base case) to 41.4 °C (see Table 5), which means a reduction by 3 °C. In this case, the profile of T_{si} is unchanged compared to the base case, as the PCM mainly accomplishes its action on the outdoor wall surface. Overall, the dynamic parameters gained from the simulations for all scenarios are reported in Table 5.

In the base case, the east and west walls show low TL values (7 and 4 hours, respectively) and DF = 0.20, because of their low surface mass. The peak values of outer and inner surface temperature are 44.8 °C and 33.8 °C, respectively. For the other solutions, the worse condition is the one where VIPs are placed on the inner side, because in this case the inner surface temperature increases by 1.1 °C with great fluctuations.

On the contrary, the optimal solution is when PCM panels are placed on the inner side, which shows TL = 10 h and DF = 0.09, with a reduction in the peak inner surface temperature of about 1.4 °C. Both the solutions with VIP and PCMs on the outer side do not provide any significant contribution to the reduction of the inner surface temperature. Furthermore, it can be highlighted that the VIPs on the outer side overheat the outer surface of the walls by about 3 °C, while the PCM panels on the outer side

reduce the peak outer surface temperature by about 3 °C.

5. Conclusions

The results show that the innovative solutions considered in this study (VIPs and PCMs) may be useful in the Mediterranean climate, but only if placed on the right side of the walls.

In particular, VIPs are very useful to reduce the heating energy needs: in this paper, the heating energy demand is reduced by 57 % and 46 % if they are placed on the inner or the outer side, respectively. However, the cooling energy needs increase by about 12 % compared to the base case.

As concerns the selected PCM, in this specific case it is not recommended with HVAC systems because in this case the set point imposed by the HVAC systems (20 °C in winter and 26 °C in summer) is lower than the melting temperature of the PCM, thus it cannot activate. Indeed, the results show that the energy demand for heating and cooling with the PCM panels are almost the same when compared to the base case.

However, if PCMs were used into a mixed-mode building with 28 or 30 °C cooling setpoint, they would be capable to activate and the application could work well.

The simulations in free-running conditions have highlighted that both the solutions with VIPs and PCMs on the outer side are the worst ones for indoor comfort conditions in summer. Placing the VIPs on the inner side leads to very high fluctuations in the indoor operative temperature (from 28.4 °C to 35.2 °C) compared to the case with PCMs placed on the inner side (from 28.8 °C to 32.9 °C). That is why the PCM panels placed on the inner side can be regarded as the optimal solution.

Nomenclature

Symbols

C_{eq}	Equivalent heat capacity ($J \cdot kg^{-1} \cdot K^{-1}$)
C_{cp}	Specific heat ($J \cdot kg^{-1} \cdot K^{-1}$)
DF	Decrement factor (-)
ES	Energy saving percentage (%)
h	Enthalpy ($J \cdot kg^{-1}$)
ITD	Intensity thermal discomfort ($^{\circ}C \cdot h$)
s	Thickness (m)
S	External surface (m^2)
S_n	Net floor area (m^2)
SHGC	Solar Heat Gain Coefficient (-)
SM	Surface mass ($kg \cdot m^{-2}$)
T	Temperature ($^{\circ}C$)
TL	Time lag (h)
U	Thermal transmittance ($W \cdot m^{-2} \cdot K^{-1}$)
V	Heated gross volume (m^3)

Greek letters

α	Solar absorptance (-)
ε	Thermal emissivity (-)
λ	Thermal conductivity ($W \cdot m^{-1} \cdot K^{-1}$)
ρ	Density ($kg \cdot m^{-3}$)
τ	Time (h)

Subscripts/Superscripts

C	Cooling
f	Frame
g	Glazing
H	Heating
i	Indoor
M	Melting point
max	Maximum
min	Minimum
o	Outdoor
op	Operative
si	Inner surface
so	Outer surface

References

- Alam, M., H. Singh, M.C. Limbachiya. 2011. "Vacuum Insulation Panels (VIPs) for building construction industry – A review of the contemporary developments and future directions". *Applied Energy* 88(11): 3592-3602. doi: 10.1016/j.apenergy.2011.04.040.
- Alotaibi, S.S., S. Riffat. 2014. "Vacuum insulated panels for sustainable buildings: a review of research and applications". *International Journal of Energy Research* 38: 1-19. doi: 10.1002/er.3101.
- Bejan, A-S., T. Catalina. 2016. "The implementation of Phase Changing Materials in energy-efficient buildings. Case Study: EFdeN project". *Energy Procedia* 85: 52-59. doi: 10.1016/j.egypro.2015.12.274.
- DesignBuilder. Energy simulation software. 2014. Version 4.2, <http://designbuilder.co.uk>.
- EnergyPlus. Engineering reference. 2011. The reference to energy plus calculation, Conduction Finite Difference Solution Algorithm. Berkeley, U.S.A: LBNL.
- Evola, G., L. Marletta, F. Sicurella. 2013. "A methodology for investigating the effectiveness of PCM wallboards for summer thermal comfort in buildings". *Building and Environment* 59:517-527. doi: 10.1016/j.buildenv.2012.09.021.
- Evola, G., L. Marletta. 2014. "The effectiveness of PCM wallboards for the energy refurbishment of lightweight buildings". *Energy Procedia* 62: 13-21. doi: 10.1016/j.egypro.2014.12.362.
- Evola, G., F. Sicurella, N. Papa, E. Wurtz. 2011. "Simulation of the behaviour of phase change materials for the improvement of thermal comfort in lightweight buildings". In: *Proceedings of the 12th international IBPSA conference*. Sydney, Australia: IBPSA.
- Gagliano, A., F. Nocera, F. Patania, A. Moschella, M. Detommaso, G. Evola. 2016a. "Synergic effects of thermal mass and natural ventilation on the thermal behaviour of traditional massive buildings". *International Journal of Sustainable Energy* 35(5): 411-428. doi: 10.1080/14786451.2014.910517.
- Gagliano, A., M. Detommaso, F. Nocera, U. Berardi. 2016b. "The adoption of green roofs for the retrofitting of existing buildings in the Mediterranean climate". *International Journal of Sustainable Building Technology and Urban Development* 7 (2): 116-129. doi: 10.1080/2093761X.2016.1172279.
- Hasse, C., M. Grenet, A. Bontemps, R. Dendievel, H. Sallée. 2011. "Test and modelling of honeycomb wallboards containing a phase change material".

- Energy and Buildings* 43: 232-238. doi: 10.1016/j.enbuild.2010.09.017.
- Johansson, P. 2014. "Building Retrofit using Vacuum Insulation Panels." *Degree thesis*. Gothenburg, Sweden: Chalmers University.
- Kuznik, F., J. Virgone, J.J. Roux. 2008. "Energetic efficiency of room wall containing PCM wallboard: a full-scale experimental investigation". *Energy and Buildings* 40: 148-156. doi: 10.1016/j.enbuild.2007.01.022.
- Kuznik, F., J. Virgone. 2009. "Experimental assessment of a phase change material for wall building use". *Applied Energy* 86: 2038-2046. doi: 10.1016/j.apenergy.2009.01.004.
- Rossi, M. 2009. "Prodotti e sistemi di involucro innovativi per il progetto di edifici energeticamente efficienti." *PhD thesis*. Naples, Italy: University of Naples Federico II.
- Seong, Y.B., J.H. Lim. 2013. "Energy saving potentials of phase change materials applied to lightweight building envelopes". *Energies* 6: 5219-5230. doi: 10.3390/en6105219.
- Sicurella, F., G. Evola, E. Wurtz. 2012. "A statistical approach for the evaluation of thermal and visual comfort in free-running buildings". *Energy and Buildings* 47: 402-410. doi: 10.1016/j.enbuild.2011.12.013.
- Thorsell, T. 2011. "Advances in thermal insulation – vacuum insulation panels and thermal efficiency to reduce energy usage in buildings". *PhD Thesis*. Stockholm, Sweden: KTH.
- Voelker, C., O. Kornadt, M. Ostry. 2008. "Temperature reduction due to the application of phase change materials". *Energy and Buildings* 40: 937-944. doi: 10.1016/j.enbuild.2007.07.008.

Pitfalls in Weather Data Management Strategies of Building Performance Simulation Tools

Livio Mazzarella – Politecnico di Milano – livio.mazzarella@polimi.it

Martina Pasini – Politecnico di Milano – martina.pasini@polimi.it

Abstract

The use of simulation for building design and performance assessment is becoming mandatory if NZEB requirements have to be met. As a matter of fact, only dynamic simulations are able to correctly account for renewable energy exploitation on the building site. Dealing with solar energy source conversion, the correct use of available standard weather data files is still more important than solar gains through the transparent envelope. When using such statistically derived weather data, however, different pitfalls might arise. In fact, when performing sub-hourly simulation, the information provided by hourly-based climatic data is insufficient. Interpolation algorithms are implemented in Building Performance Simulation tools (BPSTs) to provide intermediate weather data, which can affect the quality of the results. Specifically, solar radiation data are insufficiently represented by hourly-based values when dealing with short time-step simulations of complex building systems. In this article, a review of radiation algorithms and weather data management algorithms at sub-hourly simulation time steps will be introduced, as implemented by two well-known software, such as TRNSYS 17 and EnergyPlus 8.6.0. Further considerations will be made upon information exchange among simulation components during the simulation, and upon the possibilities offered or denied by different data management-implementations when multiple actors are involved in the simulation.

1. Introduction

In complex systems like buildings, control strategies become vital when looking for energy use reduction and renewable sources exploitation. However, when dealing with complex systems that exhibit non-linear behaviours which may also depend on thresholds, integral or averaged information over time might not be any more sufficient to assess the

performance of that particular system. In that case, the “instantaneous” time dependence of some of the input data might become important to get a realistic comprehension of the behaviour of the enquired system. Here instantaneous means short, compared to the smallest system characteristic time. Short time step simulations might therefore become the only possibility to compare different systems at design time.

Starting from these considerations, we have tried to evaluate the impact on simulation in “averaging” those inputs that show an extremely variable behaviour, as solar radiation in particular.

When using weather data in a simulation, four main aspects should be taken into consideration:

1. Are the requirements of correct timing and synchronization of weather data with the different nature (instantaneous or averaged) fulfilled?
2. Is the accuracy, by which the solar position is calculated with, consistent with small time steps?
3. What is the loss of information when averaging weather data?
4. What is the impact of different weather data interpolation strategies?

One of the basic requirements, when dealing with information exchange, for both internal and external objects involved in a simulation, is the knowledge of the nature and occurrence timing of the information. In some cases, an “accurate” synchronization of different kinds of information might not be so relevant, such as at pre-design time when the average “variation pattern” is enough to get design values to size the system. In other cases, when studying real situations, such as during the empirical validation of BPSTs against measured data or at operational time, by using monitoring weather data

to optimize the performances of the building system, the correct synchronization between data with different natures, both influencing the behaviour of the system (such as temperature and solar radiation in photovoltaics systems efficiency), becomes important.

Following these considerations, a review of the algorithms implemented in two well-known BPSTs, such as TRNSYS 17 and EnergyPlus 8.6.0, was performed.

2. Aspects to be Considered When Addressing Short or Hourly Time Steps Simulations

2.1 Information Exchange: Timing and Consistency

One of the most important aspects to be addressed when simulating systems comprised of different objects is the exchange of information among the different actors involved. The two main properties that this information should contain are: its nature and its timing.

When speaking of timing, it should be clear that:

- the *time step* is the time interval between two subsequent calculations,
- while the *time stamp* is the exact time to which the results of each calculation are referred (the difference between two subsequent time stamps is thus the time step).

The most commonly used numerical methods in solving partial differential equations, such as finite volumes, finite differences, and conduction transfer functions, provide as their results the instantaneous values of the dependent variables (temperatures and/or fluxes) at a well-defined time stamp, and not an average value on the previous time step. To get to this result it is always necessary to know the instantaneous values of their initial state and – depending on the chosen numerical scheme – of their boundary conditions at the previous and/or current time stamp. For example, to solve the problem of conductive heat transfer in a wall, the fluxes and the temperatures on their boundaries at precise time stamps need to be known.

Besides, in a simulation, a manager must always be “elected” that “conducts the orchestra”, here called *simulation manager*.

The simulation manager should ask all the actors involved in a simulation to perform their calculation and expose to all the other components their properties at each precise time stamp. These time stamps will be referred to as *global time stamps* and the time in between the two subsequent as *global time steps*.

The global time step should be as short as required by the actor that is more sensitive to a rapid variability of its boundary conditions.

That doesn’t mean that all the actors will be “forced” to repeat their calculation at each global time stamp. Each of them will be allowed to expose its properties as unvaried and store the information coming from the other objects at its convenience.

Another possibility, might be the one that sees an object which needs to perform its calculation with shorter time steps to reach more accurate results, but not that much sensitive to the “exact form” of variation of its boundary conditions (linear, random, etc.). In this case it should not “ask” the simulation manager to reduce its global time step. It will collect the needed information at the global time stamps and perform multiple calculations to give out its results at each global time stamp.

A last remark about these definitions relates to the nature of these time stamps, i.e. what kind of time (solar, universal, local, etc.) is used. The choice of the nature of the time stamp has to be made, among the other reasons, to reduce the interpolation needed on the available input data. Therefore, since in the majority of cases, other time-dependent input data, as the schedules defined for describing user habits (such as working hours, etc.), are based on local time, time stamps should be *local* instead of *solar*. Local time can be affected by legal corrections or not, and this aspect should be managed by the simulation manager and well documented to avoid confusion in the input and output reading/writing.

Therefore, we know the input data at specific local time stamps, such as users-schedules, instantaneous weather climatic data, such as dry temperature, relative humidity, wind velocity, and integral or averaged weather data, such as global and diffuse horizontal solar radiation, at a file format dependent time stamp (solar, local, etc.).

2.2 Weather Data Nature and Timing

We have said that the input data are not always available as “instantaneous”. Among the data to be exchanged, the most complex to manage are the weather-related data, due to:

- the different nature of its quantities (some of which are intensive/scalar and other extensive/vectorial)
- the relative time stamp at which these data are available.

A review performed on both the weather data file format manuals (Wilcox and Marion, 2008) and the Guide to Meteorological Instruments and Methods of Observation (Jarraud, 2008) showed that some weather data are recorded as instantaneous values associated to a time stamp, other are integral values of a variable evaluated on the previous time step.

Weather data that are relative to solar radiation are given in almost all weather data file formats as integrated over time, i.e. as the total amount of solar radiation (energy) received during the period ending at the time stamp associated with the datum and starting at the timestamp associated with the previous one.

The weather processor has instead to provide each object with the total irradiance (power) striking a specific oriented surface at each global time stamp. Thus, this information provided in terms of *energy*, should be translated in terms of *power* and used with a correctly aligned sun position, to calculate the correct amount of irradiance reaching each oriented surface.

That means that when a rule is set to assure the time alignment of provided weather climatic data (i.e. the instantaneous data and those transformed from integral to instantaneous), a consistent rule should also be set for the alignment of the sun position. In this regard, before going more into the details of how to manage instantaneous and integral weather data, a review upon sun position algorithms is introduced here to clarify the answer to the following questions:

- what is the timing of the solar position used by the different tools,
- what is the accuracy of the algorithms used for the calculation of the sun position, when the

simulation time step is of the order of magnitude of minutes.

2.2.1 Sun position timing

In some cases (TRNSYS) we have the possibility to define the weather data as instantaneous or averaged and on which time interval it has been averaged, if needed. In other cases we might need to modify the input data to time align them as required. However, there is always something that we cannot change, i.e. the way the tool manages the sun position timing. Both EnergyPlus and TRNSYS expose to all other procedures the sun position that is evaluated at the middle of the global time step regardless any other choice. Accordingly, for time consistency, we should expose to all the objects involved in the simulation all the other input data at that particular *mid time stamp* (i.e. at the mid of the time step) performing interpolations, even if we have instantaneous data available at the global time stamps. In our opinion, this is not the best choice because:

- unneeded interpolations are performed;
- integral weather data need a transformation, which could be better performed when aligning the transformed data to the time stamps of the instantaneous data;
- schedules data are usually defined at the time stamp as well, and not at the mid of the previous time step.

2.2.2 Sun position accuracy at short time steps

As far as the accuracy of the sun position calculation is concerned, we have done a review of the most broadly diffused algorithms (Duffie and Beckman, 2013) to understand if the simplified hypotheses at their basis are still applicable when dealing with short time step simulations. We detected some ambiguity among different sources concerning the definition of the fractional year; therefore we recovered the original source for the definition of the most accurate equations for the calculation of sun declination and equation of time (Spencer, 1971). We found a witness (Oglesby, 1998) that reported one error in the first coefficient of Spencer’s equation of time. We will report it here only for completeness:

$$E = 0.0000075 + 0.001868 \cos(T) - 0.032077 \sin(T) - 0.014615 \cos(2T) - 0.040849 \sin(2T) \quad (1)$$

In Spencer’s equation of time there is a fractional-year time “T” depending on the day-of-the-year number “d” which ranges from 0 on 1 January to 364 on 31 December, that has the equation: $T = 2 \pi d/365$. Since the sun declination is kept constant over one day and the author (Spencer, 1971) suggested using those equations in years in the middle of a 4-year leap cycle, we wondered:

- what might be the rate of change of declination in one day and
- what would happen if we need to compute the sun position when using monitored weather data near or for a leap year.

We noticed, by using the nautical almanac algorithms for the calculation of the sun position, that the rate of change of its declination in one day is maximum 0.4°.

To answer the second question, we calculated the error of Spencer’s simplified algorithm on the daily-average declination with respect to the more accurate algorithm of the nautical almanac. For a year before the leap one, this error depends on the longitude of the location and varies along the year, reaching maximum absolute values that are of the same order of the maximum daily declination variation. Using, in Spencer’s equations, a fractional day-of-the-year number, calculated at the beginning, mid or end of the day, a bigger or smaller error results depending on the longitude of the location, since universal time is not taken into consideration. However, the accuracy reached with Spencer’s simplified equations is still acceptable when calculating the zenith of the sun even at very short time steps.

2.3 Using Weather Data Recorded on a Particular Time Basis

Referring to weather data availability and “desired” simulation time step two scenarios might occur:

- weather data recorded on a short time step basis (minutes or seconds) are available and hourly simulations are intended,
- hourly weather data are available and short time step simulations are needed.
- In these cases, the following questions have arisen:
 - what do we lose if we use hourly weather data generated from short time step monitored data that preserve integral solar radiation?
 - which interpolation strategy is the most effective when dealing with data estimation between its recorded values?

2.3.1 From data recorded on a short time step basis to hourly data

In this first case we have weather data recorded on a minute or second time basis, but we would like to set the global time step of our simulation to 1 h. This might be the correct approach to reduce calculation time if we imagine that the components involved in the simulation do not need to know the “exact variability” of the data, while only integral values of radiation are of interest. If we want to perform hourly simulation, we cannot use the weather data recorded at those short time steps as they are. Neither of the two tools taken in consideration allows it, and in general it is difficult others might do it. Therefore, those data need to be transformed and we want to understand which error this process introduces. We used the data collected for the year 2016 (in particular the month of April) by the weather station of the Energy department of the Politecnico di Milano. The data were recorded on a 10 s time step basis. We want to know how the integral over the month of April of the solar radiation reaching the most common expositions is influenced by the integration of those data (needed to be able to run a simulation with a global time step of 1 h).

First of all, by doing this operation, we have a smoothing of the original data, as can be seen in Fig. 1.

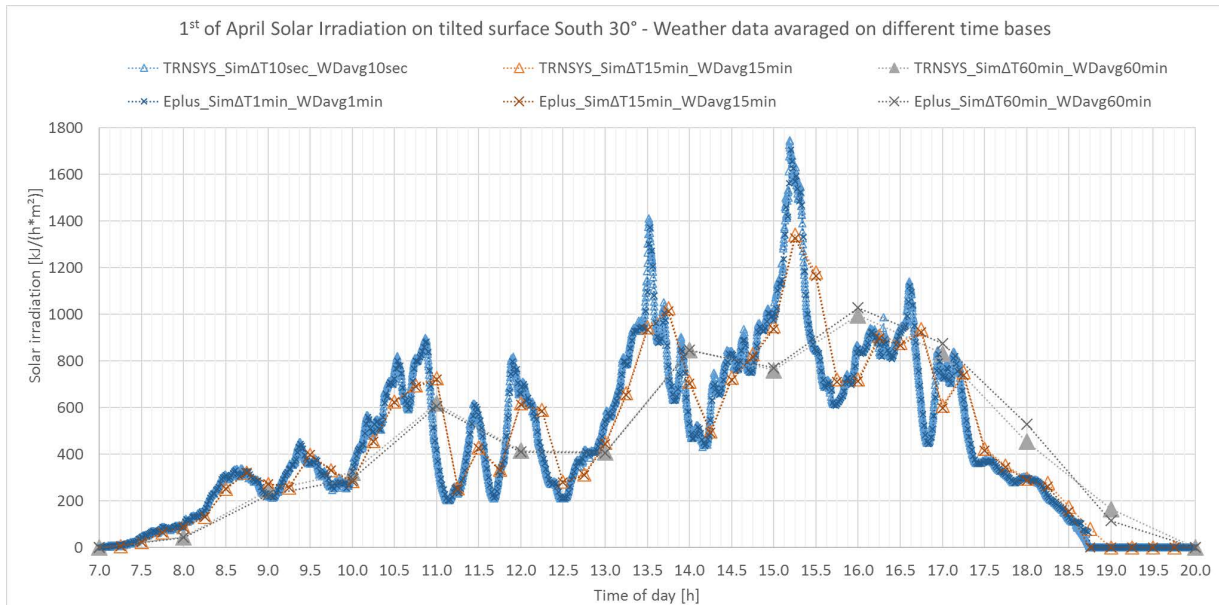


Fig. 1 – Effect of the choice of different time bases for averaging monitored data

A note about all the figures shown here: All the graphs are represented with dotted lines for an easy time series reading, even if they are intended to show discontinuous, averaged over the global simulation time step, pseudo-instantaneous values as provided by the investigated tools. These values have been associated to the time stamp provided by the tool, even if the tool calculates them as average values over the simulation time step.

Table 9 – Weather data recorded at a short time basis used on hourly simulation

Exp	WD ΔT [min]	April Sol.Rad. [MJ/m²]		Diff [%]	
		TRNSYS	Eplus	TRNSYS	Eplus
South 30°	15	565	519	0.46	0.36
	60	567	526	0.89	1.61
Hor	15	498	461	0.32	-0.1
	60	501	465	0.98	1.07
North	15	128	124	0.30	-0.47
	60	132	122	3.43	-2.12
South	15	351	333	0.55	1.16
	60	353	335	1.09	1.86
West	15	409	373	1.33	3.26
	60	430	361	6.41	-0.08
East	15	219	207	0.28	-2.82
	60	222	208	1.47	-2.36

Together with the smoothing, also the integral of the solar radiation that reaches the different expositions

is influenced. Taking as reference values those computed with the smallest global simulation time step allowed by the tool (10 seconds for TRNSYS and 60 seconds for EnergyPlus), we can see in A note about all the figures shown here: All the graphs are represented with dotted lines for an easy time series reading, even if they are intended to show discontinuous, averaged over the global simulation time step, pseudo-instantaneous values as provided by the investigated tools. These values have been associated to the time stamp provided by the tool, even if the tool calculates them as average values over the simulation time step.

Table 1 that we get a difference in the integral value of the total solar radiation incident on each exposition which depends on the particular kind of exposition. EnergyPlus gives lower solar radiation integrals with respect to TRNSYS. We report these considerations to show that preserving the integral on those input data related to solar radiation is not a guarantee of an “accurate” integral on the computed radiation reaching different expositions.

2.3.2 From hourly weather data to short time step simulation

We have seen in the previous paragraph what happens in the first scenario identified in Paragraph 2.3. Now we will consider the second scenario.

Naturally, when dealing with short time step simulations, the best solution should be to work with

weather data recorded with the same frequency. However, we are still working with hourly weather data, even if Crawley, Hand and Lawrie (1999) pointed out that this kind of data is no longer enough since interpolating between hourly observations does not accurately represent weather conditions that change much more frequently.

Given that, we need to assess the possibilities offered by the different tools to overcome such lack of information.

While for the instantaneous variable, the interpolation algorithm commonly chosen is linear interpolation with solar radiation; different tools have chosen different strategies.

In particular TRNSYS and EnergyPlus chose different interpolation algorithms for solar radiation. EnergyPlus decided to convert the integral value of solar radiation (energy) associated with a time stamp in the weather data file to an average instantaneous value of solar irradiance (power) associated to a time stamp in the middle of the current and previous ones (backward middle time). After that, the instantaneous value at each time stamp (irradiance) is calculated as linear interpolation between the average irradiance attributed to the backward middle time and that attributed to the forward middle time (Fig. 2).

TRNSYS instead, chose to interpolate the values gained from the weather data file for horizontal solar radiation by using the curve for extra-terrestrial radiation. This kind of interpolation is more heavy computationally, than the one implemented in EnergyPlus, therefore its greater effectiveness should be evaluated.

However, care should be taken when importing user defined weather data in TRNSYS, because the following two possibilities are allowed, i.e. using:

- one object, i.e. the Type 99 that combines external data reader and solar processor;
- two objects, i.e. the Type 9 for external data reading and the Type 16 for processing solar information.

These two ways give different results, as can be seen in Fig. 3 where we have the comparison between solar irradiance (power) computed by the two Types for a simulation with 15-minute global time steps, using input data averaged on a 60-minute time basis, and a 15-minute simulation using instead input data averaged on a 15-minute time basis. As written in the manual, Type 99 performs radiation "smoothing", while Type16 does not, in both cases the sky model of Perez 1999 was used, but site altitude could not be set. Table 2 shows the difference in respect to the reference values, of the integrals of the solar radiation striking different expositions as given by the smoothed, non-smoothed and linear interpolations, according to the exposition.

Table 10 – Integrals of the solar radiation with different interpolation algorithms of hourly weather data at time steps of 15 min

Exp	Diff [%] over the month of April		
	Type 99	Types 16+9	EnergyPlus
South 30°	1.13	0.94	1.34
Hor	0.86	0.74	0.75
North	1.02	1.77	-1.14
South	1.27	1.07	1.69
West	2.55	4.26	0.44
East	2.16	1.79	-1.79

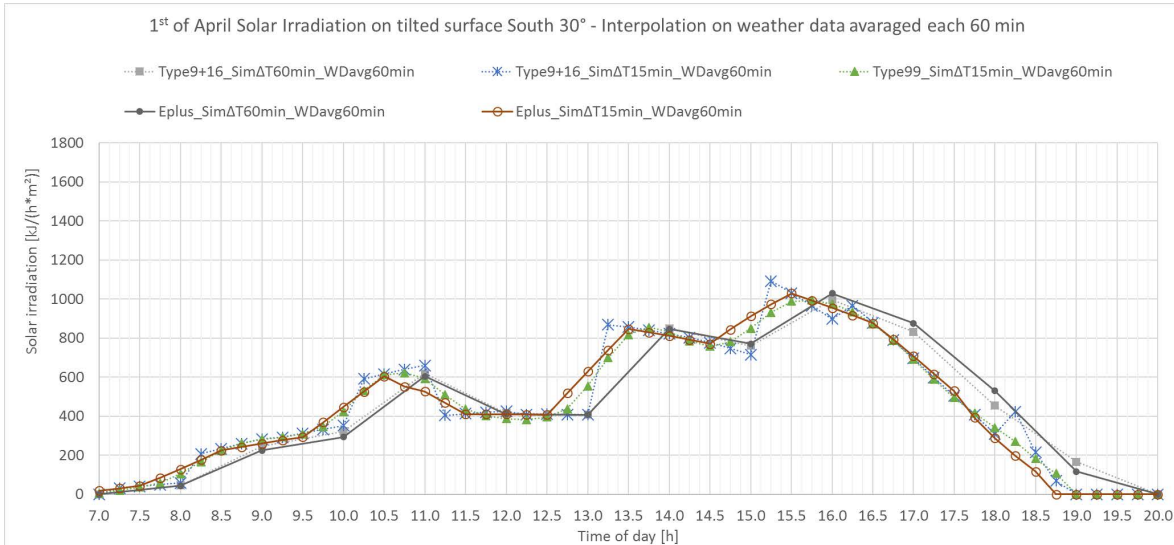


Fig. 2 – Effect of a different interpolation of 60 minutes averaged weather data for simulation with 15 min. global time steps

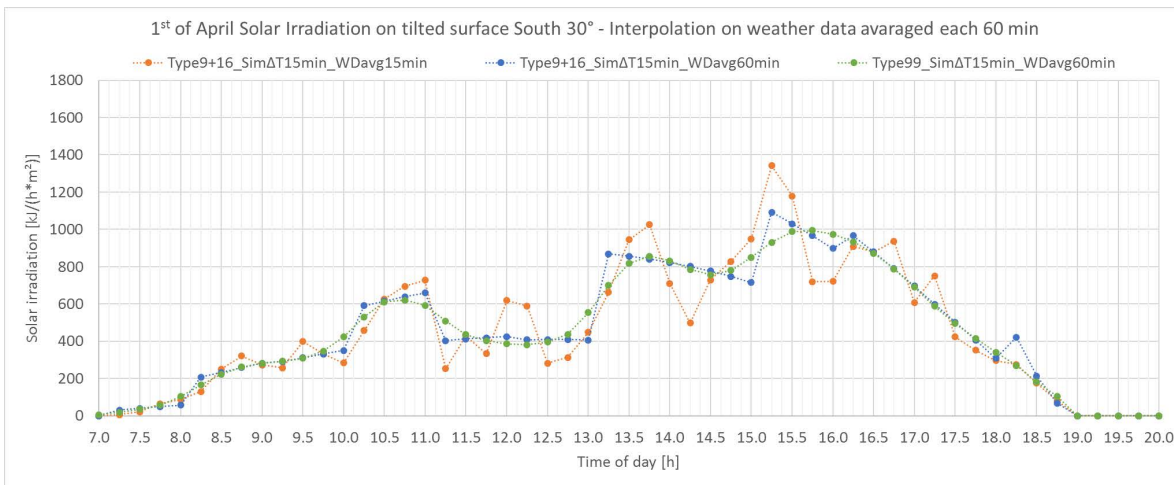


Fig. 3 – Comparing simulations with global time step of 15 min in case of weather data averaged over a time base of 15 min. or 60 min

Actually, with the exception of the west exposition, the two interpolation routines might be considered quite equivalent in terms of integral solar radiation calculation (Table 2).

However, if we want to check the performance of our solution against solar irradiance variability, the second non-smoothed interpolation might be preferable, since it is a bit more “discontinuous”.

Of course this second strategy is still not sufficient to emulate those random phenomena that occur in the atmosphere that are quite relevant when dealing with solar radiation. If we use the weather data file averaged on a 15-minute time basis, we have a different pattern of variability with respect to the interpolated ones starting from an hourly averaged weather data file (Fig. 3). Energy Plus does not allow

any choices and its linear interpolation has quite the same effect as the radiation smoothing of TRNSYS Type99.

While trying to ensure the conservation of energy received on a horizontal surface, a valuable algorithm for the estimation of those unknown values might consider the statistical variability of that specific variable. Variables such as solar radiation or wind velocity might be better estimated by applying a more realistic “pattern” to their “interpolation” than linear or smoothed regression. Statistics might be used to define a reduced number of patterns that might be applied to variables that show similar variability. Of course this apparently random behaviour should be deterministic and repeatable. Otherwise each time we repeat a simulation after having

changed a component to evaluate a different technology, we would get results that are non-comparable.

This statistical approach should have the goal to better assess the efficiency of a system and its control strategy as realistically as possible.

3. Discussion and Result Analysis

We have seen that different requirements might occur depending on:

- the sensitivity of the simulation components to input variability;
- the availability of weather data recorded at different time bases;
- the goal of the dynamic simulation (validation or evaluation at design time).

We have seen that in some cases it is necessary to describe in detail the variability of input data by using very short time step simulation (minutes), while other times, it might be sufficient to communicate to a simulation component an average value of the input required. In some cases, it might be better to align the different input data with precision, other times this synchronization might not be vital.

In the majority of the cases we have simulation components with very different time bases (heavy building construction and HVAC systems), but we do not want to use a very short time step simulation because it takes too much time.

How could we fulfil all the different requirements, in the best possible way?

A starting point might be to help the user to describe needs and input data as precisely as possible and let the tool choose what has to be done, in the most consistent way. For example, the user should not be asked to manipulate its weather data if the recorded time base is smaller than the global simulation time step.

After that, it might be better to reduce the required assumption. Since different kinds of uncertainties are already ingrained in numerical simulation, while defining the strategy to handle time-variant information inside the simulation, a relevant pursued goal should be to avoid assumptions not strictly needed, as interpolating values at mid time steps systematically.

The last but most important suggestion would be related to avoid information annihilation. If we have input data described on a short time basis, they should be kept available for whichever component might need them, without compelling all the other components as well to perform not "strictly needed" calculations. This can be managed by the singular component that should decide "by itself" if it needs to perform its calculation each time stamp or not.

4. Conclusion

The review here presented has been focused on the routines that handle weather data, as implemented by TRNSYS 17 and EnergyPlus 8.6.0. Our aim has been to point out how weather data provided on a certain time basis are used in the simulation, when the simulation time step is smaller, equal or larger than the weather data recording time basis.

When the simulation time step is the same as the weather data recording time basis, a clear architectural choice for the alignment of the different types of weather data and sun position is needed. While some possibilities are provided to the user to describe the available weather data, sun position timing is not modifiable. The more common strategy implemented by the analysed tools is to exchange the values of the simulation variable averaged over the time steps. However, this strategy prevents the numerical scheme implemented in each simulation component to directly handle the process of weighting its boundary conditions at different time stamps. A good architectural choice should preserve all the information available in input data, while managing rules should be defined and used only if strictly needed, as we have seen for solar radiation. When the simulation time step is smaller than the weather data recording time basis, interpolation is needed. We have seen that the currently available interpolation routines might not be "significant enough" to test complex components and control strategies. A stochastic "interpolation" algorithm, derived by statistical analysis on weather data fluctuations, might overcome this lack of information. This algorithm will have the purpose of mimicking the variability of variables with similar

capacity/patterns, to better evaluate the effectiveness of a system and of its control strategy when subjected to “realistic” boundary condition fluctuations.

References

- Crawley, D.B., J.W. Hand, L.K. Lawrie. 1999. “Improving the Weather Information Available to Simulation Programs”. In: *Proceedings of Building Simulation '99*. Kyoto, Japan: IBPSA.
- Duffie, J.A., W.A. Beckman. 2013. *Solar engineering of thermal processes*. Hoboken, U.S.A: John Wiley & Sons, Inc.
- Jarraud, M. 2008. *Guide to Meteorological Instruments and Methods of Observation* (WMO-No. 8). Geneva, Switzerland: World Meteorological Organisation.
- Oglesby, M. 1998. Personal correspondence. Accessed the 30th of January 2016 <http://www.mail-archive.com/sundial@uni-koeln.de/msg01050.html>.
- Spencer, J.W. 1971. “Fourier Series Representation of the Position of the Sun”. *Search* 2(5): 172.
- Wilcox, S., W. Marion. 2008. *Users manual for TMY3 data sets*. Golden, U.S.A.: National Renewable Energy Laboratory.

Comparison Among Different Green Buildings Assessment Tools: Application to a Case Study

Benedetta Mattoni – Sapienza University of Rome – benedetta.mattoni@uniroma1.it

Francesco Asdrubali – Roma TRE University – francesco.asdrubali@uniroma3.it

Giorgio Baldinelli – University of Perugia – giorgio.baldinelli@unipg.it

Francesco Bianchi – University of Perugia – bianchi.unipg@ciriaf.it

Fabio Bisegna – Sapienza University of Rome – fabio.bisegna@uniroma1.it

Luca Evangelisti – Niccolò Cusano University – luca.evangelisti@unicusano.it

Paola Gori – Roma TRE University – paola.gori@uniroma3.it

Gianluca Grazieschi – Niccolò Cusano University – gianluca.grazieschi@unicusano.it

Claudia Guattari – Roma TRE University – claudia.guattari@uniroma3.it

Abstract

The concept of green building plays a role of primary importance in the reduction of the use of resources, water, and materials, as well as on the reduction of impacts on human health and the environment, during the building lifecycle. A large number of countries has already developed energy certification procedures in order to rate the building energy performance; furthermore, a range of green building assessment tools and protocols has been developed in the past 20 years, with the aim of reducing energy consumption and the environmental impact in both the building construction and management phases. This paper compares the results of the application of three green building assessment methods on both the energy and environmental performance. Some of the most spread rating systems were chosen: Istituto per l'innovazione e Trasparenza degli Appalti e la Compatibilità Ambientale (ITACA, Italy), Comprehensive Assessment System for Built Environment Efficiency (CASBEE, Japan), and Green Star (Australia). The analysis was developed on a residential building located in central Italy, constructed by taking into account the international principles of sustainability and bioclimatic architecture. Starting from previous studies developed by the Authors, by which these protocols were compared and their scores normalized, the proposed study assesses the sustainability of the case-study building thanks to a point-based methodological approach. It is based on the identification of six common macro-areas that allow the homogeneous comparison of the three green building assessment tools. The study aims to assess the impact of these new normalized

categories on the overall sustainability performance of the building.

1. Introduction

Buildings are responsible for a considerable part of the energy consumption and greenhouse gas emissions, and according to Swan and Ugursal (2009), they account for 40 % of the total energy consumption of the European Union. This problem involves all the advanced countries in different ways, not only in terms of air pollution but also with regard to the availability of primary energy resources and balance between imported and exported energy. As a result, several actions for the energy and environmental preservation and for the rational use of resources have been recently undertaken by the national governments: in Italy the energy efficiency of buildings is the primary goal, while energy labelling is gaining importance all over the world. Several findings in literature affirm that increasing the buildings energy efficiency is a primary goal (Boyano et al., 2009; Evangelisti et al., 2015a) and many solutions have been introduced aiming at reducing the building sector environmental impacts (Gori et al., 2016; Evangelisti et al., 2015b; Mattoni et al. 2015). Furthermore, in the last years, the so-called green rating systems have been developed in order to estimate the buildings sustainability level in a

broader way, including other aspects in addition to energy consumptions. The sustainability concept is defined by ISO 15392:2008 in three ways: economic, environmental, and social. Recently the attention is focused on environmental sustainability, and different programs and methods related to this aspect are flourishing all over the world. The Life Cycle Analysis, for example, initially developed in the industrial world, is now being spread also to the building sector with the goal of quantifying the potential environmental impacts linked to the construction process. The private sector has promoted different initiatives both at a national and international level. In this framework, a huge number of green building assessment tools and protocols has been developed in the past 20 years. Among these, the most famous sustainable protocols at international level are LEED (Leadership in Energy and Environmental Design) from the U.S., CASBEE (Comprehensive Assessment System for Built Environment Efficiency) from Japan, Green Star from Australia, and BREEAM (Building Research Establishment Environmental Assessment Method) from the UK. In Italy also the public sector has promoted a sustainability protocol called ITACA (in English: Institute for Transparency of Contracts and Environmental Compatibility). Some of these protocols, such as LEED and BREEAM, are applied all over the world with different specifications according to the features of the local country. The protocols aim at defining standards and parameters to evaluate the level of sustainability in the building sector and to reduce the energy use during the life cycle of the buildings at a prescriptive and voluntary level. They consist in methodological approaches that analyze energy consumptions, the characteristics of the site, the indoor well-being, and the effects on human health. The different calculation methods and credits of the labelling tools can lead to significant differences in the final sustainability scores of a building (Suzer, 2015; Bahaudin et al., 2014). These differences are both at a national and regional level: in fact, in a country it is possible to find also different versions of the same protocol. ITACA, for example, is a federation of different protocols of the Italian regions characterized by a common methodology and by common technical-scientific requirements. This diversification allows us to take into account

local peculiarities, like climate characteristics or constructive practices. Despite the need of considering the distinctive features of each territorial context, the building sustainability level in the globalized world should be hopefully comparable among different countries. This objective could be achieved by defining common targets, aims, and requirements.

In this framework, the present study applies the well-known rating systems ITACA, CASBEE, and Green Star to the green building complex "Le Violette", located in Foligno, Perugia (Italy) with the aim of highlighting differences and similarities between the rating tools. The original and latest editions of these rating systems were taken into account considering only the residential building versions of these protocols.

The application of these systems to a real case allows us to understand which issues have more influence on the final performance rate of each protocol. The work also gives some suggestions for the reduction of the dissimilarities between the rating systems, and for the definition of a common "sustainability language".

2. Method and Tools

The goal of this paper is to evaluate the results obtained through the application of the original tools and to make a comparison among the studied protocols by means of a point-based system. In this new methodological approach, the original credits of the protocols were grouped into six new common macro-areas (Table 1). This approach allows to overcome the differences between the original categorizations of the three-certification procedures, and to assess the impact and the influence of these new normalized categories on the final sustainability performance of each analyzed rating system.

Table 1 – New categories of impact

Macro-Areas	Description
Site	Influence of the site characteristics on the building
Water	Total water use
Materials	Impact of building materials from cradle to grave
Energy	Energy use and renewable energy production
Comfort and safety	Indoor human well-being and functional characteristics of interior spaces and safety
Outdoor quality	Impacts on the outdoor environment

2.1 The Methodological Approach

The comparison among the chosen green building rating systems was carried out in order to underline similarities and differences in their approaches. Each tool is characterized by a certain number of macro-areas that are divided into credits achievable on the basis of the building characteristics; each credit is also characterized by a "weight" that stands for the importance given to the specific credit on the final score. Moreover, each rating system allows us to achieve a building labeling on the basis of the reached final score, which is the sum of the points gained for each credit, previously multiplied for their specific weights. It is worthy to notice that each certification system is characterized by a certain point total amount and it is distinguished by a precise number of achievable credits. Fig. 1 shows the original rating systems macro-areas; in this analysis only the credits related to the new residential buildings were considered. Starting from previous studies (Asdrubali et al., 2015; Bisegna et al., 2016), this work presents the comparison among ITACA, CASBEE, and Green Star sustainability rating scores by applying the six new macro-areas (see Fig. 2).

QI	Weight	CASBEE				GREEN STAR				ITACA					
		Q1	Q2	Q3	Q4	Q1	Q2	Q3	Q4	Q1	Q2	Q3	Q4		
Q1.1 - Noise & Acoustics	0.15	Q2.1 - Service Ability	0.4	Q3.1 - Preservation & Creation of Biotope	0.3	LR1.1 - Building Thermal Load	0.2	LR2.1 - Water Resources	0.2	LR3.1 - Consideration of Global Warming	0.33	LR4.1 - Efficient Operation	0.2	LR5.1 - Consideration of Local Environment	0.33
Q1.2 - Thermal comfort	0.35	Q2.2 - Durability & Reliability	0.3	Q3.2 - Townscape & Landscape	0.4	LR1.2 - Natural Energy Utilization	0.1	LR2.2 - Reducing Usage of Non-renewable Resources	0.6	LR3.2 - Consideration of Local Environment	0.33	LR4.2 - Efficient Operation	0.2	LR5.2 - Consideration of Surrounding Environment	0.33
Q1.3 - Lighting & Illumination	0.25	Q2.3 - Flexibility & Adaptability	0.3	Q3.3 - Local Characteristics & Outdoor Amenity	0.3	LR1.3 - Efficiency in Building Service System	0.5	LR2.3 - Avoiding the Use of Materials with Pollutant Content	0.2	LR3.3 - Consideration of Surrounding Environment	0.33	LR4.3 - Efficient Operation	0.2	LR5.3 - Consideration of Surrounding Environment	0.33
Q1.4 - Air quality	0.25														
Management	Pt	Indoor environmental quality	Pt	Energy	Pt	Transport	Pt	Water	Pt	Materials	Pt	Land Use Ecology	Pt	Emissions	Pt
Green Star Accredited Professional	1	Indoor Air Quality	4	Greenhouse Gas Emissions	10	Sustainable Transport	10	Peak water	12	Life Cycle Impacts	7	Ecological Value	3	Storm water	2
Commissioning and Tuning	4	Acoustic Comfort	3	Peak Electricity Demand	20		20			Responsible Building Materials	3	Sustainable sites	2	Light pollution	1
Adaptation and Resilience	2	Lighting Comfort	3							Sustainable Products	3	Heat Island Effects	1	Microbial Control	1
Building information	2	Visual Comfort	3							Construction and demolition waste	1			Refrigerant impacts	1
Commitment to performance	2	Indoor Pollutants	2												
Metering and Monitoring	1	Thermal Comfort	2												
Construction environmental Management	1														
Operationalwise	1														
Site Quality	Pt	Resource consumption	Pt	Environmental Loads	Pt	Indoor Environmental quality	Pt	Service Quality	Pt	Indoor Environmental quality	Pt	Service Quality	Pt	Service Quality	Pt
Service Accessibility	4	Primary non-renewable energy required during the lifecycle	32.1	CO ₂ equivalent emissions	6.1	Ventilation	4.55	Maintenance of operational performance	3.5	Ventilation	4.55	Maintenance of operational performance	3.5	Do notok systems	3.2
		Energy from renewable sources	6.2	Waste water	11.40	Thermal Comfort	4.55	Acoustic Comfort	4.55	Thermal Comfort	4.55	Acoustic Comfort	4.55		
		Eco-friendly materials	9.70	Drinking Water	5.60	Visual Comfort	4.55	Visual Comfort	4.55	Visual Comfort	4.55	Visual Comfort	4.55		

Fig. 1 – Original rating systems macro-areas

The credits included in the original macro-areas of each system were distributed into the new six ones and their scores were normalized in order to make the tools comparable. In the normalization process the credits related to the management aspects were not taken into account because they include bureaucratic issues that do not match the purpose of this study. Similarly, also the innovation extra points that allow to get up to 10 extra points in each protocol, were not considered in the analysis.

CASBEE			
SITE	WATER	ENERGY	COMFORT AND SAFETY
Q3.1 Preservation and conservation of Biotope	LR2.1 Water Resources	LR1.1 Control of heat load	Q1.1 Sound Environment
Q3.2 Townscape and landscape		LR1.2 Natural Energy utilization	Q1.2 Thermal comfort
		LR1.3 Efficiency in building service systems	Q1.3 Lighting and illumination
		LR1.4 Efficient operation	Q1.4 Air Quality
			Q2.1 Service Ability
			Q2.2 Durability and Reliability
			Q2.3 Flexibility and Adaptability
GREEN STAR			
SITE	WATER	ENERGY	COMFORT AND SAFETY
Ecological value	Potable water	Greenhouse gas Emission (ENERGY)	Indoor Air Quality
Sustainable sites		Peak electricity demand reduction	Acoustic comfort
Stormwater			Lighting comfort
			Visual comfort
			Indoor pollutants
			Thermal comfort
ITACA			
SITE	WATER	ENERGY	COMFORT AND SAFETY
Service accessibility	Drinking Water Waste water	Primary non-renewable energy required during the lifecycle Energy from renewable sources	Ventilation
			Thermal Comfort
			Acoustic Comfort
			Visual Comfort
			Domestic systems

Fig. 2 – Distribution of credits for the new six macro-areas

2.2 The Applied Green Building Rating Systems

2.2.1 ITACA

In Umbria, where the building analyzed in this work is located, the regional law number 17 (2008) introduces the certification of the environmental sustainability in the building sector. The law is mandatory for public buildings and voluntary for the private ones. The evaluation of the buildings is realized by means of 22 technical sheets inspired by the ITACA protocol and customized to the local features. The protocol is divided into five macro-areas:

quality of the site, resource consumption, environmental loads, indoor environmental quality, and service quality.

A score is associated to every sheet from “poor” (-1) to excellent (+5); the sum of the scores, calibrated by the different weights given to every sheet, determines the score of each macro area. In the ITACA protocol the resource consumption has the heaviest weight (53.6 %), followed by Indoor environmental quality (18.2 %) and Environmental loads (17.5 %); service quality (6.7 %) and site quality (4 %) have the lowest weight. The sum of the scores of the macro areas gives the final score that classifies the building according to one of the five classes of sustainability provided: A+, A, B, C, D (see Table 2). If a building is in the D class, it is to be considered uncertified.

Table 2 – Final achievable scores in ITACA

Total Score	Class
100-85	A+
84-70	A
69-55	B
54-40	C
<40	D

2.2.2 CASBEE

In Japan, the governmental and academic project that worked on the CASBEE protocol was developed in 2001 by two organizations: The Japan Green Build Council (JaGBC) and the Japan Sustainable Building Consortium (JSBC). CASBEE identifies two main vectors that are considered incompatible and inversely proportional: the improvement of the environmental quality (Q) and the building environmental loads (L). The certification is not based on the sum of scores obtained from the different elements analyzed but on a simple scalar indicator named “Building Environmental Efficiency” (BEE) indicated and calculated as the ratio Q/L.

In CASBEE, the Environmental Quality (Q) measures the following assessment fields: quality of the indoor environment (Q1), the building service quality (Q2), and the quality of the surrounding site within the hypothesis space (Q3). On the other

hand, the Environmental Load (L) measures the following assessment fields: energy load on the environment (L1), the resources and material loads (L2), and the building environmental loads outside the enclosed space (L3). The classification of the building is realized through a special graph (Fig. 3) in which the domains of every class are represented, the Q result should be set on the vertical axis (y-axis) and the L result should be set on the horizontal axis (x-axis). Therefore, the efficient building is the one that is characterized by the least environmental load and the highest environmental quality. The ranks provided are S (excellent), A (very good), B+ (good), B- (fairly poor), and C (poor).

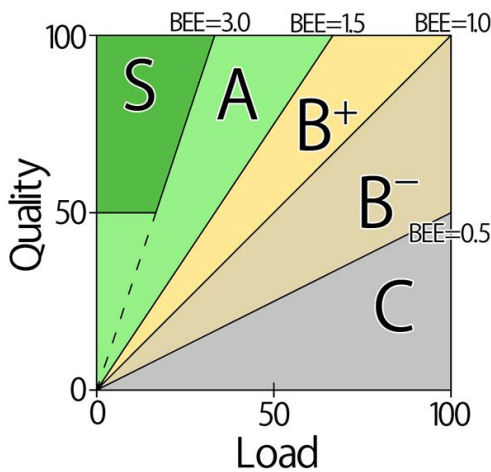


Fig. 3 – Graph for CASBEE classification

2.2.3 Green Star

Green Star was launched in 2003 by the Green Building Council of Australia and then, after having been customized and adapted to the local contexts, was adopted also in New Zealand and South Africa. The protocol identifies nine macro-areas: management, indoor environment quality, energy, transport, water, materials, land use & ecology, emissions, and innovation. Every category gives credits that address specific aspects of a sustainable building design, construction or performance with a total of 156 un-weighted points available for distribution to eight categories. Five extra points are available for the Innovation category but they are not considered in this paper. The weights of every category are: Management 9 %, Indoor Environmental Quality 17 %, Energy 19 %, Transport 8 %, Water 10 %, Materials 21 %, Land use & ecology 5 %, Emissions

11 %. The sum of the credits allows to classify the sustainability level of the building expressed through a number of Green Stars rating from 1 to 6 (Table 3). In this paper the “Design and As built” certification scheme was considered. This version of the protocol allows to certificate buildings only from Four to Six stars: scores under 45 points are insufficient for certification.

Table 3 – Green Star rating scores

Score	Rating	Category
10-19	One Star	Minimum Practice
20-29	Two Stars	Average Practice
30-44	Three Stars	Good Practice
45-59	Four Stars	Best Practice
60-74	Five Stars	Australian Excellence
75+	Six Stars	World Leadership

3. Case Study

The case study is represented by the green building complex “Le Violette”, located in Foligno, in the region of Umbria (Italy). It was built by taking into account the principles of sustainability in terms of both structural and technical solutions (Fig. 4). The building is characterized by a modern style but, nevertheless, it is well integrated in the surrounding landscape. The structure has a regular shape (organised on four floors) and has a total of twelve flats sized are 71 and 90 m². Moreover, the building has 12 basement garages.

External solar shading systems are installed; the building is equipped both with “roof garden” and inclined roofs in order to allow the positioning of solar and photovoltaic panels. The heating system is centralized and characterized by radiant floors. It is powered by geothermal energy and heat pumps. The envelope of the building is well insulated through the employment of wood panels and expanded polystyrene.



Fig. 4 – The case study: “Le Violette” complex

4. Results and Discussion

The first step of this study was the application of the original rating systems to the analyzed building. It can be seen that the building achieved 57.71 % of the total score applying the ITACA protocol, and is certified “B level” (Table 4); the CASBEE system gave a score equal to 1.8 BEE index, which represents the “A” level (4/5 Stars) (Table 5). Finally, the application of Green Star gives 45 % of the score that corresponds to a rating of “Four Stars” (Best Practice) (Table 6).

Table 4 – Points achieved by applying the original version of ITACA

Original Areas	Points
Site quality	0.80
Resource consumption	34.14
Environmental loads	15.12
Indoor environmental quality	6.37
Service quality	1.28
Certification Level: B	57.71

These dissimilarities in the results can be referred on one side to the different range of achievable credit points and on the other side to the number and typology of credits available for the sustainability assessment. For example, Green Star has a narrow range of points and generally assigns one or zero points for each credit; thus, if the building cannot achieve the strict requirements defined by the credit, the score obtained is 0.

Table 5 – Points achieved by applying the original version of CASBEE

Original Areas	Points
Q1 Indoor environment	3.6
Q2 Quality of service	3.2
Q3 Outdoor environment on site	3.5
LR1 Energy	4.2
LR2 Resources & Materials	2.8
LR3 Off-site environment	3.7
Certification Level: A	BEE:1.8

On the contrary, both CASBEE and ITACA are characterized by a wider range, and it is easier to get a better score (0÷5 points for CASBEE and -1÷5 for ITACA): even though the maximum points cannot be reached, halfway performance can be assessed anyway with a medium score (i.e. 3 points). Furthermore, CASBEE takes into account more aspects and sustainability issues compared to Green Star and ITACA. These motivations influenced the final score of CASBEE, which results in being the highest one.

In the second step, the results gained by the three rating tools were compared by applying the new six macro-areas to highlight the main differences in the composition of the total score.

Table 6 – Points achieved by applying the original version of Green Star

Original Areas	Points
Management	6
Indoor environment quality	13
Energy	4
Transport	1
Water	3
Materials	6
Land use & Ecology	3
Emissions	5
Innovation	4
Certification Level: 4 Stars	45

Once the new macro-areas were filled with credits, the scores were normalized on the basis of 100, in order to verify the importance that each rating method gives to the different aspects.

Fig. 5 shows the points achieved in each rating system after the application of the new six macro-areas. The figure allows us to understand the percentage points achieved for each new macro-area by the studied building, compared to the maximum achievable.

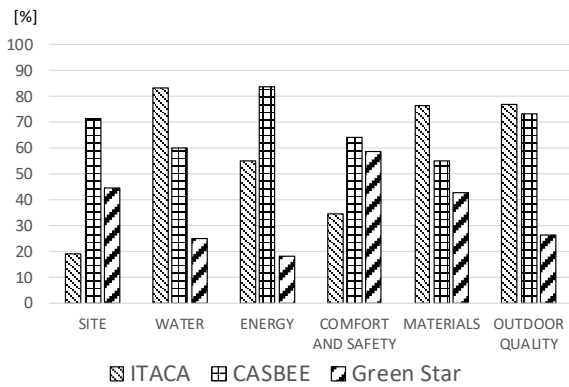


Fig. 5 – Comparison among ITACA, CASBEE and Green Star results (new macro-areas).

Moreover, Fig. 5 provides the comparison among the rating systems and highlights that:

- By applying ITACA, the building obtained the highest percentage of the reachable score in Water category (83.56 %), followed by Materials (76.60 %) and Outdoor Quality (77.20 %) categories, compared to the other protocols. On the other hand, the lowest scores were achieved in Site (where this rating system obtains a score lower than 20 %) and Comfort and Safety (where ITACA reaches a score of about 35 %);
- By employing CASBEE, the building results as the most efficient only in Energy category (84 %), Site (71 %) and Comfort and safety (63 %), compared to the other rating systems. It is possible to observe that CASBEE results are high and comparable among the six new macro-areas: all its scores range between 55 % and 84 % and, due to this, the building scores the best certification level;
- By using Green Star, the building always achieved the lowest scores, compared to the other protocols, except for the Site and Comfort and Safety categories, in which the worst was given by ITACA. In particular, by using Green Star, the building obtains scores lower than 20 % in Energy and lower than 30 % in Water. On the contrary, the highest scores were

achieved in Comfort and Safety (about 60 %) and Site (about 44 %).

It can be noticed that the highest final score reached by applying the CASBEE rating system (Level A-very good) is related to the fact that a high and homogenous amount of points in the six macro-areas was obtained (as mentioned, it ranges between 55 % and 84 % of the total achievable points). On the contrary, for the other two systems, the obtained scores for each macro-area have high variabilities. Despite the fact that ITACA is the most widely applied green rating tool in Italy and we should expect to gain the best certification level through its application, ITACA scores range between 19 % and 84 %, highlighting results that are not comparable between the new six macro-areas. Also by employing Green Star the score was quite unsatisfying, it is homogenous with ITACA, in fact it ranges between 18 % and 60 %.

5. Conclusion

This paper proposes a comparative study among three building environmental assessment methods, ITACA, CASBEE, and Green Star.

The tools were firstly applied to a residential building located in Italy; then, the results were compared by using a methodological approach based on the definition of six new macro-areas.

This approach allowed us to underline the main differences and analogies among the protocols, by subdividing and distributing their credits into the six new categories (site, water, energy, comfort and safety, materials, and outdoor quality) and by normalizing them on the basis of 100. The building achieved very different final scores with the three systems: the best was CASBEE while the worst was Green Star.

It is a bit surprising that the building achieved a better score with the CASBEE method than with ITACA, considering the fact that the latter is widely adopted in Italy. This circumstance is probably related to the different range of achievable credit points and the number and typology of credits available for the sustainability assessment.

It is worthy to notice that by analyzing in detail each macro-area, high differences among the performance rates given by each tool were observed. It is therefore possible to assert that it is difficult to achieve a common sustainability language due to different calculation models, different credits, and weights applied by each green rating systems. There is therefore the need to homologate the targets of sustainability by defining a set of sustainable issues regulated by common principles shared all over the world.

References

- Asdrubali, F., G. Baldinelli, F. Bianchi, S. Sambuco. 2015. "A comparison between environmental sustainability rating systems LEED and ITACA for residential buildings". *Building and Environment* 86:98–108. doi.org/10.1016/j.buildenv.2015.01.001.
- Bahaudin, A.Y., E.M. Elias, A.M. Saifudin. 2014. "A comparison of the green Building's Criteria". In: *Proceedings of the Emerging Technology for Sustainable Development Congress*. Bangi, Malaysia. doi: 10.1051/e3sconf/20140301015.
- Bisegna, F., B. Mattoni, P. Gori, F. Asdrubali, C. Guattari, L. Evangelisti, S. Sambuco, F. Bianchi. 2016. "Influence of Insulating Materials on Green Building Rating System Results". *Energies* 9(9):712. doi:10.3390/en9090712.
- Boyanoa, A., P. Hernandez, O. Wolf. 2013. "Energy demands and potential savings in European office buildings: case studies based on Energy Plus simulations." *Energy and Buildings* 65: 19–28. doi.org/10.1016/j.enbuild.2013.05.039.
- Evangelisti, L., C. Guattari, P. Gori. 2015a. "Energy retrofit strategies for residential building envelope: An Italian case study of an early-50s building." *Sustainability* 7:10445–10460. doi:10.3390/su70810445.
- Evangelisti, L., C. Guattari, P. Gori, R. De Lieto Vollaro. 2015b. "In situ thermal transmittance measurements for investigating differences between wall models and actual building performance." *Sustainability* 7(8):10388–10398. doi:10.3390/su70810388.
- Gori, P., C. Guattari, L. Evangelisti, F. Asdrubali. 2016. "Design criteria for improving insulation effectiveness of multilayer walls." *International Journal of Heat and Mass Transfer* 103:349–359. doi.org/10.1016/j.ijheatmasstransfer.2016.07.077
- Homepage of BREEAM. Accessed on 23 November 2016. <http://www.breeam.com>.
- Homepage of CASBEE. Accessed on 23 November 2016. <http://www.ibec.or.jp/CASBEE/english/overviewE.htm>.
- Homepage of Green Star. Accessed on 23 November 2016. <https://www.gbca.org.au/green-star/rating-tools/>.
- Homepage of Istituto per l'innovazione e Trasparenza degli Appalti e la Compatibilità Ambientale (ITACA). Accessed on 23 November 2016. <http://www.itaca.org>.
- ISO. 2008. *ISO 15392:2008 Sustainability in building construction - General principles*. Geneva, Switzerland: ISO.
- Mattoni, B., P. Gori, F. Bisegna. 2015. "A step towards the optimization of the indoor luminous environment by genetic algorithms". *Indoor and Built Environment* 26(5): 590–607. doi: 10.1177/1420326X15608229.
- Suzer, O. 2015. "A comparative review of environmental concern prioritization: LEED vs other major certification systems." *Journal of Environmental Management* 154:266–283. doi.org/10.1016/j.jenvman.2015.02.029.
- Swan, L.G., V.I. Ugursal. 2009. "Modeling of end-use energy consumption in the residential sector: a review of modeling techniques." *Renewable and Sustainable Energy Reviews* 13(8): 1819–1835. doi: 10.1016/j.rser.2008.09.033.
- U.S. Green Building Council. Accessed on 23 November 2016. www.usgbc.org.

Integrated Numerical Analysis and Building Information Modeling for Cultural Heritage

Elena Gigliarelli – ITABC, CNR – elena.gigliarelli@itabc.cnr.it

Filippo Calcerano – ITABC, CNR – filippo.calcerano@itabc.cnr.it

Michele Calvano – Sapienza University of Rome – michele.calvano@uniroma1.it

Francesco Ruperto – Sapienza University of Rome – francesco.ruperto@uniroma1.it

Mario Sacco – Studio Arcrea, Rome – arch.mariosacco@gmail.com

Luciano Cessari – ITABC, CNR – luciano.cessari@itabc.cnr.it

Abstract

The use of numerical simulation applied to heritage buildings triggers a tremendous increase in complexity and at the present time, few studies focus on this issue and the problems of their calibrations. The difficulties are affected by many factors: the complex geometry involved, the non-standardization of building elements, the inertial behaviour of the wall masses, the importance of moisture transport; in short, the complexity of managing the design workflows in a conservation project of historical buildings. The integration of numerical simulation and Building Information Modeling is not yet automated and relies heavily on the manual steps and the individual experience. The research analyses the high potential of the use of the simulation of building performance, and the computational design along with Heritage Building Information Modeling, with the aim of pushing the three technologies to their potential limits, and promote their evolution towards an easier practical application. The paper presents an experimental HBIM workflow applied to a case study of a building located in an Italian historic centre and discusses a number of problems that still exist in the application of these workflows. They range from finding a correct set of information necessary for the analysis to the lack of interoperability that still exists between the software, up to the difficulties of the methodological approach. The results show that through a combination of recent open source software constantly evolving, it is possible to overcome some of the obstacles that prevent an effective interoperability between individual software, paving the way for an increasing number of useful solutions in the built heritage conservation.

1. Introduction

The construction industry in Europe is responsible for about 40 % of the total energy consumption and 36 % of CO₂ emissions (Economidou et al. 2011; Berardi, 2015). The European Commission has undertaken several actions to reduce energy consumption in the building sector with two directives on the energy performance of buildings (EPBD 2002 and EPBD 2010 recast), but because of the difficulties in finding energy efficiency measures compatible with architectural, historical and cultural heritage values of the built environment, (also very vulnerable to climate change, Kilian et al. 2010) historical buildings have been excluded from these directives (European Parliament, 2012). However there is a large untapped potential in these interventions (Martínez-Molina et al. 2016; D’Ambrosio et al. 2015; Ascione et al. 2015), and in recent years, thanks to the adoption of the concept of energy efficiency as a tool to protect and support the conservative process, rather than a legislative restriction (Carbonara, 2015), the conflict between conservation practices and energy efficiency measures seems to be finally solved.

1.1 Building Performance Simulation and Built Heritage

Among the latest technical instruments to improve energy efficiency of the built heritage, building performance simulation (BPS) is one of the most promising. BPS is primarily a powerful tool for understanding complex phenomena (Clarke et al., 2015),

moreover it enables innovative applications in restoration design process and in non-destructive pre-diagnostics and diagnostics of cultural heritage. This depends also on its capability of providing feedback on energy and environmental implications of conservation interventions and on changes-embedded in the deterioration process. In spite of the possibilities of use offered by these tools, their applications are still few in the early stages of building design practice and even less in case of historic buildings, with a concentration of implementation examples in the Italian context (Ascione et al., 2015; Roberti et al., 2015; Cornaro et al., 2016). This is mainly due to the complexity inherent the historic building from a simulative point of view connected with the complex geometry involved, the lack of standardised building elements, the inertial behaviour of the wall masses, the importance of moisture transport, and not secondarily, the reluctant attitude of architects to use these tools in the design process (Paryudi, 2015). A major barrier to simulation tools in conservation design processes consists in fact in how to deal with a great amount and variety of information and with the complexity of architectural features (geometry representation, building envelope, survey of the passive behaviour, historical material characterisation, etc.) that must be taken into consideration with historic buildings.

1.2 The Heritage–BIM Approach and Interoperability with Building Performance Simulation

A historic building is characterized by a multitude of heterogeneous information that go beyond its physical and geometrical characteristics (Saygi et al., 2013). As demonstrated by a series of studies (Logothetis et al., 2015), the Building Information Modeling (BIM) technology seems capable of triggering a new evolution of an integrated and efficient management of the knowledge produced by the conservation process. In the field of Heritage Building Information Modeling (HBIM) after the first experiments on geometry representation (Murphy, 2012; Dore et al., 2015) the researches are gradually following other multidisciplinary studies based on interoperability with structural analysis (Oreni et al., 2014; Bassier et al., 2016), building

operation and management (Barazzetti et al., 2016), documentation and design of restoration intervention (Gigliarelli et al., 2015) and environmental and energy retrofit (Gigliarelli et al., 2016). Since an HBIM model already contains a large amount of data required for a building simulation, interoperability can save time and costs while reducing errors and mismatches (Rahmani Asl et al., 2013). Unfortunately, the integration between BIM and simulation environments is still a complex issue, still in the development phase (Ivanova et al., 2015; Senave et al., 2015; Maile et al., 2013): the attempts of the BIM world to interact with the simulations have not yet produced satisfactory results. Using IFC format or gbXML certification it is still not possible to effectively transfer all the data needed for the simulation (Ahn et al., 2014), and often the BIM-based model for a BPS ends up so heavily influenced by the purpose of simulation to be of little use at an architectural level which results in a parallel modeling. On the other hand numerical simulations are still used as a combination of science and art based on the user's experience (Hitchcock et al., 2011), a non-standardized process that suffers the dichotomy between architecture and building a thermal vision (Wilkins et al., 2008). Information modelling, interoperability and knowledge management within the Heritage BIM become even more strategic within the legislative and regulatory framework that is being developed in various European countries also as a result of the European Directive 2014/24/EU on public procurement (European Parliament, 2014). With the Article 22 c.4 4. of the Directive 2014/24/EU "For public works contracts and design contests, Member States may require the use of specific electronic tools, such as of building information electronic modelling tools or similar" the legislator seems to guide all EU member states towards a BIM-based approach for public procurement even on historic buildings and highlights the need of a conscious adoption of methodologies and tools for building information modeling based on open standards for interoperable data.

2. Methodology

2.1 Proposed Approach, Needed Expertise, and Workflow

Given the current BIM-BPS interoperability limitations and additional complexities arising from the selected historical building, we opted for a semi-automated interface that is more reliable and suited to the task compared to a fully automated interface, thanks to its possibility of human intervention in the process (Ahn et al., 2014). The undertaken solution has exploited the computational design (CD) that is used today mainly for the generation of aesthetic form but has a huge untapped potential in performance-based design (Rahmani Asl et al., 2013) as an intermediate step between the two environments. Four specific experts were involved in the process: the conservation expert who followed the entire procedure from data collection up to the control of the results in terms of architectural HBIM and energy simulation, the BPS expert who contributed from the analytical phase through all the other steps to check the interoperability between the software, the BIM expert, and the CD expert. In conventional workflows geometry and building components modelling are executed in parallel between BIM and BPS, starting from a common multidisciplinary analysis (Fig. 1).

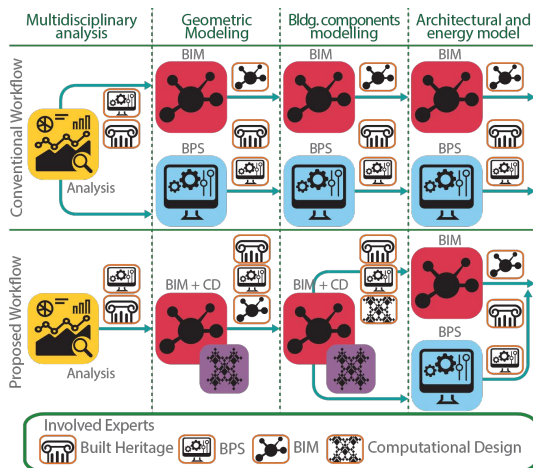


Fig. 1 – Conventional and proposed workflow to avoid parallel modeling and datasets

After a series of tests and experimentations, a new highly effective design workflow is presented, a process in which from the BIM software Archicad,

the geometry is exported through gbXML schema, the opaque and transparent building elements through spreadsheets. Both data are then acquired inside the Rhinoceros-Grasshopper CD environment and then translated into an .idf file (EnergyPlus file format) through the two plug-ins of Grasshopper Ladybug and Honeybee (Roudsari et al., 2013).

The following workflow has been used (Fig. 2) to verify, under the coordination of the conservation expert, that the HBIM-generated information was correctly received by EnergyPlus:

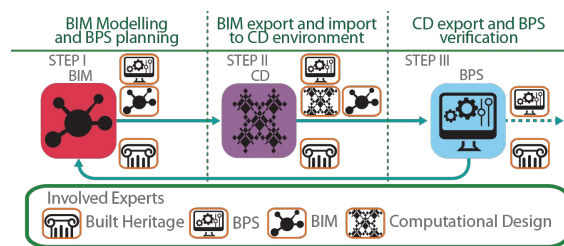


Fig. 2 – Testing workflow

- In the first step, HBIM modelling is performed while planning for the BPS the thermal zones or surfaces sub-division due to different boundary conditions or different building constructions;
- in the second step the model is exported from HBIM in a format that can be easily acquired inside the computational design environment where a first check of errors is carried out;
- in the third step, the .idf file is written by Honeybee inside the CD environment, it is then checked inside EnergyPlus Idf Editor and the simulation is launched. If the data transfer resulted inconsistencies, the process starts again from the first step.

2.2 Case Study

The case study, located in the historic centre of Frigento, is a traditional terraced house resulted by the merging of two previous units, and partly rebuilt after the earthquake in Irpinia in 1980. After conducting an in-depth historical analysis of its construction and evolution, a metric and geometric survey of its three-dimensional consistency was performed. The metric and geometric representation of the building was based on 3D laser scanner surveys and photogrammetry surveys with telescopic

3DEYE, compared with old drawings, archived documents, data concerning the historic construction techniques and architectural details, and enriched with in-situ direct specific measurements. The building walls are characterised by three different kinds of masonry (mainly Castelluccio limestone, with the exception of the North side which is in tuff, and part of the reconstructed east side that is in hollow bricks), with plaster on both sides. The windows are double-glazed, the floor is weakly insulated and ventilated with a crawl space: the first floor was rebuilt over the existing wood beams (retained) in reinforced concrete and hollow tiles with iron beams. The roofs were reconstructed in wood with weak insulation. Non-destructive diagnostic tests such as infrared thermography, magnetic analysis, and heat flux measures, were performed to determine thermo-physical characteristics and critical points. The energy request of the building was retraced through monthly energy bills.

2.3 Thermal Zoning and Energy Modelling

The first geometric interoperability tests were performed on very simplified models in a three-step process (Fig.3).

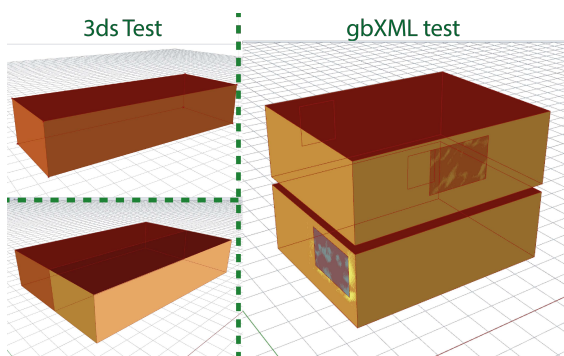


Fig. 3 – Geometric interoperability test models

First, the simple mass created by Archicad was exported in the .3dm file format of Rhinoceros, and then imported inside Rhinoceros to test the geometric functions of Honeybee (i.e. the transition from CD to BPS). Next a second simple volume was added in Archicad to verify surface matching of two adjacent surfaces for thermal zoning. In the third step a more complex geometry with walls thicknesses was modelled by Archicad and exported in .xml format through the gbXML schema. This

allows the test of a zone creation, openings and surface matching separated by a gap corresponding to the thickness of the wall.

After these tests it was possible to address the specific complexities required by a thermal zoning and geometry representation of the heritage building, starting from the architectural model in HBIM. This approach simplified the design of the simulation and its thermal zoning because it allowed planning building simulation directly on an existing model. The building was divided into three thermal zones (ground floor, first floor, and north attic) in order to maintain the geometric representation of the masses only when it becomes crucial for the numerical representation (i.e. internal floors exposed to the sun). Therefore, some internal partition geometry was not exported into the energy model, since additional masses could be added later in EnergyPlus. Due to the massive characteristic of the building and to the great differences between walls, the HBIM-based energy model preserved all the existing thickness differences. This solution generated two problems on the model: the first was the creation of additional and not required surfaces in the automated generation of Archicad spaces (every time walls of different thicknesses were present on a coplanar surface). This barrier was eliminated by setting the construction of the walls on the internal axis in Archicad before exporting the file through the gbXML schema. The manual intervention highlighted the need for a better automation of the space construction, capable to bypass a heritage building typical problem that occurs when thermal zones are different from the spaces defined by real internal partitions.

To solve the second problem, linked to the thermal zoning as well, the boundary condition for the Archicad spaces was removed from two internal partitions. Then in Archicad two virtual surfaces were modelled in parallel (Fig.4, last model, green areas) with space boundary properties in order to replace spaces as needed for thermal zoning. It is recommended a better space modification ability in Archicad to reduce the geometric issues arising from the thermal zoning.

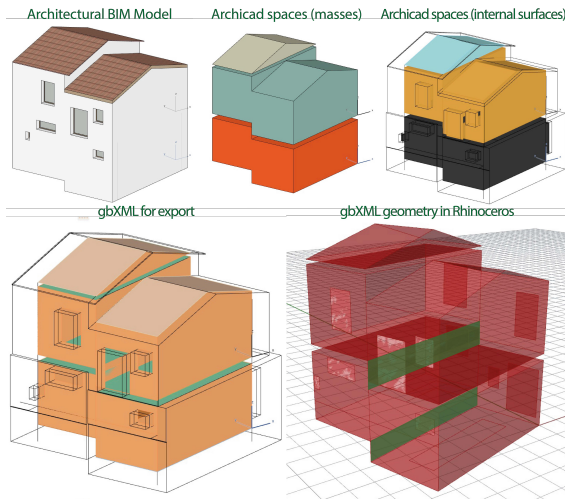


Fig. 4 – Generation of the thermal model from the BIM environment

Geometric modelling was completed by adding the geometry of the surrounding buildings as shading surfaces for the simulation (Fig. 5). The reconstruction resulting from a laser scanner survey of the historic centre of Frigento was acquired and modelled in HBIM, transferred to Grasshopper and then to EnergyPlus.

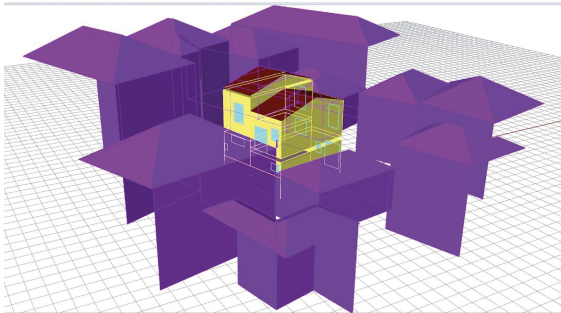


Fig. 5 – Geometry representation inside the Rhinoceros environment of the thermal zones and the context surfaces imported from the BIM model

2.4 Building Components Modelling

Building materials and construction elements were specified in Archicad and then acquired through spreadsheets generated by the software. The main problem to address in terms of compatibility concerns the different ways by which Archicad and EnergyPlus manage materials and construction elements. Firstly, in an Archicad environment the building material is defined by the thermo physical properties and the thickness is set up when creating the construction element (composites), while in an EnergyPlus environment the same material with different thicknesses has a different value and a

different name. Secondly, the materials stratigraphic sequence of some composites in Archicad is the inverse of the one required by the EnergyPlus construction elements (i.e. roofs). The solution of both problems was found in the CD environment where, once acquired from Archicad, materials were automatically duplicated and renamed according to their thickness value as required by EnergyPlus. For the construction elements the problem was solved by defining an additional value for each Archicad composites elements to be exported in the spreadsheet. This value was used to clearly indicate when and in which thermal zone a stratigraphy needed to be duplicated and reversed.

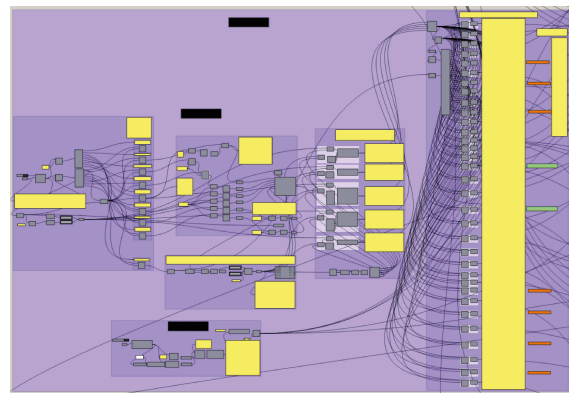


Fig. 6 – Grasshopper screenshot of the data acquisition for building materials and construction elements

These steps were needed to keep the HBIM model simple and as less as possible affected by modification generated for the simulation purpose. Although at the end of the process all the issues were addressed, the process required complex computational design software architecture (Fig. 6), this shows that a greater automation of the translation process inside the BIM environment is highly desirable.

2.5 EnergyPlus file check and simulation

In the final Grasshopper file (Fig. 7), the geometry and the building elements were manually matched inside the corresponding thermal zone, along with the rest of the input for the simulation through Honeybee. The generated .idf file and the error files of the simulation were then checked, they resulted in no errors.

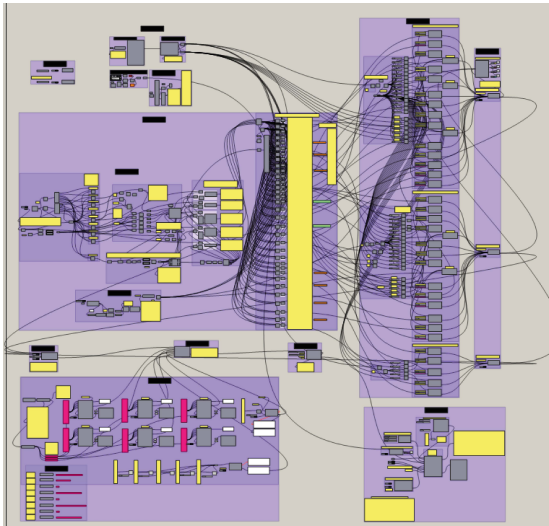


Fig. 7 – Grasshopper screenshot of the final Grasshopper file that links together Archicad and EnergyPlus

3. Results and Discussion

A new fully implemented methodology to link together Heritage-BIM and BPS is proposed that, through an integrated approach involving the joint work of a multidisciplinary team of experts (in conservation of architectural heritage, building performance simulation, building information modeling and computational design) in conjunction with the use of a set of up-to-date open source software is able to generate and modify geometry and building elements both for the thermal and the BIM model through an active and parametric link. The semi-automatic approach increases the speed by which reliable simulations can be produced and allows the team to intervene directly in all data transfers. There are still interoperability limits between the two software environments, that could be overcome through future research and tests by the team. However, its development represents a significant step towards the production of tools combining the parametric design process with performance analysis.

3.1 Future Research

Future research developments will aim to simplify and improve the proposed workflow that integrates the BIM with numerical simulations, reducing non-automated steps to limit the risk of errors and mismatch, while preserving the possibility of human

intervention, a crucial need raised by the conservation field. Additional possibilities for data exchange (i.e. schedules and internal gains) between the two environments will be further investigated along with the data visualisation of the simulation results inside the HBIM environment.

Acknowledgement

The data on the case study for the modelling come from METRICS project financed by PON Campania Research and Competitiveness 2007-2013 Programme.

Nomenclature

Acronyms

BPS	Building Performance Simulation
BIM	Building Information Modeling
HBIM	Heritage Building Information Modeling
CD	Computational Design

References

- Ahn, K.U., Y.J. Kim, C.S. Park, I. Kim, K. Lee. 2014. "BIM Interface for Full vs. Semi-Automated Building Energy Simulation". *Energy and Buildings* 68B: 671–678. doi:10.1016/j.enbuild.2013.08.063.
- Ascione, F., N. Bianco, R.F. De Masi, F. de’Rossi, G.P. Vanoli. 2015. "Energy Retrofit of an Educational Building in the Ancient Center of Benevento. Feasibility Study of Energy Savings and Respect of the Historical Value". *Energy and Buildings* 95: 172–183. doi:10.1016/j.enbuild.2014.10.072.
- Barazzetti, L., F. Banfi, R. Brumana. 2016. "Historic BIM in the Cloud". In: *Progress in Cultural Heritage: Documentation, Preservation, and Protection, Lecture Notes in Computer Science* 10058. doi: 10.1007/978-3-319-48496-9_9.
- Bassier, M., G. Hadjidemetriou, M. Vergauwen, N. Van Roy, E. Verstrynghe. 2016. "Implementation of Scan-to-BIM and FEM for the Documentation

- and Analysis of Heritage Timber Roof Structures". In: *Progress in Cultural Heritage: Documentation, Preservation, and Protection, Lecture Notes in Computer Science* 10058. doi: 10.1007/978-3-319-48496-9_7.
- Berardi, U. 2015. "Building Energy Consumption in US, EU, and BRIC Countries". *Procedia Engineering* 118: 128–36. doi:10.1016/j.proeng.2015.08.411.
- Carbonara, G. 2015. "Energy Efficiency as a Protection Tool". *Energy and Buildings* 95: 9–12. doi:10.1016/j.enbuild.2014.12.052.
- Clarke, J.A., J.L.M. Hensen. 2015. "Integrated Building Performance Simulation: Progress, Prospects and Requirements". *Building and Environment* 91: 294–306. doi:10.1016/j.buildenv.2015.04.002.
- Cornaro, C., V. Adoo Puggioni, R.M. Strollo. 2016. "Dynamic Simulation and on-Site Measurements for Energy Retrofit of Complex Historic Buildings: Villa Mondragone Case Study". *Journal of Building Engineering* 6: 17–28. doi:10.1016/j.jobe.2016.02.001.
- D'Ambrosio, F.R., L. Mazzarella, P. Romagnoni. 2015. "Special Issue: Historic, Historical and Existing Buildings: Designing the Retrofit. An Overview from Energy Performances to Indoor Air Quality". *Energy and Buildings* 95: 1–218 Amsterdam, The Netherlands: Elsevier.
- Dore, C., M. Murphy, S. McCarthy, F. Brechin, C. Casidy, E. Dirix. 2015. "Structural Simulations and Conservation Analysis -Historic Building Information Model (HBIM)". *The International Archives of the Photogrammetry, Remote Sensing and Spatial Information Sciences* XL-5/W4.
- Economidou, M., B. Atanasiu, C. Despret, J. Maio, I. Nolte, O. Rapf. 2011. *Europe's Buildings under the Microscope. A Country-by-Country Review of the Energy Performance of Buildings*. Brussels, Belgium: Buildings Performance Institute Europe (BPIE).
- European Parliament. 2012. *Directive 2012/27/EU of the European Parliament and of the Council of 25 October 2012 on Energy Efficiency*. Brussels, Belgium: European Parliament.
- European Parliament. 2014. *Directive 2014/24/EU of the European Parliament and of the Council of 26 February 2014 on Public Procurement and Repealing Directive 2004/18/EC*. Brussels, Belgium: European Parliament.
- Gigliarelli, E., F. Calcerano, L. Cessari. 2016. "Implementation Analysis and Design for Energy Efficient Intervention on Heritage Buildings". In: *Progress in Cultural Heritage: Documentation, Preservation, and Protection, Lecture Notes in Computer Science* 10058. doi:10.1007/978-3-319-48496-9_8.
- Gigliarelli, E., G. Quattrone, L. Cessari. 2015. "Documentation Tools and Decision Systems for Built Heritage Rehabilitation". In: *Proceedings of the 2nd International Conference on Preservation, Maintenance and Rehabilitation of Historic Buildings and Structures*. Oporto, Portugal: Green Lines Institute for Sustainable Development.
- Hitchcock, R.J., J. Wong. 2011. "Transforming Ifc Architectural View Bims for Energy Simulation". In: *Proceedings of Building Simulation 2011: 12th Conference of International Building Performance Simulation Association*. Sydney, Australia: IBPSA.
- Ivanova, I., K. Kiesel, A. Mahdavi. 2015. "BIM-Generated Data Models for EnergyPlus: A Comparison of gbXML and IFC Formats". In: *Proceedings of Building Simulation Applications BSA 2015 2nd IBPSA-Italy Conference Bozen-Bolzano*. Bolzano, Italy; BUPRESS.
- Kilian, R., J. Leissner, F. Antretter, K. Holl, A. Holm. 2010. "Modeling Climate Change Impact on Cultural Heritage - The European Project Climate for Culture". In: *Effect of Climate on Built Heritage, WTA-Colloquim*. Eindhoven, The Netherlands.
- Logothetis, S., A. Delinasiou, E. Stylianidis. 2015. "Building Information Modelling for Cultural Heritage: A Review". *ISPRS Annals of the Photogrammetry, Remote Sensing and Spatial Information Sciences* II-5/W3.
- Maile, T., J. O'Donnell, V. Bazjanac, C. Rose. 2013. "BIM-Geometry Modelling Guidelines for Building Energy Performance Simulation". In: *Proceedings of BS2013: 13th Conference of International Building Performance Simulation Association*. Chambéry, France: IBPSA.
- Martínez-Molina, A., I. Tort-Ausina, S. Cho, J.L. Vivancos. 2016. "Energy Efficiency and Thermal Comfort in Historic Buildings: A Review".

- Renewable and Sustainable Energy Reviews* 61: 70–85. doi:10.1016/j.rser.2016.03.018.
- Murphy, M. 2012. "Historic Building Information Modelling (HBIM). For Recording and Documenting Classical Architecture in Dublin from 1700 to 1830". *PhD Thesis*. Dublin, Ireland: Trinity College Dublin.
- Oreni, D., R. Brumana, S. Della Torre, F. Banfi, L. Barazzetti, M. Previtali. 2014. "Survey Turned into Hbim: The Restoration and the Work Involved Concerning the Basilica Di Collemaggio after the Earthquake (L'Aquila)". *ISPRS Annals of the Photogrammetry, Remote Sensing and Spatial Information Sciences II-5*.
- Paryudi, I. 2015. "Architects and Energy Simulations Tool". *International Journal of Scientific & Technology Research* 4(3):80-82.
- Rahmani Asl, M., S. Zarrinmehr, Y. Wei. 2013. "Towards BIM-based parametric building energy performance optimization". *ACADIA 2013 Adaptive Architecture*. Toronto, Canada: Riverside Architectural Press.
- Roberti, F., U. Filippi Oberegger, A. Gasparella. 2015. "Calibrating Historic Building Energy Models to Hourly Indoor Air and Surface Temperatures: Methodology and Case Study". *Energy and Buildings* 108: 236–43. doi:10.1016/j.enbuild.2015.09.010.
- Roudsari, M.S., M. Pak. 2013. "Ladybug: A Parametric Environmental Plugin for Grasshopper to Help Designers Create an Environmentallyconscious Design". In: *Proceedings of BS2013: 13th Conference of International Building Performance Simulation Association*. Chambéry, France: IBPSA.
- Saygi, G., G. Agugiaro, M. Hamamcioğlu-Turan, F. Remondino. 2013. "Evaluation of GIS and BIM roles for the information management of historical buildings." *ISPRS Annals of the Photogrammetry, Remote Sensing and Spatial Information Sciences II-5/W1*.
- Senave, M., S. Boeykens. 2015. "Link between BIM and Energy Simulation". *WIT Transactions on The Built Environment* 149: 341-352. doi:10.2495/BIM150291.
- Wilkins, C., A. Kiviniemi. 2008. "Engineering-Centric BIM." *ASHRAE Journal* December 2008.

Weather Scenario Generation for Stochastic Model Predictive Control Using Vector Autoregressive Prediction

Samuel R. Currie – University of Colorado – samuel.currie@colorado.edu

Gregor P. Henze – University of Colorado – gregor.henze@colorado.edu

Abstract

Conventional building energy simulation utilizes characteristic locational weather data to illustrate the typical operation of the modeled facility, generally to provide design or capital investment insight. Because of the uncertainty in the weather, the assumptions behind typical meteorological year (TMY) data tend to perform poorly in building energy modeling applications for real-time control such as model predictive control (MPC) of passive building thermal mass. To account for weather uncertainty in such operational context, we present a strategy for creating an arbitrary number of plausible near-future weather scenarios via a vector autoregressive (VAR) time-series prediction framework. This approach allows us to preserve the relationships between several spatiotemporally interrelated weather variables, for example dry-bulb temperature and absolute humidity, by capturing the variance in the joint time-series. Results from several climates are presented for 24-hour predictions of psychrometric and solar weather variables for a range of samples sizes and the application to stochastic MPC is highlighted.

1. Introduction: MPC for Space Temperature Setpoints

In a perfect world, in which we had perfect forecasts of future weather events, a commercial building could be controlled by adjusting the space temperature setpoints and other operational parameters in order to both keep occupants comfortable and minimize either energy consumption or utility cost according to the conditions that the building will experience in the near future. These optimized strategies would take advantage of the thermal capacitance of construction materials (structural steel and concrete) and interior furnishings (e.g. system

furniture) to store heat and release it at a later time.

This type of control would require:

1. A model to represent the behavior of the building in response to weather variables
2. A mechanism for forecasting future weather and other uncertain driving variables

Building energy modeling is common today and is typically employed during the design phase of a new construction project or during retro-commissioning of an existing facility. Unfortunately, perfect weather forecasts do not exist. Statistical models that represent plausible weather forecasts have been in use for decades; the difference between these plausible scenarios and the weather events that will eventually unfold represents our uncertainty in using this data for MPC. We can attempt to account for this uncertainty by using a range of plausible weather scenarios to account for what may occur, as opposed to a single forecast. Here, an MPC strategy would implement a control strategy that performs best over the entire range of possibilities in an attempt to protect ourselves from the mismatch between forecast and actual weather. The established methods of accounting for this range of possibilities are robust MPC, which examines and prepares for the extreme events that may occur, and stochastic MPC, which uses random but statistically likely events instead in an attempt to reduce the conservatism inherent in robust MPC.

2. Uncertainty Characterization

A typical energy model can be considered as a “grey box” representation of a building. That is, it uses physics based models of heat transfer phenomena enhanced by empirical data and statistical models to

represent equipment performance and other facets of building operation. These models are ambitious, attempting to capture the effects of weather, occupants, internal gains such as computers and lights, construction assemblies, stratification of air inside spaces, thermal mass of furnishings and more. Attempting to capture the behavior of so many features of modern buildings means that simplifications necessarily take place; occupants are modeled through immutable schedules as are lights and internal heat gains such as computers, weather is assumed to be “typical” weather rather than historic or forecast, air is assumed to be fully mixed or arbitrarily “layered”, and so on. What these energy models do not account for is the uncertainty in all of these other characteristics; the framework proposed here attempts to account for the uncertainty in weather so that these models may be used in a stochastic MPC context.

2.1 TMY Data

Energy models used for design or commissioning purposes typically make use of TMY weather data for a location reasonably close to the modeled site. The goal of TMY data is to represent the typical characteristics and patterns of local weather—it is a composite of many years of empirical data for the given location. In this case, “typical” means that many years (typically 30) of data are collated to capture a wide range of weather phenomena experienced by a location while still presenting an annual average that corresponds to the average long-term weather trends for that location. Because of this, one cannot assume that the hourly TMY weather data will match the actual weather at any given time but one can reasonably assume that the long-term data trends will tend to be similar to the actual weather.

For engineers and architects designing buildings and building systems, performing a simulation using TMY data is sufficient to determine the performance impact of design decisions and to create arguments to justify one design over another. For the operation of the building, however, one cannot assume that TMY will match the current or future weather; if we would like to optimize the operation of our HVAC systems, we would like to

know how weather will behave in the short-term. Predicting short-term weather trends is, of course, a famously difficult problem.

2.2 Uncertainty with Scenarios

The difficulty in predicting short-term weather trends is an uncertainty we wish to account for in MPC. Classically, this uncertainty might be represented by the extremes encountered for a particular location—the so called robust MPC framework (Kouvaritakis and Cannon, 2015). This however introduces a considerable amount of conservatism in our model; since extreme weather patterns are unlikely to materialize, in most situations we would expect that optimizing building operations to account for these extremes would mean that some savings are “left on the table” – meaning that there is still potential for further optimization.

Instead of relying on extreme events to characterize a location’s short-term weather patterns, we can use data to develop a hypothetical weather pattern that is likely to occur by examining the recorded weather pattern leading up to the current moment. In this approach, we assume a future time horizon, F , for which we would like to optimize over as well as a window of time directly preceding the current time for which the optimization is taking place, H . The past time window H represents the historical data that we will use to generate a likely weather scenario for the future time horizon F .

The scenario approach is naturally deterministic, unlike other stochastic MPC strategies such as the use of chance constraints, for which the feasible set of solutions have the potential to be non-convex and difficult to express (Schildbach et al., 2013). Scenario based approaches have been shown to be an effective method in estimating the solution of nonlinear optimal control problems (Mesbah, 2015), which optimization problems involving buildings tend to be.

3. Vector Autoregressive Framework

Because weather variables are not independent (i.e. dry bulb temperature has a relationship with

absolute humidity), any effective modeling approach used to produce a weather scenario must account for the joint variance between the modeled variables. Here, we use a vector autoregressive (VAR) model to represent this dependence. The VAR framework has been shown to generate useful weather scenarios that account for the stochastic nature of local weather pattern (Verdin et al., 2014). The VAR model can be summarized as an extension of the classical autoregressive time series model which allows explaining each variable's evolution in terms of its own lags (the value of the variable at previous time intervals) as well as the lags of each additional exogenous variable assumed to be interrelated. To illustrate this approach, let us first consider an example in which two variables, say dry bulb temperature (T) and absolute humidity (W) are modeled as lag 1, or rather that the current value of these variables is only a function of their values at the previous observation:

$$\begin{bmatrix} T_t \\ W_t \end{bmatrix} = \begin{bmatrix} c_1 \\ c_2 \end{bmatrix} + \begin{bmatrix} A_{1,1} & A_{1,2} \\ A_{2,1} & A_{2,2} \end{bmatrix} \begin{bmatrix} T_{t-1} \\ W_{t-1} \end{bmatrix} + \begin{bmatrix} e_1 \\ e_2 \end{bmatrix} \quad (1)$$

Here, c_1 and c_2 are some constants and e_1 and e_2 are error terms. The A matrix is solved via a least squares minimization. The current values of temperature and absolute humidity are assumed to depend only on the values at the previous time step; the number of lags represent the time window used to create the forecast, in this example the window is 1 hour.

3.1 Lag Selection

Of course, predicting future temperatures based solely on the value of temperature and humidity an hour ago are not likely to be very accurate. We would like to choose a number of lags that maximizes our confidence in the model. Following (Hastie et al., 2008), let us define our total prediction error E as in Equation 2:

$$E = \frac{1}{N} \sum_{n=1}^N L(X(n), \hat{f}(n)) \quad (2)$$

where N is the number of samples, $\hat{f}(n)$ is the fitted model, and L is some loss function relating the observed test value $X(n)$ with the prediction. Since the testing error will nearly always be smaller than

the error for new predictions, it is useful to quantify our confidence in the model and thus how optimistic our testing error is. We define this optimism O as:

$$O = E_{in} - E \quad (3)$$

where E_{in} is our in-sample error, an estimate that combines the prediction error with a term that penalizes complicated models; the justification being that complex models may be over-fitted to the training data. Two common estimates for in-sample error E_{in} are Akaike's Information Criterion (AIC) and the Bayesian Information Criterion (BIC). We can define both criteria in terms of the final prediction error FPE for autoregressive models (Akaike, 1969), which is based on the mean squared error of residuals $\overline{R^2}(A^{(M)})$ in Equation 4, the VAR model order or number of lags M :

$$\overline{R^2}(A^{(M)}) = \frac{1}{N} \sum_{n=1}^N \left[\tilde{X}(n) - \sum_{m=1}^M A_m^{(M)} \tilde{X}(n-m) \right]^2 \quad (4)$$

Where $A^{(M)}$ is the matrix of covariates from the fitted VAR model and $\tilde{X}(n)$ is the deviation from the data mean:

$$\tilde{X}(n) = X(n) - \frac{1}{N} \sum_{n=1}^N X(n) \quad (5)$$

with $X(n)$ being the observed data. Using Equation 4, we can estimate our final prediction error as:

$$FPE = \left(1 + \frac{M+1}{N} \right) S_M \quad (6)$$

where S_M is:

$$S_M = \frac{N}{N-M-1} \overline{R^2}(A^{(M)}) \quad (7)$$

Using our estimate of the final prediction error we can now formulate an information criterion to guide the selection of lags:

$$AIC = \ln|FPE| + \frac{2}{N} MP^2 \quad (8)$$

$$BIC = \ln|FPE| + \frac{\ln N}{N} MP^2 \quad (9)$$

where P is the number of variables jointly modeled. Equations 8 and 9 use similar penalty terms, BIC penalizing complex models slightly more than AIC

due to the $\ln N$ term versus factor 2 as illustrated in Fig. 1. Ideally we would like to minimize how optimistic our model is, so we should select a number of lags that minimizes either the AIC or BIC, whichever we elect to use. Because of the slightly larger penalty term in BIC, models using this selection criteria will generally have fewer lags than those using AIC.

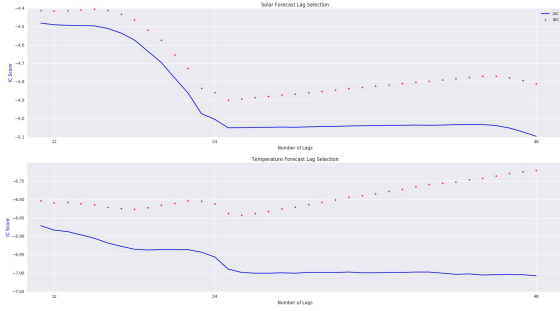


Fig. 1 – Information criterion scores for solar forecasts (top) and temperature forecasts (bottom)

After we select the number of lags, we write the general form of the VAR framework for P variables and M lags as in Equation 10.

$$X_t = c + \sum_{m=1}^M A_m^{(M)} X_{t-m} + e \quad (10)$$

or in long form for each variable $x_p, p \in [1, \dots, P]$

$$\begin{bmatrix} x_{1,t} \\ \vdots \\ x_{p,t} \end{bmatrix} = \begin{bmatrix} c_1 \\ \vdots \\ c_p \end{bmatrix} + \begin{bmatrix} A_{1,1}^{(1)} & \dots & A_{1,P}^{(1)} \\ \vdots & \ddots & \vdots \\ A_{P,1}^{(1)} & \dots & A_{P,P}^{(1)} \end{bmatrix} \begin{bmatrix} x_{1,t-1} \\ \vdots \\ x_{P,t-1} \end{bmatrix} + \dots \\ + \begin{bmatrix} A_{1,1}^{(M)} & \dots & A_{1,P}^{(M)} \\ \vdots & \ddots & \vdots \\ A_{P,1}^{(M)} & \dots & A_{P,P}^{(M)} \end{bmatrix} \begin{bmatrix} x_{1,t-M} \\ \vdots \\ x_{P,t-M} \end{bmatrix} + \begin{bmatrix} e_1 \\ \vdots \\ e_p \end{bmatrix}$$

where c is some constant and e is some error.

4. Scenario Generation

Using the VAR framework, we can take advantage of either locally measured historical or typical weather data to forecast a range of scenarios to represent what the local weather of a given location may look like over the next 24-hours.

The general process for producing weather scenarios is as follows:

1. Fit a VAR model to the data by selecting a number of lags via AIC and solving for the A matrix like that shown in Equation 1
2. Find the standard deviation σ for each weather variable over the number of lags preceding the current time t
3. For each desired scenario, perturb the observed weather data during the time window (based on the selected number of lags) with a random variable between $\pm\sigma$ and use the fitted VAR model to predict a weather scenario using the perturbed data.

The development of the stochastic weather generator gives us a tool for creating any number of plausible weather scenarios that largely relies on two parameters:

1. The length of the historical window W (the number of lags used in VAR process);
2. The number of scenarios to be generated.

These parameters can be thought of high-level tuning parameters specific to the application, building and data at hand but some general guidance on these questions is warranted. Fig. 2 illustrates how the range of predictions changes depending on the number of scenarios, in particular it indicates a widening interquartile range as the number of scenarios increases. Indeed, as the number of scenarios approaches infinity, a scenario based stochastic MPC solution will begin to approximate the robust MPC solution (Zhang et al., 2013). In addition to the temperature and humidity data we have seen thus far, we can also predict solar data like that shown in Fig. 3, which shows predictions for global horizontal and direct normal irradiance using data from Golden, Colorado.

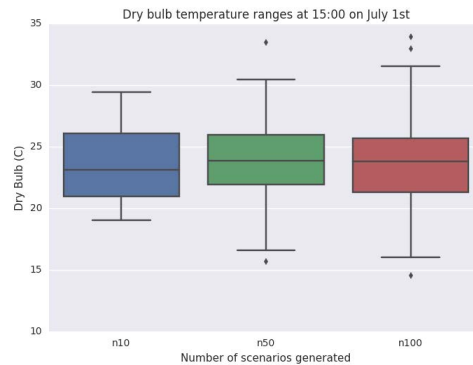


Fig. 2 – Example prediction ranges generated for an increasing number of scenarios for dry bulb temperature during 15:00 on July 1st for Golden, CO

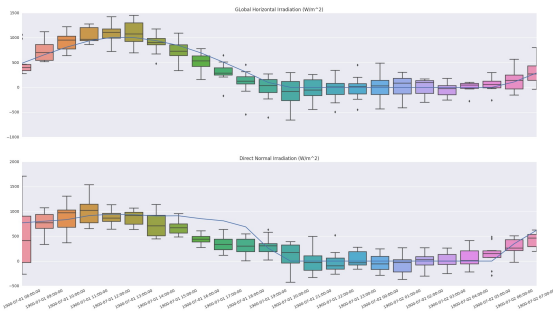


Fig. 3 – Forecast of 10 direct normal and global horizontal irradiance scenarios for 24 hours starting on July 1st in Golden, CO

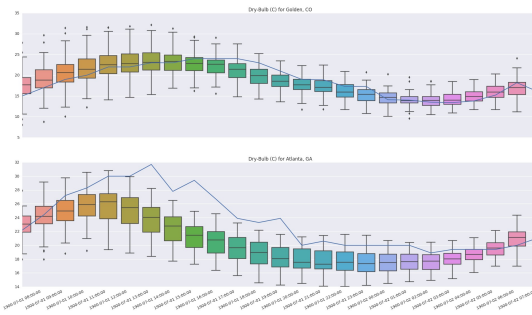


Fig. 4 – Forecast of 50 dry-bulb temperature predictions for Golden, CO (temperate, dry) and Atlanta, GA (hot, humid)

5. Summary and Conclusions

The VAR framework provides an accessible and generally applicable method of representing uncertainty with scenarios. Indeed, the VAR solution is tractable (as evidenced by rapid scenario generation times) and easy to use, the only requirement being relatively stationary time-series test data, which the seasonal nature of weather phenomena is well suited for. While the proposed VAR framework provides a simple tool for generating forecasts of short-term weather trends for MPC applications, care must be exercised in choosing which variables are assumed to be related. Assuming two tangentially related variables are dependent on each other can produce poor fits and misleading results. Additionally, the selection of an appropriate time-horizon is important for capturing the daily swings in weather behavior; locations that see large diurnal temperature differences may require a longer historical window to produce acceptable fits. Fig. 4 illustrates this using predictions for a hot, humid climate (Atlanta, Georgia) during the summer season where the diurnal temperature swing is relatively large as compared to a temperate climate (Golden, Colorado) where the diurnal swing is approximately 5 °C on the presented day.

The solution presented in this paper was developed as part of the stochastic MPC python package `smc` (Currie, 2016), the goal of which is to provide a set of open-source tools for performing stochastic time-series analysis and investigating stochastic MPC problems.

Nomenclature

AIC	Akaike’s information criterion
BIC	Bayesian information criterion
TMY	Typical Meteorological Year
VAR	Vector autoregressive
$A^{(M)}$	Covariate matrix of the fitted VAR model
c	Constant
e	Error
E	Total prediction error
$\hat{f}(n)$	Fitted VAR model
FPE	Final prediction error
F	Future time horizon
H	Past time window
M	VAR model order, lag order
N	Number of observations
O	Model optimism
P	Number of features to model
$\overline{R^2}(A^{(M)})$	Residual mean squared error
T	Dry-bulb temperature
W	Absolute humidity
$X(n)$	Observed data
$\tilde{X}(n)$	Deviation of the observed data from mean

References

- Akaike, H. 1969. "Fitting Autoregressive Models for Prediction". *Annals of the Institute of Statistical Mathematics* 21(1): 243–247. doi: 10.1007/BF02532251.
- Currie, S. 2016. smpc: A Python Framework for Stochastic Time Series and Optimization. <https://github.com/sarocu/smpc>.
- Hastie, T., R. Tibshirani, J. Friedman. 2008. *The Elements of Statistical Learning*. New York, U.S.A.: Springer.
- Kouvaritakis, B., M. Cannon. 2015. *Model Predictive Control*. New York, U.S.A.: Springer.
- Mesbah, A. 2015. "Stochastic Model Predictive Control: A Review". *IEEE Control Systems Magazine*.
- Schildbach, G., L. Fagiano, M. Morari. 2013. "Randomized Solutions to Convex Programs with Multiple Chance Constraints". *SIAM Journal of Optimization* 23(4): 2479–2501. doi: 10.1137/120878719.
- Verdin, A., B. Rajagopalan, W. Kleiber, R.W. Katz. 2014. "Coupled stochastic weather generation using spatial and generalized linear models". *Stochastic Environmental Research and Risk Assessment* 29(2): 347–356. doi: 10.1007/s00477-014-0911-6.
- Zhang, X., G. Schildbach, D. Sturzenegger, M. Morari. 2013. "Scenario-Based MPC for Energy-Efficient Building Climate Control under Weather and Occupancy Uncertainty". In: *Proceedings of European Control Conference*.

Historical Buildings in Protected Areas in Italy: A Re-Design Study of a Rural Building

Maurizio Cellura – University of Palermo – maurizio.cellura@unipa.it

Giuseppina Ciulla – University of Palermo – giuseppina.ciulla@unipa.it

Francesco Guarino – University of Palermo – francesco.guarino@unipa.it

Sonia Longo – University of Palermo – sonia.longo@unipa.it

Abstract

Historic and traditional buildings, including rural ones, are a territorial resource in Europe and constitute an integral part of the European cultural heritage. However they are often characterized by poor energy performance and a large potential for energy retrofit actions.

On the other hand, the hardest part in retrofitting such buildings is the limited invasiveness that such actions need to have on the historical and heritage value of the building itself.

The paper describes an experience of re-design of an existing rural building located in Sicily, inside the ancient Greek Valley of the Temples.

An energy audit was performed on the building, its energy uses thoroughly investigated. A building model was developed in the TRNSYS environment and its performances validated. The validated model was used for re-design studies aimed towards the improvement of the energy performances of the building in compliance with the legislation. The best performing solutions to be applied to a case-study like the Sanfilippo House are those regarding the management of the building, as in the case of the natural ventilation and the HVAC setpoints that would allow a large impact (up to a 10 % reduction in energy uses) on the energy performances of the building with no invasiveness, and those with very limited invasiveness and high impact on the energy efficiency of the building, as in the lighting scenario (up to 30 % energy use reduction). The most invasive actions can only be justified in case of high energy savings as with the insulation of the roof, otherwise they should be disregarded.

1. Introduction

Historic and traditional buildings, including rural ones, represent one important territorial resource in many European cities and are an integral part of the European cultural heritage (Tassinari et al., 2007). However, they are among the largest contributors to the poor energy performance of the building sector (Tadeu et al., 2015) in Europe since they often have poor envelopes and un-optimized HVAC systems that contribute substantially to CO₂ emissions, rising energy bills and increasing indoor environment quality issues (Bastian et al., 2014). This represents a large potential for energy efficiency that needs to be tapped if the ambitious targets of decarbonisation discussed at the latest COP meetings are to be met in the future.

For example, a study based on building energy modeling found that the refurbishment of half of Europe's buildings built before 1945 with an average of factor 4 reduction in the heat transmittance (U) of the opaque structures could result in a reduction of 5.6 % of the total energy demand of buildings (which represents 2.25 % of the total energy consumption) (Climate-KIC, 2013).

In Italy, 60.44 % of the buildings were built before 1976 (13.15 % before 1919, and 22.90 % between 1919 and 1945) (Fabbri et al., 2011). In detail, over 3,900,000 buildings were built before 1920 and several of these constructions are characterized by historical and artistic values, therefore protected as cultural heritage (Ascione et al., 2011). Furthermore, there are 1,376,304 rural buildings used in continuous or seasonal activities, 68 % of which are used to store farm machinery and equipment; 1,084,038 are

animal shelters, 45 % of which were built or restored before 1970; the stock of housing within farms amounts to a total of near one million and a half units 1,460,980, 358,422 of which are unoccupied (Candura et al., 2008).

It is often difficult to operate energy retrofits in the context of historical buildings, since the main focus is the achievement of higher energy performances without compromising the architectural and historical value of the building (Dalla Mora et al., 2015; Pisello et al., 2016; Tadeu et al., 2015).

Moreover, the regulation in Italy makes a clear difference between historical buildings and non-historical ones. Regarding the former, they are excluded from the fulfilment of minimum energy requirements, even after retrofits. Furthermore, the retrofit itself is to be subjected to a feasibility verification in order to identify whether the action configures as an “unacceptable alteration of the historical character” of the building (Presidenza Repubblica Italiana, 2015).

Since the potential for energy efficiency enhancement in existing buildings is so large (Beccali et al., 2013), the EU has paid widespread attention to this topic. In 2014 the energy efficiency Directive highlighted the need for member states to submit National Energy Efficiency Action Plans and a long-term strategy in the field of building renovation to reach a higher energy efficiency. Also, member states are required to renovate 3 % of the total area of conditioned buildings.

The Energy performance of buildings Directive, by introducing the Net Zero Energy Building concept (Cellura et al., 2015), has tried to promote energy efficiency with the built environment, as well as the on-site generation through the exploitation of renewable energy sources (Beccali et al., 2007).

In this context, the paper describes the experience of a re-design of an existing rural building located in Sicily, inside the well-known ancient Greek Valley of the Temples, that mostly hosts the administrative offices of the park.

An energy audit was performed on the building, its energy uses thoroughly investigated. A building model was developed in the TRNSYS environment (University of Wisconsin, 2012) environment and its performances was validated. The validated model was used for redesign studies to improve the energy

performances of the building in compliance with the limitations set by the legislation.

The study aims to the simulation of energy efficiency actions to be implemented inside the building in compliance with the limitations coming from its status of heritage building.

The work is one of the plans of the CRIM-SAFRI Italy Malta cross-border cooperation projects.

2. The Case Study

The building is called Sanfilippo House and it is located in the city of Agrigento, in southern coastal Sicily.

The building is very close to one of the most relevant examples of Magna Grecia in Italy and has been a UNESCO Heritage Site since 1997, the Valley of the Temples (Figs 1 and 2).



Fig. 1 – South view of the building



Fig. 2 – Aerial view of the building (Google Maps)

The main body of the building is L-shaped (Figs 3–4), with the main entrance located in the North, it leads directly into the conference hall, marked by the red arrow. All around it, in the two sections of

the L, the building houses offices. Restrooms are located outside the core of the building and are located in the smaller construction at the far North of the plan.

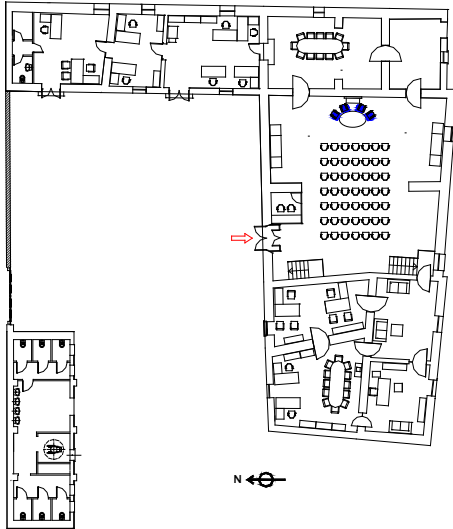


Fig. 3 – Plan of the main body of the building (first level)

The basement of the building includes more offices and technical spaces (Fig. 4).

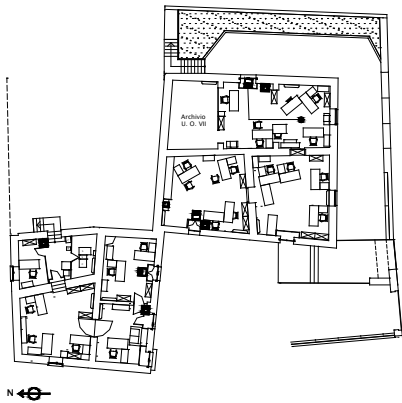


Fig. 4 – Plan of the main body of the building (basement)

The building is characterized by a total floor surface of about 730 m², a height of about 5 m and a shape factor $S/V = 0.51$. The envelope is characterized by tuff outer walls, with $U=0.74$ W/(m²K) with a total thickness of about 0.8 m; externally there is a coating with stone and mortar; internally the walls are plastered and painted with lime and gypsum.

The pitched roof ($U=2.55$ W/(m² K)) is made of brick tiles on wooden decking; the wooden beams are

exposed; all rooms are made of terracotta bricks. Floors are 160 cm thick and have a U value of 0.43 W/(m² K).

Windows use single glazing (overall average $U=6.5$ W/(m² K) while door-windows are double glazed (overall $U=1.86$ W/(m² K)); window to wall ratios are never higher than 5 % in all facades and orientations.

The use of the building is non-residential, not more than 50 occupants can be inside the building simultaneously. Work times are from 7:30 am until 2:00 pm, every day from Mondays to Fridays, while on Wednesdays from 7:30 am to 6:00 pm. Fluorescent tubes of different sizes give lighting. Internal increases are mainly based on office equipment, mostly personal computers (27 in the whole building) and printers (25). Working schedules for machines follow exactly the occupancy pattern in the building, printers' peak power due to non-contemporary use is equal to 20 % at the most. Also lightings follow a variable use pattern that takes into account both the occupancy levels and the availability of natural light during the year. Heating and cooling equipment are considered on as long as the building is occupied.

The building is conditioned through an air-water heat pump with R410A and fan coil units. The fan distribution is a function of the geometrical and thermal characteristics and based on the number of occupants. The HVAC system works from December 1st, to March 31st in heating mode and from June 10th to September 10th in cooling mode.

Thermal imaging studies were performed as well during the energy audit to determine the quality of the envelope and the presence of thermal bridges (Figs 5–7). Such an approach fits perfectly the limited invasiveness required for monitoring and diagnosing techniques to be used in a protected site.

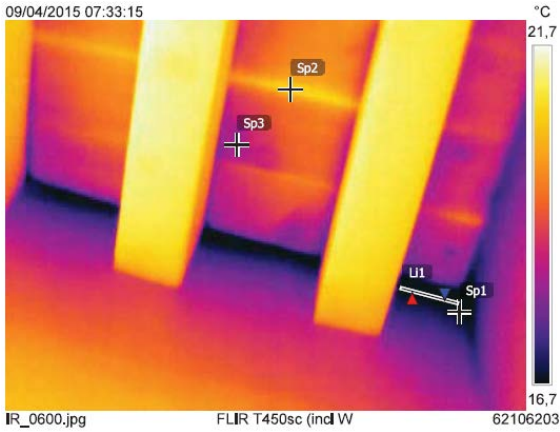


Fig.5 – IR image of the roof

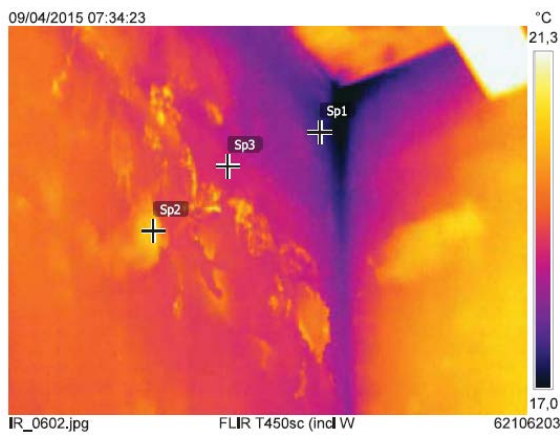


Fig.6 - IR of East oriented internal walls



Fig. 7 – IR of the main North facade

The limits of the envelope are clearly highlighted by Figs 5–6. Thermal bridges are clearly visible in both the internal roof and the external facades. In Fig.5, thermal bridges are highlighted whereas the temperature on the roof is below the average up to 4-5 °C. In Fig. 6 a defective internal plaster layer is

available and the thermal bridge in this case, causes a temperature difference with the rest of the opaque wall of 4.3 °C.

In Fig. 7 a defective insulation is evident, as the external temperature in the opaque structure is variable from 10 to 13 °C on the whole façade. This highlights one of the most problematic aspects in establishing the performances of heritage and historical buildings: the low performances of the envelope make it difficult to quantify the most correct assumptions to be implemented in building modeling. The results of the IR images have identified defective insulation in the envelope and are used to introduce corrections to the theoretical U value of the walls in the model to take into account the thermal bridges.

Another critical aspect in most historical and heritage buildings is the lack of detailed energy meters to quantify the energy flows within the building and the difficulty in installing even temporary ones.

As such, all the energy use profiles were determined based on working times, interviews of the occupants, and calculation of the maximum power installed. The only available data was deduced from the energy bills that led to the information reported in Fig. 8.

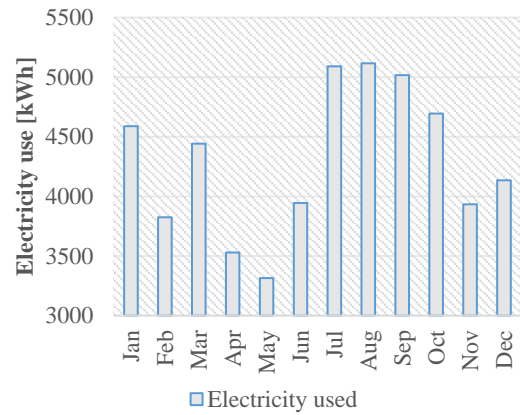


Fig. 8 – Energy bill monthly electricity use

As per the energy bill preliminary calculations, overall electricity energy uses amount to roughly 69 kWh/m² (51 MWh/year).

3. Modeling

The modelling of the building was performed in the TRNSYS environment. Due to a vast homogeneity of the building thermal zones in terms of use profiles, occupation, and adopted thermal system, also in compliance with the Italian technical regulations, we opted to define one thermal zone per plan.

The heat pump is modelled with a fixed Coefficient of Performance (2.92) and Energy Efficiency Ratio (2.4) with 27 °C and 18 °C as cooling and heating setpoints, respectively.

Internal loads for lighting are assumed to be 5 W/m² for the whole building; when active, internal loads for personal computers are assumed equal to 72 W, while for printers the value input to simulation is 50W.

Natural ventilation and infiltration is modelled through TRNFLOW (Transsolar, 2009), establishing a pressure network in the model. The nodes represent the rooms and the building surroundings (Weber et al., 2003). In the baseline model windows are to be closed throughout the year.

The TRNSYS model outputs were compared with the energy bill monthly information to validate them critically. Results are shown in Figs 9 and 10.

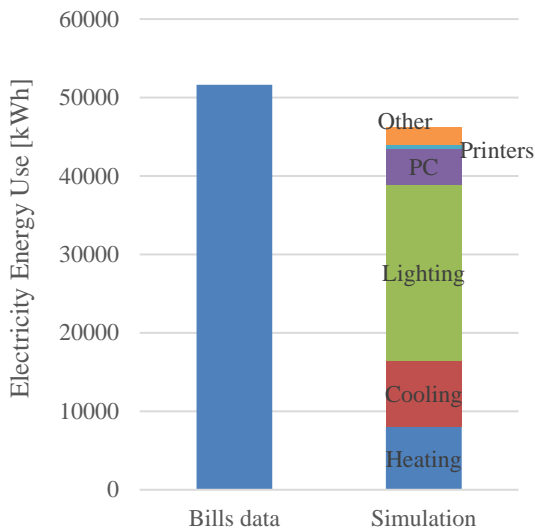


Fig. 9 – Validation of the simulation, annual data

Heating represents 17.34 % of the total electricity consumptions, cooling is very close to this value (18.38 %), while the highest contribution to the total is the electrical equipment and lighting (64.28 %).

Lighting in particular amounts to about 48 % of the electricity use in the building.

On a yearly base, the simulated results report a deviation from the bills data close to 10 %. While this is usually the threshold accepted worldwide in several standards (ASHRAE, 2014) for validation of models, a more in-depth analysis would allow relating these results to some contingent issues.

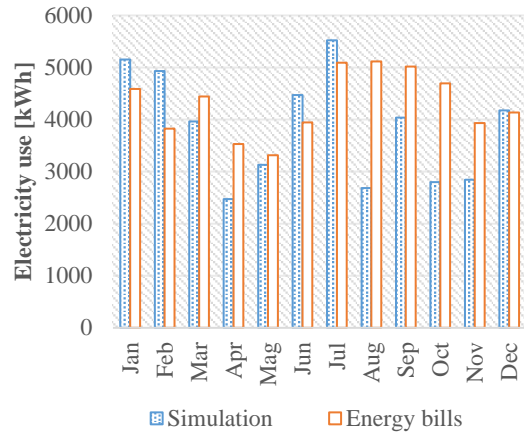


Fig. 10 – Validation of the simulation, monthly data

The analysis in Figure 10 shows some differences between the energy bills data and the simulations in some months and results nearly identical in others. These differences are connected to some behaviour of the occupants, different work hours in some specific parts of the year than what were implemented in the model and to the use of a standard weather file during the simulation. Moreover, only one year of energy bills was retained in the administrative offices of the building and as such it was the only quantitative reference available. The wide and non-quantifiable use of a portable air conditioner was registered as well for the summer period, which is one of the causes of the more pronounced differences in the hotter months.

The model is however able to reproduce the general trend with moderate differences with the energy bills, and as such, is considered appropriate for the development of the building redesign studies.

4. Redesign

From the analysis of the building and of the results, it is possible to define some retrofit actions to improve the energy performances of the building. The context in which to operate is bound by non-technical constraints. As such the approach was to target first the easiest and simplest reductions in energy use with no structural interventions, while only afterwards to include progressively more invasive retrofitting actions. In this section of the paper, the energy efficiency and retrofitting solutions proposed are reported and briefly discussed. All the retrofitting solutions proposed were analyzed singularly and the energy saving potential was evaluated comparing all the retrofitting solutions with the same baseline case.

4.1 Natural Ventilation

Benefits from promoting the use of natural ventilation in mixed mode buildings range from an increase in the air quality of the offices to a substantial reduction in energy use.

The use of natural ventilation in the building is modeled by implementing a mixed-mode building control in the simulation, that includes the manual opening of the windows when overheating occurs ($T_{\text{indoor}} > 26$) and while external temperature is below $26\text{ }^{\circ}\text{C}$ as well. If internal temperature rises higher than $27\text{ }^{\circ}\text{C}$, the standard cooling equipment will be operating.

Although cooling was not the highest contributor of the energy use in the building, this solution could allow the savings of nearly 20 % of the whole cooling energy required during the year (1650 kWh), equal to 5.50 % of the total energy savings.

4.2 Adaptive comfort considerations in the use of cooling equipment

As a complimentary measure to the previously discussed one, this scenario investigates the benefits of a variable cooling setpoint towards the reduction of energy uses.

Under the premises of UNI EN 15251 (European committee for Standardization, 2007) and its future revision prEN 16798-1 (European committee for Standardization, 2015), it is possible to associate the

concept of adaptability of subjects living in a considerably hotter environment to the capability of perceiving a higher indoor temperature as comfortable. Although adaptive comfort in mixed-mode buildings still needs further research, this scenario includes a higher setpoint temperature for the activation of cooling systems while allowing the opening of windows while temperature is below it. The setpoint is calculated as based on the equation of the comfort temperature reported in the UNI EN 15251; if the indoor temperature is higher than $29\text{ }^{\circ}\text{C}$, however, windows will be closed and the cooling system will be activated.

This scenario forecasts a 55 % reduction in the cooling energy use (5650 kWh_e) and an overall reduction of nearly 10 % in overall energy uses.

4.3 Substitution of lighting elements with LED

The largest source of potential energy efficiency actions in the building is the lighting system (nearly 50 % of overall consumptions). The existing fluorescent tubes can be substituted throughout the building with LED elements that guarantee a higher visual comfort and high electricity savings.

The modelling includes a variation in the power installed while it grants the same illuminance levels to the indoor environment.

This solution could guarantee a reduction of up to 60 % of the lighting consumptions and of nearly 30 % of total electricity use in a year.

4.4 Substitution of windows and frames

Another potential source of inefficiencies in the building energy management are the windows, since most of them are single-glazed. Double glazing windows could allow in the whole building a reduction of heating requirements due to both the reduction of infiltration airflow and transmittance values.

This scenario includes the substitution of single glazing windows with double ones, having $U=1.06\text{ W}/(\text{m}^2\text{ K})$, solar transmittance $g=0.548$ and visible transmittance $T_v=0.769$.

This scenario could reduce energy the use for heating by roughly 6 % but as a drawback could increase

cooling energy requirements by 2 %. Overall electricity use reduction on a yearly base will not be higher than 1 %.

4.5 Internal insulation

The transmittance values for all opaque structures are above the normative limitations in Italy for new buildings (roof= $U=2.55\text{W}/(\text{m}^2\text{ K})$, vertical opaque elements $U=0.74\text{ W}/(\text{m}^2\text{ K})$).

The retrofit intervention studied is to add internal insulating coatings to the vertical opaque structures and the roof. Although it would be more beneficial to the energy performances of the building to actually expose thermal mass towards the inside, altering the facades in such a deep way, is not considered a viable option.

By adding internal insulation, the U values for both the opaque vertical structures and for the roof will be reduced respectively $0.343\text{ W}/(\text{m}^2\text{ K})$ and $0.29\text{ W}/(\text{m}^2\text{ K})$. In the first case, the insulation of opaque structures can reduce the energy use during the year by 1.70 %, cooling can be reduced up to 2.3 % and heating by 7.4 %.

Higher values are reported for the insulation of the roof that can reach 8 % of the overall yearly electricity use reduction and of both heating (62 %) and cooling (51 %) energy requirements.

4.6 Recap

Several retrofit solutions have been examined in the paper, ranging from purely energy management choices to actual retrofit interventions to the existing environment.

Table 1 reports briefly all the energy savings identified, while focusing both on the single energy use (e.g. heating) and on the overall energy consumptions.

The results identify energy savings in the case of positive values while it marks an increase of energy consumptions if the values reported are negative.

Table 1 – Recap of the simulation scenarios

	Heating	Cooling	Lighting	Overall
Natural vent.	-	19.20 %	-	5.50 %
Adaptive comfort	-	54.81 %	-	9.92 %
LED	1.39 %	-6.25 %	59.10 %	30.02 %
Windows	5.94 %	-2.01 %	-	0.66 %
Vertical walls	7.41 %	2.28 %	-	1.70 %
Roof	62.02 %	51.10 %	-	7.86 %
Redesign	78.60 %	90.36 %	59.10 %	44.46 %

A contemporary application of all these solutions, indicated in Table 1 as “Redesign”, could allow an overall reduction in energy consumption of roughly 44.5 %, with very large reductions in heating, cooling and lighting energy use.

5. Discussion

The results analysed have identified several redesign solutions and actions with different potential to increase the energy efficiency of the building. However they do not have the same impact either in terms of invasiveness and feasibility in a heritage building.

Several other potential solutions were investigated at first but later removed, due to their too large invasiveness on the features of the environment and of the building itself.

It was the case of wind turbines that would disrupt the visual impact of the historical park, as well as photovoltaic systems that could have completely reworked the facades and the appearance of the rural building under study.

The easiest retrofitting scenarios are therefore the least invasive approaches that can guarantee the highest energy savings. From this perspective, the first two scenarios (natural ventilation use and application of variable setpoints) come as perfectly tailored for such a building, whereas the only needed actions are better strategies for the management of the openings and of the HVAC system. These solutions highlight relevant energy savings that could be achieved through the development of a wider energy awareness by the occupants of buildings with no costs and zero impact on the historical value of the building.

The largest energy reduction is achievable through the substitution of the lighting elements with higher performance LED. Aside from the limited impact on heating and cooling, this scenario can guarantee a relevant increase in performance with a modest impact on the building, with little to no invasiveness. This scenario, due to the specific nature of the energy consumptions of the building, proves the best and most impacting one, representing a very effective compromise between invasiveness and effectiveness.

The substitution of windows and frames, usually regarded as effective in existing buildings in similar conditions needs to be contextualized to the Sanfilippo House and in general to similar buildings, with very massive envelopes and very limited transparent surfaces. Having less than 5 % of glazed surfaces on all facades, while having even no windows in some, will indeed limit the effectiveness of a retrofit of the windows.

The solution has a very limited impact on the performances of the building. Achieving only a 6 % reduction of the overall heating consumptions, while performing a moderate invasiveness retrofit action in a heritage building, which is probably not the best choice in this context. Moreover, allowing moderately higher infiltration values could help in having healthier conditions indoor, in a building that does not have high airflow interaction with the outdoor environment.

Applying internal insulation to the vertical elements and to the roof leads to different results, mostly in accordance to the difference in the original transmittance values in the two cases. Having a transmittance equal to $U=2.55W/(m^2 K)$, the retrofit of the roof leads to the best results, up to nearly 8 % in the overall electricity use reduction, while for the vertical walls this value could reach only 1.7 %.

Although these solutions could be performed even on a heritage building, while the retrofitting of the roof is necessary, since it could cut by more than 50 % both heating and cooling, the vertical walls have only limited positive impacts on the results, and as such could be removed from the final implementation to preserve as much as possible the integrity of the historical value of the building.

6. Conclusions

The study has presented a case study of a typical rural heritage building of Southern Italy, built close to the archaeological site of the “Valley of the temples” close to Agrigento, Sicily.

The aim of the study was to develop a retrofit study to be viable in a heritage context, with the achievement of good results while being respectful of the historical value of the building itself and of the overall site in which the building is built.

The main focus was given to the selection of a range of retrofit solutions with the lowest impact and invasiveness to the value of the building.

The best performing solutions to be applied to a case study like the Sanfilippo House are those regarding the management of the building, as in the case of the natural ventilation and the HVAC setpoints, and those with very limited invasiveness and high impact on the energy efficiency of the building, as in the lighting scenario.

The most invasive actions can only be justified in the case of high-energy savings as in the case of the insulation of the roof; they should otherwise be disregarded.

Acknowledgements

The study was developed in the context of the CRIM – SAFRI project funded by Operative Programme Italia-Malta 2007-2013.

References

- Ascione, F., F. De Rossi, G.P. Vanoli. 2011. “Energy retrofit of historical buildings: theoretical and experimental investigations for the modelling of reliable performance scenarios”. *Energy and Buildings* 43(8): 1925-1936. doi: 10.1016/j.enbuild.2011.03.040.
- ASHRAE. 2014. “Measurement of Energy, Demand and water Savings”. ASHRAE Guideline 14-2014. Atlanta, U.S.A.; ASHRAE.
- Bastian, Z., M. Spiekman, A. Troi. 2014. “Energy retrofit of cultural heritage buildings”. *REHVA Journal* May 2014: 24-27.

- Beccali, M., M. Cellura, M. Mistretta. 2007. "Environmental effects of energy policy in Sicily: The role of renewable energy". *Renewable and Sustainable Energy Reviews* 11(2): 282-298. doi:10.1016/j.rser.2005.02.001.
- Beccali, M., M. Cellura, M. Fontana, S. Longo, M. Mistretta. 2013. "Energy retrofit of a single-family house: Life cycle net energy saving and environmental benefits". *Renewable and Sustainable Energy Reviews* 27: 283-293. doi: 10.1016/j.rser.2013.05.040.
- Cellura, M., F. Guarino, S. Longo, M. Mistretta. 2015. "Different energy balances for the redesign of nearly net zero energy buildings: An Italian case study". *Renewable and Sustainable Energy Reviews* 45: 100-112. doi: 10.1016/j.rser.2015.01.048.
- Candura, A., P. Dal Sasso, G. Marinelli. 2008. "Recovery and Reuse of Rural buildings: the Spread Out Building case". *Agricultural Engineering International: the CIGR E journal*. Invited Overview No. 3. Vol. X.
- Climate-KIC. 2013. "Building a market for reducing energy emissions in heritage buildings." Accessed January 21, <http://www.climate-kic.org/case-studies/building-a-market-for-reducing-energy-emissions-in-heritage-buildings/>.
- European committee for Standardization. 2007. *EN 15251: Indoor environmental input parameters for design and assessment of energy performance of buildings- addressing indoor air quality, thermal environment, lighting and acoustics*. Brussels, Belgium: CEN.
- European committee for Standardization. 2015. *prEN 16798: Energy performance of buildings - Part 1: Indoor environmental input parameters for design and assessment of energy performance of buildings addressing indoor air quality, thermal environment, lighting and acoustics - Module M1-6*. Brussels, Belgium: CEN.
- Fabbri, K., L. Tronchin, V. Tarabusi. 2014. "Energy Retrofit and Economic Evaluation Priorities Applied at an Italian Case Study". *Energy Procedia* 45: 379-384. doi: 10.1016/j.egypro.2014.01.041.
- Pisello, A, A. Petrozzi, V.L. Castaldo, F. Cotana. 2016. "On an innovative integrated technique for energy refurbishment of historical buildings: Thermal-energy, economic and environmental analysis of a case study". *Applied Energy* 162: 1313-1322. doi: 10.1016/j.apenergy.2015.05.061.
- Dalla Mora, T., F. Cappelletti, F. Peron, P. Romagnoni, F. Bauman. 2015. "Retrofit of an Historical Buildign toward NZEB". *Energy Procedia* 78: 1359-1364. doi: 10.1016/j.egypro.2015.11.154.
- Presidenza Repubblica Italiana. 2005. "D.Lgs. 192/2005, Attuazione della direttiva 2002/91/CE sul rendimento energetico in edilizia". *G.U. n. 222 del 23 settembre 2005 S.O. n.158* (come modificato dal D. Lgs. 311/2006, G.U. n. 26 del 1 febbraio 2007 S.O. n.26/L).
- Tadeu, S., C. Rodrigues, A. Tadeu., F. Frire, N. Simões. 2015. "Energy retrofit of historic buildings: environmental assessment of cost-optimal solitions". *Journal of Building Engineering* 4: 167-176. doi:10.1016/j.jobee.2015.09.009.
- Tassinari, P., D. Torreggiani, G. Paolinelli, S. Benni. 2007. "Rural Buildings and their Integration in Landscape Management." *Agricultural Engineering International. The CIGR Ejournal*. Manuscript LW 07 020. Vol. IX.
- Transsolar. 2009. "TRNFLOW: a module of an air flow network for coupled simulation with TYPE 56 (multi-zone building of TRNSYS)."
- University of Wisconsin. 2012. "TRNSYS 17: A transient system simulation program". Madison, U.S.A.: Solar Energy Laboratory.
- Weber, A., M. Koschenz, V. Dorer, M. Hiller, S. Holst. 2003. "Trnflow, a new tool for the modelling of heat, air and pollutant transport in buildings within Trnsys". In: *Eighth International IBPSA Conference*. Eindhoven, Netherlands: IBPSA.

On the Cost-Optimal Design: Comparison of Quasi-Steady-State and Dynamic Simplified Methods of Calculation of H/C Energy Needs

Ilaria Ballarini – Politecnico di Torino – ilaria.ballarini@polito.it

Andrea Costantino – Politecnico di Torino – andrea.costantino@polito.it

Domenico Dirutigliano – Politecnico di Torino – domenico.dirutigliano@polito.it

Enrico Fabrizio – Politecnico di Torino – enrico.fabrizio@polito.it

Simona Paduos – Politecnico di Torino – simona.paduos@polito.it

Vincenzo Corrado – Politecnico di Torino – vincenzo.corrado@polito.it

Abstract

The Directive 2010/31/EU promotes the improvement of the energy performance of buildings within the European Union, by taking into account indoor climate requirements and cost-effectiveness. Thus, the cost optimisation is one of the main objectives of the EU regulatory framework concerning the energy performance of both new buildings and existing buildings subject to refurbishment actions. When assessing the cost-optimal levels of energy performance, the calculation of the energy needs is usually carried out by means of CEN standards or equivalent national calculation methods, based either on steady-state or on dynamic simplified models. However, many research studies have pointed out the limitations of the steady-state approach, especially for high performance buildings.

The aim of this work is to study how the calculation method – quasi-steady or dynamic - of the energy needs for heating and cooling, impacts on the final optimal design. This is done through the application of a cost-optimal procedure to a single-family house located in Milan. The building energy needs for space heating and cooling are calculated by means of the quasi-steady-state monthly method specified by the Italian standards and the simplified hourly dynamic model of ISO 13790. The performance of the thermal systems is then assessed by means of the national standards (UNI/TS 11300), while the global cost is evaluated by means of EN 15459. Several design options with increasing levels of energy efficiency are applied to the case study.

We compare the cost-optimal solutions derived from the application of the two methods, and discuss the reasons for the deviations.

1. Introduction

1.1 Research Studies on Cost-Optimal Design

The Guidelines accompanying the Commission Delegated Regulation (EU) No 244/2012 of 16 January 2012, supplementing Directive 2010/31/EU, introduce a comparative methodology framework for calculating cost-optimal levels (European Union, 2012). It gives the possibility to compare energy efficiency measures on the basis of their energy performance and costs.

The Guidelines indicate three calculation methods of energy performance: monthly quasi-steady-state calculation method, simple hourly dynamic calculation method, and detailed dynamic simulation methods. The literature concerning the Cost Optimal Analysis (COA) shows that the quasi-steady-state method has been applied both to the design of new nZEB (Kurnitski et al., 2011) and to the refurbishment of existing buildings (Corrado et al., 2016a), while the detailed dynamic simulation method was applied in similar cases, often using TRNSYS (Ferrara et al., 2016) or EnergyPlus (Becchio et al., 2015). Comparisons of cost optimality results between the quasi-steady-state method and the detailed dynamic simulation are carried out in other works, as for instance in Corrado et al. (2015). The simple hourly dynamic calculation method has been used less than the other methods in COA studies; it is taken into account, for instance, when the analysis is focused on the energy delivered and the matching with renewable sources (Testi et al., 2016).

The Guidelines indicate two methods to deal with the iterations between the building and its systems: a holistic approach, where the heat gains from the technical building system are considered in the calculation of the energy need, or a simplified approach, where the recovered heat losses of the system are obtained by fixed conventional recovery factors. The holistic approach is more common in the dynamic models.

1.2 Aim

This paper aims to investigate how different calculation methods for heating and cooling energy needs influence the results of a cost-optimal analysis. A case study is taken into account and two out of the three calculation methods indicated by the Guidelines accompanying Commission Delegated Regulation (EU) No 244/2012 of 16 January 2012 are applied. The two methods considered are the quasi-steady-state monthly method, and the simple hourly dynamic method of ISO 13790 standard (ISO, 2008). The study considers the parameters of cost and energy performance.

2. Calculation Models and Optimization Procedure

2.1 Quasi-Steady-State Method

The quasi-steady-state calculation method is presented in ISO 13790 standard (ISO, 2008). It is based on the monthly balance of heat losses (transmission and ventilation) and heat gains (solar and internal) assessed in monthly average conditions. The dynamic effects on the net energy needs for space heating and space cooling are taken into account by introducing a utilization factor that takes into account the time mismatch between transmission *plus* ventilation heat losses and solar *plus* internal heat gains, and that considers an ideal control system which allows overheating or undercooling. The utilisation factor depends on the time constant of the building, on the ratio of heat gains to heat losses and on the occupancy/system management schedules. The space heating and cooling energy need for each month is calculated as:

$$Q_{H,nd} = Q_{H,ht} - \eta_{H,gn} \cdot Q_{gn} \quad (1)$$

$$Q_{C,nd} = Q_{gn} - \eta_{C,ls} \cdot Q_{C,ht} \quad (2)$$

where, $Q_{H/C,nd}$ is the space heating/cooling energy need, $Q_{H/C,ht}$ is the total heat transfer (transmission *plus* ventilation), Q_{gn} is the total heat gains (internal *plus* solar), $\eta_{H,gn}$ is the utilization factor of heat gains for heating mode, and $\eta_{C,ls}$ is the utilization factor of heat losses for cooling mode.

The quasi-steady-state monthly method specified in the Italian standards (UNI/TS 11300) (UNI, 2014) is applied in the present work.

2.2 Simple Hourly Method

The simple hourly dynamic method is described in Annex C of ISO 13790 standard (ISO, 2008). It consists in a simplification of the heat transfer between outdoor and indoor environment based on a similarity between the thermal behavior of the analyzed building and a resistance – capacitance network made up of 5 resistances and 1 capacitance (5R1C). The schematics of the model is reported in Fig. 1 where, θ_{air} is the indoor air temperature, θ_s is the temperature given by the mix of mean, radiant and indoor air temperature, θ_m is the temperature of the capacitive mass node, θ_e is the outdoor air temperature, θ_{sup} is the supply air temperature, H_{ve} is the ventilation heat transfer coefficient, $H_{tr,is}$ is the heat transmission coefficient between the air node and the surface node, $H_{tr,w}$ is the transmission heat transfer coefficient of doors, windows, curtain walls and glazed walls, $H_{tr,op}$ is the transmission heat transfer coefficient of opaque components, C_m is the building fabric internal heat capacity, Φ_{ia} , Φ_{st} , Φ_m are the internal and solar heat gains, $\Phi_{H/C,nd}$ is the heating or cooling heat load.

The indoor air temperature (θ_{air}), at each time step, is calculated as:

$$\theta_{air} = \frac{H_{tr,is} \cdot \theta_s + H_{ve} \cdot \theta_{sup} + \Phi_{ia} + \Phi_{H/C,nd}}{H_{tr,is} + H_{ve}} \quad (3)$$

Summing the $\Phi_{H/C,nd}$ per each time step adopted by the model (1 h), the heating/cooling energy needs during the analyzed period is obtained ($Q_{H/C,nd}$).

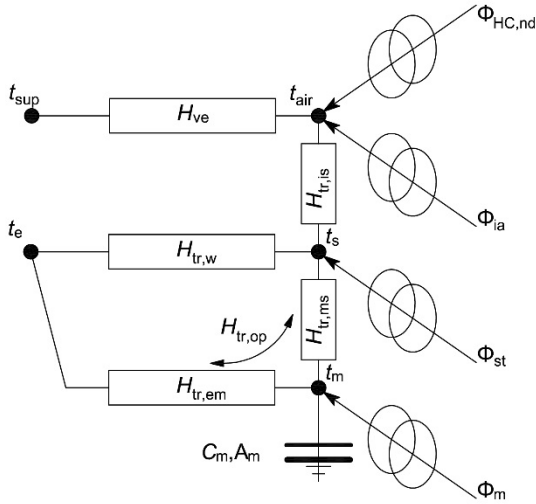


Fig. 1 – Schematic representation of the simple hourly method (ISO, 2008)

2.3 The Cost-Optimal Approach

The cost-optimal solution consists in a package of energy efficiency measures characterised by the lowest global cost compared to a reference package (starting point of the optimization). In the present work, the cost optimisation procedure was based on a sequential search-optimisation technique considering discrete options or levels of energy efficiency measures, as described in detail in Corrado et al. (2014). This procedure refers to the model developed by Christensen et al. (2006). The procedure allows to identify a sequence of “partial optimums”, each one obtained from the previous one by modifying all the parameters that characterize the levels of each energy efficiency measure one at a time.

The global cost analysis was performed by applying EN 15459 standard (CEN, 2007). The global cost (C_{gl}) is expressed as in Eq. (4). It is directly linked to the duration of the calculation period t . The calculation, referred to the starting year t_0 , may be performed by a component or system approach, considering the initial investment (C_1), and, for every component or system j , the annual costs (C_a) and the discount factor (R_{disc}) for every year i (referred to the starting year), and the final value Val_F .

$$C_{gl}(t) = C_1 + \sum_j \left[\sum_{i=1}^t (C_{a,i}(j) \cdot R_{disc}(i)) - Val_{F,t}(j) \right] \quad (4)$$

3. Case Study and Input Data

3.1 The Case Study

The case study is a single-family house built in the period 1976–1990.

It is a reference building selected within the IEE-TABULA project. The main geometric and construction data of the building are shown in Table 1, while the features of its thermal systems are listed in Table 2.

Table 1 – Main geometric and construction data of the case study

Geometric data			Construction data		
V	[m ³]	725	U_{wl}	[W m ⁻² K ⁻¹]	0.76
$A_{t,n}$	[m ²]	199	$U_{fl,lw}$	[W m ⁻² K ⁻¹]	0.98
A_{env}/V	[m ⁻¹]	0.69	$U_{fl,up}$	[W m ⁻² K ⁻¹]	0.97
A_w	[m ²]	24.9	U_w	[W m ⁻² K ⁻¹]	2.80
No. storeys	-	2	$g_{gl,n}$	[-]	0.75

Table 2 – Features of the thermal systems of the case study

Space heating (H) and DHW (W) systems			Space cooling system		
Radiators	$\eta_{H,e}$	0.94	Heat terminal units	$\eta_{c,e}$	0.97
Central distribution	$\eta_{H,d}$	0.91	Zone temp. control	$\eta_{c,c}$	0.94
Gas standard boiler for H	$\eta_{H,g}$	0.85	Zone distribution	$\eta_{c,d}$	1.00
Gas standard boiler for W	$\eta_{W,g}$	0.80	Split system (100 % load)	EER	2.35

3.2 The Energy Efficiency Measures

The cost-optimal approach considered a whole renovation of the building. The energy efficiency measures (EEMs) concern both the fabric and the technical building systems (see Table 3): EEMs from 1 to 5 consider the envelope; EEMs 6 and 7 stands for the replacement of the technical building systems for space cooling and for combined space heating and domestic hot water preparation by means of different technologies (condensing boiler, biomass generator, district heating, air-to-water heat pump). The energy production from renewables is taken into account by EEMs 8 (solar collectors for DHW)

and 9 (PV panels), while EEM 10 considers the heat recovery ventilation system. Finally, EEM 11 refers to the use of an advanced control for space heating. Several levels of performance (EELs) for each EEM were considered; for each level, the thermal parameter value and the referred specific cost are listed in

Table 3; the data results from a market survey (Corrado et al., 2016b). The costs exclude 22 % VAT but include extra-costs for lathing and technical building system adjustments.

Table 3 – Energy efficiency measures (EEMs) and related performance levels (EELs) and costs

No.	EEM	Parameter	EEL	EEL			
				1	2	3	4
1	External wall thermal insulation	U_{wl}	[W m ⁻² K ⁻¹]	0.30	0.26	0.20	
		C_i/A_{wl}	[€ m ⁻²]	25.75	28.86	35.10	
2	Upper floor thermal insulation	$U_{fl,up}$	[W m ⁻² K ⁻¹]	0.30	0.25	0.20	
		$C_i/A_{fl,up}$	[€ m ⁻²]	11.70	15.60	21.06	
3	Lower floor thermal insulation	$U_{fl,lw}$	[W m ⁻² K ⁻¹]	0.30	0.25	0.20	
		$C_i/A_{fl,lw}$	[€ m ⁻²]	23.40	27.30	31.20	
4	Window thermal insulation	U_w	[W m ⁻² K ⁻¹]	1.90	1.80	1.40	1.16
		C_i/A_w	[€ m ⁻²]	113.88	119.57	124.21	150.50
5	Solar shading system	τ_s	[-]	0.40	0.35		
		$C_i/A_{shadings}$	[€ m ⁻²]	50.00	70.00		
6	Chiller	EER	[-]	2.90	3.50	4.00	
		C_i	[€ m ⁻²]	1638	1872	2028	
7	Combined generator for heating, DHW, and appropriate emission system	$\eta_{gn,Pn,H+W}$ or COP	[-]	1.10	0.90	0.99	4.45
		C_i	[€]	2100	11700	3120	6000
		A_{coll}	[m ²]	3.00	3.40	4.00	6.60
8	Thermal solar system	C_i	[€]	3042	3354	3666	5148
		W_p	[kW]	1.00	2.00	3.00	4.00
9	PV system	C_i	[€]	1716	3090	4680	6240
		η_{ve}	[-]	0.90			
10	Heat recovery ventilation system	C_i	[€]	1716			
		$\eta_{H,c}$	[-]	0.995			
11	Heating control system	C_i	[€]	*			

* Cost computed in EEM 7

3.3 Input Data

The calculation was performed for the Milan location (2404 HDD). The weather database of the Italian Thermotechnical Committee was used.

Concerning the building energy performance evaluation: the values of the thermal transmittance of the opaque components already includes the effect of thermal bridges; the internal heat capacity of the building was calculated according to ISO 13786; the external obstacles were not considered; the heat transfer through the unheated spaces was calculated by means of the adjustment factors $b_{tr,U}$. Concerning the user behaviour, the following input data and assumptions were used:

- the sensible internal heat gains and the ventilation flow rate were defined by hourly schedule; the weekly mean values are respectively 4.5 W m⁻² and 0.04 m³ s⁻¹,
- the solar shadings were used when the incident solar radiation on the transparent components was higher than 300 W m⁻²,
- two different operational modes were considered for the heating season: a continuous and an intermittent schedule related to the user's presence. In the first case the setpoint was fixed at 20 °C; in the latter case 14 hours a day of operational time were set at 20 °C, and the set-back was fixed at 16 °C,
- the cooling setpoint was fixed at 26 °C.

In the global cost analysis, a financial perspective calculation was adopted, without considering subsidies. The calculation was performed over 30 years, with a real interest rate of 3 %. The energy costs as well as the energy trend scenarios, the annual maintenance costs and the technical lifespan of building components and systems used in the calculation process derived from previous studies (Corrado et al., 2016b).

The energy performance was calculated in accordance with ISO 52000-1 and it is expressed in terms of non-renewable primary energy (EP_{nren}). The renewable and non-renewable primary energy factors were assumed according to the Italian regulation. The electricity from PV panels is considered as a reduction of the monthly electrical energy demand, while the exported electrical energy is not considered.

3.4 Consistency options

In order to compare the two models, some consistency options were applied as follows: the monthly values of the outdoor air temperature and of the incident solar radiation derived from the correspondent hourly input data; in the quasi-steady-state method the use of the solar shadings was performed by means of the weighted fraction of the time $f_{sh,with}$, calculated from the hourly values of the simple dynamic method; the sensible internal heat gains and the ventilation flow rate in the monthly method were assumed equal to the mean value of the weekly profile used in the hourly method. Finally, the performance of the thermal building systems was assessed by means of the national standards (UNI/TS 11300, parts 2, 3 and 4) that evaluate the technical building systems performance on a monthly basis. It has to be noted that the hourly variability of the thermal building systems performance might affect the cost-optimal solution choice, however this effect is not considered in the present work.

4. Results

Fig. 2 shows the energy needs for heating and cooling of the case study before retrofit, in continuous operational mode. As a general observation, if the quasi-steady state results are taken as a reference, it can be noticed that the simple hourly method underestimates the energy use for heating and overestimates the energy use for cooling.

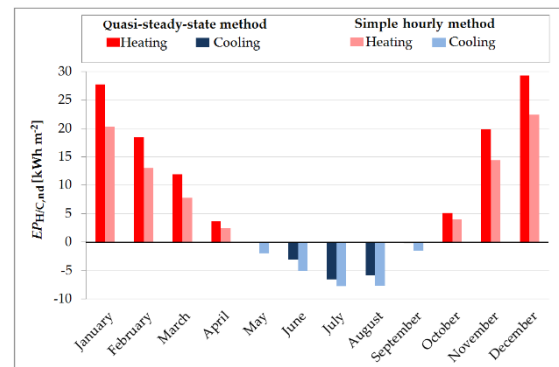


Fig. 2 – Building energy needs for space conditioning before the retrofit

The results of the cost-optimization application are reported in Table 4, in terms of energy efficiency measures and performance levels.

As regards the monthly model, in case of intermittent heating the set-point temperature for the calculation is the same as for the normal heating mode, according to mode B of ISO 13790 (ISO, 2008); that is because the time constant of the building is greater than three times the duration of the longest reduced heating period. For that reason, the energy needs and consequently the cost-optimal solution, do not change with the heating operational mode. In case of quasi-steady-state method, the optimal retrofit considers the thermal insulation of the opaque components by 0.08-0.10 m additional insulating material, the use of external movable shadings in tissue, the installation of thermostatic valves and of wall heat recovery ventilation units in combination with PV.

Table 4 – Cost-optimal packages of measures

No.	EEM	Parameter	Ante retrofit	Cost-optimal packages of measures			
				Quasi-steady-state method		Simple hourly method	
				Continuous / Intermittent mode		Continuous mode	Intermittent mode
1	External wall thermal insulation	U_{wl} [W m ⁻² K ⁻¹]	0.76	0.26	0.30	0.30	
2	Upper floor thermal insulation	$U_{fl,up}$ [W m ⁻² K ⁻¹]	0.97	0.30	0.30	0.30	
3	Lower floor thermal insulation	$U_{fl,lw}$ [W m ⁻² K ⁻¹]	0.98	0.30	0.30	0,98	
4	Window thermal insulation	U_w [W m ⁻² K ⁻¹]	2.80	2.80	2.80	2.80	
5	Solar shading system	τ_s [-]		0.40	0.40	0.40	
6	Chiller	EER [-]	2.35	2.35	4.00	4.00	
7	Combined generator for heating, DHW	$\eta_{gn,Pn,H+W}$ or COP [-]	0.85	0.85	0.85	0.85	
8	Thermal solar system	A_{coll} [m ²]					
9	PV system	W_p [kW]		2.00	2.00	2.00	
10	Heat recovery ventilation system	η_{ve} [-]		0.90			
11	Heating control system	$\eta_{H,c}$ [-]	0.85	0.995	0.995	0.995	

When the cost-optimal solution is investigated by means of the simple hourly method, it can be noticed that retrofit measures are generally oriented to the reduction of the energy use for space cooling: lower additional thermal resistance of the opaque wall with respect to the quasi-steady-state method, natural ventilation and substitution of the old splits with more efficient ones. Finally, the additional thermal resistance of the first floor facing the unconditioned space (EEM 3 of Tab. 4) is not considered an optimal retrofit measure when the intermittent operational mode is used in the simple hourly method.

Fig. 3 shows the energy, the investment and the operating and maintenance costs of the building without retrofit and for the cost-optimal solutions. In case of no refurbishment, only the energy and the operating and maintenance costs occur. Results show that, despite different values of the global cost before the refurbishment (650 € m⁻² in case of a monthly evaluation, 567 € m⁻² and 524 € m⁻² for the hourly method with continuous or intermittent heating setpoints respectively), the deviation of the cost-optimal solutions between the two calculation methods is negligible (maximum deviation of 5 € m⁻² between quasi-steady-state and intermittent

simple hourly model). In particular, the costs for operating and maintenance are similar for all the optimal solutions (115-119 € m⁻²), while the energy cost and the investment cost counterbalance one another.

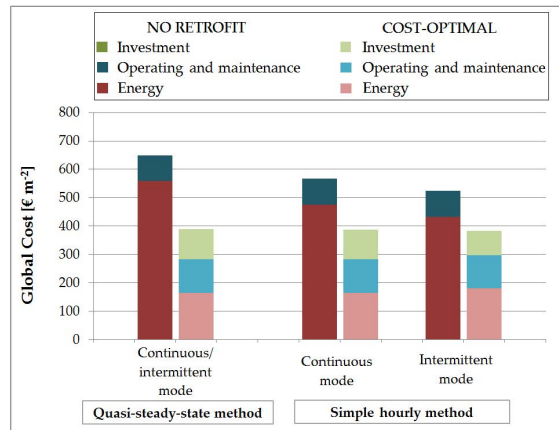


Fig. 3 – Global cost, no retrofit and cost-optimal solutions

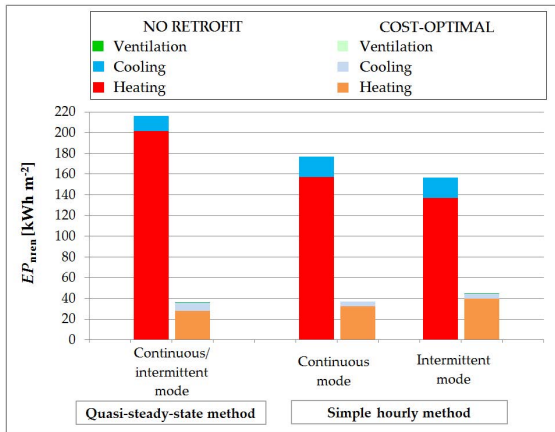


Fig. 4 – Non-renewable primary energy performance, no retrofit and cost-optimal solutions

Fig. 4 shows the non-renewable energy performance of the cost-optimal solutions compared with the building before the retrofit, calculated by means of the two methods. The cost-optimal approach allows to reduce the non-renewable primary energy use from 71 % by the intermittent mode of the simple hourly method to 83 % by the quasi-steady-state method.

Despite different values of the energy performance of the existing building (216 kWh m⁻² for monthly method, 177 kWh m⁻² and 157 kWh m⁻² for the hourly method with continuous or intermittent heating setpoints respectively), the cost-optimal EP_{nren} is in between 37 kWh m⁻² of the monthly and the continuous hourly models, and 45 kWh m⁻² of the intermittent hourly model. The non-renewable energy use for heating is increased in the hourly method (especially with the intermittency mode) because of the minimization of the global cost. Thus, the higher energy cost with respect to the monthly model is counterbalanced by a lower investment cost (Fig. 3) due to the choice of minor additional thermal insulation material and the absence of heat recovery ventilation systems. As well, the different EER values between the cost-optimal solutions of the quasi-steady-state and the simple hourly methods (EEM 6) justify the deviation in $EP_{C,nren}$.

5. Conclusion

The paper presents the application of two different calculation methods for the heating/cooling energy

needs in compliance with ISO 13790 to the cost optimization analysis. The analysed methods are the quasi-steady-state and simple hourly.

Results show that the cost-optimal set of energy efficiency measures is different if the quasi-steady-state or the simple hourly method is applied. Moreover, when the hourly model is used, a change in the operational schedule of the heating system (continuous or intermittent mode) entails a different set of cost-optimal retrofit solutions. Nevertheless, similar values of non-renewable energy performance and global cost among several refurbishment solutions, can be found despite the use of different calculation methods.

Nomenclature

Symbols

A	Area (m ²)
$b_{tr,U}$	Correction factor for unconditioned space (-)
C_I	Investment cost (€)
C_m	Heat capacity (J·K ⁻¹)
COP	Coefficient of performance (-)
EER	Energy efficiency ratio (-)
EP	Energy performance (kWh·m ⁻²)
f	Factor (-)
g_{gl}	Total solar energy transmittance (-)
H	Heat transfer coefficient (W·K ⁻¹)
Q	Thermal energy (Wh)
U	Thermal transmittance (W·m ⁻² ·K ⁻¹)
V	Volume (m ³)
W_p	Peak power (kW)
η	Efficiency (-) / utilisation factor (-)
θ	Temperature (°C)
τ_s	Solar transmittance coefficient (-)
Φ	Heat flow (W)

Subscripts/Superscripts

a	Air / annual
C	Space cooling
c	Heat control (subsystem)
coll	Solar collectors
d	Heat distribution (subsystem)
e	External / heat emission (subsystem)
env	Building envelope
f, fl	Floor

g	Heat generation (subsystem)
gl	Global
gn	Heat gains
H	Space heating
ht	Heat transfer
I	Investment
i	Internal
ls	Heat losses
lw	Lower
n	Net, normal
nd	Need (energy)
nren	Non-renewable
op	Opaque (component)
Pn	Nominal power
sh	Shading
sup	Supply (air)
tr	Transmission (heat transfer)
up	Upper
ve	Ventilation
W	Domestic hot water
w	Window
wl	Wall

References

- Becchio, C., P. Dabbene, E. Fabrizio, V. Monetti, M. Filippi. 2015b. "Cost Optimality assessment of a single family house: Building and technical systems Solutions for the nZEB target". *Energy and Buildings* 90: 173–187. doi: 10.1016/j.enbuild.2014.12.050.
- Christensen, C., R. Anderson, S. Horowitz, A. Courtney, J. Spencer. 2006. *BEopt™ Software for Building Energy Optimization: Features and Capabilities*. Golden, U.S.A.: U.S. Dep. of Energy, NREL.
- Corrado, V., I. Ballarini, S. Paduos. 2014. "Assessment of cost-optimal energy performance requirements for the Italian residential building stock". *Energy Procedia* 45: 443–452. doi: 10.1016/j.egypro.2014.01.048.
- Corrado, V., I. Ballarini, D. Dirutigliano S. Paduos. 2015. "Cost-optimal analysis of Italian office buildings through the application of a quasi-steady-state model validated by detailed dynamic simulation". In: *Proceedings of Building Simulation 2015*. Hyderabad, India: IBPSA.
- Corrado, V., I. Ballarini. 2016a. "Refurbishment trends of the residential building stock: Analysis of a regional pilot case in Italy". *Energy and Buildings* 132: 91–106. doi: 10.1016/j.enbuild.2016.06.022.
- Corrado, V., G. Murano, S. Paduos, G. Riva. 2016b. "On the Refurbishment of the Public Building Stock Toward the Nearly Zero-energy Target: Two Italian case studies". *Energy Procedia* 101:105–112. doi: 10.1016/j.egypro.2016.11.014.
- European Committee for Standardization (CEN). 2007. *EN 15459 - Energy performance of buildings - Economic evaluation procedure for energy systems in buildings*. Brussels, Belgium: CEN.
- European Union. 2012. "Guidelines accompanying Commission Delegated Regulation (EU) No 244/2012 of 16 January 2012 supplementing Directive 2010/31/EU of the European Parliament and of the Council". *Official Journal of the European Union*, 19 April 2012.
- Ferrara, M., E. Fabrizio, J. Virgone, M. Filippi. 2016. "Energy systems in cost-optimized design of nearly zero-energy buildings". *Automation in Construction* 70: 109–127. doi: 10.1016/j.autcon.2016.06.007.
- International Organisation for Standardisation (ISO). 2008. *ISO 13790 - Energy performance of buildings. Calculation of energy use for space heating and cooling*. Geneva, Switzerland: ISO.
- Italian Organisation for Standardisation (UNI). 2014. *UNI/TS 11300-1 - Energy performance of buildings. Part 1: Evaluation of energy need for space heating and cooling* (in Italian). Milan, Italy: UNI.
- Kurnitski, J., A. Saarib, T. Kalameesc, M. Vuolled, J. Niemelad, T. Tarke. 2011. "Cost optimal and nearly zero (nZEB) energy performance calculations for residential buildings with REHVA definition for nZEB national implementation". *Energy and Buildings* 43: 3279–3288. doi: 10.1016/j.enbuild.2011.08.033.
- Testi, D., E. Schito, P. Conti. 2016. "Cost-optimal sizing of solar thermal and photovoltaic systems for the heating and cooling needs of a nearly Zero-Energy Building: the case study of a farm hostel in Italy". *Energy Procedia* 91: 528–536. doi: 10.1016/j.egypro.2016.06.286.

Static and Dynamic Strategies for Improving Daylight Use in Side-Lit Classrooms: A Case Study

Vincenzo Costanzo – University of Reading – v.costanzo@reading.ac.uk

Gianpiero Evola – University of Catania – gevola@unict.it

Luigi Marletta – University of Catania – luigi.marletta@unict.it

Dario Panarelli – Freelance Engineer – dariopn@live.it

Abstract

Daylight plays a very important role in educational buildings, as it allows to create a pleasant environment, to enhance students' performance and to provide better health conditions to the occupants.

For these reasons, and also to save energy in artificial lighting, a great body of literature has dealt with the study of daylight in schools in the past years. Although some quantitative criteria are already in use for assessing daylight effectiveness for several visual tasks – e.g. minimum illuminance values and daylight factors – the distinction between well and badly daylit spaces very often rely on qualitative issues, such as the avoidance of discomfort glare conditions.

Moreover, current design practices rely on standard sky patterns, and neglect the specific climate-related issues, and the time varying appraisal of the indoor space.

The present paper contributes to this research field by exploring the use of different strategies to enhance daylight levels in a school located in Sicily and selected as a case study. The building is mainly made up of side-lit classrooms, exposed to different orientations.

The strategies that are investigated rely both on traditional static devices (e.g. light shelves and reflective glazing) and on more advanced dynamic concepts (e.g. sensor-controlled blinds and electrochromic glazing). All the selected devices are already available on the market.

The daylight performance is assessed in the Radiance-based environment provided by DAYSIM 4.0; the model is calibrated upon a measurement campaign. To this aim several Climate Based Daylight Metrics (CBDM) are used to provide a deeper insight of the potentialities of each solution. Further developments are discussed in the conclusions.

1. Introduction

Daylighting in school buildings has been a subject of interest for many years, since daylight plays a crucial role in educational spaces. Indeed, daylight in schools is able to create a pleasant environment, to enhance academic performance, to promote better health, and to provide significant energy savings. For all of these reasons, the importance of daylight in schools is internationally recognized today (Meresi, 2016). In order to optimize daylighting in school buildings, several strategies are possible, mainly aimed to improve daylight uniformity within the classroom, to reduce glare risk close to the windows, and to avoid insufficient daylight availability in the back of the room (Reinhart and Weissman, 2012).

In this regard light shelves may be an effective solution. Light shelves consist in plane elements (horizontal or slightly inclined) placed in the upper part of a window (internally, externally or both) to control and redistribute incoming daylight. In particular, light shelves are expected to redirect incoming light by reflection towards the ceiling, and from there to the back of the room, while also reducing the high levels of daylight near the window. This obviously improves illuminance uniformity (Claros and Soler, 2002).

One of the main properties of a light shelf as a daylighting device is its reflectance. Light shelves reflectance can be specular or diffuse. Studies showed that specular light shelves are more effective than diffuse ones under low and medium solar altitudes (i.e. in winter), although the latter perform better at

high solar altitudes (i.e. in summer). The appropriate height of a light shelf from the floor is around 2.00 m. The optimum width is between 80 cm and 100 cm, while the optimum position (inner or outer) usually depends on the specific boundary conditions (Meresi, 2016).

An alternative strategy to the use of light shelves to improve daylighting in classrooms is the adoption of *dynamic glazing*.

As opposed to static glazing, dynamic “smart” glazing can switch its optical properties when subject to an appropriate input, such as voltage, light or heat. Amongst smart glasses, *electrochromic glazing* (EC) is the most popular typology: when a voltage pulse is applied between two transparent electrodes, ions move between the EC glazing and an ion storage films, and the overall transparency is changed. A voltage pulse with opposite polarity makes the device restore its original properties. However, small voltage is needed for switching (Hee et al., 2015). Electric power is needed only for switching, i.e. no power is needed to maintain the windows in their clear or dark state, but only to change them from one state to the other.

In EC, the glazing transparency may be reduced from around 0.65 in the clear state to less than 0.05 after switching. If controlled according to the indoor illuminance level, EC glazing can create a building shell that is adaptive to the needs, i.e. able to reduce the solar radiation admitted into the room in case of excessive daylight illuminance or when glare occurs.

Tests using scale models showed that EC glazing would eliminate over-illumination in an office, while maintaining quite good daylight autonomy; however, when the sky is overcast, artificial lighting would be extensively used (Ajaji and André, 2015). In principle, EC glazing cannot improve daylight uniformity within the indoor spaces.

In this paper, both these technologies (light shelves and EC glazing) will be tested on a real case study. The case study is a classroom with east-facing windows, where an experimental campaign has highlighted the need to reduce light levels close to the windows, and to provide a better illuminance distribution, especially in the back of the room.

2. Methodology

When studying the exploitation of daylight in enclosed spaces, several metrics are available.

One of the most common metrics is the *Daylight Factor* (DF): it is defined as the ratio of the daylight illuminance at a given point inside a room to the daylight illuminance measured at the same time on an unobstructed horizontal plane. Direct sun light is excluded for both interior and exterior values (Carlucci et al., 2015). However, according to several authors, the daylight factor does not properly account for non-overcast skies; it makes no difference among different window exposures, and it does not describe how the illuminance varies with time. Finally, it is expressed as a percentage, hence no information is provided about absolute illuminance values.

In order to overcome all these shortcomings, other metrics have recently been introduced. Amongst these, the *Useful Daylight Illuminance* (UDI) is defined as the fraction of the time in a year when the indoor horizontal daylight illuminance at a given point falls within a given range (Carlucci et al., 2015). Three bins are usually identified, separated by a lower and an upper illuminance threshold. The upper bin represents the percentage of time when excessive daylight illuminance occurs, which might lead to visual discomfort; the lower bin represents the percentage of time when daylight illuminance is scarce. Finally, the intermediate bin is associated with the time when appropriate daylight illuminance is attained. According to the original UDI definition (Nabil and Mardaljevic, 2002), the lower and upper thresholds are set respectively to 100 lx and 2000 lx. Later studies (Mardaljevic et al., 2009) proposed to further split the intermediate bin, making a distinction between *supplementary UDI* ($E < 500$ lx) and *autonomous UDI* ($E > 500$ lx). When this latter condition occurs, the second case supplementary artificial lighting is most likely not needed.

In this paper, the UDI is calculated according to three bins: $E < 300$ lx (*fell-short UDI*), 300 lx $< E < 2000$ lx (*suitable UDI*), $E > 2000$ lx (*exceeded UDI*). Indeed, 300 lx seems to be a more suitable value than 100 lx to set a lower threshold for classrooms, and it is consistent with the actual binding prescriptions set by (UNI EN 12464-1:2011).

Finally, the *Spatial Daylight Autonomy* (sDA) is the percentage of the indoor space that meets a minimum daylight illuminance level for at least 50 % of the time of occupancy in a year (Carlucci et al., 2015). Again, the minimum threshold is set to 300 lx. The advantage of the sDA is that it returns a single value representing the whole area. However, it does not account for the amount by which the illuminance threshold is exceeded.

In any case, in order to calculate all these parameters, it is necessary to evaluate the time-varying illuminance distribution within the indoor space. In this paper, the calculation will be performed by simulating the classroom with DAYSIM. DAYSIM is a daylighting simulation software based on the RADIANCE algorithm, able to compute time-varying daylighting illuminance on a sensor grid for any building geometry (Gibson and Krarti, 2015). Real sky conditions, available as TMY weather files, may be used for simulations. DAYSIM was validated against experimental data in Reinhart and Walkenhorst (2001), and Reinhart and Breton (2009), and is nowadays regarded as a reliable tool for daylight simulations.

3. Case Study

3.1 Experimental Campaign

The building selected as a case study is a school built in the 1960s in a town located in Sicily (Southern Italy, LAT. 37°21'N, LON. 13°51'E). The classrooms are mainly oriented to the east and south, while offices and recreational rooms are oriented to the north and west (see Fig. 1).

In this paper, only one classroom representative of the whole set of spaces facing east is investigated. The classroom measures 5.4 x 6 m² and 3.5 m in height, and has two clear double-glazed windows with a fixed clerestory at the top and three panes of glass at the bottom (see Fig. 2 for the details), resulting in a total glazed area of 5.26 m². It hosts 25 students from 8:00 a.m. to 3:00 p.m., from Monday to Saturday. The installed lighting power density is 8 W/m², and no dimming control systems or shading devices are in place except for plastic rolling shutters operated manually from inside.



Fig. 1 – View of the school selected as a case study

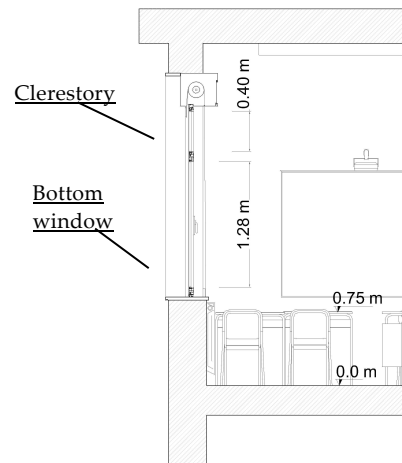


Fig. 2 – Vertical section of the classroom

The first step of the study involved a detailed field survey of the geometrical and optical features of the rooms. To this aim, a Leica X 310 laser distance meter was used to set up the geometrical model, while a Minolta T-10 lux meter and a Minolta LS-100 luminance meter were used to define the optical properties of the different surfaces. The main features of the instruments are shown in Table 1.

The values of luminance (L) and illuminance (E) measured on the opaque surfaces allowed to define their visible reflectance. Indeed, under diffuse reflection, the following relation holds:

$$\rho = (\pi \cdot L) / E \quad (1)$$

The results are reported in Table 2.

Table 1 – Main characteristics of the instruments

Solution	Range	Accuracy
Leica X 310 (laser meter)	0-150 m	±0.001m
Minolta T-10 (lux meter)	0.01-300 klx	± 3 %
Minolta LS-100 (luminance meter)	0.01-50 kcd/m ²	± 0.2 % (±1 digit of measured value)

Table 2 – Optical properties of the surfaces

Solution	Reflectance or Transmittance
Courtyard tiles (outside)	$\rho = 0.20$
Outer plaster (dark-yellow colour)	$\rho = 0.41$
Inner plaster – walls (pale-yellow)	$\rho = 0.75$
Inner plaster – ceiling (white)	$\rho = 0.85$
Marble tiles – floor	$\rho = 0.32$
Desks and seats (wooden)	$\rho = 0.55$
Blackboard	$\rho = 0.08$
Windows frames (aluminium)	$\rho = 0.78$
Glazing: clear double pane	$\tau = 0.70$

Another series of measurements allowed to quantify the illuminance levels on a horizontal grid of 72 points equally spaced within the classroom (70 cm grid resolution) at the height of 80 cm above the floor (UNI EN 12464-1:2011). The illuminance levels were measured on December 22 at 10:30 a.m. without the use of any artificial light sources, to appreciate the contribution of daylight only to the brightness of the environment.

The measured illuminance values are shown in Fig. 3 as isolux curves filled with a false colour gradient depicting different daylight intensities. Based on these results, as well as after surveying teachers and students on their perception of brightness levels throughout the year, it emerges that the main issue is represented by discomfort glare for the students seated close to the windows. Indeed, values close to 4000 lx were measured for these positions while in all the other points the illuminance is always above the minimum threshold of 300 lx (UNI EN 12464-1:2011). The peak values close to the window on the north side of the room are due to a direct spot of sunlight hitting the wall through the windows, what is clearly observable in the same Fig. 3 (upper picture) that provides an interior view of the room at that time.

3.2 Proposed Solutions

A series of different strategies employing several technological solutions are proposed to improve daylight distribution within the room, ranging from the most traditional ones like blinds or reflective windows to the most advanced concepts such as light shelves and electrochromic windows.

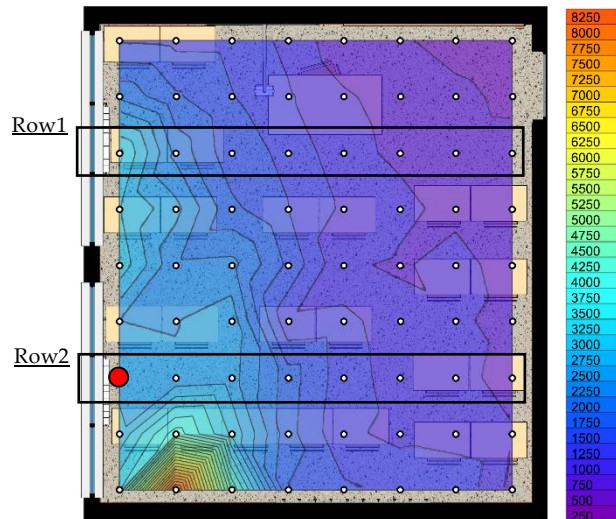


Fig. 3 – Interior view of the room (top) and measured illuminance distribution (bottom) on December 22 at 10:30 am

In particular, the following cases are investigated:

- Case B: base case (as previously discussed);
- Case BL: as in case B, but with the addition of an internal light shelf placed at the bottom of the clerestory (2.20 m above the floor);
- Case BLB: as in case BL, but with the additional use of light-colored internal blinds for the bottom glasses, triggered by an automatic control system;
- Case EC: electrochromic panes triggered by an automatic control system instead of clear ones for the bottom windows, while the clerestory retains clear glazing;
- Case ECL: as in case EC, but with the additional use of an internal light shelf placed at the bottom of the clerestory;
- Case R: reflective panes instead of clear ones for the openable parts, while the clerestory retains clear glazing.

The reasons for studying these technologies to improve daylight distribution are manifold: first, they are able to reduce light levels close to the windows without affecting the daylight availability in the back

of the room, thanks to the clerestory and to the light shelves, when used. Secondly, they allow a comparison between static (reflective windows and light shelves) and dynamic devices (automated blinds and EC windows). Finally, all the products chosen for simulation purposes are already available on the market and thus represent practical refurbishing solutions. Their main optical characteristics, as gathered from the manufacturer data sheets, are summarized in Table 3.

The proposed internal light shelf is 0.8 m in width; Preliminary simulations showed that this size optimizes illuminance values at the back of the classroom, while an external light shelf would not produce any improvements due to low sun angles. The visible reflectance of the light shelf is $\rho = 0.9$ (see Table 3); diffuse reflectance with a 10 % specular component is considered in the simulations.

As far as electrochromic (EC) glazing is concerned, the technical data sheets provided by the manufacturer report a switching time of less than 3 seconds when a voltage of 120 V is applied; the power needed for switching is 5 W/m². The values of visible transmittance in the clear and the tinted states are reported in Table 3.

The logic of activation of these devices, as well as the one to trigger the internal blinds, is to prevent high illuminance values and glare occurrence for the desks close to the windows. More specifically, whenever the illuminance in the control point (highlighted in red in Fig. 3) exceeds 2000 lx, the dynamic devices are automatically triggered in the respective scenarios. This threshold value is consistent with the one adopted by Mardaljevic and Nabil (2008) when studying the energy benefits of different daylighting solutions for sidelit office rooms.

Table 3 – Optical properties for the selected technologies

Solution	Reflectance or Transmittance
Internal light shelf (0.8 m width)	$\rho = 0.90$
Vertical light-coloured blinds	$\rho = 0.80$
Electrochromic (double glazing)	$\tau = 0.05 - 0.65$
Reflective (double glazing)	$\tau = 0.47$

Although a thermal analysis lies outside the scope of this paper, it is worth highlighting that all the proposed window solutions have an U-value close

to that of the base case scenario ($U = 2.7 \text{ W/m}^2\text{K}$), in order to not affect the amount of heat exchanged by temperature difference between the indoor and the outdoor environment. However, further studies on these aspects are needed since different optical properties lead to different g-values and thus affect the room energy balance as well.

4. Results and Discussion

In this section, the fine-tuning of the Radiance parameters is first discussed, and the model built in DAYSIM for simulation purposes is validated by comparison with the measured illuminance values. Then the results of the simulations for the solutions described in Section 3 are presented. The discussion of the results is based on the use of the metrics introduced in Section 2.

4.1 Model Validation

In order to validate the model and to fine-tune the Radiance parameters, various simulations were run by adjusting the parameters until a mean error below 20 % was achieved between measured and simulated mean illuminance profiles. Since DAYSIM is a climate-based software, it needs to know the site location (to evaluate the sun's position in the sky vault) and the time profile of direct and diffuse horizontal irradiance to estimate illuminance and luminance levels on a user-defined grid of points. These data are available on TMY weather files; in this work, the file referring to Catania Fontanarossa weather station was used.

However, it must be remarked that during the measurement campaign – launched on December 22 at 10:30 a.m. – the presence of some clouds was registered. This affected the value of the global illuminance on an unobstructed horizontal plane, which amounted to 11 klx. This value does not correspond to what reported on the weather file (60 klx on December 22 at 10:30 a.m., measured in clear sky conditions). For this reason, the simulations were run by using the data available in the weather file for December 20 at 10:00 a.m., when a global illuminance of around 12 klx is reported on the horizontal plane. The values of the Radiance parameter retained after

tuning and validation are reported in Table 4. With these parameters, the simulated illuminance profiles for the rows of points depicted in Fig. 3 are reported in Fig. 4 (dashed lines), and show a good agreement with the measured values (solid lines). A certain underestimation of the daylight illuminance close to the windows (at a distance below 1.70 m) is registered, which may be due to some inaccuracy in the exact tracing of direct sun rays, such as the one that produces the above-mentioned spot of direct sunlight. On the other hand, the contribution of the diffuse sunlight is simulated with much more accuracy. Overall, the model is considered accurate enough to compare the different proposed solutions for improving daylight exploitation.

It may be interesting to underline that the duration of the simulations was about 30 minutes, except in those cases with light shelf (around 50 minutes).

Table 4 – Radiance parameters used for the simulations

Parameter	Value
Ambient bounces (ab)	5 - 7*
Ambient divisions (ad)	2048
Ambient super-samples (as)	512
Ambient resolution (ar)	512
Ambient accuracy (aa)	0.075
Limit reflection (lr)	8
Specular threshold (st)	0.15
Specular jitter (sj)	0.70
Limit weight (lw)	0.004
Direct jitter (dj)	0.7
Direct sampling (ds)	0.15
Direct pretest density (dp)	512

(* the second value is used in the simulations with light shelves)

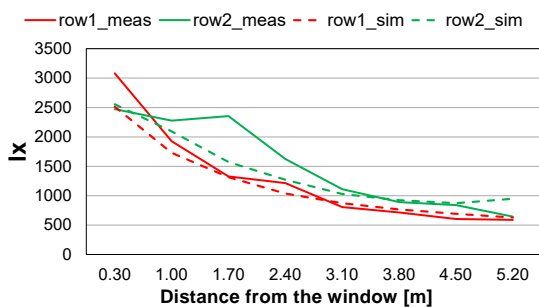


Fig. 4 – Illuminance profiles for two sections of the room

4.2 Simulation Results

The results of the simulations show a good daylight availability within the room in the base configuration (B), as observed from the values of the *spatial*

Daylight Autonomy in Fig. 5. Indeed, sDA = 91 %: this means that more than 90 % of the floor area is sufficiently daylit (i.e. the illuminance is above 300 lx) for more than 50 % of the occupancy period. However, very similar figures are expected also when using reflective windows (case R).

As far as the introduction of an internal light shelf to the existing configuration is concerned (case BL), this solution on the one hand reduces the daylight availability in proximity of the windows but, on the other hand, it increases the daylight availability at the back of the classroom. These two contrasting effects seem to balance, hence sDA is around 91 %.

The use of EC windows would reduce the sDA to 70 %, since the back of the classroom would be severely penalized. However, coupling them with an internal light shelf (case ECL) allows the distribution of daylight and the same performance as in the base-case (sDA = 91 %). The worst scenario is given by the combined use of internal blinds and light shelves (case BLB), since for this configuration the illuminance values are the lowest everywhere within the room, and sDA amounts to around 50 %. To sum up, according to the recommendations by IES (IES, 2012), the existing configuration (with or without internal light shelf), as well as the use of reflective windows and EC windows with a light shelf, all provide good spatial Daylight Autonomy (sDA > 75 %). The other solutions (BLB and EC) are only rated as *nominally acceptable* (sDA > 55 %).

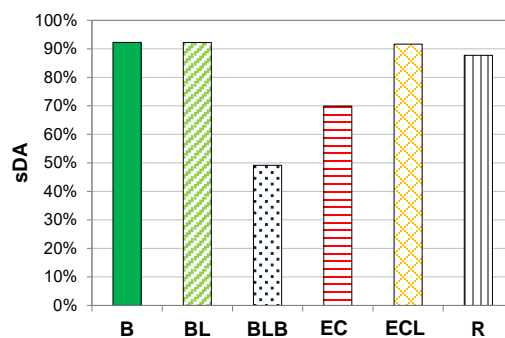


Fig. 5 – Spatial Daylight Autonomy for the proposed solutions

However, one should also take into account the magnitude and duration of the daylight levels achieved throughout the year. To this aim, one can assess the mean value of the *Useful Daylight Illuminance*, according to the three bins previously defined. This allows to evaluate for how long the amount of

daylight within the classroom is not satisfactory ($UDI < 300$ lx), acceptable ($300 < UDI < 2000$ lx) or too high ($UDI > 2000$ lx) for normal visual tasks (see Fig. 6), thus complementing the spatial analysis provided by the sDA.

As expected, the worst performance pertains to the BLB scenario, where for almost 60 % of the time the mean illuminance is too low ($UDI < 300$).

However, even the use of electrochromic windows – coupled (ECL) or not coupled (EC) with a light shelf – significantly worsen the availability of daylight in the classroom, as demonstrated by UDI values very close to those of the BLB scenario.

On the other hand, the best performing solution is the adoption of reflective windows (R): in this case, acceptable mean daylight levels are achieved for more than 80 % of the occupancy period, while potential discomfort glare occurs only 10 % of the time. In fact, reflective windows reduce the excessive illuminance measured close to the windows, and establish a more pleasant visual environment if compared with the base case (B): here, acceptable daylight levels are predicted for around 70 % of the year, but potential discomfort glare could occur for more than 20 % of the time.

Finally, the results are interpreted in terms of *mean annual illuminance uniformity*, in order to appreciate the capability of the different strategies to evenly distribute daylight. The *illuminance uniformity* is the ratio of the mean to the maximum illuminance measured within the space.

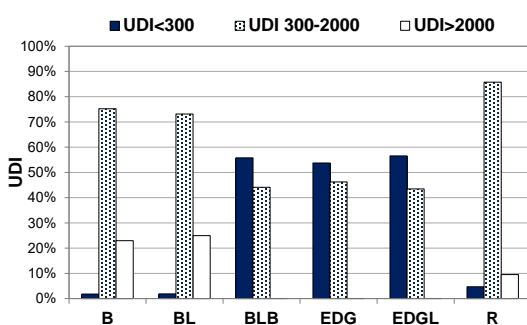


Fig. 6 – UDI values for the proposed solutions (spatial mean)

The results, reported in Fig. 7, show that none of these configurations can reach the minimum illuminance uniformity prescribed by UNI EN 12464 for classrooms in educational buildings (60 %), alt-

hough the norm does not explicitly state the duration of the period of analysis.

The reader should not be misled by the fact that EC windows – especially if coupled to a light shelf – get the highest illuminance uniformity. In fact, the previous analyses suggest that the illuminance values are just 'uniformly low' within the room for these configurations. Better results are expected with reflective windows (R), since the illuminance uniformity rises to 50 %, while the base case (B) has a value of 46 %. Slightly worse results are given with the internal blinds, with or without light shelves.

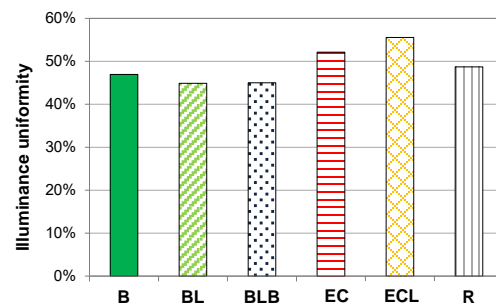


Fig. 7 – Mean illuminance uniformity for the proposed solutions

5. Conclusions

A daylight analysis of an existing classroom facing east has been carried out by means of both measurements and numerical simulations. The main issues of the classroom were found to be the too high illuminance values close to the windows and the uneven distribution throughout the space. To overcome these problems, the paper considered the adoption of different solutions already available on the market, and compared their performance by climate-based daylight metrics.

The outcomes of this analysis show that for this temperate climate, room exposure and geometrical configuration, reflective windows outperform electrochromic windows (with or without internal light shelves) and internal blinds in improving daylight distribution throughout the year. However, the exposure of the windows (south) is expected to have a great influence on the results.

The authors are conducting further analyses to study how other exposures, configurations, and logics or threshold values of activation for the dy-

dynamic devices could affect the results here presented. The energy needs for artificial lighting systems, as well as those for triggering the electrochromic windows and activating the internal blinds, will be considered as well.

Nomenclature

Symbols

A	Area (m ²)
DF	Daylight Factor (%)
E	Illuminance (lx)
I	Solar irradiance (W m ⁻²)
L	Luminance (cd m ⁻²)
sDA	Spatial daylight autonomy (%)
U	Thermal transmittance (W m ⁻² K ⁻¹)
UDI	Useful daylight illuminance (%)

Greek letters

ρ	Reflectance (-)
τ	Transmittance (-)

References

- Ajaji, Y., P. André. 2015. "Thermal comfort and visual comfort in an office building equipped with smart electrochromic glazing: an experimental study". *Energy Procedia* 78: 2464-2469. doi: 10.1016/j.egypro.2015.11.230.
- Carlucci, S., F. Causone, F. De Rosa, L. Pagliano. 2015. "Review of indices for assessing visual comfort with a view to their use in optimization processes to support building integrated design". *Renewable and Sustainable Energy Reviews* 47: 1016-1033. doi: 10.1016/j.rser.2015.03.062.
- Claros, S-T., A. Soler. 2002. "Indoor daylight climate-influence of light shelf and model reflectance on light shelf performance in Madrid for hours with unit sunshine fraction". *Building and Environment* 37: 587-598. doi:10.1016/S0360-1323(01)00074-9.
- Gibson, T., M. Krarti. 2015. "Comparative analysis of prediction accuracy from daylighting simulation tools". *Leukos* 11(2): 49-60. doi:10.1080/15502724.2014.986274.
- Hee, W.J., M.A. Alghoul, B. Bakhtyar, O. Elayeb, M.A. Shameri, M.S. Alrubaih K. Sopian. 2015. "The role of window glazing on daylighting and energy saving in buildings". *Renewable and Sustainable Energy Reviews* 42: 323-343. doi: 10.1016/j.rser.2014.09.020.
- IES, Illuminating Engineering Society of North America. 2012. Approved Method: IES Spatial Daylight Autonomy (sDA) and Annual Sunlight Exposure (ASE).
- Mardaljevic, J., L. Heschong, E. Lee. 2009. "Daylight metrics and energy savings". *Lighting Research and Technology* 41: 261-283. doi: 10.1177/1477153509339703.
- Mardaljevic, J., A. Nabil. 2008. "Electrochromic glazing and facade photovoltaic panels: a strategic assessment of the potential energy benefits". *Lighting Research and Technology* 40: 55-76. doi: 10.1177/1477153507083906.
- Meresi, A. 2016. "Evaluating daylight performance of light shelves combined with external blinds in south-facing classrooms in Athens, Greece". *Energy and Buildings* 116: 190-205. doi:10.1016/j.enbuild.2016.01.009.
- Nabil, A., J. Mardaljevic. 2006. "Useful daylight illuminances: a replacement for daylight factors". *Energy and Buildings* 38: 905-913. doi:10.1016/j.enbuild.2006.03.013.
- Reinhart, C.F., P.F. Breton. 2009. "Experimental validation of Autodesk 3ds Max Design 2009 and Daysim 3.0". *Leukos* 6(1): 7-35. doi: 10.1582/LEUKOS.2009.06.01001.
- Reinhart, C.F., O. Walkenhorst. 2001. "Validation of dynamic RADIANCE-based daylighting simulations for a test office with external blinds". *Energy and Buildings* 33(7): 683-697. doi: 10.1016/S0378-7788(01)00058-5.
- Reinhart, C.F., D.A. Weissman. 2012. "The daylight area-correlating architectural student assessments with current and emerging daylight availability metrics". *Building and Environment* 50: 155-164. doi:10.1016/j.buildenv.2011.10.024.
- UNI. 2011. *UNI EN 12464-1:2011. Luce e illuminazione - Illuminazione dei posti di lavoro - Parte 1: Posti di lavoro in interni*. Milan, Italy: UNI.

RC Building Modelling for Control Purposes: A Case Study

Erica Zavaglio – Politecnico di Milano – erica.zavaglio@polimi.it

Rossano Scoccia – Politecnico di Milano – rossano.scoccia@polimi.it

Mario Motta – Politecnico di Milano – mario.motta@polimi.it

Abstract

When dealing with models, a key factor to consider when selecting their features is the context in which the models will be used: for example, they could be used for design or for control purposes. If we focus on the second case, the model should be accurate enough to capture the principal dynamics of interest and simple enough to minimize the computational effort. In building modelling for control, a promising paradigm seems to be the use of simplified grey-box models. This paper presents a case study in which the existing temperature control strategy can be improved with the resulting possibility of considerable energy saving. More in detail, we introduce here the first step of the entire process: the choice of the model of the system. We decided to investigate the use of a grey-box model, the parameters of which were estimated using a parametric identification process. Thanks to this approach, full knowledge of the system is not required but this lack of information needs to be balanced with the use of measured data. We decided to use only measured data during the standard operation mode of the system for the parameter identification process. Thus we did not perform targeted experiments on the real system, because of all the restrictions in the specific context. Using this approach, it was still possible to achieve good results in terms of deviation between model simulation and data (indoor air: RMSE = 0.31 and $R^2 = 0.92$).

1. Introduction

Buildings account for 20–40 % of the total energy consumptions (Parry et al., 2007) and, as a result, in the past decades, great efforts have been made in trying to reduce this data.

When dealing with energy efficiency in buildings, the main research areas focus on retrofitting and modernization. On top of these, a promising

approach is the application of advanced control strategies in the building automation systems (BAS).

The potentiality of this approach is shown, for example in (Liao and Dexter, 2004): the only improvement of a boiler control can lead to an energy saving up to 20 %.

Despite the research efforts in improving advanced control techniques, the most widely used approach for temperature control in buildings, is the use of a single heating-curve, tuned according to the climatic zone and few building characteristics, and a feedback temperature control. In some cases, in addition to the heating-curve, the heating, ventilation and air conditioning system (HVAC) is locally controlled with rule-based controllers (RBC) that use an “if-then-else” strategy to maintain the desired ambient condition in each room. With this control configuration, what is immediately evident is the lack of an optimized strategy for the entire building control. Advanced control techniques can overcome this problem.

The main research directions in the above-mentioned field are: 1) Learning based approaches like neural networks, genetic algorithms, fuzzy techniques, etc.; 2) Model predictive control (MPC).

With reference to the first research field, an interesting review about neural network in building can be found in (Kumara et al., 2013), whereas for MPC in buildings, a review can be found in (Prívvara et al., 2012).

The first class of methods needs a lot of data from the real system, and on-going learning is required to face with changes of different nature, like changes in the physics of the buildings but also in the occupancy behavior.

On the contrary, building models for MPC are generally more linked to the physics of the buildings, e.g. (Bacher and Madsen, 2011), thus it is easier to deal with changes in the building structure or with the inputs. In addition, with this approach, it is easy to create scalable models for the optimization process and deal with constrained problems. As will be discussed in the next sections of this work, the second class of methods is chosen because of the purpose of the work.

The present work is, in fact, part of a larger study devoted to energy saving in public buildings. More in detail, the final aim of the work is to achieve energy saving using different control strategies.

Reading the previous text, the importance of modelling as a crucial part for advanced control strategies, can be inferred. In this paper, the chosen modelling approach will be discussed, and the results of the model tuning process will be presented and treated. It is worth remembering that the goal of the modelling step is to create a simple, but accurate enough model that can be used for control purposes.

2. Mathematical Approach

When dealing with mathematical models, two general classes can be detected: *forward* and *inverse* models (ASHRAE, 2001). Models belonging to the first class are based only on the physical knowledge of the system. This kind of approach is mainly used for design because one does not need to observe an existing system to create a model. For example, in building modelling, the design of a HVAC system can be performed by taking into account the desired behavior of the system and the physical characteristics of the involved elements.

Conversely, the inverse modelling approach is primarily used for performance monitoring, control system design, and application of on-line control strategies. This because an inverse model needs data to be tuned and it thus requires a real system.

It is worth noticing that both forward and inverse modes result in a set of equations with parameters, but the main difference between the two approaches is in how to define the values of said parameters.

For example, suppose that we need to set the value of the specific heat of a wall. In forward modelling

framework, this value is derived directly by the wall material knowledge. Conversely, in inverse modelling, the same parameter is set to its values using data collected during an appropriate experiment on the wall thermal properties, without any wall material information.

Therefore, it is clear that the second approach is particularly attractive if one has limited knowledge of the system and a big amount of data.

As said before, we decided to investigate the second approach, so the information contained in the data is used to define the value of the model parameters.

2.1 Grey-Box Model

The model chosen here to describe the building structure belongs to the inverse class just presented but more in detail, to the grey-box models class.

A grey-box model combines partial a-priori knowledge of the system with empirical knowledge obtained by data. Particularly, the first type of knowledge is used to define the structure of the building model and the second to tune parameters. This kind of tuning via data usage is called *parameter identification* and it will be discussed more in detail in the next session.

We decided to use grey-box modelling because we know the building in terms of the main characteristics but we do not know in detail all the physical elements. Through the correct use of data, we can overcome this lack of knowledge.

The building model structure results in a set of differential equations with some parameters and we decide to represent them with a simple electric equivalent, through an R-C network representation. This kind of approach is well explained for example in (Parnis and Sproul, 2010) and it is based on the use of electrical components to represent thermal quantities.

2.2 Parameter Identification: Methodology and Specific Issues

As said before, parameter identification is used to define the values of the model parameters.

This method is based on the use of a set of relevant data from a real system. This set must be divided into training and testing data. The first set is then used to perform parameter identification, while the

second is used to verify the validity of the tuned model. One of the key factors of this approach is the use of appropriate data.

In particular, during the data collection, the input to the real system must be *persistently exciting* (Bittanti, 2005). This results in the fact that all the dynamics of the system are excited by the input signal, namely in the trend of the output variable there is all the information to obtain the value of the system parameters.

Often, an experiment performed on the system is required to respect this fundamental rule of parameter identification, but, in some cases, it is not trivial to create an input to the system with the desired characteristics. In the building framework, for example, there are a lot of restrictions.

In particular, in our case study, the first restriction is caused by the configuration of the plant. What we want to handle is the power input from the heating system, but on the real plant this variable cannot be directly changed. Therefore, we need to act on other variables (e.g. valve openings) through the control unit, thus we have to face all the restrictions due to the control unit configuration and operation mode. The second important issue is linked to the inner conditions of the building. If the thermal power entering the building has the needed characteristics, the indoor air temperature fluctuations would be too large to maintain the indoor ambient comfort conditions.

These problems can be partially overcome with the choice of an appropriate period during the year in which the principal dynamics of the building are excited enough with the normal behaviour of the plant and with the other external inputs.

As said before, the parameter identification process is used to define parameter values through data usage. The mathematical problem associated to this idea is an optimization problem, the goal of which is to find the minimum of an appropriate objective function (Nocedal and Wright, 1999).

In parameter estimation, dealing with deterministic models, the most commonly used approach is to set a least-squares problem. This means that the objective function is in the form:

$$f(x) = \sum_{i=1}^n (ym_i - y_i)^2 \quad (1)$$

where ym_i is the measure of the output and y_i is the output of the model. This means that the distance between the measure and the output of the model has to be as small as possible compatibly with the model structure.

The only way to minimize the objective function is to change the model parameters in the proper way so as to change the output variable y_i and thus the objective function.

3. Case Study

We prove the validity of our approach on the basis of a real building located in Lombardy (Northern Italy), a public structure used as a primary school. The building hosts four classrooms and a canteen with a big hall in the middle. There is an underfloor heating system and no feedback control. The regulation of the heating system is performed with the use of a heating-curve, thus using the external temperature, and on the basis of time scheduled operating modes.

We decided to collect the needed data through a small set of non-invasive sensors. We used indoor temperature data logger to measure the indoor temperatures and decided to estimate the underfloor heating water temperature using PT1000 sensors, connected to embedded data collectors, on pipe surfaces.

To measure the solar radiation, a small climate station with a pyranometer was also placed near the building. The external temperature data are collected using the sensors already existing on site and used for the plant regulation. We also used PT1000 sensors to measure the flow and return water temperature of the secondary circuit.

Because of both the distribution system configuration and the control strategy, we could avoid the use of a permanent flowmeter on the secondary circuit. Namely, the heating water is always flowing in the secondary circuit and the circuit does not change its configuration.

The mass flow was thus evaluated using a portable ultrasonic flow measuring system installed for a relatively short period.

In Table 1, the accuracy of the instruments, according to the datasheets, are given.

Table 1 – Measurement equipment accuracy

Instrument	Accuracy
Indoor temperature data logger	$\pm 0.35 \text{ }^\circ\text{C}$
Outside temperature sensor	$\pm 0.2 \text{ }^\circ\text{C}$ influence of temperature <10 $^\circ\text{C}$, >40 $^\circ\text{C}$ --> $\pm 0.007 \text{ }^\circ\text{C}/^\circ\text{C}$
Pt1000	$\pm 0.15 \pm 0.002 T \text{ }^\circ\text{C}$
Pyranometer	Second class (ISO, 1999)
Flowmeter	$\pm 2 \%$ o.r. $\pm 7.5 \text{ mm/s}$

The present study is based on data collected during the winter 2014–2015.

The following time series were collected with the measurement equipment: T_{in} , T_{out} , T_{ext} , Φ_r .

In addition to the above time series, T_a , namely the mean value (weighing on volumes) of the measured temperatures inside the building, is computed and used for the parameter identification process.

On the basis of the available data and on the structure of the building, we selected a set of possible model structures.

In the present work, we only show the most appropriate one on the basis of the result analysis.

As said before, the chosen model can be represented with an electric equivalent: in Fig. 1 the RC-network of the model is shown.

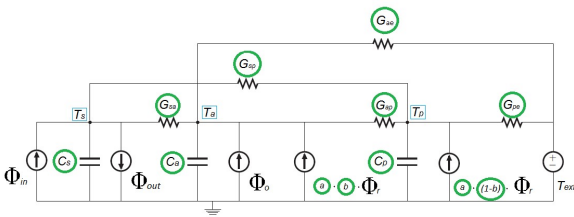


Fig. 1 – RC-network of the building model

The model has one manipulable input variable, i.e. the thermal power entering the building through the heating system, Φ_{in} , and three non-manipulable inputs: the solar global irradiance, Φ_r , the internal gain provided by the occupants and the internal supplies, Φ_o , and the external temperature, T_{ext} . It is important to notice that the thermal input from

the plant is divided into power entering the building, Φ_{in} , and power exiting the building, Φ_{out} , thus following the water flows.

There are three state variables, named T_a , T_s and T_p , which represent respectively the indoor air temperature, the floor temperature and the external walls temperature (included the roof). Each state variable is associated with the corresponding heat capacity, namely C_a , C_s and C_p .

Each G_{xy} term represents the thermal conductance between generic temperatures T_x and T_y .

Φ_o input is computed only according to the occupation schedule and with a fixed thermal coefficient per person.

The parameter a is used to scale the solar input, which is already weighted on the basis of the external area of the building, while b , is used to share the solar input into two terms: one affecting on the walls and the other directly on the indoor air temperature. This second term ideally represents the portion of the solar input entering the building through the windows. The main assumption, which supports the last statement, is that the thermal input entering the windows, and thus affecting the floor, is totally transferred to the air node because of the insulation of the floor.

In Fig. 1, the powers entering and exiting the building (Φ_{in} and Φ_{out}), are used, but, given that

$$\Phi_{in} = \dot{m} \cdot c \cdot T_{in} \tag{2}$$

$$\Phi_{out} = \dot{m} \cdot c \cdot T_{out} \tag{3}$$

and that the term $\dot{m} \cdot c$ can be considered as a constant, it can be convenient to use T_{in} as an input variable and T_{out} as output.

Another important assumption, is the chosen relation between T_{out} and the other variables.

So the following equation was derived from the stationary model of the heat exchange along a pipe:

$$T_{out} = \alpha \cdot T_{in} + (1 - \alpha) \cdot T_s \tag{4}$$

with $0 < \alpha < 1$.

In Eq. (5) the state-space representation of the system is given.

$$\begin{cases} \frac{dx}{dt} = Ax + Bu \\ y = Cx + Du \end{cases} \tag{5}$$

where:

$$x = \begin{pmatrix} T_s \\ T_a \\ T_p \end{pmatrix}, \quad y = \begin{pmatrix} T_a \\ T_{out} \end{pmatrix}, \quad u = \begin{pmatrix} T_{in} \\ \Phi_o \\ \Phi_r \\ T_{ext} \end{pmatrix}$$

$$A = \begin{bmatrix} a_1 & G_{sa}/C_s & G_{sp}/C_s \\ G_{sa}/C_a & a_2 & G_{ap}/C_a \\ G_{sp}/C_p & G_{ap}/C_p & a_3 \end{bmatrix}$$

$$a_1 = -(G_{sa} + G_{sp} + \dot{m} \cdot c \cdot (1 - \alpha))/C_s$$

$$a_2 = -(G_{sa} + G_{ap} + G_{ae})/C_a$$

$$a_3 = -(G_{ap} + G_{sp} + G_{pe})/C_p$$

$$B = \begin{bmatrix} b_1 & 0 & 0 & 0 \\ 0 & 1/C_a & a \cdot b/C_a & G_{ae}/C_a \\ 0 & 0 & a \cdot (1 - b)/C_p & G_{pe}/C_p \end{bmatrix}$$

$$b_1 = \dot{m} \cdot c \cdot (1 - \alpha)/C_s$$

$$C = \begin{bmatrix} 0 & 1 & 0 \\ 1 - \alpha & 0 & 0 \end{bmatrix}$$

$$D = \begin{bmatrix} 0 & 0 & 0 & 0 \\ \alpha & 0 & 0 & 0 \end{bmatrix}$$

Here, the output variables are T_a and T_{out} .

The use of T_a as output variable is a common practice because the focus is on the indoor condition of the building. The use of T_{out} as output is closely associated to the plant configuration and the future use of the model. This variable is indeed the link between the plant and the building models. Thus, it is very important that the trend of this variable is well represented in the model simulation.

In addition to the choice of the model outputs, it is also crucial to underline some aspects about model parameters.

In Fig. 1, the parameters involved in the identification process are circled in green. As said before, all G_{xy} and C_x terms have a physical meaning so it is worth noticing that the initialization values for the identification process can be chosen taking into account the physical knowledge of the system.

Because of the stated aim to simplify as much as possible the model structure and the consequent use of a lumped approach, these parameters included a lot of different physical elements. Therefore, the guess values for the identification process were chosen based on a generic knowledge of the system. For example, we used a single element to define a generic external wall without difference between ceiling, floor and exterior walls. This simplification led us not to consider each single layer of the wall element with the related features (thickness, specific

heat, density, etc.) but only average characteristics of the generic wall.

4. Results and Discussions

In this section, the main results are presented.

First, the results of the parameter identification process are shown and then the model validation is presented and discussed.

4.1 Identification Results

In the identification process, the focus is on the correct representation of the output variables, those involved in the minimization process.

Therefore, the first check on the results has to be performed considering the difference between data and model outputs.

In Fig. 2 and Fig. 3, the difference between simulation results (red lines) and data (blue lines) are shown for the internal ambient temperature and the return water temperature respectively.

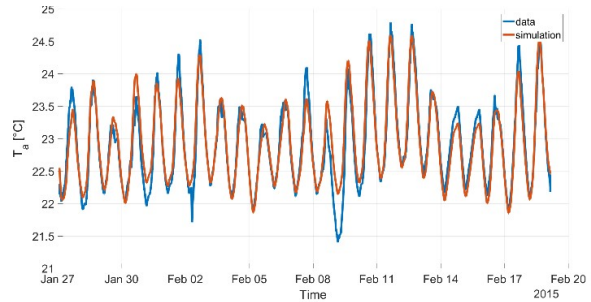


Fig. 2 – Simulation VS tuning data: indoor air temperature

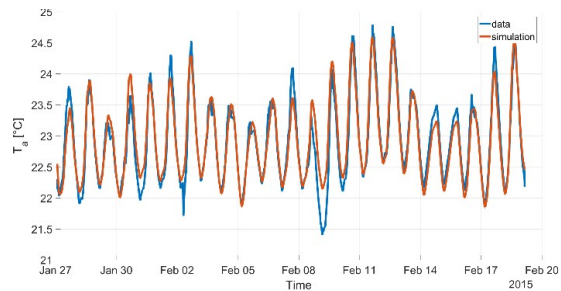


Fig. 3 – Simulation VS tuning data: return water temperature

First, it is important to analyse the simulation result dealing with the ambient temperature because the model is primarily devoted to the evaluation of the inner conditions. If we analyse Fig. 2, we can see that the maximum deviation between measurement and

simulation (0.78 °C) occurs during 09/02. Despite the fact that such a deviation could be too big for our purposes, it is necessary to understand what could be the cause of such a big difference between the data and the model simulation results.

With a good probability, this discrepancy could be due to an unpredictable disturbance on the ambient temperature. The opening of a window represents an example of this kind of disturbances. It happens in an arbitrary manner depending on the needs of the building occupants, we do not have sensors to measure this event, and it causes an abrupt decrease in temperature. If the opening continues for a considerable time, air temperatures can deviate very significantly from the simulated temperature as seems to occur on 09/02. To confirm this hypothesis, we can analyse the return water temperature, Fig. 3, in the same period. What we can immediately notice is that the simulation does not differ clearly from the measured data. This is because the variation of air temperature in the data is not due to the effective cooling of the building, but to a phenomenon that acts directly on the internal temperature.

We decided not to model this phenomenon because it is not very frequent and requires some sensors to be detected; thus, it is obvious that the model differs from the data when it occurs.

In Fig. 3, the second output variable, the return temperature, is shown.

The simulation result is slightly better than the previous one: the simulation deviates from the given measured by less than 0.5 °C and the dynamic appears to be well represented with the identified model.

Once verified the good agreement of the time series, it is also important to quantify the results using some standard performance indexes.

Therefore, in Table 2, the RMSE and R^2 values are listed in order to quantify T_a and T_{out} deviation from the data.

Table 2 – Model deviation from identification data

Index	T_a	T_{out}
RMSE	0.21	0.16
R^2	0.89	0.98

Considering the results shown in Table 2, we can confirm that the model accuracy in reproducing the return water temperature is higher if compared to the indoor air representation.

This result is not surprising if we remember that the identification process is performed using an average room temperature.

When dealing with grey-box models, as in this case, it is also possible to analyse the identification results considering the meaning of the parameters.

In Table 3, the identification results, in terms of parameter values, are listed.

For a better understanding of the numerical results, the thermal conductance and capacities are reported as a ratio of the total air volume.

Table 3 – Parameter values

Parameter	Value	Unit
Gsa	0.924	W/(K · m ³)
Gsp	0.596	W/(K · m ³)
Gap	1.481	W/(K · m ³)
Gpe	0.444	W/(K · m ³)
Gae	0.219	W/(K · m ³)
Cs	26.280	kJ/(K · m ³)
Ca	43.283	kJ/(K · m ³)
Cp	116.108	kJ/(K · m ³)
a	0.727	-
b	0.618	-
α	0.176	-

To evaluate this result, it is important to remember that we use a lamped model, so that we have to consider, for example, that the heat capacity associated to the air can be affected by the mass of the building furniture.

For the same structural reason, also other parameters deserve some clarifications.

Some layers, for example, compose the external wall, and it is not trivial to define the position of the mass centre based on the collected data. This can cause some shift in the values of G_{ap} and G_{pe} . What

can be evaluated is only the total conductance of the wall (G_{ap} composed with G_{pe}) because we only have the external temperature and the inner air temperature data without any information on the wall internal temperature.

Another important parameter to evaluate is α , which influence the heat exchange between the distribution system and the indoor air.

The result (value closer to 0 than to 1) confirms the expected behaviour of the underfloor system.

To prove the good result in parameter identification, it is also important to evaluate the time constants associated to the model. In Table 4, these time constants are listed.

Table 4 – Model time constants

Time constant	Value	Unit
tau1	1.8	h
tau2	4.5	h
tau3	40	h

The last time constant (tau3), an order of magnitude larger than the others, is associated to the walls dynamics and has a reasonable value considering the dimension of the building.

Considering what discussed above, and the results shown in Table 2, we can confirm that the identification result can be considered good enough to move to the second step: the validation of the results using a different data set.

4.2 Validation Results

Once the model is tuned, based on the tuning data set, it is crucial to confirm its validity in reproducing the main dynamics of the system in general conditions, i.e. under different inputs.

A simulation of the tuned model is performed on a different data set.

Validation data range from 14/03/2015 to 28/03/2015. It is not a huge period but what is worth noticing is a change in the control strategy: during the weekend, the heating system is switched-off.

This change is evident if we consider Fig. 4 and Fig. 5 showing simulation results (red lines) and data (blue lines) of the indoor air temperature and the return water temperature.

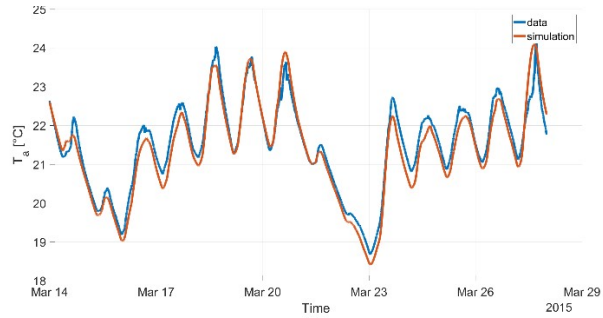


Fig. 4 – Simulation VS validation data: indoor air temperature

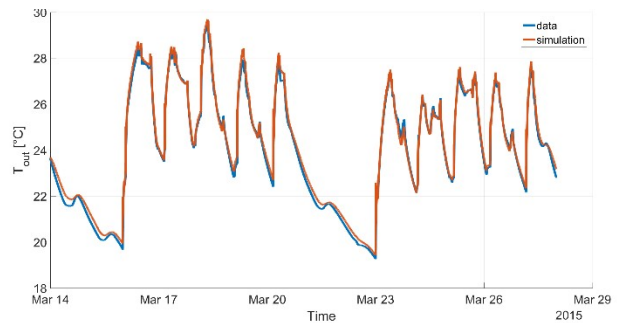


Fig. 5 – Simulation VS validation data: return water temperature

In Table 5, the same indexes used in section 4.1 are shown to evaluate the model deviation from the validation data set.

Table 5 – Model deviation from validation data

Index	T_a	T_{out}
RMSE	0.31	0.22
R^2	0.92	0.99

Considering Fig. 4, Fig. 5 and Table 5, we can confirm that the model can be used also under different conditions and the simulation results can be considered good enough for our purpose.

5. Conclusions

In the general framework of energy saving in buildings, the first step of a wider research on advanced control strategies is presented.

The choice of an appropriate model of the system is certainly a crucial part of the MPC approach chosen here.

Based on a case study, some important methodology aspects are treated.

First, the choice of the model structure and of input and output variables accordingly to the control purposes of the work is discussed.

Then the use of measured data during the normal operation mode of the system is presented and discussed as a good enough method to get data for the parameter identification process.

Unfortunately, the validation data set is not extensive enough to prove the validity of the tuned model on the entire winter period, but a future effort will be done to collect the desirable amount of data to carry out an extensive validation.

Moreover, a complete dissertation about the identification results in terms of physical meanings is here presented.

Nomenclature

Symbols

a	Solar coefficient (-)
b	Sharing coefficient for solar power (-)
C	Thermal capacity (J/K)
c	Water specific heat (J/kg/K)
G	Thermal conductance (W/K)
T	Temperature (°C)
\dot{m}	Water flow (kg/s)
α	Water temperature coefficient (-)
φ	Thermal flow (kW/m ²)
ϕ	Thermal power (kW)
o.r.	of reading

Subscripts/Superscripts

a	indoor air
ext/e	outdoor air
in	water flow
o	people and internal heat gains
out	return water flow
p	wall
r	solar global irradiance
s	floor

References

- ASHRAE. 2001. 2001 *ASHRAE Handbook-Fundamentals*. Atlanta, U.S.A.: American Society of Heating, Refrigerating and Air-Conditioning Engineers, Inc.
- Bacher, P., H. Madsen. 2011. "Identifying suitable models for the heat dynamics of buildings". *Energy and Buildings* 43(7): 1511-1522. doi: 10.1016/j.enbuild.2011.02.005.
- Bittanti, S. 2005. *Identificazione dei Modelli e Sistemi Adattativi*. Bologna, Italy: Pitagora Editrice.
- ISO. 1999. *ISO 9060:1999 - Solar energy - Specification and classification of instruments for measuring hemispherical solar and direct solar radiation*. Geneva, Switzerland: ISO.
- Kumara, R., R.K. Aggarwal, J.D. Sharma. 2013. "Energy analysis of a building using artificial neural network: A review". *Energy and Buildings* 65: 352-358. doi: 10.1016/j.enbuild.2013.06.007.
- Liao, Z., A.L. Dexter. 2004. "The potential for energy saving in heating systems through improving boiler controls". *Energy and Buildings* 36(3): 261-271. doi: 10.1016/j.enbuild.2003.12.006.
- Nocedal, J., S. Wright. 1999. *Numerical Optimization*. New York, U.S.A.: Springer.
- Parnis, G.A., A.B. Sproul. 2010. "Fast Thermal Modelling Using Micro-Cap". In: *Solar2010, the 48th AuSES Annual Conference*. Canberra, Australia.
- Parry, M., O. Canziani, J. Palutikof, P. van der Linden, C. Hanson. 2007. *Climate change 2007: impacts, adaptation and vulnerability*. Cambridge, UK: Cambridge University Press.
- Prívvara, S., Z. Váňa, E. Žáčková, J. Cigler. 2012. "Building modeling: Selection of the most appropriate model for predictive control". *Energy and Buildings* 55: 341-350. doi: 10.1016/j.enbuild.2012.08.040.

Architectural Integration of Photovoltaics: Performance Evaluation of Curved Modules

Marco Lovati – Institute for Renewable Energy, EURAC research – marco.lovati@eurac.edu

Laura Maturi – Institute for Renewable Energy, EURAC research – laura.maturi@eurac.edu

David Moser – Institute for Renewable Energy, EURAC research – david.moser@eurac.edu

Abstract

BiPV (Building integrated photovoltaics) stands on the bridge between architecture and energy production, some photovoltaic companies in the last decade are engaging in the design and production of non conventional PV technologies (Céron et al., 2013). BiPV industry aims to transform PV from power plant to building material, thus the need for features such as freedom of color and dimensions, and flexibility is coming up. In this paper a method is presented for the estimation of power production on curved active surfaces, the performance of two samples of flexible thin film photovoltaic modules are evaluated as a validation. Because of its curved application, the electrical layout and a non-uniform temperature issue affect the performance of the modules under study. The work shows a method to simulate the performance of curved photovoltaic modules subject to uneven irradiation. For the experimental set-up, a curved shelter was built (of those typically used to shield market carts outside supermarkets). Two different flexible photovoltaic modules are glued onto the curved roof of the structure, each module is equipped with an MPPT tracker connected to a data logger, and there are then 2 thermocouples to measure temperatures in the two different modules. Because of the curved shape of the photovoltaic surface the incoming irradiation cannot be measured with a pyranometer, and should therefore be accessed by geometry based computer simulation. The irradiation is simulated through ray-tracing computations (Ward, 1996). The simulation uses weather data retrieved from the weather station located at the ABD airport in Bozen (less than 1 km away). The main result is the comparison between the simulated and the measured power production. Both simulated and measured power point to a better performance linked to one electrical layout over the other. More values are of interest such as Ross coefficient on the module for this particular type of shape and integration. The study shows an

acceptable level of agreement between the simulated power production and the measured one provided that some parameters are calibrated. The possibility of simulating this technology opens the path for economic analysis and feasibility studies to access the real potential of this technology in non-flat application cases.

1. Introduction

Performance prediction and monitoring of PV performance at a system level is crucial for the effective management of renewable energy in both design and operational phases. Well established guidelines, standards, and good practices are available for the assessment of performances and the calibration of the parameters in a model (Woyte et al., 2013). Research literature presents numerous studies about the accuracy of instruments and the uncertainty of measurement. Nevertheless, the shape of the PV system can be complex and some key aspects are not known by simple measurements. This is the case for flexible PV modules glued on a curved surface Fig. 1, the incoming irradiance cannot be measured along the whole surface but needs to be estimated by means of computer simulation. The present study aims at showing a versatile and lean modelling and simulation procedure for the assessment of performances in non-conventional PV modules and systems. The method is particularly desirable for optimization purposes where the computational time is critical.

2. Methodology

2.1 Experimental Setup

In the field test the modules are bent over a curved surface (i.e. the ceiling of a shopping cart’s shelter of those typically found outside supermarkets) as in Fig. 1.



Fig. 1 – Experimental setup

The curvature of the modules is aligned north south so that each part of the module gets irradiated mainly at a particular time of the day, at noon the irradiation pattern is symmetrical over the module and the most irradiated spot is the centre. Each of the two modules is connected to an MPPT device equipped with a data logger that collects the power production each minute, the loggers are then connected to a battery which in turn is connected to a dissipating load. The two modules share the same CIGS cell technology but they are differently organized at the module level as shown in Fig. 2. M1 is transversally divided into 14 smaller modules connected in parallel with each other, while M2 is transversally divided in 44 cells connected in series. The arrangement of M2 may cause huge losses and overheating problems (hot spots) in strongly asymmetrical irradiation conditions, to mitigate these problems the manufacturer equipped each pair of cells with a bypass diode for a total number of 22 diodes.

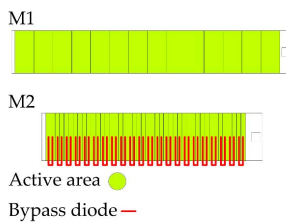


Fig. 2 – Module level organization of the two technologies

Each module is equipped with a thermocouple to measure the superficial temperature on its horizontal edge. Parameters such as ambient temperature, GH and DN are retrieved from the ABD meteorological station located about one km south of the test field.

2.2 Model and Formulas

The performance modelling and assessment methods, are based on the estimate of the incoming irradiation on the plane of the module (Sprenger et al., 2016). Usually trigonometric formulas are used to estimate the irradiation, these could become particularly cumbersome in case of a curved surface. The computation could be sped by simply dividing the curved surface into a number of flat patches. In this paper though a backward ray-tracing procedure using the software Radiance (Ward, 1996) was adopted. The main advantage of this approach is that it is geometry independent (i.e. can be performed independently from the geometry on which the radiation is calculated and on the shading bodies), therefore particularly fit for BIPV applications. The two modules were modelled by approximating the curved surface with a series of flat portions as in Fig. 3; one measuring point corresponds to each portion. The ray tracing procedure is used in this case to retrieve daylight coefficients between each measuring point and a different part of the sky vault using the software Daysim (Reinhart and Herkel, 2000), this method allows for computing the irradiation over different timesteps with one only ray tracing calculation.

Once the irradiation on the different portions of the modules in every timestep of the analysis period is known, the power production of the two modules can be estimated.

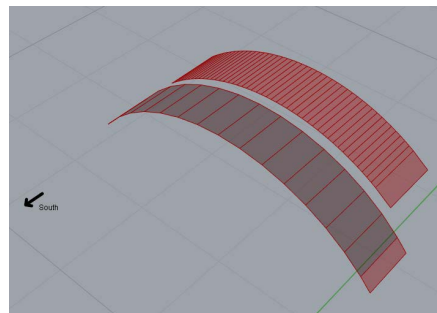


Fig. 3 – Model construction of the two modules and approximation of the curved surface with a discrete number of flat portions

2.2.1 M1

As said, the first module is formed by 14 smaller modules connected in parallel to each other, this disposition renders the power production strongly correlated to the average irradiation over the surface. To model the behavior of this technology a simple relation such as the following is shown to yield satisfying results, the power of the M1 module over one timestep “t” is therefore:

$$P(t) = A \cdot \eta \cdot N^{-1} \cdot \sum_{i=1}^N I_i \cdot c(T) \quad (1)$$

Where $c(T)$ was calibrated to better match the experimental data and found equal to $-0.002 \text{ }^\circ\text{K}$.

2.2.2 M2

The second module presents a power production that is not proportional to the average irradiation as it is influenced by the electrical disposition of its cells, to model the behavior of M2; the following relation was used, as an approximation:

$$P(t) = \min(I_i \cdot c(T)) \cdot A \cdot \eta \quad (2)$$

In this case $c(T)$ was assumed equal to the one from M1.

In this model, the least electrically producing cell in the module dominates the production output of the system, the model does not take into account the behavior of the bypass diode provoking an underestimation of the power in the morning and the evening. In this equation the temperature effect is not taken into account as the estimation of the temperature gradient along the module is strongly dependent on the formation of hot spot and on the behavior of the bypass diode.

2.2.3 Module temperature assessment

Given the present scarcity of thermal sensors in operational commercial PV systems, the estimation of the temperatures of the modules in the simulation makes sense from a technical standpoint. Furthermore the sensors were positioned only in the center of the module, thus ignoring a temperature gradient along the module length. This gradient could be accessed by estimating the temperatures. Some correlations exist to access the superficial temperature of one module (Skoplaki and Palyvos, 2009), among these the most straightforward was used:

$$T_{AMB} = T_{MOD} + k \cdot G \quad (3)$$

The Ross coefficient (Ross and Smokler, 1986) was retrieved by linear interpolation of the difference in

temperature ($T_{AMB}-T_{MOD}$) against the corresponding irradiation. Where a thermal sensor is not available, the following empirical equation can be used:

$$k = (NOCT - 20)/800 \quad (4)$$

3. Results

The power production from the two modules are shown and compared with the results of the simulation method applied.

3.1 Ross Coefficient

As with other semiconductor devices, higher temperatures reduce the power output of PV. The power reduction in the case of PV happens in an almost linear way (Skoplaki et al., 2008).

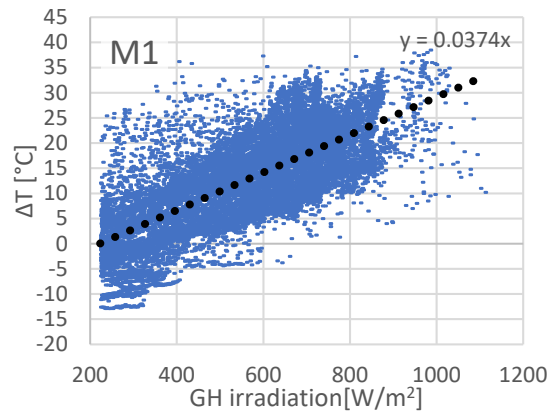


Fig. 4 – $\Delta T=(T_{MOD}-T_{AMB})$ versus irradiation for M1

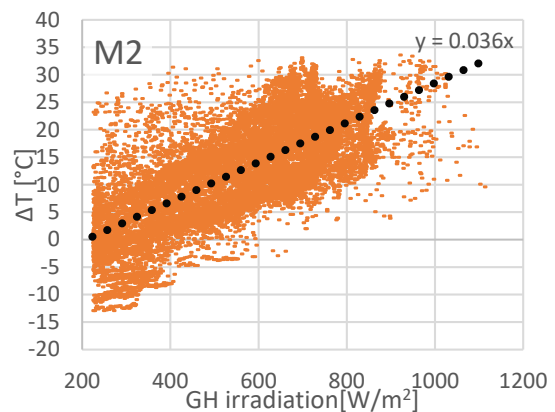


Fig. 5 – $\Delta T=(T_{MOD}-T_{AMB})$ versus irradiation for M2

Because both the technologies indicate a $48 \text{ }^\circ\text{C}$ NOCT, the Ross coefficient k would result equal to $0.035 \text{ }^\circ\text{C}/(\text{W}/\text{m}^2)$. The results shown in Figs 4 and 5

are in accordance with the values for a flat plate rack mounted CIGS module (Maturi et al., 2014), indicating that there is no detectable overheating caused by the type of integration.

3.2 Field Test Results

3.2.1 Measured electricity production

From the data collected by the loggers, it is possible to have an idea about the performances of the two modules. Examining the production curves in a clear sky day a difference is apparent in Fig. 6 Fig. 6. The difference exists despite a similar shape and irradiation pattern because of the electrical layout.

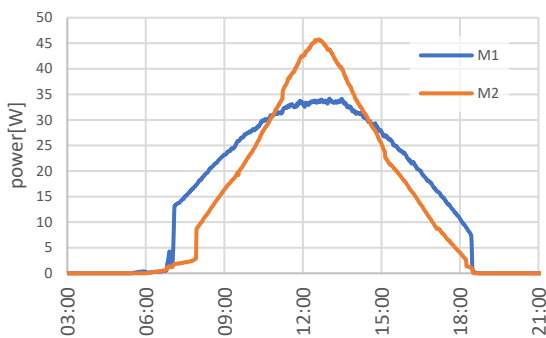


Fig. 6 – The power output of the two modules for August 8, 2016

In general M2 technology outperforms the other around noon by generating a narrower and somewhat sharper profile. Given the higher nominal power declared by the producer (M1=47 W, M2=70 W), which is almost proportional to the highest power at noon (e.g. M1 = 33 W, M2 = 45 W), it is plausible that M2 suffers a drop in efficiency in the morning and the afternoon. This could be explained by stronger current mismatch effects when the irradiation pattern is more asymmetrical (i.e. the sun is east or west). Considering the cumulative energy production over an analysis period of 10 days (from August 26 to September 5, 2016) M1 shown a higher energy production (M1≈ 126 kWh M2≈ 117 kWh).

3.2.2 Simulated electricity production

The simple formula used in equation 1 shows a good level of agreement with the measured data. An overestimation of the power is apparent during the morning hours, this is due to a lag in the sunrise time between the location of the experiment and the pyrhelimeter at ABD (Fig. 7).

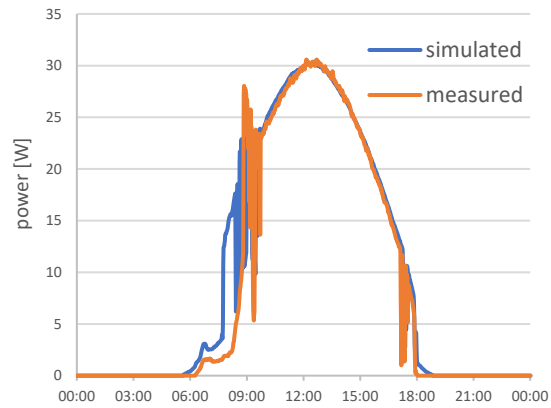


Fig. 7 – Simulated and measured power output for the M1 module for August 31

The error in the days from August 26 to September 5, 2016 was analyzed. The data were filtered and only the core hours (from 9:30 to 15:30) the simulated power production and the measured one are shown in Fig. 8.

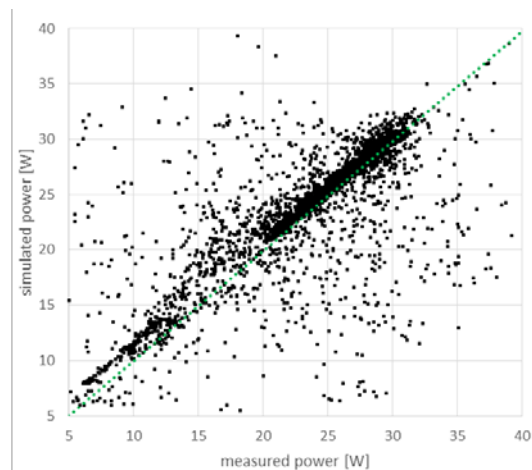


Fig. 8 – Dispersion diagram of simulated vs. measured power from August 26 to September 5, 2016. The data were filtered removing the morning hours

The error (measured – simulated power) resulted from a Kolmogorov-Smirnov test of significance level 0.1 to be drawn from a normal population of mean -0.28 W and standard deviation 1 W.

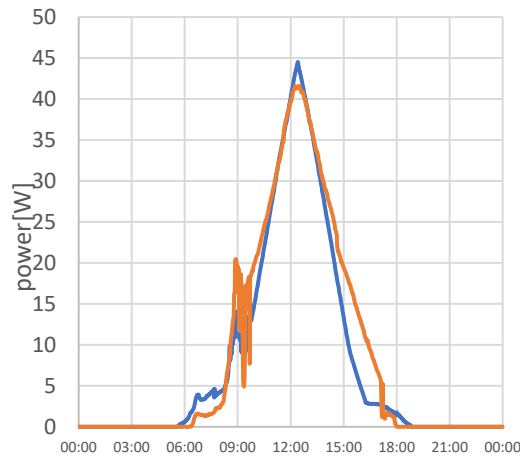


Fig. 9 – Simulated and measured power output for the M2 module for August 31

The simulation of the M2 technology proved less successful for a straightforward approach like the one proposed (Fig. 9). Equation 2 in fact assumes that the power produced by every cell is equal to the least irradiated; this does not coincide with the real behavior because of the presence of bypass diodes. The simplification in modelling leads to a severe underestimation of the output power in the hours far from noon.

4. Conclusions

The integration of this flexible technology in direct contact with a curved polycarbonate board do not show significant overheating problems compared with a standard free field application, therefore the need for ventilation is not an issue for this specific use.

The on-field data collected show a higher cumulative energy production from the technology M1 despite a lower nominal power, the efficiency loss is shown to be due to the electric layout of M2. The integration of the ray-tracing techniques in the photovoltaic simulation at a module scale proves successful for the M1 technology while M2 needs a deeper electrical modelling of the bypass diodes to avoid an underestimation of the electricity production. Is unclear whether a fast and straightforward approach can lead to sufficiently accurate results, it depends on the computational cost of simulating a

substantial number of bypass diodes. A lean approach is needed because it is computationally fit for optimization processes.

Acknowledgement

This study was developed within the CommONEnergy project and has received funding from the European Union Seventh Framework Programme FP7/2007-2013 under Grant Agreement 608678.

Nomenclature

A	Area of the module
ABD	Bolzano Dolomiti Airport
c(T)	Temperature correction coefficient
CIGS	Copper indium gallium selenide
DN	Direct normal irradiation
G	Global radiation
GH	Global-horizontal irradiation
I	Irradiation
k	Ross coefficient
M1	Module of the 1st technology
M2	Module of the 2nd technology
MPP	Maximum power point
MPPT	Maximum power point tracker
N	Number of cells in the module
NOCT	Normal operating cell temperature
OC	Open circuit
SC	Short circuit
T_{AMB}	Ambient temperature
T_{MOD}	Temperature of module
η	Efficiency of the cell

References

- Cerón, I., E. Caamaño-Martín, F.J. Neila. 2013. "State-of-the-Art' of Building Integrated Photovoltaic Products". *Renewable Energy* 58: 127–33. doi:10.1016/j.renene.2013.02.013.
- Maturi, L., G. Belluardo, D. Moser, M. Del Buono. 2014. "BiPV System Performance and Efficiency

- Drops: Overview on PV Module Temperature Conditions of Different Module Types". *Energy Procedia* 48: 1311–19. doi:10.1016/j.egypro.2014.02.148.
- Reinhart, C.F., S. Herkel. 2000. "The Simulation of Annual Daylight Illuminance Distributions – a State-of-the-Art Comparison of Six RADIANCE-Based Methods". *Energy and Buildings* 32(2): 167–87. doi:10.1016/S0378-7788(00)00042-6.
- Ross, R.G., M.I. Smokler. 1986. *Electricity from Photovoltaic Solar Cells: Flat-Plate Solar Array Project Final Report. Volume VI: Engineering Sciences and Reliability*. Springfield, U.S.A.: National Technical Information Service.
- Skoplaki, E., A.G. Boudouvis, J.A. Palyvos. 2008. "A Simple Correlation for the Operating Temperature of Photovoltaic Modules of Arbitrary Mounting." *Solar Energy Materials and Solar Cells* 92(11): 1393–1402. doi:10.1016/j.solmat.2008.05.016.
- Skoplaki, E., J.A. Palyvos. 2009. "Operating Temperature of Photovoltaic Modules: A Survey of Pertinent Correlations". *Renewable Energy* 34(1): 23–29. doi:10.1016/j.renene.2008.04.009.
- Sprenger, W., H.R. Wilson, T.E. Kuhn. 2016. "Electricity Yield Simulation for the Building-Integrated Photovoltaic System Installed in the Main Building Roof of the Fraunhofer Institute for Solar Energy Systems ISE". *Solar Energy* 135: 633–43. doi:10.1016/j.solener.2016.06.037.
- Ward, G. 1996. *RADIANCE Reference Manual*. IEA SHC Task 12.
- Woyte, A., M. Richter, D. Moser, S. Mau, N. Reich, U. Jahn. 2013. "Monitoring of Photovoltaic Systems: Good Practices and Systematic Analysis". In: *Proceedings of the 28th European Photovoltaic Solar Energy Conference*. Munich, Germany: EU PVSEC.

Validation of a PCM Simulation Tool in IDA ICE Dynamic Building Simulation Software Using Experimental Data from Solar Test Boxes

Cristina Cornaro – Tor Vergata University – cornaro@uniroma2.it

Marco Pierro – Tor Vergata University – marco.pierro@uniroma2.it

Daniele Roncarati – Tor Vergata University – daniele.roncarati3@gmail.com

Valerio Puggioni – EnUp – puggioni@enup.it

Abstract

This work aims to provide a method to validate a PCM tool implemented in a whole building dynamic simulation software (IDA ICE) using outdoor measurements coming from Solar Test Boxes (STB).

The STB method was originally conceived by ESTER lab at the University of Rome Tor Vergata, to evaluate thermal characteristics of transparent and semi transparent materials in outdoor conditions. In the approach presented here, two boxes (reference and test) were equipped with a standard double glass pane. A PCM pane, provided by RUBITHERM®, was put on the floor of the test box. Two monitoring campaigns were carried out and the thermal behaviour of the box with PCM was analyzed and compared with the thermal behaviour of the reference box. Temperature trends measured inside the “PCM box” were used to validate the PCM behaviour provided by the IDA ICE tool, comparing measured and simulated data.

1. Introduction

Since the 1930s Phase Change Materials (PCM) have been investigated thanks to the pioneering work of Telkes (1975). Many studies have been conducted on these materials since then but unfortunately their application did not take off due to technological constraint and costs. However, as recent reviews show (Khadiran et al., 2016; Souayfane et al., 2016), interest for PCM has increased again in the last years.

Many studies can be found in the literature regarding experimental and theoretical analyses of PCM behavior. It is possible to group these works into laboratory experimental activity, outdoor experimental activity, numerical and theoretical

investigation and studies involving experiments and theory.

Various works can be found on laboratory tests. Most of the examined works regard the evaluation of the thermal characteristics of gypsum boards containing microencapsulated PCM tested in simulation chambers and/or tests boxes (Lee et al., 2007; Zhang et al., 2012, 2013; Li et al., 2013; Marchi et al., 2013). Barreneche et al. (2013) incorporated PCMs with Portland cement and gypsum and investigated the best PCM quantity to be incorporated for each tested material.

The paper by Tardieu et al. (2011) on outdoor experimental activity that used two cabins built in Auckland, New Zealand, is worth mentioning. One was used as reference and one with PCM and numerical simulation using Energy Plus to evaluate the thermal behavior of the two cabins. Both simulation and experimental data collected showed that PCM in wallboards improved the thermal inertia of buildings. From simulations they also concluded that the additional thermal mass of PCM can reduce the daily indoor temperature fluctuation by up to 4 °C in summer days. Also Entrop et al. (2011) made experiments using small outdoor boxes in Denmark, equipped with different materials among which, PCM. Their results evidenced that PCM is an excellent way to store energy and small boxes are effective in studying this aspect. Also Su et al. (2012) used a box to evaluate the PCM thermal behavior in China, while Sage-Lauck and Sailor (2014) built a passive house duplex in Portland, Oregon. They found that the addition of PCM could reduce by about 60 % the over-heating number hours.

Goia et al. (2014) tested a glazing system filled with PCM in outdoor conditions during a long term monitoring campaign. They concluded that the PCM glazing is capable of smoothing and shifting solar gains, and that this result could positively contribute to the energy balance of highly glazed buildings. Numerical simulation is also used to evaluate PCM performance at different locations and climates using various simulation tools such as ESP-r (Fernandez and Costa, 2009), self-made programs (Zwanzig et al., 2013), COMSOL environment (Zhou et al., 2014), and Energy Plus (Guarino et al., 2015). All these works should be supported by experimental data as by Guarino et al. (2015).

The aim of this work is to provide valuable experimental data that could be used to validate the behavior of a custom PCM simulation tool integrated in the whole building simulation software IDA ICE by EQUA simulation. In the following sections the experimental facility used for the study is presented together with the custom PCM software module implemented in the IDA ICE environment. We introduce the results of the monitoring campaigns, and discuss a comparison between simulated and measured data to validate the tool. Once validated, the software module could be used to evaluate energy performance of PCM in buildings.

2. Simulation and Experiment

2.1 Method

Solar Test Boxes (STBs) were built with the objective of carrying out a comparative analysis of thermal and lighting performance of transparent material with respect to a double glass reference pane, and to evaluate solar heat gain and U-value of the innovative semi-transparent materials. In the present study they were used to test the thermal performance of a SP21E PCM pane provided by RUBITHERM®, the characteristics of which are listed in Table 1. The STBs were provided with two identical standard double glass panes. In the experiments one of the

boxes (PCM) contained the PCM panel while the other (Ref) was used as a reference.

Table 1 – SP21E PCM pane characteristics

Data	Value
Melting area	22–23 °C
Congeealing area	21–19 °C
Heat Storage Capacity Combination of sensible and latent heat in a temperature range of 13 °C to 28 °C.	160 kJ/kg
Specific Heat Capacity	2 kJ/(kg K)
Density solid (15 °C)	1.5 kg/l
Density liquid (35 °C)	1.4 kg/l
Volume expansion	3–4 %
Thermal conductivity	0.6 W/(m K)
Max Operation temperature	45 °C

The STBs thermal behaviour was simulated in the IDA ICE dynamic simulation environment. In particular the PCM box model was provided with the custom PCM software module to simulate the PCM pane. The temperature data, gathered during two short-term outdoor monitoring campaigns, carried out in different periods of the year, were used to validate the results.

2.2 Solar Test Boxes Description

The boxes were designed with a linear scale factor of 1:5 and a surface scale factor of 1:25 with respect to a real room. They have the dimensions of 1.00 m × 0.60 m × 0.55 m and consist of 5 opaque walls and one glazed wall. The exterior was manufactured with plywood panels of 8 mm thickness painted entirely white, to make them highly reflective. The entire not glazed inner surface of the boxes, also comprising the portion of the area behind the frame of the window, was heavily insulated with a lightweight rigid insulating material of 80 mm thickness, Stiferite GT, specific for thermal insulation in buildings. On the south facing wall a glazed area of 42 cm × 37 cm can be allocated, the remaining of this surface being occupied by a wood frame 90 mm thick, to shield the thickness of the inside insulating panes.

Table 2 – Thermal properties of STB materials

	Thickness (mm)	Density (kg/m ³)	Specific heat (J/(kg K))	Thermal conductivity (W/(m K))	Thermal resistance (m ² K/W)	SHGC
Plywood	8	545	1215	0.120	-	-
Insulation	80	36	1453	0.024 (at 10 °C)	3.33	-
Double glazed pane	20	2400	800	1.4	0.34	0.82

Each box is equipped to measure inside air temperature, illuminance, and surface temperature of the inner and outer side of the glazed pane. Temperature sensors are TT500 thermistors by Tecno.el srl with a wide temperature range (-30 to 120 °C), a resolution of 0.1 °C and an accuracy of ±0.2 °C. Illuminance is measured using a luxmeter by Delta Ohm srl with a measurement range of 200,000 lx, a sensitivity of 1.5 mV/klx and a less than 4 % calibration accuracy less than 4 W/%. Also outside temperature and relative humidity, solar irradiance on the vertical plane, and wind speed and direction are measured using a portable weather station. Temperature and relative humidity are measured by a Rotronic Hygroclip2 sensor with a ±0.1 °C accuracy for the temperature, and a ±0.8 % accuracy for relative humidity. The solar irradiance sensor is a silicon cell pyranometer provided by Apogee Instruments with an accuracy of ±5 % while wind speed and direction are measured using a 7911 anemometer model provided by Davis Instruments with an accuracy of ±1 m/s for speed and of ±7 ° for direction. Data are acquired at a minute time rate. The weather and solar station of ESTER lab (Lat. 41.9, Long. 12.6) provides direct and diffuse solar irradiance measurements useful for climate file construction in dynamic simulation software. Table 2 lists the material properties used in STBs.

2.3 STB Calibration

STBs original calibration is reported in Cornaro et al., 2015. For the purpose of this study it was necessary to reduce the glazed surface to control solar irradiance entering the boxes. In this way PCM was not exposed to too high temperatures that could damage it. For this reason, the original glazed area was reduced using a wider wood frame. A new calibration was then necessary to take this modification into account (Fig. 1).



Fig. 1 – STBs with different window frames during the calibration test

A short – term monitoring campaign was carried out at ESTER lab from November 12 to 17, 2015, to collect calibration data.

Fig. 2 shows the trends of the external and inside air temperatures, monitored in the two STBs equipped with the reference glazed pane and the two different frames. The inside temperature of both boxes increased to 50 °C and more, due to the high insulation properties of the materials and the solar heat gain of the glazing. In particular, the inside temperature of the old framed STB (Tair_OF) reached almost 80 °C, or more, while the new framed STB (Tair_NF) did not exceed 50 °C. This difference is explained by the reduction of the glazed surface due to the new frame.

First of all the air temperature trend inside the old framed box was compared to the simulation data provided by the STB model to verify the old calibration accuracy. Root mean square error (RMSE) and normalized RMSE, NMRSE, were used to evaluate the accuracy. The two indexes are defined as:

$$RMSE = \sqrt{\frac{\sum_{i=1}^n (x_i^m - x_i^s)^2}{n}} \quad (1)$$

$$NMRSE = \frac{RMSE}{x_{max}^m - x_{min}^m} \quad (2)$$

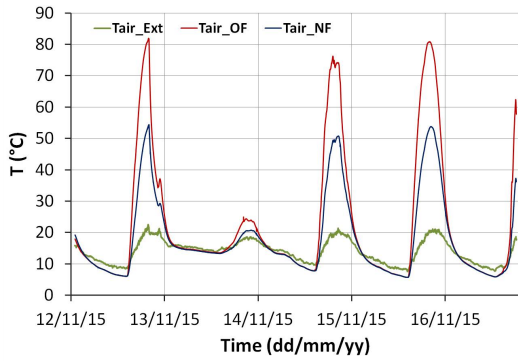


Fig. 2 – Temperature trends recorded during the calibration of the new frame (NF); OF = original frame; Ext = outside air

A RMSE of 2.72 °C was obtained over the whole test period with a 4 % NRMSE indicating good agreement with the original calibration.

To calibrate the new framed box the inside air temperature obtained by the STB simulation model was compared with the experimental data; the U-value of the frame and the ratio of opaque over glazed area (frame fraction) were changed in the model till the RMSE reached a minimum. Fig. 3 shows the inside air temperature trends of the new framed STB after calibration. A RMSE of 2.56 °C was obtained with a 5.4 % NRMSE, considering a $U = 2 \text{ W}/(\text{m}^2\text{K})$ and a frame fraction, $F = 0.55$.

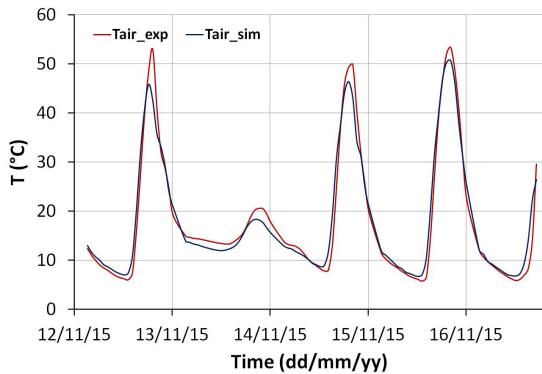


Fig. 3 – Comparison between measured and simulated temperature trends inside the new framed box after calibration

2.4 Measurement Campaigns

Two measurement campaigns were carried out, each of them including three full days of data acquisition.

2.4.1 First campaign

The first campaign was conducted from September 26 to 29, 2016. Two boxes were exposed outdoor, one with a PCM pane layered on the box floor (PCM box) and the other one without PCM (Ref box). Air

temperature inside both boxes was measured together with outdoor air temperature, relative humidity, wind speed and direction, and global irradiance on a vertical plane. Climatic conditions during the test are presented in Fig. 4 with air temperature (T_{air_ext}) and solar irradiance measured on a vertical plane (GR_V). Good weather conditions characterized the period with high temperatures (maximum peak at 29 °C) and a significant thermal range between day and night (12–13 °C). Solar irradiance reached peaks of approx. 800 W/m^2 . Fig. 5 shows the air temperature trends inside the reference box (T_{air_ref}) and the PCM box (T_{air_PCM}) during the test. A significant decrease in maximum temperature is observed in the PCM box when compared to Ref box due to the PCM melting in the 22–23 °C temperature range. An average decrease of the temperature peaks of approx. 10 °C is observed during the day while at night the opposite behavior occurs. Indeed, the air temperature inside the PCM box is higher than in the Ref box due to the PCM solidification and the thermal mass.

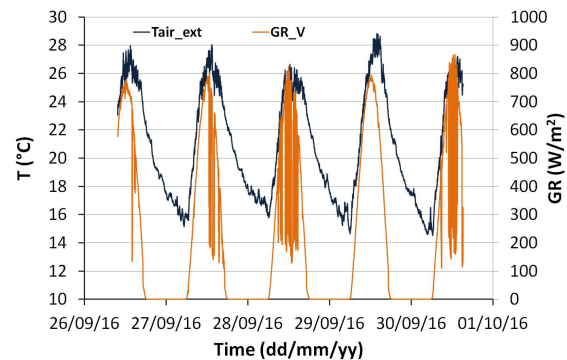


Fig. 4 – Outdoor air temperature and global irradiance on a vertical plane experienced during the first measurement campaign

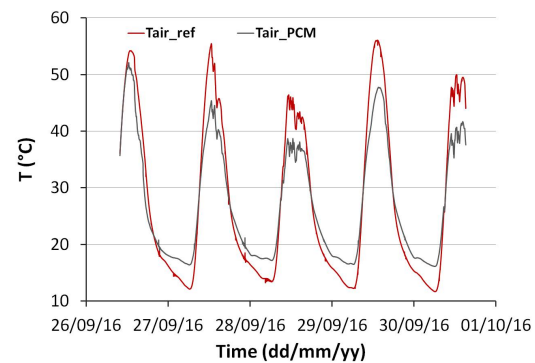


Fig. 5 – Air temperature inside the Ref box and the PCM box during the first test

No evident shift of the temperature trend due to PCM heat capacity is observed, that is because the amount of material in the box is not enough to produce this effect.

2.4.2 Second campaign

A second measurement campaign was carried out later, in winter, between December 5 and 9, 2016. We experienced nice weather during the last two days of test while the first day was overcast but not rainy, as evidenced by Fig. 6. The outdoor air temperature, in this case, was lower than in the first campaign with a maximum of approx. 21 °C, and a minimum of approx. 2 °C with a thermal range of 15 °C in the clear days. Solar irradiance reached values as high as 930 W/m². This is because in this period the sun elevation is low so a vertical surface receives higher irradiance than a horizontal one.

Fig. 7 shows the temperature trends inside Ref and PCM boxes.

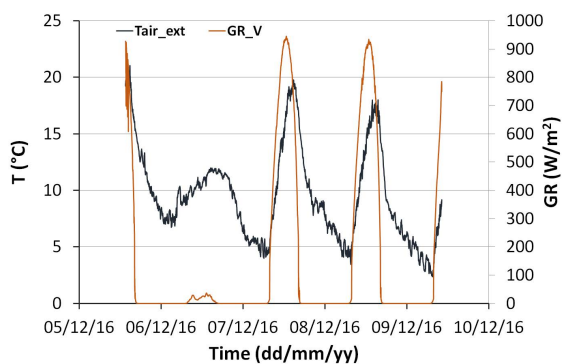


Fig. 6 – Outdoor air temperature and global irradiance on a vertical plane experienced during the second measurement campaign

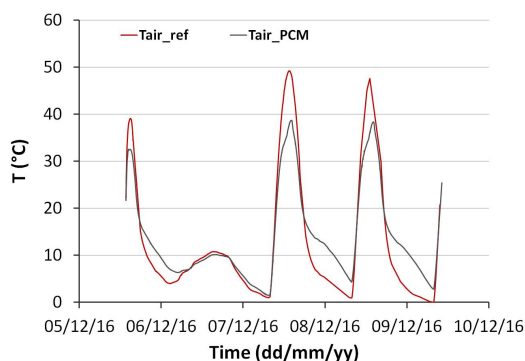


Fig. 7 – Air temperature inside the Ref box and the PCM box during the second test

Also in this case a temperature peak damping of approx. 10 °C caused by the PCM is observed during the clear days, while for the overcast day no effect of the material is observed due to the low temperatures experienced inside the box (well below melting point). PCM solidification occurs earlier in the day (around 7 pm) than in the first campaign (around midnight). Apart from this shift, we also observed a change in the curvature of the decreasing temperature trend with respect to the first campaign. This is probably due to the behavior of the solid phase at temperatures well below the solidification.

2.5 Simulation

2.5.1 STB model

STBs were simulated in the IDA ICE environment. The geographic location corresponded to ESTER lab coordinates, and customized climate files were built for all the simulations using weather data coming from the weather and solar station of the same lab. The boxes were oriented with the glazing area toward south. The thermal properties presented in Table 2 were inserted in the model. For what concerns the STB provided with the PCM, the custom software module was connected to the STB floor working in advanced level mode.

2.5.2 Custom PCM software module description

“PCM wall” is a module for IDA ICE, written in NMF language (Neutral Model Format), that allows calculating heat absorbed and/or released by phase change materials. It uses an enthalpy formulation to describe the relation between enthalpy and temperature for a PCM material with different paths during melting and solidifying phases. The partial enthalpies and the temperature coordinates are input parameter vectors describing this relation. Partial enthalpies are expressed in J/kg. Heat capacity (J/(kg K)) is calculated by dividing the partial enthalpies difference at different temperatures by the correspondent temperature interval.

The computed help variable “Mode” is used to keep track of the current state (phase) of the PCM material.

There are five different PCM conditions that can be monitored with the variable "Mode", for which heat capacity, thermal resistance, and temperature as a function of enthalpy are computed:

- Mode -2: solid phase
- Mode 2: liquid phase
- Mode -1: solidifying phase
- Mode 0: reversing during melting/solidifying phase
- Mode 1: melting phase

Fig. 8 shows the enthalpy versus temperature curves, as specified by RUBITHERM® for the SP21 PCM pane, for heating and cooling. These data were input to the PCM software module.

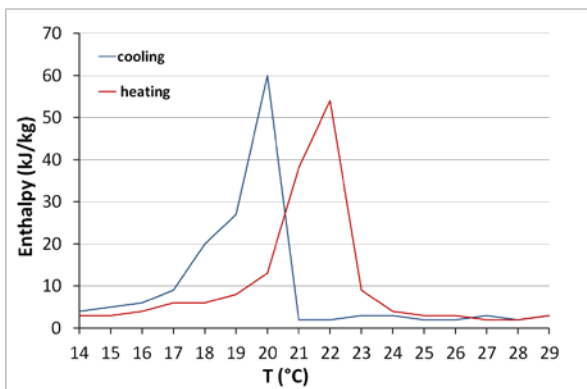


Fig. 8 – Enthalpy – Temperature curves for heating and cooling for the tested SP21 PCM pane

3. Discussion and Results

Experimental data gathered during the two experimental campaigns were used to validate the custom PCM software module with two datasets in which the PCM behaved in different ways due to different climatic conditions. During the first campaign, in the month of September, the weather conditions were such that the PCM material could work fully in its phase change temperature range, while in the month of December, even if solar irradiance was high, external air temperature limited the PCM phase status mainly to solid for most of the period. Fig. 9 A and B show the comparison between the experimental and simulated temperature trends inside the PCM box for the campaign of September and December, respectively. A very good agreement can be observed for both periods indicating the correct simulation of the boxes and the PCM. In Fig. 9B a major difference between the

experimental and simulated temperature is observed during the night, when the air temperature inside the PCM box fell to 18 °C. In this period the PCM material is in the solid phase and it continues to cool down. The model does not seem to follow the experimental trend as well as during the first campaign, this is probably due to the fact that the PCM specifications are not available in the model for such low temperatures.

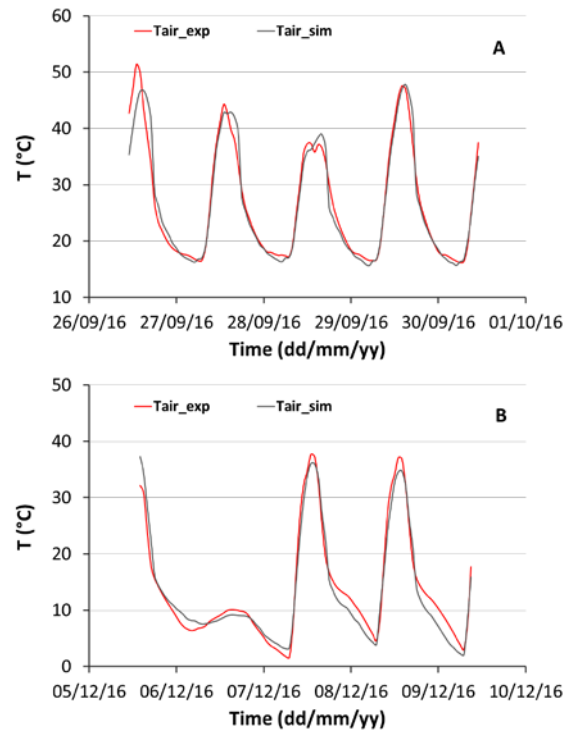


Fig. 9 – Measured and simulated air temperature, inside the PCM box for the first (A) and second (B) monitoring campaign

When overcast, day temperatures were too low so the PCM always remained in the solid phase. To quantify the accuracy of the simulation, we evaluated the RMSE and NRMSE for all cases, and listed them in Table 3. In the calculations the first and last hours of operation were discarded to evaluate the indexes on three full days for each campaign. Also the indexes referred to Ref box were evaluated to verify the correct simulation of the box itself. It can be noticed how NRMSE stays below 6 % in all cases, confirming the optimum agreement.

Table 3 – RMSE and NMRSE between measured and simulated temperature trends for the two campaigns

Campaign	Ref box		PCM box	
	RMSE	NMRSE	RMSE	NMRSE
	(°C)	(%)	(°C)	(%)
26-29/09/16	1.78	4.1	1.57	5.0
05-12/12/16	2.50	5.2	1.83	5.1

Fig. 10 A and B show the heat fluxes (HF) of PCM and of the incoming solar radiation together with the temperature experienced by PCM simulated for the two monitoring campaigns.

The pane removes approx. 15 W peak during the day compared to an incoming solar flux with peaks of around 40 W (around 40 % heat reduction) lowering the box air temperature peaks of approx. 10 °C.

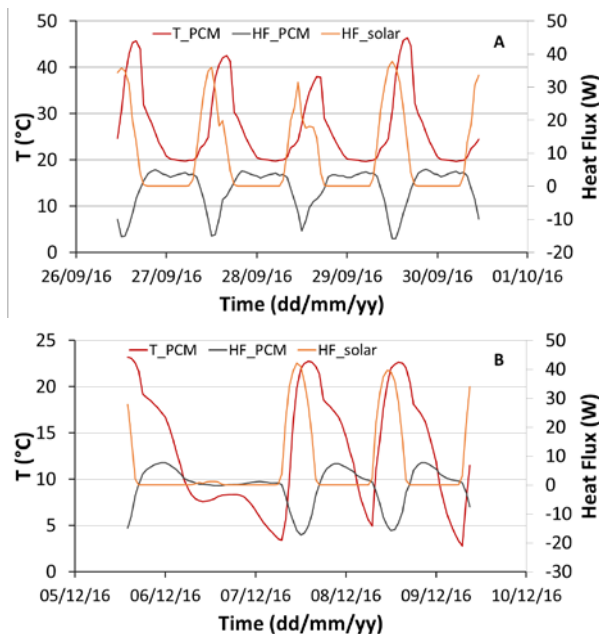


Fig. 10 – Heat flux (HF) of PCM and of incoming solar radiation and temperature trend of the PCM. A: first test; B: second test

During the night it releases heat (4–5 W) due to solidification. While during the first campaign it stays in the liquid phase all day, and in the solid phase during night, in the second campaign it is mainly in the solid phase due to low outside temperatures, melting occurring only between 11:00 am and 6:00 pm.

4. Conclusion

We have introduced a method to validate custom-made software module to simulate PCM materials. The software module was built in the IDA ICE environment and experimental data for validation were collected in two outdoor monitoring campaigns using solar test boxes. A different behaviour of the PCM could be observed due to different climate conditions during the two campaigns. We detected a very good agreement between measured and simulated temperature trends inside the boxes, which proves the good implementation of the customized software module. Small discrepancies were only identified during nighttime for the December campaign, probably due to lack of information on PCM behaviour at such low temperatures in the solid phase. However, this does not invalidate the results obtained. We also carried out the analysis of heat fluxes using the validated model. Future work will consist in the energy saving capability evaluation of PCM materials implemented in office buildings.

References

- Barreneche, C., M.E. Navarro, A. Ines Fernandez, L.F. Cabeza. 2013. "Improvement of the thermal inertia of building materials incorporation PCM. Evaluation in the macroscale". *Applied Energy* 109:428–432. doi: 10.1016/j.apenergy.2012.12.055.
- Cornaro, C., F. Bucci, M. Pierro, M.E. Bonadonna, G. Siniscalco. 2015. "A new method for the thermal characterization of transparent and semi-transparent materials using outdoor measurements and dynamic simulation". *Energy and Buildings* 104: 57–64. doi: 10.1016/j.enbuild.2015.06.081.
- Entrop, A.G., H.J.H. Brouwers, A.H.M.E. Reinders. 2011. "Experimental research on the use of micro-encapsulated Phase Change Materials to store solar energy in concrete floors and to save energy in Dutch houses". *Solar Energy* 85: 1007–1020. doi: 10.1016/j.solener.2011.02.017.
- Fernandez, N.T.A., V.A.F. Costa. 2009. "Use of phase-change materials as passive elements for climatization purposes in summer: the

- Portuguese case". *International Journal of Green Energy* 6(3):302–311. doi: 10.1080/15435070902886585.
- Goia, F., M. Perino, V. Serra. 2014. "Experimental analysis of the energy performance of a full-scale PCM glazing prototype". *Solar Energy* 100: 217–233. doi: 10.1016/j.solener.2013.12.002.
- Guarino, F., V. Dermardiros, Y. Chen, J. Rao, A. Athienitis, M. Cellura, M. Mistretta. 2015. "PCM thermal energy storage in buildings: experimental study and applications". *Energy Procedia* 70: 219 – 228. doi: 10.1016/j.egypro.2015.02.118.
- Khadiran, T., M.Z. Hussein, Z. Zainal, R. Rusli. 2016. "Advanced energy storage materials for building applications and their thermal performance characterization: a review". *Renewable and Sustainable Energy Reviews* 57: 916–928. doi: 10.1016/j.rser.2015.12.081.
- Lee, S.H., S.J. Yoon, Y.G. Kim, Y.C. Choi, J.H. Kim, J.G. Lee. 2007. "Development of building materials by using micro-encapsulated phase change material". *Korean Journal of Chemical Engineering* 24(2):332–5. doi: 10.1007/s11814-007-5054-8.
- Li, M, Z. Wu, J. Tan. 2013. "Heat storage properties of the cement mortar incorporated with composite phase change material". *Applied Energy* 103:393–399. doi: 10.1016/j.apenergy.2012.09.057.
- Marchi, S., S. Pagliolico, G. Sassi. 2013. "Characterization of panels containing microencapsulated phase change materials". *Energy Conversion and Management* 74:261–268. doi: 10.1016/j.enconman.2013.05.027.
- Sage-Lauck, J.S., D.J. Sailor. 2014. "Evaluation of phase change materials for improving thermal comfort in a super-insulated residential building". *Energy and Buildings* 79:32–40. doi: 10.1016/j.enbuild.2014.04.028.
- Souayfane, F., F. Fardoun, P.H. Biwole. 2016. "Phase change materials (PCM) for cooling applications in buildings: A review". *Energy and Buildings* 129: 396–431. doi: 10.1016/j.enbuild.2016.04.006.
- Su, J.F., X.Y. Wang, S.B. Wang, Y.H. Zhao, Z. Huang. 2012. "Fabrication and properties of microencapsulated-paraffin/gypsum-matrix building materials for thermal energy storage". *Energy Conversion and Management* 55:101–107. doi: 10.1016/j.enconman.2011.10.015.
- Tardieu, A., S. Behzadi, J.J.J. Chenand, M.M. Farid. 2011. "Computer simulation and experimental measurements for an experimental PCM-impregnated office building". In: *Proceedings of Building Simulation 2011*. Sydney, Australia: IBPSA.
- Telkes, M. 1975. "Thermal storage for solar heating and cooling". In: *Proceeding of the workshop on Solar Energy Storage Subsystems for the Heating and cooling of Buildings*. Charlottesville, U.S.A.
- Zhang, G.H., S.A.F. Bon, C.Y. Zhao. 2012. "Synthesis, characterization and thermal properties of novel nano encapsulated phase change materials for thermal energy storage". *Solar Energy* 86:1149–1154. doi: 10.1016/j.solener.2012.01.003.
- Zhang, Z., G. Shi, S. Wang, X. Fang, X. Liu. 2013. "Thermal energy storage cement mortar containing n-octadecane/expanded graphite composite phase change material". *Renewable Energy* 50:670–675. doi: 10.1016/j.renene.2012.08.024.
- Zhou, D., G.S.F. Shire, Y. Tian. 2014. "Parametric analysis of influencing factors in phase change material wallboard (PCMW)". *Applied Energy* 119:33–42. doi: 10.1016/j.apenergy.2013.12.059.
- Zwanzig, S.D., Y. Lian, E.G. Brehob. 2013. "Numerical simulation of phase change material composite wallboard in a multi-layered building envelope". *Energy Conversion and Management* 69:27–40. doi: 10.1016/j.enconman.2013.02.003.

Analysis of the Influence of Thermal Losses of the Recirculation Flow Loop in a Residential Hot Water Solar System

Paolo Valdiserri – University of Bologna – paolo.valdiserri@unibo.it

Abstract

Water heating for domestic needs contributes significantly to energy demands in the residential sector. The paper reports an energetic analysis of a solar hot water system performed on a dwelling located in Rome, Italy. The study is focused on a group of apartments, where the domestic hot water is provided by a solar system coupled with a storage tank. A recirculation loop, composed by a pump and a system of pipes from the tank to the more distant apartment is also considered in the study. The loop overcomes the problem of long waiting times for hot water for the user by keeping it flowing inside the system. Since the recirculation loop is compulsory in this kind of plants, a dynamic energetic analysis is performed in order to analyse the pipe heat loss influence on the solar fraction. Dynamic simulations are performed using TRNSYS by setting different parameters (insulation thickness, pipe length, mass flow rate) and by interrupting the flow in the recirculation loop during the night. The study shows the sizing process of the whole system, the variation of the solar fraction and heat loss fraction for all the analysed cases.

1. Introduction

Water heating for domestic needs contributes significantly to the energy demands in the residential sector. The Member States of the European Union have to achieve at least 20 % of renewable sources in the final energy consumption by 2020. Solar Water Heating (SWH) is a well-known technology able to allow energy savings and reductions in CO₂ emissions in water heating for residential needs. The performance of SWH systems has been studied theoretically and experimentally over the past several decades (Duffie and Beckman, 2013). Different computational tools have been developed to numerically evaluate the long-term performance

of solar systems and to study the effect of the design parameters. TRNSYS 17 (Klein et al., 2010) is an extensive software for transient simulation that provides good agreement with experimental data. Shrivastava et al. (2017) provide a critical review of the SWH system simulation, a comparative analysis of popular simulation tools, and their architecture in the TRNSYS perspective.

Hobbi and Siddiqui (2009) used TRNSYS to model a forced circulation SWH system for domestic hot water requirements in Montreal, Canada. In their study, they optimized the system and collector parameters by changing, among others, collector area and mass flow rate, storage tank volume, size and length of connecting pipes. The authors reported that by utilizing solar energy, the modelled system could provide 83–97 % and 30–62 % of the hot water demands in summer and winter, respectively.

For circulation of the hot water in the system piping a big amount of energy is required (Lee, 2009). Once the hot water leaves the storage tank and flows through the pipes, the water temperature drops due to the travel distance and ambient air temperature. The solution for the problem, without using a circulation loop, is to reheat the water before use.

Since water circulation in pipes has an energetic cost, it is desirable to interrupt the hot water flow in the pipes when the water requirement is low. For this reason, it is important to know the hourly hot water consumption. Moreover, data of domestic hot water consumption are pivotal to compute the energy demand and to design the SWH system. Studies based on measured data or simulations are available to estimate DHW consumption focusing on a daily average, hourly average, appliance consumption, and number of occupants (Ahmed et al., 2016; Edwards et al., 2015). Ahmed et al. derived the

hourly DHW profiles for 5 groups of a different number of people as a function of the number of occupants. In the study weekday (WD) and weekend (WE) consumption variations were reported.

In the present study, the entity of energy losses in the circulation loop between the hot water storage tank and the final hot water outlet has been analysed both in terms of *solar fraction* and *heat loss fraction*.

2. SWH System Under Investigation

In the present study a forced circulation system with a secondary flow loop and a storage tank is modelled (Fig. 1). The secondary flow, that absorbs and transports the solar energy collected by the solar collector (SC), circulates between a heat exchanger, inside a storage tank (SST), and a collector. When the produced water is cooler than the desired set temperature in the tank ($50 \pm 2.5 \text{ }^\circ\text{C}$) or during over-cast days, the water inside the tank is warmed up by a hot fluid through a heat exchanger placed inside the tank (Aux). The produced hot water reaches the final user through a system of pipes (HW). A tempering valve adds cold water (CW) to adjust the temperature in order to supply the water (ws) at the user's desired temperature ($38 \text{ }^\circ\text{C}$).

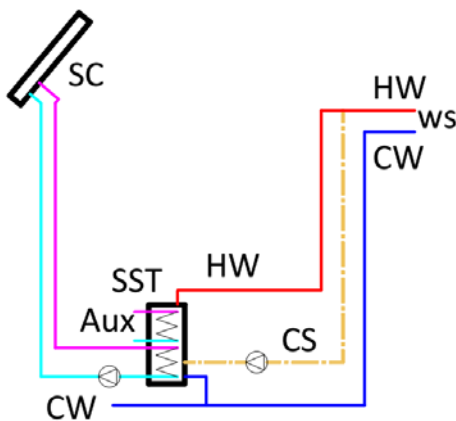


Fig. 1 – Sketch of the SWH system

A recirculation flow loop (CS) can keep the water warm from the storage tank to the final user. The described system is simulated using the TRNSYS simulation program.

The solar heating plan is located in Rome, and it provides hot water for a residential building of 20 apartments (48 people). The average daily consumption of hot water is set to 2400 litres (50 l per person). The solar radiation and ambient temperature data as a function of time are from Meteonorm.

2.1 Hot Water Load Profile

The hourly distribution of domestic hot water consumption during a day is affected by several factors. It varies from day to day, from season to season, and from family to family. The daily water profiles used in this study are presented in Fig. 2 and are derived from Ahmed et al. (2016) in the case of a community of ≥ 50 people.

In the graph, for each hour of the day the hourly water consumption (l/h) is reported for an average daily consumption of 2400 litres. Four different profiles are used in the present study according to: i) the period of year: winter (WIN), summer (SUM), and ii) the day of the week: weekday (WD), weekend day (WE). The winter period goes from the last Monday in October to the last Sunday in March, while the summer season starts on the last Monday in March and ends on the last Sunday in October.

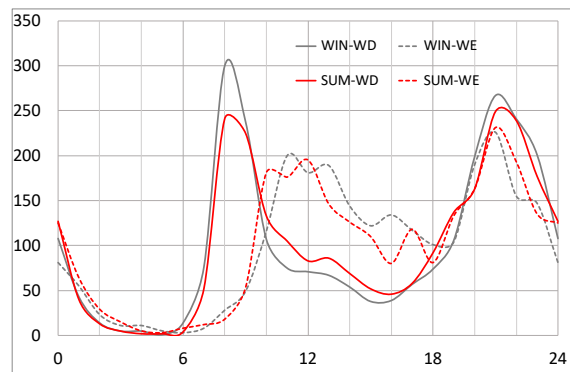


Fig. 2 – Daily water profiles for winter and summer, weekdays and weekend (from Ahmed et al. 2016)



Fig. 3 – DHW monthly consumption factor for Italian apartment buildings (modified from Ahmed et al., 2015, see text for further explanation)

The monthly correction factor was modified from the one proposed by Ahmed et al. (2016), since the majority of people in Italy are on vacation in August and therefore the consumption of hot water drops in that period of the year (Fig. 3).

2.2 Description of System Components

Solar collector (SC): Flat-plate collectors are used with a total area of 30 m², oriented toward south with a 50 ° slope. The set parameters are summarised in Table 1: η_0 indicates the optical efficiency of the collector; a_1 and a_2 represent the thermal loss parameters.

Table 1 – Solar collector characteristics

η_0	a_1 (W m ⁻² K ⁻¹)	a_2 (W m ⁻² K ⁻²)
0.807	3.766	0.0059

Storage water tank (SST): A fully stratified 3 m³ storage tank (10 nodes) is employed in the simulation. Two heat exchangers provide heat from the solar collector and from the auxiliary system.

Solar circuit: A pipe system connects the solar collector to the upper heat exchanger inside the storage water tank. A mixture of water and glycol flows in the circuit. The total length of the circuit is 60 m and the pipes are insulated with the minimum thickness of insulation required by the Italian law (DPR 412/93).

Circulation system (CS): A pipe system connects the storage water tank to the apartments where the hot water is supplied. A mass flow of 500 kg/h is moved by a pump. This is the pipe system under investigation in the present paper. Different pipe lengths and different thicknesses of pipe insulation are taken into account.

3. Results and Discussion

Monthly or annual solar fraction, which is the fraction of the total hot water energy (Q_{Load}) that is supplied by solar system, are calculated using the equation by Buckles and Klein (1980),

$$f = (Q_{Load} - Q_{Aux})/Q_{Load} \quad (1)$$

where Q_{Aux} is the energy supplied by the auxiliary system to integrate the part of the total load that is not provided by the solar energy.

In Fig. 4 the solar fraction in three different cases is shown: i) without taking into account the heat losses from the tank and the pipes of both the solar and the recirculation system (no circuit losses, NCL); ii) by considering only the losses of the solar circuit and the tank but not the recirculation flow loop (no recirculation loop losses, NRL); iii) by considering the three heat losses mentioned above (total circuit losses, TCL). In the latter case the length of the recirculation pipe is 30 m (CS in Fig. 1); the overall length of the circuit is 60 m including the hot water pipes (HW in Fig. 1). The considered insulation thickness, with an insulation material having a thermal conductivity $\lambda = 0.036$ Wm⁻¹K⁻¹, is set at 19 and 13 mm respectively for a pipe of 1"1/4 (HW in Fig. 1) and 3/4 (CS in Fig. 1). In the present work these insulation parameters are considered a *standard insulation*.

Fig. 4 shows the yearly solar fraction fall from 81.7 % (NCL) to 66.5 % (NRL) and 60.2 % (TLC). The difference between the three cases is more evident in the winter months, likely due to pipe heat losses that are not counteracted by the solar energy. Neglecting pipe losses may lead to overestimate the solar factor.

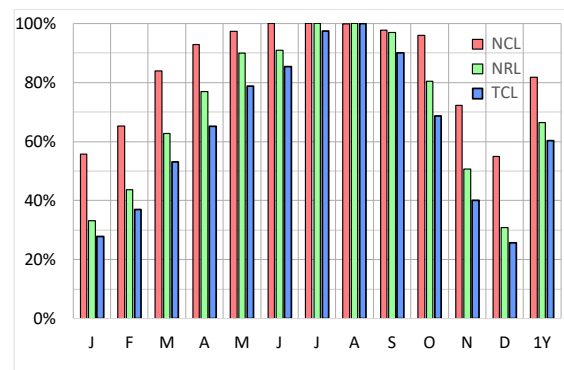


Fig. 4 – Monthly and yearly solar fraction average in three different cases (see text for more details)

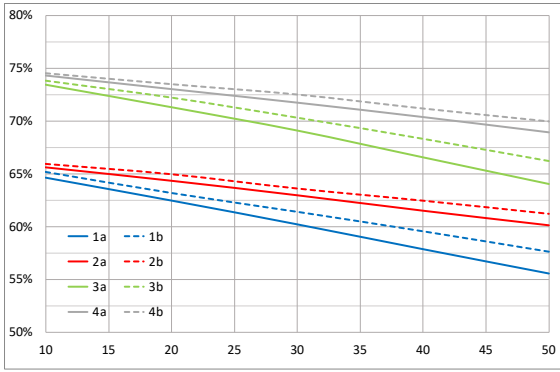


Fig. 5 – Solar fraction vs different pipe length of the circulation system

Fig. 5 shows the yearly solar fraction by varying the length of the recirculation pipes in eight different cases: 1a) *standard insulation* and an average daily consumption by the occupants of the apartments set to 2400 litres; 2a) insulation with the same insulation material as in case 1a) but with an increased thickness of 40 mm and 25 mm respectively of 1”1/4 and 3/4 pipes, the average daily consumption set to 2400 liters; 3a) *standard insulation* and an average daily consumption reduced to 1600 liters; 4a) insulation with the same insulation material and thickness as in case 2a). The average daily consumption was reduced to 1600 liters. Cases 1b-4b have the same pipe features and averaged daily consumptions as in cases 1a–4a, whilst the recirculation pump was switched off every day between 11 pm to 6 am. So, during the night, when the hot water demand is lower than during the day, no water circulates through CS pipes and only the hot water required by the users flows in HW.

As expected, the solar fraction increases by reducing the water flow from 2400 to 1600 liters per day, and by increasing the insulation thickness. Vice versa, if the length of the pipes is increased, the solar fraction decreases. Interestingly, the solar fraction increases during the night interruption of the flow, and it becomes more evident if the thickness of the insulation and the length of the pipes are reduced.

The same cases (1a–4a and 1b–4b), described above, are evaluated in terms of *heat loss fraction* (Fig. 5). The heat loss fraction is defined by:

$$hlf = \frac{Q_{Loss}}{Q_{Load}} \quad (2)$$

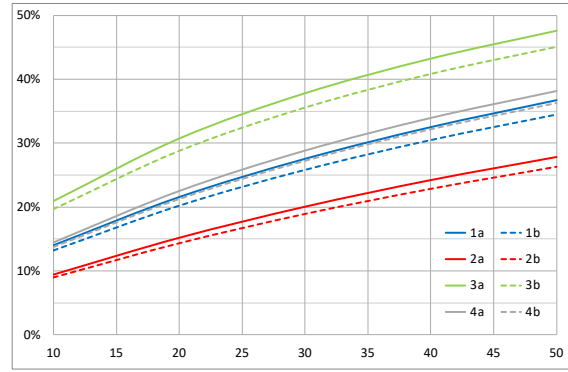


Fig. 6 – Heat loss fraction vs different pipe length of the circulation system

where Q_{Loss} is the energy waisted through the pipes from the tank to the final user and in the recirculation circuit.

As expected, increasing the pipe length leads to an increase in the heat loss fraction. Two possible strategies can be used to reduce the heat loss fraction: either by increasing the thickness of the insulation, or by switching the circulation pump off when the user demand is low (i.e. during the night). As seen in Fig. 6, better results in terms of reducing the heat loss fraction can be obtained doubling the insulation thickness instead of switching the circulation flow off during the night. Reducing the water flow from 2400 to 1600 liters per day leads to a heat loss fraction increase.

Fig. 7 shows the heat loss fraction for different values of the daily water consumption. The circulation pipes have a *standard insulation*, the same thickness and thermal characteristics of the cases 1a and 2a, and the length of 30 m (CS in Fig. 1).

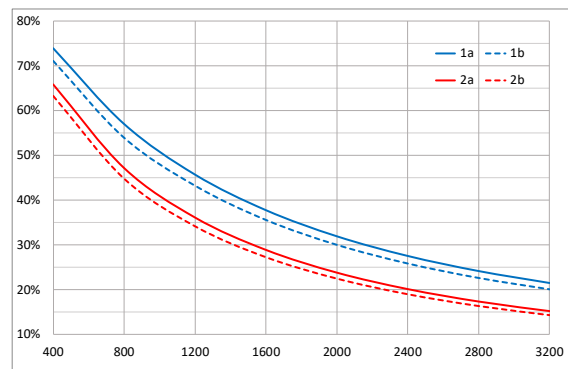


Fig. 7 – Heat loss fraction vs different daily water consumption by the occupants of the apartments

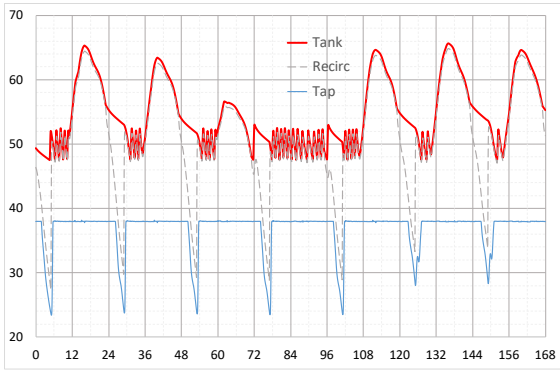


Fig. 8 – Water temperature oscillation during one week in winter, circulation pumps switch off during the night

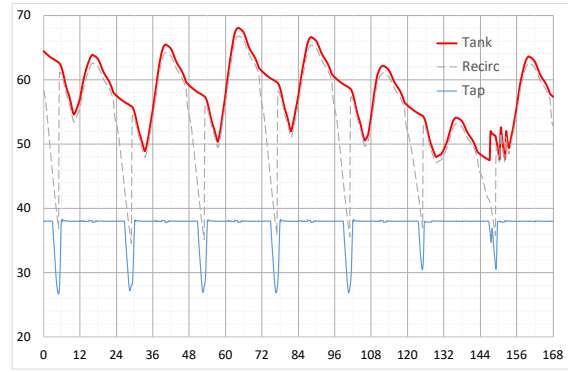


Fig. 9 – Water temperature oscillation during one week in summer, circulation pumps switch off during the night

The curves, the one with the 24 h daily circulation (cases 1a, 2a) and the one operating only during the daytime (dotted line, cases 1b, 2b), are reported in the graph. Reducing the daily water consumption leads to a dramatic increase in heat loss fraction.

Despite the advantages in energy saving obtained by switching the circulation pump off, the system is not able to provide the warm water set at 38 °C at the user level during the night period, as can be seen in Fig. 8. This figure displays the variation of the water temperature during one week in winter (middle of February) in three different sections. The pipes have a *standard insulation*, the average daily consumption by the occupants of the apartments was set to 2400 litres (case 1b). The red line represents the temperature of the hot water exiting the tank, the dotted line is the temperature of the water leaving the hot water pipes at the three way valve with the circulation pipes (end of the circuit before mixing with the cold water); the light blue line is the temperature of the water at the user's tap after mixing with the cold water. The control of the auxiliary system starts to provide energy to the tank water when the temperature falls below 47.5 °C and ends when it reaches 52.5 °C. The peak (i.e. $T > 52.5 \text{ }^\circ\text{C}$) of the red line in Fig. 8 is due to the energy from the solar collectors, while the sharp oscillations around 50 °C derive from the auxiliary energy.

During the night, the hot water at the user's tap falls below the setting point of 38 °C about 2h after the circulation pump is switched off. So to have water at 38 °C in the apartments, it is necessary to reheat the water locally (i.e. with an electric boiler).

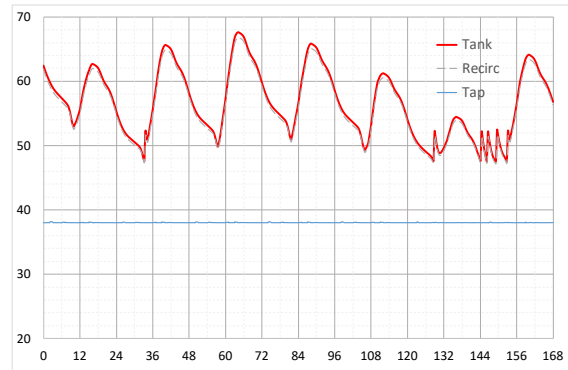


Fig. 10 – Water temperature oscillation during one week in summer, circulation pumps switch on during the night

If the pump is kept on during the night, it is not necessary to reheat the water at the user's end, but the tank water is heated in the storage tank by the auxiliary system (data not shown).

Fig. 9 shows the variation of the water temperature during one week in summer (end of June) in the three different positions previously described. As in Fig. 8, the pipes have *standard insulation* and the daily average consumption by the occupants of the apartments was set to 2400 litres (case 1b).

Like in winter, in the summer week (Fig. 9) during the night, when the circulation pump is switched off, the hot water at the user's tap falls below the setting point of 38 °C, it is therefore necessary to reheat the water locally.

Fig. 10 shows the variation of the water temperature during the same week in summer analyzed in Fig. 8 (end of June) when the circulation pump is on. By comparing the red lines of Fig. 9 and Fig. 10, it is possible to observe that during that week, the auxiliary system (heat exchanger inside the tank) provides energy 3 times when the pump is off during the night, and 6 times when the pump is

working continuously. At the user level, when the pump is on, it is not necessary to locally reheat the water, while if the pump is off this is needed.

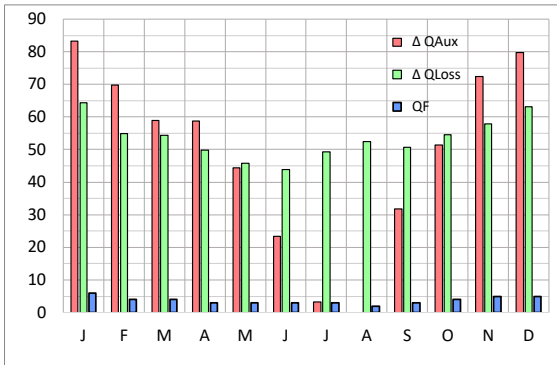


Fig. 11 – Difference in monthly energy consumption between having the circulation pump switched on or off during the night

Fig. 11 presents the difference in terms of energy (in kWh) between the case when the circulation pump is switched on 24 h/day and the case when it is off during the night. Both cases have a 30 m circulation system with *standard insulation* and a daily flow rate of 2400 liters (Cases 1a and 1b). The figure shows that: i) the energy needed to reheat the water during the night (Q_F) when the pump is switched off is always smaller than the energy dissipated through the pipes (ΔQ_{Loss}); ii) the auxiliary energy difference (ΔQ_{Aux}) between the two cases is irrelevant in July and August; iii) the energy needed to reheat the water during the night when the pump is switched off is smaller than the auxiliary energy difference in winter and in the summer months except in July and August. Since in summer the energy to heat the water is provided by the solar collector, it is not necessary to switch off the pump to save auxiliary energy.

4. Conclusion

In the present study TRNSYS software was used to model a forced circulation SWH system for domestic hot water requirements in Rome, Italy. The entity of energy losses in the circulation loop between a hot water storage tank and the final hot water outlet has been analysed both in terms of *solar fraction* and *heat loss fraction*.

The study demonstrates that neglecting pipe losses leads to an overestimation of the solar factor.

To improve the solar fraction, different strategies can be applied: increasing the thickness of the insulation, interrupting the recirculation flow when the mass flow rate is low (i.e. during the night). It was found that doubling the insulation thickness instead of switching the circulation flow off during the night ameliorates the solar fraction and reduces the heat loss fraction. In addition, reducing the daily water consumption leads to a dramatic increase in heat loss fraction.

The domestic hot water is heated by solar collectors and an auxiliary system. The study indicates that in sunny summer days, the energy to heat the water is fully provided by the solar collector, it is thus not necessary to switch off the pump to save auxiliary energy. To decide if it is economically convenient to interrupt the circulation flow during summer nights it is necessary to monitor whether the heat is provided by the solar collector or the auxiliary system. Further studies are required to set up an appropriate circulation pump control system related to the hot water mass flow rate and the temperature in the pipes. With a customer tailored control system on the pump, it would be possible to reduce or increase the switching off period during the entire day, not only during the night. Moreover, the present strategy could be applied to other cities with different climatic conditions.

Nomenclature

Symbols

Q	Energy (kWh)
T	Temperature (°C)
λ	Thermal conductivity ($W\ m^{-1}K^{-1}$)

Subscripts/Superscripts

Aux	Provided by auxiliary system
F	Necessary to reheat the water locally
Load	Necessary to heat the requested water
Loss	Waisted through the pipes

References

- Ahmed, K., P. Pylsy, J. Kurnitski. 2016. "Hourly consumption profiles of domestic hot water for different occupant groups in dwellings". *Solar Energy* 137: 516–530. doi: 10.1016/j.solener.2016.08.033.
- Buckles, W.E., S.A. Klein. 1980. "Analysis of solar domestic hot water heaters". *Solar Energy* 25(5): 417–424. doi: 10.1016/0038-092X(80)90448-X.
- Duffie, J.A., W.A. Beckman. 1974. *Solar Engineering of Thermal Processes*. Hoboken, U.S.A.: John Wiley & Sons, Inc.
- Edwards, S., I. Beausoleil-Morrison, A. Laperrière. 2015. "Representative hot water draw profiles at high temporal resolution for simulating the performance of solar thermal systems". *Solar Energy* 111: 43–52. doi: 10.1016/j.solener.2014.10.026.
- Hobbi, A., K. Siddiqui. 2009. "Optimal design of a forced circulation solar water heating system for a residential unit in cold climate using TRNSYS". *Solar Energy* 83: 700–714. doi: 10.1016/j.solener.2008.10.018.
- Klein, S.A., et al. 2010. *TRNSYS Version 17*. Madison, U.S.A.: Solar Energy Laboratory, University of Wisconsin-Madison.
- Lee, M.C. 2014. "Reducing CO₂ emissions in the individual hot water circulation piping system". *Energy and Buildings* 84: 475–482. doi: 10.1016/j.enbuild.2014.07.094.
- President of the Italian Republic. 1993. *D.P.R. 26 agosto 1993, n. 412. Regolamento recante norme per la progettazione, l'installazione, l'esercizio e la manutenzione degli impianti termici degli edifici ai fini del contenimento dei consumi di energia, in attuazione dell'art. 4, comma 4, della L. 9 gennaio 1991, n. 10.*
- Shrivastava, R.L., V. Kumar, S.P. Untawale. 2017. "Modeling and simulation of solar water heater: A TRNSYS perspective". *Renewable and Sustainable Energy Reviews* 67: 126–143. doi: 10.1016/j.rser.2016.09.005.

Calibration of the Energy Simulation Models using Tikhonov-Type Regularization: Application to a Residential Building Apartment

Maja Miletić – Institute for Renewable Energy, EURAC – maja.miletic@eurac.edu

Chiara Dipasquale – Institute for Renewable Energy, EURAC – chiara.dipasquale@eurac.edu

Roberto Fedrizzi – Institute for Renewable Energy, EURAC – roberto.fedrizzi@eurac.edu

Abstract

It is well known that the calibration of building energy models is an under-determined problem, whether subjected to hourly or monthly calibration criteria. In fact, while it is possible to identify a large number of calibrated models, it is not clear which offer a good representation of the building behaviour. For a calibration methodology of building energy models to be effective, it should automate and speed-up calibration processes. This is especially important when the number of model parameters is too large to tune manually. Moreover, when the number of model parameters is too large, the probability to find the real parameter combination using statistical sampling methods is very small. Instead, we suggest performing a guided search of the parameter space, e.g. solving a parameter optimization problem. Since Tikhonov-type regularization has been applied successfully to many ill-posed inverse problems, we propose adopting the same methodology to find optimal parameters for building energy models. The regularization term can be interpreted as imposing certain a-priori distributions on model parameters as identified by an energy audit. As an illustration, the study case of a residential apartment is calibrated and we show that regularization more accurately predicts the energy demand estimate after the retrofit of the study case.

1. Introduction

It is well known that the calibration of building energy simulation models against the monitored energy demand, is an under-determined problem (Alifanov et al., 1995), whether subjected to hourly or monthly calibration criteria. To account for model uncertainty, the identification of more than one calibrated model is advised (ASHRAE, 2002). While it is possible to identify a large number of calibrated parameter sets, it is not clear which offer

a reasonable representation of the real building. The importance of reducing parameter uncertainty in building energy models, lies in the increased confidence in the calculation of savings for the intended energy conservation measures (Heo et al., 2012), as well as in the reliable prediction for model predictive controls (Schirrer et al., 2016), to name just a couple of applications.

In order to rank different calibrated models, Reddy et al. (2007) introduce an aggregated index incorporating a number of statistical indicators representing the agreement between simulation data and data reported on monthly utility bills. However, the calibration process can result in large standard deviations for certain influential model parameters. Caucheteux et al. (2013) calibrated an energy simulation model for a house based on hourly monitoring data. They noticed that, although the deviation of some influential parameters seems to decrease as the calibration period increases, some parameters can cancel each other out, thus a significant parameter deviation remains. Alternatively, Heo et al. (2012) proposed a probabilistic approach based on the Bayesian calibration of energy models to match monthly gas consumption values. Unlike deterministic methods, in a Bayesian approach a distribution function of each model parameter is sought, it directly provides the quantification of uncertainty.

Recently, optimization-based approaches have been utilized in simulation model calibration (Tahmasebi et al., 2012), where the cost function sums up the discrepancy between simulation and monitoring data. Solving an optimization problem for a parameter combination which optimally matches the monitored data, leads to further automatization of the

calibration process. However, the danger of the cancellation effect of two or more parameters remains. In this way, parameters may also reach the boundaries of the predefined parameter range, thus taking on less plausible values.

Regularization has already been successfully applied to many ill-posed inverse problems including the calibration of financial market models (Crépey, 2003), geophysical models (Zhdanov, 2002), and even in meteorology and oceanography (Navon, 1998). We propose adopting the Tikhonov-type regularization to find optimal parameters for building energy models. When regularization is applied, priority is given to those solutions which are ranked closer to the modeller’s initial guess.

In Section 2 we introduce the proposed methodology, and its application to a residential building apartment is presented in Section 3. Finally, the conclusion and the discussion on further research are given in Section 4.

2. Calibration Methodology

The goal of developing an effective calibration methodology for building energy models is to automate and speed-up the calibration process, which is especially convenient when the number of model parameters is too large to tune manually. In the literature, there is a clear consensus that the first phase of the calibration procedure consists in an energy audit of the building and the acquisition of monitoring data, followed by an initial model development and the identification of uncertain model parameters (Coakley et al., 2012; Raftery et al., 2011). In the second stage, the dimension of the parameter space is typically reduced using a sensitivity analysis, and the calibration criteria are chosen (and potentially the validation criteria) based on the acquired monitoring data and the simulation results of the initial model (Fig. 1). However, a number of different methods for the final calibrated energy model(s) identification are used in the literature. Not all include a validation step. In earlier approaches, the parameters were tuned manually, based on the expertise of the modeller. This process was later automatized, mostly using the statistical sampling

of the parameter space to evaluate different parameter combinations.

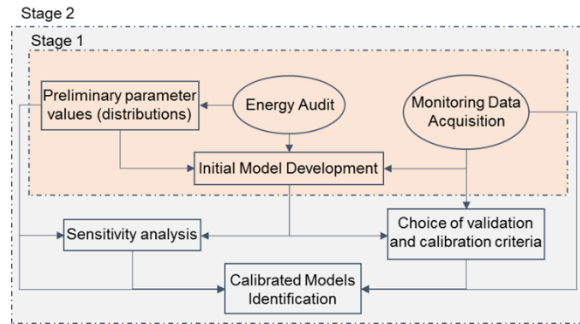


Fig. 1 – Typical building energy model calibration procedure

The calibration process can be further automatized using a guided search (e.g. optimization algorithm) to directly identify optimal parameter combinations. In the rest of this chapter, we present a regularization-augmented optimization-based approach to building energy model calibration. This approach aims at reducing the model uncertainty that arises from common practice.

2.1 Parameter Space and Probability Distribution

We assume we have an initial simulation energy model of the building, and that the number of model parameters was reduced by sensitivity analysis. Let $p = (p_1, \dots, p_n) \in \mathbb{R}^n$ be the model parameter vector, where $p_k \in [p_k^{min}, p_k^{max}]$ lies in the realistic range chosen by the modeller based on an energy audit and/or various datasheets on material properties, internal gains, etc.

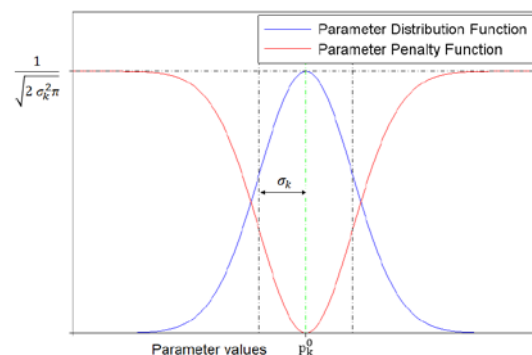


Fig. 2 – Parameter distribution and penalty function

Parameter ranges should be chosen wide enough to include all plausible values for the given case, even if their probability is low. We also assume that for some parameters it was possible to give an initial guess p_k^0 as well as choose an a-priori probability distribution function. For example, the normal distribution $p_k \sim N(p_k^0, \sigma_k)$ can be assumed (Fig. 2), where a modeller provides an appropriate deviation estimate σ_k . The higher the certainty of the initial guess p_k^0 , the lower the deviation σ_k .

2.2 Optimization Problem

In order to identify the parameter vector p that fits the monitoring data, a constrained optimization problem is defined to minimize the error between the monitored and simulated energy demand:

$$\min J(p), \quad \text{where } p_k \in [p_k^{\min}, p_k^{\max}] \quad (1)$$

In order to optimally represent the building under consideration, the cost function should also include an a-priori knowledge on the parameter probability. Hence, the cost function $J(p)$ is designed as summation of the cumulative absolute simulation error for temperature and heating demand, and a regularization term representing penalization depending on parameter probability:

$$J(p) = \sum_{j=1}^N (w_T |T_j^m - T_j^s| + w_Q |Q_j^m - Q_j^s|) + \sum_{k=1}^N w_k f_{pen,k}(p_k). \quad (2)$$

Here, T and Q denote indoor air temperature and cumulative heating demand, respectively. Superscripts m and s represent measured and simulated values respectively, and subscript j denotes the corresponding value at the j^{th} time step. Since scales for the temperature and heat demand vary largely, the corresponding error terms should be balanced using appropriate weights w_T and w_Q . However, since the goal of the calibration is to accurately predict the heating demand, the corresponding error should still be dominant. Adding a regularization term can be interpreted as imposing certain a-priori distributions on model parameters. Here $f_{pen,k}(p_k)$ and w_k denote the penalty function and weight for each parameter p_k . The penalty term $f_{pen,k}$ should increase as $|p_k - p_k^0|$ increases, i.e. when parameter p_k takes less probable values. For this reason let

$$f_{pen,k}(p_k) = \tilde{f}_{pen,k}(|p_k - p_k^0|) \quad (3)$$

such that $\tilde{f}_{pen,k} : \mathbb{R}^+ \rightarrow \mathbb{R}^+$ is a monotonically increasing function. Hence, it could be defined as (Fig. 2):

$$f_{pen,k}(p_k) = \frac{1}{\sqrt{2} \sigma_k^2} \left(1 - e^{-\frac{(p_k - p_k^0)^2}{2 \sigma_k^2}} \right). \quad (4)$$

Since the penalty term not necessarily needs to be defined as a weighted norm, it represents a generalization of the Tikhonov regularization. The problem (1) can be observed as a multi-objective optimization problem, where a trade-off is made between minimizing the simulation error and maximizing the parameter probability.

3. Study Case Model Calibration

In this section, the methodology introduced in Section 2 is illustrated on a residential building apartment model. The presented results offer evidence of regularization benefits on the retrofit prediction and model parameter estimation.

3.1 Study Case Description

The residential building under consideration is located in the south of Madrid, Spain. Built in the 1960s, with poorly fitted windows, no insulation and cracks around doors, windows, and foundations, it was deemed suitable for retrofit. On the eastern side, it is attached to a twin residential building (Fig. 3).



Fig. 3 – Study case residential building

Each block contains five 50 m² apartments. The study case apartment is located in the west block on the last floor (Fig. 4).

It used a gas boiler with five water radiators for the heating in winter and a split unit for the cooling in summer. Monitoring data is available for one year before the retrofit (September 2014 — September 2015), and two months after the installation of new windows and insulation layers on the envelope (January 2016 – March 2016).

The acquired real-time data with 15 min samplings include internal (IAT) and external (EAT) temperatures, global solar radiation, CO₂ concentration, and electric consumption. A heat meter on supply and return pipes of the gas boiler was also installed to monitor the heating energy. The heating demand at each time step is easily calculated as the increase in the measurement of heating energy. The internal temperature of the apartment below was monitored as well, but not the one of the apartment adjacent on the eastern side.



Fig. 4 – Front view

3.2 Initial Building Energy Model

The initial energy model for the whole building was developed in the dynamic environment of TRNSYS Simulation Studio (Klein et al., 2010), where the building geometry was developed in Google SketchUp and set up in TRNBuild. The model is based on the information provided by the energy audit (Garcia et al., 2014), including building plans,

envelope structure, openings, air tightness, internal partitions, shading elements, and occupancy. Each apartment is divided in two thermal zones, north and south oriented (see Fig. 5). Since the heating setpoint of the apartment is unknown, we assume an ideal heating. An infiltration coefficient is used when the windows are closed, and another when windows are open. Internal heat gains from occupants and equipment are included, where 75 W/person is assumed and heat gain from electric appliances is estimated based on real-time electric meter measurements and guidelines by ASHRAE (1985). The shading model is based on an on/off differential controller that takes into account the indoor air temperature and solar irradiance at each window according to its orientation. Shading is activated when both indoor temperature and solar irradiance on horizontal plane exceed a certain threshold. The threshold for the temperature controller is equal to the calibration parameter p_4 , and 250 W is chosen for the solar irradiance controller. The external shading factor is the calibration coefficient p_3 taken to be the same for all windows in the apartment. The new control value for each controller is the output control signal from the previous time step, by introducing a hysteresis effect. Therefore, both lower and upper deadband for the difference between actual and threshold values, also need to be defined. These deadbands are chosen to be -0.5 °C and 0.5 °C for the temperature controller, and -50 W and 0 W for the solar radiation controller. The shading activation is an adaptation of the controller values defined by Dott et al. (2013).

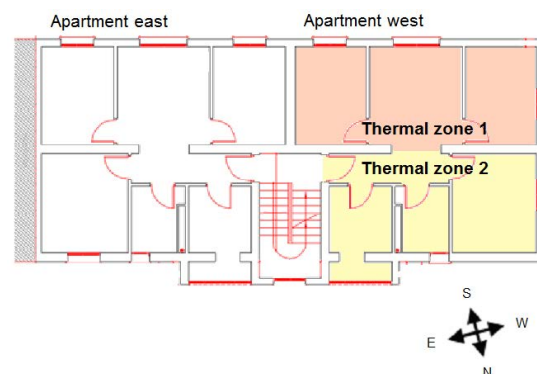


Fig. 5 – Building cross-section

The sensitivity analysis was performed using the Morris method (Saltelli, 2008), and significant

model parameters for the energy demand assessment were identified (Table 1).

Table 1 – Significant model parameters

Parameter	Description [Unit]
p_1	Internal temperature of the adjacent apartment [°C]
p_2	Occupancy multiplication factor [-]
p_3	Shading factor [-]
p_4	Shading activation temperature [°C]
p_5	Infiltration with windows closed [ACH]
p_6	Total infiltration and ventilation with windows open [ACH]
p_7	Conductivity of the concrete layer in the external walls [W/(m K)]
p_8	Conductivity of the concrete layer in the internal partitions, floors and ceilings [W/(m K)]
p_9	Conductivity of the concrete layer in the roof [W/(m K)]
p_{10}	Window U-value [W/(m ² K)]

The outcome shows that the IAT of the adjacent apartments (p_1) has a strong influence on the heat demand. Parameter p_2 represents the correction factor for the assumed occupant's heat gain. In addition, the parameters of the shading model (p_3, p_4) are mostly significant in the summer and swing period. Infiltration parameters (p_5, p_6) turn out to have a strong effect on both IAT and heat demand, as expected. To account for possible errors in layer description of the external and internal walls, floor and roof, and the fact that walls are reinforced, we have included the conductivity of the concrete as uncertain model parameters (p_7, p_8 and p_9). Parameter p_{10} represents the windows U-value. Since for a number of apartments in the building, additional windows were already installed, we want to prove our hypothesis that the monitored apartment has double windows. As an initial point, minimum

and maximum values of each parameter were defined (Table 2), based on the energy audit and by consulting various standards and datasheets.

Table 2 – Parameter range and initial guess

Parameter	p_k^{min}	p_k^{max}	p_k^0	σ_k
p_1	17.6	24.6	18.6	-
p_2	0.5	2	1	0.3
p_3	0	1	0.5	-
p_4	22	32	25	-
p_5	0.15	0.75	0.4	0.6
p_6	0.4	5.2	3	-
p_7	0.8	2.5	1.13	0.35
p_8	0.8	2	1.13	0.35
p_9	0.8	2	1.13	0.45
p_{10}	2.74	5.68	2.83	-

In particular, the initial guess for the infiltration parameter (p_5) is based on the blower-door test which was performed during the energy audit (Table 3).

Table 3 – Blower-doors test results

ΔP [Pa]	Flow [m ³ /h]	ACH
20	200	2.0
30	276	2.8
50	382	3.9
65	471	4.7

The airflow through the building envelope and the pressure difference across it are known to have the following relationship (Sherman, 1987):

$$q = C (\Delta P)^n \quad (5)$$

Here ΔP is the induced pressure difference (in Pa), q is the airflow through the building envelope (in m³/h), and C is the air leakage coefficient. To determine the parameters n and C , the least-square tech-

nique is applied to the blower-door test results following ISO standard (ISO/TC 163/SC 1, 2015). The reached values $n = 0.67$ and $C = 260$ have a standard deviation estimate 0.02 and 3 respectively, and $r^2 = 99.7\%$. In order to estimate the average air infiltration, stack-dominated and wind-dominated components are evaluated separately (Klems, 1983). From one year measurement data, the average indoor air temperature, the temperature difference between the indoor and external air, and the air density were obtained and used to calculate the average stack effect pressure difference to be $\Delta P_{se} = 1.03$ Pa. From the meteorological data, the average wind speed in Madrid is estimated to be 2 m/s, implying a wind pressure difference equal to $\Delta P_w = 1.23$ Pa. Hence, the stack effect air infiltration and the infiltration due to the wind are equal to 0.3 ACH and 0.27 ACH respectively, which implies an infiltration rate of 0.4 ACH (Klems, 1983). The occupancy multiplication parameter p_1 is estimated to be equal one, where we assume that 75 W/person provided by ASHRAE (1985) is a well-studied approximation. The conductivity of the concrete found in the walls, floors and partitions (p_8 , p_9 and p_{10}) is provided by the refurbishment architect during the energy audit (Garcia et al., 2014). These initial guesses are considered reliable and are assigned a divergence factor. The corresponding penalty is added to the cost function of the optimization problem. The window U-value and the shading coefficient are estimated with less certainty by inspecting the windows and the indoor temperature. Since ventilation rates with open windows (p_6) cannot be easily estimated, a wide parameter range was chosen and the approximate mean value was selected as the initial guess. Initial guesses that are not reliable are not included in the regularization term.

3.3 Calibration and Validation Procedure

The monitoring data was divided into three periods: the calibration period (September 11, 2014–January 31, 2015), and the validation period before (February 01, 2015–April 12, 2015) and after the renovation (January 21, 2016–March 29, 2016). Opening of the windows and occupancy in the apartment were identified on the basis of CO₂ levels. Measured IATs were set as the heating setpoint in the monitored

apartment and for the apartment below. However, the IAT measurement is not available for the apartment adjacent on the eastern side, which is therefore treated as an unknown model parameter (p_1). Although the whole building is simulated, the results for the monitored apartment were considered just in the cost function. The heating demand and the average indoor air temperature during the heating season are summarized in Table 4.

Table 4 – Monitoring data summary

Period	Heat demand [kWh]	Average heating IAT [°C]
Calibration	3755	21.91
Validation 1	2252	21.76
Validation 2	1222	22.62

Since the ideal heating is assumed and the IAT is taken as the setpoint, the temperature error is negligible in the heating periods. Therefore, it is included in the cost function only when there is no heating. Used weight coefficients are $w_T = 0.65$ and $w_Q = 5.7e - 3$, in order to approximately achieve a 1:4 ratio between temperature and energy demand error. For a regularized solution $w_k = 100$ is taken. As soon as the optimization problem was solved, the models were validated on a new set of monitoring data. Since the average measured heating power was 1.9 kW, the sensor resolution of the heating demand (1 kWh) was not suitable to take into consideration the normalized mean bias (NMB) and the coefficient of variation of root mean square error (CVRMSE) on an hourly basis. Instead, the daily NMB and CVRMSE were reported. The recommended calibration criteria per ASHRAE (2002) for hourly values are NMB $\leq \pm 10\%$ and CVRMSE $\leq 30\%$, and NMB $\leq \pm 5\%$ and CVRMSE $\leq 15\%$ for monthly data. However, according to the knowledge of the authors, there are no standard criteria for daily values. Hence, as daily criteria we use a combination of ASHRAE defined criteria: NMB $\leq \pm 5\%$ and CVRMSE $\leq 15\%$ for calibration, and NMB $\leq \pm 5\%$ and CVRMSE $\leq 30\%$ for validation. For model validation after the renovation, models were

adapted to include new windows, the corresponding infiltration parameter and insulation layers, as specified in the manufacturers' datasheets.

3.4 Regularized and Non-Regularized Solution

Hybrid algorithm combining Particle Swarm optimization and Hooke-Jeeves optimization algorithms from GenOpt (Wetter, 2009) were used to solve the optimization problems. Regularized and non-regularized solution models were obtained using the same algorithm parameters and the initial parameter set, solving optimization problem (1), where the cost function (2) in the former case includes also the regularization term. The obtained parameter sets are reported in Table 5. Both models yield zero shading since otherwise the simulated IAT would be much lower than monitored. However, four parameters of the non-regularized model reach boundary values of the pre-defined parameter range. For example, when the windows are open infiltration reaches minimal 0.4 ACH, thus contradictory since it is smaller than the infiltration with windows closed (0.62 ACH).

Table 5 – Calibrated model parameters

Parameter	Regularized	Non-regularized
p_1	18.08	18.6
p_2	1.25	2
p_3	0	0
p_4	28	30
p_5	0.35	0.62
p_6	1.46	0.4
p_7	1.13	0.88
p_8	1.51	1.99
p_9	1.13	1.99
p_{10}	2.74	2.74

We also note that the conductivity of the concrete in internal partitions and roof also reaches the maximum value of the interval. Compared with the

regularized solution, these values are significantly larger and result in larger transmission losses through the roof. And also, a larger infiltration when windows are closed results in a larger infiltration loss compared to the regularized solution. These losses are counterbalanced by a higher gain from the occupants (150 W/person, maximum value), a reduced infiltration when windows are closed, and less transmission losses through external walls. The parameters of the non-regularized model that reach minimum or maximum values represent possible, but highly unlikely, scenarios. Table 6 summarizes the calibration results for both models. Both models satisfy the calibration criteria. Also the average absolute error (AAE) for cumulative heat demand and temperature calculated at 15-minute intervals is considered.

$$AAE\ Heat = \frac{\sum_{k=1}^n \int_{t_0}^{t_k} |\dot{Q}^s - \dot{Q}^m| dt}{n} \frac{100}{\int_{t_0}^{t_n} \dot{Q}^m dt} \quad (6)$$

$$AAE\ Temp = \frac{\sum_{k=1}^n |T_k^s - T_k^m|}{n} \quad (7)$$

\dot{Q}_{sim} and \dot{Q}_{mea} are simulated and measured heating power. Average absolute heating demand error amounts to 0.45 % and 0.34 % of the total measured heating energy demand (3755 kWh, see Table 4) for the regularized and non-regularized solution.

Table 6 – Calibration error (Sep 11, 2014 – Jan 31, 2015)

	Regularized	Non-regularized
NMB	-0.85	-0.47
CVRMSE	9.57	10.3
AAE Heat [kWh]	11.64	12.6
AAE Temp [°C]	1.24	1.09

Table 7 reports the error for both solutions in the validation period before the renovation.

Table 7 – Pre-renovation (Feb 01, 2015 – Apr 12, 2015) validation results

	Regularized	Non-regularized
NMB	-3.97	-3.53
CVRMSE	22.38	22.98
AAE Heat [kWh]	82.12	78.09
AAE Temp [°C]	0.92	0.82

The total measured heating demand for the validation period reads 2252 kWh, and the values predicted by the regularized and the non-regularized solution are 2150 kWh and 2157 kWh, which represents under-prediction of 4.44 % and 4.22 % respectively.

Both models satisfy the validation criteria. The regularized solution has a slightly better performance with respect to NMB and CVRMSE, while the non-regularized solution has lower average absolute errors. The model predictions for the post-retrofit period are given in Table 8. The total monitored heating demand in that period is 1222 kWh. The predictions obtained by regularized and non-regularized solution read 1173.8 kWh and 1099 kWh, hence the models under-predict the demand by 3.9 % and 10.1 %, respectively. The regularized solution yields a better estimate of the building energy demand after the renovation. The non-regularized solution underestimates the heating demand by over 10 % because it overestimates the occupant internal gain, while it underestimates the infiltration losses.

Table 8 – Post-renovation (Jan 21, 2016 – Mar 29, 2016) validation results

	Regularized	Non-regularized
NMB	-3.66	-10.1
CVRMSE	25.3	29.9
AAE Heat [kWh]	19.66	47.9
AAE Temp [°C]	0.89	0.76

4. Discussion and Further Research

We have illustrated how calibrated and validated building models do not necessarily provide good renovation savings estimates. The parameter optimization method for complex building energy models presented in this work aims to reduce the parameter uncertainty and thus the prediction error by utilizing regularization. The proposed method is in general useful when the number of model parameters is large, since the chances to perform a good search of the parameter space by using statistical sampling, is small and the model uncertainty increases. The performance of a guided search of the parameter space instead is advantageous, e.g. it solves a parameter optimization problem.

This work also highlights the importance of a good preliminary estimation of the building parameters; otherwise, unrealistic parameter combinations may emerge as optimal in the calibration phase.

The success of the regularization strongly depends on the choice of the penalty weight in the cost function. How to optimally choose this value has not been considered here and is a topic for further research. A possible approach is to address (1) as a multi-objective optimization problem and evaluate different Pareto optimal solutions. Finally, although only the heating demand was considered, this method naturally extends to the calibration of the models with respect to both the heating and the cooling demand.

Acknowledgement

This study is performed as part of iNSPiRe project, funded by the European Commission's 7th Framework Programme 2007–2013 under GA no. 314461.

Nomenclature

Symbols

C	Air pressure leakage coefficient
$f_k(p_k)$	Penalty function for k^{th} parameter
$J(p)$	Cost function
n	Air pressure exponent coefficient
p_k	k^{th} model parameter
p	Parameter vector
q	Air flow through building envelope
Q	(Cumulative) Heating demand
\dot{Q}	Heating power
T	Indoor Air temperature
w_k	Weight for k^{th} parameter p_k penalty function
w_Q	Weight for heating demand error
w_T	Weight for temperature error
ΔP	Induced pressure difference

Subscripts/Superscripts

j	Value at the j^{th} time step
m	Monitored value
s	Simulated value
se	Stack-effect dominated value
w	Wind dominated value

References

- Alifanov, O.M., E.A. Artiukhin, S.V. Rumiantsëv. 1995. *Extreme methods for solving ill-posed problems with applications to inverse heat transfer problems*. New York, U.S.A.: Begell House.
- ASHRAE. 2002. *ASHRAE Guideline 14-2002: Measurement of Energy and Demand Savings*. Atlanta, U.S.A.: American Society of Heating, Refrigerating and Air-Conditioning Engineers.
- ASHRAE. 1985. *ASHRAE handbook: Fundamentals*. Atlanta, U.S.A.: American Society of Heating, Refrigerating and Air Conditioning Engineers.
- Caucheteux, A., E. Stephan, C. Ouest. 2013. "Transient simulation calibration of an old building using an experimental design: evaluating uncertainty results". In: *Proceedings of the 13th IBPSA Conference*. Chambéry, France: IBPSA.
- Coakley, D., P. Raftery, P. Molloy. 2012. "Calibration of whole building energy simulation models: Detailed case study of a naturally ventilated building using hourly measured data". In: *First Building Simulation and Optimization Conference*. Loughborough, UK IBPSA.
- Crépey, S. 2003. "Calibration of the Local Volatility in a Generalized Black-Scholes Model Using Tikhonov Regularization". *SIAM Journal on Mathematical Analysis* 34: 1183–1206. doi:10.1137/S0036141001400202
- Dott, R., M.Y. Haller, J. Ruschenburg, F. Ochs, J. Bony. 2013. "The Reference Framework for System Simulations of the IEA SHC Task 44/HPP Annex 38 Part B: Buildings and Space Heat Load". In: *A Technical Report of Subtask C, Report C1 Part B*.
- Garcia, J., D. Romera, C. Dipasquale, R. Fedrizzi, M. D'Antoni. 2014. "Energy audit – Case study Madrid Development of Systemic Packages for Deep Energy Renovation of Residential and Tertiary Buildings including Envelope and Systems". URL http://www.inspirefp7.eu/wp-content/uploads/2014/07/WP7_D7.1b_20140514_P15_Energy_Audit_Madrid.pdf
- Heo, Y., R. Choudhary, G.A. Augenbroe. 2012. "Calibration of building energy models for retrofit analysis under uncertainty". *Energy and Buildings* 47: 550–560. doi:10.1016/j.enbuild.2011.12.029.
- ISO. 2015. *ISO/TC 163/SC 1, 2015. ISO 9972:2015: Thermal performance of buildings – Determination of air permeability of buildings – Fan pressurization method*. Geneva, Switzerland: ISO.
- Klems, J.H. 1983. "Methods of estimating air infiltration through windows". *Energy and Buildings* 5: 243–252. doi:10.1016/0378-7788(83)90012-9.
- Navon, I.M. 1998. "Practical and theoretical aspects of adjoint parameter estimation and identifiability in meteorology and oceanography". *Dynamics of Atmospheres and Oceans* 27, 55–79. doi:10.1016/S0377-0265(97)00032-8.
- Raftery, P., M. Keane, J. O'Donnell. 2011. "Calibrating whole building energy models: An evidence-based methodology". *Energy and Buildings* 43: 2356–2364. doi:10.1016/j.enbuild.2011.05.020.

- Reddy, T.A., I. Maor, C. Panjapornpon. 2007. "Calibrating Detailed Building Energy Simulation Programs with Measured Data—Part I: General Methodology (RP-1051)". *HVAC&R Research* 13: 221–241. doi:10.1080/10789669.2007.10390952
- Saltelli, A. 2008. *Global sensitivity analysis: The primer*. Chichester, UK: John Wiley.
- Schirrer, A., M. Brandstetter, I. Leobner, S. Hauer, M. Kozek. 2016. "Nonlinear model predictive control for a heating and cooling system of a low-energy office building". *Energy and Buildings* 125: 86–98. doi:10.1016/j.enbuild.2016.04.029.
- Sherman, M.H. 1987. "Estimation of infiltration from leakage and climate indicators". *Energy and Buildings* 10: 81–86. doi:10.1016/0378-7788(87)90008-9.
- Tahmasebi, F., R. Zach, M. Schuß, A. Mahdavi. 2012. "Simulation model calibration: An optimization-based approach". In: *Proceedings of BauSim 2012: Fourth German-Austrian IBPSA Conference*.
- Wetter, M. 2009. *Generic Optimization Program User Manual Version 3.0.0*. Berkeley, U.S.A.: Lawrence Berkeley National Lab.
- Zhdanov, M.S. 2002. *Geophysical inverse theory and regularization problems*. Amsterdam; The Netherlands: Elsevier.

On-Site Measurements and Whole-Building Thermal Dynamic Simulation of a Semi-Confined Prefabricated Building for Heritage Conservation

Francesca Frasca – Sapienza University – f.frasca@uniroma1.it

Anna Maria Siani – Sapienza University – annamaria.siani@uniroma1.it

Cristina Cornaro – Tor Vergata University – cornaro@uniroma2.it

Abstract

In this study the capability of a BDFWall model (IDA Indoor Climate and Energy software) is assessed in a semi-confined site for the conservation of works of art. The case under study is the paleontological deposit of “La Polledrara di Cecanibbio” (Rome, Italy), where many valuable faunal remains from the Middle Pleistocene are preserved. The thermo-hygrometric data collected from 2009 to 2013 have allowed for a thorough investigation of the environmental conditions of the site. The calibration of the simulation-building model was performed in two phases. First, a sensitivity analysis was conducted to identify which input parameters significantly affect the discrepancy, if any, between measured and modelled hourly indoor temperature (T) data (from September to December 2013). Second, the calibration of the model was carried out by taking into account the most effective parameters. The dual approach, given by both experimental and simulation data, can support the preventive measures of risk analysis for artworks in the case of retrofit solutions of a building used for conservation purposes.

1. Introduction

Recently, the whole-building dynamic simulation has become a useful tool in preventive climate control actions in buildings which preserve cultural artefacts. However, the existing software has been developed to model the indoor climate of modern buildings having regular geometries and for which the thermo-physical properties of building materials are well known.

In historical and archaeological buildings, the libraries of the simulation codes do not include the materials of these structures and, in the case of semi-confined sites, strongly affected by external factors and/or boundary constraints, the performance of these codes has not been thoroughly investigated.

The possibility to know in advance the effect of a retrofit in buildings with conservation purposes is fundamental in order to assess the optimal solutions taking into account both conservation needs and people’s thermal comfort requirements.

This paper describes how the dynamic simulation software, IDA Indoor Climate and Energy, applied to a semi-confined site such as the paleontological deposit of “La Polledrara di Cecanibbio” in Rome (Italy) was used.

The aim was to investigate the thermal behaviour of the case under study by using both on-site measurements and simulated values. This allows a better understanding of the object/environment and building/environment interaction. This study pays particular attention to the calibration of the whole-building dynamic model using only the features of the building envelope, since the variations of the geometry and of the thermo-physical properties of the building components and boundaries do not affect the model in the same way.

2. The Case Study

“La Polledrara di Cecanibbio” (Lat. 41.9°, Long. 12.3°) is a paleontological deposit located about 15 km NW of Rome (Italy) in a rural area. Several

valuable faunal remains from the Middle Pleistocene are preserved, such as large mammals (*Palaeloxodon antiquus* and *Bos primigenius*). The largest faunal remains are held by cineritic tuffite fluvial sediments (Fig. 1). The faunal remains placed in the north side of the site suffer from biological degradation because they are directly exposed to soil hygrometric conditions.



Fig. 1 – La Polledrara di Cecanibbio, Rome (Italy)

The deposit was discovered in 1984 within a survey supported by the Soprintendenza Speciale per i Beni Archeologici di Roma (SSBAR) and was kept unearthened in the following years. In 2000, a prefabricated building was built with the main purpose to preserve the fossils from meteorological conditions and to make it a public museum.

The building covers an excavated area of 900 m² (30x30 m per side) and is placed directly on the soil. The maximum height of the building is 8 m (east side), while the minimum is 6.5 m (west side). The windows (i.e. double-pane clear glazing with aluminium frame without thermal-break) are along the north and south walls covering an area of about 1900 m² with a solar factor of 0.79 and a heat transmittance (U-value) of 5.80 W/(m²K). There are internal white PVC roller blinds which are usually never opened.

The external walls are double skin panels insulated by polyurethane with a nominal thickness of 6 cm and a U-value=0.60 W/(m²K).

The roof is a trapezoidal sheet for concrete slabs with a nominal thickness of 12 cm, a slope of 30 cm and a U-value=1.09 W/(m²K).

3. Measurement and Simulation

An on-site monitoring campaign and whole-building dynamic simulation software were used with the double purpose to investigate the thermal behaviour of “La Polledrara di Cecanibbio” and to optimize the semi-automatic calibration of the simulation model in the case of a semi-confined site.

3.1 On-Site Monitoring Campaign

Sensors for the measurement of indoor temperature (T), relative humidity (RH), and cracks (FO) parameters were installed in June 2008. The analysis was carried out taking into account data from January 2009 to December 2013. The outdoor T and RH sensors were installed in June 2013 in the south corner of the building, accurately shaded from direct solar radiation, and protected from meteorological events. T sensor is a platinum resistance thermometer Pt100 1/3 DIN (accuracy = 0.3 °C), whereas RH sensor is a film capacitor “Rotronic” C94 (accuracy = 1.5 %). The metrological features of T and RH sensors are in accordance with the European Standards EN 15758:2010 and EN 16242:2012, respectively.

FO sensor is a capacitor (accuracy = 0.25 %) and is installed on the crack of a cinerite that holds a fang of a *Palaeloxodon antiquus*.

All the sensors were connected to a datalogger CR 1000 distributed by Tecno.el S.r.l. (Italy), with acquisition and recording time set to 30 minutes.

The monitoring campaign is still in operation.

3.2 Analysis of Microclimatic Data Series

Before performing the exploratory data analysis (EDA), the quality of the T-RH data series was assessed using the Continuity Index (CI) and the Completeness Index (CoI) (Frasca et al., 2016). Both indexes range between 0 (poor quality) and unity (high quality, i.e. no missing values).

Assuming any distribution of the data, the Spearman’s rank correlation coefficient (ρ) was computed to assess whether there was a monotonic relationship between the T-RH parameters and the cracks, in order to define an empirical relationship among parameters. This relationship is useful, in combination with the simulation results, to support

preventive measures concerning risk analysis for artworks in the case of retrofit solutions of a building used for conservation purposes.

3.3 Simulation Environment

3.3.1 IDA ICE setting

A dynamic building simulation for indoor climate analysis was performed using the software tool IDA Indoor Climate and Energy (IDA ICE) 4.7.1 developed and distributed by EQUA simulation AB. The BDFWall model (finite differences model of a multi-layer component) was used to carry out the simulation of the thermal behaviour of the building.

We created the geometry of the building model of “La Polledrara di Cecanibbio” was created starting from the architectural survey provided by the SSBAR and using the thermo-physical properties reported in UNI 10351:2015 for opaque components and in EN 673:2011 and EN 410:2011 for glass components. The first guess building model was assumed as an unconditioned large area, only affected by external climate and directly placed on soil.

The soil layer was modelled according to model ICE 3, which computes the soil temperature as the mean of T of the selected climate file without 2D or 3D modelled effects.

The air infiltrations were modelled according to wind driven flow and considering air tightness at 0.5 ACH (Air Change per Hour) at a pressure difference of 50 Pa.

Lighting, equipment and people were not included, since the site has a limited number of visitors in the selected period.

A climate file was built to run the model for calibration using outdoor T and RH measured at “La Polledrara”. Wind direction and speed intensity, direct and diffuse (sky) radiation on a horizontal surface, measured at ESTER station (Energia Solare TEst e Ricerca), belonging to the Tor Vergata University of Rome (Lat. 41.9°, Long. 12.6°), were also included in the climate file.

3.3.2 Method

In this study, MatLab 2014a was used to set the configuration parameters of the building model to carry out the Sensitivity Analysis (SA) and the calibration of the simulation model, based only on the parameters that describe the building envelope.

First, the SA was carried out to identify the most effective parameters of the model. Then, the calibration based on these selected parameters was performed to minimize the difference between modelled and measured data. The aim was to identify the best settings of the thermal-physical properties of building components and boundaries.

After that, the model was validated in a different period (January 2016) given the availability of measured indoor and outdoor temperature data.

3.3.3 Sensitivity analysis

In this study, the Elementary Effects method (EEs) was applied using modelled hourly indoor T from September to December 2013 and based on the Morris random sampling method of the set of parameters (Morris, 1991) that defined the building model. The experimental plan is built by taking into account the number of EEs (r) for each parameter and the number of levels (p) in which the parameters range. In this study, we computed $r=10$ for each parameter using only $p=4$ discretized levels in the experimental plan. We selected 24 parameters (k) for screening, and defined the ranges according to a fixed uncertainty at $\pm 10\%$ from the initial value, as listed in Table 1.

In this way, the resulting computational effort was 250 runs (N) which corresponds to:

$$N = r * (k + 1) \quad (1)$$

The input set parameter matrix given by Morris sampling is N -by- k . The N -models were run in batch mode in IDA ICE. The error between simulated T and T from the first guess model was expressed in terms of the mean absolute error (MAE) that was used as a target function for the calculation of the EEs.

The EEs ascribed to each parameter are defined as the difference in the output between two following simulations divided by the variation of the input parameter (Saltelli et al., 2004). The EEs were computed according to eq. 2:

$$EEs(x) = \frac{y(x_1, x_2, \dots, x_i + \Delta x_i, \dots, x_k) - y(x)}{\Delta x} \quad (2)$$

where x is the set of parameters, y is the target function and Δx is the variation of the input parameter. Finally, the mean (μ^*) of the absolute values of the EEs associated with each parameter, the standard deviation (σ) and the ratio σ/μ^* were calculated. μ^*

provides a measure of the parameter relevance (Campolongo et al., 2011), in the rank order. The ratio σ/μ^* is an indicator of linearity of each parameter effect ($\sigma/\mu^* < 0.1$) with respect to other parameters and to the whole modelled building (Garcia

Sanchez et al., 2014). In EEs scatter plot (σ vs μ^*) four areas delimited by $\sigma/\mu^* < 0.1$, $0.1 \leq \sigma/\mu^* < 0.5$, $0.5 \leq \sigma/\mu^* < 1$ and $\sigma/\mu^* \geq 1$, allows highlighting if outcomes from SA are physically consistent.

Table 1 – Modelling parameter values used in the first guess model (initial value) and parameter ranges value used in Morris sampling for SA

Component	Parameter	Initial Value	Range for SA
External Wall - Steel	λ [W/(m K)]	52	47-57
	s [m]	0.001	0.001-0.005
	d [kg/m ³]	7800	7000-8600
	c [J/(kg K)]	550	490-600
External Wall - Polyurethane	λ [W/(m K)]	0.034	0.029-0.040
	s [m]	0.15	0.13-0.17
	d [kg/m ³]	25	22-28
	c [J/(kg K)]	1.464	1.320-1.610
Roof - Concrete	λ [W/(m K)]	0.21	0.18-0.25
	s [m]	0.15	0.14-0.17
	d [kg/m ³]	700	630-770
	c [J/(kg K)]	1050	1000-1150
Soil	λ [W/(m K)]	1.5	1.3-1.7
	s [m]	1	0.9-1.1
	d [kg/m ³]	1200	1080-1320
Window	c [J/(kg K)]	840	765-925
	U [W/(m ² K)]	3.052	2.950-3.500
	ExtW-Slab [W/(m K)]	0.05	0.04-0.06
Thermal Bridges	ExtW-IntW [W/(m K)]	0.03	0.02-0.04
	ExtW- ExtW [W/(m K)]	0.08	0.07-0.09
	WinPerim [W/(m K)]	0.03	0.02-0.04
	DoorPerim [W/(m K)]	0.03	0.02-0.04
	Roof [W/(m K)]	0.09	0.08-0.10
	Slab [W/(m K)]	0.14	0.13-0.15

Note: λ =thermal conductance; s=thickness; d=density; c=specific heat; U=heat transmittance; ExtW-Slab=external wall-internal slab; ExtW-IntW=external wall-internal wall; ExtW-ExtW= external wall-external wall; WinPerim = external window perimeter; DoorPerim = external door perimeter; Roof=roof-external wall; Slab=external slab-external wall.

3.3.4 Calibration

The simulation model was calibrated using hourly indoor T measurements from September till December 2013. The model was initialized at a start-up period from August 18, 2013 to August 31, 2013. The calibration was carried out taking into account

only the most effective parameters with the aim to minimize the root-mean-square-difference (RMSD) and the CV-RMSD (Coefficient of Variation of the RMSD) between modelled and measured indoor T. They were used to assess the quality of the changes to calibrate the building model (Cornaro et al.,

2016). The most effective parameters were ranged within the interval reported in Table 1, using a major number of levels with respect to the Morris sampling.

The modelled and measured indoor T were compared using the Taylor Diagram (Taylor, 2001). It summarizes the agreement between observed data (a) and modelled data (b) using three statistical quantities: standard deviation (SD), correlation coefficient (R), and the centred RMSD (E'), the relationship of which is given by the following equation:

$$E' = \sqrt{SD_a^2 + SD_b^2 - 2\cos(SD_a SD_b R)} \quad (3)$$

4. Results and Discussion

4.1 Microclimate Analysis

Both the T and RH data series are of high quality (CI=1.00 and CoI=0.96) and hence suitable for exploratory data analysis.

Fig. 2 shows the box-and-whiskers plots of RH data. Several outliers (indicated as circles in the figure) are observed in winter, spring, and fall. A detailed

study of RH outliers has shown that they occurred mainly in the hourly intervals between 13:00 UTC and 20:00 UTC, i.e. after the maximum solar exposure of the building.

The box plots for T (figure not shown), do not show any anomalous values, and there is no significant difference among seasons over the selected period. The mean yearly value is 17.7 °C ranging between 12.4 °C (25th percentile) and 23.1 °C (75th percentile). It was found that in summer the indoor environmental conditions were too warm and too humid, while in winter, they were too cold and humid, especially in morning. These conditions provoked thermal discomfort, as communicated by staff and visitors, and might have favoured the biological degradation in the north side of building.

The behaviour of T and RH daily span (difference between the maximum and minimum values) allows studying their short-term variability. A similar behaviour among season (except in summer) was observed: $\Delta T_{daily}=1-7$ °C and $\Delta RH_{daily}=3-40$ %. In summer, the daily span of T and RH range as follows: $\Delta T_{daily}=5-6$ °C and $\Delta RH_{daily}=20-40$ %, showing that the period is mostly characterized by large fluctuations.

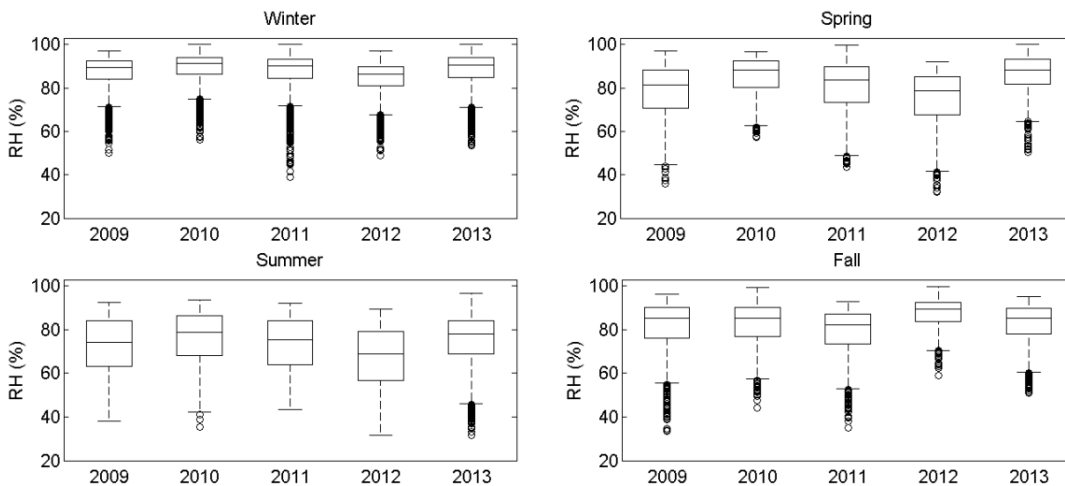


Fig. 2 – Box and-whiskers plots of indoor relative humidity (RH) for each season over the period 2009-2013. The line inside the box is the median value, with the 25th and 75th percentiles as lower and upper sides of the box, respectively. The lowest and the highest value of the data set are plotted as whiskers when they are not outliers, indicated as circles (i.e. above or below 1.5*IQR, IQR interquartile range)

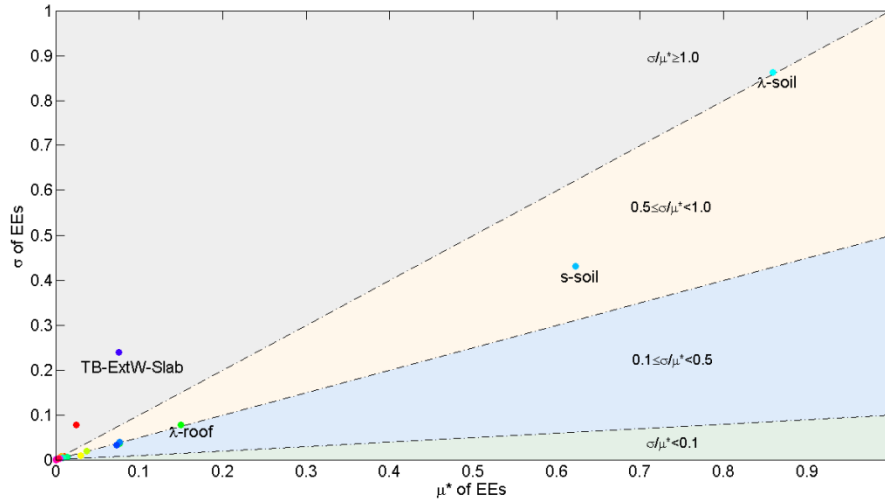


Fig. 3 – Scatter plot (σ vs μ^*) of Elementary Effects method for 250 runs by taking into account 24 input parameters (indicated as colored dots) of building envelope. Four areas delimited by the ratio σ/μ^* indicate the effect of parameter on model: light green ($\sigma/\mu^* < 0.1$, linear effect), light blue ($0.1 \leq \sigma/\mu^* < 0.5$, monotonic effect), pink ($0.5 \leq \sigma/\mu^* < 1$, almost monotonic effect), and grey ($\sigma/\mu^* \geq 1$, non-linear and/or non-monotonic effect)

Finally, T-RH parameters affect the evolution cracks measured on the cinerite that holds a fang: the correlation with T is $\rho=0.62$ whereas with UR is $\rho=-0.68$. An empirical relationship was found:

$$FO = b_1 * RH^{b_2} * T^{b_3} \quad (4)$$

where $b_1 = 6.76$, $b_2 = -0.09$ and $b_3 = 0.01$. Modelled FO data deviate from measured FO of at most 5 %.

4.2 Simulation

Fig. 3 shows the results of the EEs computed taking into account 24 parameters (see Table 1). The most effective parameters corresponding with the high values of μ^* and σ are: the thermal conductance (λ_s) and thickness (s_s) of the soil, the thermal conductance of the roof (λ_r), and the thermal bridge related to the external walls and slab ($TD_{ExtW-Slab}$).

The scatter plot shows that the effects of λ_s and $TD_{ExtW-Slab}$ are non-linear and/or non-monotonic (indicated as the grey area in figure ($\sigma/\mu^* \geq 1$)), while the effects of λ_r and s_s are almost monotonic (indicated as the pink area in the figure ($0.5 \leq \sigma/\mu^* < 1$)).

The significant influence of the soil on indoor T is due to its low resistance at heat transfer. It is controlled by several factors such as porosity and soil temperature. Further studies will be carried out taking into account the actual temperature of the soil.

The other parameters form a cluster with low μ^* and σ , which means that they have a limited influence

on the model and could be neglected in the model calibration.

Fig. 4 shows the Taylor Diagram for a comparison among modelled hourly indoor T (indicated as coloured dots) and measured hourly indoor T (indicated as A) by running several simulations varying the first two effective parameters as described above (subsection 3.3.4).

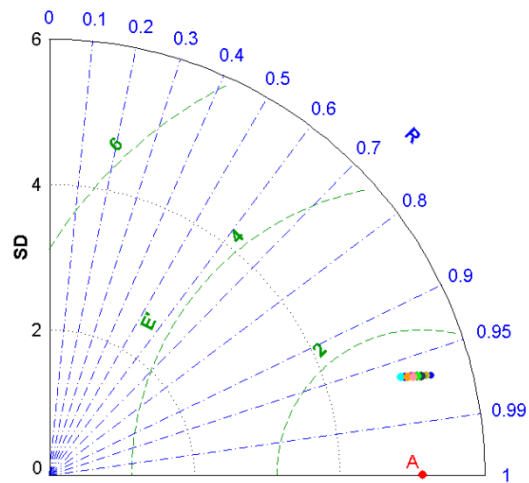


Fig. 4 – Taylor Diagram displaying a statistical comparison among observations (A) and 15 run models (clustered coloured dots). Black dotted circles are standard deviation (SD), green dashed circles are the centred root-mean-square-difference (E') and, finally, blue dash-dotted lines are the correlation coefficient (R)

Modelled indoor T data are strongly clustered showing that, even though λ_s and s_s are the most effective parameters, their variation does not play a key role in minimizing the error among modelled

and measured T. Data series are highly correlated ($R > 0.95$), the E' ranges within 1.32 °C and 1.39 °C, and the SD is between 5.0 °C and 5.5 °C.

In Table 2, the RMSD and the CV-RMSD of the indoor T over the calibration period for the first guess model and the calibrated model are reported with respect to the observations. The RMSD and the CV-RMSD of the calibrated model are quite lower than in the first guess model. Even though the most effective parameters were identified, the calibration procedure did not improve the capability of the model to well simulate the building. This would confirm that an accurate monitoring of the soil temperature should be performed and included in the analysis.

Table 2 – The RMSD and the CV-RMSD for the first guess model and the calibrated model are reported

	First Guess Model	Calibrated Model
RMSD	1.38 °C	1.32 °C
CV-RMSD	8.0 %	7.8 %

Fig. 5 shows the temporal behaviour of bias (%) calculated between measured and calibrated modelled indoor T. The mean bias is 0.6 % (indicated as a dashed blue line), while the 7th and 93rd percentile are -9.0 % and 14.5 %, respectively (indicated as dashed red lines). The calibrated modelled T usually overcomes the measured T, mainly from the end of November, when a sudden drop of outdoor T occurs.

The RMSD and the CV-RMSD of the indoor air T over the validation period (January 2016) are 1.92 °C and 20.0 %, respectively. In general, the modelled T overestimates the measured T.

The increase in RMSD and CV-RMSD can be due to a different behaviour in the heat transfer of the soil during meteorological events. Over the validation period, the amount of precipitations was about 18 mm/day, while in the calibration period heavy rainfall (about 230 mm/day), although sporadic, was recorded.

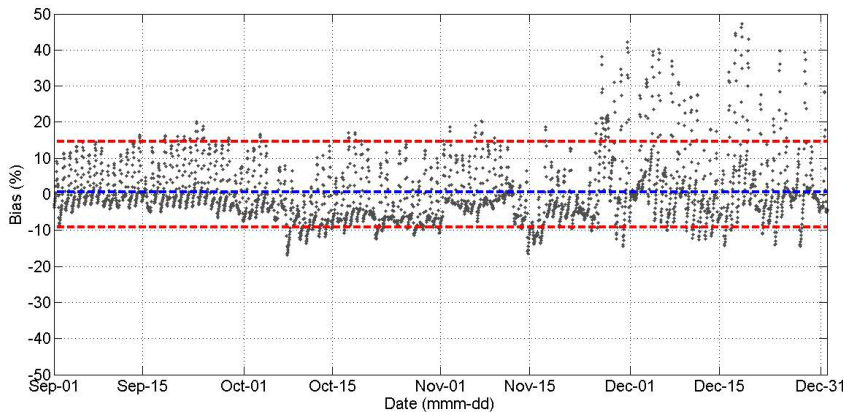


Fig. 5 – Time plot of bias (%) computed between measured indoor T and calibrated modelled indoor T data from September to December 2013. Blue line is the mean of bias (0.6 %), while red lines are 7th (-9.0 %) and 93rd (14.5 %) percentile of bias respectively

5. Conclusion

The temporal behaviour of indoor thermo-hygrometric parameters seems to be related to the solar exposure of the building and its capability to transfer the heat thorough external walls (i.e. thin double skin insulated panels). This has favoured an indoor environment unsuitable for the conservation purpose of faunal remains. The empirical relationship between cracks and T-RH (eq. 4) will be used for

preventive measures after an accurate calibration of the building dynamic simulation model.

The Elementary Effects (EEs) method allowed us to identify the most effective parameters, then used in the calibration. In this case study, the most effective parameters are the thermal conductance and the thickness of the soil. Nevertheless, the use of these parameters does not allow to minimize the error between calibrated modelled and measured indoor temperature, suggesting that other parameters, such

as the air infiltration rate, should be taken into account.

Further studies will be conducted considering the measured soil temperature and humidity, and by using the HAMWall model implemented into the IDA ICE environment. The HAMWall allows the simultaneous simulation of the transfer of heat, air mass, and moisture. In this way, it will be possible to find the most adequate thermo-hygrometric conditions to consider in the building retrofit for the conservation of faunal remains.

Acknowledgement

The authors wish to acknowledge Arch. Carmelo La Micela for the plant and section of "La Polledrara di Cecanibbio" and Tecno.El S.r.l. for microclimate data.

The authors thank all the anonymous reviewers for their precious suggestions to improve our contribution.

References

- CEN. 2011. *EN 410:2011. Glass in building - Determination of luminous and solar characteristics of glazing*. Brussels, Belgium: European Committee for Standardization.
- CEN 2011. *EN 673:2011. Glass in building - Determination of thermal transmittance (U value) - Calculation method*. Brussels, Belgium: European Committee for Standardization.
- CEN. 2010. *EN 15758:2010. Conservation of cultural property—procedures and instruments for measuring temperatures of the air and the surfaces of objects*. Brussels, Belgium: European Committee for Standardization.
- CEN. 2012. *EN 16242:2012. Conservation of cultural property—procedures and instruments for measuring humidity in the air and moisture exchanges between air and cultural property*. Brussels, Belgium: European Committee for Standardization.
- Campolongo, F., A. Saltelli, J. Cariboni. 2011. "From screening to quantitative sensitivity analysis. A unified approach". *Computer Physics Communications* 182(4):978-988. doi: 10.1016/j.cpc.2010.12.039.
- Cornaro, C., V.A. Puggioni, R.M Stollo. 2016. "Dynamic simulation and on-site measurements for energy retrofit of complex historic buildings: Villa Mondragone case study". *Journal of Building Engineering* 6:17-28. doi: 10.1016/j.job.2016.02.001.
- Frasca, F., A.M. Siani, G.R. Casale, M. Pedone, Ł. Bratasz, M. Strojceki, A. Mleczkowska. 2016. "Assessment of indoor climate of Mogiła Abbey in Kraków (Poland) and the application of the analogues method to predict microclimate indoor conditions". *Environmental Science and Pollution Research* 1-13. doi:10.1007/s11356-016-6504-9.
- Garcia Sanchez, D., B. Lacarrière, M. Musy, B. Bourges. 2014. "Application of sensitivity analysis in building energy simulations: Combining first-and second-order elementary effects methods". *Energy and Buildings* 68:741-750. doi: 10.1016/j.enbuild.2012.08.048.
- Morris, M.D. 1991. "Factorial sampling plans for preliminary computational experiments". *Technometrics* 33(2):161-174. doi: 10.2307/1269043.
- Saltelli, A., S. Tarantola, F. Campolongo, M. Ratto. 2004. *Sensitivity analysis in practice: a guide to assessing scientific models*. Chichester, UK: John Wiley & Sons.
- Taylor, K.E. 2001. "Summarizing multiple aspects of model performance in a single diagram". *Journal of Geophysical Research: Atmospheres* 106(D7):7183-7192. doi: 10.1029/2000JD900719.
- UNI. 2015. *UNI 10351:2015. Materiali e prodotti per edilizia - Proprietà termo-igrometriche - Procedura per la scelta dei valori di progetto*. Milan, Italy: Ente nazionale italiano di unificazione.

Comparison Between Simplified and Detailed Methods for the Calculation of Heating and Cooling Energy Needs of Livestock Housing: A Case Study

Andrea Costantino – Politecnico di Torino – andrea.costantino@polito.it

Ilaria Ballarini – Politecnico di Torino – ilaria.ballarini@polito.it

Enrico Fabrizio – Politecnico di Torino – enrico.fabrizio@polito.it

Abstract

Climate control (heating, cooling, and ventilation) is an important aspect of animal production, since the zootechnical performance and the health of reared animals are strongly related to their comfort conditions. Currently, there are neither specific protocols nor commercial tools to estimate the energy use for climate control in a livestock housing.

In this work (in the context of a funded project called EPAnHaus) three different energy simulation methods (QS: quasi-steady-state method, SH: simple hourly dynamic method, DD: detailed dynamic method), in compliance with the ISO 13790 standard, are applied to a broiler house. The aim of the work is to verify which method is more suitable to be applied for the estimation of heating and cooling energy needs of the animal house. A study was carried out to make consistent boundary conditions between the analysed models.

In the comparison of the results, the variability of the boundary conditions is not represented in QS model, resulting in considerable overestimations of the heating energy needs in the colder months (January, February, and December), it does not consider the simultaneity of heating and cooling needs during some months (February and March). Dynamic models (SH and DD models) correctly describe the thermal behavior of the analyzed building, in particular the trend of heating and cooling loads during the production cycles, and the temperature trend during empty periods.

It should be noted that the energy need for cooling is only theoretical since usually free cooling is provided by increased ventilation instead of mechanical cooling. Further analysis and comparison with measured data may therefore be carried out once the performance and the energy use of ventilation fans in the house are modelled.

1. Introduction

The aim of animal rearing is to maximize reared animals' zootechnical performance to increase production (e.g., meat, milk, and eggs) and, at the same time, to guarantee the best life conditions for the animals as required by the EU directives on animal welfare (e.g., European Council Directive 2007/43/CE and 2008/120/EC).

In this context, the climate control of livestock houses plays an important role, because it allows to maintain the indoor environmental conditions within a range of acceptability in terms of temperature, humidity, and indoor air quality (IAQ).

The indoor air temperature in livestock houses must be kept within the range of nominal losses, a thermal neutral air temperature range in which the animal production level is acceptable (ASHRAE, 2005). Within said temperature range, animals use most of the energy gained by feed intake for both, their own growth and the production increase.

Humidity and contaminants are other important parameters that are controlled in livestock houses in order to guarantee optimal environmental conditions by ventilation. Non-optimal levels of moisture may increment the animals' heat stress and cause health problems. Contaminants production is an important issue in livestock (European Commission, 2015): the presence of microscopic particles, ammonia and sulphides coming from feed, bedding and faecal material, may cause health problems to both, the animals and the workers inside the houses. For this reason, a ventilation flow rate to grant the IAQ is always

present in these buildings and it generally reaches high values (e.g., 5-7 ach).

Temperature, humidity, and IAQ control are therefore indispensable for maintaining high production levels and for ensuring a high-quality environment. At the same time, they represent an energy use and a financial cost factor because they are carried out by mechanical systems (e.g. gas heaters and fans). Some values of energy use related to climate control can be found in the literature (Rossi et al., 2013; Costantino et al., 2016): in meat chicken (broilers) production, climate control uses 75.5 % of the global thermal energy needed by the house, and 96.3 % of the total electricity consumption. These percentages consider heating (86–137 kWh/m²/year of thermal energy) and ventilation (4–11 kWh/m²/year of electricity, for both cooling and IAQ control). In swine production, 47.7 % of total thermal energy and 69.2 % of the total electricity is used for climate control with 34–37 kWh/m²/year of electricity used for ventilation and local heating. In dairy cow production, the energy use for climate control is lower and only equal to 20.0 % of the total electricity used into a dairy house.

Many aspects such as the species and the stocking density must be considered to estimate the energy performance of a livestock house. Currently, there are neither specific protocols nor commercial tools that allow farmers and agricultural engineers to estimate the energy use for animal house climate control. Due to the estimated growth in the consumption of livestock products e.g. meat and milk (FAO, 2011) and the projected transference of new technologies to the animal production sector in the coming future (De Corato et al., 2014), an increase in energy needs is expected in the next years. For this reason, the correct estimation of energy use in livestock houses is essential to adopt appropriate energy efficiency strategies in this sector.

1.1 The Aim of the Work

Given this picture, a project called EPAnHaus has been funded to develop a certification scheme of energy use for climate control in animal houses

through modelling and simulation, and measurements. In the present work, three different simulation methods, namely quasi-steady-state (QS), simple hourly dynamic (SH), and detailed dynamic (DD) are applied to a case study. The main purpose is to identify which method is more suitable to be used at the energy performance certification stage for determining the energy needs for the heating and cooling of a livestock house. The case study refers to a house for broiler production.

In the present work, we analyze the consistency options of the boundary conditions and assumptions made during the modelling stage, and compare the outputs of each simulation model. In this way, it is possible to understand which models can correctly describe the boundary conditions and the thermal behavior of the analyzed building.

2. Simulation

2.1 The Case Study

2.1.1 Broiler Production

In the present work three different simulation models are applied to a broiler house to estimate its heating and cooling energy needs. Humidity control is not taken into account.

The broiler house was chosen for the case study because of its interesting features from an engineering point of view.

First, broilers are bred in a closed enclosure. Another interesting element is that broilers are reared in high stocking densities, generally between 33 and 42 kg_{meat}/m², which means an animal presence between 15-23 birds/m², depending on the final live weight. These high values entail considerable heat and vapor production that strongly affect the indoor environment. For example, the flock analysed in this work (about 34,400 birds) has a maximum sensible heat emission of 385 kW and it can produce 170 kg of water in 24 hours by breathing and by faecal material. The data for the estimation of heat and vapor emission by broilers can be determined by animal physiology and homeothermy manuals (Esmay et al., 1986).

An additional feature that makes broiler production interesting is that the climate conditions that must

be kept in the house are not steady during the duration of the production cycle (batch). Conditions, like the heating set point, the cooling set point, and the IAQ ventilation flow rate vary as a function of the broiler age and weight. As shown in Fig. 1, the two-set point temperatures are negatively related to the age (older broilers need lower temperatures than younger ones), while the IAQ flow rate is positively related to the age (older broilers produce more contaminants due to their greater weight).

For this reason (high internal gains and variable set point temperatures) in broiler houses heating may be needed also in the hot season and cooling in the cold one.

In this work, a flock of 34,440 birds is considered. The considered stocking density for the flock is 16.5 birds/m², with a batch duration of 39 days. At day 1 of the batch, few-day-aged chicks are carried in the house. Between two consecutive batches, a sanitary empty period of 13 days is considered, in which there are no animals in the houses and the climate of the house is not controlled. Given these assumptions, each year, 7 completes batches can be carried out.

Using performance objectives tables by feed companies (Lohmann Meat, 2007), the live weight of the birds for each day of the batch can be considered. At the start of the batch chicks of 0.042 kg are considered, while at day 39, broilers have a final live weight of 2.5 kg, as shown in Fig.1.

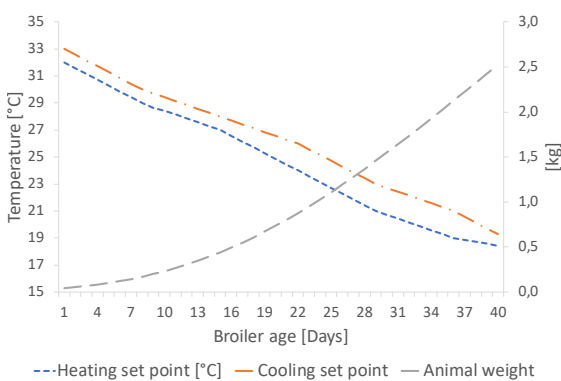


Fig. 1 – Animal weight and air set point temperatures for the batch duration

Data about set point temperatures and minimum IAQ ventilation flow rate come from guides for the management of broiler houses (Cobb, 2008). In Fig 1

the heating set point and cooling set point trends are shown.

2.1.2 The reference broiler house

Broiler production is generally carried out in low insulated buildings, with a width of 10-15 m and a length that can be greater than 100 m.

The reference building used as the case study is in Parma, in the North of Italy. The building is a gable roof broiler house built with a steel structure and prefabricated sandwich panels. It is 15 m wide and 140 m long, with the longer axis aligned on the east-west direction. The total useful floor for the broiler production is 2087 m². At the ridge level the house has a height of 5 m and it decreases to 3 m at the eave level.

The house walls and the roof are prefabricated sandwich panels made up of a double layer of pre-painted steel sheets. Between the two metal sheets a 0.04-m thick high-density spread polyurethane layer ($\lambda = 0.028$ W/(m K)) is interposed as a thermal insulation layer.

The floor is a reinforced concrete screed above a waterproofing sheet and a thermal insulation layer of cellular glass granules ($\lambda = 0.08$ W/(m K)). The thickness of the thermal insulation layer is 0.15 m, while the concrete screed has a thickness of 0.20 m. The internal heat capacity of the opaque elements was calculated according to the ISO 13786 standard (ISO, 2007).

The analysed broiler house has a guillotine opening system for the windows. They are made of metal frames and polycarbonate alveolar panels.

Table 3 – Thermo-physical properties of the building envelope

Element	U -value [W/(m ² K)]	κ_i [kJ/(m ² K)]	α [-]
Walls	0.63	4.8	0.3
Roof	0.64	4.9	0.6
Floor	0.45	67.9	/
Windows	3.6	/	/

All data used for the building envelope come from commercial products. The thermo-physical properties of the envelope are presented in Table 1.

2.2 Calculation Methods

Three different calculation methods based on the ISO 13790 standard (ISO, 2008) were adopted to create three different energy calculation models. The used methods are:

- a monthly quasi-steady-state calculation method (QS);
- a simple hourly dynamic calculation method (SH);
- a detailed (hourly) dynamic simulation method (DD).

They differ because of the chosen time step, the dynamic parameters considered, and the different details of the requested input data.

The adopted methods are described in the following sections.

2.2.1 The quasi-steady-state (QS) model

The quasi-steady-state calculation method (ISO, 2008) is based on the monthly balance of heat losses (transmission and ventilation) and heat gains (solar and internal), assessed in monthly average conditions (Corrado et al., 2007). The dynamic effects on the net energy needs for space heating and space cooling are taken into account by introducing a utilization factor for the mismatch between transmission *plus* ventilation heat losses and solar *plus* internal heat gains leading to heating/cooling loads. The utilisation factor depends on the time constant of the building, the ratio of heat gains to heat losses, and the occupancy/system management schedules. The energy need for space heating and cooling for each month is calculated as:

$$Q_{H,nd} = Q_{H,ht} - \eta_{H,gn} \cdot Q_{gn} \quad (1)$$

$$Q_{C,nd} = Q_{gn} - \eta_{C,ls} \cdot Q_{C,ht} \quad (2)$$

where, $Q_{H/C,nd}$ is the energy need for space heating/cooling, $Q_{H/C,ht}$ are the total heat losses (transmission *plus* ventilation), Q_{gn} are the total heat gains (internal *plus* solar), $\eta_{H,gn}$ is the utilization factor of heat gains, and $\eta_{C,ls}$ is the utilization factor of heat losses.

The actual lengths of the heating and the cooling seasons are determined on the basis of the limit value of the dimensionless heat-balance ratio for the heating mode and the cooling mode respectively.

The limit value is expressed as a function of a dimensionless numerical parameter depending on the time constant of the building.

2.2.2 The simple hourly dynamic (SH) model

The simple hourly dynamic model is described in Annex C to the ISO 13790 standard (ISO, 2008). It consists in a simplification of the heat transfer between outdoor and indoor environment based on a similarity between the thermal behavior of the analyzed building and a resistance – capacitance network made of 5 resistances and 1 capacitance (5R1C). The schematics of the model is reported in Fig. 2 where:

- θ_{air} : indoor air temperature
- θ_s : temperature given by the mix of mean radiant and indoor air temperature
- θ_m : temperature of the capacitive mass node
- θ_e : outdoor air temperature
- θ_{sup} : supply air temperature
- H_{ve} : ventilation heat transfer coefficient
- $H_{tr,is}$: heat transmission coefficient
- $H_{tr,w}$: transmission heat transfer coefficient through windows
- $H_{tr,op}$: transmission heat transfer coefficient through opaque components
- C_m : building fabric heat capacity
- $\Phi_{ia}, \Phi_{st}, \Phi_m$: internal and solar heat gains
- $\Phi_{H/C,need}$: heating or cooling heat load.

The indoor air temperature (θ_{air}) is calculated as:

$$\theta_{air} = \frac{H_{tr,is} \cdot \theta_s + H_{ve} \cdot \theta_{sup} + \Phi_{ia} + \Phi_{H/C,nd}}{H_{tr,is} + H_{ve}} \quad (3)$$

The heating/cooling energy need during the analyzed period ($Q_{H/C,need}$) is obtained by summing the $\Phi_{H/C,need}$ per each time step adopted by the model (1 hour).

This model was applied to a calculation tool for the estimation of the heating and cooling energy need of a broiler house, as shown in Fabrizio et al. (2015).

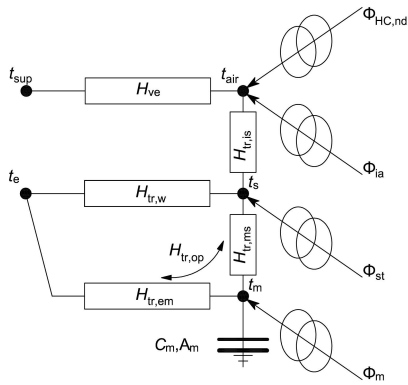


Fig. 2 – Schematic representation of the simple hourly method (ISO, 2008)

2.2.3 The detailed dynamic (DD) model

The detailed dynamic model was created in the EnergyPlus software tool (Filippi et al., 2012). The building thermal zone calculation method of EnergyPlus is the air heat balance model. It is based on the assumptions that the air in the thermal zone has, by default, a uniform temperature, the temperature of each surface is uniform, the long-wave and short wave radiation is uniform, the surface irradiation is diffusive, and the heat conduction through the surfaces is one-dimensional. The air heat balance, neglecting the heat transfer due to infiltration and to inter-zone air mixing, can be written as:

$$C_z \frac{d\theta_z}{d\tau} = \sum_{i=1}^N Q_{c,i} + \sum_{i=1}^{N_{surface}} h_i A_i (\theta_{si} - \theta_z) + m_v c_p (\theta_e - \theta_z) + \dot{Q}_{sys} \quad (4)$$

where, N is the number of convective internal loads $Q_{c,i}$, $h_i A_i (\theta_{si} - \theta_z)$ is the convective heat transfer from the zone i -surface at temperature θ_{si} to the zone air at temperature θ_z , while $c_p (\theta_e - \theta_z)$ is the heat transfer due to ventilation with the outside air, and \dot{Q}_{sys} is the system output. The capacitance C_z takes into account the contribution of the zone air as well as that of the thermal masses assumed to be in equilibrium with the zone air. In order to determine the building net energy need under ideal conditions and to make the result independent from the system features, the so-called “Ideal Loads Air System”, which can be operated with infinite heating and cooling capacity, was applied.

A time step of fifteen minutes was adopted in the simulation.

Some examples of application of this tool to animal houses can be found in literature (Fabrizio, 2014).

2.3 Consistency Options

In order to compare the net energy needs obtained with different methods, the modelling procedures should be made consistent, as shown in Corrado et al. (2015) and Ballarini et al. (2011). In the following, the consistency options applied to the models are presented.

- The hourly weather data (outdoor air temperature, solar radiation) used in the DD simulation come from a data set known as IWEC (International Weather for Energy Calculations). The same data were applied in the SH model. The monthly average values were considered in the QS model.
- Hourly schedules of heating and cooling set point temperatures, internal heat sources (sensible heat emission of broilers), and ventilation flow rate were assumed in the hourly methods (DD and SH), while monthly averages of the same quantities were used in the QS model.
- In EnergyPlus, the opaque and transparent building components were modelled by defining the detailed thermo-physical parameters of their materials (e.g., thermal conductivity, density, specific heat capacity, spectral features). The resulting thermal transmittance values of the envelope components and the total solar energy transmittance of glazing were applied to the SH and the QS model.

3. Discussion and Result Analysis

3.1 Numerical Results

The yearly energy needs for heating and for cooling estimated by the three models are reported in Table 2. From the table, it is possible to notice that the total heating energy need of the QS model is the highest value. By contrast, the SH total cooling energy need is the highest one, while the value obtained through the QS model is the lowest. For

both heating and cooling energy needs, the results of DD fall within the values obtained by the QS and SH models.

Focusing on the total heating energy needs, the differences between the outputs of the three models appear to be not negligible. Table 2 shows that, assuming the DD model value as a reference, the value estimated by the SH model is smaller by 17.0 kWh/m² (-17 %). The yearly heating need value estimated by the QS model is greater than DD by 66.9 kWh/m² (+66 %).

By contrast, when looking at yearly energy need values for cooling, all values are quite similar. Considering the detailed dynamic model (DD) result as reference, the QS model result is lower by 18.2 kWh/m² (-9 %), while the SH model value is greater by 6.7 kWh/m² (+3 %).

Table 2 – Yearly energy needs for heating and cooling (outputs of the models)

Energy use	QS model	SH model	DD model
Heating [kWh/m ²]	168.1	84.2	101.2
Cooling [kWh/m ²]	187.5	205.7	199.0

The significant difference that exists especially between the heating values of the QS model and of the DD and SH models can be explained by analyzing the monthly energy needs, as shown by Fig. 3. In colder months, the energy needs for heating, estimated by the QS model, are greatly overestimated, in particular in January, February and December. Another interesting element is that the QS model is not able to consider the simultaneity of a heating and a cooling energy need in the same month, except for those months in which heating and cooling seasons (or vice versa) change, as it occurs in October. Since it does not contemplate this aspect, the QS model does not consider important shares of energy needs, such as the cooling needs in February and in April.

For these reasons, the use of the QS model cannot be recommended for this type of application.

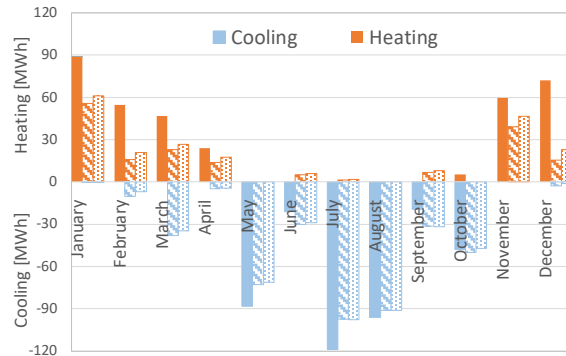


Fig. 3 – Monthly heating and cooling energy needs; (QS model: full color columns; SH model: striped columns; DD model: dotted columns)

In Fig. 4 the trends of heating and cooling loads estimated by the two dynamic models (SH and DD models) are shown during a complete batch carried out between February and April. In the first part of the chart (batch start) neither heating nor cooling loads occur because the birds are not inside the building, therefore the air temperature fluctuates in free-range conditions. When the young chicks arrive at the broiler house, there is a heating load peak which is estimated differently in the two models, while later, the trends of loads in both models appear quite close.

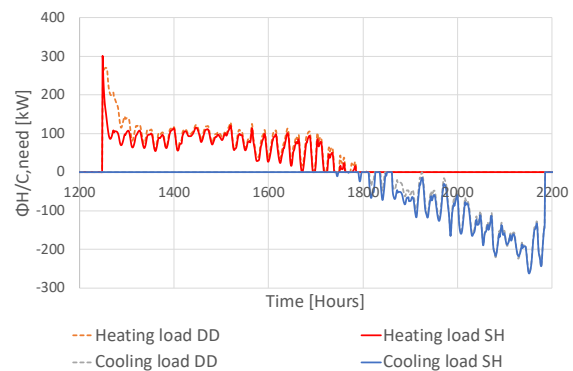


Fig. 4 – Hourly heating and cooling need during a batch (February–April)

While the animals grow, the heating load decreases, as shown in Fig. 4, as a function of the decrease in the heating set point temperature, and the cooling load increases during the last part of the batch. The RMSE between the two-load profiles, calculated over the 936 h of the batch, is equal to 22.0 kW for the heating load and to 8.1 kW for the cooling load. Not considering the first days in the calculation of

the heating load, the RMSE between the two trends decreases to 7.3 kW.

In Fig. 5 the indoor air temperature trends estimated by the SH and DD models are shown for the last days of the batch of Fig. 4, and for the following empty period. In the first part of the chart both estimated indoor air temperatures (obtained through the SH and DD models) correspond to the cooling set point. When the batch ends, the broiler house is empty, no set point temperature is requested and the indoor air temperature fluctuates in a free running condition. Both models present very close air temperature trends after some days, while just after the system shut off, the temperature decay in the DD model takes a few days when compared to the decay in the SH model that takes place in a few hours. This may be due to a difference in the heat capacity estimation of the floor in the two models.

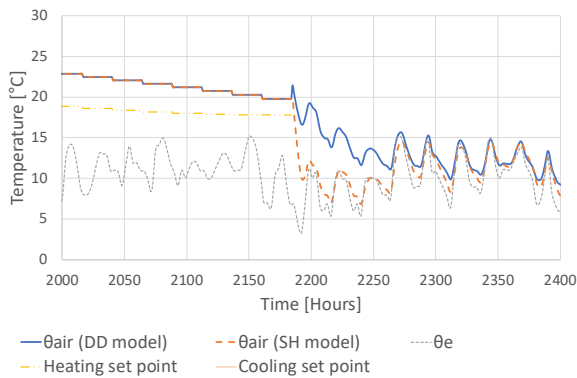


Fig. 5 – Temperature trends at the end of the batch of Fig. 4 and during the following empty period (free running conditions)

4. Conclusion

In the present paper, three simulation models for the estimation of the energy needs of a broiler house are compared.

The results show that the simple hourly dynamic method (SH) and the detailed (hourly) dynamic simulation method (DD) give similar results for heating and cooling energy needs, with a difference between 9 % and 17 %. The monthly quasi-steady-state method does seem not to be suitable for the energy analysis of such house because it considerably overestimates the heating energy need values and it is not able to correctly consider the

variation of boundary conditions (e.g., set point temperature and internal heat gains).

It should be noticed that the cooling energy need is only theoretical; in fact only free cooling techniques based on the house's tunnel ventilation are applied. Therefore, a direct comparison with the measured data cannot be made at this stage, but it should be made once the electricity use for ventilation in free cooling mode is also estimated.

The presented methodology may also be used for estimating the energy consumptions of other livestock houses for animal species commonly reared in intensive breeding, such as swine and laying hens.

Acknowledgement

This work was financially supported by the SIR (Scientific Independence of young Researchers) 2014 “EPAnHaus – Energy performance certification of livestock houses” project, grant number RBSI141A3A, funded by MIUR.

Nomenclature

Symbols

C	Effective heat capacity (kJ/K)
H	Heat transfer coefficient (W/K)
Q	Thermal energy (Wh)
U	Thermal transmittance (W/(m ² K))
α	Solar absorption coefficient (-)
η	Utilization factor (-)
θ	Temperature (°C)
λ	Thermal conductivity (W/(m K))
κ	Areal heat capacity (kJ/(m ² K))
Φ	Heat flow rate (W)

Subscripts/Superscripts

a	Air
C	Space cooling
e	External, exterior
gn	Heat gains
H	Space heating
ht	Heat transfer
i	Internal (temperature)
ls	Losses

m	Mass-related
nd	Need (energy)
op	Opaque
tr	Transmission (heat transfer)
sup	Supply (of air)
ve	Ventilation (heat transfer)
w	Windows

References

- ASHRAE (American Society of Heating Refrigeration and Air-Conditioning Engineers). 2005. *ASHRAE Handbook: Fundamentals*. Atlanta, U.S.A.: ASHRAE.
- Ballarini, I., V. Corrado. 2011. "A new thermal analysis by numerical simulation to investigate the energy performance of buildings". In: *Proceedings of Building Simulation 2011*. Sydney, Australia: IBPSA.
- Cobb. 2008. *Broiler Management Guide*. Siloam Springs, AK, U.S.A.: Cobb.
- Costantino, A., E. Fabrizio, A. Biglia, P. Cornale, L. Battaglini. 2016. "Energy use for climate control of animal houses: the state of the art in Europe". *Energy Procedia* 101: 184-191. doi.org/10.1016/j.egypro.2016.11.024.
- Corrado, V., H.E., Mechri, E. Fabrizio. 2007. "Building energy performance assessment through simplified models: Application of the iso 13790 quasi-steady state method". In: *Proceedings of Building Simulation 2007*. Beijing, China: IBPSA.
- Corrado, V., I. Ballarini, D. Dirutigliano, S. Paduos. 2015. "Cost-optimal analysis of Italian office buildings through the application of a quasi-steady state model validated by detailed dynamic simulation". In: *Proceedings of Building Simulation 2015*. Hyderabad, India: IBPSA.
- De Corato, U., F.A. Cancellara. 2014. *L'efficienza energetica nel comparto zootecnico. Analisi dei consumi energetici e miglioramento delle performance di efficienza energetica in alcune tipologie di allevamento*. Rome, Italy: ENEA.
- Esmay, M.E., J.E. Dixon. 1986. *Environmental control for agricultural buildings*. Westport, U.S.A.: The AVI Publishing company, INC.
- European Commission. 2015. *Best Available Techniques (BAT) Reference Document for the Intensive Rearing of Poultry or Pigs (Final Draft)*. Brussels, Belgium: European Commission.
- European Council. 2007. European Council Directive 2007/43/C. 28th June 2007. *Laying down minimum rules for the protection of chickens kept for meat production*. Brussels, Belgium: European Council.
- European Council. 2008. European Council Directive 2008/120/EC. 18th December 2008. *Laying down minimum standards for the protection of pigs*. Brussels, Belgium: European Council.
- Fabrizio, E., G. Airoidi, R. Chiabrando. 2014. "Study of the environmental control of sow farrowing rooms by means of dynamic simulation". *Lecture Notes in Electrical Engineering* 263(3): 3-11. doi:10.1007/978-3-642-39578-9_1
- Fabrizio, E., A. Ghiggini, M. Bariani. 2015. "Energy performance and indoor environmental control of animal houses: a modelling tool". *Energy Procedia* 82: 439-444. doi.org/10.1016/j.egypro.2015.11.833.
- FAO (Food and Agriculture Organization of the United Nations). 2011. *World Livestock 2011. Livestock in food security*. Rome, Italy: FAO.
- Filippi, M., E. Fabrizio (edited by). 2012. *Introduzione alla simulazione termoenergetica dinamica degli edifici*. Milan, Italy: Editoriale Delfino.
- ISO (International Standard Organization). 2007. *13786 - Thermal performance of building components - Dynamic thermal characteristics - Calculation methods*. Geneva, Switzerland: ISO.
- ISO (International Standard Organization). 2008. *13790 - Energy performance of buildings. Calculation of energy use for space heating and cooling*. Geneva, Switzerland: ISO.
- Lohmann Meat. 2007. *Broiler Stock Performance Objectives*. UK/USA: Aviagen.
- Rossi, P., A. Gastaldo, G. Riva, C. de Carolis. 2013. *Progetto Re Sole*. Reggio Emilia, Italy: Centro Ricerche Produzioni Animali (CRPA).

Effect of Blind Control Strategies on Energy Demand of Office Buildings and Melanopic Effect for Occupants

Daniel Plörer – University of Innsbruck – daniel.ploerer@uibk.ac.at

Matthias Werner – University of Innsbruck – matthias.werner@uibk.ac.at

Martin Hauer – University of Innsbruck – martin.hauer@uibk.ac.at

David Geisler-Moroder – Bartenbach GmbH – david.geisler-moroder@bartenbach.com

Abstract

The total energy demand of buildings consisting of heating, cooling, and artificial light demand is strongly depends on solar gains resp. daylight passing the façade. To prevent glare issues and overheating in summer, shading systems are widely used especially in office buildings. The majority of such systems involve venetian blinds. To provide a satisfying operation of the blind systems, the decision whether the façade should be opened or closed has to be based on live measurements of the external situation in terms of solar radiation, illuminance, and ambient temperature. The most commonly used control strategies operate rudimentarily, and often choose only between the two façade states, retracted blinds and deployed at a certain angle, mostly around 45°, based on simple criteria depending on single values of external sensors. This paper introduces a novel control strategy, which simulates the necessary artificial light and heating or cooling demand for each possible blind position in real time depending on external boundary conditions. This allows the determination of the best blind angle in terms of minimal total energy demand. The results show that these elaborate strategies can have a remarkable influence on the total energy demand of buildings. The evaluated test scene shows 30 % savings in terms of total primary energy demand could be achieved compared to conventional sun protection control strategies. In addition, daylight exposure of the occupants' faces can be improved and this represents an important factor for the melanopic effect. Two new strategies are applied to three different façade setups for a single office scenario and compared to a hypothetical reference system, which represents the state of the art.

1. Introduction

The transparent area and the insulation qualities of the façade define the total energy demand of the

building. Solar gains reduce the heating demand in winter but can cause overheating or a high cooling demand in summer. To avoid that, a sun protection façade system can be installed, which is usually activated by exceeding external irradiation values in summer. Such façade systems often also fulfil a glare protection function, which is controlled by the occupant. Furthermore, it has an enormous influence on the daylight input and thus on the artificial lighting demand. However, this impact is usually not taken into account in the façade control strategy and energetically optimized façade system positions in terms of minimal heating, cooling, and artificial light demand cannot be determined.

Two elaborate integral control strategies for façade systems are introduced and compared to a commonly employed "reference strategy". In contrast to other studies introducing elaborate integral control strategies, which operate blinds at cutoff angle or optimize blind angles to improve daylight redirection in deeper regions of the room (Liu et al., 2015; Chan and Tzempelikos, 2015), a full factorial simulation of all possible blind positions in every time step is provided in this study. Both introduced strategies involve a daylight simulation based on the radiance three-phase-method (Ward et al., 2011). It is used to detect glare, calculate the vertical illuminance of the occupant's faces, and assess the horizontal room illuminance on certain points by daylight. Finally, the artificial light demand results from the difference to a requested illuminance of 500 lx on the working plane. While the first strategy only deals with lighting issues, the second strategy additionally includes a simplified thermal analysis and is therefore capable of considering concerning about the total energy demand in the choice of the

optimal blind-positions. For the optimization, a target function is defined including the calculation of all possible blind-positions. The one that reaches the optimum for the target function will be chosen. A detailed description of both strategies, their optimization processes, and the daylight simulation routine is provided in Section 2.4.

Three different façade build-ups are investigated. All of them employ external blinds that form the second most investigated systems in literature (Konstantoglou and Tsangrassoulis, 2016) after the internal blinds, hardly capable of preventing overheating in summer. The systems differ in terms of adjustability and blind type. While the first and second system only use shading blinds, the third system consists of shading blinds in the lower part and daylight redirecting blinds in the upper part. System two and three differ from system one in the fact that blind angles can be chosen differently in the lower and upper part.

The influences and potential savings of this novel control strategy are evaluated with the dynamic thermal building simulation tool, TRNSYS. Only the first of the three façade-systems is operated by all three strategies, since the other two systems involve separately controllable blind systems for the upper and lower part and thus they cannot be handled by the “reference strategy”.

The annual simulations are performed on a single office with a south façade, using an EnergyPlus weather file for Innsbruck, Austria. The thermal insulation of the room is chosen to fulfil passive house standards. The windows consist of three panes where shading blinds are used and an additional glazing to protect the daylight redirecting blinds. In Sections 2.1 and 2.4 the geometry respectively other parameters of the thermal model are described in detail.

2. Model Setup

Parameters like room ventilation and envelope insulation including window build-up, have a significant influence on the thermal balance of the model, and consequently on the energy optimizing blind control strategy. Since the introduced blind systems and control strategies are not expected to

find their main application in the retrofitting of existing buildings, a new building with passive house standard is assumed for the present study.

2.1 Geometry

As a test scene, a two-person office with a floor area of 5 x 5 m, a room height of 3 m and a façade, which is opaque in the part below 1 m and fully glazed above, is assumed. For the window a three-pane glazing is considered, including an additional pane in case of the daylight redirecting blind, which measures 1 m in height.

2.2 Investigated Blind Systems and Daylight Calculation

As shown in Fig. 1 left, diffuse reflecting, downwards curved lamellae are assumed as external blinds. Highly specular reflecting lamellae, which show an upward curvature, form the daylight redirecting blinds and are shown in Fig. 1 right. For the daylight simulation, the blind systems were geometrically modelled and bidirectional scattering distribution functions (BSDF) data were calculated for eight different blind angles (0°, 10°, 15°, 25°, 35°, 45°, 60°, 75°) using the radiance genBSDF method.

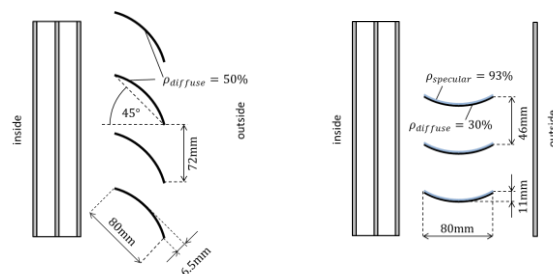


Fig. 1 – Left: External blinds; Right: Daylight redirecting blinds

The daylight calculations have to be carried out for all lamella positions in a very short timeframe to achieve real time results. Therefore daylight coefficients for diffuse and direct radiation are pre-calculated using the radiance three-phase-method (Ward et al., 2011). The BSDF-data in matrix format are multiplied by the daylight-matrix (diffuse and direct) from left, and by the view-factor-matrix from right. The multiplication of the resulting matrix by the daylight vector from the left, allows the calculation of the room illumination by daylight. The dimensions of the BSDF-matrix depend on the required angular resolution for the incoming and outgoing half-space. For

the study at hand, Klems resolution was chosen, thus, the dimensions of the BSDF-matrix equal 145×145 . For the daylight vector, the Tregenza discretization with 145 patches was chosen so the daylight-matrix also shows the dimensions of 145×145 . The view-factor-matrix represents the mapping from the inner intensity distribution of the façade system to the measurement points (MP) inside the room, where the vertical and horizontal illuminance as well as the received luminance were calculated. The positions of the four MPs are shown in Fig. 2. At MP 1 and 2, which are 0.85 m above the ground, the vertical illuminance was calculated. The resulting values were used to calculate the artificial light demand that equates to the difference of the calculated daylight illuminance at the darker of the two MPs to the required 500 lx.

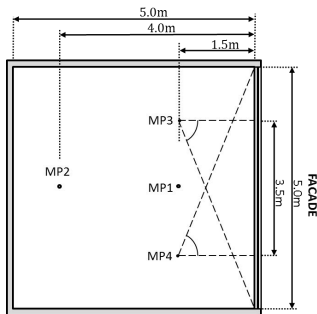


Fig. 2 – Positions of measurement points (MP) in the test room

MP 3 and 4 represent the sitting occupant's faces at a height of 1.2 m. Two different indicators are determined at these positions. The first is the vertical illuminance, used to evaluate the potential of gaining a nonvisual effect of the applied strategy and façade system. The second identifier is the maximum of the observed luminance. Glare is detected whenever this value exceeds 3000 cd/m^2 for either MP3 or MP4. This criterion was chosen according to DIN EN 12464-1, which defines an upper limit for the luminance of light fixtures that could cast reflections onto screens.

The daylight calculation was split up into a direct and a diffuse part from sun and sky respectively. The luminance of the sky is assumed to be homogeneously distributed over the entire half-space. Using the three-phase-method, for each measurement point and blind position one diffuse and 145 direct daylight factors are simulated in advance and saved

in a database. These 146 factors describe the quotient of internal and external luminance/illuminance by a diffuse sky and 145 sun positions. In each time step, the measured diffuse radiation is multiplied by the diffuse factor and the direct radiation is multiplied by the factor, which is chosen from the 145 direct values depending on the sun position. The results from direct and diffuse daylight calculation are summed up at the end resulting in internal luminance and illuminance values. These simplified calculations of two multiplications allow a real time determination of the daylight input for all possible blind positions, even in case of complex daylight redirection systems.

2.3 Coupled Thermal and Lighting Simulation

In order to evaluate the performance of this novel control strategy, the algorithm is tested within a TRNSYS simulation environment, which represents the building behavior using the multi-zone-building model Type56. Thus, the simulation routine comprises a thermal evaluation in TRNSYS, which is coupled to a thermal and lighting calculations based on the pre-calculated daylight factors described in Section 2.2 in the time step. The lighting and thermal calculations, as well as the optimization of blind positions are amalgamated in so-called VEC-modules (Visual and Energy Control), as described more closely in Section 2.5. The coupling routine works as follows: TRNSYS acts as master and hands over relevant parameters from the weather file to the particular VEC-module in every time step. The VEC-Module computes and returns values of the optimal blind position as well as the horizontal and vertical illuminances on the working plane, respectively the occupant's faces and the artificial light demand. TRNSYS considers the artificial light demand in the thermal simulation as an addition to the internal gain. Solar gains are calculated in TRNSYS using the newly introduced window model based on solar BSDFs and ISO 15099 algorithms (Hiller and Schöttl, 2014), provided by Transolar as beta-version within this research work. Thereby, additionally to the solar transmittance, also the secondary heat flux is taken into account proper-

ly. The changing of the blind angle of the VEC-module is performed in TRNSYS by choosing the appropriate thermal BSDF of the system. The calculation of the thermal BSDFs were done in Window 7 using the previously calculated optical BSDFs. Almost the entire simulation setup is equal for all strategies and façade systems, except for the set of thermal BSDFs that change according to the investigated façade system, and the VEC-module is swapped according to the evaluated strategy and façade system.

2.4 Build-Up for Thermal Simulation in TRNSYS

Since the investigated office is assumed to be part of a large office building and adjacent room temperatures are considered equally, the heat flux through adjacent walls is neglected. To achieve a realistic simulation, some basic assumptions for the test setup were made.

Table 1 – Parameters of test room for the thermal simulation

Parameter	Value
U-value façade wall	0.1 W/m ² /K
U-value window glazing (no shade)	0.7 W/m ² /K
g-value window glazing (no shade)	0.5
Sensible heat emissions*	70 W/pers.
Operating hours*	7am-6pm
Internal loads* (equipment)	9.6 W/m ²
Heating threshold*	20 °C
Cooling threshold*	26 °C
Air change rate domestic* (occupied/unoccupied)	0.96 / 0.2 h ⁻¹
Air change rate night*	3 h ⁻¹
Heat recovery rate	80 %
Infiltration rate	0.07 h ⁻¹
Reflectance (ceiling/walls/floor)	80 / 50 / 30
Luminous efficacy of artificial light	70 lm/W

*according to SIA 2024

The occupation time and a schedule for internal gains were chosen by following the SIA 2024 standard. The chosen parameters for the test room for the thermal simulation are listed in Table 1.

2.5 VEC-Module

The VEC-module holds the control logic and is adapted to the particular façade system. As described in Section 2.2 the daylight calculation in the VEC-module is based on pre-calculated values. In each time step the diffuse and the direct daylight vectors are calculated based on the global and diffuse horizontal illuminance.

According to the applied control strategies and façade systems, different variants of the VEC-module were used, but for convenience all of them use the same set of input and output parameters, listed in Table 2. The global and diffuse vertical radiation is only used in the VEC-module, which employs the energy optimizing strategy. While the artificial light demand is the only energy output delivered by the VEC-module, heating and cooling demand were calculated in TRNSYS based on the blind position chosen by the VEC-module, as described in Section 2.2.

Table 2 – Input and output parameters of VEC-modules

Inputs	Outputs
- Timestamp [hour in year]	- Deployment of blinds [bool]
- Ambient temperature [°C]	- Blind angle middle façade part [deg]
- Global vertical radiation [W/m ²]	- Blind angle upper façade part [deg]
- Diffuse vertical radiation [W/m ²]	- Vertical daylight illuminance MP3 [lx]
- Global horizontal radiation [W/m ²]	- Vertical daylight illuminance MP4 [lx]
- Diffuse horizontal radiation [W/m ²]	- Horizontal Illuminance [lx]
- Global horizontal illuminance [lx]	- Artificial light demand [W/m ²]

Each variant of the VEC-module is defined by pre-calculated daylight factors depending on the deployed façade system and the employed control strategy. The three façade systems are external

blinds with continuous hanging, external blinds whereby the blind angle can be chosen separately for the upper and middle façade part and a combination of daylight redirecting blinds in the upper part and, finally, external blinds in the middle part. The three strategies are the “reference strategy” which decides to close the façade with a blind angle of 45° whenever the vertical global radiation rises above 150 W/m^2 , the “light strategy” which always uses the blind position allowing maximal daylight entry without causing glare, and the “energy strategy” which performs an energetic analysis of all the blind positions and chooses the one generating the lowest primary energy demand. For heating and cooling heat pump systems with coefficients of performance of 3.5, respectively 2.5 are assumed. The primary energy demand is calculated by adding up heating, cooling, and artificial light demand weighted by the primary energy factors, for which values of 0.67, 0.96 and 2.4 are assumed respectively. The strategies “light” and “energy” avoid glare, since they exclude all blind positions, which meet the glare criterion during the office hours.

The energy analysis of the “energy strategy” comprises simplified calculations of the heating and cooling demand of the investigated room after the EN 13790 standard. Heating and cooling demands are calculated for every possible blind position, neglecting the thermal mass of the room. The consideration of the thermal mass is problematic, because the thermal situation in the time step before would strongly influence the decision for the optimal blind position. As an example in the morning of a hot summer day, the building’s core temperature can still be relatively cold due to night ventilation and thus the cooling demand can be strongly underestimated. In that case, the strategy would not take into consideration the possible overheating in the morning hours and thus open the blind angles up to glare limitation. Due to the thermal mass of the building, the solar gain in the morning would have a negative repercussion on the rest of the day. That means a realistically calculated cooling demand is not the optimal criterion for the choice of the blind position. The stationary cooling demand was found to form a much more useful criterion for the optimization of the blind positions, since it sets the thermal insulation of the building in relation to the solar

gain, and that parameter is directly influenced by the variation of the blind positions.

3. Evaluation of Simulated Data

The main goal of the present study is to evaluate blind control strategies according to the primary energy demand they cause, and for their ability of gaining a melanopic effect. Since control strategies interact directly with façade systems, an independent comparison is not expedient. The performed simulations involved different façade systems and different control strategies. A comparison between different façade systems controlled by the same strategy, as well as a comparison between different control strategies acting on the same façade system is shown in Section 4. For the energy evaluation of the strategies and façade systems, the primary energy demands for heating and cooling calculated in TRNSYS, and artificial light calculated in the VEC-module, were evaluated on a monthly and annual basis. To evaluate the façade systems’ and strategies’ potential of reaching a melanopic effect, the vertical illuminance was evaluated in MP 3 and 4, and integrated in the office hours of each month and for the whole year, resulting in the vertical luminous exposure. The melanopic effect comprises several non visual effects of daylight on humans. The term melanopic originates from the protein melanopsin, which can be found in intrinsically photosensitive retinal ganglion cells and plays an important role for the circadian rhythm (Hattar et al., 2002; Provencio and Warthen, 2012). A proper definition of the melanopic effect is still missing, but it strongly depends on the vertical illuminance of the occupants faces. The vertical luminous exposure is calculated as an integral of the vertical illuminance of the occupants faces during the office hours. The monthly and annual sum of these values can be used to assess the melanopic effect potential of the investigated setup. Since the melanopic effect is critical in winter and not critical in summer, the vertical luminous exposure was only evaluated for those days in which the sun rises after 7 am. It can be assumed, that workers gain sufficient daylight on their way to the office outside that time of year. The calculated values of the monthly and annual vertical

luminous exposure are used to compare the particular strategies and façade systems in terms of their ability to provide a melanopic effect for the occupants.

4. Results and Interpretation

Fig. 3 shows the annual and monthly primary energy demand of the test room for the energy, light, and reference strategies.

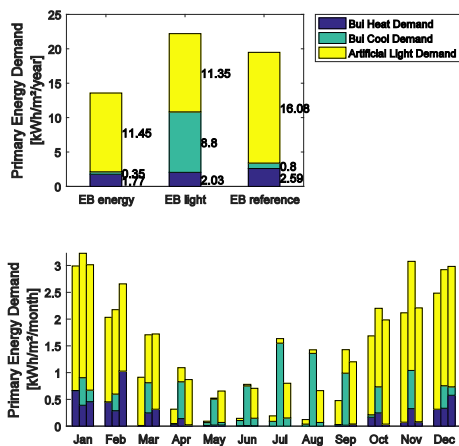


Fig. 3 – Annual and monthly primary energy demand of the test room equipped with external blinds (EB) for the energy, light, and reference strategies

The comparison of the three strategies shows that the cooling demand is the energetically most critical parameter for the control strategy. Since the investigated room was assumed to be well insulated according to passive house standards, for suboptimal control strategies a cooling demand can also be observed in winter. This is a rather hypothetical problem, since overheating in winter could be easily solved by temporarily increasing the ventilation rate or simply by opening a window. In such a case, the control strategy of the ventilation system would have to be adopted. The ventilation system defined for the thermal simulation in TRNSYS was not adjusted to that case, but to interact well with the “energy strategy”. An energetically optimized strategy can reduce the cooling demand to the minimum, and for the simulated location, Innsbruck, Austria, the blind strategy can make the difference whether a cooling system is required or not. The only strategy that really depends on a cooling system is the “light strategy”, whereby the artificial

light demand is the only parameter that was minimized, and the blind angles are always opened to a maximum just to avoid glare. This causes high solar gain also in summer. The “reference strategy” performs well enough in terms of the cooling demand, since cooling in winter must not be taken into account, and the demand in summer is comparable to the value given by the “energy strategy”. The heating demand can be reduced by more than 20 % when the “light” or “energy strategy” is applied compared to the “reference strategy”, but the absolute energy savings of 0.6 kWh/m²/year is not worth mentioning. Since the wall buildup is assumed to comprise a good thermal insulation and the ventilation system with energy recuperation is taken into account, the heating demand does not leave much room for improvement. The main energy demand remaining for a well-insulated building equipped with a solar shading system is the artificial light demand. Compared to the “reference strategy” the artificial light demand can be reduced by 28.7 % or 4.6 kWh/m²/year with the application of the “energy strategy”. The “energy strategy” achieves nearly the same artificial light demand as the “light strategy”. Due to the fact that during the winter there is less gain in heating and artificial light demand is higher, the “energy strategy” prefers open façade settings, which results in same blind position as with the “light strategy”. During the summer, the available daylight mostly suffices for the room illumination, even for the blind positions, which are chosen to prevent overheating. In this test setup the total primary energy saving for the “energy strategy” compared to the “reference strategy” is 29.6 % or 5.9 kWh/m²/year.

In Fig. 4 the annual and monthly vertical luminous exposure of the occupant’s faces is shown. When the “reference strategy” is used, the occupants gain slightly more daylight during the critical period compared to the “energy strategy”, but this result has to be considered with caution, because the “reference strategy” does not include a proper glare protection. The “light strategy” achieves the maximum quantity of daylight on the occupants, whereby glare is avoided. Although lighting energy savings are negligible, the vertical luminous exposure is increased by 18 % in the critical time compared to the “energy strategy”.

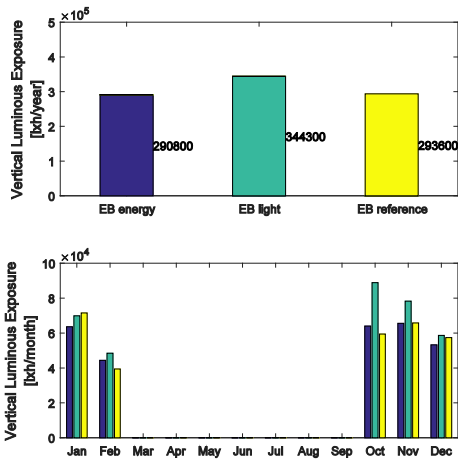


Fig. 4 – Annual and monthly vertical luminous exposure of the occupants' faces for the time range between October 5 to February 16, when sunrise is after 7 am

The reason for this discrepancy is that in time steps where several blind configurations neither cause glare nor artificial light demand, the “light strategy” tends to choose the configuration where the blinds are opened to a maximum. Since the target function of the “energy strategy” includes the heating and cooling demand in addition to the artificial lighting demand, it will choose a further closed façade configuration where still no artificial light is needed to avoid overheating in summer.

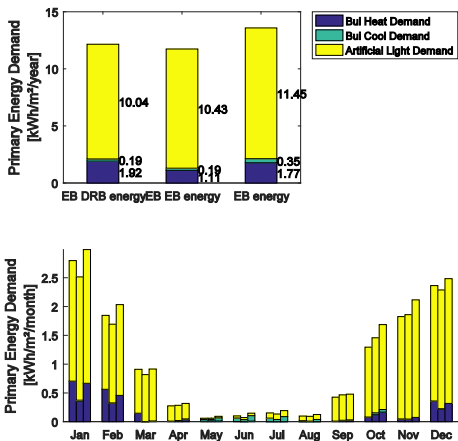


Fig. 5 – Annual and monthly primary energy demand of the test room equipped with the façade systems external blinds in combination with daylight redirecting blinds (EB DRB energy), external blinds two part hanging (EB EB energy) and external blinds (EB energy) controlled by the strategy energy

Fig. 5 shows the annual and monthly primary energy demand of the test room equipped with the façade systems external blinds (EB), external blinds with two-part hanging (EB EB), and external blinds

in combination with daylight redirecting blinds (EB DRB) controlled by the strategy energy. The greater amount of possible façade configurations allows the simultaneous decrease of all three energy demands in total by 15 % using external blinds with two-part hanging compared to external blinds with continuous hanging. The façade settings “EB EB energy” and “EB DRB energy” achieve nearly the same energetic performance.

Fig. 6 shows the annual and monthly mean value of the vertical luminous exposure of the occupants' faces.

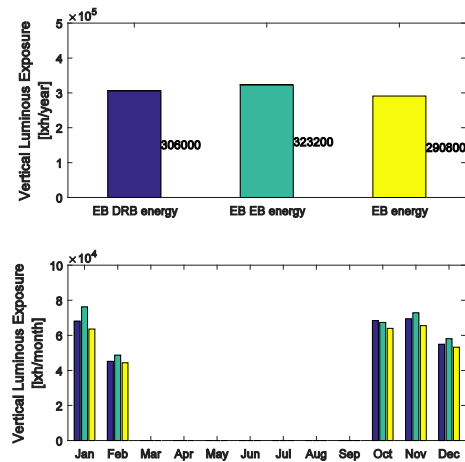


Fig. 6 – Annual and monthly vertical luminous exposure of the occupants' faces for the time range between October 5 to February 16, when sunrise is after 7 am

Even though the artificial light demand is higher, the vertical luminous exposure during the critical time is slightly higher, by 6 %, for the external blinds with two-part hanging compared to the daylight redirecting blind system. A possible reason for that curiosity is the fact that daylight redirecting blinds project daylight deeper into the room than diffuse reflecting external blinds. Since all workplaces in the test office are assumed to be close to the window, this illumination of the deeper space is not profitable for the occupants.

5. Conclusion

Energetically optimizing blind control strategies and ventilation strategies can work independently, but since they address the same optimization goal, namely minimizing the heating and cooling demand, they have to be adapted to each other in

order to keep them from working against each other.

A blind control strategy that only aims to avoid glare and has no included sun protection function can cause serious overheating problems. The addition of an energy optimization can make the installation of a cooling system unnecessary, depending on the climate at the specific site.

The performance of this integral control strategy at the evaluated test scene shows 30 % savings in terms of primary energy demand. Artificial light demand can be kept at its almost optimal level when an optimization of the total primary energy demand is performed. For the vertical luminous exposure of the occupants' faces, some room for improvement remains however still available.

6. Outlook

A scientific definition of the melanopic effect, which is still an object of research, so far is missing. Thereafter, a strategy to find a compromise between the minimal energy demand and the maximal melanopic effect can be investigated.

For future studies, a more realistic scenario could be achieved by a thermal simulation of an entire building including different façade orientations. The investigation of different sites would also be of interest.

The test room chosen for the study at hand does not show any benefits when using daylight redirecting blinds. A deeper office room with workplaces further away from the window should also be investigated to confirm or refute the expected benefit of using daylight redirecting blinds.

An implementation of the introduced energy blind control strategy at a test site and/or in a real building is necessary to investigate its applicability in the real world.

Acknowledgement

The presented work was funded as part of the research project VisErgyControl within the framework of the funding program City of tomorrow of the Austrian Research Agency (FFG) and elaborated

in cooperation with the partners Bartenbach GmbH and HELLA Automation GmbH.

References

- Chan, Y.C., T. Athanasios. 2013. "Efficient Venetian Blind Control Strategies Considering Daylight Utilization and Glare Protection". *Solar Energy* 98: 241–254. doi:10.1016/j.solener.2013.10.005.
- Hattar, S., H.W. Liao, M. Takao, D.M Berson, K.W. Yau. 2002. "Melanopsin-Containing Retinal Ganglion Cells: Architecture, Projections, and Intrinsic Photosensitivity". *Science* 295(5557): 1065–1070. doi:10.1126/science.1069609.
- Hiller, M., P. Schöttl. 2014. "Modellierung komplexer Verglasungssysteme in TRNSYS". In: *Fifth German-Austrian IBPSA Conference*.
- Konstantoglou, M., A. Tsangrassoulis. 2016. "Dynamic Operation of Daylighting and Shading Systems: A Literature Review". *Renewable and Sustainable Energy Reviews* 60: 268–283. doi:10.1016/j.rser.2015.12.246.
- Liu, M., K. Bjarne Wittchen, P. Kvols Heiselberg. 2015. "Control Strategies for Intelligent Glazed Façade and Their Influence on Energy and Comfort Performance of Office Buildings in Denmark". *Applied Energy* 145: 43–51. doi:10.1016/j.apenergy.2015.02.003.
- Provencio, I., D.M. Warthen. 2012. "Melanopsin, the Photopigment of Intrinsically Photosensitive Retinal Ganglion Cells". *Wiley Interdisciplinary Reviews: Membrane Transport and Signaling* 1(2): 228–237. doi:10.1002/wmts.29.
- Ward, G., R. Mistrick, E.S. Lee, A. McNeil, J.C. Jonsson. 2011. "Simulating the Daylight Performance of Complex Fenestration Systems Using Bidirectional Scattering Distribution Functions within Radiance". *Leukos* 7: 241–261. doi:10.1080/15502724.2011.10732150.

Introducing a Hybrid Energy-Use Model at the Urban Scale: The Case Study of Turin (Italy)

Marta Carozza – Politecnico di Torino – marta.carozza10@gmail.com

Guglielmina Mutani – Politecnico di Torino – guglielmina.mutani@polito.it

Silvia Coccolo – École Polytechnique Fédérale de Lausanne – silvia.coccolo@epfl.ch

Jérôme Kaempf – Haute École d'Ingénierie et d'Architecture Fribourg – jerome.kaempf@hefr.ch

Abstract

As in the past, urban morphology plays an important role for the livability of the city and for both outdoor and indoor human comfort. Nowadays, the relationship between the urban form and energy consumption has been estimated by many researchers, showing how the morphological aspects influence the energy consumption of the buildings, the thermal comfort of the urban spaces and the district air quality. Conversely, in recent urban planning processes, these morphological aspects are undervalued or not considered, any more. To reinforce their importance, this paper presents an optimization of a previous statistical model made by the complementary use of bottom-up and top-down models to evaluate the energy-use of residential buildings. The average intensity of energy-use data for residential buildings with a different age, shape, and heated volume has been corrected using the urban energy-modelling tool CitySim Pro. This hybrid approach describes how the urban form, the solar exposure of the buildings, the outdoor spaces and the material characteristics of the urban surfaces impact the energy performance of the buildings. This research analyzed a case study in the city of Turin (Italy) to quantify the space heating energy-use of residential buildings. To estimate the buildings heating energy-use, the urban energy simulation tool CitySim Pro was used, and the building information model of Turin was validated with the real consumptions data based on two years of monitoring data. The results of this research show a direct correlation between the buildings energy-use and the following five urban variables: Building Coverage Ratio, Aspect ratio, Main Orientation of the Streets, Solar factor, and albedo coefficients of outdoor surfaces. The building density and the urban canyon phenomenon play an important role, as they reduce the heating energy-demand in medium density urban contexts. Furthermore, the solar exposure

strongly influences energy demands, especially for high buildings density contexts, as well as the presence of green surfaces. The proposed methodology, based on a multivariate compensative approach, can support urban planning to improve the energy sustainability of the cities.

1. Introduction

According to the European Commission (European Commission, 2016), buildings are responsible for 40 % of energy consumption and 36 % of CO₂ emissions in the EU. Within this frame, the buildings energy efficiency is an increasingly important instance for environmental sustainability. Recent studies demonstrate that the building energy consumption depends not only on the climate, the envelope characteristics, and system efficiencies, but also on the surroundings urban texture (Delmastro, 2015). This means that, in order to decrease the buildings' consumption, the urban context design plays an important role, as well as the design at the building scale. Several studies show the impact of the urban form on buildings' energy consumption. The first studies date back to the '70s, when Martin and March (1972) analyzed the urban form for what concerns soil occupancy. Although this study does not take into account the effects of urban density on energy consumption for the heating or cooling demand of buildings, it laid the foundations for future research. Baker and Steemers' study (1996) focuses on the importance of using tools, in the early stages of architectural design, that can provide the annual primary energy consumption for lighting, cooling, heating, and ventilation as output results. For this purpose, Steemers

developed the LT method (Lighting and Thermal) for non-residential buildings, which takes into account the orientation of the facades and solar gains, by defining passive and not passive zones inside the buildings. Thanks to the development of new software, capable of taking into account the complexity of the urban texture, the impact of the urban form on building energy consumption is becoming an increasingly important research topic. In his study, Kaempf et al. (2010) propose a methodology to minimize the buildings' energy consumption in urban areas by using a new evolutionary algorithm, so called hybrid CMA-ES/HDE. Through this methodology, three urban typologies have been parameterized (terraces flat roofs, terrace courts, and sloped roofs) in order to find an optimal urban form for the exploitation of solar gains. The study by Ratti et al. (2005) analyze the impact of the urban form on building energy consumption, by taking into account some urban parameters such as the Aspect Ratio and the orientation of the facades, and tries to overcome the concept that the Surface to Volume ratio (S/V) is the main influential factor in urban energy consumption. In 2014, Rode et al. (2014) try to determine the theoretical energy efficiency as a function of the city's spatial conformation. For this purpose, the authors take as case studies standard urban areas of 500X500m in the cities of Amsterdam, Berlin, Paris, and Istanbul, and some urban parameters such as Building Density, Building Coverage Ratio, Building Height, and Sky View Factor. As a conclusion, this study shows that the highest and compact buildings have greater energy efficiency than the low and isolated buildings. Moreover, Delmastro's study (Delmastro et al., 2015) takes into account some urban parameters (such as the Building Coverage Ratio, Building Density, Building Height, Aspect Ratio, and Solar Factor) to show how the urban form influences the heating demand of residential buildings in Turin (Italy). The vastness and variety of the studies carried out in the field of energy sustainability at an urban scale show how a good design of the urban texture is crucial for buildings' energy consumption reduction. Conversely, there are still few researches that demonstrate the impact of the urban form on buildings' energy demand in a quantitative manner.

This study aims to propose a methodology to analyse how some urban parameters affect the buildings' heating energy-use.

2. Methodology

This study starts from the energy consumption models for residential buildings at an urban scale, developed from the research project "Cities On Power" (Mutani, 2015; Mutani et al., 2016). With these simplified models, the energy-use for space heating and hot water production was represented for about 50 municipalities of the Metropolitan City of Turin. The energy-use models were based on energy consumptions data at buildings and municipal scales with a statistical approach and applied with a GIS-based tool. The results of this paper will improve the previous models, taking into account the differences in buildings' heating energy needs, due to their surrounding context. The assumption is that the buildings' measured heating consumption is partly influenced by its characteristics and climate but also by the surrounding context and its micro-climate variations:

$$\frac{kWh}{m^2 \cdot year} \Big|_{measured} = \frac{kWh}{m^2 \cdot year} \Big|_{building} \pm \frac{kWh}{m^2 \cdot year} \Big|_{context} \quad (1)$$

For this analysis, a territorial unit called "census parcel", corresponding to a block of buildings, was considered and the buildings' heating demand variations were correlated to the urban form, the solar exposure, and the outdoor materials. In particular, six urban parameters, calculated with ArcGIS 10.1.2 (ESRI), were taken into account:

- the Building Coverage Ratio (m^2/m^2) is the ratio between the built area and the total census parcel area;
- the Aspect Ratio, or H/W ratio, (m/m) is the ratio between the building height (H) and the distance between buildings (W);
- the Main Orientation of the Streets (-) defines the quality of the streets' orientation. A MOS=1.3 defines the best orientation (East-West), while a MOS=0.8 corresponds to the worst one (North-South) (Delmastro, 2015).
- the Albedo of external surfaces (-) indicates the reflecting power of a surface;

- the Solar Exposure, or H/H_{av} , (m/m) is the ratio between the building height (H) and the surrounding buildings average height (H_{av});
- the Solar Factor, a statistical parameter equal to $MOS \cdot H/H_{av}$ (Delmastro, 2015).

In order to analyse different urban layouts, the software CitySim Pro was used, proposing consistent variations on the urban form and outdoor materials, compared to the real case study. CitySim is an urban energy modelling tool (Robinson et al., 2009), able to quantify the energy demand from the building to the urban scale. The thermal model of buildings is based on an analogy with the electrical circuit, more precisely on a resistor-capacitor network (Robinson et al., 2009; Kämpf and Robinson, 2007). The radiation model is based on the Simplified Radiosity Algorithm (SRA), where the radiant external environment is represented by two hemispheres, discretized into several solid angles (Robinson and Stone, 2005). CitySim was also certified by the IEA BESTEST (Walter and Kämpf, 2015). In order to understand the impact of greening the outdoor environment, further models are under development, able to quantify the evapotranspiration as well as the impact of trees on the urban microclimate (Upadhyay et al., 2015; Coccolo et al., 2015). CitySim provides the energy needs of buildings on hourly values, by including the interactions within the built environment. As an example, the interrelations between buildings, as well as the mutual shading, are calculated. In order to perform the calculations, hourly weather data are required, as the one created by the software Meteonorm (Remund et al., 2015), or by on-site monitoring. The geometry of urban layouts is created by CAD modelling tools, and it is directly imported in the software. The physical properties of buildings (i.e. envelope, glazing ratio, occupancy profile, and energy systems) as well as the ground covering are defined within CitySim Pro. The proposed case study is a traditional settlement in the central district of the city of Turin (IT) called "Crocetta" characterized by old and high-rated row buildings.

3. Results

Turin is an important city in the northwestern part of Italy with about 900,000 inhabitants, 10 Districts, 3,839 census parcels, and about 40,000 residential buildings. 86 % of residential buildings in Turin were built before the '70s, and 43 % are characterized by a Surface to Volume ratio $S/V < 0.4$ and a compact form. The Crocetta district (Fig. 1) is a portion of District 1, in the historic centre of Turin, with 16 census parcels and a total area of about 160 km². The data on the buildings' period of construction were obtained thanks to a Geographical Information System model. This information allowed us to assign to each building its construction system, in terms of materials, type of envelope and level of thermal insulation (Table 1).

Table 1 – Physical characteristics of Crocetta buildings (in brackets the number of buildings used for the energy-use models validation)

Construction period	U_{wall} W/m ² /K	U_{window} W/m ² /K	g_{value} (-)	Glazing ratio(%)	N° of Buildings
Before 1945	1.5	4.7	0.85	18	150 (24)
1946-1970	1.15	4.2	0.75	19	69 (16)
1971-1980	0.81	4.9	0.75	34	18 (2)

The roads and the courtyards in the Crocetta district are made of asphalt with an average albedo coefficient of 0.17. The average building height is about 20 meters and the urban form can be considered homogenous, as the urban parameters of the census parcels are similar (Table 2).

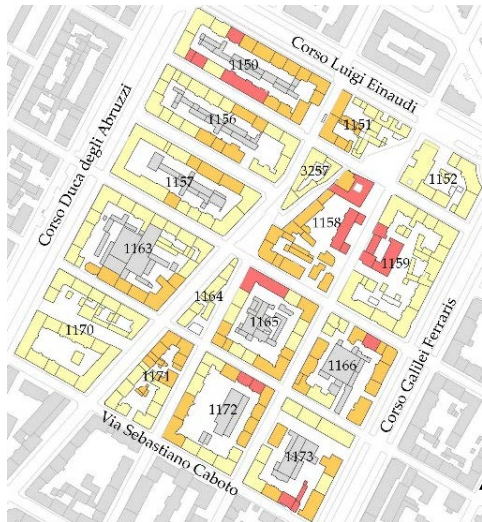


Fig. 1 – The Crocetta district with census parcel numbers and the buildings' period of construction: before 1945 (yellow), from 1946 to 1970 (orange), and from 1971 to 1980 (red)

Table 2 – Crocetta urban parameters: Building Coverage Ratio (BCR), Aspect Ratio (H/W), Main Orientation of the Streets (MOS), and Albedo (A)

Crocetta	BCR m ² /m ²	H/W m/m	MOS (-)	A (-)	H/H _{av} (m/m)
Average	0.41	0.89	1.3	0.17	1.02
Dev.st	0.07	0.17	0.25	0.01	0.34

The building heating energy-use was calculated with CitySim Pro by considering the following input data: an internal temperature of 20 °C, a number of air changes per hour of 0.5 as infiltration rate, an occupancy profile based on ASHRAE Standard for residential buildings (ANSI/ASHRAE/IESNA Standard 90.1-2007 - Energy Standard for Buildings Except Low-Rise Residential Buildings), and a traditional heating system connected with the district heating network. As regards the outside temperature, two hourly climate files were generated by Meteonorm, and further calibration of the air temperatures according to the data measured by the weather station “Via della Consolata” in Turin. Meteonorm is a worldwide well-known meteorological database; the hourly data provided by the software are based on the average irradiance data for the period 1991-2010 and the average temperature data for the period 2000-2009. For the dynamic simulations two heating seasons were considered (in Table 3 the average monthly air temperatures): the season from October 15, 2013 to April 15, 2014

and the season from October 15, 2014 to April 15, 2015.

Table 3 – Average monthly air temperatures in Turin for the heating seasons 2013-14 and 2014-15

Air temp. [°C]	Oct	Nov	Dec	Jan	Feb	Mar	Apr
2013-14	14.6	9.2	5.5	5.7	7.1	12.0	15.6
2014-15	16.2	10.6	6.6	5.6	5.4	10.8	15.1

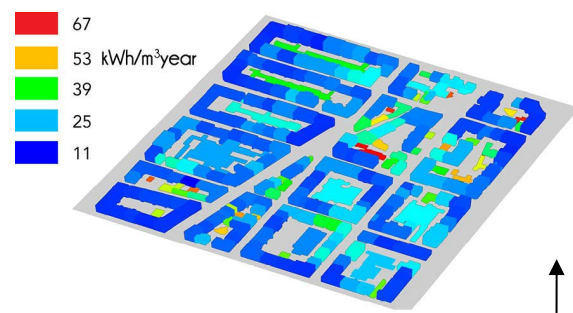


Fig. 2 – Yearly heating demand of Crocetta District calculated by CitySim Pro

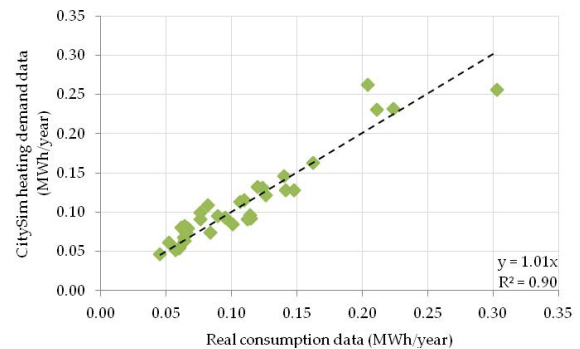


Fig. 3 - Linear relationship between the buildings heating demand calculated by CitySim Pro and the real consumption data

The building space heating consumption data calculated by the software (Fig. 2), were compared to the real building consumption data, provided by the district heating company “IREN”. The validation of the model took into account 42 buildings, with different periods of construction. As shown in Fig. 3, there is a strong correlation between the calculated data and the real data (R²=0.9). As mentioned before, the aim of this research was to define how urban variables can influence space heating consumptions. Since the urban texture in the Crocetta district

is very homogeneous, new urban layouts were created in order to achieve greater changes in the urban form, useful for determining major differences in buildings' heating energy-use. For this purpose, the census parcel numbers 1,154 and 1,163 (Fig. 4), that have the highest number of validated buildings belonging to the same construction period (before 1945), were taken into account.

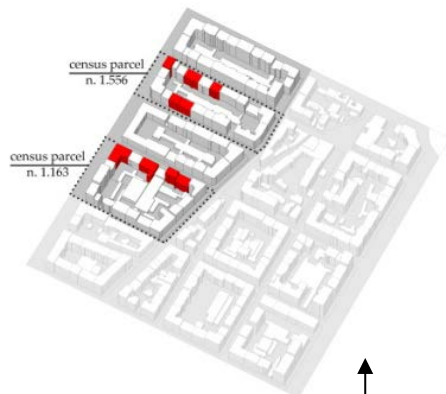


Fig. 4 – Census parcel n. 1,156 (top) and 1,163 (bottom) taken into account in order to analyse the influence of urban form on buildings' heating demand

In this research, every single urban variable was changed one at the time to evaluate their influence on energy consumptions, while the buildings' characteristics, such as the surface to volume ratio, the physical characteristics of the envelope, and system performances, remain unchanged. First of all, new urban layouts were created by varying BCR from 0.25 to 0.55 (Fig. 5). Next, the width of the roads was changed to evaluate the H/W parameter effect. In this case new models were created with values of aspect ratio H/W from 0.4 to 1.9. New layouts were also created by rotating the blocks of 30°, 60° and 90° in order to have configurations with MOS of 0.9, 1 and 1.1 (Fig. 6). Finally, new configurations were created with different values of Albedo coefficient: 0.07 (new dark asphalt), 0.5 (light asphalt), 0.25 (dark green), and 0.35 (light green).

After creating the new configurations, the dynamic simulations were performed with CitySim Pro, in order to obtain the new buildings heating consumption data.

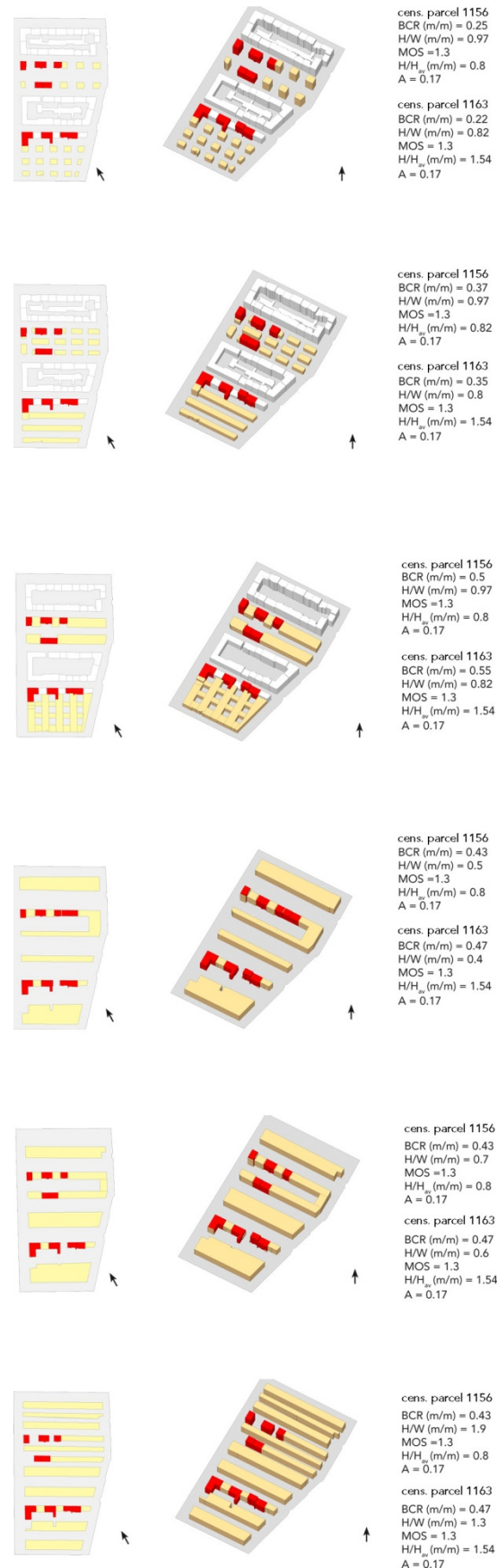


Fig. 5 – New layouts of BCR and H/W

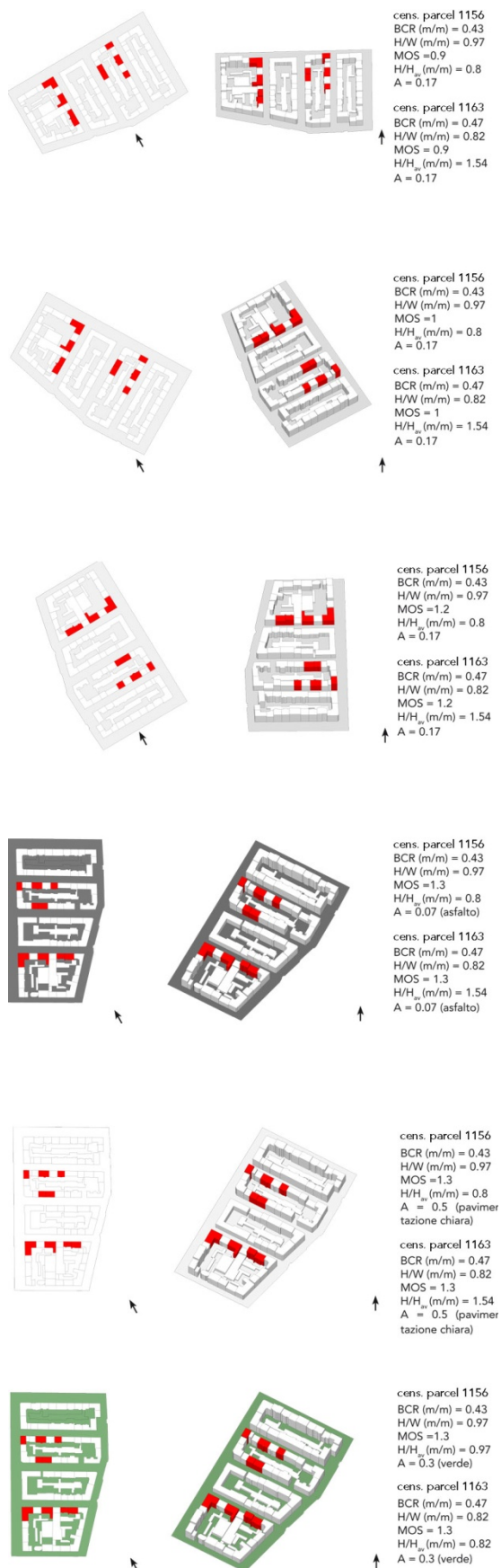


Fig. 6 – New layouts of Albedo and MOS

The results show how energy consumption varies in the different urban layout as a function of the urban variables. The trend of the heating energy-use as a function of the BCR and H/W parameters is parabolic as shown in Fig. 7. In particular, for high and very low values of BCR and H/W the heating demand is higher, while for medium values of the parameters, energy consumptions are lower.

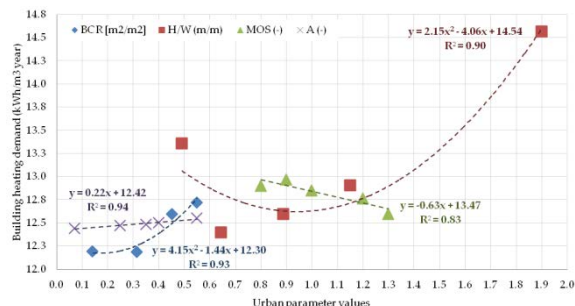


Fig. 7 – Buildings heating demand trend as a function of urban parameters: BCR (rhombus), H/W (squares), MOS (triangles) and Albedo (crosses)

The results show an inversely proportional correspondence between the buildings’ heating energy-use and MOS: the best orientation, in order to reach reductions in heating consumption, is West-East (MOS=1.3). Heating consumptions increase linearly by varying the albedo coefficient A: the buildings’ heating energy-uses are lower with darker surfaces in the surrounding outdoor spaces (i.e. with new asphalt: A=0.07). Finally, knowing how the buildings’ heating energy-use varies with the different urban variables BCR, H/W, MOS, H/Hav and A, a further analysis was performed considering all the buildings’ heating consumption results. Starting from Equation 1, the aim of this analysis was to define a correlation that allows calculating the buildings heating energy-use as a function of the urban parameters, specifically for the Turin case study. For this purpose, a multiple regression analysis was performed, considering the urban variables mentioned in paragraph 2, minimizing the differences between measured and calculated energy consumption data:

$$\begin{aligned}
 \text{heating energy-use intensity [kWh/m}^3\text{/year]} = & -0.40*(BCR)^2 + 1.23*BCR - 0.05*(H/W)^2 \\
 & + 1.95*H/W - 1.96*H/H_{av} - 3.52*MOS \\
 & + 0.63*A + 0.12*G + 17.78.
 \end{aligned}
 \tag{2}$$

In Equation (2), the G value is a discrete variable that indicates the presence of greenery: equal to 1 when the surrounding ground surface is green or equal to 0 if there are no green outdoor surfaces. In Fig. 8 the influence of the different urban variables of Equation 2 is represented for the analysed urban layouts. The aspect ratio H/W , the solar exposure H/H_{av} , and the main orientation of the streets MOS are the most energy-consumption related variables. This demonstrates the high influence of the urban canyon phenomenon and the solar exposure in space heating energy consumptions.

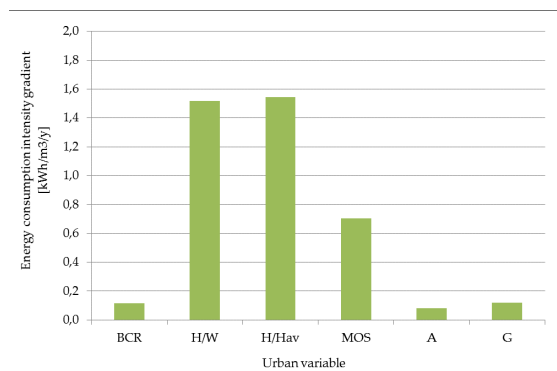


Fig. 8 – Heating intensity gradients related to variations in the urban variables (on 199 buildings' simulations)

Figs 7 and 8 reveal also how the surrounding environment can play an important role in energy sustainability. It is possible to guide the urban design with compensatory measures, to reduce energy consumptions; for example, the high buildings density requires high values of H/W and then high heating consumptions, but with a good solar exposure (high MOS and H/H_{av}) the energy-use decreases. Also the selection of materials for outdoor spaces (i.e. A and G) can help in increasing the energy sustainability of a district.

4. Discussion and Conclusions

Reducing buildings' energy consumption is one of the crucial problems that architects and urban planners are called to solve every time they face the design of new buildings or the renovation of existing parts of the city. The initial goal was to demonstrate the incidence of the urban form on buildings' space heating demands. The results show that the heating energy-use trend, as a function of BCR and

H/W parameters, is parabolic. In a very dense urban context, in fact, solar gains are lower and the shadows, generated by the buildings, cause a lowering of the outdoor air temperature, and so, an increase of the buildings' heating demand. In less dense urban contexts, instead, the buildings are more exposed to solar radiation but there is no urban canyon effect, i.e. the incident solar radiation is not trapped in the urban texture and the outside air temperature is not increased. For this case study, the optimum values of BCR , in order to reach a reduction in heating demand, is 0.3, which means an urban context in which the built area is the 30 % of the total site area. Moreover, very high values of the H/W parameter (considering the buildings' height constant) indicate the presence of very narrow streets. In these conditions too, there is not the urban canyon effect and the solar radiation cannot penetrate. For very low Aspect Ratio values, however, the roads are very wide and, even in this case, the effect of the urban canyon does not occur, since the solar radiation is not trapped within the external walls of the buildings. The optimal situation is when H/W values are equal to 0.9, a situation in which the street width is approximately equal to the building height. Additionally, the results show that the best orientation of the streets is West-East, which means that if a census parcel (or a building block, or a district) has that main orientation, the building energy efficiency is optimal. The trend of energy consumption as a function of Albedo is increasing linear, which means that very dark surfaces (characterized by low values of Albedo) absorb more solar radiation and cause a rise in the outside air temperature. This corresponds to a decrease of the thermal gradient between the buildings' internal air temperature and the outside air, and a reduction of heat losses. This study doesn't want to be the arrival point in the definition of new urban strategies to reduce the buildings' energy consumptions, in fact it tries to define a common methodology. The future developments of this research may provide for the application of the illustrated methodology in situations of hot or arid climates. In South America or Saudi Arabian cities, in fact, the control of the incident solar radiation plays an important role in the reduction of buildings' cooling energy demands. By analyzing how the urban parameters influence the buildings'

cooling demand, a complete picture of the problem could be delineated, because the rules found for a temperate climate (such as the case of Turin) may not be valid for an arid context.

This research tries to define a method for the determination of the urban form influence on the buildings' heating demands. In this sense, the illustrated methodology could be useful for the design of the new Zero Energy Building districts as it could provide a valuable tool to increase the buildings' energy efficiency, since it would not only optimize the envelope or system performances, but also the form of the urban context in which the building is located.

References

- ASHRAE. 2007. *ANSI/ASHRAE/IESNA Standard 90.1-2007 - Energy Standard for Buildings Except Low-Rise Residential Buildings*. Atlanta, U.S.A.: ASHRAE.
- Baker, N., K. Steemers. 1996. "LT Method 3.0: A strategic energy-design tool for Southern Europe". *Energy and Buildings* 23: 251–256. doi: 10.1016/0378-7788(95)00950-7.
- Coccolo, S., J. Kämpf, J.L. Scartezzini. 2015. "Outdoor Human Comfort and Climate Change. A Case Study in the EPFL Campus in Lausanne". In: *ICUC9 - 9th International Conference on Urban Climate jointly with 12th Symposium on the Urban Environment*.
- Delmastro, C., G. Mutani, G. Vicentini, M. Pastorelli. 2015. "Energy consumption and urban morphology". In: *Proceedings of ICRERA: 4th International Conference on Renewable Energy Research and Applications*.
- European commission. "Energy Performance of Buildings." Accessed on November 2016. <https://ec.europa.eu/energy/en/topics/energy-efficiency/buildings>.
- Kämpf, J.H., M. Montavon, J. Bunyesc, R. Bolliger, D. Robinson. 2010. "Optimization of buildings' solar irradiation availability". *Solar Energy* 84: 596–603. doi: 10.1016/j.solener.2009.07.013.
- Kämpf, J.H., D. Robinson. 2007. "A Simplified Thermal Model to Support Analysis of Urban Resource Flows". *Energy and Buildings* 39(4):445–53. doi: 10.1016/j.enbuild.2006.09.002.
- Martin, L., L. March. 1972. *Urban space and structure*. Cambridge, UK: Cambridge University Press.
- Mutani, G. 2015. "Buildings' energy efficiency and RES potential in urban contexts". In: *Spatial Data for Modelling Building Stock Energy Needs, JRC Conference and Workshop Report*.
- Mutani, G., A. Gamba, S. Maio. 2016. "Space heating energy consumption and urban form. The case study of residential buildings in Turin (Italy)". In: *11th Conference on Sustainable of Energy, Water and Environmental Systems*.
- Ratti, C., N. Backer, K. Steemers. 2005. "Energy consumption and urban texture". *Energy and Buildings* 37: 762–776. doi: 10.1016/j.enbuild.2004.10.010.
- Remund, J., S. Müller, S. Kunz. 2015. *Meteonorm. Global Meteorological Database. Version 7*.
- Robinson, D., F. Haldi, J. Kämpf, P. Leroux, D. Perez, A. Rasheed, U. Wilke. 2009. "Citysim: comprehensive micro-simulation of resource flows for sustainable urban planning". In: *Proceedings of the 11th International IBPSA Conference*. Glasgow, UK: IBPSA.
- Robinson, D., A. Stone. 2005. "A Simplified Radiosity Algorithm for General Urban Radiation Exchange". *Building Services Engineering Research Technology* 26(4): 271–84. doi: 10.1191/0143624405bt1330a
- Rode, P., C. Keim, G. Robazza, P. Viejo, J. Schofield. 2014. "Cities and energy: urban morphology and residential heat-energy demand". *Environment and Planning B: Planning and Design* 41: 138–162. doi: 10.1068/b39065.
- Upadhyay, G., D. Mauree, J. Kampf, J.L. Scartezzini. 2015. "Evapotranspiration Model to Evaluate the Cooling Potential in Urban Areas - a Case Study in Switzerland". In: *Proceedings of Building Simulation 2015 - 14th International IBPSA Conference*. Hyderabad, India: IBPSA.
- Walter, E., J. Kämpf. 2015. "A verification of CitySim results using the BESTEST and monitored consumption values". In: *Proceedings of the 2nd Building Simulation Applications BSA 2015*. Bolzano, Italy: BUPRESS.

OpenBPS: A New Building Performance Simulation Tool

Livio Mazzarella – Politecnico di Milano – livio.mazzarella@polimi.it

Martina Pasini – Politecnico di Milano – martina.pasini@polimi.it

Abstract

A new generation building energy performance simulation program, OpenBPS™, is currently under development. It overcomes some of the drawbacks typical of many of the popular building energy simulation programs around the world. This Building Performance Simulation Tool is primarily a set of libraries dedicated to building energy analysis and performance simulation, which can be included in any user-oriented interface or commercial software that aims to perform such analysis. The basic goal of the project is to provide a robust, validated, and high-performing calculation engine that can be shared, and grow with the contribution of a community of developers and users. To maximize its possible deployment and to facilitate its development and extension by a growing community, it has been built as an open source cross-platform (Windows, Mac, and Linux) software library. For this reason, OpenBPS™ will be distributed under a Copyleft Software License (EURL) and is coded with a cross-platform object oriented programming language, C#, which is an open source language for .NET Framework based on ECMA standards. The main features of this tool are the object-oriented modelling of physical phenomena and building and HVAC system components, the native code parallelization to take advantage of multi-thread/multi-core processors today available, the multi-scale calculation time step (each object can work using its own time step, scaling down or up with respect to the chosen simulation time step), etc. Not only the technical systems are described and simulated modularly, being their components objects, but also the building fabric is natively modular. Any building envelope component is an object that interacts with other objects, which represent the world around it (air node included). This allows the use of different modelling approaches for different wall components during the same simulation (linear, non-linear, with phase-change, ventilated, etc.). The input and output data structures are tailored to facilitate third party integration with high efficiency, using today's technologies. Other

planned capabilities include multi-zone airflow simulation and dynamic models for HVAC system components.

1. Introduction

Over the last years at the Technical University of Milan (Politecnico di Milano), a research group has been working on developing a “next generation” building energy performance simulation tool. In 2009 a preliminary research project, carried out through a Ph.D. work (Pasini, 2009), traced the route to the re-conceptualisation and development of an object-oriented model for the simulation of the building system (Mazzarella and Pasini, 2009). The main idea was to combine the power of the object-oriented programming languages today available with the object-oriented nature of a building. In developing the tool, great care has been taken in its design to ensure modularity and maintainability through an open source (OS) development approach. The development methodology was itself part of the development work, aimed at creating a common framework for a community of developers able to manage the complete software development lifecycle (Mazzarella and Pasini, 2015a). Code validation was then a second key point along the development of the tool: both analytical and comparative tests have been employed to assess the quality of the implemented algorithms. The first results of a comparative validation done on such tool, following the BESTEST standard, have been presented at the 2013 IBPSA International Conference (Mazzarella and Pasini, 2013). Some other comparative tests between different numerical solutions of the heat conduction differential equation have been presented at the 6th International Building Physics Conference, IBPC 2015 (Mazzarella and Pasini, 2015b). Most of the

work has since been documented in technical reports, which will be made available with the tool in the future. Since part of the developing work was financed by Regione Lombardia, the final decision, about how to deploy and support it, is still pending. The name of the tool has already been chosen and is OpenBPS (Open Building Performance Simulator). This paper describes the structure, features, and capabilities of OpenBPS.

2. What is OpenBPS

OpenBPS is a new building performance simulation program primarily designed as an open source cross-platform (Windows, Mac, and Linux) software library. It is a simulation engine and there is no formal user interface. For developing and testing purposes, a simple GUI is provided, which is able to import building geometry provided by the OpenStudio plug-in for SketchUp or to directly import projects defined through EnergyPlus input files (.idf), although not yet fully implemented. It is coded from scratch with a cross-platform object oriented programming language, C#, which is an open source language for .NET Framework based on the ECMA standards. This language has easily allowed native code parallelization to take advantage of multi-thread/multi-core processors today available.

2.1 Object Oriented Code

One of the main goals for OpenBPS is to create an enhanced modular structure that facilitates adding new features and allows the library to be used by any hosting program. An object-oriented programming language, as C#, was selected to achieve this goal because it:

- is a rich implementation of the object-oriented paradigm, which includes encapsulation, inheritance, polymorphism, and method overriding;
- is an easy and efficient object oriented language: developers can translate their ideas/algorithms to solve complex problems more easily than with C++;
- is one of the leading languages which works on cross-platform using .NET framework: it is

available in Windows, Linux and MacOS operating systems;

- is more type safe than C++; the only implicit conversions by default are those that are considered safe, such as widening of integers; the managed memory cannot be explicitly freed; it is instead automatically garbage collected;
- may produce applications that run as fast as C++ applications, using the Just In Time (JIT) compiler, which can finely tune code optimization on the running machine hardware;
- is today a standard and open-source programming language (ECMA-334 and ISO/IEC 23270:2006).

An object-oriented structure is natively modular and simplifies the reuse of pieces of code through the concept of class inheritance. Different kinds of objects often have a certain amount of “attributes” and “behaviours” in common with each other. Phase-change walls, breathing walls and ventilated walls, for example, all share the characteristics of walls (geometry, layers composition, orientation, etc.). Yet each also defines additional features that make them different: phase-change walls have phase-change material properties to account for together with nonlinear performance; breathing walls have additional properties like porosity and their solver has to account for advection through the wall porous material; ventilated walls have additional channel properties which account for inner wall mass forced/natural ventilation. Object-oriented programming allows classes to inherit commonly used states and behaviours from other classes. In this example, *Wall* is the *superclass* of the classes “phase-change walls”, “breathing walls”, and “ventilated walls”.

Objects are class instances. For instance, the class “Building” describes the concept of what a building is. When the class “Building” is specified, by loading specific data, the object, “Building-XYZ” is built, representing a particular instance of the class Building.

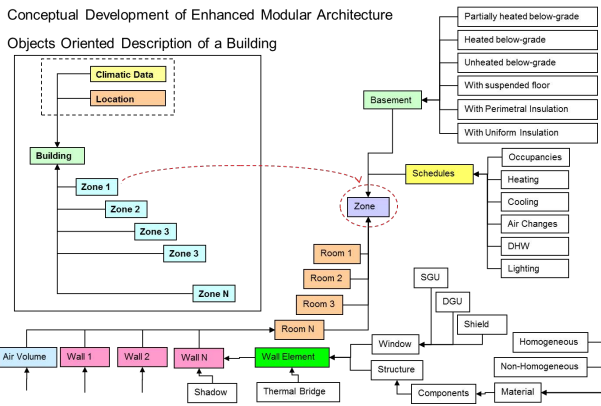


Fig. 1 – Enhanced modular structure of OpenBPS based on the building’s object-oriented descriptions

The object-oriented structure helps parallel calculations at the object’s management level. Since each wall in a building is a separate object, at each time step its performance can be calculated in parallel to other walls (how many depends on how many CPUs are available) (Mazzarella et al., 2014). Also, the object-oriented approach naturally allows the use of different integration time steps inside each object and lets them optimize their performances regardless of the global simulation time step imposed by the user.

2.2 OpenBPS Structure

The enhanced modular structure of OpenBPS, shown in Fig. 1, follows a hierarchical organization, with the “Building” class at the top, hierarchically encapsulating all the instances of the other classes that contribute to its definition. To implement such structure in a manageable code, OpenBPS has been developed inside MS Visual Studio development framework, and is organized in a “Solution” that contains all the necessary elements to build its exe code, debug, and test, or continue its development. This Solution comprises several “projects” that have been created to manage different aspects of software development, according to the modular nature of the whole project. As shown in Fig. 2, there are seven projects in the solution, each of them with a specific functionality:

- *GUI*, the executable project containing a simple user interface provided for developing and testing purposes only;

- *ExtendedMath*, a dll (dynamic link library) project containing the math algorithms used for simulation;
- *SimulationManager*, a dll project containing the simulation manager implementation;
- *SimulationComponents*, a dll project containing the description of the building system components;
- *InputOutputUtilities*, a dll project containing the tools for the management of inputs and outputs;
- *ModelingProject1*, an executable project that supports the development stage by checking for interdependence among code components, and assessing if they comply or not with predefined dependency rules;
- *TestProject1*, an executable project that implements a set of automatized tests with known solutions to verify code integrity after code modifications.

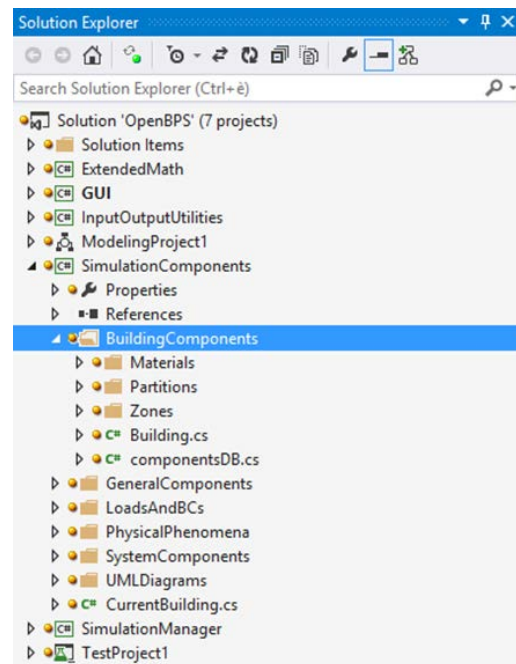


Fig. 2 – OpenBPS Solution modular structure

2.3 Simulation Management

Among the four main libraries, which constitute the simulation engine of OpenBPS, the *SimulationManager* dll project, contains the Simulator code. This is the top-level object that manages the simulation, controlling the interactions among all the objects constituting the building. Due

to the object-oriented nature of the whole code, the components management is handled via iterations until convergence is reached inside each global simulation time step. This approach allows separating the global simulation time step (the time step the Simulator uses to update its information) from each local time step any single object may use. In this way, it is also possible to implement in each object strategies to prevent the user to force such component to work with an inconsistent time step (in respect to the characteristic time of that component). Basically, the Simulator organizes and synchronises the work of all objects, instructing them to take actions such as initialize, simulate, export results, etc. It can manage from sub-hourly up to several-hour time steps over a simulation period ranging from a day to several years.

The simulation manager that concentrates in one object all management rules, allows:

- to better define the priorities in objects execution;
- to allocate the parallelization to a specific group of objects, which can benefit more than others of such technique;
- to consistently control the work flow;
- to easily add new classes and objects.

In Fig. 3 a simplified scheme shows how the parallel calculations are applied to the building: a first parallelization is applied among zones, given the priority of some calculations at their level, and a second parallelization is applied among all the other simulation components involved in the calculation.

2.4 Energy and Mass Balance

The underlying building thermal zone calculation method in OpenBPS is an integral enthalpy balance model in which room air is modelled under the fully mixed assumption, i.e. with the assumption of uniform temperature throughout the room space (Mazzarella, 2013). The object-oriented structure of OpenBPS of course allows more detailed room air convection calculations, such as CFD or zonal methods, which can be added in a future development. The “sensible” part of the enthalpy balance constitutes the so-called “air node” ordinary differential equation, here simply referred to as the Air-Node object.

The Air-Node object deals with various advective mass flows such as ventilation air, exhaust air, and infiltration, other than the convective heat transfer with the room surfaces (walls, windows, ceilings, and floors), assumed with uniform surface temperature. It accounts for the thermal capacity of room air and evaluates direct convective heat gains from people and equipment.

The heat transfer through each building fabric component, here simply called Partition, determines the room surface temperatures used in the Air-Node object to calculate the convective heat transfer. The Partition class allows different solvers to integrate the second-order differential equation that describes the diffusive heat conduction: finite difference method, conduction transfer functions and harmonic quadrupole (for comparison tests purposes). Any Partition object can use a different solver when a simulation is run, according to its needs (i.e. one wall can be modelled using finite difference explicit scheme, another full implicit, and another one conduction transfer function).

The long wave internal radiative heat transfer among room surfaces is modelled using the Grey Body Model based on mutual radiation factors, which can be calculated at the initialization stage from the view factor (geometrically defined) and surface emissivities. The mutual radiative heat transfer among all internal surfaces is accounted for when the boundary conditions (BCs) of each object (component) are updated. When the BCs are updated, also short wave irradiation is determined for both external and internal Partition surfaces through the solar radiation processor and the Short-Wave Radiation module (SWRadModule).

This module has the responsibility of:

- setting shaded perimeters in external surfaces by considering external obstructions, such as other buildings, self-shadings, overhangs and fins, (without, however, considering them also as possible direct and diffuse reflectors)
- setting the solar radiation transmitted through the transparent envelope component and non-uniformly distributed among the room surfaces.

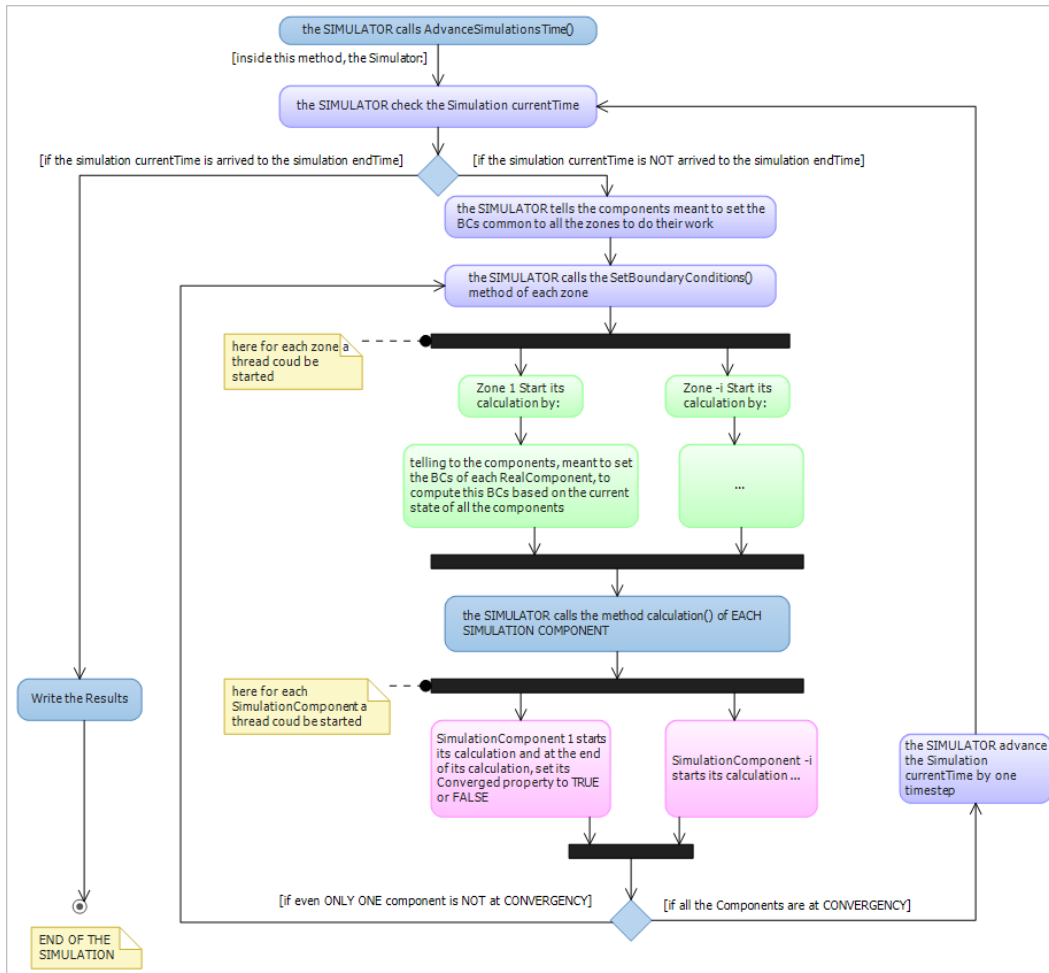


Fig. 3 – OpenBPS: Parallelism handling at different levels, simplified scheme

When dealing with transparent Partitions (windows, etc.), OpenBPS performs an accurate calculation using angular dependence of transmission and absorption for both solar and visible radiation, and temperature dependent U-value calculated at run-time entering a layer-by-layer window description, or simplified calculation entering the windows description taken from third party projects, such as the Berkeley Lab WINDOW 7.4.

Solar control has not yet been introduced, but new models for shadings and shadings control could be introduced easily thanks to the object-oriented structure of the project. A finite number of view factors might be pre-calculated for different positions of the shading and a “transparent layer like” description could be used for handling the SW radiation part, while air convection should be considered with simplified or detailed calculations.

An improved calculation for diffuse solar radiation on tilted surfaces has been implemented as described by (Perez et al, 1990). This non-isotropic model accounts for circumsolar, horizon brightening, and isotropic diffuse radiation through empirically derived "brightening coefficients". These coefficients, function of sun position and cloud cover, have been implemented following the last curve fit performed by Perez in 1999, as reported in both the technical documentation of TRNSYS 17 and EnergyPlus 8.6.0.

2.5 Building Systems Simulation

The Simulator prioritizes the building fabric components before starting to manage the building system simulation. The objects that represent the components of HVAC and electrical systems, energy conversion equipment, and any other needed building technical systems component, are then

asked to expose their outputs at the actual time stamp in organized sequences. The natural modularity of the adopted object oriented scheme supports the realization a fully integrated simulation of loads, systems, and plant, but at the same time it can raise stability issues. To avoid or limit, as much as possible such instabilities, the objects belonging to a specific technical system are organized in “queues” as in the real word, i.e. solved in sequence according to their energy transfer direction. With “queue” we mean a sequence of objects that are solved sequentially one after the other as they interact mainly sequentially, like, for instance, an emitter, the distribution pipes, the boiler, and their thermostatic controls. Of course, networks of pipes and ducts represent close-loop “queues”. Thus, each global time step, the Simulator has to iterate among all components, managing to solve at first the unknowns for the building fabric components (mainly in parallel) and then for the building technical systems (mainly serially). This integrated simulation allows capacity limits and control strategies to be modelled more realistically and provides a tighter coupling between the building fabric components and the technical system components, allowing a specific object requirement to override this general management structure, as in active double-skin façades where a HVAC system closely interacts with an envelope component.

The building system part is currently under development because, instead of using performance maps and/or steady state models for the HVAC and plant components, true dynamic models have been targeted, though simplified. This to overcome one of the most significant drawbacks that characterize many of the popular building energy simulation programs: the use of steady state modelled equipment with few-minute simulation time steps. The introduction of a component characteristic time can avoid this misleading use that can lead to unreliable results.

2.6 Input, Output and Weather Data

As mentioned several times, OpenBPS is a set of dynamic link libraries that are mainly designed to be used by third party software. Thus, the user front

end is not in the project goal, even though a simple GUI has been developed for developing and testing purposes. This interface allows to import EnergyPlus input files, with some limitations, or files created with the TRNSYS17 or OpenStudio plug-in in SketchUp, always with some limitations. Drag-and-drop features are also implemented to manage tests on components, and assign to them, for instance, different solvers, and so on. For the same reason an output manager allows to print out almost all the necessary variables to analyse the building performance.

The real input to the code is anyhow the Building Object itself: the GUI is just filling up all the required properties of all included objects, simulation requirements included, and then passes it to the *SimulationManager* dll library for simulation execution. During the simulation, the Output Object is filled with the required output variables, warnings and any other information. At the end of the simulation, the Output Object is exposed to the caller program that takes over the task of producing graphs, synopses, and any other specifically formatted output.

The other major data input is weather, provided through weather data files directly read by the simulation engine. The code can directly read standard weather data formats, like TMY and EPW, or custom-made data format. In any case, the weather processor is able to produce the required quantities regardless of the matching between provided data frequency and required data frequency. After a time alignment, the weather processor produces via interpolation the required data if required by an object, with a frequency higher than the recording frequency. If, instead, this frequency is lower than the recording frequency, we have two possibilities. We can communicate to all the simulation components all the climatic data and let them decide if they want to perform multiple calculations without iteration, or if they prefer to store and manipulate the data in accordance with their numerical scheme, and perform their calculation only once. Or we can manipulate the climatic data before exposing them to the components, in which case two different cases arise: the frequency is a multiple of the recording frequency or is not. In the first case, non-integral

data are directly provided to the object, while integral data are cumulated before exposing them to the object. In the second case an additional interpolation is performed to provide the required information.

2.7 Contributing to New Developments

One of the main goals for OpenBPS is to encourage continuous development and enrichment with new features. To achieve this goal, it was decided to adopt an open source approach and to build around it a community of developers who can take care of that. This idea and the tools provided to realize it were already described in a previous paper (Mazzarella and Pasini, 2015a). Nevertheless, the contributing procedure can be summarised as follows: Anyone can download the source code and can do, according to the open source license agreement, what he likes. In order to be a recognized contributor (i.e. to be able to upload to the developing repository his own code that will become part of the version following the official version), a developer has to join the community and follow its rules. The production of new classes of building components is highly encouraged, and it is in principle quite easy. Due to the object-oriented structure and the developing environment (MS Visual Studio under Windows, MonoDevelop under Linux, and MacOS), the process is relatively simple. First, a developer defines a new component by writing down its mathematical and numerical model and identifies the model parameters and needed equations, the specialized coefficients and any other needed data. Next the developer writes the code (using the OpenBPS programming standard) and identifies the “parent” class from which to inherit common properties and methods. If a detailed class is not available, this father class must be the “SimulationComponent” class. In fact, the Simulator at the beginning of the simulation scans all the components to find the one that inherits from that class, thanks to polymorphism. The simulation component class exposes methods that are always called by the Simulator, such as the initialization method, the calculation method, the methods needed to manage convergence and the method for output writing. All new components,

while implementing their specific properties and methods, have to inherit from their particular “father” class or override the available implementation of those particular methods defined for the “SimulationComponent” class, to be correctly called by the simulator to get input from other objects and to deliver their output.

3. Validation

OpenBPS is continuously under validation, since it is still in its developing phase. Some references to earlier validations can be found in Mazzarella and Pasini (2013, 2015b). Fig. 4 shows several ASHRAE 140 Standard (ASHRAE, 2014) cases: case 600FF, free floating internal temperature (FF) and light walls; case 650FF, i.e. 600FF with night ventilation; case 900FF and case 950FF, respectively free floating with heavy wall without and with night ventilation. These BESTEST validations have been carried out with the actual version of OpenBPS and show quite a good agreement with the provided information.

4. Conclusion and Perspectives

The OpenBPS object oriented building performance simulation tool is not yet ready to be deployed within the energy simulation community because it lacks the building system component models. This part is currently under development by trying to model the system components as dynamic components, even if simplified. On the other side, a decision has to be made on how to initiate the developers’ community, to create a true open source project. The main idea that can support and increase its development and diffusion, is to launch it as a “standard de facto” replacing the whole EPBD standard set that will be in force at the end of 2017. This new EPBD set of standards implies that each technical software house that sells programs to assess building energy performance, has to rewrite its calculation engine according to the new standards. Thereafter, they have to require a legal validation before putting it on the market. A joint venture between OpenBPS and the technical software houses may solve the problem of both: a unique full validated calculation engine that can be

used inside any software on any platform, completely documented and expandable time by time.

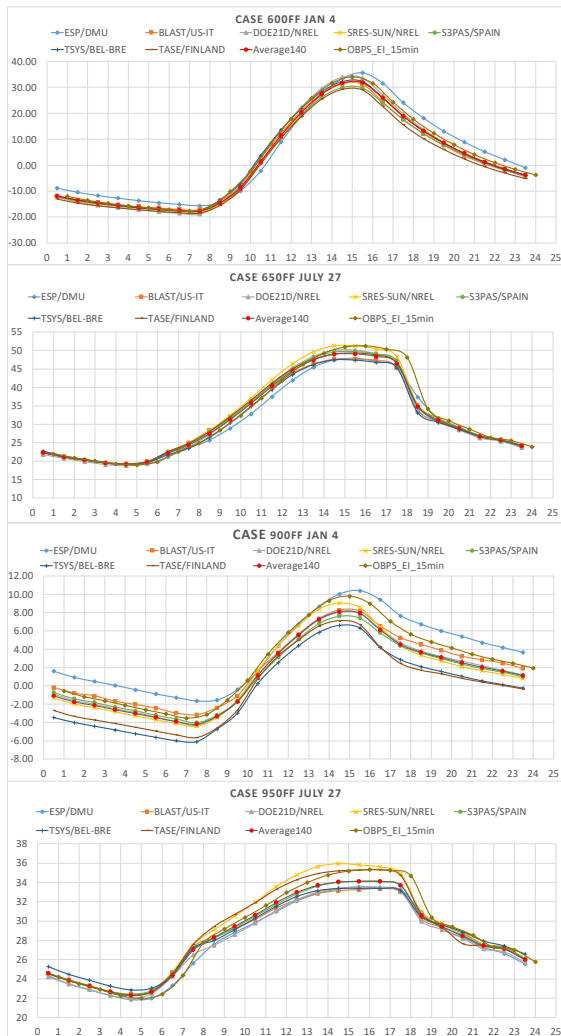


Fig. 5 – ASHRAE 140 Standard OpenBPS validations

Acknowledgement

The development of the code presented in this paper was partially supported by Regione Lombardia through financing under the main project "TRIBOULET: Carbon Footprinting of Products".

References

ASHRAE. 2014. *ASHRAE Standard 140:2014 -- Standard Method of Test for the Evaluation of Building Energy Analysis Computer Programs*. Atlanta, U.S.A.: ASHRAE.

Mazzarella, L., M. Pasini. 2009. "Building energy simulation and object-oriented modelling: review and reflections upon achieved results and further developments". In: *Proceedings of Building Simulation 2009*. Glasgow, UK: IBPSA.

Mazzarella, L. 2013. "The air energy balance equation paradox". In: *Proceedings of Building Simulation Applications BSA 2013, the 1st IBPSA-Italy conference*. Bolzano, Italy: BUPRESS.

Mazzarella, L., M. Pasini. 2013. "Development of a new tool for the co-simulation of multiple autonomous object". In: *Proceedings of Building Simulation 2013*. Chambéry, France: IBPSA.

Mazzarella, L., M. Pasini, N. Shahmandi Hoonejani. 2014. "Challenges, limitations, and success of cloud computing for parallel simulation of multiple scenario and co-simulation". In: *Proceedings of ASHRAE/IBPSA-USA Building Simulation Conference*. Atlanta, U.S.A.: ASHRAE.

Mazzarella, L., M. Pasini. 2015a. "Advancement in the development of an Open Source Object Oriented BPSt: development methodology". In: *Proceedings of Building Simulation Applications BSA 2015, the 2nd IBPSA-Italy conference*. Bolzano, Italy: BUPRESS.

Mazzarella, L., M. Pasini. 2015b. "CTF vs FD based numerical methods: accuracy, stability and computational time's comparison". *Energy Procedia* 78: 2620–2625. doi: 10.1016/j.egypro.2015.11.324.

Pasini, M. 2009. *Towards an Enriched Modularity of Building Performance Simulation's Programs: Reconceptualisation and development of an Object-Oriented model*. Ph.D. Thesis, Milano, Italy: Politecnico di Milano.

Perez, R., P. Ineichen, R. Seals, J. Michalsky, R. Stewart. 1990. "Modeling Daylight Availability and Irradiance Components from Direct and Global Irradiance". *Solar Energy* 44, 271-289. doi: 10.1016/0038-092X(90)90055-H.

A Comparative Study of Computational Algorithms Used in the Automatic Generation of Reduced-Order Models from CFD Simulations

Thibault Marzullo – National University of Ireland Galway – t.marzullo1@nuigalway.ie

Sajjad Yousefian – National University of Ireland Galway – s.yousefian2@nuigalway.ie

Marcus M. Keane – National University of Ireland Galway – marcus.keane@nuigalway.ie

Marco Geron – Queen’s College of Belfast – m.geron@qub.ac.uk

Rory F.D. Monaghan – National University of Ireland Galway – rory.monaghan@nuigalway.ie

Abstract

In indoor thermal environment modelling applications where dynamic local effects of fluid flows are critical, classic zonal models are not always suitable. On the other hand, CFD simulations can give accurate solutions at very high computational cost. Reduced-order models (ROMs), extracted from CFD simulations, can preserve CFD model accuracy while being characteristically of low computational cost. The authors propose a method, known as CFD-ROM, capable of rapidly and automatically generating, from CFD simulations, zones, mass, and heat flows, and boundary conditions (BCs) for ROMs. This paper presents a comparative study of automatic zone generation algorithms as a necessary initial step to developing the CFD-ROM method. Zone generation algorithms compared in this paper are: (1) Mean Values Segmentation; (2) Classic Watershed; and (3) Coarse Grid Interpolation. The methods were compared on the bases of their accuracy against the original validated CFD simulation results, and their time to zone generation. The Mean Values Segmentation method yields promising results, providing a mean error below 0.2 K for 15-zone models generated in under 28 seconds. The next immediate steps for the development of CFD-ROM are (i) construction of a ROM solver, and (ii) testing its ability to predict thermal conditions when CFD BCs and ROM BCs differ.

1. Introduction

The buildings sector and people’s activities in buildings are responsible for 31 % of the global final energy demand, one-third of energy-related CO₂ emissions, two-thirds of halocarbon emissions, and 25–33 % of black carbon emissions (GEA, 2012). Sustainability, as defined by the ASHRAE Handbook of

Fundamentals (ASHRAE, 2013), is "providing for the needs of the present without detracting from the ability to fulfil the needs of the future". A key approach to improve the sustainability of energy use is the reduction of waste through careful planning, optimization and management of demand. In the built environment, the use of models of building thermal conditions during both the design and operation phases is recognised as a powerful method to increase energy efficiency and reduce energy demand (Harish and Kumar, 2016).

These computer models can be grouped into three categories: (1) physics-based models, (2) experimental models, and (3) mixed models (Harish and Kumar, 2016). Physics-based (theoretical) models describe in detail the studied system and its subsystems, and define an output based on mathematical equations constrained by physical laws. They are typically used during the preliminary design and energy audit phases. Experimental models on the other hand are tailored to a particular system. Through experimentation, the system’s response to various inputs is evaluated and the model is developed accordingly. Finally, mixed models are physics-based models for which parameters are estimated using statistical and/or experimental analysis.

Among physics-based models, Computational Fluid Dynamics (CFD) is a powerful and increasingly widespread tool for simulating fluid domains, which yields models of high fidelity (van Hooff and Blocken, 2013; Tamura and Van, 2014; Antonioni et al., 2012). However its large computational expense frequently renders it too time-consuming for design tasks. Designers and operators therefore often choose lower fidelity but faster methods when

available (Li and Wen, 2014). Unfortunately lower fidelity methods lose information that could be otherwise beneficial to the overall system performance. In order to overcome some of these issues we propose a method called CFD-ROM (Computational Fluid Dynamics – Reduced Order Model) which will automatically extract ROMs from CFD simulations and solve them rapidly for a wide range of conditions, including those for which no CFD solutions are available. The method aims to develop ROMs that will retain a high level of accuracy, similar to the CFD simulations, but at a significantly lower computational cost (Mullen et al., 2015; Tan and Glicksman, 2005; Mora et al., 2003; Lucia et al., 2001). A flowchart for the CFD-ROM method is shown in Fig. 1. The method uses as its input, results obtained from a CFD simulation (Step 1). It then clusters computational cells together to create zones (Step 2). Zones' physical properties and inter-zone interactions are calculated (Step 3). Afterwards, a multi-zone ROM is generated and passed to the ROM solver (Step 4). It is solved (Step 5) and the results are remapped to the original CFD domain (Step 6). Operations performed by the CFD-ROM method can be categorised as online or offline. Online operations are tasks that need to be repeated to obtain a new ROM solution, while offline operations are those tasks executed only once for a given indoor environment. Zone generation (Step 2) represents a major portion of offline method computational expense and is executed only once to generate a set of ROMs. ROM solving, on the other hand, is an online operation, as yielding new results involves computing ROMs for new boundary conditions.

The purpose of the study presented in this paper is to perform an evaluation of different zone generation algorithms to inform the development of the CFD-ROM method. This is important as the zoning algorithm has an influence on the quality of the information passed to the ROM solver and preliminary studies showed that this step can represent a large portion of the offline total time to solution (Mullen et al., 2015).

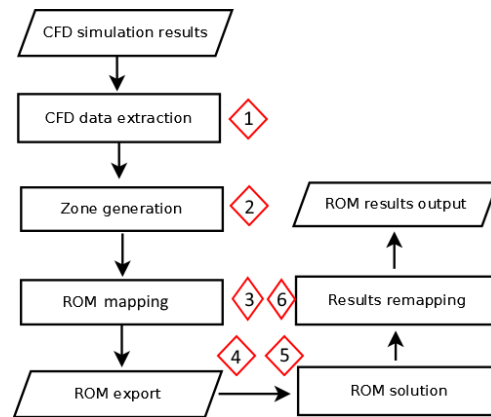


Fig. 1 – CFD-ROM method flowchart

2. Description of Zoning Algorithms

As previously stated, a crucial step in the development of the CFD-ROM method is the selection of a zone generation algorithm to develop a multi-zone ROM. It is important to note that these algorithms do not output a complete ROM; their scope is limited to the optimal clustering of cells into zones of similar physical properties. Three methods have been considered in the present study: (1) Mean Values Segmentation (MVS), (2) Classic Watershed (CW), and (3) Coarse Grid Interpolation (CGI). All three algorithms, which are explained in the following sections, have been coded in Python v2.7 (Python Software Foundation.). MVS has been developed from the results obtained during preliminary CFD-ROM development (Mullen et al., 2015) as it provided satisfactory proof-of-concept results. CW is directly adapted from the eponymous image processing method (Soille and Vincent, 1990). Finally, CGI interpolates the CFD solution to a very coarse mesh.

The use of higher computational power such as Graphic Processing Unit (GPU) processors and parallel computing are not within the scope of this study, but their use will be investigated in the future once a zoning method has been selected.

2.1 Mean Values Segmentation

This method successively splits the domain depending on the zone criteria. Zone criteria are the physical properties that are used to identify uniform regions of the simulation domain. Examples of zone

criteria include temperature, air velocity and carbon dioxide concentration. For the purpose of the present comparative study, temperature is the only zone criterion used. Zone generation is achieved through three main steps described by Mullen et al. (2015): (1) zone-type generation, (2) zone creation, and (3) zone number reduction. A zone-type is an interval containing all the cells sharing similar values of the zone criteria independently from their spatial position.

Fig. 2.a describes the MVS method. The algorithm extracts the values of the zone criteria from the entire domain (Step 1), computes the average value of the zone criteria (Step 2), then divides the domain into two zone-types (Step 3). The first zone-type containing cells with zone criteria values greater

than the average value, and the second containing the remaining cells. The algorithm successively splits the zone-types until the required number of zone-types has been achieved (Step 4).

After generating the required number of zone-types the algorithm will cluster adjacent cells together within a zone-type. During this step a new zone is generated at each time a cell that has not been assigned a zone yet, is found. The algorithm then searches all adjacent cells within the same zone-type and assigns them the same zone. The process continues until no adjacent cells are found in the zone-type any more, at which point the process is repeated for a new zone until all cells within the zone-type have been assigned a zone. At this point

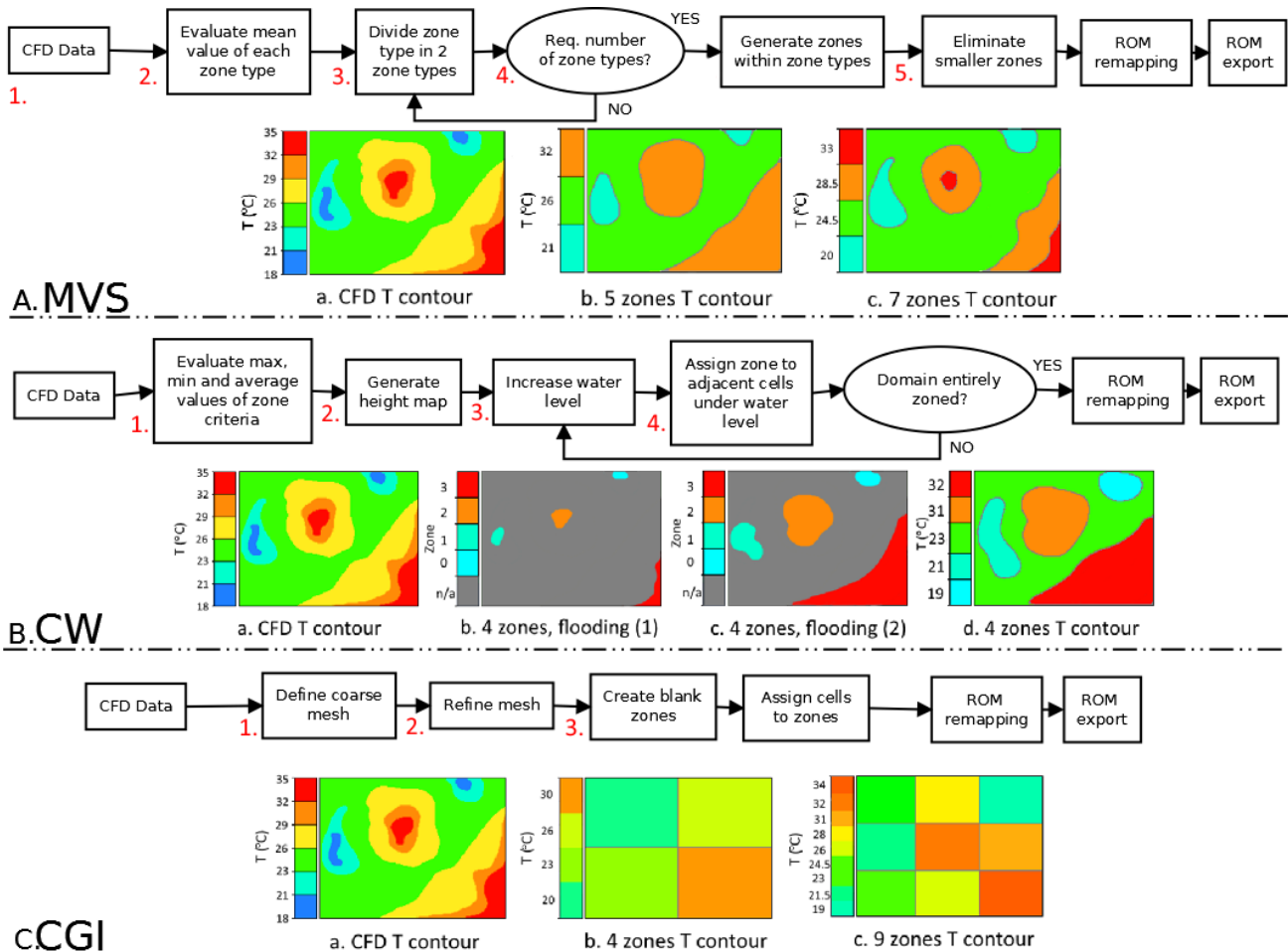


Fig. 2 – Flowcharts of the Mean Values Segmentation (A), Classic Watershed (B) and Coarse Grid Interpolation (C) algorithms

a large number of zones has been created. The algorithm scans the domain one last time to incorporate the smallest zones into larger ones (Step 5) until the desired number of zones is reached.

2.2 Classic Watershed

The Classic Watershed (CW) is a method used in image processing for image segmentation (Soille and Vincent, 1990; Tsukahara et al., 2008). It has been adapted by the authors to ROM generation because its principle is very similar to zone creation. In fact, the CW algorithm is mainly used for gray-scale image segmentation but its fundamental basis can be used for any n-dimensional dataset provided a height map which is defined below can be extracted.

The CW algorithm comprises 4 steps highlighted in Fig. 2.b and described in detail by Soille and Vincent (1990): (1) a height map is generated from the dataset, assigning lower heights to data points that are more relevant to the study; (2) working only with the height map, a water level is defined. The water level will rise (3) at each new iteration, and the data points belonging to the same basin (i.e. adjacent data points under the water level) are clustered together (4). Basins will grow until either they come in contact with another basin or a maximal height is reached. At this point, watersheds are raised.

The CW has many variations depending on the application, such as aerial photography (Wei and Xin, 2010) or medical imaging (Tsukahara et al., 2008).

In this study the height map is generated from temperature values and is normalized so that a lower height (i.e. greater importance) is assigned to local temperature maxima and minima. This ensures that the algorithm prioritizes sections of the domain where temperature differences are important.

Once the height map has been generated and it has been iteratively flooded, a set of clusters of cells belonging to the same basin is obtained. The clusters are remapped to the original domain to obtain a multi-zone model.

2.3 Coarse Grid Interpolation

In the CGI method the CFD results are interpolated to a coarse mesh. For this study the mesh was coarsened from 1.5 million cells to 2–30 cells (see the Results section). In this method, the only zone criteria are the X, Y, Z coordinates of each cell. The algorithm developed for this study is straightforward and is shown in Fig. 2c. The algorithm (1) scans the domain and defines a coarse mesh based on the desired number of zones, (2) refines the coarse mesh to ensure that boundary cells cannot be part of more than one zone, (3) creates empty zones, and (4) assigns cells to a zone depending solely on their coordinates. Similarly to the MVS and CW methods, the mean values of the zone criteria of each zone are computed and assigned to the zone.

3. Results

The data used in this comparative study are taken from the previously validated CFD model of a north-facing office in the Environmental Research Institute (ERI) building at University College Cork (UCC) (Mullen et al., 2015). CFD models were developed using the Phoenix modelling software to generate a database of test cases. For all simulations turbulence is modelled using the steady-state Reynolds Average Navier-Stokes (RANS) approach coupled with the Re-Normalisation Group (RNG) $k-\epsilon$ turbulence model. Air is modelled as an incompressible ideal gas. Phoenix utilises an immersed body technique and consequently the domain is discretized using a Cartesian structured grid with 1,572,165 cells (115x147x93). Constant temperature boundary conditions have been utilised for the ceiling, and the floor, and east and west walls. All other objects are considered adiabatic. All CFD simulations used have been validated with experimental data and previously published (Mullen et al., 2015). All the multi-zone models used to obtain the results are automatically extracted with the only input from the user being the required number of zones. As described in section 1, zone generation is one of the CFD-ROM method's key steps in creating ROMs. It is not possible to predict CFD-ROM's output based

solely on the results of the zone generation algorithm, so the bases of comparison for this study are (1) the accuracy of the multi-zone models, and (2) the time it takes to generate them.

3.1 Accuracy

Quantifying error of multi-zone models provides an indication on the quality of zone generation algorithms. The present study uses a weighted Mean Absolute Error, or WMAE (Equation 1) in Kelvin, to account for differences in cell volumes. The unitary error is defined by the AE or Absolute Error in Kelvin, as shown in Equation 2.

$$WMAE = \sum_{i=0}^n \frac{V_i \times AE_i}{n \times V_{domain}} \quad (1)$$

$$AE_i = |T_{CFDi} - T_i| \quad (2)$$

Where n is the number of cells in the domain, V_i is the volume of cell i , AE_i is the absolute error of cell i , V_{domain} is the total volume of the domain, T_{CFDi} is the original CFD temperature of cell i , and T_i is the temperature assigned to the cell after the zoning process is completed. The motivation for weighting the original MAE is to account for varying cell volumes, as the computational grid is finer close to boundaries, where the largest temperature differences also occur. The following results have been obtained for zone numbers ranging from 2 to 27 for CGI, from 3 to 27 for CW, and from 2 to 29 for MVS. Fig. 3 shows a plot of the WMAE versus number of zones N for the three algorithms described above. The results indicate that for this range of numbers of zones the CGI method produces multi-zone outputs in which accuracy is highly dependent on the geometry of the coarse grid. In fact, the more accurate results (for 3, 8, 12, 18, and 27 zones, as shown in Fig. 3) correspond to grids which were divided more finely in the vertical direction in order to better capture thermal stratification.

The mean error of the outputs produced with the CGI algorithm is still higher than the mean error obtained with the MVS algorithm. The mean error of the latter rapidly decreases as more zones are generated before gradually stabilizing. The results presented by Mullen et al. (2015) show a similar trend for the solved ROM.

The results obtained for the CW algorithm indicate that the mechanics of the algorithm are not optimal. The watersheds are placed whenever one basin comes into contact with another, which excludes the possibility of including an intermediate zone between two others to characterize a smooth transition from one zone to another: a zone of high temperature can come in direct contact with a zone of cold temperature without a transition zone in between. Future work includes the investigation of techniques that could address this issue.

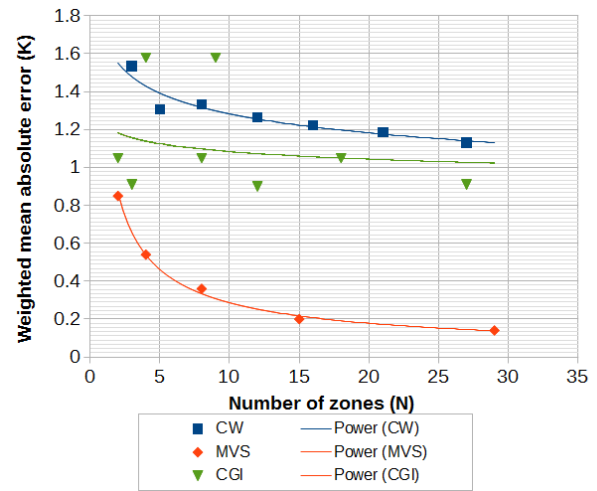


Fig. 3 – Weighted mean absolute error versus number of zones

3.2 Time to Generation

The time to generate multi-zone models is measured with Python's `time()` function found in the `time` library. Python 2.7 `time()` documentation states that whether the code is run on a UNIX system or not, "[time] is the function to use for benchmarking Python or timing algorithms" and that "the resolution is typically better than one microsecond" (Python Software Foundation). The timer is set to start after the initialization step and stops after the algorithm outputs the results in order to capture only the time for the zoning process. Each algorithm was run 15 times and an average time was calculated.

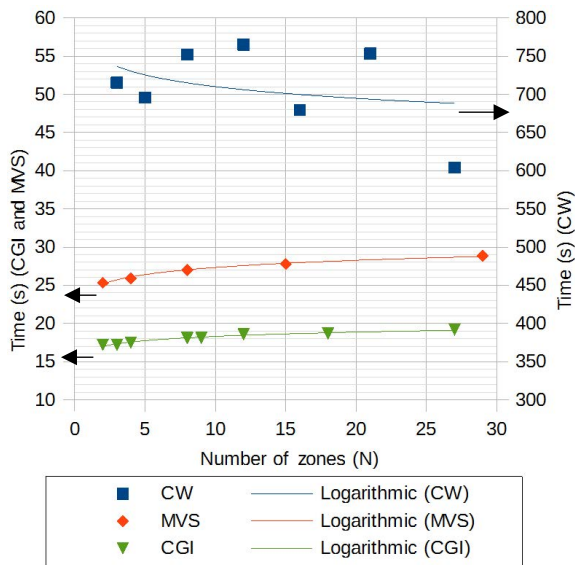


Fig. 4 – Time to generation versus number of zones

It is important to note that zone generation is considered an offline operation, meaning that each ROM has to be generated only once. This is in contrast to ROM solution, an online operation, which is performed multiple times. Therefore the time for zone generation cannot provide an indication of the overall ROM generation and solution performance.

The time to completion for the CGI algorithm is relatively constant, varying only from 17.2 s to 19.2 s across the range of 2–27 zones as shown in Fig. 4. This result was expected, as the CGI algorithm does not divide the domain according to cell conditions but only according to cell coordinates. MVS on the other hand demands more time to generate multi-zone models as the number of zones increases.

This study found times to generation ranging from 25.3 s to 28.9 s for 2–29 zones. Finally, CW in this configuration proved to be very time consuming (right-hand y-axis). The iterative mechanism of the algorithm involves much longer times to completion, as shown in Fig. 4. The decrease in time to completion with increasing zone numbers for CW is explained by the involvement of a height map in zone generation and the creation of watersheds. As watersheds are created during zone generation, some zones will stop growing in size and will then be ignored at the next iteration. The watersheds are

automatically placed at different locations depending on the desired number of zones, therefore the size of each zone is not inversely proportional to the number of zones. An improvement in the method could be the creation of watersheds on small slopes (i.e. areas with low temperature differences) rather than points of contact between two zones.

4. Discussion

This study has shown encouraging results for the MVS algorithm, as it yields multi-zone models with a lower error than the CGI algorithm with comparable times to generation. The CW algorithm could benefit from a modification in the mechanics of watershed creation when considering the WMAE, but its high times to generation may prove problematic if its accuracy is not greatly improved. It should however be noted that in the case of a ROM being generated only once, but being solved with different BCs a large number of times, the time for zone generation might be of secondary importance compared to that for ROM solution. Estimates of ROM solution times will be needed to clarify this. Likewise the characterization of error based on the generated zone temperatures rather than the solved ROM temperatures represents only a first step in comparing these algorithms. Additionally it will be important to characterize the ability of ROMs generated by the different algorithms to predict thermal conditions in cases where the ROM BCs differ from the CFD BCs. This is an important capability for the CFD-ROM method as it would enable the replacement of large numbers of CFD simulations with a smaller number of CFD simulations complemented by very large numbers of ROMs spanning the conditions between them.

Nevertheless this comparison has proven extremely valuable as a first step towards the development of a truly systematic CFD-ROM method that can reduce the need for computationally expensive CFD simulations in determining thermal conditions in realistic indoor environments.

The principal limitation of this study is the restriction to zone generation. In fact, the final goal of the CFD-ROM method is the ability to generate

multiple ROMs from a reduced set of CFD simulations. The algorithms described in this study could present different results when solved (1) for the same BCs and (2) for different BCs.

5. Conclusion

The main objective of this study was to compare zone generation algorithms to be used in a novel CFD-ROM method for thermal modelling of indoor environments. At this stage, MVS was found to be the most suitable method. However, the multi-zone models generated by these algorithms could yield different results when solved for sets of BCs different from the original CFD BCs.

Future plans for the CFD-ROM methods include, in order: (1) the development of a ROM solver in the Modelica language, (2) the validation of the CFD-ROM method for the extraction of a single ROM from a CFD simulation, (3) the extension of the method to multiple zone criteria, and (4) the evolution of the method to allow ROM generation for off-design BCs (multi-ROM approach).

This study is the first step towards the ultimate goal which is a rigorous and systematic design of the CFD-ROM method.

Acknowledgements

The authors wish to acknowledge the following funding. T. Marzullo is supported by a Scholarship from the College of Engineering and Informatics at NUI Galway and by HIT2GAP (EU/H2020 Grant Agreement No.: 680708). S. Yousefian is supported by a Scholarship from the College of Engineering and Informatics at NUI Galway and by the Science Foundation Ireland-backed Research Centre for Marine and Renewable Energy (MaREI) with industrial support from the Gas Networks Ireland Gas Innovation Group.

Nomenclature

Symbols

AE	Absolute Error (K)
n	Number of computational cells
T	Temperature (K)
V	Volume (m ³)

Subscripts

CFDi	Computational cell i of the CFD solution
domain	Domain
i	Computational cell i of the multi-zone model

Acronyms

BC	Boundary Condition
CFD	Computational Fluid Dynamics
CFD-ROM	Computational Fluid Dynamics – Reduced Order Model
CGI	Coarse Grid Interpolation
CW	Classic Watershed
GPU	Graphic Processing Unit
MAE	Mean Absolute Error
MVS	Mean Values Segmentation
ROM	Reduced Order Model
WMAE	Weighted Mean Absolute Error

References

- Antonioni, G., S. Burkhart, J. Burman, A. Dejoan, A. Fusco, R. Gaasbeek, T. Gjesdal, et al. 2012. "Comparison of CFD and Operational Dispersion Models in an Urban-like Environment". *Atmospheric Environment* 47: 365–372. doi:10.1016/j.atmosenv.2011.10.053.
- ASHRAE. 2013. *ASHRAE Handbook Fundamentals*. Atlanta, U.S.A.: American Society of Heating, Refrigerating, and Air Conditioning Engineering, Inc.
- GEA. 2012. *Global Energy Assessment - Toward a Sustainable Future*. Cambridge, UK and New York, U.S.A.: Cambridge University Press; and Laxenburg, Austria: International Institute for Applied Systems Analysis.

- Harish, V.S.K.V., A. Kumar. 2016. "A Review on Modeling and Simulation of Building Energy Systems". *Renewable and Sustainable Energy Reviews* 56: 1272–1292. doi:10.1016/j.rser.2015.12.040.
- Li, X., J. Wen. 2014. "Review of Building Energy Modeling for Control and Operation". *Renewable and Sustainable Energy Reviews* 37. Elsevier: 517–537. doi:10.1016/j.rser.2014.05.056.
- Lucia, D.J., P.S. Beran, W.A. Silva. 2001. "Reduced-Order Modeling - New Approaches for Computational Physics". *Progress in Aerospace Sciences* 40(1-2): 51–117. doi:10.2514/6.2001-853.
- Mora, L, A.J. Gadgil, E. Wurtz. 2003. "Comparing Zonal and CFD Model Predictions of Isothermal Indoor Airflows to Experimental Data". *Indoor Air* 13(2): 77–85. doi:10.1034/j.1600-0668.2003.00160.x.
- Mullen, D.T., M.M. Keane, M. Geron, R.F.D. Monaghan. 2015. "Automatic Extraction of Reduced-Order Models from CFD Simulations for Building Energy Modelling". *Energy and Buildings* 99: 313–326. doi:10.1016/j.enbuild.2015.04.015.
- Python Software Foundation. *Python Language Reference, Version 2.7*.
- Soille, P., L. Vincent. 1990. "Determining Watersheds in Digital Pictures via Flooding Simulations". *Visual Communications and Image Processing* 1360: 240–250. doi: 10.1117/12.24211.
- Tamura, Y., P. Pham Van. 2014. "Development of CFD and Applications: Monologue by a Non-CFD-Expert". *Journal of Wind Engineering and Industrial Aerodynamics* 144: 3–13. doi:10.1016/j.jweia.2015.05.003.
- Tan, G., L.R. Glicksman. 2005. "Application of Integrating Multi-Zone Model with CFD Simulation to Natural Ventilation Prediction". *Energy and Buildings* 37(10): 1049–1057. doi: 10.1016/j.enbuild.2004.12.009.
- Tsukahara, M., S. Mitrović, V. Gajdosik, G. Margaritondo, L. Pournin, M. Ramaioli, D. Sage, Y. Hwu, M. Unser, T.M. Liebling. 2008. "Coupled Tomography and Distinct-Element-Method Approach to Exploring the Granular Media Microstructure in a Jamming Hourglass". *Physical Review E* 77(6).
- van Hooff, T., B. Blocken. 2013. "CFD Evaluation of Natural Ventilation of Indoor Environments by the Concentration Decay Method: CO₂ Gas Dispersion from a Semi-Enclosed Stadium". *Building and Environment* 61: 1–17. doi:10.1016/j.buildenv.2012.11.021.
- Wei, W., Y. Xin. 2010. "Rapid, Man-Made Object Morphological Segmentation for Aerial Images Using a Multi-Scaled, Geometric Image Analysis". *Image and Vision Computing* 28(4): 626–633. doi:10.1016/j.imavis.2009.10.002.

Comparison of Direct Radiation Split Algorithms for Energy Simulation of Buildings

Giorgio Lupato – University of Trieste – s232454@stud.units.it

Marco Manzan – University of Trieste – manzan@units.it

Stefano Cirilli – University of Trieste – cirilli@units.it

Abstract

Direct normal radiation (DNI) has great importance for both energy building simulations and solar energy systems. The data is seldom available from measurements but usually is recovered from global radiation data using split algorithms. The present paper analyses the performance of 33 different split radiation models and the error which arises when applied to building energy simulations using generated hourly weather files.

The split models have been applied to an observed dataset composed by 525888 points, which comprises global and diffuse radiation on the horizontal plane, related to -year measurements, starting from 2001 with 10-minute time steps.

The generated weather files have been employed as input for energy simulations with EnergyPlus on a building generated using DesignBuilder software. We investigated the impact of the weather files in building energy simulation highlighting the performances of four models selected among the 33 models by means of statistical indicators, during different periods of the dataset, since its amplitude allowed us to decompose and analyse 10 different years.

1. Introduction

Dynamic building energy simulations, usually carried out at least on an hourly basis, require detailed environmental data such as temperature, humidity, wind velocity and direction usually available from a number of climatic stations. However, in order to compute solar loads, direct normal radiation and diffuse horizontal radiation are also required. Unfortunately, continuous records of DNI are scarce due to the cost of the equipment: the monitoring stations equipped with solar trackers are very rare. An intermediate solution is to record diffuse and global irradiance, but

global insolation is the unique parameter monitored in numerous locations around the world, therefore a great number of climatic data report only this value.

Starting from the work by Liu and Jordan (1960), many efforts were undertaken to develop separation models to estimate the diffuse horizontal irradiation component and, by subtraction, the direct horizontal component. Thereafter, the direct radiation is obtained by dividing it by the cosine of the zenith angle, properly averaged on the interval monitored. In literature, more than 150 models have been developed with numerous comparison papers. Nevertheless, the definition of a universal model able to provide the best possible result at any specific location is still very complicated, because algorithms are usually expressed in terms of first or fourth degree polynomial functions, empirically derived from site-specific measurements. This technique usually tends to suffer for excessive model localization and/or overfitting which implies that one model can lead to accurate results for a location, while performing poorly for a different one.

This paper describes the performance of different split algorithms using a dataset containing global and diffuse irradiance measurements recorded in Trieste. The availability of a large number of climatic data, which spans for a period of ten years, allows for a deep comparison among split methods. Therefore, the former part of this paper is focused on the statistical analysis of the models while the latter explores the effect of the different split methods on building energy simulations.

2. Dataset

The data used is composed of 10-year records of Trieste (45°,65°,13.76°) collected by the Meteorology and Oceanography Laboratory of the University of Trieste containing global and diffuse horizontal irradiation measurements with 10-minute interval detection. The total number of available points is 525888 and includes the following exogenous measurements: dry bulb temperature, relative humidity, wind speed and wind direction too.

Solar position has been considered in the middle of the measurement interval, shifting the time detection back 5 minutes for all the datasets, since the row data were originally recorded as mean solar measurement in Wh/m² reported at the end of the interval.

The global horizontal irradiation has been used as the input data for the application of split methods, while the diffuse, and hence the direct horizontal data, have been used as the reference value.

3. Model Selection

Since the first split model proposed by Liu and Jordan in 1960, many models were developed in literature. According to Lannini (2010), three different types of models can be considered: polynomial models, exponential models, and logistic models. All of these categories use predictors, intended as a measurement, or an evaluated variable, required for applying the model. In all the proposed models of this paper clearness index kt , defined in Equation 1, is used as a predictor in order to obtain the diffuse fraction kd , defined in Equation 2.

$$kt = \frac{GLO}{E_{0h}} \tag{1}$$

$$kd = \frac{DIF}{GLO} \tag{2}$$

The extraterrestrial solar radiation was calculated with Spencer Fourier series expansion.

Other predictors can be used as well. They can be grouped in kt class predictors and exogenous predictors as dry bulb temperature, dew point temperature or relative humidity. Table 1 presents the list of the models chosen and analyzed in this article.

4. Quality Control

The posteriori quality control of the measured data was followed as described in Gueymard et al. (2016) and summarized in Table 2. With the application of this quality check, the number of valid points was reduced from the original 525888 to 239594, taking into consideration night hours, too.

Table 1 – Models analyzed with total number of required predictors and number of exogenous predictors in brackets

Id	Model	# predictors
1	Orgill and Hollans	1
2	Reindl1	1
3	Reindl2	2
4	Hawladar	1
5	De Miguel	1
6	Karatasou	1
7	Erbs	1
8	Chandrasekaran	1
9	Oliveira	1
10	Soares	1
11	Lam Li	1
12	Furlan 1	1
13	Lee	1
14	Maxwell	2
15	Macagnan	2
16	Boland 2001	1
17	Louche	2
18	Spencer	1
19	Jacovides	1
20	Boland 2008	1
21	Reindl3	4(2)
22	Perez	4(1)
23	Ulgen Hepbash	1
24	Ruiz-Arias	2
25	Chikh	1
26	Engerer2+Bird	5
27	Paulescu and Blaga 1	1
28	Paulescu and Blaga 3	1
29	Paulescu and Blaga 4	4(2)
30	Paulescu and Blaga 5	2
31	Elminir	1
32	Al Riahi	1
33	Torres	1

The PSA algorithm (Blanco-Muriel et al., 2001) was used to calculate the position of the sun.

Finally, the maximum allowable value of clearness index kt has been forced to 1, but this condition had to be enforced 3 times only.

Table 2 – Quality checks applied and number of eliminated points (Npe) for each rule

Id	Limit	Npe
a	$Z < 85^\circ$	284736
b	$GLO > 0$ and $DIF > 0$ and $DIR \geq 0$	267586
c	$DIF < 0.95 \cdot E_0 \cdot \cos^{1.2} Z + 50$	95
d	$GLO < 1.5 \cdot E_0 \cdot \cos^{1.2} Z + 100$	71
e	$DIF/GLO < 1.05$ and $Z < 75^\circ$	934
f	$DIF/GLO < 1.10$ and $Z > 75^\circ$	1120

An additional correction has been adopted by limiting minimum and maximum values of the estimated diffuse fraction to values of 0 and 1 respectively in order to prevent unphysical results. This quality check avoids negative diffuse irradiation or diffuse irradiation greater than the global irradiation. It is worth noticing that the diffuse radiation lower limit of 0 represents an unreal value too, since even with the clearest sky condition, the diffuse fraction should be present, too.

5. Statistical Indicators

Three statistical errors were used: mean bias deviation, mean absolute deviation, and root mean square deviation, defined in Equations 3–5.

$$MBD = \frac{\sum_{i=1}^n (DIFe_i - DIFm_i)}{n} \quad (3)$$

$$MAD = \frac{\sum_{i=1}^n |DIFe_i - DIFm_i|}{n} \quad (4)$$

$$RMSD = \sqrt{\frac{\sum_{i=1}^n (DIFe_i - DIFm_i)^2}{n}} \quad (5)$$

Subscript e indicates the estimated value, subscript m the measured values, and n is the number of valid points after the quality check.

The purpose of this paper is to investigate the error that occurs in building energy simulations because of the split model selection in defining climatic datasets. The statistical analysis could help the designer in making a conscious choice between the proposed models. In this paper, four models have been selected for a subsequent energy simulation analysis.

6. Results: Statistical Indicators

Tables 3 to 5 present for each statistical indicator the results obtained for the top five performing models considering the whole dataset and separate heating and cooling periods.

Table 3 – Models with lowest mean bias deviation

Model	MBD [Wh m ⁻²]		
	year	Heating	Cooling
Oliveira	0.2	4.23	8.86
Maxwell	2.6	-3.37	26.25
Ulgen Hepbasli	3.6	-3.04	12.78
Torres	4.1	6.38	15.30
Perez	4.5	-1.37	8.35

Table 4 – Models with lowest mean absolute deviation

Model	MAD [Wh m ⁻²]		
	year	Heating	Cooling
Perez	26.0	16.12	32.59
Louche	27.7	14.94	35.99
Spencer	27.8	15.23	35.61
Soares	28.3	14.54	35.55
Ruiz-Arias	28.6	14.06	37.25

Table 5 – Models with lowest root mean square deviation

Model	RMSD [Wh m ⁻²]		
	year	Heating	Cooling
Perez	45.6	30.51	53.33
Oliveira	46.6	24.81	54.54
Erbs	46.6	26.94	56.66
Torres	46.8	26.71	56.17
De Miguel	47.3	27.71	58.57

From the analysis of the results, the Perez model shows remarkable results in the cooling period, but the performance degrades for heating. Since the number of day hours is greater in the cooling period, the Perez model performs better than the other models on an annual basis. Taking into account the full results, of which Tables 3, 4, and 5 are just a summary, the Perez, Oliveira and Torres models were chosen to carry out building energy simulations.

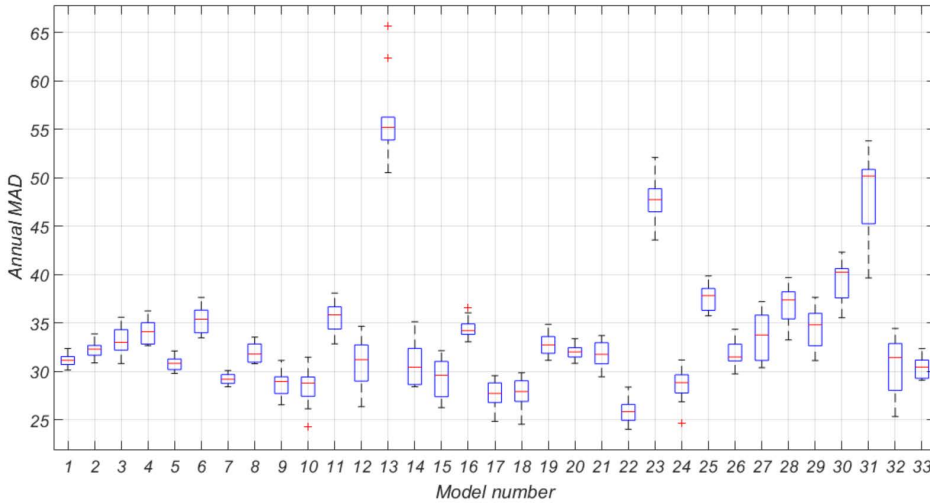


Fig. 1 – Distribution of MAD computed for every year of the dataset and each model

It is interesting to consider that the Oliveira and Torres models were obtained by linear regression applied to datasets collected in San Paulo, Brazil, and Pamplona, Spain, respectively. These models perform well also with the present dataset of Trieste because those locations have similar solar irradiation.

Fig. 1 presents the performance of each model by applying the statistical indicator for each year of the dataset. Therefore for each model a distribution of ten values is obtained. To compare the performance of the complete set of models, the results are reported as box plots, where the box extends from the first to the third quartile, the upper and lower whisker represent the minimum and maximum values of the set, while the line drawn into the box represents the median of the distribution. In this way an idea of the performance distribution can be obtained at a glance.

The inspection of Fig. 1 shows which model performs better compared to the others, not only in an absolute manner, but also considering the dispersion of the results: one model can perform well for one year but can give unsatisfactory results for other situations with large dispersed values. Due to this consideration, we focused on the Al Riahi model. As can be seen in Fig. 1, the Torres model (model n. 33) and the Al Riahi model (model n. 32) have comparable MAD over the entire dataset (red line within the box). However, we can also notice that the amplitude of Al Riahi box is

remarkably greater than the Torres box. The Al Riahi model has therefore been added to the selected models: the goal is to observe how the performance discrepancy between different years influences the building energy simulation. In detail, the Al Riahi model has its lowest MAD for 2003 (MAD 25.4), and its highest for 2004 (MAD 34.5). This can be explained through the inspection of Fig. 2: the year 2003 is characterized by high mean global and direct irradiation, with a low diffuse fraction; on the contrary, the year 2004 shows low global and direct solar radiation paired with high diffuse fraction. The last condition is different from Trieste’s solar irradiation and from the original Al Riahi dataset, monitored in Baghdad. For the same reasons also the Torres model, collected in Pamplona, Spain, has its lowest MAD in 2003, while the highest is recorded in 2004.

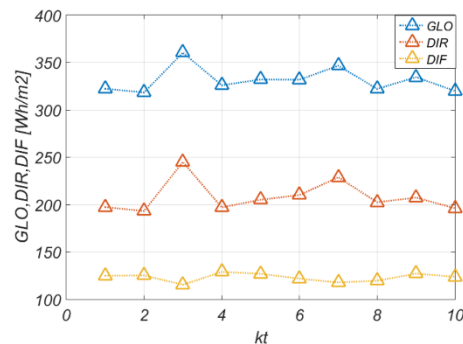


Fig. 2 – The mean yearly values of irradiance: Global, Direct and Diffuse on the horizontal plane

7. Model Choice

Following the observation explained in the previous paragraph, we selected four split models: Oliveira, Perez, Al Riahi, and Torres models. According to Lannini et al. (2010), except the Perez model that is classified as an exponential model, the three others are polynomial models. Fig. 3 presents the dispersion of diffuse fraction over the clearness index for the Perez model, while Fig. 4 compares the same dataset with the Oliveira, Al Riahi, and Torres models.

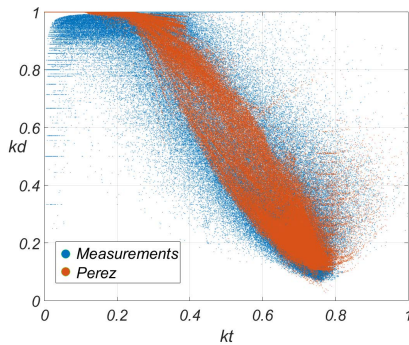


Fig. 3 – The Perez model

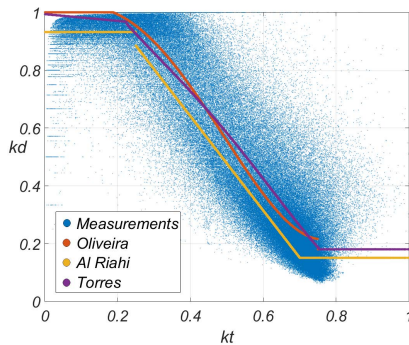


Fig. 4 – The Oliveira, Al Riahi, and Torres models

8. Building Envelope

The selected models were to generate climatic data in order to check the effect on building simulations. According to Pernigotto et al. (2016), a simple test building was simulated. It consists of a prism shape building with a square base, oriented to the main cardinal directions. Its internal floor area is 100 m² with 3 m internal height. All the opaque constructions are composed by two-layer structures with external isolation and 30 cm of concrete

internal structure. Thermal bridges are neglected. The material characteristics are reported in Table 6. The insulation thickness, reported in Table 7, was set in order to obtain the reference thermal transmittance, according to the Italian regulations for climatic zone E. Windows have thermal transmittance $U_w = 1.8 \text{ W m}^{-2} \text{ K}^{-1}$ with $g = 0.35$.

Table 6 – Layer material thermal proprieties

Layer	λ	Cp	ρ
Concrete	0.13	1.88	399
Insulation	0.04	1.47	40

Table 7 – Thermal transmittance and insulation layer thickness

Construction	U	s [cm]
External wall	0.30	9.41
External roof	0.25	12.2
Ground floor	0.30	9.25

Wall solar absorbance was set to 0.3, except for the internal floor and the external roof where a value of 0.6 was set. Ground temperature at building surface and at ground deep temperature was considered as constant, respectively of 18 °C and 14 °C.

In summary, the test building is composed of a well-insulated envelope with external windows on the east, south, and west facade, each one of 9.707 m² (29.12 m² of total area). This last choice was made to analyze a building with a wide window size that, as highlighted by Pernigotto et al. (2016), is critical for possible high cooling loads.

Internal gains are constant equal to 4 W/m² with radiant and convective fraction of 0.5. Ventilation air change was set at 0.3 vol/h. Heating and cooling systems were simulated as an ideal system, 100 % convective and with a unitary coefficient of performance. Heating and cooling systems are available according to Table 8.

Table 8 – Beginning, end and setpoint temperature related to heating and cooling systems

System	Begin	End	Setpoint [°C]
Heating	1/10	31/03	20
Cooling	1/04	30/09	26

9. Weather Files

EnergyPlus simulation files require input variables, all monitored or derived from the dataset such as the DNI. Except for the Perez model that calculates DNI directly, in the other cases it was estimated through Equation (6).

$$DNI = DIR / \cos(Z) \tag{6}$$

Due to the uncertainty of the measuring instrument at high zenith angles, Equation (6) can return extremely high values (that were previously eliminated from the quality control, Equation 3). This can lead to unphysical values, even higher than extraterrestrial solar radiation, which can cause simulation errors if used in building simulation codes. The issue was solved, as was recommended by Spinelli F. (personal communication, 2016, ENEA - Italian National agency for new technologies, Energy and sustainable economic development) with the substitution of out of range values. The problematic points were identified by applying the check reported in Equation (7) (Gueymard et al., 2016), with the DNI values obtained using the Bird clear-sky model according to Sengupta and Gotseff (2013).

$$DNI < 1100 + 0.03 \cdot Elev \tag{7}$$

The application of Eqn. 7 resulted in 95 points replacement in the dataset, 499 in Oliveira, 533 for Al Riahi, and 499 for Torres, and none for the Perez model. For all the variables previously described, the dataset was reduced from 10-minute detection to hourly weather files by averaging.

10. Simulation Results

Ten-year measurements and four selected models were used to obtain 40 simulations related to the split models. The results were compared to a reference simulation with weather files obtained using the original dataset. In the following paragraphs, the energy required for heating and cooling are analysed. As previously explained, we focused mainly on two different years, 2003 and 2004.

Tables 9 and 10 report the error in seasonal cooling or heating energy, as defined in Equation (8), where

subscripts “*se*” and “*sm*” represent respectively the simulation result with estimated and measured weather files.

$$Error = \frac{Energy_{se} - Energy_{sm}}{Energy_{sm}} \tag{8}$$

Table 9 – Cooling energy errors for the various models

Year	Sim [kWh]	Oliveira [%]	Perez [%]	Al Riahi [%]	Torres [%]
2001	2678	+1,9	+0,5	+1,9	+1,6
2002	2539	+1,7	+0,2	+1,5	+1,4
2003	3852	+1,8	+0,4	+1,4	+1,4
2004	2585	+2,4	+0,5	+2,2	+1,9
2005	2377	+2,9	+1,3	+2,6	+2,6
2006	2718	+3,2	+0,8	+3,5	+2,7
2007	3001	+3,6	+1,4	+3,3	+3,1
2008	2910	+2,7	+1,8	+2,4	+2,5
2009	3190	+3,9	+2,5	+3,8	+3,6
2010	2580	+3,6	+2,2	+3,3	+3,3

Table 10 – Heating energy errors for the various models

Year	Sim [kWh]	Oliveira [%]	Perez [%]	Al Riahi [%]	Torres [%]
2001	2516	-0,3	+3,0	-2,9	+0,1
2002	2381	-1,5	+2,0	-3,9	-1,1
2003	2234	-1,3	+2,8	-4,4	-0,6
2004	2706	-1,8	+1,4	-4,4	-1,3
2005	2839	-2,4	+1,4	-5,1	-2,0
2006	2403	-1,5	+2,6	-4,2	-0,9
2007	2040	-2,7	+2,1	-5,8	-2,3
2008	2429	-2,9	+1,0	-5,5	-2,4
2009	2544	-3,6	+0,6	-6,0	-3,3
2010	3249	-3,0	-0,4	-5,0	-2,8

As can be seen from Table 9, the Perez model in estimating the cooling energy preforms remarkably better than the others, with errors ranging from 0.2 % to 2.5 %. However, when considering heating energy, the Perez model shows the same performance of the Oliveria and Torres models. The result confirms the statistical analysis presented in Tables 3 to 5 where the Perez model showed the best results in the cooling period, but with lower performance during the heating one.

Furthermore, the numerical simulation confirms the distribution of the statistical error with the box plots presented in Fig. 1: a model can perform very differently if applied to different years on the same location. Considering Table 9, the Torres and Al Riahi models present the same error for the year 2003, while the latter shows consistently higher errors for different years.

Finally Figs 5 and 6 graphically show the errors trend reported in Tables 9 and 10, showing the good performance of the Perez model in cooling simulations, and the comparable performance of the Torres and Oliveira models for heating.

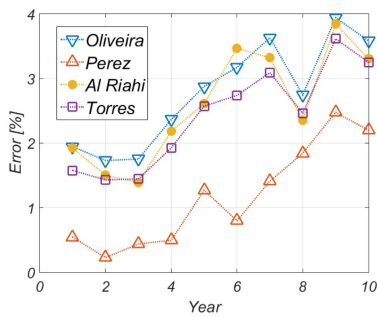


Fig. 5 – Cooling energy, percentage error between models and measured data

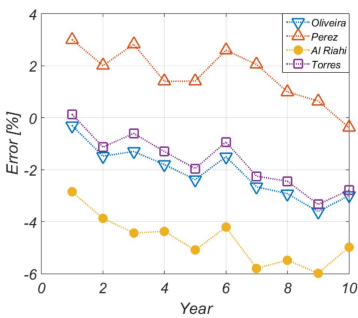


Fig. 6 – Heating energy, percentage error between models and measured data

11. Conclusions

33 split models were implemented in order to study their impact in building energy simulations. This analysis was developed both with statistical indicators and with simulation results, through EnergyPlus software. Considering the whole 10-year dataset, the Perez model performs significantly better than the others, both for MAD and RMSD statistic parameters, but with remarkable differences between cooling and heating periods. It

shows also consistency if applied to different years of the same location. Regarding the polynomial models, they can perform with satisfying accuracy if the current dataset has similar climatic characteristics to the one originally used to obtain the model. Those that behave better in this case are Oliveira and Torres.

Simulation results, applied on a test building with a well-insulated envelope, have shown that the Perez model performs extremely well for what concerns the cooling energy. On the other hand, the model shows higher energy needs during the heating period, but with a performance comparable to the other models.

The Al Riahi, with a greater range of variability between different years, for this reason included in the set of tested models, showed a trend similar to the Torres and Oliveira, but with more errors for the selected years, and critical results for heating due to its constant underestimation of the required energy. Finally, the Perez model shows the best overall performance. Nevertheless, the issue of lower performance in simulations concerning the heating period, especially for insulated buildings, cannot be neglected. Therefore, further investigation is required to identify the different behavior of the Perez model between heating and cooling periods. Regarding the influence of split models in simulation applied to insulated buildings, the choice can affect the simulation error from 0.2 % up to 4 %, this result is remarkable and has to be considered when dealing with building detailed energy analysis.

Nomenclature

Symbols

C_p	Thermal capacity ($\text{kJ kg}^{-1} \text{K}^{-1}$)
DIF	Diffuse horizontal solar radiation (Wh m^{-2})
DNI	Normal solar radiation, (Wh m^{-2})
DIR	Horizontal direct solar radiation, (Wh m^{-2})
E_0	Extraterrestrial solar radiation, (Wh m^{-2})
E_{0h}	Extraterrestrial solar radiation, horizontal (Wh m^{-2})
$Elev$	Elevation (m)
GLO	Global horizontal solar radiation, (Wh m^{-2})
kd	Diffuse fraction (-)

kt	Clearness index (-)
U	Thermal transmittance ($W m^{-2} K^{-1}$)
Z	Zenith angle ($^{\circ}$)
λ	Thermal conductivity ($W m^{-1} K^{-1}$)
ρ	Density ($kg m^{-3}$)

References

- Al-Riahi, M., N. Al-Hamdani, K. Tahir. 1992. "An empirical method for estimation of hourly diffuse fraction of global radiation". *Renewable Energy* 2(4): 451-456. doi:10.1016/0960-1481(92)90079.
- Bird, R.E., R.L. Hulstrom. 1981. *A Simplified Clear Sky Model for Direct and Diffuse Insolation on Horizontal Surfaces*, SERI/TR-642-761. Golden, U.S.A.: Solar Energy Research Institute.
- Blanco, M.J., D.C. Alarcon-Padilla, T. López-Moratalla, M. Lara-Coira. 2001. "Computing solar vector". *Solar Energy* 70(5): 431-441. doi:10.1016/S0038-092X(00)00156-0.
- Boland, J., B. Ridlay, B. Brown. 2007. "Models of diffuse solar radiation". *Renewable Energy* 33(4): 575-584. doi:10.1016/j.renene.2007.04.012.
- Chikh, M., A. Mahrane, M. Haddadi. 2012. "Modeling the diffuse part of the global solar radiation in Algeria". *Energy Procedia* 18: 1068-1075. doi:10.1016/j.egypro.2012.05.121.
- Elminir, H. 2005. "Experimental and theoretical investigation of diffuse solar radiation: data and models quality tested for Egyptian sites". *Energy* 32(1): 73-82. doi:10.1016/j.energy.2006.01.020.
- Engerer, N.A. 2015. "Minute resolution estimates of the diffuse fraction of global irradiance for southeastern Australia". *Solar Energy* 116: 215-237. doi:10.1016/j.solener.2015.04.012.
- Furlan, C., A.P. Oliveira, J. Soares, G. Codato, J.F. Escobedo. 2011. "The role of clouds in improving the regression model for hourly values of diffuse solar radiation". *Applied Energy* 92: 240-254. doi:10.1016/j.apenergy.
- Gueymard, C., J.A. Ruiz-Arias. 2016. "Extensive worldwide validation and climate sensitivity analysis of direct irradiance predictions from 1-min global irradiance". *Solar Energy* 128: 1-30. doi:10.1016/j.solener.2015.10.010.
- Jacovides, C.P., F.S. Tymvios, V.D. Assimakopoulos, N.A. Kaltsounides. 2006. "Comparative study of various correlations in estimating hourly diffuse fraction of global solar radiation". *Renewable Energy* 31(15): 2492-2504. doi:10.1016/j.renene.2005.11.009.
- Lannini, F., S. Wunderle, M. Lehning, C. Fierz. 2010. "Division of global radiation into direct radiation and diffuse radiation". *Master thesis*. Bern, Switzerland: University of Bern.
- Lee, K., H. Yoo, G.J. Levermore. 2013. "Quality control and estimation hourly solar irradiation on inclined surfaces in South Korea". *Renewable Energy* 57: 190-199. doi:10.1016/j.renene.2013.01.028.
- Liu, B.Y.H., R.C. Jordan. 1960. "The interrelationship and characteristic distribution of direct, diffuse and total solar radiation". *Solar Energy* 4(3): 1-19. doi:10.1016/0038-092X(60)90062-1.
- Macagnan, M.H., E. Lorenzo, C. Jimenez. 1993. "Solar radiation in Madrid". *International Journal of Solar Energy* 16(1): 1-14. doi: 10.1080/01425919408914262.
- Perez, R., P. Ineichen, E. Maxwell, R. Seals, A. Zelenka. 1992. "Dynamic Global-to-Direct Irradiance Conversion Models". *ASHRAE Transactions* 98(1):354-369.
- Pernigotto, G., A. Prada, P. Baggio P., A. Gasparella, A. Mahdavi. 2016. "Solar irradiance modelling and uncertainty on building hourly profiles of heating and cooling energy needs". In: *Proceedings of the IV International High Performance Buildings Conference*. West Lafayette, U.S.A.: Purdue University.
- Reindl, D.T., W.A. Beckman, J.A. Duffie. 1990. "Diffuse fraction correlations". *Solar Energy*, 45(1): 1-7. doi:10.1016/0038-092X(90)90060-P.
- Sengupta, M., P. Gotseff. 2013. *Evaluation of Clear Sky models for satellite-based irradiance estimates*, Technical Report NREL/TP-5D00-60735. <http://www.nrel.gov/GPO/gpo53784>
- Spencer, J.W. 1982. "A comparison of methods for estimating hourly diffuse solar radiation from global solar radiation". *Solar Energy* 29(1):19-32. doi:10.1016/0038-092X(82)90277-8.
- Torres, J.L., M. De Blas, A. Garcia, A. de Francisco. 2010. "Comparative study of various models in estimating hourly diffuse solar irradiance". *Renewable Energy*, 35(6): 1325-1332. doi:10.1016/j.renene.2009.11.025.

Introduction of a New Dynamic Simulation Screening Tool to Support Early-Stage Building Design

Marco Picco – University of Brighton – m.picco@brighton.ac.uk

Giorgio Ghisalberti – giorgio.ghisa@gmail.com

Gaetano Fabio Graziano – gf.graziano@gmail.com

Marco Marengo – University of Brighton – m.marengo@brighton.ac.uk

Abstract

The paper introduces a newly designed dynamic building energy simulation screening tool to help integrate the use of advanced simulation techniques to early stage building design and feasibility studies. The tool will help the design process to move toward an integrated design approach, including energy analyses and expertise from the first stages of design when time constraints and information requirements are still a hindrance for the use of other existing simulation tools. The paper focuses on the integration of the user input and output interfaces and automatic model generation algorithms while referring to previously existing papers in term of model definition, case studies and validation. The tool is able to simulate building energy performances starting from a limited number of inputs received through a specifically designed user interface supported by databases and suggested values. Based on those inputs, a simplified building model is generated and simulated in EnergyPlus and results are post processed and visualized on the user interface. The tool is fully web based and can be used through any web-enabled device as only the input and output interfaces are managed by the user device, with all other components being allocated to the server. The tool is able to run building performance simulations based on a simplified building model description with a limited number of inputs and in a short span of time, ranging from minutes to less than an hour. Nonetheless, the simulations are still returning results with an acceptable margin of accuracy compared to a detailed simulation, considered to generate useful information during early stage design and still higher compared to the use of traditional stationary models. The proposed tool will help the design process evolve toward an integrated approach and adapt to the foreseeable changes in regulations and market demand of low- and zero-carbon buildings.

1. Introduction

Buildings have been identified as one of the major targets for the reduction of energy use and greenhouse gas (GHG) emissions for many years. Studies show how buildings are responsible for around 40 % to 50 % of the global GHG emissions (Chen, 2009; Economidou, 2011).

Consequently, a strong push toward more efficient buildings is currently ongoing on a world scale, with the aim of Zero Carbon (ZCB) or Zero Energy (ZEB) Buildings. Private initiatives such as LEED or BREEAM are already targeting those high goals, while national and supranational regulations are quickly settling for slightly less ambitious goals, such as Net Zero (NZEB) and Nearly Zero (nZEB) Energy Buildings to be mandatory in the next few years (Executive Order No. 13514, 2009; European Parliament, 2010).

Design processes of buildings need to adapt to reach those standards, they have to become more attentive to energy and performance problems and move toward an integrated approach, such as IDP. Building performance simulation can greatly help the design process by fuelling it with essential information on the building expected behaviour (Hensen, 2004), as well as feasibility studies, and it is in fact already used in high calibre projects and design validation.

The constant push toward a new standard of highly efficient buildings such as nZEBs requires the creation of energy models during the early design phases (Utzinger and Bradley, 2009; Ferrero et al., 2015). However, such analyses require a high level of expertise and significant time commitment, in addition to a significant amount of information, all

usually unavailable during the first stages of the building design or the feasibility study.

The proposed simulation tool tries to solve this dilemma by providing a quick and easy way to perform simplified energy simulation with a limited number of essential user input, to be used as a screening tool to evaluate different design options. At the same time, the simulations need to deliver an adequate level of accuracy in order to provide useful information to fuel the decision process. This need is strongly related to the time and information requirement previously cited and therefore the accuracy of the simulation can be still acceptable even if lower compared to more traditionally detailed ones. This is granted by the tool through the use of specifically developed simplified models as seen below.

2. The Simulation Tool

2.1 The Idea

Research in the direction of a simplified simulation and screening tool stems from the need to overtake those well known barriers that are currently pre-

The tool allows the dynamic simulation of buildings in a timeframe compatible with the needs of the design process, while at the same time it achieves an acceptable level of accuracy. Additionally, the tool is designed to be used on any web-enabled device, without the need of installing any specific simulation software by the user, although it requires an Internet connection. Instead, the user will have access to the web interface and obtain the results as a service, in what could be considered an automated consultancy delivery.

Through the use of this tool, the user only needs to input a limited number of details through the input interface on his device. Those details are then sent to the server where the simulation model is created and the simulation performed, output from the simulation is then post-processed, and relevant information on the performance of the building is sent to the user through the user result interface.

An explanatory infographic summarizing the structure of the proposed tool can be seen in Fig. 1, highlighting each component that is needed for the process to work from when the user inputs the data on his device to the moment the results are visualized under the form of readily usable information.

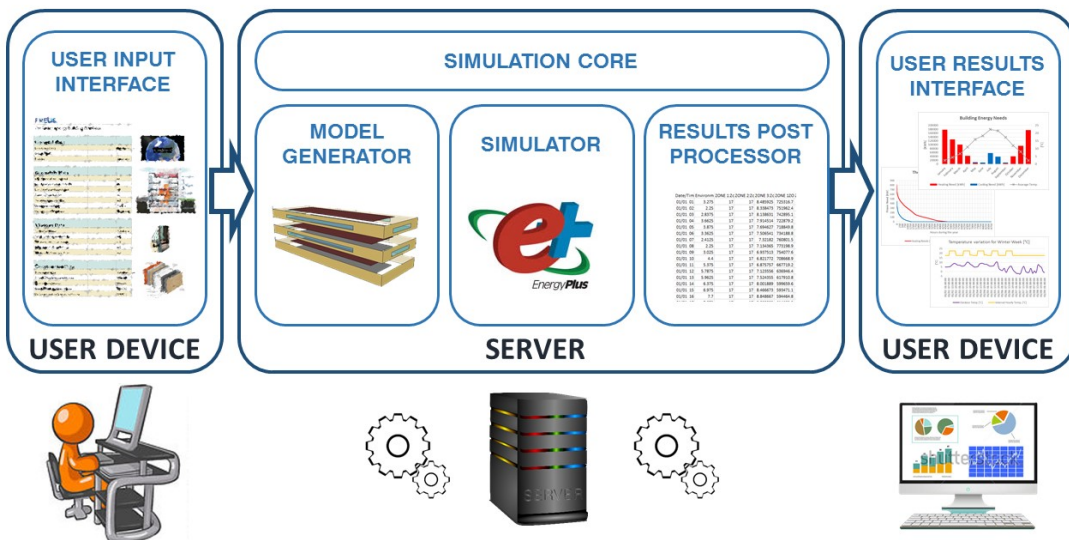


Fig. 1 – Structure of the proposed Simulation Tool

venting or limiting the diffusion of advanced building performance analysis during the first steps of the integrated building design process or feasibility study of renovations.

The tool is structured in three different blocks:

- the simulation Core,
- the user input interface,
- the user results interface.

Each part is discussed more in detail in the following paragraphs. Although the graphical aspect of the interfaces is currently under work and is not finalised, each element has already been defined and implemented in the tool.

2.2 The Simulation Core

The simulation core is composed by all the elements the user does not have direct contact with, and is subsequently hosted on a server, only exchanging data with the user device through an Internet connection.

The simulation core can be decomposed into three different elements:

- the simulator,
- the model generator,
- the results post processor.

The simulator is, in fact, the simulation code that runs the dynamic performance simulation of the building, based on the model received in input. For this application, the research team decided to use an already existing and reliable simulation code developed by the US Department of Energy named EnergyPlus (Crawley et al., 2004; Henninger and Witte, 2010). This allows to maintain the complexity and versatility of an advanced simulation code, while at the same time it lets the research team focus on the other aspects of the tool, as highlighted previously, and discussed in the following paragraphs. Not only this, but the reliance on an already existing calculation code will allow the final user to export the simulation model to EnergyPlus at any point, if needed, to extend the range of accessible features, if necessary, and it easily allows for future expansions of the tool itself.

The authors focused most of the research on the model generator. To be able to perform dynamic simulations, EnergyPlus requires a complex and specific input file containing the building model. As mentioned, this is one of the barriers for the extensive application of building simulation, as such models are usually time-consuming, and require a significant amount of information.

By applying the knowledge gathered during past research work and integrating the previously developed simplified building description model (Picco et. al, 2014), this pre-processor is able to collect the

limited number of details provided by the user and automatically generate a fully functional, although simplified, building model that EnergyPlus can use to perform dynamic simulations.

The last element of the simulation core is the results post-processor that automatically reads the output .csv file obtained by EnergyPlus, and processes the contained data in usable information for the user in the form of tables and graphs, ready to be sent to the user interface, an example of such results can be seen in Chapter 4 of this paper.

2.3 The Input Interface

The input interface is a web-based application that will be accessible to the user from a web-browser of any web-enabled device. Here, the user will be able to input the essential data required by the tool through a series of intuitive fields varying from value fields to database selection.

In its current state, a total of 25 inputs are required from the user, divided in 20 values and 5 database selections, once all the fields are filled the user will be able to send the data to the server to start the simulation process.

The input interface is divided into 5 categories:

- General Data: Contains general information on the building, for a total of 1 value and 2 database selections;
- Geometric Data: containing details on the shape and size of the building for a total of 6 values and 1 database selection;
- Windows Data: containing details related to the transparent surfaces, for a total of 4 values and 1 database selection;
- Construction Data: containing details on the materials and structure type used within the building, for a total of 1 database selection and 4 values;
- HVAC Data: giving basic details on the HVAC configuration and HR for the simulation, for a total of 5 values.

As the amount of input is extremely limited, and the tool could be used by professionals with limited expertise on the topic, it is particularly important that every field is clearly defined and accompanied by an acceptable amount of details allowing the user to correctly utilize the tool.

For this reason, in the final version of the tool, every field will feature a comprehensive explanatory tag, and will include both visual help and recommended values for different situations.

At the same time, the databases cover the important role of delivering all the information required to the model that is usually not available at the required level of detail during the stages in which the tool is potentially being used.

For this reason, a significant level of thought has been and will be devoted to the definition of comprehensive and suitable database entries able to effectively cover most, if not all the possible cases with limited assumption and approximation.

2.4 The Output Interface

Lastly, the output interface is constituted by a webpage where the results from the simulation are visualized after being elaborated into readily usable information. The data containing relevant graphs and tables is sent directly by the server and visualized on the user device.

Although this could be considered the least research-intensive part of the tool, it is still essential to identify and convey the useful information in a comprehensive and clear way for the final user to understand it. At the same time the information needs to be concise and specific to avoid the risk of less expert users to lose themselves in an unmanageable amount of data.

The authors identified a list of useful information that was included in the interface and is directly visualized on the user device in the form of tables and graphs. An example of those results is shown in Chapter 4 and can be summarized in 3 groups:

- Monthly Energy Needs for Heating and cooling: useful to immediately understand the performance of the building in terms of consumption and to compare different design options;
- Thermal power curves for heating and cooling needs: essential as a starting point for plant design and feasibility analysis of different plant options;
- Hourly temperature variation for a Winter and Summer Typical week: useful to form a qualitative idea of the internal comfort conditions and

to compare different design choices in term of user comfort.

Lastly, both the output .csv file obtained from the EnergyPlus simulation and the .idf file containing the model used for the simulation, are given to the user as an optional download. The user is therefore able to perform more detailed analysis either by post-processing the already generated output from the simulation or, for more expert users, to add elements to the simulation itself to perform a more detailed analysis, e.g., by following the development of the building design while new information becomes available. The option of generating an automated report including all the results in a readily presentable form is currently under evaluation. The option to visualize an internal comfort chart for the building is currently under discussion as the simplified nature of the tool can only allow for a qualitative evaluation of comfort conditions and cannot consider localized effects that could greatly influence it. Nonetheless even a qualitative information on comfort condition could be of great use while comparing different design choices to identify the best option not only in terms of energy use but in terms of the building performance in general.

3. Validation and Case Studies

As mentioned at the beginning of the paper, one of the most important aspects of this research has been the focus on accuracy, although limited by the necessity of using simplified models. As mentioned, a simplified screening tool such as the one proposed here, still needs to ensure an adequate level of accuracy, although lower when compared to a detailed building simulation due both to its nature and its purpose, being used when a detailed simulation is not possible or feasible due to time and information constraints.

Validation was therefore approached in two different phases: validation of the simplified model and validation of the simplified tool. A third phase associated with the validation of the simulation code is deemed unnecessary thanks to the use of EnergyPlus, a well-known and reliable simulation code (Crawley et al., 2004; Henninger and Witte, 2010).

The validation of the simplified model has been performed following its definition and extensively discussed in previous publications (Picco et al., 2015). During this study, three different buildings were selected and modelled, both through the use of the simplified model and a detailed model using all available information. The detailed model was calibrated thanks to the use of historic data and for each analysed case, the difference in results in terms of heating and cooling energy needs and heating and cooling peak power was verified to be below the threshold of 20 %. This threshold was derived by the authors based on market expectations and, although not directly related, the recommended acceptable value of mean bias error for detailed and calibrated simulation models as presented in the Measurement and Verification guidelines from DOE (DOE, 2008) equal to 10 %.

Following the initial validation, the simplified model was applied to a number of other buildings to evaluate their energy performances. When suitable, a detailed model was also simulated, for validation and research purposes. For each case, the difference between simplified and detailed model, in terms of heating and cooling energy needs and peak power needs always resulted under the aforementioned 20 % margin; a further confirmation of the validity of the simplified model.

The second part of the validation process focuses instead on the tool itself, verifying that the automatic model generator is able to correctly recreate the simplified model of a building starting from the data of the input interface, and at the same time the output post-processor is able to correctly recreate useful information both in numerical and graphical form.

This phase of the validation process is currently undergoing, in parallel with the finalizing and improvement of the user interface, although initial results can be seen in the following chapter through an example of application of the tool, proving that both the model generator and output post-processor work correctly, as expected.

4. Example of Application

As an example of the application of the presented tool in its current form, the Castelli clinic building was selected. The building is one of the case studies used during the definition of the simplified model; we are therefore able to verify the tool is correctly creating the simplified model and compare the obtained results to the ones of the detailed model, developed for the validation of the simplified model results.

The building, located in Bergamo, is considered a medium-large building with an approximate floor area of 5000 m² on a total of five floors. Built before the second Great War, and currently used as a hospital, the building is characterized by poor thermal performances of the envelope and old plants.

The building data summarized in Table 1 is input in the simulation tool's user interface through relevant database selections and the direct input of values. Names of the specific inputs are coded in the table based on their category as the authors decided to not divulge them prior to the official launch of the tool.

The simulation is then launched from the same interface. Following this, as previously detailed, the information is sent to the simulation core, where the pre-processor generates the EnergyPlus input file and performs the simulation. Results from EnergyPlus are then loaded by the post-processor and elaborated to generate readily usable information.

Although the amount of data that could be obtained from EnergyPlus is extremely large in size and variety, a series of essential details were identified as the most important to be directly shown to the user through the output interface.

Table 11 – Input data for application example

Entry	Value	Unit
GENERAL_DATA_1	Bergamo [IT]	-
GENERAL_DATA_2	-70.8	°
GENERAL_DATA_3	Hospital	-
GEOMETRIC_DATA_1	4	-
GEOMETRIC_DATA_2	53.4	m
GEOMETRIC_DATA_3	83.5	m
GEOMETRIC_DATA_4	3.5	m
GEOMETRIC_DATA_5	1124	m ²
GEOMETRIC_DATA_6	Yes	-
GEOMETRIC_DATA_7	Hospital	-
WINDOW_DATA_1	Double Clear	-
WINDOW_DATA_2	59.1	m ²
WINDOW_DATA_3	230.4	m ²
WINDOW_DATA_4	130.3	m ²
WINDOW_DATA_5	125.0	m ²
CONSTRUCTION_DATA_1	Masonry	-
CONSTRUCTION_DATA_2	1.60	W/m ² K
CONSTRUCTION_DATA_3	1.65	W/m ² K
CONSTRUCTION_DATA_4	1.21	W/m ² K
CONSTRUCTION_DATA_5	1.65	W/m ² K
HVAC_DATA_1	22.5	°C
HVAC_DATA_2	28.0	°C
HVAC_DATA_3	18.0	°C
HVAC_DATA_4	28.0	°C
HVAC_DATA_5	0.0	%

Figs 3 to 6, shown below, exemplify the current visual output obtained by the user through the output interface following the execution of the simulation. Fig. 2 shows a monthly summary of heating and cooling energy needs of the building through stacked bars, coupled with the monthly average outdoor

temperature as a reference. This graph, coupled with optional tabular data gives a good representation of the energy performances of the simulated building.

Fig. 3 shows the Thermal power curves of the system, for both heating and cooling, this is useful information to select the optimal plant configuration and size, and to estimate the annual hours of activity of a different plant equipment.

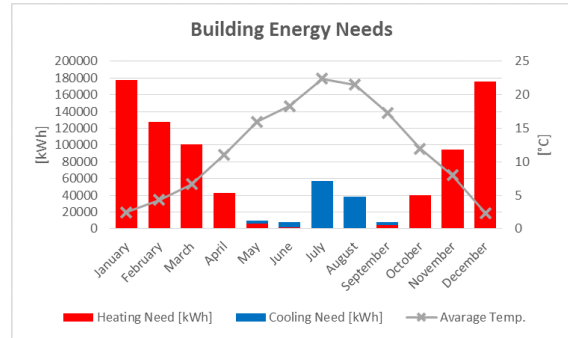


Fig. 2 – Output: Monthly Energy Needs

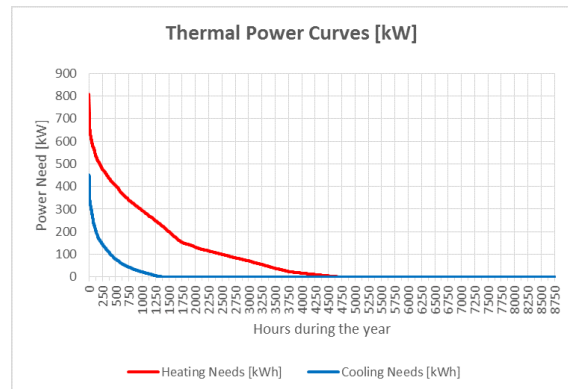


Fig. 3 – Output: Thermal Power Curves

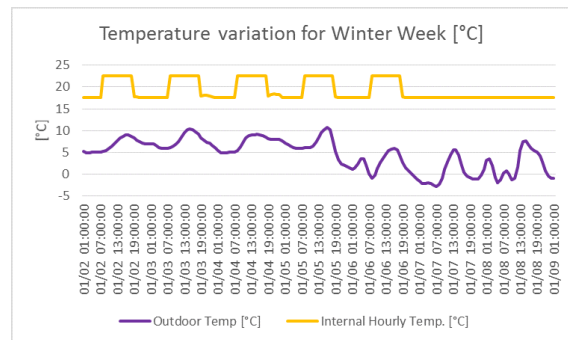


Fig. 4 – Output: Hourly Temperature Variation for Winter Week

Figs 4 and 5, respectively, show the hourly temperature variation for a zone within the building for a typical winter and summer week, coupled with

the outdoor temperature. Those graphs are useful for the user to immediately have an idea of the thermal conditions within the building and the operation of the systems.

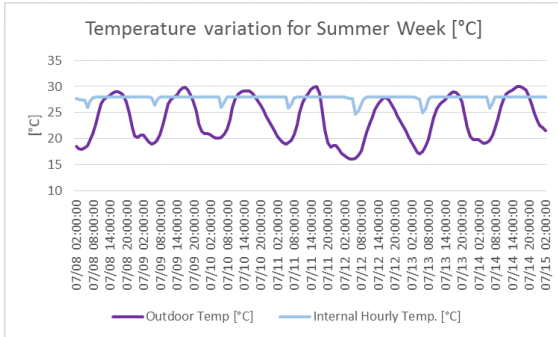


Fig. 5 – Output: Hourly Temperature Variation for Summer Week

Finally, the results in terms of total heating and cooling needs, are reported in Table 2 below to compare results obtained by the tool with the ones obtained from the simplified and detailed model previously developed and discussed in previous papers.

Table 12 – Comparisons between models

Model	Heating [kWh]	Cooling [kWh]
Tool	769473	110219
Simplified Model	774493	126788
Detailed Model	791075	128102

As evident by the table, the tool delivers the same results as the simplified model, which confirms that the model generation and post-processing algorithms have been implemented correctly in the tool; and starting from the input data, the generated model is equivalent to the manually created simplified model.

5. Conclusions

As we are moving toward a carbon free future, our buildings are becoming increasingly more complex, due to the constantly increasing performance requirements and new surfacing technologies. As a consequence, the design of the building is becoming

an increasingly complex process, that requires additional expertise and attention to energy and performance issues.

Building performance simulation could be considered a possible solution, however, a gap is still present between the available tools and the needs of the design process during the first stages of the building design, due to the lack of available time and information.

The proposed screening tool aims to fill this gap by providing a quick and simple way to perform simplified dynamic performance simulations with minimum time commitment and information required to identify preferable design choices during the early stage design and feasibility studies. Thanks to the use of a validated simulation code EnergyPlus and a purposely developed simplified description model, the tool is able to deliver results within an acceptable margin of difference compared to the detailed simulations, within the 20 % difference on all evaluated case studies.

The tool is currently being delivered in its initial form and it focuses on the most essential design parameters such as the envelope, materials, and basic HVAC parameters. Once the first version is fully operational, various possible developments are under evaluation, such as the inclusion of specific building features, the expansion of the plant side of the model, and the inclusion of renewable technologies. The inclusion of optimization techniques such as genetic algorithms is under evaluation, too. Meanwhile databases will be constantly expanded to cover for a larger range of options.

The authors believe, based on the obtained results, their personal experience in the field of building performance simulation, and the market expectations, that the proposed tool will have a significant impact on the integration of computer simulation during the early-stage design and feasibility study, providing useful information and fuelling the constant improvement in building performance.

Nomenclature

Symbols

GHG	Greenhouse Gas
ZCB	Zero Carbon Buildings
ZEB	Zero Energy Buildings
NZEB	Net Zero Energy Buildings
nZEB	Nearly Zero Energy Buildings
EPBD	European Performance of Buildings Directive
IDP	Integrated Design Process
BPS	Building Performance Simulation
HR	Heat Recovery
SGHC	Solar Heat Gain Coefficient
CSV	Comma Separated Value
IDF	EnergyPlus input data files

References

- Chen, A. 2009. *Working Toward the Very Low Energy Consumption Building of the Future*. <http://newscenter.lbl.gov/2009/06/02/working-toward-the-very-low-energy-consumption-building-of-the-future/>.
- Crawley, D.B., L.K. Lawrie, C.O. Pedersen, F.C. Winkelmann, M.J. Witte, R.K. Strand, R.J. Liesen, W.F. Buhl, Y.J. Huang, R.H. Henninger, J. Glazer, D.E. Fisher, D.B. Shirey, B.T. Griffith, P.G. Ellis, L. Gu. 2004. "EnergyPlus: An Update". In: *Proceedings of SimBuild 2004*.
- DOE. 2008. *U.S. DOE M&V Guidelines: Measurement and Verification for Federal Energy Project, Version 3.0*.
- DOE. 2009. *Exec. Order No. 13514 (2009). Executive Order 13514—Federal Leadership in Environmental, Energy, and Economic Performance*.
- Economidou, M. 2011. *Europe's buildings under the microscope. A country by country review of the energy performance of buildings*. Buildings Performance Institute Europe (BPIE).
- European Parliament. 2010. *Directive 2010/31/EU of the European parliament and of the council, of 19 May 2010 on the energy performance of buildings (recast)*. Brussels, Belgium: European Parliament.
- Ferrero, A., E. Lenta, V. Monetti, E. Fabrizio, M. Filippi. 2015. "How to apply building energy performance simulation at the various design stages: a recipes approach". In: *Proceedings of BS2015: 14th Conference of International Building Performance Simulation Association*. Hyderabad, India: IBPSA.
- Henninger, R.H., M.J. Witte. 2010. *EnergyPlus Testing with Building Thermal Envelope and Fabric Load Tests from ANSI/ASHRAE Standard 140-2007*. Washington, U.S.A.: DOE.
- Hensen, J. 2004. "Towards more effective use of building performance simulation in design". In: *Proceedings of the 7th International Conference on Design & Decision Support Systems in Architecture and Urban Planning*.
- Picco, M., R. Lollini, M. Marengo. 2014. "Towards energy performance evaluation in early stage building design: A simplification methodology for commercial building models". *Energy and Buildings* 76: 497-505. doi: 10.1016/j.enbuild.2014.03.016.
- Picco, M., M. Marengo. 2015. "On the impact of simplifications on building energy simulation for early stage building design". *Journal of Engineering and Architecture* 3(1):66-78.
- Uttinger, D.M., D.E. Bradley. 2009. "Integrating energy simulation in the design process of high performance building: a case study of the Aldo Leopold Legacy center". In: *Proceedings of Building simulation 2009*. Glasgow, UK: IBPSA.

On the Influence of Storage Size and Management on the Consumption of Air Source Heat Pumps in High Performance Buildings

Elena Bee – University of Trento – elena.bee@unitn.it

Alessandro Prada – University of Trento – alessandro.prada@unitn.it

Paolo Baggio – University of Trento – paolo.baggio@unitn.it

Abstract

Air-source heat pumps can be coupled with photovoltaic panels, a water storage tank and low temperature hydronic terminals (radiant floor) with the purpose of using renewable sources for domestic heating. Some kind of storage solution is required since the availability of solar energy is most of the time out of sync with the heating needs. In principle the energy storage could take place in water filled storage tanks, acid-lead batteries, and in the building envelope. The thermal capacity of the storage tank depends on the tank size and it could affect the performance of the system. Hence, the system management strategy should consider such inertia in order to correctly control the system, also by taking into account the current availability of solar energy.

This work investigates whether the correct sizing of the water storage tank and its correct management can increase the energy self-consumption and, consequently, the renewable share of the primary energy used. The work analyses the behaviour of such a system configuration during the heating season in different climate conditions. Four European climates and two types of building envelopes, with different thermal capacities (timber and concrete), were considered.

Results show that a control logic oriented to self-consumption can significantly reduce the energy taken from the power grid, with respect to the more typical control systems that reset the supply temperature based on the outdoor temperature. However, increasing the tank size in the range of the typical installations has only a slight effect on the percentage of self-consumed energy. In the case of the control strategy that includes outdoor temperature reset, it was found that this percentage does not change, regardless of the tank size.

1. Introduction

Air-to-water heat pumps have an increasing share in the European heating market. According to the European Heat Pump Market and Statistics Report 2015 (EHPA, 2015), they represent the fastest growing heat pump segment across Europe. The performance of the average commercial products has consistently improved in recent years both at nominal operating conditions and part load conditions, the latter because of the adoption of the inverter-driven compressors.

Moreover, air-source heat pumps (ASHP) will have an important role in order to fulfil the requirements of covering primary energy consumption using renewable energy sources, since the aerothermal energy is considered a renewable source by the Italian Legislative Decree 28/2011 and by the European directive 2009/28/EC. The renewable percentage of energy consumption further increases in the case that a share of the electric input energy comes from a photovoltaic system.

The performance of the heating system depends on many parameters. The thermal inertia of the storage tank (i.e. tank size) could be one of these. Other authors (Arteconi et al., 2013) found that with regard to the established sizing procedures, there is no need for larger storage, except in the case of large PV sizes or highly fluctuating electricity prices. It was also found (Alimohammadisagvand et al., 2016) that with small tank sizes, both the electric consumption and the life cycle cost of the thermal energy storage are lower. However, in literature few works have focused on the increment of the PV self-consumption in high performance buildings.

Moreover, the influence of storage tanks in the performance of heating systems with ASHP has been scarcely investigated in the literature.

This work investigates whether the correct sizing of the water storage tank and its correct management can increase energy self-consumption. The work analyses the behaviour of such a system configuration during the heating season in different climate conditions. Four European climates and two types of building envelopes, with different wall thermal capacitance were considered.

2. Methods

2.1 Simulation Layout

A coupled simulation of the simplified reference building and its heating system was set up in the TRNSYS simulation suite. The reference building is a well-insulated semi-detached house (Fig. 1), presented in Penna et al. (2015). In this work the reference building was modified to consider the influence of the thermal capacitance of the building envelope, consequently, concrete block and timber envelope were considered, respectively with an internal areal capacity of $50.6 \text{ kJ m}^{-2} \text{ K}^{-1}$ and $36.5 \text{ kJ m}^{-2} \text{ K}^{-1}$. In both cases, the walls have a thermal transmittance of $0.29 \text{ W m}^{-2} \text{ K}^{-1}$, according to the EN ISO 13786 procedure.

The heating system is based on an air-to-water heat pump with a variable speed compressor and coupled with a photovoltaic array. The system is combined with a reference building with radiant floor. The model was set up in the TRNSYS simulation suite (Fig. 2). Standard and TESS libraries are used for many of the system components, whereas a subroutine was adapted to simulate the part load operation of the ASHP, in order to model the behaviour of the latest generation machines (Bee et al., 2016). The tank model is a stratified liquid storage tank with two inlet and two outlet flows and no internal heat exchangers. The tank is a vertical cylinder and its height was calculated in order to maintain the same shape while varying the volume. The model includes calculation of losses from the tank to the ambient and assumes that all stratification nodes of the tank are uniform in size. The loss coefficient per

unit area was set equal to $0.35 \text{ W m}^{-2} \text{ K}^{-1}$ on the base of the average market product performance.

The part-load operation of the ASHP is described by a function that can be considered representative of the last generation units. The part load and full load performance data are given as inputs to the ASHP model and the instantaneous behaviour depends on the outdoor condition and the required thermal power. The heat pump was sized in order to cover the peak load without auxiliary generators. That results in different HP sizes for different climates and/or buildings.

The radiant floor was modelled with an “active layer” (TRNSYS documentation, 2012). The design specifications are referred to a commercial configuration with 0.12 m pipe spacing and PEX pipes with a diameter of 0.016 m, a thickness of 0.002 m and a thermal conductivity of $0.44 \text{ W m}^{-1} \text{ K}^{-1}$.

The heating system is powered by either grid or photovoltaic electric power in an “UPS like mode” avoiding battery operation in parallel with the grid. Hence, the system is re-connected to the grid only when the battery has been completely discharged. In the morning, the photovoltaic generated power is used to charge the batteries. As soon as the batteries have been charged, the system uses the residual photovoltaic power, if still available, and then it exploits the stored energy until it is finished. The photovoltaic array is made of 12 modules with an area of 1.6 m^2 each. The total generated energy depends on the radiation input and it changes for the different studied climates.

Four European cities were considered in order to broaden the validity of the results. The simulation code read the weather data for the investigate cities that are Helsinki (Finland), Berlin (Germany), Milan and Rome (Italy). These climates are classified respectively as 6A, 5C, 4A and 3C, according to the ASHRAE 90.1 classification. From each TRY, a six-months period (October 15 – April 15) was selected for the simulations.

2.2 Management Approaches

The water supply to the radiant floor is controlled by means of the thermostat signal (setpoint at 20°C ,

proportional band of 1°C). The flow rate varies linearly between 100 and 400 kg h⁻¹.

Two management approaches were implemented in the simulation layout in order to investigate the possibility to increase the renewable coverage factor during the heating period. The heat pump is controlled setting the desired supply temperature, by means of either:

- a. an outdoor temperature reset (OTR) of the supply temperature;
- b. a logic that considers a constant supply temperature when the delivered energy comes from the grid whereas a higher temperature when self-produced energy is used (batteries discharging or directly from the panels). That will be called a self-consumption-oriented logic (SCO).

The control system ensures an indoor temperature between 19.5 °C and 23 °C.

2.3 Storage Volumes

Simulations were performed for the four mentioned climates, the two types of envelopes, five tank sizes (in the range of 100 to 1000 litres), and with the two management strategies. The lower storage volumes (up to 500 litres) correspond to the typical tank sizes in residential single unit applications. The range was extended to 1000 litres in order to explore potential benefits from a larger storage, even if those solutions are not easily applicable in practice.

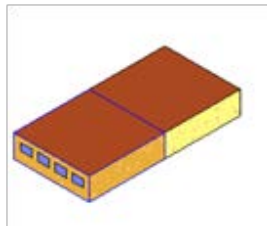


Fig. 1 – Reference building

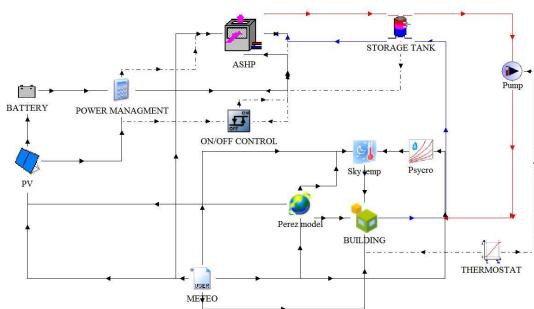


Fig. 2 – Layout of the simulations in TRNSYS Simulation Studio

3. Discussion and Result Analysis

The results of the analyses are the energy consumption of the ASHP and the PV power production use for the heating system. These results are obtained on an hourly basis as shown in Fig. 3.

3.1 Management Approaches

We compared the management approaches, in the cases with a storage volume of 300 litres and 700 litres. The SCO approach increases the self-consumption percentage with regard to the OTR logic, in all the simulations (Fig. 4). With reference to a tank size of 300 litres, the maximum increase is 10 %. That is a consequence of two main facts. First, although the supply temperature range is the same for the two control approaches, with the SCO one the lower supply temperature is more frequent over the season and that results in a more efficient operating condition for longer time (higher COP). Second, the heat pump is turned off (no consumption) for some hours over the season, with a frequency that does not depend on the time of the day or the outdoor temperature (as shown in Fig. 3), but it is rather linked to the radiation and the batteries capacitance. It is necessary to point out that the mentioned increase of self-consumption percentage means, simultaneously, a reduction of total energy needs and an increase of the self-produced share.

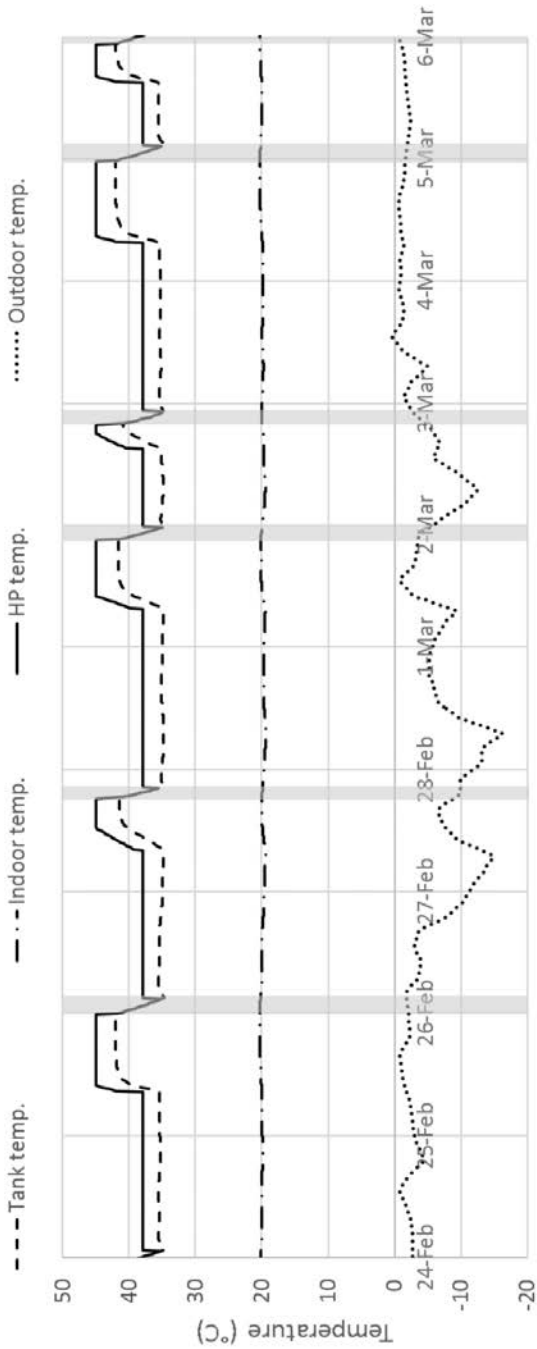
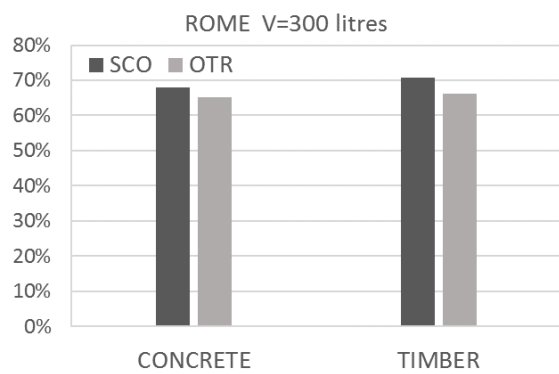
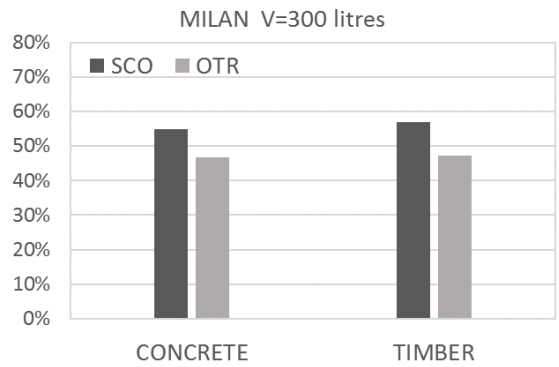
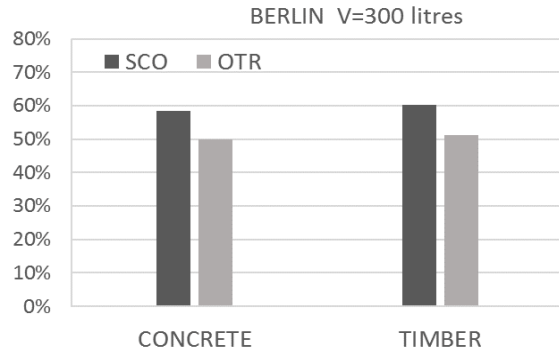
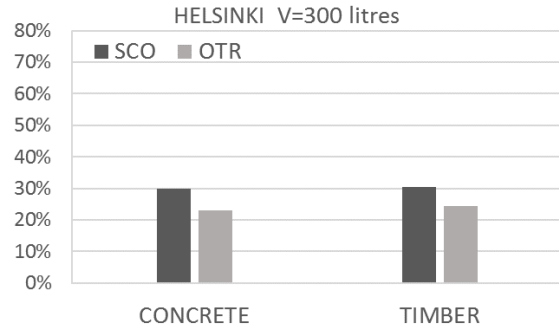


Fig. 3 – Sample of a simulation with the climate of Helsinki and the concrete envelope. The figure is intended to show the behaviour of the system (heat pump and tank) with the SCO management. The shaded areas correspond to the stages in which the HP is off: in these hours the HP supply temperature overlaps the tank temperature (no thermal power is transferred to the water). In the preceding hours the stored water has been overheated using the self-produced energy



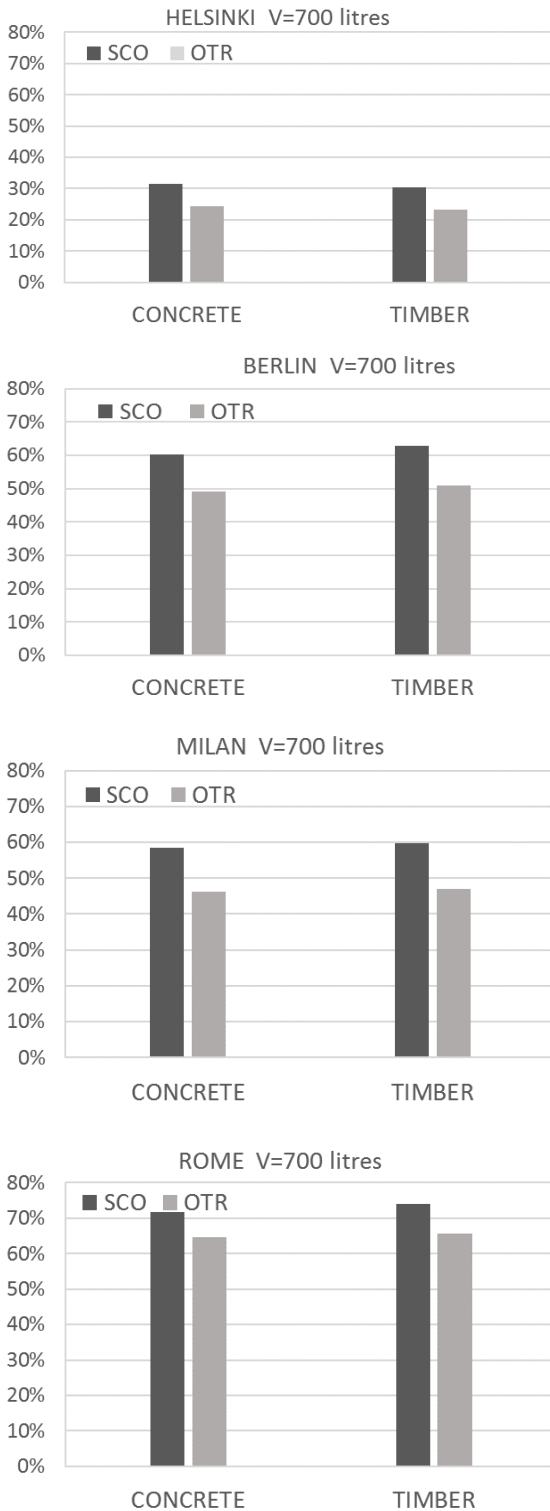


Fig. 4 – Comparisons in terms of self-consumption percentage between the two management approaches: the self-consumption oriented logic (SCO) and the outdoor temperature reset (OTR); results presented with the tank volume equal to 300 litres e 700 litres, for the four climates and the two envelope types

3.2 Storage Volume

The second aspect we analysed is the impact of the storage volume. We found that it does not have any impact on the OTR logic (as can be deduced by comparing the graphs for 300 litres and 700 litres in Fig. 4) and only a moderate impact with the SCO logic. For this second case, results are shown in Fig. 5. The differences reach a 9 % (maximum) increase between 100 and 1000 litres, but only 3 % between 100 and 500 litres, which is a more likely range for the typical residential installations. Here, the increase of the self-consumption percentage is the net effect of a slight increase of total energy needs (1 % for Helsinki, 2 % for Berlin and Milan, and 3 % for Rome) as shown in Fig. 6, and a great increase of the self-produced energy (up to 15 % for the climate of Rome).

Finally, it is interesting to notice some differences between the timber and the concrete envelopes, in average, the systems with a timber envelope seem to take greater advantage from the increase of the tank size (Fig. 5). That is to be expected, since the wooden ones have a lower thermal capacity.

4. Conclusions

This paper is a simulation work on the influence of the storage size and management in air-source heat pump systems for residential space heating, integrated with a photovoltaic array. We compared two management approaches and results show that a very simple logic oriented to self-consumption can significantly reduce the use of energy from the grid. Regarding the tank size, we found that, among the investigated cases, a 500-litre tank allows a maximum of 3 % increase of self-consumption share with respect to a 100-litre tank, and that gain also includes a slight increase of the total consumption. Hence, increasing the storage size does not lead to significant benefits in terms of energy saving.

The findings of this study will be further investigated, in particular the system will be integrated with a more sophisticated management strategy that may include a scheduled working rate of the system, also depending on the occupants' behaviour. By means of an optimization we will also

analyse the effect of some parameters such as the heat pump characteristics or the PV and battery sizes.

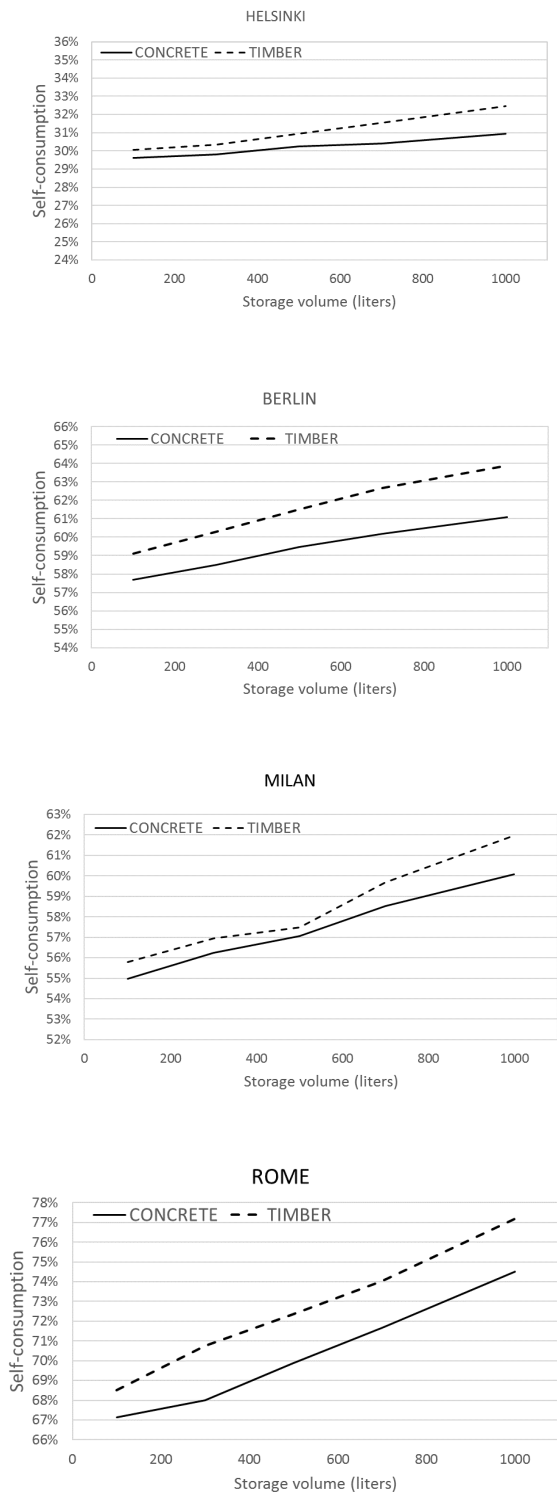


Fig. 5 – Variation of the self-consumption percentage as a function of the storage tank size (volume) for the timber and concrete envelopes and with the SCO strategy

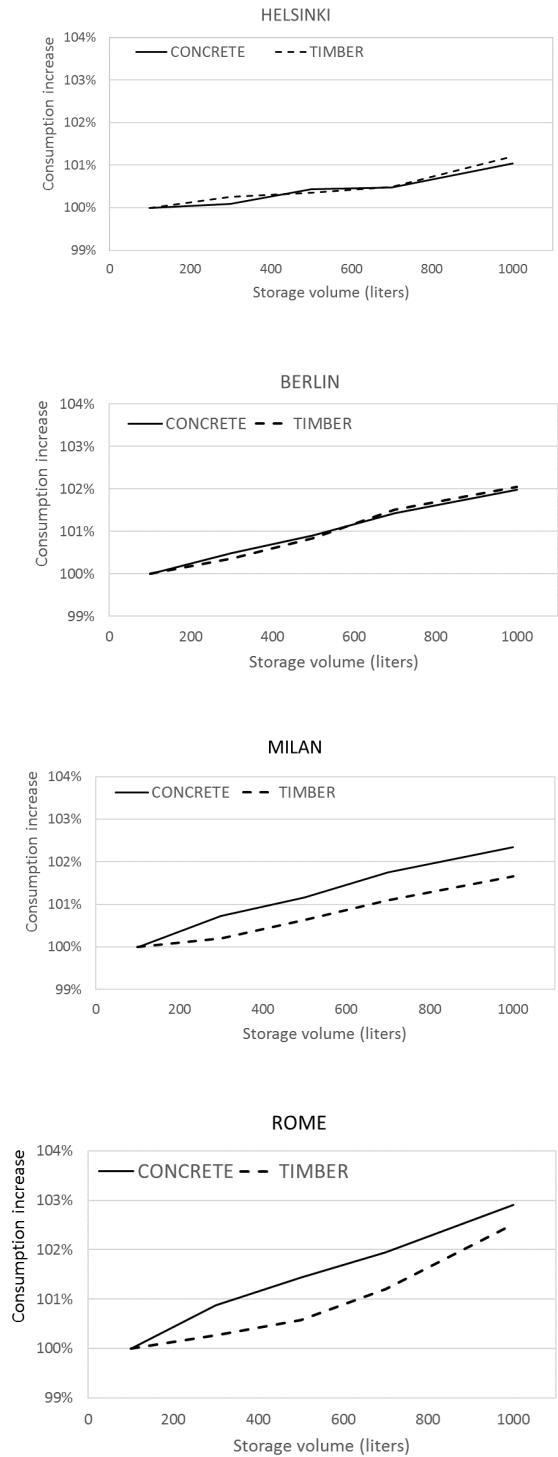


Fig. 6 – Variation of the consumption as a function of the storage tank size (volume) normalized on the case with the lower storage volume (100 litres). Simulations with the SCO strategy

References

- Arteconi, A., N.J., Hewitt, F. Polonara. 2013. "Domestic demand-side management (DSM): Role of heat pumps and thermal energy storage (TES) systems". *Applied Thermal Engineering* 51: 155-165. doi: 10.1016/j.applthermaleng.2012.09.023.
- ASHRAE 2007. *ASHRAE 90.1. 2007. Energy standard for buildings except low rise residential buildings. Technical report*. Atlanta, U.S.A.: ASHRAE - American Society of Heating, Refrigerating, and Air-Conditioning Engineers.
- Alimohammadisagvand, B., J. Jokisalo, S. Kilpeläinen, M. Ali, K. Sirén. 2016. "Cost-optimal thermal energy storage system for a residential building with heat pump heating and demand response control". *Applied Energy* 174: 275–287. doi: 10.1016/j.apenergy.2016.04.013.
- Bee, E., A. Prada, P. Baggio. 2016. "Variable-speed air-to-water heat pumps for residential buildings: evaluation of the performance in northern Italian climate". In: *Proceedings of the 12th Rehva World Congress*. Aalborg, Denmark: DTU.
- CEN. 2007. *EN ISO 13786 - Thermal performance of building components - dynamic thermal characteristics calculation methods*. Brussels, Belgium: European Committee for Standardization.
- EHPA. 2015. *European Heat Pump Market and Statistics Report 2015*. EHPA, European Heat Pump Association.
- Penna, P., A. Prada, F. Cappelletti, A. Gasparella. 2015. "Multi-objectives optimization of Energy Efficiency Measures in existing buildings". *Energy and Buildings* 95: 57–69. doi:10.1016/j.enbuild.2014.11.003.

Energy Refurbishment of Social Housing Stock in Italy: Analysis of Some Scenarios from the Impact of Climate Change to Occupant Behaviour

Leone Pierangioli – University of Florence – leone.pierangioli@unifi.it

Cristina Carletti – University of Florence – cristina.carletti@unifi.it

Gianfranco Cellai – University of Florence – gianfranco.cellai@unifi.it

Fabio Scieurpi – University of Florence – fabio.sciurpi@unifi.it

Abstract

In the period from the '40s to the late '70s, Italy implemented an extensive public social housing plan (INA-CASA and GESCAL) that is widely representative of the national residential building stock. Obviously, its energy performance is extremely poor and its refurbishment plays a key role in the national targets of GHG emissions reduction.

For these reasons, through historical research and survey of 145 social housing buildings, a building typology matrix with six-reference buildings has been developed following the IEE TABULA project method. Some typical refurbishment measures have been analysed, in term of global costs and total primary energy demand, considering different economics and climate change scenarios. The research has been carried out for Tuscany, central Italy, using both weather data sets for inland (Florence) and seaside (San Vincenzo). The input assumptions consider a constant thermal comfort level, in order to identify the measures that can provide comfort conditions to the occupants with the lowest value of energy demand. The results of this study, taking into account the impact of global warming on the Mediterranean climate, the high thermal inertia of typical buildings, and different user's behaviours, show that the combination of measures with advanced and standard performance level can be considered optimal in terms of global costs reduction.

1. Introduction

The European Directive 2010/31/EU, which aims to reduce energy consumption and the environmental impact of buildings, was implemented with the

identification of a set of reference buildings, representative of the national stocks of the member states, through the TABULA research project followed by the EPISCOPE project (IWU, 2016).

In Italy, the TABULA research project (Corrado et al., 2014) defined the typological and technological characteristics of the reference buildings on the basis of the Piedmont Region building stock.

According to the common European methodology (European Commission, 2012) several combinations of energy efficiency measures have been applied to reference buildings in order to identify the optimal solutions under a cost-benefit profile. Finally, the results were used to issue the Italian decree 26/6/2015 on the minimum energy performance requirements for different types of intervention and the building energy rating system.

The most critical aspects of the application of the European methodology are:

- representativeness of the regional reference buildings compared to the national buildings stock;
- the energy performance calculation doesn't consider climate change, though the economic analysis is performed over the service life of the reference buildings;
- EN ISO 13790:2008 seasonal calculation methods (quasi-steady state) could fail in precisely evaluating the effects of high thermal inertia of the typical Italian residential buildings.

This research, starting from the European methodology framework (European Commission, 2012), has addressed these three aspects by taking into

account a new set of reference buildings and climate change projections for Tuscany in central Italy.

2. Reference Buildings

Two major plans of social housing construction were activated in Italy, from 1949: INA-CASA (1949-1963) and GESCAL (1963-1973) that continued until the '80s (Acocella, 1980; Capomolla and Vittorini, 2003). INA-CASA buildings are characterized by very simple construction technologies and the most common types of buildings are the detached multifamily house and its combination in larger apartment blocks (INA-CASA, 1949).

From these premises, we selected a sample of 145 multi-family houses and apartment blocks, constructed in Pistoia (Beneforti and Ottanelli, 2012) between 1946 and 1977 under the INA-CASA and GESCAL plans.

This sample was analysed following the methodology developed for the TABULA and EPISCOPE projects that conform to the national housing census classification (ISTAT, 2011). By means of statistical analysis a strong correlation between A_e and V_G ($R^2 = 0.93$) and A_w and A_f ($R^2 = 0.83$) was observed and the dependence of space heating and cooling demands on these geometrical parameters was analysed. Starting from the results at this preliminary stage (Pierangioli and Cellai, 2016), the Building Type Matrix shown in Table 1 was developed by arranging the sample into two historical periods characterized by different construction technologies (from 1946 to 1960 with 67 buildings, and from 1961 to 1977 with 78 buildings), and three building size classes based on V_G and the number of apartments (Pierangioli and Cellai, 2016). Tables 2 and 3 show the Building Type Matrix envelope construction technologies and the HVAC system typologies.

The data derived from the TABULA project database (Corrado et al., 2014), local INA-CASA and GESCAL archives, and technical references (UNI, 2014-a).

Table 1 – Building Type Matrix (Pierangioli and Cellai, 2016)

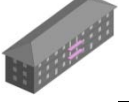
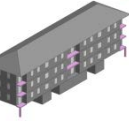
		DIMENSIONAL CLASS		
		(1) SMFH $V_G \leq 2700$ $nU \leq 8$	(2) MMFH $2700 < V_G < 4800$ $8 < nU \leq 15$	(3) AB $V_G \geq 4800$ $nU > 15$
(1) 1946 1960		Type 1.1	Type 1.2	Type 1.3
				
		sample size: 26 buildings	sample size: 28 buildings	sample size: 13 buildings
		6 apartments $A_f=496.2 \text{ m}^2$ $V_G=1987.0 \text{ m}^3$ $A_e/V_G=0.6 \text{ m}^{-1}$ $A_w=79.1 \text{ m}^2$ $A_w/A_f=0.16$	12 apartments $A_f=872.4 \text{ m}^2$ $V_G=3428.2 \text{ m}^3$ $A_e/V_G=0.54 \text{ m}^{-1}$ $A_w=129.6 \text{ m}^2$ $A_w/A_f=0.15$	24 apartments $A_f=1618.8 \text{ m}^2$ $V_G=6293.7 \text{ m}^3$ $A_e/V_G=0.47 \text{ m}^{-1}$ $A_w=266.0 \text{ m}^2$ $A_w/A_f=0.16$
		Type 2.1	Type 2.2	Type 2.3
				
(2) 1961 1977		sample size: 30 buildings	sample size: 26 buildings	sample size: 20 buildings
		6 apartments $A_f=485.7 \text{ m}^2$ $V_G=1893.1 \text{ m}^3$ $A_e/V_G=0.61 \text{ m}^{-1}$ $A_w=89.7 \text{ m}^2$ $A_w/A_f=0.18$	12 apartments $A_f=954.3 \text{ m}^2$ $V_G=3697.5 \text{ m}^3$ $A_e/V_G=0.58 \text{ m}^{-1}$ $A_w=176.4 \text{ m}^2$ $A_w/A_f=0.18$	16 apartments $A_f=1633.2 \text{ m}^2$ $V_G=6201.9 \text{ m}^3$ $A_e/V_G=0.50 \text{ m}^{-1}$ $A_w=286.4 \text{ m}^2$ $A_w/A_f=0.18$
	(1) Small Multi-Family House (2) Medium Multi-Family House (3) Apartment Block			

Table 2 – Thermal properties of building envelope components

	BLDG. TYPES 1.1, 1.2, 1.3	BLDG. TYPES 2.1, 2.2, 2.3
External walls	Load bearing brick and stone masonry no thermal insulation $U=1.55 \text{ W}/(\text{m}^2 \text{ K})$	Multilayer masonry (hollow brick, air gap, hollow brick) no thermal insulation $U=1.25 \text{ W}/(\text{m}^2 \text{ K})$
Semi-exp. walls	Load bearing brick masonry; $U=1.80 \text{ W}/(\text{m}^2 \text{ K})$	Hollow brick masonry; $U=1.60 \text{ W}/(\text{m}^2 \text{ K})$
Floors and ceilings	Reinforced brick concrete slab no insulation: - external floor: $U=1.70 \text{ W}/(\text{m}^2 \text{ K})$ - semi-exposed floor: $U=1.40 \text{ W}/(\text{m}^2 \text{ K})$ - semi-exposed ceiling: $U=1.75 \text{ W}/(\text{m}^2 \text{ K})$	
Roof	Pitched roof with brick-concrete slab; $U=2.00 \text{ W}/(\text{m}^2 \text{ K})$	
Basement	Concrete floor on soil; $U=2.20 \text{ W}/(\text{m}^2 \text{ K})$	
Window glass	Double 3-6(air)-3 clear glazing; Wood frame; $U_w= 3.1 \text{ W}/(\text{m}^2 \text{ K})$; $g = 0.76$;	

Table 3 – HVAC system of reference buildings

	BLDG. TYPES 1.1, 1.2, 1.3	BLDG. TYPES 2.1, 2.2, 2.3
Heating	Traditional gas boiler (individual system); hot water radiators (70 °C/60 °C) with zone thermostat	
Cooling	Direct expansion multi-split system (individual system)	
Ventilation	Natural ventilation provided by window opening.	

3. Research Method

3.1 Climate Boundary Conditions

Previous studies (De Wilde and Coley, 2012) highlight the importance of evaluating the climate change impact in order to assess energy refurbishment strategies. For this reason, the climate boundary conditions used in this research incorporate possible results of global warming projections.

In particular, energy simulations were carried out with three different weather data sets. The first was assumed as representative of the current climate up to the year 2035. The other two represent the future climate change, as projected for the periods 2036–65 and 2066–95, within the worst-case Representative Concentration Pathways 8.5 scenario. The current weather data sets used in this study are Test Reference Years built by CTI (Italian Thermotechnical Committee) on the basis of data collected between 2000 and 2009 for the city of Florence, and by ItMeteoData on the basis of data collected between 1990 and 2009 for San Vincenzo. Both locations lie in the Hot Summer Mediterranean climate (Köppen climate classification Csa). The first was chosen to represent the Italian climatic zone D (inland sublittoral climate), the second, as an example of the more mild climatic zone C (coastal climate). The Florence climate, in particular, is interesting because it features one of the hottest summers and coldest winters among the big cities in the central and southern part of Italy. Moreover, HDD and CDD of the Florence weather station are used by ENEA to define the Super Index parameter for the performance evaluation of Italian energy end-use consumption in different economic sectors (ENEA,

2016). HDD and CDD of the current weather data sets are reported in Table 4.

Table 4 – Heating and cooling degree days for the study locations

Site	HDD (20 °C)	CDD (23 °C)
Firenze	2037	277
San Vincenzo	1831	118

The future weather data sets were processed by means of the “morphing” method (Belcher et al., 2005), adjusting the current weather on the basis of the results of high-resolution regional climate model COSMO CLM developed by the Euro-Mediterranean Centre on Climate Change. Future weather data present an annual average temperature higher than current one of 1.8 °C in the medium-term and of 4.3 °C on the long-term for Florence and, respectively, 2.1 °C and 4.5 °C for San Vincenzo.

3.2 Energy Efficiency Measures (EEMs)

The EEMs analysed were selected on the basis of the official data on the energy refurbishment measures that have been mostly applied under the tax benefit programs promoted by the Italian Government since 2006 (Nocera, 2015).

In order to carry out a preliminary analysis, EEMs were applied to Building Type 2.1 and 1.3. Every EEM is characterized by two levels of performance: one moderate level (level 1) which just complies with the Italian Decree 26/6/2015 (minimum energy performance requirements for buildings and building elements) and a second level with advanced energy performance (level 2).

Tables 5 and 6 report the performance parameters, the investment and maintenance costs, and the service life of the different EEMs. In order to take into account the interaction between different measures as, for example, the external envelope thermal insulation that allows the reduction of the boiler size, the selected EEMs were combined in 54 EEMs packages.

Table 5 – EEM on building elements

	LEVEL 1	LEVEL 2
Name	ETI1	ETI2
Ext. walls	EPS insulation layer on the external side	
	<u>Climatic zone C</u> U = 0.40 W/(m ² K) C _I =C _R : 75.5÷77.9 €/m ²	U = 0.24 W/(m ² K) C _I =C _R : 85.2÷87.7 €/m ²
Semi exposed ceiling	Glass wool insulation layer on the upper side	
	<u>Climatic zone C</u> U = 0.34 W/(m ² K) C _I =C _R : 12.2 €/m ²	U = 0.20 W/(m ² K) C _I =C _R : 17.2 €/m ²
Semi exposed and ext. floors	EPS insulation layer on the lower side	
	<u>Climatic zone C</u> U = 0.42 W/(m ² K) C _I =C _R : 65.0 €/m ²	U = 0.24 W/(m ² K) C _I =C _R : 75.6 €/m ²
Name	WDG(S)	WTG(S)
Windows	Double low e. clear glass with wooden frame	
	<u>Climatic zone C</u> U _w = 2.35 W/(m ² K) C _I =C _R : 440 €/m ²	Triple low em. Glass with PVC frame; U _w = 1.1 W/(m ² K) C _I =C _R : 625 €/m ²
Shading	External venetian blind activated from May to September when global solar irradiation on windows exceeds 300 W/m ² (UNI, 2014-b); C _I =C _R : 105 €/m ²	
	Service life of external thermal insulation: 30 years (40 years for ceiling insulation) Service life of windows: 30 years Service life of shading devices: 20 years	

The EEMs combinations include the possibility to leave the current building envelope or HVAC system un-refurbished.

Table 6 – EEM on heating generation system

	LEVEL 1	LEVEL 2
Name	CB	DX
Gen. system	Condensing gas boiler C _I =C _R : 2600 €/apt. CM: 39 €/year*apt. Service life: 20 years	Direct expansion multi-split system C _I =C _R : 5800 €/apt. CM: 232 €/year*apt. Service life: 15 years

3.3 Simulation and Cost Analysis Assumptions

The 54 EEMs packages were simulated by means of dynamic energy simulation software EnergyPlus v.8.0; in order to calculate annual energy carriers demand and total primary energy demand for heating and cooling (kWh/(m² y)) the following assumptions were adopted:

- heating and cooling systems are available 24 h/day and 7 days/week in order to keep operative temperature constant at 20 °C winter and 26 °C in summer;
- constant (00-24 from Monday to Sunday) natural ventilation rate equals to 0.3 h⁻¹;
- simplified calculation of thermal bridges by the increase of the the U-value of the building elements according to technical standard EN ISO 13790:2008;
- internal heat gains from occupants, lighting and appliances are considered constant and equal to 3.0 W/m² (TABULA Project Team, 2013);
- window additional thermal resistance due to night closing of shutters and energy needed for hot water and lighting are not considered;
- the total primary energy demand is calculated by the official Italian conversion factors (2.42 for electricity and 1.05 for natural gas).

In order to identify cost-optimal energy refurbishment strategies, a global cost analysis was carried out for every EEM package, according to the general principles and methodology of the EU Regulation 244/2012 and accompanying guidelines (European Commission, 2012), and according to market-based data. The service life duration and the maintenance costs of building elements and HVAC components were gathered from UNI, 2008, and Di Giulio (1999). The electricity price includes taxes

and ranges from 0.20 (preferential rate for heat pumps) to 0.29 €/kWh. The gas price includes taxes and varies from 0.75 €/Sm³ to 0.81 €/Sm³ depending on the yearly demand (AEEG, 2016). The following assumptions were adopted for the global cost calculation:

- costs related to refurbishment works, which have no influence on the energy performance or do not change between different EEM packages have been omitted;
- disposal costs have not been considered since, in long calculation periods, their influence is marginal due to discounting rate (EU Commission, 2012);
- n° 8 economic scenarios (Table 7) were analysed combining the following assumptions:
 - two calculation periods (building service life): 50 and 80 years;
 - two levels of real discount rate: 3 % and 5 % (EU Commission, 2012);
 - two future trajectories of energy carrier prices: high increase projection (Capros et al., 2010) recommended by the European calculation methodology and updated moderate increase scenario (E3M-Lab, 2016).

Table 7 – Economic scenarios

Scenario	Service life	Energy price increase	Discount rate
1	50 years	moderate	5 %
2	50 years	moderate	3 %
3	50 years	high	5 %
4	50 years	high	3 %
5	80 years	moderate	5 %
6	80 years	moderate	3 %
7	80 years	high	5 %
8	80 years	high	3 %

4. Discussion and Result Analysis

The global cost and the energy performance of the different EEMs packages is shown for:

- Building Type 1.3 with economic scenario 1, which is the most favourable to moderate performance – low initial cost measures (Fig. 1a);

- Building Type 2.1 with economic scenario 8, which is the most favourable to high performance – high initial cost measures (Fig. 1b).

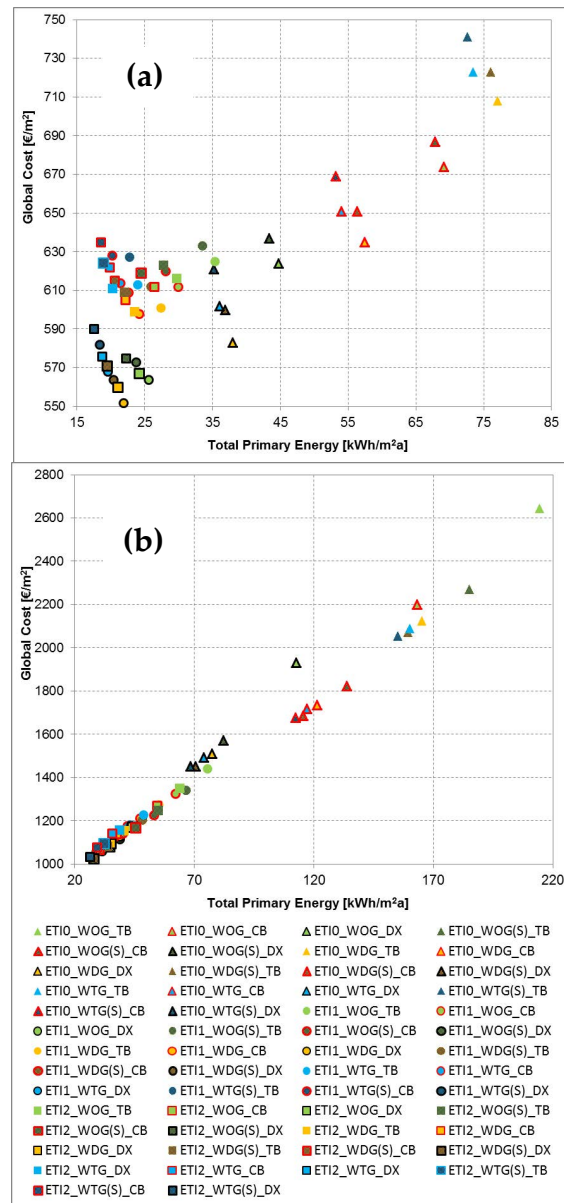


Fig. 1 – (a) building type 1.3 - C_e / EP plots West/East oriented, climatic zone C; (b) building type 2.1, South/North oriented, climatic zone D

Due to mild climate (zone C), South orientation, low V_c/A_e (0.47) and A_w/A_f (0.16) ratios the non-refurbished Building Type 1.3 presents a reduced primary energy need and therefore less sensitivity to redevelopment actions.

The results, shown in Fig. 1a, clearly show that, starting from not very high energy need and considering short-term economic scenarios, the solutions with the

best energy performance do not coincide with the cost-optimal ones; the linear correlation between energy performance and global cost of different EEMs packages is very low. In this case, the cost-optimal solution features a standard level of external thermal insulation, standard windows (double low emissivity glazing), and a direct expansion multi-split system heat pump (ETI1_WDG_DX) with a $C_G = 552.3 \text{ €/m}^2$ and $EP_H + EP_C = 21.9 \text{ kWh/m}^2$.

On the contrary, Building Type 2.1 is more energy-intensive, due to higher V_G/A_e (0.61) and A_w/A_f (0.18) ratios, colder climate (zone D) and unfavourable orientation (high-summer, low-winter solar gains). Consequently, it has a more pronounced sensitivity to energy efficiency interventions. In this case the solutions with the best energy performances are also the cost-optimal ones, and there is a strong linear correlation between energy performance and the global cost of EEMs packages. The cost-optimal solution has an advanced level of external thermal insulation, standard windows with solar shading, and a direct expansion multi-split system heat pump (ETI2_WDG(S)_DX) with $C_G = 1027.3 \text{ €/m}^2$ and $EP_H + EP_C = 27.8 \text{ kWh/m}^2$.

For each building-type, climatic zone and facade orientation, 24 simulations (8 economic scenarios times 3 climatic scenarios) were performed and the resulting C_G/EP plots were processed in order to identify the most robust energy refurbishment solutions. These solutions present the lowest global cost output with the highest frequency on varying economic and climatic scenarios. The results are summarized in Table 8.

From the analysis of the results, it can be seen that:

- None of the analyzed EEMs, if applied alone, represents a cost-optimal solution. Thus, cost-effective energy refurbishment implies a combination of different EEMs, featuring the proper level of performance;
- Advanced level of thermal insulation (current Italian National requirements DM 26/6/2015) is a cost-optimal solution in any case except for the building with low V_G/A_e ratio (building type 1.3), located in the mild climatic zone C where the standard level implies a lower global cost. When this type of building is located in the climatic zone D, the standard level of external thermal insulation, even if not the cost-optimal

solution, yields a global cost that lies within the range of 10 €/m^2 from the optimal solution.

- Double low emissivity glazing, compliant with current national requirements, represents the cost-optimal solution in most cases, while triple glazing could be considered a cost/benefit solution only when considering building-type 1.3, West/East oriented located in climatic zone D.
- The economic feasibility of shading devices is determined primarily by the orientation of the building. For West/East orientation solar shading devices are always a cost-optimal intervention due to the greater amount of solar gains received from the facades during the summer.

Table 8 – Most robust solutions and frequency of EEMs package

Building-type, climatic zone, orientation	EEMs package	Freq. (%)
Type 1.3, zone C, or. S/N	ETI1_WDG_DX	100
Type 1.3, zone C, or. W/E	ETI1_WDG(S)_DX	100
Type 2.1, zone C, or. S/N	ETI2_WDG_DX	50
	ETI2_WDG(S)_DX	50
Type 2.1, zone C, or. W/E	ETI2_WDG(S)_DX	100
Type 1.3, zone D, or. S/N	ETI2_WDG_DX	69
	ETI2_WTG_DX	31
Type 1.3, zone D, or. W/E	ETI2_WTG(S)_DX	69
	ETI2_WDG(S)_DX	31
Type 2.1, zone D, or. S/N	ETI2_WDG_DX	100
Type 2.1, zone D, or. W/E	ETI2_WDG(S)_DX	100

- In case of a higher A_w/A_f ratio and mild climate shading devices are cost-optimal even for the South/North orientation, just in case of low discount rate (3 %) scenarios;
- The direct expansion multi-split heat pump is by far the cost-optimal solution for the HVAC system, regardless of building-type, orientation and climatic zone;
- The economic factor that most influences the global cost results is the discount rate followed by service life;

- Climate change effect on global cost results is moderate, while a more relevant influence can be observed looking at the energy performance: in un-refurbished buildings, climate change causes a decrease in primary energy demand for heating that rather exceeds the increase of cooling demand, resulting in a total annual primary energy demand decrease, both on a medium and long-term scale. The opposite happens to energy refurbished buildings since the most robust EEMs combinations, listed on Table 8, worsen their medium and long-term energy performance; this happens because cost-optimal measures are more effective in reducing heating demand than cooling demand, with the latter growing much more than the former in future scenarios. These findings well match the conclusion of previous studies by the authors (Pierangioli et al., 2017).

Finally a simplified evaluation of the reliability of these findings in consideration of the more realistic user's behavior was performed. User presence and the related internal gains were derived from UNI/TS 11300-1 tailored rating profile (UNI, 2014 b). It was assumed that window opening for natural ventilation and solar shading devices operations match this profile as well. By the way of example, for building type 2.1, located in the climatic zone D, South/North oriented, a more realistic user profile implies an increase of primary energy demand and global cost of EEM's. This happens mainly because of the cooling demand rise due to the less efficient use of solar shading devices that are not operated during the central hours of weekdays. Moreover, increased cooling demand is not effectively balanced by a natural ventilation increase. Cost-optimal solution identification and ranking is affected as well, especially regarding windows selection: the economic feasibility for solar shading devices obviously weakens in favour of low g-value glazing.

5. Conclusion

This research investigated global costs and primary energy demand of common energy refurbishment measures applied to a couple of building models, representative of the Italian social housing stock build

from 1946 to 1977 in Central Italy. Different climatic and economic scenarios have been considered. Although the results cannot be used to provide general and conclusive solutions, they are useful to highlight the trend of the effectiveness of climate change adaptation measures in Mediterranean climate.

The coupled energy-economic analysis shows that the selection of the cost-optimal refurbishment solution is significantly affected by the typological characteristics of the building, its orientation and climatic zone, in addition to the discount rate value which represents the most influential factor among the analysed economic parameters. These findings result in the necessity of an accurate preliminary assessment of the different refurbishment strategies in order to avoid non-optimal solutions.

In summary, the preliminary results of this research indicate that for most typological, economic, and climatic scenarios, cost-optimal solutions feature:

- advanced levels of external thermal insulation (beyond current national requirements);
- standard glazing system (double low emissivity) that complies with the current national requirements;
- operable solar shading devices in case of West/East orientation;
- a reversible direct expansion multi-split heat pump featuring a standard system efficiency that is already required by the Italian regulations.

Nomenclature

Symbols

A_f	Useful floor area of conditioned space (m ²)
A_e	Surface area of gross cond. volume (m ²)
V_G	Gross conditioned volume (m ³)
A_w	Window area (m ²)
U	Thermal transmittance (W/(m ² K))
U_w	Window thermal transmittance (W/(m ² K))
g	Solar factor (-)
EP_H	Heating Primary Energy/ A_f (kWh/m ²)
EP_C	Cooling primary energy/ A_f (kWh/m ²)
C_G	Global Cost (€/m ²)
C_i	Initial investment costs (€/m ²)

C _R	Replacement costs (€/m ²)
C _M	Maintenance costs (€/m ²)
HDD	Heating degree days (Kd)
CDD	Cooling degree days (Kd)
ETI0	Current level of ext. thermal insulation
ETI1	Standard level of ext. thermal insulation
ETI2	Advanced level of ext. thermal insulation
WOG	Current double glazing
WDG	Double low emissivity glazing
WTG	Triple low emissivity glazing
(S)	Windows with shading system
TB	Traditional boiler
CB	Condensing boiler
DX	Direct expansion multi-split system

References

- Acocella, A. 1980. *L'edilizia residenziale pubblica in Italia dal 1945 ad oggi*. Padova, Italy: CEDAM.
- AEEG (Italian Regulatory Authority for Electricity Gas and Water). 2016. "Prices and tariffs". <http://www.autorita.energia.it>.
- Belcher, S.E., J.N. Hacker, D.S. Powell. 2005. "Constructing design weather data for future climates". *Building Services Engineering Research and Technology* 26: 49-62. doi:10.1191/0143624405bt112oa.
- Beneforti, G., A. Ottanelli, 2012. *Le case popolari di Pistoia*. Pistoia, Italy: Vannini.
- Capomolla, R., R. Vittorini. (edsited by). 2003. *L'architettura INA-CASA 1949-1963. Aspetti e problemi di conservazione e recupero*. Rome, Italy: Gangemi.
- Capros, P., L. Mantzos, N. Tasios, A. De Vita, N. Kouvaritakis. 2010. *EU energy trends to 2030*. Luxembourg, Luxembourg: Publications Office of the European Union.
- Corrado, V., I. Ballarini S.P. Corgnati. 2014. *Building Typology Brochure – Italy*.
- De Wilde, P., D. Coley. 2012. "The Implications of a Changing Climate for Buildings". *Building and Environment* 55: 1–7. doi: 10.1016/j.buildenv.2012.03.014.
- Di Giulio, R. 1999. *Manuale di manutenzione edilizia*. Rimini, Italy: Maggioli.
- E3M-Lab, 2016. *EU Reference Scenario 2016 Energy, transport and GHG emissions. Trends to 2050*. Luxembourg, Luxembourg: Publications Office of the European Union.
- ENEA - National Agency for New Technologies, Energy and Sustainable Economic Development. 2016. *Bulletin quarterly analysis of the Italian energy system. N°2 third quarter*. Roma, Italy: ENEA.
- European Commission. 2012. *Commission delegated regulation No. 244/2012 on the energy performance of buildings by establishing a comparative methodology framework for calculating cost-optimal levels*. Brussels, Belgium: European Commission.
- INA-CASA. 1949. *Piano incremento occupazione operaia: case per lavoratori – Bandi di concorso*. Roma, Italy: Damasso.
- ISTAT - National Institute of Statistics. 2011. *Population and housing census*. Rome, Italy: ISTAT.
- IWU (Institut Wohnen und Umwelt). 2016. EPISCOPE and TABULA website. Accessed December 20. <http://episcope.ue/welcome>
- Nocera, M. 2015. *Le detrazioni fiscali del 55-65% per la riqualificazione energetica del patrimonio edilizio esistente nel 2013*. Roma, Italy: ENEA.
- Pierangioli, L., G. Cellai. 2016. "The impact of climate change on the energy-efficient refurbishment of social housing stock in Italy". In: *Proceedings of the 3rd IBPSA - England Conference*. Newcastle, UK: Newcastle University.
- Pierangioli, L., G. Cellai, R. Ferrise, G. Trombi, M. Bindi. 2017. "Effectiveness of passive measures against climate change: Case studies in Central Italy". *Building Simulation* 10: 459–479. doi: 10.1007/s12273-016-0346-8.
- Tabula Project Team. 2013. *TABULA Calculation Method. Energy use for heating and domestic hot water*. Darmstadt, Germany: InstitutWohnen und Umwelt GmbH.
- UNI Ente di Unificazione Italiano. 2008. *UNI EN ISO 15459. Energy performance of buildings. Economic evaluation procedure for energy systems in buildings*. Milan, Italy: UNI.
- UNI Ente di Unificazione Italiano. 2014-a. *UNI/TR 11552. Opaque envelope components of buildings. Thermo-physical parameters*. Milan, Italy: UNI.
- UNI Ente di Unificazione Italiano. 2014-b. *UNI/TS 11300. Energy performance of buildings. Part 1: Evaluation of energy need for space heating and cooling*. Milan, Italy: UNI.

Analysis of Simplified Lumped-Capacitance Models to Simulate Thermal Behaviour of Buildings

Jacopo Vivian – University of Padova – jacopo.vivian@dii.unipd.it

Angelo Zarrella – University of Padova – angelo.zarrella@unipd.it

Giuseppe Emmi – University of Padova – giuseppe.emmi@unipd.it

Michele De Carli – University of Padova – michele.decarli@unipd.it

Abstract

Lumped-capacitance models for the simulation of the dynamic thermal behaviour of buildings have recently received growing attention due to their low computational cost and ease of implementation in city district simulation models. This work looks at two simplified dynamic models to evaluate the energy performance of buildings in both heating and cooling. In particular, the xRyC models proposed by the International Standard ISO 13790 and the German Guideline VDI 6007 are analysed in detail and compared with TRNSYS, in both long- and short-term, under the same boundary conditions. The analysis has been carried out considering an apartment with different types of building structures (high-low thermal capacitance, high-low thermal insulation). Four European climates (Helsinki, Venice, Vienna and Palermo) have been taken into account. The comparison has been done in terms of energy need, peak load, and hourly heating/cooling load profile during both seasons. The simulation results show that the simplified 7R2C model of the VDI 6007 is in good agreement with TRNSYS, in terms of both energy needs and transient behaviour. The improvement over the 5R1C model of the Standard EN 13790 increases when the cooling season is considered.

1. Introduction

Appropriate dynamic models are necessary both during early design stages of buildings and neighbourhoods as well as when retrofitting solutions for existing ones are being evaluated. The most frequently used software for building simulation - e.g. TRNSYS (Klein et al., 2010), EnergyPlus (Crawley et al., 2001) - rely on models that require a detailed description of the building in terms of both its

geometry and physical properties. As these methods require a high computational effort and cannot readily be interfaced with optimization solvers, they are unsuitable for applications such as model predictive control (Privara et al., 2013) and simulations of neighbourhoods or city districts (Kämpf et al., 2007). Secondly, due to the high number of input parameters they can hardly be approached by inexperienced users. Thus, simplified dynamic models of buildings have been receiving growing attention in recent times. In these models, the system domain is discretized into a set of nodes connected by thermal resistances and capacitances (i.e. the parameters of the model). These parameters can be identified analytically, by model order reduction (Gouda et al., 2002) or by tuning the model to a temperature and energy consumption dataset (Madsen and Holst, 1995). The first attempt to describe the dynamic behaviour of building elements using the electrical analogy dates back to 1936 when Beuken (1936) derived the equations for a generic network with n thermal capacitances. That study formed the basis for the n -capacitances room model proposed by Rouvel (1972) that was implemented in the GEBSIMU software (Rouvel, 2015). A few years later, Laret (1980) proposed a simple analytical method to represent each construction element with a one-node model consisting of two resistances and one capacitance. The subdivision of the thermal resistance was carried out by calculating a variable referred to as the 'accessibility factor'. Based on this approach, Lorenz and Masy (1982) lumped all the construction elements of the thermal zone considered in a simple model with two time constants: one for the air volume and one for the building structure. In accordance with the same approach

used for the n-capacitances model (Rouvel, 1972; Rouvel and Zimmermann, 2004) the building elements are split into those under symmetric load and those under asymmetric load, which are typically internal partitions and external walls, respectively. The 7R2C model of Rouvel and Zimmermann has been recently implemented in the German Guideline VDI 6007-1 (German Association of Engineers, 2012). The International Standard ISO 13790 (ISO, 2008) fully prescribes a quasi-steady-state calculation method - monthly method - and a simple dynamic method - simple hourly method - based on a lumped-capacitance model with five thermal resistances and one thermal capacitance (5R1C).

In this work, an apartment was simulated with the one-capacitance (1C) model described in ISO 13790 and with the two-capacitances (2C) model described in VDI 6007, by taking into consideration four diverse building structures under four different climate conditions (Palermo, Venice, Vienna, and Helsinki). The results of the simplified models were then compared with those obtained from the well-established TRNSYS software (used as benchmark), in both heating and cooling seasons in terms of seasonal energy needs, peak load, and transient thermal behaviour.

2. Methods

2.1 Weather Conditions

One-hour time steps were used over a one-year simulation period including a heating season (from October 15 to April 15), a cooling season (from May 15 to September 15); the remaining periods of the year had free-floating indoor air temperatures. The test reference year (TRY) files of four reference European locations were used to examine a wide range of weather conditions. Table 1 summarizes the main characteristics of the climates mentioned. Both heating and cooling degree-days are calculated with a baseline of 18.3 °C. Solar irradiation refers to the annual amount of global radiation on the horizontal surface.

Table 1 – Characteristics of the considered reference climates

	PA	VE	WI	HE
Max. temp. [°C]	34.6	33.6	31.7	28.7
Min. temp. [°C]	5.9	-5.8	-18.3	-21.7
Heating degree days	801	2267	3180	4856
Cooling degree days	1002	474	212	39
Ann. solar irr. [kWh/m ²]	1458	1102	1123	947

2.2 Buildings Structures

Four building structures representing different combinations of weight and thermal insulations [heavyweight not insulated (H1), heavyweight insulated (H2), lightweight not insulated (L1) and lightweight insulated (L2)] were considered. The building components are outlined in Table 2.

Table 2 – Characteristics of the building components

Building components		U [W/m ² K]	<i>m_f</i> [kg/m ²]
External walls	EW_H1	1.06	410
	EW_H2	0.26	410
	EW_L1	1.04	50
	EW_L2	0.28	70
Internal partitions/ boundary walls Ceilings/ floors	IW_H	2.53	150
	BO_H	0.95	310
	IW_L	1.59	30
	BO_L	0.95	50
	CE_H	0.73	590
	FL_H	0.73	590
Windows	CE_L	0.33	290
	FL_L	0.33	290
	SP	5.68	-
	DP	2.83	-

Both simplified models used the solar heat gain obtained from the detailed simulation as the input signal. This was done because many authors have indicated that solar gains are one of the main sources of uncertainty (Reynders et al., 2014). Solar gains were calculated using Type 56 of TRNSYS. At each time step, the solar heat entering the building was given by the sum of shortwave transmission and secondary heat flux through external windows. The apparent sky temperature and the ground temperature were calculated according to the equations

proposed by the Standard VDI 6007. Table 3 outlines the combination of building components of each building structure.

Table 3 – Building components of the reference envelopes

Envelope \ building comp.	Non-Adiabatic	Adiabatic
Heavyweight uninsulated (H1)	EW_H1 SP	IW_H, BO_H, CE_H, FL_H
Heavyweight well insulated (H2)	EW_H2 DP	IW_H, BO_H, CE_H, FL_H
Lightweight uninsulated (L1)	EW_L1 SP	IW_L, BO_L, CE_L, FL_L
Lightweight well insulated (L2)	EW_L2 DP	IW_L, BO_L, CE_L, FL_L

Other boundary conditions for both simplified and detailed building models are: emissivity of surfaces for long-wave thermal radiation (0.9); absorption coefficient of exterior surfaces (0.6); convection heat transfer coefficient of internal surfaces (2.7 W/(m² K) for horizontal heat flow and 1.7 W/(m² K) for vertical heat flow) and convection heat transfer coefficient of external surfaces (20 W/(m² K)).

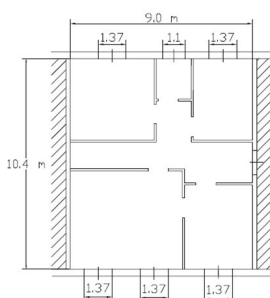


Fig. 1 – Floor plan of the apartment

The considered building was a 93.6 m² single-storey apartment (see Fig. 1). The apartment has two external walls oriented along the east-west direction - or north-south, depending on the considered simulation - and the construction elements in all the other directions were considered adiabatic. The latter include internal partitions, boundary walls towards conditioned spaces (adjacent apartments), floor and ceiling. All glazed components on the east side are windows of height 1.3 m (overall glazed area of 5 m²), whereas all glazed components on the opposite side are doors of height 2.3 m (overall glazed area of 9.4 m²). The height of the apartment was 3 m and the overall surface of the internal partitions was 95 m².

Both the air mass flow rate due to infiltration and/or natural ventilation and the heat flow rate due to internal heat gains were assumed constant in time and uniform within the thermal zone.

They were calculated in accordance with the Italian Standard UNI/TS 11300-1 (UNI, 2008). The internal heat gain was calculated according to Eq. (1) and the air change rate was assumed to be 0.5 volumes per hour, as is generally assumed for domestic dwellings.

$$\Phi_{\text{int}} = 5.294 A_{\text{fl}} - 0.01557 A_{\text{fl}}^2 \text{ [W]} \quad (1)$$

For sake of simplicity, this paper includes only the numerical results of the apartment oriented along the east-west axis. Analogue results were obtained for the north-south case.

2.3 Evaluation of Models Accuracy

The different load profiles obtained by the RC models were compared to assess their accuracy with respect to the TRNSYS model as far as the dynamic response and overall energy needs were concerned. The dynamic response was evaluated by calculating the distance between the heat load profiles of the RC models and the heat load profile obtained with TRNSYS, i.e. the root mean squared error (RMSE). In order to compare the RMSE obtained with reference to different building structures and under different weather conditions, the latter was successively normalized with respect to the mean heat load of the case considered, thus obtaining the relative error ε . The mean heating/cooling load was obtained by dividing the energy needed for space heating/cooling by the number of hours with HVAC systems turned on.

3. Simplified Models

Lumped-capacitance models assume that the distributed thermal mass of the dwelling is lumped into a discrete number of thermal capacitances, depending on the model type (Reynders et al., 2014). The lumped-capacitance model was solved by a linear system composed of n heat balance equations, where n is the number of nodes of the corresponding thermal network. As is usual in building simulations, the system has one degree of freedom unless

one variable is fixed by the user. This leads to two possible model uses:

Calculation of the heat load: The indoor air temperature $\theta_i = \theta_{set}$ is set by the user and the output of the model is the heat load ϕ_{hc} ;

Calculation of the indoor air temperature: The user sets the heat load ϕ_{hc} and the output of the model is the indoor air temperature θ_i .

The models considered do not include the balance of water vapour in the indoor ambient, which means that the calculation of the latent heat load (to be delivered to or extracted from conditioned spaces) is not included. The models were developed in the MATLAB environment (Mathworks, 2010); their main features are briefly described in the following.

3.1 The 5R1C Model

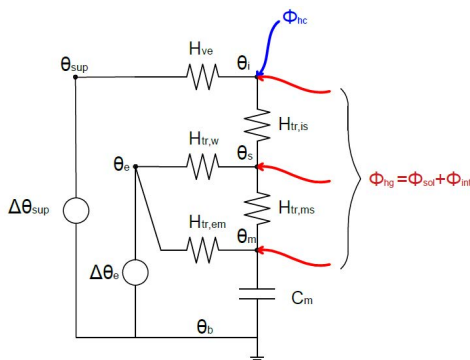


Fig. 2 – 5R1C model of EN ISO 13790

The International Standard ISO 13790 presents two methods that rely on the same inputs to calculate the building’s energy use at different levels of detail: the *monthly method* with one month time intervals and the *simple hourly method* with one hour time intervals. The simple hourly method is based on the equivalent resistance-capacitance (RC) circuit shown in Fig. 2.

3.2 The 7R2C Model

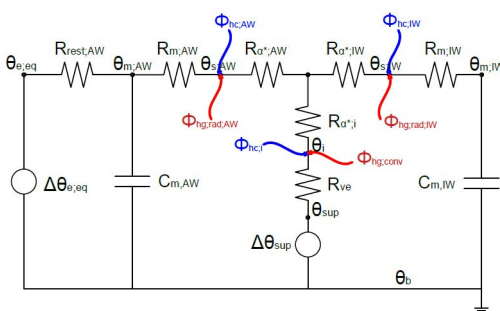


Fig. 3 – 7R2C model of VDI 6007

The model distinguishes between adiabatic and non-adiabatic building components and assigns the thermal capacity to each of the two groups. In the 5R1C model, the entire thermal mass of the building is lumped into one single element, thereby making this distinction impossible. Both models use the ISO 13786 Standard (ISO, 2007) for the calculation of the thermal capacitances. The equivalent circuit is shown in Fig. 3.

4. Results

4.1 Peak Loads and Energy Needs

Table 4 shows that lumped-capacitance models tend to slightly underestimate the peak load for the space heating of uninsulated building structures (down to -5.5 % with the 1C model and to -2.2 % with the 2C model) and to overestimate it for well insulated buildings (up to +8.1 % with the 1C model and to +4.0 % with the 2C model).

Tables 6 and 7 seem to extend the patterns found for the peak load to the energy needs calculation. In fact, the energy needs for space heating is slightly underestimated by the RC models for buildings with low thermal insulation (approx. -4 % for both models), while it is overestimated for highly insulated building envelopes (+5 % for the 1C model and +3 % for the 2C model). The trends in the space cooling mode remained almost entirely unaltered, although in this case the error in the lumped-capacitance models was not as significant as that in the peak load calculation: the mean error of the simulations with the 1C model is approx. -2.2 % and drops to -0.3 % with the 2C model. This fact suggests that although they do not accurately follow the fluctuations of the heat load, simplified models are better able to estimate the energy needs season. On the other hand, the peak load for space cooling is systematically underestimated (from -6.3 % to -14.5 %) by the 1C model, as it can be observed in Table 5. The 2C model seems instead to be quite accurate, with an error that ranges from -2.7 to +4.1 % and a mean error of +0.3 %.

Table 4 – Peak load for space heating

Env.	Clim.	Peak load for space heating [W]		
		TRNSYS	5R1C	7R2C
H1	PA	1564	-0.5 %	-2.2 %
	VE	3321	-3.6 %	-1.7 %
	WI	4882	-1.2 %	-0.3 %
	HE	6037	-2.6 %	-1.7 %
H2	PA	717	+8.1 %	+4.0 %
	VE	1745	+2.0 %	+2.5 %
	WI	2629	+2.5 %	+3.4 %
	HE	3277	+2.0 %	+2.0 %
L1	PA	1761	-4.8 %	+0.1 %
	VE	3560	-5.5 %	-0.7 %
	WI	5355	-4.6 %	-0.9 %
	HE	6223	-3.8 %	-1.5 %
L2	PA	803	+6.6 %	+2.9 %
	VE	1831	+2.9 %	+2.0 %
	WI	2796	+2.7 %	+3.4 %
	HE	3378	+1.7 %	+1.7 %

Table 5 – Peak load for space cooling

Env.	Clim.	Peak load for space cooling [W]		
		TRNSYS	5R1C	7R2C
H1	PA	2720	-10.5 %	-1.5 %
	VE	2678	-6.3 %	-0.8 %
	WI	3810	-7.7 %	+0.4 %
	HE	2582	-5.7 %	+2.5 %
H2	PA	2346	-11.1 %	-1.2 %
	VE	2307	-8.1 %	-0.4 %
	WI	3390	-9.9 %	+1.4 %
	HE	2571	-9.1 %	+1.8 %
L1	PA	3164	-14.5 %	+1.3 %
	VE	3184	-12.9 %	+1.7 %
	WI	4602	-13.8 %	+2.0 %
	HE	3290	-13.1 %	+4.1 %
L2	PA	2637	-13.8 %	-2.7 %
	VE	2572	-10.8 %	-2.1 %
	WI	3895	-13.4 %	-0.8 %
	HE	3003	-12.6 %	-0.4 %

Table 6 – Seasonal energy needs for space heating

Env.	Clim.	Energy needs for space heating [kWh]		
		TRNSYS	5R1C	7R2C
H1	PA	1293	-2.5 %	-6.5 %
	VE	7377	-4.0 %	-4.2 %
	WI	9304	-4.3 %	-4.0 %
	HE	13557	-4.2 %	-3.6 %
H2	PA	137	+33 %	+16 %
	VE	3055	+5.7 %	+3.4 %
	WI	3890	+5.7 %	+3.8 %
	HE	6528	+3.7 %	+2.4 %
L1	PA	1336	-5.2 %	-6.3 %
	VE	7300	-3.5 %	-3.5 %
	WI	9203	-3.8 %	-3.3 %
	HE	13291	-3.3 %	-2.9 %
L2	PA	179	+14 %	+7.3 %
	VE	3129	+4.8 %	+2.7 %
	WI	3989	+4.6 %	+3.2 %
	HE	6531	+4.0 %	+2.5 %

Table 7 – Seasonal energy needs for space cooling

Env.	Clim.	Energy needs for space cooling [kWh]		
		TRNSYS	5R1C	7R2C
H1	PA	3353	-3.6 %	-1.3 %
	VE	2170	-3.0 %	-0.4 %
	WI	2282	-0.1 %	0.0 %
	HE	809	+4.2 %	+3.3 %
H2	PA	3402	-2.9 %	-1.3 %
	VE	2589	-3.0 %	-1.0 %
	WI	3071	-3.2 %	-1.9 %
	HE	1811	-5.1 %	-2.8 %
L1	PA	3313	-2.4 %	+0.1 %
	VE	2228	-3.5 %	+1.2 %
	WI	2409	-2.1 %	+1.7 %
	HE	952	-3.7 %	+4.7 %
L2	PA	3337	-2.9 %	-1.4 %
	VE	2578	-3.2 %	-1.1 %
	WI	3017	-2.9 %	-1.5 %
	HE	1794	-5.1 %	-2.5 %

4.2 Transient Behaviour

The accuracy in the transient response of the lumped-capacitance models is measured here as the mean distance (RMSE) between their heating/cooling load profiles and those obtained by TRNSYS simulations. Fig. 4 shows the RMSE of the simplified models and the peak load in the corresponding season for the apartment facing east west. The peak load, which was extracted from the heat load profile produced by TRNSYS, serves as a valid reference for both simplified models. The RMSE of the simplified models in heating mode increased from Palermo to Vienna but showed a smaller increase with reference to the snow-dominated climate of Helsinki. Fig. 4(a), for example, shows that while the peak load in Vienna is more than three times the peak load in Palermo (from 1564 W to 4882 W) and the $RMSE_{1C}$ is more than twice (from 81 W to 184 W), this proportion is no longer valid when we turn our attention from Vienna to Helsinki (+23 % of peak load and only +5 % of the $RMSE_{1C}$). This trend could be linked to the different patterns of temperature differences between the indoors and outdoors, which represents the main driving force for space heating load in winter months. Indeed, temperatures are less prone to register significant diurnal fluctuations in the Nordic climate of Helsinki than in the other locations considered in this study. This trend seems to be valid for both simplified models regardless of the building envelope. During the warm season, instead, the cooling load is a result of the overlapping effects of outdoor air temperature and solar radiation. Fig. 4 shows that the accuracy of the 7R2C model is greater than that of the 5R1C one in all the cases considered and that such improvement is particularly relevant in the cooling season. Indeed, the RMSE from 1C to 2C drops from -35 % to -53 % in heating mode and from -44 % to -76 % in cooling mode.

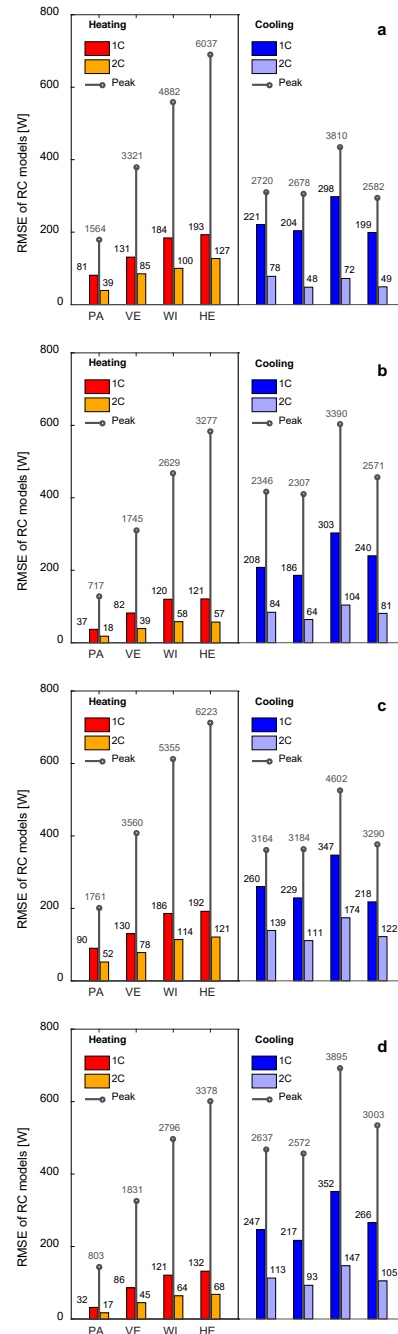


Fig. 4 – RMSE of lumped-capacitance models and peak load for the apartment with envelopes: (a) H1, (b) H2, (c) L1 and (d) L2

The trivial reason for this improvement is linked to the presence of the second thermal capacitance that makes it possible to distinguish between adiabatic and asymmetrically loaded building components, as explained in Section 3.2. Moreover, the presence of two internal surface temperature nodes (θ_{IW} and θ_{AW} in Fig. 3) may lead to further improvement with respect to the 1C model due to both a more coherent distribution of heat gains throughout the

wall surfaces and the introduction of the radiative heat exchange between the inside surface of external walls and the surfaces of internal building components.

The relative errors ε of both simplified models are presented graphically in Fig. 5 for the 32 simulations of the apartment (with both orientations). Here, it is evident that the type of building structure does not significantly affect the accuracy of the simplified models in the heating mode, as the effect of climate conditions prevails. In fact, the blue indicators that represent the climate of Helsinki are always lower than the red ones that represent the climate of Palermo, while the green and the orange indicators are always somewhere in between. This holds true both for the 1C and 2C models, although the error of the former presents a higher dispersion. The improvement of the 2C model over the 1C one is evident for both seasons. Fig. 5 shows that while the error ε_{1C} of the 1C model shoots to very high values (20–30 %) when the transition is made from the heating to cooling mode, the error ε_{2C} of the 2C model does not undergo such a sharp increase and always remains below the threshold of 12.5 %.

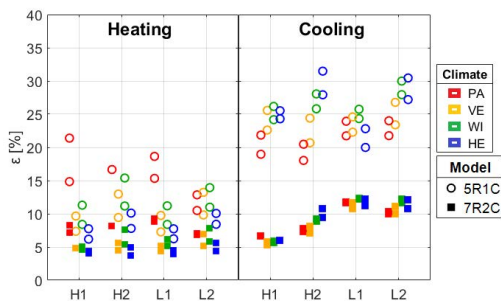


Fig. 5 – The relative error ε in the heating and cooling seasons

Contrary to what takes place in the heating mode, the type of building envelope does seem to affect the accuracy of the models during the warm season. Indeed, lightweight building structures present a higher error than heavyweight ones. This is particularly evident when the error of the 2C model is compared, since ε_{2C} increases from 6–7 % to 12 % when there is low thermal insulation (i.e. from H1 to L1) and from 7–11 % to 10–12 % when it is high (i.e. from H2 to L2). This may be due to the difficulty that lumped capacitance models have in following the reaction of lightweight structures to rapid fluctuations of air temperature or heat gains.

5. Conclusions

The 5R1C and 7R2C lumped-capacitance models described in the International Standard ISO 13790 and in the German Guideline VDI 6007 were used to simulate the thermal behaviour of an apartment using four reference building envelopes in four different climates. The accuracy was evaluated by comparing the resulting profiles with those obtained by the well-established software TRNSYS.

Both lumped-capacitance models appear to reliably calculate the overall energy needs of buildings in both heating and cooling seasons.

As far as the transient behaviour is concerned, the second-order model of VDI 6007 provides more accurate results. Indeed, the first-order model systematically underestimated the peak load for space cooling (-11 % on average), while the second-order model showed a fairly accurate calculation. The accuracy of the 7R2C model in terms of relative error ε (ratio between the RMSE and the mean load) was approximately 6 % and 9 % in the heating and cooling seasons, respectively.

Acknowledgement

The Interdepartmental Centre funded this research activity for Energy Technology and Economics “G. Levi Cases” of the University of Padova.

Nomenclature

Symbols

A	Surface area (m^2)
C	Thermal capacitance (J/K)
H	Heat transfer coefficient (W/K)
m_f	Frontal mass (kg/m^2)
R	Thermal resistance (K/W)
$RMSE$	Root mean squared error
U	Thermal transmittance ($\text{W}/(\text{m}^2 \text{K})$)
ε	Relative error (-)
θ	Temperature (K)
ϕ	Heat flow rate (W)

Subscripts/Superscripts

<i>AW</i>	Non-adiabatic building elements
<i>conv</i>	Convective
<i>e</i>	External air
<i>fl</i>	Floor
<i>hc</i>	Heating/cooling load
<i>i</i>	Indoor air
<i>int</i>	Internal gains
<i>IW</i>	Adiabatic building elements
<i>m</i>	Thermal mass (node)
<i>rad</i>	Radiative
<i>s</i>	Surface (node)
<i>set</i>	Set-point
<i>sup</i>	Supply (air)
<i>tr</i>	Transmission
<i>ve</i>	Ventilation

References

- Beuken, K.L. 1936. *Wärmeverluste bei periodisch betriebenen Öfen*. Dissertation. Freiburg, Germany.
- Crawley, D.B., L.K. Lawrie, F.C. Winkelmann et al. 2001. "EnergyPlus: Creating a new-generation building energy simulation program". *Energy and Buildings* 33: 319–311. doi: 10.1016/S0378-7788(00)00114-6.
- Ente Nazionale Italiano di Unificazione (UNI). 2008. *UNI/TS 11300-1: Energy performance of buildings. Evaluation of energy need for space heating and cooling*. Milan, Italy: UNI.
- German Association of Engineers. 2012. *Calculation of transient thermal response of rooms and buildings -modelling of rooms (VDI 6007-1)*. Düsseldorf, Germany: Beuth Verlag GmbH.
- Gouda, M.M., S. Danaher, C.P. Underwood. 2002. "Building thermal model reduction using nonlinear constrained optimization". *Building and Environment* 37: 1255–65. doi: 10.1016/S0360-1323(01)00121-4.
- International Organization for Standardization - ISO. 2008. *ISO 13790: Energy performance of buildings: calculation of energy use for space heating and cooling*. Genève, Switzerland: ISO.
- International Organization for Standardization - ISO. 2007. *ISO 13786: Thermal performance of building components -- Dynamic thermal characteristics -- Calculation methods*. Genève, Switzerland: ISO.
- Kämpf, J.H., D. Robinson. 2007. "A simplified thermal model to support analysis of urban resource flows". *Energy and Buildings* 39: 445–53. doi: 10.1016/j.enbuild.2006.09.002.
- Klein, S.A. et al. 2010. *TRNSYS 17: A Transient System Simulation Program*. Madison, U.S.A.: Solar Energy Laboratory, University of Wisconsin-Madison.
- Laret, L. 1980. "Use of general models with a small number of parameters: Part 1 – theoretical analysis". In: *Proceedings of the 7th International Congress of Heating and Air Conditioning CLIMA 2000*. Budapest, Hungary.
- Lorenz, F., G. Masy. 1982. *Méthode d'évaluation de l'économie d'énergie apportée par l'intermittence de chauffage dans les bâtiments. Traitement par différences finies d'un model a deux constantes de temps*. Report N. GM820130-01. Liege, Belgium: University de Liege.
- Madsen, H., J. Holst. 1995. "Estimation of continuous-time models for the heat dynamics of a building". *Energy and buildings* 22: 67-79. doi: 10.1016/0378-7788(94)00904-X.
- MathWorks Inc. 2010. "MATLAB version 7.10.0" Natick, U.S.A.: MathWorks Inc.
- Privara, S., J. Cigler, Z. Vaňa et al. 2013. "Building modeling as a crucial part for building predictive control". *Energy and Buildings* 56: 8-22. doi: 10.1016/j.enbuild.2012.10.024.
- Reynders, G., J. Diriken, D. Saelens. 2014. "Quality of grey-box models and identified parameters as function of the accuracy of input and observation signals". *Energy and Buildings* 82 263–274. doi: 10.1016/j.enbuild.2014.07.025.
- Rouvel, L. 1972. "Berechnung des wärmetechnischen Verhaltens von Räumen bei dynamischen Wärmelasten". *Brennst-Wärme-Kraft* 24 (6).
- Rouvel, L. 2015. "Thermische Gebäudesimulation GEBSIMU- Berechnungsverfahren zum instationären thermischen Gebäudeverhalten". Accessed on 01/01/2017. <http://www.gebsimu.de>
- Rouvel, L., F. Zimmermann. 2004. "Berechnung des instationären thermischen Gebäudeverhaltens". *LH* 55 (3): 39-46; *LH* 55 (4): 24-30.

Measurement of the Impact of Buildings on Meteorological Variables

Dasaraden Mauree – Ecole Polytechnique Fédérale de Lausanne – dasaraden.mauree@epfl.ch

Laurent Deschamps – Ecole Polytechnique Fédérale de Lausanne – laurent.deschamps@epfl.ch

Paul Bequelin – Laboratory, Ecole Polytechnique Fédérale de Lausanne – paul.becquelin@epfl.ch

Pierre Loesch – Ecole Polytechnique Fédérale de Lausanne – pierre.loesch@epfl.ch

Jean-Louis Scartezzini – Ecole Polytechnique Fédérale de Lausanne – jean-louis.scartezzini@epfl.ch

Abstract

A meteorological tower was installed on the EPFL campus in a semi-urban environment for the high frequency monitoring of the microclimate. This project was done in the larger framework of the measurement of the meteorological profiles, and also for a quantification of the energy consumption and the outdoor human comfort. A long-term monitoring of various meteorological variables like wind speed, air temperature, turbulence, humidity is realized by the use of 3D sonic anemometers, surface temperature sensor, and a meteorological station so as to analyse the micro-climate in an urban context.

The preliminary results from the experimental setup confirm that the wind speed is considerably modified in the urban canopy. We show that the decrease in the wind speed will have a significant effect on the heat convection coefficient. Furthermore, we demonstrate that it is possible to reconstruct the air temperature along the vertical axis with a correction using the data from the meteorological station. In the near future, a net radiometer will be installed to analyse the influence of the incoming and outgoing radiation in the urban setup on the energy balance of the district.

1. Introduction

The Fifth Assessment Report (AR5) issued by the IPCC (Intergovernmental Panel on Climate Change) in 2013, stated that there is clear evidence that the current global warming is being caused by human activities. There is compelling proof this is due to the release of greenhouse gases (GHG) such as carbon dioxide (CO₂) from the combustion of fossil fuels to produce energy (IPCC, 2013). A large proportion of global energy demand has been related to buildings that are therefore, one of the main sources

of air pollution. Approximately half of the primary energy use in Switzerland occurs in buildings. Of this energy, about 30 % is consumed by space heating, cooling, and water heating; 14 % by electricity use, and 6 % by construction and maintenance (SFOE, 2011). In addition, the building sector accounts for more than half of the CO₂ emissions in Switzerland, which shows that it is among the most significant contributors to carbon emissions. This implies also that the building sector provides a real opportunity for a large improvement with regards to energy efficiency and reduction of CO₂ emission. The efficient planning of future buildings and districts will only be possible if urban planners have the appropriate tools and information at their disposal. For example, the future development of the EPFL campus shows the need to densify the existing building stock (Coccolo et al., 2015), but the question still remains on its design in order to reduce energy consumption while at the same time increase the liveability of the outdoor environment. It is now well known that the urban climate depends on a series of processes taking place at different spatial (from global to local) and temporal scales (Oke, 1982); building energy demand and urban climate are also closely related and interdependent (Ashie et al., 1999; Salamanca et al., 2011; Mauree et al., 2015). It is thus essential to have access to tools, which can evaluate - with precision - the interactions that exist between buildings, their energy use, as well as the local climate. Several models have been developed in the recent years to better represent the various phenomena that influence the energy use and the urban climate (Krpó et al., 2010; Mauree et al., 2017; Mauree et al., 2017a). One of the major drawbacks of these models

is the lack of data to validate and to further understand the various processes taking place in the urban areas.

The monitoring of high resolution vertical meteorological profiles is essential to determine the impact of urban areas / buildings on these variables: it is necessary to represent these effects when evaluating building energy use, air pollutant dispersion, and renewable energy potential in urban planning scenarios. Monitored meteorological data are scarcely available with high vertical resolution. Campaigns such as the BUBBLE (Rotach et al., 2005) observation period provide useful information and data to develop and generalize new parameterization schemes. However, there is a strong need for such data and in multiple configurations in order to develop new tools and methodologies which can then be used in the evaluation of building energy use. The vertical profiles of variables such as wind speed and direction, and the air temperature in the vicinity of buildings are crucial in the determination of the momentum and heat fluxes.

In the current study, we first give an overview of the experimental setup, the type of instruments that have been installed, and details related to their configuration. We then give the preliminary results from the setup and provide a sensitivity analysis of the heat convection coefficient. Finally, we conclude and give a few perspectives for the current study.

2. Experimental Setup

This experiment was set up in the framework of the MoTUS (Measurement of Turbulence in an Urban Setup) project (motus.epfl.ch). In the following sections we describe the setup, instruments, and calculations done for the various instruments.

2.1 Mast

For this purpose of the study, a 27 m mast was installed on the EPFL campus in Lausanne, Switzerland, to measure various meteorological parameters (see Fig. 1). The average building height in this district is around 10 m.

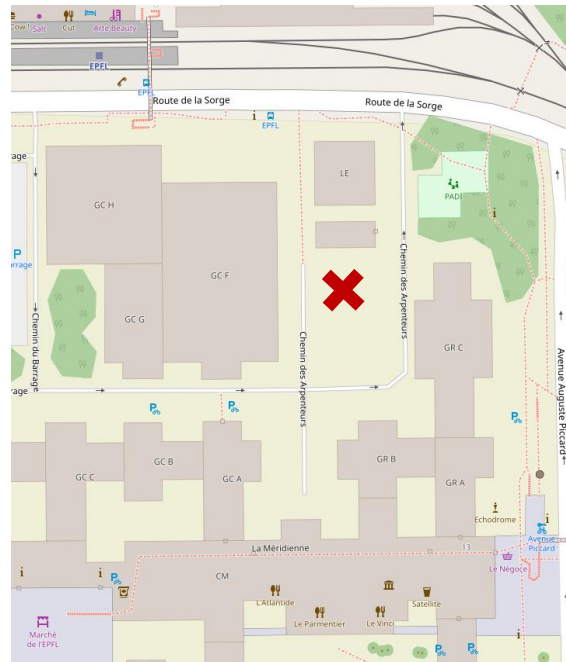


Fig. 1 – Location of the setup on the campus (indicated with the red cross). This image is taken from Open Street Map whose copyright notices can be found here: <https://www.openstreetmap.org/copyright> (CC-BY-SA-2.0).

2.2 Instruments

Table 1 lists the various instruments installed on the mast. Seven 3D sonic anemometers have been placed along the vertical axis every 4 m. A meteorological station was set at the bottom of the installation (1.5 m above ground level) to measure the relative humidity and the atmospheric pressure. Both of these variables will then be used to correct the sonic temperature measurement from the anemometers to calculate the air temperature. A surface temperature sensor was also installed at 1.5 m to measure the ground temperature. At the top of the tower two AXIS-cameras have been installed; one looking at the sky and the other one at the campus. The objective of these cameras is, for example, to provide useful information on cloud coverage. Data from the instruments are collected with a frequency of 1Hz based on the recommendations by Kaimal and Finnigan (1994) and stored in a database at EPFL.

Table 1 – List of instruments

Instrument	Brand	Type
3D sonic anemometers	Gill	WindMaster
Meteorological station	Gill	GMX 300
Surface temperature sensor	Optris	OPTCSLT15K

The sonic anemometers as well as the weather stations work with a frequency of 1 Hz. Fig. 2 gives an illustration of the experimental setup of the meteorological tower.

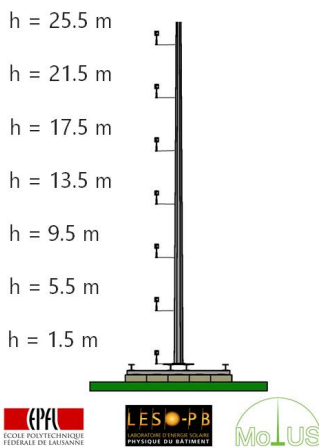


Fig. 2 – Experimental setup

A complete schematic of the setup as well as the communication protocols used can be found in Fig. 3.

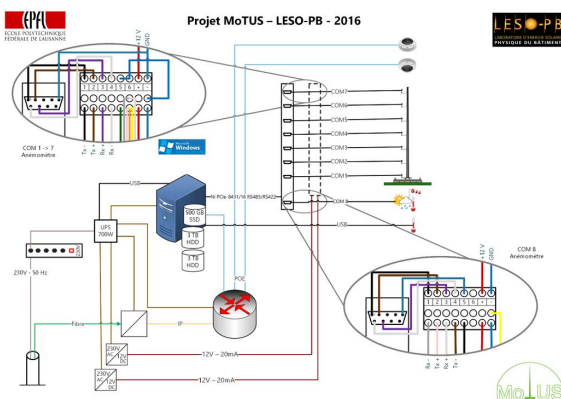


Fig. 3 – MoTUS schematic and protocols

2.3 Air Temperature Calculation

The sonic anemometers measure the sonic temperature. As these values do not correspond to the air temperature, we use a formula developed by Cassardo et al. (1995) to correct the sonic temperatures in order to determine the air temperature. To do this we needed the vapour pressure as well as the air pressure for every time step. These values were obtained from the Maximet weather station. The air temperature can be calculated as follows:

$$\theta_a = \frac{\theta_s}{1 + 0.32 \left(\frac{e}{P} \right)} \quad (1)$$

where θ_a is the corrected air temperature in Kelvin, θ_s is the sonic temperature (K), P is the air pressure (Pa), and e is the vapour pressure (Pa) that is calculated using:

$$e = RH * 100 * \left(6.11 * 10^{\left(\frac{7.5\theta_m}{237.3 + \theta_m} \right)} \right) \quad (2)$$

where RH is the relative humidity and θ_m is the air temperature measured using the Maximet weather station. Note that here we assume that the relative humidity is constant along the vertical axis and that hence the vapour pressure is as well.

2.4 Convection Coefficient

The convective heat flux can be calculated as a product of the heat convection coefficient and the difference in the surface and air temperature. A detailed review of the more commonly used formulations can be found in Mirsadeghi et al. (2013). For the purpose of the study we evaluate the impact of using localized wind speed on two formulations of the McAdams heat transfer coefficients, and analyse their sensibility to local wind speed. Firstly, in its original form, the coefficient is given by:

$$h_c = 5.678 \left[m + n \left(\frac{U}{0.3048} \right) \right] \quad (3)$$

where h_c is the convective heat transfer coefficient (in $W/m^2.K$), m and n are constants with a value of 0.99 and 0.21, U is the wind speed (in m/s) calculated on the wind attack angle on a particular surface in the windward or leeward-direction. For the purpose of this study we will simply assume U to be the horizontal wind speed. Note that this is the formulation used for $U < 4.88 \text{ ms}^{-1}$.

Secondly, we choose the linearized form as commonly used in software such as CitySim (Robinson, 2012) for example:

$$h_c = 2.8 + 3U. \tag{4}$$

3. Results Analysis and Discussion

3.1 Wind Speed

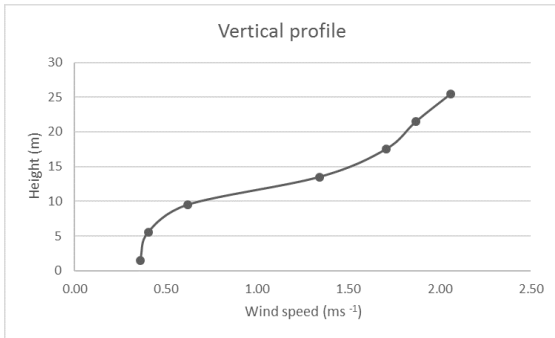


Fig. 4– Vertical profile of the horizontal wind speed ($m s^{-1}$) for the night of 01/09/2016 measured from the sonic anemometer

As can be expected in an urban context, the wind profile is highly impacted by the presence of buildings. It can be noted from Fig. 4, that the characteristic logarithmic profile is present above the building roof, and that below in the canopy layer, there is low horizontal wind speed. This corresponds to results and findings previously reported (Rotach et al., 2005; Santiago and Martilli, 2010; Mauree et al., 2017).

3.2 Air Temperature

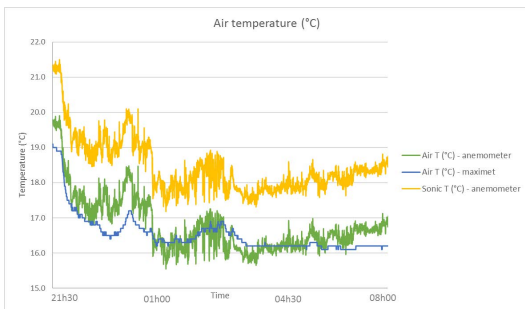


Fig. 5 – Air temperature ($^{\circ}C$) for the night of 04/09/2016 measured from the sonic anemometer, the weather station and the corrected air temperature

We can see from Figs 5 and 6, that the calculated air temperature from the sonic anemometers corrected by the sonic temperature has a very good agreement

(correlation coefficient is equal to 0.81) with the values from the Maximet weather station.

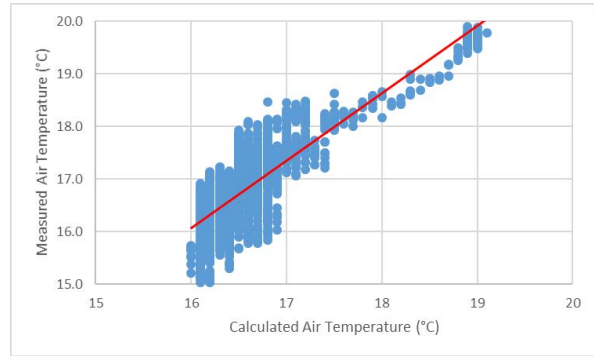


Fig. 6 – Measured and corrected air temperature ($^{\circ}C$)

We can highlight that there seems to be an overestimation of the temperature ($\sigma=0.44^{\circ}C$).

3.3 Heat Convection Coefficient

A sensitivity analysis is done using the wind speed usually taken at the standard meteorological height (10m), and the wind actually measured using the anemometers that corresponds to each floor of the LESO-PB building.

Table 2 – Convection coefficient at each floor using Equation 3

Floor	$h_c (W/m^2.K)$	Relative difference
1 st	7.0	35 %
2 nd	7.2	34 %
3 rd	8.1	26 %

Table 3 – Convection coefficient at each floor using Equation 4

Floor	$h_c (W/m^2.K)$	Relative difference
1 st	3.9	43 %
2 nd	4.0	41 %
3 rd	4.7	32 %

As can be seen from Tables 2 and 3, there is a significant difference between the convection coefficient calculated using the localized wind speed and the one typically taken at 10 m. The difference can go up to 43 % if we consider the 1st floor. Although

the original formulation of McAdams seems to present slightly better results, it should be highlighted that this formulation is recommended when wind speed is measured far enough from the surface, without any disturbance. In addition to the fact that building energy software generally uses data from meteorological stations that are not taking into account the urban microclimate, it is also demonstrated that the use of local meteorological data will have a significant impact, according to which formulation of the convection coefficient is adopted. We additionally compared the coefficient from CIBS and they showed results (not shown here) close to the original formulation by McAdams.

4. Conclusions and Perspectives

This paper presents an experimental setup used for the high frequency and long-term measurement meteorological variables in an urban setup. Seven 3D sonic anemometers have been installed along a vertical axis to provide high frequency measurements of the wind speed and air temperature. A meteorological station installed at the bottom of the mast provides local weather conditions such as the relative humidity, and the air temperature and pressure.

It was shown that the wind speed is highly impacted in an urban setup and that this considerably influences the calculation of the heat convection coefficient. Differences of up to 43 % were noted for the LESO case. An analysis of the sensitivity of two heat convection coefficients was performed. It was established that the use of local climatic data does not have the same effect on their calculation. This can have significant influence when evaluating strategies such as natural ventilation or when conceiving high-energy efficiency building.

The current study will in the near future be expanded to include an analysis of the temperature difference along the vertical axis on the calculation of the convective heat flux, and how this impacts the building energy consumption simulation. Furthermore, high frequency monitoring will be used to calculate turbulent fluxes (momentum and heat) in an urban context, and to develop new parameterization for the Canopy Interface Model (Mauree et al.,

2017). Additionally, a net radiometer will be installed at the beginning of 2017 to complete the setup.

5. Acknowledgements

The authors wish to thank EPFL and the ENAC faculty for their financial support for the equipment and the Commission for Technology and Innovation of the Swiss Confederation for the funding of the Swiss Competence Center for Energy Research, Future Energy Efficiency Buildings and Districts, FEEB&D (CTI.2014.0119). The authors would also like to thank the LESO IT Team (Michael Divia, Jonathan Marquez, Pascal Roulin, and Alexandre Stoll) for their help in the experimental setup.

Nomenclature

Symbols

RH	Relative humidity (-)
θ	Air temperature (K)
e	Vapour pressure (Pa)
P	Air pressure (Pa)
U	Horizontal wind speed (ms^{-1})
m, n	Constants
h_c	Convective heat transfer coefficient ($\text{W/m}^2\cdot\text{K}$)

Subscripts/Superscripts

m	Maximet weather station
s	Sonic measurement
a	Corrected air temperature

References

- Ashie, Y., Vu Thanh Ca, T. Asaeda. 1999. "Building canopy model for the analysis of urban climate". *Journal of Wind Engineering and Industrial Aerodynamics* 81(1-3): 237-48. doi:10.1016/S0167-6105(99)00020-3.
- Cassardo, C., D. Sacchetti, M.G. Morselli, D. Anfossi, G. Brusasca, A. Longhetto. 1995. "A Study of the Assessment of Air Temperature,

- and Sensible-and Latent-Heat Fluxes from Sonic-Anemometer Observations". *Il Nuovo Cimento C* 18 (4): 419-40. doi:10.1007/BF02511367.
- Coccolo, S., J. Kaempf, J.L. Scartezzini. 2015. "The EPFL Campus in Lausanne: New Energy Strategies for 2050". *Energy Procedia* 78: 3174-3179. doi:10.1016/j.egypro.2015.11.776.
- IPCC. 2013. *Working group I contribution to the IPCC 5th assessment report climate change 2013: the physical science basis*. Geneva, Switzerland: Intergovernmental Panel on Climate Change.
- Kaimal, J.C., J.J. Finnigan. 1994. *Atmospheric Boundary Layer Flows: Their Structure and Measurement*. Oxford, UK: Oxford University Press.
- Krpo, A., F. Salamanca, A. Martilli, A. Clappier. 2010. "On the Impact of Anthropogenic Heat Fluxes on the Urban Boundary Layer: A Two-Dimensional Numerical Study". *Boundary-Layer Meteorology* 136(1): 105-27. doi:10.1007/s10546-010-9491-2.
- Mauree, D., N. Blond, M. Kohler, A. Clappier. 2017. "On the Coherence in the Boundary Layer: Development of a Canopy Interface Model". *Frontiers in Earth Science* 4. doi:10.3389/feart.2016.00109.
- Mauree, D., S. Coccolo, J. Kaempf, J.L. Scartezzini. 2017. "Multi-scale modelling to evaluate building energy consumption at the neighbourhood scale". *PLOS ONE* 12 (9): e0183437 doi:10.1371/journal.pone.0183437.
- Mauree, D., J.H. Kämpf, J.L. Scartezzini. 2015. "Multi-scale modelling to improve climate data for building energy models". In: *Proceedings of the 14th International Conference of the International Building Performance Simulation Association*. Hyderabad, India: IBPSA.
- Mirsadeghi, M., D. Cóstola, B. Blocken, J.L.M. Hensen. 2013. "Review of external convective heat transfer coefficient models in building energy simulation programs: Implementation and uncertainty". *Applied Thermal Engineering* 56(1-2): 134-51. doi:10.1016/j.applthermaleng.2013.03.003.
- Oke, T.R. 1982. "The Energetic Basis of the Urban Heat Island". *Quarterly Journal of the Royal Meteorological Society* 108(455): 1-24. doi:10.1002/qj.49710845502.
- Robinson, D. 2012. *Computer Modelling for Sustainable Urban Design: Physical Principles, Methods and Applications*. Routledge.
- Rotach, M.W., R. Vogt, C. Bernhofer, E. Batchvarova, A. Christen, A. Clappier, B. Feddersen, et al. 2005. "BUBBLE – an Urban Boundary Layer Meteorology Project". *Theoretical and Applied Climatology* 81(3-4): 231-261. doi:10.1007/s00704-004-0117-9.
- Salamanca, F., A. Martilli, M. Tewari, F. Chen. 2011. "A study of the urban boundary layer using different urban parameterizations and high-resolution urban canopy parameters with WRF". *Journal of Applied Meteorology and Climatology* 50(5): 1107-1128. doi: 10.1175/2010JAMC2538.1.
- Santiago, J.L., A. Martilli. 2010. "A Dynamic Urban Canopy Parameterization for Mesoscale Models Based on Computational Fluid Dynamics Reynolds-Averaged Navier-Stokes Microscale Simulations". *Boundary-Layer Meteorology* 137(3): 417-39. doi:10.1007/s10546-010-9538-4.
- SFOE, Swiss Federal Office of Energy. 2011. *Public Energy Research in Switzerland*. http://www.bfe.admin.ch/php/modules/publikationen/stream.php?extlang=en&name=en_898824905.pdf&endung=Public%20Energy%20Research%20in%20Switzerland.

Improving Local Wind Estimation for the Automated Control of Blinds

Dasaraden Mauree – Ecole Polytechnique Fédérale de Lausanne – dasaraden.mauree@epfl.ch

Ali Motamed – Ecole Polytechnique Fédérale de Lausanne – ali.motamed@epfl.ch

Laurent Deschamps – Ecole Polytechnique Fédérale de Lausanne – laurent.deschamps@epfl.ch

Jean-Louis Scartezzini – Ecole Polytechnique Fédérale de Lausanne – jean-louis.scartezzini@epfl.ch

Abstract

Blinds are usually installed on building façades to improve the visual and thermal comfort of the occupants. They are now often linked to an automated system that helps control the glare and decrease overheating. These automated systems are linked to a weather station that is located on top of the buildings in which they are installed. In the current study, we show that the use of such stations does not provide accurate and reliable information to the control algorithm. It is proposed to couple a model that can calculate wind speed and direction in an urban canopy to the control algorithm. The model is compared to data from an experimental setup on the EPFL campus, Switzerland. We demonstrate that there is very good agreement between the models and the data that have been collected. Furthermore, a new control algorithm is proposed in order to improve the response of the system during strong gusts and to prevent an erratic behaviour of the automated system.

1. Introduction

Several control mechanisms have been developed in recent years to implement automation systems in buildings to enhance the thermal and visual comfort of the occupants.

The replacement cost of blinds, due to damage caused by strong wind gusts and turbulence patterns, is substantial for the building owner and installer. To protect such installations, a weather station is usually set on top of the buildings to provide information to an automatic control system. However, the location and limited number of weather stations for a particular building give an incorrect or unreliable source of information as these do not always reflect properly the meteorological conditions on the building façade (e.g., wind

speed or turbulence patterns). Thus, the trigger command given to the algorithm to raise the blinds in order to protect them against breakage is based on unreliable information. This frequently contributes to the perception of the occupants that there is an erratic behaviour of the system that often leads to a complete shutdown of the system, often with a visual and thermal discomfort in the building.

It is well known that the urban climate depends on a series of processes taking place at different spatial (from global to local) and temporal scales (Oke, 1982); building energy demand and urban climate are also closely related and interdependent (Ashie et al., 1999; Salamanca et al., 2011; Mauree et al., 2015). It is thus essential to have access to tools, which can evaluate precisely the interactions that exist between buildings and their local climate. Several models have been developed in recent years to better represent the various phenomena influencing the urban climate (Masson 2000; Martilli et al., 2002; Krpo et al., 2010; Mauree et al., 2017).

The monitoring of high resolution vertical meteorological profiles is essential to determine the impact of urban areas/buildings on these variables: it is necessary to represent these effects when evaluating building energy use, air pollutant dispersion and renewable energy potential in urban planning scenarios. Monitored meteorological data are scarcely available with at a vertical resolution. Campaigns such as the BUBBLE (Rotach et al., 2005) observation period provide useful information and data to develop and generalize new parameterizations schemes. However, there is a strong need for such data and in multiple configurations in order to develop new tools and methodologies which can then be used in the evaluation of building energy use. The vertical profiles of variables such as wind speed

and direction, and the air temperature in the vicinity of buildings are crucial in the determination of the momentum and heat fluxes.

In the current study, we first give an overview of the experimental setup, the model used and the new algorithm to control the blind movements. We then give the preliminary results from the setup and compare them with the model. Finally, we conclude and give a few perspectives for the current study.

2. Materials and Methods Setup

This experiment was set up in the framework of the MoTUS (Measurement of Turbulence in an Urban Setup) project (motus.epfl.ch). In the following sections, we describe the setup, the model used to calculate high-resolution vertical profiles and new control algorithm implemented for the control of the blinds.

2.1 Mast

For this purpose of the study, a 27 m mast was installed on the EPFL campus in Lausanne, Switzerland to measure various meteorological parameters. The average building height in this district is around 10 m. Seven 3D sonic anemometers have been placed along the vertical axis every 4 m. Data from the instruments are collected with a frequency of 1 Hz based on the recommendations by Kaimal and Finnigan (1994) and stored in a database at EPFL.

Fig. 1 gives an illustration of the experimental setup of the meteorological tower.

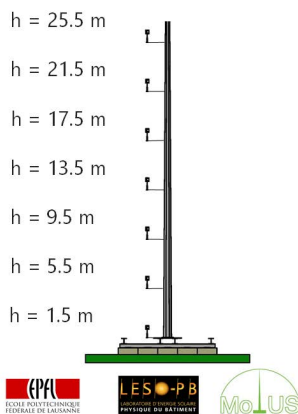


Fig. 1 – Experimental setup

A KNX meteorological station measuring the traditional variables (wind speed and temperature) is

also available on the top of the LESO building. Similar meteorological stations are usually used in automated system to control the blinds.

2.2 Canopy Interface Model

A one-dimensional Canopy Interface Model (CIM) was recently developed (Mauree, 2014; Mauree et al., 2017) to improve the surface representation in meso-scale meteorological models and to prepare the coupling with microscale models, too. For the purpose of this study, CIM will provide high-resolution vertical profiles that will be used as input for the control algorithm.

CIM uses a diffusion equation derived from the Navier-Stokes equations but reduced to one direction only. Equations 1 and 2 are used to calculate the wind speed and potential temperature profiles.

$$\frac{du}{dz} = \frac{d}{dz} \left(\mu_t \frac{du}{dz} \right) + f_u^S \quad (1)$$

$$\frac{d\theta}{dz} = \frac{d}{dz} \left(\kappa_t \frac{d\theta}{dz} \right) + f_\theta^S, \quad (2)$$

where U is the horizontal wind speed in either the x - or y -direction, θ is the potential temperature, μ_t and κ_t are the momentum and heat turbulent diffusion coefficients and f_u^S and f_θ^S are the source terms representing the fluxes (from the surface or buildings) that will impact the flow.

CIM solves for a 1.5-order turbulence closure using the turbulent kinetic energy (TKE). The TKE is calculated using Equation 3:

$$\frac{de}{dt} = \frac{d}{dz} \left(\lambda_t \frac{de}{dz} \right) + C_\epsilon \frac{\sqrt{e}}{l} (e_\infty - e) + f_e^S \quad (3)$$

where e is the TKE, λ_t is the diffusion coefficient (assumed here to be equal to μ_t) is a constant equal to 1, e_∞ is considered to be a stationary value of the TKE, and f_e^S is source term representing the additional production of TKE due to the obstacles.

The momentum and heat diffusion coefficients are calculated using:

$$\mu_t = C_e \sqrt{e} l \quad (4)$$

$$\kappa_t = Pr \mu_t \quad (5)$$

where C_e is a constant equal to 0.3. l is defined as the mixing length and is taken from Mauree et al. (2017)

to account for the obstacles density and height in the canopy.

The CIM has been developed to function in an offline mode and can hence be forced directly at the top using traditional meteorological boundary conditions.

2.3 Control Algorithm

In order to increase the reliability of the system, as well as to decrease the perception of an erratic behaviour of the automation system a new control algorithm was proposed. The objective was to couple the CIM results with the automation system to have more reliable information that could be used to protect the blinds.

Fig. 2 gives an overview of the decision process by the system. CIM calculates at every time step T (every minute in our case) a vertical profile. The simulated value for the wind is then used as an input for the control algorithm. Since we do not want to raise the blind every time there is a gust, we used an additional condition to verify that the wind is blowing above a pre-determined threshold (5 ms^{-1} in our case). Note that the control algorithm also accounts for the daylighting needs of the user, as well as the glare index calculated using sensors inside the controlled offices.

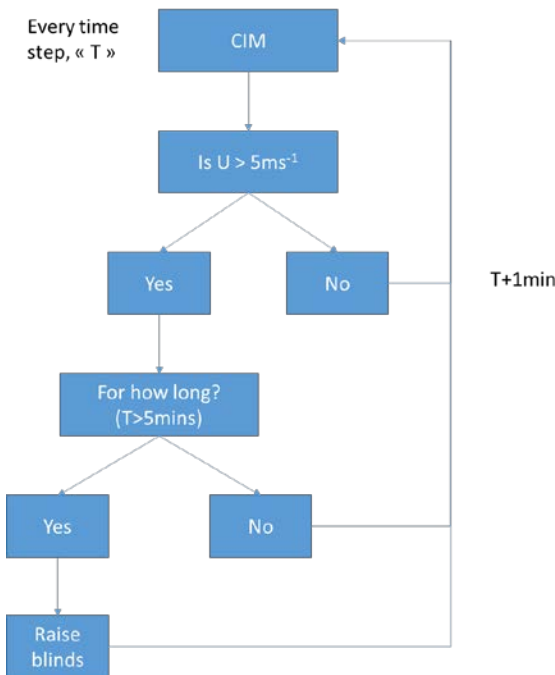


Fig. 2 – Proposed algorithm flow chart

The blinds that are controlled are located on the south-eastern part of the LESO-PB building on the EPFL campus.

3. Results Analysis and Discussion

3.1 Measured Wind Speed

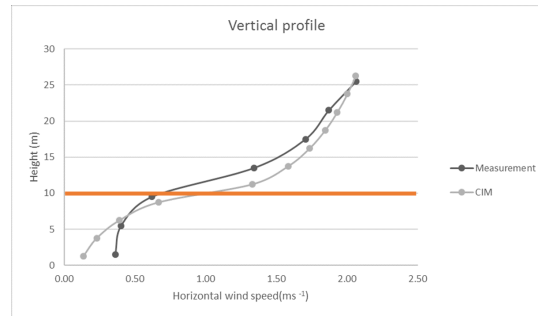


Fig. 3 – Vertical profile of the horizontal wind speed (ms^{-1}) from the sonic anemometers (in black) and results from CIM (in grey) with the height (m) on the vertical axis. The orange line represent the building height (10 m)

As can be expected in an urban context, the wind profile is highly impacted by the presence of buildings. It can be noted from Fig. 3 that the characteristic logarithmic profile is present above the building roof and that below in the canopy layer there is a low horizontal wind speed. This corresponds to results previously reported (Rotach et al., 2005; Santiago and Martilli, 2010).

Table 1 – Wind speed measured at each floor v/s at top

Floor	$U \text{ (ms}^{-1}\text{)}$	Relative difference
1 st	0.36	73%
2 nd	0.40	71%
3 rd	0.62	54%

Table 1 shows the variation of the wind speed measured at each floor with respect to the wind speed measured on top of the building, as usually done with the current automated system. It should be highlighted here that the wind measured can be up to 73 % less strong than the wind measured at the top. Furthermore, the turbulent patterns (not shown

in the present paper) can be significantly altered in the urban canyon.

3.2 Simulated Wind Speed

Boundary conditions from the highest anemometer are then used to force the CIM model. The results are shown in Fig. 3. It can be seen that CIM can reproduce with a very good agreement the measurement. There is however a slight underestimation of the wind speed close to the ground. This might be due to the drag force coefficient parameterization that is usually overestimated (Santiago and Martilli, 2010). The drag force parameterization used in this study is based on the occupied volume (density of the neighbourhood). Since CIM is a 1D model, there is a simplification of the 3D representation of the buildings. This can be the reason for the over-estimation of the drag force close to the ground.

3.3 Control of Blinds

Based on the results that we have obtained, we implemented the new control algorithm in our system to improve the automation of the blinds on the LESO façade.

It was shown that a more realistic and appropriate behaviour of the blinds was possible in an urban context, where the wind speed is usually erratic and can have a significant impact on turbulent patterns.

4. Conclusions and Perspectives

This paper presents the results from an experimental setup that measures meteorological variables in an urban setup. Seven 3D sonic anemometers have been installed along a vertical axis to provide high frequency measurements of the wind speed.

It was shown that the wind speed is highly impacted by the urban context and that this can considerably influence the decision of an automated system to control blinds on a building façade. Differences of up to 73 % were noted in the current case. The vertical profiles from the measurement campaign were then compared with the simulation from CIM. The results showed very good agreement between the computed and measured data. A new control algorithm was then derived to improve the

automation system installed in a building on the EPFL Campus.

The current study will be expanded in the near future to include six more sonic anemometers that will be installed directly on the façade. Furthermore, the experiments will be prolonged for one whole year and the results will be analysed in more details to understand the behaviour of the blinds and of the control algorithm.

5. Acknowledgements

The authors wish to thank EPFL and the ENAC faculty for their financial support for the equipment, and the Commission for Technology and Innovation of the Swiss Confederation for the funding of the Swiss Competence Centre for Energy Research, Future Energy Efficiency Buildings and Districts, FEEB&D (CTI.2014.0119).

Nomenclature

Symbols

U	Wind speed (ms^{-1})
θ	Air temperature (K)
e	Turbulent Kinetic Energy ($\text{m}^2 \text{s}^{-2}$)
e_∞	Stationary TKE value
λ_t	TKE diffusion coefficient ($\text{m}^2 \text{s}^{-1}$)
μ_t	Momentum diffusion coefficient ($\text{m}^2 \text{s}^{-1}$)
κ_t	Heat diffusion coefficient ($\text{m}^2 \text{s}^{-1}$)
z	Height (m)
l	Mixing length (m)
Pr	Prandtl Number
C_e	TKE constant
C_ϵ	Dissipation constant
f_u^s	Momentum surface fluxes
f_ϑ^s	Heat surface fluxes
f_e^s	TKE surface fluxes

Subscripts/Superscripts

t	Referring to turbulent coefficient
s	Referring to surface fluxes

References

- Ashie, Y., Vu Thanh Ca, T. Asaeda. 1999. "Building canopy model for the analysis of urban climate". *Journal of Wind Engineering and Industrial Aerodynamics* 81(1-3): 237-248. doi:10.1016/S0167-6105(99)00020-3.
- Kaimal, J.C., J.J. Finnigan. 1994. *Atmospheric Boundary Layer Flows: Their Structure and Measurement*. Oxford, UK: Oxford University Press.
- Krpo, A., F. Salamanca, A. Martilli, A. Clappier. 2010. "On the Impact of Anthropogenic Heat Fluxes on the Urban Boundary Layer: A Two-Dimensional Numerical Study". *Boundary-Layer Meteorology* 136(1): 105-27. doi:10.1007/s10546-010-9491-2.
- Martilli, A., A. Clappier, M.W. Rotach. 2002. "An Urban Surface Exchange Parameterisation for Mesoscale Models". *Boundary-Layer Meteorology* 104(2): 261-304. doi:10.1023/A:1016099921195.
- Masson, V. 2000. "A Physically-Based Scheme For The Urban Energy Budget In Atmospheric Models". *Boundary-Layer Meteorology* 94(3): 357-397. doi:10.1023/A:1002463829265.
- Mauree, D. 2014. "Development of a multi-scale meteorological system to improve urban climate modeling". Strasbourg, France: Université de Strasbourg.
- Mauree, D., N. Blond, M. Kohler, A. Clappier. 2017. "On the Coherence in the Boundary Layer: Development of a Canopy Interface Model". *Frontiers in Earth Science* 4. doi:10.3389/feart.2016.00109.
- Mauree, D., J.H. Kämpf, J.L. Scartezzini. 2015. "Multi-scale modelling to improve climate data for building energy models". In: *Proceedings of the 14th International Conference of the International Building Performance Simulation Association*. Hyderabad, India: IBPSA.
- Oke, T.R. 1982. "The Energetic Basis of the Urban Heat Island". *Quarterly Journal of the Royal Meteorological Society* 108(455): 1-24. doi:10.1002/qj.49710845502.
- Rotach, M.W., R. Vogt, C. Bernhofer, E. Batchvarova, A. Christen, A. Clappier, B. Feddersen, et al. 2005. "BUBBLE – an Urban Boundary Layer Meteorology Project". *Theoretical and Applied Climatology* 81(3-4): 231-261. doi:10.1007/s00704-004-0117-9.
- Salamanca, F., A. Martilli, M. Tewari, F. Chen. 2011. "A study of the urban boundary layer using different urban parameterizations and high-resolution urban canopy parameters with WRF". *Journal of Applied Meteorology and Climatology* 50(5): 1107-1128. doi: 10.1175/2010JAMC2538.1
- Santiago, J.L., A. Martilli. 2010. "A Dynamic Urban Canopy Parameterization for Mesoscale Models Based on Computational Fluid Dynamics Reynolds-Averaged Navier–Stokes Microscale Simulations". *Boundary-Layer Meteorology* 137(3): 417-39. doi:10.1007/s10546-010-9538-4.

Modelling of Complex Fenestration Systems – Validation Results by Long-Term Measured Data

Martin Hauer – University of Innsbruck – martin.hauer@uibk.ac.at

Michael Grobbauer – SFL technologies GmbH – grobbauer.michael@sfl-technologies.com

Stefan Holper - normconsult OG - office@normconsult.at

Daniel Plörer - University of Innsbruck – daniel.ploerer@uibk.ac.at

Abstract

This paper shows comparative results between simulated and measured values on a complex façade system. The simulation was carried out with the newly implemented model in TRNSYS for complex glazing systems based on the ISO 15099 standard and using BSDF data. Long-term measurements were done on a test façade under real weather conditions. Investigations were made on a major diffuse-reflecting and a highly specular blind system to examine the model capabilities. We compared modelled and simulated layers and air gap temperatures. The overall model results show a satisfying correlation. Nevertheless, model simplifications are reflected in the results and discussed in the conclusion of the paper.

1. Introduction

An integral evaluation of thermal and daylighting performance of complex façade systems (CFS) is a crucial aspect to achieve optimized results in minimizing the energy demand of heating, cooling, and artificial light, while enhancing thermal and visual comfort. By implementing the RADIANCE flux matrix methods, an efficient annual daylight simulation even for complex fenestration systems could be achieved. Therefore, a new model algorithm “ArtLight 2.0” was implemented in TRNSYS in order to enable coupled thermal and daylight simulations with efficient run times in the dynamic building simulation (Hauer et al., 2015).

For the daylight modelling as well as for the thermal modelling, the bi-directional scattering distribution function (BSDF) is used to treat the transmitted part

of the incident radiation. For the thermal part a flexible approach was introduced by Klems (Klems, 1994a, 1994b) to calculate the bi-directional solar transmittance of a CFS by multiplying several matrices - each representing a layer of the complex glazing setup. The hemispherical front and back side of a shading layer is discretized into 145 patches, which allows the description of the transmittance behavior by 145 ingoing and outgoing directions.

For the detailed longwave radiation modelling, the algorithms according to ISO 15099 are used. The detailed longwave radiation exchange between glazing layers and non-planar layers (e.g. shading blinds, screens...) is calculated using “layer-equivalent” parameters specifying the thermal characteristics, based on LBNLs layer-method. This includes the thermal emissivity (front and back) as well as the infrared transmittance of such a non-planar layer. Additionally, a dimensionless and almost free to choose front openness factor describes the permeability of the shading and subsequently its influence on the convective air circulation around and through the slat stack.

Although these model algorithms tend to describe the physical phenomena in detail, a fundamental comparison and validation against measured data is still rarely available in the literature. First, detailed verifications of mathematical models describing complex shades against measurements were carried out within the framework of the IEA Task 34/Annex34. This comprehensive work, conducted by different research laboratories around Europe, included several simulation tools (EnergyPlus, DOE-2, ESP-r, TRNSYS). Results and conclusions are found

in several publications (Loutzenhiser et al., 2008; Simmler and Binder, 2008). Nevertheless, the testing in the previously mentioned studies was short-term and supposed to cover almost ideal situations (e.g., clear sky or cloudy sky) for a significant model validation. Furthermore, the modeling capabilities have improved significantly by the initially mentioned methods in the last years - especially in terms of modelling complex daylight re-directing blinds. The present work contributes to the comparison and validation of a newly introduced CFS modelling method in TRNSYS Type56 (Hiller and Schöttl, 2014). Within the Austrian national research project “lightSIMheat”, beside several simplified approaches, this method is used as a thermal modelling part within the coupled ArtLight-routine. In cooperation with SFL technologies in Stallhofen an extensive long-term monitoring on different façade types was carried out to test these models under real environmental conditions.

2. Thermal Modelling of CFS

2.1 Type56_BSDF in TRNSYS

The latest model implementations based on bi-directional scattering distribution functions (BSDF) are available (Hiller and Schöttl, 2014) for the detailed thermal modelling of CFS within the multi-zone building model in TRNSYS. In contrast to the previous standard window model based on one-dimensional angular dependent input values for transmission, reflection and absorption (WIN-DOE file), the new model uses BSDF-data. (Fig. 1). This enables a detailed optical modelling of multiple scattered reflection and transmission of blind systems - especially in case of specular, daylight redirecting systems. Subsequently, a detailed thermal modelling is done according to the algorithms defined by ISO 15099 standard. Based on the established concept of a layer-by-layer calculation for glazing systems (Fig. 2), the shading blind is thermally treated as a homogenous layer by pre-calculated factors for infrared transparency and effective emissivity that define the longwave radiative exchange. The modelling of the convective

behavior around the shading layer is simply covered by an effective openness factor that describes the “permeability” of the slat stack. These values are calculated for each slat angle.

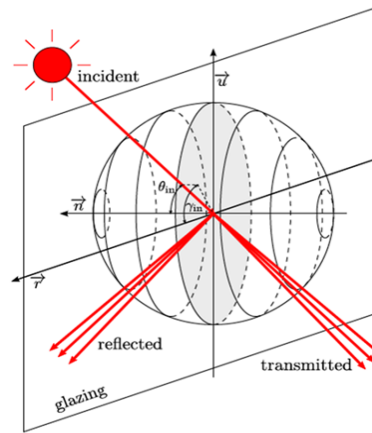


Fig. 1 – Thermal modelling of transmitted solar gains by BSDF datasets (Hiller and Schöttl, 2014)

A comparison between the BSDF-model and the simplified approaches was presented at the Building Simulation Application Conference 2015 in Bolzano (Hauer et al., 2015). As a further step these models are now validated in terms of accuracy and practicability against long-term measurement data from a real office façade carried out within the present work.

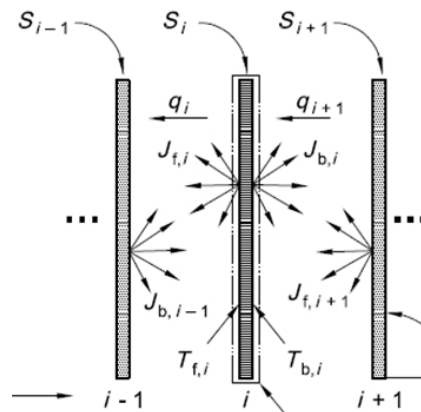


Fig. 2 – Layer-by-layer modelling according to ISO 15099

3. Monitoring

3.1 Façade Description

The monitoring façade is located in one of the Cell-Labs of SFL technologies GmbH (Fig. 3) in Stallhofen/Austria. The Cell Lab is a cubic space with glazing and opaque façade elements in two directions (west and south). The south façade with an exact orientation towards south-south-east (Azimuth = 335°) is an experimental façade that includes different function modules (BIST, BIPV, shading, fan coil) (Mach et al., 2015). The east and north enclosures are convertible internal office walls.



Fig. 3 – Cell-Lab at areal of SFL technologies GmbH

The measurement took place in the south façade within a transparent façade element consisting of a room-height window layer (thermally separated aluminum profiles) as thermal envelope with a rear ventilated impact pane at approx. 150 mm distance to the inner window layer. The window layer consists of a lower door and a fixed overhead window, both with a triple-pane insulated glazing. The impact pane is made of a 12 mm thick double-layer laminated safety glass. The proper description of the window layer setup is documented in Table 1. The investigated venetian blind is mounted between the window layer and the impact pane. During testing the rear ventilation was blocked by an airtight sealing tape.

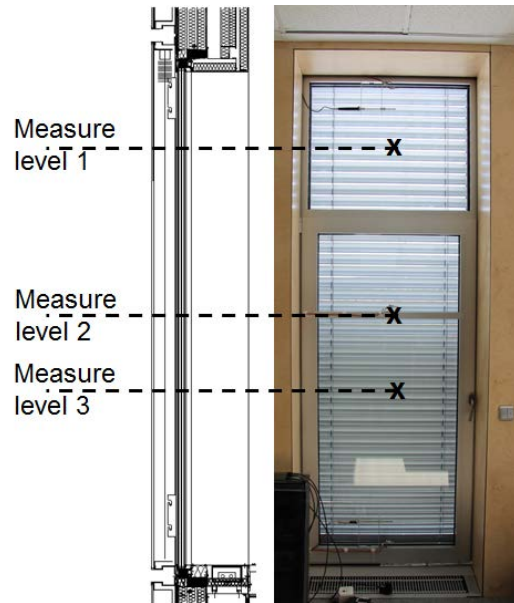


Fig. 4 – Height levels of measurement at the test façade

3.2 Sensor Positions and Radiation Measurements

Sensors were mounted at three different height levels in the façade (Fig. 4) in order to verify differences in the temperature profile over the height. Fig. 5 schematically shows the sensor positions along the façade depth at the different levels. Naming is as follows: the first number indicates the height level; the second number the corresponding system-layer.

Sensors for surface temperatures (OT, Pt100-type 1/3 DIN B) at glazing and blind were mounted on the front and back side of the respective layer (except the outer side of the safety glass): OT10 - OT16 for level 1 and OT30 - OT36 for level 3. On level 2 no surface temperature sensors were used.

Sensors for air temperature (LT, Pt100-type 1/3 DIN B) are situated within the air gap in front and behind the blind stack: LT12 – LT14 for level 1 and LT32 – LT34 for level 3. Additional air sensors in front of the impact pane and behind the windows (seen from outside) are positioned to determine boundary temperatures for the model setup (LT20, LT17, LT27, LT37, LT00).

The vertical airflow velocity is recorded within the air gap between impact pane and blind stack (LT/LG21) respectively on the inner side along the triple-pane glazing (LT26/LG26) on level 2 by hot wire anemometers. These sensors also measured the

air temperature (Ahlborn Almemo FVA935TH4, 0,05–0,2 m/s, bidirectional, resolution 0,0001 m/s, accuracy +/-0,04 m/s).

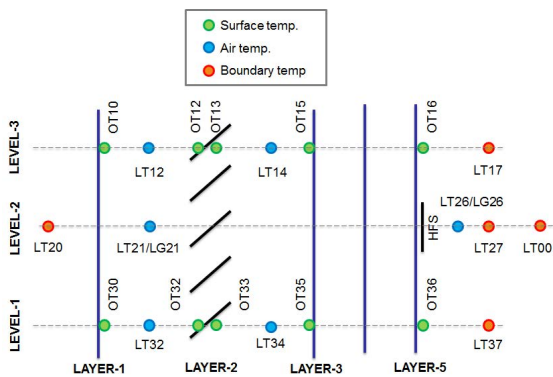


Fig. 5 – Sensor positions on the three measuring levels

Additionally, a heat flux plate (HFS) was mounted on the inner side of the glazing to detect the heat flow to the inside (just valid in times without irradiance on the flux plate).

Irradiance was determined by a secondary standard temperature compensated pyranometer (Kipp & Zonen CMP11) at 285–2800 nm, 0–4.000 W/m², IT_CMP11). In addition, a Daylight measuring instrument (LM-TLM) from company Zumtobel was installed on the rooftop to measure the vertical illuminances for each direction as well as the direct and diffuse component for horizontal illuminance. Thus, the direct-diffuse ratio by the illuminance values was used to split the irradiance value of the CMP11.

During the measuring period a non-standard complex pyranometer with excellent standards was added (Sunshine SPN1, 400–2700 nm, 0–2.000 W/m², IT_SPN1). SPN1 was able to measure direct and diffuse irradiance by means of seven sensors and a shadow ring, which results in one sensor unshaded and one totally shaded, while the others are partly shaded in each measurement. Thus the respective values could be calculated. The vertical global irradiation (perpendicular to the facade) was also measured for the validation of the model by a photo diode sensor, that doesn't cover the whole solar spectrum (EMS11, calibrated in comparison with Kipp & Zonen CMP12, IT_FAS).

In Fig. 6 a comparison between the reference measurements in the façade (IT_FAS), the simulated radiation based on horizontal measurements with

the CMP11 (IT_CMP11) respectively SPN1 (IT_SPN1) are diagramed. Both simulated values show an excellent accordance, even in clear sky as well as in cloudy days. A constant lower measurement result for the vertical global irradiation on the façade (IT_FAS) by photo diode sensor can be mentioned, which can also be partly caused through dust on the sensor.

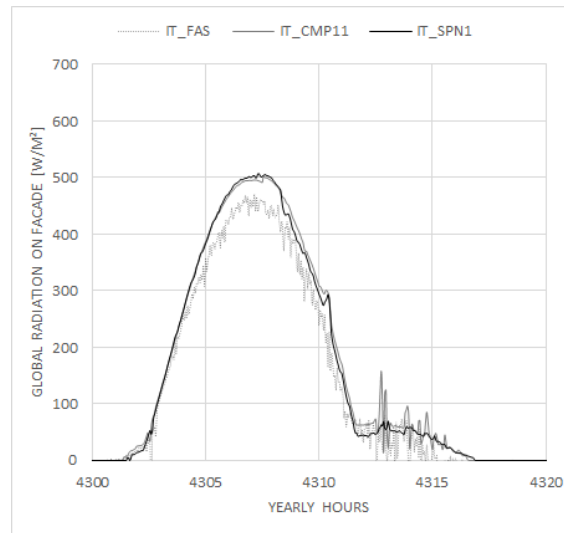


Fig. 6 - Irradiance on Façade: measured vs. simulated

For the model input, the actual radiation on the vertical test façade, which is SSE-oriented (Azi=335°), was calculated based on the measurements by using the Perez 1999 model in TRNSYS Type99.

To get realistic assumptions for the convective heat transfer coefficient, wind velocity and direction on the outer façade were measured by an ultrasonic-sensor, installed in vertical façade orientation (Gill Windsonic, 0–60 m/s, resolution 0,01 m/s, accuracy +/-2 % at 12 m/s, 360 degrees, north facing upwards).

4. Model setup

4.1 System Description Data Acquisition

The system setup of the CFS was done in WINDOW7 according to the glazing layer definition available from manufacturers (Table 1).

Table 1 – Monitoring facade at SFL - layer setup and configuration in WINDOW7

Layer	ID	Product	d
1	893	Impact pane	12 mm
2	1	Shader + Air gap	150 mm
3	11006	Planilux*	6 mm
	9	Air/Argon (10%/90%)	16 mm
4	11393	Planitherm One*	4 mm
	9	Air/Argon (10%/90%)	16 mm
5	11398	Planitherm One II*	6 mm

*Manufacturer: Saint-Gobain

For the monitoring phase two different blind systems were investigated: one diffuse reflective blind with a non-curved geometry and a concave (upward-curved) blind with a highly specular surface on the upper slat side.

According to the geometrical model of the blind, the BSDF dataset was modelled with the RADIANCE tool genBSDF.

Table 2 – Blind Definition

	SYS 1	SYS 2
width	80 mm	80 mm
spacing	72 mm	46 mm
rise	15 mm	11 mm
ϵ_{front}	0.69	0.04
ϵ_{back}	0.93	0.80
material _{front}	Millfinish MP	Miro3
material _{back}	RAL7035	RAL7030

The layer-equivalent factors for the thermal specification of the BSDF-layer are calculated using WINDOW7. The calculation of these factors is based on the view-factor-method and is calculated internally in WINDOW7 by using blinds defined by their geometrical dimensions (Hauer et al., 2014). Through the modelling a geometrically representative slat and their blind material properties (Table 2), the required factors for

infrared transparency (TIR), layer emissivity front ($\epsilon_{\text{ps_f}}$) and layer emissivity back ($\epsilon_{\text{ps_b}}$) are determined to define the thermal characteristic of the BSDF-layer (Table 3).

Table 3 – Results for the effective layer specifications

SYS-1	00deg	45deg	85deg
TIR	0.3565	0.2392	0.0020
$\epsilon_{\text{ps_f}}$	0.5823	0.5957	0.7097
$\epsilon_{\text{ps_b}}$	0.5823	0.7256	0.9391
EOF	0.95	0.5	0.05
SYS-2			
TIR	0.3250	0.1817	0.0037
$\epsilon_{\text{ps_f}}$	0.5385	0.4447	0.04
$\epsilon_{\text{ps_b}}$	0.5385	0.6900	0.8098
EOF	0.95	0.5	0.05

The effective openness factor (EOF) that describes the permeability of the shading layer concerning convection (0=air tight, 1=fully permeable) is treated linear corresponding to the slat angle. Several investigations showed a very low influence of the EOF on the results, while the other thermal parameters showed a clear higher influence. After including these factors into the modelled System-BSDF file and combining them with the glazing layers according to Table 1, a representative BSDF set for the whole CFS was generated and implemented in Type56_BSDF.

4.2 Façade Model Setup in Type56

The thermal model that represents the measuring site includes the outside oriented glazing façade (BSDF-model) and adiabatic walls in all other directions. The geometric expansion in depth (0.175 m) describes the reveal of the window (cf. Fig. 4). The emissivity values of the walls are equally set to 1 and the construction kept massless. The setting of the model boundary conditions is shown in Fig. 7. The best agreement between measured and simulated values could be achieved by using the measured temperature directly in front of the façade (LT20) as the external model temperature, instead of using the measured ambient temperature on the rooftop.

Exterior sky-temperature and the ground-temperature were set equal to the measured

ambient temperature. For the boundary conditions on the inner side of the model, the mean value between the measured air temperatures directly behind the inner glazing (LT17/27/37) was used. This showed a better accordance between measured and simulated values than with the measured air temperature in the room behind. Additionally, the back wall of the thermal model was connected with the measured back-wall temperature of the room.

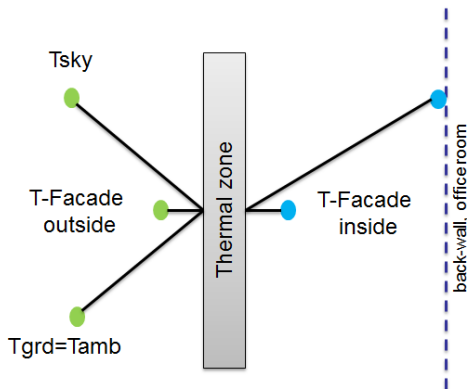


Fig. 7 – Boundary conditions for the thermal model

To model the convective heat transfer coefficient on the outer and inner side of the façade most accurately, an available model in TRNSYS library (Type1232) was used. It calculated an hourly value for the heat transfer coefficient on a vertical flat-plate according to ambient temperature on the surface (outside: LT20; inside: mean value of LT17/27/37), temperature of the surface (outside: mean value of OT30/OT10; inside: mean value of OT16/OT36), as well as the measured air velocities on the outer and inner glazing surface. After implementing these values in the BSDF model of Type56, the results improved significantly, especially for the inner and outer glazing surface temperatures.

5. Results

5.1 System 1

For system 1, several measuring periods were investigated for slat angles of 0°/45° and 85° (fully closed). The comparison of the measurements against the simulation model was done for each layer temperature as well as for the gap temperatures before and behind the slat stack.

Fig. 8 shows a weekly trend of the measured slat temperature (measured on back side) and a tilt angle of 45° compared to the simulations. Especially the rise of the temperature shows a very good agreement. The model underestimates the maximum temperature slightly, although the difference is almost less than 5 K. Due to missing thermal capacity in the blind model, the simulated values fluctuate much more according to the changing irradiance values. The mean deviation between measurement and simulation is in the range of ±5 K.

5.2 System 2

In a second monitoring phase, measurements on system 2 were evaluated similarly for the slat angles of 0°/45° and 85° (fully closed). Fig. 9 shows the weekly temperature trend of the slat temperature (measured on the back side) for a slat angle of 45° compared to the simulations. Although the overall accordance is satisfying, higher deviations are detected compared to the results with system 1. Mainly, an overestimated temperature as well as a faster temperature rise can be recognized by the simulation model. The mean deviation between measurement and simulation is in the range of ±10 K. In Table 4 the Root-mean square errors (1) are summarized for all measured layer and gap temperatures at each slat position and each system. Systematically, the lowest deviations are at the layers on the outer and inner side of the glazing system (OT10/OT16). And generally, highest deviations are reached in both systems for closed blind positions.

$$RMSE = \sqrt{\frac{1}{n} \sum_{i=1}^n (y_{meas} - y_{sim})^2} \quad (1)$$

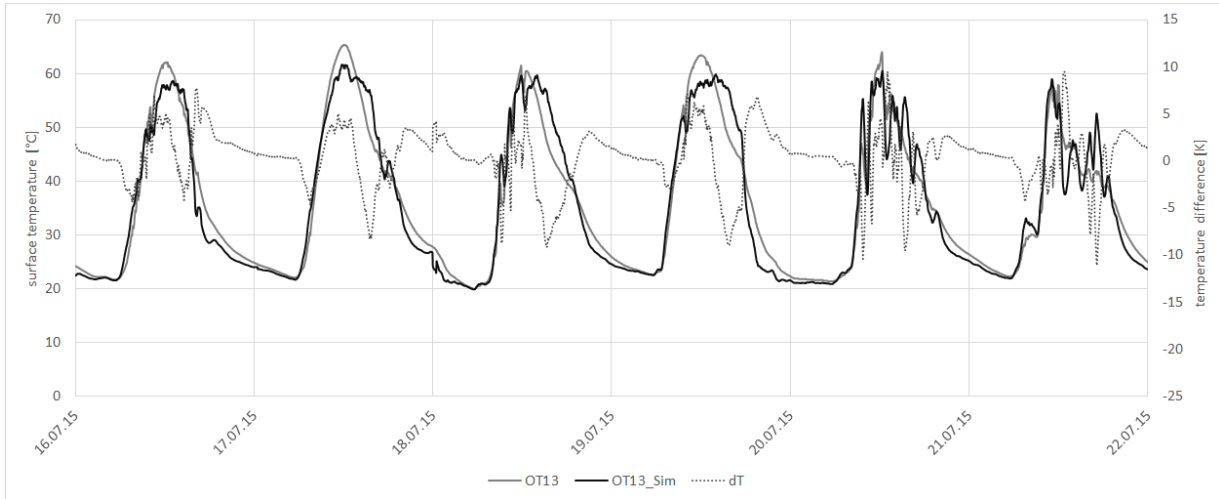


Fig. 8 – Blind temperature, System 1 - 45° slat angle

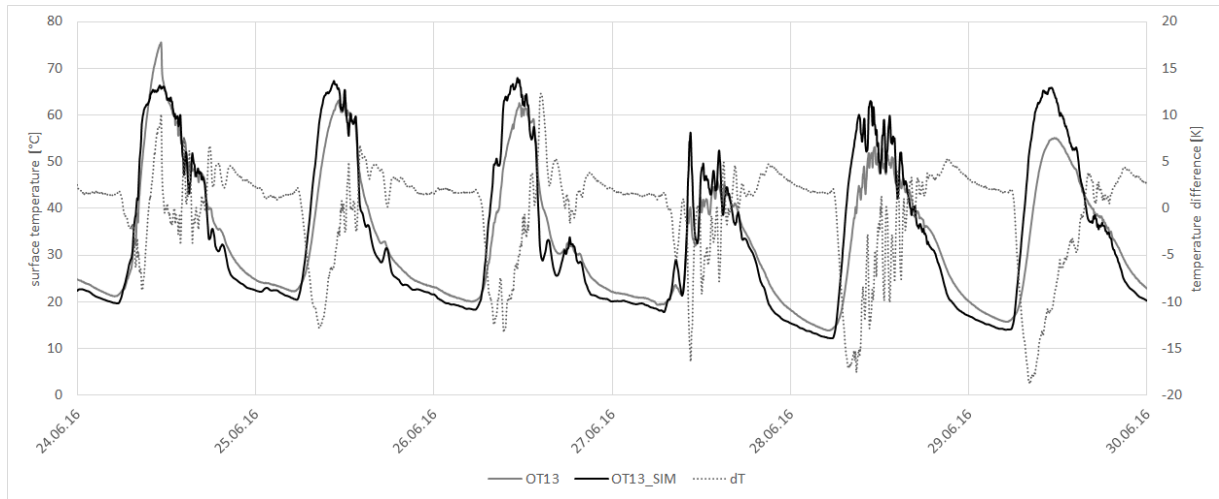


Fig. 9 – Blind temperature, System 2 - 0° slat angle

Table 4 – RMSE for temperature differences (in K) measured vs. simulated values (level 1)

SYS1	dT_OT10 [K]	dT_LT12 [K]	dT_OT12 [K]	dT_OT13 [K]	dT_LT14 [K]	dT_OT15 [K]	dT_OT16 [K]
00deg	2.575	4.187	3.249	3.111	3.981	4.542	2.572
45deg	1.889	2.806	2.323	2.277	2.682	3.137	1.169
85deg	4.433	5.765	5.455	5.432	5.387	6.524	1.694
SYS2							
00deg	4.702	5.149	6.243	6.248	6.027	6.820	1.322
45deg	3.112	3.794	4.962	5.266	6.223	6.844	0.943
80deg	2.594	3.793	10.327	10.79	9.902	12.395	3.251

6. Conclusions

By collecting long-term measurement data for two different façade systems, an extensive proof of the model validity of the recently implemented BSDF/ISO-model in TRNSYS Type56 could be shown. The results are very satisfying in general. Deviations between measurement and modelling are shown especially for peak values. Reasons for this can be either through model simplifications done by ISO 15099 (convective model, layer emissivity) or either by a limited resolution for the optical modelling by the BSDF data based on Klems resolution. Especially for system 2 (specular blind surface) this aspect could be critical.

In the overall results by the RMSE-analyse, the highest deviations are mentioned for closed blind conditions that are not satisfying. In this case, an individual analysis for the measured values on level 3 (bottom) showed much better accordance compared to level 1. A strong stack effect by temperature layering could be obtained, which is not sufficiently represented in the modelling.

In general, neglecting the thermal mass of the single glazing could show a significant influence on the modelled layer temperatures. With an increasing layer number (from outside to inside) an increasing time shift of approx. 0,5-1 hour between measured and simulated values occurred. In case of future trends in modelling glazing systems up to 4 panes including a shading layer, this aspect gains significant relevance. A model adoption towards including the thermal mass is recommended.

Based on these conclusions, further in-deep analysis of the model will be done by static measurements in a g-value test chamber as well as dynamic measurements with a newly developed measuring method for in-situ g-value measurements. Beside the gained validation results, this work successfully represents the full workflow, starting from the manufacturers' information, the use of powerful (partly free) tools (genBSDF, WINDOW7, IGDB) to generate the needed simulation data and built up of the model for simulating complex fenestrations systems.

References

- Hauer, M., D. Geisler-Moroder, M. Hiller. 2015. "Thermal modelling of complex fenestration systems. Comparison of a BSDF-based model with simplified approaches". In: *Proceedings of BSA 2015 - Building Simulation Applications*. Bolzano, Italy: BUPRESS.
- Hauer, M., M. Hiller, C. Kofler. 2014. "Comparative thermal simulation of conventional and daylight deflecting systems with BSDF-based Models in TRNSYS and EnergyPlus". In: *Proceedings of EuroSun 2014*.
- Hiller, M., P. Schöttl. 2014. "Modellierung komplexer Verglasungssysteme in TRNSYS". In: *Proceedings Bausim 2014*.
- ISO. 2003. *ISO 15099:2003: Thermal performance of windows, doors and shading devices — Detailed calculations*. Geneva, Switzerland: ISO.
- Klems, J.H. 1994a. "A new method for predicting the solar heat gain of complex fenestration systems. I. Overview and derivation of the matrix layer calculation". *ASHRAE Transactions* 100: 1064–1072.
- Klems, J.H. 1994b. "A new method for predicting the solar heat gain of complex fenestration systems. II. Detailed description of the matrix layer calculation". *ASHRAE Transactions* 100: 1073–1086.
- Loutzenhiser, P.G., H. Manz, S. Carl, H. Simmler, G.M. Maxwell. 2008. "Empirical validations of solar gain models for a glazing unit with exterior and interior blind assemblies". *Energy and Buildings* 40(3): 330–340. doi: 10.1016/j.enbuild.2007.02.034.
- Mach, T., M. Grobbauer, W. Streicher, M.J. Müller. 2015: *mppf - The Multifunctional Plug&Play Approach in Facade Technology*. Graz, Austria: Verlag der Technischen Universität Graz.
- Simmler, H.; B. Binder. 2008. "Experimental and numerical determination of the total solar energy transmittance of glazing with venetian blind shading". *Building and Environment* 43(2): 197–204. doi: 10.1016/j.buildenv.2006.10.011.

Cooling Energy Needs in Non-Residential Buildings Located in Mediterranean Area: A Revision of the Quasi-Steady Procedure

Roberto Bruno – University of Calabria – roberto.bruno@unical.it

Natale Arcuri – University of Calabria – natale.arcuri@unical.it

Cristina Carpino – University of Calabria – cristina.carpino@unical.it

Abstract

With the Italian Interministerial Decree of 25 June 2015, the evaluation of the cooling energy requirements for residential and non-residential buildings has become mandatory. In Italy the UNI TS 11300-1 is the reference standard for the calculation of cooling energy requirements, by integrating the quasi-steady models of the international standard EN ISO 13790. The Italian standard takes into account some corrections in order to obtain even more precise results, but the deviances are still evident for non-residential buildings equipped with large glazed surfaces. Therefore, these models have to be calibrated further for Mediterranean climatic characteristics because the results are still discordant with those obtained by dynamic simulation codes. With reference to Mediterranean climatic conditions, a new correlation to use in the quasi-steady calculation procedure, derived from summer gain utilization factors, is proposed. The latter were calculated by means of TRNSYS simulations, varying the percentages and the typologies of the windowed surface and the time constant class of a reference non-residential building. The main factors causing the divergences in the results were identified and a proper calibration of the quasi-steady procedure contextualized to the summer Italian climatic conditions is proposed, in order to obtain cooling requirements closer to those provided by TRNSYS.

1. Introduction

For many years, designers have been looking for simplified procedures for the calculation of energy demands in buildings, to use as alternative to complex dynamic simulation codes. This need is still more evident in summer, where the variability of the external forcing on the building envelope makes the calculation of the cooling energy requirements difficult. In this field, the literature provides

different simplified procedures that can be derived by direct and indirect methods (ASHRAE, 2005). Quasi-steady procedures employed at monthly level were proposed (Bauer and Scartezzini, 1999) by introducing the concept of the gain utilization factor (in winter) and the loss utilization factor (in summer) in order to take into account the dynamic effects on the thermal energy demands. Moreover, the summer procedure is similar to those employed in winter by inverting the role of thermal losses and energy gains. Other simplified methods for the cooling energy demand calculation are the Dutch model (NEN 2916, 1994; Van Dijk and Spiekman, 2003; Van Dijk et al., 2005) and the so-called Schibuola model (Schibuola, 1999). The first uses a loss utilization factor, while the second a gain utilization factor. Beccali et al. (2001) carried out a comparison between the two models, highlighting how difficult it is to assess a cooling energy model similar to those already employed for the calculation of heating energy requirements. Other analyses concerning the quasi-steady procedures to use in the cooling period can be found in Mazzarella (2000) and in Prada et al. (2011) to investigate the role of the loss utilization factor. Finally, also international standards have adopted the quasi-steady procedure for the summer calculation such as CEN (CEN, 2005) and ISO (ISO, 2008). The latter represents the reference document for the determination of the energy required for space heating and cooling, from which the Italian regulation UNI 11300-1 was derived (UNI, 2014). However, the original procedure was developed for continental climates where the differences between summer energy gains and thermal losses are limited. Instead, in the Mediterranean climatic context the opposite occurs, especially in well-

insulated building envelopes equipped with large glazed surfaces, typical of the non-residential sector. Despite the fact that an appropriate procedure to correct the loss utilization factor contextualized to the Mediterranean climate was proposed by Corrado et al. (2007), the deviations of the cooling energy requirements determined by dynamic codes remain large for the mentioned building typology.

2. The Quasi-Steady Approach

The calculation method described in the ISO 13790 standard is based on a monthly energy balance between thermal losses and heat gains in steady-state conditions. Successively, the dynamic effects on the cooling energy needs are taken into account by the loss utilization factor, which considers the mismatching between thermal losses and energy gains, and an adjustment of the setpoint temperature for intermittent cooling or set-back. Both depend on the time constant of the building and on the monthly heat balance ratio (defined in ISO 13790 as the ratio between the monthly energy gains and the monthly thermal losses). So, the cooling energy demand can be determined in function of the loss utilization factor as:

$$Q_{C,nd} = Q_{C,gn} - \eta_{C,ls} \cdot Q_{C,ht} \quad (1)$$

where the latter is calculated by the relation (if the heat balance ratio is higher than zero):

$$\eta_{C,ls} = \frac{1 - \gamma_C^{-a_C}}{1 - \gamma_C^{-(a_C + 1)}} \quad (2)$$

According to the Italian UNI 11300-1 standard, the superscript a_C depends not only on the building time constant, but also on the ratio between glazed and floor surfaces. This coefficient was calibrated by means of different cases study developed for Mediterranean climates and can be determined by the following correlation (Corrado et al., 2007):

$$a_C = 8.1 - 13 \cdot \xi + \frac{\tau}{17} \quad (3)$$

strongly different from the correlation suggested by ISO 13790 for continental climates:

$$a_C = 1 + \frac{\tau}{15} \quad (4)$$

The coefficients that appear in Equations (3) and (4) were evaluated by multiple regression of different values of the loss utilization factor calculated by the inverse solution of Equation (1). The actual cooling energy needs, and the equivalent values to the steady-state thermal losses and energy gains, can be provided by dynamic codes, by applying procedures as the "Black Box" method (ISO, 2008). The ISO 13790 standard provides also another method to calculate the cooling energy demands, which employs a gain utilization factor:

$$Q_{C,nd} = (1 - \eta_{C,gn}) \cdot Q_{C,gn} \quad (5)$$

where the thermal losses appear indirectly because involved in the calculation of the same factors. It is easy to demonstrate that:

$$\eta_{C,gn} = \frac{\eta_{C,ls}}{\gamma_C} \quad (6)$$

In this paper, regarding a reference non-residential building located in two different places of the Italia peninsula, a new correlation for the " a_C " parameter derived from the summer gain utilization factors, is proposed. The latter were calculated by the inverse solution of Equation (5) employing results provided by TRNSYS v.17 code (Klein et al., 2012). Successively, the cooling energy requirements obtained with the proposed procedure were compared with the TRNSYS results, in order to quantify the result deviances.

3. The Reference Building

The energy evaluations were carried out with reference to an office building (Fig. 1) varying the glazed surface, the glazed system, the building time constant, and climatic data. In the latter case, the same building was located in Rome (Lat. 41.9°N) and Cosenza (Lat. 39.3°N) by employing monthly

average daily climatic data listed in the Italian UNI 10349-1 standard (UNI, 2016). It consists of ten storeys with a conditioned volume lower than 10,000 m³. The ground floor is equipped with “pilotis” to avoid heat transfer towards the soil. The remaining nine floors have the same size with a rectangular form (10×30 m) and a longitudinal development in the east-west direction. The overall height is 33 m and the stairway is externally located in the north façade to avoid the presence of non-air-conditioned spaces. The reference building was considered as a single thermal zone conditioned by a centralized plant with the same indoor air temperature regulation. Table 1 shows the cases studied and indicates the percentage of the windowed surface (WWR, in function of the vertical opaque walls), the windowed system, the ratio of the glazed area to floor area, and the building time constant. The case studies were conducted for both localities. Time constant values variation was obtained by modifying the glazed surface area, the windowed system and the surface of internal walls. Their calculation was carried out by considering a mono-capacitive model of the building fabric.



Fig.1 – Non-residential reference building with WWR of 50 %

Table 1 – Cases study conducted on the reference building located in Rome and Cosenza

Case	WWR	Windowed System	ξ	τ [h]
1	50 %	Double	0.37	47.9
2	25%	Double	0.19	64.5
3	50%	Double	0.37	87.0
4	10%	Double	0.07	79.7
5	75%	Double	0.52	39.0
6	50%	Single	0.37	29.6
7	50%	Triple	0.37	53.4

4. Simulation Results

By applying the “Corrado” method in alternative to the Black Box approach (Corrado et al., 2007), the TRNSYS simulations allowed us to determine the gain utilization factors from Equation (5), for every case in the considered locations. The mentioned method allowed us to calculate energy gains and energy losses “equivalent” to the steady-state conditions. These values, together with the actual cooling demands, are requested for the inverse solution of Equation (5). The indoor set-point temperature was set to 26 °C supposing a continuous operation regime of the cooling plant. The calculation of the gain utilization factors was preferred to the calculation of the loss utilization factors because the latter, derived from Equation (1), could tend to infinity in presence of reduced thermal losses. Moreover, the procedure has highlighted two critical aspects:

- the utilization factors are calculated by considering the involved energies in the whole months, while the UNI TS 11300-1 considers the fraction of month included in the cooling period. Consequently a mismatch between the equivalent and the steady-state values of the heat balance ratios was detected;
- the “ac” correlations were formulated considering equivalent heat balance ratios, but the latter could be strongly different from those determined in steady-state conditions, which will be used in Equation (2), providing different values of the utilization factors.

Regarding the locality of Rome, in Fig. 2 the cooling energy requirements (in kWh) determined by TRNSYS and by the ordinary UNI TS 11300-1 steady-state procedure, are presented for the seven

considered cases. The results concern the seasonal cooling requirements determined as the sum of the monthly needs. The deviations among the obtained results (TRNSYS results as reference) range between 4.9 % (Case 4) and 21.2 % (Case 5). Similar values were determined for the other locality.

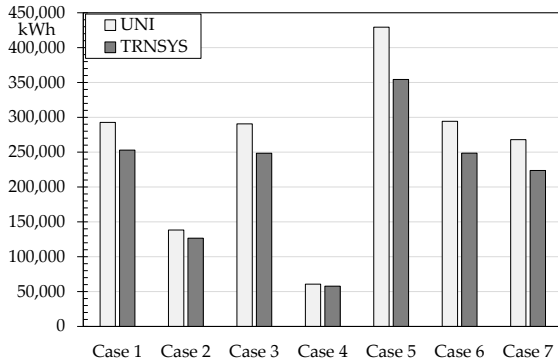


Fig. 2 – Rome: cooling energy requirements for the reference building in the considered cases (in kWh per year)

The deviations are limited for envelopes equipped with limited windowed surfaces, contrarily the differences are more marked with the glass surface growth. Except for Case 4, percentage differences always greater than 10 % were detected. If we suppose that the reference building is conditioned by electric heat pumps with seasonal EER of 2.5, in Case 5 the deviation between the UNI procedure and TRNSYS produces an electric energy overestimation greater than 75000 kWh at seasonal level, corresponding to 18750 € in expenses for electricity (in continuous regime operation). Therefore, these percentages cannot be neglected and they produce an evident mistake in the summer energy performances reported in the building energy certificate. Regarding the comparison between equivalent and steady-state monthly energies, the observed deviances can be summarized as follows:

- noticeable errors are detected for the thermal losses when the monthly average daily temperature value of external air is next to the internal setpoint;
- solar gains determined with the UNI procedure are always overestimated compared to TRNSYS results, but the deviances among the monthly energy remain almost constant.

5. Discussion

The evaluations of the monthly energy gains and monthly thermal losses in steady-state conditions are “adjusted” by the application of the utilization factors. However, in the UNI 11300-1 the latter are calculated by Equation (2) using heat balance ratios different from those employed for the identification of the parameter a_C . Therefore, a more precise evaluation of the steady-state heat balance ratio is recommended in order to calculate utilization factors more similar to those derived from the “Corrado” method. Thus, a better quantification of the summer thermal losses and summer energy gains is required. However, it is very difficult to assess the envelope thermal losses in steady-state conditions, because the external air temperature can rise or drop below the internal setpoint. In the Mediterranean climatic context, the thermal losses can be very limited during the cooling period, therefore elevated heat balance ratios could be achieved. In order to avoid this condition, the use of the reciprocal value of the heat balance ratio seems to be more appropriate. From the energy gains point of view, instead, the constant monthly difference between the steady-state and the equivalent solar gains suggests that other geometrical and optical aspects concerning the building have to be analysed in detail. Fig. 3 presents the trend of the gain utilization factors determined through the 14 examined cases, in function of the reciprocal value of the heat balance ratio. The dependence of the dynamic coefficient on the time constant is less pronounced when compared with the loss utilization factor. If we suppose to use Equation (7) for the interpolation of the gain utilization factors derived from TRNSYS, a multiple regression allowed us to identify the superscript “ a_C ” values that better fit the equivalent heat balance ratios.

$$\eta_{C,gn} = \frac{\gamma_C^{-1} - \gamma_C^{-(a_C+1)}}{1 - \gamma_C^{-(a_C+1)}} \quad (7)$$

Successively, by setting the dependence of the coefficient a_C from the time constant and the ratio between windowed and floor surfaces, the following correlation was determined:

$$a_C = 7.25 \cdot \xi + \frac{\tau}{10} \quad (8)$$

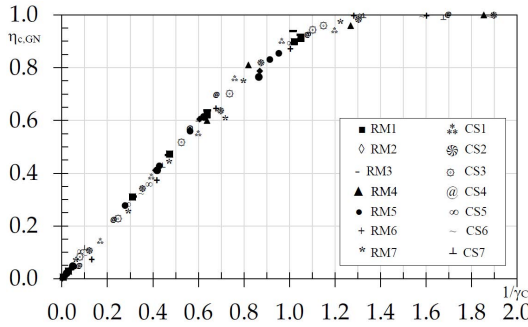


Fig. 3 – Trend of the gain utilization factor vs. reciprocal of the heat balance ratio for Rome (RM) and Cosenza (CS)

Negative values of the gain utilization factor can be obtained when also the heat balance ratios assume negative values (thermal losses are an additional load). This condition happens when the monthly average daily temperature value of external air is higher than the internal setpoint. In this case, the gain utilization factor can be set equal to the heat balance ratio. In Fig. 4 the energy requirements determined by utilization factors evaluated with the ordinary procedure exploiting the Equation (3) (UNI_1) and determined with the new proposed correlation (UNI_mod), are shown. In the same figure, the actual cooling needs determined by TRNSYS are also reported. In every case, the second correlation allows for better results when compared with those provided by TRNSYS. The deviations are more limited, in particular for the examined cases the percentage errors detected are reduced respectively:

- from 15.7 % to 11.5 % for Case 1;
- from 10.3 % to 4.5 % for Case 2;
- from 16.9 % to 12.7 % for Case 3;
- from 4.9 % to -3 % for Case 4;
- from 21.2 % to 15.1 % for Case 5;
- from 18.4 % to 13.2 % for Case 6;
- from 19.8 % to 15.5 % for Case 7.

Similar results were achieved for the second city, therefore they are not reported. If in Equation (7) heat balance ratios closer to the equivalent ones are employed, better results can be achieved. A noticeable improvement can be obtained with a more precise determination of solar gains in steady-state conditions and by using the reciprocal of the heat balance ratio. By setting:

$$\gamma_{C,gn} = \frac{1}{\gamma_C} \quad (9)$$

Equation (7) can be rewritten as:

$$\eta_{C,gn} = \frac{\gamma_{C,gn} - \gamma_{C,gn}^{(a_C + 1)}}{1 - \gamma_{C,gn}^{(a_C + 1)}} \quad (10)$$

with $\gamma_{C,gn}$ that assumes compact values.

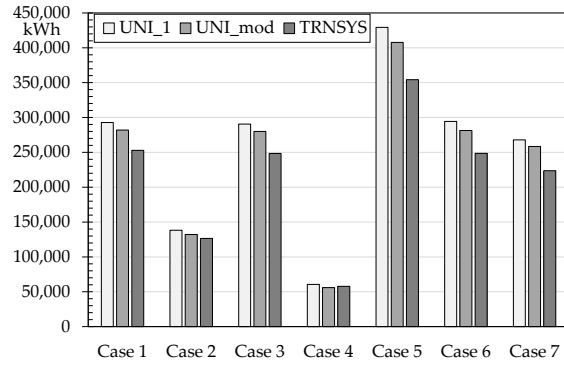


Fig. 4 – Rome: comparison among the cooling energy requirements (in kWh per year) for the reference building determined with ordinary a_C values (UNI_1), the proposed a_C values (UNI_mod) and with TRNSYS

5.1 Improvement in Steady-State Solar Gains Evaluation

The difference determined at a monthly level between steady-state energy gains and equivalent energy gains is almost constant; a comparison is shown in Fig. 5 for Rome for Cases 4 and 5. Therefore, a common aspect concerning solar gains calculation in steady-state conditions has not been adequately considered. Regarding building envelopes equipped by large glazed surface, in fact, the part of solar radiation reflected by the inner surface in the air-conditioned volume, escaping newly through the same glazed surface, is not quantified. This fraction of solar radiation does not become a cooling load for the internal environment, and it cannot be neglected. Moreover, this aspect is cited by ISO 13790 as a “noise” source for the evaluation of the utilization factors, and in the calculation of the equivalent energy gains, TRNSYS considers this solar gain rate adequately. In order to evaluate the missed contribution related to the escaping solar irradiation, an absorption coefficient of the indoor environment (or cavity absorption coefficient) can be introduced.

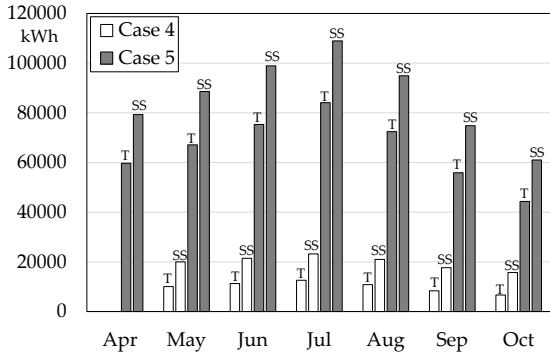


Fig. 5 – Rome: comparison between solar gains obtained with steady-state model (SS) and TRNSYS (T) for Cases 4 and 5

Fig. 6 shows the trend of this coefficient, in function of the ratio between glazed surface and global opaque surface Ψ (including floor, ceiling, and inner surface areas) and for three types of the usual clear glass by assuming a mean solar absorption coefficient of internal walls equal to 0.35 (Oliveti et al., 2011). The difference among the three considered windowed surfaces is related to the different optical properties of the glasses that determine a different amount of entering and escaping solar radiation. For a Ψ factor of 0.1, corresponding usually with a whole glazed wall, the cavity absorption coefficient is about 0.7, therefore 30 % of the incoming solar radiation does not become a cooling load for the indoor environment. Contrarily, for Ψ ratios lower than 0.05 (typical in residential buildings), the role of α_{cav} can be neglected. The relations to use for α_{cav} calculation for clear single, double, and triple pane are respectively:

$$\begin{aligned} \alpha_{cav} &= 1 - 2.00 \cdot \exp\left[-1.60 \cdot \left(\frac{0.35}{\Psi}\right)^{0.33}\right] \\ \alpha_{cav} &= 1 - 1.87 \cdot \exp\left[-1.64 \cdot \left(\frac{0.35}{\Psi}\right)^{0.33}\right] \\ \alpha_{cav} &= 1 - 1.86 \cdot \exp\left[-1.78 \cdot \left(\frac{0.35}{\Psi}\right)^{0.31}\right] \end{aligned} \quad (11)$$

By modifying the steady-state solar radiation transmitted through windowed surfaces by the cavity absorption coefficient, the new comparison with solar gains determined by TRNSYS at seasonal level, is shown in Fig. 7.

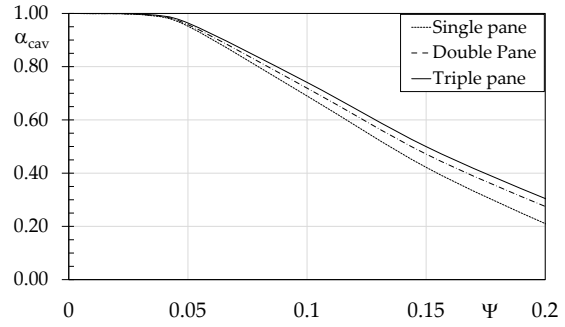


Fig. 6 – Cavity absorption coefficient of the solar radiation in function of the ratio Ψ and for three types of clear glass

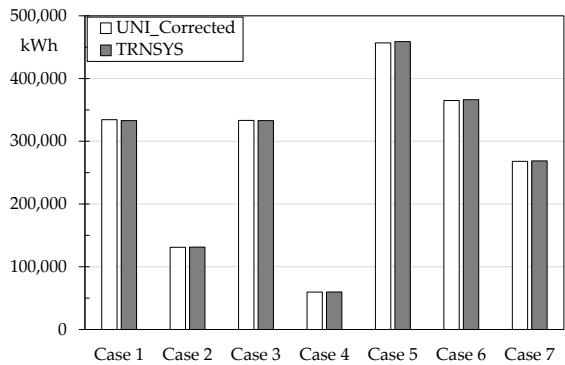


Fig. 7 – Rome: seasonal solar gains obtained by considering the cavity absorption coefficient in the steady-state procedure and comparison with TRNSYS

The values concerning the equivalent heat balance ratio provided by TRNSYS, those determined by the ordinary steady-state model, and those calculated by the corrected solar gains, are listed for Rome in Table 2. Despite the errors concerning the thermal loss evaluations, the correction of the solar gains allows for a calculation of the heat balance ratios close to the equivalent ones, and the deviances are reduced when the lower is given by the outside air temperature. Similar deviations were obtained for the second locality. Finally, the cooling energy requirements was calculated in function of the gain utilization factor determined by Equation (10) by employing the coefficient α_c determined by Equation (8) and the heat balance ratios calculated with corrected solar gains. Considering that Equation (8) was derived by TRNSYS results, where the aspects concerning the “escaping” solar radiation were already taken into account, the monthly energy gains that appear in Equation (5) have to be calculated without solar gains correction. The latter aspect, in fact, is successively adjusted by the application of the gain utilization factor. Fig. 8 shows the results for Rome for the 7 analysed cases by observing a reduction of the

deviances in the cooling energy requirements. The proposed quasi-steady approach provides a slight overestimation, but the detected percentage errors now are always lower than 5%. In particular, these errors are equal respectively to 4% for Case 1, -0.9% for Case 2, 4.6% for Case 3, 4% for Case 4, 4.5% for Case 5, 1.8% for Case 6, and 2.8% for Case 7. Similar

	Case 1			Case 2			Case 3			Case 4			Case 5			Case 6			Case 7		
	$\gamma_{C,gn1}$	$\gamma_{C,gn2}$	$\gamma_{C,gn3}$																		
Apr	1.02	0.88	1.01	-	-	-	1.05	0.87	1.00	-	-	-	0.91	0.75	0.89	-	-	-	1.03	0.86	1.09
May	0.64	0.55	0.64	0.87	0.76	0.85	0.64	0.54	0.63	1.27	1.18	1.28	0.56	0.47	0.56	0.87	0.68	0.72	0.64	0.54	0.69
Jun	0.31	0.24	0.28	0.41	0.34	0.38	0.31	0.24	0.28	0.64	0.54	0.59	0.28	0.21	0.25	0.42	0.30	0.32	0.31	0.24	0.30
Jul	0.03	0.02	0.02	0.03	0.03	0.03	0.04	0.02	0.02	0.05	0.04	0.05	0.03	0.02	0.02	0.05	0.02	0.03	0.03	0.02	0.02
Aug	0.01	0.04	0.04	0.00	0.05	0.06	0.01	0.04	0.04	-0.01	0.08	0.09	0.01	0.03	0.04	0.02	0.05	0.05	0.00	0.04	0.05
Sep	0.47	0.40	0.46	0.61	0.54	0.61	0.47	0.40	0.46	0.82	0.83	0.89	0.43	0.35	0.41	0.62	0.50	0.53	0.47	0.39	0.50
Oct	1.05	0.95	1.09	1.34	1.26	1.39	1.02	0.94	1.08	1.85	1.81	1.94	0.95	0.83	0.97	1.49	1.18	1.24	1.04	0.93	1.16

Table 2 – Rome: heat balance ratios determined by TRNSYS ($\gamma_{C,gn1}$), by ordinary steady-state procedure ($\gamma_{C,gn2}$) and by correcting solar gains with the cavity absorption coefficient α_{cav} ($\gamma_{C,gn3}$)

results were obtained for Cosenza. The detected errors are mainly linked to the employment of the correlations appearing in Equation (8) and Equation (11).

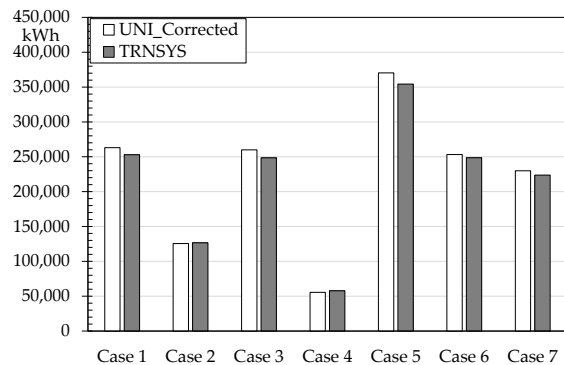


Fig. 8 – Rome: comparison of the cooling energy requirements determined with the proposed procedure and evaluated by TRNSYS for the reference building and for the 7 examined cases

6. Conclusion

An alternative correlation to determine the utilization factors required for the calculation of cooling energy requirements with the quasi-steady approach, is proposed. The correlation was derived by interpolating the values of the summer gain utilization factors, because in the Mediterranean climatic context the calculation of the loss utilization factor could be affected by reduced thermal losses. The equivalent monthly energy values, concerning energy gains and energy losses and the actual cooling needs, required for the evaluation of the gain utilization factor, were determined by the TRNSYS code. Successively, the results provided by the proposed procedure were compared with the TRNSYS cooling demands in order to quantify the deviances. A noticeable improvement in the results has been achieved by introducing a correction factor for the solar gains through glazed surfaces. For a building equipped with large glazed surface, the steady-state procedure does not consider the fraction of solar radiation “escaping” from the air-conditioned space due to the inner surface reflection. By correcting the steady-state solar gains by an appropriate cavity absorption coefficient, heat balance ratios close to the equivalent ones determined by TRNSYS, were achieved. This aspect allowed a more precise calculation of the utilization factors, as well as the evaluation of cooling energy demands similar to those provided

by TRNSYS for a reference non-residential building. Regarding the 14 examined cases, the percentage errors on the cooling requirements, calculated by using the TRNSYS results as reference values, are always lower than 5 % considering different building configuration and two different localities.

Nomenclature

Symbols

a	Utilization factor parameter [-]
α	Absorption coefficient [-]
γ	Heat balance ratio [-]
η	Utilization factor [-]
Q	Monthly energy [kWh]
τ	Time constant [-]
ξ	Glazed/floor area ratio [-]
Ψ	Glazed/opaque area ratio [-]

Superscripts/Subscripts

C	Cooling
cav	Cavity
gn	Gain
ht	Thermal loss
ls	Loss
nd	Energy requirement

References

- ASHRAE. 2005. ASHRAE Handbook of Fundamentals. Atlanta, U.S.A.: ASHRAE.
- Bauer, J., J.L. Scartezzini, 1998. "A simplified correlation method accounting for heating and cooling loads in energy-efficient buildings". *Energy and Buildings* 27(2): 147–154. doi: 10.1016/S0378-7788(97)00035-2.
- Beccali, M., L. Mazzarella, M. Motta. 2001. "Simplified models for building cooling energy requirement". In: *Proceedings of the 7th International IBPSA Conference*. Rio de Janeiro, Brazil: IBPSA.
- CEN. 2005. EN 15265:2005 - *Thermal performance of buildings—calculation of energy use for space heating and cooling—general criteria and validation procedures*. Brussels, Belgium: European Committee for Standardization.
- Corrado, V., E. Fabrizio. 2007. "Assessment of building cooling energy need through a quasi-steady state model: Simplified correlation for gain-loss mismatch". *Energy and Buildings* 39: 569-579. doi: 10.1016/j.enbuild.2006.09.012.
- ISO. 2008. ISO/DIS 13790:2008 - *Thermal performance of buildings—calculation of energy use for space heating and cooling*. Geneva, Switzerland: International Organization for Standardization.
- Klein, S.A., et al. 2012. TRNSYS Vers. 17. Madison, U.S.A.: Solar Energy Laboratory, University of Wisconsin-Madison.
- Mazzarella, L. 2000. *Modello quasi-stazionario per la stima del fabbisogno energetico utile di raffrescamento, Report R3-Cofin Murst 1998*. Milan, Italy: Politecnico di Milano.
- NEN. 1994. NEN 2916:1994, *Energy Performance of Non-Residential Buildings – Determination Method*. Delft, The Netherlands: Nederlands Normalisatie Instituut.
- Oliveti, G., N. Arcuri, R. Bruno. 2011. "An accurate calculation model of solar heat gain through glazed surfaces". *Energy and Buildings* 43: 269-274. doi: 10.1016/j.enbuild.2010.11.009.
- Prada, A., G. Pernigotto, P. Baggio, A. Gasparella. "Summer load evaluation in the Italian climate: sensitivity of the loss utilization factor to the weather data". In: *Proceeding of Building Simulation 2011*. Sydney, Australia: IBPSA.
- Schibuola, L. 1999. "Simplified summer energy demands of buildings". *CDA* 2: 131-138.
- UNI. 2014. UNI 11300-1 - *Energy performance of buildings, Part 1: Evaluation of energy need for space heating and cooling*. Milan, Italy: UNI.
- UNI. 2016. UNI 10349-1 - *Heating and cooling of buildings - Climatic data - Part 1: Monthly means for evaluation of energy need for space heating and cooling and methods for splitting global solar irradiance into the direct and diffuse parts and for calculate the solar irradiance on tilted planes*. Milan, Italy: UNI.
- van Dijk, D., M.E. Spiekman, 2003. *Monthly method to calculate cooling demand of EP regulations, CEN/TC89 N870*. Brussels, Belgium.
- van Dijk, D., M.E. Spiekman, P. de Wilde. 2005. "A monthly method for calculating energy performance in the context of European building regulations". In: *Proceedings of Building Simulation 2005*. Montreal, Canada, IBPSA.

Steady-State and Transient Simulation of a Radiant Heating System

Fabian Ochs – University of Innsbruck – fabian.ochs@uibk.ac.at

Mara Magni – University di Bologna – mara.magni@studio.unibo.it

Michele Bianchi Janetti – University of Innsbruck – michele.janetti@uibk.ac.at

Dietmar Siegele – University of Innsbruck – dietmar-siegele@uibk.ac.at

Abstract

Radiant heating generally addresses all heat emission systems that have a share of radiant heat emission greater than 50 %, compared to a convector or fan coil where the heat is transferred mainly by means of convection. Recently, so-called infrared-heating systems are increasingly discussed as a cost-effective heating system. Relative small areas with high surface temperatures of typically up to 120 °C are used. In order to investigate in detail radiant heating systems, building models able to reproduce accurately the occurring physics phenomena are required. Physics-detailed steady state and transient room models have been developed in Matlab®. The required view factors for the radiative exchange between all surfaces and between each surface and a sphere representing a person are calculated using COMSOL®. Moreover, the thermal comfort in different positions of the room has been evaluated.

1. Introduction

The implementation of the concept of NZEB (Kurnitski et al., 2013) will lead to a further reduction of the heating demand of new buildings. Also the heating demand of the building stock will decrease by applying deep renovation. The technology to achieve very low energy demands has been available for about 25 years, when the first Passive House was built in Darmstadt, Germany (Feist, 2016). Since then, technology and products have been further improved and cost-effectiveness has significantly increased. However, in order to improve the economic feasibility of these very efficient buildings, cost-effective heating systems are required. In parallel the share of renewable energies (such as PV or wind) in the electric grid will further increase. Both these developments make

electric heating interesting again in spite of the fact that, because of thermodynamic principles, electricity should not be used for heating.

2. Motivation and Objective

Recently so-called infrared-heating systems are increasingly discussed as a cost-effective heating system. Relative small areas of typically 0.6 m x 1.2 m with high surface temperatures of up to 120 °C are used. The following questions have to be answered:

- What is the appropriate dimensioning of the radiant system depending on the load of the building?
- What are the comfort conditions with radiant heating systems and how should they be determined and evaluated?
- What is the energy performance compared to reference systems such as hydronic heat emission systems e.g. with an air-sourced heat pump?
- Is there a benefit in the intermittent operation due to the relative fast response of these heating systems?

3. Radiative Heating – Definition

With a convective heat emission system, such as e.g. a convector or a fan coil, thermal energy is emitted mainly convectively (either through free and/or forced convection) directly into the air. Contrariwise, with a so-called radiative heat emission system, i.e. a heated area where min. 50 % of the heat emission occurs as long-wave radiation, the major

share of the heat is distributed to the surrounding surfaces. Radiation heat emission systems are in principle independent of the type of heat supply (i.e. electrical or hydronic), however, often electrically heated systems are addressed (infrared heating system). Remark: The so-called supply air heating in a Passive House is with regard to the supply air rooms also a radiant heating system. The warm supply air flows close to the ceiling due to the Coanda effect (Felder, 1993). In turn, the ceiling is heated up in an area close to the air outlet and, consequently, it emits heat as long-wave radiation to the other surfaces.

In case of a radiant heat emission system, the temperature of the surrounding surfaces increases compared to a predominantly convective heating system, assuming the same heating power. As a consequence, a lower convective (i.e. air) temperature is required for the same operative temperature, which consists of about 40 % to 50 % of the convective temperature and 50 % to 60 % of the surface temperature of the surrounding areas. This means for the energy balance of a room, that with a radiant heating system compared to a convective heating system the same thermal comfort can be obtained with slightly reduced ventilation losses, but also slightly increased transmission losses (especially when the radiant heater is mounted on an external wall or when external walls form the radiation partner of the radiant heater). In buildings with very high quality of the thermal envelope, the increase of the transmission losses is almost negligible (unless the direct radiation partner is a window). In case of very efficient buildings, as demanded by the EU energy performance of the buildings directive (European Commission, 2012), the ventilation losses are also low (due to the heat recovery required for achieving high thermal comfort and low heating demands), hence, also the reduction of ventilation losses is of minor importance. Decreased and increased losses are more or less balanced. The difference of the heating demand between a radiant and a convective heating system increases with better quality of the building envelope and higher energetically effective air exchange rate (the equivalent air change that is not covered by the heat recovery). In case of poor quality of the envelope the energy consumption for

heating can even increase compared to a convective heating system.

4. Thermal Comfort

The radiant temperature asymmetry (half-space and small hot surfaces) has to be considered when dimensioning a radiant heat emission system. The ISO 7730 (2005), as well as the ASHRAE 55 (2013), specifies a maximum radiant temperature asymmetry of 5 K for heated ceilings and 23 K for a heated wall. More recent studies, such as e.g. Glück (1994) indicate slightly higher values with about 8 K for heated ceilings. Here, it is important to note that slightly different results might be obtained for the heating demand depending on whether optimal thermal comfort at the most unfavorable location in the room or in average with respect to the occupied area is demanded. For a meaningful comparison, equal room air quality and equal thermal comfort are prerequisite.

In addition to the potential energy savings due to reduced ventilation losses, there is a further reduction potential due to the possibility to provide thermal comfort only locally. This can refer to a specific place in the room (e.g., the working place) or on separate heating of the occupied areas (in contrast to heating the entire inhabited space). A correct sizing and a temporally and spatially correct functioning control of the radiant heating system is a prerequisite to achieve thermal comfort.

5. Modelling and Building Simulation

A building model with a detailed calculation of the radiation exchange (between each of the surrounding surfaces, as well as between all surrounding surfaces and a sphere (or ellipse or cube), simulating a person in the room and used for calculating the operating temperature) is required to represent these effects with sufficient accuracy. With such a model, the effects can be determined with higher accuracy compared to a two-star e.g., Dynbil (EnergyPlus) or star node e.g. EN ISO 13790 (CEN, 2008), TRNSYS model that are usually used for building simulations (Crawley et al., 2005; Davies, 2004) (Fig. 1).

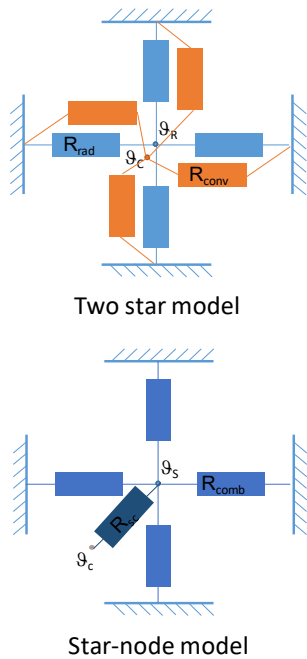


Fig. 1 – Star-node model (top) and two-star model (bottom) with four surfaces: θ_r radiative node, θ_c convective node, θ_s star node (mixture of surface and air temperature), R_{rad} radiative resistance, R_{conv} convective resistance; R_{comb} combined radiative and convective resistance and R_{sc} the resistance between the star node and the convective node

With such a detailed physical model of a room a possible influence on the heating demand with a radiant heating system compared to a convective heating system can be calculated depending on the building standard (i.e. the quality of the building envelope and the energetically effective air exchange rate). Here, a low linear temperature stratification in the room (i.e. an ideal mixing) is assumed, see Fig. 2. This assumption is acceptable in rooms with a very good insulation level and ventilation with heat recovery. However, it will not hold in case of radiant ceilings and/or cold air supply. For a more accurate analysis, in addition, a computational flow simulation (CFD) to determine the temperature stratification would be needed. The convective heat transfer coefficients are calculated with well-known power law correlations, see Awbi (1999):

$$h_{conv} = C \cdot \Delta \theta^n \quad (1)$$

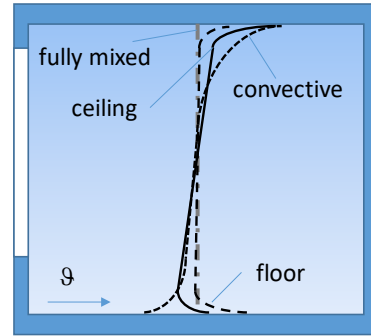


Fig. 2 – Temperature stratification for different heating situations, ceiling and floor heating, convective heating and fully mixed

6. Physical Room Model

Detailed steady state and transient physical room models have been developed in Matlab® based on the radiosity approach, see Davies (2004), see Fig. 3. The required view factors for the radiation exchange between all surfaces and between each surface and a sphere representing a person or a thermal comfort in different positions of the room are calculated using COMSOL Multiphysics® software, see section below for details. H_i is the radiosity. The resistances R_{ij} can be calculated with the view factor F_{ij} the area A_i and r_i is the emissivity resistance.

$$R_{ij} = \frac{1}{A_i F_{ij}} \quad (2)$$

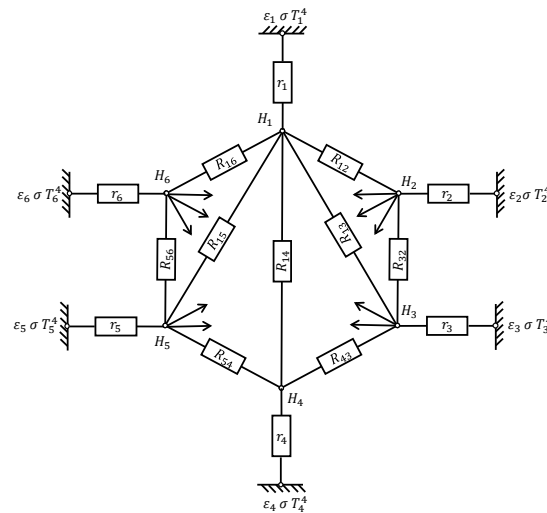


Fig. 3 – Model for long-wave radiation exchange with 6 surfaces

6.1 View Factor Calculation

The view factor F_{ij} represents the fraction of the radiation that leaves the surface A_1 and strikes the surface A_2 , as shown in Fig. 4.

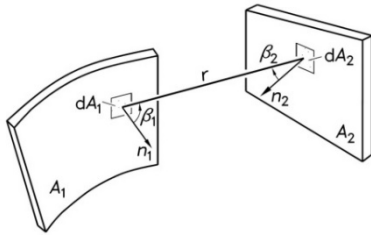


Fig. 4 – Calculation of View Factor (Baehr and Stephan, 2010)

6.2 Analytic Calculation of View Factors

If the radiation intensity is constant over the surface the view factor can be calculated analytically by solving Eq. 3. the view factor F_{12} does not depend only on the geometrical configuration.

$$F_{12} = \frac{1}{\pi A_1} \iint_{A_1, A_2} \frac{\cos \beta_1 \cos \beta_2}{r^2} dA_1 dA_2 \quad (3)$$

For many simple geometries view factors are available in the literature, e.g. in Baehr and Stephan (2010) or VDI-HA. For complex geometries, numerical methods have to be used. If the surfaces radiate diffusely, have constant temperature and radiation properties over the entire area numerical integration can be applied.

6.3 Numerical Integration

In Matlab® CDIF (contour double integral formula) can be used to calculate view factors between planar surfaces (i.e. polygons) for any shape and orientation e.g. with Lauzier (2004).

6.4 View Factor Calculation with radiosity approach

In COMSOL® surface to surface radiation problems can be solved using the radiosity approach with the irradiation G (here G is the mutual irradiation coming from the other boundaries), the radiosity H and the emissivity ε :

$$(1 - \varepsilon) \cdot G = H - \varepsilon \cdot \sigma \cdot T^4 \quad (4)$$

The emissivity can be a function of wavelength (λ) and surface temperature (T). Complex geometries also with obstructions can be considered. But the hypothesis of a diffuse grey surface has to hold i.e. every surface has the absorption coefficient equal to the emissivity coefficient, and emissivity and absorptivity are independent of the angle of emission or absorption, respectively.

Here, two different methods are studied and compared:

- 1) Surface to surface radiation physics, where it is necessary to run one simulation for every view factor which has to be calculated. The COMSOL® operators $\text{radopd}(H_{\text{up}}, H_{\text{down}})$ and $\text{radopu}(H_{\text{up}}, H_{\text{down}})$ are used.
- 2) Heat Transfer with Surface-to-Surface Radiation physics where surfaces are presented as solid objects.

$$H_i = -\dot{Q}_i \frac{(1 - \varepsilon_i)}{\varepsilon_i A_i} + \sigma \cdot T_i^4 \quad (5)$$

6.5 Numerical Integration

In Matlab® CDIF (contour double integral formula) can be used to calculate view factors between planar surfaces (i.e. polygons) for any shape and orientation e.g. with Lauzier (2004).

7. Model Validation

For a room with 6 surfaces, the view factors are calculated with the three numerical methods (numerical integration with Matlab® and the two methods using COMSOL®) and are compared against the analytical solution. For six surfaces, there are 36 unknown view factors. Considering that the surfaces are plane and there are symmetries and applying reciprocal conditions the unknowns are reduced to four. With one simulation with COMSOL method 2, for six surface temperatures six heat fluxes are determined. The remaining linear system of equations can be solved, e.g. with Matlab®. The view factors of the analytical solution are reported in the Table 1. Maximum deviations for each case are summarized in Table 2.

Table 1 – View factors for the six surface problems

	(1)	(2)	(3)	(4)	(5)	(6)
(1)	0	0.1125	0.1257	0.1125	0.3246	0.3246
(2)	0.1500	0	0.1500	0.0668	0.3166	0.3166
(3)	0.1257	0.1125	0	0.1125	0.3246	0.3246
(4)	0.1500	0.0668	0.1500	0	0.3166	0.3166
(5)	0.1461	0.1068	0.1461	0.1068	0	0.4942
(6)	0.1461	0.1068	0.1461	0.1068	0.4942	0

Table 2 – Max and mean deviations with respect to the analytical solution

	COMSOL® Method 1	COMSOL® Method 2	Numerical integration (Matlab®)
Max	6.1409E-06	0.09540322	4.0868E-06
Mean	1.7281E-06	0.03366432	2.1446E-06

Numerical integration with Matlab® and COMSOL® Method 1 deliver sufficiently accurate results with respect to the analytical solution. The reason for the deviations in case of the method 2 has to be further investigated. The main advantage of using COMSOL® for the determination of the view factors is that the problem can be coupled to further physic problems such as CFD simulations.

8. Simple Case Study

8.1 Description of the Room Model

For a simple room model with the dimensions 8 m x 6 m x 2.7 m (WxDxH) the theoretical change of the heating power and the (annual) heating demand were calculated exemplarily. The room has one external façade with a share of window surface of 30 % (or 60 % as a variant) and an external ceiling (insulated flat roof, or adiabatic as a variant) each in Passive House quality. Different sizes and positions of the radiant heater have been investigated, (see Table 3) and compared against the reference case with convective heating.

Table 3 – Investigated cases – different position and size of radiant heater; c: centric and ac: acentric, see Fig. 5

	Large	Medium	Small centric	Small acentric
Side wall	x	x	x	x
Rear wall	x	x	x	x
Floor	x	x		
Ceiling	x	x	x	x

Fig. 5 shows a scheme of the case with small radiant heater centred and acentric and Fig. 6 shows the corresponding spatial distribution of the radiative temperature in 1.5 m height as a result of a steady state calculation for an operative temperature of 20 °C.

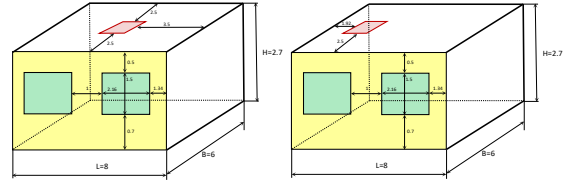


Fig. 5 – Scheme of small radiant heater centered (left) and acentric (right)

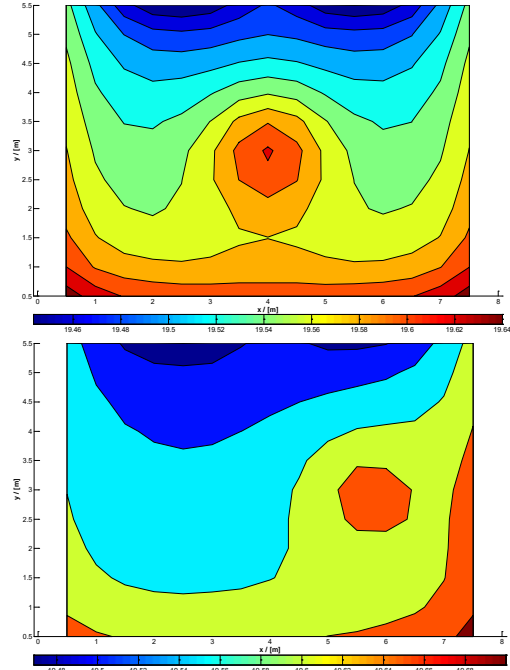


Fig. 6 – Spatial distribution (depth over with of the room) of the radiation temperature in 1.5 m height for the small radiant heater centred (top) and acentric (bottom)

8.2 Results

The calculated reduction of the heating demand depends on the energetically effective air exchange rate, see Fig. 7.

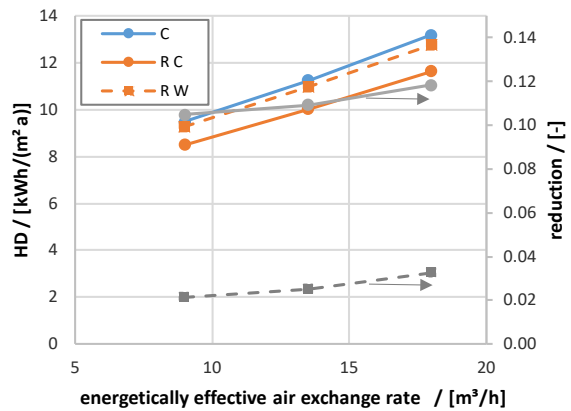


Fig. 7 – Heating demand (HD) for the small radiative heater on the ceiling (R C) and wall (R W) and reduction with respect to convective heating (C) depending on the energetically effective air exchange rate

It is in case of a specific heating demand (HD) of about 10 kWh/(m² a) corresponding to an air change rate of 60 m³/h with heat recovery with an effectiveness of 85% (with correspondingly very low energetically effective air exchange rate of only 9 m³/h) in the range of 10 % for a small ceiling mounted radiant heater and 6 % for a small wall mounted radiant heater (each with 1 m²), see Table 4. This reduction results from the fact that good thermal comfort in this constellation is given only locally. For the same temporal and spatial comfort, no significant differences between a predominantly convective heat emission system and one which emits predominantly long-wave radiation can be determined within the model accuracy. Differences in the heating demand, which are based on differences in local comfort cannot be valued as energy savings. The radiant temperature asymmetry is in case of the small ceiling mounted radiant heater at the limit of the thermal comfort range. The maximum radiant temperature asymmetry permitted according to ISO 7730 is 5 K and can be exceeded with a small radiant heater with a correspondingly high surface temperature.

Considering that, in case of a comfort ventilation, the air is further heated in the exhaust air rooms (especially in the bathroom, where according to the standards a temperature of 24 °C should be maintained), the difference between predominantly convective heat emission and radiative heat emission is likely to be further reduced in reality, i.e. the calculated difference will be lower when related to the entire building.

Table 4 – Heating Demand (HD) for different sizes and positions of the radiant heater compared to pure convective heating, climate in Innsbruck

Case	Heating Demand / [kWh/(m ² a)]
Convective	10.2
Floor Heating (large)	10.7
Ceiling Heating (large)	10.5
Ceiling Heating (small)	9.1
Wall Heating (small)	9.6

With large radiative surfaces, the possibility of providing local comfort is limited and the reduction of the ventilation losses is (over-) compensated by

increased transmission losses. For an increased effective air exchange (i.e. in the case of window ventilation or an exhaust air system) the difference of the heating demand would be theoretically larger, however the heating demand would then have an order of magnitude such that an electric heater as a sole heating system cannot be recommended. It must further be noted that without heat recovery, due to cold air drop and due to the high radiant temperature asymmetry, thermal comfort cannot be provided. A radiant heating system as a sole heating system is generally not recommended without heat recovery. Without heat recovery, a convective heating part is required to preheat the occasionally very cold fresh air in order to avoid cold air drop and cold air stratification.

9. Discussion

The savings potential is relatively low with respect to the heating demand. However, not only the heating demand but the entire production, transport and storage chain must be considered in a comprehensive comparison, i.e. eventually, the primary energy consumption of the whole building must be compared. It has to be taken into account that heat storage and distribution losses can occur with conventional heating systems, if they are placed outside the thermal envelope.

Compared to e.g. an air heat pump heating system, which generally has a relatively low seasonal performance factor (SPF) of around 2 to 3 for heating due to low air temperatures in winter, the electricity and primary energy demand is higher for an electric radiant heating system even by taking into account all thermal losses. Assuming a specific heating demand of 15 kWh/(m² a), 10 % reduction of the heating demand in the case of radiant heating system and 10 % distribution and storage losses for the conventional heating system, an electricity consumption of 13.5 kWh/(m² a) results for the radiant heating system and 8.25 kWh/(m² a) for the heat pump heating system with a SPF of 2.

Electric radiant heaters are with regard to the investment, a low-cost alternative to conventional heating systems. Based on the life cycle cost, the price of electricity can have an important influence,

especially if it is subject to seasonal fluctuations, which might be expected with an increasing share of renewables in the electricity mix.

The solution for the hot water preparation should be considered in addition for a final comparison.

10. Summary and Conclusions

For a meaningful comparison of the heating demand of different heat emission systems, for the investigated variants, the indoor air quality and the thermal comfort (evaluated according to ISO 7730) with the operating temperature in the living area (generally in the center of the room) and the maximum acceptable radiation temperature asymmetry (as well as taking the draught risk into account) must be identical.

In order to compute the differences of a heat emission system, which is predominantly convective or predominantly radiative with sufficient accuracy, a building model with a detailed calculation of the radiation exchange (between each of the surrounding areas, as well as between the surrounding surfaces and a sphere that is used for calculating the operative temperature) is required. With such a model, these effects can be figured out more precisely than with a two-star or star node model, as usually used for building simulations. The assumption of an ideal mixing of air is acceptable in rooms with a very good insulation level and mechanical ventilation with heat recovery; however, it does not apply to the case of radiative ceiling and/or ventilation without heat recovery. A computational flow simulation (CFD) for determining the temperature stratification would be required additionally for a more accurate analysis.

For the same temporal and spatial thermal comfort, within the model accuracy no significant differences in the heating demand can be obtained between a heat emission which is predominantly convective and one which is predominately radiative.

A numerically or experimentally determined reduction of the heating demand, which results from either a reduction of indoor air quality or of the thermal comfort, cannot be called a reduction in the strict sense (i.e. in the sense of a better efficiency of the heat emission system – in the same way as a

reduction of the heating demand by reducing the air exchange cannot be accounted for energy savings, but represents a deterioration of the indoor air quality, or energy savings through temporary heating or local heating is not energy saving but a temporal or spatial reduction of the thermal comfort).

If comfort is only defined for the occupied space, i.e. traffic area (in the same way as in the case of ventilation on demand, indoor air quality is defined only during presence, i.e. there is no loss of comfort with regard to the temporal and local presence of the user), a low energy saving can be achieved without loss of comfort (i.e. with local comfort). It must be noted that the potential to create thermal comfort only locally is greater for small (and consequently hot) areas while the radiant temperature asymmetry in this case can even exceed the limit defined in ISO 7730.

Careful planning and proper sizing of the radiative heater is essential. A precise temporal and spatial control of the radiant heater is also crucial to achieve good thermal comfort.

A radiant heater as a sole heating system is generally not recommended without heat recovery. A convective heating part is required to preheat the occasionally very cold air in order to avoid cold air drop and cold air stratification.

Not only the heating demand, but also the entire production, transport, and storage chain must be considered in a comprehensive assessment. In contrast to a central heating system there are no storage and distribution losses in case of an electric radiant heating system. Eventually, the primary energy consumption of the whole building needs to be compared. The technical solution for domestic hot water preparation has to be considered, too.

11. Outlook

Especially for a deep energy renovation of buildings (e.g. according to the EnerPHit standard) the radiant heating can represent an interesting solution in combination with air heating (e.g. exhaust air HP or split unit) for room-wise control (instead of an electrical re-heating of the air), in particular if there is no (uniform) heat distribution and emission infrastructure.

Acknowledgements

IFI Institut für Infrarotwärme GmbH initiated this work. The authors thank the IFI Institut für Infrarotwärme GmbH for this initiative and for their support. For part of this work financial support was provided by the Austrian research funding association (FFG) under the scope of "Innovationscheck Plus".

References

- ASHRAE. 2013. *ASHRAE 55:2013 -- Thermal Environmental Conditions for Human Occupancy*, Atlanta, U.S.A.: ASHRAE.
- Awbi, H.B., A. Hatton. 1999. "Natural convection from heated room surfaces." *Energy and Buildings* 30(3): 233-244. doi: 10.1016/S0378-7788(99)00004-3.
- Baehr, H.D., K. Stephan. 2010. *Wärme- und Stoffübertragung*. Berlin, Germany: Springer.
- CEN. 2008. *EN ISO 13790: Energy Performance of Buildings: Calculation of energy Use for Space Heating and Cooling*. Brussels, Belgium: CEN.
- Crawley, D.B., J.W. Hand, M. Kummert, B.T. Griffith. 2005. "Contrasting the Capabilities of Building Energy Performance Simulation Programs." In: *Proceedings of Building Simulation 2005*. Montréal, Canada: IBPSA.
- Davies, M.G. 2004. *Building Heat Transfer*. Hoboken, U.S.A.: Wiley.
- Dynbil. Accessed in 2016. http://www.passiv.de/de/01_passivhausinstitut/02_kompetenzbereich/e/02_simulation/01_gebaudesimulation/01_gebaudesimulation.htm
- EnergyPlus. Accessed in 2016. <https://energyplus.net/>
- European Commission. *EPBD*. Accessed in 2016. <https://ec.europa.eu/energy/en/topics/energy-efficiency/buildings>
- Feist, W. 2016. "Passivhaus - die langlebige Lösung". In: *Proceedings of the 20th International Passive House Conference*. Darmstadt, Germany: PHI.
- Felder, A. 1993. *Untersuchungen zum Coanda-Effekt-mögliche Anwendung im Bauingenieur-wesen*. PhD Dissertation, München, Germany: TU München.
- Glück, B. 1994. "Zulässige Strahlungs-temperatur-Asymmetrie." *Gesundheitsingenieur* 115(6): 285 – 293.
- ISO. 2005. *ISO 7730, Ergonomics of the thermal environment - Analytical determination and interpretation of thermal comfort using calculation of the PMV and PPD indices and local thermal comfort criteria*. Geneva, Switzerland: ISO.
- Kurnitski, J. (Ed.). 2013. *Cost Optimal and Nearly Zero-Energy Buildings (nZEB) Definitions, Calculation Principles and Case Studies*. London, UK: Springer.
- Lauzier, N. Accessed in 2016. <https://de.mathworks.com/matlabcentral/fileexchange/5664-view-factors>
- Passive House/ EnerPHit. Accessed in 2016. <http://www.passiv.de>
- TRNSYS. Accessed in 2016. <http://sel.me.wisc.edu/trnsys/>
- VDI-HA. *VDI Heat Atlas*. Berlin, Germany: Springer.

Comparison Between Energy-Optimized and Cost-Optimized Design of Multi-Family Buildings Through Automated Optimization

Maria Ferrara – Politecnico di Torino – maria.ferrara@polito.it

Elisa Sirombo – Politecnico di Torino – elisa.sirombo@polito.it

Enrico Fabrizio – Politecnico di Torino – enrico.fabrizio@polito.it

Abstract

Living in multi-family buildings is very common in Italy. Towards the implementation of economic sustainability principles, it is important to consider the effect of the design strategies in the energy demand of these buildings and their related operational costs. This is particularly important for low-income tenants, and is pursued by many social housing developments by which a good energy performance design is reached. In this work, a simulation-based optimization methodology that combines the use of TRNSYS® with GenOpt® is applied in order to minimize two different objective functions, one related to the primary energy demand and the other related to the operational energy cost, and to verify the extent to which an energy-optimized design differs from a cost-optimized design in the northern Italian climate. The study is performed on a 7-flat typical floor of a real multi-family building for social housing. The design of the building envelope is optimized, leading to reduce the primary energy demand for heating and cooling of the floor by 36 % and the energy costs by 35 %. Higher equality between the energy performances of the flats is also reached. Both objectives lead to very close values of primary energy and costs, but the resulting optimal building design is different according to optimization objective. The comparison between the energy-optimized and the cost-optimized scenarios leads to the conclusion that, in order to reduce the risk of energy poverty, the design solution that minimizes the energy cost can be preferred, as it can minimize the energy bill of low-income tenants while being close to the environmental optimum.

1. Introduction

In Italy, more than 50 % of people live in multi-family buildings. That is why increasing the energy

efficiency of new and existing multi-family buildings can have a significant impact on the reduction of the energy consumption of the Italian residential building stock. Furthermore, multi-family is the common building typology for social housing interventions; therefore improving their energy performance also constitutes a challenge for contrasting the risk of energy poverty for low-income households (Faiella et al., 2014).

Copiello (2016) demonstrates that energy efficiency allows the low-income tenants to be neutral about the rent increase that may occur for new social housing interventions under the current Italian regulation. Moreover, after the introduction of the 2012/27/EU Directive and the principles of heat accounting, many problems have emerged related to cost repartition and the non-homogeneity between the different flats in multi-family buildings (Ficco et al., 2016; Fabrizio et al., 2017).

The development of a building dynamic simulation and its combination with automated optimization constitutes a powerful tool for designers to evaluate thousands of different building design solutions (Xing et al., 2016), leading to accurately optimize the building design according to different objective functions that imply the dynamic calculation of the building energy consumption (i.e. primary energy, life-cycle cost, etc.). The choice of the optimization objective clearly affects the resulting building design and many researchers are dealing with the problem of developing strategies for the economic feasibility of an environmentally optimal building design, as there is often a gap between economic optimum and environmental optimum (Ferrara et al., 2014; Pikas et al., 2015; Zacà et al., 2015).

1.1 Aim of the Work

The aim of this work is to further develop some previous works of the Authors (Ferrara et al., 2016a, and 2016b), where primary energy and energy cost optimization objectives were addressed separately. The aim of this paper is to study and compare the two objectives in parallel by providing an answer to the following questions:

- Which is the potential performance optimization of a new multi-family building for social housing in Italy?
- How and to what extent does cost-optimized design differ from energy-optimized design?
- Which design variables are mostly influenced by optimization objectives?
- Which design variables are mostly resilient to the variation of the optimization objectives?
- What are the differences in energy performance and thus in energy costs between the different flats of a multi-family building? How and to what extent a design optimization can help in reducing the differences?

The analysis is based on a case study that is representative of recent social housing in Italy.

2. Simulation

2.1 Case Study

The case study is a real multi-family building located in Cremona, Italy. The construction of external wall includes bricks (30 cm) and an external thermal insulation (10 cm), for a wall thermal transmittance U equal to $0.26 \text{ W}/(\text{m}^2 \text{ K})$. Transparent surfaces are double low-e glass windows with metal frame, with a mean thermal transmittance equal to $1.45 \text{ W}/(\text{m}^2 \text{ K})$, and a solar factor equal to 0.59. As shown in Fig.1, some windows are shaded by external loggias, a typical feature of the Italian architecture. Details can be found in Ferrara et al. (2016a). For the purpose of this study, one typical floor of the case study building was selected for carrying out optimization studies. As reported in Fig. 1, the floor is composed of 7 flats, each with a different floor area and surface-to-volume ratio (Table 1), for a total floor conditioned floor area of 466 m^2 .



Fig. 1 – Case study building. South façade view and plan of the typical 7-flat floor

The building is connected to a district-heating network with radiant panels as heating terminals (the total seasonal efficiency ratio of the heating system is 0.88, based on the Energy Performance Certificate; the primary energy conversion factor declared by the supplier is equal to 0.62). A gas boiler produces DHW (energy efficiency ratio equal to 0.85, primary energy conversion factor equal to 1.05). A mechanical ventilation system with a heat exchanger is also present; the medium seasonal efficiency of the heat recovery was considered equal to 0.5. For calculating the cooling energy consumption and primary energy, a reference air conditioner system was considered (energy efficiency ratio EER equal to 2.05; total primary energy conversion factor for electricity equal to 2.42). For energy cost calculation, the prices of 0.10 €/kWh_t for the thermal energy provided by the district heating system (Linea Reti e Impianti, 2016), 0.08 €/kWh_t for gas, and 0.20 €/kWh_e for electricity (Eurostat, 2016) were considered. The energy simulations were carried out with the IWEC weather data for Milan.

Table 1 reports the specific primary energy consumption and the operational costs related to each flat and the average value related to the entire floor of the case-study building in its actual configuration, which is the so-called “initial scenario” for the optimization. The energy rating, according to the current Italian energy performance certification regulation (DM 26/06/2015), is A1 for each flat and for the floor.

Table 1 – Initial scenario. Annual primary energy consumption and annual energy costs for each apartment and floor values.

	A	B	C	D	E	F	G	Floor
Floor area (m ²)	86.0	48.7	77.5	77.5	47.4	47.6	81.1	465.8
S/V (m ⁻¹)	0.74	0.66	0.26	0.26	0.32	0.27	0.45	0.46
Heating EP _H (kWh/m ²)	26.5	17.7	19.2	18.9	15.5	13.6	26.9	20.7
CH (€/m ²)	4.27	2.85	3.10	3.04	2.50	2.20	4.34	3.34
Cooling EP _C (kWh/m ²)	15.3	18.3	10.0	9.7	20.7	20.2	14.4	14.7
Cc (€/m ²)	1.26	1.52	0.82	0.80	1.72	1.68	1.18	1.22
DHW EP _W (kWh/m ²)	21.9	25.0	22.4	22.4	25.2	25.1	22.2	23.1
Cw (€/m ²)	1.58	1.80	1.62	1.62	1.82	1.82	1.60	1.66
Vent EP _V (kWh/m ²)	15.1	15.1	15.1	15.1	15.1	15.1	15.1	15.1
Cv (€/m ²)	1.24	1.24	1.24	1.24	1.24	1.24	1.24	1.24
Tot EP _{gl} (kWh/m ²)	78.8	76.1	66.7	66.0	76.5	74.2	78.6	73.6
C _{gl} (€/m ²)	8.35	7.41	6.78	6.70	7.28	6.94	8.36	7.46
Energy rating	A1							

2.2 Optimization Methodology

The methodology that was used to investigate the objectives presented in the scope of the work was set up in previous works (Ferrara et al., 2016c) and involves the coupling between TRNSYS® and GenOpt® in a simulation-based optimization process, as shown in Fig. 2.

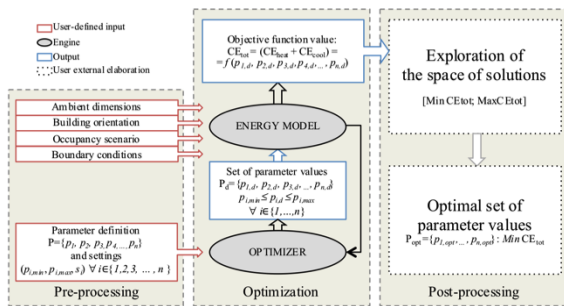


Fig. 2 – Simulation-based optimization methodology

In the pre-processing stage, the TRNSYS model is created including the building boundary conditions, and the set of design parameters to be optimized is defined. These parameters are related to the thermal resistance of the insulation panels and the solar absorption coefficient of the external walls, the type and size of the windows, the horizontal overhang and fin dimensions of the south-oriented

windows, the depth of the loggias facing north and south. The range and the step of their variation were set according to regulation requirements, technical feasibility, and market criteria. Table 2 reports the selected options for variation of window type parameters, which are related to different combinations of glass thermal transmittance, solar factor, and visible transmittance. In the nomenclature, all defined parameters are reported. The set of parameters with their dimension and constraints, defines the space of solutions of the problem, in which the search for the optimal design solutions according to the objective is conducted. See (Ferrara et al., 2016c) for details about the parameter definitions.

Table 2 – Options for window type parameters

ID	Design	U _g (W/m ² K)	g (-)	τ _v (-)
1	4/16/4	1.27	0.59	0.71
2	4/15/4	1.10	0.61	0.78
3	6/12/4/12/4	0.70	0.29	0.58
4	6/16/6	1.10	0.33	0.64
5	6/16/6	1.29	0.33	0.66
6	2.5/12.7/2.5/12.7/2.5	2.00	0.70	0.74
7	4/16/4/16/4	0.70	0.50	0.64

At the optimization stage, the iterative process driven by the optimization algorithm leads to evaluate a great number of design solutions, each related to a different value of the objective function, until the objective function is minimized. The optimization process was run with two different objective functions, calculated for the all the floors (Fig. 2 refers to the energy cost optimization process). The primary energy objective function is defined in (1), as the total sum of heating and cooling primary energy annual consumption of the entire case-study floor (kWh/m²).

$$PE_{H+C} = \frac{Q_H}{r_H} \cdot f_H + \frac{Q_C}{EER} \cdot f_C = \frac{Q_H}{0.88} \cdot 0.62 + \frac{Q_C}{2.05} \cdot 2.42 \quad (1)$$

The energy cost objective function is defined in (2), as the total sum of heating and cooling annual operational cost of the case-study floor (€/m²).

$$C_{H+C} = \frac{Q_H}{r_H} \cdot c_H + \frac{Q_C}{EER} \cdot c_C = \frac{Q_H}{0.88} \cdot 0.1 + \frac{Q_C}{2.05} \cdot 0.2 \quad (2)$$

Only the heating and cooling energy needs (Q_H and Q_C) were included in objective functions, as DHW and ventilation needs cannot be reduced with the variation of the defined set of parameters.

The optimization process was run also to maximize the objective functions, so that at the final stage, as post-processing, the space of solution could be explored from its minimum to its maximum. This process led to the evaluation of 6,893 different design solutions. Then, the optimal set of parameter values related to the minimization of one or the other objective function was found. Once the performance of the floor was optimized, the values of primary energy and energy costs were calculated for each flat of the floor in the resulted optimal design configurations.

3. Results and Discussion

Fig. 3 reports all points evaluated within the optimization processes that were run for the primary energy objective Function (1) and for the cost objective Function (2). Each point is reported in the graph having its PE_{H+C} value on the horizontal axis and its C_{H+C} value (heating and cooling energy cost) on the vertical axis. The points of the space of the solution that were evaluated within the energy optimization

are reported in orange, while blue points are referred to the cost optimization. Since the optimization process was run for both minimizing and maximizing the objective function, the graph shows that the space of solution led to primary energy values within the range of 20-70 kWh/m² and to operational energy cost values in the range between 2.9 and 7.4 €/m².

It is interesting to note that the two objective functions lead to a similar range of possible solutions in both dimensions and thus to optimal points that are very close to each other in the graph. The graph clearly shows that reducing the primary energy consumption also leads to a reduction of operational energy costs.

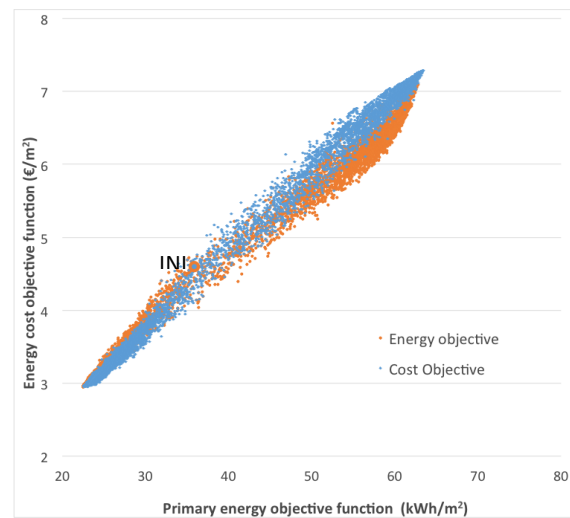


Fig. 3 – Primary energy (x-axis) and cost values (y-axis) of the points in the space of solution evaluated within the energy optimization (orange) and the cost-optimization (in blue)

However, looking at the parameter values related to the optimal scenarios (Table 3), it appears that similar objective function values can be reached with different building design configurations.

This means that different combinations of parameter values can lead to similar values of primary energy consumption and cost with different shares of cooling and heating demand.

This is because of the different weights given to the heating and cooling needs. According to the definition of the objective Functions (1) and (2), cooling energy needs have the highest weight in the primary energy objective function, while heating needs weight the most in calculating the operational energy costs. However, it has to be noted that, in the

initial scenario, the heating needs are 40 % higher than the cooling energy needs.

In Table 3, the parameter values defining the initial, the energy-optimized, and the cost-optimized building design configurations are reported.

It is shown that the values of the parameters related to the external wall insulation in all orientations (sISOLN, sISOLEW, sISOLS) are significantly increased to the upper bound of the variation range of parameters in both optimal scenarios. Also the parameters related to the window dimensions (WWidth parameters, where the letter indicates the flat in which the window is located) have equal values in both energy and cost optimized scenarios, in which the width of all windows is equal or smaller than in the initial scenario.

The grey color highlights the parameter values where differences occur. These are related to the absorption coefficients of the opaque envelope, to the external shadings and to the window type.

It is clear that cost-optimization is heating- driven. In fact, higher values of solar absorption coefficients and a smaller depth of horizontal overhangs and of loggias increase heating gains in winter, allowing solar radiation to enter the cost-optimized building more than in the energy-optimized building.

Following the same principle, window type 7 that is selected for the south windows in the cost-optimized scenario, has the same thermal transmittance of window type 3, but a higher solar factor.

The different shares of cooling and heating energy needs in the two optimal scenarios are also shown in Table 4, where the different values of heating and cooling primary energy, and the related energy costs are reported for each flat of the floor in both the energy-optimized (Eopt) and the cost-optimized (Copt) scenario. Savings in terms of percentage reduction of each term with respect to initial scenario are also indicated. Fig. 4 reports the reduction achieved by optimal scenarios considering also DHW and ventilation energy uses (that are not affected by optimization). Interestingly, the energy cost of the Eopt scenario is close to the one obtained in the Copt scenario, and the same is for the primary energy in the Copt scenario, where the related primary energy is close to the minimum found in the Eopt scenario.

The data related to each flat, reported in Table 4 and in Figs 5 and 6 clearly show that the optimization of

the energy performance of the floor (Fig. 5) leads to different reductions of the energy consumptions between flats, where the highest reductions are achieved for flats related to the highest energy needs in the initial scenario. As a secondary effect, the optimization of the performance of the floor as a whole leads to a greater equality between flats in terms of energy performance. In fact, the difference between the highest (flat G) and the lowest (flat F) PE_{H+C} values decreases from 12.8 kWh/m² in the initial scenarios to 6.3 kWh/m² in the Eopt scenario. Concerning the cost objective function (Fig. 6), results follow similar trends. Major reductions are achieved by the flats A and G (the ones related to the highest energy cost in the initial scenario) and the difference between the highest and the lowest C_{H+C} values decreases from 1.69 €/m² in the initial scenario to 1.23 €/m² in the cost-optimized scenario, leading to major equality between flats in terms of specific energy costs for heating and cooling.

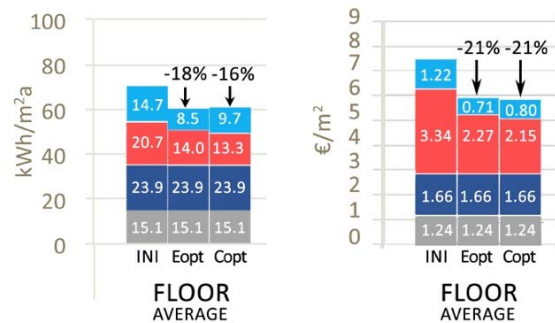


Fig. 4 – Primary energy and energy costs of the initial (INI), energy-optimized (Eopt), and cost-optimized (Copt) scenarios, floor values of ventilation (grey), DHW (dark blue), heating (red), cooling (light blue)

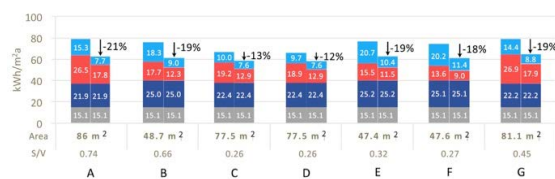


Fig. 5 – PE reduction for all flats in an energy-optimized scenario with respect to the initial scenario. Colors are the same as in Fig.4

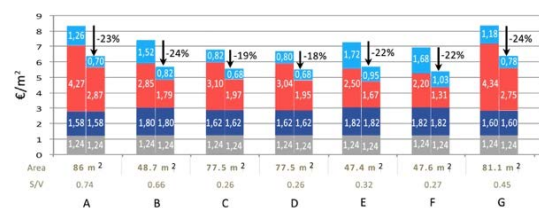


Fig. 6 – Cost reduction for all flats in a cost-optimized scenario with respect to the initial scenario. Colors are the same as in Fig.4

Table 3 – Value assumed by parameters in the initial scenario and in the two optimal solutions (energy and cost). The grey color indicates the parameters of which the optimal value changes according to the objective function

Parameter name	Initial value	Energy-optimal value	Cost-optimal value	Parameter name	Initial value	Energy-optimal value	Cost-optimal value
sISOLN (m ² K/W)	1.73	5.40	5.40	WWidthA1 (m)	1.0	1.0	1.0
sSOLEW (kWh/m ² K)	1.73	5.40	5.40	WWidthA2W(m)	0.9	0.9	0.9
sISOLS (m ² K/W)	1.73	5.40	5.40	WWidthA2S (m)	1.2	0.8	0.8
abs-back (-)	0.2	0.2	0.5	WWidthA3 (m)	1.8	1.8	1.8
abs-backS (-)	0.2	0.2	0.2	WWidthB1 (m)	1.8	1.6	1.6
abs-backEW (-)	0.2	0.2	0.5	WWidthB2 (m)	1.2	1.2	1.2
S _{overhproj} (m)	0	0.8	0.6	WWidthC1 (m)	2.4	2.0	2.0
S _{LRwproj} (m)	0	0.8	0.6	WWidthC2 (m)	2.7	2.7	2.7
PLOGGIA (m)	1.8	1.8	1.4	WWidthD1 (m)	2.4	2.0	2.0
LRw _{LOGGIA} (m)	1.8	1.8	1.4	WWidthD2 (m)	2.7	2.7	2.7
PLOGGIAN (m)	1.8	1.8	0.6	WWidthE1 (m)	1.2	1.2	1.2
LRw _{LOGGIAN} (m)	1.8	1.8	0.6	WWidthE2 (m)	1.8	1.6	1.6
WT (-)	1	3	3	WWidthF1 (m)	1.2	1.2	1.2
WTS (-)	1	3	7	WWidthF2S (m)	0.9	0.9	0.9
WTW (-)	1	3	3	WWidthF2 (m)	1.8	1.6	1.6
WTL (-)	1	3	7	WWidthG1N (m)	0.9	0.9	0.9
				WWidthG1L (m)	3.0	2.2	2.2
				WWidthG2L (m)	1.2	1.2	1.2
				WWidthG3 (m)	1.2	1.0	1.0

Table 4. Comparison of the heating and cooling energy demand between the energy-optimized and the cost-optimized solution. Colors refer to Fig. 1; the reported energy and cost savings are referred to the initial scenario (Table1)

Flat	PE _H (kWh/m ²)	PE _H savings	CH (€/m ²)	CH savings	PE _C (kWh/m ²)	PE _C savings	C _C (€/m ²)	C _C savings	Energy rating
A (E_Opt)	17.8	-33 %	2.87	-33 %	7.7	-50 %	0.64	-49 %	A2
A (C_Opt)	16.0	-39 %	2.87	-33 %	8.5	-45 %	0.70	-44 %	A2
B (E_Opt)	12.3	-31 %	1.99	-30 %	9.0	-51 %	0.75	-51 %	A2
B (C_Opt)	11.1	-37 %	1.79	-37 %	9.9	-46 %	0.82	-46 %	A2
C (E_Opt)	12.9	-33 %	2.09	-33 %	7.6	-24 %	0.63	-23 %	A2
C (C_Opt)	12.2	-36 %	1.97	-36 %	8.2	-18 %	0.68	-17 %	A2
D (E_Opt)	12.9	-32 %	2.08	-32 %	7.6	-22 %	0.63	-21 %	A2
D (C_Opt)	12.1	-36 %	1.95	-36 %	8.2	-15 %	0.68	-15 %	A2
E (E_Opt)	11.5	-26 %	1.86	-26 %	10.4	-50 %	0.86	-50 %	A2
E (C_Opt)	10.4	-33 %	1.67	-33 %	11.4	-45 %	0.95	-45 %	A2
F (E_Opt)	9.0	-34 %	1.46	-34 %	11.4	-44 %	0.94	-44 %	A2
F (C_Opt)	8.1	-40 %	1.31	-40 %	12.5	-38 %	1.03	-39 %	A2
G (E_Opt)	17.9	-33 %	2.89	-34 %	8.8	-39 %	0.72	-39 %	A2
G (C_Opt)	17.0	-37 %	2.75	-37 %	9.5	-34 %	0.78	-34 %	A2
Floor (E_Opt)	14.0	-32 %	2.27	-32 %	8.5	-42 %	0.71	-42 %	A2
Floor (C_Opt)	13.3	-36 %	2.15	-36 %	9.7	-34 %	0.80	-34 %	A2

4. Conclusion

This study deals with the envelope design optimization (passive energy efficiency measures) of a recent multi-family building for social housing in Italy according to different objectives. With the defined design parameters, based on the current design of the building, both energy optimization and cost optimization can decrease the amount of heating and cooling primary energy consumptions by more than 35 % and the energy costs for heating and cooling by around 35 %. This demonstrates that there is still a large potential for performance improvement with respect to the current construction practice of multi-family buildings in Italy.

This has a significant impact on the design, as performance improvements derive from increasing wall insulation, selecting window types with an optimal combination of thermal transmittance and solar factor according to the orientation, modifying the depth of loggias, with obvious implications on the flat layout, and adding fixed shadings elements of a specific depth, with implications on the façade design.

Despite the differences in weights assigned to the heating and cooling needs by the two objective functions, the performance improvements achieved in both energy-optimized and cost-optimized scenarios are very close to each other. However, because of these weights, in the analysed climatic conditions of the northern Italy the cost-optimized design results to be heating driven, while the energy-optimized design results to be cooling driven.

It has to be noted that these results were achieved by optimizing the floor as a whole. Better results could be probably achieved by optimizing the performance of each flat, but investigations on how to deal with the possible increase of construction costs due to a greater differentiation of construction components should be carried out.

The comparison between the energy-optimized and the cost-optimized scenarios leads to conclude that, in order to reduce the risk of energy poverty, the design approach that minimizes the energy cost can be preferred, as it minimizes the energy bill of the tenants while being close to the environmental optimum.

Further work should complete the present study and investigate the problem from the building

owner perspective, including in the cost objective function also investment and maintenance costs. Moreover, future developments of the work will investigate the problem in different climate conditions and in different energy tariff scenarios.

Acknowledgements

This work was carried out within the Starting Grant 2016 project funded by Compagnia di San Paolo.

Nomenclature

Symbols

abs-back	North wall absorption factor (-)
abs-backS	South wall absorption factor (-)
abs-backEW	East/West wall absorption factor (-)
C _{opt}	Cost-optimized scenario
E _{opt}	Energy-optimized scenario
f _c / f _H	Total primary energy conversion factor for cooling (C) or heating (H)
c _c / c _H	Unit energy cost for cooling (C) or heating (H)
LRw_LOGGIA	Left/right projection length for South loggia (m)
LRw_LOGGIA N	Left/right projection length for North loggia (m)
PLOGGIAN	Overhang projection length for North loggia (m)
PLOGGIAS	Overhang projection length for South loggia (m)
r _H	Seasonal heating efficiency ratio
sSOLEW	East/West walls - thermal resistance of the insulation layer (m ² K/W)
sISOLN	North walls - thermal resistance of the insulation layer (m ² K/W)
sISOLS	South walls - thermal resistance of the insulation layer (m ² K/W)
S_LRwproj	Left/right projection length for South windows (m)
S_overhproj	Overhang projection length for South windows (m)

WT	North window type (-)
WTL	Loggia window type (-)
WTS	South window type (-)
WTW	West window type (-)
WWidthA1	Window width A1 (m)
WWidthA2W	Window width A2 West (m)
WWidthA2S	Window width A2 South (m)
WWidthA3	Window width A3 (m)
WWidthB1	Window width B1 (m)
WWidthB2	Window width B2 (m)
WWidthC1	Window width C1 (m)
WWidthC2	Window width C2 (m)
WWidthD1	Window width D1 (m)
WWidthD2	Window width D2 (m)
WWidthE1	Window width E1 (m)
WWidthE2	Window width E2 (m)
WWidthF1	Window width F1 (m)
WWidthF2S	Window width F2 South (m)
WWidthF2	Window width F2 Loggia (m)
WWidthG1N	Window width G1 (m)
WWidthG1L	Window width G1 Loggia (m)
WWidthG2L	Window width G2 (m)
WWidthG3	Window width G3 (m)

References

- Copiello, S. 2016. "Leveraging Energy Efficiency to Finance Public-Private Social Housing Projects". *Energy Policy* 96: 217-230. doi:10.1016/j.enpol.2016.06.003.
- European Parliament and Council. 2012. *Directive 2012/27/EU of the European Parliament and of the Council of 25 October 2012 on energy efficiency, amending Directives 2009/125/EC and 2010/30/EU and repealing Directives 2004/8/EC and 2006/32/EC*.
- Eurostat. Energy Price Statistics, data extracted in 2016. http://ec.europa.eu/eurostat/statistics-explained/index.php/Energy_price_statistics
- Fabrizio, E., M. Ferrara, V. Monetti. 2017. "Smart heating systems for cost-effective retrofitting", in F. Pacheco-Torgal, C. Granqvist, B. Jelle, G. Vanoli, N. Bianco, J. Kurnitski (Eds.), "Cost-effective energy efficient building retrofitting. Materials, technologies, optimization and case studies", 277-302. Elsevier.
- Faiella, I., L. Lavecchia. 2014. "Energy Poverty in Italy". Occasional Paper 240. Rome, Italy: Bank of Italy.
- Ferrara, M., E. Fabrizio, J. Virgone, M. Filippi. 2014. "A simulation-based optimization method for cost-optimal analysis of nearly Zero energy Buildings". *Energy and Buildings* 84:442-457. doi: 10.1016/j.enbuild.2014.08.031
- Ferrara, M., E. Sirombo, A. Monti, M. Filippi, E. Fabrizio. 2016a. "Influence of Envelope Design in the Optimization of the Operational Energy Costs of a Multi-family Building". *Energy Procedia* 101: 216-223. doi: 10.1016/j.egypro.2016.11.028.
- Ferrara, M., E. Sirombo, A. Monti, M. Filippi, E. Fabrizio. 2016b. "Influence of Envelope Design in the Optimization of the Energy Performance of a Multi-family Building". *Energy Procedia* 111: 308-317. doi: 10.1016/j.egypro.2017.03.095.
- Ferrara, M., E. Fabrizio, J. Virgone, M. Filippi. 2016c. "Energy systems in cost-optimized design of nearly zero-energy buildings". *Automation in Construction* 70: 109-127. doi: 10.1016/j.autcon.2016.06.007.
- Ficco, G., L. Celenza, M. Dell'Isola, P. Vigo. 2016. "Experimental comparison of residential heat accounting systems at critical conditions". *Energy and Buildings* 130:477-487. doi: 10.1016/j.enbuild.2016.08.068.
- Linea Reti e Impianti. Data related to II trimester 2016. http://www.linea_ri.it/teleriscaldamento/servizi-cliente/tariffe-cremona
- Pikas, E., M. Thalfeldt, J. Kurnitski, R. Lias. 2015. "Extra cost analyses of two apartment buildings for achieving nearly zero and low energy buildings". *Energy* 84:623-633. doi: 10.1016/j.energy.2015.03.026
- Xing, S., Z. Tian, W. Chen, B. Si, X. Jin. 2016. "A review on building energy efficient design optimization from the perspective of architects". *Renewable and Sustainable Energy Reviews* 65:872-884, doi: 10.1016/j.rser.2016.07.050.
- Zacà I., D. D'Agostino, P.M. Congedo, C. Baglivo. 2015. "Assessment of cost-optimality and technical solutions in high performance multi-residential buildings in the Mediterranean area". *Energy and Buildings* 102:250-265. doi:10.1016/j.enbuild.2015.04.038.

Effective Building Modelling for Energy Performance Contracting

Alberto Giretti – Università Politecnica delle Marche – a.giretti@univpm.it

Massimo Lemma – Università Politecnica delle Marche – m.lemma@univpm.it

Miquel Casals – Universitat Politècnica de Catalunya – miquel.casals@upc.edu

Marcel Macarulla – Universitat Politècnica de Catalunya – marcel.macarulla@upc.edu

Alba Fuertes – Plymouth University – alba.fuertes@plymouth.ac.uk

Rory Jones – Plymouth University – rory.jones@plymouth.ac.uk

Abstract

Energy Performance Contracts (EPC) are contractual agreements between beneficiaries and energy service providers, where budgets are established in relation to a determined level of energy performance. Hence, the problem of forecasting the energy performance of buildings in the EPC tendering phase becomes relevant for the reliability of the overall contract. Unfortunately, fuzziness and incompleteness often characterize the technical information supporting EPC call for tenders. Furthermore, buildings that are the subjects of EPCs are normally quite complex public buildings (hospitals, schools, etc.) usually relatively old and not technically well known. Gathering information about such buildings is a time consuming and expensive process within the usually short time frame of EPC call for tenders. This paper investigates the application of Grey-Box modelling to the energy performance forecast of complex buildings, in perfectly and poorly informed operational cases. The proposed methodology offers a potential solution to the EPC operational requirements since it requires a substantially reduced parameter set. Results show that the proposed Grey-Box modelling can be used to arrange a calibration set-up with good forecasting performance. Furthermore, Grey-Box modelling allows an effective management of the information uncertainty usually present in the EPC context.

1. Introduction

An Energy Performance Contract (EPC) is a contractual agreement between a beneficiary and an energy service provider (usually an Energy Service Company - ESCO), where budgets are established in relation to a contractually bounded level of energy performance (Directive 2006/32/CE). According to

the U.S. Department of Energy (DOE), there are several proven benefits from using EPCs, such as guaranteed improvements, cost savings, and enhanced performance (DOE, 2014). However, the results of the Transparence EPC survey (Garnier, 2013) shows that the application of the EPC concept in daily practice is somewhat difficult. Besides the financial and regulatory barriers witnessed by EU ESCOs, the application of the EPC concept has a technical implication that raises a fundamental issue in the building modelling research. In fact, the overall balance of EPCs substantially depends on the estimation of the building energy performance in real operating conditions. This is a totally new perspective for the procurement phase of an energy contract: the reliable forecast of the building energy performance during the tendering phase becomes essential for the reliability of the overall contract. Unfortunately, fuzziness and incompleteness often characterize the technical information supporting EPC call for tenders. Buildings that are the subjects of EPCs are usually quite complex public buildings (hospitals, schools, etc.) sometime relatively old. Gathering information about such buildings is time consuming and expensive. Furthermore, the time that is usually available from the call for tenders to the submission deadline is quite short; hence, on-site surveys are necessarily limited. Within this scenario, ESCOs can formulate reliable offers, minimizing the risks of a mismatch between forecasted and real costs, only if they are able to model the energy behaviour of the building, thoroughly exploiting the information available in the tendering phase, despite its fuzziness and uncertainty.

New modelling approaches are necessary for this task. Standard detailed building energy models are not suitable. They require a large amount of details, (wall geometry and section details, layouts, etc.), and a lot of human resources. Furthermore, their calibration is a time consuming and brittle process. To overcome these barriers, this paper investigates the application of the Grey-Box modelling technique, a recent advance in the building energy modelling technology (Bacher and Madsen, 2011; Reynders et al., 2014), to the EPC tendering phase. Grey-box is a reduced-order building modelling technology that estimates the parameters of a reduced-order model of the building thermal behaviour, from sets of measured data. Despite the reduced set of parameters Grey-Box modelling has been proven effective in predicting the building energy performance with good accuracy. This paper proposes an adaptation of the Grey-Box modelling procedure to the EPC context. Since no extended monitoring data sets are usually available in the EPC tendering phases, the Grey-Box model has been configured so that the parameters can be estimated by means of a manual calibration process. The proposed Grey-Box modelling approach has a number of key features that fit well in the EPC framework. First, the reduced model structure is fixed and shared among a wide range of buildings. Second, the detailed building geometry is missing, causing a relevant speed-up of the modelling phase. Third, the building is represented by a reduced set of parameters that can be quite easily estimated in time-limited surveys. Fourth, the remaining modelling uncertainty is concentrated on a very limited set of parameters, and can be reduced through a quite simple calibration procedure, based on data set that are usually available to the building managers (e.g., monthly energy bills). Finally, the model size is extremely limited even for large buildings, and the simulation time is consequently negligible.

This paper exemplifies the application of the Grey-Box modelling approach in two case studies, characterized by different levels of knowledge about geometry, technology and systems: a university library located in Terrassa (Spain) and a multi-use building (offices and laboratories) located in Plymouth (England). Details about information pro-

cessing and the reliability of the forecasted performances are discussed. Section 2 details the case studies. Section 3 discusses the Grey-Box model used in both cases. Section 4 reports about the calibration process and the reliability of the achieved results in the EPC context. A conclusion section summarises the paper achievements and introduces future works.

2. The Case Studies

Two case studies with different information background have been considered in this research.

2.1 The UPC Terrassa Library

The UPC Terrassa library (Fig. 1) is a three-storey building. The ground floor contains shops and the library entrance. The main reading rooms are located in the second and third floor, which contains also some offices and small meeting rooms. The UPC Terrassa Library building is rather well known, since it is regulated by a BEMS system. Detailed energy consumption, monitored occupancy rates and local weather files provide reliable information about external gains and energy consumptions.



Fig. 1 – The south east façade of the UPC Terrassa library building

The building and the systems' main features have been collected through the analysis of technical project drawings. The net floor area is about 754 m² and the floor to ceiling height is about 2.70 m. The external walls are made of bricks plus two layers of insulation separated by an air gap. All the external façades have windows and those facing south have aluminum louvre solar shadings. The currently

heating and cooling system is the result of renovation works carried out in 2012: it consists of five heat pumps that serve fan coil units. At the second floor, air exchange is supplied by a mechanical ventilation system. Detailed energy consumption and occupancy rate are available through BEMS monitoring.

2.2 The Smeaton Building in Plymouth

The second case study is the Smeaton Building of the Plymouth University Campus located in Plymouth, UK (Fig. 2). In this case we have encountered the typical modelling conditions of a not well-known building.



Fig. 2 – The Smeaton Building in Plymouth, UK

The Smeaton Building is a four-storey building. The net floor area is about 2484 m² and the floor to ceiling height is about 2.90 m. The boundary walls' outside is made of sandwich panels, while the interior surface has concrete blocks with air gap and bricks, finished with plaster. On the ground floor, the sandwich panels of the outside face are missing. The building has single glazing system on the south side, and double-glazing on the north side. Every window has internal shades. Information about the Smeaton building systems was collected by visual inspection. The occupation profile is not monitored and it is different for each room since a lot of teaching rooms are present. Information about the maximum number of people and the teaching hours is available for every teaching room. The energy consumption was estimated from monthly bills that include other two nearby buildings.

2.3 Summary of the Case Studies

Table 1 summarises the main features of the two case studies.

Table 1 – Summary of the case studies' parameter

UPC Terrassa Library	Smeaton Building
Floor area: 797 m ² Volume: 9325 m ³	Floor area: 2484 m ² Volume: 29808 m ³
Envelope: brick (0.14 m), expanded polystyrene (0.04 m), air gap, expanded polystyrene (0.04 m), plasterboard (0.025 m) Floor: reinforced concrete, hollow slab (0.4 m) Windows: single and double glazing (U-value 5.6 W/m ² K - 2.5 W/(m ² K)) with solar shadings	Envelope: aluminium sheet (0.0015 m), mineral wool (0.09 m), aluminium sheet (0.0015 m), concrete blocks (0.3 m), air gap (0.18 m), brick (0.105 m), plaster (0.013 m) Floor: cast concrete (0.1 m), cement screed (0.1 m), linoleum (0.05 m) Windows: single and double glazing
Heating/Cooling: Heat pumps with fan-coil units	Heating: Boiler
Lighting: 17868 W	Lighting: N.A.
Operation: Monday to Friday: 9:00 am – 9:00 pm	Operation: Monday to Friday: 9:00 am – 18:00 pm
Setpoint temperature: winter 21 °C – summer 25 °C	Setpoint temperature: winter 20 °C
Annual electrical energy: 159674.85 kWh (year 2014)	Annual electrical energy: N.A.

Table 2 summarises the knowledge level reached for each class of information. A high knowledge level means reliable information and low uncertainty.

Table 2 – Knowledge level reached for each information class

Information	UPC Terrassa	Smeaton
Climate	High	High
Geometry	High	High
Envelope	Medium	Medium
Systems	Medium	Low
Operation	High	Low
Consumption	High	Low

3. The Grey-Box Model

The same Grey-Box model was used to simulate both buildings. It is made of four main blocks: the building envelope, internal walls and floors; the weather; the heating/cooling system and the internal gains block (see Fig. 3 and Table 3).

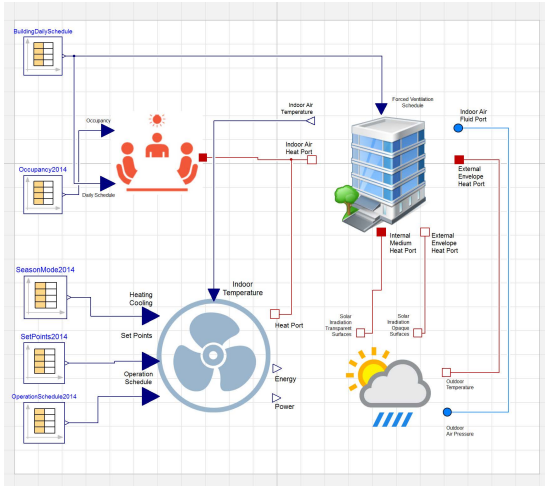


Fig. 3 – The Grey-Box model used to simulate both case studies

A single zone, third order model was used for the envelope and the internal walls and floors (Reynders, 2014). The indoor air volume is represented as a single volume. The building envelope and internal partitions and slabs are represented by means of a couple of lumped thermal resistances and capacities. The model was implemented using the basic thermal and fluid components of the Modelica Standard Library (Fritzon, 2004) in the Dymola simulation environment. No detailed representation of the building geometry is required. Only the overall geometric and physical parameters, like areas, thermal resistance and capacities are necessary. They can be easily and, quite reliably, estimated from design data, if available, or by a brief on-site survey. The weather block calculates the solar gains through the windows and the envelope, and provides the external temperature. Weather data are usually available from the web, and the consequent solar gains can be calculated by standard physics equations. More specifically, the following physics were implemented using the Modelica Buildings Library components (Wetter et al., 2011).

Distribution of room’s solar gain - The solar gains per unit area for the room surfaces is calculated by

assuming that all solar radiation that enters the room first hits the floor, and that the floor diffusely reflects the radiation to all other surfaces. Multiple reflections are neglected. Area-weighted solar distribution factors are used, instead of view factors between the floor and the other surfaces.

Solar irradiation - Both the direct solar irradiation on a tilted surface and the hemispherical diffuse irradiation are computed using an anisotropic sky model (Perez et al., 1990).

G-value - The reduction of the total solar energy transmittance caused by the external solar protection device is taken into account with a parameter (G-value) calculated according to UNI EN 13363-1. Heat gain due to air infiltration through windows is represented by a single resistance. This parameter depends on the user behaviour and may significantly affect the overall building thermal performance. Data concerning the infiltration and air exchange rates are available from the regulation (e.g., UNI TS 11300-1:2014). However, to get a reliable figure for the specific case study, this parameter should be estimated indirectly through a calibration process. The thermal gains due to the occupancy are simply modelled by two components multiplied by an occupancy schedule: a fixed thermal source (default 130 W for each person) and a thermal source that corresponds to the fixed equipment gains.

Table 3 – The Grey-Box Model parameter set

Parameter	Availability
Building Volume	Project data and/or surveying
Opaque envelope area divided as per orientation	Project data and/or surveying
Window area divided as per orientation	Project data and/or surveying
Average monthly occupancy level	Monitored or estimated
System operation schedule	Monitored or defined indirectly by interviews or opening data
Indoor temperature set-points	Monitored or defined indirectly by interviews

Outdoor air - envelope coupling resistance	Regulation
Averaged resistance of the opaque envelope	Project data, estimated
Averaged heat capacity of the opaque envelope	Project data, estimated
Thermal resistance between the interior and the interior air	Regulation
Heat capacity for the interior walls and furniture	Project data and surveying
Internal air volume	Project data and surveying
Air infiltration resistance	Regulation
Mass flow rate through forced ventilation	Project data
Weather data file	Available through the web
Solar shading coefficient	Project data and survey
Heat gain per person	Regulation
Heat gain due to fixed equipment and systems	Survey
Thermal resistance between the HVAC system and the interior	Technical data-sheets
Heat capacity for the HVAC system	Technical data-sheets
Efficiency of the HVAC system	Technical data-sheets
Installed heating/cooling power	Technical data-sheets

Monthly occupancy data can be available, as in the Terrassa Library case, or not, as in the Smeaton Building case. If not, they can be quite reliably estimated by interviews, or extrapolated from observation.

Finally, the heating/cooling system is modelled by a simple thermal source, with positive/negative flux respectively, that performs at a given efficiency rate. The indoor temperature setpoint is controlled by a PID. Setpoints are generally known, as in our case studies, since they are explicitly stated in the system operation schedules. The non-linear closed loop

control of the fluid temperature is regulated by a second internal PID. The heating/cooling system coupling with the indoor environment is modelled by a resistance and a capacity. These parameters can be estimated from standard technical data, but since they are subject to change during the lifetime of the system they should be fine-tuned through calibration.

Summarising, the proposed Grey-Box building energy model is described by 22 parameters. Among them, 14 parameters can be quite reliably estimated by analysing technical data or through on-site survey, the remaining 8 can be only roughly estimated, hence they should be fine-tuned, starting from standardised values, through calibration.

4. The Calibration Process

The calibration phase is a critical step in standard modelling since it is usually a complex and time-consuming process, dealing with hundreds or even thousands of variables (Coakley et al., 2014). The small number of parameters in the proposed Grey-Box modelling approach makes the calibration phase a manageable process. This is indeed an essential factor for the effective implementation of modelling procedures in the EPC context. When the knowledge level about the building is high, like in the UPC Terrassa Library case, some simple guidelines can be used to converge rapidly to a calibrated solution. When the knowledge level is low, the modeller should assume a paradigm shift. In these cases the standard modelling approach, aimed at building a detailed and trustworthy description of the portion of the reality under investigation, is not feasible. Rather, a new epistemic approach aimed at exploiting the available knowledge and minimizing the negative effects of the uncertainty on the final results should be assumed. In other words, instead of building a detailed picture of the reality, modelling should be aimed at constructing the best possible explanation of the building energy behaviour on the basis of the available data. In this perspective, the calibration process is essentially an explanation forming process, or, from a logical viewpoint, and abductive inference. Initially, information is ranked according to its reliability. Then, since the

knowledge is incomplete, some assumptions must necessarily be formulated in order to compensate for the uncertainty. Consequently, the calibration process can be used to verify the plausibility of the assumptions made, within the context of the set of constraints imposed by the known parameters and by the implemented physics. We will exemplify this modelling perspective in the following section.

4.1 The calibration of the UPC Terrassa Library

The UPC Terrassa library is a rather well known building. Uncertainty is low and no critical assumptions must be made to start the calibration process. In this case it is possible to speed up the calibration procedure further by applying simple heuristics to prioritize the selection of the parameters. The first step of the calibration process is the construction of the baseline. Energy consumption data are usually available through the energy bills. Collected consumption data must be analysed and eventually purged if some deviation from the standard operation schedule occurred (e.g., system breakdown period, malfunctioning, maintenance, etc.). The second step involves ranking the model parameters according to their uncertainty degree. Since the number of parameters is low, the standard ranking based on sensitivity analysis is less strategic than the uncertainty control that is consequent from the uncertainty based ranking. Despite, in principle, the uncertainty degree about a model parameter varies from case to case; usually data concerning the passive surfaces, walls transmittances, air masses and capacities can be estimated rather reliably. Hence, they usually score low uncertainty values. Weather data and solar gains are usually quite reliable as well. On the contrary, occupancy gains, ventilation and some system parameters affected by variation due to ageing, like system efficiency and coupling resistance, are quite fuzzy. Hence they should be adjusted first in the calibration process. All in all, as a general assumption we can use an Occam razor like principle, fixing reliable parameters and limiting the variable parameter sets to the most uncertain.

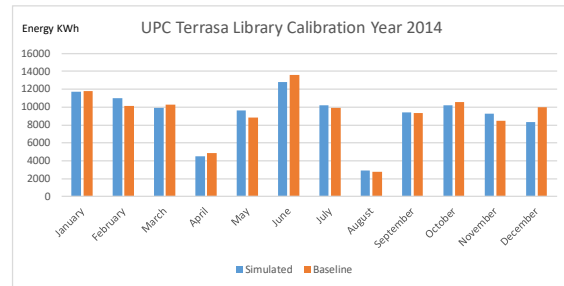


Fig. 4 – The baseline and the calibrated simulation of the UPC Terrassa Library - Year 2014 data set

In the UPC Terrassa Library case, this procedure rapidly converges to a satisfying calibration condition just after two iterations: initially the system efficiency was adjusted to compensate an offset occurring in both seasons; secondly, the ventilation rate was slightly increased to minimize the varying monthly offset. ASHRAE provides NMBE and CV(RMSE) indexes for assessing the model calibration (ASHRAE, 2002). For the UPC Terrassa library case NMBE= -0.65 % and CV-RMSE = 8.00 % was achieved using the 2014 data set. Fig. 4 shows the baseline and the calibrated model simulation of energy consumption for the year 2014.

4.2 The Calibration of the Plymouth Smeaton Building

The knowledge about the Smeaton building was affected by severe uncertainty about the system parameters, the operation, and the energy consumption. Since the building’s heating energy is supplied by a boiler shared with other buildings, very strong assumptions were made to extrapolate the energy baseline and the supplied heating power. No direct metering was available; hence the energy consumption extrapolation was made assuming a proportion between supplied energy and floor surfaces. The occupancy assumption was even weaker, since no monitoring data was available, an average daily occupancy rate, based on observation, was used. Under these uncertainty conditions, the calibration process was used to find a credible parameter arrangement based on the evidences provided by the simulated internal energy dynamic.

Initially, the same heuristic procedure of the previous case was used. Hence, the first iteration involved the set-up of the supplied power and of the system efficiency. The supplied power parameter

was increased until the system was able to drive the indoor temperature to the setpoint of 20 °C. Then, in a second iteration, the system efficiency was adjusted to minimize the overall energy consumption offset. These two initial iterations mostly affected the NMBE factor. A third iteration involved the ventilation rate, that was adjusted to compensate mismatches between cold and mid-season months, and occupancy rate. After three iterations, promising NMBE= -1.03% and CV-RMSE = 17.86% were reached. Fig. 5 shows the baseline and the simulated energy consumption for the heating months. Nevertheless, according to (ASHRAE, 2002) the model was not yet calibrated. This is essentially due to the prediction mismatch in May, which amounts to -46 %. There may be multiple reasons of this mismatch. It could have been caused by unknown operational conditions, system maintenance or other totally occasional and unknown factors. But it is unlikely that the mismatch could be the result of a simulation fault. According to the simulation, the low consumption in May was due to favourable climatic conditions. The outdoor temperature rose to about 19 °C for about a couple of weeks. Hence, the indoor temperature was kept close to the setpoint by wall inertia and by solar and occupancy gains, and the system didn't switch on.

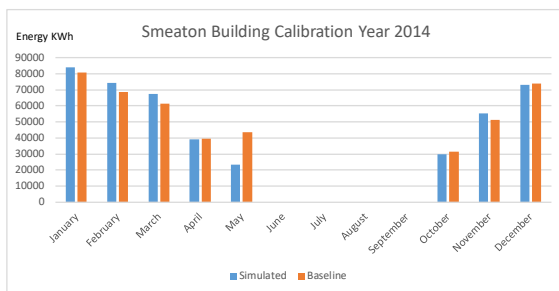


Fig. 5 – The baseline and the simulated energy consumption of the Smeaton Building in Plymouth - Year 2014 data set

Sensitivity analysis shows that neither wall inertia nor solar and occupancy gains can be reasonably adjusted to compensate the energy consumption mismatch registered in May, without corrupting the results of other months. Therefore, the most likely explanation that can be given in this context of uncertainty is that May can be considered an anomaly. If May is cancelled from the calibration data set, the model can be considered calibrated, scoring

NMBE= 3.40% and CV-RMSE = 7.06%. Of course the validity of this calibration is bounded by the limits imposed by the discussed assumptions. However, this is the best explanation of the Smeaton building energy dynamics that can be given with the available information. These insights provide the ESCO decision maker an information background that can be used to drive his/her contractual strategies in the EPC contexts, because they combine the estimation of the energy dynamics and of the saving potentials with the analysis of the accompanying uncertainty.

5. Conclusion

A Grey-Box modelling methodology to forecast building energy performance, has been proposed. The paper shows how it can be effectively used to provide decisional support in the EPC tendering phase, when modelling time and costs must be minimised, and when the uncertainty significantly affects the technical and operational knowledge. It has been shown how the proposed method allows the exploitation of all available knowledge by increasing the confidence level on simulation outcomes that are based on uncertain assumptions. A number of improvements and extensions are still necessary to implement the proposed procedure at an industrial level. The modelling is limited to energy consumption and does not include comfort. Cost benefit analysis concerning multiple zoning has not been carried out. Finally, the overall conceptualization and guidelines must be refined, as well as the uncertainty management approach that is still in its initial formulation stage.

Acknowledgement

This work emerged from the Annex 60 project, an international project conducted under the umbrella of the International Energy Agency (IEA) within the Energy in Buildings and Communities (EBC) Programme. Annex 60 developed and demonstrated new generation computational tools for building and community energy systems based on Modelica, Functional Mock-up Interface and BIM standards.

The ESCO vision has been formulated within the research agreement between Cofely s.p.a Italia and Università Politecnica delle Marche. A special acknowledgment in this context is due to Dott. Giovanni Pescatori and Dott. Oscar Merendoni. Many PhD and master students contributed to this research. Among them, special thanks are due to Sara Ruffini, Simona Marinelli, Elisa Gregori, Alessandro Defranco, and Adriano Morresi.

References

- ASHRAE. 2002. *ASHRAE Guideline 14-2002: Measurement of Energy and Demand Savings*. Atlanta, U.S.A: ASHRAE.
- Bacher, P., H. Madsen. 2011. "Identifying suitable models for the heat dynamics of buildings". *Energy and Buildings* 43:1511-1522. doi: 10.1016/j.enbuild.2011.02.005.
- Coakley, D., P. Raftery, M. Keane. 2014. "A review of methods to match building energy simulation models to measured data". *Renewable and Sustainable Energy Reviews* 37:123-141. doi: 10.1016/j.rser.2014.05.007.
- DOE. 2014. Energy Savings Performance Contracts (ESPCs), accessible at: <http://energy.gov/eere/femp/energy-savings-performance-contracts>
- European Parliament. 2006. *Directive 2006/32/EC of the European Parliament and of the Council of 5 April 2006 on Energy End-Use Efficiency and Energy Services*, accessible at: <http://eur-lex.europa.eu/legal-content/EN/TXT/PDF/?uri=CELEX:32006L0032&from=EN>
- Fritzson, P. 2004. *Principles of Object Oriented Modelling and Simulation with Modelica 2.1*. New York, U.S.: Wiley.
- Garnier, O. 2013. *D2.1 European EPC market overview, Deliverable of the Transparence EU project*, accessible at: <http://www.transparence.eu/eu/publications/markets>
- Perez, R., P. Ineichen, R. Seals, J. Michalsky, R. Stewart. 1990. "Modeling Dyalight Availability and Irradiance Componets From Direct and Global Irradiance". *Solar Energy*, 44(5):271-289. doi: 10.1016/0038-092X(90)90055-H.
- Reynders, G., J. Diriken, D. Saelens. 2014. "Quality of grey-box models and identified parameters as function of the accuracy of input and observation signals". *Energy and Buildings* 82: 263-274. doi: 10.1016/j.enbuild.2014.07.025.
- UNI. 2013. *UNI EN 13363-1:2013. Solar protection devices combined with glazing - Calculation of solar and light transmittance - Part 1: Simplified method*. Milan, Italy: UNI.
- UNI. 2014. *UNI/TS 11300-1:2014. Energy performance of buildings - Part 1: Evaluation of energy need for space heating and cooling*. Milan, Italy: UNI.
- Wetter, M., W. Zuo, T.S. Noudui. 2011. "Modeling of Heat Transfer in Rooms in the Modelica "Buildings" Library". In: *Proceedings of Building Simulation 2011*. Sydney, Australia: IBPSA.

Integrated Energy Modelling to Support District Cooling Optimisation: Methodological Approach

Francesco Passerini – R2M solution – francesco.passerini@r2msolution.com

Andrea Bassani – R2M solution – andrea.bassani@r2msolution.com

Pietro De Cinque – R2M solution – pietro.decinque@r2msolution.com

Raymond Sterling – National University of Ireland Galway – raymond.sterling@nuigalway.ie

Jesus Febres – IK4-Tekniker - jesus.febres@tekniker.es

Anna Magrini – Università di Pavia – magrini@unipv.it

Andrea Costa – R2M solution – andrea.costa@r2msolution.com

Marcus M. Keane – National University of Ireland Galway – marcus.keane@nuigalway.ie

Abstract

In a district cooling system different kinds of cooling production can be combined (e.g., vapour compression chillers, absorption chillers, and free cooling). Controlling those systems in an efficient way is a complex problem: the cooling demand is much more difficult to predict than the heat demand and, as for absorption chillers, heat sources such as the solar energy and the waste heat are not predetermined by the designers.

The EU project INDIGO deals with the improvement of District Cooling (DC) systems. Its main goal is the development of a more efficient, intelligent, and cheaper generation of DC systems. The results of INDIGO will include the development of:

- predictive controllers;
- system management algorithms;
- an open-source planning tool.

To validate the results, the consortium is analysing some case studies. The proposed solutions for DC systems will be installed in the Basurto Hospital campus in Bilbao. Different parts of models that regard the buildings and all the relevant components of the DC system are being developed:

1. generation systems;
2. distribution and storage systems;
3. HVAC systems;
4. thermal behaviour of the buildings, considering also internal loads and building use.

The first three parts are being simulated by means of Modelica, an open-source object-oriented modeling language that provides dynamic simulation models for building energy and control systems. The fourth part is being modelled with EnergyPlus. They are going to be

integrated through the Functional Mock-up Interface (FMI) for co-simulation.

The models of some building envelope elements are being validated considering experimental measurements (heat flow rates, temperatures, entering solar radiation).

Component models for the air handlers and for the fan-coils found in the studied buildings are developed in Modelica. Different kinds of chillers are modelled. Particular attention is paid to the distribution system, where thermal and hydraulic effects must be considered jointly.

All the developed models will be validated, both independently and considering the integration, using data acquired at the test-site.

The validated models will be considered a reference point for the development of the innovative controllers, of the management strategy, and of the planning tool. The new models developed in Modelica will be part of a District cooling open-source library (DCOL).

1. Introduction

This paper presents the role of the energy models in the development of INDIGO, a research project that is funded by the European Union in the context of the Horizon 2020 research and innovation program. The project started in March 2016 and will end in August 2019. Its main goal is the improvement of the district cooling (DC) systems.

In comparison with the heating systems, the cooling systems present problematic aspects related to the greater difficulty in the prediction of the energy

demand. The reason is that the energy demand can change quickly because it is influenced by factors such as the solar radiation and the internal heat loads.

Another problematic issue is that the difference between the supply water temperature and the return water temperature for DC loops is generally around 8 °C, while in district heating loops the difference is usually greater than 40 °C. That causes an increase in the cost of the piping system and of the energy requested for pumping.

The improvement of the DC systems shall be achieved through the development of new tools for the design and for the management of district cooling systems:

- predictive controllers that will be responsible for determining the setpoints of the mechanical systems (some of them will include self-learning algorithms), at all levels (generation, distribution, storage, AHUs, and fan-coil units). They will develop on the basis of “reduced” and validated versions of the energy models;
- an innovative management strategy, on which the controllers will be based, will consider energetic aspects, environmental aspects, and economical aspects;
- an open-source planning tool for the evaluation of existing systems and for the design of new district cooling systems. It will be based also on the results of simulations;
- an open library including physical/mathematical models developed in Modelica of the components that compose a DC system that will be called *District cooling open-source library* (DCOL).

The models regard mainly the real situation of the Basurto Hospital, in Bilbao, which is divided in 20 buildings, among them 9 are mechanically cooled. The results of INDIGO will be applied and measured in the plants relative to that facility. The DC system was installed in 2003 and extended in 2011 by Veolia-Giroa. The chilled water is produced by two absorption chillers and by four vapour compression chillers. The system supplies chilled water always at 7 °C (as setpoint temperature) and it modulates the water flow rate. The absorption chillers are cooled by water loops, one vapour compression chiller is water-cooled while the other three electric

chillers are air-cooled (Fig. 1). The hot water, which is used by the absorption chillers and to heat the buildings, is heated by the waste heat of a cogeneration system. That heat can be stored in a water tank. The cogeneration system is activated on the basis of the economic convenience of producing electricity.

In this case the cooling demand is particularly variable because it depends on the number of scheduled surgeries and on the occupancy level as well.

The internal zones are conditioned mainly through Air Handling Units (AHUs) or through fan-coil units. Since the local regulations for hospitals do not permit air recirculation, an important amount of energy is requested for the treatment of the outdoor air.

In the other two pilot cases, located in Barcelona, the models and the INDIGO solutions (controllers and management system) will be tested without a physical installation. They are not considered in this paper.

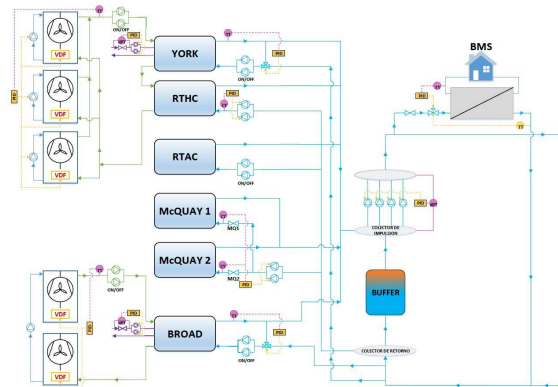


Fig. 1 – Scheme reporting the situation of the cooling production/distribution plant in the hospital (INDIGO project, 2016)

2. The Integrated Model

2.1 FMI

Different partners of the project consortium are developing different parts of models that regard the buildings and the DC system of the Basurto hospital. The different parts will be integrated and they are:

1. generation systems;
2. distribution and storage systems;
3. HVAC systems inside the buildings;

4. building geometry, thermal behaviour of the building structures, internal loads, and building use.

The fourth part will be developed in EnergyPlus and will be converted into functional mock-up units (Blochwitz et al., 2012; Nouidui et al., 2014) that will be then imported and used in a Modelica model that includes the AHUs. The weather data will be integrated in the same functional mock-up unit (FMU) of the building. The FMU will have as input variables latent and sensible heat gains provided by the AHUs to each conditioned thermal zone and as output variable room conditions (zone air temperature and relative humidity) and outdoor air conditions. The combined Modelica-AHUs with EnergyPlus-FMUs will be then converted into another FMU and used for training an advanced control algorithm to be developed in INDIGO and for the integration with the distribution-storage-generation models, which are being created in Modelica.

The integration of different tools allows the exploitation of their different capabilities. EnergyPlus is a whole building energy simulation software, the development of which is funded by the U.S. Department of Energy – Building Technologies Office. It is free, open-source, and cross-platform. In EnergyPlus many physical-mathematical models relative to the building physics (as well as to the HVAC systems) are already available and validated. Modelica is a non-proprietary, object-oriented, equation based language. The use of a Modelica library (Wetter et al., 2014) and the development of new models require the use of a Modelica simulation environment (some environments are commercial, a few environments are free). The use of Modelica allows for a greater flexibility than EnergyPlus.

2.2 Validation

The models will be validated, at different levels, using measured data. The quality of the measured data will be checked in order to eliminate the unreliable ones. The validation process will consider statistical test methods, with the definition of an acceptable range of accuracy with respect to the model goal. It will be an iterative process.

The validated models will be then used as a tool for the improvement of the plant and for the development of other tools, such as the controller, the management strategy, and the planning tool.

A monitoring campaign has started in summer 2016 and is going to be completed in summer 2017. A Building Management System (BMS) is installed and some data used for the validation were already being measured, while other data are being measured or are going to be measured because it was requested by the measurement plan developed for this project.

2.3 Generation Systems

The models of the generation system that are being developed are: water cooled vapour compression chillers, air cooled vapor compression chillers, absorption chillers, cooling towers, heat exchangers (plates and shell & tube), and pumps. The development is being carried out in Modelica. The following measurements, with a time step equal to 1 minute, are available:

- cooling energy produced by each chiller (elaboration from water flow rate and temperatures);
- total cooling energy produced by the plant (elaboration from water flow rate and temperatures);
- electric consumption in each chiller;
- gas consumption of the cogeneration engines;
- supply and return temperature of the hot water loop for each absorption chiller;
- supply and return temperature of the heat rejection loops (cooling towers);
- water temperature in the supply and return manifolds;
- outdoor temperature.

2.4 Distribution and Storage Systems

Outside the building where the generation system is located, there is a buffer tank for cold water that is installed between the return and supply manifolds (its volume is 25 m³). The chilled water temperature is measured at the top and at the bottom of the tank. The length of the distribution piping is about 2 km (supply pipes plus return pipes), split in two branches. The DC grid sends chilled water to 9 buildings where substations are installed. The total

substations are 11 because in two of the buildings there are two substations. Only in a substation there is a heat exchanger, while in other ones there are hydraulic separators between the DC loop and the loop inside the buildings. In some cases, energy meters are installed in the building side of the substation.

The central pumps are connected to a frequency converter that allows the variation of their speed.

As for the models of valves, pumps and fittings, the relative models available in the Modelica Standard Library are being used. As for the pipes, a new model, based on the “plug-flow” approach, is being developed. The roughness of the pipes, since it influences the hydraulic resistance and it raises the water temperature, the heat losses through the pipes, and the thermal inertia of the distribution system are being considered.

As for the water tanks, phenomena like the thermal energy charging and discharging process, the stratification, and the heat losses are being considered.

2.5 HVAC Systems

Several libraries exist in Modelica for modelling and simulation of HVAC systems. The INDIGO team decided to use the Annex60 (Wetter et al., 2015) Modelica library as a basis for the component models and develop whichever component was not included in the library.

This section deals with the modelling and simulation of the Air Handling Units (AHUs) that serve one of the demonstrator buildings, the Aztarain Block in Basurto Hospital. Aztarain is served by two main AHUs as the one shown in Fig. 2.

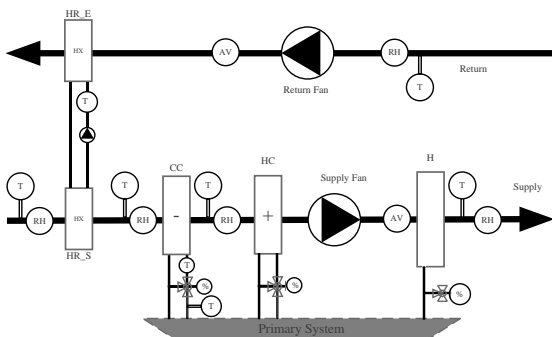


Fig. 2 – Schematic of Aztarain AHUs (Sterling, 2016)

The unit is composed of:

- heat recovery (HR) based on two heat exchangers with a close water circuit as transfer fluid;
- cooling coil (CC);
- heating coil (HC);
- supply and return fans;
- humidifier (H);
- sensors: temperature (T), relative humidity (RH), air velocity (AV), valve position (%).

In the Aztarain building an AHU serves pressure positive rooms for immuno-depressed or critical patients. Another AHU serves all the other areas. For the underground floor the supplied air can be post-heated or post-cooled by water coils installed in local boxes, where the renovation airflow rate is mixed with recirculated air.

The Annex60 library contains models for the fans, the heating coil, and the humidifier. However, a model for the cooling coil is not implemented yet. An initial implementation of the cooling coil model has been made based on the efficiency-NTU method.

These models will be validated using real operation data from the facility after the monitoring and instrumentation is upgraded to match the instrumentation shown in Fig. 2. Attention will be focused on the cooling coil given the aim of the INDIGO project to improve operations of district cooling systems.

To calibrate and validate the cooling coil models a procedure based on (Febres et al., 2015) has been proposed whereby the full range of operation of the coil is explored at discrete steps. This is done by modulating the cold-water control valve as shown in Fig. 3.

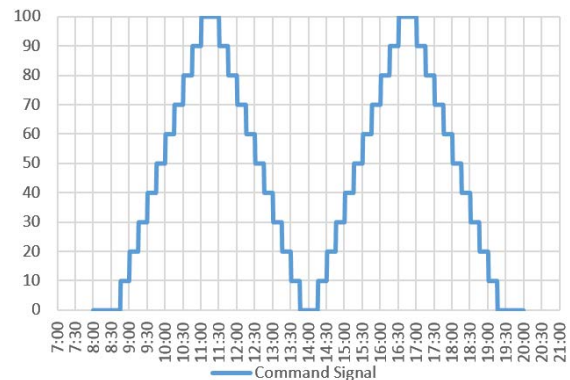


Fig. 3 – Controlling variable signal (Sterling, 2016)

In this validation scenario, the input and output air temperature and relative humidity are monitored at 1-minute intervals over the validation period. With this approach, it is possible to characterise the relationship between valve command and output conditions and hence validate the suitability of the model for the specific coil.

The rest of the components will be validated during normal operations to avoid disrupting the hospital functioning.

2.6 Building, Internal Loads, Users

Some measurements relative to the building have started in summer 2016. They regard the building envelope.

The thermographic camera has been used for detecting irregularities in the building envelope. In this way, the best position for the heat flow meter can be evaluated. The heat flow meter was used to measure the heat flow rate through the roof and the external walls of the Aztarain building. During the same period the outdoor and the indoor air temperature, the outdoor and the indoor surface temperature were measured (Fig.s 4 and 5). The data relative to the solar radiation and to the wind velocity and direction are available through the weather station C039 - Deusto of the Basque agency of meteorology Agencia vasca de meteorología. A new solar radiation sensor will be installed in the next months. Generally, the measurements made through the heat flow meter are indicative when there is an important difference (at least 10 °C) for some consecutive days between the indoor temperature and the outdoor temperature. Normally this happens during the winter season. Nevertheless, in this case the measurements were carried out in summer because the research is interested in modelling the cooling demand and therefore in analysing the behaviour of the structures in hot conditions and when they are stricken by a high solar radiation.



Fig. 4 – Internal measurement equipment for heat flow rate, surface temperature, and air temperature (Passerini, 2016)

The validation of the models of the walls and of the roof is considering: amplitude of peak, time between two peaks, minimum, maximum and mean values, slope and the number of inflection points, attenuation factor relative to the external and the internal oscillations, time delay between external surface temperature and internal surface temperature or internal heat flow rate. The surface emissivity is being evaluated through a thermographic camera: the surface temperature is measured at the same time with a thermographic camera and with a surface thermometer and the emissivity considered by the thermographic camera is adjusted until it measures the same value measured by the surface thermometer.

The surface solar absorptance considered in the model is adjusted in order to have an acceptable agreement between measured and calculated outside surface temperatures. The results obtained with different models of the outdoor convection coefficient are going to be compared with measured data in order to select the most appropriate one for the analysed case.

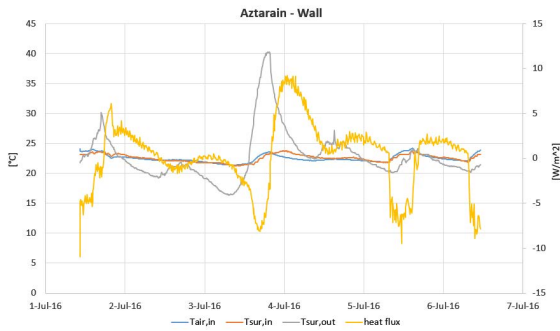


Fig. 5 – Elaboration of measured data relative to an external wall of Aztarain building (Passerini, 2016)

A pyranometer was used with different sky conditions in order to evaluate the ratio between the solar radiation flux density (W/m^2) entering the windows and the external solar radiation on a plane parallel to the window.

Additional measurements to be carried out in order to improve the input accuracy regarding mainly the internal loads and the behaviour of the users are:

- internal heat gains (metering of the consumption of medical equipment, communication racks, UPS systems, IT equipment, and any other relevant equipment);
- window openings (magnetic sensors);
- CO_2 concentration.

The correlation between the opening of the windows and other parameters (e.g., CO_2 concentration, indoor and outdoor temperatures) will be investigated.

Since the control of the HVAC system is based on the return air temperature, the rooms have been divided in thermal zones by gathering all the rooms of a floor that are supplied by the same AHU. For the underground floor of the Aztarain building the division has considered also the distribution of the reheating/recooling boxes.

3. Conclusions

In the INDIGO project an important role is played by the creation of dynamic models of a DC system and of the connected cooling demand.

The geometry of the buildings and the thermal properties of the structures, as well as some AHUs, the water buffer tank, some chillers, and other components have been modelled. The integration of the building model with the AHUs models was tested.

In the next weeks, the parameters will be adjusted and validated on the basis of the data monitored in summer 2016. The validation will be completed after the elaboration of the data that will be measured in the next months and in summer 2017. Through the validated models, improvements of the technical plants and of their management will be tested. Some proposed improvements will regard the control logics, while other improvements will regard the installation (e.g., the installation of a new solar thermal system that can feed the absorption chillers).

The models will be useful in evaluating whether there are discrepancies between the expected performance and the real performance, in finding the causes of the possible discrepancies and in quantifying the energy and economic savings in comparison with the previous situation (before the implementation of INDIGO solutions).

Acknowledgements

INDIGO has received funding from the European Union’s Horizon 2020 research and innovation programme under grant agreement n° 696098.

Osakidetza is the public health service of the Basque countries and it is the owner of the Basurto hospital, where Veolia-Giroa (partner of the project consortium) manages the DC systems. Osakidetza and Veolia-Giroa have given permission to use the Basurto hospital as a pilot case. In particular, Veolia-Giroa is involved as WP leader in information collection and in the validation of the performed developments.

Nomenclature

Symbols

DC	District cooling
FMI	Functional mockup interface
FMU	Functional mockup unit

References

- Agencia vasca de meteorologia <http://www.euskalmet.euskadi.eus>
- Blochwitz, T., et al. 2012. "Functional Mockup Interface 2.0: The Standard for Tool independent Exchange of Simulation Models". In: *Proceedings of the 9th International Modelica Conference*. he Modelica Association.
- EnergyPlus. Accessed December 2016. <https://energyplus.net/>
- Febres, J, R. Sterling, M. Keane. 2015. "Automated calibration of Air Handling Unit models using a modified Preisach model". In: *Proceedings of Building Simulation 2015*. Hyderabad, India: IBPSA.
- FMU export of EnergyPlus <http://simulationresearch.lbl.gov/fmu/EnergyPlus/export/index.html>
- Modelica. Accessed December 2016. <https://www.modelica.org>
- Nouidui, T.S., M. Wetter, W. Zuo. 2014. "Functional mock-up unit for co-simulation import in EnergyPlus". *Journal of Building Performance Simulation* 7(3): 192–202. doi: <http://dx.doi.org/10.1080/19401493.2013.808265>.
- Wetter, M., Z. Wangda, T.S. Nouidui, X. Pang. 2014. "Modelica Buildings library". *Journal of Building Performance Simulation* 7(4): 253–270. doi: <http://dx.doi.org/10.1080/19401493.2013.765506>.
- Wetter, M., M. Fuchs, P. Grozman, et al. 2015. "IEA EBC Annex 60 Modelica Library - An international collaboration to develop a free open-source model library for buildings and community energy systems". In: *Proceedings of Building Simulation 2015*. Hyderabad, India: IBPSA.

The Development and Verification of a Computational Tool for the Evaluation of the Visual Accessibility of Architectural Spaces

Dawid Wolosiuk – TU Wien – dawid.wolosiuk@tuwien.ac.at

Harald Hofstätter – TU Wien – harald.hofstatter@tuwien.ac.at

Ardeshir Mahdavi – TU Wien – amahdavi@tuwien.ac.at

Abstract

The present paper presents a tool for the assessment of the visual performance of spaces, especially with regard to the requirements of visually impaired people. This tool was one of the key deliverables of a recently completed project (ViDeA) addressing the special architecturally relevant needs of the visually impaired building users. Implementation of building regulations related to visual accessibility in a reliable manner (during design process) requires expert knowledge and the use of sophisticated visual simulation software. Toward this end, the tool attempts to facilitate the accurate evaluation of visual conditions in the proposed designs. The paper describes the general structure and implementation details. It also documents the preliminary verification of the tool based on a case study of an underground metro station.

1. Introduction

Partially sighted people constitute a large part of the population (over 246 million worldwide, WHO, 2012). The specific requirements of this population in view of the universal design has not been sufficiently addressed. International and national standards (e.g., ISO, 2011; DIN, 2009; SIA, 2009; ASI, 2013; BSI, 2009) provide some information on the threshold levels for certain relevant visual indicators (e.g., luminance contrast and average illuminance). Less attention seems to have been paid to further visual performance indicators (for example, light distribution uniformity), which are equally relevant in evaluation of visual quality of spaces. The threshold values for these indicators had to be derived in a process of original optometric

experiments in the ViDeA project involving both partially and full sighted participants.

There is a long list of visual simulation applications that can support the building design process. However, to our knowledge there is a lack of visual performance simulation tools that would be suited to specifically address the needs of visually impaired people.

2. A Visual Performance Assessment Tool

2.1 General Structure

The standard workflow in ViDeA begins on the client's side where a 3d model is created or imported to a CAD software (see Fig. 1). Utilizing software's GUI (Graphical User Interface) it is semantically enriched. Thereby, visual properties of the surfaces and lighting system details are specified.

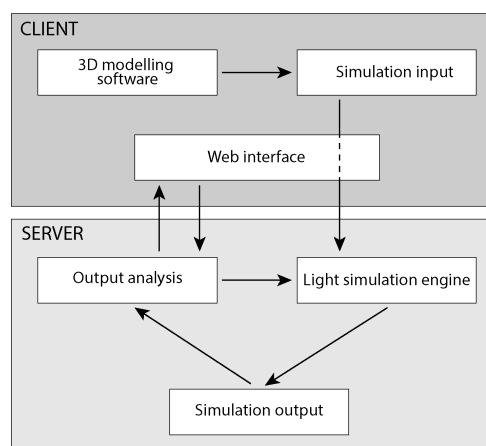


Fig. 1 – ViDeA tool workflow (Wolosiuk et al. 2015)

This data set together with user-specified observer positions constitute the input for an advanced lighting simulation engine. Simulation results in the values of a number of view dependent visual indicators such as UGR (Unified Glare Rating). The user is presented with the results of the simulation via a dedicated Web interface, where rendered images can be further analyzed in whole or in parts (e.g., mean luminance or contrast ratio for a selected segment of the rendered image).

Computed values of numeric indicator values are compared with pertinent threshold values, which are determined via optometric experiments (conducted in the course of the ViDeA project) and literature. The set of relevant visual indicators that was selected for the projected space evaluation is as follows:

Luminance contrast according to Michelson (Rea, 2000):

$$C_M = (L_{max} - L_{min}) \cdot (L_{max} + L_{min})^{-1} \quad (1)$$

Luminance contrast according to Weber (Rea, 2000):

$$C_W = (L_g - L_l) \cdot L_g^{-1} \quad (2)$$

Mean Luminance (L_m) and mean Illuminance (E_m)

Light Distribution Uniformity (DIN, 2011):

$$U_o = L_{min} \cdot L_m^{-1} \quad (3)$$

Unified Glare Rating (CIE, 2011):

$$UGR = 8 \cdot \log[(0,25 \cdot L_b^{-1}) \cdot \sum[(L^2 \cdot \Omega) \cdot p^2]] \quad (4)$$

The indicators set was based on examination of related literature (e.g. CIE, 2011; DIN, 2009 and 2010; ISO, 2011; SIA, 2009; Bright et al., 1997; Buser et al., 2008; Joos et al., 2012; Schmidt and Buser, 2014; BMG, 1996) approved and supplemented by recommendations from optometrists involved in the project.

2.2 Implementation

To cater for the ViDeA tool's requirements in view of 3D modelling, camera tools, "layers" grouping, and material selection functionality, Trimble SketchUp was selected (Trimble, 2014). This tool comes with a built-in Ruby API that allows for a further functionality extension through various plug-ins. The already existing "su2rad" (Bleicher, 2015) plug-in, was altered to support the project goals. The original plug-in functions as a bridge between SketchUp and RADIANCE advance lighting simulation software (Ward, 1994) (Fig. 2). It facilitates

access to the initial simulation settings, allows for the assignment of Radiance compliant materials to groups of 3D objects (per layer, per color), and exports stored camera positions.

The output of the original plug-in is a folder containing simulation files structured in accordance with RADIANCE guidelines. To perform a simulation of an exported scene, Radiance and operating systems command line interface (CLI) knowledge is required. The ViDeA extension alters this original plug-in to make it possible to import into the model, luminaire source geometry and photometric data extracted from IES photometric data files (IESNA, 2002). Moreover, the developed plugin allows to easily exchange imported luminaire instances against other options in the luminaire database.

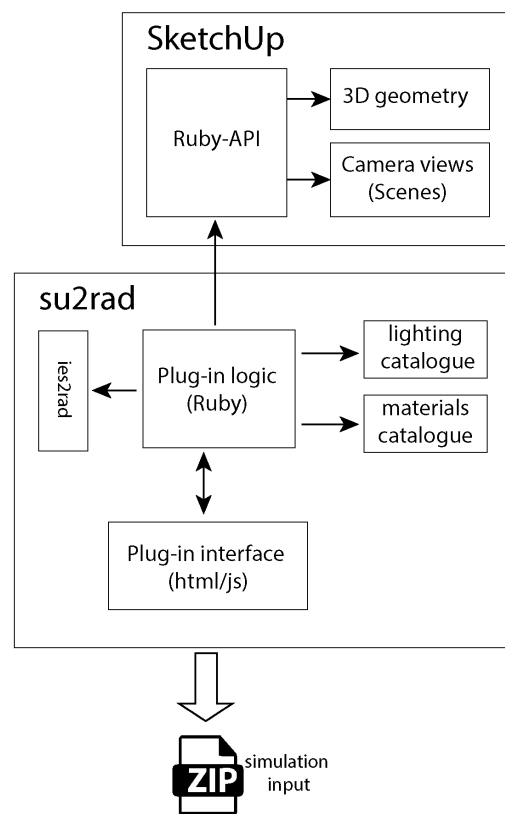


Fig. 2 – Plug-in architecture

The plug-in also enables users to import Radiance compliant materials list stored in a text file and add them to the native SketchUp materials list. This allows for the use of the native "paint bucket" tool for the custom Radiance material assignment. It also adds additional view and renders settings that are

required for calculation of the visual performance indicators.

To remove CLI, a web-application was created (Fig. 3). It presents the user with numeric and visual simulation results together with warning information in case the values are outside the recommended ranges. Likewise, tools are provided for an interactive analysis of the rendered views.

Simulation files are automatically compressed during the export process to facilitate the upload process. Uploading is done via dedicated web-interface. The simulation is automatically initialized on the server by the execution of the relevant Radiance executable and system commands. All relevant simulation output (indicators, rendered images) is processed and stored in a database for rapid queries.

During image analysis, an R-tree data structure (multi-dimensional tree data structures that provide efficient spatial access to their elements, see Guttman, 1984) is generated from values obtained from each pixel.

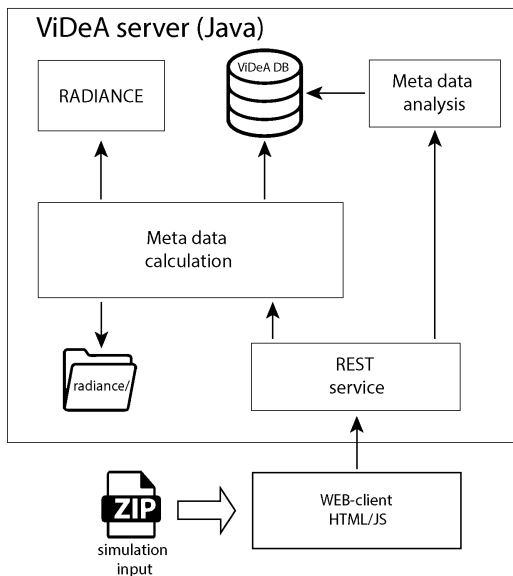


Fig. 3 – Web application architecture

The interface offers the possibility to select a point, segment, or surface of interest in the image. Multiple descriptive statistics are calculated based on pixels' meta-data (e.g. luminance values) including minimum and maximum values, mean, variance, and standard deviation. This data is then used to calculate visual performance indicators for selected segments of the image.

3. Illustrative Example

3.1 Input Data

In order to illustrate the workflow and verify the ViDeA tool, an existing metro station in Vienna was selected as a study case. Toward this end, the following data was acquired:

- Blueprints and photographic documentation for the recreation of 3D space;
- Photometric profiles of electric lighting;
- Luminance images;
- Optical properties of the building materials.

The project partners supplied the blueprints as well as the photometric lighting profiles (in form of IES files). The station was also well documented in a set of luminance images captured using a fish-eye lens. These images are later used for model validation.

Using a portable spectrophotometer, a series of on-site measurements was performed to determine the average reflectance of the building materials. The collected data had to be converted to a radiance compliant format.

3.2 Modelling

The 3D model of the station was recreated in Archicad (BIM software) and exported in a Sketchup compliant format (Fig. 4). Given the added functionality in the modified "su2rad" plug-in, the luminaire source geometry (extracted from IES file) was imported to the 3D model and then duplicated and positioned according to the plan documentation. In the following step, the 3D model was semantically enriched by associating previously gathered material properties to the surfaces. This was done using another new plug-in' feature that allowed to add the on-site collected materials (in radiance compliant format) to the native Sketchup material collection, thereby enabling the use of the built-in "paint bucket" tool.

Finally, using native Sketch-Up camera and 3d view storing functionality, a number of viewer positions (matching those from luminance camera) were selected for rendering.

Simulation is carried out automatically after the upload of a ZIP file (outcome of the modeling phase) via ViDeA web interface to the dedicated server.

The end product of the simulation is a set of rendered views with pre-calculated view dependent visual indicators (UGR, mean luminance/illuminance, light distribution uniformity), ready for analysis. Rendered images and those obtained from the luminance camera were compared toward model performance evaluation.

3.3 Simulation Results and Verification

Figs. 5 and 6 contrast the false color images obtained from the luminance camera with the computationally rendered images. Table 1 shows the resulting average luminance values for the specific segments of the images (see Figs. 5 and 7).



Fig. 4 – 3D model of the metro station

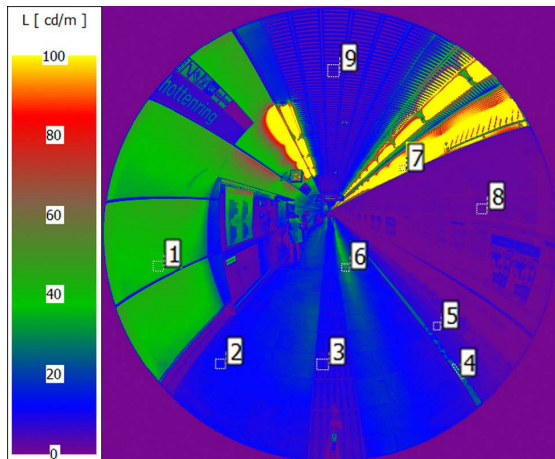


Fig. 5 – False color image obtained from the luminance camera

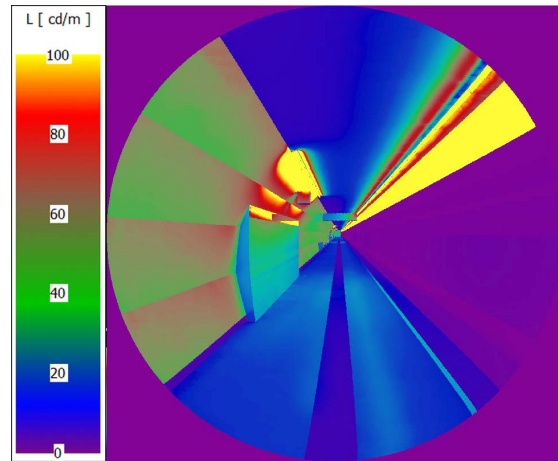


Fig. 6 – False color rendered image

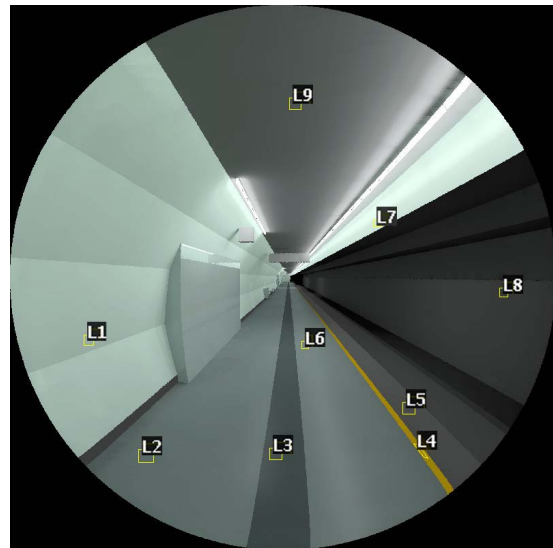


Fig. 7 – Rendered image

Table 1 – Luminance result comparison

Region	Average Luminance [cd/m ²]	
	Camera	Simulation
1/L1	41.5	43.5
2/L2	12.6	12.7
3/L3	8.7	7.7
4/L4	23.4	22.6
5/L5	7.4	7.3
6/L6	25.2	23.8
7/L7	218.2	217.0
8/L8	2.3	2.1
9/L9	7.9	8.5

The good correlation between the simulations and the measurements are arguably the result of two factors. One factor is attributable to the reliability of the adopted computational engine (Radiance). The other factor pertains to the deployment potential of the developed environment toward a proper and effective generation of simulation input models. Hereby, the effectiveness relates to the circumstance that the components of the model (geometry, surface properties, luminaire specifications) can be conveniently obtained and reliably assembled. Likewise, consideration and inclusion of empirically obtained information regarding the specific requirements of visually impaired people enriches the informational background for the evaluation of the calculated values of pertinent visual performance indicators.

4. Conclusion

This paper reported on a visual simulation and analysis tool that was developed as a part of the ViDeA research project. The project addressed the needs of visually impaired people by focusing on the specific requirements for creation of visually accessible spaces. Toward this end, the project partners carried out interviews and optometric experiments. Moreover, a systematic set of key visual performance indicators and associated computational routines was generated, which served as a base for the developed tool. The ViDeA tool aims at providing the necessary means to support designers in simulating and analyzing 3D scenes. To obtain detailed and high fidelity simulation results, a well-established simulation engine was deployed. A set of analytical tools was provided to facilitate the extraction of data necessary for a comprehensive visual performance assessment of the rendered scenes. The comparison of simulated and real-world numeric results presented in this paper, shows a promising correlation. This points to the potential of the developed environment as a design and retrofit decision support tool. The next developmental steps pertain to tool performance optimization. Specifically, computational efficiency is to be increased. Toward this end, recent developments in the use of advanced GPUs in the ray tracing process (Jones,

2014) and the associated rendering time reduction are to be harnessed.

Acknowledgement

The ViDeA project was funded under the Austrian Research Promotion Agencies program "Mobility of the Future" (grant No. 844158) by the Austrian Federal Ministry for Transport, Innovation and Technology (bmvit). The project team included, aside from the authors, Ulrich Pont, Matthias Schuß, Magdalena Maringer, and Nico Hauck.

Nomenclature

Symbols

E_m	Average Illuminance (lux)
L_b	Background Luminance ($E \cdot \pi^{-1}$) ($\text{cd} \cdot \text{m}^{-2}$)
L_g	Higher Luminance ($\text{cd} \cdot \text{m}^{-2}$)
L_l	Lower Luminance ($\text{cd} \cdot \text{m}^{-2}$)
L_m	Average Luminance ($\text{cd} \cdot \text{m}^{-2}$)
L_{\max}	Maximum Luminance ($\text{cd} \cdot \text{m}^{-2}$)
L_{\min}	Minimum Luminance ($\text{cd} \cdot \text{m}^{-2}$)
Ω	Solid angle (sr)
p	Guth position index
U_o	Luminance uniformity

References

- ASI. 2013. *Barrierefreies Bauen – Planungsgrundlagen (ÖNORM B1600:2013)*. Vienna, Austria: Austrian Standards Institute.
- Bleicher, T. 2015. Radiance plug-in for SketchUp. URL: <http://sites.google.com/site/tbleicher/Home>.
- BMG. 1996. *Verbesserung von visuellen Informationen im öffentlichen Raum – Handbuch für Planer und Praktiker*, Bundesministerium für Gesundheit. Hof Saale, Germany: Fach Media Service Verlagsgesellschaft.
- Bright, K., G. Cook, J. Harris. 1997. *Colour, Contrast and Perception - Design Guidance for Internal Built Environments*. Reading, UK: The University of Reading.

- BSI. 2009. *Design of buildings and their approaches to meet the needs of disabled people – Code of practice (BS 8300:2009)*. London, UK: British Standards.
- Buser, F., A. Scheidegger, R. Joos. 2008. *Untersuchung zur verbesserten Lesbarkeit von Bildschirminformationen für Sehbehinderte im öffentlichen Verkehr im Auftrag des Bundesamtes für Verkehr*. Olten, Switzerland: Fachhochschule Nordwestschweiz.
- CIE. 2011. *Guide to increasing Accessibility in Light and Lighting (CIE 196:2011)*. Vienna, Austria: International Commission on Illumination.
- DIN. 2009. *Gestaltung visueller Informationen im öffentlichen Raum zur barrierefreien Nutzung (DIN 32975:2009)*. Berlin, Germany: Deutsches Institut für Normung, Beuth Verlag.
- DIN. 2010. *Barrierefreies Bauen – Planungsgrundlagen – Teil 1: Öffentlich zugängliche Gebäude (DIN 18040-1:2010)*. Berlin, Germany: Deutsches Institut für Normung, Beuth Verlag.
- DIN. 2011. *Licht und Beleuchtung – Grundlegende Begriffe und Kriterien für die Festlegung von Anforderungen an die Beleuchtung (DIN 12665:2011)*. Berlin, Germany: Deutsches Institut für Normung, Beuth Verlag.
- Guttman, A. 1984. "R-Trees: A Dynamic Index Structure for Spatial Searching". In: *Proceedings of the 1984 ACM SIGMOD*.
- IESNA. 2002. *Standard File Format for Electronic Transfer of Photometric Data and Related Information (ANSI/IESNA LM-63-02)*. New York, U.S.A.: Illumination Engineering of Northern America.
- ISO. 2011. *Building construction – Accessibility and usability of the built environment (ISO 21542:2011)*. Geneva, Switzerland: International Standards Organization.
- Joos, R., F. Buser, A. Scheidegger, F. Horlacherer, S. Hinni, F. Gogniat. 2012. *Eruierung des für Sehingeschränkte relevanten Blickwinkels auf Objekte im öffentlichen Verkehr bezüglich Kontrolle des gesetzlich geforderten Kontrastes*. Olten, Switzerland: Fachhochschule Nordwestschweiz.
- Jones, N., C. Reinhart. 2015. "Validation of GPU Lighting Simulation in Naturally and Artificially Lit Spaces". In: *Proceedings of the 14th International Conference of the International Building Performance Simulation Association*. Hyderabad, India: IBPSA.
- Rea, M.S. 2000. *The IESNA Lighting Handbook Reference Application (9th ed.)*. New York, U.S.A.: Illumination Engineering of Northern America.
- Schmidt, E., F. Buser. 2014. *Planung und Bestimmung visueller Kontraste*. Zürich, Switzerland: Schweizerische Fachstelle für behindertengerechtes Bauen.
- SIA. 2009. *Hindernisfreie Bauten (SIA 500:2009)*. Zürich, Switzerland: Schweizerischer Ingenieur- und Architektenverein.
- Trimble. 2014. SketchUp Version 15.1.104. Sunnyvale, U.S.A.: Trimble Navigation Limited.
- Ward, G.J. 1994. "The RADIANCE Lighting Simulation and Rendering System". In: *SIGGRAPH '94 Proceedings of the 21st Annual Conference on Computer graphics and interactive techniques*.
- WHO. 2012. *Global Data on Visual Impairments*. Geneva, Switzerland: World Health Organization.
- Wolosiuk, D., U. Pont, M. Maringer, M. Schuss, N. Hauck, A. Mahdavi. 2015. "Supporting visual design for all: The ViDeA approach". In: *Proceedings of the 14th International Conference of the International Building Performance Simulation Association*. Hyderabad, India: IBPSA.

The Diversity Challenge in Models of Occupants' Presence in Buildings

Ardeshir Mahdavi – TU Wien – amahdavi@tuwien.ac.at

Farhang Tahmasebi – TU Wien – farhang.tahmasebi@tuwien.ac.at

William O'Brien – Carleton University – liam.obrien@carleton.ca

H. Burak Gunay – Carleton University – burak.gunay@carleton.ca

Abstract

This contribution is concerned with a number of basic questions regarding inhabitants' presence in buildings: How diverse are office inhabitants' presence patterns? Aside from the differences in the absolute values of the defining markers of such patterns (e.g. arrival and departure times), to which extent do the respective distributions of the marker values differ from inhabitant to inhabitant? Are tendencies regarding presence patterns in one location transferrable to other locations? Can the diversity of presence patterns among the inhabitants be reproduced via the randomisation of the markers' mean values? To explore these questions, we use monitored presence data from two offices in two different locations. The findings point to considerable differences amongst inhabitants and locations. Moreover, an empirically observable diversity of the office workers' presence patterns cannot be simply reproduced based on the randomisation of generic presence patterns.

1. Introduction

Multiple efforts in the past have pursued the development of advanced mathematical models of people's presence in buildings (e.g. Page et al., 2008; Richardson et al., 2008; Mahdavi and Tahmasebi, 2015a; Wang et al., 2016). The effectiveness of such models depends arguably on the representativeness of the underlying empirical data. This pertains also to the existence of inter-individual differences in patterns of inhabitants' presence and behaviour in buildings (O'Brien et al., 2016; Tahmasebi and Mahdavi, 2016; Feng et al., 2015).

In a previous study, we used data from an office building in Vienna, Austria, to analyse the presence patterns of a small but diverse number of inhabitants (Mahdavi and Tahmasebi, 2015b). Thereby,

differences in general long-term characteristics of individual presence profiles were studied to determine the statistical variance of the defining markers of such profiles, including arrival and departure times, presence and absence durations. We hypothesised that, even if the tendency of the specific values of these markers could be different for different occupants, the respective data distribution shapes could be comparable. If so, randomisation of general schedules could be conducted without any consideration of the occupants' diversity.

Given the limitation of this study (just one office building and a small number of inhabitants), the results were not deemed to be conclusive. The present contribution thus incorporated additional data from an office building in Canada. The respective data was similarly treated to identify central tendencies and dispersion of the marker values for inhabitants' presence patterns.

2. Approach

2.1 Selected Offices

For the Vienna study, we used one-year-long data obtained from an office area (including a single-occupancy closed office, two single-occupancy semi-closed offices, and an open plan office zone) in a university building. The collected data included indoor environmental conditions, state of devices (luminaires, radiators, windows and doors), and specifically presence patterns of eight inhabitants (academic and administrative staff).

In case of the Ottawa office, data was obtained from 16 private offices located in an academic building. The building's automation system monitors the inhabitants' presence using passive infrared (PIR)

sensors. The duration of observations varies from 19 days to 264 days across the offices.

2.2 The Occupancy Markers

We considered a number of markers (parameters) to capture presence patterns as follows:

- First arrival time (AT);
- Last departure time (DT);
- Presence duration (PD);
- Number of transitions (NT);
- Working hours (WH);
- Absence duration (AD);
- Mean break duration (MBD);
- Fraction of presence (FOP).

First arrival time (FA) and last departure time (LD) are derived by detecting the first and last occupied interval in a day (in the present study, data was structured in terms of 15-min intervals). The occupancy duration (OD) is calculated by counting the number of occupied intervals in a day. Number of transitions (NT) denotes the number of daily occupied-to-vacant transitions. Working hours (WH) are calculated by subtracting arrival time from departure time. Absence duration (AD) equals working hours (WH) minus presence duration (PD). Mean Break Duration (MBD) is obtained by dividing Absence duration (AD) by the number of transitions (NT). Fraction of presence is derived by dividing presence duration (PD) by working hours (WH).

2.3 Statistics

Presence data was processed in terms of four statistics, namely mean, median, standard deviation (SD), and coefficient of variation (CV). In addition, the values of the eight markers for all inhabitants were displayed (in aggregate and individually) in terms of probability distribution plots. This was done based on the original marker values as well as their normalized variation (i.e. difference between the marker value and the mean value of that marker).

Data analysis and interpretation targeted the following questions:

- 1) Considering both within-group and between-group standpoints, are the absolute values of inhabitants' presence markers similar across different inhabitants?

- 2) Does the between-group view of the tendencies in the two locations reveal similar overall tendencies in the absolute values of the presence markers?
- 3) Considering both within-group and between-group standpoints, is the statistical shape of distributions (dispersions) of the inhabitants' presence marker values comparable across different inhabitants?

3. Findings

The cumulative probability distributions of individual occupants' presence markers obtained from the offices in Austria and Canada are given in Fig. 1. Fig. 2 shows the probability distributions of normalized markers (representing the deviations from the average marker values) for aggregate data obtained from two office areas. Fig. 3 illustrates the distribution of CV values of the presence pattern markers across different occupants for the two locations. These results provide a number of insights regarding the previously stated research questions:

- i. There are obviously significant differences amongst the inhabitants with regard to absolute values of the presence markers (see Fig. 1). This is true for both populations.
- ii. Likewise, the between-group comparison of the tendencies in the two locations reveals significant differences with regard to the distribution of the inhabitants' presence markers (Fig. 2).

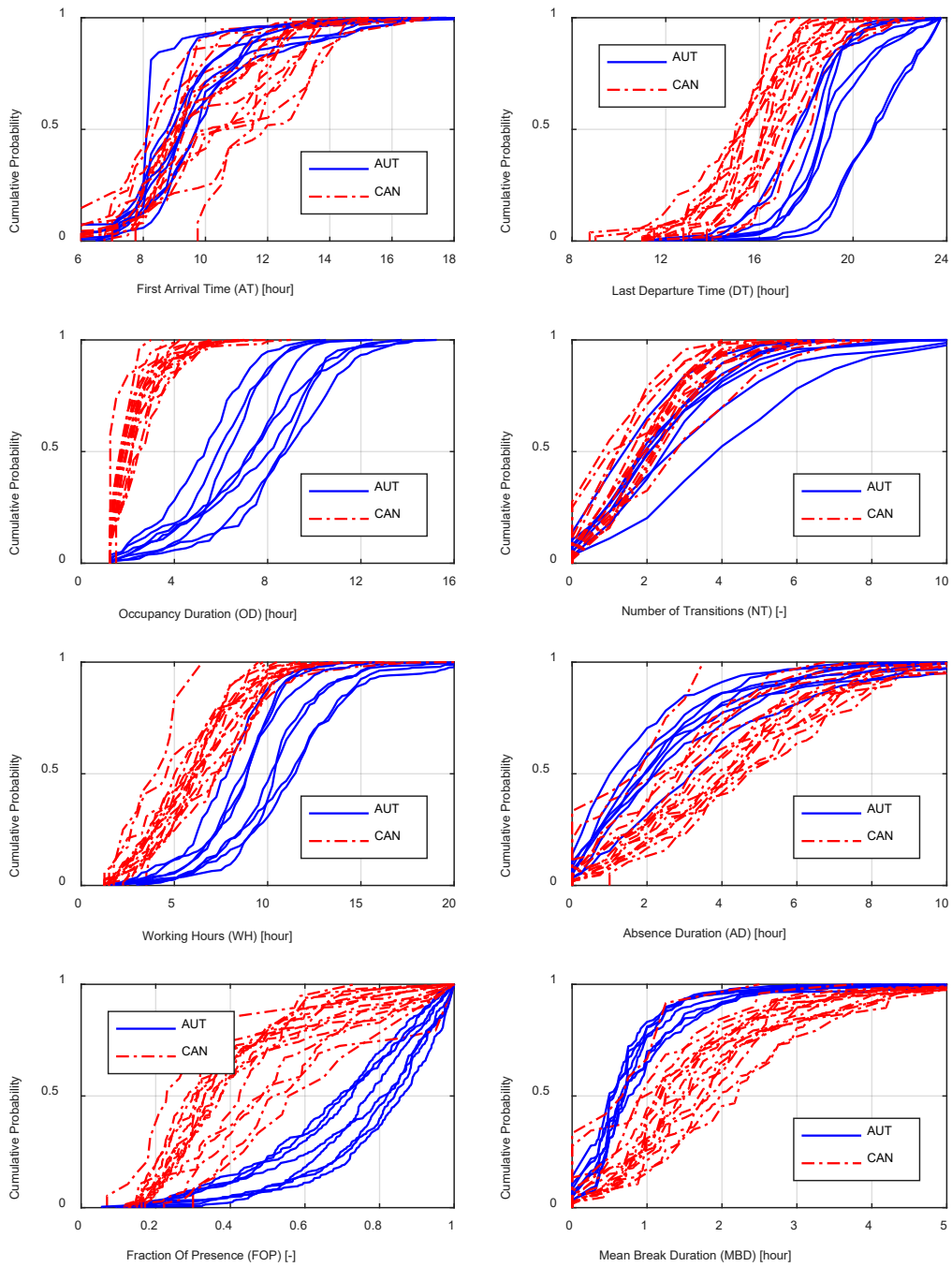


Fig. 1 – Cumulative distributions of individual occupants' presence markers obtained from the office areas in Vienna, Austria (AUT) and Ottawa, Canada (CAN)

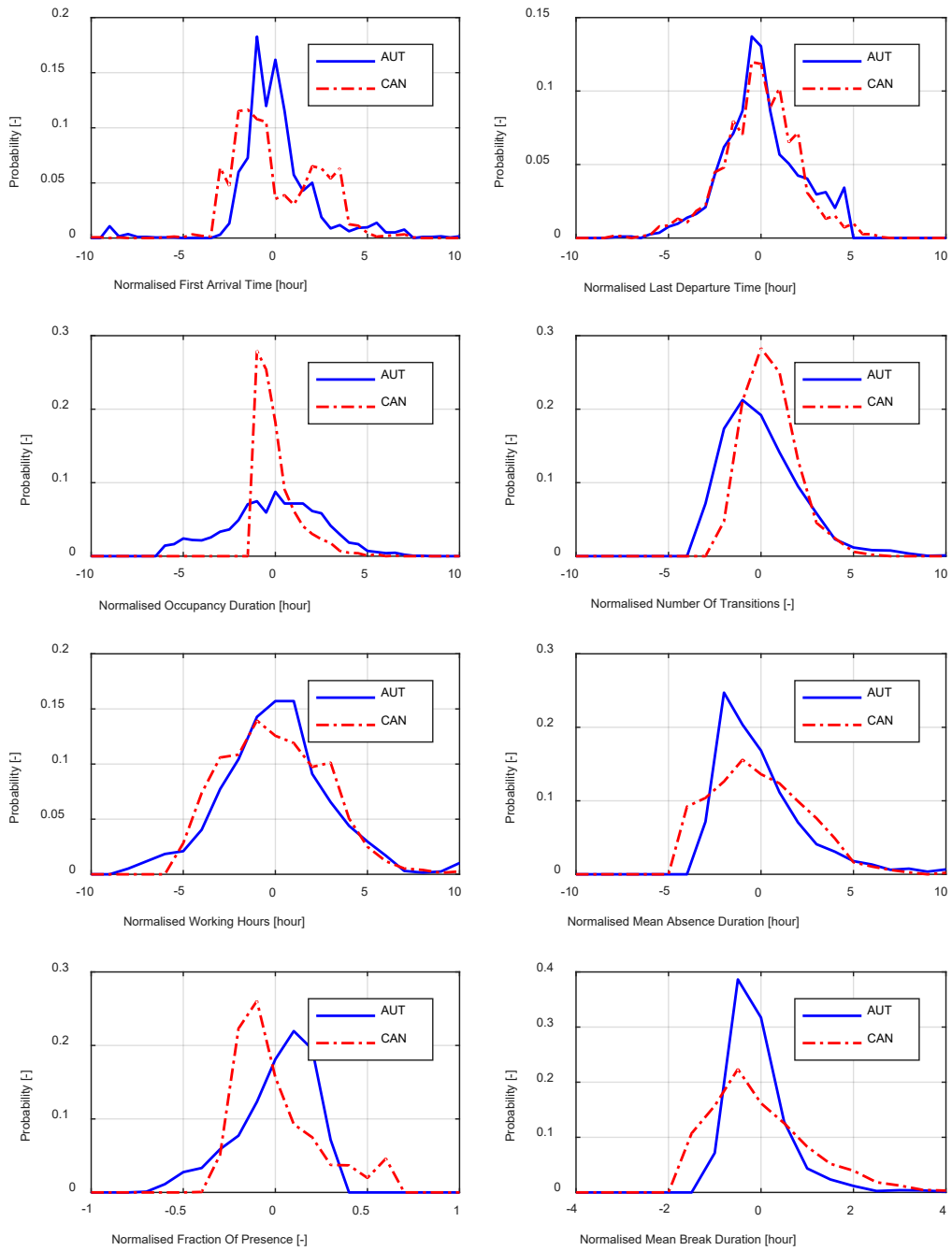


Fig. 2 – Distributions of aggregated normalized occupants' presence markers obtained from the office areas in Vienna (AUT) and Ottawa (CAN)

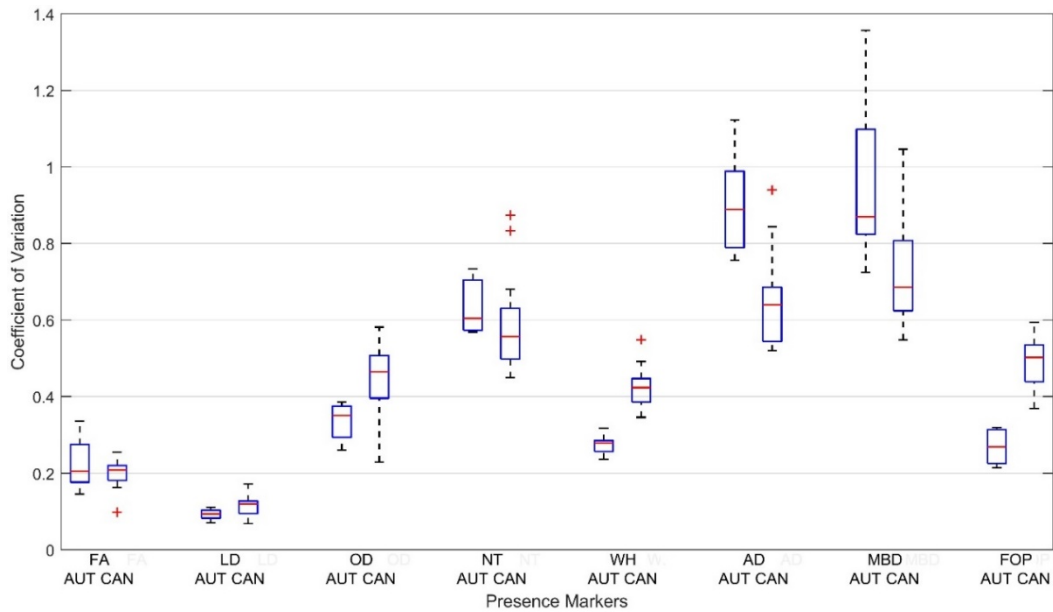


Fig. 3 – Boxplot of the coefficient of variation of the presence markers

- iii. Moreover, the spread of the marker values (as expressed in terms of CV) is not small (see Fig. 3). Hence, the reproduction of the inhabitants' diversity via randomisation requires not only empirical information on the diversity of the mean marker values, but also on the diversity of respective distributions' spread and shape. As such, the generation of stochastic presence patterns would have been easy, if the statistical distributions of the marker values were similar, thus resistant to diversity. Inter-inhabitant diversity could have been thus reduced to the mean marker values. The presented data clearly suggests that this is not the case. Moreover, distributions are not only different in view of the spread, but also between the two locations.
- iv. Even if we could ignore the diversity of the data distribution ranges, there would be still the problem of distribution morphologies. The two locations differ not only significantly in terms of the spread of the data (see Fig. 3), but also in terms of the distribution shapes. For instance, in the Ottawa office, AT displays a markedly bi-modal distribution. Likewise, FOP markers in the two locations display a distinct morphological asymmetry.

4. Concluding Remarks

This contribution empirically addressed the diversity of the inhabitants' presence patterns based on the inhabitants' monitored presence patterns in two office buildings in Vienna and Ottawa. The results suggest that the inhabitants' presence patterns can be significantly different and not reducible to just a few standard ones. Moreover, diversity amongst the inhabitants applies not only to the absolute values of the presence patterns' markers, but also to the spread and shape of the individual marker values' distributions.

Moreover, even if certain patterns could be suggested to apply to a specific building or location (for instance, LD and WH indicators display a very narrow range of CV values for the Vienna office), they cannot be suggested to apply to other locations. As such, without reliable empirical information regarding mean values and distributions of the marker values of inhabitants' presence patterns, simple randomisation of occupancy schedules cannot be expected to reproduce reliable representations of diversity. Seen from this specific viewpoint, the diversity of inhabitants' presence patterns in office buildings may be suggested to be irreducible.

Acknowledgements

The research presented in this paper benefited from the authors' participation in the ongoing efforts of the IEA-EBC Annex 66 (Definition and Simulation of Occupant Behaviour in Buildings) and the associated discussions.

References

- Feng, X., D. Yan, T. Hong. 2015. "Simulation of occupancy in buildings". *Energy and Buildings* 87: 348–359. doi: 10.1016/j.enbuild.2014.11.067.
- Mahdavi, A., F. Tahmasebi. 2015a. "Predicting people's presence in buildings: An empirically based model performance analysis". *Energy and Buildings* 86: 349–355. doi: 10.1016/j.enbuild.2014.10.027.
- Mahdavi, A., F. Tahmasebi. 2015b. "The inter-individual variance of the defining markers of occupancy patterns in office buildings: a case study". In: *Proceedings of BS2015*. Hyderabad, India: IBPSA.
- O'Brien, W., H.B. Gunay, F. Tahmasebi, A. Mahdavi. 2016. "A preliminary study of representing the inter-occupant diversity in occupant modelling". *Journal of Building Performance Simulation* 10: 509–526. doi:10.1080/19401493.2016.1261943.
- Page, J., D. Robinson, N. Morel, J.L. Scartezzini. 2008. "A generalized stochastic model for the simulation of occupant presence". *Energy and Buildings* 40(2): 83–98. doi: 10.1016/j.enbuild.2007.01.018.
- Richardson, I., M. Thomson, D. Infield. 2008. "A high-resolution domestic building occupancy model for energy demand simulations". *Energy and Buildings* 40: 1560–1566. doi: 10.1016/j.enbuild.2008.02.006.
- Tahmasebi, F., A. Mahdavi. 2016. "An inquiry into the reliability of window operation models in building performance simulation". *Building and Environment* 105: 343–357. doi: 10.1016/j.buildenv.2016.06.013.
- Wang, Q., G. Augenbroe, J.H. Kim, L. Gu. 2016. "Meta-modeling of occupancy variables and analysis of their impact on energy outcomes of office buildings". *Applied Energy* 174: 166–180. doi: 10.1016/j.apenergy.2016.04.062.

Accounting for the Diversity of Use Patterns in Representations of Office Plug Loads in Building Performance Simulation

Ardeshir Mahdavi – TU Wien – amahdavi@tuwien.ac.at

Farhang Tahmasebi – TU Wien – farhang.tahmasebi@tuwien.ac.at

Abstract

This paper explores the relationship between inhabitants' presence, the installed power for office equipment, and the resulting electrical energy use. This exploration is based on long-term observational data obtained from a continuously monitored office area in Vienna, Austria. The findings facilitate the formulation of both simplified and probabilistic models to estimate annual and peak office plug loads. Aside from a general comparison of the performance of simple and stochastic models, the present contribution focuses on the question if and to which extent consideration of the diversity of the inhabitants influences the reliability of plug load predictions.

1. Introduction

Plug loads denote office buildings' energy requirements due to computers, peripheral devices, telephones, etc. Plug loads can constitute more than 20 % of primary energy used in office buildings, and this ratio has been suggested to further increase in the future (Roth et al., 2008). Hence, simulation tools need reliable methods to estimate the magnitude of plug loads. Compared to a relatively broad range of research efforts regarding inhabitants' presence models (Wang et al., 2016; Tahmasebi and Mahdavi, 2017; Feng et al., 2015), only few studies have gone beyond the use of typical profiles of plug loads to provide more advanced models of plug loads for building simulation (e.g. Gunay et al., 2016; Gandhi and Brager, 2016; Menezes et al., 2014).

Given this context, we have been working on developing methods to compute both aggregated annual and detailed time-dependent electrical energy use patterns. In the present contribution, we specifically

focus on the problem of the diversity of the inhabitants (Mahdavi and Tahmasebi, 2015) and its implications for plug loads modelling.

2. Method

Previously, we have suggested that plug loads in office buildings could be estimated based on the knowledge of: i) installed equipment power and ii) presence patterns of inhabitants (Mahdavi et al., 2016). The corresponding findings are based on data from an office area (with both single-occupancy and open-plan office zones) in a University building in Vienna, Austria (see Table 1). For the purposes of this paper, high-resolution data (monitored presence and plug loads) collected over a three-year period (2013 to 2015) were used to develop and evaluate the plug loads models.

2.1 Simplified Approach

We hypothesised that plug load fraction F (ratio of actual plug load to the installed equipment power) of occupant j at time interval i is a function of presence probability p . A linear version of this relationship could be formulated as follows (with a and b as empirically grounded coefficients):

$$F_{j,i} = a \cdot p_{j,i} + b \quad (1)$$

Consequently, plug loads E for an office with m inhabitants over n intervals with a total length of T could be computed using Equation 2. Note that the coefficients a and b in equation 1 may be specified in an aggregated manner (i.e. for the entire population), or – given that sufficient empirical data is available – for individual office inhabitants.

$$E = T \times \sum_{i=1}^n \sum_{j=1}^m (F_{j,i} \times Q_{e,j}) \quad (2)$$

Table 1 – Selected office zones with information on inhabitants (denoted as U1 to U7), areas, and installed equipment power.

Space	Inhabitants	Installed power [W]	Area [m ²]
Open-plan	U1, U2, U3, U4	640	43
Office 1	U5	180	19
Office 2	U6	90	34
Office 3	U7	130	17

2.2 Stochastic Approach

To compute plug loads stochastically, we utilized three specific Weibull distributions to capture:

- 1) Plug load fractions during occupied periods or intermediate absences shorter than one hour;
- 2) Plug load fractions during intermediate absences longer than one hour;
- 3) Plug load fractions outside working hours.

A Weibull distribution is generally formulated as using Equation 3, where λ is the scale parameter and k is known as the shape parameter. Plug load fractions are picked randomly via inverse transform sampling method, whenever the occupancy state falls within one of the above possibilities.

$$f(x|\lambda, k) = \frac{k}{\lambda} \left(\frac{x}{\lambda}\right)^{k-1} e^{-\left(\frac{x}{\lambda}\right)^k} \quad (3)$$

Electrical energy use can thus be calculated in a manner similar to the aforementioned simplified model (see Equation 2). Note that, to use this model, the occupancy states (occupied or vacant) at each time interval need to be provided as input. In the current study, we used a presence model (Page et al., 2008) that uses a profile of presence probability and average parameter of mobility (μ : the ratio of state change probability to state persistence probability). The latter was set to 0.1 (O'Brien et al., 2016). As output, the model produces a set of randomly generated non-repeating Boolean occupancy profiles.

As with the linear regression model, we provided the stochastic model with presence profiles for weekdays and weekends, either averaged across all occupants or for individual inhabitants, depending on the diversity representation approach. In this case, too, the stochastic representation can be real-

ised both for the whole population and for individual inhabitants.

2.3 Representation of Diversity

To address diversity representation among inhabitants, we used empirical data (from the year 2014) to generate models in two different ways: i) occupancy and plug load profiles averaged across all occupants, and ii) individual occupancy and plug load profiles. Using 2014 data, Table 2 gives the resulting simple plug load model's coefficients (slope and intercept) for the individual inhabitants as well as in aggregate. Table 3 provides the coefficients (scale and shape) of the stochastic model's Weibull distributions based on individual and aggregate presence and plug load data.

2.4 Simulated Alternatives

A non-random relationship can be shown to exist between inhabitants' presence, their respective installed equipment power, and the resulting electrical energy use (Fig. 1). A stronger correlation can be revealed considering individual inhabitants as opposed to the population as a whole (Fig. 2). This may be interpreted as the consequence of considering inhabitants' diversity with regard to the electrical energy used for equipment. The difficulties associated with obtaining necessary observational data on inhabitants' diversity highlight the relevance of the initially addressed research question: To which extent can the calculated values of standard performance indicators such as annual and peak office plug loads be influenced by inter-inhabitant diversity?

To systematically explore this question, we used data from the year 2014 to calibrate models of annual and peak plug loads for the aforementioned office area. The calibrated model was used to predict plug loads for the years 2013 and 2015. Thereby, both simplified and stochastic models were generated with and without consideration of diversity (Table 4). Moreover, to put the model's performance in a more familiar context, we provided, for the same office area, the electrical energy use estimations based on plug load profiles from ASHRAE 90.1.

Table 2 – Coefficients of the simple plug loads model

Inhabitants	Slope (a)	Intercept (b)
U1	0.55	0.05
U2	0.76	0.06
U3	0.25	0.21
U4	0.33	0.07
U5	0.73	0.13
U6	0.72	0.04
U7	0.36	0.08
All	0.53	0.09

Table 3 – Parameters of the stochastic model's Weibull distributions

Inhabitants	Weibull 1		Weibull 2		Weibull 3	
	λ	k	λ	k	λ	k
U1	0.50	2.05	0.29	1.20	0.07	1.30
U2	0.46	2.52	0.30	1.24	0.07	1.28
U3	0.35	1.62	0.24	1.51	0.18	1.45
U4	0.35	1.67	0.27	1.60	0.22	2.48
U5	0.51	1.80	0.41	1.12	0.12	0.99
U6	0.57	4.62	0.42	1.95	0.20	1.07
U7	0.41	2.00	0.21	1.09	0.09	1.14
All	0.56	1.89	0.38	1.32	0.14	1.07

Table 4 – Explored modelling scenarios with information regarding the modelling technique (simplified versus stochastic) and inhabitants' representation (aggregate versus diverse)

Modelling scenario	Modelling technique	Diversity
S1_A	Simplified	No
S1_D	Simplified	Yes
S2_A	Stochastic	No
S2_D	Stochastic	Yes
S3_A	ASHRAE profile	No

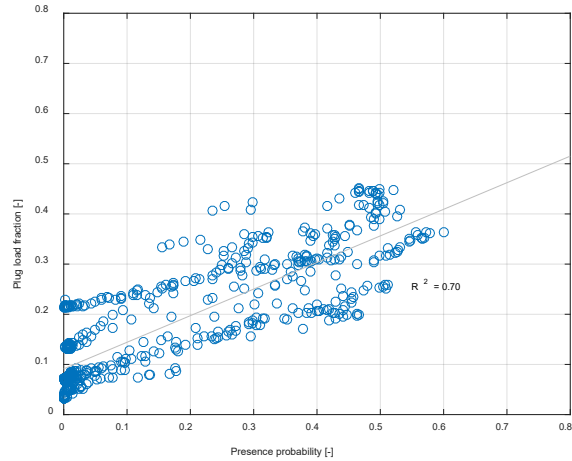


Fig. 1 – The relationship between plug load fraction and presence probability for all office inhabitants

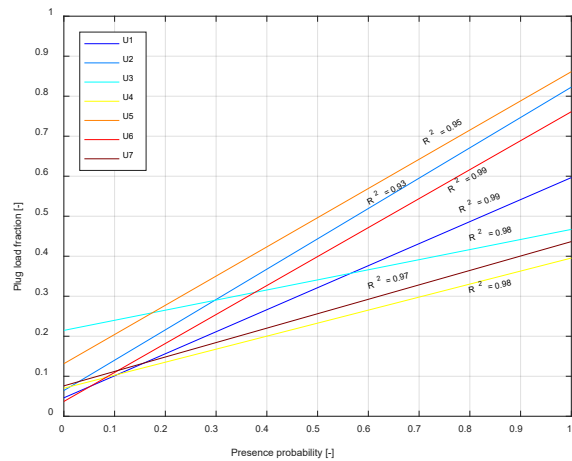


Fig. 2 – The relationship between plug load fraction and presence probability for individual office inhabitants

The comparison of computed annual and peak plug load values with observational data was expressed in terms of Relative Errors. For interval-by-interval comparison of monitored and calculated energy use, standard statistical indicators, namely Root Mean Square error (RMSE), Normalised Root Mean Square Error (NRMSE), and Mean Bias Error (MBE) were considered. To compare the distribution of predicted and monitored plug loads, the Jensen-Shannon divergence metric was used (for details see Mahdavi et al., 2016). This metric expresses the distances between two probability distributions and it is bounded between 0 and $\ln(2)$.

3. Results and Discussion

Table 5 provides a summary of the monitored and calculated total and peak equipment-related electrical energy use in the selected office area for the years 2014, 2013, and 2015, together with the values of the aforementioned error statistics.

The simplified method provides reasonable predictions of annual plug loads (Fig. 3). However, the probabilistic plug load model performs better than the simplified model in terms of peak load (Fig. 4) and the distribution of predictions. The latter conclusion can be inferred from the lower values of JSD for the probabilistic model (Table 5). Independently of the diversity treatment, the non-stochastic model displays a slightly better performance in predicting time interval plug loads (see MBE, RMSE, and NRMSE values in Table 5).

As to the primary question of the present treatment, namely the diversity consideration, the results may be interpreted as follows. Inclusion of diversity does not improve the predictive performance of the models with regard to annual and peak plug loads (see Fig. 3 and 4, as well as Table 5). Indeed, the inclusion of diversity has either very little impact on the predicted value of the energy use indicators or it even slightly worsens the prediction performance.

The summary representation of Table 6 illustrates this observation in simple terms. It indicates if the inclusion of diversity in plug load modelling improves the results or not. Thereby, the values of the statistics RE_a (Relative Error of annual load predictions), RE_p (Relative Error of peak load predictions), JSD, MBE, RMSE, and NRMSE were taken into consideration. Aside from rather small improvements for simplified model's results for 2013, the inclusion of diversity seems to worsen, rather than improve, the results. Notably, the intuitively expected positive effect of such inclusion on RE_p and JSD values is not supported by the results.

4. Conclusion

This contribution explored the performance of simple and stochastic office plug loads models. Thereby, the focus was on the implications of inhabitants' diversity. The results suggest the following:

- Plug load fractions strongly correlate with the inhabitants' presence probability.
- Both simple and probabilistic can exploit this correlation to provide reasonable predictions of annual peak plug loads. The stochastic model however, more reliably predicts peak plug loads.

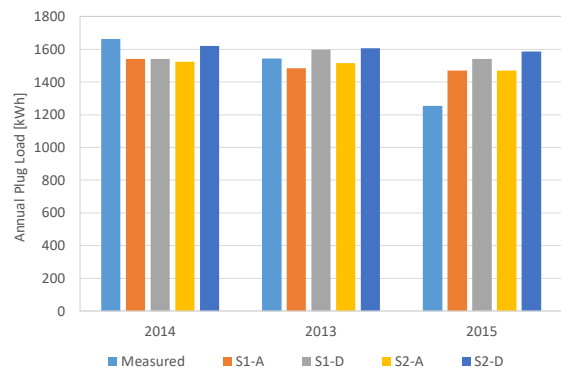


Fig. 3 – Annual plug load obtained via different modelling approaches, along with the respective monitored values

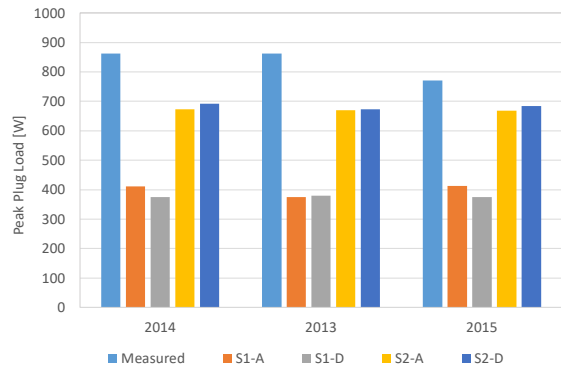


Fig. 4 – Peak plug load obtained via different modelling approaches, along with the respective monitored values

Table 5 – Statistical comparison of the monitored plug loads for the years 2013 to 2015 with the respective calculations according to various modelling scenarios: S1_A (simple model, average occupant); S1_D (simple model, individual occupants); S2_A (stochastic model, average occupant); S2_D (stochastic model, individual occupants)

Model	Run period	Run period sum		Run period peak		Distribution	Time interval values		
		Value [kWh]	RE [%]	Value [W]	RE [%]		JSD [-]	MBE [W]	RMSE [W]
Measured	2014	1662.7	0.0	861.7	0.0	0.00	0.0	0.0	0.0
S1_A	2014	1540.8	-7.3	411.6	-52.2	0.43	-13.9	119.6	14.7
S1_D	2014	1541.2	-7.3	374.3	-56.6	0.46	-13.9	120.6	14.8
S2_A	2014	1524.5	-8.3	672.5	-22.0	0.30	-15.8	131.3	16.1
S2_D	2014	1620.5	-2.5	691.9	-19.7	0.36	-4.8	131.7	16.2
Measured	2013	1543.4	0.0	861.9	0.0	0.00	0.0	0.0	0.0
S1_A	2013	1484.7	-3.8	374.7	-56.5	0.53	-6.7	99.8	12.5
S1_D	2013	1596.5	3.4	380.3	-55.9	0.52	6.1	99.7	12.5
S2_A	2013	1514.2	-1.9	669.4	-22.3	0.32	-3.3	121.2	15.2
S2_D	2013	1606.8	4.1	673.6	-21.8	0.39	7.2	122.4	15.3
Measured	2015	1255.0	0.0	770.6	0.0	0.00	0.0	0.0	0.0
S1_A	2015	1470.5	17.2	412.2	-46.5	0.41	24.6	102.6	13.9
S1_D	2015	1541.2	22.8	374.3	-51.4	0.46	32.7	123.1	16.7
S2_A	2015	1469.8	17.1	667.7	-13.4	0.28	24.5	120.2	16.3
S2_D	2015	1587.5	26.5	684.6	-11.2	0.33	38.0	124.6	16.9
ASHRAE 90.1	-	3025.7	141.1	936.0	21.5	0.42	202.1	352.3	47.8

- In the present case study, the inclusion of diversity (i.e. implementation of individual functions for individual occupants) in the course of simple and stochastic prediction of annual and plug loads did not improve model predictions.
- The performance differences between simple and stochastic plug loads was found to be much less important for the quality of predictions when compared to the availability of reliable information on inhabitants' presence and installed plug loads. This circumstance, which is independent of the diversity inclusion issue, can be inferred from the very large deviations of standard-based plug load estimations (see Table 5, last row).

Table 6 – Improvement test of the values of the statistical indicators RE_a (Relative Error of annual load predictions), RE_p (Relative Error of peak load predictions), JSD, MBE, RMSE, and NRMSE as a result of inclusion of diversity in plug load modelling

Statistics	Simplified model		Stochastic model	
	2013	2015	2013	2015
RE _a [%]	Yes	No	No	No
RE _p [%]	Yes	No	Yes	Yes
JSD [-]	-	No	No	No
MBE [W]	Yes	No	No	No
RMSE [W]	Yes	No	No	No
NRMSE [%]	-	No	No	No

Needless to say, we do not suggest that the above observations generally apply, given various shortcomings of our case study – particularly in view of the limited magnitude of available data and the small number of inhabitants. Nonetheless, we believe the study does provide valuable initial observations and insights: independently of the choice of specific mathematical formalisms, the observed significant correlation between plug load fractions and presence patterns has the potential to offer a solid basis for developing plug load prediction models. Our study also suggests that, to support simulation-based design processes, it is important to obtain dependable basic information regarding the nature of occupancy and the technical specification of the office equipment: The sole reliance on standard-based procedures could be misleading.

As to the implications of the diversity consideration for the prediction of annual and peak plug loads, the case study did not show that the inclusion of inhabitants' diversity is beneficial in principle. However, this matter, too, requires further in-depth studies before ultimate conclusions can be formulated.

Acknowledgements

The presented research has benefited from the authors' participation in the ongoing efforts of the IEA-EBC Annex 66 and the associated discussions.

References

- Gandhi, P., G. S. Brager. 2016. "Commercial office plug load energy consumption trends and the role of occupant behavior". *Energy and Buildings* 125: 1–8. doi: 10.1016/j.enbuild.2016.04.057.
- Gunay, H.B., W. O'Brien, I. Beausoleil-Morrison, S. Gilani. 2016. "Modeling plug-in equipment load patterns in private office spaces". *Energy and Buildings* 121: 234–249. doi: 10.1016/j.enbuild.2016.03.001.
- Feng, X., D. Yan, T. Hong. 2015. "Simulation of occupancy in buildings". *Energy and Buildings* 87: 348–359. doi: 10.1016/j.enbuild.2014.11.067.
- Mahdavi, A., F. Tahmasebi. 2015. "The inter-individual variance of the defining markers of occupancy patterns in office buildings: a case study". In: *Proceedings of BS2015*. Hyderabad, India: IBPSA.
- Mahdavi, A., F. Tahmasebi, M. Kayalar. 2016. "Prediction of plug loads in office buildings: Simplified and probabilistic methods". *Energy and Buildings* 129: 322–329. doi: 10.1016/j.enbuild.2016.08.022.
- Menezes, A.C., A. Cripps, R. A. Buswell, J. Wright, D. Bouchlaghem. 2014. "Estimating the energy consumption and power demand of small power equipment in office buildings". *Energy and Buildings* 75: 199–209. doi: 10.1016/j.enbuild.2014.02.011.
- O'Brien, W., H.B. Gunay, F. Tahmasebi, A. Mahdavi. 2016. "A preliminary study of representing the inter-occupant diversity in occupant modelling". *Journal of Building Performance Simulation* 10: 509–526. doi:10.1080/19401493.2016.1261943.
- Page, J., D. Robinson, N. Morel, J.L. Scartezzini. 2008. "A generalized stochastic model for the simulation of occupant presence". *Energy and Buildings* 40(2): 83–98. doi: 10.1016/j.enbuild.2007.01.018.
- Roth, K., K. Mckenny, C. Paetsch, R. Ponomou. 2008. "US residential miscellaneous electric loads electricity consumption". In: *ACEEE study on energy efficiency in buildings*.
- Tahmasebi, F., A. Mahdavi. 2017. "The sensitivity of building performance simulation results to the choice of occupants' presence models: a case study". *Journal of Building Performance Simulation* 10: 625–635. doi:10.1080/19401493.2015.1117528.
- Wang, Q., G. Augenbroe, J.H. Kim, L. Gu. 2016. "Meta-modeling of occupancy variables and analysis of their impact on energy outcomes of office buildings". *Applied Energy* 174: 166–180. doi: 10.1016/j.apenergy.2016.04.062.

A Comparison Between Numerical Methods for Evaluating Ground-Coupled Heat Pump Systems Performance

Angelo Zarrella – University of Padova – angelo.zarrella@unipd.it

Roberto Zecchin – Manens-Tifs – rzecchin@manens-tifs.it

Diego Guzzon – Manens-Tifs – dguzzon@manens-tifs.it

Michele De Carli – University of Padova – michele.decarli@unipd.it

Giuseppe Emmi – University of Padova – giuseppe.emmi@unipd.it

Michele Quaggia – Manens-Tifs – mquaggia@manens-tifs.it

Abstract

Ground coupled heat pumps are increasingly used for HVAC systems. The difficulty in sizing and predicting their behaviour and performance is well known. A suitable simulation is often advisable to help in the design choices. The code EnergyPlus is widely used in the field of building simulation and, since it includes a routine dealing with borehole heat exchangers, based on the well-known concept of g-functions, it can be profitably used for the considered purpose. On the other hand a numerical tool, namely CaRM, based on a detailed finite difference model of both the ground and borehole heat exchangers has been developed. A comparison between the use and the results of the EnergyPlus g-functions approach and CaRM in ground subsystem modelling was carried out with particular reference to an office building with quite a critical unbalance between heat extracted from and heat injected into the ground.

1. Introduction

EnergyPlus (U.S. Dept. of Energy, 2016) is a well known computer simulation software widely used for design analysis and certification procedures (e.g. LEED). It allows for a detailed description of the building characteristics and the analysis of several HVAC systems.

Among these characteristics, the borehole ground-coupled heat pumps are nowadays receiving particular attention. An efficient computational handling of the borehole field is not easy because of the complex geometry and the strong significance of

its thermal capacitance. For this purpose, the relatively simple and powerful technique of the “transfer functions” has been adopted within the EnergyPlus code to model the borehole heat exchangers and calculate fluid temperatures and related energy fluxes. For this approach a mathematical tool called *g-functions* was introduced by Eskilson (1987).

The downloadable version of EnergyPlus includes precalculated g-functions for only three cases of borehole fields, namely 1x2, 4x4, 8x8 regular grids, with 4.6 m spacing and 0.74 or 1.47 W/(m K) grout thermal conductivity. The effectiveness of the model drops dramatically as the considered characteristics differ even slightly from the default ones.

A specific evaluation of the g-functions, for a given design case, requires an external computer code, and the commercial software GLHEPro (Spitler, 2000) by the Oklahoma State University, is suggested in the EnergyPlus handbook. The latest version of GLHEPro implements the simulation of the whole geothermal system, as it includes the model of the heat pump. The characteristics of the geothermal field can be specified in such a way to allow the simulation with one hour or shorter time step, via EnergyPlus or HVACSYS software. For vertical boreholes the long time-step (LTS) g-functions developed by Eskilson (Eskilson, 1987) using a finite difference model, are used and a data base of 307 precomputed functions is included in the package, and equation fits have been developed to approximate larger rectangular borehole fields. For short-time step (STS) other g-functions (Yavuzturk and Spitler, 1999; Xu and Spitler, 2006) are used to consider the thermal capacitance of the borehole heat

exchanger when a more detailed simulation is required.

In the past, several researches have been carried out to develop more accurate but less computer time-consuming models. In the literature several analytical models can be found for a simplified sizing of ground heat exchangers, based on the infinite line source (ILS) (Carslaw and Jaeger, 1959) or cylindrical source, or finite line source (FLS) (Zeng et al., 2002) concept. The latter was used by Cimmino (Cimmino and Bernier, 2013) for a simplified calculation of g-functions, as an approximation of Eskilson's ones; this tool is available upon request. As an alternative to the above mentioned solutions it is possible to simulate the behaviour of the geothermal field by resorting to numerical methods like finite differences, finite elements, or finite volume. These methods require higher computational time, but they describe perfectly the field, as they represent a direct application of Fourier's law. One of such methods is CaRM (CApacity Resistance Model) (Zarrella et al., 2011 and 2013a). With the last release (Zarrella et al., 2013b), the entire ground source heat pump system (i.e. both the heat pump and borehole heat exchangers) can be simulated. The prediction of the performance of the geothermal system is useful for both the design and the energy analysis of the borehole field. Each building requires a specific design of the geothermal field because it has a different impact on the entire building-plant system. Additionally, it is important for the geothermal system simulation to accurately describe the real effect of a different solicitation, e.g., long time and low amplitude or short time and high amplitude.

The purpose of this paper is to compare the results obtained from g-functions and a finite difference algorithm. The comparison starts from a long-term hourly profile of the heating and cooling load of an office building, characterised by an appreciable unbalance between the energy exchanged with the ground in summer and winter. The same load profile, estimated by means of EnergyPlus, has been used in all the cases.

2. Method

2.1 The g-functions

In the last decades, several design tools have been developed to simulate ground heat exchangers. The basic ones rest on some analytical solutions for line source (Carslaw and Jaeger, 1959) and cylindrical source (Ingersoll et al., 1954).

In the approach by Eskilson (Eskilson, 1987) the borehole wall temperature is calculated by making use of transient finite difference method; he proposed dimensionless parameters, the so-called *g-functions*, to describe the performance of a borehole's inhomogeneous ground. Each borehole field configuration is represented by the corresponding g-functions. For each time step the bore wall temperature is calculated according to the following equation:

$$T_{borehole} = T_g + \sum_{i=1}^n \left(\frac{q_i - q_{i-1}}{2\pi\lambda} \cdot g \left(\frac{\tau_n - \tau_{n-1}}{\tau_s}, \frac{r_b}{H} \right) \right) \quad (1)$$

Eskilson's model was implemented in the simulation tools EED (Hellström and Sanner, 1994) and GLHEPro (Spitler, 2000), where several configurations of bore fields are considered.

These models are often not suitable to analyse the borehole's short-time behaviour. For example, in his model Eskilson (1987) proposed to apply no variations of the heat extraction-injection rate on a time-scale below the following limit:

$$\tau = \frac{5r_b^2}{a_g} \quad (2)$$

For a borehole in typical applications this time step might lie between 2 and 6 hours. In many cases, this may not be important since the time of interest is in the order of months or even years. In some applications, short-time simulations of ground-coupled systems are needed for a more accurate model dealing with small time intervals (e.g. intermittent operation). Yavuzturk and Spitler (1999) analysed this problem and they solved the numerical heat diffusion problem in the ground by taking into account the heat capacity of the pipe and the grout; their numerical results were expressed in terms of short-time g-functions. This method was then improved by Xu and Spitler (2006) in order to decrease the calculation time. In particular the borehole heat exchanger is modelled as one pipe with grouting material, whose thermal properties are assumed in

such a way to have the same borehole thermal resistance making use of the multipole method (Bennet et al., 1987).

Cimmino and Bernier (2013, 2014) analytically calculated the g-functions using the finite line source method (Zeng et al., 2002). Their approach considers the position of the head of the borehole in the ground and the heat rate can be different for the boreholes of the field; however, as in Eskilson’s model, the heat rate is assumed to be constant along the borehole depth.

2.2 The CaRM Approach

The CaRM tool solves the Fourier’s equation of the thermal field via a numerical way using the electrical analogy. The most recent version of CaRM (Zarrella et al., 2013a) gives a considerable improvement on the first releases (De Carli et al., 2010). The borehole heat exchanger and ground are discretized with thermal nodes, and the heat balance equations are based on these. The new version (Zarrella et al., 2013a) calculates the heat exchange between the heat-carrier fluid inside the boreholes and the surrounding ground and also accounts for the axial heat conduction within both grout and ground. Convective heat transfer, temperature, and short-long wave radiation exchange at ground surface are also modelled. This approach allows the analysis also of short-borehole heat exchangers that are generally placed where the ground temperature is affected by near-surface effects. The model also considers the shape of the borehole field. Fig. 1 outlines the CaRM approach.

The model resorts to thermal resistances and capacitances in order to solve the unsteady state heat transfer phenomenon. The ground is divided into three main zones: the surface, the borehole, and the deep zones (Fig. 1a). The adopted heat transfer model varies depending on the zone being considered: one-dimensional heat conduction (i.e. along the depth direction) is modelled in both the surface and deep zones, while the heat transfer is in both the radial and axial directions in the borehole (middle) zone. For each thermal node (Fig. 1b-c) of the domain, the heat balance equation is written. The CaRM tool can investigate several types of borehole heat exchangers: single and double U-tube, coaxial

pipes, helical shaped pipe, and also energy piles, whose characteristics do not conform to the above g-functions application and require a specific analysis (Zarrella et al., 2017). In CaRM the building load profile is an input, and the tool calculates the ground temperatures and the inlet and outlet heat-carrier fluid temperatures of the boreholes for each time step of the simulation.

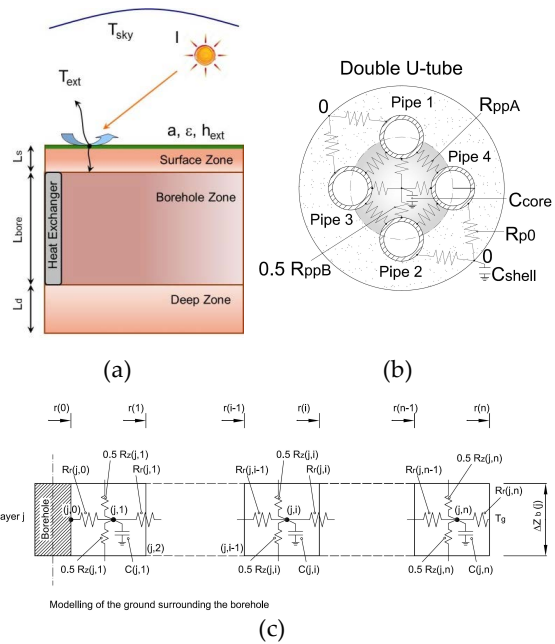


Fig. 1 – Scheme of the modelling approach of CaRM

3. Case Study

The building used as case study is located in the city of Padova, in the north of Italy. It is a four-storey office building with a total floor area of 2,200 m². Three floors are above ground and one level is underground (Fig. 2, top). Approximately 90 people work inside this building. The north and south facades are completely glazed (the south is a double-skin type). The west-side wall is opaque with a large central window on the first two floors, while the top west-side floor is fully glazed. The construction was completed in 2003 and the whole building has been operational since 2004. A radiant and primary air HVAC system is installed: during the daytime the air handling unit is on, whereas the thermally activated radiant building system is switched on during the night (Currò Dossi et al., 2003). The heating and cooling demand of the building is

provided by a 4-step water to water heat pump coupled to 16 borehole heat exchangers, 95 m long and 7 m apart and arranged in an L-shape (Fig. 2, bottom). The heat pump runs with refrigerant R407c and is used for both spaces heating and cooling; its capacities are 111 kW and 93 kW in cooling and heating, respectively. The heat pump operates with one temperature setpoint in heating mode, i.e. 35 °C, and with two different setpoints in cooling mode, i.e. 7 °C and 17 °C in daytime and night time, respectively, to improve the energy efficiency when no air handling is required.

The borehole heads are buried at about 1 m beneath the ground surface. A double U-tube heat exchanger was installed inside the borehole and the outside (inside) diameter of the pipe is 32 mm (26 mm); the borehole diameter is 140 mm. All the circuits (double U-tube) inside each borehole heat exchanger are coupled in parallel. The heat-carrier fluid inside the ground heat exchangers is pure water with a total constant mass flow rate equal to 5.56 kg/s.

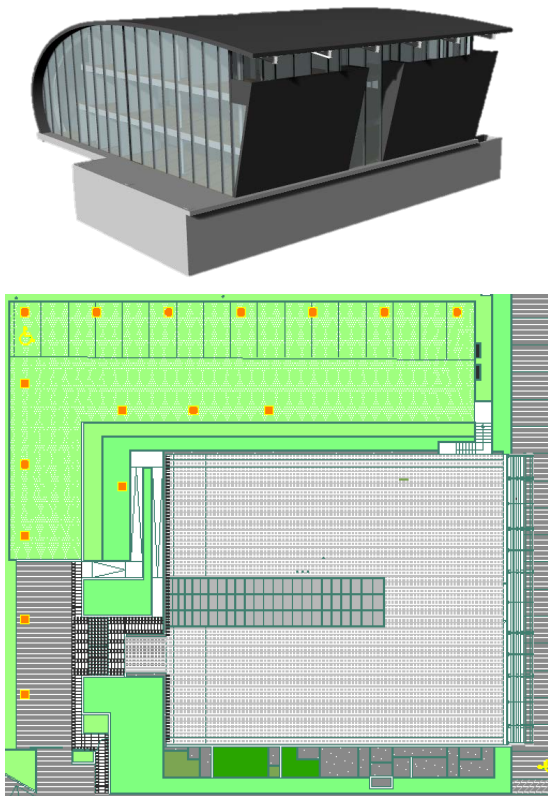


Fig. 2 – North and West view of the building of the EnergyPlus model (top) and plant of the real boreholes field (bottom)

On the building side, the total mass flow rate of water (i.e. the heat-carrier fluid) is equal to 6.10 kg/s.

The fluid mass flow rates in the loops were considered constant over the simulation time.

An equivalent ground layer was used to carry out the simulations: the mean weighted thermal conductivity was 1.9 W/(m K) and the volumetric heat capacity was 2.24 MJ/(m³ K). The undisturbed ground temperature was assumed to be 14 °C. The area's groundwater flow effect was considered negligible.

The heating and cooling demand of the building was calculated by means of the EnergyPlus tool over eleven years. To this purpose, real weather data provided by the regional environmental agency ARPAV for the weather station of Legnaro (at about ten kilometers from the building) were used.

The energy model of EnergyPlus was built dividing the whole building in 59 thermal zones, and for each of them, the geometric and thermal properties of the opaque walls, glazed surfaces, and solar shading surfaces were assigned. Then, for each zone the internal heat gains were set.

Fig. 3 shows the thermal loads of the heat pump. The ratio between the annual heating and cooling energy demand ranges from 0.56 initially, to 0.4 at the end of the considered period. This confirms that the building's annual load profile is cooling dominant.

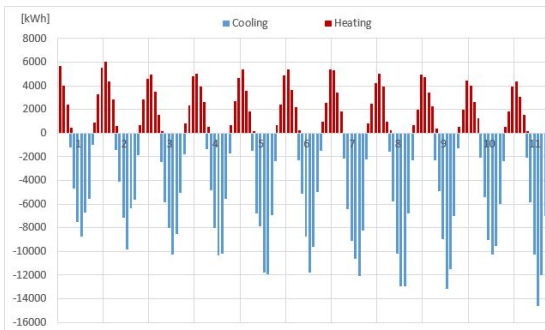


Fig. 3 – Synthesis of building load profile derived from hourly calculations

4. Computer Simulations

The comparison between the models was carried out considering the real layout of the borehole field of the case study. Moreover, two other configurations were assumed in order to make the comparison more complete. In all the layouts considered,

the total borehole length was kept constant and the position of the boreholes was only modified. Table 1 reports the three cases investigated.

The heat pump was simulated considering the data provided by the manufacturer. In particular the energy efficiency was calculated at each time step according to the following equations:

Cooling mode:

$$\frac{Q_c}{Q_{c,ref}} = -0.25 + 7.3574 \left(\frac{T_{L,in}}{T_{ref}} \right) - 2.3973 \left(\frac{T_{S,in}}{T_{ref}} \right) - 1.5156 \left(\frac{\dot{V}_L}{\dot{V}_{ref}} \right) - 2.25 \left(\frac{\dot{V}_S}{\dot{V}_{ref}} \right) \quad (3)$$

$$\frac{Power_c}{Power_{c,ref}} = 0.5625 + 1.4518 \left(\frac{T_{L,in}}{T_{ref}} \right) + 5.9483 \left(\frac{T_{S,in}}{T_{ref}} \right) - 3.125 \left(\frac{\dot{V}_L}{\dot{V}_{ref}} \right) - 4.125 \left(\frac{\dot{V}_S}{\dot{V}_{ref}} \right) \quad (4)$$

Heating mode:

$$\frac{Q_h}{Q_{h,ref}} = 0.8125 - 1.6888 \left(\frac{T_{L,in}}{T_{ref}} \right) + 8.6281 \left(\frac{T_{S,in}}{T_{ref}} \right) - 2.8594 \left(\frac{\dot{V}_L}{\dot{V}_{ref}} \right) - 3.7187 \left(\frac{\dot{V}_S}{\dot{V}_{ref}} \right) \quad (5)$$

$$\frac{Power_h}{Power_{h,ref}} = 3.4375 + 6.1243 \left(\frac{T_{L,in}}{T_{ref}} \right) + 1.4024 \left(\frac{T_{S,in}}{T_{ref}} \right) - 5.3125 \left(\frac{\dot{V}_L}{\dot{V}_{ref}} \right) - 5.1094 \left(\frac{\dot{V}_S}{\dot{V}_{ref}} \right) \quad (6)$$

where T_{ref} is a fix value equal to 283.15 K.

Table 1 – List of simulations

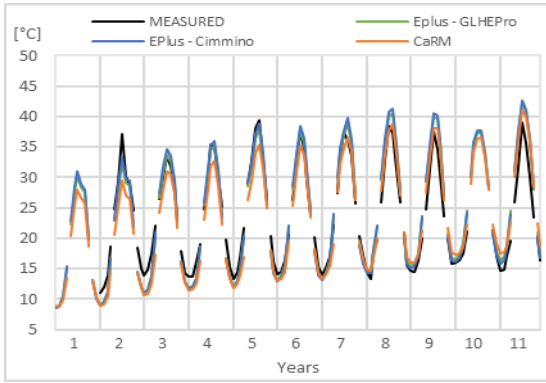
Case	Spacing (m)	Total length (m)
Case A - L shape (Real)	7	1520
Case B - Grid 4 x 4	7	1520
Case C - U shape	7	1520

The comparison between the models was carried out in terms of the outlet temperature of the heat carrier fluid from the boreholes, seasonal energy efficiency of the heat pump, and seasonal electrical energy consumption.

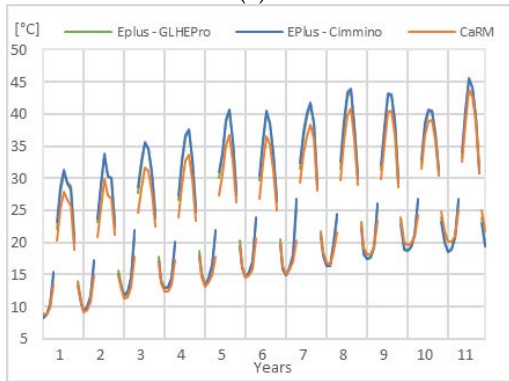
5. Results and Discussion

The computer simulations allow to determine several parameters representing the behaviour of the building-plant system. For the purpose of this work the outlet temperature from the borehole heat exchangers and the seasonal performance of the heat pump (S-COP in heating and S-EER in cooling mode) were chosen. In Fig. 4 the monthly average outlet temperatures are reported for the three considered configurations of the borehole field; in particular for the L-shaped case, which is the real one, also the values of the temperature measured and recorded are shown. It can be seen that the agreement is quite good over the full eleven-year period for all the three approaches of ground heat exchangers modelling. The actual temperature drift due to the unbalance between heating and cooling loads is well reproduced.

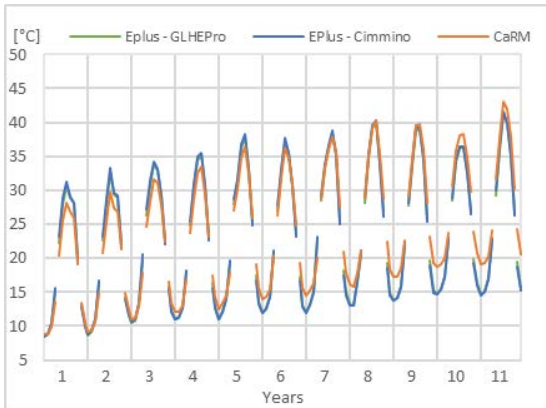
In Fig. 5 the calculated values of the S-COP and S-EER of the heat pump are shown for the same eleven-year period of simulation. The simulations give evidence of an appreciable change in the efficiency of the heat pump over the considered period.



(a)

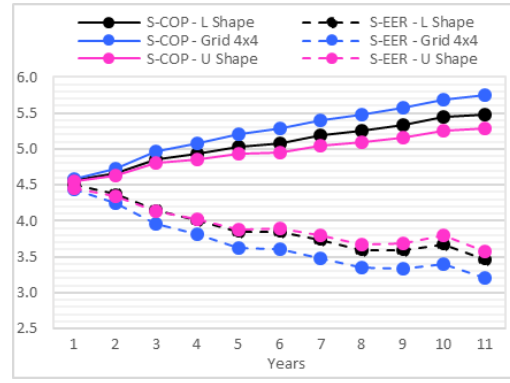


(b)

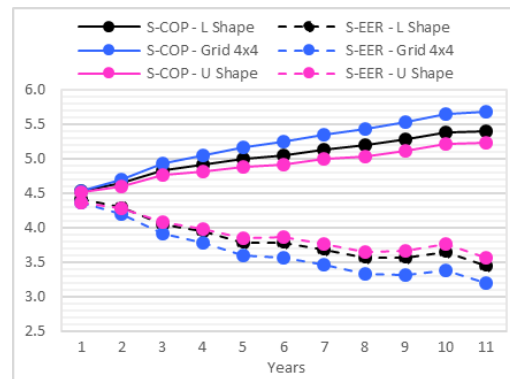


(c)

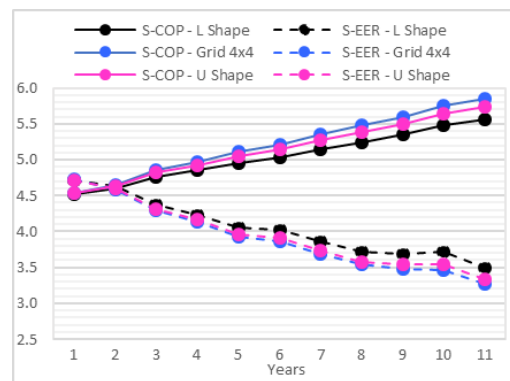
Fig. 4 – Monthly average outlet temperature of the fluid from the boreholes for L-shape (real) (a), grid 4x4 (b) and U shape (c) configurations of field



(a)



(b)



(c)

Fig. 5 – Monthly values of heat pump efficiency calculated with GLHEPro (a), Cimmino (b) and CaRM (c) for the three configurations of field

6. Conclusions

Having ascertained that the predefined default g-functions included in the EnergyPlus original package are not suitable to handle the multiplicity of possible cases, a specific method to determine such functions should be adopted to perform a reliable simulation. In this paper two calculation methods of g-functions have been applied to a significant case study of a real office building showing a multi-year ground temperature drift. These two methods result in more than reasonable agreement, and are in agreement with the long term monitoring of the building as well. Moreover a third method, CaRM, based on the numerical time dependent solution of Fourier's equation applied to the ground field, has been applied, starting from the same heating and cooling loads calculated by EnergyPlus; also this method shows consistency with the measured values of the ground leaving water temperature. It has to be pointed out that the CaRM tool, being based on the mere actual representation of the borehole field, does not exhibit any limits of applicability, as the other methods do due to their preliminary and boundary assumptions. The only penalty is the need to break into two parts the process of simulation.

Acknowledgements

The authors are grateful to M. Cimmino, Ecole Polytechnique de Montréal, and J.D. Spitler, Oklahoma State University, for making available the g-functions softwares used in this work.

Special thanks are due to HiRef S.p.A. for providing the full set of performance data concerning the water-to-water heat pump considered in this work.

Nomenclature

Symbols

$T_{borehole}$	Average borehole temperature (°C)
T_g	Undisturbed ground temperature (°C)
q	Step heat rejection pulse (W/m)
r_b	Borehole radius (m)
τ	Time (s)

$\tau_s = H^2 / (9\alpha_g)$	Time scale (s)
α_g	Ground diffusivity (m ² /s)
H	Borehole length (m)
λ	Ground thermal conductivity (W/(mK))
Q	Heat pump capacity (W)
$Power$	Heat pump electric power (W)
V	Volumetric flow rate (m ³ /s)
$T_{L,in}$	Load side inlet temperature (K)
$T_{S,in}$	Source side inlet temperature (K)
S-COP	Seasonal Coefficient Of Performance
S-EER	Seasonal Energy Efficiency Ratio

Subscripts/Superscripts

i	Index of a time step
n	Number of time steps
ref	Reference conditions
c	Cooling value
h	Heating value
S	Source side
L	Load side

References

- Bennet, J., J. Claesson, G. Hellstrom. 1987. *Multipole Method to Compute the Conductive Heat Flow to and between Pipes in A Composite Cylinder*. Lund, Sweden: University of Lund, Department of Building and Mathematical Physics.
- Carslaw, H.S., J.C. Jaeger. 1959. *Conduction of Heat in Solids*. Oxford, UK: Clarendon Press.
- Cimmino, M., M. Bernier. 2014. "A semi-analytical method to generate g-functions for geothermal bore fields". *International Journal of Heat and Mass Transfer* 70: 641-650. doi: 10.1016/j.ijheatmasstransfer.2013.11.037.
- Cimmino, M., M. Bernier. 2013. "Preprocessor for the generation of g-functions used in the simulation of geothermal systems." In: *Proceedings of BS2013: 13th Conference of International Building Performance Simulation Association*. Chambéry, France: IBPSA.
- Currò Dossi, F., M. De Carli, R. Del Bianco, F. Fellin, M. Tonon, R. Zecchin. 2003. "A pilot project for a low energy building equipped with thermal

- slabs, heat pump and ground heat storage". In: *8th International IBPSA Conference*. Eindhoven, The Netherlands: IBPSA.
- De Carli, M., M. Tonon, A. Zarrella, R. Zecchin. 2010. "A computational capacity resistance model (CaRM) for vertical ground-coupled heat exchangers". *Renewable Energy* 35: 1537-1550. doi: 10.1016/j.renene.2009.11.034.
- Eskilson, P. 1987. *Thermal analysis of heat extraction boreholes*. Ph.D Thesis. Lund, Sweden: Lund Institute of Technology, Department of mathematical physics.
- Hellström, G., B. Sanner. 1994. *Earth energy designer: software for dimensioning of deep boreholes for heat extraction*. Lund, Sweden: Department of Mathematical Physics, Lund University.
- Ingersoll, L.R., O.J. Zobel, A.C. Ingersoll. 1954. *Heat Conduction: With Engineering and Geological Applications*. New York, U.S.A.: McGraw-Hill.
- School of Mechanical and Aerospace Engineering Oklahoma State University. 2016. *GLHEPRO 5.0 For Windows Users' Guide*. Stillwater, U.S.A.: School of Mechanical and Aerospace Engineering Oklahoma State University.
- Spitler, J.D. 2000. "GLHEPRO a design tool for commercial building ground loop heat exchangers". In: *Proceedings of fourth international heat pumps in cold climates conference*. Aylmer, Quebec.
- U.S. Department Of Energy. 2016. *Engineering Reference Manual*. In EnergyPlus V8.5.
- U.S. Department Of Energy. 2016. *Getting Started Manual*. In EnergyPlus V8.5.
- Xu, X., J.D. Spitler. 2006. "Modeling of Vertical Ground Loop Heat Exchangers with Variable Convective Resistance and Thermal Mass of the Fluid". In: *Proceedings of the 10th international conference on thermal energy storage*. Pomona, U.S.A.
- Yavuzturk, C., J.D. Spitler, S.J. Rees. 1999. "A Transient Two-dimensional Finite Volume Model for the Simulation of Vertical U-tube Ground Heat Exchangers". *ASHRAE Transactions* 105(2): 465-474.
- Zarrella, A., G. Emmi, R. Zecchin, M. De Carli. 2017. "An appropriate use of the thermal response test for the design of energy foundation piles with U-tube circuits". *Energy and Buildings* 134: 259-270. doi: 10.1016/j.enbuild.2016.10.053.
- Zarrella, A., A. Capozza, M. De Carli. 2013a. "Analysis of short helical and double U-tube borehole heat exchangers: A simulation-based comparison". *Applied Energy* 112: 358-370. doi: 10.1016/j.apenergy.2013.06.032.
- Zarrella, A., A. Capozza, M. De Carli. 2013b. "Performance analysis of short helical borehole heat exchangers via integrated modelling of a borefield and a heat pump: A case study". *Applied Thermal Engineering* 61: 36-47. doi: 10.1016/j.applthermaleng.2013.07.021.
- Zarrella, A., M. Scarpa, M. De Carli. 2011. "Short time step analysis of vertical ground-coupled heat exchangers: The approach of CaRM." *Renewable Energy* 36: 2357-2367. doi: 10.1016/j.renene.2011.01.032.
- Zeng, H.Y., N.R. Diao, Z.H. Fang. 2002. "A finite line-source model for boreholes in geothermal heat exchangers". *Heat Transfer Asian Research* 31(7):558-67. doi: 10.1002/htj.10057.

Data Transfer from BIM to Building Performance Simulation Tools: A Case Study

Mirjana Bucevac – TU Wien – mirjana.bucevac@gmail.com

Ulrich Pont – TU Wien – ulrich.pont@tuwien.ac.at

Sigrun Swoboda – TU Wien – swoboda@iemar.tuwien.ac.at

Ardeshir Mahdavi – TU Wien – amahdavi@tuwien.ac.at

Abstract

Recent developments in building planning and delivery processes point to an increased deployment of BIM (Building Information Modelling) and corresponding tools in the AEC (Architecture-Engineering-Construction) domain. BIM is understood as the digital representation of the physical and functional characteristics of a facility that can offer a reliable informational basis for decision-making throughout a building's life cycle in different domains. Given this context, the present contribution addresses data transfer from commonly used BIM-software environments and a specialized simulation tool for thermal bridge analysis in view of heat flow, surface temperatures, condensation, and mould growth risk. Interestingly, much of the input data required for such in-depth assessments is already available in basic design models. However, there is a paucity of related fully functional data transfer solutions. This paper documents and evaluates data transfer issues based on sample building details. The objective is thereby to support software developers toward a better integration of state-of-the-art assessment methods in building design.

1. Introduction

The AEC domain is generally considered to be slow in technological advances. However, in recent years different concepts utilizing the ubiquitous availability of computational power, software tools and the World Wide Web pervaded this branch of economy. The term Building Information Modelling (BIM) was promoted as a key concept for the current and future planning practice. A commonly used description of BIM is: "Building Information Modelling (BIM) is a digital representation of physical and functional characteristics of a facility.

A BIM is a shared knowledge resource for information about a facility forming a reliable basis for decisions during its life cycle; defined as existing from earliest conception to demolition. A basic premise of BIM is collaboration by different stakeholders at different phases of the life cycle of a facility to insert, extract, update or modify information in the BIM to support and reflect the roles of that stakeholder" (NIBS, 2012).

Another trend in recent building planning is the increased use of state-of-the-art numeric simulation tools. These tools – if well understood by the user – offer a very fast and rather inexpensive possibility to explore in-depth different performance aspects of yet-to-be-built buildings, such as structural stability, energy use, and thermal performance of building components. Such tools allow new approaches in building construction, which can be extensively tested prior to realization. Moreover, typical uncertainties and issues regarding different aspects of building performance can be clarified to a certain extent or even solved with such tools.

One of the premises of Building Information Modelling is the reduction of redundancies regarding building-related data, and a high degree of compatibility with specialized stakeholder's tools. However, the current practice does not fully follow this premise: Many specialists generate their own building models, although a common building representation created by building planners is available. Borrmann et al. (2015) attribute this practice to the fact that the data exchange is currently not working satisfactorily, due to the high complexity of commonly used BIM-formats such as IFC (industry foundation classes, buildingsmart 2016). Moreover,

they state that the programmers of specialized software tools often struggle with the high variety of how buildings and building components can be described within IFC files of third parties. To ensure compatibility with all possibilities of data representation would generate an implementation effort that is too large for most producers. A possible relief for this situation is described by Beetz et al. (2015): In the future, the concept of the so called Model View Definitions (MVDs) will offer exact definitions and rules for an easy representation of buildings and building parts.

Only few publications address the data transfer between BIM environments and thermal bridge simulation tools. Narowski et al. (2011) discuss the modelling of conduction transfer functions for typical thermal bridges that were identified out of BIM data. They provide a list of correction factors based on thermal bridge simulations that can be used to modify the 1-dimensional heat transfer coefficients usually derived from whole building simulations (which can be performed based on BIM-models). Ingelaere (2016) gave a talk in the framework of the Qualicheck initiative (Qualicheck, n.d.) about the impact of BIM on energy performance calculations, and stated “detailed calculations (thermal bridges, ...) require a lot of input data and extra calculation tools.” In contrast, recent developments in one of the leading BIM environments, ArchiCad (Graphisoft, 2016), include the integration of a proprietary building performance simulation environment. This encompasses a (simplified) thermal bridge simulation tool for 2D thermal bridges. This feature was highly appreciated by the user community of ArchiCad (graphisoftus, n.d.). A downside of the feature is the limitation to 2D-bridges. Moreover, it is controversially discussed, if the full integration of a thermal bridge simulation module within an existing drafting/modelling tool can be considered as “BIM” following the definition of NIBS. Borrmann et al. (2015) define such an environment as “closed BIM”. If used only by a single stakeholder (e.g. the planner), they name it “little closed BIM”. On the contrary, the transfer of data between different software tools (of different producers) is defined as “little” or “big open BIM” (Fig. 1).

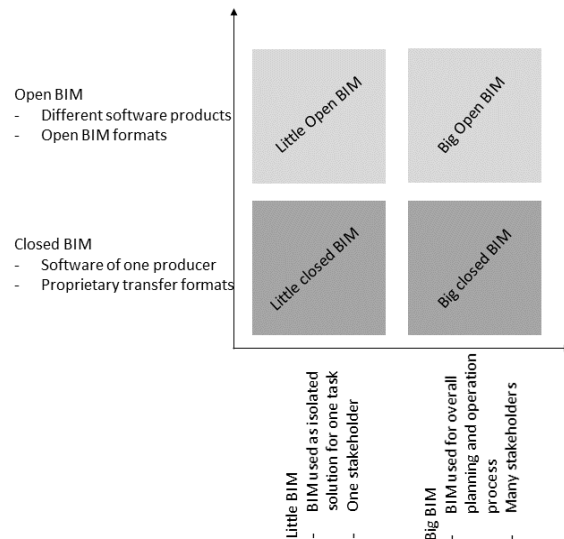


Fig. 1 – BIM classification, based on Borrmann et al. (2015)

2. Objective

In this contribution, we document and analyse the current data transfer possibilities between (architectural) BIM tools and a specialised building performance tool addressing the numeric simulation of thermal bridges. The majority of the required input data for numeric thermal bridge simulation should be included in a BIM representation of a building. Therefore, it can be considered interesting, which part of the data transfer between these environments works properly, and which aspects require improvement. Case studies as the one described might offer valuable insights for future development of the appropriate interfaces between such tools. Another objective of this paper is to suggest potential improvements regarding the data transfer between the mentioned environments, which, from a user’s point of view, seem to be feasible in realization.

This research paper is based on a master thesis addressing the topic of interoperability between BIM and building performance tools (Bucevac, 2016).

3. Methodology

3.1 Used Software Environments

3.1.1 BIM environments

Autodesk Revit

Revit has been developed since 1997 and was integrated in Autodesk's product portfolio in 2002. As a third party tool, it was not derived from Autodesk's key product AutoCad, but rather a stand-alone development. One key feature determined the name: Revit is the abbreviation of Revise instantly, and refers to the capability of the tool to instantly update any plan, section, and view after any change. All building components in Revit are processed as 3D representations, and organized in so called families. A family represents a group of elements with a common set of properties. Revit features so-called System families (categories of objects) that include the basic building elements such as walls, floors, ceilings, and other building constituents. Note that in such a family/category all layered components of such a building assembly are stored (as subcategories). For a wall, for instance, these subcategories could refer to the finishing layers on both sides, the thermal insulation, etc.

Moreover, additional so-called component families can be imported to a project from external sources. The basic idea behind this concept was that System families resemble generic building elements, while component families are customized families, originating from producers or system specialists. Within Revit, a wide range of properties of the different building components can be set or taken from a library, including basic properties important for performance assessments. These properties include (amongst others) thermal conductivity, specific heat, density, emissivity, permeability, porosity, reflectivity, and electrical resistivity. Fig. 2 illustrates the "thermal properties" dialogue available for building materials in Revit.

Graphisoft ArchiCad

ArchiCad is considered the first commercial BIM environment, as the use of "building objects" and "virtual building" was already integrated in its first launch in 1987. ArchiCad models are constituted of data-enhanced parametric objects, often referred to

as "smart objects". Similar to Revit, the attachment of certain properties is possible, both via manual input, and data from an integrated library. Fig. 3 illustrates the material editor in ArchiCad (for a specific material).

Numeric thermal bridge simulation

The tool used within this study was Antherm 8. Antherm is a software environment focusing on conductive heat and mass transfer within building components and utilizes a finite point method for the assessment of heat flows. It can be used to evaluate two- and three-dimensional thermal bridges, and it features a graphical user interface, drafting possibilities, and different reporting and visualization possibilities for temperature distributions in and on building assembly surfaces as well as for condensation and mold growth risk. The tool is under constant development. Recent developments were described in Kornicki et al. (2012) and Pont et al. (2016).

To perform basic thermal bridge evaluations, Antherm requires both geometric and semantic information. Geometric information includes dimensions and adjacency situations of different building components (represented as "material boxes" in Antherm), as well as adjacent spaces (represented as "space boxes" in Antherm). Semantic information includes the building material properties (conductivity λ , specific heat capacity c , diffusion resistance μ , and density ρ), as well as the temperature and relative humidity of the adjacent spaces.

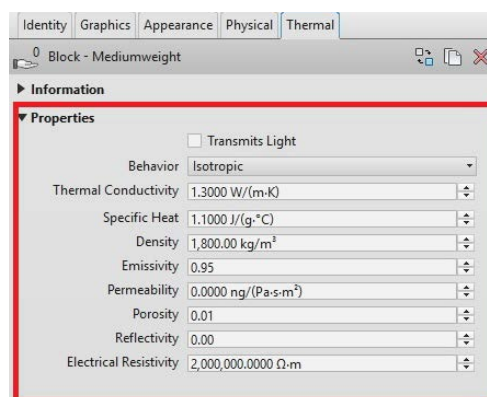


Fig. 2 – Thermal properties dialogue for building materials in Revit

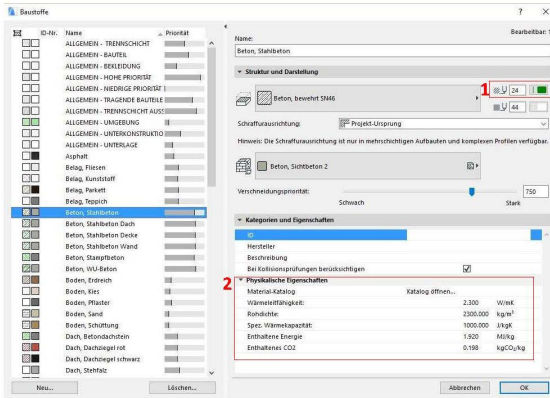


Fig. 3 – Material editor in ArchiCad

Table 1 – Import and export capabilities of Revit, ArchiCad, and Antherm

Tool	Application	Input file formats	Output file formats	Interoperable file Formats
Revit	BIM platform	dwg dxg	dwg <u>dxg</u>	dwg dxg
ArchiCad	for modelling	gbxml ifc	gbxml ifc	gbxml ifc
Antherm	Thermal bridge simulation tool	xml	xml	<u>dxg</u>
		waebru	csv	
		heat2	jpg	
		heat3 kobra86	3D scene	

3.2 Principal Data Transfer Capabilities in the Software Tools

Basically, all described tools feature a range of accepted file formats for import and export. The BIM applications offer “native” BIM formats (gbXML, gbXML 2016; ifc, buildingsmart 2016), but they can also generate commonly used CAD formats (dwg, dxg). Antherm offers import capabilities for different typical file formats of other thermal bridge assessment environments (waebru, heat2, heat3, kobra86), and additionally for dxg files and xml files. Due to the finite-point-based simulation kernel of Antherm, which generates a rectangular grid, dxg files are required to fulfill certain conventions: All imported geometry needs to be constituted from axis-parallel lines. Moreover, only 2D drawings will be accepted for import, and components have to be constituted by closed polylines (other elements will be neglected in import). Table 1

illustrates the different file formats that can be imported and exported from the different tools used in this study.

The dxg format is the only file format integrated as file interchange interface in all involved tools. The dxg-format (drawing interchange format) was developed by Autodesk, and due to its simple structure and clear documentation, is considered the industry standard for CAD-drawing interchange (Autodesk n.d.). However, as dxg is a pure drawing interchange format, no additional information (e.g., semantic data) can be attached to the geometric data inside the file.

Both Revit and ArchiCad offer the gbXML format as export possibility. This is an extended markup schema for (green) buildings. Antherm accepts XML as import file format. Therefore, a potential data transfer track, including both geometry and semantic data could be based on XML or gbXML structured information.

3.3 Case Study Building Assembly Joints

A set of typical construction details was chosen to extensively experiment with the data transfer possibilities and to discover strengths and weaknesses of different approaches. All of these details were created based on the specifications given in relevant standards (cut planes based on DIN 2008, thermal properties based on ASI 2013). A full description of all details including simulation results can be found in Bucevac (2016). To document the different transfer processes in this contribution we chose the construction joint of an insulated external wall with a concrete slab. Fig. 4 illustrates this construction detail and its constituent properties.

All details were drafted both in Revit and ArchiCad. Thereby, in both tools the option of setting hierarchies between different constitutive elements was utilized to generate full 3D-representations of correct building constructions. As far as possible, the thermal properties were also set in the environments (both BIM environments do not feature property settings to determine the diffusion resistance of components).

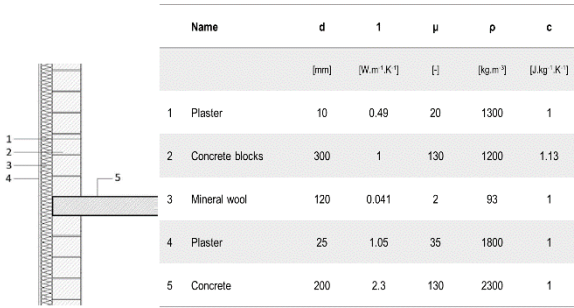


Fig. 4 – Wall/Slab detail and its thermal properties

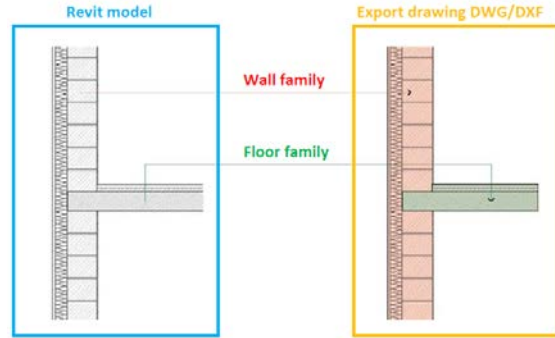


Fig. 5 – Translation process in Revit (categories and subcategories to dsf layers)

4. Data Transfer Documentation

4.1 Data Transfer via Drawing Interchange Format (dxf)

In both BIM environments, it is required to define the export settings in an appropriate fashion. This is necessary to apply the conversion of elements and parameters into pieces of geometrical information that can be stored in dxf. The export settings, once established, can be stored in a “translator” file and repetitively applied to different models and details.

In Revit, in a first step, a section (cut) plane needs to be defined. Afterwards the categories and subcategories of elements are mapped to a layer name and color for the dxf. Fig. 5 illustrates this translation principle in Revit. A split of parts of a family or subcategory to different layers seems not to be possible in recent versions of Revit. In terms of further workflow for the export to the thermal bridge simulation, this can be considered a problem. Moreover, a Revit engineered dxf file does not comply with the requirements for dxf import as described in section 3.2 (the exported dxf file does not contain building components in the required closed polylines form). To be able to use the generated dxf file for Antherm, manual postprocessing via a CAD-environment such as AutoCad (Autodesk, n.d.) is required. Fig. 6 illustrates the adjustment process in AutoCad (deleting unnecessary lines and hatches, conversion of boundaries to closed polylines).

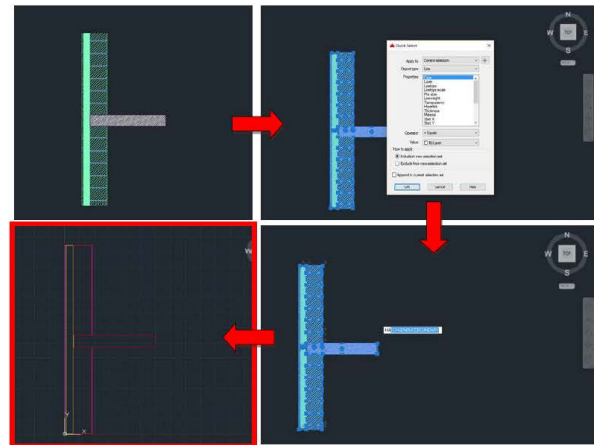


Fig. 6 – Postprocessing of a Revit-generated dxf File in AutoCad

In ArchiCad a section (cut) plane has to be defined, similar to the Revit case. The generation of “Detail” views, considering the required dimensions and scale of such sections tailored for thermal bridge simulation assessment, can be performed with ease. Moreover, in its current version Archicad features an elaborated import/export settings wizard, which allows customizing the properties of the exported files. However, similar as in Revit, it is not possible to automatically generate a dxf comprising closed polylines as required for Antherm. While Revit requires the detour via a CAD environment, it is possible to manually modify the detail drawing in ArchiCad, so that an exported dxf is already compliant for import in Antherm.

Regarding the import in the Antherm environment, it is possible to instruct the tool to distinguish between different materials based on Layer name, on Line color, or on Line type, allowing a wide range of different drafting styles being successfully transferred to Antherm. A certain amount of post processing in Antherm – no matter how good or bad

a dxf file is prepared – will be required. This is due to the fact that – as already mentioned – the dxf file cannot transport semantic information, such as the thermal building material properties. Therefore, these properties require a manual data entry, even if they were set correctly in the BIM environments. Moreover, the setup of space cells (adjunct boundary conditions for the thermal bridge simulation) needs to be performed, as this is not foreseen in any of the BIM environments.

Given the requirement for manual post processing in Antherm, it seems feasible – out of practical reasons – to generate layers based on the different materials in the imported dxf files. Moreover, if layers are named with appropriate and clear names, the later assignment of thermal properties (manual or from the material database integrated in AnTherm) can be facilitated.

Fig. 7 summarizes the data transfer via the dxf format from Revit and ArchiCad to Antherm.

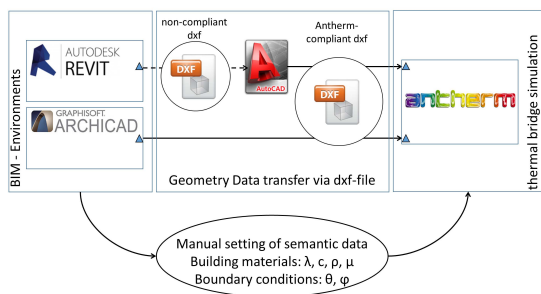


Fig. 7 – Illustration of the principal data transfer process from BIM environments to the thermal bridge simulation via dxf format (triangles indicate required pre-/post-processing steps)

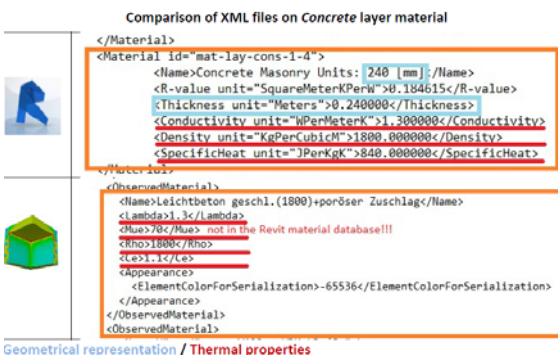


Fig. 8 – Example of xml-files generated by Revit and Antherm (concrete element)

4.2 Data Transfer via (gb)XML

Due to the fact that the common extended markup language schemes are supported both by the BIM environments and the used thermal bridge simulation tool, a data transfer via XML seems to be a viable solution at first sight. Indeed, the XML-file structure that can be read (and written) by Antherm encompasses a major portion of the gbXML file structure that can be read (and written) by the BIM environments (Fig. 8). However, a seamless data transfer from one XML structure to the other without a major effort in later postprocessing of the data is currently not possible. Third party mapping tools, such as Altova MapForce (Altova, 2016), might offer the possibility to map data from one scheme to another. However, some fundamental differences in the way data is stored would persist, such as the geometric definition of elements in one case (Revit gbXML) as extrusion width from a base plane, and in the other case (Antherm) as Cartesian coordinates. While technically a full data transfer from one scheme to another seems to be possible, the effort required is barely feasible. Moreover, this task can hardly be requested by the stakeholders involved in the building delivery process, as this would require the skills and knowledge of a software engineer (especially if data transfer routines are to be used generically).

5. A Potential Improvement for the dxf Data Transfer Approach

Both presented data transfer tracks show issues from a user perspective: The XML-approach in its current state does not allow a comprehensive data transfer. Therefore this approach cannot be used – until improved by the software engineers of either side of the transfer. Whereas the dxf-approach does show a set of weaknesses (the generation of dxf files requires cumbersome intermediate processing, no possibility to transfer semantic data), it can at least be utilized to transfer geometry information to Antherm. As the generation of building models is known to require the major portion of time in building performance simulation (Mahdavi and El-Bellahy, 2005), this can still be considered superior

to manual (re)drafting of existing geometry in the simulation environment in terms of time and effort. However, the existence and utilization of databases with thermal material properties would allow a simple, but effective, “workaround” solution for the issue that dxf files cannot transport semantic data. This approach would only require little programming effort, and could reduce the post-processing time significantly. If both the BIM-environment (Revit or ArchiCad) and Antherm access the same material catalogues, the unique identifiers of the data lines within these catalogues could be utilized as part of the layer names in the dxf-format used for data transfer. Based on the unique ID of the material, the corresponding library entry could be searched within Antherm, and automatically assign found properties to all components on this layer. For instance, in ArchiCad and Antherm the material catalogue of the Austrian Standard 8110-7 (ASI, 2013) is integrated (amongst a large number of vendor provided catalogues). Therefore, such an improvement would only require a slight adaptation of the already existing “search and assign material” option within Antherm.

Even without the use of unique IDs of a database, e.g., if generic materials are used, the sketched approach could be beneficial. A regular search and find utility could suggest – assuming the corresponding layer in the dxf file is named appropriately – materials matching this name from the catalogue to the user, who then simply selects one of the data entries. In this way the time for the semantic enrichment of the model can be shortened. Fig. 9 illustrates this improvement suggestion.

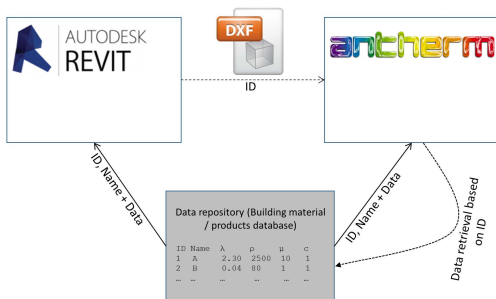


Fig. 9 – Scheme of improved data transfer via dxf format, including data retrieval via Unique ID from a shared database

6. Conclusion

The present contribution has shed some light on the current possibilities of data transfer between commonly used BIM environments and a state-of-the-art numeric bridge simulation tool. It was illustrated that the current data transfer procedures are far from satisfactory. Although the majority of data is already stored in the BIM environments, the data transfer to the simulation tool allows only the transfer of the geometry information in a reasonable form. Even for this transfer - to be successfully completed - a number of cumbersome pre- and post-processing steps are required. We illustrated a straightforward improvement suggestion, which could help to overcome some of the obstacles in data transfer to the thermal bridge simulation environment. Interestingly, the transfer between BIM environments and other building performance assessment tools, such as overall building performance simulation seem to work more conveniently than the transfer to thermal bridge simulation tools.

Future research and development efforts in the improvement of data transfer should encompass a fundamental model view definition (MVD) for the data transfer, which facilitates the implementation of data exchange routines for software engineers on the source (BIM tools) and target side (numeric thermal bridge simulation). Furthermore, the routines presented in this research contribution were checked on a generic base (other BIM-environments, other tools addressing thermal bridge issues). Moreover, as some important pieces of information can currently not be defined in the existing BIM environments (e.g. vapour diffusion resistances), respective integration in the workflow should be put on to the development agenda.

References

- Altova. 2016. Accessed on 23.12.2016. www.altova.com
- ASI. 2013. *Austrian Standard 8110 – 7: Thermal insulation in building construction — Part 7: Tabulated design values for thermal insulation*, Vienna, Austria: Austrian Institute of Standardization.
- Autodesk. 2016. *Revit 2016 and Revit 2017*. Accessed on 23.12.2016. <http://www.autodesk.de/>
- Autodesk. n.d. AutoCAD2000 DXF Reference available via <http://www.autodesk.com/techpubs/autocad/acad2000/dxf/> (last accessed 23.12.2016)
- Beetz, J., A. Borrmann, M. Weise. 2015. "Prozessgestützte Definition von Modellinhalten". In: *Building Information Modeling – Technologische Grundlagen und industrielle Praxis*. Springer Vieweg VDI-Buch.
- Borrmann, A., M. König, C. Koch, J. Beetz. 2015. "Einführung". In: *Building Information Modeling – Technologische Grundlagen und industrielle Praxis*. Springer Vieweg VDI-Buch.
- Bucevac, M. 2016. *Generation and Application of a BIM-based repository of highly insulated building construction details*. Vienna, Austria: TU Wien.
- Buildingsmart. 2016. www.buildingsmart.org (last accessed 23.12.2016)
- DIN. 2008. *Thermal bridges in building construction – Heat flows and surface temperatures – Detailed calculations (ISO 10211:2007)*. Berlin, Germany: Deutsches Institut für Normung e.V. Berlin.
- Gbxml. 2016. www.gbxml.org (last accessed 23.12.2016)
- Graphisoft. 2016. ArchiCad 20. www.archicad.com (last accessed 23.12.2016)
- Graphisoftus. n.d. <http://blog.graphisoftus.com/sustainability/eco-designer-star-thermal-bridging-simulation-part-1> (last accessed: 23.12.2016)
- Ingelaere, B. 2016. *The potential impact of BIM uptake regarding EPC calculations. Presented at the 3rd Qualicheck conference – Better compliance and quality of the works in practice*. Brussels, Belgium.
- Kornicki, T., C. Volko, M. Kornicki, U. Pont. 2015. "Numeric thermal bridges simulation: Approaching optimized usability for sloped and rounded surfaces". In: *Proceedings of the 10th International Conference on Buildings & Environment*. Bratislava, Slovak Republic: STU.
- Mahdavi, A., S. El-Bellahy. 2005. "Effort and effectiveness considerations in computational design evaluation: A case study". *Building and Environment* 40(12): 1651-1664. doi: 10.1016/j.buildenv.2004.11.014.
- Narowski, P., J. Stasiński, P. Wereszczynski. 2011. "Modelling of Conduction Transfer Functions for Typical Thermal Bridges Identified in BIM data". In: *Proceedings of Building Simulation 2011: 12th Conference of International Building Performance Simulation Association*. Sydney, Australia: IBPSA.
- NIBS. 2012. *National BIM Standard United States Version 2*. Washington, U.S.A.: National Institute of Building Sciences.
- Pont, U., O. Proskurnina, M. Kornicki, C. Volko, T. Kornicki. 2016. "Recent Developments in Application of Simplifications for Numeric Thermal Bridging Evaluation: A work Report". In: *Proceedings of CESB 2016: Central Europe towards sustainable building 2016 - innovations for sustainable future*. Prague, Czech Republic.
- Qualicheck. n.d. <http://qualicheck-platform.eu/> (last accessed 23.12.2016)

A Comparison of the Performance of Two- and Three-Dimensional Thermal Bridge Assessment for Typical Construction Joints

Ulrich Pont – TU Wien – ulrich.pont@tuwien.ac.at

Ardeshir Mahdavi – TU Wien – amahdavi@tuwien.ac.at

Abstract

The consideration of thermal bridges in building envelopes has gained importance in recent years. This is due to their potential impact on the overall thermal building performance of highly insulated buildings. Moreover, energy-efficient buildings tend to be more sensitive to problems associated with thermal bridges, such as surface condensation, mould growth, and thermal comfort issues. Therefore, planners must minimize the negative impact of thermal bridges. Although user-friendly thermal bridge simulation tools are available, they are not yet widely used in practice. Instead, planners often rely on generic details from the building construction literature. The thermal performance of such details often remains unknown given the wide range of possible building materials (and their thermal properties). In this contribution, we present the results of a thermal bridge simulation of a set of such standard details. Thereby, we assessed vertical sections through typical constructions via 2D thermal bridge simulation, as well as 3D corner situations constituted by such 2D sections. The aim was to address two research questions: i. How do typical details perform, given the large range of thermal properties of applied materials? ii. How does the performance of the 3D-thermal bridges compare to their constituent 2D-details, and is it possible to use 2D results to approximate the results of 3D thermal bridges?

1. Introduction

The quality of building envelope has a significant impact on buildings' energy use, indoor conditions and hygiene, and overall durability. Overall building assessment routines regularly utilize a simplified, one-dimensional approach for the assessment of heat and mass flow through building envelope components such as EN ISO 6946 (ISO, 2007). In recent years, as a consequence of more stringent building regulations, the relative importance of

thermal bridges within highly insulated envelopes has increased. The behaviour of thermal bridges regarding heat and mass flow cannot be captured via simplified (1D) models. Thermal bridges can increase heat losses and reduce indoor surface temperatures. They can cause surface condensation, mould growth, water-induced degradation of building components. In the past decades, detailed numeric evaluation methods (Heindl et al., 1987; Heindl et al., n.d.; Mahdavi et al., 1992) and powerful computational assessment tools have been developed (Kornicki et al., 2012; Pont et al., 2016; Antherm, 2016). However, even with such tools, planners face a number of challenges, such as the lack of input data, handling problems with the model and simulation setup conventions (Ward and Sanders, 2007), and – more generally – lack of time, knowledge, and financial resources. In this context, we address two research questions: i. How well do typical details perform, given the large range of thermal properties of applied materials? ii. How does the performance of the 3D thermal bridges compare to their constituent 2D details? Is it possible to use 2D results to approximate the behaviour of 3D thermal bridges? To address these questions, we obtained a number of 2D construction details (vertical sections through building assemblies) from the pertinent literature and assessed those using a numeric simulation tool. Thereby, we varied the input data (thermal conductivity) based on material property catalogues to answer the first question. Subsequently, we converted the 2D details to 3D details, repeated the simulation, and compared the 2D and 3D results.

2. Methodology

2.1 Material Properties, Boundary Conditions and Scenarios

The basic assessment of thermal bridges (steady state boundary conditions, focus on heat flow and temperature distribution) requires at least the thermal conductivity (λ) of the materials and conditions of the adjacent spaces (surface resistance values, room temperatures). In the building planning process, performance specialists are required to make assumptions regarding the physical properties of the used materials. Normative documents, such as the ÖNORM B 8110-7 (ASI, 2013), include design values, which are intended for use in different performance-related inquiries, when detailed values are not available. However, the standard offers a multitude of generic materials and does not include a guideline as to which values should be used in which type of assessment. Thus, this decision needs to be made by the planners, and leaves a wide range of values open.

A number of simulation scenarios were defined as per Table 1. Regarding boundary conditions, we assume temperatures of -10 °C (outdoor), 20 °C (conditioned indoor spaces), and 5 °C (unheated indoor spaces). Surface heat transfer resistance values are set to $0.04\text{ m}^2\cdot\text{K}\cdot\text{W}^{-1}$ (outdoor) and $0.25\text{ m}^2\cdot\text{K}\cdot\text{W}^{-1}$ (indoor) (DIN, 2012). Table 2 provides an overview of standard-based minimum, maximum, and average λ values for different types of materials (such as insulation, concrete, bricks, etc.).

Table 1 – Simulation scenarios

Scenario	Description
S1	All conductivities set to minimum
S2	All conductivities set to maximum
S3	All conductivities set to average
S4	As S3, but insulation materials set to min.
S5	As S2, but insulation materials set to min.

The construction joints are assessed as 2D thermal bridges. To generate 3D details we follow two

approaches: For a number of details, we generate corner details based on the 2D sections (Details A to D, see section 2.2 below). Thereby, the sections are revolved by 90 degrees (Fig. 1). The other approach is a “layered” approach. Thereby, successive 2D sections with respective dimensions on the z-coordinate are layered together resulting in the 3D representation of the construction (Fig. 2). All scenarios are applied to both 2D and 3D details.

Table 2 – Conductivity values, as stated in ÖNORM B 8110-7 for different building materials

ID / Hatch	Name	Min. λ [W.m ⁻¹ .K ⁻¹]	Max. λ [W.m ⁻¹ .K ⁻¹]	Average λ [W.m ⁻¹ .K ⁻¹]
1 	Flexible insulation	0.031	0.066	0.049
2 	Rigid insulation	0.031	0.066	0.049
3 	Concrete (reinforced)	2.300	2.500	2.400
4 	Masonry (<30 cm)	0.230	0.577	0.404
5 	Masonry (≥30 cm)	0.089	0.130	0.110
6 	Insulated wall element	0,230	0,577	0,404
7 	Plaster (inside)	0.180	0.570	0.375
8 	Plaster (outside)	0.120	1.050	0.585
9 	Screed	0.470	1.580	1.025
10 	Foil	0.130	0.400	0.265
11 	Water proofing	0.130	0.400	0.265
12 	Perimeter protection	0.100	0.500	0.300
13 	Soil / gravel	1.500	2.000	1.750
14 	Natural stone element	0.120	6.000	3.060
15 	Glass	1.000	1.000	1.000
16 	(Stainless) Steel	30.000	50.000	40.000
17 	Timber	0.110	0.240	0.175
18 	Vacuum	0.00001	0.00001	0.00001

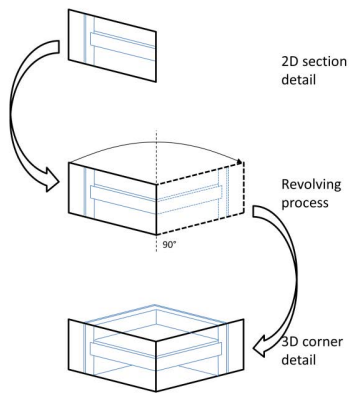


Fig. 1 – Conversion from 2D model to (revolved) 3D corner detail model

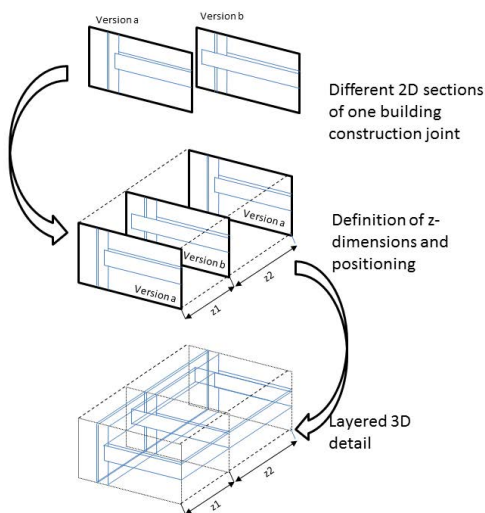


Fig. 2 – Conversion from 2D model to layered 3D detail model

2.2 Assessed Building Construction Joints

Five construction joints were selected for this study, based on Beinhauer (2003), Antherm (2016), Baubook (2016), and previous research work related to vacuum glass (Proskurnina et al., 2016). These details are:

- A: Connection of a slab and an external wall over a soil-adjacent basement (Fig. 3).
- B: Connection of a slab in an external wall between two conditioned floors (Fig. 4).
- C: Connection of a flat roof and an external wall (surrounding an Attica) (Fig. 5).
- D: Lower corner of a bay construction (Fig. 6).
- E: Vacuum glass, between two adiabatic boundary planes (E1 without pillars, E2 with pillars; Fig 7.)

The hatch patterns in the Figures indicate the material assumed for the specific components in Details A to D (see Table 2).

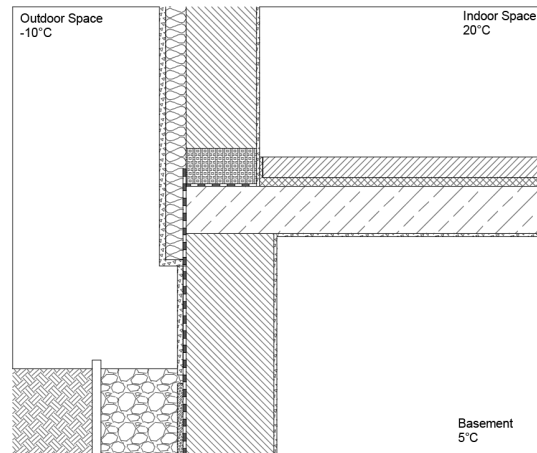


Fig. 3 – Detail A, Section 1:25

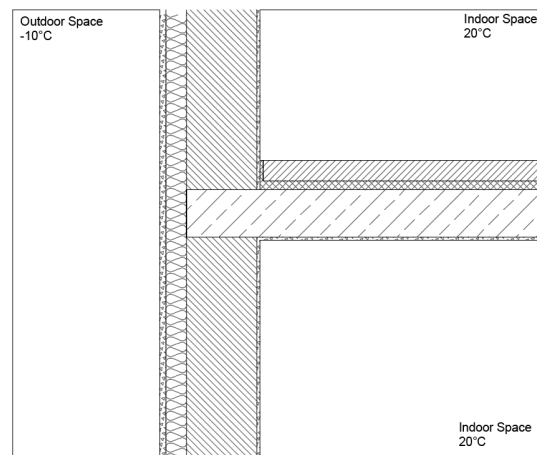


Fig. 4 – Detail B, Section 1:25

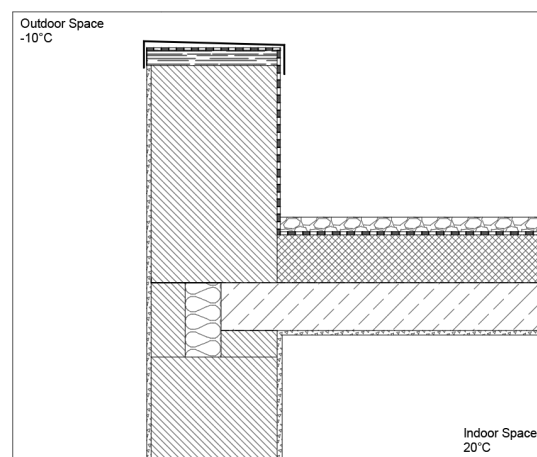


Fig. 5 – Detail C, Section 1:25

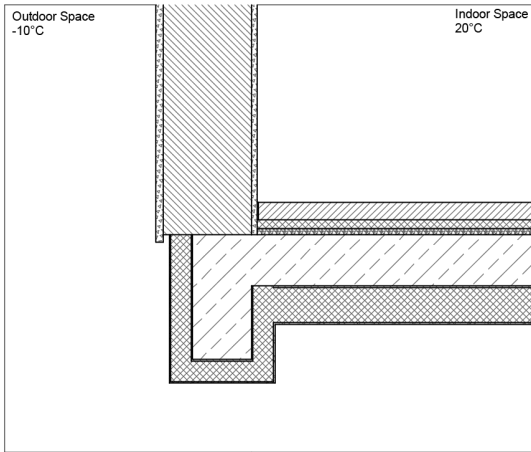


Fig. 6 – Detail D, Section 1:25

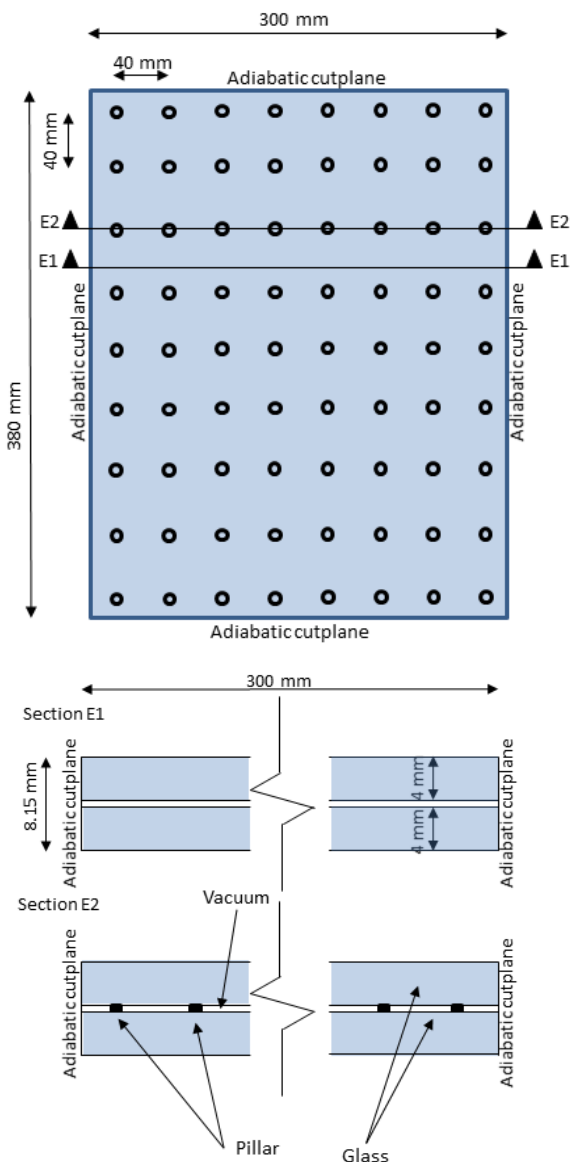


Fig. 7 – Scheme and sections (Detail E1 and E2)

Note that simulation models are distinguished via abbreviations. For instance, A_2D_S1 denotes the 2D simulation model for detail A and scenario S1.

Simulation Settings and Indicators

The applied numeric simulation tool used was Antherm 8 (Antherm, 2016). The geometry was drafted in a CAD tool (Draftsight, 2016) and exported to Antherm. The level of detail for the calculation in Antherm was set to 2 mm minimum cell size for Details A-D, and to 0.02 mm minimum cell size for Detail E.

The following indicators were selected for assessment purposes:

Temperature and **saturation relative humidity** of the coldest point of the internal surface.

Temperature factor f_{Rsi} (Equation 1), that is the temperature difference between the lowest indoor surface temperature (θ_{si}) and outdoor temperature (θ_e) divided by the indoor (θ_i) outdoor temperature difference.

$$f_{Rsi} = \frac{\theta_{si} - \theta_e}{\theta_i - \theta_e} [-] \quad (1)$$

Standards (DIN, 2014) state values for f_{Rsi} equal or lower to 0.57 (surface condensation), 0.70 (mould growth) and 0.88 (corrosion of metallic surfaces) as critical.

Heat Flow Q denotes heat transfer from an indoor (warmer) space to outdoor environment.

Thermal coupling coefficient L^{2D} / L^{3D} (Equation 2 and 3). This is the quotient of the total heat flow Q from the internal to the external environment of a detail and the temperature difference between inside and outside.

$$L^{2D} = \frac{Q}{\theta_i - \theta_e} [W \cdot m^{-1} \cdot K^{-1}] \text{ (2D-models)} \quad (2)$$

$$L^{3D} = \frac{Q}{\theta_i - \theta_e} [W \cdot K^{-1}] \text{ (3D-models)} \quad (3)$$

A Comparison of the Performance of Two- and Three-Dimensional Thermal Bridge Assessment for Typical Construction Joints

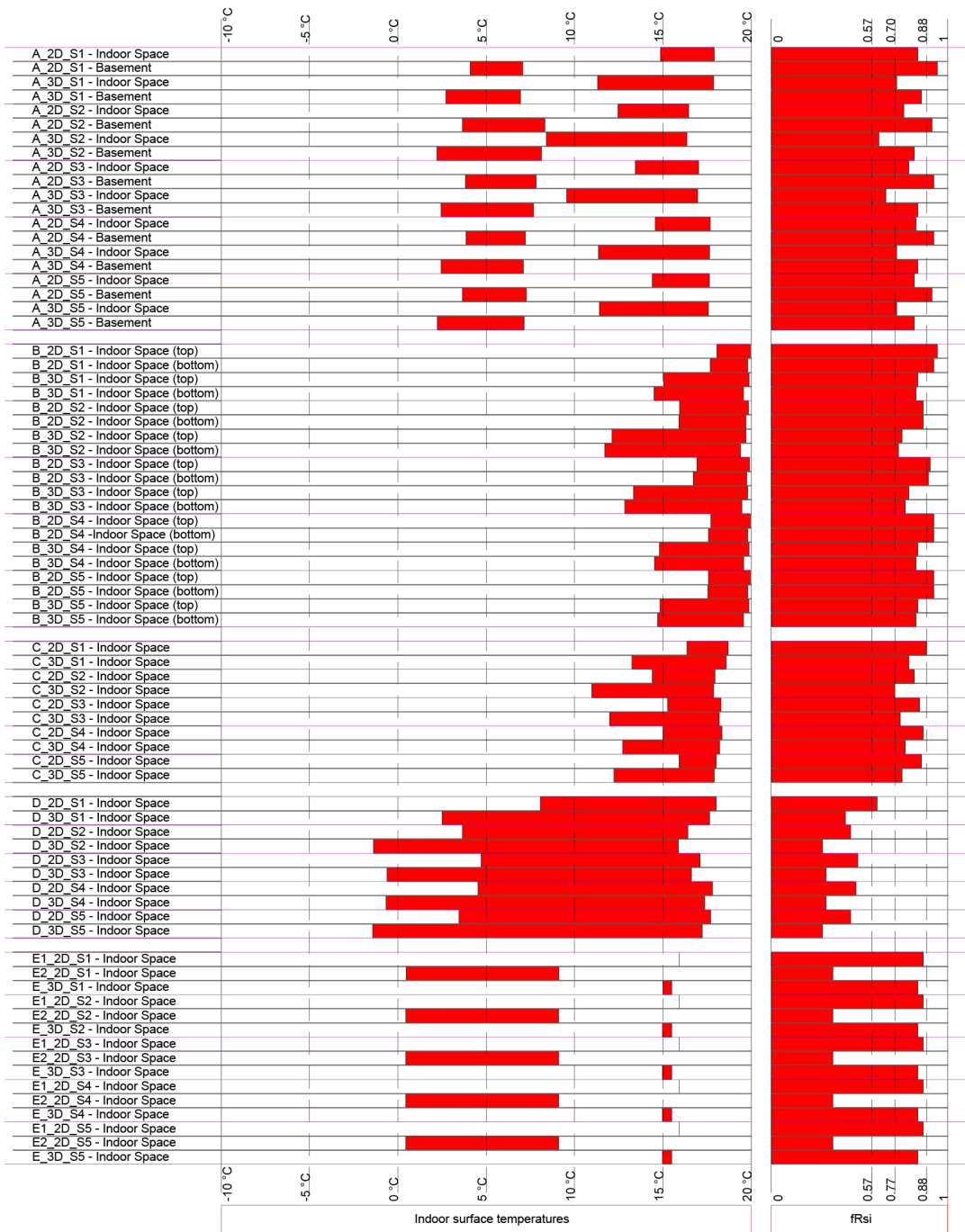


Fig. 8 – Results overview (surface temperatures and fRsi values). Calculations are coded as {Detail_2D/3D-Simulation_Scenario}

3. Results and Discussion

3.1 Impact of Different Conductivity Assumptions

Fig. 8 illustrates the minimum and maximum surface temperatures for all scenarios, together with the f_{Rsi} values. In general, a significant impact due to different material assumptions can be seen for details A-D, but not for detail E, whose composition did not involve variation in conductivity assumptions. For Detail A-D, S1 shows the best results (high surface temperatures, high f_{Rsi} value, and low heat flow), whereas S2 shows the poorest results. In case of 2D simulation, the S2 temperature results are between 1.77 (detail B) and 4.43 K (detail D) lower than the S1 results. In 3D simulations for details A-D, the temperature difference ranges from 2.28 (detail C) to 3.88 K.

Regarding the f_{Rsi} values, S2 scenarios show in 2D evaluation values that are between 7 (detail C) and 25 % (detail D) lower than S1 scenarios. This deviation amounts to relative differences between 10 (detail C) and 31 % (detail D) in 3D evaluation. Note that some of the details fulfill certain standard-based requirements (such as the limit for surface condensation), if executed with highly insulating materials, but fail otherwise. For instance, detail A features an f_{Rsi} value higher than 0.71 (mold growth criteria) in 3D simulation in scenario S1, but fails in scenario S2 (f_{Rsi} of 0.61).

Fig. 9 shows surface temperature distributions in A_3D_S1 and A_3D_S2.

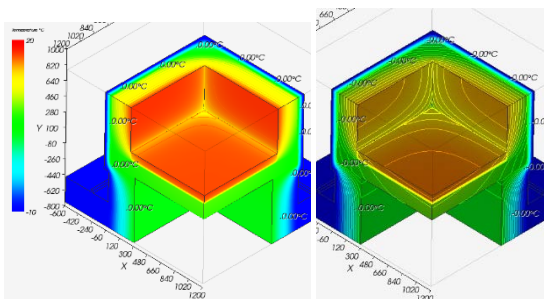


Fig. 9 – Surface temperature distribution: A_3D_S1 (left) and A_3D_S2 (right)

From the viewpoint of thermal transmittance, the heat flow rates in S2 scenarios are 158–232 % (2D simulation), respectively 150–230 % (3D simulation)

higher than in S1. Results of S3, S4, and S5 fall between S1 and S2.

3.2 Comparison Between 2D and 3D Assessment

Fig. 8 contrasts the results of 2D and 3D simulations against each other. The results for details A to D show a significant impact of the corner situation, resulting in colder surface temperatures and reduced f_{Rsi} values in the 3D-simulation. The temperature differences 2D and 3D simulation for these details range from 2.74 (detail B, Scenario 5) to 5.58 K (detail D, Scenario 1).

The 2D simulations of E1 (no pillars) and E2 (section with pillars) show significant differences, but do not allow to predict the overall result of the element. The 3D-simulation (see Fig. 10), which considers the small z-dimension of the pillars, shows a result closer to E1. The lowest surface temperature is close to 1 K lower than in the E1 simulation, but more than 14 K larger than in the E2 simulation.

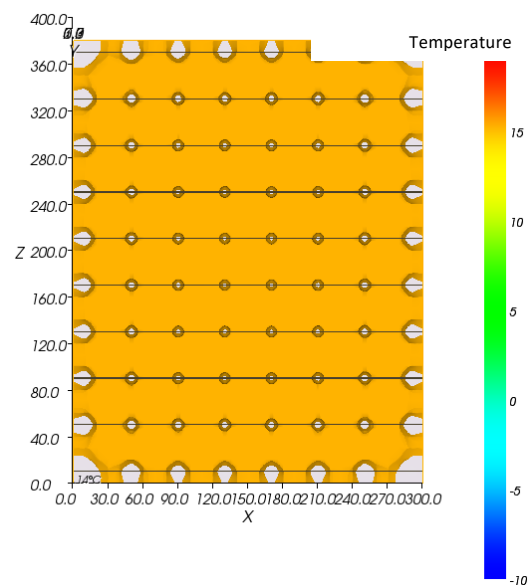


Fig. 10 – Surface temperatures for detail E (3D simulation)

4. Conclusion and Future Research

We numerically analysed a number of thermal bridges to answer two research questions, namely the impact of the thermal property assumptions on the performance of the details, and the potential of 2D simulation for the estimation of 3D details' behaviour.

Regarding material properties assumptions, the results suggest that:

- Material properties can have a significant impact on the simulated thermal performance of the detail.
- Construction details such as A-D, which can be found in the building construction literature, do not necessarily perform well, if the underlying material qualities are not sufficiently high. Numeric thermal bridge simulation can facilitate the definition of minimum material properties requirements for product selection.

Regarding the utility of 2D simulation to infer the behaviour of 3D details, the results suggest that:

- 2D simulation of 3D thermal bridges needs to be assessed carefully, given potentially large differences between 2D and 3D results. In critical cases, 3D simulation should be understood as a necessary requirement.
- Needless to say, differences between 2D and 3D results depend on the nature of the details. In the present study, 3D thermal bridge simulations yielded, for the same boundary conditions, surface temperatures up to 6 K below those in 2D analysis. Such differences need to be considered, given the increased condensation and mould growth risk due to lower surface temperatures, even at rather low indoor relative humidity.

Future research efforts shall address a broader set of construction instances. Moreover, assumptions regarding the surface resistance values in corner situations (3D thermal bridges) should be further scrutinised.

Acknowledgements

The research presented in this contribution was partly conducted within the framework of the following two research projects: VIG-SYS-RENO (P. 845225) and MOTIVE (P. 854690), both funded by the Austrian Research Promotion Agency (FFG) in the framework of the programme "Stadt der Zukunft".

References

- Antherm. 2016. www.antherm.eu (last accessed 23.12.2016).
- ASI. 2013. *Austrian Standard 8110 – 7: Thermal insulation in building construction — Part 7: Tabulated design values for thermal insulation*. Vienna, Austria: Austrian Institute of Standardization.
- Baubook. 2016. www.baubook.info (last accessed 23.12.2016)
- Beinhauer, P. 2003. *Standard-Detail-Sammlung*. Rudolf Müller GmbH & Co KG.
- DIN. 2012. *DIN EN ISO 13788 Wärme- und feuchtetechnisches Verhalten von Bauteilen und Bauelementen – Raumseitige Oberflächentemperatur zur Vermeidung kritischer Oberflächenfeuchte und Tauwasserbildung im Bauteilinneren – Berechnungsverfahren (ISO 13788:2012)*. Deutsches Institut für Normung e.v.
- DIN. 2014. *DIN 4108-3 Thermal protection and energy economy in buildings – Part 3: Protection against moisture subject to climate conditions – Requirements and directions for design and construction*. Deutsches Institut für Normung e.v.
- Draftsight. 2016. <http://www.3ds.com/> (last accessed 23.12.2016).
- Heindl, W., K. Krec, E. Panzhauser, A. Sigmund. 1987. *Wärmebrücken – Grundlagen, einfache Formeln, Wärmeverluste, Kondensation – 100 durchgerechnete Baudetails*. Vienna, Austria: Springer.
- Heindl, W., E. Panzhauser, K. Krec, A. Sigmund, T. Kornicki, n.d. *WAEBRU – 2D and 3D Wärmebrücken-Berechnungsprogramm*.

- ISO. 2007. *EN ISO 6946 – Building Components and building elements – Thermal resistance and thermal transmittance – Calculation method*. 2007. Geneva, Switzerland: International Standardization Organization.
- Kornicki, T., J. Nackler, K. Krec. 2012. "4D Simulation – Implementation of a periodic thermal conduction model in a 4D simulation program." *Czasopismo Techniczne – Technical Transaction 2-B/2012 Issue 3*, 109.
- Mahdavi, A., T.Y. Jeung, P. Mathew. 1992. "Conductive Heat Transfer through Insulated Building Enclosure Components; A Cross-Section Analysis of Constructions Typical to Low-Rise Residential and Commercial Buildings in North America". *Journal of Thermal Insulation and Building Envelopes* 16(2): 161-182. doi: 10.1177/109719639201600208.
- Pont, U., O. Proskurnina, M. Kornicki, C. Volko, T. Kornicki. 2016. "Recent Developments in Application of Simplifications for Numeric Thermal Bridging Evaluation: A work Report". In: *Proceedings of CESB 2016: Central Europe towards sustainable building 2016 - innovations for sustainable future*", P. Hájek, J. Tywoniak, A. Lupisek (Ed.). Prague, Czech Republic.
- Proskurnina, O., U. Pont, A. Mahdavi. 2016 "The Performance of Vacuum Glazing in existing window constructions: A case study". In: *Proceedings of the Central European Symposium on Building Physics*, J. Grunewald (ed.). Fraunhofer IRB Verlag.
- Ward, T., Sanders, C. 2007. *Conventions for Calculating Linear Thermal Transmittance and Temperature Factors*. Watford, UK: BRE press.

Comparison Between Simulated and In-Situ Measured Speech Intelligibility in the Multilingual Context of the Free University of Bozen-Bolzano

Simone Torresin – Free University of Bozen-Bolzano – simone.torresin@natec.unibz.it

Chiara Visentin – University of Ferrara - vsnchr@unife.it

Nicola Prodi – University of Ferrara– prdncl@unife.it

Francesca Cappelletti – University IUAV of Venezia – francesca.cappelletti@iuav.it

Andrea Gasparella – Free University of Bozen-Bolzano – andrea.gasparella@unibz.it

Abstract

Classrooms acoustics can affect students' speech intelligibility and learning performance depending on its background noise level and/or reverberation. Speech intelligibility is usually assessed in real classrooms through a subjective approach, by performing speech intelligibility tests, or through an objective approach, by evaluating speech transmission index (STI) from impulse response, speech and noise level measurements. An acoustic simulation technique makes it possible to assess acoustical conditions for speech reception in virtual environments, thus allowing for predicting intelligibility before a classroom is built or renovated. However, in order to obtain reliable results, the simulation model needs to be calibrated and validated with in-situ measurements.

The aim of this work is to compare tests performed in-situ on a group of people, with tests performed on the same people by reproducing the auralized test signal through headphones, in terms of intelligibility scores (IS), response times (RT), listening efficiency values (DE) and related STI values. Simulations have been carried out using the room acoustic software Odeon version 14.01. The investigation focused on a university classroom, which is part of the Classroom Spaces Living Lab of the Free University of Bozen-Bolzano, currently equipped with devices for monitoring energy and indoor comfort conditions, as well as detailed external weather conditions. By exploiting the bilingual context in South Tyrol, Diagnostic Rhyme Tests (DRT) in the Italian language were administered to both Italian and German native speaker students, the latter with an Italian level at least equal to B2, according to the common European framework of reference for languages. In this way, speech reception performance of the two groups has been investigated and compared.

1. Introduction

The effect of adverse acoustical conditions in learning environments has been widely investigated in literature and turned out to be detrimental for students' performance (Shield and Dockrell, 2003; Klatt et al., 2010).

Excessive reverberation and/or background noise lead to poor speech intelligibility, and affect negatively students' listening, learning and behaviour. Acoustical comfort in classrooms can be achieved when both teacher's speech results highly intelligible and students' effort is minimized.

Speech intelligibility can be estimated in real classrooms through an objective approach, by evaluating the speech transmission index (STI) from measurements of impulse response, and speech and noise level (IEC, 2011), or through a subjective approach, by performing on people speech intelligibility tests based on sentences, isolated words or non-sense items.

In this latter case, the speech recognition accuracy is measured by the percentage of correctly understood items, defined as intelligibility score (IS). Beside IS, the effort paid by the listener in the recognition of the speech material needs to be considered, which can be tracked by the time required to the participant to give a response, defined as response time (RT). Intelligibility scores and response time have thus been combined into a joint metric called listening efficiency (DE), which describes both accuracy and effort put in the speech recognition process (Prodi et al., 2010).

Besides objective or subjective in-situ evaluations, the acoustic simulation technique makes it possible to assess acoustical conditions for speech reception in virtual environments, even before a classroom is built or renovated. Through computer simulation, subjective speech reception performance can be assessed by reproducing the auralized listening conditions through loudspeakers in an anechoic chamber or via headphones, after convolving the anechoic speech material with simulated binaural room impulse responses (BRIRs). Similarly, the objective evaluation metric STI can be derived from simulated impulse responses, noise and signals.

Acoustic models are usually calibrated based on a comparison between measured and simulated room-acoustical parameters. However, there are many perceptual features of a sound field which may not be completely described by standard room acoustical parameters (Postma and Katz, 2016). This may result in significant differences in speech reception between real and auralized conditions.

Several studies were intended to validate the assessment of speech intelligibility based on auralized signals (Yang and Hodgson, 2007; Hodgson et al., 2008; Zhu et al., 2015). Objective metrics and IS obtained from the simulated sound field were compared with the ones obtained from in-situ measurements and direct listening. However, to the authors' knowledge, no study has so far integrated RT and DE metrics in the validation procedure.

The main objective of the present study is thus to investigate how accurately STI values can be predicted by acoustic simulation and how auralized listening conditions can lead to a reliable assessment of speech recognition performance, in terms of IS, RT and, as a consequence, DE values.

By exploiting the multilingual context of South Tyrol, a region in northern Italy, listening tests in the Italian language have been proposed both to Italian and German native speaker students and academic staff. A comparison of effort and speech recognition performance between the two groups is thus provided.

2. Methods

One existing university classroom, part of the Classroom Spaces Living Lab of the Free University of Bolzano-Bozen, has been selected for in-situ and virtual speech intelligibility tests. The room is currently equipped with devices for monitoring energy and comfort indoor conditions, as well as detailed external weather conditions. The classroom has a parallelepiped shape with dimensions of 7.29 m (width), 7.62 m (length) and 3.55 m (height), resulting in a volume of 197 m³.

The façade of the room has a concrete painted wall with two large windows of approximately 6 m² each. Partitions with adjacent classrooms are made of a double layer of painted plasterboard on each side, with insulation in the cavity, whereas the partition with the corridor is acoustically treated with a Topakustik® 6/2 type finishing. The ceiling is made of unpainted concrete and the floor is raised, with a linoleum finishing. Twenty-four not-upholstered wooden chairs are distributed in the seating area. Reverberation times measured in the fully occupied condition (25 persons) are shown in Fig. 1.

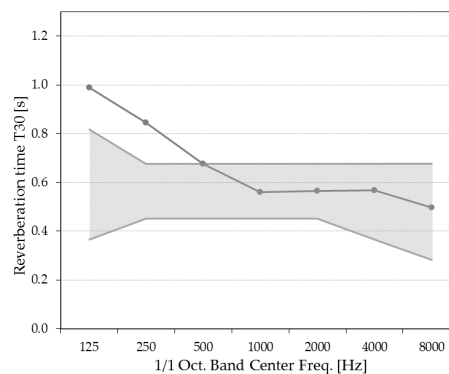


Fig. 1 - Reverberation times T_{30} [s] measured in the fully occupied classroom compared with target values suggested by the DIN 18041 standard (DIN, 2016)

Values were obtained from impulse response measurements and are the spatial average of 6 microphone positions evenly distributed over the seating area.

The mid-frequency reverberation time is equal to 0.62 s, close to the target value suggested by the DIN 18041 standard, $T_{soll}=0.56$ s (DIN, 2016).

In Fig. 1 measured reverberation times are compared with the tolerance range derived, according to the standard, from the target value T_{soll} . Measured

octave-band values above 500 Hz comply with the standard requirements.

2.1 In-Situ Intelligibility Tests and Measurements

This section describes speech intelligibility tests performed in the university classroom and the objective characterization of listening conditions. This allowed the collection of reference values for the calibration of the corresponding virtual model and the validation of the auralized listening conditions.

2.1.1 Participants, test material and procedures

A Diagnostic Rhyme Test (DRT) in the Italian language was used for this study (Bonaventura et al., 1986). Test words were meaningful disyllabic words, with a phoneme distribution representative of the Italian language. The speech material, consisting in the target words embedded in a carrier phrase, was read by an Italian native female speaker and recorded in a silent room. The material was split into 6 lists of 18 words and played back inside the classroom by a B&K type 4720 artificial mouth with a level of 63 dBA measured at 1 m in front of the loudspeaker. The signal source was located at 1.5 m above the floor at the teacher's position and oriented towards the seating area. The test setup is shown in Fig. 2.

Listening tests were performed under three acoustic conditions, called, respectively, "actual ambient noise" (A), "stationary noise" (S), and "fluctuating noise" (F).

In the first condition, no disturbing noise was added. The background noise consisted in the emission from the classroom projector and from the ventilation system. The two masking signals were a speech-shaped stationary noise (S) and a fluctuating noise (F), created by processing a signal according to the ICRA instructions (Dreschler et al., 2001). During the test session, S and F were played back with a B&K type 4292-L omnidirectional source located on floor, exactly below the speech source, as to screen the direct noise path towards the listeners and thus guaranteeing a diffuse noise condition. Noise levels were varied as to obtain, at 1 m in front of the signal source, a null signal to noise ratio

(SNR) for the stationary noise and a SNR equal to 1 dBA for the fluctuating noise.

- ⊕ S1+S2 Signal and noise sources
- TV Illuminance and microclimatic sensors
- n Tester
- ⊗ Rn Microphone and head and torso simulator

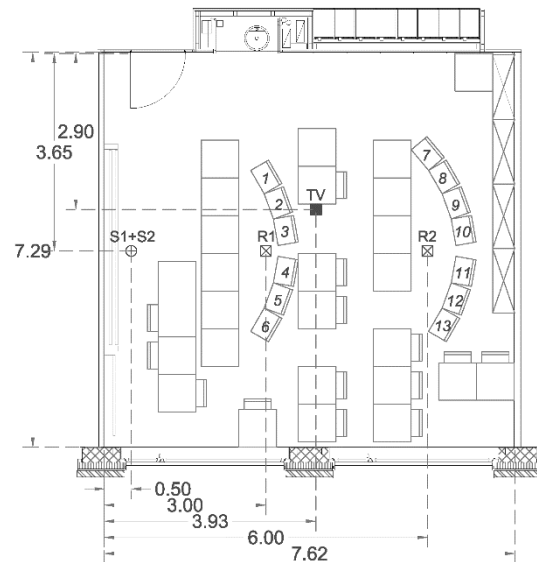


Fig. 2 – Test and measurement setup during in-situ speech intelligibility tests

The tests were administered to 26 normal-hearing young adults, half of them Italian native speakers, and, the other half, German native speakers with an Italian level at least equal to B2, according to the Common European Framework of Reference for Languages. Participants were selected from students and academic staff on the basis of their self-declared language skills.

The tests were administered to the two sample groups in two subsequent one-hour sessions. In each session, the subjects sat around two receiver positions, R1 and R2, as illustrated in Fig. 2, located, respectively, at 3.9 m and 7.6 m from the classroom front-end wall. After a training session, the participants completed three tests, each under a different noise (A, S, F). The subjects were then asked to listen again to the three listening conditions and to rate on three Visual Analogue Scales the effort paid in speech comprehension. The participants were then invited to change their sitting positions: the testers sitting on the back of the classroom were asked to move forward, and vice

versa. With this new arrangement, the three listening tests and related effort evaluations were repeated, under the same noise conditions but with a different exposure order (S, F, A) and with different word lists. In this way, each participant experienced each of the three noise conditions at each receiver position. The two-phase experiment was then repeated for the second sample group.

The tests were administered through *Intelligo*, a system that manages the synchronous audio playback and response collection, also enabling automatic recording of response times (Prodi et al., 2012). The participants, after hearing a carrier phrase followed by a target word, had to select the word they had heard on a mobile phone touchscreen by choosing between three options, two-word alternatives or the “none of the above” option, as shown in Fig. 3.

Following the tests, German native speakers were asked to fill out a brief questionnaire aimed at a deeper understanding of their language background. The answers regarding their age of acquisition of the German and Italian languages, their language use at home, with friends and at university, their country of origin, their language proficiency certifications and their parents’ mother tongues were collected. The questionnaire confirmed that all German native speakers had been exposed to the German language from birth and started the study of the Italian language at primary school (around 6 years of age).

2.1.2 Objective measurements

At the end of each one-hour experiment, the objective description of the test acoustic conditions was performed. With participants sitting quietly, monaural and binaural impulse responses were measured, and signal and noise levels collected at the two receiver positions by means of two B&K type 4128-c head and torso simulators and two omnidirectional microphones located on the top of each manikin. Speech level measurement was carried out recording a continuous speech sample. Indoor microclimatic parameters – i.e. air temperature, relative humidity, air velocity – were monitored during the test sessions and used as input data for the subsequent acoustic model. A DeltaOHM Thermal Microclimatic logger type HD 32.1 was positioned as shown in Fig. 2, as to collect

a mean value inside the space area. Even if a denser measurement grid would be required, a rough estimation of thermal comfort conditions can be performed by calculating Fanger’s comfort indices PMV (Predicted Mean Vote) and PPD (Percentage of People Dissatisfied). The average PMV value calculated for the test period is equal to 0.0 (PPD = 5 %), considering people in sedentary activity (1.2 met) while wearing 0.8 clo. This confirms that testers were in thermo-neutral conditions and that during the tests the classroom could be included in the I Category of comfort according to UNI EN 15251 prescriptions (CEN, 2008).

In addition, illuminance level measurements were conducted at the same monitoring position by the use of a LI-210 Photometric Sensor (LI-COR), in order to obtain a rough estimation of the horizontal illuminance level on the task area (i.e. the surface at the desks’ height). An average illuminance level of 522 ± 60 lx was measured.



Fig 3 – Example of Intelligo test screen

2.2 Acoustic Simulation and Intelligibility Tests

A classroom model was created and calibrated based on measured room-acoustical parameters. Auralized speech intelligibility tests were then created and reproduced via headphones, in such a way to virtually replicate the listening conditions experienced in the real room as accurately as possible.

2.2.1 Room modelling and model calibration

The space was modelled using the room acoustics software Odeon version 14.01 (Odeon A/S, 2016). The software employs a hybrid approach that combines, below a selected reflection transition order, a mixture of the image source method and ray-tracing

and, above this transition order, a special ray tracing process that generates secondary sources radiating energy locally from the surfaces (ray-radiosity).

A geometric model, made of 261 surfaces, was created in SketchUp and imported in Odeon. Desks and unoccupied chairs were simulated as suspended planes. Occupied chairs were modelled as parallelepipeds with sides of 0.6 m (depth), 0.5 m (width) and 0.4 m (height), corresponding to the seat and parallelepipeds with sides of 0.2 m (depth), 0.5 m (width) and 0.4 m (height) as the seatback.

For room-acoustical parameter predictions, the virtual source was defined as to represent the directivity pattern of the speech source used in real classroom measurements. The *Tlknorm* source available in Odeon was used, having the directivity of a human talker, but it was shaped with a typical female spectrum according to IEC 60268-16 (IEC, 2011).

Concerning the noise source, it was modelled as an omnidirectional source (*Omni*), as to replicate the dodecahedral source employed in real classroom measurements.

Two receiver points were set corresponding to R1 and R2 receiver positions. Simulations were performed with a transition order of 2, 2000 early rays and 16000 late rays. Air temperature and relative humidity were set according to average values measured during the tests (T=23 °C, RH=23 %).

Mid-frequency scattering coefficients were assigned to surfaces, taking into account only scattering due

to surface roughness, being diffraction phenomena handled directly by Odeon. A scattering coefficient of 0.50 was applied for occupied chairs and of 0.70 for radiators. A coefficient of 0.05 was assigned to all other surfaces.

The initial absorption coefficients were assigned to surfaces based on Odeon’s material library and on data available from literature. These values were then adjusted to calibrate T30 values. The calibration procedure was performed with slight adjustments in order to keep physically realistic values for material properties. The calibrated octave-bands absorption coefficients are shown in Table 1.

2.2.2 Participants, test material and procedures

Auralized listening conditions were created by convolving anechoic signals with the binaural impulse responses (BRIRs) calculated in Odeon. The BRIRs were calculated by introducing in Odeon the signal and noise sources with a white spectrum, in order not to include twice the overall frequency response after convolution with anechoic signals.

The virtual listener was defined by the head-related transfer function (HRTF), previously measured for the B&K type 4128-c manikin. The generic headphone equalisation filter *Subject_021Res10deg_diffuse.wav* was employed as to compensate for a non-linear frequency response of the headphones.

Table 1 – Octave-band absorption coefficients of the main linings in the classroom

Material	125	250	500	1000	2000	4000
Painted concrete wall	0.02	0.02	0.03	0.04	0.05	0.05
2 · 13 mm plasterboard on steel frame, mineral wool in cavity, surface painted	0.12	0.08	0.06	0.04	0.04	0.05
Rough concrete ceiling	0.02	0.03	0.03	0.03	0.04	0.07
Desks and furniture	0.04	0.05	0.05	0.05	0.03	0.01
Perforated wood panel, Topakustik 6/2	0.30	0.32	0.42	0.66	0.70	0.45
Audience on wooden chairs	0.22	0.25	0.56	0.69	0.81	0.78

The auralization procedure involved creating separate BRIRs at each receiver position (R1 and R2), for both speech and noise sources. The BRIRs were then convolved through AudioMulch software with the

anechoic speech and noise signals to recreate a subset of the listening conditions proposed during the in-situ experiment. Specifically, the two conditions

(position R1 and R2) with the stationary masker (S) were selected.

Listening tests with auralized material were proposed in a quiet environment, by reproducing signals over Audio Technica type ATH-m50x headphones.

In order to calibrate the reproduction level of the signals and measure the STI of the virtual conditions, auralized speech and noise signals were measured with headphones placed on the head and torso simulator.

The test in virtual conditions was proposed to 21 listeners who took part in the in-situ experiment. Details are given in Table 2.

Following a training session, participants completed two tests respectively at the R1 and R2 virtual receiver positions, under stationary noise (S). Tests were administered again through the Intelligo system and self-evaluation of effort was performed through visual analogue scales after each test completion.

Table 2 – Participants to the auralized speech intelligibility test

Italian native speakers	Age
Female (n=5)	23.4 (± 0.8)
Male (n=5)	25.4 (± 1.6)
All (n=10)	24.4 (± 1.6)
German native speakers	Age
Female (n=6)	23.0 (± 2.5)
Male (n=5)	29.4 (± 9.7)
All (n=11)	25.9 (± 7.5)

3. Results

3.1 Room Acoustical Parameters

Measured and simulated T30 and C50 values are provided in Fig. 4 and 5, as mean values over the two receiver positions. Differences are related to the just noticeable differences (JND) indicated in EN ISO 3381-1 standard, assuming for C50 the same threshold as for C80 (CEN, 2009).

As a consequence of the model tuning, good agreement is found between simulated and in-situ measured T30 values. T30 differences are within the one-JND threshold, except for 8000 Hz where the difference reaches 2 JNDs (10 %).

Simulated C50 values are within the one-JND threshold from measured ones, except for 1k, 2k and 8k octave-bands where C50 differences are, respectively, equal to 1.28 dB, 1.45 dB and -2.55 dB.

3.2 Speech and Noise Levels

Fig. 6 presents a comparison between simulated and measured speech and noise levels, as mean values between the two R1 and R2 receiver positions. Simulated values were derived from recordings of speech and noise signals reproduced over headphones on a head and torso simulator.

Differences are generally above the JND threshold. Signal prediction is up to 5 dB above measurement at 8k, while noise prediction is up to 5 dB above measurements at 125 Hz.

3.3 STI

STI values were derived from in-situ measured impulse responses and signal and noise levels, according to IEC 60268-16 standard (IEC, 2011). Similarly, STI values related to auralized sound fields were calculated from simulated BRIRs and from recordings of speech and noise signals reproduced over headphones on a head and torso simulator. Final STIs were obtained as average values between the two ears. Female STI values are considered. As illustrated in Table 3, good agreement is found between simulated and measured STI values.

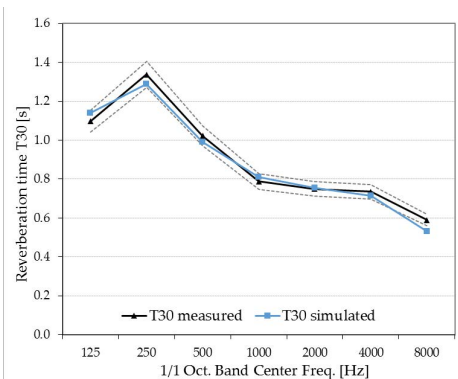


Fig. 4 – Comparison between mean measured (± 1 JND) and simulated T30

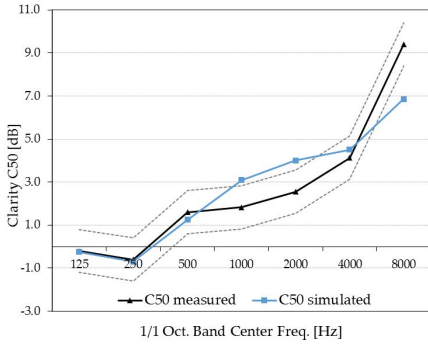


Fig. 5 – Comparison between mean measured (± 1 JND) and simulated C50

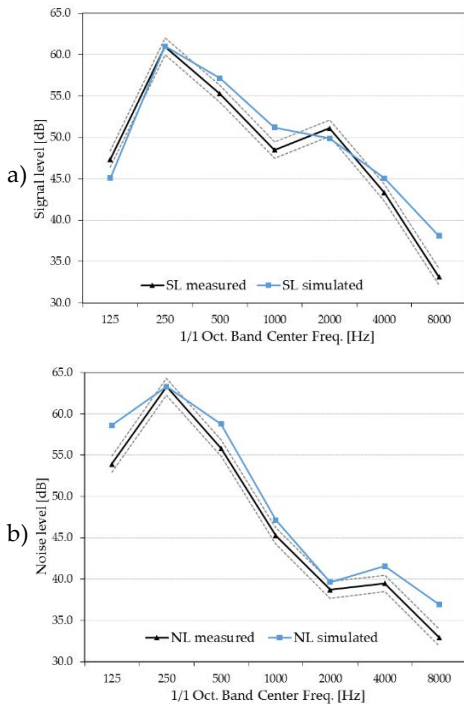


Fig. 6 - Comparison between mean measured (± 1 JND) and simulated signal (a) and noise (b) levels

Table 3 – Comparison between STI values obtained from in-situ measurements and from auralization

STI female	In-situ	Auralized
R1	0.55	0.54
R2	0.46	0.46

3.4 Intelligibility scores

Single IS values were calculated as follows:

$$IS = (raw\ score + 1) \cdot 0.5 \quad (1)$$

where the raw score is equal to “+1” for correct answers, “-1” for incorrect answers and “-0.5” for the “none of the above” option (Prodi et al., 2010).

Pooled IS values were averaged, for each acoustical condition, separately for the Italian (n=10) and German (n=11) native speakers and for in-situ and auralized tests. Results are analyzed by comparing IS, along with their standard deviations, with STI values, as shown in Fig. 7.

Even though a statistical analysis of data has not been yet performed, some tendencies can be outlined and preliminarily discussed, relying on mean values and standard deviations.

Differences between measured and simulated listening conditions are always within the standard deviations, suggesting that the real and auralized conditions cannot be discriminated by the IS metric. As expected, IS at position R1, closer to the speech source, are higher than IS at the rearward position R2. In addition, data show a tendency towards higher IS for the Italian group compared to the German one, at both listening positions.

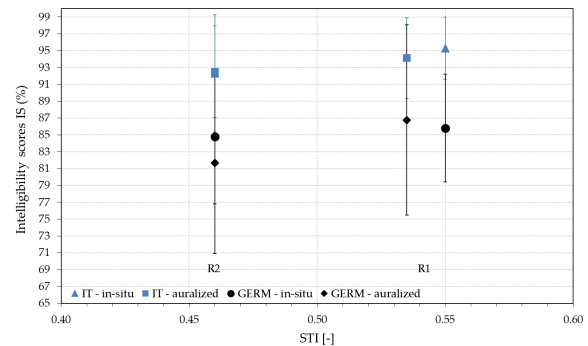


Fig. 7 – Comparison of intelligibility scores (IS) and speech transmission index (STI) from in-situ and auralized tests, for Italian (IT) and German (GERM) native speakers

3.5 Response Time

RT values from in-situ and auralized tests are presented in Fig. 8, by distinguishing the two sample groups (IT and GERM) and the two listening conditions (position R1 and R2).

Differences between in-situ and auralized tests are lower than individual standard deviations. A tendency can be observed towards shorter RTs for the Italian group compared to the German one and for position R1, closer to the sound source, compared to position R2.

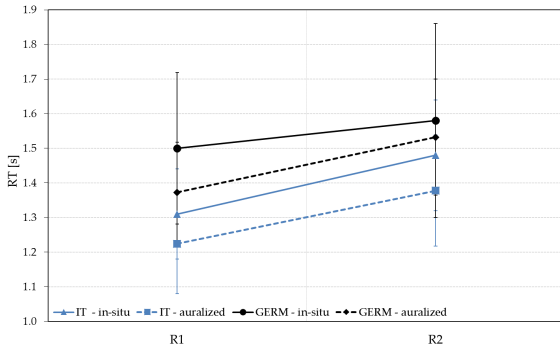


Fig. 8 - Comparison of response times (RT) from in-situ and auralized tests, for Italian (IT) and German (GERM) native speakers

3.6 Listening Efficiency

DE values were calculated as the ratio of IS and RT values. Values from in-situ and auralized tests for the two sample groups are provided in Fig. 9. By comparing differences between real and simulated conditions with their standard deviations, it could be concluded that no differences are found in the DE metric. Differences between Italian and German native speakers are, in this case, larger than standard deviations, suggesting a difference between the two groups, with a higher efficiency for Italians.

In accordance with IS and RT results, a higher listening efficiency is reached at position R1.

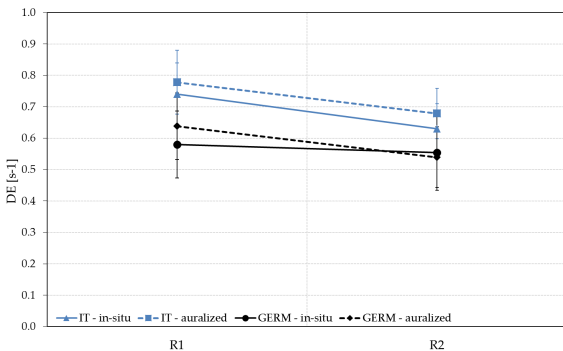


Fig. 9 – Comparison of listening efficiency values (DE) from real and auralized tests, for Italian (IT) and German (GERM) native speakers

3.7 Self-Evaluated Effort

Data collected from subjective effort assessments were normalized on a 0-10 scale and averaged for the two sample groups and for in-situ and auralized tests, as shown in Fig. 10.

Differences between real and simulated conditions are lower than standard deviations for individual results, suggesting a lack of differences. However, it

should be noticed that the more scattered nature of data makes it difficult to recognize differences clearly also between IT and GERM groups. The only clear tendency is towards higher effort paid by listeners at the furthest position.

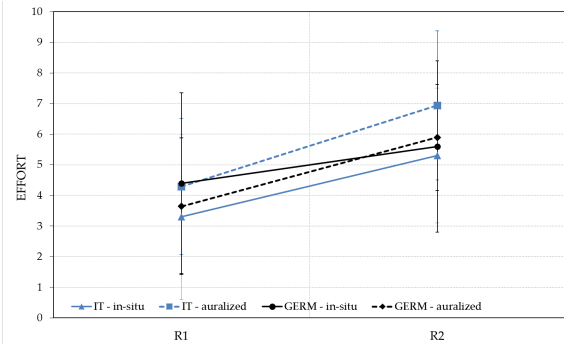


Fig. 10 – Comparison of subjective effort assessments from in-situ and auralized tests, for Italian (IT) and German (GERM) native speakers

4. Conclusion

The present study investigates the effectiveness of a calibrated acoustical model in providing valid auralized sound fields for speech-intelligibility evaluation. Listening tests at two positions inside a real and an auralized university classroom were proposed both to Italian and German native speakers, in the presence of a masking stationary noise. Descriptive statistics results suggest good agreement between STI, IS, RT, and DE values and thus an overall consistency of the two procedures. Moreover, the GERM group showed a tendency to achieve lower IS, longer RT, and lower DE values compared to their Italian peers. To assess the significance of the trends outlined by data a detailed statistical analysis is under course for both IS, RT, and DE and the perceived subjective effort.

Acknowledgements

This study has been funded by the project “Klimahouse and Energy Production” in the framework of the programmatic “financial agreement with the Autonomous Province of Bozen-Bolzano of Research Capacity Building and by the internal project “Human Centred Design of the Built Environment: definition of a methodology for the experimental assessment of the overall Indoor Environmental Quality” of the Free University of Bozen-Bolzano.

The authors gratefully acknowledge students and academic staff for their kind collaboration in the listening tests. Part of the instrumentation used for this research has been provided by FISTEC laboratory of University IUAV of Venezia. Additional thanks go to Lorenza Pistore for her kind support during tests and microclimatic measurements.

References

- Bonaventura, P., A. Paoloni, F. Canavesio, P. Usai. 1986. *Realizzazione Di Un Test Di Intelligibilità per La Lingua Italiana. Rapporto Tecnico 3C1286*. Rome, Italy: Fondazione Ugo Bordoni.
- CEN - European Committee for Standardization. 2008. *EN 15251 - Indoor Environmental Parameters for Assessment of Energy Performance of Buildings, Addressing Indoor Air Quality, Thermal Environment, Lighting and Acoustics*. Brussels, Belgium: CEN.
- CEN - European Committee for Standardization, . 2009. *EN ISO 3382: Acoustics - Measurement of Room Acoustic Parameters - Part 1: Performance Spaces*. Brussels, Belgium: CEN.
- DIN - German Insitut for Standardization. 2016. *DIN 18041: Acoustic Quality in Rooms - Specifications and Instructions for the Room Acoustic Design*.
- Dreschler, W.A., H. Verschuure, C. Ludvigsen, S. Westermann. 2001. “ICRA Noises: Artificial Noise Signals with Speech-like Spectral and Temporal Properties for Hearing Instrument Assessment”. *Audiology* 40(3): 148–57. doi: 10.3109/00206090109073110.
- Hodgson, M., N. York, W Yang, M. Bliss. 2008. “Comparison of Predicted, Measured and Auralized Sound Fields with Respect to Speech Intelligibility in Classrooms Using CATT-Acoustic and ODEON”. *Acta Acustica United with Acustica* 94(6): 883–90. doi:10.3813/AAA.918106.
- IEC - International Electrotechnical Commission. 2011. *IEC 60268 Sound System Equipment - Part 16: Objective Rating of Speech Intelligibility by Speech Transmission Index*.
- Klatte, M., T. Lachmann, M. Meis. 2010. “Effects of Noise and Reverberation on Speech Perception and Listening Comprehension of Children and Adults in a Classroom-like Setting”. *Noise and Health* 12(49): 270–82. doi:10.4103/1463-1741.70506.
- Odeon A/S. 2016. *Odeon - User’s Manual*.
- Postma, B.N.J., B.F.G. Katz. 2016. “Perceptive and Objective Evaluation of Calibrated Room Acoustic Simulation Auralizations”. *The Journal of the Acoustical Society of America* 140:4326. doi:10.1121/1.4971422.
- Prodi, N., C. Visentin C. Bellettini. 2012. “Listening Efficiency Testing”. In: *Proceedings of the AES International Conference*.
- Prodi, N., C. Visentin A. Farnetani. 2010. “Intelligibility, Listening Difficulty and Listening Efficiency in Auralized Classrooms”. *The Journal of the Acoustical Society of America* 128(1): 172–81. doi:10.1121/1.3436563.
- Shield, B.M., J.E. Dockrell. 2003. “The Effects of Noise on Children at School: A Review”. *Building Acoustics* 10(2): 97–116. doi:10.1260/135101003768965960.
- Yang, W., M. Hodgson. 2007. “Validation of the Auralization Technique: Comparative Speech- Intelligibility Tests in Real and Vir-tual Classrooms”. *Acta Acustica United with Acustica* 93(6): 991–99.
- Zhu, P., F. Mo, J. Kang, G. Zhu. 2015. “Compar-isons between Simulated and in-Situ Meas-ured Speech Intelligibility Based on (Binaural) Room Impulse Responses”. *Applied Acoustics* 97: 65–77. doi:10.1016/j.apacoust.2015.04.005.

Simulation-Assisted Monitoring-Based Performance Evaluation of a Historically Relevant Architectural Design

Matthias Schuss – TU Wien – matthias.schuss@tuwien.ac.at

Ulrich Pont – TU Wien – ulrich.pont.tuwien.ac.at

Mahnameh Taheri – TU Wien – mahnameh.taheri@tuwien.ac.at

Christoph Lindner – TU Wien – christoph.lindner@architektur2000.at

Ardeshir Mahdavi – TU Wien – amahdavi@tuwien.ac.at

Abstract

In this contribution, we describe ongoing research efforts to assess the performance of a number of buildings by the Austrian architect Konrad Frey, a pioneer of energy-efficient architecture. A number of his buildings, planned in the 1970s, adapted the principles of modern solar houses. These key projects are the subject of an ongoing nationally funded research project. Thereby, we deploy building simulation to assess the energy performance of one of his buildings (Kindergarten Pachern, located in Hart, close to Graz, Styria, completed in 1997). Moreover, the object was subjected to detailed performance monitoring. The building implements two design strategies: On the one hand, its envelope design is optimized for solar gains, on the other, the building is embedded in the local landscape's morphology, utilizing the benefits of reduced transmission losses via ground-adjacent building components. The building contains standard facilities for kindergarten usage (three group rooms, a gym, a kitchen, and sanitary facilities). The intensive monitoring phase started in summer 2016. The monitored data is expected to support the documentation of the building's actual performance. Moreover, a simulation model of the current state of the building will be calibrated via the collected data. Based on this calibrated model, previous states of the building (subtracting later adaptations) can be simulated. We thus can virtually reconstruct the building's originally intended state and assess its performance.

1. The Architect's Work

Konrad Frey was born in 1934 and is considered one of the pioneers in solar architecture in Austria and central Europe. Considered a key representative of the avangardistic *Graz School* of architecture (alongside with Günter Domenig, Helmut Richter, and others), Frey's work encompasses a wide range of different buildings and structures, spanning from social housing to private residences, schools, and office buildings. Konrad Frey's approaches to energy-efficient buildings date back to his study years in Graz and to his first office, which was created in London in the early 1970s (with Florian Beigel). His pioneering work regarding the integration of passive (and active) solar components is represented by his contribution to the "Sonnenhaus Österreich" (1976), and the planning of the Haus Fischer (see Fig. 1 and 2) in Grundlsee, Styria. However, Frey later admitted that he was disappointed by the output of the solar collector units in Haus Fischer, and conceptually changed his design approach.



Fig. 1 – External view Haus Fischer Grundlsee – Austria (Nextroom, 2016)



Fig. 2 – Internal view of Haus Fischer, Grundlsee, Austria (Nextroom, 2016)



Fig. 3 – External view of Haus Zankl, Geneva, Switzerland (Wagner and Böck, 2013)

For the well-known Haus Zankel (Fig. 3), built from 1976 to 1985 in Geneva, Switzerland, he suggested to understand the building as a solar collector itself, rather than applying solar collector units to the façade. Haus Zankel provided an opportunity to test a number of concepts

regarding solar house design thanks to Frey's very ambitious and adventurous client.

The related experiences resulted in multiple publications. For instance, one of the first handbooks for energy-efficient building designs published in Austria was co-authored by Konrad Frey (Wagner and Böck, 2013).

2. The Case Study Building

The Kindergarten Pachern in Graz, Styria was opened in 1997 and can be considered the rigorous further development of Frey's architectural approach to energy-efficient building design. The south-oriented parts (Fig. 4) of the complex's envelope allow both daylight and shortwave radiation to penetrate the building. Industrial rolling doors (Fig. 5) offer the opportunity to open a large part of the south façade in the summer season, creating thus a seamless transition from inside to outside.



Fig. 4 – External view of the Kindergarten Pachern Hart near Graz, Austria



Fig. 5 – South facing wall with the large garage-type rolling door (pictures by the authors)

The building design makes clever use of its location, as major parts of the building's envelope are embedded in the slope of the topography. The building appears well integrated in the surroundings. Moreover, the roof area can be used as playground, including a slide from the upper level to the ground level (Fig. 6).

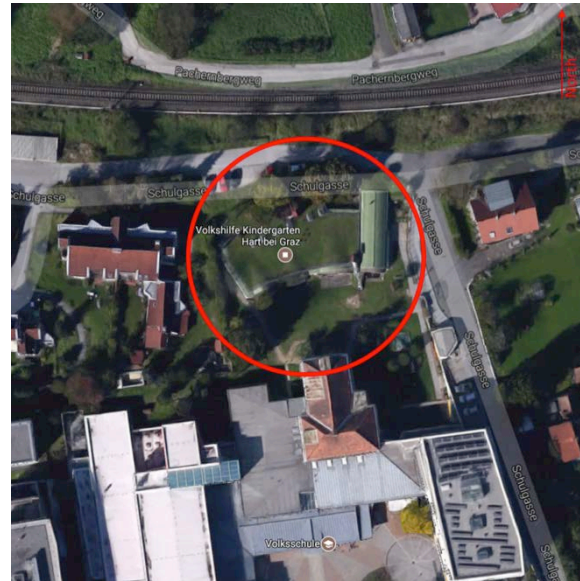


Fig. 6 – Plan of the building site (Google maps 2016, modified)

The interior layout includes three large group rooms (Fig. 7) and a gym on the south side. Sanitary rooms, cloak room, a kitchen, and an office are mainly illuminated by skylights and a small light shaft.



Fig. 7 – Internal view of a group room at the Kindergarten Pachern Hart near Graz, Austria

3. Performance Monitoring

A detailed monitoring of the indoor conditions started at the beginning of summer 2016. The data acquisition focuses on air temperature, humidity, and carbon dioxide concentration in the three group rooms, the gym, and the corridor. To capture occupancy patterns, two motion detection sensors were installed in each group room. The state of windows and doors were recorded with contact sensors (Fig. 9).

All sensors are standard wireless energy independent sensors equipped with EnOcean transmitters. An Arduino YUN based data logger recorded the collected sensor data locally and forwarded it via UMTS-Modem to our central monitoring data repository (Schuss et al., 2016, for more details on the general monitoring strategy and configuration). In addition, local external weather conditions were recorded with a wireless weather station directly from the flat roof (Fig. 8). Additional details on sensors are given in Table 1.

Table 1 – Deployed monitoring devices

Device	Range / Accuracy
Davis Vantage Pro2 Wireless Weather station	Temperature: -40 to +65 °C ± 0.5 °C Humidity: 0 to 100 % ± 3 % Solar radiation: 0 to 1800 W ± 5 % Wind speed: 1 to 67 m/s ± 1 m/s or ± 5 % Wind direction: 0 to 360° ± 4°
Pressac CO ₂ , Temperature and Humidity Sensor	Temperature: 0 to 51 °C ± 0.5 °C Humidity: 0 to 100 % ± 5 % CO ₂ : 0 to 2550 ppm ± 125 ppm
Thermokon SR-MDS Solar	Occupancy / Motion: 0 / 1 Light level: 0 to 510 lx
Thermokon SRW01 Window contact	Status: 0/1



Fig. 8 – Wireless local weather station



Fig. 9 – Floor map with locations of the performance monitoring sensors installed at the Kindergarten Pachern Hart near Graz, Austria

4. Performance Simulation

An initial thermal model of the building was developed based on construction plans and site visits. EnergyPlus (2016) was selected as simulation tool. Generated and calibration of simulation models are expected to help explore the influence of adaptations in the building and its usage on building's actual performance.

Fig. 10 illustrates the complex geometry of the EnergyPlus model (visualized by OpenStudio plugin for SketchUp). The energy model of the building involves five monitored zones, including three group rooms, a gym, and the corridor (Table 2). Thus, performance indicators such as mean air temperature in each zone can be calculated. Moreover,

four non-monitored zones are also included in the EnergyPlus model.

Table 2 – Studied thermal zones

Zone	Area [m ²]	Volume [m ³]
Group room 1	77.5	124.4
Group room 2	76.2	220.7
Gym	96.7	280.5
Group room 3	81.4	223.6
Corridor	170.4	460.0

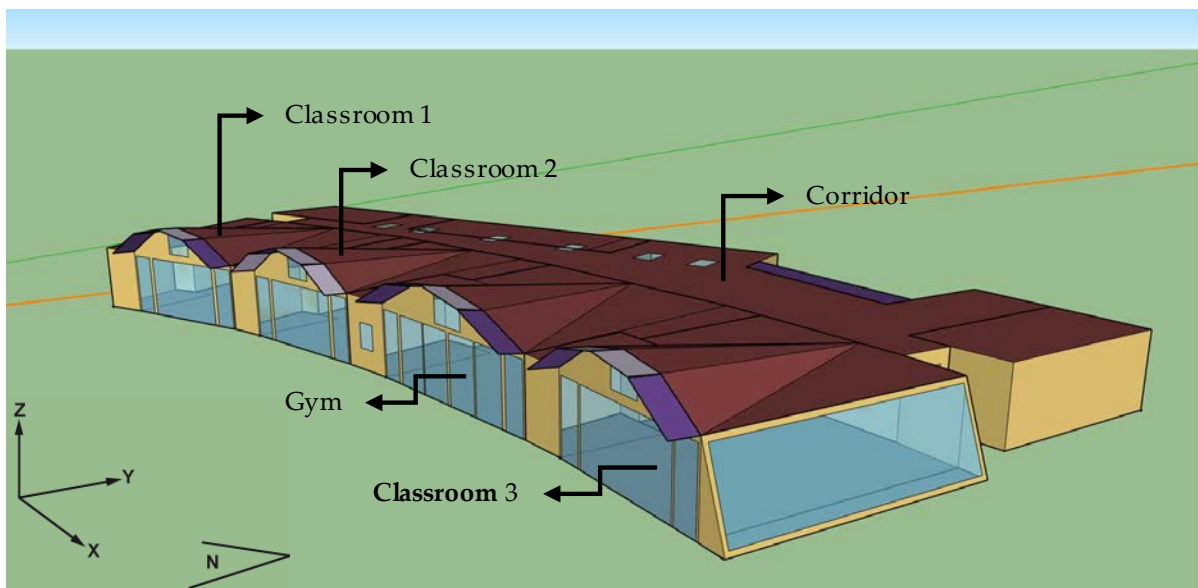


Fig. 10 – EnergyPlus model geometry for the kindergarten building

4.1 Thermal Properties of the Construction

Besides the geometrical modelling, the thermal properties of the constitutive materials were set according to the real existing setup. Table 3 summarizes information on the thickness and the estimated U-Value of the different opaque elements. Layer structure and solar transmittance of the transparent building elements are listed in Table 3.

4.2 Operation Schedules

In the initial model, occupancy schedules were defined for the rooms considering the working hours of the kindergarten and each group room. Moreover, lighting was modelled in the initial model based the installed power and the daily occupied hours.

In order to define the schedules in the calibrated models, sensor data (occupancy, windows) was used to generate more accurate operation schedules. The observed data was integrated via csv-files and assigned to the related variables such as state of

windows (open/closed), occupancy (absence/presence), and lights (on/off).

Table 3 – Opaque building elements

Building element	Thickness [m]	U-Value [W m ⁻² K ⁻¹]
Outside wall – Type 1	0.37	0.493
Outside wall – Type 2	0.47	0.164
Outside wall – Type 3	0.38	0.460
Inside wall – Type 1	0.14	0.224
Inside wall – Type 2	0.30	4.226
Floor – Type 1	0.56	0.317
Floor – Type 2	0.47	0.313
Green roof – Type 1	0.76	0.211
Green roof – Type 2	0.48	0.218
Flat roof	0.46	0.227
Outside door	0.10	0.497
Inside door	0.02	3.864

Table 4 – Transparent building elements

Building element	Layers	Solar transmittance [-]
Window type 1	Clear glass	0.781
	Air	
	Clear glass	
Window type 2	Coated glass	0.165
	Air	
	Coated glass	

4.3 Local Weather Data

For the initial model we obtained hourly weather data from the EnergyPlus weather file database for the closest city to the case study, namely the city of Graz, Austria. For more accurate simulations, we generated a local weather file based on the measured values from our locally installed weather station. An exported data set for an entire year together with our measured data from the weather station was used to create an hourly data import file for Meteororm (2016) and to process the generation of an EPW-file for EnergyPlus.

4.4 Simulation Results

Figs 11 to 14 illustrate the simulated indoor air temperatures (in the group rooms 1 to 3 as well as in the gym) based on the previously mentioned tree models together with the corresponding monitored values for the later part of August 2016.

For a comparison between the simulated and measured room air temperatures in August 2016, values for the following statistics were calculated (Table 5): Mean Bias Error (MBE), Root Mean Square Error (RMSE), and the Coefficient of Variation of the Root Mean Square Error (CV(RMSE)).

The initial model simulation results (with general operational schedules based on working hours, maximum internal gains, and the Graz weather file) showed significant deviations from the monitored results and displayed a strong trend toward overheating. A second variation with a weather file based on the local measurements further increased this overestimation of indoor temperatures: The local data involved comparatively higher outdoor temperatures and radiation values.

The third set of simulations used more realistic operation patterns (lower internal gains and different ventilation rates) and resulted in a significantly higher agreement with the measured values. However, the group room 1 shows, even for the calibrated model, significantly higher temperatures as compared to the measurements. The inaccurate modelling of the surrounding trees and external canvas blind could explain this circumstance. Further model improvements, especially for the autumn and winter period, are to be implemented in the near future. As in this case the building will not be operated in the free-running mode, additional sensors will be required for model calibration (e.g., surface temperature probes for radiators for the calculation of thermal energy magnitudes introduced in the spaces).

The resulting final calibrated model of the building will be used to generate different virtual variants of the building to account for the past adaptations. The results are expected to explain how the initial design concept and the related performance could have been influenced by such adaptations. For instance, a cross ventilation possibility was an important part of the original design. Adaptations during the

construction phase and the actual use patterns, however, significantly reduce the natural cooling possibility in summer. A virtual building setup and simulations using a calibrated model can document (possibly validate) this original design intention for the provision of thermal comfort via passive cooling.

Table 5 – Simulation errors (room air temperature), expressed in terms of the statistics values (four rooms, three simulation models)

Model	Group room				
	1	2	3	4	
Initial model EPW Graz	MBE [%]	8.1	1	-3.5	-2.5
	RMSE [K]	2.7	2.1	2.4	3.1
	CV(RMSE) [%]	11.4	8.9	9.5	12.1
Initial model EPW Hart	MBE [%]	16.0	8.6	4.3	5.3
	RMSE [K]	4.2	2.9	2.0	2.8
	CV(RMSE) [%]	18.0	11.7	8.1	10.9
Calibrated model	MBE [%]	8.5	1.8	0.17	-2.2
	RMSE [K]	2.7	1.8	1.6	2.3
	CV(RMSE) [%]	11.3	7.4	6.4	8.7

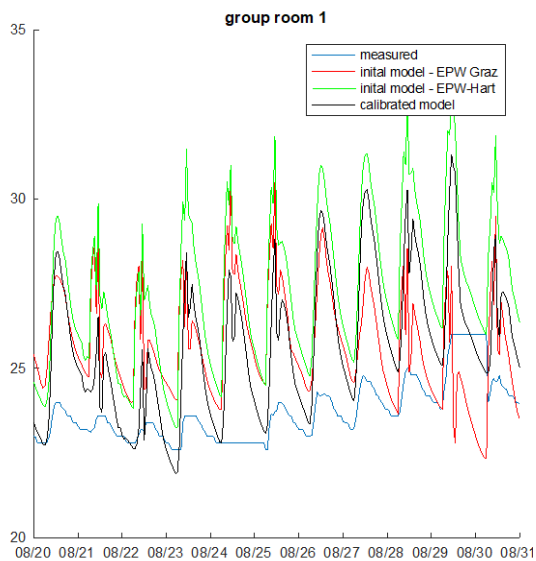


Fig. 11 – Trend of measured and simulated room temperature in group room 1

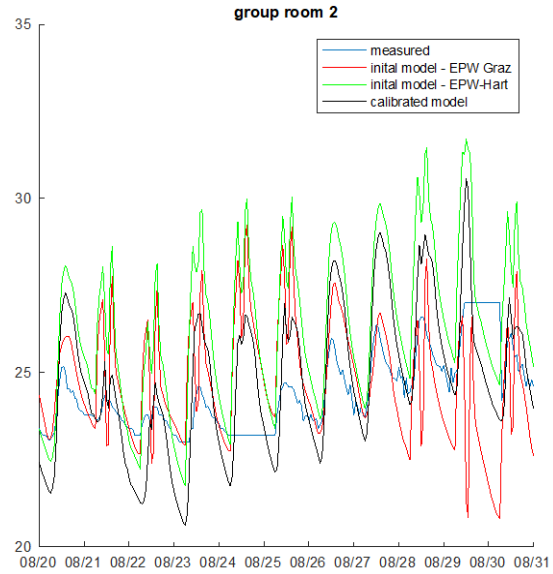


Fig. 12 – Trend of measured and simulated room temperature in group room 2

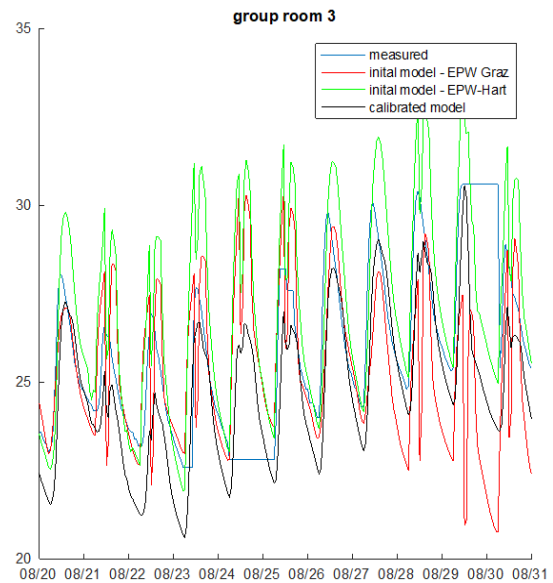


Fig. 13 – Trend of measured and simulated room temperature in the gym

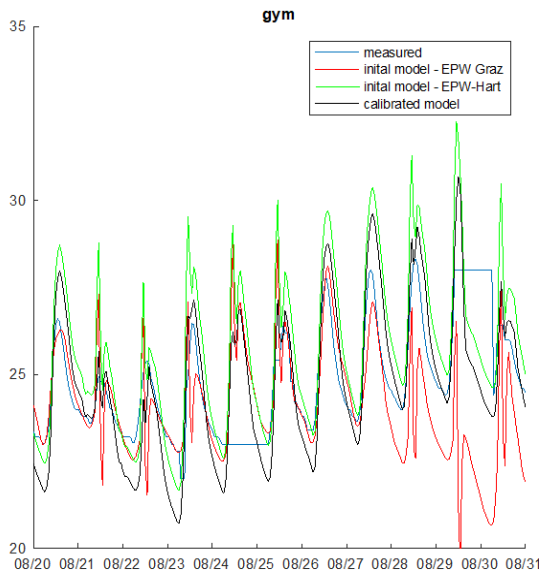


Fig. 14 – Trend of measured and simulated room temperature in group room3

5. Conclusion

The present paper illustrates the use of monitored data to generate a more accurate simulation model compared to standard design assumptions for operational schedules and external climate. The differences in the mean room temperature derived by simulation and measured values highlight the importance of realistic operation schedules and internal gains. The calibrated models will be used to virtually reconstruct the building in accordance with the architects original design intentions. The effectiveness of the underlying design strategies in view of energy and environmental performance could thus be objectively examined.

Acknowledgements

This contribution was written in the framework of the project “Solar houses of Konrad Frey: Environmental Research and Solar Design Knowledge”. This project is funded by the Austrian Science Fund (Grant No. P28677-G26). The authors would also like to acknowledge project collaborators A. Wagner and I. Böck (Institute of Architectural Theory, Art History and Cultural Studies of TU Graz).

References

- Google maps 2016. <https://www.google.at/maps/>; accessed in January 2017.
- EnergyPlus. 2016. “EnergyPlus 8.6.0.” Energy Plus. Accessed 2016 December 28. <http://energyplus.net>
- Meteonorm. 2016. “Meteonorm 7” Meteotest. Accessed 2016 December 20 <http://www.meteonorm.com/de/downloads>
- Nextroom. 2016. “Haus Fischer am Grundlsee” Nextroom Accessed 2016 December 20 <http://www.nextroom.at/building.php?id=29880>
- Schuss, M., S. Glawischnig, A. Mahdavi. 2016. “A flexible and scalable approach to building monitoring and diagnostics”. In: *Proceedings of the 11th European Conference on Product and Process Modelling*.
- Wagner, A., I. Böck. 2013. “Konrad Frey: Haus Zankel. Experiment Solararchitektur”. Berlin, Germany.

Bio-Based and Recycled-Waste Materials in Buildings: A Study of Energy Performance of Hemp-Lime Concrete and Recycled-PET Façades for Office Facilities in France and Italy

Chadi Maalouf - University of Reims Champagne-Ardenne - chadi.maalouf@univ-reims.fr

Carlo Ingrao - University of Foggia - carlo.ingrao@unifg.it

Flavio Scrucca - University of Perugia - scrucca.unipg@ciriaf.it

Tala Moussa - University of Reims Champagne-Ardenne – tala.moussa@univ-reims.fr

Caterina Tricase - University of Foggia – caterina.tricase@unifg.it

Francesco Asdrubali - University of Roma Tre - francesco.asdrubali@unipg.it

Abstract

Energy efficiency and Greenhouse Gases emission reduction are actual key issues in all the economic sectors and, in particular, in the building sector that is one of the most energy-consuming. This paper reports on the performance of sustainable materials produced from natural resources as hemp-concrete or from recycled-waste non-biodegradable materials including Recycled PolyEthylene Terephthalate (R-PET). Three façades employing three different materials (hemp-concrete, hemp-concrete with brick and R-PET) were investigated in three cities in France (Nancy and Carpentras) and in Italy (Perugia) with different climates. The energy performance of each façade was assessed in terms of cooling and heating demands, electrical consumptions and indoor thermal comfort including indoor temperature and relative humidity. The effects of two ventilation modes were tested using a constant airflow rate or humidity sensitive flow rate.

1. Introduction

Nowadays, the building sector is considered one of the most energy and resources consuming: buildings consume about 40 % of the world global energy, 25 % of the global water and 40 % of the global resources (United Nation Environment Program, 2016). Within the global aim of energy and resources saving, recent studies investigated buildings considering them as a fundamental part of the environment (Rossi et al., 2015), and also characterized innovative construction materials in detail (D'Alessandro et al., 2014). In this regard, the

building sector has recently undergone a notable evolution towards sustainable materials (Asdrubali et al., 2015), thus contributing to both improving and promoting energy efficiency and renewable energy in sustainable development contexts. Also, climate changes are increasing as a result of growing atmospheric concentrations of carbon dioxide and other Greenhouse Gases (GHGs); this sets several challenges to be faced in the building sector. Therefore, it has become crucial to accelerate the shift from classical to environmentally friendly materials, in order to contribute to the transition to equitable, sustainable, post fossil-carbon societies. The use of bio-sourced materials as hemp-lime concrete or recycled-waste materials including Recycled Poly-Ethylene Terephthalate (R-PET) as insulating panels seems to be a promoting solution. In that context, this paper aims at performing a numerical assessment of the hygrothermal behaviours of three different walls. The latter incorporates hemp-lime concrete as shown in Fig. 1 (Elfordy et al., 2008; Arnaud and Gourlay, 2012; Collet et al., 2013; Ingrao et al., 2015) known as “hemp concrete” or “hempcrete”, (Pretot et al., 2014; Ingrao et al., 2015) or R-PET which is PET, a thermoplastic polyester widely used for bottles and containers of food or pharmaceutical products (Massey et al., 2008). It can also be introduced in building applications in the form of insulating panels, with significant environmental benefits coming not only from the good thermal insulation performance but also, from the avoided use of virgin PET in the panel production phase (Ingrao et al., 2014; 2016).

The numerical study employs the simulation tool SPARK in which heat and moisture transfer equations are implemented. The annual electrical energy consumption values are also calculated through the simulations.



Fig. 1 – Hemp-lime concrete for building applications

2. Mathematical Model

This section is devoted to present the equations that were developed to assess the heating and cooling loads, on both the room and the air level.

The thermal performance of an envelope including the durability of the material highly depends on the moisture transport through the envelope. Thus, understanding the humidity transfers is crucial to improve performance and indoor thermal comfort especially when using a bio-sourced material like hemp-concrete (Lelievre et al., 2014; Tran Le et al., 2010). Along the years, several investigators have developed models of moisture transport in buildings and, in particular, in single building materials, among others: Kunzel (1995), Pedersen (1992), and Mendes (1997).

Most of these models nearly have a similar physical basis: heat and mass equation, Philip and de Vries model (Philip and De Vries, 1957), and the laws of Fourier, Fick and Darcy. In contrast, the Umidus model (Mendes, 1997) which, as known, takes into account the liquid and vapour phase transfer is employed in this work. The wall thickness L is presented in Fig. 2 as well as the different transport phenomena, including mass and heat convections. The governing partial equations to model heat and mass transfer are given as follows:

$$\frac{\partial \theta}{\partial t} = \frac{\partial}{\partial x} \left(D_T \frac{\partial T}{\partial x} \right) + \frac{\partial}{\partial x} \left(D_\theta \frac{\partial \theta}{\partial x} \right) \quad (1)$$

With the boundary conditions at the external surface ($x = 0$) and the internal surface ($x = L$):

$$\rho_l \left(D_T \frac{\partial T}{\partial x} + D_\theta \frac{\partial \theta}{\partial x} \right) \Big|_{x=0,e} = h_{M,e} (\rho_{ve,a,e} - \rho_{ve,s,e}) \quad (2)$$

$$\rho_l \left(D_T \frac{\partial T}{\partial x} + D_\theta \frac{\partial \theta}{\partial x} \right) \Big|_{x=L,i} = h_{M,i} (\rho_{ve,s,i} - \rho_{ve,a,i}) \quad (3)$$

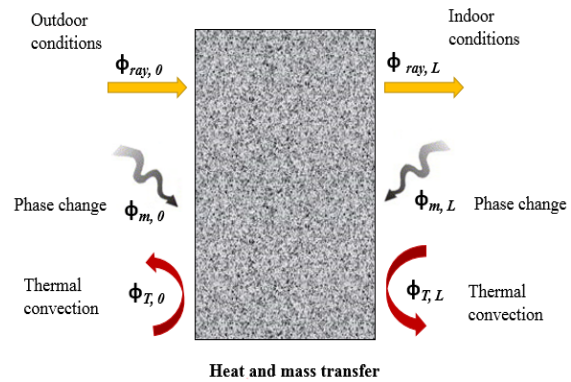


Fig. 2 - Heat and mass transfer through a material envelope

The energy conservation equation with coupled temperature and moisture for porous media is considered, and the effect of the absorption or desorption heat is added. This equation is written as follows:

$$\rho C p_m \frac{\partial T}{\partial \tau} = \frac{\partial}{\partial x} \left(\lambda(T, \theta) \frac{\partial T}{\partial x} \right) \quad (4)$$

$$+ L_v \rho_l \left(\frac{\partial}{\partial x} \left(D_{T,v} \frac{\partial T}{\partial x} \right) \right.$$

$$\left. + \frac{\partial}{\partial x} \left(D_{\theta,v} \frac{\partial \theta}{\partial x} \right) \right)$$

$$C p_m = C p_0 + C p_l \frac{\rho_l}{\rho_\theta} \quad (5)$$

where $C p_m$ is the average specific heat which takes into account the dry material specific heat and the contribution of the specific heat of liquid phase. λ is the thermal conductivity depending on moisture content. For a better understanding, it is underscored that the used boundary conditions take into account radiation, convection, and phase change.

$$-\lambda \frac{\partial T}{\partial x} \Big|_{x=0,e} - L_v \rho_l \left(D_{T,v} \frac{\partial T}{\partial x} + D_{\theta,v} \frac{\partial T}{\partial x} \right)_{x=0,e} \quad (6)$$

$$= h_{T,e} (T_{a,e} - T_{s,e}) + L_v h_{M,e} (\rho_{ve,a,e} - \rho_{ve,s,e}) + \Phi_{ray,e}$$

$$-\lambda \frac{\partial T}{\partial x} \Big|_{x=L,i} - L_v \rho_l \left(D_{T,v} \frac{\partial T}{\partial x} + D_{\theta,v} \frac{\partial T}{\partial x} \right)_{x=L,i} \quad (7)$$

$$= h_{T,i} (T_{s,i} - T_{a,i}) + L_v h_{M,i} (\rho_{ve,s,i} - \rho_{ve,a,i}) + \Phi_{ray,i}$$

Since the wall comprises several material layers, equations at the interface between layers are added. In this case study, the contact between layers is assumed perfect, moisture and thermal resistances at the interface are neglected, and the temperature and capillary pressure are considered continuous, according to Tran Le et al. (2009), Mendes and Philippi (2005).

$$(T)_A = (T)_B \quad (8)$$

$$(\psi)_A = (\psi)_B$$

where T is the temperature and ψ is the capillary pressure.

According to Kelvin's law:

$$\phi = \exp(\psi g / R_v T) \quad (9)$$

Then, it can be deduced that:

$$\frac{R_v(T)_A}{g} \ln(\phi)_A = \frac{R_v(T)_B}{g} \ln(\phi)_B \quad (10)$$

where R_v is the constant of water vapour, ϕ is the relative humidity and g is the gravity acceleration. Because the temperatures for both materials are the same at the interface, the above equation can be written as:

$$(\phi)_A = (\phi)_B \quad (11)$$

which means that relative humidity is the same at the interface for both materials, whilst moisture content is discontinuous because of the different pore structures of those materials.

2.1 Air Model

The air in the zone is assumed to be well mixed respecting the perfect gas law. The net heat transferred into the zone across its faces must equal the heat stored in the volume of air in the cell. This involves heat fluxes through the envelope (transmission, long and short-wave radiation input), additional thermal loads, air exchange due to natural convection or 'Heating, Ventilating and Air Conditioning' (HVAC). The energy equation can be written as:

$$(\rho_i c_p V + I) \frac{\partial T}{\partial \tau} = \Phi_{West} - \Phi_{East} + \Phi_{South} - \Phi_{North} + \Phi_{Bottom} - \Phi_{Top} + \Phi_{Source} \quad (12)$$

where I is the room's thermal inertia.

The humidity condition in the room is due to moisture transfer from interior surfaces, moisture production rate, and the gains or losses due to air infiltration, natural and mechanical ventilation, as well as sources or sinks due to the room occupancy. This yields the following mass balance equation for room air:

$$V \frac{\partial \rho_i}{\partial \tau} = Q_{mWest} - Q_{mEast} + Q_{mSouth} - Q_{mNorth} + Q_{mBottom} - Q_{mTop} + Q_{mSource} \quad (13)$$

2.2 Radiation Exchange

For the short-wave radiation transmitted through the walls, it can be considered that radiant energy enters the room by pane window. However, the mean radiant temperature method is used to calculate long-wave radiation exchange between walls. A linear equation expressing the radiative flow between a wall and all the other walls of the room is written as:

$$\Phi_{rad,LW}^{int} = h_r S (T - T_m) \quad (14)$$

The value of h_r is expressed by:

$$h_r = 4 \varepsilon \sigma_0 T_m^3 \quad (15)$$

where T_m is the mean radiant temperature of the walls and is given by:

$$T_m = \frac{\sum S_j T_{Sj}}{\sum S_j} \quad (16)$$

3. Study Conditions

The composition of the first façade includes an external hemp-concrete layer of $0.095 \text{ W}\cdot\text{m}^{-1}\cdot\text{K}^{-1}$ thermal conductivity associated with 20 cm hollow brick (HCB façade). The second comprises a 36 cm hemp-concrete wall with indoor lime plaster (HC façade). The third façade is based on a thermal block, a thermal insulation layer realised with R-PET mats of $0.036 \text{ W}\cdot\text{m}^{-1}\cdot\text{K}^{-1}$ thermal conductivity and a ventilated cavity associated with a cladding layer (PER façade). The characteristics of each façade are presented in Tables 1, 2, and 3.

The energy performances of the façades were compared through annual energy analyses; each façade is coupled with a virtual office considering different climatic conditions in two cities in France (Nancy and Carpentras) and one in Italy (Perugia). Two types of ventilation are compared: the constant flow rate ($36 \text{ m}^3/\text{h}$) and the relative humidity sensitive rate ($16 - 43 \text{ m}^3/\text{h}$).

With reference to the standard NF EN 12831, the air infiltration rate is estimated to 0.2 h^{-1} . An additional night free cooling of 2 h^{-1} is considered in the summer season (from 3 am to 8 am) to optimise cooling energy consumption. Because of lack of data for the hollow bricks, moisture transfer was neglected in this layer (for both HCB and R-PET façades). Room temperature was kept constant from October to late March and was allowed to float between $19 \text{ }^\circ\text{C}$ and $26 \text{ }^\circ\text{C}$ for the remaining period. Simulations were run for a period of 24 months, the results of the first twelve months were neglected and used to initialize the calculation, then the final results were presented for the last twelve months from January to December. The time step was set to 10 minutes.

The cooling and heating energy demands as well as the electrical energy consumptions were calculated taking into account the heat and moisture within the façade (especially for the hemp-concrete material).

Table 1 – Hemp-concrete brick façade (HCB) properties

Façade (HCB)	Layers (from inside to outside)	Mass density (kg m^{-3})	Thermal conductivity ($\text{W m}^{-1} \text{K}^{-1}$)	Specific heat ($\text{J kg}^{-1} \text{ }^\circ\text{C}^{-1}$)	Transmittance ($\text{W m}^{-2} \text{K}^{-1}$)
	A - Gypsum plaster	900	0.25	850	0.3
	B - Optibric PV3+ Imeris	700	0.187	850	
	C - Sprayed hemp concrete	420	0.095	1000	
	D - Lime sand plaster (2cm)	1650	0.4	830	

Table 2 – Hemp-concrete façade (HC) properties

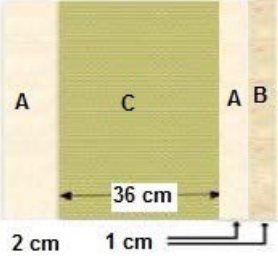
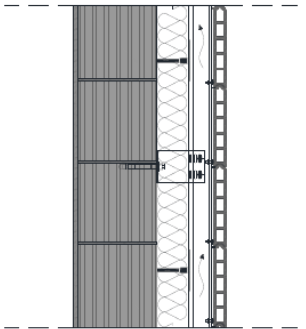
Façade (HC)	Layers (from inside to outside)	Mass density (kg m ⁻³)	Thermal conductivity (W m ⁻¹ K ⁻¹)	Specific heat (J kg ⁻¹ °C ⁻¹)	Transmittance (W m ⁻² K ⁻¹)
	B - Hemp-lime plaster	930	0.2	1000	0.26
	A - Lime sand plaster	1650	0.4	830	
	C - Sprayed hemp-concrete	420	0.095	1000	

Table 3 - R-PET façade properties

Façade (R-PET)	Layers (from inside to outside)	Mass density (kg m ⁻³)	Thermal conductivity (W m ⁻¹ K ⁻¹)	Specific heat (J kg ⁻¹ °C ⁻¹)	Transmittance (W m ⁻² K ⁻¹)
	Lime sand plaster (1.5 cm)	1650	0.4	830	0.22
	Thermal block (25 cm)	531	0.18	900	
	Thermal insulation (10 cm)	30	0.0365	240	
	Ventilated cavity				
	Cladding (4 cm)	750	0.3		

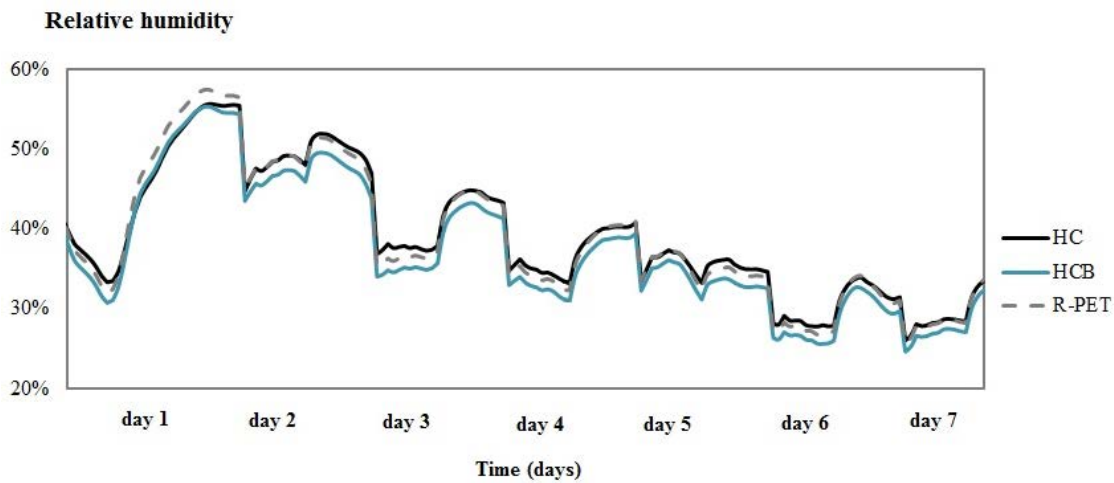


Fig. 3 - Indoor relative humidity variation during one week of December in Nancy using a constant flow rate ventilation mode

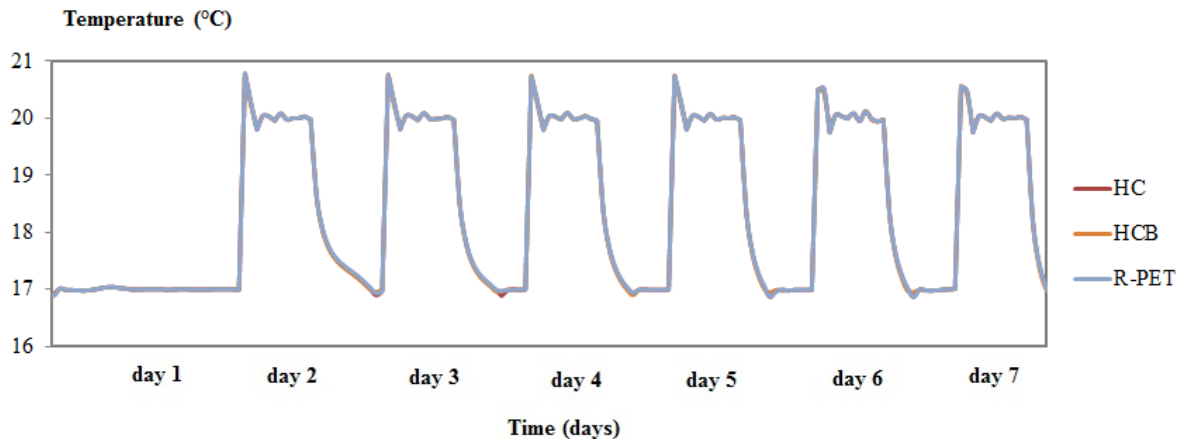


Fig. 4 - Indoor temperature variation of the PI controller during one week in Nancy using a constant flow rate ventilation mode

4. Results

4.1 Constant Air Flow Rate Case

Detailed analyses of the indoor air conditions in Nancy city, during the winter and in Carpentras city, during the summer, were developed and are discussed in this section on the constant air flow rate. For a better understanding, it needs to be clarified that Perugia's air conditions are not presented since the variations are close to Carpentras.

For Nancy, the indoor relative humidity profiles are depicted for a period of one week in the winter season (mid-December) and for the three façades. In Fig. 3 one can see that during occupancy hours, the indoor relative humidity varies between 27 % and 49 %. The relative humidity for HC and R-PET façades are close since the lime hemp and lime mortar plasters have close buffering moisture values higher than gypsum. In vacancy hours, the relative humidity increases since the indoor temperature setpoint decreases from 20 °C to 17 °C as depicted in Fig. 4. For the three cases, indoor relative humidity profiles are close and less affected by the façade material because of the air ventilation rate.

4.2 Heating and Cooling Energy Consumption

The yearly heating and cooling needs for each façade are calculated and presented in Fig. 5 and 6, or the constant flow rate ventilation mode and for

relative humidity sensitive air flow rate, respectively. Based upon the findings one can see that, for Nancy city, (located in the North of France with semi-continental weather) the main energy demand comes from the heating phase, whereas for Carpentras and Perugia cities, the cooling energy demand is higher than the heating one, mainly because of their locations in the related regions. In addition, it can be noticed that the heating energy demands decrease sharply in the case of humidity sensitive flow rate ventilation with a slight increase in the cooling energy demands, independently of the considered façades. For Nancy, the heating demand decreases by about 28 %, whereas for Carpentras it decreases by 56 %, and for Perugia by 61 %.

Concerning the cooling demand, we can see an average increase by about 10 % in Nancy, 8.5 % in Carpentras, and 7.5 % in Perugia. These growths are similar for the three façades except for the HCB in Carpentras where the cooling need increase reaches 18.5 % due to the indoor high relative humidity.

In the light of this, it appears that cooling is not needed for Nancy and, so, other passive means are recommendable like day window opening for natural ventilation in summer.

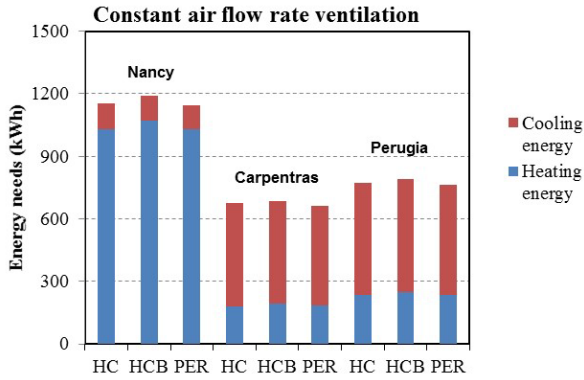


Fig. 5 - Annual heating and cooling energy consumption for the three studied building façades for the constant flow rate ventilation case in the cities of Nancy, Carpentras, and Perugia

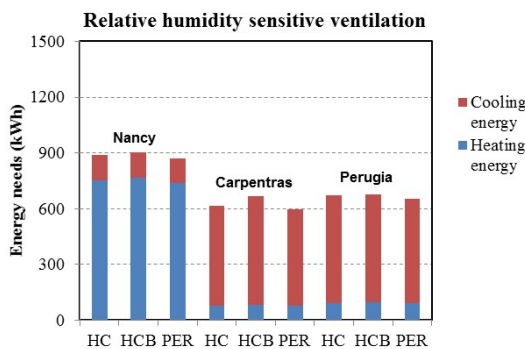


Fig.6 - Heating and cooling needs for the three façades using relative humidity sensitive ventilation

Table 4 - Total electrical energy consumption (kWh.y⁻¹) for the three building façades considered (constant air ventilation rate)

	HC	HCB	R-PET
Nancy, Fr	373.8	386.3	372.8
Carpentras, Fr	254.6	258.3	250.2
Perugia, It	286.9	293.2	284.5

Table 5 - Total electrical energy consumption (kWh.y⁻¹) for the three building façades considered (humidity sensitive flow rate ventilation)

	HC	HCB	R-PET
Nancy, Fr	281.0	285.0	276.3
Carpentras, Fr	234.8	252.3	229
Perugia, It	253.5	256.0	248.3

4.3 Electrical energy consumption

The annual electrical energy consumption for the aforementioned cities using the two air ventilation systems are shown in Table 4 and 5. There is evidence that the lowest values of overall electricity

consumption were recorded in Carpentras, thanks to the three façades' thermal behaviour with the best performance in winter, and rather acceptable in summer (compared to the other two cities). Additionally, it can be clearly seen that the use of a humidity sensitive air ventilation rate decreases the annual energy consumption by about 24 % for Nancy, 7 % for Carpentras, and 11.6 % for Perugia with a hemp-concrete façade. The same observations are applied for the other façades. Moreover, the usage of R-PET mats allows for very good thermal behaviours of the related façade, which makes the latter the less electricity demanding one, with the lowest consumption rate recorded in Carpentras when using the humidity sensitive flow rate ventilation.

5. Conclusion

In this paper, a numerical study of the hygrothermal behaviour of three different walls was performed via the simulation tool SPARK. Three façades including hemp-concrete (HC), hemp-concrete with a brick layer (HCB), and Recycled PolyEthylene Terephthalate (R-PET) were tested for three cities (Nancy, Carpentras in France, and Perugia in Italy) with constant and relative humidity sensitive air flow rates. For each case, heating and cooling demands were computed and used to calculate the annual electrical energy consumption. Our results suggest that relative humidity sensitive ventilation reduces electrical energy consumption when compared to the constant air flow rate. For Nancy city, electrical consumption is reduced by about 24 % whereas for Carpentras and Perugia cities, the reduction is by about 7 % and 11.6 %, respectively. Besides, the thermal behaviour of the HC façade is close to that of the R-PET one in cold climates and its energy performance slightly decreases when summers get warmer as in Carpentras and Perugia, because of the low thermal inertia of the hemp-concrete.

Nomenclature

Symbols

w	Moisture content by mass	kg/kg
C	Specific heat	J.kg ⁻¹ .K ⁻¹
C ₀	Specific heat of dry material	J.kg ⁻¹ .K ⁻¹
C _i	Specific heat of water	J.kg ⁻¹ .K ⁻¹
D _T	Mass transport coefficient associated to a temperature gradient	m ² .s ⁻¹ .K ⁻¹
D _{T,v}	Vapor transport coefficient associated to a temperature gradient	m ² .s ⁻¹ .K ⁻¹
D _θ	Mass transport coefficient associated to a moisture content gradient	m ² .s ⁻¹
D _{θv}	Vapor transport coefficient associated to a moisture content gradient	m ² .s ⁻¹
h _M	Mass transfer convection coefficient	kg.m ⁻² .s ⁻¹
h _T	Heat transfer convection coefficient	W.K ⁻¹ .m ⁻²
I	Room's thermal inertia	
L _v	Heat of vaporization	J.kg ⁻¹
R _v	Constant of water vapor	J.kg ⁻¹ .K ⁻¹
T	Temperature	K
T _a	Indoor air temperature	K
T _m	Mean radiant temperature of the walls	K
T ₀	Operative temperature	K
τ	Time	s
θ	Moisture content	m ³ .m ⁻³
λ	Thermal conductivity	W.m ⁻¹ .K ⁻¹
ρ ₀	Mass density of dry material	kg.m ⁻³
ρ _i	Mass density of water	kg.m ⁻³
ρ _v	Mass density of vapor water	kg.m ⁻³
ρ _i	Air density	kg.m ⁻³
φ	Relative humidity	%
φ	Time shift	h
Φ	Heat flux	W
Q _m	Air flow rate	kg.s ⁻¹
Φ _{source}	Heat source power	W
ψ	Capillary pressure	Pa
ε	Wall emissivity (long wave)	
σ ₀	Stephan-Boltzmann constant	W.m ⁻² .T ⁻⁴

References

- Arnaud, L., E. Gourlay. 2012. "Experimental study of parameters influencing mechanical properties of hemp concretes". *Construction and Building Materials* 28(1): 50–56. doi: 10.1016/j.conbuildmat.2011.07.052.
- Asdrubali, F., F. D'Alessandro, S. Schiavoni. 2015. "A review of unconventional sustainable building insulation materials". *Sustainable Materials and Technologies* 4: 1–17. doi: 10.1016/j.susmat.2015.05.002.
- Collet, F., J. Chamoin, S. Pretot, C. Lanos. 2013. "Comparison of the hygric behaviour of three hemp concretes". *Energy and Buildings* 62: 294–303. doi: 10.1016/j.enbuild.2013.03.010.
- D'Alessandro, F., F. Asdrubali, G. Baldinelli. 2014. "Multi-parametric characterization of a sustainable lightweight concrete containing polymers derived from electric wires". *Construction and Building Materials* 68: 277–284. doi: 10.1016/j.conbuildmat.2014.06.075.
- Elfordy, S., F. Lucas, F. Tancret, Y. Scudeller, L. Goudet. 2008. "Mechanical and thermal properties of lime and hemp concrete ("hemcrete") manufactured by a projection process". *Construction and Building Materials* 22(10): 2116–2123. doi: 10.1016/j.conbuildmat.2007.07.016.
- Ingrao, C., F. Scrucca, C. Tricase, F. Asdrubali. 2016. "A comparative Life Cycle Assessment of external wall-compositions for cleaner construction solutions in buildings". *Journal of Cleaner Production* 124: 283–298. doi: 10.1016/j.jclepro.2016.02.112.
- Ingrao, C., A. Lo Giudice, J. Bacenetti, C. Tricase, G. Dotelli, M. Fiala, V. Siracusa, C. Mbohwa. 2015. "Energy and environmental assessment of industrial hemp for building applications: A review". *Renewable and Sustainable Energy Reviews* 51: 29–42. doi: 10.1016/j.rser.2015.06.002.
- Ingrao, C., A. Lo Giudice, C. Tricase, R. Rana C. Mbohwa, V. Siracusa. 2014. "Recycled-PET fibre based panels for building thermal insulation: Environmental impact and improvement potential assessment for a greener production". *Science of the Total Environment* 493: 914–929. doi: 10.1016/j.scitotenv.2014.06.022.

- Künzel, H.M. 1995. *Simultaneous Heat and Moisture Transport in Building Components One- and two-dimensional calculation using simple parameters*.
- Lelievre, D., T. Colinart, P. Glouannec. 2014. "Hygrothermal behavior of bio-based building materials including hysteresis effects: Experimental and numerical analyses". *Energy and Buildings* 84: 617–627. doi:10.1016/j.enbuild.2014.09.013.
- Massey, S., P. Cloutier, L. Sanche, D. Roy. 2008. "Mass spectrometry investigation of the degradation of polyethylene terephthalate induced by low-energy (<100eV) electrons". *Radiation Physics and Chemistry* 77(7): 889–897. doi: 10.1016/j.radphyschem.2008.01.002.
- Mendes, N. 1997. *Models for prediction of heat and moisture transfer through porous building element*. Florianopolis, Brazil: Federal University of Santa Catarina.
- Mendes, N., P.C. Philippi. 2005. "A method for predicting heat and moisture transfer through multilayered walls based on temperature and moisture content gradients". *International Journal of Heat and Mass Transfer* 48(1): 37–51. doi: 10.1016/j.ijheatmasstransfer.2004.08.011.
- Pedersen, C.R. 1992. "Prediction of moisture transfer in building constructions". *Building and Environment* 27(3): 387–397. doi: 10.1016/0360-1323(92)90038-Q.
- Philip, J.R., D.A. De Vries. 1957. "Moisture movement in porous materials under temperature gradients". *Transactions of American Geophysical Union* 38(2): 222. doi: 10.1029/TR038i002p00222.
- Pretot, S., F. Collet, C. Garnier. 2014. "Life cycle assessment of a hemp concrete wall: Impact of thickness and coating". *Building and Environment* 72: 223–231. doi: 10.1016/j.buildenv.2013.11.010.
- Rossi, F. B. Castellani, A. Presciutti, E. Morini, M. Filipponi, A. Nicolini, M. Santamouris. 2015. "Retroreflective façades for urban heat island mitigation: Experimental investigation and energy evaluations". *Applied Energy* 145: 8–20. doi: 10.1016/j.apenergy.2015.01.129.
- Tran Le, A.D., C. Maalouf, K. Cordeiro Mendonça, T. Hoang Mai, E. Wurtz. 2009. "Study of moisture transfer in a double-layered wall with imperfect thermal and hydraulic contact resistances". *Journal of Building Performance Simulation* 2(4): 251–266. doi: 10.1080/19401490903082459.
- Tran Le, A.D., C. Maalouf, T.H. Mai, E. Wurtz, F. Collet. 2010. "Transient hygrothermal behaviour of a hemp concrete building envelope". *Energy and Buildings* 42(10): 1797–1806. doi: 10.1016/j.enbuild.2010.05.016.
- United Nation Environment Program. 2016. Environment for development. Available at: <http://www.unep.org/sbci/AboutSBCI/Background.asp>.

Case Study for Energy Efficiency Measures of Buildings on an Urban Scale

Domenico Dirutigliano - Politecnico di Torino – domenico.dirutigliano@polito.it

Mark-Alexander Brüntjen – RWTH Aachen University - bruentjen@e3d.rwth-aachen.de

Christian Fliegner – RWTH Aachen University – fliegner@e3d.rwth-aachen.de

Jérôme Frisch – RWTH Aachen University - frisch@e3d.rwth-aachen.de

Vincenzo Corrado - Politecnico di Torino – vincenzo.corrado@polito.it

Christoph van Treeck – RWTH Aachen University – treeck@e3d.rwth-aachen.de

Abstract

The energy efficiency of existing buildings is one of the challenges launched by the EPBD recast. The RWTH Aachen University accepted this challenge and started the project EnEff: Campus - Roadmap aiming at reducing the specific primary energy consumption of the university campus building stock (about 300 buildings) by 50 % until 2025. For the estimation of refurbishments for this kind of big data, data mining techniques can be used like the CART method (Classification and Regression Tree). In this investigation, the method applied on the RWTH Aachen buildings stock and the estimated results will be compared to results from a simple data mining technique, called visual method. The comparison is performed by using low-order dynamic building model (LOM) performance simulation through the Modelica AixLib. The determined results of the recommendation of the CART method will be discussed and evaluated in this paper.

1. Introduction

This paper deals with work within the project “EnEff: Campus - RoadMap RWTH Aachen” (EnEff: Campus). The central aim of the project is to develop a road map for the RWTH Aachen University which leads to a cost-effective reduction of the specific primary energy consumption at RWTH Aachen University by 50 % until 2025, based on the energy consumption of 2013/14. The RWTH Aachen building stock counts about 300 buildings which differ for instance in the following characteristics: usage type, year of construction, and building structure typology. To reach the central aim of the

project, a city district performance simulation is applied and a systematic approach has to be followed, by using LOM and distribution network energy performance models. The city district performance simulation needs the LOM to calculate the heating performance and demand in satisfying computation time. The parametrization of the LOM is set up by archetype buildings. Lauster’s investigations show that the used LOM leads to high accuracy compared to detailed simulation models (Lauster et al., 2014b). Concerning the usage of statistical data for enriching LOM parameters, Schiefelbein describes the generation of archetype buildings by only five input parameters: “building type, year of construction, floor height, number of floors, net floor area” (Schiefelbein et al., 2015a). As the accuracy of statistical data depends on the dataset, the parametrized LOM characterized by the five input parameters were investigated with respect to a similar building stock as the one of the RWTH Aachen Campus. The results achieved a corresponding compliance for the thermal city district simulation with respect to measurements (Lauster et al., 2014a). All things considered, Lauster showed that the LOM is suitable for city district simulation due to the accurate estimation of the heating load and energy demands (Lauster et al., 2014a).

This paper shows the possibility to identify the buildings, offering an efficient recommendation of measures for energetic retrofitting.

2. Data Mining Methods

The aim of the investigation is to apply data mining methods for the determination of efficient energetic retrofit measures on a city district scale. Data mining methods enable the examination of a large number of parameters, for instance those, which influence the energetic behaviour of a building stock, like building construction parameters, such as U-Values, transmission heat loss coefficient, average efficiency ratio of the energy supply, and ventilation rate. In this investigation, two different approaches will be compared. The first one is a visual method, which determines boundary sets in diagrams for filtering data, and the second one is the usage of the CART algorithm. The different approaches are compared by LOM building performance simulation. Therefore, the dataset is set up with the “Tool for Energy Analysis and Simulation for Efficient Retrofit”, in short: TEASER (TEASER, 2016). This tool enriches a data set based on statistical approaches if information is scarce. Successively, the data set is applied to the recommended analysis.

2.1 Visual Method

There are simple methods to determine energetic building retrofit measures with a potential of energy savings, however, they do not always provide high savings. One of these simple processes to determine buildings is to set up diagrams of the building stock, as shown in Fig. 1 and 2. The visual information can be used for setting filters and estimating retrofit measures.

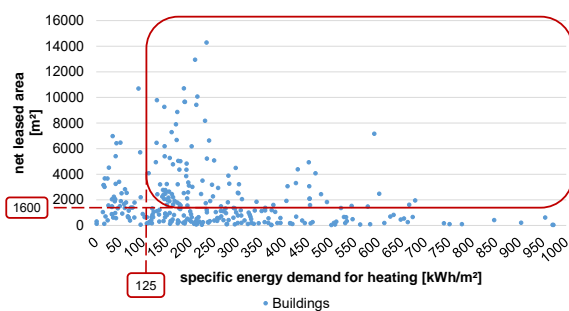


Fig. 1 – Qualitative overview of buildings with a huge net leased area and a high specific energy demand for heating

Fig. 1 is a typical illustration which helps to characterize a building stock. It is possible to extract huge buildings with a high-energy demand in the

upper right part of the diagram, as highlighted by the frame. Nevertheless, there is no information about the distribution of the energy losses. Therefore, Fig. 2 illustrates a method to highlight buildings. On the abscissa in the diagram represents the average U-value [W/(m²K)] and on the ordinate the transmission heat loss coefficient [W/K] is plotted. The highlighted frame represents the buildings which have a high U-value and, due to the high H_T -value of the façade, high-energy losses are caused by transmission.

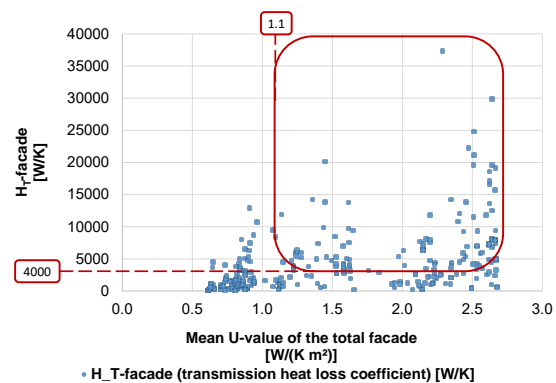


Fig. 2 – Qualitative overview of buildings with a high total facade U-Value and a big transmission heat loss coefficient H_T

These visual illustrations and analyses point out buildings, which could have a potential for retrofiting. Nevertheless, it has to be mentioned, that these are processes accounted by only four to five parameters, they hence represent a very simple way of filtering. On city district level, it is common that the energetic behaviour is influenced by more than these parameters. Thus, the data mining method will be applied to the building stock of the RWTH Aachen Campus.

2.2 Decision Tree with CART Algorithm

Data mining aims to determine models for decision making. In the energy context, the models used in this investigation represent two different types and depend on the scope: classification on the one hand and regression models on the other hand. The first kind of models try to assign a class for each observation (each line in a data set), considering information derived from a data set with classes which are already known (called learning sample). The second kind of models predict the attributes of a

dataset which influence a given outcome stronger than other attributes. Common techniques of classification are decision trees. The algorithms which are frequently associated with decision trees are: ID3, C4.5, CART, CHAID, SLIQ, SPRINT. In this paper, a decision tree is chosen to show a group of rules of classification in a tree scheme and it is matched with the CART algorithm (Breiman et al., 1984). A regression tree is used to predict problems in case the response variable is numeric or continuous. This algorithm is adopted for a supervised multistage decision-making process to classify the observations in a finite number of classes. In the literature, this approach has already been tested to rank flats based on calculated normalized primary energy demands calculated with a quasi steady-state method (Capozzoli et al., 2016).

The decision tree starts with the root node which contains the complete data set and is used as learning sample. Successively, the decision tree subdivides the data set using a binary split in homogeneous subsets, considering 2^k-1 ways of creating a partition of k attribute values, and gives the origin to a new node. The last nodes in the tree are called leaves and each node is labelled with the attribute's name. The tree branches show the path which respects a series of rules and classifies the samples. With a rising number of rules, the tree appears more and more complex which should be avoided to maintain the usability. For this reason, a so-called pruning can be applied. The criterion used is called Gini Index, which evaluates the degree of impurity of each node. The data are split for each node that maximizes the decrease of impurity.

Another element to characterize the tree is to evaluate the statistical performance of the model if a new dataset is used. In this investigation, a k -fold cross-validation is applied. This technique divides the dataset in equal k -parts and for each step; one part is used for the validation of the data set, while the other one is used for training the dataset.

The models are developed with Rapid Miner 7.3.001.

2.3 TEASER and Low Order Building Model

TEASER uses statistical approaches based on the IWU (Loga et al., 2005) building typology (Schiefelbein et al., 2015b). The minimum required input data consist of the following five parameters: year of construction/ year of retrofit, building height, net leased area, number of storeys, and usage type.

These parameters are the basis to estimate envelope areas for exterior walls, windows, rooftops, and basement. Furthermore, the constructions of envelope structures are parameterized. This data enrichment provides a full dataset for the "MultizoneEquipped.mo" zone model of the Aixlib library. In this investigation, TEASER is applied to set up building models of the RWTH Aachen Campus building stock and is used to highlight the differences of recommended estimated retrofit measures.

The mentioned LOM "MultizoneEquipped.mo" is an RC-Model based on the German Guideline VDI 6007-1 (Lauster et al., 2014b). Lauster modified the guideline model by adding an extra resistance representing the thermal behaviour of window elements. To keep the information content low, a minimum number of zones should be the aim of low order modelling. Therefore, only a small number of zones represent the building in the thermal building performance model.

The accuracy of the TEASER tool chain for enriching the data by the mentioned five parameters to set the lumped parameters was evaluated by Lauster (Lauster et al., 2014a), and assessed to be suitable for city district energy performance simulation.

3. Data Set

3.1 Origin of the Data Set

The building stock of the RWTH Aachen University campus consists of about 300 buildings.

For this investigation, some energy-related facts and specific particularities are of interest, for instance, the campus' total energy demand for heating amounting to 126,000 MWh or the specific value of the energy consumption (EC) with respect to the net

leased area of about 236 kWh/m² (Facility Management, 2014). The distribution of the parameters relevant for the description of heating energy losses is illustrated in Fig. 3 and 4.

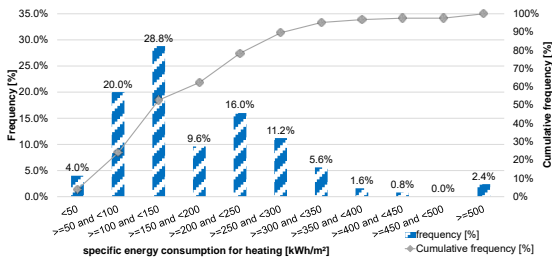


Fig. 3 – Distribution of the energy consumption of the RWTH Aachen University Campus, divided into efficiency classes

Fig. 3 shows the distribution of the EC of the RWTH Aachen building stock (only 125 consumption values are available). The following Fig. 4 describes the distribution of the estimated energy demand (ED) by applying TEASER and LOM (299 data of ED are available); the estimated average of the yearly ED for heating is about 249 kWh/m² with respect to the net leased area.

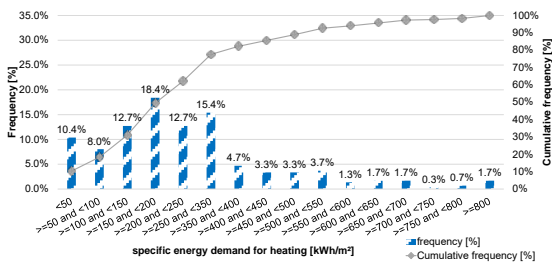


Fig. 4 – Distribution of the energy demand of the RWTH Aachen University Campus, estimated with TEASER and LOM

Fig. 3 and 4 illustrate that about 60 – 80 % of the buildings have a high specific ED for heating. This could yield to the assumption that a lot of buildings should have a high potential for energetic retrofitting. In the further reading, some characteristics of the data set are presented.

3.2 Characteristics of the Data Set

To show some important characteristics for the description of the energetic behaviour of the buildings, like U-values of the total vertical façade or the opaque facade following histograms are illustrated in Fig. 5 and 6.

The distribution of the total mean U-value of the facades is shown in Fig. 5. The figure shows that

there are about 35 % of buildings with a U-value above 2.1 W/(m² K) and approximately another 20 % above 1.2 W/(m² K). Hence, the focus of the investigation is indispensable and the main goal is the determination of facade retrofit measures.

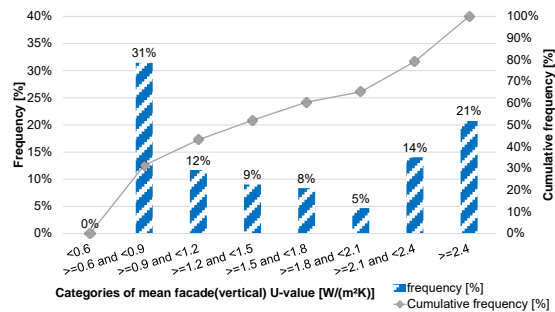


Fig. 5 – Distribution of the total mean U-value of the building facades, based on data estimated with TEASER

Fig. 6 shows the allocation of U-values from the opaque part of the facade.

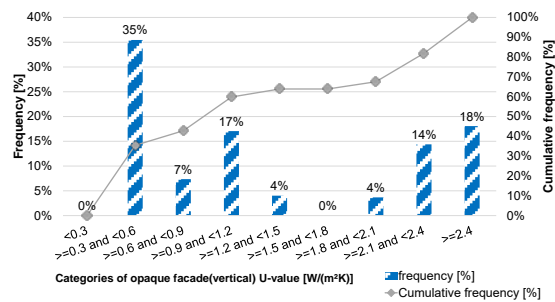


Fig. 6 – Distribution of the U-value of the opaque building facades, based on data estimated with TEASER

Furthermore, Fig. 6 illustrates that the opaque U-values are responsible for about 30 % above 2.1 W/(m² K) and approximately 42 % under 0.9 W/(m² K). This leads to the allocation of window U-values. As mentioned before, the data set which describes the campus was emulated by TEASER; therefore, only two categories of windows are available. The values are between 1.5 W/(m² K) and 2.0 W/(m² K), and above 2.8 W/(m² K).

3.3 Determination of Retrofit Measures by the Visual Method

As mentioned in section 2, the filter settings for determining the buildings which have to be retrofitted are indicated by the diagrams in Fig. 1 and 2. For this investigation two filters are set and applied on the data emulated with TEASER.

Fig. 1 shows the boundaries of the first visual method filter (VM filter setting 1): a high specific ED of 125 kWh/m² and a high total ED (considered by a high net leased area of 1600 m²). These boundaries result in a dataset of about 136 buildings. Moreover, retrofit measures would never be performed, unless they are absolutely necessary. Thus, it is indispensable to consider the U-value, which is set to 1.1 W/(m²K), as highlighted in Fig. 2. Based on to the U-value, the first retrofit recommendation is given and results in 70 buildings with a potential to retrofit the opaque facade. To determine buildings with high transmission heat losses, a high Hr-value, here 4000 W/K, is considered and leads to a second visual filter (VM filter setting 2). This results in a potential data set of about 57 buildings.

3.4 Pre-processing of the Data Set

In this phase, different strategies are considered to prepare the data for an analysis. Firstly, outliers are detected and the values are normalized. Secondly, the variables which influence attributes are selected. Finally, a data transformation is carried out.

To detect the outliers of the data set, a distance-based outlier detection algorithm is applied. Thereby, the Euclidean distance is calculated between the data points, and the ones with the greatest distance from other data points are marked as outliers.

In order to grant equal consideration of the attributes, it is necessary to normalize the data set.

After the data analyses and the review of similar studies in literature (Capozzoli et al., 2016), the following attributes are selected: aspect ratio S/V , heat transfer surface on heated volume in [m⁻¹]; U-value opaque, U-value of the vertical opaque envelope in [W/(m² K)]; Hr-value wall, the mean overall heat transfer coefficient by thermal transmission of the opaque components in [W/K]; U-value window, U-value of the vertical opaque envelope in [W/(m² K)]; Hr-value window, the mean overall heat transfer coefficient by thermal transmission of the opaque components in [W/K].

The attributes are chosen based on the information gain they can give. For this reason, it is common that the attributes of the data set are independent and only the label attribute is clearly dependent of the

other attributes. In this paper, Data Sets 1 and 3 are used with all the variables showed before with the exclusion of Hr. Data Sets 2, 4, and 5 take all the previously shown variables into account. The latest data set is shown in section 6.4 to compare the results and to investigate how the information gain using Hr variables can be used, despite the correlation with the U-values.

Data transformation introduces criteria to label each building according to the “high”, “medium” or “low” category. These labels are necessary, as the classification tree is based on a categorical response variable. Each “high” category starts from the median value to the maximum value of energy performance. The thresholds between the categories “high-medium” and “medium-“low” of the ED data set are 241.05 kWh/m² and 50.00 kWh/m², respectively. The thresholds between the categories of the EC data set are similar with 177.84 kWh/m² and 74.00 kWh/m², respectively. The threshold limit of the “low” category applying ED comes from the energy efficiency class of EnEv2014 (BMW_i, 2014). The threshold limit of the “low” category applying EC is based on a similar percentage of buildings as in the “low” category applying ED. The percentage of buildings in the categories “high”, “medium”, “low” with the ED data set is 36 %, 54 % and 10 %. The categories with the EC data set have the following percentages 41 %, 50 % and 9 %.

4. Limitations

In the following, some boundary conditions shall be mentioned. The applied low order models used for this investigation are supplied by the AixLib library version “The Modelica _Annex60_ library”. This library is currently still under development and, furthermore, TEASER enriches the parameter sets for LOM and uses statistical approaches.

5. Decision Trees

In this investigation, two different approaches are evaluated and a set of buildings of the RWTH Aachen building stock with opaque facades should

be retrofitted. Two different decision trees are evaluated with CART algorithms; the first one is determined with the input of the specific EC for heating with Data Set 1. It is illustrated in Fig. 7.

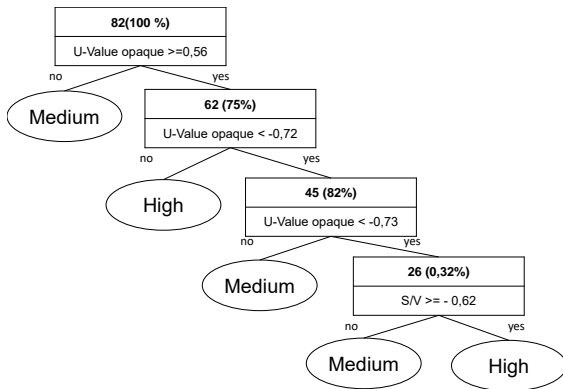


Fig. 7 – Decision tree, based on EC with Data Set_1

After the pre-processing of Data Set 1 with EC, the decision tree classifies 82 buildings.

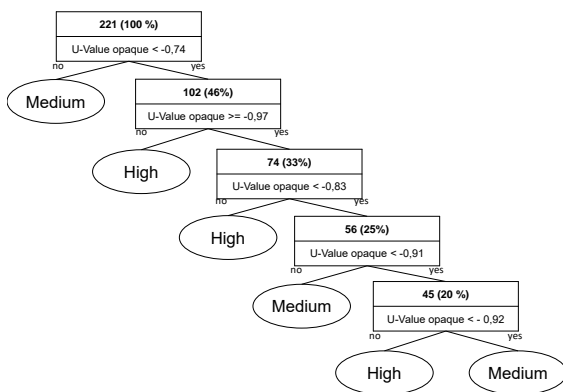


Fig. 8 – Decision tree, based on ED with Data Set 3.

The decision tree of Data Set 3 (normalized data) with ED is shown in Fig. 8. It classifies 221 buildings, thus, more buildings than the first one.

6. Supervised Classification Process

6.1 Analysis of the Classification Tree Split Attributes

The first attribute enables us to split the data in the Root Node, representing the one with the most influence on the energy consumption or demand. The decision tree based on EC has 5 leaf nodes and a tree size of 9. The main attribute is if the U-value of the opaque facade is bigger or equal than 0.56.

Furthermore, in this decision tree, there aren't any attributes about transparent components.

The decision tree, based on ED, has 6 leaf nodes and the size of 11. The main attribute of this decision tree is if the U-value of the opaque facade is smaller than 0.7 (with normalized data).

6.2 Classification Accuracy

The training records which are correctly classified by the decision tree based on EC are about 66 % of all buildings. The accuracy of the same model is 52.97 % with 5 k- folders of the cross validation.

The training records of the decision tree based on ED are about 78 % of the whole considered buildings, and the model accuracy about 72.28 % with 10 k-folders of the cross validation. The accuracy of the whole classification of about 70-80 % (Gao et al. 2010; Yu et al., 2010) is considered acceptable. A lower number of buildings influences the model based on energy consumption negatively. The model of classification based on ED is recommended to evaluate retrofitting measures for higher accuracy.

6.3 Evaluation of Retrofit Actions

The decision trees visualize the main attributes which classify buildings and influence the energy consumption or demand. In the upper part of the tree, close to the Root Node, there are attributes that classify most of the buildings.

Each node could consider a retrofit action. In this study, for each building the following retrofit measures are considered: retrofitting of only transparent components or retrofitting of only opaque components. The retrofit actions are applied only in leaf nodes.

An attribute doesn't necessarily give the possibility of a refurbishment, such as in the case of the S/V-ratio (last node of the Fig. 7). The retrofit actions are applied on all the buildings with the characteristics indicated by the attributes in the leaf nodes, including the buildings not classified by the decision tree. The excluded buildings from retrofit actions belong to the "low" categories (both with EC and ED). These are not considered, because priority is given to the buildings which are classified as "high" and "medium".

6.4 Results

With the visual approach and the CART approach, four different recommendations of a data set are evaluated. These contain the buildings with a high potential for retrofitting the opaque facade. With the visual method, the following filters are used: filter setting 1 with spec. energy demand > 125 kWh/m² AND net leased area > 1600 m² AND U-value > 1.1 W/(m²K); filter setting 2 with spec. energy demand > 125 kWh/m² AND net leased area > 1600 m² AND U-value > 1.1 W/(m²K) AND H_T-value > 4000 W/K. The visual method filter recommends about 70 buildings, whereas the second filter selects about 57. The first CART method based on EC recommends 73 buildings and the second, based on ED, recommends 268 buildings. All the results of retrofit actions are analysed by applying a building performance simulation using LOM. The results are illustrated in Fig. 9. They show that with the CART method, it is possible to save more energy while refurbishing more buildings. In order to investigate possible recommendations, an analysis is conducted with the Data Set 2 (with H_T and U values). Fig. 9 shows that both recommendations of the visual methods yield an energy saving percentage of about 7 % and 8.25 %. This means that the influence of 13 buildings which are retrofitted in addition to the second data set offer no great advantages.

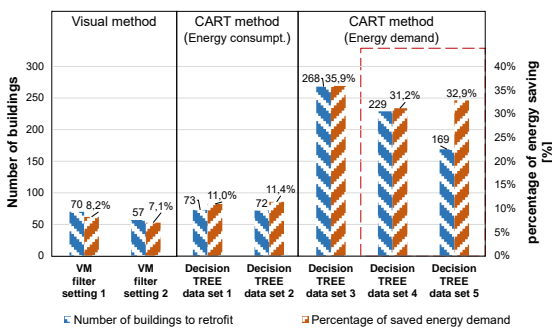


Fig. 9 – Comparison of different evaluated recommendations by the two different methods: visual method and CART method

Data Sets 1 and 2 do not show large differences. It is possible to see that Data Set 3 has the most energy saving potential but also the highest number of buildings to refurbish. Data Sets 4 and 5 consider the same data set but with different retrofit actions. In Data Set 4, the buildings are refurbished following

the attributes of the decision tree and, therefore, with actions on opaque and transparent components. In Data Set 5 all the buildings are object of only opaque retrofit actions.

The estimated recommendation by applying Data Set 2 of the CART method results in energy savings of about 11.4 % and with Data Set 4 of about 31 %. However, Data Set 5 saves about 33 % with fewer buildings, as in the case of Data Set 4. This proves that also retrofit actions should be analysed. Concerning Data Set 5, it has to be mentioned that more than half of the building stock is recommended to be retrofitted. This value seems to be high, but in contrast to a theoretical investigation of retrofitting all 299 campus buildings, the percentage of energy savings was calculated to be 36 %.

Hence, the CART method identifies the main influencing parameter, as it recommends 169 buildings to be optimized (57 % of the building stock) and offers a reduction of about 33 % energy savings, which is very close to the theoretical investigation. However, the accuracy of the decision tree of ED with Data Sets 4 and 5 is lower than the decision tree of ED with Data Set 3.

7. Conclusion

In this paper, two different data mining approaches, namely the visual method and the CART method are analysed and evaluated. The result of each data mining concept is a list of buildings. These buildings are recommended to be retrofitted concerning their opaque vertical facade. The first method depends on human interpretation and is subjective, whereas the latter method is based on a statistical data mining process, which is more objective. The main differences between the methods are the handling (time), reliability, and accuracy. Thus, for a quick recommendation to estimate data sets, the visual method could be considered. But if the input data are reliable and recommendations should be dependable, the CART method should be preferred.

In further investigations, the estimated recommendations of combined retrofit measures will be analysed and discussed.

References

- Breiman, L., J.H. Friedman, R.A. Olshen, C.J. Stone. 1984. *Classification Regression Trees*. Chapman and Hall/CRC.
- Capozzoli, A., G. Serale, M.S. Piscitelli, D. Grassi. 2016. "Data mining for energy analysis of a large data set of flats". In: *Proceedings of the Institution of Civil Engineers - Engineering Sustainability* 170: 3-18. doi: 10.1680/jensu.15.00051.
- Facility Management. 2014. "Energiebericht 2013". RWTH Aachen University. Accessed January 04. 2017. <http://www.rwth-aachen.de/cms/root/Die-RWTH/Einrichtungen/Verwaltung/Dezernate/~pvm/Facility-Management/>
- Federal Ministry for Economic Affairs and Energy (BMWi). 2014. "Energieeinsparverordnung (EnEV 2014)". 2014. Accessed on November 18th 2013. http://www.bmwi.de/Redaktion/DE/Download_s/E/envkv-entwurf-lesefassung-aenderung.pdf?__blob=publicationFile&v=1
- Gao, Y., E. Tumwesigye, B. Cahill, K. Menzel. 2010. "Using data mining in optimisation of building energy consumption and thermal comfort management". *Software Engineering and Data Mining*: 434-439.
- Lauster, M., J. Teichmann, M. Fuchs, R. Streblow, D. Müller. 2014a. "Low order thermal network models for dynamic simulations of buildings on city district scale". *Building and Environment* 10: 223-231. doi: 10.1016/j.buildenv.2013.12.016
- Lauster, M., M.A. Brüntjen, H. Leppmann, M. Fuchs, J. Teichmann, R. Streblow, C. van Treeck, D. Müller. 2014b. "Improving a low order building model for urban scale application". In: *Proceedings of BAUSIM 2014, German –Austrian of IBPSA Conference*.
- Loga, T., N. Diefenbach, J. Knissel, R. Born. 2005. "Entwicklung eines vereinfachten statistisch abgesicherten Verfahrens zur Erhebung von Gebäudedaten für die Erstellung des Energieprofils von Gebäuden". Online resource. Accessed on November 25th 2016. http://www.iwu.de/fileadmin/user_upload/dateien/energie/werkzeuge/iwu-kurzverfahren_energieprofil-endbericht.pdf
- Schiefelbein, J., A. Javadi, M. Lauster, P. Remmen, R. Streblow, D. Müller. 2015a. "Development of a city information model to support data management and analysis of building energy systems within complex city districts". In: *International Conference Future Buildings & Districts Sustainability from Nano to Urban Scale Lausanne 2*: 949-954. doi:10.5075/epfl-cisbat2015-949-954.
- Schiefelbein, J., M. Diekerhof, A. Javadi, G. Bode, R. Streblow, D. Müller, A. Monti. 2015b. "Development of a tool chain for complex city district energy system modeling and simulation". In: *Proceedings of Building Simulation 2015*. Hyderabad, India: IBPSA.
- TEASER. 2016. Energy Efficient Buildings and Indoor Climate, TEASER – "Tool for Energy Analysis and Simulation for Efficient Retrofit" released. Online resource. Accessed February 4th 2017. <https://www.ebc.eonerc.rwth-aachen.de/go/id/gips/?lidx=1#aaaaaaaaaagipu>
- Yu, Z., F. Haghghat, B.C.M. Fung, H. Yoshino. 2010. "A decision tree method for building energy demand modelling". *Energy and Buildings* 42: 1637-1646. doi:10.1016/j.enbuild.2010.04.006.

Investigating the Suitability of the WRF Model for Improving Prediction of Urban Climate Boundary Conditions

Kristopher Hammerberg – TU Wien – kristopher.hammerberg@tuwien.ac.at

Oscar Brousse – KU Leuven – oscar.brousse@kuleuven.be

Ardeshir Mahdavi – TU Wien – amahdavi@tuwien.ac.at

Abstract

Urban populations continue to increase in parallel with global temperatures. The result is an increasing number of people affected by increasingly severe urban heat conditions. Understanding these effects and being able to accurately account for the effects of the urban climate on building energy use is important for urban and architectural design decision making. This paper presents part of an on-going research effort to evaluate the Weather Research and Forecasting (WRF) model as a tool for improving prediction of boundary conditions in urban climates. WRF is a regional climate model that is capable of down-scaling global weather data to a fine resolution and includes detailed urban canopy models. The use of a numerical model in urban climate studies would allow for computational experiments involving changes to the urban fabric and future climate scenarios. In this study, Vienna, Austria, was used as a test case. The weather was simulated over five 48-hour periods, which were selected using cluster analysis to best represent typical weather conditions in Vienna. The model results were then compared to data collected from a network of 170 weather stations throughout the region of interest. Additionally, the land-use classification and urban parameterization in the model domain were improved using high-resolution GIS data from the city of Vienna. Results show a great deal of variation in the accuracy of the model under different weather conditions. Although individual problems can be identified during specific intervals, there is no obvious trend or bias to the variation across all time periods. The extent of the variation indicates the model results are not suitable for use as boundary conditions for building performance models throughout an entire year.

1. Introduction

In recent years, cities have been increasingly considered to be both contributors and stakeholders in the global climate change discussion, yet scientific precedents for the study of the climate impact of cities stretch back over two centuries (Hebbert and Jankovic, 2013). The commonly understood concept of the urban heat island, for instance, finds its roots in the work of Luke Howard in London (1833) and James Gordon's temperature survey of the Salt River Valley (1921). In our current context of mass urbanization and global warming, urban planners and architectural designers could benefit from improved urban climate representations. An accurate urban climate model would allow for quantitative decision support in both the response of buildings to altered boundary conditions and the response of the local climate to changes in urban development.

The misrepresentation of external boundary conditions in building simulation can result in fairly large errors. A study in Bahrain showed that using outdated weather files can underestimate annual electricity consumption by 14.5 % and cooling loads by up 8.9 % (Radhi, 2009). Weather data for the typical meteorological year (TMY) are frequently used in building simulation models and are often derived from airport weather stations (Barnaby and Crawley, 2011). These locations do not represent the semantic and geometric complexities of urban environments or the resulting microclimate effects (Perinotto et al., 2014). Bhandari et al. (2012) investigated the use of synthesized location specific weather files from third party providers and found that monthly building loads can vary up to ± 40 %. In another study, Chan (2011) examined the range of impact of climate change variation by morphing the

TMY based on the projections of a general circulation model (GCM). This revealed the potential for a substantial increase in A/C energy demand ranging from 3.7 to 24 % for residential buildings.

Together, advances in numerical weather models, the increasing availability of highly accurate GIS data, and the proliferation of weather monitoring stations allow for new avenues for exploring the complexities of the urban climate. In this study, we investigated the performance of the WRF model over the city of Vienna, Austria, under various weather conditions with the aim of using the output to improve the boundary conditions of building energy models set in urban areas. The WRF model was chosen as it incorporates a detailed subgrid representation of the urban morphology, called the building environment parameterization and building energy model (BEP+BEM).

2. Methodology

2.1 Study Area

This study was centered on the city of Vienna, Austria. In comparison to other Central European cities with intact historic centers, Vienna is morphologically rather typical. According to the Köppen climate classification, it lies at the edge of the oceanic/subtropical zone (Cfb) that covers most of Western Europe and shares characteristics with both the warm summer continental climate to the East (Dfb) and the humid subtropical conditions (Cfa) of some Northern Italian cities (Kottek et al., 2006). Its municipal boundaries inscribe an area of 414.87 km² and approximately 1.8 million residents (Lukacsy and Fendt, 2015). It lies at the eastern edge of the Alps with the western edge of the city rising into the Wienerwald, and the eastern edge stretching over the Danube River and into the Vienna Basin. Our area of interest contains the municipal boundary of Vienna as well as the surrounding suburban and rural areas (Fig. 1).

The availability of both weather data records as well as high-resolution geospatial data informed our decision to select Vienna as our case study. Additionally, with the notable exception of Stuttgart (Fallmann et al., 2014), Berlin (Jänicke et al., 2016),

and Madrid (Brousse et al., 2016) relatively few European cities have been examined in WRF modeling studies.

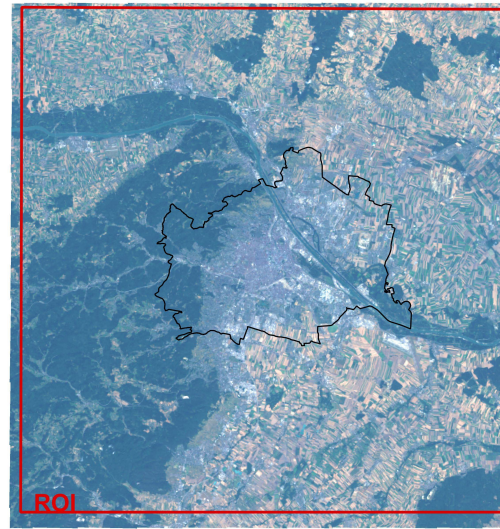


Fig. 1 – Vienna, Austria. Region of interest (red). Municipal boundary (black)

2.2 Study Period

Although numerical weather models can be excellent tools for computational experiments and weather prediction, they are resource intensive. In this study, we hoped to examine the utility of WRF across different weather conditions. Rather than run simulations with season-long or year-long durations, we selected 5 representative periods each with a 48-hour duration.

These representative dates were selected with a k-means cluster analysis method and daily means for the Schwechat Airport provided by Austria's Zentralanstalt für Meteorologie und Geodynamik (ZAMG). This station is well calibrated and sited in an open area that allows for good mixing and less impact of extreme micro-climate effects, making it well suited for classifying regional weather types. Then, three uncorrelated climatic variables were selected to use as key indicators in clustering: temperature, diurnal temperature range, and wind speed. There is no objective or automated method for selecting an optimal number of clusters with the k-means approach. For this study, we needed to achieve a balance between investigating the widest range of weather conditions and reducing the total number of simulations. In order to achieve this

balance, we chose to use 5 weather categories after an iterative testing process (Fig. 2).

The final step was to select the most representative 48-hour period within the cluster for simulation. In order to guarantee that each period best represents the aspects of the category that distinguish it from the other four, we selected days from each category with values furthest from the mean of the other clusters (Table 1).

2.3 Land Cover and Urban Canopy Parameters

2.3.1 WUDAPT Land Cover

The WRF model requires a land cover map to describe the surface condition and calculate its interaction with the atmosphere. For this study we used the World Urban Database and Access Portal Tool (WUDAPT) to provide the land cover map. WUDAPT is a state-of-the-art web portal that pro-

duces land cover maps of cities using the Local Climate Zone (LCZ) concept developed by Stewart and Oke (2012). These maps are created for use in urban climate modeling. The method classifies Landsat satellite imagery with a Random Forest Classification algorithm (Bechtel et al., 2105). Training areas, which best represent each LCZ, are selected by the user. Then the algorithm uses the distinct reflective signature in each spectral band to classify each 100x100 m pixel within the region of interest (ROI).

Table 1 – Representative dates and key climate indicators

Dates	Mean Temp. [°C]	Diurnal Range [K]	Mean Wind Speed [m/s]
January 7-9	-1.62	5.13	1.64
February 8-10	-0.32	4.31	5.00
March 20-22	6.93	15.24	0.69
April 21-23	15.00	12.30	2.49
July 5-7	27.26	16.13	1.56

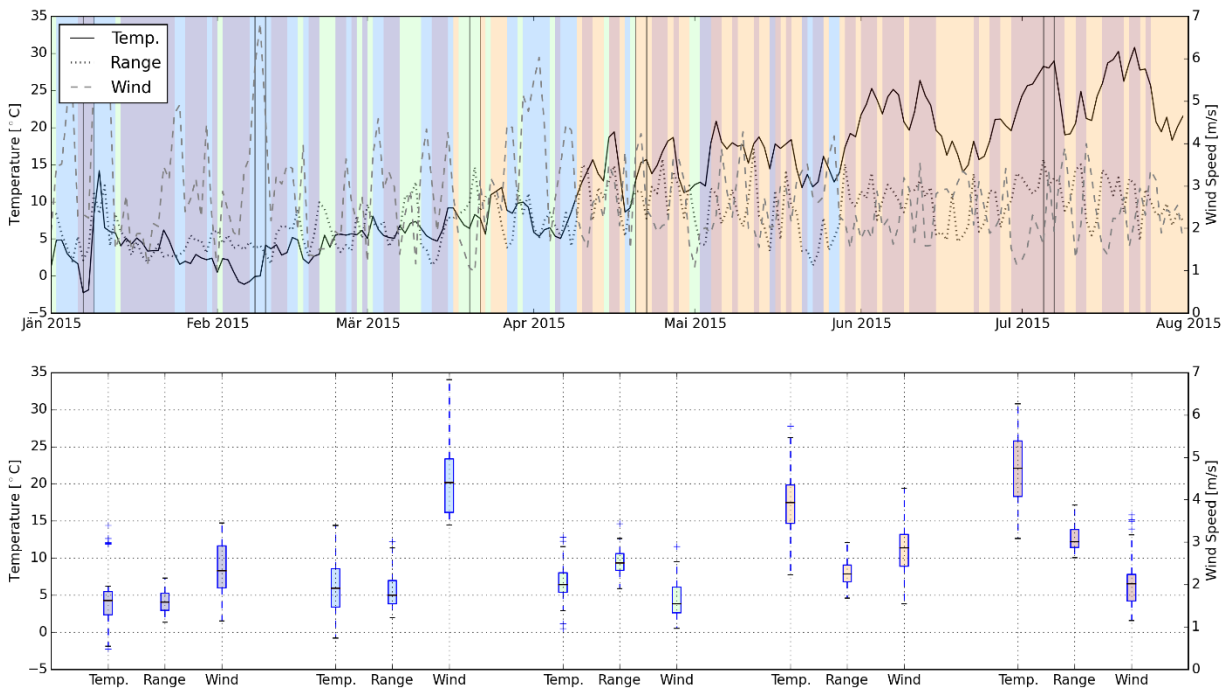


Fig. 2 – Key indicator time series with clustering (top) and boxplot by cluster (bottom)

2.3.2 Urban Canopy Parameters from GIS

In addition to the land cover map, the sub-grid urban model in WRF, the BEP+BEM, requires a morphological description or urban canopy parameters (UCPs) for each urban class in the land cover map. Although there are typical ranges

provided by Stewart and Oke (2012), in Vienna we could extract these values directly from a detailed database of geospatial data made available by the City of Vienna (“Open Government in Vienna,” 2016). This database includes a high-resolution vector map of all the building and land cover

features within the city. It allows for the precise calculation of most of the required UCPs (e.g. height-to-width ratio, pervious fraction, average building height).

In order to extract these values, an algorithm was created with the Quantum GIS software (Quantum GIS Development Team, 2016). It iterates over the region of interest on a 100x100 m grid and calculates the UCPs for each cell. Building height and land use type are included in the metadata of each polygon. With the use of the metadata and the polygon areas, it was straightforward to calculate the necessary area fractions (i.e. pervious, impervious, and urban fractions). The average building height was calculated by weighting the height values with the building footprint area. Likewise, the histogram of height distribution was calculated using the percentage of total building footprint area in 5 ft bins. The height-to-width ratio was computed with a 4-pass raster method (Fig. 3) adopted from Burian et al. (2003).

This algorithm produced a gridded data set with unique UCP values for each cell. However, this level of detail could not be used directly with WRF, as the GIS data is only available within the municipal boundaries and did not cover the entire ROI. Thus, mean values were used for each LCZC.



Fig. 3 – Example of the 4 pass height-to-width ratio results

2.4 Model Setup

The BEP+BEM (Martilli, 2002; Salamanca et al., 2010), under the Bougeaut-Lacarrère at 1.5 degree turbulence scheme, was chosen for this study for its

multilayer urban canopy representation. This sub-grid urban model is currently the most detailed urban representation within the WRF model. The meteorological boundary conditions used for the simulations were derived from the NCEP Final Analysis (FNL from GFS) data at 1° resolution and taken every 6h for each of the two-day simulations. Three nested domains were used to downscale the results to an inner domain with a 500 m resolution (Fig. 4).

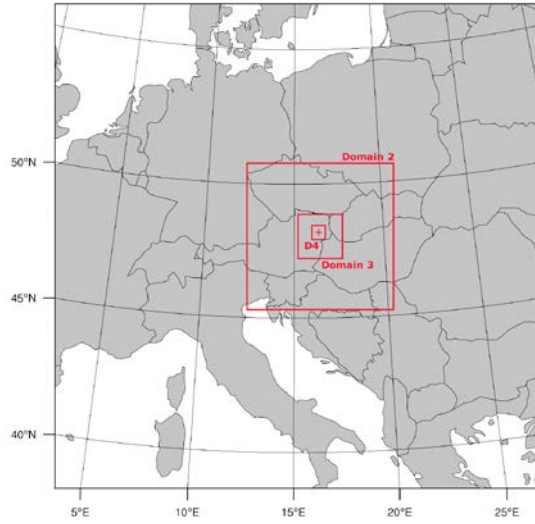


Fig. 4 – WRF nest domain configuration

2.5 Observational Data

We used three different sources for weather data in this study: the Austrian ZAMG, the City of Vienna Department for Environmental Protection (MA22), and Wunderground's Personal Weather Station Network (PWSN). The stations from ZAMG and the MA22 are installed and maintained by official organizations, however they provide sparse coverage (11 stations). On the other hand, the PWSN provides excellent coverage, however these stations are installed and maintained by amateur weather enthusiasts. At the beginning of the study period, January 2015, there were 310 active PWSN stations in our ROI. Although this number has increased to 873 at the time of writing, only those initial stations were included (Fig. 5).

While the PWSN's crowdsourcing approach provides a weather station network with excellent spatial coverage, it introduces several sources of uncertainty. There is no guarantee that recommended standards for installation are followed. In fact, a

number of stations in a similar crowdsourced network in Berlin were setup indoors (Meier et al., 2015).

Furthermore, there is no standard for the type of hardware used. Of the stations that provide information about their hardware type, the majority (78.8 %) are Netatmo stations. While the manufacturer claims acceptable sensor accuracy, these stations are not ventilated or shielded so they have to be set up where they are not in direct sunlight or they risk overheating. Rain and wind gauge accessories are optional and not included with many stations.

In order to address the potential for increased measurement errors as a result of using these unverified stations, we used several data quality control filters to remove erroneous data. These filters reduced the number of stations from 310 to 160. First, all data that greatly exceeded historic global extremes at the Earth's surface were removed. Such extreme values usually represent error codes.

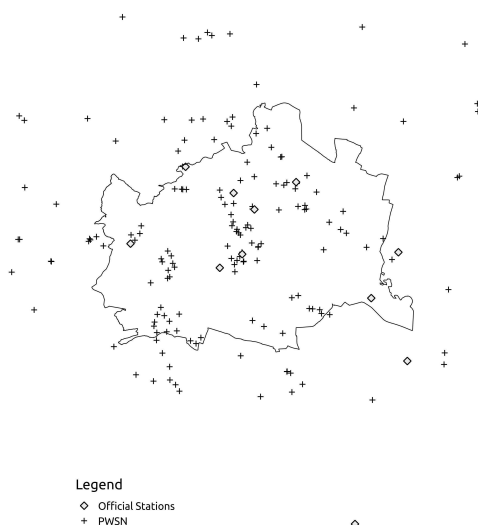


Fig. 5 – Weather station network

Then, outliers were identified with a two-tailed median absolute deviation (double MAD) test to account for skewed distributions and to prevent the outliers from influencing the selection process. The outlying data were then removed and stations that had more than 25 % of their values flagged as outliers were entirely removed from the dataset.

In the final step, the remaining PWSN stations were compared to nearby official stations. The compari-

son included two additional filters designed to target specific types of error. The first targeted weather stations that were installed indoors by comparing the average daily minimum temperature. The second filter targeted overheating due to lack of radiation shielding, ventilation or improper positioning.

3. Results

3.1 Near-Surface Temperature

The modelled temperatures at 2 meters were compared against a network of official stations and the PWSN. In general, the deviations between the model and observations were large (Table 2).

The model tended to overestimate near surface temperature in the cold study periods and underestimate during the warmer two periods. Also, the model tended to perform better during the day when it had both lower RMSE and less bias. However, at a closer examination of the diurnal variation there is no clear pattern between study periods that might allow for a consistent correction factor or transformation (Fig. 6a): (1) both in January and February, the modeled temperatures rose drastically on the second day; (2) despite that temporary deviation, February had the lowest overall RMSE; (3) in March temperatures were overestimated during the night, but daily temperatures showed good agreement; (4) April is the only period to underestimate the temperatures for the whole duration; (5) overall, July and April cases accurately represented the daily temperature ranges and fluctuation.

Table 2 – 2 m Temperature results [°C]

	RMSE	MB	Mean	SD	Min	Max
Overall	3.04	0.62	10.06	10.48	-8.69	33.71
Day	2.65	-0.10	12.48	11.17	-7.54	33.71
Night	3.40	1.34	7.65	9.15	-8.69	32.23
January	3.62	1.87	0.24	3.91	-8.69	10.34
February	1.94	0.84	0.46	2.25	-5.67	5.19
March	3.76	2.66	9.49	3.48	0.46	16.03
April	2.82	-1.74	13.17	3.92	2.11	19.46
July	2.82	-0.31	26.91	4.39	15.02	33.71

3.2 Global Radiation

Global shortwave radiation was overestimated by the model in nearly every study period. This is likely due to both the obstruction of weather station sensors by surrounding obstacles and cloud formation inaccuracies in the model. The February study period had the most accurate modelled solar radiation and even underestimates the solar radiation on the second day, which indicates that the shortwave radiation was not driving the extreme overestimation of temperature during the same period (Table 3).

Table 3 – Global shortwave radiation results [W/m²]

	RMSE	MB	Mean	SD	Min	Max
Overall	87.75	26.88	175.53	274.35	0.00	947.25
January	57.27	14.36	38.12	82.46	0.00	311.11
February	43.88	2.12	38.10	73.94	0.00	420.89
March	90.38	35.38	202.76	266.78	0.00	722.62
April	98.07	26.82	258.62	303.51	0.00	867.09
July	123.31	54.47	340.05	358.25	0.00	947.25

3.3 Wind Speed

Wind speed measurements showed consistently large differences between official weather stations and the PWSN. This was likely due to the difficulty of properly positioning wind gauge instruments. Therefore, for wind measurements only the official stations were used in the analysis (Fig. 6b).

Table 4 – Wind speed results [m/s]

	RMSE	MB	Mean	SD	Min	Max
Overall	2.54	0.42	3.76	2.95	0.00	14.17
Day	2.33	0.19	3.70	2.80	0.00	13.14
Night	2.73	0.65	3.82	3.10	0.05	14.17
January	2.25	0.51	3.15	2.04	0.11	12.72
February	3.69	1.16	7.82	2.16	2.83	14.17
March	1.46	0.41	1.57	0.95	0.01	5.17
April	2.67	0.33	4.05	2.50	0.12	11.86
July	2.07	-0.30	2.22	1.89	0.00	8.85

3.4 Comparison to Reference Station

In an effort to give some context to the magnitude of these errors, the deviations of the model results from near surface temperature observations were compared to the deviation of the airport reference station from all other stations. In effect, we wanted to test how well the model performed relative to the naïve use of nearby airport weather station data in predicting urban conditions (Fig. 7).

The median of the absolute model error was only lower in February and the spread of that error was only significantly smaller in July. Therefore, the model failed both in terms of accuracy and precision when compared to the airport reference station.

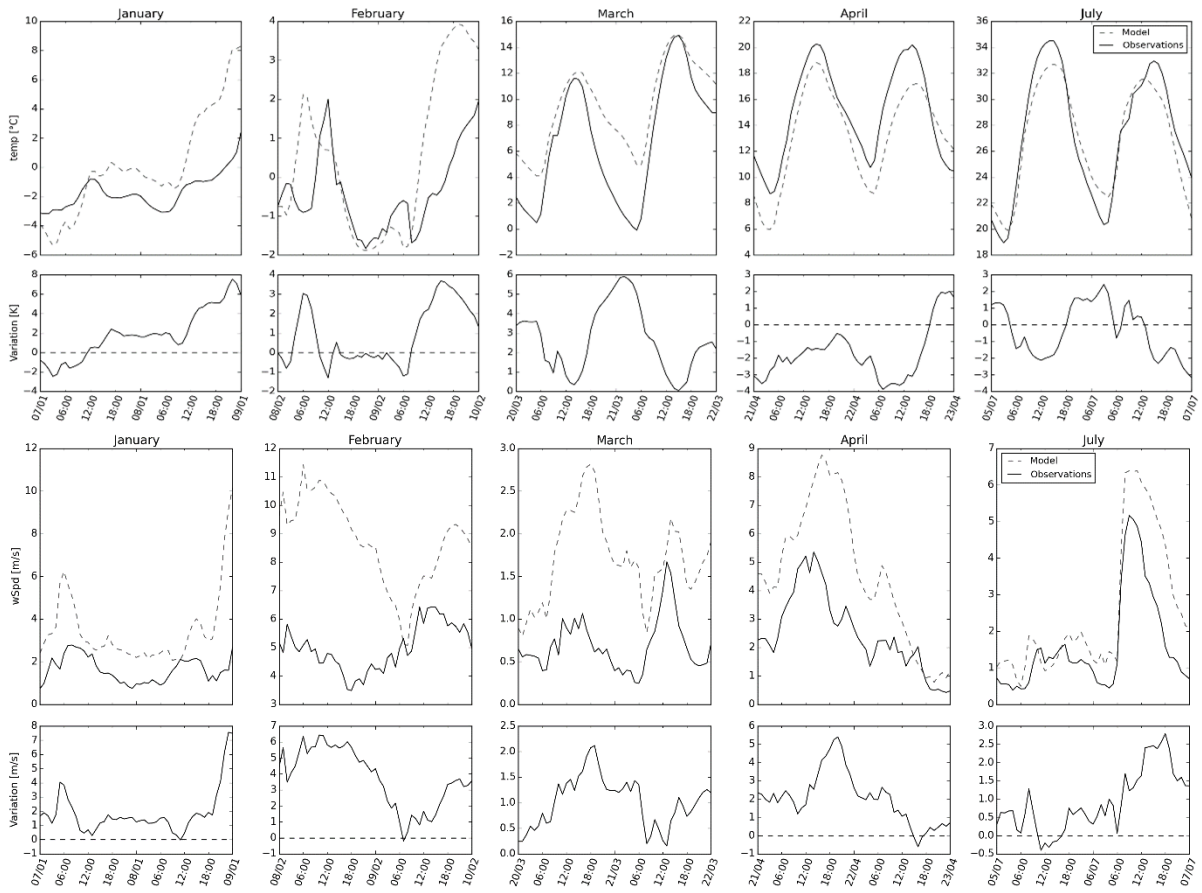


Fig. 6a, 6b – Model vs. Observations for 2 m Temperature (top) and Wind Speed (bottom)

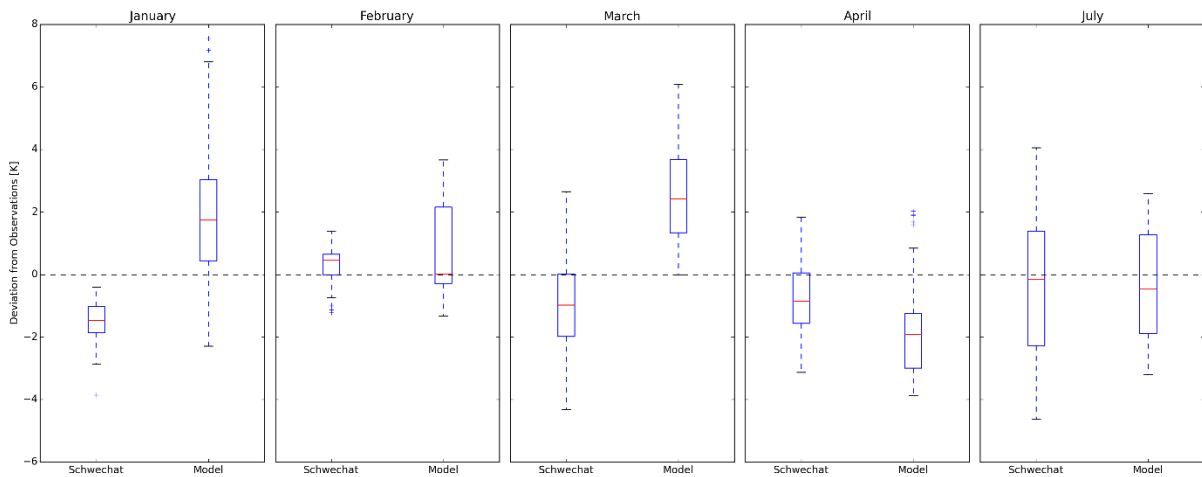


Fig. 7 – Distribution of deviation from 2 m temperature observations for airport reference station and WRF model

4. Discussion

4.1 Suitability for Building Energy Model Boundary Condition

Despite the use of a detailed description of the urban areas, core climatic variables, such as air temperature, were inconsistently reproduced. In fact, as Jänicke et al. (2016) show in their study over the Berlin-Brandenburg region, increasing complex multi-layered UCMs might actually be a source of increased error when compared to a simple slab model.

With such a large degree of error and no consistency in the direction of bias that is both seasonally and diurnally stable, the present study cannot identify the WRF model as an appropriate tool for deriving urban boundary conditions for building energy modeling. Furthermore, the model more often provided worse estimates of the urban near surface temperature than the airport reference station. This suggests that morphing approaches that modify reference measurements or TMY records may be more suitable for urban studies.

4.2 Sources of Error

In order to better isolate the sources of modeling error, a correlation analysis was conducted between the overall RMSE per station and station properties that could be contributing to the observed error. Only the station elevation showed any significant correlation with the error with a correlation coefficient of 0.28. It is a weak relationship and may be related more to the land cover typology than elevation as in Vienna, the urban density decreases with elevation to the West and we have seen a higher rate of error associated with lower density LCZCs (e.g. LCZ 6 and 9) in another ongoing research effort.

Due to the use of unofficial personal weather station data, it was also of interest to examine the stations that showed the best and worst agreement with model results. Interestingly, we saw no consistency between study periods or within types of stations (i.e. official vs. amateur). This indicates that any consistent measurement error that might exist is obscured by the magnitude and spatial variation of the modeling error.

References

- Barnaby, C.S., D.B. Crawley. 2011. "Weather Data for Building Performance Simulation". In: *Building Performance Simulation for Design and Operation*. Abingdon, UK: Taylor & Francis Group.
- Bechtel, B., P.J. Alexander, J. Böhrner, J. Ching, O. Conrad, J. Feddema, G. Mills, L. See, I. Stewart. 2015. "Mapping Local Climate Zones for a Worldwide Database of the Form and Function of Cities". *ISPRS International Journal of Geo-Information* 4(1): 199–219. doi:10.3390/ijgi4010199.
- Bhandari, M., S. Shrestha, J. New. 2012. "Evaluation of Weather Datasets for Building Energy Simulation". *Energy and Buildings* 49: 109–18. doi:10.1016/j.enbuild.2012.01.033.
- Brousse, O., A. Martilli, M. Foley, G. Mills, B. Bechtel. 2016. "WUDAPT, an Efficient Land Use Producing Data Tool for Mesoscale Models? Integration of Urban LCZ in WRF over Madrid". *Urban Climate* 17: 116–34. doi: 10.1016/j.uclim.2016.04.001.
- Burian, S.J., W.S. Han, M.J. Brown. 2003. "Morphological Analyses Using 3D Building Databases: Oklahoma City, Oklahoma". Los Alamos, U.S.A.: LA-UR, Los Alamos National Laboratory.
- Chan, A.L.S. 2011. "Developing Future Hourly Weather Files for Studying the Impact of Climate Change on Building Energy Performance in Hong Kong". *Energy and Buildings* 43(10): 2860–68. doi:10.1016/j.enbuild.2011.07.003.
- Fallmann, J., S. Emeis, P. Suppan. 2014. "Mitigation of Urban Heat Stress—a Modelling Case Study for the Area of Stuttgart". *DIE ERDE—Journal of the Geographical Society of Berlin* 144 (3-4): 202–16.
- Gordon, J.H. 1921. "Temperature Survey of the Salt River Valley, Arizona". *Monthly Weather Review* 49(5): 271–74. doi:10.1175/1520-0493(1921)49<271:TSOTSR>2.0.CO;2.
- Hebbert, M., V. Jankovic. 2013. "Cities and Climate Change: The Precedents and Why They Matter". *Urban Studies* 50(7): 1332–47. doi:10.1177/0042098013480970.

- Howard, L. 1833. *The Climate of London: Deduced from Meteorological Observations Made in the Metropolis and at Various Places around It*. Vol. 2. London, UK: Harvey and Darton, J. and A. Arch, Longman, Hatchard, S. Highley and R. Hunter.
- Jänicke, B., F. Meier, D. Fenner, U. Fehrenbach, A. Holtmann, D. Scherer. 2016. "Urban–rural Differences in near-Surface Air Temperature as Resolved by the Central Europe Refined Analysis (CER): Sensitivity to Planetary Boundary Layer Schemes and Urban Canopy Models". *International Journal of Climatology*, August. doi:10.1002/joc.4835.
- Kotttek, M., J. Grieser, C. Beck, B. Rudolf, F. Rubel. 2006. "World Map of the Köppen-Geiger Climate Classification Updated". *Meteorologische Zeitschrift* 15(3): 259–63.
- Lukacsy, M., C. Fendt. 2015. "Vienna in Figures". Vienna: Vienna City Administration MA23. Accessed on December 15th. <https://www.wien.gv.at/statistik/pdf/viennainfigures.pdf>.
- Martilli, A. 2002. "Numerical Study of Urban Impact on Boundary Layer Structure: Sensitivity to Wind Speed, Urban Morphology, and Rural Soil Moisture". *Journal of Applied Meteorology* 41(12): 1247–66. doi:10.1175/1520-0450(2002)041<1247: NSOUIO>2.0.CO;2.
- Meier, F., D. Fenner, T. Grassmann, B. Jänicke, M. Otto, D. Scherer. 2015. "Challenges and Benefits from Crowd-Sourced Atmospheric Data for Urban Climate Research Using Berlin, Germany, as Testbed". In: *Proceedings of ICUC9 - 9th International Conference on Urban Climate jointly with 12th Symposium on the Urban Environment*. Toulouse, France.
- "Open Government in Vienna" 2016. *Für Eine Offene Stadt*. Accessed February 9. <https://open.wien.gv.at/>
- Pernigotto, G., A. Prada, D. Cóstola, A. Gasparella, J.L.M. Hensen. 2014. "Multi-Year and Reference Year Weather Data for Building Energy Labelling in North Italy Climates". *Energy and Buildings* 72 :62–72. doi:10.1016/j.enbuild.2013.12.012.
- Quantum GIS Development Team. 2016. Quantum GIS Geographic Information System. Open Source Geospatial Foundation Project. <http://qgis.osgeo.org>
- Radhi, H. 2009. "A Comparison of the Accuracy of Building Energy Analysis in Bahrain Using Data from Different Weather Periods". *Renewable Energy* 34(3): 869–75. doi:10.1016/j.renene.2008.06.008
- Salamanca, F., A. Krpo, A. Martilli, A. Clappier. 2010. "A New Building Energy Model Coupled with an Urban Canopy Parameterization for Urban Climate Simulations—part I. Formulation, Verification, and Sensitivity Analysis of the Model". *Theoretical and Applied Climatology* 99(3-4): 331–44. Doi: 10.1007/s00704-009-0142-9.
- Stewart, I.D., T.R. Oke. 2012. "Local Climate Zones for Urban Temperature Studies". *Bulletin of the American Meteorological Society* 93(12): 1879–1900. doi:10.1175/BAMS-D-11-00019.1.

On the Global Performance of Offices with Different Complex Fenestration Systems

Anna Maria Atzeri – Free University of Bozen-Bolzano – annamaria.atzeri@unibz.it

Francesca Cappelletti – University IUAV of Venezia – francesca.cappelletti@iuav.it

Athanasios Tzempelikos – Purdue University – ttempel@purdue.edu

Andrea Gasparella – Free University of Bozen-Bolzano – andrea.gasparella@unibz.it

Abstract

Complex fenestration systems influence indoor comfort conditions and energy consumption in a complex way. If all the involved aspects are not considered jointly since the design phase, buildings can show a deep gap between their planned and real performance, especially when dealing with low energy buildings (Vanhoutteghem et al., 2015). This can be avoided by identifying the design configurations able to provide a trade-off between contrasting requisites: improving comfort conditions while minimizing energy use. This work analyzes and compares different design solutions for an open space office from a global performance perspective. Dependence on the building characteristics and operation strategy has been assessed by comparing two different windows sizes, three glazing systems, and three different approaches to control the shading devices, for a South oriented façade in the climate of Rome. The study has been conducted combining a RADIANCE/DAYSIM lighting simulation with EnergyPlus for the thermal comfort and energy analysis. A set of metrics, able to express both the time constancy and the spatial uniformity of visual and thermal comfort conditions, has been evaluated together with the energy demand for heating, cooling, and lighting. The results show how a global approach allows obtaining a more comprehensive building performance evaluation and, consequently, identifying design solutions capable of enhancing both energy efficiency and occupant comfort.

1. Introduction

Fenestrations with shading devices, or Complex Fenestration Systems (CFSs), due to their thermal and optical complexity can influence indoor visual and thermal conditions, daylight availability and energy consumption in a complicated way. Failure

to consider since the early design phase all the concurrent performance aspects, including comfort conditions, which affect occupants' interactions with the building, is one of the causes for the gap between planned and real performance, especially in low energy buildings.

Even if it is possible to identify different approaches for describing thermal and visual comfort conditions and energy use, a common thread can be unveiled in the recent scientific literature: the need to define an optimal trade-off between energy efficiency and indoor well-being. All the studies clearly underline the importance of considering both energy and comfort performance, when designing a building or a façade component.

The evaluation of the global building performance has been conducted by analyzing energy consumption and indoor comfort conditions in Ferrara et al. (2015), Liu et al. (2015), Mainini et al. (2015), Roetzel et al. (2014), Yao (2014a), David et al. (2011).

In Zhang et al. (2017), a Pareto front representation on a 3D space allows to recognize the non-dominated solution in terms of thermal, visual comfort, and energy consumption for heating and lighting.

Vanhoutteghem et al. (2015) used a contour plot representation of the space heating demand imposing three fixed parameters (U-value, windows orientation and room width-to-depth ratio), and plotting the results for different g-values and glazing-to-floor ratio. Thermal and visual comfort are evaluated defining specific boundaries for overheating occurrences and daylighting availability.

Regardless of the indices used for evaluating the building performance, or the software employed for calculating them, there is the need of synthesizing hourly profiles calculated for some specific points in

the building, and derive zonal and long-term metrics. In Atzeri et al. (2016a), a set of zonal and long-term metrics has been proposed with this aim. Time constancy or spatial uniformity of the considered comfort aspects are at the base of their definition.

In this work, daylight, visual and thermal comfort and global energy consumption for heating cooling and lighting performance have been analysed for a set of 18 open space office building modules in the climate of Rome.

They have been derived from the same reference module, modifying glazing systems, windows size, and control strategies for the shading devices, according to a full factorial plan. The metrics and representations introduced by Atzeri et al. (2016b) have been used to contrast the performances of different CFSs and their operation strategy.

2. Simulation Method and Metrics Calculation

In order to calculate energy and comfort performance of the analyzed building configurations, different simulation codes have been combined. The building model has been developed through Rhinoceros, a commercial 3D computer graphics and computer-aided design (CAD) application software. Grasshopper, a graphical algorithm editor tightly integrated with Rhinoceros 3D modelling tools, has been used for the parametric definition of the different configurations. Daylight, glare, and electric lighting annual profiles have been calculated in a RADIANCE/DAYSIM based lighting simulation software (Roudsari et al., 2013) and then they have been post-processed through MatLab to obtain artificial lighting and roller shades operation schedules useful for energy and thermal comfort simulations with EnergyPlus and to calculate daylighting, visual, and thermal comfort metrics. Indoor visual comfort conditions have been assessed by means of the enhanced Daylight Glare Probability simplified (eDGP_s) index, calculated on an annual basis according to Wienold (2009):

$$eDGP_s = c_1 \cdot E_v + c_2 \cdot \log_{10} \left[1 + \sum_{i=1}^n \left(\frac{L_{s,i}^2 \cdot \omega_{s,i}}{E_{s,i}^{1.87} \cdot p_i^2} \right) \right] + c_3 \quad (1)$$

Thermal comfort conditions have been assessed by means of the Predicted Mean Vote according to EN ISO 7730:2005 but using a modified Mean Radiant Temperature (MRT) that takes into account the direct and diffuse solar radiation passing through the transparent surfaces and striking the occupants, according to La Gennusa et al. (2005; 2007):

$$MRT_{irr}^4 = \sum_{i=1}^n F_{s \rightarrow j}^{in} + \frac{\alpha_{irr,b}}{\epsilon \sigma} f_p J_{bn}^{in} \quad (2)$$

For all the RADIANCE based simulations, the ambient bounce (-ab) parameter has been set to 5, in order to be able to consider even the inter-reflection influence deeper in the room.

The natural light distribution has been obtained on a grid of 81 points located 0.8 m above the floor and excluding a peripheral band 0.5 m deep along the walls, even if the results are averaged for being represented for 9 positions to be consistent with the comfort analysis. Thermal and visual comfort indices have been calculated on a grid of 9 points. Thermal comfort points are 0.6 m above the floor, corresponding to the height of a sitting person's stomach. Instead, 1.2 m has been chosen for visual comfort analysis, as the reference height for the line of sight for a sitting person in studies dealing with visual comfort, suggested by several regulations.

The annual energy demand for heating, cooling, and lighting have been calculated by means of EnergyPlus and expressed in terms of primary energy per unit of surface. The simulation has been performed with an hourly time step.

All the other simulation settings (observers' view direction, HVAC, and artificial lighting system characteristics) have already been described in more detail in Atzeri et al. (2016b).

3. Model Setup

Being used especially during daytime, offices are characterized by an even more urgent necessity of balancing thermal and visual comfort requisites, in order to be able, for example, to maximize as much as possible solar gains and daylight contributions, avoiding high cooling demand, glare, and thermal discomfort. These aspects make them an ideal target for this study.

An open space office located in Rome, Italy (Lat. N 42° 54' 39'' HDD18: 1420 K d - CDD18: 827 K d) has been chosen for the analysis. Hourly weather data for one year have been used as climatic inputs (US DOE, 2009).

The workspace floor area is 100 m² and the internal height is 3 m. The opaque envelope is made of an internal clay block layer, 0.2 cm thick, and an external insulation layer, 0.12 m thick, with a thermal transmittance of 0.26 W m⁻² K⁻¹ complying with the requisites of the national legislation for the considered climatic conditions. The entire envelope disperses to the outdoor environment, except the floor, which is in contact with a conditioned space, and is considered adiabatic. To model the interaction between light and the room surfaces, walls and ceiling, have been assumed with a reflectance of 70 %, the floor 30 % and the ground 20 %. Different design configurations have been analysed, combining two values for the window dimensions and three glazing types. Roller shades have been chosen due to their widespread availability, especially in buildings belonging to the tertiary sector. Table 1 shows the configuration parameters used, together with the labelling key to represent the different cases in the following.

The optical and solar properties of the roller shades, characterized by a nominal solar and visual transmittance of 0.05, were determined through angular measurements, and calibrated using a validated model (Atzeri et al., 2016b).

Table 1 – Design configuration parameters

Parameters	Values	Labels
Window Wall Ratio (WWR)	45 %	S1
	75 %	S2
Glazing Systems (GS)	1) $U_{gl} = 1.1 \text{ W m}^{-2} \text{ K}^{-1}$; $\tau_{vis} = 0.77$; SHGC = 0.62;	HH
	2) $U_{gl} = 1.1 \text{ W m}^{-2} \text{ K}^{-1}$; $\tau_{vis} = 0.72$; SHGC = 0.36;	HL
	3) $U_{gl} = 1.1 \text{ W m}^{-2} \text{ K}^{-1}$; $\tau_{vis} = 0.33$; SHGC = 0.33;	LL

3.1 Roller Shades Control Strategies

Several researchers underlined that shading devices can lead to a reduction of the building cooling energy needs together with an increase of the indoor environmental quality, related to thermal and visual comfort. Regardless of the physical properties that

characterize the fabric material, the possibility to change progressively the shades position can facilitate the balance between solar and glare protection, daylight availability and external view. Even if shades can be operated directly by the occupants, different studies underlined that the manual operation tends to show some hysteresis. Once completely closed, the shades tend to remain in this state for a long period (Konstantoglou and Tsangrassoulis, 2016). The possibility to control them automatically is essential, in particular to avoid the gap between the planned and the real performance of buildings. Different configurations and control approaches have been proposed and analysed in literature. Kapsis et al. (2010) proposed a motorized roller shade that opens from top to bottom. In this way, the roller shade covers the bottom part of the window, while allowing daylight to enter from the top part of the window, thus ensuring uniform light distribution. Two algorithms, aiming at maximizing solar heat gains while reducing heat losses during the heating season, have been suggested by Bastien and Athienitis (2012). One, called *global solar control*, operates the shades based on the global horizontal radiation level, independently of the shades orientation. The other, defined as *individual solar control*, allows controlling shades with different orientations using their respective incident solar radiation level. Both the controls consider only an open-closed shades position. An open-closed operation is also described in Shen and Tzempelikos (2012), where the shades are automatically closed when incident beam radiation on the facade is higher than 20 W m⁻² and outside work hours. The same authors (Shen and Tzempelikos, 2014) defined a control based on the effective daylight transmitted into the space, used also in Konstantzos et al. (2015). The effective daylight control has been compared to a work plane protection control, where the shading position is a function of the solar profile angle and the distance between the occupant and the window, and to a fully closed state of the shades. Also, in Singh et al. (2015) an open-closed control mode has been used, closing the shade when the glare threshold is exceeded. Xiong and Tzempelikos (2016) considered 11 possible shades positions, choosing the more convenient as the highest that is able to maximize daylight while maintaining visual comfort.

Three visual comfort criteria have been used, respectively based on DGP, vertical illuminance (E_v) and effective illuminance. If all shading positions fail to pass the criterion, the shades are left closed. In this study, three different approaches to control the roller shades have been considered:

1. Open-closed operation (CTRL1 in the following)
The shades state is determined according to the illuminance level measured on the workplane position closest to the transparent surface: 500 lx is the opening threshold and represents the desired work plane illuminance; 2000 lx is considered the limit value to avoid visual discomfort (Nabil and Mardaljevic, 2006). The shades state depends also on their state in the previous time step: if the shades were already closed and in the current the workplane illuminance is still larger than 500 lx, the shades will be kept closed.

The two next controls are based on the certainty that to ensure a comfortable visual environment it is not necessary for shades to operate in an open/closed mode. On the contrary, they can move to intermediate positions that depend on solar position, sky conditions, and solar penetration depth relative to the occupant position.

2. Solar adaptive operation (CTRL2)

The shade height (h_{sh}) with respect to the work plane height is calculated as:

$$h_{sh} = D \cdot \tan(\Omega) \quad (3)$$

where D is the distance of the working plane from the facade, and Ω is the solar profile angle (function of solar altitude α and surface solar azimuth γ).

This control method (Tzempelikos and Shen, 2013) allows preventing direct sunlight from falling on the work plane area but can cause glare and overheating problems especially in summer. Moreover, when French windows are considered, this control does not allow closing completely the shades, due to the reference height used in the equation. At the same time, it is very simple to implement, because a pre-calculated schedule can be applied according to the specific building location.

3. Effective daylight operation (CTRL3)

The effective illuminance E_{eff} (Shen and Tzempelikos, 2014) represents the overall illuminance transmitted through the window, measured on the same plane, considering both the shaded (E_{sh}) and unshaded (E_g) parts of the window:

$$E_{eff} = \frac{\sum_i (E_{gi} \times A_{gi} + E_{shi} \times A_{shi})}{\sum_i (A_{gi} + A_{shi})} \quad (4)$$

Once fixed a reference value for the work plane illuminance, it is possible to determine a limit value for E_{eff} that represents a threshold, called E_{esp} , analyzing the correlation between the two quantities in the case of CTRL2. Using this threshold, a new equation to calculate the shades height can be defined:

$$h_{sh} = \frac{(E_{esp} - E_{sh}) \cdot H}{E_g - E_{sh}} \quad (5)$$

Where H represents the total window height. Then, the final shades height can be iteratively chosen as the smaller value between those calculated using Equations (1) and (3):

$$h_{sh} = \min \left\{ D \cdot \tan \Omega, \frac{(E_{esp} - E_{sh}) \cdot H}{E_g - E_{sh}} \right\} \quad (6)$$

All the three controls close the shades completely during the unoccupied hours.

4. Results and Discussion

Results will be represented and discussed by means of the zonal and long-term performance metrics as described in Atzeri et al. (2016b), namely availability, spatial availability, usability, time, and through the energy demand for heating, cooling, and lighting. Since the performance depends on the shade operation, Fig. 1 compares the shades position obtained by applying the three different controls previously described. For space reasons, only the small windows equipped with HH glazing systems have been considered. The yellow color ramp allows recognizing the shades opening percentage from 0 (black) to 100 % (white).

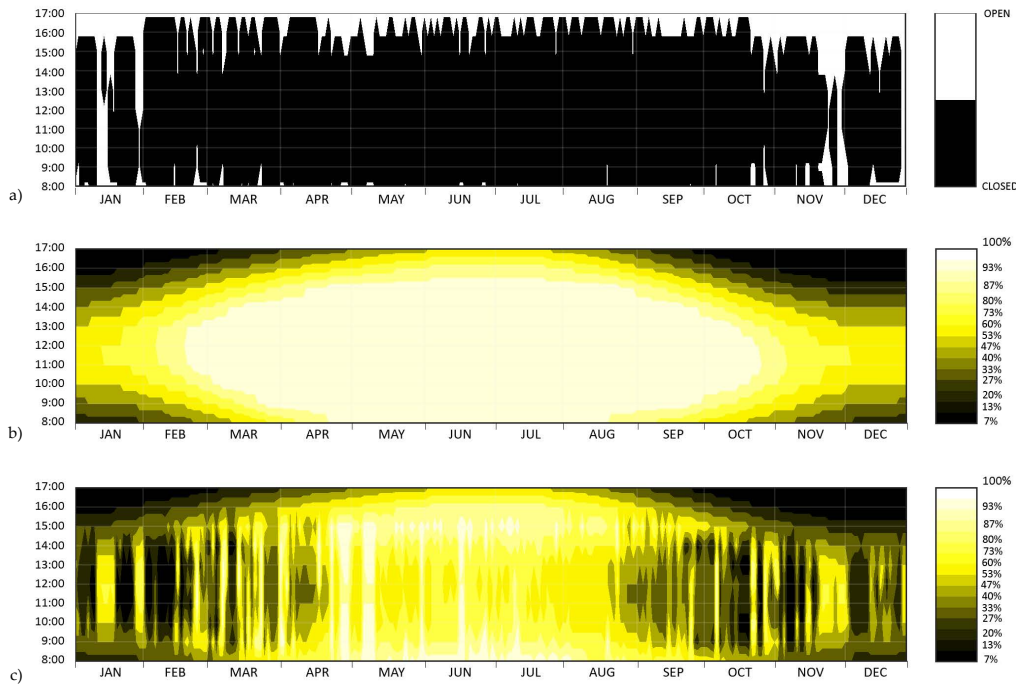


Fig. 1 – Temporal plot for the shades' opening percentage according to CTRL1 (a), 2 (b) and 3 (c) for the small window S1, with HH glazing system

Fig. 2 allows the comparison of the shades operation according to the three control strategies for all the glazing systems. The yellow columns represent the number of hours during which shades are open, the black ones the number of hours with closed shades, and the grey ones the number of hours when shades are in an intermediate position (only for CTRL2 and 3). With the exception of CTRL2, which considers only the sun position to manage the shades, the shades position frequency changes with the control strategy and with the type of glazing.

Tables 2 and 3 point out for how long, considering CTRL2 and CTRL3, the roller shades remain at a certain distance from the windowsill. The duration is expressed as time percentage compared to the annual occupation hours. In particular, looking at Table 3 it can be noticed that, since the reference height of the working plane is 0.8 m, with CTRL2 the shades cannot assume a distance from the windowsill lower than 0.8 m.

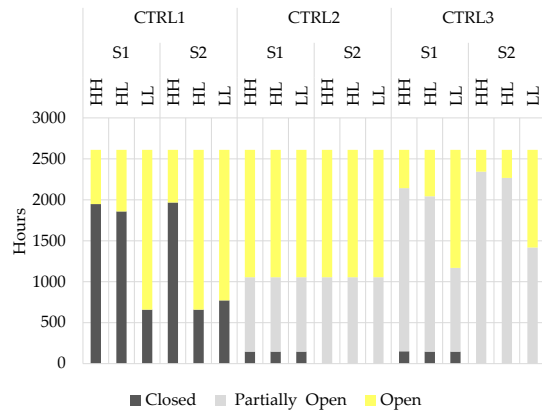


Fig. 2 – Shades opening state during occupancy period according to the control strategy for the different glazing systems

On the contrary, when the CTRL3 equation is used, the shades can overcome this limit to reduce excessive workplane illuminance and with some impact on possible overheating and discomfort conditions, as underlined in the following.

Table 2 – Shades position in small windows S1: percentage of occupancy period for different heights from windowsill

Height (m)	CTRL2			CTRL3		
	HH	HL	LL	HH	HL	LL
1.5	60	60	60	18	22	55
1.4	2	2	2	4	3	2
1.3	2	2	2	3	4	2
1.2	2	2	2	4	6	3
1.1	2	2	2	6	7	3
1	3	3	3	7	6	2
0.9	3	3	3	7	6	4
0.8	4	4	4	7	6	5
0.7	6	6	6	7	7	7
0.6	3	3	3	8	7	3
0.5	3	3	3	6	6	3
0.4	1	1	1	4	5	1
0.3	2	2	2	5	5	2
0.2	1	1	1	5	4	1
0.1	0	0	0	3	2	0
0	6	6	6	6	6	6

Table 3 – Shades position in large windows S2: percentage of occupancy period for different heights from windowsill

Height (m)	CTRL2			CTRL3		
	HH	HL	LL	HH	HL	LL
2.5	60	60	60	10	13	46
2.4	2	2	2	2	1	2
2.3	2	2	2	2	1	2
2.2	2	2	2	1	3	3
2.1	2	2	2	2	2	3
2	3	3	3	3	3	2
1.9	3	3	3	4	3	4
1.8	4	4	4	4	3	4
1.7	6	6	6	4	4	5
1.6	3	3	3	3	4	4
1.5	3	3	3	5	5	4
1.4	1	1	1	4	5	3
1.3	2	2	2	6	6	4
1.2	1	1	1	6	5	3
1.1	0	0	0	4	4	1
1	1	1	1	5	4	2
0.9	1	1	1	5	5	2
0.8	4	4	4	9	9	6
0.7	0	0	0	5	4	1
0.6	0	0	0	4	3	0
0.5	0	0	0	2	2	0
0.4	0	0	0	2	2	0
0.3	0	0	0	3	3	0
0.2	0	0	0	3	3	0
0.1	0	0	0	3	1	0
0	0	0	0	0	0	0

4.1 Daylighting Performance

Table 4 shows the spatial distribution of Daylight Autonomy, DA₅₀₀ through the office, for all the design configurations and the three shading controls proposed.

Starting with S1 cases, with CTRL1, DA₅₀₀ is insufficient regardless of the position analyzed, and, comparing the three glazings, only LL guarantees a slight sufficient DA in the first row close to the windows.

As expected, with CTRL2, DA values and distribution improve for all the glazings. HH and HL have the best performance in all the positions and with HH the highest DA is obtained in the third row. With LL the DA distribution is similar to the one obtained with CTRL1, even if in this case useful values can be reached at least in the row close to the window.

With CTRL3, again HH and HL guarantee the best performance, even if the DA distribution is less homogeneous. With glazing LL, DA is acceptable only in the first row and useless in the second and third rows. Compared to CTRL2, the values of DA in the first row are almost the same, in the second almost half, and, in the third row, the situation is as negative as with CTRL1.

Cases with windows S2 have the same trend as cases S1, but the large windows allow higher DA in the second rows in almost all the cases and controls.

Table 5 shows the spatial Daylight Autonomy, sDA, for the three controls, the three glazings and the two window areas: with CTRL1, glazings HH and HL have sDA null, while glazing LL guarantees an sDA of 33 % that coincides with the first row from the window. With CTRL2, glazings HH and HL perform in the same way and guarantees 67 % sDA, that means the acceptable DA in the first two rows, while glazing LL guarantees adequate DA only in the first row. Finally, with CTRL3, adequate DA is guaranteed only in the first row with all the three glazings. The situation is very similar with large windows even though with CTRL2 100 % sDA is reached using HH and HL glazings. Concluding CTRL2 allows obtaining the best performance in terms of daylight availability, regardless of the window dimensions and with all the glazing types.

Concerning the usability of the space, in terms of the fraction of space with a sufficient daylighting level, e.g. 500 lx, in the same moment, Fig. 3 shows the percentage of the occupancy time for different values of Daylight Usability. The control that guarantees the higher DU is CTRL2 with HH and HL glazing: with small windows, DU is 90 % for the 22 % of

the time with HH and 13 % of the time with HL glazing, and it is about 50 % for large windows, with both HH and HL glazing. Nevertheless CTRL3 always perform better than CTRL1. These quantities represented by a red solid line in the figure, are the time Daylight Usability (tDU), summarized in Table 5. The threshold of 90 % of Daylight usability is never reached by the other cases with both S1 and S2.

4.2 Visual Comfort

The VCA distribution (Table 4), underlines that for almost all the glazing systems, regardless the control approach, the window dimension and the occupant's position, are able to ensure a comfortable environment from a visual point of view.

The only design configurations that are not able to fulfil the required environmental conditions, are those coupling CTRL2 with HH and HL glazing systems, for the left and central points on the first row. Particularly critical are the values related to the larger windows, where the DGP lies above 0.35 for more or less half of the occupancy time. sVCA values in Table 5, confirm what has been previously pointed out.

When applying CTRL2 to HH or HL glazing systems, the fraction of space in the room in visual comfort conditions for at least 90 % of the reference period lies always under the threshold selected. The most critical condition is associated to the largest windows equipped with HH glazing; where DGP is lower than 0.35 only for 66 % of the room.

When VCU is considered (Fig. 3), HH and HL glazings coupled with CTRL2 show a reduced fraction of space simultaneously in visual comfort with respect to CTRL1 and 2.

4.3 Thermal Comfort

Thermal comfort availability is very high (higher than 90 %) in all the points in the space for almost all the cases (Table 4). In particular, CTRL1 ensure a good homogeneity with HH and HL glazings, while with LL, TCA falls between 80 % and 90 % in the row close to the windows and in the middle point in particular. The performance with CTRL3 is similar: TCA is very homogeneous in the space and only the position in the middle of the first row has a TCA between 80 % and 90 %. CTRL2 assures higher TCA

than the other controls in the rows far from windows, while in the points closer to the windows TCA is particularly low (57 %) in the point in the middle of the first row, close to the window. Consequently, it is possible to see that Spatial Thermal Comfort Availability, sTCA, is 100 % with CTRL1 and glazing HH and LL, with both large and small windows, and with CTRL3 is 100 % with HH and HL but only for small windows. With glazing HH and HL, CTRL1 and CTRL3 are the best controls for small windows, while CTRL1 is the best for large windows. With glazing LL the three controls perform in the same way guaranteeing 89 % of sTCA in cases with small windows and 67 % with large windows. Concerning the contemporaneity of the comfort achievement over the space, Table 5 reports time Thermal Comfort Usability: CTRL1 guarantees 90 % of usability for about the 90 % of the time with HH and HL glazings, with both large and small windows, while the percentage decreases with LL glazing (87 % with small windows and 76% with large windows). CTRL2 gives the worst results in terms of time usability especially with HH glazing, while CTRL3 gives intermediate results: with small windows the performance is better than with large windows and HL glazing performs better than HH and LL glazings.

4.4 Energy Consumption

A previous work (Atzeri et al., 2014) underlined how the use of shading devices can affect the energy performance in different ways, depending on their optical properties and position, on windows orientation and size. In this study, the analysis has been concentrated mainly on the effect of different shades controls, pointing out their possible influence in terms of energy consumption. The primary energy demand for heating, cooling, and artificial lighting is plotted in Fig. 4 for all the cases investigated.

Generally, CTRL2 and CTRL3 give the best results in terms of artificial light demand, reducing considerably energy consumption compared to CTRL1. When the shades position mainly depends on the glazing system properties, as it happens for CTRL1, LL glazing systems perform better. Their lower visual transmittance allows shades to stay open for longer period than with other glazing, maximizing the use of natural light. On the contrary, when

CTRL2 and CTRL3 are considered, the best performance derives from HH and HL. These glazing systems are characterized by a very similar trend across the different design configurations, due to their close visual transmittance. On the contrary, when cooling consumption is considered, different control systems can produce different trends. It happens especially using CTRL2. It determines a longer shades opening period along the year and, when it is applied to the larger windows, it does not allow the shades to be less than 0.80 m from the bottom edge of the windows, thus increasing solar gains. The same behavior can be pointed out considering CTRL3 results, but in this case, the difference between HH and HL glazing systems is less evident.

HH and HL, except for CTRL2 applied to large windows for the reason described above, perform better than LL for the cooling aspects.

Actually, when a control system based on illuminance values, is applied, glazing systems allow a bigger amount of natural light entering the confined environment, together with the solar radiation. It can be particularly critic when a climatic location, as Rome, where cooling demands represent the main source of energy consumption, is considered.

Concerning the total energy demand, HL glazing systems, coupled with CTRL3, provide the best performance, reducing simultaneously both artificial lighting and cooling demand.

Table 4 – DA₅₀₀, VCA₃₅ e TCA₁₀ for small and large windows. Tables represents the room plan, the thick border the walls, and the missing border the window position

		CTRL 1			CTRL 2			CTRL 3		
		HH	HL	LL	HH	HL	LL	HH	HL	LL
DA	SS1	0 0 0	0 0 0	0 0 0	25 31 26	16 24 18	0 0 0	0 0 0	0 0 0	0 0 0
	SS2	1 1 2	2 3 3	3 4 3	62 67 66	63 66 64	10 14 11	38 47 40	42 48 39	4 8 6
	SS2	16 17 17	19 20 20	53 58 56	84 86 85	83 85 84	70 75 73	83 86 85	82 85 84	70 75 73
VCA	SS1	100 100 100	100 100 100	100 100 100	100 100 100	100 100 100	100 100 100	100 100 100	100 100 100	100 100 100
	SS2	100 100 100	99 100 100	99 100 100	100 100 100	100 100 100	100 100 100	100 100 100	100 100 100	100 100 100
	SS2	99 99 100	99 99 100	97 98 100	74 76 94	78 82 96	99 99 100	98 99 100	98 99 100	99 99 100
TCA	SS1	91 92 91	91 92 91	92 92 92	95 93 95	93 93 93	93 93 93	92 92 92	92 92 92	93 93 93
	SS2	91 91 91	92 91 92	92 92 92	93 93 93	93 93 93	93 93 93	92 92 92	92 92 92	93 93 93
	SS2	91 91 91	91 91 91	92 88 92	89 76 89	92 88 92	93 89 93	92 90 92	92 91 92	93 89 93
TCA	SS1	91 92 92	92 92 92	92 92 92	95 93 94	94 94 94	94 93 93	92 92 92	92 92 92	93 93 93
	SS2	92 92 92	92 92 92	92 92 92	92 92 92	93 93 93	93 93 93	92 92 92	92 92 92	93 93 93
	SS2	91 90 91	92 91 92	88 78 87	73 57 73	87 73 86	87 73 87	89 87 89	91 89 91	89 81 89

Table 5 - Spatial Availability and Time Usability for small and large windows

		Spatial Availability									Time Usability								
		CTRL1			CTRL2			CTRL3			CTRL1			CTRL2			CTRL3		
		HH	HL	LL	HH	HL	LL	HH	HL	LL	HH	HL	LL	HH	HL	LL	HH	HL	LL
D	SS1	0	0	33	67	67	33	33	33	33	0	0	0	23	17	0	0	0	0
	SS2	0	0	33	100	100	33	33	33	33	0	0	0	53	49	0	0	0	0
VC	SS1	100	100	100	78	78	100	100	100	100	99	99	97	72	77	99	98	98	99
	SS2	100	100	100	67	67	100	100	100	100	99	99	98	46	51	99	99	99	99
TC	SS1	100	100	89	67	89	89	100	100	89	90	90	87	75	86	87	89	90	88
	SS2	100	100	67	67	67	67	67	89	67	89	90	76	56	71	71	85	87	79

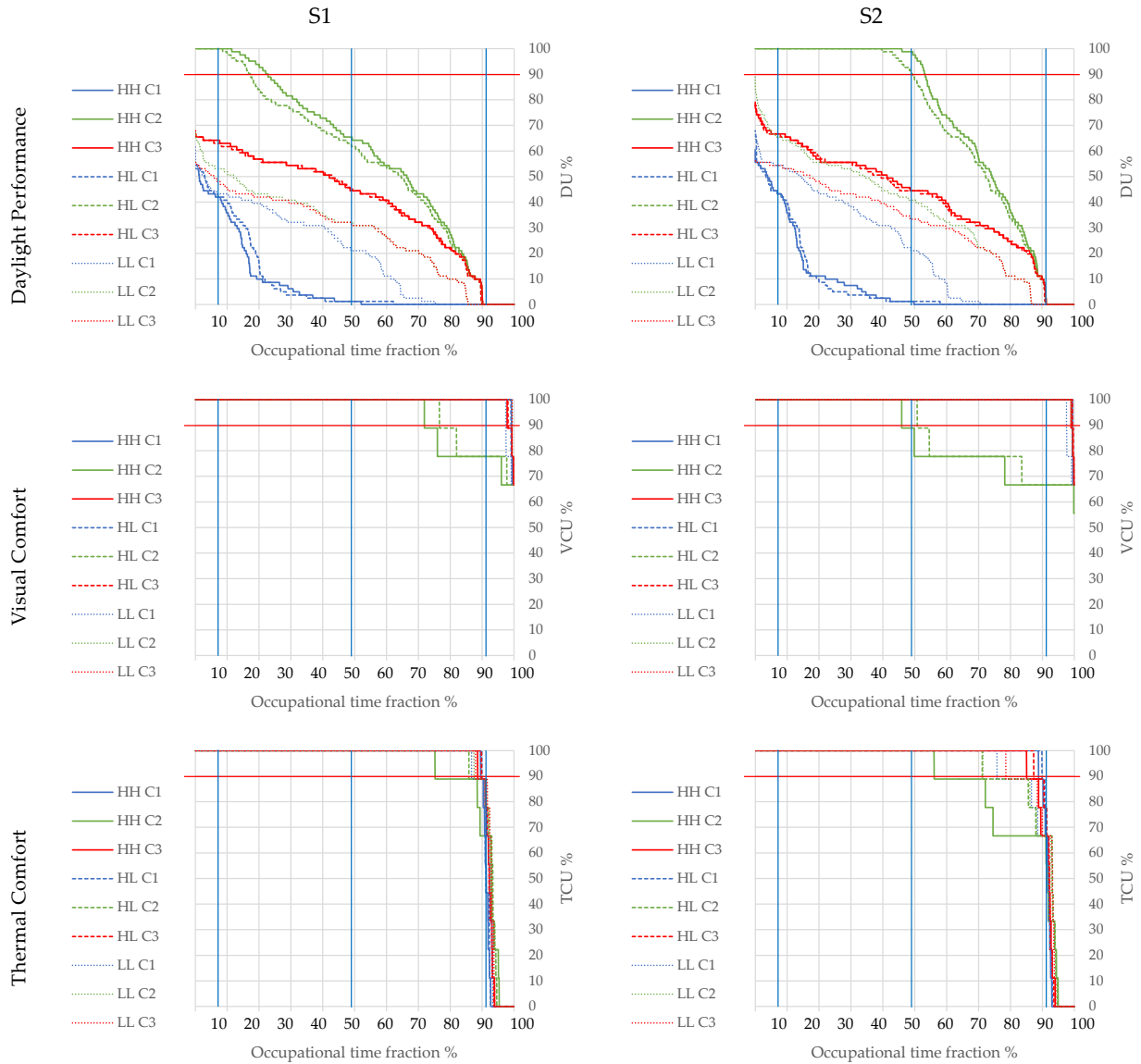


Fig. 3 – Daylight Usability, Visual Comfort Usability, and Thermal Comfort Usability for small and large windows

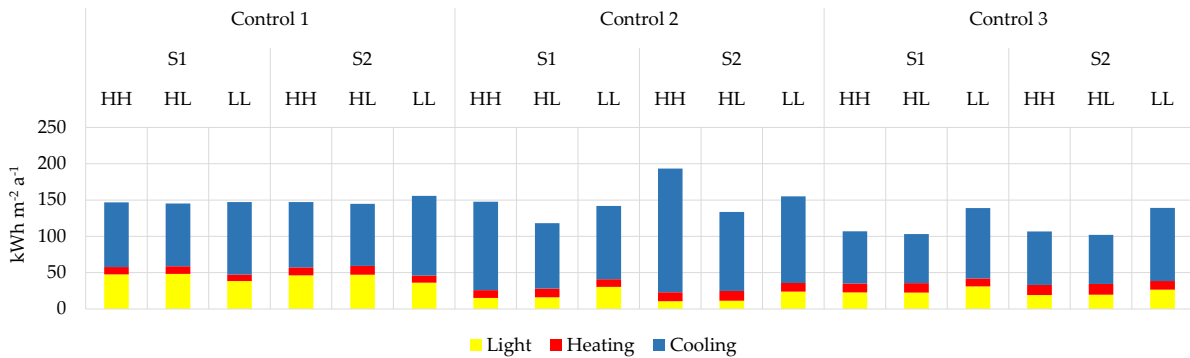


Fig. 4 – Primary Energy demand for artificial lighting, heating and cooling

5. Conclusion

In this paper, the integrated performance of different CFSs coupled with three control approaches for shading devices is presented. The first is characterized by a standard open-closed operation, while the others are able to assume intermediate positions according to solar position and effective daylight. The building's *global* performance has been assessed, considering thermal and visual comfort conditions and daylighting availability besides overall energy demand. Results have been expressed in terms of availability, spatial availability, usability, time usability (Atzeri et al., 2016b), and energy demand for heating, cooling, and lighting.

Outcomes underline that advanced controls for shades operation, not working with an on-off mode, are able to ensure a suitable indoor environment and to reduce energy consumption. However, performance obtained with advanced controls is more affected by the type of glazing system adopted which determines different amounts of energy demand. Furthermore, it has been demonstrated that CTRL3 guarantees a more homogeneous distribution of the natural light, even in a deep space as the one used in this study.

Concerning CTRL2, as already underlined in Tzempelikos and Shen (2013), the results confirm that, although this operation mode is very simple to apply, it is not able to ensure the same comfort performance, in terms of visual and thermal quality, nor the same energy demand, as CTRL1 and CTRL3. Beyond the previous advantages, the possibility to locate the shades on intermediate positions can help the occupants to maintain a closer connection to the outdoor environment, improving their perception of the confined space.

Acknowledgement

This study has been funded by the project "Klimahouse and Energy Production" in the framework of the programmatic-financial agreement with the Autonomous Province of Bozen-Bolzano of Research Capacity Building and by the internal project "IBAS - Intelligent Building Automation System for

optimization of energy consumptions and indoor environmental quality" of the Free University of Bozen-Bolzano.

References

- Atzeri, A.M., F. Cappelletti, A. Gasparella. 2014. "Internal versus external shading devices performance in office buildings". *Energy Procedia* 45: 463–472. doi: 10.1016/j.egypro.2014.01.050.
- Atzeri, A.M., F. Cappelletti, A. Gasparella, A. Tzempelikos. 2016a. "On the representation of the thermal and visual behavior of a roller shade material: comparison between different simulation models". In: *Proceedings of the 3rd High Performance Buildings Conferences at Purdue*. West Lafayette, U.S.A.: Purdue University.
- Atzeri, A.M., F. Cappelletti, A. Tzempelikos, A. Gasparella. 2016b. "Comfort metrics for an integrated evaluation of buildings performance". *Energy and Buildings* 127: 411–424. doi: 10.1016/j.enbuild.2016.06.007.
- Bastien, D., A.K. Athienitis. 2012. "A Control Algorithm for Optimal Energy Performance of a Solarium/Greenhouse with Combined Interior and Exterior Motorized Shading". *Energy Procedia* 30: 995–1005. doi: 10.1016/j.egypro.2012.11.112.
- David, M., M. Donn, F. Garde, A. Lenoir. 2011. "Assessment of the thermal and visual efficiency of solar shades". *Building and Environment* 46(7): 1489–1496. doi: 10.1016/j.buildenv.2011.01.022.
- Ferrara, M., M. Filippi, E. Sirombo, V. Cravino. 2015. "A simulation-based optimization method for the integrative design of the building envelope". *Energy Procedia* 78: 2608–2613. doi: 10.1016/j.egypro.2015.11.309.
- Kapsis, K., A. Tzempelikos, A.K. Athienitis, R.G. Zmeureanu. 2010. "Daylighting performance evaluation of a bottom-up motorized roller shade". *Solar Energy* 84(12): 2120–2131. doi:10.1016/j.solener.2010.09.004.
- Konstantoglou, M., A. Tsangrassoulis. 2016. "Dynamic operation of daylighting and shading systems: A literature review". *Renewable and Sustainable Energy Reviews* 60: 268–283. doi: 10.1016/j.rser.2015.12.246.

- Konstantzos, I., A. Tzempelikos, Y.C. Chan. 2015. "Experimental and simulation analysis of daylight glare probability in offices with dynamic window shades". *Building and Environment* 87: 244–254. doi: 10.1016/j.buildenv.2015.02.007.
- La Gennusa, M., A. Nucara, M. Pietrafesa, G. Rizzo. 2007. "A model for managing and evaluating solar radiation for indoor thermal comfort". *Solar Energy* 81(5): 594–606. doi: 10.1016/j.solener.2006.09.005.
- La Gennusa, M., A. Nucara, G. Rizzo, G. Scaccianoce. 2005. "The calculation of the mean radiant temperature of a subject exposed to the solar radiation - A generalised algorithm". *Building and Environment* 40(3): 367–375. doi: 10.1016/j.buildenv.2004.06.019.
- Liu, M., K.B. Wittchen, P.K. Heiselberg. 2015. "Control strategies for intelligent glazed façade and their influence on energy and comfort performance of office buildings in Denmark". *Applied Energy* 145: 43–51. doi: 10.1016/j.apenergy.2015.02.003.
- Mainini, A.G., D. Bonato, T. Poli, A. Speroni. 2015. "Lean Strategies for Window Retrofit of Italian Office Buildings: Impact on Energy Use, Thermal and Visual Comfort". *Energy Procedia* 70: 719–728. doi: 10.1016/j.egypro.2015.02.181.
- Nabil, A., J. Mardaljevic. 2006. "Useful daylight illuminances: A replacement for daylight factors". *Energy and Buildings* 38(7): 905–913. doi: 10.1016/j.enbuild.2006.03.013.
- Roetzel, A., A. Tsangrassoulis, U. Dietrich. 2014. "Impact of building design and occupancy on office comfort and energy performance in different climates". *Building and Environment* 71: 165–175. doi: 10.1016/j.buildenv.2013.10.001.
- Roudsari, M.S., M. Pak. 2013. "Ladybug: a parametric environmental plugin for grasshopper to help designers create an environmentally-conscious design". In: *Proceedings of the 13th International IBPSA Conference*. Chambéry, France: IBPSA.
- Shen, H., A. Tzempelikos. 2012. "Daylighting and energy analysis of private offices with automated interior roller shades". *Solar Energy* 86(2): 681–704. doi: 10.1016/j.solener.2011.11.016.
- Shen, H., A. Tzempelikos. 2014. "A Global Method for Efficient Synchronized Shading Control Using the 'Effective Daylight' Concept". In: *Proceedings of the 3rd International High Performance Buildings Conference at Purdue*. West Lafayette, U.S.A.: Purdue University.
- Singh, R., I.J. Lazarus, V.V.N. Kishore. 2015. "Effect of internal woven roller shade and glazing on the energy and daylighting performances of an office building in the cold climate of Shillong". *Applied Energy* 159: 317–333. doi: 10.1016/j.apenergy.2015.09.009.
- Tzempelikos, A., H. Shen. 2013. "Comparative control strategies for roller shades with respect to daylighting and energy performance". *Building and Environment* 67: 179–192. doi: 10.1016/j.buildenv.2013.05.016.
- Vanhoutteghem, L., G.C.J. Skarning, C.A. Hviid, S. Svendsen. 2015. "Impact of façade window design on energy, daylighting and thermal comfort in nearly zero-energy houses". *Energy and Buildings* 102: 149–156. doi: 10.1016/j.enbuild.2015.05.018.
- Wienold, J. 2009. "Dynamic daylight glare evaluation". In: *Proceedings of the 11th International IBPSA Conference*. Glasgow, UK: IBPSA.
- Xiong, J., A. Tzempelikos. 2016. "Model-based shading and lighting controls considering visual comfort and energy use". *Solar Energy* 134: 416–428. doi: 10.1016/j.solener.2016.04.026.
- Yao, J. 2014. "An investigation into the impact of movable solar shades on energy, indoor thermal and visual comfort improvements". *Building and Environment* 71: 24–32. doi: 10.1016/j.buildenv.2013.09.011.
- Zhang, A., R. Bokel, A. Van Den Dobbelsteen, Y. Sun, Q. Huang, Q. Zhang. 2017. "Optimization of thermal and daylight performance of school buildings based on a multi-objective genetic algorithm in the cold climate of China". *Energy and Buildings* 139: 371–384. doi: 10.1016/j.enbuild.2017.01.048.

Sensitivity of WRF/Urban Simulations to Urban Morphology Parameters: A Case Study in the City of Bolzano

Gianluca Pappaccogli – Free University of Bozen-Bolzano – gianluca.pappaccogli@natec.unibz.it

Lorenzo Giovannini – University of Trento – lorenzo.giovannini@unitn.it

Francesca Cappelletti – University IUAV of Venezia – francesca.cappelletti@iuav.it

Dino Zardi – University of Trento – dino.zardi@unitn.it

Abstract

The recent progress in numerical weather prediction modelling, and in particular the possibility to reach increasingly finer spatial resolutions, allowed researchers to reproduce building-atmosphere interactions in a more accurate and realistic way, especially in urban areas.

The present work aims at evaluating the impact of high-resolution gridded datasets of urban morphology parameters on the results of numerical simulations of atmospheric processes performed with the WRF/Urban suite in the city of Bolzano (Italy), and to analyze how they affect near-ground temperature fields.

A sensitivity test was carried out, combining the WRF model with the Building Effect Parameterization (BEP) scheme to simulate two typical clear-sky summer days, respectively with and without the input gridded data of urban morphology. The structure and the morphology of the city of Bolzano were carefully reproduced through several fine-scale morphometric parameters from surface and terrain models (0.5 m resolution).

The results highlight that urban morphological parameters display a high spatial variability, moderately affecting the distribution of the temperature field near the ground. High-resolution meteorological fields inside urban areas can be valuable information for building energy simulations. Accordingly, a scheme of model chain coupling WRF and TRNSYS codes is proposed, in order to enhance the future assessment of urbanization effects and in the same way to provide more realistic and accurate building energy simulations.

1. Introduction

In densely urbanised areas, buildings are among the most important factors controlling energy, mass and

momentum exchanges between the earth surface and the atmosphere. This interaction has close influence on the Urban Heat Island (UHI) phenomenon, which consists in a significant increase of air temperature in the city center compared to the surrounding areas. Nowadays, recent progress in numerical weather prediction modelling, along with increasing availability of high-power computational resources, allow for reaching much higher spatial resolutions, even in operational model runs for routine weather forecasting. Accordingly, a more detailed parameterisation of these processes can be included, reproducing building-atmosphere interactions in a more precise and realistic way, especially in urban areas. Numerical models involve different spatial scales. In particular, two main models can be distinguished: mesoscale models (representing the atmospheric structures and working at horizontal resolutions of 1–10 km) and microscale models (e. g. Computational Fluid-Dynamics (CFD) models, Building Energy Simulations, working at much finer resolutions). Focusing on urban areas, microscale models require detailed information about buildings structure, while meso-scale models need a parameterization of averaged urban morphology features. In this context, mesoscale meteorological models, estimating the mean thermal and dynamical effects of the cities on the atmosphere have been increasingly applied to urban areas (Salamanca et al., 2011). Indeed, implementing urban schemes with detailed urban morphological parameters can provide better tools for evaluating the urban morphology impacts on the urban microclimate and the surrounding buildings. For this reason, the National Urban Database and Access Portal Tool (NUDAPT) was designed to

provide gridded datasets of urban canopy parameters for 44 US cities. Many recent studies highlighted the importance of using fine-resolution input datasets of urban morphology parameters to keep pace with the increasingly high resolution of operational model runs, in order to improve the accuracy of the results (Solazzo et al., 2010; Salamanca et al., 2011; Giovannini et al., 2014). The Weather Research and Forecasting (WRF) model can be coupled either with a single-layer urban canopy model (Kusaka et al., 2001) or with a multi-layer canopy model (Martilli et al., 2002), providing a valuable approach to represent the heterogeneities of urban morphology, considering three different urban surfaces (walls, roofs, and roads) and infinitely long street canyons (cf. Giovannini et al., 2013). Moreover, the BEP scheme can be coupled with a simple Building Energy Model (BEP+BEM), which provides a multilayer urban parameterization that takes into account the exchanges of energy between building and atmosphere (Salamanca and Martilli, 2010). The embedded building energy module estimates the heat diffusion through building envelopes and the radiation exchange between indoor surfaces, the heat generation of occupants and equipment, the energy consumption of air conditioning systems and natural ventilation.

The present work adopts the most advanced urban parameterization scheme coupled with the WRF model, i.e. the Building Effect Parameterization (BEP) (Martilli et al., 2002), in order to evaluate climatic conditions in the city of Bolzano. The city is located in the northeastern Italian Alps, in a basin where three valleys join (Fig. 1). Climatic conditions in the city are tightly connected with the complex topography of the surrounding area that influences in particular the flow field, mainly characterized by daily-periodic up- and down-valley winds from tributary valleys, especially in the warm season. Many studies investigated the interaction between

urban area and these phenomena, emphasizing the important influence of local winds on the urban environment (Kuttler et al., 1996; Piringer and Baumann, 1999; Giovannini et al., 2011).

The objective of the present work is to develop a complete dataset of fine-scale urban canopy parameters (UCPs) in Bolzano, in order to assess their impact in WRF-urban canopy models. This methodology, besides providing an accurate description of the temperature field in the urban area, can be used also to evaluate the effects of particular urban heat island mitigation strategies, or to assess the energy consumption in buildings.

This work is organized as follows. The datasets and the methodologies used to obtain urban canopy parameters are described in detail in section 2. Section 3 describes the results of sensitivity tests performed by means of the WRF/urban scheme. Finally, section 4 presents some conclusions and the proposal of a model chain including the mesoscale model (nested WRF-urban from 10.8 to 0.4 km resolution) and the well-known building energy simulation code TRNSYS.

2. Input Datasets and Modelling Setup

2.1 Input Datasets – UCPs

As reported in the study of Giovannini et al. (2014), high-resolution meteorological simulations in complex terrain require a high-resolution topography dataset. For this reason, here the topographical data obtained from the Viewfinder Panoramas (original horizontal spatial resolution ~ 30 m) were used. Fig. 1 (right) shows the topography of the inner domain, highlighting the urban area of Bolzano. The dataset Corine was used for the land cover parameters, reclassifying the 44 Corine categories into the 20 (+3 special classes for urban land use) Modis categories, in order to fit the WRF look-up tables.

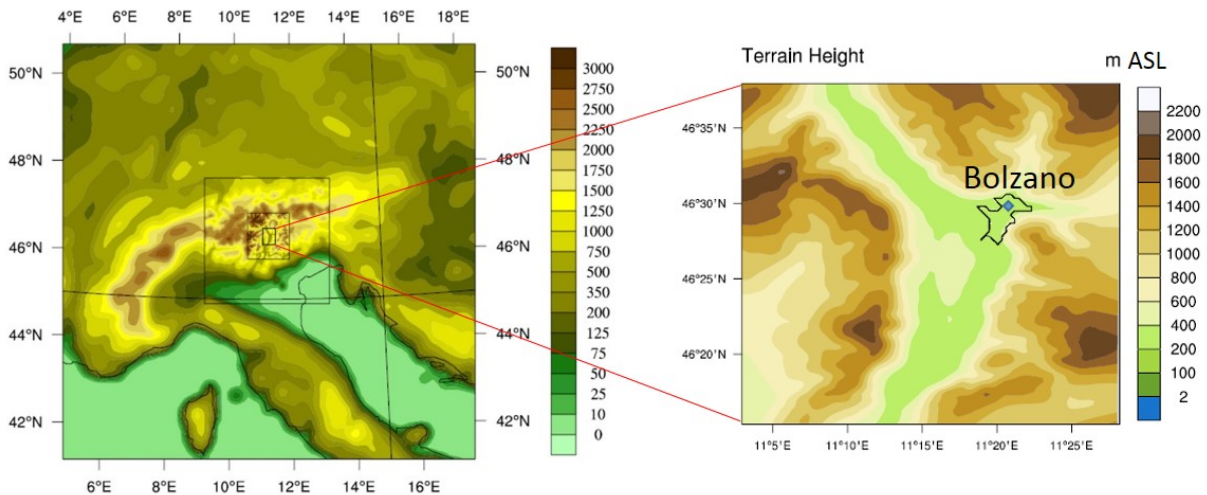


Fig. 1 – The four nested domains used for the numerical simulations (left). The zoomed-in area (right) represents the inner domain and the black line contours the urban area of the city of Bolzano

The land cover dataset is shown in Fig. 2. As the goal of this research concerns the urban environment, detailed maps of urban morphology were developed. Using digital surface and terrain models (0.5 m resolution) from the GeoCatalogo of the Autonomous Province of Bolzano (<http://geocatalogo.retecivica.bz.it/geocatalog>), fine resolution maps of urban morphology parameters were calculated by means of the QGIS + Urban Multi-scale Environmental Predictor (UMEP) and Matlab© software. Collected data and maps were processed in order to obtain gridded urban canopy parameters (UCPs) with a horizontal spatial resolution of 100 m, directly used as input for the BEP scheme. The structure of the city of Bolzano was carefully reproduced using a set of seven morphometric parameters: the average and standard deviation height of the buildings named respectively h_m and h_s , the building plan area fraction $\lambda_p = A_p/A_{tot}$ (where A_p is the plan area of buildings and A_{tot} is the total area of the cell) and plan-area-weighted mean building height $h_{aw} = (A_p \cdot h_m)/A_p$; the building envelope area to plan area ratio $\lambda_b = (A_p + A_w)/A_{tot}$ (where A_w is the wall surface area); the frontal area index $\lambda_f = A_{proj}/A_{tot}$ (where A_{proj} is the total area of buildings projected into the plane normal to the approaching wind direction at 0° - 45° - 90° - 135°), the urban fraction λ_u (percentage of the cell covered by urban land use). Finally, the distribution of building heights h_i (that corresponds to the plan area fraction of the buildings every five meters in each

computational cell) at 5 m vertical intervals was calculated on fifteen vertical urban levels. The methodology used to calculate the main urban morphological parameters is reported in Burian et al. (2008). Fig. 3 shows respectively the distribution of λ_p (a), λ_b (b), h_m (c) and λ_u (d), on a 100 m grid resolution. The same parameters have been used as input for the BEP scheme in the WRF model, averaging those previously calculated in order to adapt them to the 400 m WRF resolution. Results are shown in Fig. 4. Fig. 3 and 4a, 4b, and 4c highlight, as expected, that the highest values of these urban morphology parameters are mainly located in the central part of the city, which is characterized by a typical South Tyrolean architectural design, consisting of 4-5-storey historic buildings flanking narrow (often arcaded) street canyons. In particular, the highest values of λ_p and λ_b occur in this area, which underlines the high density of the urban area. Furthermore, high values occur also in the southern area of the city, which is the industrial and commercial areas, and in the northwestern part of the residential area, where high residential buildings are present (Fig. 4c). Finally, in order to check the consistency of the gridded morphology data, they were overlaid on Google Earth maps.

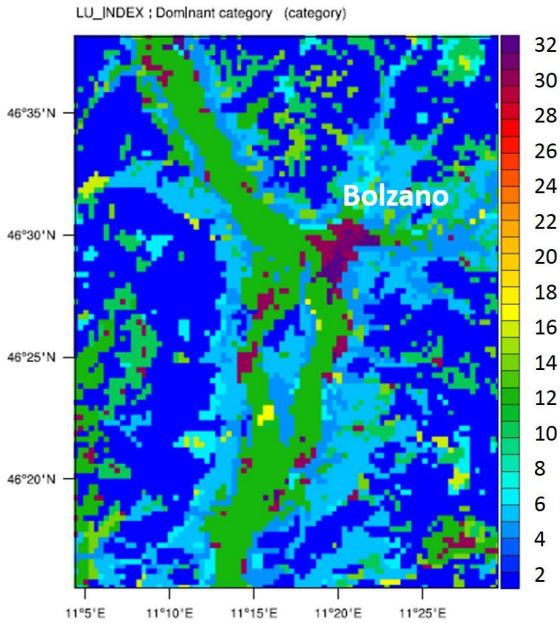


Fig. 2 – Modis land use categories in the inner model domain. Categories 31-33 indicate urban land use, namely 31: Low intensity residential, 32: High intensity residential, 33: Industrial or commercial

2.2 WRF Numerical Simulation

In order to assess the impact of the urban canopy parameters on the WRF simulation output, the non-hydrostatic version of the WRF model (version 3.8) coupled with Building Effect Parameterization BEP scheme (Martilli et al., 2002) was used (Skamarock et al., 2016). The 54-h WRF-urban simulations started at 1800 UTC (LST=UTC+1 h) 19 July 2015 and ended at 0000 UTC 21 July 2015. Simulations were carried out using four two-way nested domains (nesting ratio=3) with the grid resolution for the inner domain of 400m×400m (Fig. 1 and Tables 1 and 2 show details about domains dimension and resolution). Initial and boundary conditions derive from the National Center for Environmental Prediction (NCEP), where meteorological data have 1-deg grid resolution (about 120 km) and 6 h time resolution. 30 eta levels (terrain-following hydrostatic-pressure vertical coordinate) are used in the vertical. The simulations were run with the Bougeault and Lacarrère (1989) scheme for the Planetary Boundary Layer (PBL) parameterization, while the Noah land surface model (Chen and Dudhia, 2001) for the land surface processes parameterization.

Table 1 – Details of resolution of nested WRF domains

Domain	n.points_we	n.points_sn	dx(m)	dy(m)
d01	100	100	10800	110800
d02	91	91	3600	3600
d03	91	100	1200	1200
d04	82	106	400	400

3. Sensitivity Test

In order to analyze in detail the impacts of the gridded datasets of the urban morphology parameters, sensitivity simulations were performed with and without these input data. The simulation considering urban morphology parameters is referred to as BEP_PAR, while the one using only standard input for the BEP scheme (i.e. without the gridded datasets of urban morphology) is referred to as BEP_NOPAR. In this case, since the grid data of urban morphology are absent, the three urban classes describe the urban settlements (Fig. 2), i.e. the ancient and high-intensity residential class (class number 31), the recent high- or low-intensity residential class (class number 32), and the industrial and commercial class (class number 33), from which the urban scheme looks up the morphology parameters.

The simulation results show that the strongest temperature differences between the two simulations occur in the central part of the city, where the influence of the morphology parameters on the performance of the urban scheme is higher. At night temperatures are slightly higher (~ 0.5 - 1 °C) in BEP_PAR than in BEP_NOPAR, especially in the central part of the urban area, while in the central hours of the day the opposite occurs, mainly in the downtown area, which is characterized by densely packed buildings and narrow street canyons. These results (obtained from BEP_PAR) are in reasonable agreement with observations performed in Trento (Giovannini et al., 2011), showing a quite strong nocturnal urban heat island (UHI), especially under low wind speed and clear sky conditions, whereas an urban cool island is likely to develop in the morning.

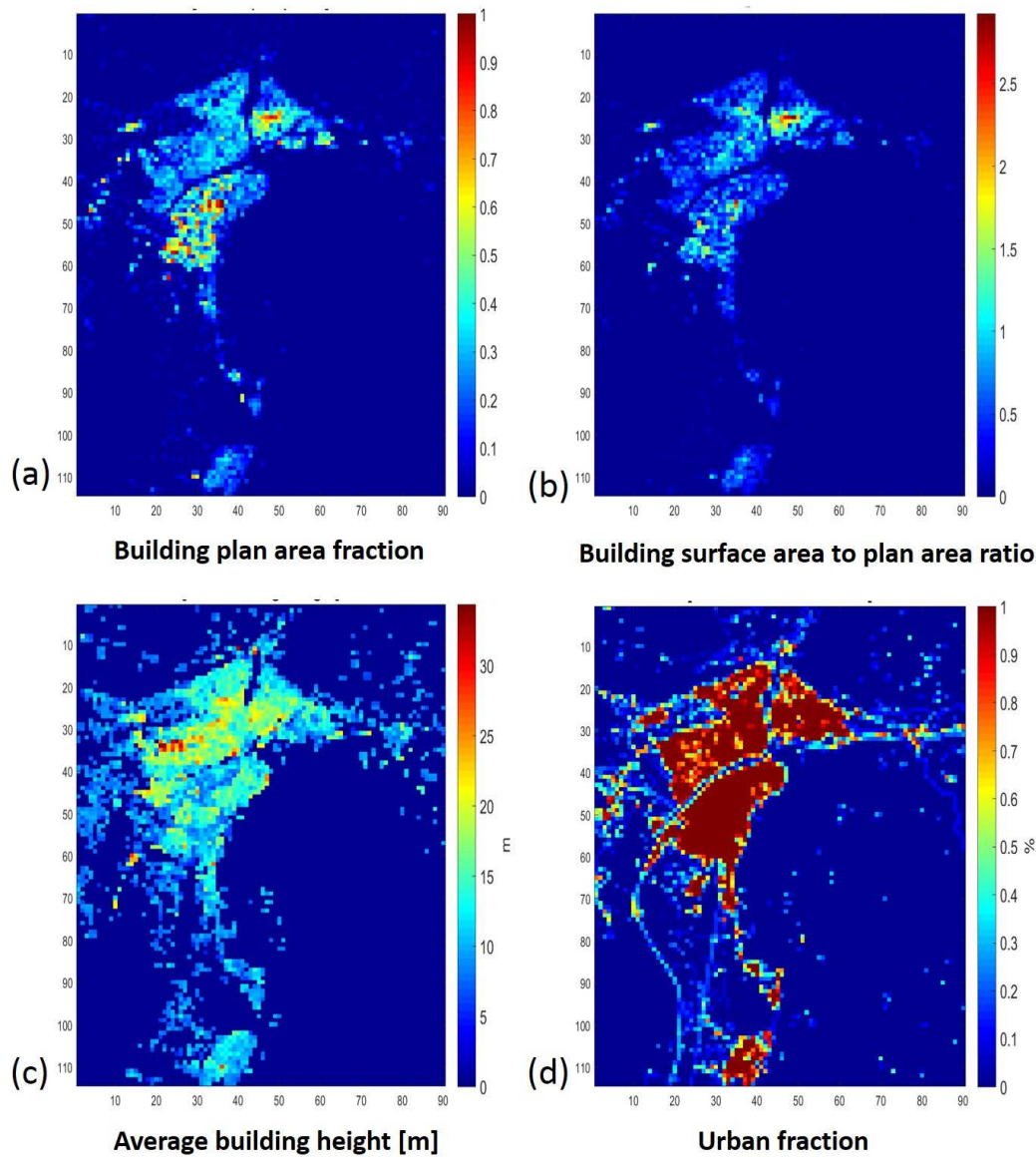


Fig. 3 – Urban morphology parameters calculated by means of MATLAB-QGIS software from digital surfaces and terrain model for the urban area of Bolzano (fine resolution-100 m). (a) Building plan area fraction λ_p , (b) building surface area to plan area ratio λ_b , (c) average building height h_m , (d) urban fraction λ_u .

Focusing on Fig. 5a, referring to nighttime (2315 UTC), the highest differences occur in the central part of the urban area, in accordance with the average values of the UCPs used in BEP_PAR, which, unlike the default urban classes, well capture the detail of the denser morphology and greater height of the buildings in that area. On the contrary, negative differences occur during daytime (Fig. 5b), especially in the morning, due to the density of urbanization which prevents solar radiation to penetrate inside narrow street canyons. However, this

difference decreases until the central hours of the day, when the temperature differences between the two schemes are less than 0.5 °C. Summing up, as can be seen in Fig. 5a and 5b, areas with low positive and negative differences are present throughout the urban area, depending closely on the local values of the gridded morphology parameters. The maximum differences between the two simulations (i.e. BEP_PAR-BEP_NOPAR) are more than 1 °C, both during the day and the night, when negative and positive differences occur respectively.

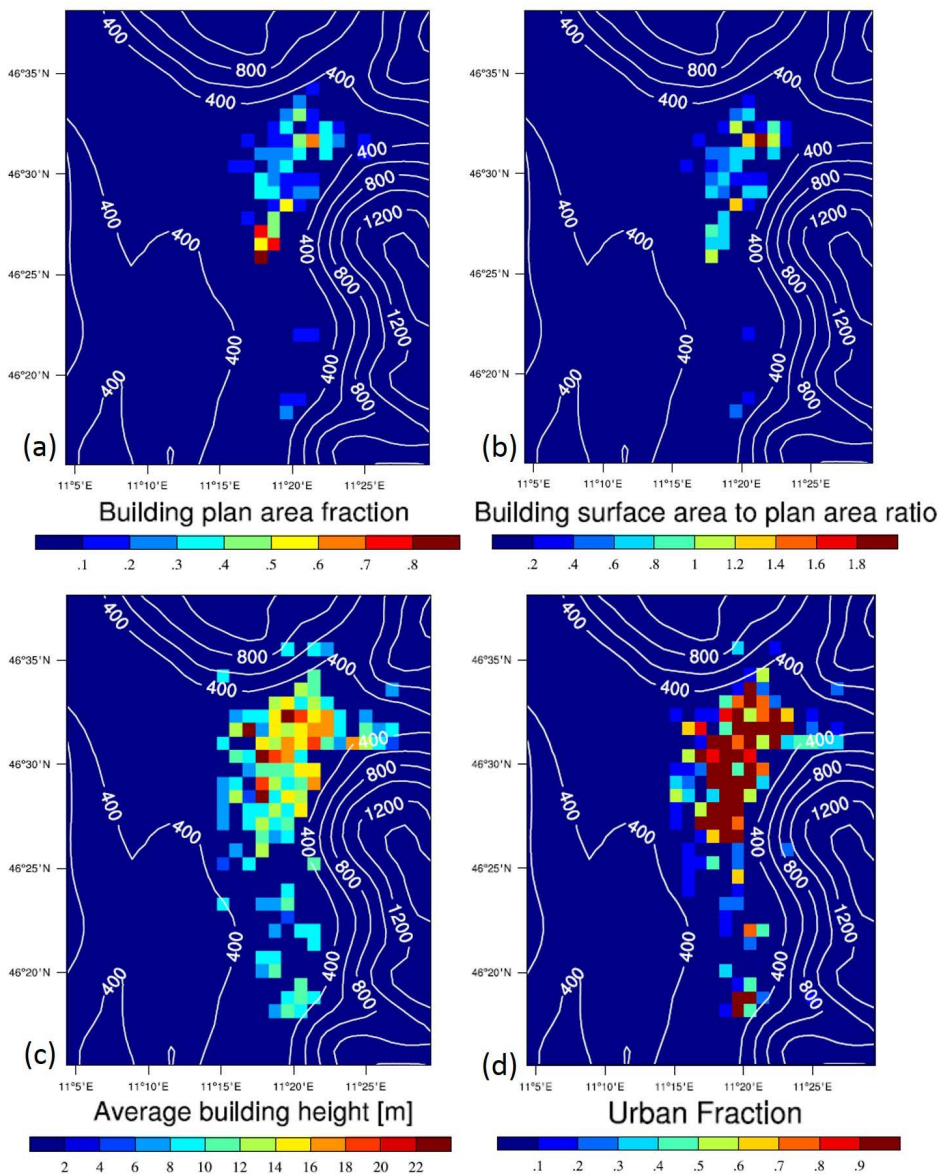


Fig. 4 – Urban morphology parameters averaging the finer-resolution previously calculated in Fig.3 and used in the BEP scheme. (a) Building plan area fraction λ_p , (b) building surface area to plan area ratio λ_b , (c) average building height h_m , (d) urban fraction λ_u . Detailed explanations of the parameters are given in section 2.1. Height contours are in above sea level (ASL)

4. Discussion and Conclusion

The WRF/BEP coupled model was applied, with and without urban morphology parameters, to simulate the atmospheric processes in the city of Bolzano during the hottest days in the summer 2015. A sensitivity test was performed to assess the impact of the gridded datasets of the urban morphology in the BEP scheme. The results show that the detailed urban parameters influence significantly the spatial and temporal variability of the urban temperatures throughout the day. In particular, the BEP_PAR

simulation shows higher temperature than BEP_NOPAR in the historical city center already in the first nocturnal hours. On the contrary, the temperature in the downtown area tends to remain lower in BEP_PAR than in BEP_NOPAR throughout the morning (~1 °C), due to a cool island effect. Further analyses are ongoing in order to investigate the model sensitivity with respect to fluxes and other micrometeorological variables. Based on the results of this paper, on the ongoing research activities, and on the continuous improvement of numerical capabilities at all scales, modelling building elements in more detail seems the further effort in

order to represent in a more accurate way the interaction between buildings and the urban atmosphere. To this regard there are some issues to overcome. On one hand the resolution typically used in mesoscale model simulations is not enough to provide details about the single building in the urban context. On the other hand, building energy simulations (BES) often focus on the single building without considering the urban context and the surrounding building effect on radiative and convective surface exchanges on the external envelope. Furthermore, providing proper initial conditions for these models remains a difficult task, as they are usually derived from observations (mostly taken within rural environment) limited to a single-point, which negatively affect model reliability. These criticalities pose a challenge when it comes to coupling these models with mesoscale models, especially when the impact of urbanization effects (UHI) on building energy performance is investigated.

In this context, WRF/Urban output can provide information that are not typically available from conventional climate data, e.g. Typical Meteorological Year, leading to a more robust source (spatially averaged) for initial conditions as compared to local observations. The possible advantages arising from the use of WRF/Urban output in building energy simulation may be shortly recalled in the following list:

- 1) Better knowledge of micrometeorological conditions representative of specific urban areas free from potential bias due to instrument location;
- 2) a more precise evaluation of temperatures on impervious urban surfaces, upper soil layers and overlying urban canopy layers;
- 3) a better prediction of future scenarios by assessing the feedback between buildings and the surrounding microclimate, which are directly affected by climate change mitigation strategies (e.g. green roofs, trees and vegetation).

A challenging opportunity that may be pursued in future developments of this research is the coupling of WRF/Urban with models dynamically reproducing building energetics (e.g. TRNSYS).

Table 2 Main features of the simulations in this paper

Schemes	BEP_PAR	BEP_NOPAR
Urban land use	Yes	Yes
Urban scheme	BEP	BEP
Gridded dataset of urban morphology	Yes	No

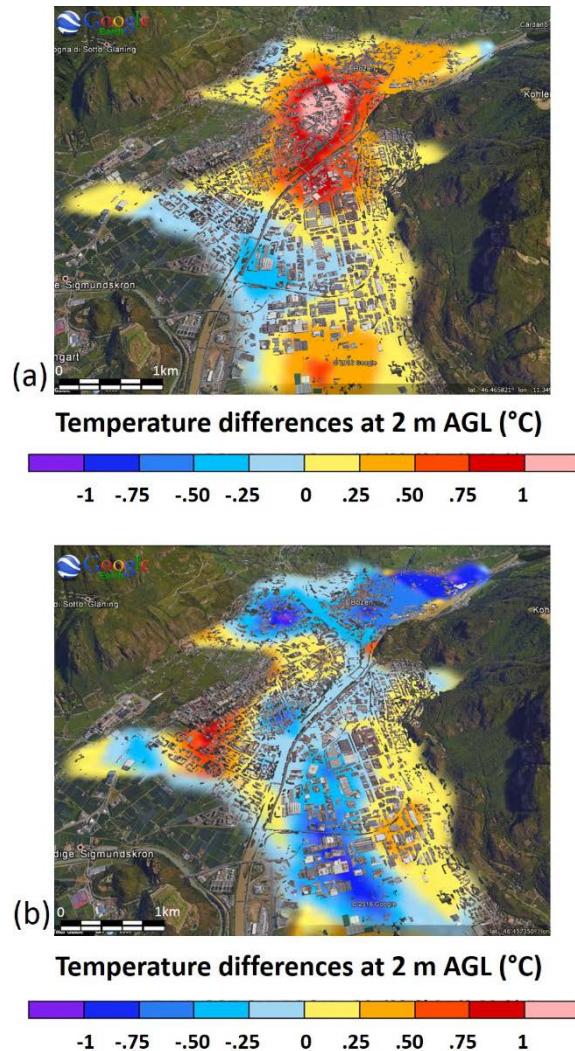


Fig. 5 – Temperature differences at 2 m AGL in the urban area of Bolzano at (a) 2315-nighttime, (b) 1200–daytime UTC respectively 19 and 20 July 2015

Acknowledgement

The first author thanks the Faculty of Science and Technology of the Free University of Bolzano, and in particular the PhD Program in Sustainable Energy and Technologies, for supporting his research project.

References

- Bougeault, P., P. Lacarrère. 1989. "Parameterization of orography-induced turbulence in a mesobeta-scale model". *Monthly Weather Review* 117: 1827-1890. doi: 10.1175/1520-0493(1989)117<1827:POOITI>2.0.CO;2.
- Burian, S., N. Augustus, I. Jeyachandran, M.J. Brown. 2008. *Final Report for the National Building Statistics Database, Version 2*. Los Alamos, U.S.A.: Los Alamos National Laboratory.
- Chen, F., J. Dudhia. 2001. "Coupling an advances land surface-hydrology model with the Penn State-NCAR MM5 modeling system. Part I: model implementation and sensitivity". *Monthly Weather Review* 129: 569-585. doi: 10.1175/1520-0493(2001)129<0569:CAALSH>2.0.CO;2.
- Giovannini, L., D. Zardi, M. de Franceschi. 2011. "Analysis of the urban thermal fingerprint of the city of Trento in the Alps". *Journal of Applied Meteorology and Climatology* 50: 1145-1162. doi: 10.1175/2010JAMC2613.1.
- Giovannini, L., D. Zardi, M. de Franceschi. 2013. "Characterization of the Thermal Structure inside an Urban Canyon: Field Measurements and Validation of a Simple Model". *Journal of Applied Meteorology and Climatology* 52: 64-81. doi: 10.1175/JAMC-D-12-06.1.
- Giovannini, L., D. Zardi, M. de Franceschi, F. Chen. 2014. "Numerical simulations of boundary-layer processes and urban-induced alterations in an Alpine valley". *International Journal of Climatology* 34: 1111-1131. doi: 10.1002/joc.3750.
- Kusaka, H., H. Kondo, Y. Kinogawa, F. Kimura. 2001. "A simple single-layer urban canopy model for atmospheric models: comparison with multi-layer and slab models". *Boundary-Layer Meteorology* 101: 329-358. doi: 10.1023/A:1019207923078.
- Kuttler, W., A.B. Barlag, F. Roßmann. 1996. "Study of the thermal structure of a town in a narrow valley". *Atmospheric Environment* 30: 365-378. doi: 10.1016/1352-2310(94)00271-1.
- Martilli, A., A. Clappier, M.W. Rotach. 2002. "An urban surface exchange parameterization for mesoscale models". *Boundary-Layer Meteorology* 104: 261-304. doi: 10.1023/A:1016099921195.
- Piringer, M., K. Baumann. 1999. "Modifications of a valley wind system by an urban area—Experimental results". *Meteorology and Atmospheric Physics* 71: 117-125. doi: 10.1007/s007030050049.
- Salamanca, F., A. Martilli. 2010. "A new building energy model coupled with an urban canopy parameterization for urban climate simulations—Part II. Validation with one dimension off-line simulations". *Theoretical and Applied Climatology* 99, 345-356. doi: 10.1007/s00704-009-0143-8.
- Salamanca, F., A. Martilli, M. Tewari, F. Chen. 2011. "A study of the urban boundary layer using different urban parameterizations and high-resolution urban canopy parameters in WRF". *Journal of Applied Meteorology and Climatology* 50: 1107-1128. doi: 10.1175/2010JAMC2538.1.
- Skamarock, W.C., J.B. Klemp, J. Dudhia, D.O. Gill, D.M. Barker, M. Duda, X.Y. Huang, W. Wang J.G. Powers. 2016. "NCAR Technical Note 2016. A description of the Advanced Research WRF version 3". *NCAR Technical Note* TN-475+STR, 125. doi: 10.5065/D68S4MVH..
- Solazzo, E., S. Di Sabatino, N. Aquilina, A. Dudek, R. Britter. 2010. "Coupling mesoscale modelling with a simple urban model: the Lisbon case study". *Boundary-Layer Meteorology* 137: 441-457. doi: 10.1007/s10546-010-9536-6.

Numerical Analysis of Thermal Bridges in Dynamic Conditions

Alessandra Romagnoli – Università Politecnica delle Marche – a.romagnoli@pm.univpm.it

Costanzo Di Perna – Università Politecnica delle Marche – c.diperna@univpm.it

Davide Barbaresi – davidebarbaresi@hotmail.it

Elisa Di Giuseppe – Università Politecnica delle Marche – e.digiuseppe@univpm.it

Abstract

Thermal bridges play a significant role in the heat loss of nearly Zero Energy Buildings (nZEB). In the case of existing buildings, the underestimation of thermal bridges can lead to errors of about 20 % in the assessment of their energy requirements.

Nowadays, proper simulation tools for evaluating the building energy performance in dynamic conditions are increasingly needed. Their outputs are important inputs for life cycle costs (LCC) and life cycle assessment (LCA) as well as for energy audits. A weak point is that the tools which are currently well established on the market, do not consider the contribution given by thermal bridges to the overall building energy balance as they rely on a one-dimensional approach to recreate heat flows.

Several scientific studies deal with different methods that can be applied to evaluate the dynamic behaviour of thermal bridges, but they disregard the wall capacity to accumulate/release heat loads and the role played by internal temperatures.

This work analyses some numerical methods proposed by different authors based on the discretization of thermal bridges and their characterization in dynamic regime.

A calculation procedure is evaluated to underline its potential as a rapid dynamic calculation algorithm to be integrated in the current software for dynamic analyses. The surface temperatures and the heat fluxes are taken into account.

In the present work, the method of the equivalent thermal wall has been implemented to get the input parameters required to dynamically assess the thermal bridges energy contribution. Afterwards a finite volume analysis is developed to compare the outputs coming from different methods in terms of crossing fluxes, surface temperatures and thermal storage capacities.

A low percentage error is found between the equivalent thermal wall and the real one in terms of surface temperatures. This achievement allows to carry out proper superficial condensation assessments.

Anyway the above-exposed procedure is quite complex and time-consuming. The algorithm is then expected to be refined in the future by simplifying the necessary operations for the evaluation of thermal bridges.

1. Introduction

The Directive 2010/31/EC of the European Parliament and of the Council of 19 May 2010, on the energy performance of buildings (EPBD Recast) has established a common framework of measures for the promotion of energy efficiency within the Union in order to ensure the objectives of the "climate-energy package 20/20/20."

Buildings account for about 40 % of total energy consumption in the Union (Ascione et al., 2012) it is necessary to reduce their greenhouse gas emissions by using energy from renewable sources and by reducing energy consumption in the buildings sector.

Italy, under the existing rules, has issued a new Ministerial Decree on June 26, 2015 for the energy efficiency of buildings. The decree imposes more restrictive limits than before in order to achieve nearly Zero Energy Buildings (nZEB).

Designers can use two main approaches for building energy calculation: a simplified approach and a dynamic simulation.

The first is based on UNI EN ISO 13790:2004 (Thermal performance of buildings - Calculation of energy use for space heating) developed according

to the European Energy Performance of Buildings Directive (EPBD- Directive 2002/91/EC).

This standard proposes a quasi steady-state approach based on algebraic equations. Heating and cooling energy demands are calculated on the basis of a balance between the transmission and ventilation heat losses, and the internal and solar gains.

The simplified calculation has several advantages over the dynamic approach because it is simpler and more intuitive, but it is considered insufficient to properly describe the dynamic behaviour of the building envelope and its system controls (Kim et al., 2013).

The dynamic approach is preferable to design high-efficiency buildings. It requires extensive inputs and the correlation between inputs and outputs is often not intuitive, but it has relevant advantages. Designers have a high level of modeling possibilities for the integrated performance assessment. In addition, simulations in dynamic regime give more precise outcomes.

Anyway it is necessary to underline the importance of the contribution of thermal bridges on energy demands, whatever simulation method is used.

According to the International Standard EN ISO 10211/2008, a thermal bridge is “a part of the building envelope where the otherwise uniform thermal resistance is significantly changed by full or partial penetration of the building envelope by materials with a different thermal conductivity, and/or a change in thickness of the fabric, and/or a difference between internal and external areas, such as occur at wall/floor/ceiling junctions”. Numerically, it is estimated that thermal bridges can increase the thermal loads and needs of a building up to 20 % (Ascione et al., 2012). Other authors showed that, under certain conditions, neglecting thermal bridges can lead to errors on energy needs calculation over 40 % (Kosny et al., 2002).

A proper correction or elimination of thermal bridges is hardly achievable. In nZEB, where a great envelope thermal resistance is advisable, thermal bridges play a significant role.

In the quasi steady-state approach, proposed by the recent Italian decree, the value H'_{τ} has been introduced. It represents the average value of the envelope's thermal transmittance that is the sum of

transparent and opaque surfaces' thermal transmittances, including thermal bridges (UNI EN ISO 6946: 2008; UNI EN ISO 14683: 2008). Previous studies have demonstrated that in order to reach the actual targets established for H'_{τ} by the Italian law, the designer needs to plan a building envelope with very small thermal transmittance in order to balance the heat loss through thermal bridges.

On the other hand, in the dynamic approach, the impact of thermal bridges has not been properly calculated yet. Dynamic simulation programs, as EnergyPlus™, adopt a zero-dimensional analysis that assumes a constant indoor air temperature. Many authors have published studies proposing several methods for the analysis of thermal bridges, according to both statistical and numerical approaches (Ascione et al., 2014; Seem et al., 1989; Renon, 2002).

An option consists on using a specific software for the calculation of thermal bridges that considers them as a linear heat transfer resistance (i.e. THERM or KOBRA).

Another possibility is to use numerical methods programs, but the computational effort increases (e.g., COSMOS, Fluent, Femlab). These programs can be used for calculating any type of thermal bridge without implementing them in the building. In this paper, a finite volume method is compared with the “equivalent wall method” developed by Kossecka and Kosny (Kossecka et al., 1997; Aguilar et al., 2014), for modelling the effects of thermal bridges on buildings. This method allows to include thermal bridges in dynamic simulation programs for the whole building energy assessment: once the equivalent wall has been calculated, it has to be included in place of the real wall.

2. Equivalent Thermal Wall Concept

The equivalent thermal wall concept allows to switch from a thermal bridge to a thermally similar wall made of three layers, obtained through the following steps:

- 1) get the temperature distribution and wall heat fluxes from the solution of the steady-state heat conduction problem through Fourier equation;

- 2) calculate the dimensionless factor φ (through the method of Kossecka and Kosny);
- 3) obtain the equivalent thermal properties (thermal capacity C , thermal resistance R , density ρ , thermal conductivity λ) with an iterative algorithm.

2.1 Boundary Conditions

This work considers a two-dimensional typical problem of thermal bridge. The heat transfer is based on the Laplace equation in (1).

Usually, energy simulation software implement one-dimensional operations for the energy balance: starting from the Laplace equation in 2D, through the decomposition of the thermal bridge, the geometric node of the structure is simplified into parts with the advantage of having a one-dimensional heat flow in each.

The boundary conditions taken into account are convection and radiation; on the sides a temperature difference of 1 K is set (2), on the interfaces the elements have the same temperature and heat flux (3).

$$\frac{\delta^2 T}{\delta x^2} + \frac{\delta^2 T}{\delta y^2} = 0 \quad (1)$$

$$\left. \begin{aligned} -\lambda_e \frac{\delta T}{\delta \eta} &= \frac{1}{R_e} (T_e - T_{W,e}) \\ -\lambda_i \frac{\delta T}{\delta \eta} &= \frac{1}{R_e} (T_i - T_{W,i}) \end{aligned} \right\} \quad (2)$$

$$T_i = T_j; \quad -\lambda_1 \frac{\delta T}{\delta \eta} = -\lambda_2 \frac{\delta T}{\delta \eta} \quad (3)$$

2.2 Approach and Finite Difference Method

The study needs the use of a simple calculation software (as a spreadsheet), in which the thermal bridge is discretized into elements in the steady-state heat conduction problem, or Computational Fluid Dynamics programs (CFD) where the analysis is launched in transient conditions.

The technique of finite differences is considered for the conduction heat transfer in 2D:

- each node represents the temperature of a point on the surface considered;

- temperature at the node represents the average temperature of that region of the surface;
- algebraic expressions are used to define the relationship between adjacent nodes on the surface;
- by increasing the number of nodes on the surface it is possible to increase the spatial resolution of the solution and potentially increase the accuracy of the numerical solution, however this increases the number of calculations needed to obtain a solution to the problem.

The diagram in Fig. 1 represents the differential temperature increase compared to the spatial coordinates; it also expresses the first balancing law for volume control.

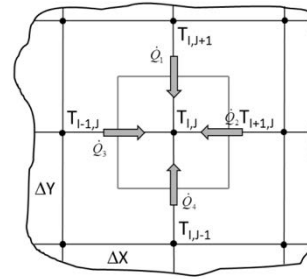


Fig. 1 – Differential temperature increases

2.3 Exemplary Case (Wall Corner)

The thermal bridge analysed for the method validation is a corner originated by two multi-layer walls with a concrete pillar (typical mid XX century building, Fig. 2). The outside surfaces are in contact with the outdoor environment with a conventional temperature $T_e = 1^\circ\text{C}$, while internal surfaces face an indoor conventional temperature $T_i = 0^\circ\text{C}$.

Materials and thermal properties of each component of the thermal bridge are included in Table 1.

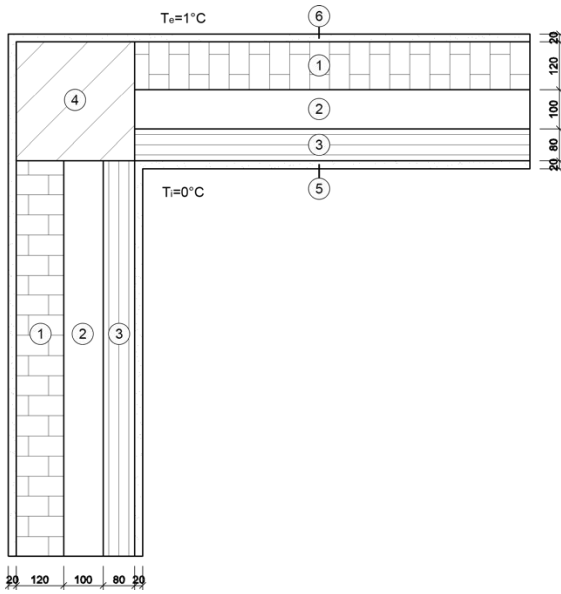


Fig. 2 – Layers of thermal bridge originated by two walls with pillar

Table 1 – Building materials and thermal properties of the corner

Material	ρ [kg/m ³]	C_p [J/(kg K)]	λ [W/(m K)]
1 Solid brick	900	1000	0.512
2 Air gap	1.2	1000	0.026
3 Hollow brick	630	1000	0.212
4 Concrete pillar	1090	1000	1.22
5 Interior plaster	1150	1000	0.57
6 Exterior plaster	1150	1000	0.57

Concerning the corner section, it is very important to delete the node resulting from the intersection of the two walls to obtain a mono-directional heat flow, following few geometric guidelines. It is important to note that when isolines become perpendicular to the section, the thermal bridge influences the finish area. The study is carried out with a distance of up to 1m from the intersection of the two wall blocks.

Therefore, the following lengths are defined and summarized (Fig. 3): $L1/2$: 1.0 m; $N1/2$: 0.2 m; $W1/2$: 0.8 m ($L1/2 - N1/2$); $A1/2$: (0.2 m²).

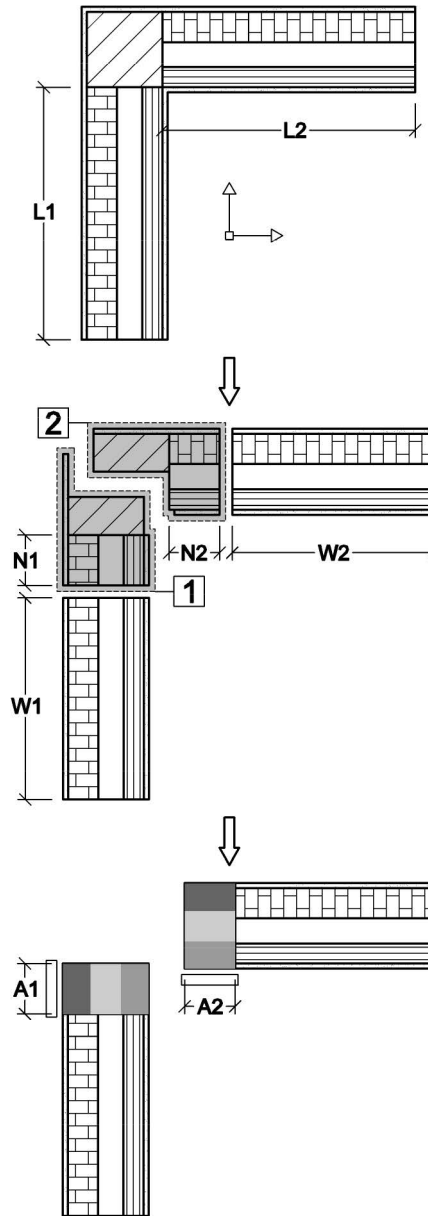


Fig. 3 – Decomposition of the thermal bridge in the equivalent thermal wall with indexes

2.4 Definition of Temperatures and Dimensionless Factors

In accordance with the above considerations regarding the discretization of the nodes by a finite difference method, an Excel matrix is developed (Fig. 4) in which each node is represented by a temperature value.



Fig. 4 – The thermal bridge model set out in Excel with highlighted board and interface cells

All links of the mesh are 1 cm x 1 cm squares; the intersections of the plot lines are the nodes, the points where the temperatures are calculated. All nodes are interconnected by equations so that the result is a set of simultaneous equations equal to the number of nodes; the number of unknown factors is the same of the equations. When the number of nodes grows, the size and complexity of the system increases.

Being the heat capacity C (4), after calculating the flow Q [W] in the external/internal interfaces as the sum of specific flows in each row or column of the spreadsheet, we proceed to the determination of dimensionless factors φ_{ii} , φ_{ee} , φ_{ie} (5).

$$C = \int \rho C_p dV \quad (4)$$

$$\left. \begin{aligned} \varphi_{ii} &= 1/C \int \rho C_p (1-T_n^2) dV \\ \varphi_{ee} &= 1/C \int \rho C_p T_n^2 dV \\ \varphi_{ie} &= 1/C \int \rho C_p T_n (1-T_n) dV \end{aligned} \right\} \quad (5)$$

The following condition must be satisfied:

$$2\varphi_{ie} + \varphi_{ii} + \varphi_{ee} = 1 \quad (6)$$

It is very important to define the geometry of the portion of the thermal bridge that will refer to the defined equivalent thermal wall.

2.5 Algorithm Development

From the heat capacity C , the dimensionless factors and the thermal transmittance U (7) it is possible to get thermal variables (C_m , R_m , ρ_m , λ_m) of the three layers of equivalent thermal wall, where $m = 1, 2, 3$. Some equations, expressed by Kossecka and Kosny (8) rule the method. The aim is to find the thermal resistance of the external layer R_1 to which the heat capacity C_2 of the intermediate level is close to zero but positive. A set of calculations has been improved to get to the solution faster (Table 2) assuming a fictitious α value (0.1-0.3).

$$U = Q/(A \cdot \Delta T) \quad (7)$$

$$\varphi_{ii} + \varphi_{ie} = \frac{1}{RC} \sum_1^3 C_m \left(\frac{R_m}{2} + R_m - e \right) \quad (8)$$

$$\varphi_{ie} = \frac{1}{R^2 C} \sum_1^3 C_m \left(\frac{-R_m^2}{3} + \frac{R_m R}{2} + R_i - m R_m - e \right) \quad (9)$$

$$R = \sum_1^3 R_m \quad (10)$$

$$C = \sum_1^3 C_m \quad (11)$$

Table 2 – Scheme for the calculation of the thermal properties

R_T	$1/U$	$j=$	$1+j$
$R_{1,\min}$	0.01	$R_{1,\min}$	0.01
$R_{1,\max}$	0.01	$R_{1,\max}$	$R_{1,j-1} \cdot \alpha$
$R_{1,j}$	$(R_{1,\min} + R_{1,\max})/2$	$R_{1,j}$	$(R_{1,\min} + R_{1,\max})/2$
$R_{2,j}$	$R_T - R_S - R_{1,j} - R_{3,j}$	$R_{2,j}$	$R_T - R_S - R_{1,j} - R_{3,j}$
$R_{3,j}$	$(R_{1,\min} + R_{1,\max})/2$	$R_{3,j}$	$(R_{1,\min} + R_{1,\max})/2$

Finally, the properties of the equivalent thermal wall are calculated (Tables 3 and 4).

Note that a standard value is considered for the specific heat for the three layers $C_p = 1000$ J/(kg K) whereas, regarding the thickness e (m) of the layers, it is a third part of the equivalent wall thickness.

Table 3 – Thermal variables of the three layers in the equivalent thermal wall

Layer	R	C_m	e	ρ_m	λ_m
m	($m^2 K/W$)	($kJ/(m^2 K)$)	(m)	(kg/m^3)	($W/(mK)$)
Se	0.04				
1	0.165	68.456	0.11	622.33	0.667
2	2.390	0.101	0.12	0.84	0.050
3	0.165	418.013	0.11	3800.12	0.667
Si	0.13				
Σ	2.8902	486.6	0.34		

Table 4 – Thermal transmittance and dimensionless factors for the equivalent thermal wall

Q [W]	U [$W/m^2 K$]	φ_{ii}	φ_{ee}	φ_{ie}
0.346	0.3460	0.738	0.134	0.064

3. Results

With a Computational Fluid Dynamics program, two simulations are launched, with the same boundary conditions first through the thermal bridge, then in an equivalent thermal wall (the section is specular) in dynamic conditions. The results are extracted and compared in some graphics.

3.1 Method Validation

The geometric model and mesh are defined using a CAD pre-processor (Fig. 5); the idea is to draw the thermal bridge by dividing it into mesh and having the *.msh file read by a CFD software to solve the heat transfer equations.

The first simulation is a steady-state heat conduction analysis carried out to obtain the temperature field and the heat fluxes, in order to better compare the values of the flows and to determine the isolines where the flow is one-dimensional.

After that the final simulation is in transient regime by applying a 20 K temperature difference between environments: inner temperature is fixed a constant; instead the external air temperature changes with a sinusoidal profile. The indoor temperature is a fixed constant $T_i = 20\text{ }^\circ\text{C}$, the law for outside temperature is $T_e(t) = F\sin(\omega t)$ where the amplitude $F = 5\text{ }^\circ\text{C}$ and the period $T = 2\pi/f = 24\text{ h}$.

The results are repeated in the same way already after about 12 hours; thus, generally the simulations will run for a period of 2 days to make it independent from the initial conditions.

3.2 Discussion

Some Iso-Surfaces are created to determine the temperature on time throughout the section thickness. The Iso-Surfaces considered are: $y = 0.0\text{ m}$; $y = 0.4\text{ m}$; $y = 0.8\text{ m}$; $y = 0.9\text{ m}$.

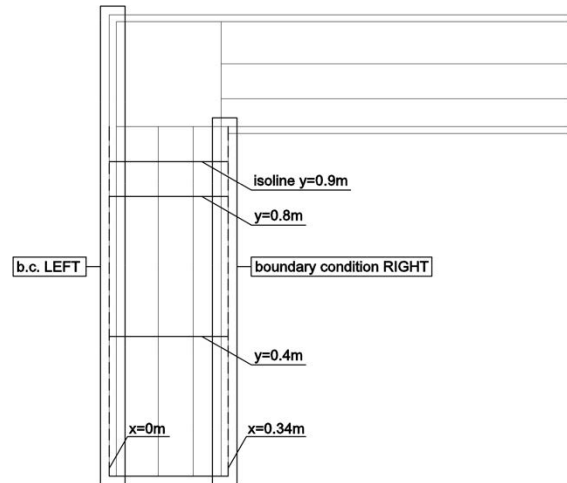


Fig. 5 – Schematization of the thermal bridge with relative nomenclature

The temperature profile of each Iso-Surface is traced by placing it in a defined point (Fig. 6), such as the simulation of the 24th hour of the second day). It can be noted that close to the thermal bridge ($y = 0.9\text{ m}$), the line has a different trend as influenced by the node (a). On the contrary, in the case of the equivalent wall, there are no differences in the temperature profiles based on their location because there is not a two-dimensional flow (b). Trying to overlap two graphs of the same Iso-Surface ($y = 0.8\text{ m}$), the surface temperatures are exactly the same, as opposed to the internal temperatures that show a different behavior (c).

Internal temperatures are different because the three equivalent layers are assumed constant but we need to consider the permeability factor; the hygrometric aspect is not to be considered for the variations of interstitial condensation. Simulations includes 24 consecutive analyzes, setting always the Time Step at 600 s, but changing the Number of time steps from 150 to 288 (simulations every hour from the 25th to the 48th); the temperature profiles on Iso-Surface are extrapolated at various distances from the bottom left point, considered the origin of the Cartesian axes.

When comparing the graphics of the middle Iso-Surface ($y = 0.9\text{ m}$) (Fig. 7); note that the two graphs do not differ particularly, less than a small margin.

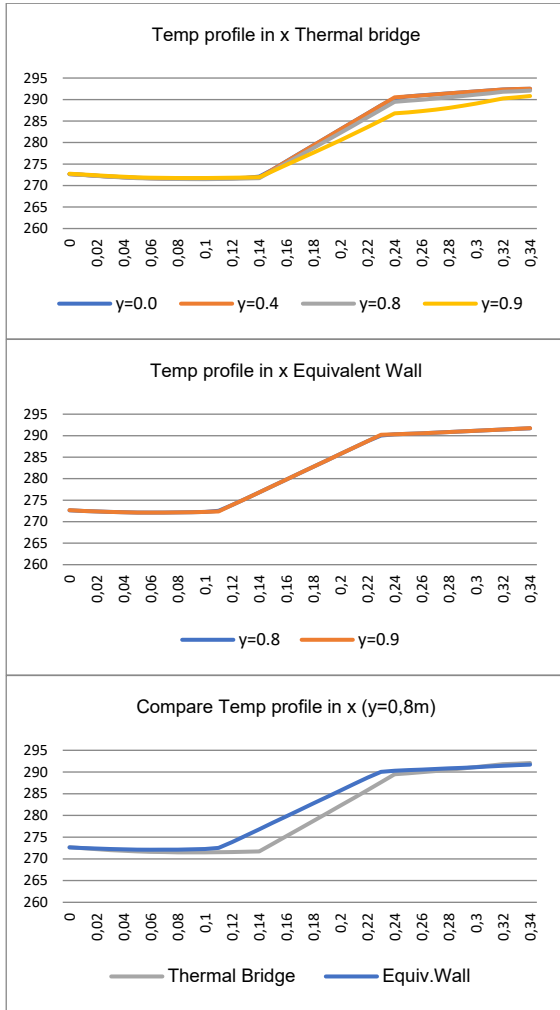


Fig. 6 – Temperature profile x-axis of thermal bridge (a), equivalent wall (b) and comparison (c)

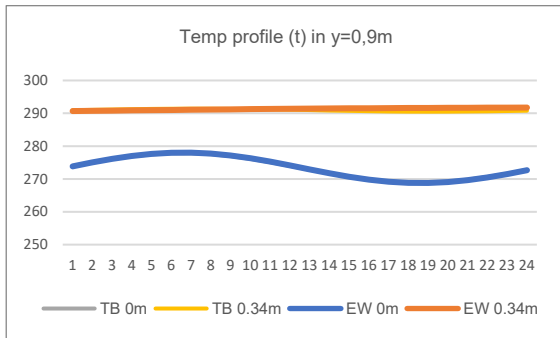


Fig. 7 – Trends of surface temperatures of the left and right boundary conditions, of the thermal bridge and the equivalent wall respectively.

When analyzing the heat flow trend in time (Fig. 8) the uncertainty on the total value is undefined, but there is a non-negligible error.

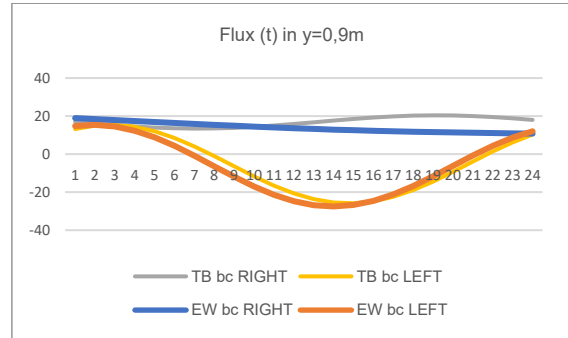


Fig. 8 – Uncertainty on heat flow trend

4. Conclusion

This paper presents the decomposition methodology of a thermal bridge that can be used to treat any type of thermal bridge which can be inserted into a dynamic modeling software for the calculation of the dispersions for transmission in dynamic regime. A good accuracy regarding the surface temperatures has been proved, therefore the method can be used effectively for energy assessments. This allows to evaluate the incidence of the thermal bridges, in winter and in summer, on a low-energy building and then to analyse their impact in terms of energetic consumption. Obviously, this method can be used only if there is a software development: it should be possible to automatically insert the geometries of thermal bridges to make their discretization faster.

Nomenclature

Symbols

A	Reference area for 1m depth (m ²)
C	Heat capacity (m ² kg/W)
C _p	Specific heat (J/(kg K))
e	Thickness of layer (m)
L	Length of wall (m)
N	Distance between the point where the vectors of the heat flux are not perfectly perpendicular to the first/second wall and the thermal bridge node (m)
Q	Heat flow (W)
R	Thermal resistance (m ² K/W)

T	Temperature (°C or K)
T _n	Temperature in a node (K)
t	Time (s)
U	Thermal transmittance (W/(m ² K))
V	Volume (m ³)
W	Length of first/second wall affected by a mono-directional flow (m)
α	Fictitious value
λ	Thermal conductivity (W/(m K))
ρ	Density (kg m ³)
φ	Dimensionless factor

Subscripts/Superscripts

bc	Boundary condition
e	External
EW	Equivalent wall
i	Internal
m	m-th layer
TB	Thermal bridge
W	Wall

References

- Aguilar, F., J.P. Solano, P.G. Vicente. 2014. "Transient modeling of high-inertial thermal bridges in buildings using the equivalent thermal wall method". *Applied Thermal Engineering* 67: 370-377. doi: 10.1016/j.applthermaleng.2014.03.058.
- Ascione, F., N. Bianco, F. de' Rossi, G. Turni, G.P. Vanoli. 2012. "Different methods for the thermal bridges into Energy simulation programs: Comparisons of accuracy for flat heterogeneous roofs in Italian climates". *Applied Energy* 97: 405-418. doi: 10.1016/j.apenergy.2012.01.022.
- Ascione, F., N. Bianco, R.F. De Masi, G.M. Mauro, M. Musto, G.P. Vanoli. 2014. "Experimental validation of a numerical code by thin film heat flux sensors for the resolution of thermal bridges in dynamic conditions". *Applied Energy* 124: 213-222. doi: 10.1016/j.apenergy.2014.03.014.
- European Parliament and European Council. 2002. *Directive 2002/91/EC of the European Parliament and of the council of 16 December 2002 on the energy performance of buildings*. Brussels, Belgium.
- European Parliament and European Council. 2010. *Directive 2010/31/EC of the European Parliament and of the council of 19 May 2010 on the energy performance of buildings*. Brussels, Belgium.
- Kim, Y.J., S.H. Yoon, C.S. Park. 2013. "Stochastic comparison between simplified energy calculation and dynamic simulation". *Energy and Buildings* 64: 332-342. doi: 10.1016/j.enbuild.2013.05.026.
- Kosny, J., E. Kossecka. 2002. "Multi-dimensional heat transfer through complex buildings envelope assemblies in hourly energy simulation programs". *Energy and Buildings* 34: 445-54. doi: 10.1016/S0378-7788(01)00122-0.
- Kossecka, E., J. Kosny. 1997. "Equivalent wall as a dynamic model of a complex thermal structure". *Journal of Building Physics* 20(3): 249-268. doi: 10.1177/109719639702000306.
- Ministero dello Sviluppo Economico. 2015. *Decreto del Ministero dello Sviluppo Economico 26 giugno 2015 - "Applicazione delle metodologie di calcolo delle prestazioni energetiche e definizione delle prescrizioni e dei requisiti minimi degli edifici"*. Rome, Italy: Italian Government.
- Renon, O. 2002. "Thermal bridges modeling in EnergyPlus". *Building Energy Simul User News* 23(4).
- Seem, J.E., S.A. Klein, W.A. Beckman, J.W. Mitchell. 1989. "Transfer function for efficient calculation of multidimensional transient heat transfer". *ASME Journal of Heat Transfer* 111: 5-12. doi: 10.1115/1.3250659.
- UNI. 2004. *UNI EN ISO 13790:2004. Thermal performance of buildings - Calculation of energy use for space heating*. Milan, Italy: UNI.
- UNI. 2008a. *UNI EN ISO 6946: 2008 - Thermal bridges in building construction. Heat flows and surface temperatures. Detailed calculations*. Milan, Italy: UNI.
- UNI. 2008b. *UNI EN ISO 10211: 2008. Thermal bridges in building construction. Heat flows and surface temperatures. Detailed calculations*. Milan, Italy: UNI.
- UNI. 2008c. *UNI EN ISO 14683: 2008. Thermal bridges in building construction. Linear thermal transmittance. Simplified methods and default values*. Milan, Italy: UNI.

Building Integrated Photovoltaics/Thermal (BIPV/T) System: A New Dynamic Simulation Model and a Case Study

Andreas Athienitis – Concordia University – aathieni@encs.concordia.ca

Giovanni Barone – University of Naples Federico II – giovanni.barone@unina.it

Annamaria Buonomano – University of Naples Federico II – annamaria.buonomano@unina.it

Adolfo Palombo – University of Naples Federico II – adolfo.palombo@unina.it

Abstract

In this paper, the energy performance of a façade open loop Building Integrated Photovoltaic/Thermal (BIPV/T) system with air as working thermal fluid is investigated. For this aim a new dynamic simulation model based on a detailed transient finite difference thermal network is developed. For a complete building energy performance analysis, such model was implemented in a suitable computer tool written in MatLab (called DETECT 2.3, suitably modified). The presented simulation model includes a parametric analysis tool useful to minimize the building energy demand.

In order to show the potential of the developed code, a comprehensive case study related to a multi-floor office building located in several climate zones is developed. In particular, with the aim to identify the design and operating parameters minimizing the overall energy consumptions, while guaranteeing the comfort of occupants, a suitable optimization procedure is carried out. Results show that through the produced electricity and thermal energy it is possible to balance the overall building energy demand approaching the NZEB goal.

1. Introduction

BIPV/T systems represent an innovative and effective measure for achieving net-zero energy buildings. Using this innovative technology, electricity and useful heat are simultaneously produced by solar energy. Therefore, the reduced building energy consumption is obtained by also boosting the share of renewables, as required for reaching the nearly-zero energy building target (Yang and Athienitis, 2016).

In order to carry out feasibility analysis as well as for the best design of such BIPV/T system, the use of

suitable energy performance simulation tool is recommended. Different numerical approaches can be followed and are commonly used by researchers. Specifically, the performance of the BIPV/T system are analysed through the use or development of one or two dimensional thermal network models (based on finite-difference schemes), through the modified Hottel-Whillier model or computational fluid dynamics (CFD) techniques (Yang and Athienitis, 2016). The active and passive energy performance of BIPV/T systems can also be assessed by using commercial software such as TRNSYS, EES, etc. (Lamnatou et al., 2015). Yet, in terms of energy, thermal, optical simulations, the available literature highlights the need of more studies focusing on the building and on the building/system configuration (Lamnatou et al., 2015). In addition, for suitable consideration of critical design and operating details, often neglected in commercial tools, novel mathematical models are being developed (Rounis et al., 2016). In this context, with the aim at investigating the BIPV/T performance, by taking into account both passive and active effects, this paper presents a new in-house developed simulation model for the dynamic analysis of BIPV/T systems. In particular, it refers to opaque photovoltaic panels integrated in the building skin façade or roof with air as working thermal fluid (Fig. 1).

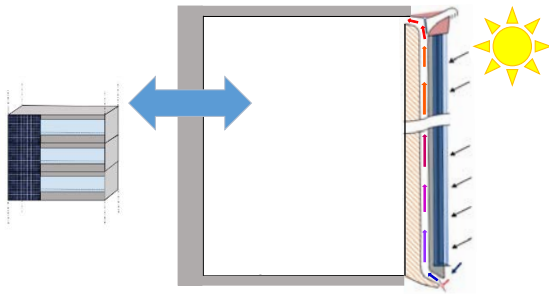


Fig. 1 – Modelled façade BIPV/T system

The developed model is implemented in a suitable computer tool, suitably modified for the simulation of BIPV/T system. The model is written in MatLab, called DETECt 2.3, validated through a recognised code-to-code procedure (Buonomano et al., 2016), and allows performing complete building energy performance analyses (Buonomano and Palombo, 2014). Particular attention is paid to:

- assessing the system energy fluxes, temperatures and airflow distribution into the BIPV/T system (air gap included);
- obtaining dynamic energy performance results also referred to the BIPV/T system active effects (e.g., space heating through the air heated by the BIPV/T system, increased electricity production efficiency by the outdoor air flow, increased coefficient of performance of heat pumps) and passive ones (winter free heating and summer overheating through BIPV/T wall heat transfer);
- achieving optimal design and operating parameters for minimizing the building energy demand (by simultaneously guaranteeing the hygrothermal comfort). Such outcomes can be easily calculated through a single simulation run (through a suitable optimization tool implemented in the presented computer code);
- assessing economic and environmental impact performance indexes of the system as a function of climate, building envelope features and use.

The developed model is particularly suitable for the simulation of the thermal behaviour of multi-zone and multi-floor buildings, with facades/roofs partially or totally integrated with PV/T. Helpful results for the process of BIPV/T systems design and feasibility analysis in case of new or retrofitted buildings can be also obtained (Buonomano et al.,

2016). Furthermore, for comparison purposes, additional dynamic simulation models related to conventional building-plant systems are also implemented in the code.

In order to show the capability of the code and the potential of BIPV/T systems, four different case studies were developed. They refer to a multi-floor office building located in four different weather zones: Freiburg (South-Germany); Bolzano (North-Italy); Naples (South-Italy); Almeria (South-Spain).

2. Simulation Model

In this section, the developed dynamic simulation model for the performance analysis of the above-mentioned innovative BIPV/T system is described. The model, written in MatLab, is embedded in a new release, appropriately modified, of DETECt 2.3, a tool for the whole building energy, economic and environmental performance analysis (Buonomano and Palombo, 2014). Dynamic building-plant system performance results can be assessed starting by building envelope features, design and operating BIPV/T parameters, hourly climate data.

The mathematical model of BIPV/T system is based on a finite volume approach. A set of explicit equations is obtained for each node of the adopted thermal resistance capacitance (RC) network, including conductive, radiative, and convective heat transfer occurring within and through the BIPV/T system. A sketch of the considered BIPV/T system thermal network adopted to model the system behaviour is shown in Fig. 2. Here, 2-D transient heat transfer is simultaneously taken into account in: PV panels; air flow gap between PV panels and the back plates; back wall integrated with the BIPV/T. 1-D transient heat transfer is taken into account between the BIPV/T system and the outdoor and the indoor environment. In the following, the description of the mathematical models relative to the BIPV/T system, including the integrating wall, is reported; all model details related to the heat transfer phenomena taking place within the building interior zone are reported in Buonomano and Palombo (2014). In order to calculate the gradient of the air temperature within the BIPV/T cavity, each element of the system (i.e. PV, air gap channel, back plate) is subdivided, along the vertical

direction, in N equal control volumes (e.g., strips). The same assumption is considered for the perimeter wall integrating with the PV/T. However, different from the PV and back plate, for the wall integrating the PV/T, N capacitive nodes are modelled according to the occurring thermal mass. Note that building indoor / outdoor air temperature gradients are neglected.

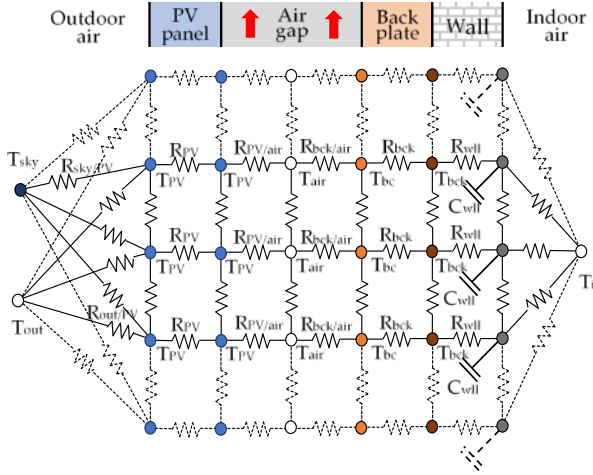


Fig. 2 – BIPV/T system RC thermal network

In order to solve the modelled thermal network for the BIPV/T system and to calculate each nodal temperature, an explicit finite difference method is used. In each time step interval $[(t + 1) - t]$ and for each i -th PV node, the discretised differential equation describing the energy rate of change is:

$$(\rho c V)_{PV} (T_{PV(i)}^{(t+1)} - T_{PV(i)}^{(t)}) = \sum_{n=i-1}^{i+1} \frac{(T_{PV(n)}^{(t)} - T_{PV(i)}^{(t)})}{R_{PV,PV}^{cond}} \Delta \vartheta + \dot{Q}_{sol,PV} + \left[\frac{(T_{out}^{(t)} - T_{PV(i)}^{(t)})}{R_{out,PV}^{conv}} + \frac{(T_{sky}^{(t)} - T_{PV(i)}^{(t)})}{R_{sky,PV}^{rad}} + \frac{(T_{air}^{(t)} - T_{PV(i)}^{(t)})}{R_{cavity,PV}^{conv}} + \frac{(T_{bc}^{(t)} - T_{PV(i)}^{(t)})}{R_{bc,PV}^{rad}} \right] \Delta \vartheta \quad (1)$$

where T is the temperature of the i -th PV node; $Q_{sol,PV}$ is the incident solar radiation on PV; $R_{m,PV}$ are the thermal resistances between the i -th node of the PV panel and other neighbours components (Fig. 2). $R_{m,PV}^{cond}$, $R_{m,PV}^{conv}$ and $R_{m,PV}^{rad}$ are, respectively, conductive, convective and radiative thermal resistances. Note that, in Equation (1) the temperature of i -th PV panel layer is the unknown variable.

The differential equation describing the energy rate of change of each control volume linked to the i -th air temperature node is:

$$L \cdot \bar{h}_{c,cavity} (T_{PV(i)}^{(t)} - T_{air(i)}^{(t)}) + L \cdot \bar{h}_{c,cavity} (T_{bc(i)}^{(t)} - T_{air(i)}^{(t)}) = \dot{m}_{air} c_{p,air} \frac{dT}{dz} \quad (2)$$

According to previous studies, in the developed model an exponential profile is taken into account for simulating the air temperature in the ventilated gap of the BIPV/T system (Pantic et al., 2014):

$$T_{(z)air} = T_{(in)air} \cdot e^{\left(\frac{2\bar{h}_{c,cavity}Lz}{\dot{m}_{air} c_{p,air}} \right)} + \left(\frac{\bar{h}_{c,cavity} T_{PV(i)}^{(t)} + \bar{h}_{c,cavity} T_{bc(i)}^{(t)}}{2\bar{h}_{c,cavity}} \right) \left(1 - e^{\left(\frac{2\bar{h}_{c,cavity}Lz}{\dot{m}_{air} c_{p,air}} \right)} \right) \quad (3)$$

The heat transfer coefficient inside the cavity, $\bar{h}_{c,cavity}$ is approximated by an experimental linear correlation, which is a function of the air velocity (Chen et al., 2010). The following correlation, recommended for design purposes, is:

$$\bar{h}_{c,cavity} = 3.94 \cdot v_{air} + 5.45 \quad (4)$$

In each t -th time step and for each i -th back plate layer node, the same approach used for PV layers is used. Thus, the discretised differential equation describing the energy rate change for each temperature node of the back plate is:

$$(\rho c V)_{bc} (T_{bc(i)}^{(\tau+1)} - T_{bc(i)}^{(\tau)}) = \sum_{n=i-1}^{i+1} \frac{(T_{bc(n)}^{(\tau)} - T_{bc(i)}^{(\tau)})}{R_{bc,bc}^{cond}} \Delta \vartheta + \left[\frac{(T_{wall}^{(\tau)} - T_{bc(i)}^{(\tau)})}{R_{wall,bc}^{cond}} + \frac{(T_{air}^{(\tau)} - T_{bc(i)}^{(\tau)})}{R_{cavity,bc}^{conv}} + \frac{(T_{PV}^{(\tau)} - T_{bc(i)}^{(\tau)})}{R_{PV,bc}^{rad}} \right] \Delta \vartheta \quad (5)$$

where $R_{m,bc}^{cond}$, $R_{m,bc}^{conv}$ and $R_{m,bc}^{rad}$ are respectively a conductive, convective and radiative thermal resistance due to the interaction between the system back-plate and others building elements. Note that in Fig. 2, the back-plate nodes are linked to the wall capacitive nodes that are subsequently linked to the indoor air temperature node T_{in} .

The discretised differential equation for each i -th façade layer describing the energy rate of change of each façade temperature node (wall in Fig. 2) is:

$$(\rho c V)_{fac} (T_{fac(i)}^{(t+1)} - T_{fac(i)}^{(t)}) = \sum_{n=i-1}^{i+1} \frac{(T_{fac(n)}^{(t)} - T_{fac(i)}^{(t)})}{R_{fac,fac}^{cond}} \Delta \vartheta + \left[\frac{(T_{in}^{(t)} - T_{fac(i)}^{(t)})}{R_{ind,fac}^{conv} + R_{fac,fac}^{cond}} + \frac{(T_{out}^{(t)} - T_{fac(i)}^{(t)})}{R_{out,wall}^{conv} + R_{fac,fac}^{cond}} \right] \Delta \vartheta + \dot{Q}_{sol,fac} \quad (6)$$

where T is the temperature of the i -th façade node and $Q_{sol,PV}$ is the solar radiation incident on the building façade.

Within the thermal zone, the calculation of the indoor air temperature T_{in} , as well as of the interior wall comprising the thermal zone is carried out by following the mathematical approach embedded in DETECT (Buonomano and Palombo, 2014). In particular, the discretized differential equation on the indoor air node is:

$$C_{in} \frac{dT_{in}}{dt} = \sum_{n=1}^N \frac{T_n^{(t)} - T_{in}^{(t)}}{R_{n,PVTwall}^{conv}} + \sum_{p=1}^P \frac{T_p^{(t)} - T_{in}^{(t)}}{R_{p,wrf}^{conv}} + \dots + Q_g^{(t)} + Q_v^{(t)} + Q_{HVAC}^{(t)} \quad (7)$$

where C_{in} is the thermal capacitance of the zone indoor air, whose temperature, T_{in} , is assumed as homogeneous in the space. The heat exchange between the $2 \times N$ internal surfaces nodes of the wall integrating the PV/T (*wll*) and the indoor air one is proportional to the internal convective resistances, $R_{n,PVTwall}^{conv}$, calculated as a function of the surfaces condition (e.g., ascendant or descendant flow, wall inclination); similarly the heat exchange between the P internal surfaces nodes of the interior building elements (walls, roof, and floor (*wrf*)) and the indoor air one is proportional to internal convective resistances, $R_{p,wrf}^{conv}$. In addition, with the exception of the radiative thermal load, all the sensible heat gains are networked to the indoor air node only (as purely convective). They are: Q_g is the internal gains due the occupants, lighting and electrical appliances; Q_v is the ventilation thermal load (including both the infiltration and ventilation terms); Q_{HVAC} is the sensible heat to be supplied to or to be removed from the building space by an ideal heating and cooling system (necessary to maintain the indoor air at the desired set point temperatures). Details about the assessment and handling of the solar radiation within the zone, and on calculation of the long-wave radiation exchange on the internal surfaces are available in (Buonomano and Palombo, 2014). The gross electricity power production is obtained by:

$$P_{el} = \eta_{PV} \cdot Q_n \cdot A_n \quad (8)$$

where η_{pv} is the PV efficiency, assumed linearly decreasing with the increasing operating temperature, taken from Pantic et al. (2010). Note that the

solar radiation incident on the PV modules, operating at their maximum power point condition, is assumed as uniform.

Finally, by the presented code it is possible to take into account the heat recovered through the PV/T channel on the heating energy consumptions. Specifically, such thermal energy can be directly supplied, as free heating, to the air thermal zone or supplied to the evaporator of a heat pump to increase its performances. To this aim, for the assessment of the coefficient of performance of air-to-air, as well as air-to-water heat pump/chiller ($COP_{HVAC,heat}$ and $COP_{HVAC,cool}$), it is possible to follow two methods within the code: i) a manufacturers data look up approach and ii) recommended analytical equations. In both methods, COPs are calculated by means of the nominal values (given by constructors) and as a function of the occurring operating conditions and the part-load ratio f_{PLR} .

3. Case Studies

The developed case studies refer to a ten-floor building (East–West oriented longitudinal axis) for open office spaces. In particular, the simulation is referred to a singular South facing perimeter thermal zone. On its South-façade a BIPV/T system and a window (4-6-4 air filled double-glazed system) of 10 m² are modelled (Fig. 3).

The thicknesses of building walls (U-value = 1.30 W/(m² K)) and floor/ceiling (U-value = 1.10 W/(m² K)) are 30 and 25 cm respectively. The wall layers include hollow bricks ($\lambda = 0.33$ W/(m K), $\rho = 1600$ kg/m³, $c = 1200$ J/(kg K)) and thermal insulation ($\lambda = 0.05$ W/(m K), $\rho = 13.0$ kg/m³, $c = 1100$ J/(kg K)). The direct solar radiation transferred through the windows to the inside zone is assumed to be absorbed by the floor and the interior walls with absorption factor of 0.4 and 0.2, respectively. For such zone, a ventilation rate equal to 1 Vol/h and a crowding index of 0.12 person/m² are taken into account. The interior thermal loads include people (95 W/p at 26 °C, varying with T_{in}), lighting, and equipment (9 W/m²). Interior walls are modelled as adiabatic. The simulation starts on 0:00 of January 1 and ends at 24:00 of December 31. Both the

innovative and traditional simulated buildings are heated/cooled through a 10 kW air-to-air electric heat pump/chiller. The HVAC system is switched on from 08:00 to 20:00 (week days only).

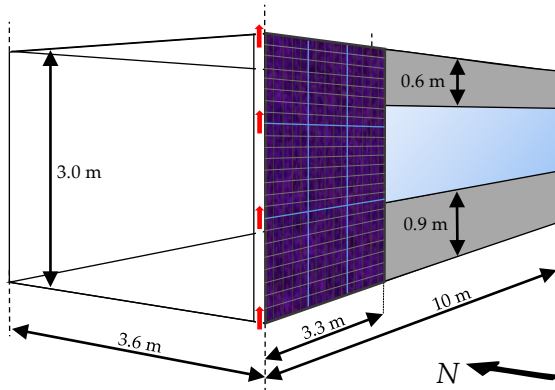


Fig. 3 – Perimeter zone of one sample building floor

The heating and cooling set points are 20 and 26 °C. The simulations were carried out through DETECT 2.3 and refer to 4 different weather zones, Table 1. Here, heating and cooling degree days (HDD and CDD), incident solar radiation (ISR) and the considered heating and cooling periods are also reported.

Table 1 – Climatic zones, climatic indexes and system scheduling

	HDD Kd	CDD Kd	ISR kWh/m ² y	Heating	Cooling
Freiburg	3110	253	1114	No limitations	
Bolzano	2641	475	1251	10/15 - 4/15	6/01 - 9/30
Naples	1479	727	1529	11/15 - 3/31	6/01 - 9/30
Almeria	783	961	1724	12/01 - 3/31	6/01 - 9/30

For the innovative system layout, the BIPV/T system outlet air is exploited in the winter to supply the evaporator of the adopted air-to-air heat pump for space heating. A minimum gap air flow rate of 0.1 m³/s is obtained through a fan. If the natural convection allows higher flow rates the fan is switched off. In this case study, the potential direct free heating (for $T_{inlet} > 20$ °C) is neglected. The BIPV/T system air flow enhances the PV efficiency.

4. Results and Discussion

In Fig. 4 for the weather zone of Naples, the time

histories of the indoor air temperature at the 9th floor for both the innovative and traditional building layouts are reported for two sample winter and summer days (January 10–11 and June 29–30, respectively). Here, it possible to observe that during the hours in which the HVAC system is switched on, the setpoint temperatures are always reached. During night time, the passive effect of BIPV/T can be easily observed: the free floating indoor air temperature increases due to the heat gain due to the thermal inertia of the wall integrating the PV/T. In particular, during the winter season the resulting free floating temperatures approaches the setpoint better than the ones obtained in the traditional building, whereas the contrary occurs in the summer.

The BIPV/T system passive effect can be also observed in Fig. 5. Here, for Naples, the calculated sensible thermal loads (Q_{HVAC}) profiles detected on the 9th building floor are depicted for the same time hours of Fig. 4, for both the innovative and traditional building configurations. During the heating season a reduction of the thermal loads vs. the traditional building (Fig. 4, top) is obtained through the BIPV/T system passive effects (space free heating). Note that in this case study the winter BIPV/T system active effect is the enhanced heat pump efficiency obtained by exploiting the heat extraction through the solar collectors. Conversely, during the summer HVAC running, an increase of cooling loads is obtained through the passive effect (space overheating) due to the BIPV/T system adoption (Fig. 4, bottom).

For a winter sample day (January 10), in Fig. 6 the temperature profiles of the PV panels and of the related gap air are reported vs. the length of the BIPV/T system gap (building height) and of the time hours (Fig. 6). Note that, the gap air temperatures follow and approach the PV panels ones (ranging between 35 and 52 °C), which obviously depends on the solar irradiation incident on the solar collector surface. The maximum temperature increase detected between the outlet and inlet air is about 20 °C (therefore, the temperature gain achieved per building floor is about equal to 2 °C). Note that, such air temperature growth is due to the slow air velocity (minimum level set at 0.45 m/s). During summer an overheating of the gap air temperatures

can be observed (mostly in hot summer climates). In this case, an increase of the gap air fan speed is recommended. It is noteworthy to observe that the calculated nighttime temperature of the PV can be lower than that of the traditional building envelope and of the outdoor air.

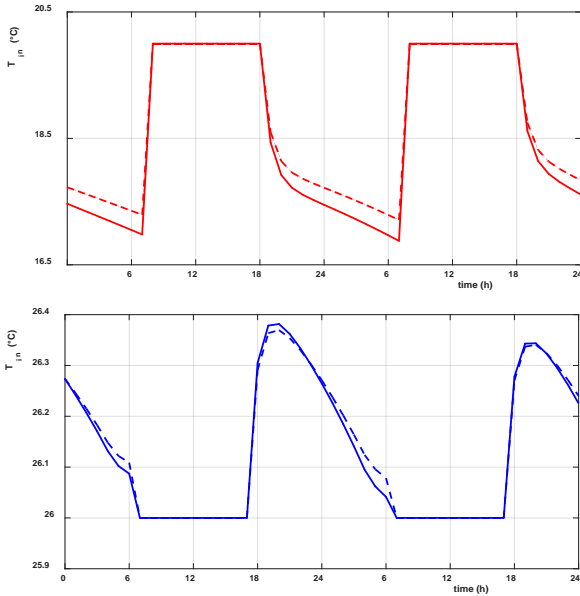


Fig. 4 – Indoor air temperatures in January 10 and 11 (up) and June 29 and 30 (down). Dashed lines: BIPV/T system layout. Solid lines: traditional building

This result is due to the long-wave infrared radiative heat exchange between the building external surfaces and the sky.

In Fig. 7 for the weather zone of Naples the temperature profile of the BIPV/T panels, gap air, and outdoor air are reported as a function of the length of the BIPV/T system gap for a sample winter time instant (January 10 at 13:00). In this figure, it can be observed that the gap air temperature reaches the selected indoor air setpoint (20 °C) at a building height corresponding to the 4th floor (12 m). Note that such occurrence is related to an inlet outdoor air temperature of 12 °C. By Fig. 6 and 7 it can be also observed that the PV panels are suitably cooled by the air flowing in the gap (an increased PV efficiency is achieved). Simultaneously, the outdoor air is gradually heated along the BIPV/T gap (the obtained thermal energy is usefully recovered). A decreasing difference trend of such temperatures can be observed in Fig. 7.

In Fig. 8, for the weather zone of Naples, the calculated monthly heating and cooling demands, are shown for both the innovative and conventional building. It is possible to observe the month-by-month effects of the BIPV/T system on the building energy requirement.

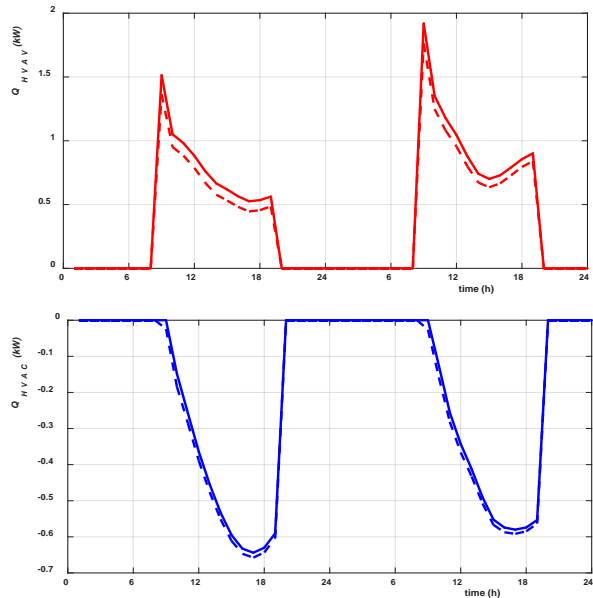


Fig. 5 – Sensible thermal loads (Q_{HVAC}) in January 10 and 11 (up) and June 29 and 30 (down). Dashed lines: BIPV/T system layout. Solid lines: traditional building

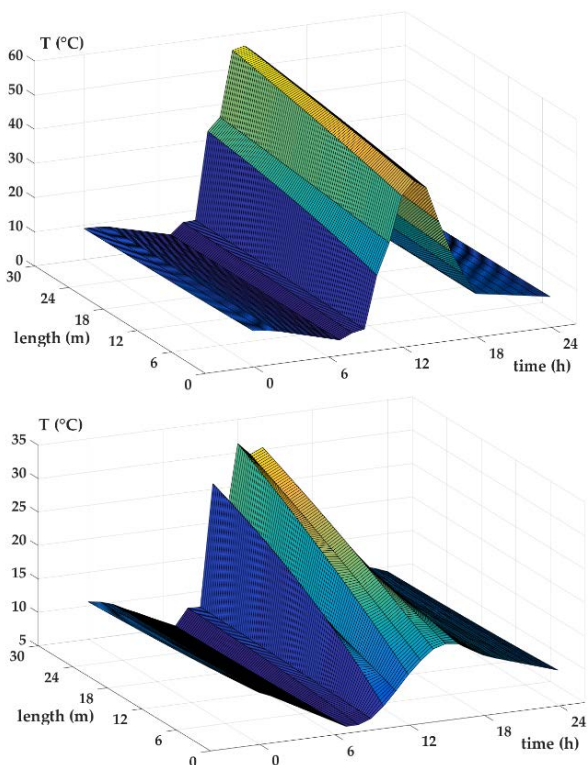


Fig. 6 – Temperatures of BIPV/T collectors (up) and gap air (down) in January 10

In Table 2 for all the investigated weather zones the yearly heating and cooling demands of the traditional and the innovative system are reported for 3 sample floors and the whole building.

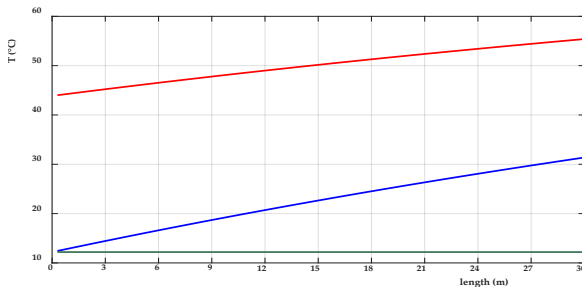


Fig. 7 - Temperatures of the BIPV/T panel (red line), gap air (blue line) and outdoor air (green line) for January 10 at 13:00

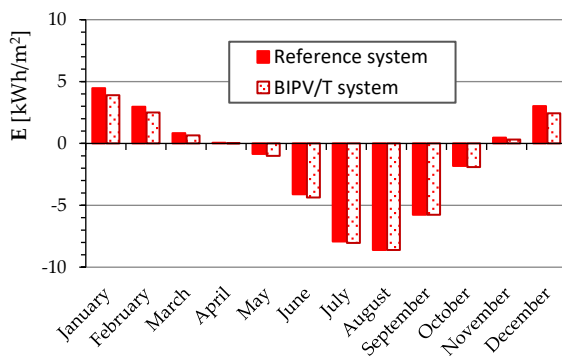


Fig. 8 – Monthly heating and cooling demands

Table 2 – Reference and BIPV/T system: energy demand for heating (H) and cooling (C) expressed as [kWh/m²y]

Reference system		Freiburg	Bolzano	Naples	Almeria
Floor 1 st	H	58.6	47.1	11.8	0.3
	C	-5.6	-16.4	-29.0	-34.6
Floor 5 th	H	58.6	47.1	11.8	0.3
	C	-5.6	-16.4	-29.1	-34.7
Floor 10 th	H	58.7	47.1	11.8	0.3
	C	-5.6	-16.4	-29.1	-34.7
Building [MWh/y]	H	21.1	17.0	4.2	0.11
	C	-2.0	-5.9	-10.5	-12.5
BIPV/T system		Freiburg	Bolzano	Naples	Almeria
Floor 1 st	H	53.5	43.3	10.2	0.2
	C	-5.9	-16.6	-28.8	-34.4
Floor 5 th	H	53.0	42.8	9.8	0.2
	C	-6.2	-17.1	-29.6	-35.2
Floor 10 th	H	52.5	42.2	9.5	0.2
	C	-6.5	-17.7	-30.5	-36.0
Building [MWh/y]	H	19.1	15.4	3.5	0.07
	C	-2.2	-6.2	-10.7	-12.7

The obtained results vary as a function of the building floor height, due to the different corresponding temperatures of the BIPV/T system wall. In general, the building heating energy savings are higher than

the increase of the cooling demands. Obviously, heating and cooling demands are strongly dependent on the weather conditions. In Table 3 the yearly electricity production calculated for all the weather zones is reported. Note that the production efficiency is enhanced through the cooling air flowing in the BIPV/T system gap. Table 3 shows that higher productions are achieved at lower building floors (i.e. stronger heat extraction potential causes lower cooling air temperatures, Fig. 7). Of course, larger electricity productions are obtained where the ISR is higher.

Table 3 – BIPV/T system: electricity production

	Freiburg	Bolzano	Naples	Almeria
Floor 1 st	29.0	34.7	37.5	41.1
Floor 5 th [kWh/y]	28.8	34.5	37.2	40.8
Floor 10 th	28.6	34.3	37.0	40.5
Building [MWh/y]	10.4	12.4	13.4	14.7

In Table 4 the yearly final electricity uses calculated for all the investigated weather zones are reported. The calculated results include the PV production and the electricity consumption of the electric heat pump/chiller, gap air fan, lighting and machineries. Here, the influence of the building floors height results to be very weak. It is noteworthy to observe that, for all the case studies the adoption of the BIPV/T system allows to reach the nearly or net zero energy building target.

Table 4 – Final electricity use expressed as [kWh_e/(m²y)]

		Freiburg	Bolzano	Naples	Almeria
Floor 1 st	Ref.	54.5	52.2	39.5	36.8
	BIPV/T	26.3	18.3	2.4	-4.4
Floor 5 th	Ref.	54.5	52.2	39.5	36.8
	BIPV/T	26.4	18.4	2.8	-3.9
Floor 10 th	Ref.	54.5	52.2	39.6	36.8
	BIPV/T	26.4	18.6	3.1	-3.5
Building [MWh _e /y]	Ref.	19.6	18.8	14.2	13.2
	BIPV/T	9.5	6.6	1.0	-1.4
[y]	SPB	8.2	6.8	6.3	6.0

In fact, in addition to the building self-consumption fulfilment an electricity export can be achieved. The best results are obtained in Almeria, with an electricity export of 1.4 MWh_e/y. By such results a swift and simplified economic feasibility analysis can be carried out by taking into account an incentive of 50 % on the system capital cost and an electricity purchase and feed-in tariff of 0.18 and 0.08 €/kWh_e, respectively. In particular, satisfactory

paybacks are achieved, Table 4. In Table 5 the yearly primary energy saving and avoided overall CO₂ emission for all the investigated weather zones are reported. An average primary energy factor of 0.46 kWh_e/kWh_p and an average CO₂ conversion factor of 0.423 kg_{CO2}/kWh_e are considered. Remarkable primary energy savings are obtained. Note that results lower than zero (Almeria) suggest energy exports (innovative building). Interesting results are also obtained in terms of avoided CO₂, confirming (besides the economic convenience), the overall feasibility of such technology.

Table 5 – Primary energy savings expressed as [kWh_p/m²y] and avoided CO₂ emissions

		Freiburg	Bolzano	Naples	Almeria
Floor 1 st	Ref.	118.4	113.4	85.8	80.0
	BIPV/T	57.2	39.8	5.3	-9.5
Floor 5 th	Ref.	118.5	113.5	85.9	80.0
	BIPV/T	57.3	40.1	6.1	-8.6
Floor 10 th	Ref.	118.5	113.5	86.1	80.0
	BIPV/T	57.4	40.3	6.8	-7.6
Building [MWh _p /y]	Ref.	42.6	40.9	30.9	28.8
	BIPV/T	20.6	14.4	2.2	-3.1
[tCO ₂ /y]	ΔCO ₂	4.3	5.1	5.6	6.2

5. Conclusion

In this paper, a new dynamic simulation model for the energy performance assessment of façade building integrated photovoltaic/thermal (BIPV/T) systems is presented. For a complete building energy performance analysis, such model was implemented in a computer tool written in MatLab (called DETECT 2.3). The developed model takes into account both the active and passive BIPV/T system effects. The active effects pertain to the efficiency increase through the air flowing in the system gap of both the PV panels and the electric heat pump for space heating.

In order to show the potentiality of the presented tool a suitable case study is developed. It refers to an office building located in four different weather zones. Here, a BIPV/T façade is suitably designed for electricity and thermal energy productions. Simulations show interesting benefits vs. traditional buildings in terms of energy efficiency, economic savings, system payback, and avoided CO₂ emissions. As evidenced by the results, useful design

and operating data are achieved for reaching the nearly or net zero energy building goal for both new and renovated buildings.

Nomenclature

Symbols

\dot{m}	flow rate (kg/s)
Q	thermal load (W)
R	thermal resistance (K/W)
T	temperature (K)

Subscripts/Superscripts

<i>air</i>	air-gap air
<i>bck</i>	back-plate
<i>faç</i>	façade
<i>in</i>	indoor air
<i>out</i>	outdoor air
<i>PV</i>	photovoltaics panel

References

- Buonomano, A., G. De Luca, U. Montanaro, A. Palombo. 2016. "Innovative technologies for NZEBs: An energy and economic analysis tool and a case study of a non-residential building for the Mediterranean climate". *Energy and Buildings* 121: 318-343. doi: 10.1016/j.enbuild.2015.08.037.
- Buonomano, A., A. Palombo. 2014. "Building energy performance analysis by an in-house developed dynamic simulation code: An investigation for different case studies". *Applied Energy* 113: 788-807. doi: 10.1016/j.apenergy.2013.08.004.
- Chen, Y., K. Galal, A.K. Athienitis. 2010. "Modeling, design and thermal performance of a BIPV/T system thermally coupled with a ventilated concrete slab in a low energy solar house: Part 2, ventilated concrete slab". *Solar Energy* 84(11): 1908-1919. doi: 10.1016/j.solener.2010.06.012.
- Lamnatou, C., J.D. Mondol, D. Chemisana, C. Maurer. 2015. "Modelling and simulation of Building-Integrated solar thermal systems: Behaviour of the coupled building/system configuration". *Renewable and Sustainable Energy Reviews* 48: 178-191. doi: 10.1016/j.rser.2015.03.075.

- Pantic, S., L. Candanedo, A.K. Athienitis. 2010. "Modeling of energy performance of a house with three configurations of building-integrated photovoltaic/thermal systems". *Energy and Buildings* 42(10): 1779-1789. doi: 10.1016/j.enbuild.2010.05.014.
- Rounis, E.D., A.K. Athienitis, T. Stathopoulos. 2016. "Multiple-inlet Building Integrated Photovoltaic/Thermal system modelling under varying wind and temperature conditions". *Solar Energy* 139: 157-170. doi: 10.1016/j.solener.2016.09.023.
- Yang, T., A.K. Athienitis. 2016. "A review of research and developments of building-integrated photovoltaic/thermal (BIPV/T) systems". *Renewable and Sustainable Energy Reviews* 66: 886-912. doi: 10.1016/j.rser.2016.07.011.

Buildings Integrated Phase Change Materials: Modelling and Validation of a Novel Tool for the Energy Performance Analysis

Giovanni Avagliano – University of Naples Federico II – g.avagliano12@gmail.com

Annamaria Buonomano – University of Naples Federico II – annamaria.buonomano@unina.it

Maurizio Cellura – University of Palermo – maurizio.cellura@unipa.it

Vasken Dermardiros – Concordia University – vdermardiros@gmail.com

Francesco Guarino – University of Palermo – francesco.guarino@unipa.it

Adolfo Palombo – University of Naples Federico II – adolfo.palombo@unina.it

Abstract

In this paper a novel dynamic energy performance simulation model for the Phase Change Materials (PCM) analysis is presented. The model is implemented in a suitable computer code, written in MatLab and called DETECT, for complete building energy analyses. In the presented model, the “effective specific heat” method is implemented. Here, the specific heat of each PCM layer changes as a function of the system phase and temperature in both melting and freezing processes. A model validation is carried out by comparing numerical results vs. measurements obtained at Solar Laboratory of Concordia University (Montreal, Canada). The simulation model allows exploring the potential of PCMs to increase the thermal inertia of building envelopes and to assess the effects/weight of several design parameters (e.g. PCMs melting temperature, etc.) on the building heating and cooling energy demand and on the related thermal comfort. In order to show the potentiality of the presented simulation model, suitable case studies referred to residential and office buildings, to three different weather conditions and to two alternative PCM layouts in the building envelope, are developed.

1. Introduction

Recently, the research of innovative solutions aimed at improving the energy efficiency and comfort of buildings, has become increasingly significant. Among the available techniques, the integration in the building envelope of Phase Change Materials (PCMs) can be considered (Kuznik et al., 2011). Basically, through such mate-

rials the thermal inertia of the building envelope can be increased by exploiting the latent heat stored in PCM during its melting process and by taking advantage of the latent heat of solid and liquid transformation. Thus, by the integration of PCM in the building envelope, the storage and release of thermal energy occurring during the phase change can effectively reduce heating/cooling consumptions and increase thermal comfort (Dutil et al., 2014). In fact, the decrease and delay of the thermal loads implies a reduced fluctuation of the indoor air temperature with the enhancement of the building comfort (to avoid system overheating by dissipating or recovering the stored heat during late/night hours). Nevertheless, the proper exploitation of the latent heat stored in PCM is highly influenced by the building usage (Buonomano et al., 2016a). In addition, the use of PCMs in buildings also implies some criticisms such as: still high initial costs and some design and operating difficulties due to the variation of specific heat, thermal conductivity, and density during the phase change process (Liu et al., 2016).

In order to assess the potentiality of the building integration of PCMs, a number of computer tools for energy performance analyses of PCMs have recently been developed (Dutil et al., 2014). However, the knowledge of the thermodynamics properties of PCMs and phenomena governing their variation is crucial to select the suitable materials for the specific building and to model the system for the energy performance assessment. In case of conduction dominated phase change, e.g.,

microencapsulated PCMs (Kuznik et al., 2011), in literature the heat transfer phenomenon is modelled by means of both the apparent specific capacity and the enthalpy method, which can alternatively be used as a function of the available thermodynamics properties and the selected methodology (Al-Saadi and Zhai, 2015; Tittlein et al., 2015). Despite of their capability in predicting the thermal and energy behaviour of PCMs in buildings, different models based on these methods are available in literature (Kuznik et al., 2011; Dutil et al., 2014). Nevertheless, for the PCM characterization (such as the assessment of PCMs specific heat, c_p) the most widely adopted technique consists in the use of a Differential Scanning Calorimeter (DSC-method) (Dutil et al., 2014; Tittlein et al., 2015), together with the T-history method (Tittlein et al., 2015). Today, the measurement of the PCMs thermodynamics properties is an open problem for researchers and manufacturers due to several issues related, for example, to the mechanical confinement, chemical interaction, different enthalpy of melting and freezing, incomplete melting and freezing, nucleation process, measurement conditions (sample mass, heating and cooling rates), etc. vs. real ones (Kuznik et al., 2011). Therefore, review studies on this topic highlight the need of improved thermal characterization procedures (Dutil et al., 2014). Such procedures are also necessary for the proper design of effective PCMs for building applications, carried out through suitable building dynamic simulation modelling. In this framework, the authors carried out the characterization of a commercially available PCM wall-board by calculating the thermodynamic PCMs properties from available experimental data. The obtained set of measurements (collected in diverse conditions) was used in order to tune the c_p profiles, variable as a function of the occurring temperature. Such novel profiles are implemented in a dynamic building energy performance simulation tool written in MatLab (DETECT 2.2) (Buonomano and Palombo, 2014), for whole building energy performance analyses. Finally, in order to show the potential of such tool, the authors developed a case study on a building integrating PCMs, located in a different weather zone.

2. Simulation Model

The simulation model used for the analysis of the PCM building integration is based on the finite difference method, assuming a one-dimensional thermal domain. By such model, called DETECT 2.2 and validated through a code-to-code validation procedure (Buonomano, 2016), the assessment of temperatures and humidity dynamics, as well as of heating and cooling loads and demands, can be carried out (Buonomano and Palombo, 2014).

The physical building model consists in a resistive-capacitive (RC) thermal network obtained by distributed parameters (Tsilingiris, 2006). Fig. 1 shows a sketch of the modelled RC thermal network for one thermal zone.

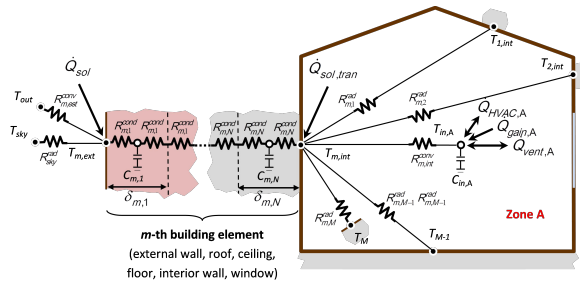


Fig. 1 – Simulation model: RC thermal network

The following model simplifications are considered: i) the indoor air of each thermal zone is considered as uniform and modelled as a single indoor air temperature node; ii) the building envelope is subdivided into M multi-layer elements (a high order RC thermal network); iii) each m -th multi-layer building element of a single zone is subdivided in N sub-layers, where thermal masses and conductivities are uniformly discretised; iv) $N+2$ capacitive and surface nodes are considered for each m -th envelope component; v) each PCM node is characterized by a dynamic variation of the heat capacity, dependent on:

- the temperature of the considered element;
- phase transition (melting/solidification).

In each (t) -th time step and for each (n) -th capacitive node of the (m) -th element, the differential equation describing the energy rate of change of each temperature node of the building envelope is:

$$C_{m,n} \frac{dT_{m,n}}{dt} = \sum_{j=n-1}^{n+1} \frac{T_{m,j} - T_{m,n}}{R_{m,j}^{eq}} \quad (1)$$

where $R_{m,j}^{eq}$ is the sum of the halves sub-layers thermal resistances $R_{m,j}^{cond}$ linking the n -th node to their neighbours (Fig. 1). For non-capacitive outer ($n = 0$) and inner ($n = N+1$) surface boundary nodes, the heat transfer is calculated by:

$$\sum_{j=n-1}^{n+1} \frac{T_{m,j} - T_{m,n}}{R_{m,j}^{cv}} + \dot{Q}_{m,n} = 0 \quad (2)$$

where $R_{m,j}^{cv}$ is either a convective (external $R_{m,0}^{conv}$ or internal $R_{m,N+1}^{conv}$ non-capacitive nodes) or a conductive resistance ($R_{m,n}^{cond}$), depending on the side layer of the considered node (Fig. 1). $\dot{Q}_{m,n}$ is a forcing function including incident solar and long-wave radiation exchange acting on outer and inner surfaces of thermal zone (Buonomano, 2016).

The differential equations on the thermal network nodes must be solved simultaneously with the system of Equations (1) and (2). The sensible energy rate of change of indoor air masses can be calculated as:

$$C_{in} \frac{dT_{in}}{dt} = \sum_{m=1}^M \frac{T_{m,N} - T_{in}}{R_{m,N+1}^{conv}} + \dot{Q}_{gain} + \dot{Q}_{vent} \pm \dot{Q}_{ac} \quad (3)$$

where \dot{Q}_{gain} is the internal load due to occupants, lights, and equipment; \dot{Q}_{vent} is the ventilation thermal load; \dot{Q}_{ac} is the sensible heat to be supplied to or removed from the thermal zone by an ideal heating and cooling system. Additional details are reported in (Buonomano and Palombo, 2014).

The modelling approach is suitable for the assessment of the phenomenon of phase change, taken into account by using the effective heat capacity method (Tittlein et al., 2015). By such technique, a temperature dependent thermal capacitance c_p is assumed, during both the melting and solidification processes (i.e. to take into account the hysteresis phenomenon typical for paraffin materials). It is worth noting that the whole building model is partially implicit, and the effective heat capacity of each node (by varying the thermal capacitance in Equation (1) as a function of the time) is calculated at the previous time step (Kuznik et al., 2015; Buonomano et al., 2016b). In order to model the PCM building integration, the effective heat capacity curve of the PCM, together with the

conductivity one, as suggested by literature (Kuznik et al., 2008), was first implemented in the model and then calibrated as a function of the available experimental data. Such inverse approach was adopted to enhance the reliability of PCM specific heat during phase change processes.

3. Experimental analysis

The PCM behaviour in the indoor environment was assessed through experimentation (Guarino et al., 2015; Guarino et al., 2017). A small test room with a large window was fitted with PCM modules on the (opposing) back wall. The test room (Fig. 2) has interior dimensions: 2.80 m width \times 1.30 m depth \times 2.44 m height, with an overall conductance of 0.2 W/(m² K). The window is double-glazed (2 m \times 2 m, U = 1.7 W/(m² K), visible transmittance of 0.616, SHGC = 0.262) with 6 mm low-e glass and a 12 mm gap filled with Argon.

The PCM used in the experiment is a commercially-available PCM wallboard, described in Kuznik et al. (2008). It is a mixture of 40 % ethylene-based polymer and 60 % paraffin wax, with a density of 900 kg/m³. The panels (5.2 mm thick, 1000 mm wide and 1198 mm long) are encapsulated with 100 μ m aluminum layer on both sides. The latent heat is 70 kJ/kg, with a melting point peaking at 21.7 °C. 20 PCM sheets were installed on the back wall of the test room.

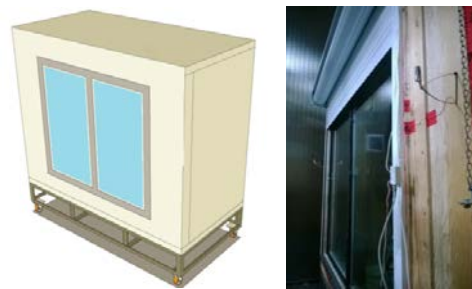


Fig. 2 – Schematic and front view of the test room

They were divided in four groups, each with 5 layers of PCM panels, for a total of roughly 100 kg. The experimental setup took place in the Solar Simulator Environmental Chamber facility at Concordia University (Montreal, Canada).

Basically, it is featured by two solar simulators and a climatic chamber in which temperatures and relative humidity can be varied between $-40\text{ }^{\circ}\text{C}$ and $+50\text{ }^{\circ}\text{C}$ and 20 % and 95 %, respectively. The test room, placed inside the climatic chamber was subjected to radiation emitted by a full-scale solar simulator (Fig. 3a). In combination with glass filters, 6 metal halide lamps provide a spectral distribution close to natural sunlight, fulfilling the EN12975: 2006 and ISO 9806-1:1994 specifications.

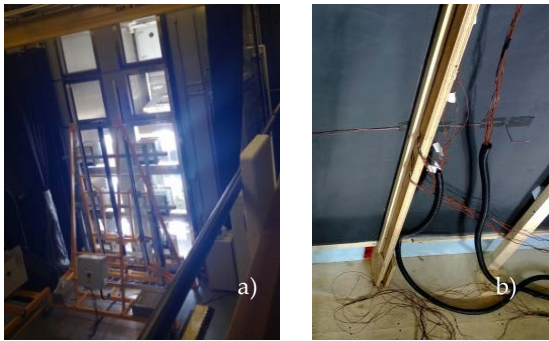


Fig. 3 – a) Solar simulator – b) Back wall PCM panels

Test room temperatures were monitored by using Type T thermocouples placed: in each PCM inter-layer interface; on the back wall (at different heights and at 5 cm distance from the PCM panels, Fig. 3b); on the remaining room interior surfaces. Air temperature in the test room was monitored at 4 different heights.

The carried out tests can be summarized as follows:

Test 1: Duration: 75 hours. Environmental chamber temperature: $16\text{ }^{\circ}\text{C}$. Test room heating obtained with a 350 W fan-coil for 21 hours (free-floating temperature for the remaining time);

Test 2: Duration: 75 hours. Quasi-sinusoidal air temperature profile in the environmental chamber with a peak of $20\text{ }^{\circ}\text{C}$ (every day) and a minimum of $10\text{ }^{\circ}\text{C}$ (first day) and $6\text{ }^{\circ}\text{C}$ (second and third day), the average solar radiation was 500 W/m^2 (9:30 am - 1:00 pm for the first day and 9:30 am - 12:30 am for the second and the third day).

For both tests the measured data were logged every 3 minutes, by averaging readings performed every 30 seconds).

4. Model validation

The model validation was performed by simulating both the experimental tests described in the previous section. Specifically, two suitable case studies were modelled in order to faithfully repeat all the above-mentioned boundary conditions. Several simplification assumptions were taken into account in the developed simulation code, such as: i) a single PCM layer (suitably divided into 5 capacitive nodes) was considered for both tests; ii) mono-dimensional heat flux is considered in the modelled PCM; iii) in Test 1 the fan coil outlet air interacts with the PCM wall only by natural convection heat transfer (e.g. considered as convective input (as \dot{Q}_{hc}) in Equation (3)); iv) in Test 2 the incident radiation on the PCM wall is considered uniform and perpendicular to the surface (whereas a difference ranging from 430 to 590 W/m^2 was effectively detected on the radiated surface).

Initially, the PCM melting and solidification c_p profiles were considered equal to those suggested in Kuznik et al. (2008). Nevertheless, the curve taken from publication was not suitable for the all the simulated tests (numerical results did not agree with all the experimental ones). Thus, the authors performed a subsequent model refinement, where the PCM c_p was iteratively obtained as a function of the reduction to the minimum of the deviation between the temperature $T_{k,i}$ (of the k -th node in the i -th time step) measured in the experimental tests and the one calculated by the simulation model. It is worth noting that convective and radiative external coefficients were suitably tuned in order to replicate the external boundary conditions occurring in the test chamber. By following this approach, new $c_p(t)$ curves, for solidification and melting were shaped. The resulting hysteresis is very slight, different from the majority of publications, but according to few authors as reported in Dutil et al. (2014). In fact, a remarkable presence of hysteresis (as the one of the first $c_p(t)$ curves) effectively created modelling inaccuracies in continuous simulated charging and discharging processes (as in Test 2). This might be ascribed to the dependence of the thermal behaviour on the history of heat loading, the heating rate, and on

incomplete melting/solidification (Dutil et al., 2014).

By taking into account the new curves, a comparison between experimental and model temperatures for the outermost PCM layer (Node 1), the innermost one (Node 5) and test cell indoor air is reported and showed in Fig. 4 and 5 for Test 1 and Test 2, respectively. A good agreement between measurements and numerical results is detected in both cases.

Such achievement is evident by observing also Fig. 6 and 7, depicting the time histories of the detected errors between experimental and simulation results, for all PCM and indoor air temperature nodes. Except for few brief time steps, model errors are always lower than ± 0.7 °C.

Note that, such errors are probably due to some uncertainties in the system modelling, as well as in measurements operations, mainly due to several occurrences, as: i) absence of radiation shading of the thermocouples for the measurement of the test chamber air temperature; ii) lack of uniform vertical temperature profile especially for Test 2; iii) conduction defect between the 5 overlapping PCM layers mainly due to the presence of the thermocouples (thin air-gap among PCM panels, simulated by slightly reducing their conductivity).

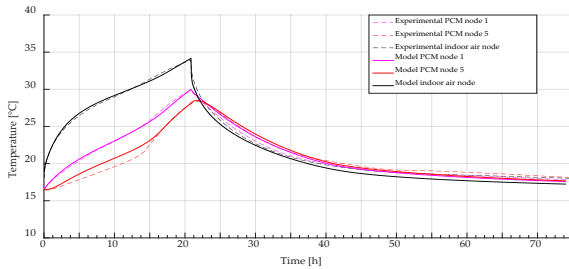


Fig. 4 – Test 1: experimental data vs. model result

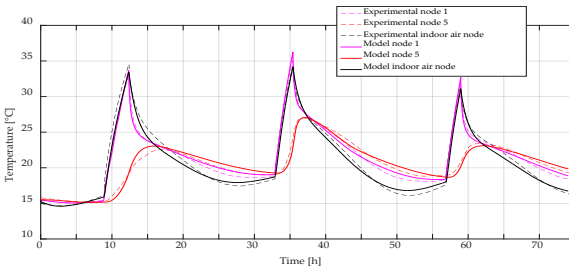


Fig. 5 – Test 2: experimental data vs. model result

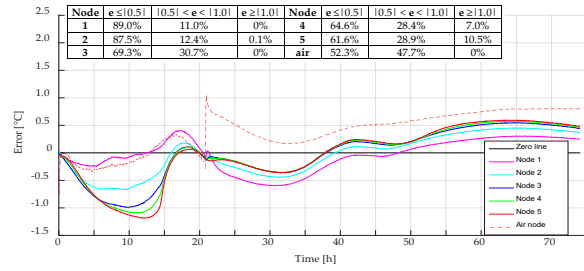


Fig. 6 – Test 1: error time history

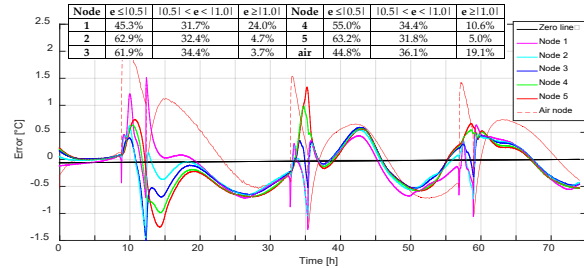


Fig. 7 – Test 2: error time history

5. Case Study

A suitable case study was developed in order to show the potentiality of the presented simulation model as well as the feasibility of PCM integration in interior walls (of external building rooms subjected to solar gains) toward the reduction of energy consumption and indoor air temperature fluctuations. For such analysis, an example of building integration of PCM was considered for a dwelling and an office building located in Naples, Palermo, and Montreal, calculating the related energy savings and the avoided CO₂. Specifically, a sample 8.0 × 6.0 m rectangular shaped lightweight building (with East-west oriented longitudinal axis), 3.0 m height, was modelled. The U-values of vertical walls, roof, and windows are respectively 0.49, 0.30, and 1.70 W/(m² K). A window SHGC of 0.262 is considered. More details are reported in Buonomano and Palombo (2014). The air flow rate for residential and office use is 0.5 and 1.2 Vol/h. A night free cooling ventilation strategy was also taken into account (2.0 Vol/h) if the outdoor air temperature is lower than the indoor one. Dynamic simulations were performed for one year by using Meteororm weather data. The HVAC system is modelled by an electric air-to-water chiller/heat pump (heating and cooling COP = 3.5 and 3.0),

necessary to maintain the indoor air temperature between 20 °C and 26 °C. The system operation was scheduled as reported in Table 1. As initial investigation, the PCM panels were integrated on the East and West walls and on the roof only. Two different layouts were simulated, where PCM panels were integrated internally and externally to the building envelope.

Table 1 – Climatic zones, climatic indexes, and system scheduling

Weather zone	HDD Kd	CDD Kd	ISR kWh/m ² y	Use	Heating Months (hours)	Cooling Months (hours)
Montreal	4567	297	1350	House Office	15/9-31/3 (0-24) (8-20)	1/6-15/9 (11-18) (8-20)
Naples	1479	499	1470	House Office	15/11-31/3 (7-10, 14-21) (8-20)	1/6-30/9 (11-18) (8-20)
Palermo	760	987	1664	House Office	1/12-31/3 (7-10, 14-21) (8-20)	1/6-30/9 (11-18) (8-20)

5.1 Results and Discussion

The monthly results for Naples are reported in Fig. 8 and 9, where the electricity demand of the chiller/heat pump is reported as a function of the different investigated system layouts. For residential applications (Fig. 8), the best configuration was reached by integrating the PCM externally to the building envelope. Simulations show that the overall summer cooling energy savings are maximized by boosting the PCM charge/discharge effect through a night free cooling ventilation. It is also worth noting that the PCM also causes a lower heating demand during the colder winter months. This is due to the heat required by the PCM charge (energy storage) basically obtained by an increase of the HVAC system demand vs. the reference case (no PCM). Such heat is dissipated during the time interval in which the heat pump is switched off (10:00 - 14:00). For office use (Fig. 9), the potential of a night free cooling strategy is higher vs. that observed for the residential use. In fact, in the office, during night hours, the absence of internal heat gains allows the PCM to complete a charge/discharge cycle. For office use, by adopting PCM a small winter saving is achieved because of the continuous HVAC system running from 08:00 to 20:00. Here, energy saving is achieved by

exploiting the free solar heat stored by PCM during the winter sunny days. A similar behaviour is observed for Palermo.

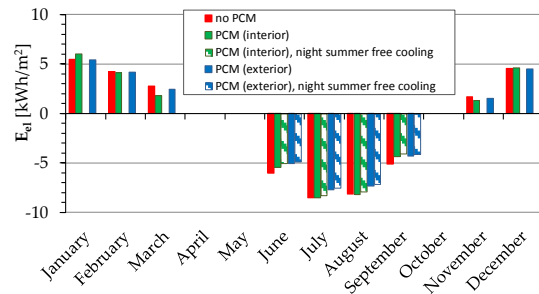


Fig. 8 – Residential building in Naples: monthly results

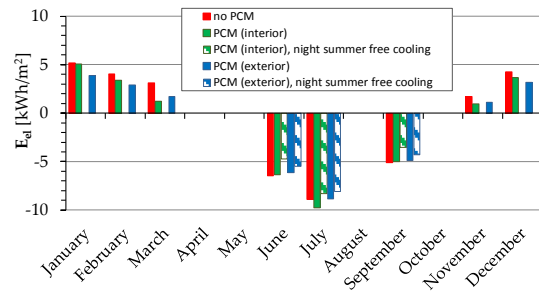


Fig. 9 – Office building in Naples: monthly results

The opposite result is achieved in winter in Montreal, where an increase of the heating demand is obtained by adopting PCM. For this climate zone, in Fig. 10 the time histories of the office indoor air temperature (T_{in}) and sensible heating load (Q_{ac}) are reported for the two PCM layouts, as well as in case of no PCM, for two winter sample days (January 5 and 6). Note that, on the second day (Saturday) the office is closed (the HVAC system is switched off). Whereas during the daytime when the HVAC system is switched on, the required indoor air temperature setpoint (26 °C) is always reached, in the nighttime a free-floating air temperature occurs. Due to the use of PCM, the minimum indoor air temperature decrease is obtained in case of interior PCM position, as expected (higher thermal comfort). Concerning the corresponding heating load (shown in Fig. 10 by averaging the predicted heating energy every hour), it is clearly visible that the lowest peak is obtained by placing the PCM on the interior position in the envelope (because of the higher indoor air temperature occurring at the start of the

HVAC system). As a result, the corresponding reduction of the heating peak load (occurring at the HVAC running start) is counterbalanced by an increase of the heating demand obtained during daytime (in Fig. 10 the green virtual area is larger than the other ones). In Fig. 11 for four summer sample days (July 13-16), the time histories of the indoor surface temperature of the West-building wall (with PCM), as well as the outdoor air temperature, are reported for the residential building use. Here, due to the PCM use, the obtained surface temperature peaks are attenuated and delayed vs. those related to the reference case without PCM, highlighting the effects due to the stored heat, delivered toward the indoor zone during nighttime. Note that a complete PCM charge/discharge cycle occurs.

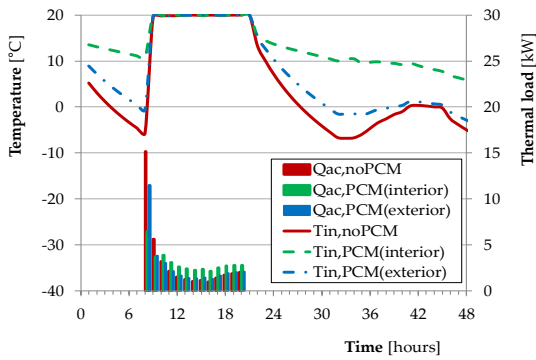


Fig. 10 – Two winter sample days in Montreal: office temperatures and loads

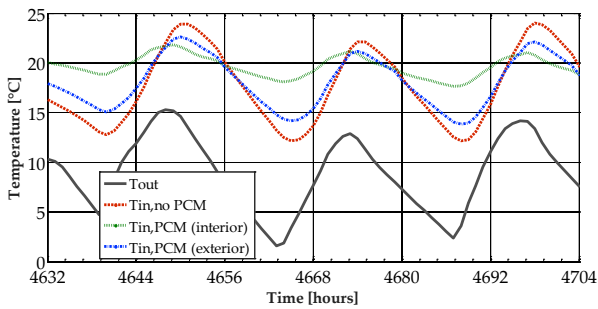


Fig. 11 - Four summer sample days in Montreal: outdoor air and interior surfaces temperatures for the residential building

In Fig. 12 for three winter sample days in Palermo (March 5-7) the time histories of the indoor air temperature with and without PCM, as well as the outdoor air temperature, are reported for the residential building. As expected the air temperatures approaching the comfort requirement occur especially in case of interior PCM positioning.

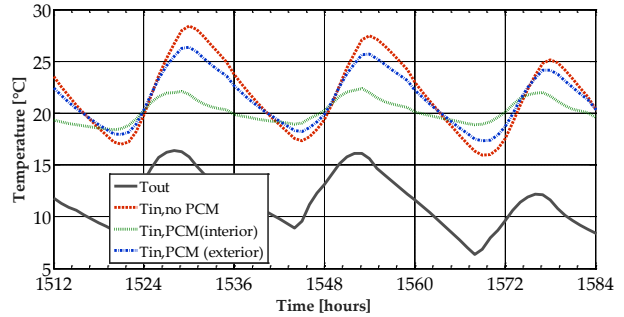


Fig. 1 – Free floating for three winter sample days in Palermo: outdoor and indoor air for the residential building

The obtained overall yearly results are reported in Table 2 and in Table 3. Here, the electricity demand of the chiller/heat pump of the traditional building (no PCM) as well as the achieved energy savings obtained by the PCM adoption are reported for all the investigated weather zones and system layouts. In the same tables the avoided CO₂ and the economic operative savings are also shown. For both the heating and cooling requirements interesting electricity savings are obtained (except for the heating demand in Montreal). For the standard system and the best system layout (exteriorly placed PCM) the overall energy savings range from 12 % to 15 %, whereas the avoided CO₂ from 21 to 42 kg/y (Table 2).

Table 2 – Yearly results for office use (standard)

Weather zone	Without PCM			PCM position	With PCM				
	E _{el,heat}	E _{el,cool}	E _{el,tot}		ΔE _{el,heat}	ΔE _{el,cool}	ΔE _{el,tot}	ΔCO ₂	ΔC
	kWh _{el} /(m ² ·y)				kWh _{el} /m ² ·y (%)			kg/y	€/y
Montreal	25.3	3.5	28.8	in	3.3 (+12.9)	-0.6 (-17.9)	2.6 (+9.2)	23.6	4.4
				out	-3.0 (-12.0)	-0.3 (-9.3)	-3.4 (-11.7)	-30.0	-16.7
Naples	5.2	6.8	12.1	in	-1.1 (-21.9)	0.2 (+3.1)	-0.9 (-7.7)	-21.8	-6.7
				out	-1.6 (-30.1)	-0.2 (-3.0)	-1.8 (-14.8)	-41.6	-12.8
Palermo	2.4	7.8	10.2	in	-1.8 (-75.8)	0.7 (+9.3)	-1.1 (-10.6)	-25.0	-7.7
				out	-1.3 (-55.6)	0.0 (+0.1)	-1.3 (-12.9)	-30.5	-9.4

Table 3 – Yearly results for office use (summer night ventilation)

Weather zone	Without PCM			With PCM					
	$E_{el,heat}$	$E_{el,cool}$	$E_{el,tot}$	PCM position	$\Delta E_{el,heat}$	$\Delta E_{el,cool}$	$\Delta E_{el,tot}$	ΔCO_2	ΔC
	kWh _{el} /(m ² ·y)				kWh _{el} /m ² ·y (%)			kg/y	€/y
Montreal CF _{CO2} = 0.186 [kg/kWh]	As in Table 2			in	-1.7 (-48.1)	1.6 (+5.5)		14.3	2.6
				out	-0.7 (-21.5)	-3.8 (-13.1)		-33.8	-18.8
Naples CF _{CO2} = 0.486 [kg/kWh]				in	-1.3 (-19.3)	-2.5 (-20.4)		-57.5	-17.7
				out	-0.9 (-13.1)	-2.5 (-20.5)		-57.7	-17.8
Palermo CF _{CO2} = 0.486 [kg/kWh]				in	-0.5 (-6.2)	-2.3 (-22.4)		-53.1	-16.4
				out	-0.6 (-8.3)	-2.0 (-19.4)		-45.9	-14.2

By the night free cooling ventilation strategy and for the same system layout, the overall energy savings range from 13 % to 21 % and the avoided CO₂ from 34 to 58 kg/y (Table 3). For all the investigated system configurations, the operating economic savings are still too low to balance the current initial PCM cost for acceptable paybacks.

6. Conclusions

The paper presents a validation procedure of a mathematical model (DETECT 2.2) for building simulation analyses involving the use of PCM wallboards. For the model validation procedure and the PCM characterization, measurements obtained by using PCM integrated in the back wall of a small test-cell under controlled conditions were used. The obtained numerical modelling is in good agreement with experimental data obtained during different tests (i.e. one charging cycle by a convective heating system and three charging cycles by solar irradiation). The tool allows the simulation of different scenarios (e.g., different PCM configurations, variable weather conditions, etc.), and the performance of parametric and sensitivity analyses to optimize the PCM building integration.

A case study analysis, carried out for a residential and an office building in three weather zones, shows the crucial influence of the building use (e.g., occupancy schedules, internal gains) on the exploitation of the latent heat stored in PCM layers. Finally, interesting design criteria for the development and adoption of building integrated PCMs

are provided. Further analyses will be performed to investigate the relationships among PCM properties (e.g., peak melting temperature, melting range, etc.).

Nomenclature

Symbols

C	thermal capacitance (J/K)
\dot{Q}	thermal load (W)
R	thermal resistance (K/W)
T	temperature (K)

Subscripts/Superscripts

ac	HVCAC system
in	indoor air
out	outdoor air

References

- Al-Saadi, S.N., Z. Zhai. 2015. "Systematic evaluation of mathematical methods and numerical schemes for modeling PCM-enhanced building enclosure". *Energy and Buildings* 92: 374-388. doi: 10.1016/j.enbuild.2015.01.044.
- Buonomano, A. 2016. "Code-to-Code Validation and Application of a Dynamic Simulation Tool for the Building Energy Performance Analysis". *Energies* 9(4): 301. doi:10.3390/en9040301.
- Buonomano, A., G. De Luca, U. Montanaro, A. Palombo. 2016a. "Innovative technologies for NZEBs: An energy and economic analysis tool and a case study of a non-residential building for the Mediterranean climate". *Energy and Buildings* 121: 318-343. doi: 10.1016/j.enbuild.2015.08.037.
- Buonomano, A., U. Montanaro, A. Palombo, S. Santini. 2016b. "Dynamic building energy performance analysis: A new adaptive control strategy for stringent thermohygrometric indoor air requirements". *Applied Energy* 163: 361-386. doi: 10.1016/j.apenergy.2015.10.182.
- Buonomano, A., A. Palombo. 2014. "Building energy performance analysis by an in-house developed dynamic simulation code: An investigation for different case studies". *Applied Energy* 113: 788-807. doi:10.1016/j.apenergy.2013.08.004.

- Dutil, Y., D. Rousse, S. Lassue, L. Zalewski, A. Joulin, J. Virgone, F. Kuznik, K. Johannes, J.P. Dumas, J.P. Bédécarrats, A. Castell, L.F. Cabeza. 2014. "Modeling phase change materials behavior in building applications: Comments on material characterization and model validation". *Renewable Energy* 61: 132-135. doi: 10.1016/j.renene.2012.10.027.
- Guarino, F., A. Athienitis, M. Cellura, D. Bastien. 2017. "PCM thermal storage design in buildings: Experimental studies and applications to solarium in cold climates". *Applied Energy* 185: 95-106. doi: 10.1016/j.apenergy.2016.10.046.
- Guarino, F., V. Dermardiros, Y. Chen, J. Rao, A. Athienitis, M. Cellura, M. Mistretta. 2015. "PCM Thermal Energy Storage in Buildings: Experimental Study and Applications". *Energy Procedia* 70: 219-228. doi: 10.1016/j.egypro.2015.02.118.
- Kuznik, F., J.P. Arzamendia Lopez, D. Baillis, K. Johannes. 2015. "Phase change material wall optimization for heating using metamodeling". *Energy and Buildings* 106: 216-224. doi: 10.1016/j.enbuild.2015.06.021.
- Kuznik, F., D. David, K. Johannes, J.J. Roux. 2011. "A review on phase change materials integrated in building walls". *Renewable and Sustainable Energy Reviews* 15(1): 379-391. doi: doi.org/10.1016/j.rser.2010.08.019.
- Kuznik, F., J. Virgone, J. Noel. 2008. "Optimization of a phase change material wallboard for building use". *Applied Thermal Engineering* 28(11-12): 1291-1298. doi: 10.1016/j.applthermaleng.2007.10.012.
- Liu, L., D. Su, Y. Tang, G. Fang. 2016. "Thermal conductivity enhancement of phase change materials for thermal energy storage: A review". *Renewable and Sustainable Energy Reviews* 62: 305-317. doi: 10.1016/j.rser.2016.04.057.
- Tittlein, P., S. Gibout, E. Franquet, K. Johannes, L. Zalewski, F. Kuznik, J.P. Dumas, S. Lassue, J.P. Bédécarrats, D. David. 2015. "Simulation of the thermal and energy behaviour of a composite material containing encapsulated-PCM: Influence of the thermodynamical modelling". *Applied Energy* 140: 269-274. doi: 10.1016/j.apenergy.2014.11.055.
- Tsilingiris, P.T. 2006. "Parametric space distribution effects of wall heat capacity and thermal resistance on the dynamic thermal behavior of walls and structures". *Energy and Buildings* 38(10): 1200-1211. doi: 10.1016/j.enbuild.2006.02.007.

From Energy Signature to Cluster Analysis: Comparison Between Different Clustering Algorithms

Lorenza Pistore – Free University of Bozen-Bolzano – lorenza.pistore@natec.unibz.it

Giovanni Pernigotto – Free University of Bozen-Bolzano – giovanni.pernigotto@unibz.it

Francesca Cappelletti – University IUAV of Venezia – francesca.cappelletti@iuav.it

Piercarlo Romagnoni – University IUAV of Venezia – piercarlo.romagnoni@iuav.it

Andrea Gasparella - Free University of Bozen-Bolzano – andrea.gasparella@unibz.it

Abstract

The energy audit on the existing buildings has become a priority in the last years, as a consequence of the adoption of the European Directives on building energy efficiency. In particular in Italy, public buildings are often the most inefficient among the stock and, thus, those with the highest potential for improvements. Many methods can be applied to perform an energy diagnosis; one of them is “Energy Signature” simplified method, ES, described in the Annex B of the technical standard EN 15603:2008. The ES can actually be seen as a very simplified model of the building, based on a linear regression between energy consumption and degree-days in a set of reference periods. If applied year after year, the ES allows a fast detection of system faults, changes of use patterns, and to assess the efficacy of different energy management strategies or retrofitting interventions, discounting the effect of weather variations. When the stock of buildings is large, individual energy audits can be too onerous and time consuming and building simulation impracticable. For this reason, ES can be combined with clustering techniques in order to identify groups of buildings with similar behaviour among which a reference case can be identified and deeply investigated either experimentally or through detailed building energy simulation (BES). In this respect, ES and clustering can be seen as the key element to allow the extension of BES also to the analysis of building stocks. In this work, ES and different clustering techniques have been used to analyse a set of 41 schools in the province of Treviso, north of Italy, pointing out the buildings features that most affect their energy signatures through multiple linear regressions. A comparison between two non-hierarchical clustering algorithms, K-means and K-medoids, has been conducted. Particular attention has been paid to the approaches for the evaluation of closeness of schools in the same group and the identification of the reference school

for each set. As the final outcome of this research, the impact of the clustering algorithms is discussed, in order to assess to which extent the selection of the schools with the most representative energy signatures can be affected by the choice of the data mining techniques.

1. Introduction

The energy audit of existing buildings is a crucial point in order to identify the potential improvements and interventions to achieve a better energy performance. In particular, the last European Directive (European Parliament and Council of the European Union, 2012) indicated public buildings as pioneers of new energy efficiency policies, because they are both community exposed and, in many cases, the least efficient of the building asset. Among them, school buildings represent an important target: in fact, they have not only to be efficient from an energetic point of view, but also to ensure adequate indoor environmental thermal conditions and pupils’ thermal comfort.

In the recent years, building simulation models have been largely used in order to evaluate the energy consumptions of school buildings and the impact of different energy renovation interventions, both from an energetic and an economic point of view. In the research by Niemelä et al. (2016), simulation-based optimization analyses have been implemented to determine cost-optimal refurbishment solutions in typical educational buildings built between 1960 and 1970 in cold climate regions. Stavrakakis et al. (2016) have used dynamic simulation to assess the effect of a cool-roof installation on the

thermal and energy performance of a school building in Greece. Moreover, model calibration has been implemented using simulated indoor air temperature and the measured one, considering *ex-ante* and *ex-post* condition. In the same country, Androulakis et al. (2016) have pointed out the contribution of simulation tools for designing complex heating systems combined with renewable sources. However, when a large stock of buildings is taken into account, a case-by-case energy analysis and building simulation modelling is onerous, time-consuming, and expensive. Consequently, if BES has to be adopted, there is the need for a method to detect buildings' energy behaviour quickly, and to identify the best improvement actions, focusing on a subset of representative buildings. In a previous work (Pistore et al., 2016), the authors proposed a method based on the Energy Signature approach (CEN, 2008) coupled with cluster and multiple regression analyses applied to a stock of 41 schools located in the province of Treviso, Italy. The Energy Signature simplified method is described as a useful diagnostic technique consisting in plotting for several times the energy consumptions for space heating or cooling of a building versus the external temperature averaged over a suitable period, and determining their linear relationship (CEN, 2008). Subsequently, K-means clusterization was applied to group schools in clusters using ES parameters, e.g., the slope of linear regression function and the zero of the function, as dependent variables to group schools in clusters. Homogeneous subsets of schools were identified by means of the buildings' features that most affect the signature parameters, and a building reference case was pointed out for each cluster in order to find the parameters that most affect the energy behaviours and, consequently, the best set of interventions able to improve the buildings' energy efficiency. These efficiency measures can be applied on the reference cases, on which more detailed analyses, such as dynamic simulation modelling, can be performed, and then the solutions can be extended to the other buildings in the same cluster by means of the ES method.

In this framework, the methodology applied for the building stock clusterization assumes a great importance in the success of final goal. In fact, the cluster analysis can be implemented according to

different algorithms, which have to be carefully selected without any preconception (Kaufman and Rousseeuw, 2005) since they can be suitable for different purposes according to the type of available data. In some cases, several algorithms are applicable and a priori arguments may not suffice to narrow down the choice to a single method, which leads to the necessity of a comparison between results (Kaufman and Rousseeuw, 2005).

In this paper, a comparison between two widespread non-hierarchical clustering algorithms, K-means and K-medoids (Reynolds et al., 2004) is presented. The comparison is conducted on the same stock of schools analysed by Pistore et al. (2016). Assuming that there is a clear resemblance in the running mode and in the object function of the two clustering algorithms, according to the literature, K-medoids algorithm is considered to be more robust with respect to outliers (Arora and Varshney, 2016; Kaufman and Rousseeuw, 2005; Park et al., 2009). Differently from K-means, the clusters determined following K-medoids are ball-shaped and the representative object (i.e. the medoid) is one element of the dataset. Moreover, various non-Euclidean approaches are available for the calculation of the distances. In the considered case, with a dataset a number of elements n lower than 100, the PAM (Partitioning Around Medoid) algorithm has been adopted, since it is often recommended when the aim is to look for representative objects and characteristics.

2. Method

2.1 Energy Signatures

A building energy audit can be performed by the ES method described in the annex B of the EN 15603:2008 (CEN, 2008). This approach consists in plotting for several time periods the average heating or cooling uses versus the average external temperature, and this allows the user to fast gather useful information about the building energy behaviour and, in a subsequent phase, to verify the refurbishment interventions effect and to forecast the energy consumptions in the further years. In this method, the indoor air temperature is assumed to be constant

and equal to the setpoint (generally 20 °C) during the occupancy time, so that the external air temperature is the most influential parameter. Its application requires gathering data about energy uses for heating or cooling, as well as average external temperatures or, when possible, cumulated differences between actual indoor and outdoor temperatures recorded at regular intervals, from one hour to a week. This latter time period has been adopted in this work, since it is long enough to capture a characteristic occupation or use pattern, while being short enough not to hide climatic variations along the seasons. Weekly natural gas consumptions have been recorded and the mean consumption for hot water production during the non-heating period has been subtracted in order to isolate the energy uses for space heating. The weekly average power per unit of heated air volume, ϕ , obtained by dividing the energy use during one week EP_h per unit of volume V by the number of opening hours per week τ , as in Eq. (1), has been plotted versus the weekly-average temperature differences during the opening hours, $\Delta T_{20,occ}$ as in Eq. (2)).

$$\Phi = \frac{\sum_{i=1}^7 EP_{h_i} / V}{\tau} \quad [W / m^3] \quad (1)$$

$$\Delta T_{20,occ} = \sum_{i=1}^n (20 - T_{ext})_i \quad [K] \quad (2)$$

with n = opening hours
of a week

Energy signatures can be characterized by two main parameters: the slope of the regression function, which represents the energy performance of the building, and the intersection with the x-axis, hereafter called zero of the function, which is the minimum temperature difference for which the system is turned on, or the maximum that does not require heating.

2.2 Multiple Linear Regression

According to the methodology already developed and described in Arambula et al. (2015), before implementing clusterization, it is necessary to define a list of independent variables describing the building to be used as predictors of the parameters

of the energy signatures. The list of 12 candidate descriptive quantities includes:

- (A) the area of the external vertical walls,
- (B) roof area,
- (C) floor area,
- (D) ground floor area,
- (E) total area of opaque envelope,
- (F) total area of transparent envelope,
- (G) windows to vertical walls ratio,
- (H) windows to floor ratio,
- (I) opaque and transparent envelope area ratio,
- (J) average thermal transmittance of the envelope,
- (K) envelope compactness ratio,
- (L) heating system capacity.

Each quantity is indicated by a letter (A to L) in the next tables. The highest value of each of the 12 descriptive quantities in the building set has been used to normalize the values for each building.

A multiple linear regression has been applied to find the sets of the candidate quantities which better define homogenous groups and to develop the clustering. Starting from groups of 2 to groups of 12 variables, 4083 possible combinations of the 12 normalized descriptive quantities have been defined and used as predictors in multiple linear regression models. For each regression, the adjusted index of determination R^2_{adj} has been calculated, as well as F-tests and the p-values, to check the model's statistical significance, and variance inflation factors VIF, for the analysis of multi-collinearity issues. Only models with significant p-value with respect to a significance level of 10 % and without multi-collinearity issues (i.e. $VIF < 10$) have been considered for the definition of the quantities for the clustering. The combinations of predictors with the highest R^2_{adj} have been selected as sets of coordinates of each element in the sample of schools. After a preliminary study, the zero of the function has been found poorly correlated to the set of proposed variables and has been discarded from the analysis, focused only on the slope of the energy signatures.

2.3 Clustering and Maximization of the Explained Variance

A comparison between two partitioning methods, K-means and K-medoids PAM has been performed. Both approaches imply that each cluster contains at least one element; each element belongs to only one

cluster and the number of clusters is $k \leq n$, where n is the number of elements to be grouped. Once defined the desired number of clusters k , an equivalent number of centroids or medoids is randomly selected and data points are assigned (Junjie, 2012). In this work, since the whole dataset for the clustering includes 41 elements, k has been imposed equal to 2, to facilitate the definition of groups with $n \geq 12$ in accordance with the statistical central limit theorem. After the attribution of the elements to the different clusters, it is checked if the variance explained by the predictors can be increased further: if for a given cluster there is a combination of predictors with higher R^2_{adj} , statistically significant F-value and p-value and limited VIF, then it is adopted as new coordinate systems for the elements belonging to it. If for a cluster the explained variance cannot be improved but at least 25 elements are present, it is possible to sub-cluster with k equal to 2 using the best set of coordinates available for that cluster. As a final step, the school closest to the centroid (K-means method) and the medoid schools (in K-medoids method) in each cluster have been selected.

The main difference between the two methods are the followings: in the K-means, initial virtual centroids are randomly generated within the domain of the dataset and objects are assigned to the clusters using the square Euclidean distance calculation, which is implemented by the algorithm itself at each iteration. Each cluster is defined around a centre-type (the centroid), whose coordinates are the mean of the coordinates of all the cluster's elements. In K-medoids, the calculation of the distances is not repeated in each iteration, but the algorithm seeks distance information from a distance matrix. The representative object of each group, i.e. the medoid, is chosen at each iteration in order to minimize the distances between it and the other elements in the data set, so as to refine the clusters themselves each time.

2.4 Comparison Method

In order to make a comparison between the two approaches, some criteria and indicators have been identified and used:

1. Number of elements in each cluster.
2. Composition of clusters in terms of specific schools grouped in the same cluster.
3. Equivalence of the identified reference buildings in the two methods.
4. Variance explained by the selected variables in the multiple linear regression. For this purpose, the indicator used is the adjusted index of determination.
5. Homogeneity and level of similarities of cluster elements. Two indicators have been considered in this case: the standard deviation from the centroid/medoid for each variable of the elements within each cluster and the sum of the square Euclidean distances in each cluster.

3. Results

The characteristics of the clusters obtained by K-means and K-medoids approaches are reported respectively in Tables 1 and 2. All the top-ten combinations of descriptive quantities (identified through an ID-string, composed by the letters representing the descriptive quantities included) have been used for clustering. Then, one of the combinations has been chosen considering its statistical significance. In particular, R^2_{adj} , F-value, p-value, and VIF have been analysed in order to obtain at least one cluster with significant values, and the other one, even if inconsequential, with such a number of elements that allows a subclustering. For these reasons, configuration AHIJ has been chosen as the initial model for both algorithms as the best performing one, leading to 30 and 11 elements in K-means, and vice versa for K-medoids. From now on, the clusters' names have been assigned with respect to the decreasing order of R^2_{adj} values and number of elements: for example, the cluster with the highest R^2_{adj} and the largest number of elements is CL1. For K-means algorithm (Table 1), configurations BEGHLI and BCJ are found maximizing the explained variance in the two clusters, with R^2_{adj} respectively equal to 0.591 and 0.679. While the latter can be considered satisfactory and identified as CL1, the former cluster can be divided into 2 sub-clusters and the explained variance further optimized, using configuration FJ for CL2 and ADGHK

for CL3. CL2 and CL3 are composed of respectively 20 and 11 buildings. Three final clusters have been obtained: CL1 with a R^2_{adj} of 0.679, and CL2 and CL3 with R^2_{adj} respectively of 0.312 and 0.868.

The same approach has been implemented with K-medoids algorithm (Table 2). Configurations CGHIL and BJCLI, both made of 5 variables, maximize the explained variance in the two clusters with R^2_{adj} equal to 0.954 (CL1) and 0.132 (CL2), respectively. The latter cluster has been divided again into 2 subclusters and the explained variance further optimized, using EHKL variables for CL2 and BEHJK variables for CL3. CL2 and CL3 are composed of respectively 10 and 20 buildings, with a R^2_{adj} of 0.939 and 0.311 respectively.

K-medoids algorithm gives higher R^2_{adj} for two over three clusters, while R^2_{adj} of CL2-kmeans and CL3-kmedoids is the same for the two algorithms. Looking at the number of elements in the three clusters, we can highlight that for both approaches we have obtained three clusters of 11, 10, and 20 objects but the distribution of the schools among the groups is different and the two methods are different.

Table 3 reports the standardized coefficients of the building variables included in the linear models defined at each step. In both algorithms, the variables selected by regression for the initial model are changed when the explained variance is maximized

for the single clusters. Indeed, the variables included in the final models have the highest explanatory power for each cluster and differentiate each group of schools from the others. Furthermore, these final models could be used, in a next phase, for the preliminary assessment of the energy efficiency measures. Comparing K-means and K-medoids algorithms, it can be observed that both final models and included variables are different.

In Fig. 1 the school position inside clusters is shown with respect to K-means algorithm first, and K-medoids second. As it can be observed, elements generally change from one cluster to another by changing the clustering algorithm and, moreover, also the identified reference buildings change between the two different approaches.

However, in order to identify the best performing algorithm, it is necessary to analyse also the output of the predictive models. A comparison between the standard deviation of each variable with respect to the centroid / medoid in each cluster, and the sum of the square Euclidean distances, have been performed as shown in Figs 2 and 3. As it can be observed, in K-medoids clusters, standard deviation and the sum of square Euclidean distances is lower, pointing out a more compactness and homogeneity of the groups of schools.

Table 1 - K-means. Results of the clustering and maximization of the explained variance. In bold those p-values significant with respect to a significance value of 10 %. The red square highlights the final clusters obtained and the best predictive models inside them

	First clustering		Subclustering	
	Initial Model	Best Model	Initial Model	Best Model
ID-string	AHIJ	BEGHLI	BEGHLI-a	FJ (CL2)
R^2_{adj}	0.539	0.591	0.046	0.312
F value	9.773	8.213	1.154	5.299
p-value	< 0.001	< 0.001	0.387	0.016
N	31	31	20	20
ID-string			BEGHLI-b	ADGHK (CL3)
R^2_{adj}			0.896	0.868
F value			15.390	14.167
p-value			0.010	0.006
N			11	11
ID-string	AHIJ	BCJ (CL1)		
R^2_{adj}	0.007	0.679		
F value	1.016	7.332		
p-value	0.479	0.020		
N	10	10		

Table 2 - K-medoids. Results of the clustering and maximization of the explained variance. In bold those p-values significant with respect to a significance value of 10 %

	Clustering		Subclustering	
	Initial Model	Best Model	Initial Model	Best Model
ID-string	AHIJ	CGHIL (CL1)		
R^2_{adj}	0.632	0.954		
F value	5.299	42.410		
p-value	0.036	< 0.001		
N	11	11		
ID-string	AHIJ	BJCLI	BJCLI-a	EHKL (CL2)
R^2_{adj}	0.038	0.132	-0.323	0.939
F value	1.284	1.882	0.561	35.863
p-value	0.303	0.135	0.731	0.001
N	30	30	10	10
ID-string			BJCLI-b	BEHJK (CL3)
R^2_{adj}			0.191	0.311
F value			1.900	2.712
p-value			0.158	0.065
N			20	20

Table 3 – K-means and K-medoids: involved variables and standardized coefficients of the linear models

ID-string	I regr. AHIJ Coeff.	K-means			K-medoids		
		CL1 ADGHK Coeff.	CL2 FJ Coeff.	CL3 BCJ Coeff.	CL1 CGHIL Coeff.	CL2 EHKL Coeff.	CL3 BEHJK Coeff.
Descriptors							
A	-0.06	-0.59					
B				-2.18			1.55
C				1.98	-1.08		
D		0.71					
E						-1.31	-0.82
F			0.35				
G		0.71			0.89		
H	0.33	1.01			0.14	-0.75	-0.57
I	-0.34				-0.79		
J	0.35		0.69	0.40			0.31
K		-0.45				0.61	0.40
L					0.24	1.07	
R^2_{adj}	0.21	0.87	0.31	0.68	0.95	0.94	0.31
F value	3.64	14.17	5.30	6.87	42.41	35.86	2.71
p-value	0.01	0.01	0.02	0.03	<0.01	<0.01	0.06

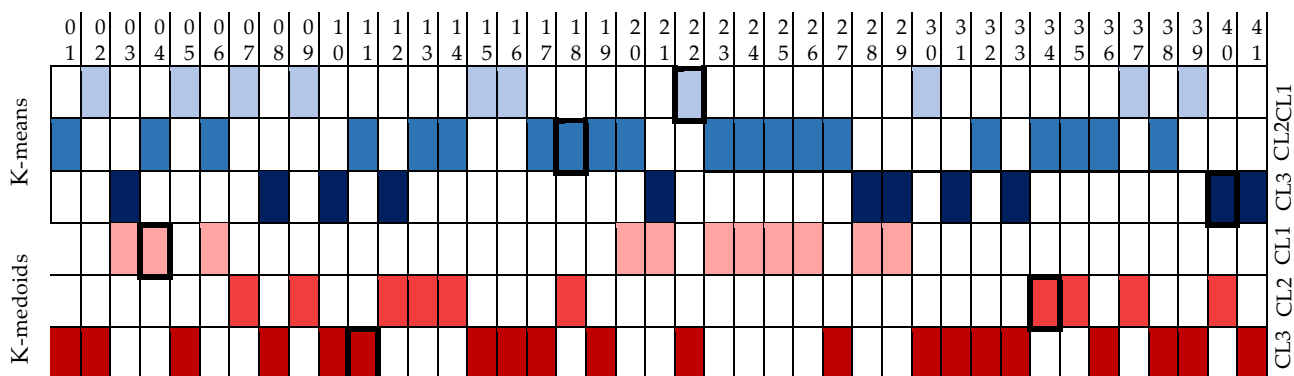


Fig. 1 - Schools position inside clusters by K-means and K-medoids algorithm. The reference buildings are indicated with the thicker black border

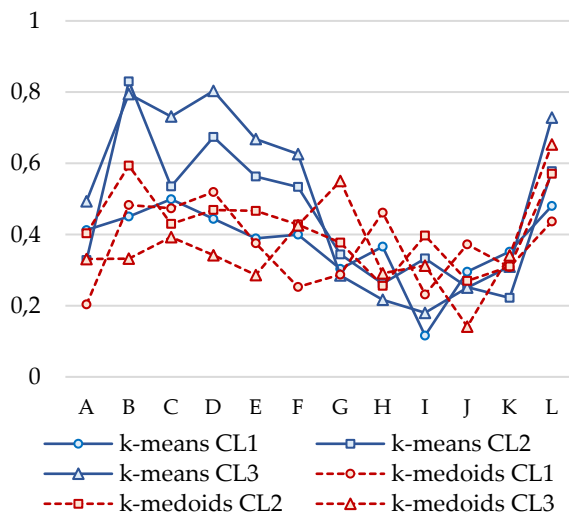


Fig. 2 - Comparison between the standard deviation for each variable with respect to the centroid / medoid of each cluster. K-means in blue colour, K-medoids in dotted red

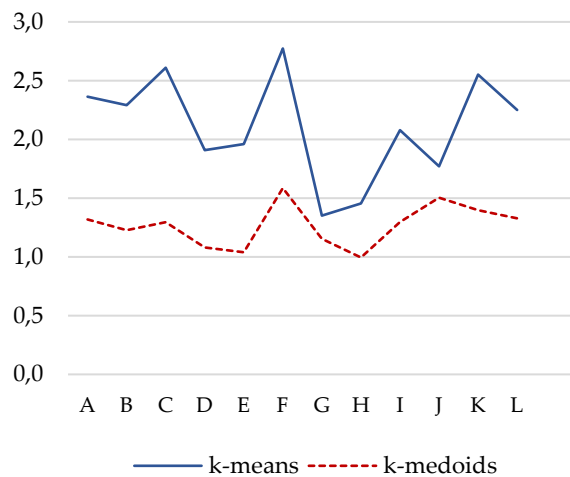


Fig. 3 - Comparison between the addition of the square Euclidean distances in the three clusters. K-means in blue colour, K-medoids in dotted red

Finally, Fig. 4 compares the energy signature slope predicted by the linear regression models with the largest explanatory power with the actual ones, for each cluster. As it can be observed, two of three models fit better for K-medoids clusters, since a greater number of elements in the stock are within the error band of $\pm 20\%$. There is one exception for CL3, which already showed a lower R^2_{adj} .

4. Conclusions

In this paper, a comparison between two different clustering algorithms has been performed. Even if the two approaches run similarly, K-medoids results to be better performing instead of K-means, for the following reasons:

- The whole set of schools has been divided in the same number of clusters, 3, and in the same numerical parts (11, 10, 20 elements), but the sets obtained are different for their composition and for the identified reference building, too.
- With K-medoids it was possible to obtain clusters with a higher Adjusted Index of Determination R^2_{adj} .
- With K-medoids, centro-types are identified in real objects included in the initial dataset, which is really useful to find a representative building.

- With K-medoids, standard deviation and the sum of square Euclidean distances result to be lower, confirming the more compactness and homogeneity of K-medoids models.
- Predictive models obtained with K-medoids generally result to fit better.

Acknowledgement

The authors would like to thank the Province of Treviso (Provincia di Treviso) for having made the schools database available for this research. The present study has been funded by the project "Klimahouse and Energy Production" in the framework of the programmatic-financial agreement with the Autonomous Province of Bozen-Bolzano of Research Capacity Building.

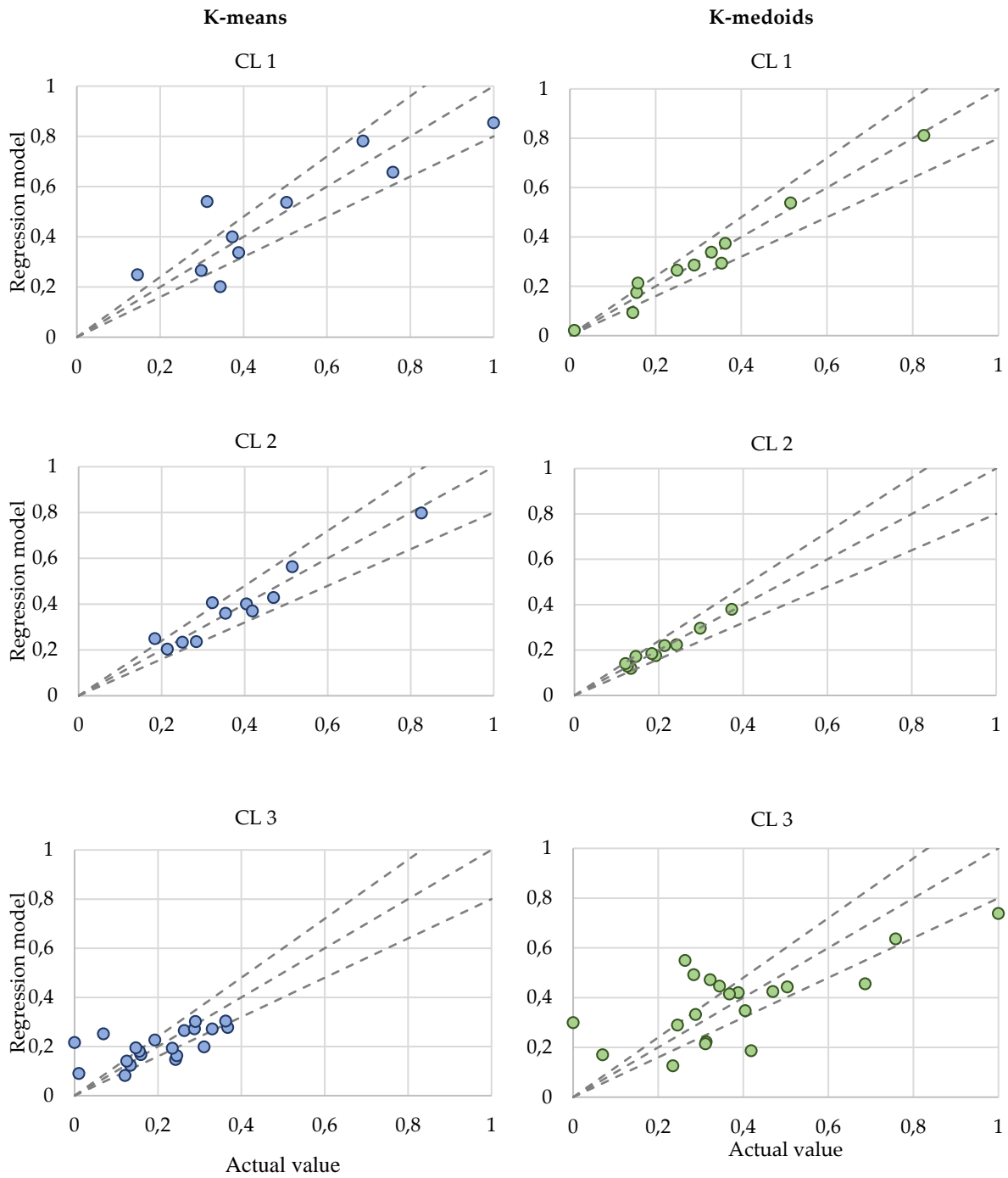


Fig. 4 - Estimated vs actual slopes of energy signatures of the schools in the three clusters. K-means clusters in blue colour, K-medoids ones in green colour. The dashed lines indicate a deviation of $\pm 20\%$

References

- Arambula Lara, R., G. Pernigotto, F. Cappelletti, P. Romagnoni, A. Gasparella. 2015. "Energy audit of schools by means of cluster analysis". *Energy and Buildings* 95: 160-171. doi:10.1016/j.enbuild.2015.03.036.
- Androulakis, N.D., K.G. Armen, D.A. Bozis, K.T. Papakostas. 2016. "Simulation of the thermal performance of a hybrid solar-assisted ground-source heat pump system in a school building". *International Journal of Sustainable Energy* 1-14. doi: 10.1080/14786451.2016.1261865.
- Arora, P., S. Varshney. 2016. "Analysis of K-Means and K-Medoids Algorithm For Big Data". *Procedia Computer Science* 78: 507-512. doi: 10.1016/j.procs.2016.02.095.
- CEN. 2008. *EN 15603 - Energy performance of buildings. Overall energy use and definition of energy ratings*. Brussels, Belgium: CEN.
- European Parliament and Council of the European Union. 2012. "Directive 2012/27/EU, on energy efficiency, amending directives 2009/125/EC and 2010/30/EU and repealing Directives 2004/8/EC and 2006/32/EC". *Official Journal of the European Union* L315/1, 14 11.
- Junjie, W. 2012. *Advances in K-means clustering. A data mining thinking*. Springer Thesis, Springer.
- Kaufman, L., P.J. Rousseeuw. 2005. *Finding groups in data. An introduction to cluster analysis*. Wiley.
- Niemelä, T., R. Kosonen, J. Jokisalo. 2016. "Cost-optimal energy performance renovation measures of educational buildings in cold climate". *Applied Energy* 183: 1005-1020. doi:10.1016/j.apenergy.2016.09.044.
- Park, H., J. Lee, C. Jun. 2009. "A simple and fast algorithm for K-medoids clustering". *Expert Systems with Applications* 36(2): 3336-3341. doi:10.1016/j.eswa.2008.01.039.
- Pistore, L., G. Pernigotto, F. Cappelletti, P. Romagnoni, A. Gasparella. 2016. "From energy signature to cluster analysis: an integrated approach". In: *Proceedings of the 4th International High Performance Buildings Conference*. West Lafayette, U.S.A.: Purdue University.
- Reynolds, A. P., G. Richards, V.J. Rayward-Smith. 2004. The application of K-medoids and PAM to the clustering of rules. In *Intelligent Data Engineering and Automated Learning – IDEAL 2004. Lecture Notes in Computer Science* 3177.
- Stavarakakis, G.M., A.V. Androutsopoulos, J. Vyörykkä. 2016. "Experimental and numerical assessment of cool-roof impact on thermal and energy performance of a school building in Greece". *Energy and Buildings* 130: 64-84. doi:10.1016/j.enbuild.2016.08.047

The Building Information Model and the IFC Standard: Analysis of the Characteristics Necessary for the Acoustic and Energy Simulation of Buildings

Costantino Carlo Mastino – University of Cagliari – mastino@unica.it

Roberto Baccoli – University of Cagliari – rbaccoli@unica.it

Andrea Frattolillo – University of Cagliari – andrea.frattolillo@unica.it

Martino Marini – University of Sassari – marini@uniss.it

Antonino Di Bella – University of Padova – antonino.dibella@unipd.it

Valerio Da Pos – Cadline Software srl – valerio@cadlinesw.com

Abstract

The new European Directive 2014/24/EU requires the use of BIM procedures in the construction of public buildings for all member States. The countries belonging to the European Union shall be obliged to transpose the Directive and adapt their procedures to that effect. The paper analyzes the IFC format, the only one recognized by the European Directive Standards for BIM procedures, to assess its use for simulations of buildings. IFC, described by the ISO 16739:2013 standard (ISO, 2013), is a standard that describes the topology of the constructive elements of the building and what belongs to it, overall. The format includes geometrical information on the rooms and on all building components, including details of the type of performance (transmittance, fire resistance, sound insulation), in other words it is an independent object file for the software producers to which, according to the European Directive, it will be compulsory to refer in the near future, during the different stages of the life of a building from the design phase, to management, and the possible demolition at the end of its life. The present study aims at carrying out a first analysis on the IFC data format, which will be further studied in-depth in the following phases. The study will compare the information and data contained in it, with those in other formats already used for energy simulations of buildings such as the gbXML (Green Building XML), highlighting the required information missing, and proposing the inclusion of new data for energetic and acoustic simulation. More generally the attention is focused on

the building physics simulation software which is implemented to exploit the BIM model potential enabling interoperability.

1. The Introduction to the BIM Concept and to the IFC Data Format

The IFC initiative began in 1994, when an industry consortium invested in the development of a set of C++ classes that can support the development of integrated applications. Twelve US companies joined the consortium: these companies that were initially included, are called the consortium "Industry Alliance for Interoperability". In September 1995 the Alliance opened the membership to all interested parties, and in 1997 changed its name to "International Alliance for Interoperability". The new alliance was reconstituted as a non-profit organization with the aim of developing and promoting the "Industry Foundation Class "(IFC) as a neutral data model for the building product useful to gather information throughout the life cycle of a building/facility. Since 2005 the Alliance has been carrying out its activities through its national chapters called SMART building. The above data relate to 2015, the first analysis in 2016 led to the consideration of a significant increase not only in the number of applications but also in the precision of procedure management based on the experience gained in the meantime by the contracting authorities. Conducting a project with BIM methodology is now necessary and a mandatory condition to achieve a "good

design". But what does "good design" mean? What are the goals and uses of a BIM model? The technical literature on the BIM topic shows different uses, but very little about how a BIM model can be considered a plausible model for the analysis and simulation of energy and/or acoustic building performance.

Today, it is generally recognized that BIM/IFC standards are capable to centralize the project information throughout its life cycle, information that can potentially serve all disciplines and sub-disciplines, and ensure an integrated and coordinated project. However, to support the work of the operators and at the same time its interoperability, many conditions must be met and many problems have to be solved. One of the basic problems is modeling (model quality), linked to the purpose for which the model was made (quantity and quality of the current information in the model) and how this information can be interpreted by the model software.

For energy and acoustics analysis, there are many reliable applications on the market, but most of them do not directly support the IFC data model. Usually they use a proprietary data scheme specifically designed to represent the analytical models. This creates a number of challenges in the field of BIM/IFC:

A. Appropriate models. The models for energy-acoustics analysis and simulation require explicit definition of the spaces (rooms and zones) and of their use, the clear specification of the exterior walls, the correct specifications of openings, etc. An IFC model should be represented not only visually but also at semantic level.

B. Appropriate geometry. The analysis/simulation requires for both thermal and acoustic spaces (zones and rooms) to be completely bounded by objects with known physical properties (thermal, acoustic), taking into account how they are connected with adjacent spaces. This requires a direct connection between the perimeters of the spaces in the model, the objects correspondences along the boundary, the subdivision in homogeneous parts (homogeneous by the analysis criteria) of walls and slabs, checking that there are no gaps along the perimeter or, on the contrary, objects overlapping

C. Integration with non-BIM data. The correct integration of the necessary external data from external non-BIM sources, such as climate data, used and unused times etc. of the spaces, data that must be appropriately associated with the BIM/IFC objects

D. Correct definition of BIM/IFC objects. The model must contain details of the physical properties of the objects regardless of the detailed graphical representation level, because this is required by the analysis/simulation tools to determine their properties correctly (e.g., total weight, thermal resistance, U values, etc.)

E. Proximity information, i.e. option to manage information of topology and proximity. This is a kind of information supported by the IFC scheme, but not common for the CAD tools typically used to create BIM. Unfortunately, the energy-acoustics analysis/simulation tools require such information; therefore if it is missing there is the need to be re-defined from building geometry.

F. Output Editing. The capabilities to edit the output, that is, how "added" information should be properly associated/integrated into the BIM data to enable management, visualization and evaluation of results.

Many of the problems require an extension of the IFC model scheme to an advanced model able to contain the necessary information for the energy-acoustics analysis and simulation. In this work we will focus our attention on the characteristics of the building (geometry and physical properties of the building components).

2. IFC Format and Other Formats for Interoperability

We consider two data formats used to facilitate interoperability: the first gbXML format, developed by Green Building Studio and the second IFC format, developed by building SMART.

In this paragraph we will describe the IFC2x3 format, IFC4 and other formats such as gbXML considering the main frame (wall, floor, slab, roof, windows, and door) and their physical properties associated with the components. We will also assess the

interaction between the different components such as nodes and joints fundamental for the energetic and acoustic analysis. As mentioned before the IFC format is only part of the BIM processes that are actually designed to manage and contract the procurement procedures and the building management.

2.1 IFC Format

Industry Foundation Classes, or IFC, is the official international standard for open BIM and is registered with the International Standardization Organization (ISO). The IFC adopts the "top-down" approach, which creates a complex, hierarchical scheme, developed in a large data file (Dong et al., 2007).

Additionally, building SMART developed a standard for the information flow in an integrated project called Information Delivery Manual (IDM).

The IFC format (Industry Foundation Classes) as mentioned in the introduction, is designed to be an interoperability format between different applications, so as to allow its use in different stages of the construction process in the perspective of a greater industrialization of the construction sector (building components, building structure, management, disposal). The very complex data structure of the IFC format includes these fundamental concepts. The scheme, as found on the building site SMART (BuildingSMART, 2016) is shown in Fig. 1. The ISO 16739 standard (ISO, 2013) specifies a conceptual data scheme and an exchange file format for Building Information Model (BIM) data.

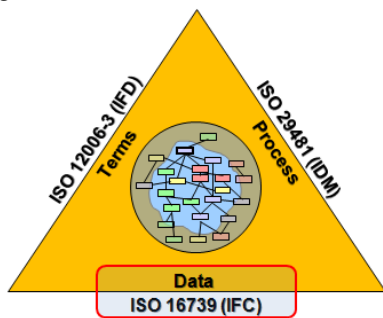


Fig. 1 –Example of data structure organization

The conceptual scheme is defined in the EXPRESS data specification language. The standard exchange file format for exchanging and sharing data according to the conceptual scheme uses the Clear text encoding of the exchange structure. Alternative

exchange file formats can be used if they conform to the conceptual scheme. Currently there are two types of IFC formats: IFC2x3 and IFC 4. In the following the schemes of data formats found on the website (BuildingSMART, 2016) are shown in Fig. 2, 3, 4, and 5.

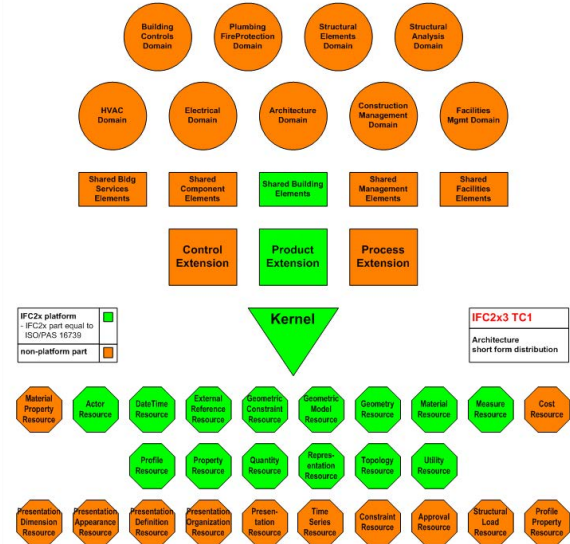


Fig. 2 – Architecture diagram, IFC 2x3 format (BuildingSMART, 2016)

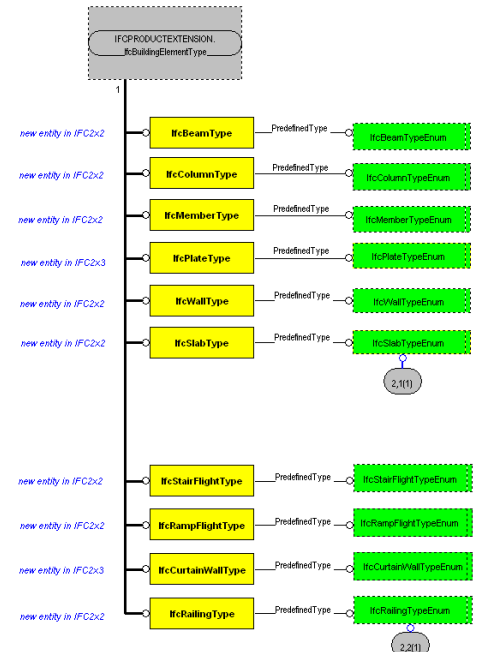


Fig. 3 – Example of data structure IFC 2x3 for building elements

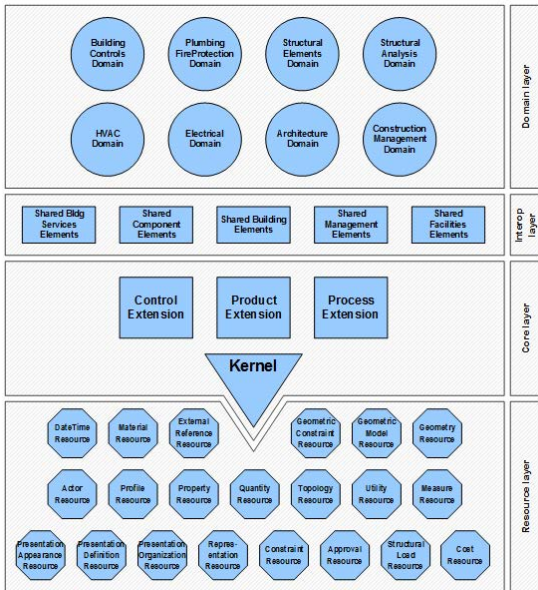


Fig. 4 – Data schema architecture with conceptual layer, IFC 4 format (BuildingSMART, 2016)

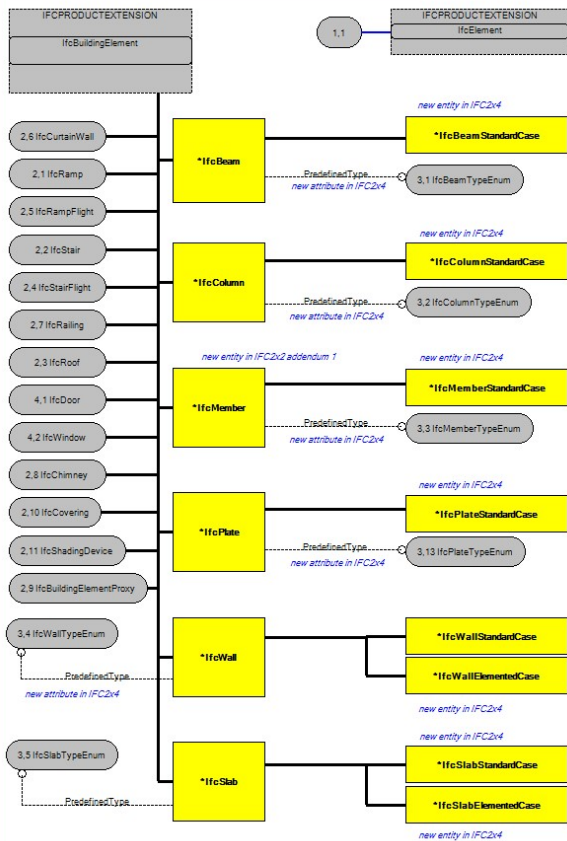


Fig. 5 – Example of data structure, IFC 4 format for building elements (BuildingSMART, 2016).

2.2 gbXML Format

The Green Building XML scheme, or "gbXML", was developed to facilitate the transfer of building information stored in CAD-based building information models, enabling interoperability between disparate building design and engineering analysis software tools (gbXML, 2016). This is all in the name of helping architects, engineers, and energy modelers to design more energy efficient buildings. Today, gbXML has the support of the industry and has been widely adopted by leading Building Information Modeling (BIM) vendors. In 2009, gbXML was spun off from Green Building Studio to become a stand-alone entity. Today, the developed gbXML is funded by organizations such as the U.S. Department of Energy (DOE), the National Renewable Energy Lab (NREL), software houses and others. Within the standard it uses geometrical and non-geometrical information available from the model and saves it in a text format under predefined labels. The information is divided into three different categories: ShellGeometry, SpaceBoundary, and Surface. Software tools employing gbXML do not always use all three categories in order to retrieve geometry. Most of them implement ShellGeometry and SpaceBoundary since in combination they represent geometry more accurately (Ivanova et al., 2015).

2.3 Features of the IFC Format

The characteristics of the IFC format are manifold, they range from the description of the geometry of the building, to information on individual building components, and various accessories (Marini et al., 2015). In this section the main classes that describe the geometric-dimensional information, the building components and their positioning will be detailed (ISO, 2004; ISO, 2016; ISO, 2007; ISO, 2013; ISO, 2014).

As an example of geometry information representation, Fig. 6 (BuildingSMART, 2016) shows how the IFC scheme represents the coordinates and dimensions of an IfcWall object. IfcWall is a subtype of IfcBuildingElement.

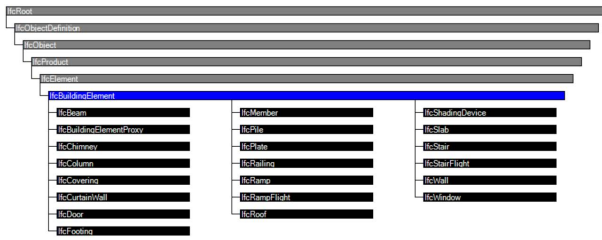


Fig. 6 – Example of IFC 4 format, Building Element - Entity inheritance

IfcBuildingElement is a subtype of IfcElement, which generalizes all components that make up an AEC product such as a wall, window, or door. IfcElement is a subtype of IfcProduct. IfcProduct has two attributes named ObjectPlacement and Representation. ObjectPlacement defines the starting point of IfcWall. It can be given by an absolute value relative to the world coordinate system by IfcGridPlacement; by a relative value, relative to the object placement of another product by IfcLocalPlacement; by grid reference i.e. by the virtual intersection and reference direction given by two axes of a design grid through IfcGridPlacement. Fig. 7 gives and shows an example of how IfcWall is represented as IfcProductRepresentation to elaborate the relational and organized data (representation of IFC).

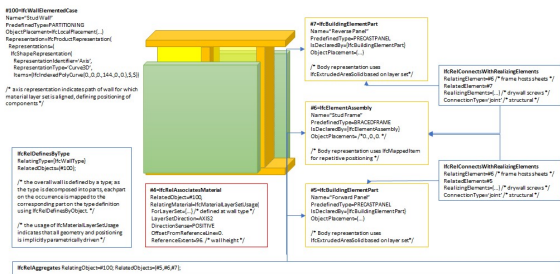


Fig. 7 – Example of IFC 4, format Building Element - object Wall elemented case

For example, the default properties/template of a wall are shown in Table 1.

Table 1 – IfcWall Property Sets for Objects

Predefined Type	
IfcWallType	Pset_WallCommon
IfcWallType	Pset_ConcreteElementGeneral
IfcWallType	Pset_PrecastConcreteElementFabrication
IfcWallType	Pset_PrecastConcreteElementGeneral
IfcWallType	Pset_ReinforcementBarPitchOfWall
IfcWallType	Pset_EnvironmentalImpactIndicators
IfcWallType	Pset_EnvironmentalImpactValues
IfcWallType	Pset_Condition
IfcWallType	Pset_ManufacturerOccurrence
IfcWallType	Pset_ManufacturerTypeInfo
IfcWallType	Pset_ServiceLife
IfcWallType	Pset_Warranty

The IfcProductRepresentation defines the representation of a product, including its geometric or topological representation. It has two attributes: IfcProductDefinitionShape and IfcMaterialDefinitionRepresentation. The IfcProductDefinitionShape defines all shape relevant information about an IfcProduct. It allows for multiple geometric shape representations of the same product. The IfcRepresentation defines the general concept of representing product properties. IfcPlacement locates a geometric item with respect to the coordinate system of its geometric context. It has two attributes called Location and Dim, where Location refers to the geometric position of a reference point, such as the center of a circle, of the item to be located. Dim refers to the space dimensionality of this class and is an IfcDimensionCount object, derived from the dimensionality of the location. IfcPlacement has three subtypes: IfcAxis1Placement, which defines the direction and location in the three dimensional space of a single axis; IfcAxis2Placement2D is used to locate and originate an object in a two dimensional space, and to define a placement coordinate system; finally IfcAxis2Placement3D is used to

locate and originate an object in a three dimensional space, and to define a placement coordinate system. These are just some of the information data encoded in the data structure of the IFC format

2.4 gbXML Format Characteristics

As mentioned before, gbXML has been developed based on XML, which incorporates data information representation but not the relationships among the data. All the geometry information imported from CAD tools is represented by the "Campus" element. The global child element "Surface" represents all the surfaces in the geometry. There are several attributes defined in "Surface" such as "id" and "surfaceType". Every "Surface" element has two representations of geometry: "PlanarGeometry" and "RectangularGeometry". Both of them carry the same geometry information. The purpose of this is to double-check whether the translation of geometry from the CAD software is correct or not. Every "RectangularGeometry" has four "CartesianPoint" elements which represent a surface. Every "CartesianPoint" has a three dimensional representation by three coordinates (x, y, z).

3. The Characteristics Necessary for Energetic and Acoustic Analyses

The physical, geometrical, environmental characteristics that are necessary for the simulation of the performance of a building through the use of BIM are many.

The tools that allow for the use of the geometrical data or more generally of the data of the building from a three-dimensional model, to modify and complete the information on the building, on climate, or on different environmental aspects with the need for energy simulations are numerous (Maile et al., 2007, Bazjanac, 2008, Chiaia et al., 2015, Pinheiro et al., 2016, Marini et al., 2015). Several of them allow to import gbXML and IFC formats automatically or in a semi-automatic way to simplify the input of geometrical data and sometimes of those related to the physical properties of the building components. A very important aspect when working with different data formats, is the congruence of

geometric information data, which is not always guaranteed, by taking into account the input mode required by the software or by the calculation model used for energy simulation (Ivanova et al., 2015). This fundamental aspect, if not considered, can spearhead results affected by errors (Ivanova et al., 2015).

In the following the main features needed by each application are described:

3.1 For Energy Simulation

The characteristics mainly missing in the IFC (Anafyo, 2016) data format as far as the energy simulation is concerned are related to the environmental forcers as, for example, the temperature trend, be it monthly or hourly scheduled, as a function of the type of simulation to be performed. Currently, calculation standards (CEN, 2008; CEN, 2012; CEN, 2007a; CEN, 2007b; CEN, 2005; CEN, 2007c) require for energy aspects the knowledge of different physical quantities, factors, or procedures not included in the IFC format. For instance, the EN ISO 13790:2008 standard (CEN, 2008) lays down the simplification of the calculation of geometry, the subdivision of the whole building into zones according to the type of energy service considered (this means that different areas can share the same space or part of space). Such aspects are not managed in a comprehensive manner by the IFC at present. For energy simulation, the IFC format should include the following key figures:

- data relating to environmental inputs (external temperature, solar radiation, vapor pressure, etc.);
- detailed physical characteristics for dynamic calculations (such as the data required by Energy Plus)
- data relating to the building's intended use, in particular, the usage profiles;
- data on the energetic zones to apply to the building;
- data on energy consumption of the building in case of energy audits;
- data relating to the characteristics of the energy generation systems (for example heat output power supplied by generators at part loads).

We reported the main information needed for the

energy simulation that is missing; they result from the analysis performed in this study, which will be further developed in successive stages.

3.2 For Acoustic Simulation

The simulation of the passive acoustic performance, which can be performed according to the EN 12354:2000 standard (CEN, 2000) requires a distinct knowledge of the individual building component performance, as measured in the laboratory, and the knowledge of the interaction among these components once installed (junctions). The geometrical identification of the rooms (Marini et al., 2015), by means of the various components involves very different performance results with respect to those measured in the laboratory for each individual component. Currently, IFC lacks the data required for the calculation of passive acoustic aspects.

As far as acoustics are concerned, it is evident that the building element performance is not a direct outcome from the individual components in particular as sound insulation and insulation against impact noise are concerned.

It is consequently necessary for the IFC format to include all of the parameters that depend on the junction of more elements or by constraint conditions, in particular:

- K_{ij} - parameter that accounts for the lateral vibration transmission;
- resonance frequency under load for materials for floating floors;
- ΔR due to the coatings that depends on the characteristics of air gap and on the mass of the rear structure;
- for noise transmission from plant operation, the possibility (as for the thermal aspects) of including reference data in the dynamic input (sound power released in the structures) is not permitted;
- for the acoustic insulation of the facade it should be noted that the performance depends on geometric and architectural parameters for the same structural components (ratio opaque surface/transparent surface, depth of the rearward room and the façade form factor ΔL_{fs}).

In addition, as regards both thermal aspects and acoustic aspects, there is the performance problem

related to the dynamic data input (L_{den} like solar radiation, with a value of the annual figure but not of the daily or hourly figure).

4. Conclusion

The present work shows the characteristics of the BIM IFC standards, highlighting the limitations and procedures that their use involves in generating energy and acoustic building performance simulations.

It also points out that the IFC standard, unlike the gbXML standard, is born for procedural, contractual, and managerial purposes. In order to use the IFC format for the prediction of energy and acoustic performance without having to resort to tools in an unidirectional way or to ensure interoperability, a lot of development work is still needed to combine the building contractual and managerial aspects, as well as their physical and environmental data.

Nomenclature

Symbols

BIM	Building Information Model
BEM	Building Energy Model
BPS	Building Performance Application
IFC	Industrial Foundation Class
gbXML	Green Building xml
xml	Extensive Markup Language
CAFM	Computer Aided Facilities Management
COBie	Construction Operations Building Information Exchange
AEC	Architecture Engineering Construction
IDM	Information Delivery Manual
IDF	Data format for Energy Plus software

References

- Anafyo. 2016. <http://www.anafyo.com>
- Bazjanac, V. 2008. "IFC BIM-Based Methodology for Semi-Automated Building Energy Performance Simulation". In: *Proceedings of the CIB-W78 25 International Conference on Information Technology in Construction*. Santiago, Chile.
- Building SMART. 2016. International home of open BIM. <http://buildingsmart.org/>
- CEN. 2000. EN 12354:2000, *Building acoustics Estimation of acoustic performance of building from the performance of elements*. Brussels, Belgium: CEN.
- CEN. 2005. EN ISO 7730:2005 - *Ergonomics of the thermal environment - Analytical determination and interpretation of thermal comfort using calculation of the PMV and PPD indices and local thermal comfort criteria*. Brussels, Belgium: CEN.
- CEN. 2007a. EN ISO 6946:2007 - *Building components and building elements Thermal resistance and thermal transmittance. Calculation method*. Brussels, Belgium: CEN.
- CEN. 2007b. EN ISO 13786:2007 - *Thermal performance of building components Dynamic thermal characteristics. Calculation methods*. Brussels, Belgium: CEN.
- CEN. 2007c. EN 15251:2007 - *Indoor environmental input parameters for design and assessment of energy performance of buildings addressing indoor air quality, thermal environment, lighting and acoustics*. Brussels, Belgium: CEN.
- CEN. 2008. EN ISO 13790:2008 - *Energy performance of buildings Calculation of energy use for space heating and cooling*. Brussels, Belgium: CEN.
- CEN. 2012. EN ISO 13788:2012 - *Hygrothermal performance of building components and building elements Internal surface temperature to avoid critical surface humidity and interstitial condensation Calculation methods*. Brussels, Belgium: CEN.
- Chiaia, B., S. Davardoust, A. Osello, N. Aste, M. Mazzon. 2015. "BIM and Interoperability for energy simulations". In: *Proceedings of BSA 2015*. Bolzano, Italy: BUPRESS.
- Dong, B., K.P. Lam, Y.C. Huang, G.M. Dobbs. 2007. "A Comparative Study of the IFC and gbXML Informational Infrastructures for Data Exchange in Computational Design Support Environments". In: *Proceedings of BS 2007*. Beijing: IBPSA.
- gbXML. 2016. Industry supported schema for sharing building information between disparate building design software tools. <http://www.gbxml.org/index.html>
- ISO. 2004. *ISO 10303-11:2004, Industrial automation systems and integration — Product data representation and exchange — Part 11: description methods: The EXPRESS Language Reference Manual*. Geneva, Switzerland: ISO.
- ISO. 2007. *ISO 10303-28:2007, Industrial automation systems and integration — Product data representation and exchange — Part 28: Implementation methods: XML representations of EXPRESS schemas and data, using XML schemas*. Geneva, Switzerland: ISO.
- ISO. 2013. *ISO 16739:2013, Industry Foundation Classes (IFC) for data sharing in the construction and facility management industries*. Geneva, Switzerland: ISO.
- ISO. 2014. *ISO 15686-4:2014, Building Construction — Service Life Planning - Part 4: Service Life Planning using Building Information Modelling*. Geneva, Switzerland: ISO.
- ISO. 2016. *ISO 10303-21:2016, Industrial automation systems and integration — Product data representation and exchange — Part 21: Implementation methods: Clear text encoding of the exchange structure*. Geneva, Switzerland: ISO.
- Ivanova, I., K. Kiesel, A. Mahdavi. 2015. "BIM-generated data models for EnergyPlus- A comparison of gbXML and IFC Formates". In: *Proceedings of BSA 2015*. Bolzano, Italy: BUPRESS.
- Maile, T., M. Fischer, V. Bazjanac. 2007. "Building Energy Performance Simulation Tools -a Life-Cycle and Interoperable Perspective". *CIFE Working Paper #WP107*. Stanford, U.S.A.: Stanford University.
- Marini, M., R. Baccoli, C.C. Mastino, V. Da Pos, Z. Tòth. 2015. "A new computational model: G.E.A.R. Graphical Expert Analytical Relations". In: *Proceedings of BSA 2015*. Bolzano, Italy: BUPRESS.
- Pinheiro, S., J. O'Donnell, R. Wimmer, V. Bazjanac, S. Muhic, T. Maile, J. Frisch, C. Van Treeck. 2016. "Model View Definition For Advanced Building Energy Performance Simulation". In: *Proceedings of BauSIM 2016*. Dresden, Germany.

Mapping Savings in Energy Demand by Heat Recovery for European Countries Under Consideration of Humidity Control

Stefanie Tafelmeier – Free University of Bozen-Bolzano – stefanie.tafelmeier@natec.unibz.it

Giovanni Pernigotto – Free University of Bozen-Bolzano – giovanni.pernigotto@unibz.it

Andrea Gasparella – Free University of Bozen-Bolzano – andrea.gasparella@unibz.it

Abstract

Sensible (SHR) and total heat recovery (THR) can play a significant role in energy savings in mechanical ventilation usage. Apart from the technical characteristics of the heat exchangers, the savings on the ventilation load depend on the air conditions for the two airstreams, namely the conditions maintained for the indoor air and the actual outside conditions, and on the proper control strategies deployed to minimize the impact on the air processes required after the heat recovery device. In this respect, humidity control can conflict with heat recovery whenever excessive humidity requires dehumidification of the ventilation air. In particular, SHR in heating mode should be preferably by-passed if the outside humidity exceeds the supply conditions required to compensate internal latent loads. For THR, moreover, the control strategy has also to account for the device's latent effectiveness, which may require an even earlier limitation of heat recovery or a by-pass if the system effectiveness cannot be controlled. Depending on the specific climate, the actual heat recovery can be much lower than the expected one and needs to be evaluated in order to avoid overestimating its energy and economic performance. The humidity supply limit required in the analysis of the actual recovery can be defined considering the target indoor humidity ratio (corresponding to the relative humidity setpoints of 50 %) reduced by the amount needed to compensate any indoor humidity source. This reduction can be expressed in terms of a specific latent load, SLL, calculated as the ratio between the mass rate of water vapor produced indoor, and the mass rate of the ventilation air, no matter whether some recirculation exists or not. Since both vapor production and ventilation air mass rate depend on sources and occupants' density inside the conditioned space (0.8, 1.2, 1.6, 2.0 or 2.4 g_v/kg_{da}), SLL is largely independent of the remaining building characteristics. In this research, we studied the savings from ventilation heat recovery in different European climatic zones and countries by applying

different control strategies to avoid excess humidity. Only the ventilation system had to be modelled through a simplified effectiveness model, considering different SLL as the only relevant building characteristic. Savings were expressed in terms of energy demand per flow rate, averaged over climatic Köppen-Geiger classes.

1. Introduction

High performance buildings, with enhanced airtight envelopes, often need a mechanical ventilation system for fresh air supply. Furthermore, the maintenance of an adequate indoor air quality for the occupants requires also humidity control. Even though results from field studies (Kosonen and Tan, 2004) lead to a weak sensation of relative humidity by occupants, some works (Tsutsumi et al., 2007) report a negative impact of high relative humidity on the performance of occupants. Moreover, health problems can be caused by excessive humidity, and it may lead to building material damage (Sterling et al., 1985). However, since the share of final energy uses by mechanical ventilation may be relevant for highly insulated buildings, an effective strategy to reduce the overall energy consumption can be based on heat recovery but its impact has to be carefully assessed, considering all air treatment stages. When dehumidification is required, for example, heat recovery is counterproductive and can even enhance the necessity of dehumidification because of excessive humidification, especially in case of latent heat recovery as indicated by the study of Smith and Svendsen (2016).

Developing further the analysis of a previous work by the authors (Tafelmeier et al., 2017), the current

research investigates the influence of humidity control on the potential energy and economic savings in heating mode, achieved by sensible and total heat recovery (respectively, SHR and THR). The study is performed for the 9 main Köppen-Geiger climate classes present in Europe, including 66 reference cities.

2. Simulation

2.1 Mechanical Ventilation System

The air treatment in the mechanical ventilation configuration is considered as in Fig. 1: outside air (OA) passes through the heat recovery device (HR), after which the exiting air (R) is mixed with the recirculated air (CA) to form the mixed air (MA). The MA is adjusted to meet the supply air (SA) condition by an air handling unit (AHU) equipped with devices for preheating, cooling and dehumidification, humidification and reheating. The return air (RA), is split up into the CA and the exhaust air (EA). The latter one passes through the HR device, whose sensible (ϵ_s), latent (ϵ_l) and total effectiveness (ϵ_t) is described as:

$$\epsilon_s = (m_{OA}/m_{min}) \cdot (T_R - T_{OA}) / (T_{RA} - T_{OA}) \quad (1)$$

$$\epsilon_l = (m_{OA}/m_{min}) \cdot (x_R - x_{OA}) / (x_{RA} - x_{OA}) \quad (2)$$

$$\epsilon_t = (m_{OA}/m_{min}) \cdot (h_R - h_{OA}) / (h_{RA} - h_{OA}) \quad (3)$$

where T is temperature, x is humidity ratio and h is enthalpy.

A unitary mass flow rate ratio is assumed, hence the OA mass flow rate, m_{OA} , and minimum mass flow rate, m_{min} , are considered to be the same. For the THR devices, ϵ_s , ϵ_l and, so, ϵ_t are taken as equal while for SHR devices ϵ_l is clearly null.

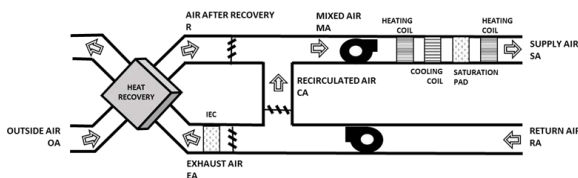


Fig. 1 – Mechanical ventilation configuration with HR device

2.2 Relative Humidity in Winter Mode

The SA humidity ratio has to be high enough to reach the comfort setpoint and low enough to balance the internal latent load m_L . Equation (4)

follows from the mass balance and gives the connection between the RA and the m_L .

$$x_{SA} = x_{RA} - m_L/m_{MA} \quad (4)$$

Even though in winter mode humidification is often necessary, when x_{MA} is greater than or equal to x_{SA} dehumidification is required. In common AHUs, it is performed by cooling the air below its dew point, with a consequent pre-heating before air is supplied to the environment.

Hence, the energy consumption in winter mode is the lowest if:

$$x_{MA} \leq x_{SA} = x_{RA} - m_L/m_{MA} \quad (5)$$

and for HR use:

$$x_R \leq x_{RA} - m_L/m_{OA} \quad (6)$$

Equation (6) describes the limitation of x_R as a function of x_{RA} and the latent load per OA flow rate.

If there is no HR or SHR (6) turns to:

$$x_{OA} \leq x_{RA} - m_L/m_{OA} \quad (7)$$

with

$$\Delta x = m_L/m_{OA} \quad (8)$$

being the specific latent load, SLL. Its value is derived by considering the suggested minimum fresh air rate per person and the latent load per person, which is classified in different activity levels. In that way, a SLL value is given independently of the building characteristics just knowing the activity of the occupants (Lazzarin et al., 2000). In this work, five SLL values were considered: 0.8, 1.2, 1.6, 2.0, and 2.4 g_v/kg_{da} .

2.3 Control Strategies and Saving Considerations

Two control strategies, A and B, have been defined for the SHR and THR. For determining the limits of control strategy A, it is assumed that HR is beneficial for heating as soon as the OA temperature or enthalpy for SHR or enthalpy for THR is below the EA temperature or enthalpy, respectively (dashed red lines in Figs 2 and 3). Control strategy B, instead, has been defined in order to avoid counter-productive dehumidification, which occurs if the humidity limitation of Equation (6) is exceeded. For SHR devices, control strategy B can be implemented through bypass as soon as Equation (7) does not apply (white area in Fig. 2). In the case of THR, Equation (6) can be rewritten by considering that x_R is given by the humidity ratio of OA, EA and ϵ_l

(Equation (2)). x_R is depending on ϵ_l , consequently it can be controlled by regulating ϵ_l by a partial bypass or rotational speed modification:

$$\epsilon_{l,op} \leq \min[\epsilon_l; 1-\Delta x/(x_{RA}-x_{OA})] \tag{9}$$

The maximum $\epsilon_{l,op}$, which in principle could be one, yet is limited to the nominal effectiveness, accounts for x_{OA} smaller than $x_{RA}-\Delta x/(1-\epsilon_l)$ (blue area in Fig. 3). The partialized $\epsilon_{l,op}$ is from the maximum value at $x_{RA}-\Delta x/(1-\epsilon_l)$ to zero at $x_{RA}-\Delta x$ (yellow area in Fig. 3).

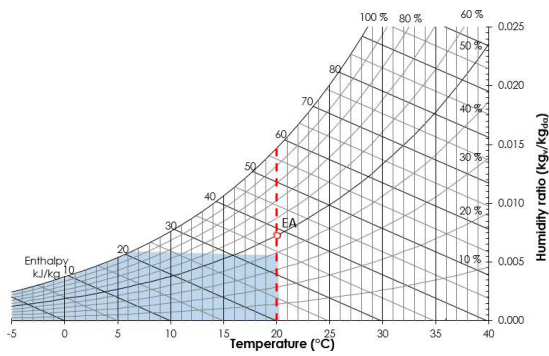


Fig. 2 – Psychrometric chart with highlighted limits in case of SHR for control A (red line) and control B (blue area)

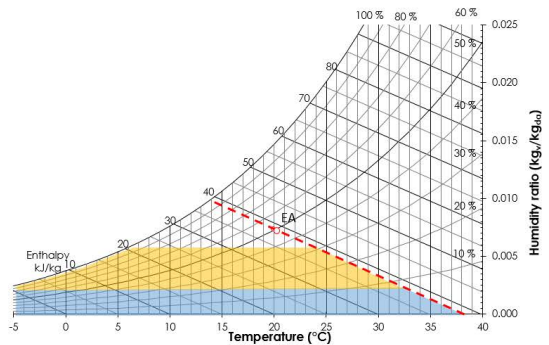


Fig. 3 – Psychrometric chart with highlighted limits in case of THR for control A (red line) and control B (blue and yellow areas)

The simulation is performed by calculating the energy savings on an hourly basis considering a steady state performance during this duration. Energy savings result from enthalpy difference between the OA and R. In order to calculate R, the EA condition equals the setpoint of the conditioned space, i.e. temperature of 20 °C and relative humidity of 50 %. The OA conditions are given by hourly weather data of a representative year provided by the EnergyPlus database (2016) for 66 reference cities in Europe. The energy savings are averaged for each Köppen-Geiger climate class (Table 1), for

which a representative city is identified by means of a Kolmogorov-Smirnov test, performed on the cumulative distributions of OA hourly enthalpy values. The cost savings are computed by consulting the natural gas prices and averaged at a national level. Energy and cost savings are given as savings per unit of flow rate and, consequently, they can be generalized independently of the building size.

Table 1 – details about climate classification and considered cities (Peel et al., 2006)

		Description	Number of cities and representative	
Cold	D	s b Dry + warm summer	1	Ankara
		f Without dry season		
		a + hot summer	3	Bucharest
		b + warm summer	16	Ostrava
		c + cold summer	5	Ostersund
Temperate	C	s Dry summer		
		a + hot summer	15	Bari
		b + warm summer	3	La Coruna
		f Without dry season		
		a + hot summer	4	Bologna
		b + warm summer	16	Amsterdam
arid	B S k	Steppe + cold	3	Madrid

Table 1 – Price for natural gas [EUR/kWh] for the main countries

State	natural gas cost	State	natural gas cost	State	natural gas cost
A	0.071	FIN	0.040*	PL	0.05
BG	0.039	GR	0.075	ROM	0.034
CZ	0.058	I	0.091	S	0.12
D	0.068	N	0.07**	SRB	0.04
DK	0.077	NLD	0.077	TK	0.035
E	0.093	P	0.098	UK	0.071
F	0.073				

* (StatisticsFinland, 2016); ** (Gasnor AS, 2016)

The following assumptions have been made:

- The nominal effectiveness for sensible, latent and total heat recovery is chosen to be 70 %.
- The gas boiler for the hot water supply for the heating coils installed in the AHU has an efficiency of 80 %.

- The natural gas prices are provided by the European Union Eurostat (2016) for the considered countries. Exceptions are Finland and Norway, for which a different source is considered, and Belarus, Cyprus, Iceland, Russia and Ukraine, which are excluded due to the lack of price information (Table 2).
- Impacts on the energy and cost savings independent of the HR device choice, such as pressure losses, were not included as well as an eventual reduction in downscaling of the AHU devices in case of HR.

3. Discussion and Result Analysis

Durational-plots (Fig.s 4 and 5) are used to show how the control strategies affect the energy savings in case of SHR and THR. They illustrate the hourly energy savings per flow rate sorted in decreasing order. Bologna, the representative city of the climate class Cfa, is chosen as an example.

As described above, control strategy A for SHR is not correlated to SLL, while control strategy B defines whether the device is bypassed or not and, consequently, if the energy saving becomes zero or remains unchanged. From Fig. 4, it can be seen that the highest energy savings achieved for SHR do not fall into the bypass region, even for the highest SLL value.

Differently from SHR, THR savings depend on the SLL value for both control strategies. In case of control strategy B for THR, the highest energy saving is reduced by the partialization of the effectiveness for SLL values of 2.0 and 2.4 g_v/kg_{da} (i.e. with those SLL, the air condition is included in the yellow region in Fig. 3). Savings in case of control strategy A for THR are generally higher than those for the control B, as the SLL raises the EA enthalpy, and allows a higher recovered energy. Nevertheless, this might reduce the indoor air quality or increases the dehumidification need.

The areas in Fig.s 4 and 5 represent the annual energy savings in heating for a SLL of 1.6 g_v/kg_{da} . Specifically, savings achieved by control strategy A are illustrated by the plane red areas and those by

control strategy B by striped red areas. An increasing SLL value in control strategy B for SHR and in both controls for THR leads to a shrinking area and so, to the reduction in savings. In this example, the total saving for heating by SHR considering a SLL of 1.6 g_v/kg_{da} in Bologna are 76.77 kWh/(l/s) and 53.00 kWh/(l/s) for SHR, and 151.50 kWh/(l/s) and 54.78 kWh/(l/s), respectively with control strategy A and B.

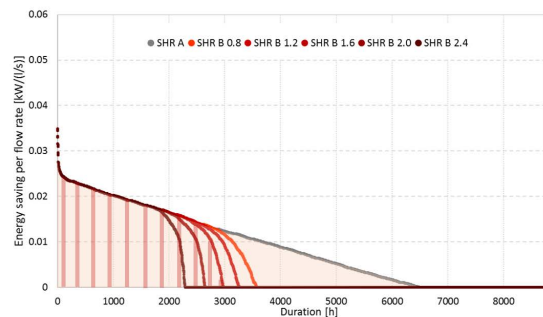


Fig.4 – Durational-plot of energy savings by SHR for Bologna

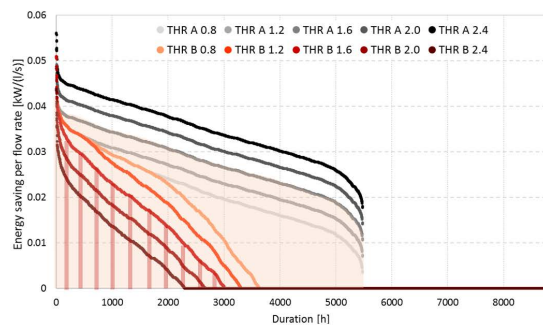


Fig. 5 – Durational-plot of energy savings by THR for Bologna

The hourly savings over the year are represented by means of carpet-style plots in order to visualize when, in terms of daytime and season, the savings due to HR is effected by the control.

Fig. 6 shows the hourly energy savings by SHR throughout the year for each climate class representative city. The order of the climate classes from the top to the bottom equals the increasing ranking of the averaged energy savings for SHR with control strategy A. As in this work only the savings regarding the heating were considered, the lowest saving potential occurs for the months from May to September, the highest from December to February. The cold climates (initial letter D) benefit from the SHR

also in the intermediate seasons, especially compared to the temperature climates with dry summer (Csa and Csb). The highest saving potential occurs in the hours between 22:00 to 8:00. Applying the control strategy B leads to an increase of zero-saving occasions, particularly for the temperate climates during the intermediate seasons in the afternoon, and during the summer in the morning and nights. In case of the THR, again, the order of the climate classes aligns with the computed increasing average savings in energy (Fig. 7). Lowest savings occur between June and September, highest similar as for SHR between December and February. The duration of zero-savings due to bypassing in summer, extents strongly for all climates into the intermediate seasons once the control strategy B is applied. The effect of the partialization of the effectiveness is the most visible in the winter months. The consequences of the above discussed impact of the humidity control on the potential in achieving energy savings by HR are given in the following paragraphs.

The ventilation load – calculated as enthalpy difference between OA and SA air conditions - and the energy savings, expressed in terms of averages and standard deviations for each climate class, are given in Table 3 for SHR with a SLL of 1.6 g_v/kg_{da}. The order is again in line with the increasing savings potential for control strategy A. The savings are the least for the temperate climates with dry summer and the highest for all cold climates in the order of the sub classes: hot, warm and cold summer. The orders do not change for control strategy B, except for BSk and Cfa, since the latter one is slightly more affected by control strategy B. The reduction itself ranges from 49.7 % for the Csa to 9.3 % for Dfc if an SLL of 1.6 g_v/kg_{da} is considered. As a whole, the energy savings contribute to a reduction of the ventilation load, which is in average 50 % for control A and 37 % for control B.

Table 3 – Average energy savings and standard deviation for heating by SHR with a SLL of 1.6 g_v/kg_{da} and the ventilation load [kWh/(l/s)]

	Ventilation load	SHR control A	SHR control B
Csa	86.25±29.40	47.35±11.36	23.82±13.63
Csb	121.19±68.66	67.83±19.86	35.38±35.43
BSk	156.48±34.70	71.46±12.67	57.50±15.96
Cfa	140.08±22.72	73.97±9.03	51.08±11.91
Cfb	178.52±36.50	93.28±15.38	64.01±18.43
Dfa	187.32±14.79	94.14±5.39	75.69±5.31
Dsb	228.75	103.67	91.26
Dfb	242.48±28.84	118.76±3.18	98.91±13.95
Dfc	345.33±47.06	163.21±21.29	148.08±24.75

Table 4 represents the results for THR equivalently to Table 3 for SHR. The ranking of the climate classes in terms of saving potential has changed but, likewise for control strategy A and a SLL of 1.6 g_v/kg_{da} for SHR, the least savings occur for the temperate climate class with hot and dry summers, the highest can be achieved in the cold climate class without dry seasons and cold summers.

Table 4 – Average energy savings and standard deviation for heating by THR with a SLL of 1.6 g_v/kg_{da} and the ventilation load [kWh/(l/s)]

	Ventilation load	THR control A	THR control B
Csa	86.25±29.40	111.90±22.86	23.68±14.65
Cfa	121.19±68.66	148.13±13.47	55.05±18.15
Csb	156.48±34.70	153.77±43.01	34.00±43.29
BSk	140.08±22.72	165.09±24.03	62.30±23.84
Dfa	178.52±36.50	176.59±9.21	90.15±10.32
Cfb	187.32±14.79	193.32±26.43	65.55±22.46
Dsb	228.75	208.36	121.25
Dfb	242.48±28.84	223.11±19.09	123.42±21.60
Dfc	345.33±47.06	284.65±25.29	196.81±41.66

The magnitude of savings and the order of the climate classes are affected more by the control strategy than for SHR. Indeed, with control strategy B, the cold climate Dfa shows higher savings than the temperate climate Cfb without dry seasons and warm summers. However, the savings in Cfb are reduced more by adopting the control strategy B than for Dfa. The climate classes representing the lowest

savings (Csa) and the highest three ones (Dsb, Dfb and Dfc) are, in terms of ranking, not affected by the HR or control choice. The maximum reduction is found for Csa, equal to 78.8 %, and the minimum for Dfc, equal to 30.9 %, with a SLL of 1.6 g_v/kg_{da}. Also in that case, the contribution of the energy savings by the THR on reducing the ventilation load has been considered. The average for a SLL of 1.6 g_v/kg_{da} and control strategy A is 104 % while for control strategy B it is 42 %. The reason for the contribution higher than 100 % is due, on the one hand, to no limitation in the effectiveness and, on the other hand, to EA humidity and enthalpy higher than those for SA, which also indicate excessive humidification.

Table 5 – Average national cost savings by SHR [EUR/(l/s)]

Country	SHR control A	SHR control B
SRB	3.53	2.83
BG	3.76	3.04
GR	3.94±0.63	2.25±0.96
TK	4.18±0.82	3.23±0.08
P	4.56±1.10	1.26±0.47
PL	5.55±0.10	4.37±0.16
F	5.63±0.95	3.57±1.02
FIN	5.72±0.22	5.03±0.24
I	5.79±1.63	3.65±1.75
ROM	5.81	4.57
E	6.26±1.40	4.24±2.18
CZ	6.63±0.18	5.42±0.14
UK	6.64±0.44	4.48±0.62
A	6.98	5.82
D	7.12±0.55	5.66±0.60
NLD	7.32	4.58
DK	8.38	6.58
N	8.61±0.21	7.05±0.89
S	17.78±3.86	15.80±4.63

The cost savings achieved by SHR are given in Table 5 for control strategies A and B, considering a SLL of 1.6 g/kg. The highest savings are for both cases for Sweden, due to the high saving potential plus the high natural gas costs. On the contrary, the lowest savings for control strategy A account for Serbia, mainly due to the low natural gas costs. This changes as soon as the control strategy B is applied,

and the weakest saving potential is in Portugal, followed by Greece. This control leads to a reduction of more than 70 % for Portugal and more than 35 % for Greece, the Netherlands, Italy, and France. Equally is the trend of the cost savings for THR with both strategies (Table 6). The maximum cost reduction accounts for Portugal, with more than 90 %, and Greece, Spain, and the Netherlands for more than 70 %. However, it should be noted that a large spread of results in the cost calculation occurs for Spain and Italy, because of the many climate classes present in those countries.

Table 6 – Average national cost savings by THR [EUR/(l/s)]

Country	THR control A	THR control B
SRB	6.70	3.20
BG	7.33	3.69
GR	8.36±1.05	1.95±1.18
TK	8.77±2.17	3.75±0.65
P	10.19±2.16	0.81±0.49
FIN	10.24±0.25	6.54±0.44
PL	10.53±0.16	5.27±0.34
ROM	10.74	5.46
I	11.64±2.60	3.55±2.19
F	11.78±1.60	3.68±1.17
CZ	12.92±0.66	6.29±0.25
A	13.85	7.02
E	13.91±3.13	3.91±2.74
D	14.00±0.72	6.19±0.95
UK	14.04±0.76	4.31±0.52
NLD	14.68	4.15
N	16.67±0.14	8.45±2.01
DK	16.79	7.28
S	31.88±4.70	20.68±7.47

4. Conclusion

This work investigates heat recovery in mechanical ventilation systems in heating mode in Europe, focusing on two aspects: 1) the impact of the humidity control on the energy and cost savings, as well as 2) the applicability of Köppen-Geiger climate class based mapping for large scale assessments.

Concerning 1), for a sensible heat recovery with humidity control strategy B, more hours with zero-

savings occur, proportionally with the specific latent load, especially in the intermediate seasons. For a total heat recovery, the behavior of the potential saving is similar but, due to an additional partialization to avoid excessive humidification, hourly and annual potential savings are often more affected than for sensible heat recovery, especially in the intermediate seasons, in the morning and night hours. The climate rankings of energy saving potentials do not vary significantly regarding the control strategies, but the humidity control strategy B causes a strong reduction, particularly for temperate and arid climate classes. In terms of cost savings, it follows from the results that heat recovery combined with humidity control reduces the annual savings for heating, especially in Portugal and, with a lower magnitude, in Greece, the Netherlands, Italy, France, and Spain. Conversely, this means that, in those countries, a saving calculation without consideration of the humidity control might overestimate the economic benefits of the heat recovery device.

Regarding 2), as soon as the control is applied the deviation increases. This raises the question of how appropriate the Köppen-Geiger classification is for humidity-correlated investigations. Since the classes are distinguished in terms of temperature and precipitation, it stands to reason that a more sophisticated classification is necessary for a convenient visualization of the saving. Future works shall overcome this limitation by investigating different solutions such as combining the Köppen-Geiger classification with the air humidity and enthalpy, consulting other climate classifications if suited or define a classification based on a larger number of examples on a tighter grid, particularly tailored for heat recovery control.

Acknowledgement

This study has been funded by the project "Klimahouse and Energy Production" in the framework of the programmatic-financial agreement with the Autonomous Province of Bozen-Bolzano of Research Capacity Building.

Nomenclature

Symbols

ε	Effectiveness
h	Specific enthalpy(kJ/kg)
m	Mass flow rate (kg/s)
T	Temperature (°C)
x	Humidity ratio (kg _v /kg _{da})

Subscripts/Superscripts

l	Latent
L	Load
MA	Mixed air
min	Minimum
OA	Outside air
R	Air after recovery
RA	Return air
S	Sensible
SA	Supply air
t	Total

References

- Energyplus. Accessed on Dec. 23rd 2016. Retrieved from <https://energyplus.net/weather>
- Eurostat. Accessed on Dec. 23rd 2016. Retrieved from <http://ec.europa.eu/eurostat/about/overview>
- Gasnor. Accessed on Dec. 23rd 2016. Retrieved from <http://gasnor.no/bolig/priserbetjeningser/>
- Kosonen, R., F. Tan. 2004. "Assessment of productivity loss in air-conditioned buildings using PMV index." *Energy and Buildings* 36(10): 987–993. doi: 10.1016/j.enbuild.2004.06.021
- Lazzarin, R.M., A. Gasparella, G.A. Longo, M. Perbellini. 2000. "Gli scambiatori di calore aria aria: potenzialità applicative nella riduzione del carico di ventilazione degli edifici". In: *Atti Del 55° Congresso Nazionale ATI*.
- Peel, M.C., B.L. Finlayson, T. McMahon. 2006. "Updated world map of the Köppen-Geiger climate classification". *Meteorologische Zeitschrift* 15(3): 259–263. doi:10.1127/0941-2948/2006/0130.
- Smith, K.M., S. Svendsen. 2016. "The effect of a rotary heat exchanger in room-based ventilation on indoor humidity in existing apartments

- in temperate climates". *Energy and Buildings* 116: 349–361. doi: 10.1016/j.enbuild.2015.12.025.
- StatisticsFinland. Accessed on december 23rd 2016. Retrieved from http://www.stat.fi/til/ehi/2015/04/ehi_2015_04_2016-03-09_tau_002_en.html
- Sterling, E.M., A. Arundel, T.D. Sterling. 1985. "Criteria for Human Exposure To Humidity in Occupied Buildings". *ASHRAE Transactions* 91(pt 1B): 611–622.
- Tafelmeier, S., G. Pernigotto, A. Gasparella. 2017. "Annual Performance of Sensible and Total Heat Recovery in Ventilation Systems: Humidity Control Constraints for European Climates". *Buildings* 7(2): 28; doi:10.3390/buildings7020028.
- Tsutsumi, H., S.I. Tanabe, J. Harigaya, Y. Iguchi, G. Nakamura. 2007. "Effect of humidity on human comfort and productivity after step changes from warm and humid environment". *Building and Environment* 42(12): 4034–4042. doi: 10.1016/j.buildenv.2006.06.037.

Mapping Savings in Energy Demand by Heat Recovery for European Countries Under Consideration of Humidity Control

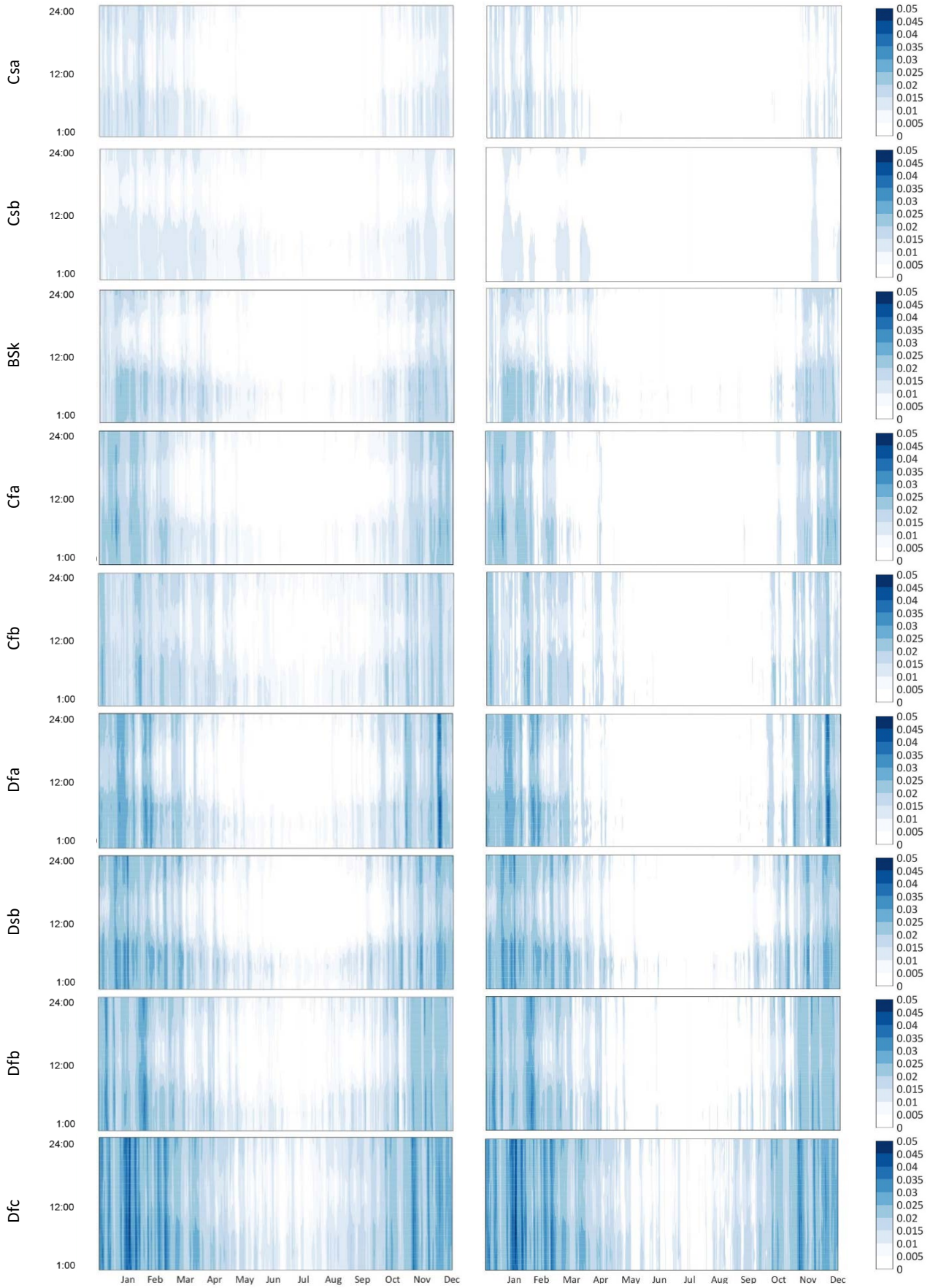


Fig. 6 – Carpet-plot of hourly energy savings for the representative cities for SHR control A (left) and control B and a SLL of 1.6g/kg_{da} (right)

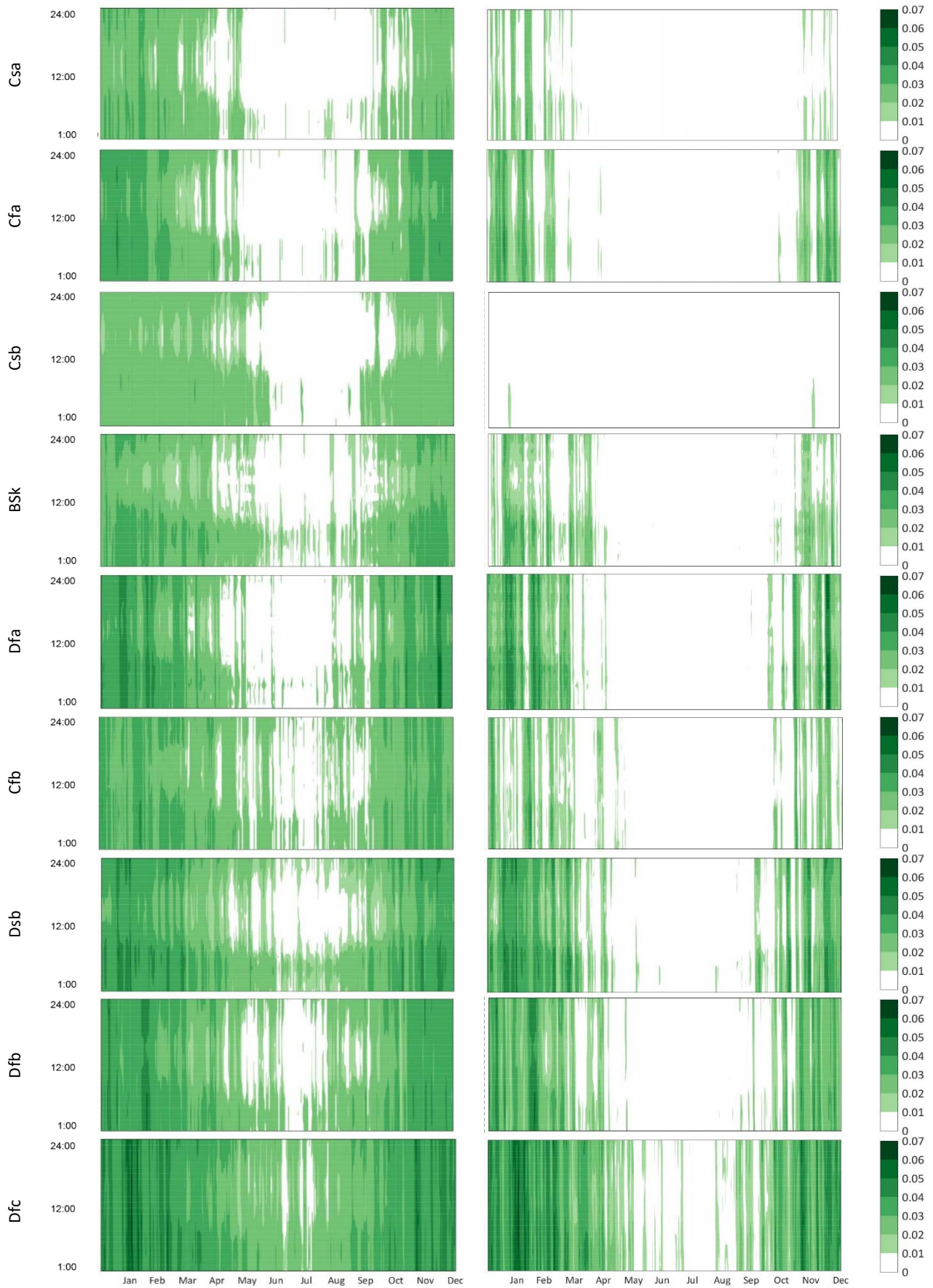


Fig. 7 – Carpet-plot of hourly energy savings for the representative cities for THR control A (left) and control B and a SLL of 1.6g/kg_{da} (right)

Calibrated Simulation Models for Indoor Comfort Assessment: The Case of a Healthcare Facility in Vienna

Luca Zaniboni –Free University of Bozen-Bolzano – luca.zaniboni@natec.unibz.it

Giovanni Pernigotto –Free University of Bozen-Bolzano – giovanni.pernigotto@unibz.it

Matthias Schuß –Vienna University of Technology – matthias.schuss@tuwien.ac.at

Kristina Kiesel –Vienna University of Technology – kristina.kiesel@tuwien.ac.at

Andrea Gasparella –Free University of Bozen-Bolzano – andrea.gasparella@natec.unibz.it

Ardeshir Mahdavi –Vienna University of Technology – bpi@tuwien.ac.at

Abstract

Design activity on healthcare buildings cannot be limited to the energy aspects and must account also for the indoor thermal comfort conditions. Indeed, the occupants of this category of buildings are affected by different kinds of unhealthy statuses and particular attention is required in order to ensure conditions adequate to therapies and medical treatments. Even if simulation can be a helpful tool in designing new buildings, also in case of complex clinics and hospitals, a proper calibration is a necessary step for the existing building stock. In this way, discrepancies between simulated and measured building energy performance and thermal behavior can be reduced, improving the reliability of the model itself and allowing its use for many purposes, from the assessment of energy performance to the evaluation of indoor thermal comfort. In this work, experimental and numerical modelling activities have been performed in order to develop a calibrated model of part of a healthcare building in Vienna, Austria, for the assessment of both thermal performances and comfort conditions. The facility was built in the early '90s, with later expansions, and is composed of many environments characterized by different therapeutic activities. Many properties of the building envelope and system are unknown and initial values have been assumed from direct inspections and documentation on construction standards. After zoning the healthcare, for each ambient, long-term measurements of the air temperature were recorded every 10 minutes from March to June 2015 and used to calibrate the model. During the same period, occupants were interviewed about their thermal comfort sensations and detailed short-term measurements were collected to calculate Fanger's Predicted Mean Votes and Percentages of Dissatisfies. The simulated air temperature

and internal surface temperature profiles have been used to evaluate the same indexes by comparing them with those calculated from the measured data and people's votes.

1. Introduction

Design and renovation of existing buildings into high efficiency ones require taking into account also the occupants' thermal comfort, which depend on both building's use and occupants' activity and personal conditions. Among different types of buildings, healthcare facilities are particularly critical to design, with the aim to ensure high standards of indoor comfort, since employees' and patients' comfort perceptions are different (Hwang et al., 2007; Khodakarami et al., 2012; Skoog et al., 2005; Verheyen et al., 2011). To this extent, building energy simulation, BES, can be a helpful tool to support the designers' activity. As regards existing facilities, however, simulation models require calibration. Only with a good estimation of input and boundary conditions, it is possible to simulate in an effective way the thermal comfort of healthcare environments' occupants.

To meet the design targets, moreover, BES codes have often to be coupled with optimization tools. For example, Ferrara et al. (2015a and 2015b) focused on school buildings and used GENOPT to run TRNSYS simulations aimed at optimizing a classroom from the point of view of both total energy demand and thermal comfort. Ascione et al. (2016) coupled EnergyPlus and a genetic algorithm

written with Matlab to optimize the hourly setpoint temperatures, based on weather forecasting and occupancy profiles, selecting the best solutions according to economic and comfort constraints. Arambula et al. (2017) exploited the genetic algorithm implemented in jEPlus+EA to calibrate and simulate an EnergyPlus model of an Italian school building.

In this work, a portion of a healthcare facility in Vienna, Austria, has been analyzed. After collecting short and long-term measurements, global comfort according to Fanger’s model (ASHRAE 2013; ISO, 2005) has been assessed and contrasted with the results by interviews submitted to occupants. A TRNSYS model has been developed and calibrated by means of two steps: first, by comparison with the collected air temperature measurements, and then against the calculated Fanger’s indexes - predicted mean votes, PMV, and predicted percentage of dissatisfied, PPD. After calibration, the developed model can be useful for several redesign tasks, encompassing the analysis of scenarios for long term thermal comfort optimization, able to manage effectively the discrepancies among the different occupants’ perceptions and to minimize overall energy costs.

2. Methods

2.1 Case Study and Measurements

This study regards the “Physikalisches Institut Leopoldau” (Fig. 1), a private physiotherapy center, located on the ground floor of a 20-year old building in Vienna, Austria. The analysed area, equal to about 103 m², includes 22 therapy rooms, where therapies are performed from 7:00 am until 8:00 pm, from Monday to Friday.

Two kinds of measurements were collected: detailed short-term measurements and long-term measurements. Short-term measurements regarded air temperature, relative humidity, mean radiant temperature, and air speed. An Ahlborn ALMEMO 2590 system with 4 probes was used. The monitored quantities were recorded with accuracies of 0.1 °C for air and mean radiant temperatures, 2 % for relative humidity and 0.01 m s⁻¹ for air velocity.

Short-term measurements were repeated 3 times in all rooms of the therapy zone: on 12/03/2015 from 3:00 pm until 7:00 pm, on 25/03/2015 from 2:00 pm until 8:00 pm and on 21/04/2015 from 11:00 am until 4:00 pm. The time interval was set at 200 s for the first two measurement campaigns and 60 s for the last one.



Fig. 1 – Physiotherapy Center layout with the area of interest for this analysis highlighted in red

Long-term measurements of temperature were collected with 8 HOBO U12 data loggers and probes, with nominal accuracies of ± 0.35 °C. Each sensor was positioned at a height of 1 m, chosen to match the need of registering air temperatures and relative humidity sufficiently representative of the indoor conditions, without disturbing the activities performed in the rooms. Considering an average duration of 30 minutes for treatments, a measurement time-step of 10 minutes was set. The measurement campaign started on 08/03/2015 and ended on 18/06/2015. The collected data were compared first with short-term measurements, in order to check the presence of errors. Furthermore, short-term measurements were used to derive correlations for the

estimation of the mean radiant temperature, not directly recorded during the long-term campaign.

2.2 Questionnaires

In order to evaluate the employees' and patients' opinions about comfort conditions, questionnaires were based on ASHRAE 7-points thermal sensation scale and developed according to ASHRAE Standard 55 (2013), ISO 7730 (2005), and other previous case studies in the literature (Azizpour et al., 2013; Huang et al., 2007; Skoog et al., 2005; Van Gaever et al., 2014; Verheyen et al., 2011). Date, time, and room where therapy was performed were asked, in order to match the answers with the measurements in the data analysis. The questionnaires were divided into three sections, one to be filled in by the employee (section A) and two by the patient, before (B) and after the therapy (C). All sections included questions about the opinion on the temperature when completing the survey ("too cold", "cold", "slightly cold", "neutral", "slightly warm", "warm", "too warm").

2.3 Simulation Model Definition

The simulation was performed using TRNSYS 3D 2017, while the calibration was made partially manually and by means of the software GENOPT. The analysis included only one thermal zone, the area with therapy rooms located in the old part of the building, highlighted in Fig. 1. The model was prepared using Google SketchUp (Fig. 2), and imported into TRNSYS 17.

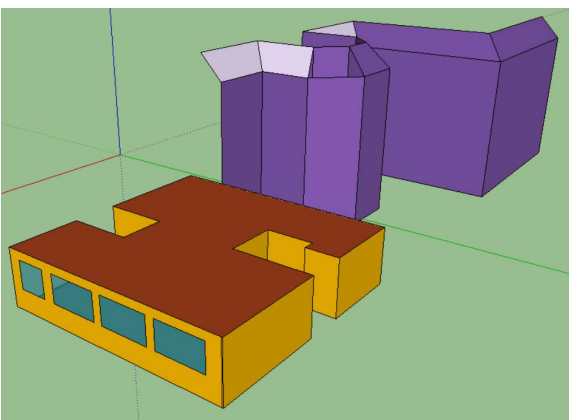


Fig. 2 – The 3D model of the analyzed area of the physiotherapy center prepared by Google SketchUp 8

The weather data were provided by the ZAMG (Zentralstalt für Meteorologie und Geodynamik), the Austrian central office of meteorology and geodynamic, and included dry bulb temperature and global horizontal irradiation in Vienna from 1 March to 30 June 2015, with a 10-minute time-step. A first hypothesis about the walls composition was made looking at the building schematic plans and sections. The walls were set as slightly externally insulated (5 cm of polystyrene) and made of 25 cm of concrete. The initial values of the thermal conductivity, density and thermal capacity of the layers materials were taken from ISO 10456 (ISO, 2008). Initial convection factors were set according to the standard pre-set values used by TRNSYS. Solar absorptance was set to 0.3 for walls and ceiling, and 0.6 for the floor. All surface emissivity were set equal to 0.9. The thermal bridges initial values were taken from UNI 14683 (UNI, 2008), considering the internal dimensions. The windows were analyzed in a previous work (Zaniboni et al., 2016a and 2016b), which involved in-situ survey and modelling of glazing parameters by means of LBNL Window 6, considering two layers of 4 mm clear glass separated by 32 mm air gap. Internal shading devices were modelled but no control was implemented since they were used for most of the time for privacy reasons. The ventilation rate was calculated equal to 2.64 ACH, taking the values recommended by UNI 10339 (1995) for physical therapies and daily staying.

Three types of internal gains were present: 1. lighting gains; 2. electrical gains due to other electrical equipment (comprising also the therapy machines); 3. metabolic gains due to the people's activities in the facility. The lighting system and electrical equipment were monitored in detail. For the first one, the capacity installed in each room, together with its utilization factor, was already known (Zaniboni et al., 2016a) and the corresponding thermal gain was set at 60 % radiative and 40 % convective. On the contrary, the utilization factors of the electrical equipment were more uncertain and set to be able to match with the overall electrical energy recorded for the whole facility for some weeks. In this case, the heat gain was set half convective and half radiative. Averaging the thermal gains by patients and employees estimated starting from their

metabolic rates, first attempt values of 52 W per occupant were set for each of the convective and the radiative part. Since the occupancy profiles of the building were known, the total gains from the metabolic rate were calculated from the sum of the gains from the patients and therapists who were present.

No data about the heating system were available and, consequently, heat capacity was modelled as ideal, half radiative and half convective, and without nighttime or weekend setbacks, since the focus of the analysis was put on the occupancy period. The system ON/OFF control was modelled with TRNSYS Type 2, a function switching the system ON and OFF if the air temperature overpasses the temperature setpoint plus or minus a default band. The band was set to 0.5 °C and the temperature setpoint was set to 24 °C, coherently with observations on the measured air temperature profiles.

2.4 Simulation Model Calibration

Since many uncertain variables were present, a preliminary sensitivity analysis was performed. It was decided, concerning the materials of opaque components, to calibrate the most affecting properties, i.e. the conductivity of the insulation layer and the specific heat capacity of the massive concrete layer. All convection coefficients were calibrated while all absorptance and emissivity were left equal to their initial values. Regarding the windows, only the thermal transmittance of frames was calibrated since the glazing properties were already assessed in a previous study (Zaniboni et al., 2016a). Among thermal bridges, only those between the window's frame and the surrounding opaque component were involved in calibration. The internal gains, the lighting ones, were not calibrated, since they had already been determined with sufficient precision in a previous contribution (Zaniboni et al., 2016a). On the other hand, the gains from other electrical equipment and occupants required calibration. The same held for the air-change rate by infiltration and ventilation and for the equivalent air specific heat capacity, which was varied to take into account the effect on thermal inertia of additional internal

elements, such as furniture. Finally, setpoint temperature was calibrated while the ON/OFF band range was not.

Material properties were varied by 50 %, because of the lack of knowledge about the material conditions. Assuming a poor ventilation rate, confirmed also by negative answers about indoor air quality in questionnaires, air-change rate was varied from 0.15 to 2.64. The equivalent air specific heat capacity was varied from 0.812 to 5.012 kJ kg⁻¹ K⁻¹ and setpoint temperature was varied between 21 and 27 °C. All other parameters were changed by 30 %.

Considering that the temperature setpoint was the most impactful variable, in order to minimize the calibration time and optimize the GENOPT code, it was manually calibrated first, with a step of 0.5 °C. The value leading to the minimization of the root mean square difference, RMSD, with respect to the long-term air temperature measurements (i.e. from 09/03/2015 to 18/06/2015, weekends excluded), was adopted and the remaining variables calibrated with GENOPT. Ten steps were set per each variable, with 90 particles and 100 generations, which means a total of 9000 simulation attempts.

2.5 Simulation Model Validation Through Comfort Indexes

PMV and PPD indexes (ASHRAE, 2013; ISO, 2001 and 2005) were derived from both measured and simulated data during occupancy time in order to validate the calibrated model. In both cases, a metabolic rate of 2 met was assigned to employees while 1 met was assumed for patients (ASHRAE, 2013; ISO, 2005). The clothing level values were determined from the answers to the questionnaires according to ASHRAE Standard 55 (ASHRAE, 2013).

Regarding the indexes calculated from measurements, air temperature, and humidity, they were taken from long-term measurements while the mean radiant temperature was estimated as functions of the air temperature. Specifically, we used only regression models derived from short-term measurements correlating mean radiant and air temperatures with indexes of determination R² larger than 0.7. When those models were not available, i.e. for therapy rooms 9, 11, 12, 13, and 14,

mean radiant temperature was assumed equal to air temperature. Short-term measurements of air speed were used as average conditions in calculations.

Considering the indexes determined from simulations, TRNSYS temperature outputs were used in calculations, together with average humidity and air speed by measurements. Since one thermal zone was simulated, we determined the mean radiant temperature as an area-weighted average of simulated surface temperatures of externally exposed components (i.e. floor, ceiling, windows, external walls) and internal components assumed at a simulated air temperature.

Finally, in both cases, the PMV and PPD, evaluated at the same time in which votes were collected, were compared for both patients and employees.

3. Results

3.1 Calibration

After calibration, RMSD decreased from 1.86 °C to 0.92 °C. The calibrated variables and the values reached after the calibrations are reported in Table 1. The profile of the measured and simulated air temperature inside the thermal zone are reported in Fig. 3, during the whole period and for 20 days at the end of March.

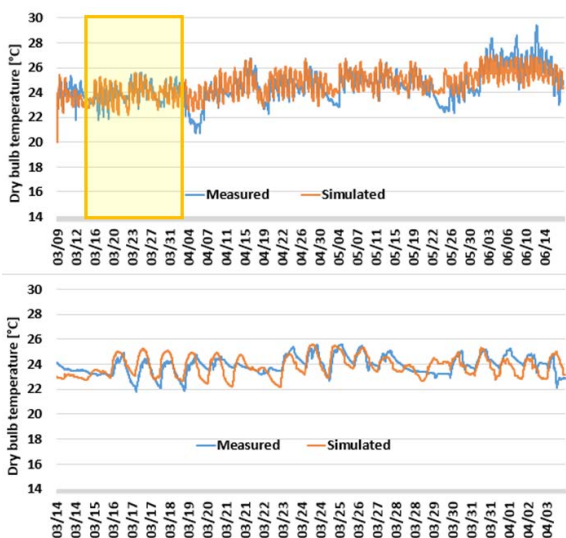


Fig. 3 – The comparison between the air temperature profiles (measured and simulated) during the whole period and for the last 20 days of March, 2015

Table 1 - List of the variables varied in calibration

Variable	Initial	Final
Thermal conductivity (insulation layer) [W m ⁻¹ K ⁻¹]	0.044	0.062
Linear thermal resistance of wall-window thermal bridge [m K W ⁻¹]	2.232	1.339
Specific heat capacity of massive concrete layer [kJ kg ⁻¹ K ⁻¹]	1.000	1.000
Internal surface wall convection coefficient [W m ⁻² K ⁻¹]	3.056	3.056
External surface wall convection coefficient [W m ⁻² K ⁻¹]	17.778	22.044
Internal surface ceiling convection coefficient [W m ⁻² K ⁻¹]	0.700	0.826
Internal surface floor convection coefficient [W m ⁻² K ⁻¹]	0.694	0.694
Window's frame thermal transmittance [W m ⁻² K ⁻¹]	1.667	1.267
Internal gains by electrical equipment [W]	696.50	487.55
Internal sensible gains by occupants [W]	52.00	39.52
Air-change rate [ACH]	2.640	0.897
Setpoint temperature [°C]	24.0	26.0
Equivalent air specific heat capacity [kJ kg ⁻¹ K ⁻¹]	1.012	2.312

As we can observe, the main discrepancies regard nighttime and weekends. This may be caused by the presence of a nighttime and weekend setback, neglected in the current calibration, which focused on the occupation period. Larger differences can be detected also in some days in June. In this case, the source of deviations may be related to solar gains and shading.

3.2 PMV and PPD Indexes

Analyzing the collected long-term measurements, air temperature resulted always between 23 °C and 25 °C during the occupancy time. The comparison

with short-term measurements, confirmed that temperatures were within the range of 24 - 26 °C and showed that relative humidity was in the range of 25 - 55 %. Air speed was very slow and well under the 0.2 m s⁻¹ and 0.1 m s⁻¹ was taken as a reference for thermal comfort calculations. 83 questionnaires were collected for the interested area.

The comparison between the PMV and PPD indexes at the time in which questionnaires were filled in by the occupants and the corresponding votes is reported in Fig. 4. Considering the patients, there is a good agreement between the average values of comfort indexes evaluated from measurements, votes collected by questionnaires and indexes calculated from the simulated model. On the contrary, there are discrepancies when considering the employees, with the average PMV calculated from measurements slightly larger than average PMV calculated from simulation outputs and both significantly larger than the employees' votes. As a whole, comfort indexes overestimate the fraction of the dissatisfied employees.

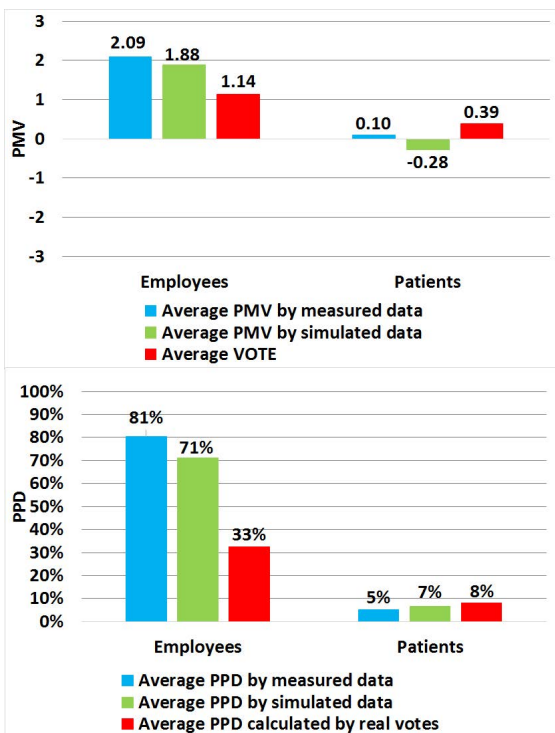


Fig. 4 - Comparison among PMV and PPD indexes obtained by measured and simulated internal temperatures and real votes

The same quantities are represented in box and whiskers charts in Fig. 5. They show that, in the case of the employees, interquartile range is significantly larger for real votes, while it has approximately the same size for PMV. Considering the patients, the three interquartile ranges are more homogeneous. Fig. 6 reports a comparison between average hourly PMV and PPD indexes calculated by measured and simulated data. In this case, the indexes do not refer to the time in which the employees and the patients compiled the questionnaires but to the whole occupancy time. Also in this case, the two groups of indexes are similar. A slightly overestimation of PMV and PPD calculated by simulation data can be registered in the morning but the trend is reversed during the afternoon.

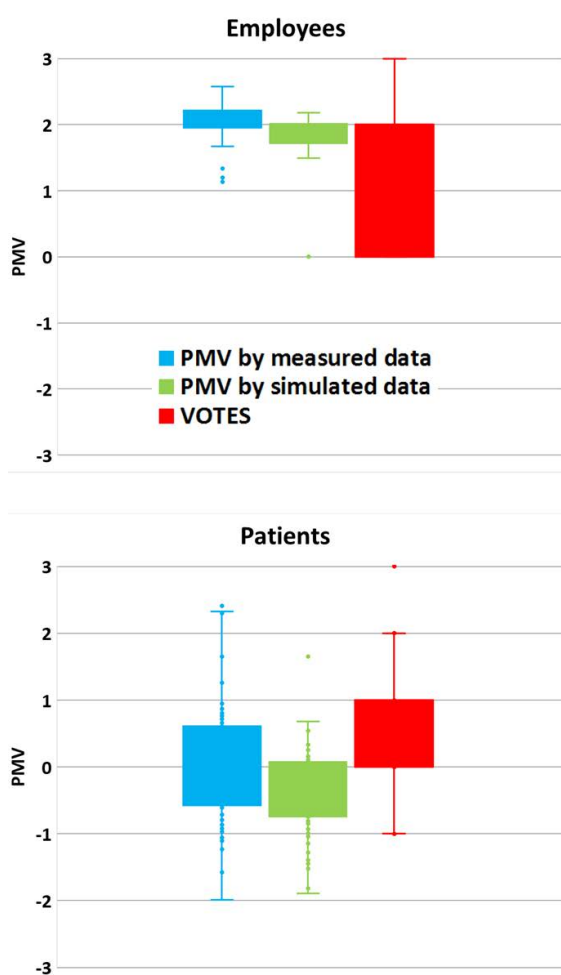


Fig. 5 – Comparison among PMV and PPD indexes obtained by measured and simulated internal temperatures and real votes – box and whiskers chart

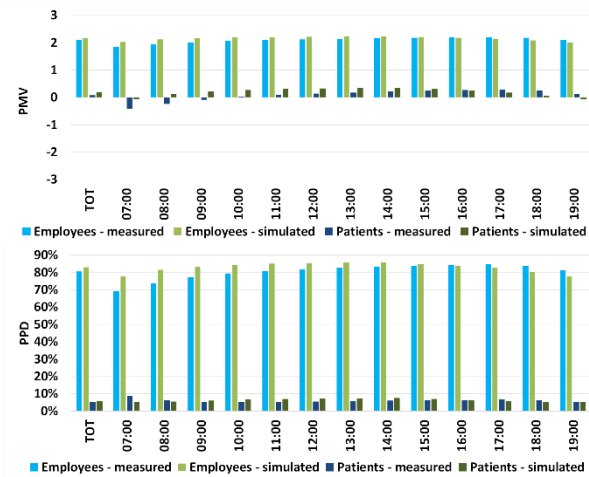


Fig. 6 – Hourly and daily comparison between PMV and PPD indexes obtained by measured and simulated internal temperatures

4. Conclusion

In this work, a calibrated model for a thermal zone of a healthcare building in Vienna, Austria, was developed for the assessment of both thermal behavior and comfort conditions. Many properties of the building envelope and system were not known and initial values were assumed from direct inspections and documentation on technical standards. Air temperature measurements taken during the months of March, April, May and June 2015 were used to calibrate the model. During the same period, the occupants were interviewed about their thermal comfort sensations and detailed short-term measurements were collected to calculate Fanger's Predicted Mean Votes and Percentages of Dissatisfied. Simulated air and surface temperature profiles were used to evaluate the same indexes, then compared to the ones calculated by the measured data and people's votes for validation purposes.

Thanks to these analyses, we observed that, although we started with a limited amount of data, it was possible to develop a calibrated model able to estimate, with sufficient accuracy, the Fanger's indexes for the considered thermal zone and allow for further analyses regarding retrofitting and control strategies.

Acknowledgements

This study has been funded by the project "Klimahouse and Energy Production" in the framework of the programmatic-financial agreement with the Autonomous Province of Bozen-Bolzano of Research Capacity Building. The authors kindly thank the Zentralanstalt für Meteorologie und Geodynamik (ZAMG) for providing the meteorological data.

References

- Arambula Lara, R., E. Naboni, G. Pernigotto, F. Cappelletti, Y. Zhang, F. Barzon, A. Gasparella, P. Romagnoni. 2017. "Optimization Tools for Building Energy Model Calibration". *Energy Procedia* 111:1060-1069. doi: 10.1016/j.egypro.2017.03.269.
- ASHRAE. 2013. *ASHRAE Standard 55: Thermal environmental conditions for human occupancy*. Atlanta, U.S.A.: ASHRAE.
- Ascione, F., N. Bianco, C. De Stasio, G.M. Mauro, G.P. Vanoli. 2016. "Simulation-based model predictive control by the multi-objective optimization of building energy performance and thermal comfort". *Energy and Buildings* 111: 131-144. doi: 10.1016/j.enbuild.2015.11.033.
- Azizpour, S., S. Moghimi, E. Salleh, S. Mat, C.H. Lim, K. Sopian. 2013. "Thermal comfort assessment of large-scale hospitals in tropical climates: A case study of University Kebangsaan Malaysia Medical Centre (UKMMC)". *Energy and Buildings* 64: 317-322. doi: 10.1016/j.enbuild.2013.05.033.
- Ferrara, M., M. Filippi, E. Sirombo, V. Cravino. 2015. "A simulation-based optimization method for the integrative design of the building envelope". *Energy Procedia* 78: 2608-2613. doi: 10.1016/j.egypro.2015.11.309.
- Ferrara, M., E. Sirombo, E. Fabrizio, M. Filippi. 2015. "Comfort filters in a total energy demand optimization method for the passive design of a building". *Energy Procedia* 83: 418-427. doi: 10.1016/j.egypro.2015.12.161.
- Hwang, R.L., T.P. Lin, M.J. Cheng, J.H. Chien. 2007. "Patient thermal comfort requirement for

- hospital environments in Taiwan". *Building and Environment* 42: 2980–2987. doi: 10.1016/j.buildenv.2006.07.035.
- ISO. 2001. *ISO 10551. Ergonomics of the thermal environment - Assessment of the influence of the thermal environment using subjective judgement scales*. Geneva, Switzerland: ISO.
- ISO. 2005. *ISO 7730:2005. Ergonomics of the thermal environment -- Analytical determination and interpretation of thermal comfort using calculation of the PMV and PPD indices and local thermal comfort criteria*. Geneva, Switzerland: ISO.
- ISO. 2008. *ISO 10456. Building materials and products – Hygrothermal properties – Tabulated design values and procedures for determining declared and design thermal values*. Geneva, Switzerland: ISO.
- Khodakarami, J., N. Nasrollahi. 2012. "Thermal comfort in hospitals – A literature review". *Renewable and Sustainable Energy Reviews* 16: 4071– 4077. doi: 10.1016/j.rser.2012.03.054.
- Skoog, J., N. Fransson, L. Jagemar. 2005. "Thermal environment in Swedish hospitals: summer and winter measurements". *Energy and Buildings* 37: 872-877. doi: 10.1016/j.enbuild.2004.11.003.
- UNI. 1995. *UNI 10339. Air-conditioning systems for thermal comfort in buildings – General, classification and requirements – Offer, order and supply specifications*. Milan, Italy: UNI.
- UNI. 2008. *UNI EN ISO 14683. Thermal bridges in building construction - Linear thermal transmittance - Simplified methods and default values*. Milan, Italy: UNI.
- Van Gaeve, R., V.A. Jacobs, M. Diltoer, L. Peeters, S. Valanduit. 2014. "Thermal comfort of the surgical staff in the operating room". *Building and Environment* 81: 37-41. doi: 10.1016/j.buildenv.2014.05.036.
- Verheyen, J, N. Theys, L. Allonsius, F. Descamps. 2011. "Thermal comfort of patients: Objective and subjective measurements in patient rooms of a Belgian healthcare facility". *Building and Environment* 46: 1195-1204. doi: 10.1016/j.buildenv.2010.12.014.
- Zaniboni, L., K. Kiesel, M. Schuß, G. Pernigotto, A. Gasparella, A. Mahdavi. 2016. "Evaluation of on-site PV-based electrical energy production: a case study". In: *Proceedings of the 12th REHVA World Congress 2016*. Aalborg, Denmark.
- Zaniboni, L., K. Kiesel, M. Schuß, G. Pernigotto, A. Gasparella, A. Mahdavi. 2016. "Indoor evaluation of a health care facility: a case study". In: *Proceedings of the 12th REHVA World Congress 2016*. Aalborg, Denmark.

Temporal and Spatial Predictability of Occupants' Presences in a Library Building

Ki Uhn Ahn – Sungkyunkwan University – ahnkiuhn@skku.edu

Won Jun Suh – Sungkyunkwan University – qqq000feel@skku.edu

Cheol Soo Park – Sungkyunkwan University – cheolspark@skku.ac.kr

Abstract

Although it has been widely acknowledged that occupants play a critical role in building energy consumption, the characteristics of the occupants' presences and actions are not accurately represented in building simulation tools.

In this study, the authors aim to identify the temporal and spatial difference in the characteristics of the occupants' presences in a library building located in South Korea. The data of each individual entering and leaving rooms in the building were recorded for weeks from 15 to 31 January by Radio-Frequency Identification (RFID) tags. Based on the data, the periodicity and predictability of the occupants' presences were investigated in terms of (1) spatial variation (individual room vs. entire floor vs. entire building), and (2) temporal variation (5 minutes vs. 30 minutes vs. 1 hour sampling times). The periodicity and predictability of the occupants' presences were quantified using a Normalized Cumulative Periodogram (NCP).

The occupants' presences in an individual room were less periodic or less predictable than those in the entire building. The predictability of the occupants' presences was influenced by the sampling time. The greater the sampling time (5 minutes vs. 1 hour), the better predictable the occupants' presences were. In other words, it is much easier to predict the aggregated number of occupants over the entire building with a longer sampling time (e.g. a couple of hours) than to predict the number of people in individual rooms with a shorter sampling time (e.g. 10 minutes). These findings could be further applied to an energy simulation study of the building and its relevance to energy prediction will be studied.

1. Introduction

Recently, the study of occupant behavior has attracted significant attention from the Building Performance Simulation (BPS) community (IBPSA,

2011-2015). It has been widely acknowledged that the occupant is one of the major factors contributing to the performance gap (IEA Annex 66, 2016). In this regard, a number of occupant behavior models have been developed to describe the occupants' presences (Page et al., 2008; Feng et al., 2015). One of the most popular stochastic approaches is a Markov chain model. The model is based on a large amount of observed data and addresses a statistical relationship between occupants' presences and actions, and other environmental factors. In addition, a sophisticated Markov chain model adopts an agent-based modeling approach to take into account human sensation, perception, cognition, and psychomotor responses (Yan et al., 2015). Another approach for the prediction of the occupants' presences, so-called 'random walk' was recently published (Ahn and Park, 2016). It is based on the belief that the predictability of the occupants' presences can vary, depending on the type of buildings (process-driven buildings such as schools, residences vs. 'random walk' buildings where the occupants' presences are not predictable).

It is still unsolved and untouched whether such predictability of the occupants' presences varies spatially and temporally. In this paper, the authors aim to investigate the periodicity and predictability of the occupants' presences in terms of spatial and temporal variation. The number of people entering and leaving rooms in a library building recorded for two weeks was used. Then, for the quantification of the periodicity and predictability, the Normalized Cumulative Periodogram (NCP) was used.

2. Random Walk

A random walk is a mathematical formalization consisting of a succession of random steps. The term “random walk”, first introduced by Pearson (1905), has been used in many fields (e.g. ecology, economics, psychology, etc.) to explain observed time-series behavior. Fig. 1 shows an example of twenty random walks in one dimension, showing the current position on the y-axis over time (x axis) (Ahn and Park, 2016).

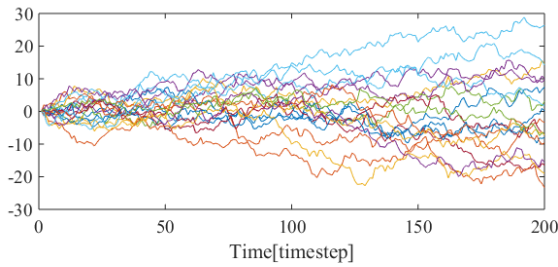


Fig. 1 – Example of twenty random walks

The mathematical form of random walk for time-series data is as follows (Gelb, 1974):

$$x_{k+1} = x_k + w_k \tag{1}$$

where x_k is the state of the k^{th} time-step, x_{k+1} is the state of the $(k+1)^{\text{th}}$ time-step, and w_k is the difference between x_k and x_{k+1} , meaning the difference in the state over time.

The time series w_k can be characterized by a frequency analysis with Fourier transform. The Normalized Cumulative Periodogram (NCP) is a common method to identify the periodicity of a given time series in a frequency domain (Hipel and McLeod, 1994).

Fig. 2 shows the NCP of 1,000 random numbers (bold blue line) and dotted lines indicate 95 % confidence intervals. It can be said that w_k follows the random walk if it is drawn within a confidence interval (pink area) along with a straight line joining (0, 0) and (0.5, 1) in the NCP (Hipel and McLeod, 1994). More details on the random walk can be found in (Ahn and Park, 2016).

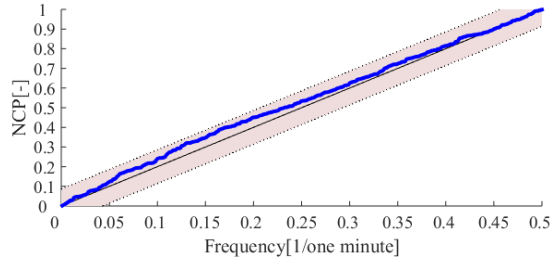


Fig. 2 – Example of NCP for 1,000 random numbers

3. Target Building

The target building is a library building of Sungkyunkwan University located in South Korea. The building has two underground floors and seven aboveground floors, and its total floor area is about 23,742 m². A circular seven-story high atrium is located at the center of the building (Fig. 3).

All library entrance gates are operated with an access management system that records each individual entering and leaving through the use of Radio-Frequency Identification (RFID) tags. In addition, six rooms (Room #: B101, B102, 101, 201, 301, 302) in the building are equipped with a RFID system that issues and records a seat number of each individual (Fig. 3). In this study, the authors used two weeks’ data of the six rooms from 15 to 31 January (Table 1 and Fig. 3).

Table 1 – Selected six rooms

Room #	Use	Location	Area (m ²)	Max. # of people
B101	Reading Room	B1	560	84
B102	ReadingRoom	B1	265	67
101	Computer Room	1F	1,029	56
201	Media Room	2F	420	9
301	Reading Room	3F	863	9
302	Reading Room	3F	733	9
Total	-	-	3,870	234

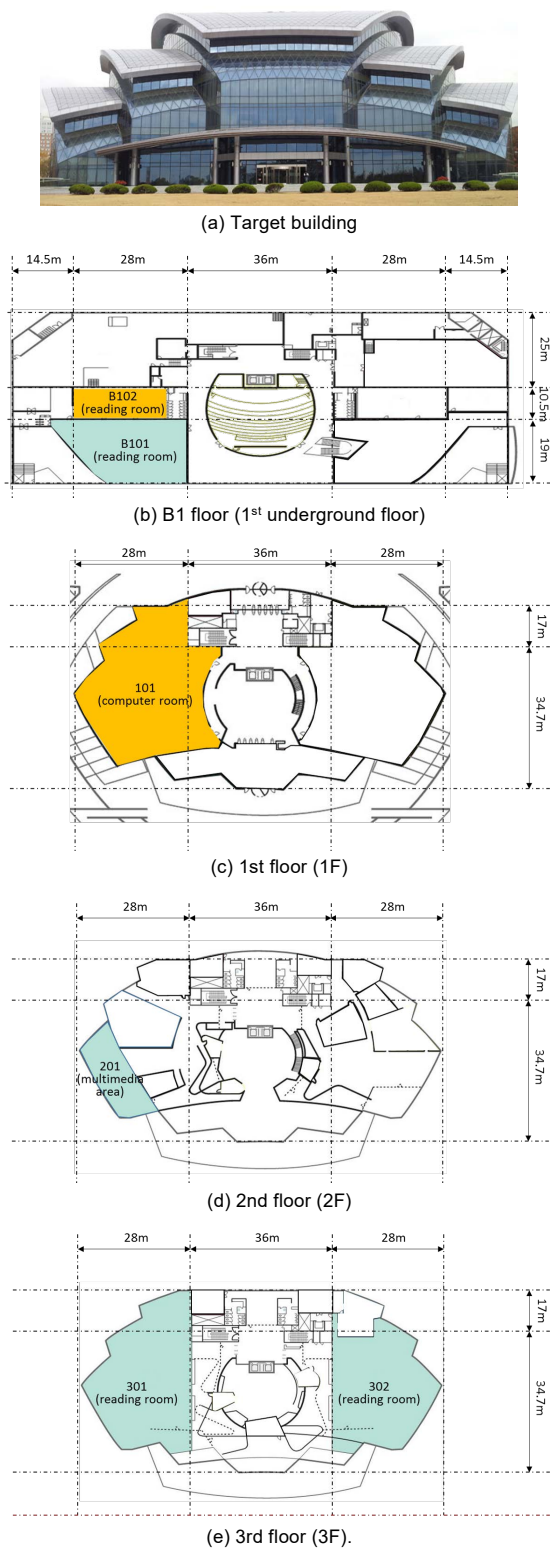


Fig. 3 – Floor plan of the target building

4. Results

To investigate the spatial characteristics of the occupants' presences, the authors categorized the six rooms into three levels: room level, floor level (B1 level: B101+B102, 1F: 101, 2F: 201, 3F: 301+302), and the entire building level. Fig. 4 shows the number of occupants based on the three levels.

Fig.s 5-10 show the NCP of the occupants' presences (x_k) and the variations in the occupants' presences (w_k).

The NCPs of w_k in Rooms #201, #301 and #302 ((Fig. 5 (h), (j), (l)) prove the random walk. The blue lines are located inside the confidence interval and are evenly distributed over the entire period. This means that w_k of Rooms #201, #301 and #302 are unpredictable (Fig. 5).

It is interesting that when the NCP of w_k is analyzed in the building level, w_k of the entire building becomes predictable (Fig. 6(f)). In other words, the variation in the occupant's presences for the small groups of people (accommodating only 9 people in Rooms #201, #301 and #302, Table 1) is unpredictable, while that of the entire building is predictable. It means that it would be difficult to predict the variation in the small group of occupants in a room, while it is possible to predict the aggregated number of people in the entire building.

In addition, the degree of randomness in w_k varies depending on the sampling time (Fig.s 5-6 vs. Fig.s 7-8 vs. Fig.s 9-10). As mentioned above, w_k in Rooms #201, #301 and #302 (Fig. 5 (h), (j), (l)) follows the random walk when the sampling time is 5 minutes. However, w_k in the same rooms (#201, #301, and #302) do not follow the random walk when the sampling time is 30 minutes (Fig. 7 (h), (j), (l)). It also applies when the sampling time is 1 hour (Fig. 9 (h), (j), (l)).

It means that it is difficult to predict the variation (w_k) in the occupants' presences with a short time interval (5 minutes), while it would be easier to predict w_k with long-enough sampling times (e.g. 30 minutes, 1 hour).

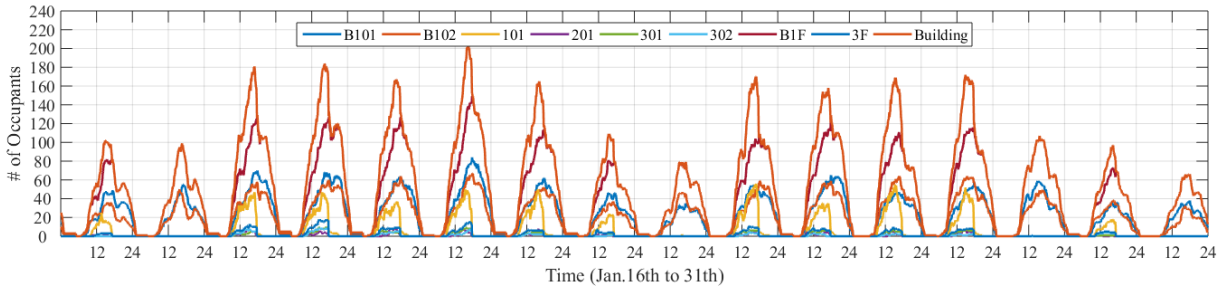


Fig. 4 – The number of occupants (sampling frequency: 5 minutes)

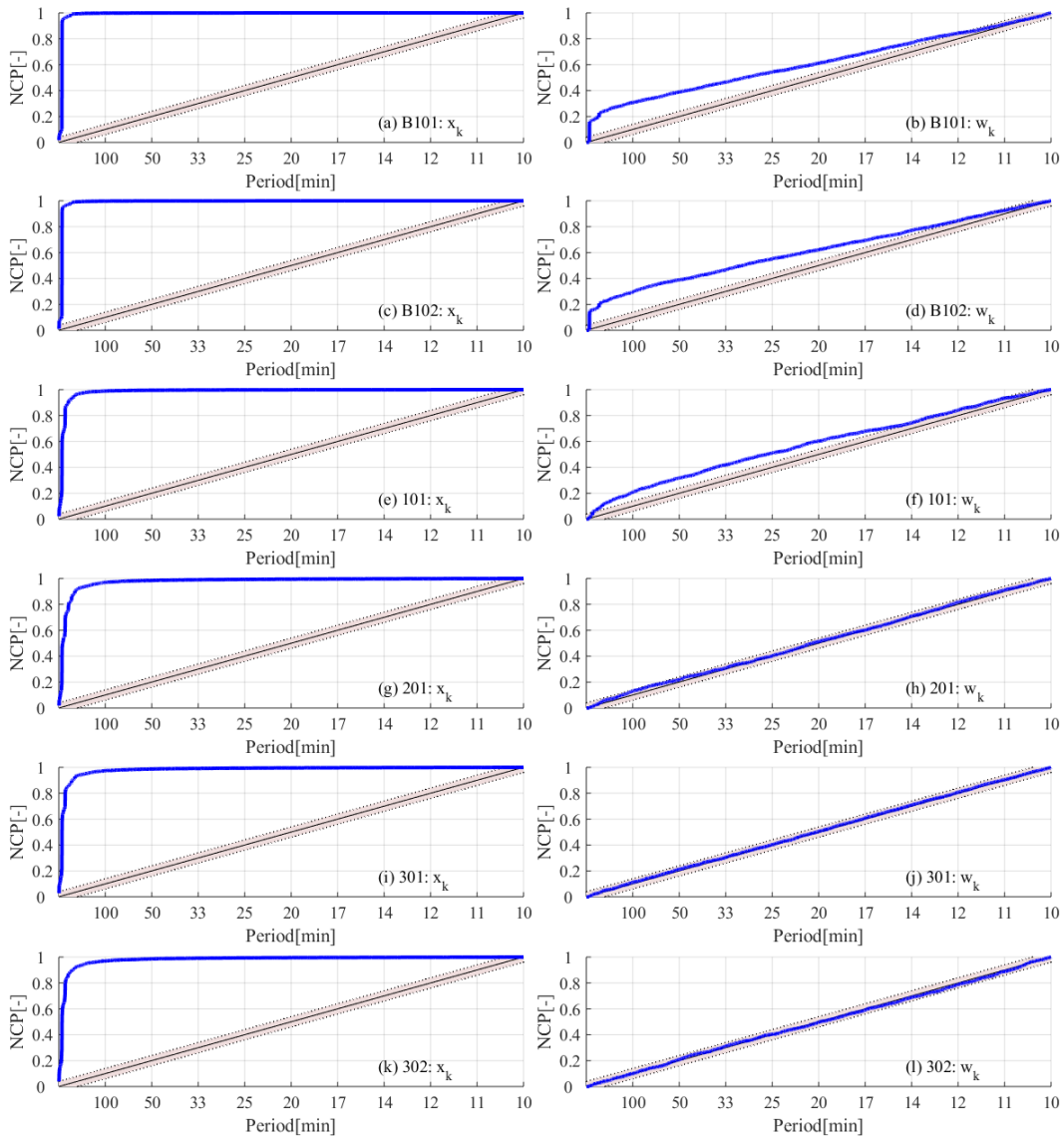


Fig. 5 –NCPs of individual room (sampling time: 5 minutes)

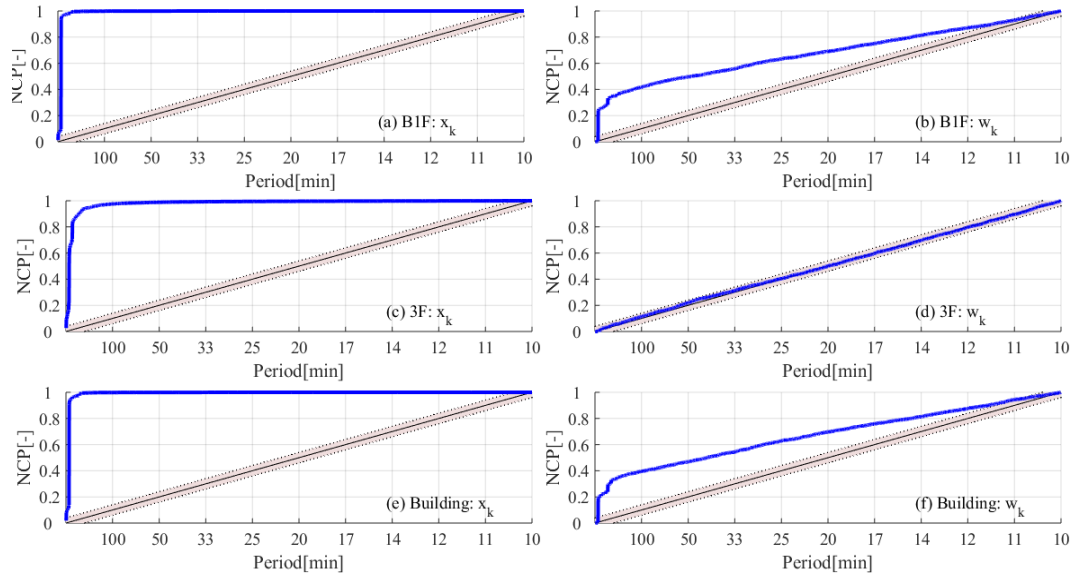


Fig. 6 – NCPs of floor and building level (sampling time: 5 minutes)

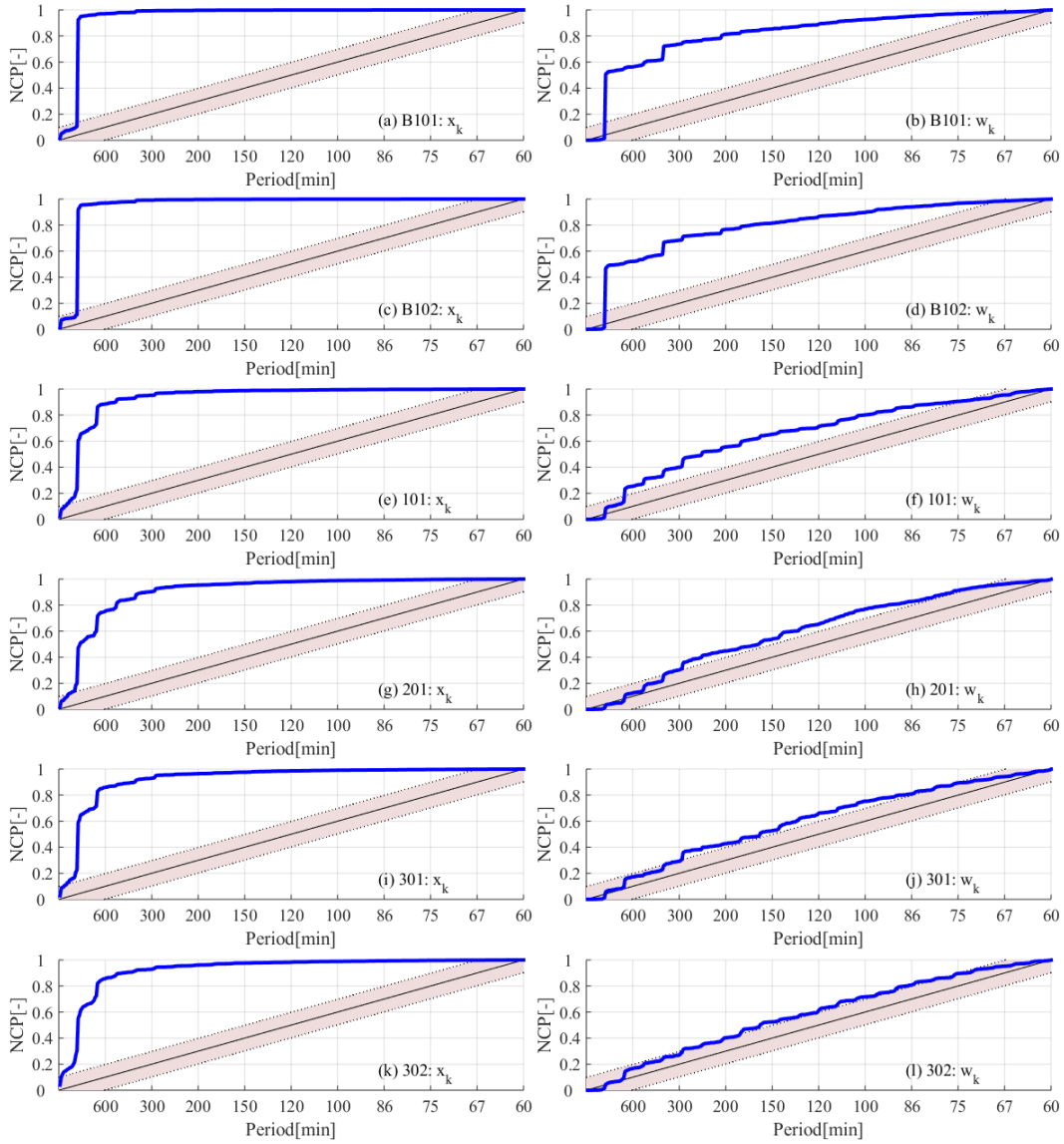


Fig. 7 – NCPs of individual room (sampling time: 30 minutes)

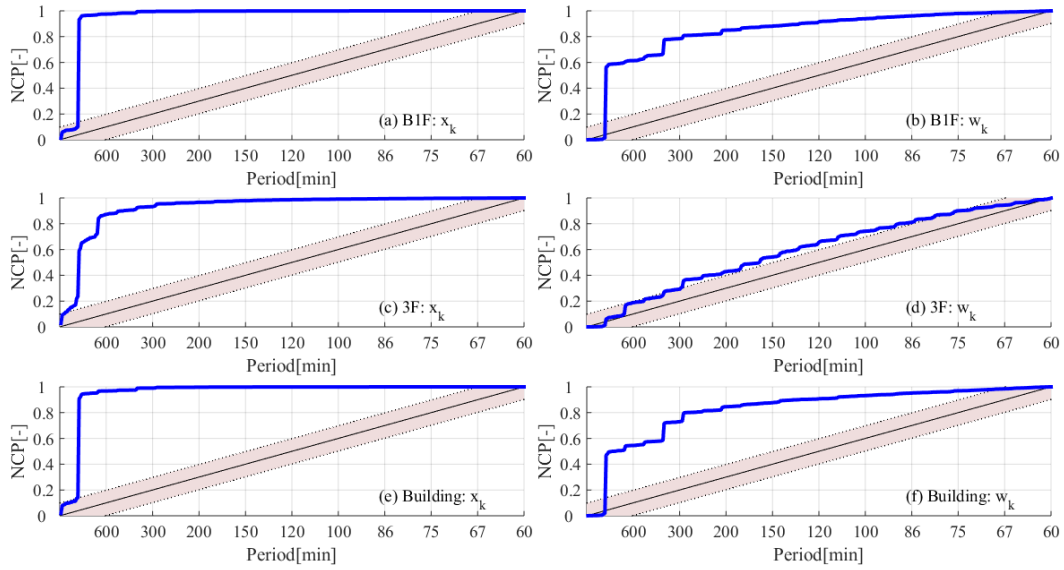


Fig. 8 – NCPs of floor and building level (sampling time: 30 minutes)

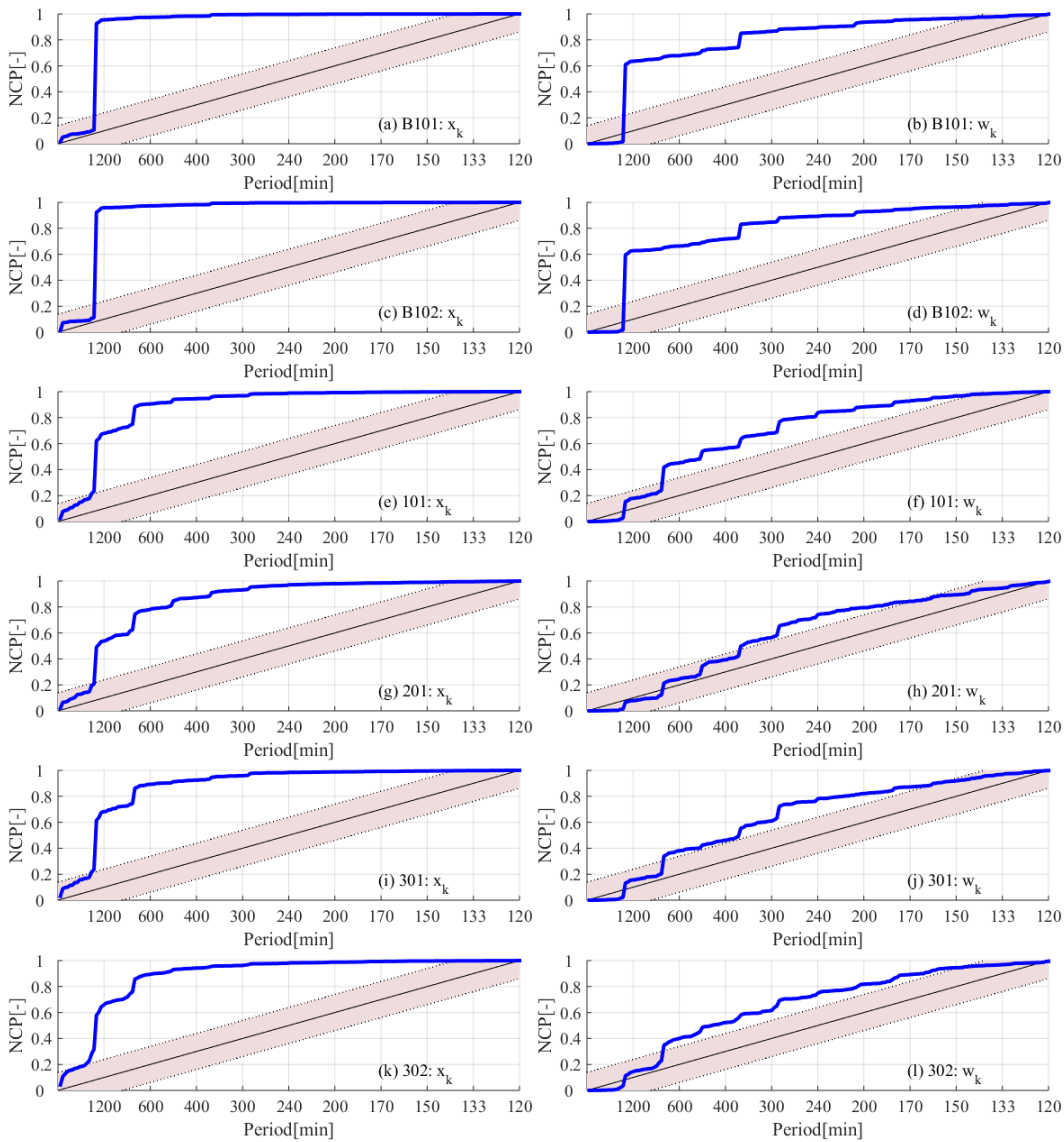


Fig. 9 – NCPs of individual room (sampling time: 1 hour)

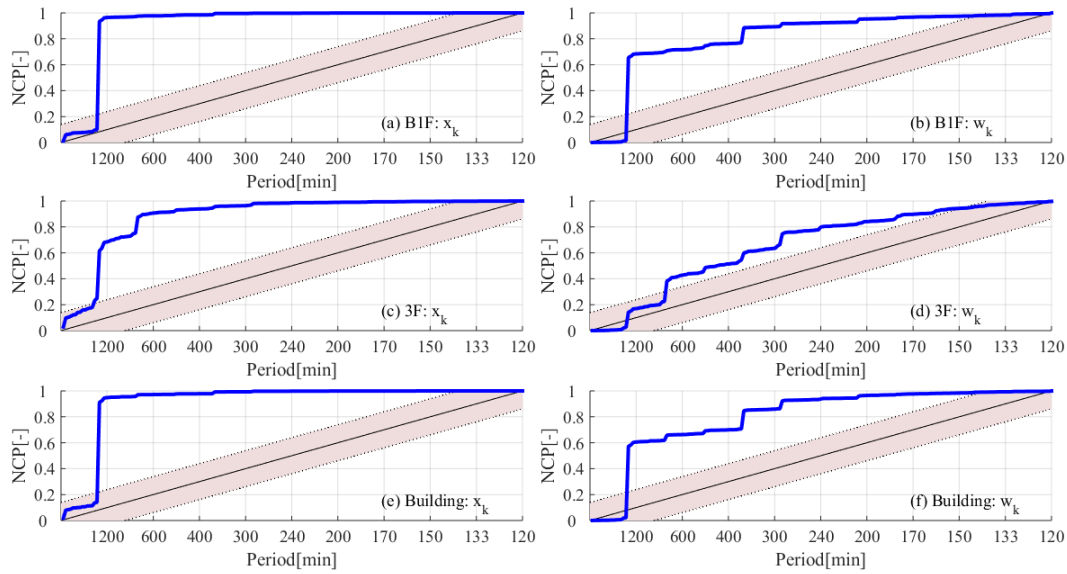


Fig. 10 – NCPs of floor and building level (sampling time: 1 hour).

5. Conclusion

The authors investigated the predictability of the occupants' presences in terms of the number of occupants (e.g. individual room level, floor level, building level) and in terms of the sampling times (e.g. 5 minutes, 30 minutes, 1 hour). This study was based on the monitored data for two weeks (from Jan 16 to Jan 31) at a library building in South Korea. The findings of this study are as follows:

- It is quite difficult to predict the variation (w_k) in the number of occupants of a small group, e.g. comprising 9 people. In contrast, the variation in the number of occupants of the entire building is predictable.
- The predictability of w_k depends on the sampling time. When the sampling time is as short as 5 minutes, w_k in a small group is unpredictable. When the sampling time becomes as long as or longer than 30 minutes, w_k in a small group is even predictable.

The aforementioned findings will be used for the uncertainty analysis of the energy prediction of the building in the near future. In addition, the quantification of the relation between the sampling time and the group size will be further investigated.

Acknowledgements

This work was supported by the Korea Institute of Energy Technology Evaluation and Planning (KETEP) and the Ministry of Trade, Industry & Energy (MOTIE) of the Republic of Korea (No. 20152020105550).

This research was supported by Global P.H.D Fellowship Program through the National Research Foundation of Korea(NRF) funded by the Ministry of Education (No. 2015H1A2A1030287).

References

- Ahn, K.U., C.S. Park. 2016. "Correlation between occupants and energy consumption". *Energy and Buildings* 116: 420-433. doi: 10.1016/j.enbuild.2016.01.010.
- Feng, X., D. Yan, T.Z. Hong. 2015. "Simulation of occupancy in building". *Energy and Buildings* 87: 348-359. doi: 10.1016/j.enbuild.2014.11.067.
- Gelb, A. 1974. *Applied optimal estimation*. Boston, U.S.A.: MIT Press.
- Hipel, K.W., A.I. McLeod. 1994. *Time series modeling of water resources and environmental systems*. Elsevier.
- IEA-EBC Annex 66. 2016. "Definition and Simulation of Occupant Behavior in Buildings". Accessed December 29. <http://www.annex66.org>
- International Building Performance Simulation Association (IBPSA). 2011-2015. *In Proceedings of the 12th to 14th international IBPSA conference*.
- Page, J., D. Robinson, N. Morel, J.L. Scartezzini. 2008. "A generalized stochastic model for the simulation of occupant presence". *Energy and Buildings* 40(2): 83-98. doi: 10.1016/j.enbuild.2007.01.018.
- Pearson, K. 1905. "The problem of the random walk". *Nature* 72: 204. doi: 10.1038/072318a0.
- Yan, D., W. O'Brien, T. Hong, X. Feng, H.B. Gunay, F. Tahmasebi, A. Mahdavi. 2015. "Occupant behavior modeling for building performance simulation: Current state and future challenge". *Energy and Buildings* 107: 264-278. doi: 10.1016/j.enbuild.2015.08.032.

Stochastic Multi-Criteria Decision Making of Energy Recovery Ventilation Systems using Cumulative Prospect Theory

Young Jin Kim –Sunmoon University – yjkim9943@sunmoon.ac.kr

Abstract

Recently, an Energy Recovery Ventilator (ERV) in a residential building was seen as an attractive ventilation option in terms of energy saving and indoor air quality. In order to identify a feasible set among many ventilation strategies in this situation, various decision-making approaches (deterministic or stochastic) using Building Performance Simulation (BPS) tools have been suggested. As a simulation-based decision-making approach, a Stochastic Multi-Criteria Decision Making (SMCDM) method based on Cumulative Prospect Theory (CPT) is presented in this paper to find the best ventilation strategy under model uncertainties. For this study, two ventilation strategies, considering air inlet positions and CO₂ sensor positions, were chosen and modelled using two simulation tools: CONTAMW 3.1 for the airflow model and EnergyPlus for the thermal model. In addition, Latin Hypercube Sampling (LHS) was used to reflect the model uncertainties. In this study, it is shown that CPT can provide a more realistic and trustworthy framework than the Bayesian decision theory.

1. Introduction

Due to the high attention given to passive houses and the increase in toxic air environments, an Energy Recovery Ventilator (ERV) in a residential building is being installed in order to attain acceptable Indoor Air Quality (IAQ) and to reduce energy consumption. The ERV is critical for people who spend about 90 % of the day in indoor spaces (Laverge and Janssens, 2013), and a ventilation strategy decision-making is emerging as a major issue. Building Performance Simulation (BPS) tools can obtain predicted outputs (energy consumption, thermal comfort, CO₂ concentration, etc.) through a kernel engine in a mathematical model, considering the indoor and outdoor physical environmental conditions. Such predicted outputs can be used to

determine the optimal design of the ERV. However, the BPS tools have many unknown inputs that generate uncertainty of the predicted outputs. Furthermore, such uncertainty is a major issue in finding a highly reliable design alternative (de Wit, 2001; Macdonald, 2002; Hopfe, 2009; Kim et al., 2014; Sun et al., 2014).

Previous studies (de Wit, 2001; Kim et al., 2014) have suggested the Monte Carlo Simulation (MCS) and the Multi-Criteria Decision Making (MCDM) under uncertainties using the Bayesian decision theory to deal with the stochastic decision-making issues. They showed the differences between the deterministic and stochastic approach, as well as the possibility of reaching a meaningful decision-making result. The Bayesian decision theory is used to calculate the utility function reflecting the preferences or attitudes of decision makers toward risk, and determine a design alternative with high-expected utility. However, the Bayesian decision theory based on utility function is problematic since the decision-making problem is solved under the assumption that the decision makers behave rationally (Kahneman and Tversky, 1979; Tversky and Kahneman, 1992). Because the individual cognitive ability varies among general decision makers, it is difficult to assume they are rational participants. To handle the aforementioned issue, Cumulative Prospect Theory (CPT) has been presented (Lahdelma and Salminen, 2009; Wakker, 2010; Krohling and de Souza, 2012).

In this study, to solve a Stochastic Multi-Criteria Decision Making (SMCDM) problem, the CPT is developed as an alternative to utility function and is used to identify a feasible set among many ventilation strategies of the ERV in a given residential building.

2. Stochastic Multi-Criteria Decision Making (SMCDM)

Most decision-making problems using BPS tools are based on many criteria rather than a single criterion. The optimal alternative is identified using predicted outputs. It should be noticed that the predicted outputs are probabilistic rather than deterministic, due to various uncertainty sources (aleatory or epistemic uncertainties). In other words, decision-making problems using BPS tools are Stochastic Multi-Criteria Decision Making (SMCDM) that must reflect various risks under uncertainties and multi-criteria simultaneously.

The SMCDM methods can be used as follows: (1) Bayesian decision theory, (2) Cumulative Prospect Theory (CPT). The Bayesian decision theory can reflect the preferences for risks under uncertainty and determine an alternative with high-expected utility (Von Neumann & Morgenstern, 1947). To present the decision-making process with the Bayesian decision theory in the area of building simulation, de Wit (2001) selected initial cost and thermal comfort as multi-criteria problems and treated a MCDM problem using stochastic predicted outputs propagated by MCS and the joint utility function. Kim et al. (2014) showed the feasibility of Bayesian inference based on the Markov Chain Monte Carlo (MCMC) to consider the different expected utilities of multiple decision makers, rather than of only a single decision-maker. The aforementioned previous studies are significant in terms of making reference to which multi-criteria decision-making was conducted by reflecting the risks of stochastic predicted outputs.

However, the Bayesian decision theory is problematic since it assumes that decision makers rationally recognize utility and behave with a consideration of the risks (Kahneman and Tversky, 1979; Tversky and Kahneman, 1992). It is difficult for decision makers to find a highly reliable alternative, considering they are based on vague information or data, and each decision maker has different cognitive abilities. In contrast, the CPT can resolve the decision-making problem based on the utility theory by reflecting reference point setting, diminishing sensitivity, and loss aversion (Lahdelma and Salminen, 2009; Wakker, 2010; Krohling and de Souza, 2012).

- Reference point setting: when making a valuable decision about gains and losses, decision makers decide a value relatively, rather than absolutely, by comparing against the predefined individual reference point. This relative valuation differs considerably from the utility theory based on the absolute value. Since decision makers' preferences toward gains and losses differ based on the reference point, difference value functions must be applied. The CPT can distinguish gains and losses according to the reference point setting and express them as value functions having an asymmetrical s-shape, as shown in Fig. 1.
- Diminishing sensitivity: even if two design alternatives have the same difference in gain or loss, they have a large value change if the difference between gain or loss and the reference point is small. Otherwise, they have a small value change. It is called diminishing sensitivity. As shown in Fig. 1, the slope of the value function decreases if the difference between gain or loss and the reference point increases. The CPT can reflect the diminishing sensitivity of the decision makers by varying the weighting function of gain or loss based on the reference point.
- Loss aversion: decision makers tend to show higher loss aversion for losses than for gains according to previous studies (Wakker, 2010; Krohling and de Souza, 2012). In other words, decision makers are more sensitive to losses than to gains. The CPT can distinguish the value functions of gains and losses according to the reference point and reflect a loss aversion coefficient for losses.

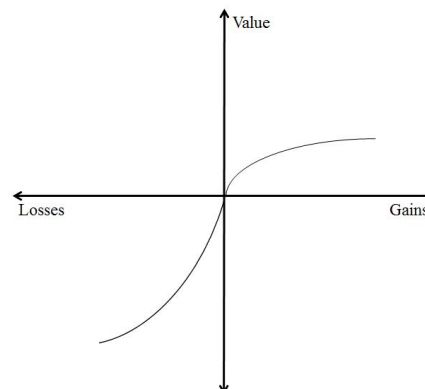


Fig. 1 - Value function of CPT

Within the aforementioned mind, this study uses the CPT for SMCDM. The prospect value $V(f)$ of CPT can be expressed as Equation (1) using the value function $v(x)$, the decision weight function π , and the probability of event p . The value function is a function according to gains if the difference between criteria value (predicted output) and reference point is positive, or a function according to losses if the difference is negative (Equation (2)). The parameters α, β related gains and losses capture the concave and convex curvature of the value function (Krohling and de Souza, 2012), and λ is the loss aversion coefficient that is used to reflect a high loss aversion toward loss. Kahneman and Tversky (1979) proposed $\alpha=0.88$, $\beta=0.88$, $\lambda=2.25$, and these parameters were used in this study. The weighting function reflects the diminishing sensitivity using the attitude coefficients γ, ϕ of gains and losses for risk as shown in Equations (3)-(6). The attitude coefficient of gains and losses were set as $\gamma^{+-}=0.8$ and $\phi=1.0$, respectively, as suggested by Prelec (1998). The propagated stochastic predictions (heating energy and CO2 concentration) using the MCS were used in this study to calculate the probability of an event.

$$V(f) = V(f^-) + V(f^+) = \sum_{i=1}^h \pi_i^- v(x_i) + \sum_{i=h+1}^n \pi_i^+ v(x_i) \quad (1)$$

$$v(x) = \begin{cases} x^\alpha & x \geq 0 \\ -\lambda(-x)^\beta & x < 0 \end{cases} \quad (2)$$

$$\pi_i^+ = \omega^+ \left(\sum_{j=i}^n p_j \right) - \omega^+ \left(\sum_{j=i+1}^n p_j \right) \quad (3)$$

$$\pi_i^- = \omega^- \left(\sum_{j=1}^i p_j \right) - \omega^- \left(\sum_{j=1}^{i-1} p_j \right) \quad (4)$$

$$\omega^+ \left(\sum_{j=h}^n p_j \right) = \exp \left(-\gamma^+ \left(-\ln \left(\sum_{j=h}^n p_j \right) \right)^\phi \right) \quad (5)$$

$$\omega^- \left(\sum_{j=1}^h p_j \right) = \exp \left(-\gamma^- \left(-\ln \left(\sum_{j=1}^h p_j \right) \right)^\phi \right) \quad (6)$$

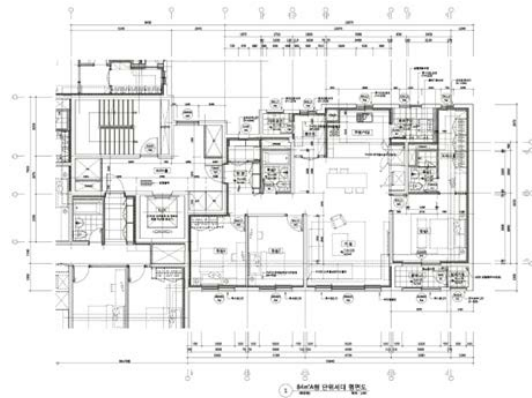
where, $V(f)$ is the prospect value, $v(x)$ is the value function, x is the difference between the critical value and the reference point, α, β are the parameters related to gains and losses, λ is the loss aversion coefficient, π is the decision weight function (+ and - superscript denote gain and loss, respectively), ω is the weighting function, γ is the risk gain attitude coefficient, and ϕ is the risk loss attitude coefficient.

3. Target Building and Unknown Inputs

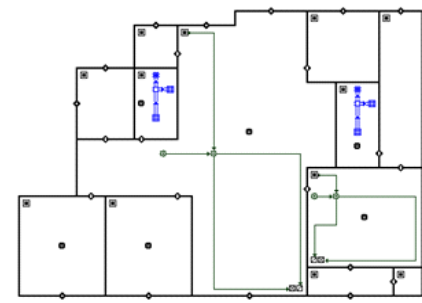
3.1 BPS Tools

For the target building of this study, a 15-story residential building in Seoul, Korea was selected for the analysis of the ventilation strategies (Fig. 2(a)). To simulate thermal and airflow phenomena, CONTAMW 3.1 and EnergyPlus 8.0 were chosen (Fig. 2(b)-(c)). EnergyPlus has been used extensively to calculate transient heat and mass flow. But it cannot perform duct modelling. Otherwise, CONTAMW 3.1, adequate for determining macro flow phenomena such as overall ventilation rates, enables the duct modeling, although it cannot reflect dynamic energy flows such as indoor air temperature. To solve these problems, the present study integrated two BPS tools using a Ping-Pong method (decoupled approach).

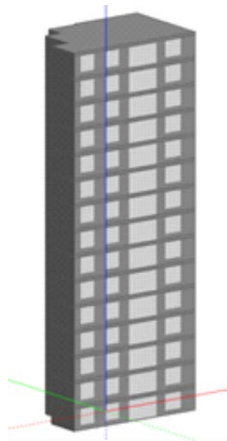
The simulation period was one day in winter (January 21), and the Seoul climate data was used. It was assumed that all doors of the room were open and the windows were closed. Since most occupants do not actively open windows in winter and this is appropriate to assess the IAQ (Kim and Park, 2009). An adult was assumed to generate 0.31 liters per minute. Infiltration was taken into consideration. The occupant schedules employed the data provided by Hyun and Park. (2006).



(a) Floor plan



(b) CONTAMW 3.1



(c) DesignBuilder

Fig. 2 - Target residential building and BPS tools

Fig. 3 shows the average occupant schedules. And the same occupant schedule for the adjacent rooms (master room, living room) was used for the bathroom. The radiant floor heating system was controlled per room and on/off control method was applied based on the heating set-point temperature (20 °C). For the ERV, the CO₂-sensor based Demand-Controlled Ventilation (DCV-CO₂) was selected. The DCV-CO₂ is operated using the on/off control method based 1,000 PPM. The air supply and exhaust rate were set as 100 CMH

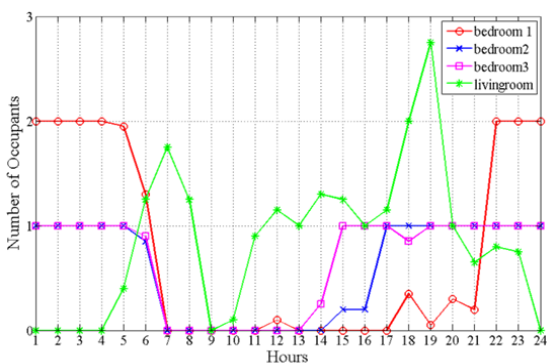


Fig. 3 - Occupant schedule (Hyun and Park, 2006)

(Cubic Meter per Hour) and 60 CMH for the air exhaust system in the bathroom.

As mentioned above, the Ping-Pong method was used to complement the shortcomings of the two simulation models. The EnergyPlus model was applied to the radiant floor heating system and ERV, and CONTAMW 3.1 was only applied to ERV. And each system is operated by automatic control logic (on/off control for radiant floor heating system, DCV-CO₂ control for ERV). For the Ping-Pong approach, the two simulation models were integrated in MATLAB platform. For each time step, EnergyPlus calculates indoor air temperatures and then CONTAMW 3.1 recalculates the airflows of the openings (windows and doors) and/or ducts, air supply rate of ERV, and CO₂ concentration using the calculated indoor air temperatures. The calculated airflows were automatically input to EnergyPlus and the heating energy consumption was recalculated. The aforementioned coupling process was repeated every 20 minutes.

3.2 Selection of Unknown Inputs

The unknown inputs of the BPS tools were chosen as shown in Table 1 by referring to the previous studies (Hyun and Park, 2006; ASHRAE, 2013; DOE, 2013a; DOE 2013b, Kim et al., 2014; Macdonald, 2002; Hopfe, 2009; Walton & Dols, 2005). The unknown inputs were assumed to have a triangular distribution (T[0.9, 1.0, 1.1]) consisting of the minimum, maximum, and base values. The triangular distribution is propagated as ratio of the definite values of the unknown inputs. The occupant schedule was chosen as the discrete uniform distribution (D[1, 30]).

Table 1 – Unknown inputs

Descriptions	
Construction materials	Density, specific heat, and conductivity of gypsum board
	Density, specific heat, and conductivity of brick
	Density, specific heat, and conductivity of concrete
	Density, specific heat, and conductivity of insulation board
	Density, specific heat, and conductivity of acoustic tile

	Solar transmittance, reflectance, emissivity, conductivity of clear window
Numerical algorithm	Loads or temperature convergence tolerance value
Grounds	Temperature and reflectance
Set-point temperature	Heating set-point temperature
Internal heat gains	Number of person, activity level, fraction radiant of people (master room)
	Number of person, activity level, fraction radiant of people (bedroom1)
	Number of person, activity level, fraction radiant of people (bedroom2)
	Number of person, activity level, fraction radiant of people (living room)
	Number of person, activity level, fraction radiant of people (bathroom1)
	Number of person, activity level, fraction radiant of people (bathroom2)
	Internal gains and fraction radiant of lights
Schedule	Internal gains and fraction radiant of electric equipment
	Occupants' schedules
	Fan efficiency, pressure rise, and motor efficiency of supply fan
ERV	Fan efficiency, pressure rise, and motor efficiency of return fan
	Sensible or latent effectiveness
	Fan efficiency and pressure rise of exhaust fan (bathroom1)
Exhaust fan	Fan efficiency and pressure rise of exhaust fan (bathroom2)
	Rated pump head and motor efficiency of heating water circulation pumps
Pumps	Maximum or minimum loop temperature
Plants	
Airflows	Flow exponent, discharge coefficient, wind pressure coefficient, wind velocity profile exponent, local terrain constant, terminal loss coefficient, leakage class#1(oval), leakage class#2(rectangular), duct roughness, leakage area of doors, leakage area of windows

4. Uncertainty Results

For the propagation of uncertainties, Latin Hypercube Sampling (LHS), appropriate for complex non-linear models, was used. The number of sampling case was set to 200. The heating energy consumption is the sum total of the radiant floor heating system and ERV. The CO2 concentration was expressed as CO2 performance φ using the total occupation time of each room T and total time δ when CO2 concentration is below 1,000 PPM as shown in Equation (7). In other words, the uncertainty results are represented as total heating energy consumption (kWh) and CO2 performance (%). And the goal of this study was to determine the air inlet position of the ERV and CO2 sensor positions. In other words, it is a SMCDM problem. For this study, two ventilation strategies were used as shown in Table 2.

$$\varphi = \left(\sum_{k=1}^m \frac{\delta_k}{T_k} \times 100 \right) / m \tag{7}$$

where, φ is the CO2 performance (%), δ is the total time when the CO2 concentration of each room is below 1,000PPM (hour), T is the total occupation time of each room (hour), and m is the number of rooms (master room, bedroom 1, bedroom 2, and living room).

Table 2 – Two ventilation strategies according to outdoor air supply rate, air inlet position, and CO2 sensor position

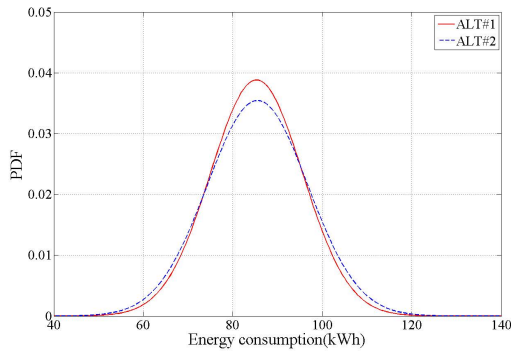
ALT.	Outdoor air supply rate	Air inlet position	CO2 sensor position
1		Living room	Living room
2	DCV-CO2	Living room + Master room	Living room + Master room

Table 3 shows the uncertainty results of two design alternatives. In terms of total energy consumption, ALT #1 is superior by a difference of 1.37 (kWh), but the difference is insignificant. In terms of CO2 performance (%), ALT #2 is superior owing to the additional CO2 sensors in the master room. In the results of the coefficient of variation, which expresses the degree of uncertainty, ALT #2 is superior in terms of total heating energy consumption and CO2 performance, but the difference in the degree of

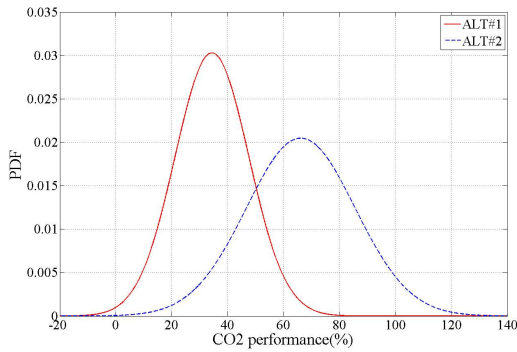
uncertainty is insignificant. Fig. 4 shows the uncertainty results of each alternative using the Probability Distribution Function (PDF).

Table 3 – Uncertainty results (STDEV: Standard deviation, COV: Coefficient of Variation)

	ALT #1		ALT #2	
	Heating energy (kWh)	CO2 performance (%)	Heating energy (kWh)	CO2 performance (%)
Min	40.86	12.61	42.23	29.27
Max	99.07	85.70	100.44	135.72
Mean	84.16	34.39	85.53	66.14
STDEV	11.25	13.17	11.26	19.49
COV	0.134	0.383	0.132	0.295



(a) Total heating energy consumption (kWh)



(b) CO2 performance (%)

Fig. 4 - Uncertainty results using PDF (ALT. #1 vs. ALT. #2)

5. SMCDM Results

In this study, reference points and weighting factors were selected to calculate the prospect values (Tables 4-5). The weighting factors were used to transfer into a single cost function. However, it

should be noticed that the selection of reference points and weighting factors can be changed according to the preferences of the real decision makers.

Table 4 – What-if scenarios of reference points

Case	Heating energy (kWh)	CO2 performance (%)
1	70	20
2	70	25
3	75	20
4	75	25

Table 5 – What-if scenarios of weighting factors for multi-criteria

Weight	Heating energy (kWh)	CO2 performance (%)
1	0.8	0.2
2	0.2	0.8
3	0.5	0.5

Table 6 shows the prospect values of the CPT according to the scenarios of reference points and weighting factors. The prospect value is expressed as a normalized prospect value matrix (Table 7) using Equations (8) and (9). As shown in Table 8, the total prospect value reflecting the two performance criteria (heating energy consumption and CO2 performance) can be calculated using Equation (10).

$$r_{i,j} = \frac{v_{i,j}}{\max(v_{i,j})}, \quad i \in M, j \in N_1 \quad (8)$$

$$r_{i,j} = \frac{\min(v_{i,j})}{v_{i,j}}, \quad i \in M, j \in N_2 \quad (9)$$

$$v(\alpha_i) = \prod_{j=1}^n r(x_j)^{w(j)} \quad (10)$$

where, r is the normalized prospect value, v is the prospect value of each alternative (refer to Table 6), N_1 is the benefit criteria for CO2 performance, and N_2 is the cost criteria for the heating energy consumption.

Table 6 – Prospect values of alternatives

ALT	Case #1		Case #2		Case #3		Case #4	
	Heating energy	CO2 performance						
1	67.81	80.93	67.81	49.50	21.58	56.27	21.58	30.62
2	79.06	204.54	79.06	170.13	34.37	203.59	34.37	170.13

Table 7 – Normalized prospect matrix results

ALT	Case #1		Case #2		Case #3		Case #4	
	Heating energy	CO2 performance						
1	1	0.396	1	0.291	1	0.276	1	0.180
2	0.858	1	0.858	1	0.628	1	0.628	1

Table 8 – SMCDM results of ERV using CPT

ALT	Case #1			Case #2			Case #3			Case #4		
	Weight #1	Weight #2	Weight #3	Weight #1	Weight #2	Weight #3	Weight #1	Weight #2	Weight #3	Weight #1	Weight #2	Weight #3
1	0.83	0.48	0.63	0.83	0.37	0.54	0.77	0.36	0.53	0.77	0.25	0.42
2	0.88	0.97	0.93	0.88	0.97	0.93	0.69	0.91	0.79	0.69	0.91	0.79

Comparing with the total prospect values according to the reference point scenarios (Table 4) under the Weight #1 condition (Table 5), ALT #2 (total prospect value: 0.88) is the optimal alternative for Cases #1-2 and ALT #1 (total prospect value: 0.77) is the optimal alternative for Cases #3-4. When the weight scenario is changed (Weights #1-3 in Table 5), a different optimal alternative is determined for Cases #3-4 among the reference point scenarios. For Cases #1-2, ALT #2 is determined as the optimal alternative, but the total prospect value is changed depending on the weighting factor.

As shown in the above results, the SMCDM using CPT results in a different optimal alternative for the ERV depending on the reference point and weighting factor, that are determined based on the subjective preferences and attitudes of decision makers toward risks. The reference point selection reflects the value function for gains and losses, unlike the Bayesian decision making based on the utility theory, and is one of the major advantages of the CPT. These merits can be useful in finding a more

rational and reliable optimal alternative than the utility theory.

6. Conclusion

In this study, SMCDM was implemented to find an optimal ventilation strategy for the ERV using the stochastic predicted outputs of the BPS tool. In the building simulation domain, Bayesian decision-making based on the utility theory is generally used for handling SMCDM. This solves MCDM problems by reflecting the preferences of decision makers. However, the utility theory is not practical because it assumes that decision makers are rational beings. In contrast, the CPT proposed in this study can reflect (1) reference point setting, (2) diminishing sensitivity, and (3) loss aversion, and this is useful in solving the problem of the utility theory. In this study, the CPT was developed and the SMCDM of the ERV was conducted by selecting two ventilation strategies. In particular, reference points and

weighting factors were randomly selected for each scenario and their effects on deciding the optimal alternative were examined.

In the results, decision makers could obtain different total prospect values depending on the selection of reference point, which has considerable effect on the decision of the optimal alternative. It means that the decision-making results using the CPT can provide more realistic and trustworthy information compared to the utility theory.

Acknowledgements

This work was supported by the National Research Foundation of Korea (NRF) grant funded by the Korean government (MSIP) (No. 2015R1C1A1A01052976).

References

- ASHRAE. 2013. *ASHRAE Handbook Fundamentals*. Atlanta, U.S.A.: ASHRAE.
- de Wit, S. 2001. *Uncertainty in prediction of thermal comfort in Buildings*. Ph.D. Dissertation. Delft, the Netherlands: TU Delft.
- DOE. 2013a. *EnergyPlus 8.0 Input/Output Reference: The Encyclopedic Reference to EnergyPlus Input and Output*. Washington, U.S.A.: US Department of Energy.
- DOE. 2013b. *EnergyPlus 8.0 Engineering Reference: The Encyclopedic Reference to EnergyPlus Calculations*. Washington, U.S.A.: U.S. Department of Energy.
- Hopfe, C.J. 2009. *Uncertainty and sensitivity analysis in building performance simulation for decision support and design optimization*. Ph.D. Dissertation. Eindhoven, the Netherlands: TU Eindhoven.
- Hyun, S.H., C.S. Park. 2006. *Uncertainty analysis of natural ventilation phenomena*. (1st year report submitted to the Korea Institute of Construction & Transportation Technology Evaluation and Planning (KICTEP)).
- Kahneman, D., A. Tversky. 1979. "Prospect theory: An analysis of decision under risk". *Econometrica: Journal of the Econometric Society* 47 (2): 263-291. doi: 10.2307/1914185.
- Kim, Y.J., C.S. Park. 2009. "Comparative Study of Ventilation Strategies in Residential Apartment Building under Uncertainty". In: *Proceedings of the 11th IBPSA Conference*. Glasgow, UK: IBPSA.
- Kim, Y.J., K.U. Ahn, C.S. Park. 2014. "Decision Making of HVAC System using Bayesian Markov Chain Monte Carlo method". *Energy and Buildings* 72: 112-121. doi: 10.1016/j.enbuild.2013.12.039.
- Krohling, R.A., T.T.M. de Souza. 2012. "Combining prospect theory and fuzzy numbers to multi-criteria decision making". *Expert Systems with Applications* 39: 11487-11493. doi: 10.1016/j.eswa.2012.04.006.
- Lahdelma, R., P. Salminen. 2009. "Prospect theory and stochastic multicriteria analysis". *Omega* 37: 961-971. doi: 10.1016/j.omega.2008.09.001.
- Laverge, J., A. Janssens. 2013. "Optimization of design flow rates and component sizing for residential ventilation". *Building and Environment* 65: 81-89. doi:10.1016/j.buildenv.2013.03.019.
- MacDonald, I.A. 2002. *Quantifying the effects of uncertainty in building simulation*. Ph.D. thesis, Strathclyde, UK: University of Strathclyde.
- Prelec, B.D. 1998. "The probability weighting function". *Econometrica* 66 (3): 497-527. doi: 10.2307/2998573.
- Sun, Y., L. Gu, C.F.J. Wu, G. Augenbroe. 2014. "Exploring HVAC system sizing under uncertainty". *Energy and Buildings* 81: 243-252. doi: 10.1016/j.enbuild.2014.06.026.
- Tversky, A., D. Kahneman. 1992. "Advances in prospect theory: Cumulative representation of uncertainty". *Journal of Risk and Uncertainty* 5(4): 297-323.
- Von Neumann, J., O. Morgenstern. 1947. *Theory of Games and Economic Behavior*. Princeton, U.S.A.: Princeton University Press.
- Walton, G.N., W.S. Dols. 2005. *CONTAMW 2.4 User Guide and Program Documentation*. NISTIR 7251. Gaithersburg, U.S.A.: National Institute of Standards and Technology.
- Wakker, P.P. 2010. *Prospect Theory: for risk and ambiguity*. Cambridge, UK: Cambridge University Press.

Proposing a Life Cycle Energy Efficiency Index for Comparative Assessment of Insulation Materials' Performance

Hashem Amini Toosi – University of Tehran – HashemAmini@ut.ac.ir

Ali Vakili-Ardebili – University of Tehran – avakiliardebili@ut.ac.ir

Nasim Hasheminejad – Politecnico di Milano – nasim.hasheminejad@mail.polimi.it

Abstract

In this paper, a new method is presented to compare different scenarios of insulation by assigning a Life Cycle Energy Efficiency (LCEE) index, which includes operational energy use and embodied energy of materials. For this purpose, a sensitivity analysis has been performed to determine the relation between insulation thickness and total energy consumption, then the new method to assign the LCEE index has been used and the results have been compared.

Our methodological approach consists of the following steps: (i) Simulate a 27 m³ cubic simple zone with a double glazed air filled window on south surface in EnergyPlus 8.3 software; (ii) Determine the thermal comfort boundaries for each studied city including Tehran, Bandar Abbas, Tabriz and Kerman; (iii) Vary installation materials and insulation thickness and calculate the total energy demand for heating and cooling in each city that includes 128 insulating scenarios; (iv) Calculate the embodied energy of different insulating alternatives based on LCI databases; (v) Perform a sensitivity analysis for each insulation material in each city to figure out the relationship between thickness of insulation materials and total energy demand in each city; (vi) Use the new method to assign the LCEE index in order to compare different scenarios.

The analysis showed that both operational energy and embodied energy have considerable impacts in decision-making processes in order to select the best insulation type and thickness. Moreover, the new method to assign the LCEE index was used as a useful method to assign a concise comparative index in order to compare different decisions by building designers.

1. Introduction

The building sector is responsible for 40 % of the total energy consumption in Europe. This sector is known as the major contributor to the environmental impact (European Union, 2013; Arena et al, 2003; Iribarren et al, 2015). It is crucial to understand the flow of energy in the buildings life cycle in order to meet global energy efficiency program targets. Energy is consumed in all the life cycle phases of a building, including material production, construction, operation, and demolition. Therefore, it's vital to understand the importance of each phase of a building life cycle. Several studies, showed the growing significance of embodied energy in a building life cycle (British Department for Communities and Local Government, 2007). In the UK, embodied emissions in new construction and renovation each year account for about 10 % of the total CO₂ emissions. Within this, approximately half is used in the extraction of raw materials and manufacture of the materials.

Nowadays in Iran and other developing countries, both the improvement of energy-efficiency standards and the deployment of low-energy buildings typically focus on reducing the operational energy consumption of buildings. Studies on low energy buildings show a reverse relation between operational energy with embodied energy. This means that while utilizing new technologies and high performance materials reduces the operational energy of a building's life cycle, the embodied energy of building is increased and this increase is mainly attributed to energy consumption in high performance material production processes (Keoleian et al., 2001; Yao et al., 2014).

As a result, it will be increasingly important to consider the primary energy-use for materials in buildings that are designed and constructed to be more energy-efficient (Thormark, 2002; Blengini et al., 2010; Dadoo et al., 2011). In order to optimize the total energy demand in a building's life span, a whole life cycle energy analysis, including all phases of a building's life cycle should be performed. In this paper, the performance of different insulation materials will be compared. For this purpose, a comparative assessment method on building insulation materials will be presented. In this method, the embodied energy and operational energy in a building life cycle are considered in calculations, and the results of each insulation material are compared with other materials.

There are various efforts to define methods with the purpose of calculating the embodied energy of insulation materials that will be reviewed in the next section, but the aim of this paper is to define a clear and concise index that could help the architects understand the differences of insulation material performance.

1.1 Literature Review

Many studies performed in order to assess the environmental impacts of different insulation materials and each study focused on different materials or different environmental targets (Tingley et al., 2015).

Winther and Hestnes (1999) compared total energy use during the life span of buildings, with different insulation scenarios, different ventilation strategies, and different energy saving equipment. Mithraratne et al. (2004) described a method for LCA based on the embodied and operating energy and costs of buildings. Shukla et al. (2009) developed a simple methodology to calculate the embodied energy of an adobe house. Ardente et al. (2008) conducted a life cycle assessment on a kenaf-fiber insulation board in comparison with stone wool, flax, paper wool, PUR, glass wool and mineral wool.

Whilst Shrestha et al. (2014) suggested a protocol to assess the environmental impacts of insulation over their life; La Rosa et al. (2014) performed a comparative LCA of four external wall alternatives with cork insulation and PVC foam. Pargana et al. (2014)

conducted an LCA on different types of insulation in Portugal. Bojic et al. (2014) performed an optimization for the entire life cycle of different thermal insulations.

2. Materials and Methods

Life Cycle Energy Analysis (LCEA) is a simplified version of life cycle assessment, which only focuses on the evaluation of energy inputs in different phases of the life cycle (Chau et al., 2015).

Our methodological approach consists in the following steps: (i) Simulate a 27 m³ cubic simple zone with a double glazed air filled window on south surface in EnergyPlus 8.3 software; (ii) Determine the thermal comfort boundaries for each studied city including Tehran, Bandar Abbas, Tabriz and Kerman; (iii) Vary installation materials and insulation thickness and calculate the total energy demand for heating and cooling in each city; (iv) Calculate the embodied energy of different insulating alternatives based on LCI databases; (v) Perform a sensitivity analysis for each insulation material in each city to figure out the relationship between thickness of insulation materials and the total operating energy demand in each city; (vi) Use the new method to assign the Life Cycle Energy Efficiency index (LCEE) in order to compare different scenarios.

To calculate the total embodied and operational energy demand of different insulating scenarios during the 30 years of life span, the Equation 1 will be used.

$$LCE_j = \sum_{i=1,12} (n OE_i + V EE_j) \quad (1)$$

where:

LCE_j: the total operating and embodied energy in 30 years life span for j(th) scenario

OE_i: heating and cooling operating energy demand of each month in a year

n: life span of insulation materials (years), (in this case study, n = 30 years)

V: the total volume of insulation materials

EE_j: embodied energy of the insulation material for j(th) scenario

To assign the LCEE index, equation 2 will be used.

The mathematical meaning of this equation is a

comparative index that helps the architects find the best insulation scenario in technical design phases. By dividing the LCE of a single scenario by the sum of the LCE for all the considered scenarios according to this equation, a clear and concise index between 0 and 100 will be obtained which could help the architect understand the differences between insulation materials' performance quickly and easily.

$$LCEE\ index_j = (1 - LCE_j / \sum_{j=1,n} LCE_j) \quad (2)$$

Where:

LCCE index_j: for j(th) scenario

LCE_j: the total operating and embodied energy in a 30-year life span for j(th) scenario

N: the all insulating scenarios

Fig. 1 and Table 1 show the thermal zone and thermal specifications of materials and construction assemblies, modeled in EnergyPlus 8.3. The values in Table 1 are the average values of Iran's building technology industry.

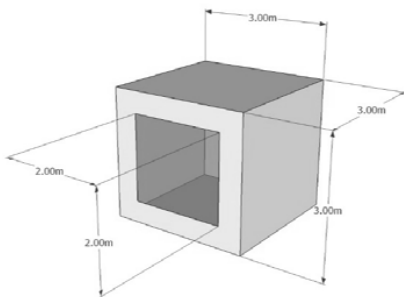


Fig. 1 – The thermal zone which is modeled in EnergyPlus 8.3

Table 1 – Thermal specification of materials (an average based on common construction materials in Iran)

Assembly	Thick-ness (m)	Density (kg/m ³)	Thermal conductivity (W/(m K))
Wall (Brick)	0.1	1800	0.9
Roof (Lightweight concrete)	0.1	1400	0.5
Floor (Lightweight concrete)	0.1	1400	0.5
Insulation (External insulating for walls, roof and floor)	Variable	Variable	Variable
Window (double glazed, air filled)	-----	-----	0.15 (equivalent thermal conductivity)

2.1 Life Cycle Inventory and Weather Data

Life cycle inventory has a high importance in any LCA analysis process, because the quality and reliability of the results in a life cycle assessment process completely depend on the quality of LCI data (SAIC, 2006). Table 2 presents the physical properties and embodied energy of the studied insulation materials.

Table 2 – LCI data of insulation materials (Hegner, 2007)

Insulation material	Thermal conductivity (W/(m K))	Density (kg/m ³)	Embodied Energy (MJ/m ³)
XPS	0.03	50	2823
GMW	0.035	20	505
PU	0.026	31	2880
Foam Glass	0.041	117	197
GMW unforced rolled	0.032	32.5	538
Wood fiber	0.044	210	1362
EPS	0.035	30	3057
Cork Slab	0.044	120	3156

Iran is located in West Asia and borders the Caspian Sea, the Persian Gulf, and the Gulf of Oman in the region known as the Middle East. It lies between latitudes 24° and 40° N, and longitudes 44° and 64° E. Iran has a variable climate. In the northwest, winters are cold with heavy snowfalls and subfreezing temperatures in December and January. Spring and fall are relatively mild, while summers are dry and hot. In the south, winters are mild and the summers are very hot with virtually continuous sunshine, the daily average temperatures in July exceed 38 °C (Bagheri et al, 2013).

In the present paper, Tehran, Kerman, Bandar Abbas, and Tabriz have been selected for the mild, warm–dry, warm–humid, and cold regions respectively. According to the National Center of Climatology of Iran, the climatic characteristics of each of the selected cities are presented in Table 3.

Table 3 – Climatic characteristic of studied cities

City	Latitude	Longitude	Elevation
Tehran	35.68 ° N	51.30° E	1219 m
Kerman	30.29° N	57.06° E	1755 m
Bandarabbas	27.20° N	56.15° E	10 m
Tabriz	37.80° N	46.25° E	1365 m

Table 4 presents the average temperature of the warm and cold months of each studied city, also the maximum and minimum comfort temperature boundaries are presented.

Table 4 represents the maximum and minimum comfort temperature based on a research that was

performed in Iran according to the adaptive theory described in EN 15251.

Table 4 – Thermal comfort boundaries (Max CT, Min CT) for studied cities and the average of warm and cold months temperatures (WMT, CMT) (Heidari, 2014)

City	WMT (°C)	CMT (°C)	Humidity (%)	Max CT (°C)	Min CT (°C)
Tehran	28.4	21.1	44	30.1	20.9
Bandar Abbas	29.3	22	66	31.3	18.3
Kerman	30.0	22.7	37.6	27.3	14.7
Tabriz	26.3	18.5	54	30.7	16.5

3. Result and Discussion

The following figures, present the sensitivity analysis of insulation thickness to total embodied and operating energy demand over a 30-year life span in each studied city. Fig. 2 presents the sensitivity analysis of insulation thickness in Tehran, and shows different rates of upward trends for different insulation materials. As these results are shown in this figure, extruded polystyrene, polyurethane, expanded polystyrene, wood fiber panels, and cork slab have a rising trend in results, and there is a direct relation between the thickness of insulation and total energy demand.

The reason for a direct relation between insulation thickness and total energy demand is the fact that infiltration is not taken into account in this study. Therefore, by increasing the thickness of insulation, the thermal resistance of walls, roof, and floor will be increased, naturally the conductive heat loss (which is the only way of natural cooling) and the rate of cooling will be decreased, as a result the cooling energy demand in warm months (dominant energy demand in Iran) will be increased.

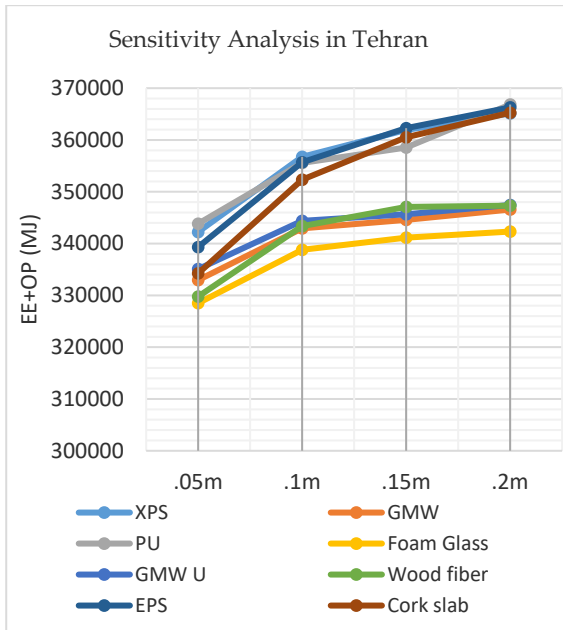


Fig. 2 – Sensitivity analysis of insulation thickness and total energy demand in Tehran

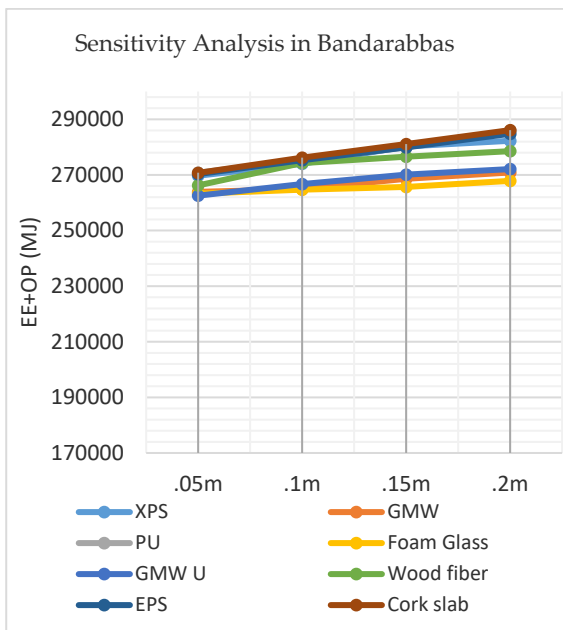


Fig. 3 – Sensitivity analysis of insulation thickness and total energy demand in Bandar Abbas

Also unfurced glass mineral wool, foam glass, and glass mineral wool represent different results, and show two different trends that indicate the importance of these simulation and sensitivity analyses to find the optimum thickness of the insulation materials.

Fig. 3 shows a weak relation between the thickness of insulation and the total embodied and operating energy demand in Bandar Abbas.

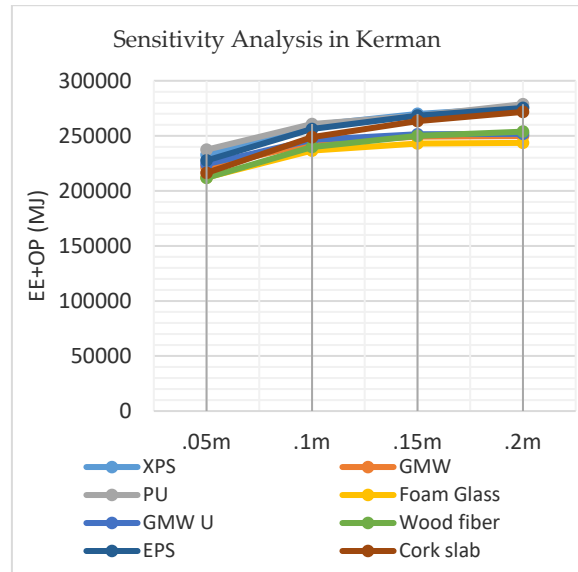


Fig. 4 – Sensitivity analysis of insulation thickness and total energy demand in Kerman

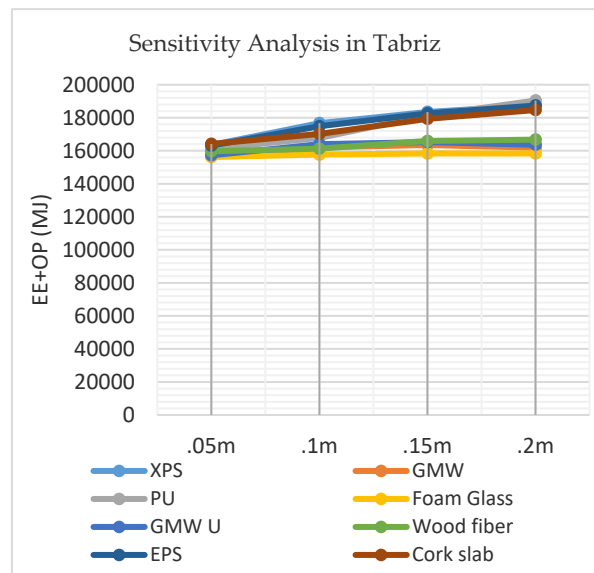


Fig. 5 – Sensitivity analysis of insulation thickness and total energy demand in Tabriz

This can be attributed to an equivalence of increasing in embodied energy and decreasing in operating energy demand by increasing the thickness of insulation in Bandar Abbas.

Fig. 4 shows a direct relation in the total energy demand and thickness of insulation material for all studied insulation materials in Kerman, the increase in operating energy demand because of a decreasing natural cooling rate and increasing the embodied energy due to the increase of the volume of

insulation materials are the reasons of this trend in the diagram

From Fig.s 5 and 3, we can understand that the sensitivity analysis results in Tabriz and Bandar Abbas are almost similar. The direct relation in the increase of insulation thickness and total energy demand for extruded polystyrene, polyurethane, expanded polystyrene, wood fiber panels, and cork slab are similar to the results of Tehran, but with a difference in the rate of the increase. Also a weak direct relation between energy demand and insulation thickness is found for unforced rolled glass mineral wool, glass mineral wool, and foam glass, this relative independence can also be attributed to the equivalence of an increase in embodied energy and decrease in operating energy demand by increasing the thickness of insulation.

By using Equation 2, the LCEE index has been assigned to each insulation scenario in different climatic conditions. The LCEE index indicates the life cycle energy efficiency in each insulating scenario. The higher index means the higher efficiency and vice versa.

Different trends and results have been observed in each city. In Tehran the highest Index is assigned to Foam glass and Wood fiber, and the lowest Index is assigned to PU, XPS and EPS. In Bandar Abbas there is not much difference between the insulation materials, but the lowest index is assigned to PU.



Fig. 6 – Life cycle energy efficiency index for different insulation scenarios in Tehran



Fig. 7 – Life cycle energy efficiency index for different insulation scenarios in Bandar Abbas

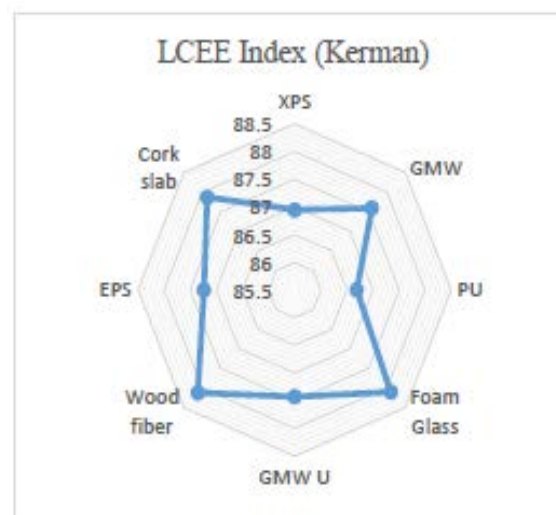


Fig. 8 – Life cycle energy efficiency index for different insulation scenarios in Kerman



Fig. 9 – Life cycle energy efficiency index for different insulation scenarios in Tabriz

Analysis in Kerman shows that the lowest index is assigned to PU and the highest index is assigned to foam glass and wood fiber. Also analysis in Tabriz shows similar results to Bandar Abbas.

By considering the results in Figs 2 to 9, we can conclude that insulating materials behave in different ways in each studied city. As these cities are located in different climatic conditions and the thermal comfort boundaries are not similar (according to a research based on adaptive theory). This fact (different behavior of insulation materials) can be attributed to differences in total operating energy demand for providing thermal comfort in each climate, and also to different humidity in each city that can affect the performance of the insulating materials.

4. Conclusion

The main aim of this study was to present a new method to comparative life cycle energy analysis for insulation scenarios under different climatic conditions. By this method the operational energy and embodied energy of each insulation scenario were considered in calculations. The analysis showed that both operational energy and embodied energy have a considerable impact on decision-making processes in order to select the best insulation type and thickness. Moreover, the new method to assign the LCEE index was used as a useful method to assign a concise comparative index in order for building designers to easily compare different options. The differences in analysis and results for each scenario can be attributed to the embodied energy of the insulation materials, the thermal performance of the insulation materials, and the differences in climatic conditions and energy demand.

In addition, this is recommended to consider the effect of different fuels used in energy systems in future studies. It is expected that the embodied energy of the energy systems has also considerable effects on the whole life cycle energy demand of a building.

Acknowledgements

The Authors would like to thank the School of Architecture, College of Fine Arts, University of Tehran, for having provided the required facilities for this research.

References

- Ardente, F., M. Beccali, M. Cellura, M. Mistretta. 2008. "Building energy performance: a LCA case study of kenaf-fibres insulation board". *Energy and Buildings* 40(1): 1-10. doi: 10.1016/j.enbuild.2006.12.009.
- Arena, A.P., C. de Rosa. 2003. "Life cycle assessment of energy and environmental implications of the implementation of conservation technologies in school building in Mendoza Argentina". *Building and Environment* 38(2): 359-368. doi: 10.1016/S0360-1323(02)00056-2.
- Bagheri, F., V. Mokarizadeh, M. Jabbar. 2013. "Developing energy performance label for office buildings in Iran". *Energy and Buildings* 61: 116-124. doi: 10.1016/j.enbuild.2013.02.022.
- Blengini, G.A., T. Di Carlo. 2010. "The changing role of life cycle phases, subsystems and materials in the LCA of low energy buildings". *Energy and Buildings* 42(6): 869-880. doi: 10.1016/j.enbuild.2009.12.009.
- Bojic, M. 2014. "Optimization of thermal insulation to achieve energy savings in low energy house (refurbishment)". *Energy Conversion and Management* 84: 681-690. doi: 10.1016/j.enconman.2014.04.095.
- British Department for Communities and Local Government. 2007. *Building a Greener Future: Policy Statement for Target of Zero Carbon Homes by 2016*. London, UK: Department for Communities and Local Government.
- Chau, C.K., T.M. Leung, W.Y. Ng. 2015. "A review on Life Cycle Assessment, Life Cycle Energy Assessment and Life Cycle Carbon Emissions Assessment on buildings". *Applied Energy* 143: 395-413. doi: 10.1016/j.apenergy.2015.01.023.

- Dodoo, A., L. Gustavsson, R. Sathre. 2011. "Building energy-efficiency standards in a life cycle primary energy perspective". *Energy and Buildings* 43(7): 1589-1597. doi: 10.1016/j.enbuild.2011.03.002.
- European Union and European Commission. 2013. *EU Energy in Figures Statistical Pocketbook*. Luxembourg, Luxembourg: European Union.
- Hegner, S. 2007. *Embodied Energy for Energy Efficiency Measures An Assessment of Embodied Energy's Relevance for Energy Saving in the Swiss Residential Building Sector*. Diploma Thesis: Zurich, Switzerland: Department of Environmental Science ETH Zurich.
- Heidari, S. 2014. *Thermal Adaption in Architecture, First step of Energy Saving*. Tehran, Iran: University of Tehran Press.
- Iribarren, D., A. Marvuglia, P. Hild, M. Guiton, E. Popovici, E. Benetto. 2015. "Life cycle assessment and data envelopment analysis approach for the selection of building components according to their environmental impact efficiency: a case study for external walls". *Journal of Cleaner Production* 87: 707-716. doi: 10.1016/j.jclepro.2014.10.073.
- Keoleian, G.A., S. Blanchard, P. Reppe. 2001. "Life-cycle energy, costs, and strategies for improving a single-family house". *Industrial Ecology* 4(2): 135-156. doi: 10.1162/108819800569726.
- La Rosa, A.D., A. Recca, A. Gagliano, J. Summerscales, A. Latteri, G. Cozzo, G. Cicala. 2014. "Environmental impacts and thermal insulation performance of innovative composite solutions for building applications". *Construction and Building Materials* 55: 406-414. doi: 10.1016/j.conbuildmat.2014.01.054.
- Mithraratne, N., B. Vale. 2004. "Life cycle analysis model for New Zealand houses". *Building and Environment* 39(4): 483-492. doi: 10.1016/j.buildenv.2003.09.008.
- Pargana, N., M. Duarte Pinheiro, J. Dinis Silvestre, J. de Brito. 2014. "Comparative environmental life cycle assessment of thermal insulation materials of buildings". *Energy and Buildings* 82: 466-481. doi: 10.1016/j.enbuild.2014.05.057.
- SAIC. 2006. *Life Cycle Assessment: Principles & Practice*. Cincinnati, U.S.A.: EPA.
- Shrestha, S.S., K. Biswas, A.O. Desjarlais. 2014. "A protocol for lifetime energy and environmental impact assessment for building insulation materials". *Environmental Impact Assessment Review* 46: 25-31. doi: 10.1016/j.eiar.2014.01.002.
- Shukla A., G.N. Tiwari, M.S. Sodha. 2009. "Embodied energy analysis of adobe house". *Renewable Energy* 34(3): 755-761. doi: 10.1016/j.renene.2008.04.002.
- Thormark, C. 2002. "A low energy building in a life cycle—its embodied energy energy need for operation and recycling potential". *Building and Environment* 37(4): 429-435. doi: 10.1016/S0360-1323(01)00033-6.
- Tingley, D., A. Hathway, B. Davison. 2015. "An environmental impact comparison of external wall insulation types". *Building and Environment* 85: 182-189. doi: 10.1016/j.buildenv.2014.11.021.
- Winther, B.N., A.G. Hestnes. 1999. "Solar versus green: the analysis of a Norwegian row house". *Solar Energy* 66(6): 387-393. doi: 10.1016/S0038-092X(99)00037-7.

Development of a Design Numerical Model of a Hybrid Cooler

Matteo D'Antoni – Institute for Renewable Energy, Eurac Research – matteo.dantoni@eurac.edu

Roberto Fedrizzi – Institute for Renewable Energy, Eurac Research – roberto.fedrizzi@eurac.edu

Abstract

This paper presents the development of the numerical model of a hybrid cooler. It is based on a modular and generic coil geometry that deals with any staggered coil and pipe arrangement. Particular attention is given to model the spray water system and to the calculation of water evaporation on the coil surface. It is validated by monitored data from a pilot system installation in which a commercial hybrid cooler is operated under typical summer south European working conditions. The numerical model has an average error of 7 % for the rejected heat and 0.1 % for the fan power consumption. The model is compatible with TRNSYS simulation software. It can be used for design and product development purposes by HVAC manufactures and thermal engineers.

1. Introduction

An efficient and cost-effective heat rejection system is a key requisite of any cooling system. Two categories of air-based condenser units are typically distinguished: dry coolers (DCs) and wet cooling towers (WCTs).

Thanks to the evaporation of water deposited on the coil surface, WCTs can reach an outlet water temperature lower than dry-bulb ambient temperature. Their average specific nominal consumption is therefore lower ($0.017 \text{ kW}_{el}/\text{kW}_t$) when compared to DCs ($0.033 \text{ kW}_{el}/\text{kW}_t$) (D'Antoni et al., 2014). Conversely, they are characterized by higher operation (e.g. water consumption) and maintenance (e.g. legionella growth risk) costs (D'Antoni et al., 2014). On the other hand, DCs are relatively cheaper ($22\text{-}27 \text{ €/kW}_t$ against $49\text{-}107\text{€/kW}_t$) and lighter ($97\text{-}185 \text{ kg/m}^2$ against $208\text{-}376 \text{ kg/m}^2$) than WCTs (D'Antoni et al., 2014).

Both WCTs and DCs have technological limitations that can turn into important economic issues up to

the extent to prevent their installation in certain climatic conditions. These problems can be partly overcome by hybrid coolers (HCs). A hybrid cooler is a dry cooler that wets the coil surface by spraying water upwards in a co-current direction with the airflow. Thanks to this solution, the use of water can be largely limited with respect to WCTs by spraying water only when necessary, thus achieving at the same time electricity savings compared to DCs due to fan operation.

HCs are not a new concept and several studies have been produced in the past 30 years (Sen, 1973; Yang and Clark, 1975; Nakayama et al., 1988; Dreyer et al., 1992). An extended literature review (Romeli, 2014) has revealed that numerical models of hybrid cooler still show room for further improvements.

- The calculation of the surface wettability is in some cases estimated through empirical correlations valid only for some specific geometries and in other fixed as a constant.
- None of the reviewed models has a modular definition of coil geometry.
- The level of detail in the control volume definition is quite diversified, ranging from the control volume identified as the whole coil, a single row, a single pass in a row or a fraction of a single tube.
- Effectiveness-NTU methods are more suitable for heat and mass transfer problems when inlet fluid conditions are imposed and for a given coil geometry, whereas mean-log enthalpy difference (LMED) can be successfully used for design purposes.

The ambition of the present paper is to present the development of a hybrid cooler numerical model characterized by:

- a modular and generic coil geometry that deals with any staggered coil and pipe arrangement;

- a model for the spray water system specifically conceived for hybrid coolers;
- a detailed calculation of wettability factors for fins and tubes at each row in which specificities of coil geometry, nozzles characteristics and position are taken into account;
- dedicated control strategies to regulate the fan's speed and the amount of sprayed water.

The numerical code is compatible with TRNSYS (Klein et al., 2010), which allows for the assessment the performance of a hybrid cooler in a whole system simulation. By reviewing already existing TRNSYS models ("Types"), we can observe that they lack:

- the possibility of specifying a generic coil geometry (e.g. Type 32);
- fins surfaces are assumed fully wet (e.g. Type 51, Type 510) and the use of the wettability factor concept;
- a clear focus on the control strategy for fans and spray water system operations.

2. Heat and Mass Transfer Balances

2.1 Governing Equations and Infinitesimal Control Volume

The heat and mass transfer problem in a hybrid cooler can be studied on an infinitesimal control volume $dA=b \times dl$ (Fig. 1). It is characterized by the presence of three fluids: (1) process fluid flowing in coil pipes (water or a water-glycol mixture), (2) water sprayed by nozzles onto the coil surface and (3) moist air passing across both fins and tubes. For each of these a subsystem is identified on which heat balance and mass conservation is written. In order to do this, a list of assumptions and simplifications are necessary and in particular:

- The system is in a steady state and it is well insulated from the surrounding environment.
- Radiative heat transfer between the coil's external surface and the environment is negligible.
- Heat and mass transfer coefficients are assumed as a constant within the infinitesimal volume.
- The model is one-dimensional.
- The spray water temperature is assumed as a constant.

- The temperature of the interface T_{int} between the water film on the external surface (fins and tubes) and the air is equal to the average bulk temperature of the film.
- The Lewis factor $Lef = hc / (hm \times cp,a) \approx 1$.

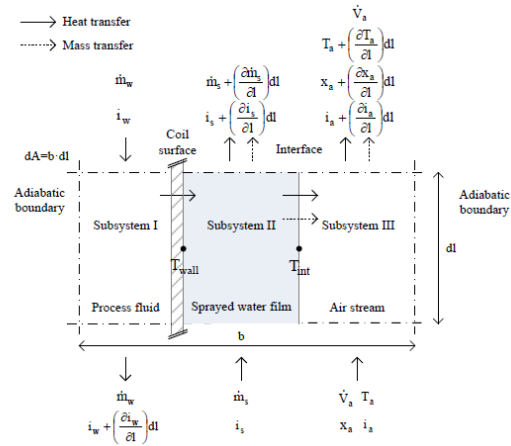


Fig. 1 – Infinitesimal control volume dA of the hybrid cooler

Looking at the overall infinitesimal control volume dA , a mass balance is written as:

$$dx_a = -\frac{dm_s}{m_a} dl \quad (1)$$

The mass balance on the subsystem II permits to calculate the evaporated rate of sprayed water on coil surface.

$$dm_s = -h_m (x_{a,sat}(T_{int}) - x_a) dl \quad (2)$$

Here $x_{a,sat}(T_{int})$ is the humidity ratio of the air stream at saturation conditions and at temperature T_{int} and h_m is the mass transfer coefficient.

The air stream (subsystem III) varies its thermohygro-metric conditions as a consequence of water evaporation from coil surface and heat release from process fluid. The consequent variation in terms of enthalpy can be expressed as follows:

$$di_a = \frac{h_m}{m_a} (i_{a,sat}(T_{int}) - i_a) dl \quad (3)$$

As done for subsystems II and III, the variation of process fluid temperature results from an energy balance imposed on subsystem I.

$$dT_w = -\frac{U_i (T_w - T_{wall})}{m_w c_{p,w}} dl \quad (4)$$

In Equation 4 U_i is the overall internal heat transfer coefficient, which is a function of the average internal convective heat transfer coefficient and of the tube thermal conductivity as calculated in (Shah and London, 1978; Gnielinski, 1976).

Therefore, the heat and mass transfer problem reduces to solving the system of differential equation of Equation 5.

$$\begin{cases} dx_a = -\frac{d\dot{m}_s}{\dot{m}_a} dl \\ d\dot{m}_s = -h_m(x_{a,sat}(T_{int}) - x_a) dl \\ di_a = \frac{h_m}{\dot{m}_a}(i_{a,sat}(T_{int}) - i_a) dl \\ dT_w = -\frac{U_i(T_w - T_{wall})}{\dot{m}_w c_{p,w}} dl \end{cases} \quad (5)$$

2.2 Mass Balance and Wettability Factors

The calculation of the wet surface area in a hybrid cooler is fundamental in order to predict the performance of the unit under different working conditions. Most of the numerical models of the sprayed water coils assume the existence of fully dry or wet conditions on tubes and fins. This assumption cannot be made because it is hard to wet uniformly the surface coil with a water jet sprayed upwards (Fig. 2 and Fig. 3).

When water sprinklers are activated, only a fraction of the spray water rate \dot{m}_s deposits on the coil surface since the remaining part passes through. The deposited spray water rate (\dot{m}_{dep}) determines the so-called wettability factor R_{wet} of fins and tubes. When the spray water forms a film deposit on the coil surface, this might result in evaporation. The evaporation rate depends on the humidity ration difference at the water-air interface (considered at saturation conditions) and the airflow. The evaporated mass flow rate can be calculated for each j row as:

$$\dot{m}_{evap} = \eta_{o,wet} h_m (x_{a,sat}(T_{int}) - x_a) A_{wet} \quad (6)$$

Water droplets that do not evaporate are removed either by gravitational forces or by the air stream. In both cases, these forces have to overcome the water surface tension driving the water retention.

The retained water on the coil surface increases the pressure drop across the heat exchanger by restricting the flow of air (McQuiston, 1978; Wang et al. 1997; Korte & Jacobi, 1997). The dominance of airflow forces on gravity (causing a trailed spray mass flow rate) or the opposite situation (water dripping) is determined through the comparison between the critical film velocity v_{crit} and the maximum air velocity $v_{a,max}$ evaluated on the minimum free-flow area (Dreyer et al., 1992; Kriel, 1991; Wallis, 1969).

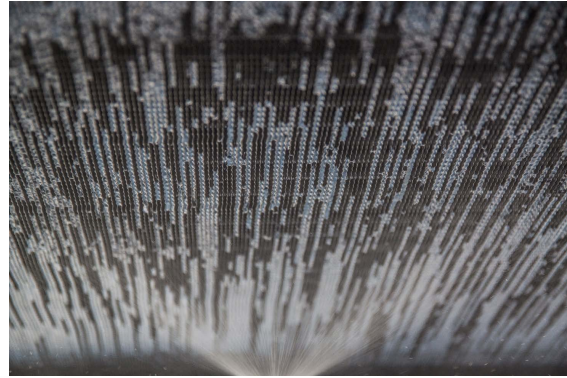


Fig. 2 – Picture of the 1st row (bottom part) of the coil while sprinkles are active

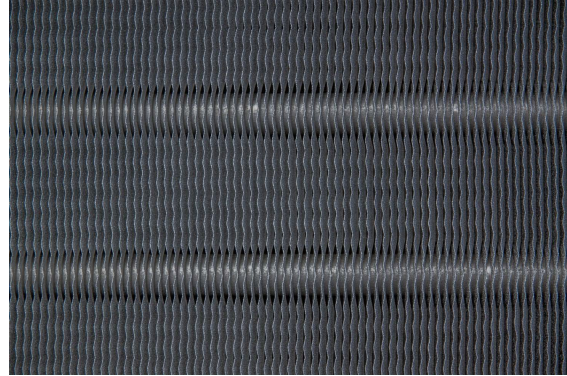


Fig. 3 – Picture of the 6th row (upper part) of the coil while sprinkles are active

2.2.1 Wettability factor

The wettability factor is defined as the ratio of wet finned-tube surface A_{wet} over the total finned-tube area. It is a fraction that depends upon several factors such as the type of nozzles, the size of droplets, the coil-geometry or the spray water pressure, just to name a few.

The research on the droplet impact is in continuous progress (Cossali et al., 2005). A physical model of the spray water system is elaborated here. Five

main assumptions are required in order to formulate the solution of the problem.

- The trajectory of water droplets is linear.
- The water is sprayed in a cone of a variable height.
- The spray water devices are designed in a way that nozzles wet potentially the entire coil frontal area A_{fr} .
- The spray evaporation before the deposit on coil surface has been neglected.
- The sprayed water that impacts the coil surface is accounted as completely deposited (specific studies on water deposition on heat exchanger are not in complete agreement).

The spray water rate deposited on the coil's surface is calculated using the notion of collection efficiency for fins E_{fin} and tubes E_{tube} . These parameters can be calculated as a function of Stoke number and Langmuir's parameter as proposed in Stuempfle (1973) and Finstad et al. (1987).

$$\dot{m}_{dep,fin} = E_{fin} \cdot \dot{m}_s \quad (7)$$

$$\dot{m}_{dep,tube} = E_{tube} \cdot (1 - E_{fin}) \cdot \dot{m}_s \quad (8)$$

After some simplifications (Romeli, 2014), the wet fin $A_{wet,fin}$ and tube $A_{wet,tube}$ surfaces are calculated as follows:

$$A_{wet} = \frac{3 \cdot d_{drop,max}^2 \cdot \dot{m}_{dep} \cdot SFT \cdot \Delta\tau}{2 \cdot \rho_s \cdot d_{drop}^3} \quad (9)$$

Where:

- $d_{drop,max}$ is the maximum diameter of deposited droplets (Cossali et al. 2005; Scheller and Bousfield, 1995);
- d_{drop} is the volume median diameter maximum diameter of deposited droplets (J.E. Braun, 1988);
- SFT is the average spray cycle;
- $\Delta\tau$ is the simulation time step.

3. Development of a Numerical Model

3.1 Geometrical Model

Typically, the coil used in a hybrid cooler is a multirow-multipass overall counter flow configuration with unmixed cross flow at each row. Tubes are arranged in a staggered configuration with their axes perpendicular to the air stream.

In a real HC configuration and with reference to the pipe coil length, it is possible to identify fans in series $N_{fan,series}$ or in parallel $N_{fan,paral}$. Then each single fan is defined by a length l_{fan} and width w_{fan} . The geometry of commercial coils can be very different and in order to adapt the geometry model for a generic coil, it is of practical use to define a modular equivalent coil arrangement. The following features characterise it:

- real and equivalent coils have the same internal and external pipe diameters, a staggered arrangement of tubes, the same longitudinal and transversal tube pitch;
- the equivalent coil geometry has one single pass for each row by defining an equivalent fan length l_{fan}^* and width w_{fan}^*

$$l_{fan}^* = l_{fan} \cdot \frac{N_{tubes}}{N_{rows} \cdot N_{circuits}} \quad (10)$$

$$w_{fan}^* = w_{fan} \cdot \frac{l_{fan}}{l_{fan}^*} \quad (11)$$

where l_{fan} is the length of the fan, N_{tubes} is the sum of all the tubes that can be counted in a vertical cross section of the coil, N_{rows} is the number of finned tube banks crossed by the airflow and $N_{circuits}$ identified by the number of parallel fluid loops in which the process fluid is divided when entering the coil.

In the present work, a single row-finned tube is selected as the finite control volume Σ on which the system of differential equations is solved (Equation 5).

This approach is compatible for the application of the ϵ -NTU method under incomplete wet conditions (Braun, 1988; Braun et al., 1989), where the heat transfer is the sum of dry and wet contributions as follows:

$$\dot{Q} = \varepsilon \cdot \dot{Q}_{\max} = \varepsilon_{\text{dry}} \cdot \dot{Q}_{\max,\text{dry}} + \varepsilon_{\text{wet}} \cdot \dot{Q}_{\max,\text{wet}} \quad (12)$$

where $\dot{Q}_{\max,\text{dry}}$, $\dot{Q}_{\max,\text{wet}}$ and ε_{dry} , ε_{wet} are the maximum heat transfer rate and the efficiency (as calculated in ESDU, 1991) under dry and wet conditions, respectively.

Kriel studied the impact of this decision (Kriel, 1991). They demonstrate that despite 1 % loss in the calculation of the rejected heat, a simplified control volume (identified with a single row) in favour of a more detailed approach (a fraction of a tube) takes 1/8 of the simulation time of the latter.

3.2 Convergence Method

For a counter-flow arrangement of cooling coil with n-rows (Fig. 4), the following continuity conditions hold:

$$T_{w,1}^{(n)} = T_{w,i} \quad \text{and} \quad T_{w,1}^{(j-1)} = T_{w,2}^{(j)} \quad (13)$$

$$T_{a,1}^{(i)} = T_{a,i} \quad \text{and} \quad T_{a,2}^{(j-1)} = T_{a,1}^{(j)} \quad (14)$$

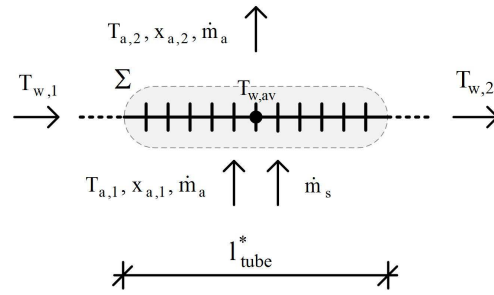
$$x_{a,1}^{(i)} = x_{a,i} \quad \text{and} \quad x_{a,2}^{(j-1)} = x_{a,1}^{(j)} \quad (15)$$

$$\dot{m}_a = \dot{m}_a^{(j-1)} = \dot{m}_a^{(j)} \quad (16)$$

$$\dot{m}_w = \dot{m}_w^{(j-1)} = \dot{m}_w^{(j)} \quad (17)$$

In Equations 13-17 subscripts 1 and 2 denote inlet and outlet conditions for the j row. Inlet temperature $T_{w,\text{in}}$ and mass flow rate \dot{m}_w of the process fluid as well as the thermo-hygrometric conditions ($T_{a,\text{in}}$, $x_{a,\text{in}}$) and mass flow rate \dot{m}_a of the air stream are typically given as inputs. In order to find the zeros of the system of equations (Equation 5), a root-finding method is necessary. After having reviewed several alternatives, Brent's method (Brent, 1973) is chosen. Brent's method is a hybrid root-finding method and it combines secant method, bisection method and inverse quadratic

Control volume Σ



Coil counter-flow arrangement

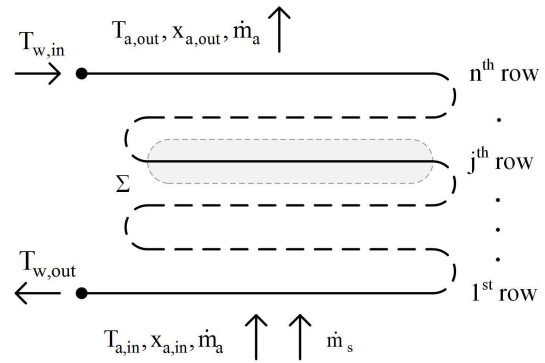


Fig. 4 – Identification of the finite control volume Σ as a coil row and its arrangement in a counter-flow configuration

interpolation based on Dekker's method (Dekker, 1969). It incorporates the guarantee of convergence as in the bisection method, but also takes advantage of the rapid rate of convergence of the less reliable methods (secant method or inverse quadratic interpolation).

This method can be used to determine a root α in the interval $[a,b]$ as long as $f(a)$ and $f(b)$ have different signs. In this problem the function f is the difference $\Delta\dot{Q}$ between the heat transfer rate on the air and process fluid. This function is calculated at any time step, and convergence is reached when the absolute value of the difference between the actual (k) and previous ($k-1$) iteration is lower than a user-defined tolerance σ (in Watt units).

$$\left| \Delta\dot{Q}^{(k)} - \Delta\dot{Q}^{(k-1)} \right| \leq \sigma \quad (18)$$

These convergence properties can be applied for a different set of operational conditions. In real applications outlet water temperature $T_{w,\text{out}}$ is controlled by varying the fan speed. In alternative

when the fan speed is set to the maximum value, the outlet temperature is sought.

The performance of Brent's convergence method is compared to the bisection method for the cases listed in Table 1.

Table 1 – Simulation boundary conditions

		Cases				
Inputs		01	02	03	04	05
Relative fan speed	ω/ω_{max} [-]	1	0.5	-	-	-
Process fluid inlet temp.	$T_{w,in}$ [°C]			40		
Process fluid mass flow rate	\dot{m}_w [kg/h]			3000		
Air inlet temp.	$T_{a,in}$ [°C]			25		
Air relative humidity	$\varphi_{a,in}$ [%]			50		
Process fluid	-			Water		
Setpoint outlet process fluid temp.	$T_{w,out,set}$ [°C]	-	-	35	30	25

For each of these, dry and wet conditions (denoted with "D" and "W", respectively) are considered. Wet conditions are determined by spraying water at a rate of 100 kg/h. When convergence is reached, equal values of rejected heat and fan electrical consumption is achieved. A relative measure of the convergence efficiency is proportional to the number of iterations. It can be appreciated as Brent method reaches.

Comparing the number of iterations, we can notice that the computational efforts determined by Brent's method are less than bisection method in the range of 10-69 % (Fig. 5).

Furthermore, the influence of the convergence tolerance σ for cases "D03", "D04" and "D05" of Table 1 is further investigated. The overall number of iterations and the relative error in the dissipated heat is calculated. Assuming that a low tolerance value ($\sigma=1 \times 10^{-4}$ W) will lead to an exact solution, we can notice that for the considered cases a good

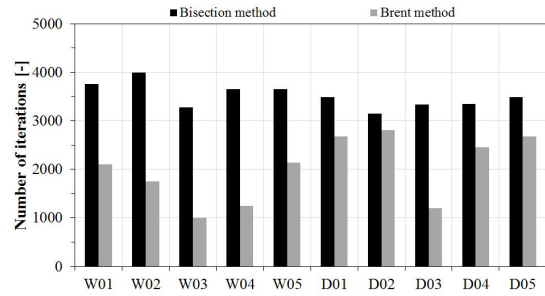


Fig. 5 – Influence of the convergence tolerance on the accuracy of the model and the related computational time for cases "D03", "D04", and "D05": comparison of bisection and Brent methods

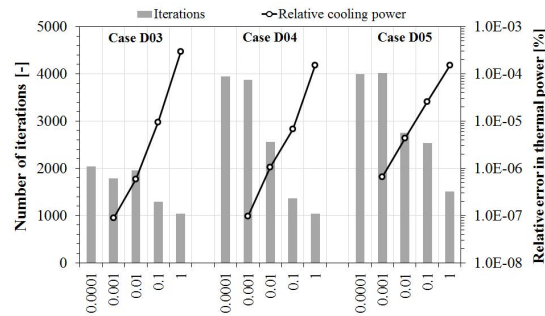


Fig. 6 – Influence of the convergence tolerance σ on the accuracy of the model and the related computational time for cases "D03", "D04", and "D05"

compromise between accuracy and computational time can be found (Fig. 6). This trade-off might change from case to case, according to the coil configuration and application.

3.3 Model Validation

Heat and mass transfer equations are written in FORTRAN with the aim of deriving a numerical model for TRNSYS simulation environment.

Geometry and technical characteristics of a commercial air-to-water hybrid cooler (model "RCS-08" provided by SorTech AG, Table 2) are used to setup the numerical model. Then it is validated using experimental data from a real installation where the hybrid cooler is operated under typical summer south European working conditions.

The process fluid is a mixture of 60 % water and 40 % glycol. This component was monitored continuously between May and September 2013 with a measurement interval of 1 minute. During this period, the following measurements were taken: dry-bulb temperature and relative humidity of ambient air, inlet/outlet process fluid temperature, mass flow rate and fan electrical consumption. The

spray water system was active for 10 seconds in a minute with an average mass flow rate of 200 kg/h. Tap water is used for the spray water system with an average temperature of about 10°C.

The uncertainty in water mass flow rate and temperature measurements is about 2 % and ± 0.3 K, respectively. The experimental error of the electrical sensor is identified at 0.25 % of measured values.

Table 2 – Nominal performance characteristics of the hybrid cooler "RCS-08" SorTech AG

Description		Value
Process fluid inlet temp.	$T_{w,in}$ [°C]	31.8
Process fluid mass flow rate	\dot{m}_w [kg/h]	3684
Air inlet temp.	$T_{a,in}$ [°C]	24.5
Air relative humidity	$\varphi_{a,in}$ [%]	50
Process fluid	-	Water
Spray water mass flow rate	\dot{m}_{spray} [kg/h]	0
Process fluid outlet temp.	$T_{w,out}$ [°C]	27
Heat transfer rate	\dot{Q} [W]	21000
Air volumetric flow rate	\dot{V}_a [m ³ /h]	13000
Max fan speed	ω_{max} [rpm]	890
Max fan electrical power	\dot{P}_{el} [W]	1320

3.3.1 Wettability factor

The validation of the wettability factor is not an easy task to perform, in particular on a real installation. The compactness of a coil assembly prevents the observation or the measurement of the water deposited on tubes and fins for each row.

Although a detailed validation of the wettability factor cannot be performed, the sensitivity analysis to a possible error in the calculation of the wet area could already provide a good insight.

This approach consists in assuming a given error in the calculation of the fins and tubes wet surface ΔA_{wet} . The wettability factors R_{wet} for each row are

then calculated together with the total transfer rate $\Delta \dot{Q}_{tot}$. For practical reasons, the variation of the wet area and the total heat transfer rate variations are provided in relative terms.

$$\delta A_{wet} = \Delta A_{wet} / A_{wet} \quad (19)$$

$$\delta \dot{Q}_{tot} = \Delta \dot{Q}_{tot} / \dot{Q}_{tot} \quad (20)$$

This test is carried out by operating the hybrid cooler with an inlet water temperature of 40 °C, an inlet air dry-bulb temperature of 25 °C, an air relative humidity of 50 %, and water mass flow rate of 3000 kg/h. The fan speed is operated at its maximum speed rate (890 rpm). Sprayed water rate amounts to 100 kg/h with a spray water cycle SFT of 0.1667.

The deviation in relative and absolute terms is shown in Fig. 7 and Fig. 8. It can be seen that despite a large deviation of wet surface area (± 60 %), the total heat transfer varies less than ± 5 %. On the contrary, a much larger variability is shown latent heat transfer (+30/-36 %). In absolute terms the deviation for the total heat transfer is between 42.9 kW and 46.4 kW.

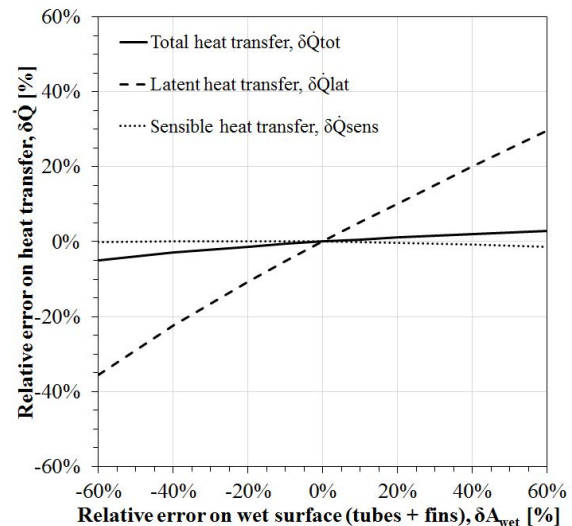


Fig. 7 – Relative error on heat transfer as a function of the relative error on wet surface calculation

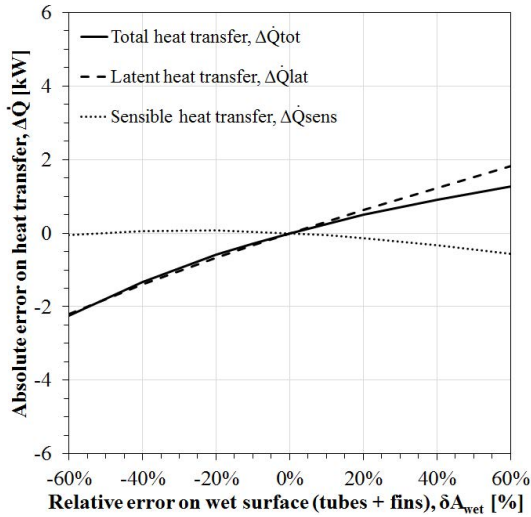


Fig. 8 – Absolute error on heat transfer as a function of the relative error on wet surface calculation

3.3.2 Heat transfer and electrical power

Fig. 9 and Fig. 10 show the comparison between the predicted and monitored instantaneous performances of the hybrid cooler with respect to the rejected heat \dot{Q}_{ch} and the fans electrical power \dot{P}_{el} , respectively.

The numerical model has an average error of 7 % for the rejected heat and 0.1 % for the fan power consumption. The major discrepancies are observed at low values of relative fan speed. This is due mainly to the fact that the pressure loss curve of the fan provided by the manufacturers does not contain specifications for an installed component.

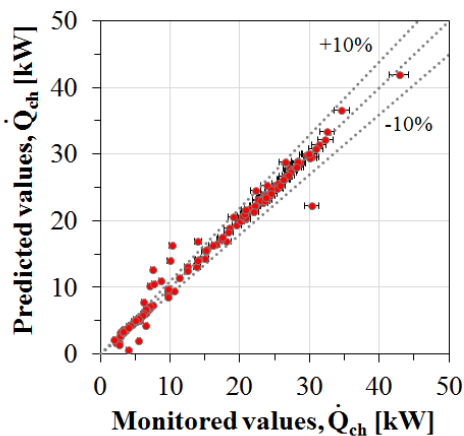


Fig. 9 – Comparison of rejected heat power between monitoring (x-axis) and experimental (y-axis) data

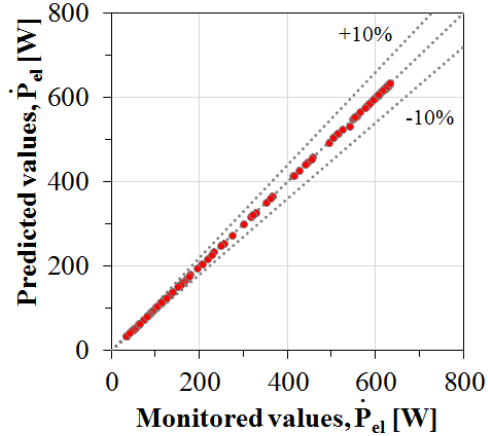


Fig. 10 – Comparison of fan electric power between monitoring (x-axis) and experimental (y-axis) data

4. Conclusion

The aim of the present work is the development of the numerical model of a hybrid cooler to be used for transient simulations purposes. The work is motivated by a raising interest in HVAC manufacturers due to its adaptability to a wide range of applications and the limitation of operation and maintenance costs with respect to traditional air-based condensing units.

The main features of the code elaborated are: (1) the definition of a modular geometry of the cooling coil, (2) the definition of water collection efficiency on coil surface due to a water jet sprayed upwards, (3) the possibility to develop tailored control strategies for water spray cycles, and (4) the implementation of dedicated control strategies to modulate the fan speed.

The model can be exploited for different purposes by HVAC industries and system designers. The influence of a hybrid cooler as an alternative heat rejection component for a whole system layout can be quantified. Dedicated control strategies for fan and spray water systems can be developed and easily implemented by the users in the simulation. Coil geometry and fans arrangements can be optimized for designing a custom-made water coil.

The numerical model was validated by using the monitored data of a pilot plant installation from May throughout September 2013. The model demonstrated to be in good agreement with the monitored performance, with errors of 7 % of the rejected heat and 0.1 % regarding the fan power.

Nomenclature

Symbols

A	Area (m ²)
C	Thermal capacity (W/K)
$c_{p,a}$	Specific heat of dry air (kJ/(kg K))
d	Diameter (m)
E	Collection efficiency (-)
h_c	Heat transfer coefficient (W/(m ² K))
h_m	Mass transfer coefficient (kg/(m ² s))
i	Enthalpy (kJ/kg)
l	Length (m)
l^*	Equivalent length (m)
Le	Lewis number (-)
\dot{m}	Mass flow rate (kg/s)
NTU	Number of transfer units (-)
K	Heat and mass transfer coefficient (kg/(m ² s))
\dot{P}_{el}	Electrical power (W)
\dot{Q}	Thermal power (W)
R_{wet}	Wettability factor (%)
SFT	Average spray cycle (-)
T	Temperature (K)
t	Thickness (m)
U	Heat transfer coefficient (W/(m ² K))
\dot{V}	Volumetric flow rate (m ³ /s)
v	Velocity (m/s)
w	Width (m)
x	Humidity ratio (kg _v /kg _a)
Δ	Variation / difference
ε	Effectiveness (-)
η	Fin efficiency (-)
λ	Thermal conductivity (W/(m K))
ϕ	Relative humidity (%)
ω	Rotational speed (rpm)
σ	Tolerance
Σ	Finite control volume
τ	Time (s)

Subscripts/Superscripts

a	Air
dep	Deposited
H	Referred to heat transfer
H+M	Referred to heat and mass transfer
i	Internal
in	Inlet
int	Interface

j	Generic row number
k	Iteration number
n	Row number
o	External
out	Outlet
s	Spray water
Sat	Saturation
W	Referred to process fluid
Wall	Coil surface

References

- Braun, J.E., S.A. Klein, J.W. Mitchell. 1989. "Effectiveness models for cooling towers and cooling coils". *ASHRAE Transactions* 92(2):164-174.
- Braun, J.E. 1988. *Methodologies for the design and control of central cooling plants*. PhD Thesis. Madison, U.S.A.: University of Wisconsin.
- Brent, R.P. 1973. *Algorithms for Minimization without Derivatives*. New Jersey, U.S.A.: Prentice Hall, Englewood Cliffs.
- Cossali, G.E., M. Marengo, M. Santini. 2005. "Single-drop empirical models for spray impact on solid walls: a review". *Atomization spray* 15: 699-736. doi: 10.1615/AtomizSpr.v15.i6.50.
- D'Antoni, M., D. Romeli, R. Fedrizzi. 2014. "Techno-economic analysis of air-to-water heat rejection systems". In: *Proceedings of EuroSun Conference*. Aix-les-Bains, France.
- Dekker, T.J. 1969. "Finding a zero by means of successive linear interpolation". In: *Constructive Aspects of the Fundamental Theorem of Algebra* edited by Wiley-Interscience. London, UK: Wiley.
- Dreyer, A.A., D.E. Kriel, P.J. Erens. 1992. "Analysis of spray-cooled finned-tube heat exchangers". *Heat Transfer Engineering* 13(4):53-71. doi: 10.1080/01457639208939788.
- ESDU 86018. 1991. *Effectiveness-NTU relations for the design and performance evaluation of two stream heat exchangers*. Engineering Science Data Unit 86018. London, UK: ESDU.
- Finstad, K.J., E.P. Lozowski, E.M. Gates. 1987. "A computational investigation of water droplets trajectories". *Journal of atmospheric and oceanic technology* 5: 160-169. doi: 10.1175/1520-0426(1988)005<0160:ACIOWD>2.0.CO;2.

- Gnielinski, V. 1976. "New equation for heat and mass transfer in turbulent pipe and channel flow". *International Chemical Engineering* 16: 359-368.
- Klein, S.A., et al. 2010. *TRNSYS v.17. A transient system simulation program*. Madison, U.S.A.: Solar Energy Laboratory, University of Wisconsin.
- Korte, C.M., A.M. Jacobi. 1997. *Condensate retention and shedding effects on air-side heat exchanger performance*. ACRC TR-132 report. Campaign, U.S.A.: Air Conditioning and Refrigeration Center, University of Illinois.
- Kriel, D.E. 1991. *Prediction and measurement of the performance of spray cooled heat exchangers*. Master Thesis. Stellenbosch, South Africa: University of Stellenbosch.
- McQuiston, F.C. 1978. "Heat, mass and momentum transfer data for five plate-fin-tube heat transfer surfaces". *ASHRAE Transactions* 84: 266-293.
- Nakayama, W., H. Kuwahara, S. Hirasawa. 1988. "Heat transfer from tube banks to air/water mist flow". *International Journal of Heat and Mass Transfer* 31 (2): 449-460. doi: 10.1016/0017-9310(88)90027-0.
- Romeli, D., 2014. *Modelling of spray cooling air-water heat exchanger*. Master. Thesis. Bergamo, Italy: University of Bergamo.
- Scheller, B.L., D.W. Bousfield. 1995. "Newtonian drop impact with a solid surface". *AIChE Journal* 41: 1357-1367. doi: 10.1002/aic.690410602.
- Sen, G.N. 1973. *Heat transfer during air-water mist flow across annular finned-tube banks*. PhD Thesis. Strathclyde, UK: University of Strathclyde.
- Shah, R.K., A.L. London 1978. *Laminar Flow Forced Convection in Ducts*. New York, U.S.A.: New York Academic Press.
- Stuempfle, A.K. 1973. *Impaction efficiency of cylindrical collectors in laminar and turbulent fluid flow*. Edgewood Arsenal Technical Report. Edgewood, U.S.A.: Department of Army.
- Wallis, G.B. 1969. *One-dimensional two-phase flow*. New York, U.S.A.: McGraw-Hill.
- Wang, C.C., Y.C. Hsieh and Y.T. Lin. 1997. "Performance of plate finned tube heat exchangers under dehumidifying conditions". *Journal Heat Transfer* 119: 109-117. doi: 10.1115/1.2824075.
- Yang, W.J., D.W. Clark 1975. "Spray cooling of air-cooled compact heat exchangers". *International Journal of Heat and Mass Transfer* 18: 311-317. doi: 10.1016/0017-9310(75)90162-3.

Selecting Roller Shades Properties Based on Glare Mitigation, Energy Performance and Connection to the Outdoors

Iason Konstantzos – Purdue University – ikonsta@purdue.edu

Athanasios Tzempelikos – Purdue University – ttempel@purdue.edu

Abstract

Visual comfort is one of the main priorities in designing working and living environments. Several indicators have been developed to quantify the degree of visual discomfort; however, there is a lack of studies in spaces with roller shades on the windows, commonly used in North America. Roller shades transmit direct and diffuse daylight and therefore their effect on visual comfort is complex. A recent study with human subjects proposed two alternative approaches in quantifying visual discomfort for the case of roller shades, based on (i) a modification of the Daylight Glare Probability (DGP) and (ii) an index based on the direct and the total portion of vertical illuminance on the eye of the observer. This paper uses a methodology based on the newly developed indices in an inverse way in order to propose suitable ranges for optical properties of the shade fabrics, in terms of openness factor and visible transmittance. A complex fenestration model that calculates the angular beam-beam and beam-diffuse shading optical properties is implemented within an advanced hybrid ray-tracing and radiosity daylighting model. Then, the concepts of annual discomfort frequency (Chan et al., 2015) and View Clarity Index (Konstantzos et al., 2015b) are used as a basis for the extraction of ranges of shade optical properties with respect to glare mitigation, energy performance and connection to the outdoors, for different sets of input parameters (location, orientation, glazing visible transmittance and distance from the window). The use of these extracted ranges can help architects select the most suitable shading products for their designs, minimizing glare complaints with the minimum cost in terms of lighting energy use and connection to the outdoors.

1. Introduction – Literature Review

Roller shades are an efficient and widely used shading approach, especially in perimeter office spaces; they combine solar and visual protection with aesthetically appealing presence. The selection of their properties can affect all three important aspects of the visual environment; visual comfort, in terms of mitigating glare, energy potential, by means of reducing required lighting energy, and connection to the outdoors.

There have been quite a few studies associating the fabric properties with energy performance, especially when combined with efficient shading control algorithms (Tzempelikos and Athienitis, 2007; Shen and Tzempelikos, 2012). However fewer studies take into account the important factor of visual comfort (Konstantzos et al., 2015a; Chan et al., 2014; Atzeri et al., 2014; Chan et al., 2015). The latter paper proposed a systematic method of selecting appropriate shading properties towards mitigation of glare and increase of energy performance. For the investigation of glare, based on concerns expressed in a study by Konstantzos et al. (2015a) about potential inconsistencies of Daylight Glare Probability – DGP (Wienold and Christoffersen, 2006) when used in cases of facing the sun through fully applied shading fabrics, used a reasonable approach of a double illuminance criterion; using a threshold for the direct part of vertical illuminance to account for annual hours with the sun in the field of view and a threshold for the total vertical illuminance for the rest of the annual hours. In a recent study, Konstantzos and Tzempelikos (2016a) conducted an experiment with human subjects to evaluate the applicability of such a double criterion, and proposed two new discomfort indices, one luminance-based and one illuminance-based, to be used when the sun is visible

through shading fabrics. Konstantzos et al. (2015b) investigated the impact of fabric properties in the clarity of view, shedding light on the connection to the outdoors with roller shades and introduced the View Clarity Index, a quantification of clarity based on the two most commonly available fabric properties, openness factor and visible transmittance.

This paper will propose a methodology to select suitable ranges for the optical properties of shading fabrics in terms of openness factor and visible transmittance with respect to glare mitigation, energy performance, and connection to the outdoors, using the newly proposed GlareEV and VCI indices to assess visual comfort and connection to the exterior respectively.

2. Methodology

2.1 Optical Properties of Roller Shades

Shading fabrics are characterized by a set of properties that identify their color and optical characteristics. That includes the openness factor (OF), the visible transmittance (TV) and the front and back reflectivities (RV). Among these, the ones that are primarily connected with the visual environment are the openness factor and the visible transmittance.

The openness factor reflects the weave density of the fabric and is an indication of the direct light being transmitted within it. Openness factors theoretically range from 0 (translucent fabrics) to 20 %, however most widely used fabrics are ranging from 1 % to 7 %, as higher values are often associated with conditions of visual discomfort and disability glare, while lower values have a negative impact on the outside view.

The visible transmittance reflects the total portion of illuminance transmitted through the fabric and is also an indirect indicator of the fabric's color; light-colored fabrics have higher T_v compared to darker fabrics of the same openness factor due to the additional allowed direct-to-diffuse light transmission.

The two aforementioned optical properties are commonly available by the fabrics' manufacturers, and their impact is highly dependent on the incidence angle of the incident light transmitted through the window.

2.2 A Suite of Metrics to Assess the Visual Environment

A strategy of maximizing lighting energy performance and connection to the outdoors while keeping visual comfort as a constraint constitutes a straightforward decision making process, which can be used either in existing buildings, in terms of retrofitting, or to optimize the design of new spaces, in terms of orientations, façade configurations, control methods or even spatial layouts according to the specific needs and functions of the space. The above can be all linked in one main annual metric, the Visual Environment Index (Konstantzos and Tzempelikos, 2016b), which consists of three parts: VEIc, related to visual comfort, VEIe, focusing on lighting energy performance and VEIv covering the connection to the outdoors (outside view). In this study, the same principles are used to propose a method of selecting optimal fabric properties for a given space.

The Visual Comfort Autonomy or VCA is defined as the portion of annual working hours when a person in a specific position and under a selected viewing direction is under visually comfortable conditions. VCA is a framework to evaluate discomfort, and can use any fitting discomfort index on a case-specific basis. For the needs of this study, where the shading fabrics are considered to be fully applied, the newly proposed discomfort index GlareEv (Konstantzos and Tzempelikos, 2016a) is used for the instances where the sun is within the field of view (Eq. 1), while a threshold for DGPs (Wienold, 2007) of 0.35, essentially associated with a 2760 lux threshold for the total vertical illuminance, is applied for all other cases.

$$Glare_{Ev} = 0.13 \cdot E_{v,dir(sun)}^{0.27} + 0.04 \cdot \left(\frac{E_v}{E_{v,dir(sun)}} \right)^{0.84} - 0.48 \quad (1)$$

$$\begin{cases} Glare_{Ev} < 0.41, sun \in FOV \\ DGPs < 0.35, sun \notin FOV \end{cases} \quad (2)$$

$$DGPs = 6.22 \times 10^{-5} \times E_v + 0.184 \quad (3)$$

where $E_{v,dir(sun)}$ is the direct vertical illuminance from the sun in the field of View and E_v is the total

vertical illuminance on the eye level. GlareEV is preferred over other luminance-based metrics as, due to its illuminance-based nature, it involves simpler calculations and faster simulations compared to more accurate metrics as DGPmod that require the calculation of detailed luminance mappings for each time step.

In order to comply with the VCA restrictions and constitute a space as comfortable, and also based on the study of Chan et al. (2015), there are two approaches to consider; (i) a reasonable standard of accepting a total of 5 % of annual working hours to be associated with discomfort (equivalent to $VCA \geq 0.95$) and (ii) a stricter consideration, of maintaining comfortable conditions for the entire working time of the year (equivalent to $VCA=1$). In lack of related literature focused on annual human subjects studies, it is unclear which of the two better complies with everyday practice; as visual discomfort does not occur in a transient form, it is important to eliminate every possible instance of discomfort in order to design glare-free indoor environments. Therefore, in this study only the safest approach ($VCA=1$) will be investigated, targeting to eliminate every single instance of glare. It can be inferred by reason that more flexible considerations might be also feasible, and the extent to which a space is protected from discomfort glare can be a decision of the architect, depending also on the operational objective of a space.

To account for the connection to the outdoors, the recently proposed View Clarity Index (Konstantzos et al., 2015b) is utilized (Eq. 4), associating the clarity of view with the openness factor and visible transmittance of the applied fabric.

$$VCI = 1.43 \cdot (OF)^{0.48} + 0.64 \cdot \left(\frac{OF}{T_v}\right)^{1.1} - 0.22 \quad (4)$$

The latter was extracted in a human subjects study using a diverse questionnaire, defining clarity through various aspects (subjective and objective questions about visual acuity, color perception, distinguishability of given targets e.a.), and associates the clarity of view with the two most commonly available optical properties.

For the consideration of the energy performance, the continuous Daylight Autonomy (cDA) is used (Rogers, 2006). The latter index is mostly efficient

for cases of light dimming, which is becoming a standard in green building, and gives partial credit for the times in which daylight illuminance is below the level of 300 lux, in order to comply with the IES standard LM-83-12 (IESNA, 2012).

2.3 Method Description

The proposed method targets to recommend fabric properties to be used in perimeter office spaces with respect to visual comfort, connection to the exterior, and lighting energy performance.

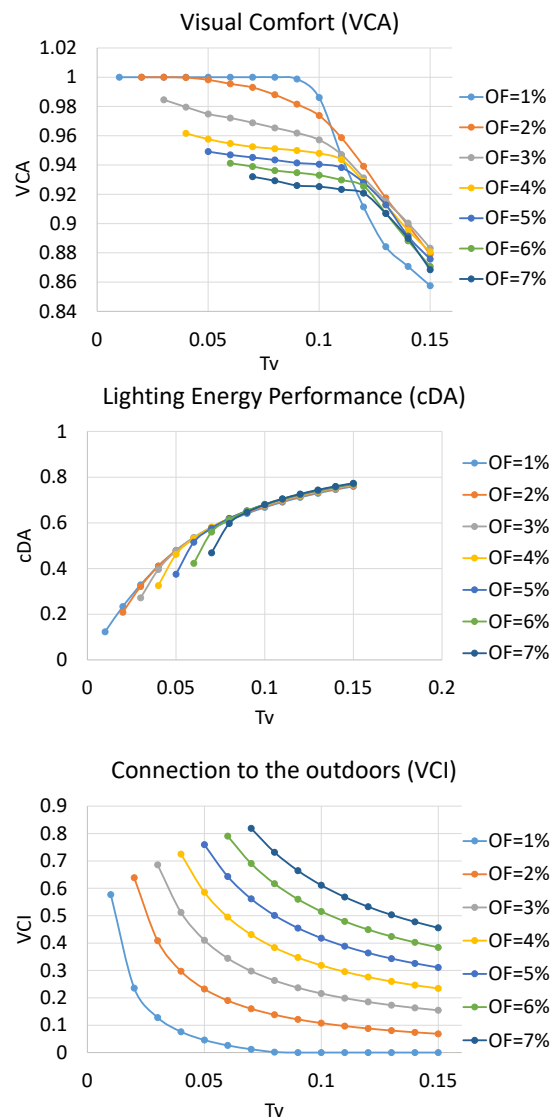


Fig. 1 – Impact of fabric properties on the three main factors of the visual environment; examples for south orientation and 1.75 m distance from window.

Among these goals, visual comfort is considered to be the most important, as discomfort can have negative effects, ranging from slight decrease in per-

formance to serious disability of performing office work. Therefore, in the proposed method, visual comfort is used as a constraint, using the strict approach presented in 2.1 for the total elimination of discomfort instances. The use of VCA as a constraint gives acceptable ranges of fabrics, in terms of openness factor and visible transmittance.

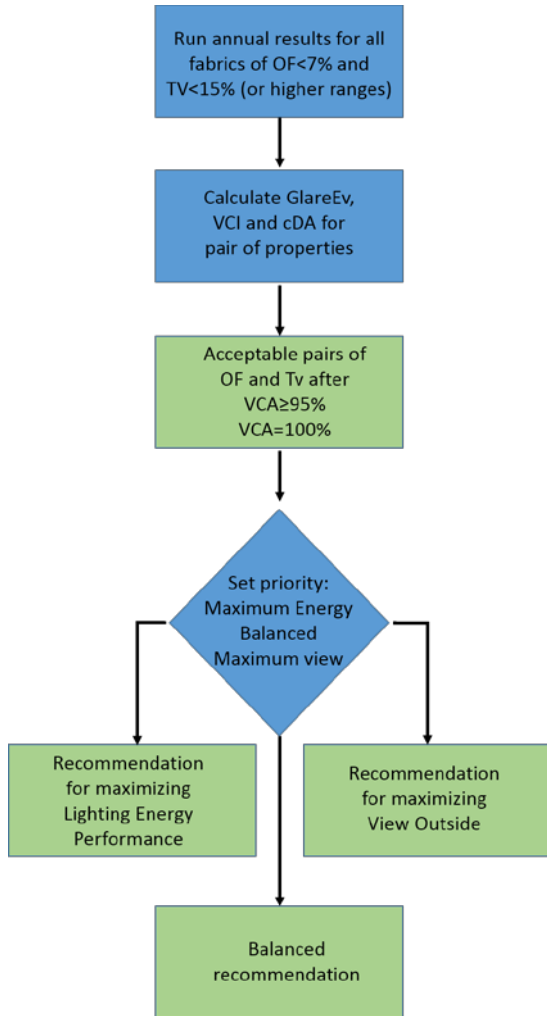


Fig. 2 – Proposed method flow-chart

However, lighting energy performance and connection to the outdoors are two contradicting objectives; lighting energy performance is by definition higher with increasing visible transmittance (portion of transmitted light through the fabric), while connection to the outdoors is negatively affected by the same increase (Konstantzos et al., 2015b). Therefore, in this study, three main different approaches are being presented when it comes to the two secondary objectives (view and lighting energy performance); proposing the optimal fab-

rics for (i) maximizing view, (ii) maximizing energy performance, and (iii) provide a balanced result of the two. Fig. 1 shows the impact of the fabric properties on the three main factors of the visual environment, while Fig. 2 shows a comprehensive flow chart of the proposed methodology.

While the cases of maximizing energy or view can be straightforward, the weighting of the two attributes for the balanced case cannot be conclusively decided due to the difference in nature of the two parameters. Therefore, and until more light is shed on that matter, for this study, two different objectives will be used to extract the optimal results for the balanced case: (i) a criterion of having the two attributes equally weighted (Bal.EW), which will at times compromise both view and energy performance to very low values and (ii) a flexible criterion (Bal.FL) which will first require each of the attributes to be over a minimum value of 0.25, and then search for the pair which will lead to the two attributes as much equally weighted as possible given that none of the two would get very low values. The objective for the balanced approach is shown in Equations 5 and 6, as the pair of points with the minimum distance from the dichotomous line of the Cartesian system without or with the minimum restrictions respectively.

$$\min\left(\frac{VCI_i - cDA_i}{\sqrt{2}}\right) \tag{5}$$

$$\min\left(\frac{VCI_i - cDA_i}{\sqrt{2}}\right), \text{ with } VCI_i, cDA_i \geq 0.25 \tag{6}$$

The authors believe that a compromise of the connection to the outside would affect the perception of daylight in the space, so it shouldn't be underestimated. A sample Pareto front chart of the four decision making approaches can be seen in Fig. 3; the points of the graph represent the combinations of OF and Tv that are eligible for use after the VCA≥95 % restriction, the green point is the optimal fabric to maximize view (OF=4 %-Tv=4 %), the yellow point the optimal fabric to maximize lighting energy performance (OF=2 %-Tv=11 %), the red point reflects the equally weighted balance of the two attributes (here fabric OF=1 % and Tv=2 %), and the black point shows the flexible balance (here OF=4 %-Tv=6 %).

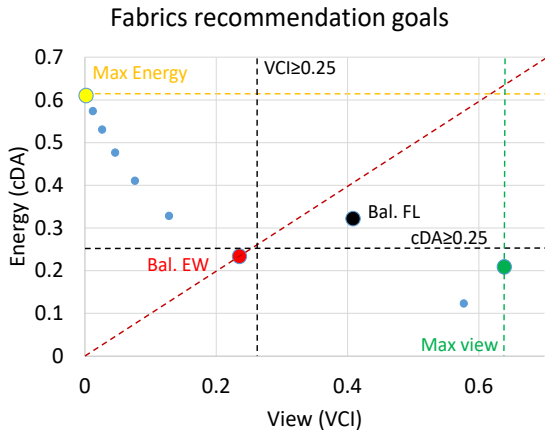


Fig. 3 – Pareto Front chart showing the logic of optimal pairs selection – results for south orientation, 1.75 m from the window and the strict VCA restriction (VCA=1)

2.4 Modeling Methodology

A hybrid ray-tracing and radiosity daylighting model with a glare module is used for the calculations of VCA and continuous daylight autonomy for the suggested configurations. The model consists of four main parts, the first simulating the exterior lighting conditions (direct and diffuse illuminance on the exterior of the window), based on TMY3 weather files, the second simulating the properties of the complex fenestration system (glazing and dynamic shading), the third calculating the interior mapping for luminances and illuminances over a specified grid, and the fourth finally calculating the glare index for each position and viewing direction of interest. We use the model by Perez et al. (1987) to calculate the diffuse sky illuminance distribution. For the interior illuminance and luminance distributions calculations, the hybrid ray tracing and radiosity module (Chan and Tzempelikos, 2012) was implemented. Ray tracing is used to capture the sun's position and the directly lit areas in the interior. Then, the radiosity method uses the initial exitances obtained above to apply the inter-reflections of the interior surfaces and calculate the final luminance and illuminance distribution in the interior for the desired grid of positions, while all surfaces densely discretized in order for the glare module to accurately identify the glare sources which will be taken into account in the equations. The model has been validated with experiments (Chan et al, 2014). The detailed beam-diffuse and off-normal properties of the roll-

er shades were calculated using the semi-empirical method introduced by Kotey et al. (2009). This model, which proved to be accurate and reliable for several types of standard (PVC-coated and vinyl) fabrics, calculates the beam-beam and beam-total visible transmittance angular variation as a function of the incidence angle and the normal OF and Tv properties, provided by manufacturers. The latest version of EnergyPlus (2015) includes this angular model in the “window thermal calculation module”, as part of the new “equivalent layer fenestration model”. In summary, the angular beam-beam shade transmittance (τ_{bb}) is calculated from:

$$\tau_{bb}(\theta) = \tau_{bb}(0) \times \left(\cos \left(\frac{\pi}{2} \times \frac{\theta}{\theta_{cut-off}} \right) \right)^b \quad (6)$$

where θ is the solar incidence angle, $\tau_{bb}(0)$ is the beam-beam transmittance at normal incidence, assumed equal to the OF of the fabric (provided by manufacturers), and b and $\theta_{cut-off}$ are parameters that depend on $\tau_{bb}(0)$, as explained in Kotey et al. (2009). The angular beam-total transmittance (τ_{bt}) is calculated from:

$$\tau_{bt}(\theta) = \tau_{bt}(0) \times (\cos\theta)^d, \left\{ \theta < \theta_{cut-off} \right\} \quad (7)$$

where $\tau_{bt}(0)$ is the beam-total transmittance at normal incidence (total visible transmittance provided by manufacturers) and d is a parameter that depends on openness factor and total visible transmittance. The cut-off angle should not be applied to light-colored fabrics, to account for direct light scattering at higher angles, while small corrections might be needed for dark-colored fabrics (Tzempelikos and Chan, 2016). The beam-diffuse transmittance, necessary for the accurate modeling of light transfer through shades, is then equal to $\tau_{bt} - \tau_{bb}$ for each angle. Finally, integrating τ_{bt} over the hemisphere yields the diffuse-diffuse shade transmittance (τ_{dd}), which cannot be measured or calculated otherwise.

As a geometry for the current study, a private office space is selected with a floorplan of 5m x 5m and height of 3.4m with a 70% WWR. Also, a standard double clear glazing system is used, to be compatible with most existing perimeter office spaces. The results are presented for two different distances from the window (0.75 m, 1.75 m) and for

the four main orientations (S,W,E,N). The location of the simulations was chosen to be Lafayette, IN.

3. Results - Discussion

Table 1 shows the allowed combinations of fabric properties based only on visual comfort, for a viewing distance of 1.75 m from the window. The number in brackets characterizes the maximum permitted visible transmittance (Tv) for the given openness factor.

Table 1 – Allowed fabric combinations for 1.75 m (VCA=1)

S	1 % (8 %), 2 % (3 %)
W	1 % (8 %), 2 % (3 %)
E	1 % (10 %), 2 % (8 %)
N	No restriction

The above permitted combinations can be used in order to comply with the visual comfort constraint. However, in order to take advantage of the full potential in terms of lighting energy performance, outside view or a balanced combination of the two, the method presented in 2.3 can propose the optimal pairs for each case. These can be seen in Table 2:

Table 2 – Fabric recommendations for 1.75 m (VCA=1)

	View	Energy	Bal. EW	Bal. FL
S	2%-2%	1%-8%	1%-2%	2%-3%
W	2%-2%	1%-8%	1%-2%	2%-3%
E	2%-2%	1%-10%	2%-4%	2%-4%
N	N/A	N/A	N/A	N/A

In cases where the immediate area near the window needs to host occupants, the results are modified as seen in Tables 3 and 4. Due to the poor sunlight exposure of northern facades in the northern hemisphere, no recommendations are stated for this orientation, as all fabrics in the evaluated range meet the strict VCA criterion of zero glare hours.

It can be derived by the results that the impact of the direct-to-direct and direct-to-diffuse portion of the fabrics, depending on their properties, can affect the results in different ways for different objectives; to maximize the clarity of view, the objective is to achieve an openness factor close to the visible

transmittance, in order to minimize the direct-to-diffuse portion of the light transmission. The latter however is essential to increase the lighting energy performance of the space by maximizing daylight illuminance. Therefore, when focused on energy performance, the objective is for a given openness factor to use the maximum permitted visible transmittance.

Table 3 – Allowed fabric combinations for 0.75 m (VCA=1)

S	1 % (5 %), 2 % (2 %)
W	1 % (5 %), 2 % (2 %)
E	1 % (6 %), 2 % (6 %)
N	No restriction

Table 4 – Fabric recommendations for 0.75 m (VCA=1)

	View	Energy	Bal. EW	Bal. FL
S	2%-2%	1%-5%	1%-2%	2%-2%
W	2%-2%	1%-5%	1%-2%	2%-2%
E	2%-2%	2%-6%	1%-2%	2%-3%
N	N/A	N/A	N/A	N/A

When attempting to balance the two attributes, it can be clear by the results that at times there is a significant compromise in both of them, if the criterion is a strict consideration of equal weights. If however this criterion switches to a more flexible approach, it is possible to achieve satisfactory results for both secondary aspects of the visual environment.

In addition, the results also reflect the definition of the GlareEV index, which was used to form the visual comfort constraint; the latter takes into account both direct and total parts of the vertical illuminance, and due to its form, having the portion of the two as a variable, also accounts for the interaction of the two, in terms of direct-to-direct and direct-to-diffuse light transmission. Positions closer to the window are more prone to be affected by the increased total vertical illuminance of brighter fabrics, therefore the recommended upper limits of visible transmittance are lower when approaching the window.

Should a less strict criterion be selected, allowing a minimum of 95 % of the annual working hours to be complying with the visual comfort restrictions, the upper limits of the fabric properties become more flexible, as shown in Table 5.

Table 5 – Allowed fabric combinations for 0.75 m (VCA>0.95)

S	1 % (6 %), 2 % (7 %), 3 % (6 %), 4 % (4 %)
W	1 % (6 %), 2 % (7 %), 3 % (5 %)
E	1 % (8 %), 2 % (9 %), 3 % (9 %), 4 % (8 %)
N	No restriction

However, glare occurrences for up to 5 % of annual working hours, associated with the VCA>0.95 limitation, get essentially translated to up to 200 hours of visually uncomfortable conditions annually. Due to the nature of visual discomfort (potentially instantaneous) and the resolution of the annual simulations (hourly time steps reflecting the available weather data), the authors believe that a strict consideration of zero glare hours, as reflected in Tables 1 to 4 is the most conservative approach towards glare-free zones in indoor environments.

4. Conclusion

This paper presented a methodology to recommend optical properties of shading fabrics in terms of openness factor and visible transmittance with respect to glare mitigation, energy performance, and connection to the outdoors, using the newly proposed GlareEV and VCI indices to assess visual comfort and connection to the exterior respectively. Visual comfort was used as a constraint, aiming to ensure glare free conditions for the entire portion of annual working hours, while the two contradicting objectives of lighting energy performance and connection to the outdoors were handled using four different objectives.

The results showed that openness factors should be always kept within 2 % in order to ensure visual comfort throughout the entire year, with visible transmittance upper limits ranging from 8% for southern facades to 10 % for eastern facades. For positions closer to the window, and in order to account for the potential increase of the total vertical illuminance due to the higher visible window surface, lower limits of visible transmittance are recommended. To maximize view to the outside, openness factor values close to the visible transmittance are recommended in order to minimize the direct to diffuse portion of the light transmission, while to maximize lighting energy performance,

the key is increasing the aforementioned portion by using a visible transmittance much higher than the openness factor.

Future work includes the development of a unified fabric rating index that will be used in design as a fabric selection tool, as well as an investigation of the thermal implications caused by fabric selection based on the visual environment performance. Annual comfort metrics, zonal, spatial and temporal, with respect to usability and availability (Atzeri et al., 2016), should be used for such an analysis.

Acknowledgement

This work is supported by Alcoa Foundation and Lutron Electronics Co Inc.

References

- Atzeri A.M., F. Cappelletti, A. Gasparella, H. Shen, A. Tzempelikos. 2014. "Assessment of long-term visual and thermal comfort and energy performance in open-space offices with different shading devices". In: *Proceedings of 3rd High Performance Buildings conference at Purdue*. West Lafayette, U.S.A.: Purdue University.
- Atzeri A.M., F. Cappelletti, A. Tzempelikos, A. Gasparella. 2016. "Comfort metrics for an integrated evaluation of buildings performance". *Energy and Buildings* 127: 411-424. doi: 10.1016/j.enbuild.2016.06.007.
- Chan, Y.C., A. Tzempelikos. 2012. "A hybrid ray-tracing and radiosity method for calculating radiation transport and illuminance distribution in spaces with venetian blinds". *Solar Energy* 86(11): 3109-3124. doi: 10.1016/j.solener.2012.07.021.
- Chan Y.C., I. Konstantzos, A. Tzempelikos. 2014. "Annual daylight glare evaluation for typical perimeter offices: simulation models versus full-scale experiments including shading controls". In: *Proceedings of ASHRAE Annual Conference*. Seattle, U.S.A.: ASHRAE.
- Chan, Y.C., A. Tzempelikos, I. Konstantzos. 2015. "A systematic method for selecting roller shade properties for glare protection". *Energy and*

- Buildings* 92: 81-94. doi: 10.1016/j.enbuild.2015.01.057.
- EnergyPlus 2015. *Energyplus Engineering Reference – the reference for Energyplus Calculations*. Berkeley, U.S.A.: Lawrence Berkeley National Laboratory (LBNL).
- IESNA. 2012. *Approved Method: IES Spatial Daylight Autonomy (sDA) and Annual Sunlight Exposure (ASE)*. Illuminating Engineering Society of North America
- Konstantzos, I., A. Tzempelikos, Y.C. Chan. 2015a. "Experimental and simulation analysis of daylight glare probability in offices with dynamic window shades". *Building and Environment* 87: 244-254. doi: 10.1016/j.buildenv.2015.02.007.
- Konstantzos, I., Y.C. Chan, J. Seibold, A. Tzempelikos, R.W. Proctor, B. Protzman. 2015b. "View Clarity Index: a new metric to evaluate clarity of view through window shades". *Building and Environment* 90: 216-214. doi: 10.1016/j.buildenv.2015.04.005.
- Konstantzos, I., A. Tzempelikos. 2016a. "Daylight Glare Evaluation with the Sun in the Field of View through Window Shades". *Building and Environment* 113: 65-67. doi: 10.1016/j.buildenv.2016.09.009.
- Konstantzos, I., A. Tzempelikos. 2016b. "A holistic Approach for Improving Visual Environment in Private Offices". In: *Proceedings of SBE 16*. Thessaloniki, Greece.
- Kotey N.A., J. Wright, M.R. Collins. 2009. "Determining off-normal solar optical properties of roller blinds". *ASHRAE Transactions* 117 (1).
- LBNL 2013. *WINDOW 7 simulation manual*. Berkeley, U.S.A.: Lawrence Berkeley National Laboratory.
- Perez, R., R. Seals, P. Ineichen, R. Stewart, D. Menicucci. 1987. "A new simplified version of the Perez diffuse irradiance model for tilted surfaces". *Solar Energy* 39(3): 221-231. doi: 10.1016/S0038-092X(87)80031-2.
- Rogers, Z. 2006. *Daylighting Metric Development Using Daylight Autonomy Calculations in the Sensor Placement Optimization Tool*. Boulder, U.S.A.: Architectural Energy Corporation.
- Shen, H., A. Tzempelikos. 2012. "Daylighting and energy analysis of private offices with automated interior roller shades". *Solar Energy* 86(2): 681-704. doi: 10.1016/j.solener.2011.11.016.
- Tzempelikos, A., A.K. Athienitis. 2007. "The impact of shading design and control on building cooling and lighting demand". *Solar Energy* 81 (3): 369-382. doi: 10.1016/j.solener.2006.06.015.
- Tzempelikos, A, Y.C. Chan. 2016. "Estimating detailed optical properties of window roller shades from basic available data and modeling implications on daylighting and visual comfort". *Energy and Buildings* 126: 396-407. doi: 10.1016/j.enbuild.2016.05.038.
- Wienold, J. 2007. "Dynamic simulation of blind control strategies for visual comfort and energy balance analysis". In: *Proceedings of IBPSA 2007 Conference*, Beijing, China: IBPSA.
- Wienold, J., J. Christoffersen. 2006. "Evaluation methods and development of a new glare prediction model for daylight environments with the use of CCD cameras". *Energy and Buildings* 38(7): 743-757. doi: 10.1016/j.enbuild.2006.03.017.

Dynamic Simulation of the Influence of Fenestration on Buildings Energy Consumption. A Comparison Between Northern and Southern Europe

Angelo Spena – University of Roma Tor Vergata – spena@uniroma2.it

Viola Iaria – University of Roma Tor Vergata – iaria.viola@libero.it

Carlo Mazzenga – University of Roma Tor Vergata – mazzengacarlo@gmail.com

Abstract

Dynamic simulation allows us to foresee the actual behavior of a building as a whole, namely of the envelope, its occupants, and HVAC equipments. This approach requires a huge amount of data of current inhomogeneous variables related to local climate, shelter's shapes and materials, fenestration and lighting technologies, mechanical and electrical facilities, air quality needs, etc. Consistency and accuracy of input data, together with a comprehensive and integrated knowledge of the performance of all the parts involved, act as the crucial points of the process. The paper, by means of a proprietary simulation SW proposed and used in the past by one of the Authors, shows first results in terms of impact of different degrees of buildings fenestration on needs of energy for either lighting and air conditioning. Conflicting opportunities when comparing locations in Southern (Rome) and in Northern (Berlin) Europe are found. A focus on crucial points is made using a case study as a reference.

1. Introduction

The correct evaluation of energy consumption of buildings is a necessity either to fulfill legal obligations, either to find the fittest improvements for existing buildings. Dynamic simulation models allow us to enhance the representation of the physical characteristics of the materials and to deeply forecast the effects of any change of the envelope and/or the plant facilities (Hensen and Nakahara, 2001; Hensen and Lamberts, 2011; Reddy, 2006). In the present paper we will stress a basic aspect often underestimated: the study of the lighting system with respect to the daylighting contribution (Fon-

toynont, 1999). This actually influences the overall energy consumption of buildings, as much as they are highly performing from the merely thermal point of view (Bazjanac, 2004; Fumo et al., 2009).

2. Aim of the Work

The purpose of the work is to evaluate and compare the different energy needs of an overall building-plant system (in terms of thermal, cooling, and electric demand) when varying both fenestration and climatic conditions, through the implementation and execution of a computer code (Spena, 1984) acting as a dynamic simulation model. The comparison will be carried out on different scenarios referring to a base-case, focusing on the influence of different kinds of glass of the frames, as follows:

- Fenestration:
 - Double glass, low emissivity (base-case)
 - Single glass, low emissivity
 - Triple glass, low emissivity.
- Locations and scenarios:
 - South Europe (city of Rome), standard building broadly exposed to insolation (base-case)
 - South Europe (Rome), building with smaller window's areas, and actually sun-shaded
 - South Europe (Rome), fully shaded building (no direct sunlight)
 - North Europe (city of Berlin), standard building broadly exposed to insolation
 - North Europe (Berlin), building with smaller windows areas, and actually sun-shaded

- North Europe (Berlin), fully shaded building (no direct sunlight).

The case study is the model of a real building located in Rome, used as an office from Monday to Friday in the daily range of 7 am–8 pm. The characteristics of the overall building-plants system together with the input data considered will be displayed in § 4, 5, 6.

3. Climate Simulation

3.1 The Stabilized-Periodic Regime

In order to get a correct energy need for HVAC plants, a detailed knowledge of the thermal behavior of the building during time is necessary. For this purpose, the study of heat transfer must be taken considering the stability of a harmonic thermal fluctuation (Clarke, 2001; Fisher and Pedersen, 1997). The temperature-response of the system was obtained from the Fourier’s general equation resolution under realistic boundary conditions. For the wall’s temperature on the inner face we used:

$$T_{pi}(s, t) = \bar{T}e + \theta * e^{-\beta s} * \text{sen}(\omega t - \beta s) \quad (1)$$

Inside the wall, anywhere at an x -distance from the outer face, we supposed a temperature periodic oscillation delayed and damped when compared with the fluctuation acting on the outer side.

Both damping and phase-delay are functions of the parameter β : it depends on material’s properties, according to the expression:

$$\beta = \sqrt{\frac{\pi}{a * \tau_0}} \quad (2)$$

This assumption, valid for a single-layer, may be extended to multi-layer walls by introducing (Tabunschikov, 1993) an equivalent homogeneous wall. Solar radiation on the outer surface is also taken into account, by means of the “sun-air temperature” (ASHRAE, 2000).

3.2 Insolation and IR Radiation

Solar radiation on the building surfaces affects both the thermal loads due to transmission through opaque and transparent walls, and the loads due to solar gains by transparency (Gugliermetti et al., 2004). The radiation intensity on the building sur-

faces not only depends on geographical coordinates, hour of the day, and sky conditions, but also varies according to the exposure of the lighted area (Spena et al., 1997). Calculations of the three components of global solar radiation have been performed following the semi-empirical model of atmosphere provided by Spena et al. (2010). No IR radiative transfer is considered at nighttime, assuming all windows as fully shaded.

4. Building Simulation



Fig. 1 - The case-study building (Google Earth)

The architecture of the simulated building (Fig. 1) fits well with both sites (Rome and Berlin). It is 8 floors tall, with a total height of 27 m and an aspect ratio of roughly 0.3. The window/total wall surface ratio varies along the three main building facades, with values: 0.48, 0.28, 0.20.

5. HVAC Facilities Simulation

5.1 Air Conditioning

Thermal comfort within the building is provided by a fully conditioned air system (air-water mixed type, namely primary air + fan-coil) that controls: ambient temperatures, relative humidity, airflow, and renewal. Primary air is treated in several AHU (Air Handling Units) and sent to spaces to balance latent-heat loads. Sensible-heat loads are balanced by the fan-coil water system. Space inner temperatures were set according to the current standard comfort requirements. External air handling acts as follows:

- winter: pre-heating, humidification, post-heating
- summer: cooling & dehumidification, post-heating.

Renewal air flow-rates were calculated as:

$$\dot{V} = n * V \left(\frac{m^3}{h}\right) \tag{3}$$

$$n = 0.15 * \left(\frac{24-t_{oc}}{24}\right) + \frac{t_{oc} * \phi * i_a * A_p}{2400 * V_a} \tag{4}$$

5.2 Inner Lighting

The lighting system is designed to guarantee and maintain given levels and uniformities of light on the work-field; to this purpose, according to UNI EN 12464, for offices and connecting spaces lighting levels were respectively averaged to 300 and 50 lx. Current standards on natural lighting in Italy (UNI 10840: 2000) impose an "average daylight factor" to be higher than 2 %, and the fenestration area to be greater than 1/8 of the floor area. It is then possible to evaluate the artificial lighting needs during time. The case study actual lighting system was based on halogen incandescent lamps with an efficiency of 22 lm/W. It was roughly assumed that 90 % of the electrical lighting power was released into the rooms, and the remaining 10 % wasted to the outer environment through the windows.

6. The Input Data of the Model

The listing of the code (Spena, 1984) is composed of a main routine and of four different subroutines operating iteratively to be applied simultaneously to the different scenarios, while composing a unique code that can inherently generate the results of each comparison. In order to correctly take into account the radiation and sun-air temperatures dependence on both time and exposure, in the iterative control procedures the execution of paths was stepped with reference to:

- day of the year (one reference day per month)
- surfaces exposure
- hourly building usage range (7 am – 8 pm).

A lean flow-chart is given in Fig. 2.

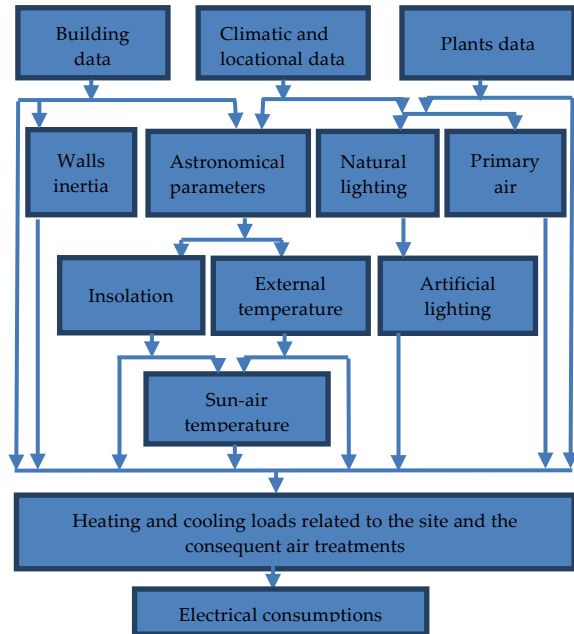


Fig. 2 – Simulation flow-chart

The daily results were then extended prior monthly and then yearly in terms of total heating, cooling, and electrical energy loads. Heating and cooling loads are supposed to be respectively covered by boilers, and electrical chillers. The corresponding electrical needs are then computed in the overall electrical energy (Spena, 1984; Spittler, 2009; Pedrini et al., 20002).

The following main input quantities are considered.

- Weather data:
 - Daily maximum and minimum external air temperatures; sunny hours per day; maximum and minimum shading; urban surfaces albedo;
- Building data:
 - Total area of walls, roof, windows, floor, connective, inner surfaces; inter-storey height; total building volume; thermo-physical characteristics of walls, roof, floors; characteristics of the windows; solar radiation absorptance from walls and from the roof;
- Facilities data:
 - airflow-rates; room temperature setpoints; performances of the major components; conversion efficiencies of the plants.

7. Simulation Results

7.1 The Base-Case: South Europe, Rome

7.1.1 Site

The reference site for the base-case is Rome.

The windows have the following properties (Table 1):

Table 1 – Base-case windows properties

Properties	Values
Glass type	Low-emissivity double glass
Transparency	0.64
Window factor	0.35
Alignment factor	0.8
Shading factor	0.5
Solar factor	0.32
Chassis factor	1.17
Transmittance	1.3 kcal/(h*m ² *K)

7.1.2 External conditions, inner lighting

The hourly outside temperature maximum value is attributed to 3 pm of each day. The absolute maximum was recorded in August (31.9 °C), the absolute minimum (2.5 °C) in December. As far as insolation is concerned, when clear sky is recorded we assume for the considered building that the maximum values are reached before midday for exposures that include South, after midday for exposures that include West (Gugliermetti et al., 2004). The cover receives maximum insolation at noon. The artificial lighting needs are closely related to the contribution of the sunlight, due to their intrinsic complementarity; so lighting needs occur mainly at sunrise and at sunset, while lacking around the midday (Pedrini et al., 2002; Li and Wong, 2007). This range is wider in summer.

7.1.3 Energy loads

As a matter of main interest, the amounts of the fan-coil loads of each different exposure are reported in Figs 3 and 4.

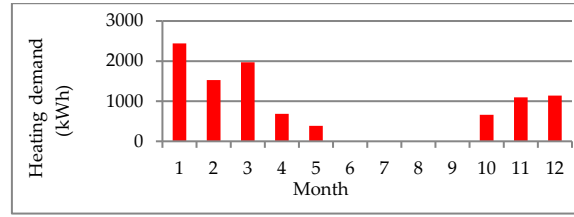


Fig. 3 – Fan-coil loads, heating demand

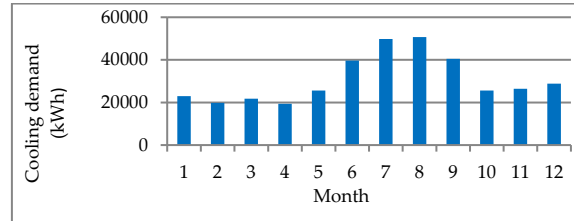


Fig. 4 – Fan-coil loads, cooling demand

The month requiring more local heating is January (2441 kWh), while the higher demand for local cooling occurs in August (50 676.5 kWh). The entity of those loads shows that relatively low thermal dissipation and high internal loads characterize the considered building. Monthly electrical requests are dominated by the use of lighting systems and chilling units.

Adding AHU demand, and reassuming:

- Thermal energy required: 391 765.8 kWh/year
- Cooling energy required: 624 801.9 kWh/ year
- Electrical energy required: 778 846.3 kWh/ year

7.1.4 Glass sensitivity

The kind of glass (Tables 2 and 3) influences either thermal and daylighting contributions (due to different transparencies), either loads due to the transmission through the glass (due to different transmittances).

Single glass

Table 2 – Single glass properties

Properties	Values
Transmittance	2.6 kcal/(h*m ² *K)
Transparency	0.8
Solar factor	0.4

The monthly thermal needs keep on growing (the higher transmittance and the lower artificial lighting contribution prevail over the higher transparency to insolation); the cooling requests decrease in winter and rise in summer (the combination of greater

transmittance and transparency prevail over the low artificial lighting contributions). Electricity is mostly influenced by the lower cooling demand.

The annual need relative departures (%) from the base-case are as follows:

- Heating: +8.7 %; Cooling: -6.4 %;
Electricity: -2.9 %.

Triple glass

Table 3 – Triple glass properties

Properties	Values
Transmittance	1.1 kcal/(h*m ² *K)
Transparency	0.51
Solar factor	0.25

The heating demand results lower in all months. The cooling demand increases in winter and decreases in summer, because of the lower transmittance and transparency. Electrical consumption increases, following the artificial lighting needs.

Departures from the base-case:

- Heating: -1 %; Cooling: -0.37 %;
Electricity: +1.1 %.

7.2 Lower Fenestration: The Case of Rome

In the reference site of Rome, the building was modified by reducing the window surfaces and their outer shield (shading factor = 0.9). The new window/total wall surfaces ratios are respectively equal to 0.05-0.10-0.20. The glass type of the initial configuration is the base case one. The reduction of the glass surfaces affects both the loads due to radiation and the loads due to artificial lighting, as the average daylight factor diminishes. Departures from Case 1 in standard configuration are:

- Heating: -2.28 %; Cooling: +8.8 %;
Electricity: +10 %.

Single glass

Departures from the initial configuration:

- Heating: +1 %; Cooling: -4.6 %;
Electricity: -3.4 %.

Similarly to the previous case, the transition from double to single glass leads to a greater heat consumption (due to greater transmittance) and to a lower electrical (related to lighting devices) and cooling request: the latter due to the lower dissipa-

tion by internal light that prevails over the greater solar gain. Departures from Case 1 with the same kind of glass:

- Heating: -9.2 %; Cooling: +10.9 %;
Electricity: +9.4 %.

These departures show how the same kind of glass over greater surfaces (and greater outer shield) requires: less cooling and electricity, more heating.

Triple glass

Departures from the initial configuration:

- Heating: -0.1 %; Cooling: +1.1 %;
Electricity: +1.1 %.

For this different building configuration the effect of the triple glass gives a greater cooling request.

Departures from Case 1 with the same kind of glass:

- Heating: -1.4 %; Cooling: +10.4 %;
Electricity: +11.9 %.

7.3 Total Shading: The Case of Rome

The new outer condition accounts for the lack of direct radiation on the building surface in the standard configuration. The presence of solely diffuse radiation implies a lower global radiation intensity that leads to both sun-air temperature and solar gain reductions. Spaces inner lighting doesn't undergo any changes. Departures from Case 1 in the standard configuration:

- Heating: +0.3 %; Cooling: -9.8 %;
Electricity: -2.9 %.

Single glass

For this scenario we considered true to evaluate the relative departures only from Case 1. In the standard configuration they resulted in:

- Heating: +9.7 %; Cooling: -18.2 %;
Electricity: -6.48 %.

Departures from Case 1 with the same kind of glass:

- Heating: +0.9 %; Cooling: -12.6 %;
Electricity: -3.7 %.

The lower insolation leads to smaller cooling and electricity request, and to higher heating

Triple glass

Departures from Case 1 in standard configuration:

- Heating: -0.72 %; Cooling: -8.4 %;
Electricity: -1.3 %.

The general reduction of all annual loads enable us

to conclude that using a triple glass in the absence of direct radiation performs better than using a double glass in standard insolation conditions.

Departures from Case 1 with the same kind of glass:

- Heating: +0.28 %; Cooling: -8 %;
- Electricity: -2.4 %.

7.4 The Case of North Europe: Berlin

7.4.1 Site, insolation, outer daylighting

The selected site is Berlin. The building is assumed to be the same of base case, in the standard configuration.

A different siting involves variations of climatic conditions such as temperature, insolation, duration of the day and of actual hours of sunshine, external average illumination values. In Berlin, temperatures are always lower than in Rome. As the absolute maximum temperature is recorded in summer in Rome (31.9 °C), the absolute minimum occurs in winter in Berlin (-2 °C). The irradiation trend for the different exposures is similar to that of Rome, while the intensity values are in general lower. A higher latitude also means that days are shorter in winter and longer in summer (Fig. 5).

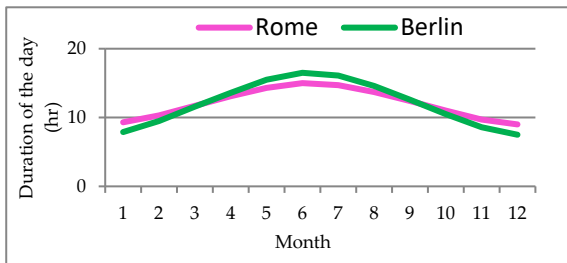


Fig. 5 – Durations of the reference days vs. months of the year

7.4.2 Energy loads

The maximum fan-coil heating demand occurs (see Fig. 6) in February, with a value of 12 085 kWh (almost 5 times the maximum monthly in Rome). The chilling fan-coil request (Fig. 7) is highest in July, namely up to 43 378 kWh (lower than the maximum cooling load occurred in Rome); high values are also recorded in January and December as the consequence of a high artificial lighting demand. The results reflect what above exposed in terms of climatic diversity between the two

locations. The electrical energy performance (peak of 88 656 kWh in December, mainly due to lighting need) corroborates what said until now.

Adding AHU demand, and reassuming:

- Thermal energy required: 567 271.6 kWh/year
- Cooling energy required: 390 216.5 kWh/year
- Electrical energy required: 703 721 kWh/year.

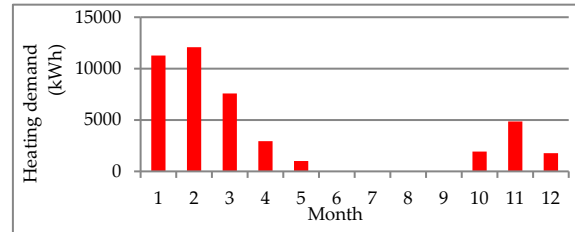


Fig. 6 – Fan-coil loads, heating demand

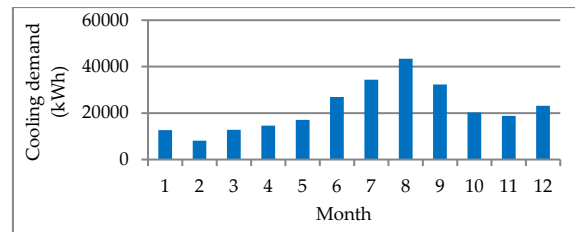


Fig. 7 – Fan-coil loads, cooling demand

Departures from Case 1 in standard configuration:

- Heating: +44.8 %; Cooling: -37.5 %;
- Electricity: -9.6 %.

7.4.3 Sensitivity to the kind of glazing

Single glass

Heating demand keeps on growing; cooling request is instead always decreasing, the highest departures occurring in months with low external solar radiation (in other months higher solar gains are offset by low lighting devices thermal dissipation).

Departures from initial configuration:

- Heating +15.6 %; Cooling: -17.3 %;
- Electricity: -4.7 %.

Departures from Case 1 with the same kind of glass:

- Heating: +53.9 %; Cooling: -44.8 %;
- Electricity: -11.3 %

Lower outdoor temperatures, lower radiation and external lighting lead to: a greater demand for heating; a lower demand for cooling and electricity.

Triple glass

Heating needs departures are again negative, but lower in absolute values. Cooling requirements instead grow in colder months and decrease in warmer months (due to lower heat transmission and lower transparency).

Departures from the initial configuration:

- Heating: -2.2 %; Cooling: +2.5 %;
Electricity: +2.1 %.

We can observe that, unlike Rome, triple glazing leads to an increase of the cooling need (the lower external insolation makes the artificial lighting dissipation dominant in the overall energy balance).

Departures from Case 1 with the same kind of glass:

- Heating: +43 %; Cooling: -35.7 %;
Electricity: -8.8 %.

7.5 Lower Fenestration: The Case of Berlin

Still in Berlin; reference building the same of Case 2.

Departures from Case 4 in the standard configuration:

- Heating: -2.3 %; Cooling: +8.9 %
Electricity: +17 %.

Single glass

Departures from the initial configuration:

- Heating: +3 %; Cooling: -12.5 %;
Electricity: -6 %.

The trend is similar to the previous cases of single glazing. Departures from Case 4, same kind of glass:

- Heating: -16.6 %; Cooling: +31.8 %;
Electricity: +15.5 %

Departures result similar to those of Case 2.

Triple glass

Departures from the initial configuration:

- Heating: -0.4 %; Cooling: +4.6 %;
Electricity: +2.1 %.

The use of a more insulating and less transparent glass, in this site reduces the transmission and solar gain loads; but globally amplifies the effect of the other inner loads. Departures from Case 4 with the same kind of glass:

- Heating: -4.8 %; Cooling: +27 %;
Electricity: +19.9 %.

7.6 Total Shading: The Case of Berlin

Still in Berlin; outer conditions changed as in Case 3.

Departures from Case 4 in the standard configuration:

- Heating: +0.6 %; Cooling: -8.1 %;
Electricity: -1.7 %.

Single glass

Departures from Case 4 in the standard configuration:

- Heating: +17.1 %; Cooling: -26.4 %;
Electricity: -6.6 %

Using the single glass instead of the double one, when adverse changes in insolation occur, involves: higher heating demand; lower cooling demand; lower electrical demand. Departures from Case 4 with the same kind of glass:

- Heating: +1.3 %; Cooling: -11 %;
Electricity: -1.9 %.

Triple glass

Departures from Case 4 in the standard configuration:

- Heating: -1.7 %; Cooling: -4.2 %;
Electricity: +0.7 %.

Departures from Case 4 with the same kind of glass:

- Heating: +0.5 %; Cooling: -6.5 %;
Electricity: -1.3 %.

8. Discussion

Consistently with the results reported in § 7, in the following pictures it may be observed, as a consequence of the transmittance and transparency reductions (transition from single to triple glass), a general heating (fan-coils+AHU) needs decrease (Fig. 8) together with a cooling (fan-coils+AHU) needs increase (Fig. 9).

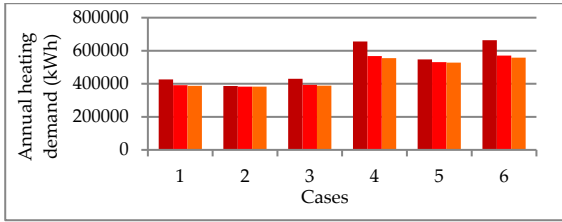


Fig. 8 – Heating overall demand for different glasses (from left: single, double, triple) in the 6 analyzed cases

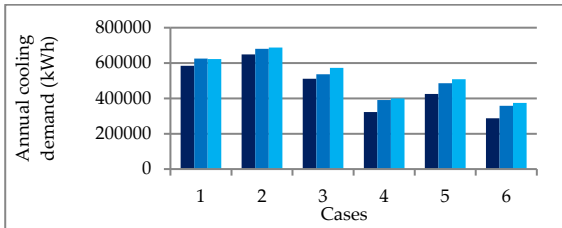


Fig. 9 – Cooling overall demand for different glasses (from left: single, double, triple) in the 6 analyzed cases

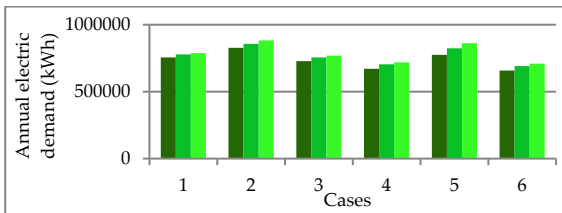


Fig. 10 – Electricity demand for different glasses (from left: single, double, triple) in the 6 analyzed cases

The highest thermal needs for the same site are recorded in case of lack of direct radiation; while the highest cooling needs occur in case of reduced windows area (electrical needs trends follow the cooling ones). The merely electrical demand (which inherently compounds all the HVAC facilities) is represented in Fig. 10, while in Fig. 11 the total energy required for the overall building performance is shown.

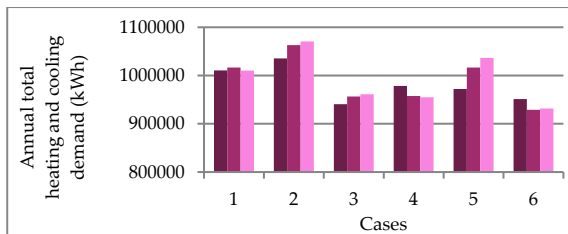


Fig. 11 – Annual total heating and cooling demand for different glasses (from left: single, double, triple) in the 6 analyzed cases

In this last picture we can observe that the overall heating and cooling demand doesn't follow a predictable trend. Considering the scenarios #1 and #4 (Rome and Berlin in standard configuration), and

not taking into account the final building system electrical consumptions, we could conclude that by replacing single glasses with triple ones (of the given properties) could be beneficial to both the sites of Rome and Berlin. A general assessment of this kind, however, is not always predictive for the actual suitability for dedicated, specific solutions. As a matter of fact, a more comprehensive analysis should consider indeed the global amount of the final energy requirement, especially if energy for the HVAC service is partly electrical (chillers, fans, pumps) and partly thermal (boilers), while the energy used by the lighting systems is merely electrical (Spena, 1984; Zhu, 2006). This could correctly lead to assess the solution that – the same comfort levels given - involves smaller overall values of both terms. And, in case of conflicting demand trends, the choice of the best solution would require an additional analysis in terms of primary energy, to be expressed in economic terms (Fumo et al., 2009). It appears necessary, as an example, in the two previously mentioned cases when, moving from single to triple glazing, thermal and electrical performances oppose.

9. Conclusion

Methodology appears validated by the intrinsic coherence of the results, and the tool fit for building comprehensive simulations. Actions and retro-fittings on fenestration made with the aim of optimizing the building performance not always lead to intuitive goals: as a matter of fact, with respect to the site we can obtain different performances for the same category of glass. The critical issue of glasses resides in their wide field of influence on building energy consumption: mainly inner room HVAC (due to the influence on heat transmission, solar gains, artificial lighting) together with lighting system energy needs. The mere assumption that single, double, triple glasses can undoubtedly - in this order - increasingly reduce building energy needs in any climatic condition, has been demonstrated to be not self-evident. Further insights will explore the sensitivity of the results to the use of led lamps at a user's level, and of heat pumps at a central level.

Nomenclature

Symbols

T_{pi}	Internal wall temperature ($^{\circ}\text{C}$)
$\overline{T_e}$	Average outside temperature ($^{\circ}\text{C}$)
θ	Fluctuations half-amplitude (-)
t	Time (s)
ω	Frequency of fluctuations (s^{-1})
s	Wall thickness (m)
β	Damping factor (m^{-1})
a	Thermal diffusivity ($\text{m}^2 * \text{s}^{-1}$)
τ^0	Time of oscillation (h)
\dot{V}	Ventilation air flow-rate ($\text{m}^3 * \text{h}^{-1}$)
n	Renewal air rate (h^{-1})
V	Room volume (m^3)
t_{oc}	Room occupancy time (h)
ϕ	Specific flow-rate ($\text{m}^3 * \text{h}^{-1} * \text{person}$)
ia	Occupancy ($\text{person} * (100 \text{ m}^2)^{-1}$)
A_p	Useful floor area (m^2)
V_a	Air volume in HVAC service (m^3)

References

- ASHRAE. 2000. *ASHRAE Handbook of Fundamentals*. Atlanta, U.S.A.: ASHRAE.
- Bazjanac, V. 2004. "Building energy performance simulation as part of interoperable SW environment". *Building and Environment* 39: 879-883. doi: 10.1016/j.buildenv.2004.01.012.
- Clarke, J.A. 2001. *Energy simulation in building design*. Oxford, UK: Butterworth-Heinemann.
- Fisher, D.E., C.O. Pedersen, 1997. "Convective Heat Transfer in Building Energy and Thermal Load Calculation". *ASHRAE Transactions* 103(2): 137-148.
- Fontoynt, M. 1999. *Daylight Performance of Buildings*. Brussels, Belgium: European Commission.
- Fumo, N., P. Mago, L. Chamra. 2009. "Energy and economic evaluation of cooling, heating, and power systems based on primary energy". *Applied Thermal Engineering* 29: 2665 -2671. doi: 10.1016/j.applthermaleng.2008.12.027.
- Gugliermetti, F., G. Passerini, F. Bisegna. 2004. "Climate models for the assessment of office buildings energy performance". *Building and Environment* 39: 39-50. doi: 10.1016/S0360-1323(03)00138-0.
- Hensen, J.L.M., N. Nakahara. 2001. "Energy and building performance simulation: current status and future issues". *Energy and Buildings* 33(4): vii-ix. doi: 10.1016/S0378-7788(00)00110-9.
- Hensen, J.L.M., R. Lamberts. 2011. *Building Performance Simulation for Design and Operation*. Abingdon Oxon, UK: Spon Press.
- Li, D.H.V., S.L. Wong. 2007. "Daylighting and energy implications due to shading effects from nearby buildings". *Applied Energy* 84: 722-29. doi: 10.1016/j.apenergy.2007.04.005.
- Pedrini, A., F.S. Westphal, R. Lamberts. 2002. "A methodology for building energy modeling and calibration in warm climates". *Building and Environment* 37 (8-9): 903-912. doi: 10.1016/S0360-1323(02)00051-3.
- Reddy, T.A. 2006. "Literature review on calibration of building energy simulation programs: uses, problems, procedures, uncertainty and tools". *ASHRAE Transactions* 112(1): 226-240.
- Spena, A. 1984. "Studio comparativo, mediante simulazione, della produzione combinata di energia elettrica, calore e freddo per la copertura dei fabbisogni di un comprensorio edilizio per attività terziarie". In: *Proceeding of the XXXII ATI National Congress*. L'Aquila, Italy: ATI.
- Spena, A., A. Vitaliti, F. Cardarelli. 1997. "Primi risultati di un metodo per la generazione di congruenti valori orari della componente della radiazione solare al suolo". In: *Proceedings of the LII ATI National Congress*. Cernobbio, Italy: ATI.
- Spena, A., C. Strati, G. D'Angiolini. 2010. "First Correlations for a Mediterranean Cloud Cover Model". In: *Proceedings of SPIE Solar Energy Plus Technology*. San Diego, U.S.A.
- Spitler, J.D. 2009. *Load calculation applications manual*. Atlanta, U.S.A.: ASHRAE.
- Tabunshikov, Y.A. 1993. *Mathematical Models of Thermal Conditions in Buildings*. Boca Raton, U.S.A.: CRC Press.
- Zhu, Y. 2006. "Applying computer-based simulation to energy auditing: a case study". *Energy and Buildings* 38: 421-428. doi: 10.1016/j.enbuild.2005.07.007.

A New Control Strategy for Variable Refrigerant Flow Systems

Xiaojie Lin – University of Maryland – xiaojie@umd.edu

Yunho Hwang – University of Maryland – yhhwang@umd.edu

Reinhard Radermacher – University of Maryland – raderm@umd.edu

Byungsoon Kim – CAC R&D Lab., LG Electronics – bs.kim@lge.com

Abstract

In the US, more than 45 % of the building primary energy is used for space cooling, space heating, and water heating. Advanced HVAC systems are key to building energy consumption reduction. A variable refrigerant flow (VRF) system is a promising solution to this problem, because it can precisely provide space cooling and/or space heating for different zones. A literature review of previous VRF modeling studies shows that the use of existing simulation tools, such as EnergyPlus, can result in more than 20 % deviation in both capacity and energy consumption. In this study, a new VRF model is proposed to improve the accuracy over conventional models. Simulation results show that the proposed model agrees with experimental field test data within a 10 % deviation in hourly capacity and 5 % in hourly energy consumption. After the validation of the VRF system model, a new VRF control strategy was proposed based upon evaporating/condensing temperature controls. The seasonal performance of VRF system with the new control strategy was simulated for the same building design in four different climates representing these US cities: Miami, Houston, Baltimore, and Chicago.

1. Introduction

The variable refrigerant flow (VRF) system is an air conditioning solution introduced by Japanese manufacturers in mid-1980s. It is well known for its excellent systematic modularity and installation flexibility as compared to ducted air conditioners. Among various VRF types, two types of VRF systems, the heat pump type (HPVRF) and the heat recovery type (HRVRF), are of interest. The differ-

ences and similarities between HPVRF and HRVRF are illustrated in Figs. 1 and 2. In Fig. 1, the HPVRF system works in a cooling mode while HRVRF works in a cooling main mode where the system provides more cooling than heating to the building. Both systems have four indoor units (IUs) and one outdoor unit (OU).

In addition, HRVRF has one extra component, which is a heat recovery unit (HRU). In the OU of HPVRF system (Fig. 1), the discharged refrigerant from the compressor rejects heat to the ambient air and is cooled down to subcooled state. The subcooled refrigerant bypasses the main electronic expansion valve (EEV) via the check valve, and flows into the IU side where it is distributed among different IUs. As shown in Fig. 1, a typical IU is made of one crossflow fan, direct expansion coils and one EEV. The subcooled refrigerant expands through the EEV and cools down room air by forced convection. Then, the refrigerant is sent back to the suction port of the compressor.

In the heating season, the four-way valve is reversed and refrigerant flow direction is alternated so that the system is working in the heat pump mode where the room air is heated. Fig. 2 shows the cooling main operation of the HRVRF. Therefore, in order to meet the demands of the rooms, a HRU has three pipes of refrigerant: low pressure vapor, high pressure vapor, and high pressure liquid. HRU distributes the refrigerant based on demands of the IUs. For example, in Fig. 2, part of the high-pressure refrigerant vapor is delivered to the IU via the HRU, instead of it being sent to the OU, when one or more rooms need heating. For the rest of the rooms, the HRU also delivers the subcooled liquid to these IUs. Finally, HRU also sends the superheated vapor back to the suction port of the

compressor. As can be seen in Figs 1 and 2, HRVRF is preferred over HPVRF where the cooling and heating loads from different parts of the building need to be satisfied at the same time, such as hospitals and office buildings.

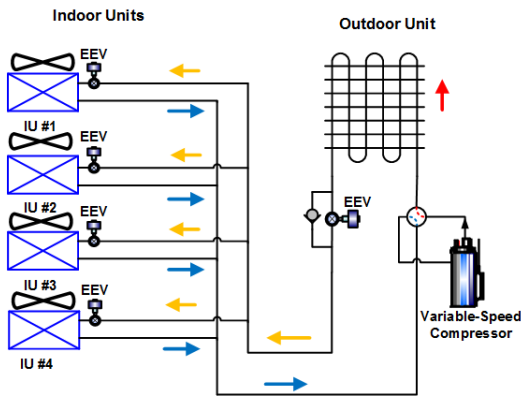


Fig. 1 – HPVRF operated in cooling mode

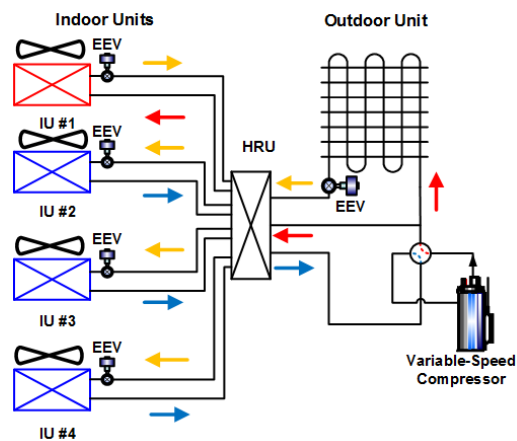


Fig. 2 – HRVRF operated in cooling main mode

However, in the buildings, the occupants could actually have more demands than space cooling or heating. For example, occupants also need ventilation and hot water. As a comprehensive and flexible building HVAC solution, VRF systems could also provide other functionality than cooling or heating. Zhu et al. (2015; 2014a; 2014b) proposed a VRF system incorporated with a dedicated outdoor cooling system. Simulation results showed that the proposed system could provide a better indoor thermal comfort with a 12.2 % higher coefficient of performance (COP) in cooling season than conventional AC systems.

Similarly, Aynur et al. (2010a; 2010b; 2008) and Aynur (2008) tested an integrated system made of HPVRF system and a solid desiccant heat pump unit. They found that the CO₂ concentration of the room could be kept within 450-500 ppm. In addition, another perspective in building VRF research is to use the simulation tools to evaluate the performance of the system. For example, eQuest and EnergyPlus are the two most popular tools used in open literature.

Most of the existing VRF models in building simulation tools are based on performance mapping method. This method is effective only with a carefully tuned model with accurate onsite parameters and schedules, as found by Lin et al. (2015a). For example, the performance mapping model developed by Zhou et al. (2008; 2007) and Zhou and Wang (2006) could yield weekly cooling energy and power consumption errors of 25.2 % and 28.3 %, respectively when applied to a real building. Researchers also observed that the model could lead to a higher uncertainty when the focus of the study switched from weekly data to hourly data. Moreover, another disadvantage of performance mapping method is the insufficiency in adopting new control strategies when focusing on hourly performance. Lin et al. (2015b) suggested and developed a first-principle based VRF model. In this paper, the development of the model is explained before the extended modeling work with the new control. After the model was validated, a new ambient temperature based evaporating/condensing temperature control strategy was applied to the model and the seasonal energy saving potential was demonstrated.

2. VRF Model

2.1 Model Flow Chart

Performance mapping model was firstly developed by Zhou et al. (2007a; 2007b; 2008) and Zhou and Wang (2006). A model of similar concept was later incorporated into EnergyPlus 6.0 as part of the official engine developed by Raustad and Sharma (2013); Nigusse and Raustad (2013); and Sharma and Raustad (2013). The basic idea is illustrated in

Fig. 3. The first step is to process the building geometry file and weather data specified by the user. The model then calculates the required space cooling and heating loads of the rooms. In the earlier versions of building model, the VRF model does not have its own IU module. Therefore, some researchers would use the window AC module instead of VRF IU module. Based on the room load, the required IU (or window AC) cooling or heating capacity is calculated. Once the engine has obtained all the information from the IU and building side, the OU module of the VRF model is called. This module reads two maps as the lookup tables. The first one is the system capacity map based on indoor and outdoor temperatures. The second map is the energy consumption map. The OU module searches the operation point in the cooling capacity map. The ideal operation point should deliver the required IU load to the building. Once the operation point is found, the energy consumption of the system is calculated accordingly.

Lin et al. (2015b) analyzed the uncertainty of performance mapping method and concluded that a thermodynamic model could be a proper way to reduce the model uncertainty. The flow chart of the new model is shown in Fig. 4. As compared to Fig. 3, the model still begins with the estimation of room load and IU load. After that, the model calls a thermodynamic OU module to find the energy consumption of the system. The required inputs for the OU module are the polynomial equations of the compressor performance and user-specified control parameters such as the degree of superheating. In order to quantify the accuracy of the new model, the normalized mean bias error (NMBE) concept (Eq. 1) from ASHRAE guideline (ASHRAE, 2002) was used. The target NMBE value was less than 5 %.

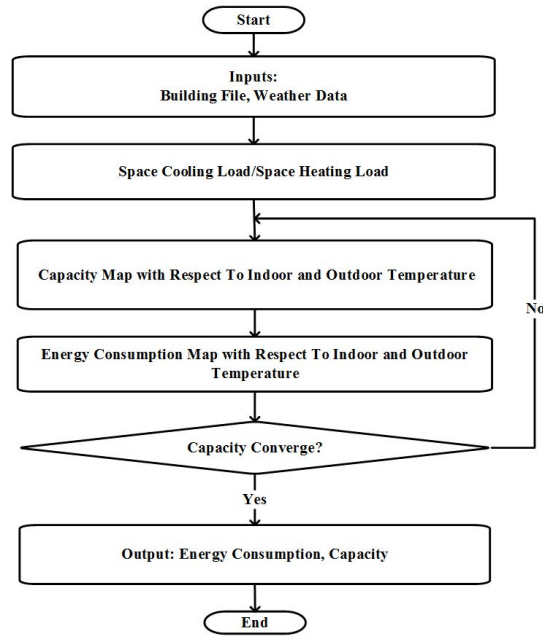


Fig. 3 – Flow chart of performance mapping method

$$NMBE = 100 * \frac{\sqrt{\sum_{i=1}^n (y_i - \hat{y}_i)^2}}{(n-1) * \bar{y}} \quad (1)$$

where y_i is the simulation result, \hat{y}_i is the experimental result, n is the amount of points, and \bar{y} is the mean of experimental results.

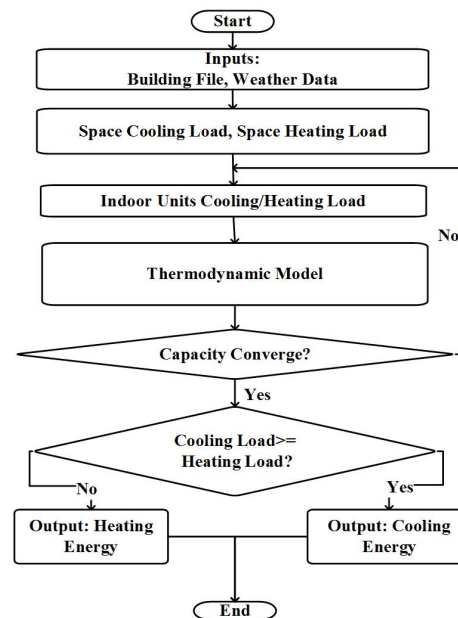


Fig. 4 – Flow chart of the new method

The model was validated in the cooling season while focusing on hourly operation data with a VRF system having seven IUs. The system has a

rated cooling capacity of 28.1 kW. The hourly energy consumption validation result is shown in Fig. 5. The obtained NMBE value was 3.7 %, which means the hourly model uncertainty is less than 5 %. The details of the model could be found in Lin et al.'s study (2015b).

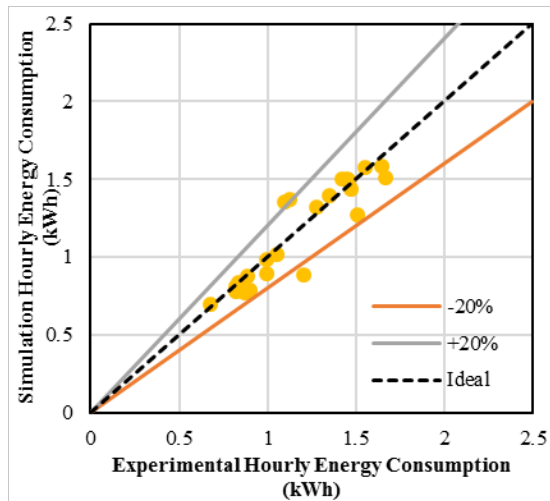


Fig. 5 – Hourly energy consumption validation

2.2 New Control Strategy

As mentioned by Chen et al. (2005), the control mechanism of VRF system is less discussed in existing literature as compared to the field tests or simulation studies due to commercial confidentiality. Even though the details of control mechanism are not available and vary with products, manufacturers generally use lookup tables to control compressors (LG Electronics 2015), as mentioned by Tu et al. (2010).

The controller estimates the building load based on ambient condition. Then it references a table to find out the proper compressor frequency meeting the estimated building load. The map is generated by laboratory testing. For example, during the cooling operation, the evaporating temperature is designed based upon the rated condition where the ambient temperature is 35 °C. When the ambient temperature decreases, the cooling demand also decreases. In a conventional fix-speed air conditioning system, the evaporating temperature decreases with ambient temperature. However, in the VRF system the evaporating temperature can be maintained by reducing the compressor frequency.

The energy consumption of the system is thereby reduced. Therefore, increasing the evaporating temperature can achieve energy saving. As shown by the experimental work from Anyur et al. (2008) and Shao et al. (2004), the compressor could operate under a further lower frequency with a higher evaporating temperature, but still delivers sufficient amount of refrigerant to the IUs, which reduces the energy consumption. Zhao et al. (2015) found that by increasing the evaporating temperature from 8 °C to 12 °C, 15 % energy saving could be achieved. Typically, the latent cooling load in the room is lower at a lower ambient temperature. When a higher evaporating temperature is used, the latent cooling capacity is decreased. Therefore, using a higher evaporating temperature at lower ambient temperature can save energy while delivering a proper sensible cooling. This means that the control of evaporating temperature is critical to energy saving in the cooling season. Similarly, in the heating operation, the condensing temperature of the system could be a key design parameter for energy saving. Therefore, in this study, a new control strategy was proposed. Instead of using single linear map based on single evaporating/condensing temperature, this new control strategy determines the compressor frequency under a varying evaporating/condensing temperature. The control strategy follows two simple rules:

- The evaporating temperature of the system is adjusted linearly from 11 °C to 4.2 °C when the ambient air temperature increases from 20 °C to 35 °C.
- The condensing temperature of the system is adjusted linearly from 50 °C to 40 °C when the ambient air temperature increases from -10 °C to 5 °C.

3. Results and Discussion

The specifications of the VRF system used in this study are listed in Table 1. The floor map of the building where the system was installed is shown in Fig. 6. The test VRF system has seven IUs and a rated OU cooling capacity of 28.1 kW. The IU #1 was installed in Room A. IU #2 and #3 were installed in Room B. IU #4 and IU #5 were installed

in Room C. IU #6 was installed in Room D. IU #7 was installed in Room E. For the cooling operation, the running period was set from July 1 to September 1. The set point of the rooms was 25 °C in cooling season. The TMY3 weather data in Baltimore, MD was used. Fig. 7 shows the daily energy consumption reduction when compared to the default VRF control strategy in the cooling season. Overall, in the cooling season, the seasonal energy consumption is reduced from 1,938 kWh to 1,764 kWh with energy savings of 8.9 %. For heating operation, the running period was set from February 1 to April 1. The set point of the rooms was 22 °C. Similarly, Fig. 8 shows the daily energy consumption reduction of the new control strategy. In heating season, the energy consumption is reduced from 2,753 kWh to 2,329 kWh with energy savings of 15.4 %.

Table 4 – VRF system specifications

Component	Cooling (kW)	Heating (kW)
OU	28.1	31.6
IU #1	2.2	2.5
IU #2	3.6	4.0
IU #3	3.6	4.0
IU #4	5.6	6.0
IU #5	5.6	6.0
IU #6	2.2	2.5
IU #7	2.2	2.5

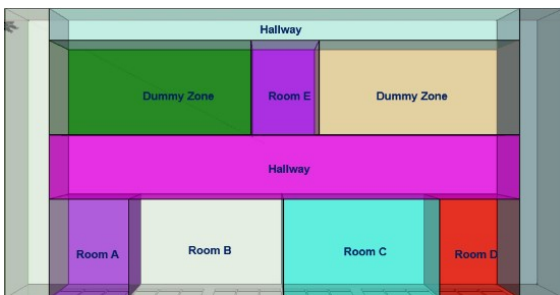


Fig. 6 – Building floor map

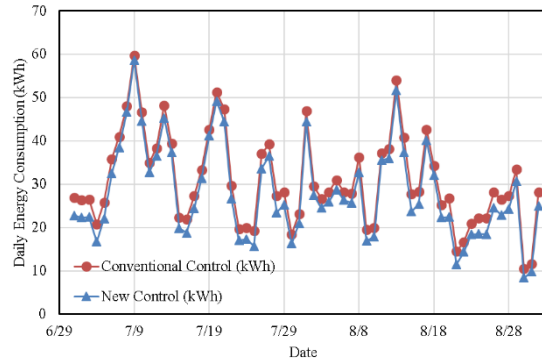


Fig. 7 – Cooling seasonal energy savings by new control strategy in Baltimore, MD

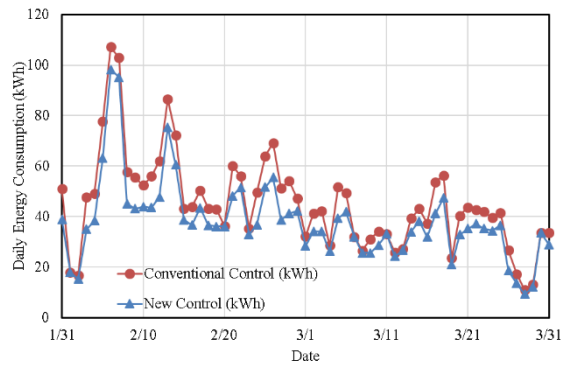


Fig. 8 – Heating seasonal energy savings by new control strategy in Baltimore, MD

The same building and VRF system were also simulated in Miami, Houston, and Chicago, which are the representative cities of the respective climate zones. The seasonal performance in different climates is listed in Table 2. Energy saving potential of the new control strategy is reduced when it is applied to Miami. That is because the key of the new control strategy is the applicable temperature range. In this case, the applicable range is selected based on the climate of Baltimore, MD. Therefore, the applicable range is relatively narrow as compared to the weather conditions in Miami, which leads to a degradation of the performance.

Table 5 – Cooling and heating energy savings in different climates

City	Cooling Season Energy Savings (%)	Heating Season Energy Savings (%)
Miami, FL	6.8 %	10.5 %
Houston, TX	5.2 %	11.2 %
Baltimore, MD	8.9 %	15.4 %
Chicago, IL	10.8 %	14.1 %

4. Conclusion

In this study, a new control strategy based on evaporating/condensing temperature control was proposed and embedded on a validated VRF model. The seasonal performance of the new control strategy was simulated in a seven-IU VRF system with a rated cooling capacity of 28.1 kW. The simulation results show that the VRF system with the new control strategy could save 8.9 % and 15.4 % of energy during the cooling and heating seasons in Baltimore, MD.

Acknowledgements

This work was supported by LG Electronics Inc. and the sponsors of the Energy Efficiency and Heat Pumps Consortium, the Center for Environmental Energy Engineering (CEEE) at the University of Maryland, College Park, MD, USA.

Nomenclature

Symbols

COP	Coefficient of performance
EEV	Electronic expansion valve
HRU	Heat recovery unit
HPVRF	Heat pump variable refrigerant flow
HRVRF	Heat recovery variable refrigerant flow
IU	Indoor unit

NMBE	Normalized mean bias error
OU	Outdoor unit
VRF	Variable refrigerant flow

References

- ASHRAE. 2002. *ASHRAE Guideline 14-Measurement of Energy and Demand Savings*. Atlanta, U.S.A.: American Society of Heating, Refrigerating and Air-conditioning Engineers, Inc.
- Aynur, T., Y. Hwang, R. Radermacher. 2008. "Experimental Evaluation of the Ventilation Effect on the Performance of a VRV System in Cooling Mode—Part I: Experimental Evaluation". *HVAC&R Research* 14(4): 615–30. doi:10.1080/10789669.2008.10391029.
- Aynur, T.N., Y. Hwang, R. Radermacher. 2010a. "Integration of Variable Refrigerant Flow and Heat Pump Desiccant Systems for the Cooling Season". *Applied Thermal Engineering* 30(4): 917–27. doi:10.1016/j.applthermaleng.2010.01.002.
- Aynur, T.N., Y. Hwang, R. Radermacher. 2010b. "Integration of Variable Refrigerant Flow and Heat Pump Desiccant Systems for the Heating Season". *Energy and Buildings* 42(4): 468–76. doi:10.1016/j.enbuild.2009.10.016.
- Aynur, T.N. 2008. *Experimental and Simulation Evaluation of a Multi-Split Type Air Conditioning System Under Steady-State and Transient Conditions*. College Park, U.S.A.: University of Maryland.
- Chen, W., X. Zhou, S. Deng. 2005. "Development of Control Method and Dynamic Model for Multi-Evaporator Air Conditioners (MEAC)". *Energy Conversion and Management* 46(3): 451–65. doi:10.1016/j.enconman.2004.03.004.
- LG Electronics. 2015. *Multi V IV Service Manual*.
- Lin, X., H. Lee, Y. Hwang, R. Radermacher. 2015a. "A Review of Recent Development in Variable Refrigerant Flow Systems". *Science and Technology for the Built Environment* 21(7): 1–13. doi:10.1080/23744731.2015.1071987.
- Lin, X., H. Lee, Y. Hwang, R. Radermacher, B. Kim. 2015b. "A New Variable Refrigerant Flow System Simulation Approach in EnergyPlus". *International Journal of Air-Conditioning and Refrigeration* 24(1). doi:10.1142/S2010132516500012

- Nigusse, B., R. Raustad. 2013. "Verification of a VRF Heat Pump Computer Model in EnergyPlus". In: *Proceedings of ASHRAE Annual Conference*. Denver, U.S.A.
- Raustad, R. 2013. "A Variable Refrigerant Flow Heat Pump Computer Model in EnergyPlus". *ASHRAE Transactions* 119: 299–308.
- Shao, S., W. Shi, X. Li, H. Chen. 2004. "Performance Representation of Variable-Speed Compressor for Inverter Air Conditioners Based on Experimental Data". *International Journal of Refrigeration* 27(8): 805–815. doi:10.1016/j.ijrefrig.2004.02.008.
- Sharma, C., R. Raustad. 2013. "Compare Energy Use in Variable Refrigerant Flow Heat Pumps Field Demonstration and Computer Model". In: *Proceedings of ASHRAE Annual Conference*. Denver, U.S.A.
- Tu, Q., Z. Feng, S. Mao, K. Dong, R. Xiao, W. Song. 2010. "Heating Control Strategy for Variable Refrigerant Flow Air Conditioning System with Multi-Module Outdoor Units". *Energy and Buildings* 42(11): 2021–27. doi:10.1016/j.enbuild.2010.06.010.
- Zhao, D., X. Zhang, M. Zhong. 2015. "Variable Evaporating Temperature Control Strategy for VRV System under Part Load Conditions in Cooling Mode". *Energy and Buildings* 91: 180–86. doi:10.1016/j.enbuild.2015.01.039.
- Zhou, Y., R. Wang. 2006. "Module Development and Simulation of the Variable Refrigerant Flow Air Conditioning System under Cooling Conditions in EnergyPlus". In: *Proceedings of the International Conference for Enhanced Building Operations*. Shenzhen, China.
- Zhou, Y., J. Wu, R. Wang. 2007a. "Definition Identification of Two Kinds of Part Load Ratio (PLR)". *Refrigeration And Air Conditioning*: 5–7.
- Zhou, Y., J. Wu, R. Wang, S. Shiochi. 2007b. "Energy Simulation in the Variable Refrigerant Flow Air-Conditioning System under Cooling Conditions". *Energy and Buildings* 39(2): 212–20. doi:10.1016/j.enbuild.2006.06.005.
- Zhou, Y.P., J.Y. Wu, R. Wang, S. Shiochi, Y.M. Li. 2008. "Simulation and Experimental Validation of the Variable-Refrigerant-Volume (VRV) Air-Conditioning System in EnergyPlus". *Energy and Buildings* 40(6): 1041–47. doi:10.1016/j.enbuild.2007.04.025.
- Zhu, Y., X. Jin, Z. Du, B. Fan, X. Fang. 2014a. "Simulation of Variable Refrigerant Flow Air Conditioning System in Heating Mode Combined with Outdoor Air Processing Unit". *Energy and Buildings* 68(1–2): 385–95. doi:10.1016/j.enbuild.2013.09.042.
- Zhu, Y., X. Jin, X. Fang, Z. Du. 2014b. "Optimal Control of Combined Air Conditioning System with Variable Refrigerant Flow and Variable Air Volume for Energy Saving". *International Journal of Refrigeration* 42: 14–25. doi:10.1016/j.ijrefrig.2014.02.006.
- Zhu, Y., X. Jin, Z. Du, X. Fang. 2015. "Online Optimal Control of Variable Refrigerant Flow and Variable Air Volume Combined Air Conditioning System for Energy Saving". *Applied Thermal Engineering* 80: 87–96. doi:10.1016/j.applthermaleng.2015.01.030.

Development of an Energy Performance Benchmark Using Quantitative Analysis of Energy Consumption of Office Buildings

HyeGi Kim – Ajou University – kimhyegi@ajou.ac.kr

SunSook Kim – Ajou University – kss@ajou.ac.kr

Abstract

Building energy benchmarking is a system to evaluate and compare the energy performance of a building over time, relatively to other similar buildings, or to a reference building, which can be used to continuously manage the energy performance of the building. An energy-benchmarking model is a mechanism to develop the benchmarks necessary for the benchmarking process. It should be selected appropriately considering the availability of building energy performance information and building specification data. The purpose of this study is to develop an energy performance-benchmarking model for existing office buildings by analysing energy consumption data from the national building energy consumption database (DB) in Korea. The results of this study can be used as the energy performance evaluation and diagnostic criteria for existing office buildings

1. Introduction

Building energy use benchmarking can help building owners and facility managers to assess building energy performance and to identify energy efficiency opportunities. With the advanced information technologies, many countries have provided databases, tools, and evaluation frameworks to assess energy performance as well as to compare buildings to standards or their peer group based on the real energy data collection. As a way to improve energy efficiency in the building sector, the Korean government developed a nation-wide integrated energy consumption DB with about 6.8 million building records and has operated an energy benchmarking system based on the DB. The current energy performance-benchmarking model uses the annual primary energy consumption of electricity and heat energy as a benchmark. The

primary energy or CO₂ emissions are appropriate to compare national consumption of natural resources such as petroleum and coal, or to check implementation status on GHG reduction targets. However, stakeholders such as building owners and facility managers in individual buildings are less aware of the concept of primary energy. Therefore, it seems difficult to evaluate the heating and cooling energy consumption by the seasonal change thoroughly as well as to identify potential energy waste and the savings opportunities for improvement.

The purpose of this study is to improve the building energy benchmarking model for office buildings that can provide benchmarks with more detailed information to compare the energy performance of buildings. For this purpose, the building specification data and the final energy consumption data (end-use data) were collected from the Korean National Energy Performance Integrated Information System (EPIIS). By use of ASHRAE inverse modelling methods, parameterized models were derived from weather-dependent energy use and weather-independent use, and then an energy performance benchmarking model was developed by a more detailed analysis of the building information and energy use data.

2. Methods

To develop the energy performance-benchmarking model, building specifications, and energy consumption data of 4,304 office buildings were collected from the EPIIS. The monthly and annual electricity and heat energy consumption data for 36 months of the recent three years (2013–2015) were collected. Next, buildings with too high or low

energy consumption that could cause distortion in the analysis (399 office buildings) were excluded using the box-plot outlier removal method. To offer benchmarking information to energy consumers such as building owners and facility managers, we analyzed the energy consumption data of 3,905 buildings selected from the initial 4,304 buildings and developed the benchmarking model based on the following contents.

2.1 Energy Consumption by Usage

Different types of energy performance information were used as benchmarks to easily determine the current level of energy performance of the buildings. Energy performance indicators that are familiar to energy consumers include the final energy consumption by an energy source, such as electricity and gas, and energy performance according to the purpose of use. The final energy consumption is the energy sources provided to consumers to meet the energy demands for each purpose of use, such as heating and cooling, and it can be constructed easily based on the utility data. Accordingly, the energy consumption DB of each energy source can be used as a criterion to compare the performance level. However, in order for energy consumers to make retrofitting decisions to improve energy performance, the energy consumption for each purpose of use should be analyzed in detail.

Based on the utility data, we separated the energy performance by the purpose of usage for detailed analysis. For this separation, the change point method was applied among the ASHRAE inverse modelling techniques, which uses the point where the energy performance changes based on the ambient temperature. This method derives a regression equation for energy performance by climate in order to separate heating, cooling, and base load from final energy consumption. Therefore, this method requires monthly energy consumption of electricity and heat, and the dry bulb temperature. The EPIIS collected monthly and yearly electricity and heat consumption data in detail via a meter. However, these data were made from the meas-

ured values for the building own billing period and require correction for various periods. Thus, before separating energy consumption data by usage, the monthly mean dry bulb temperature data provided by the National Meteorological Administration were collected. Then, the monthly consumption data were corrected based on the collected billing periods information of the 3,905 buildings, and matched the temperature data and energy consumption data.

Fig. 1 shows the change point method that will derive five parameters according to the graph shapes, as follows:

- b_0 Base-load (kWh/m²·monthly)
- b_1 Heating sensitivity (slope coefficient)
- b_2 Cooling sensitivity (slope coefficient)
- b_3 Heating start temperature (°C)
- b_4 Cooling start temperature (°C)

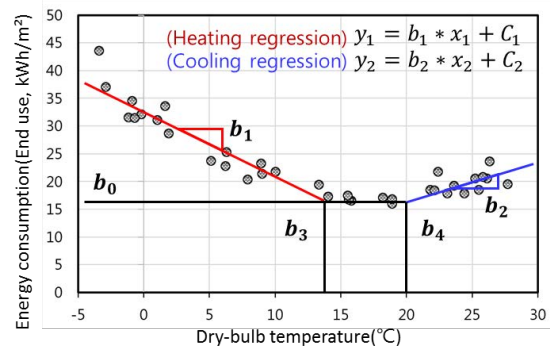


Fig. 1 – Five-Parameters of the cooling and heating models

Also, the following equations show a method to separate the heating and cooling energy consumption using a separated base-load.

$$A = EC_M - b_0$$

$$B = EC_A - 12 \times b_0$$

$$C = \sum(EC_{Ms} \text{ of the month which the } T(^\circ\text{C}) \text{ is lower than } b_3)$$

$$D = \sum(EC_{Ms} \text{ of the month which the } T(^\circ\text{C}) \text{ is higher than } b_4)$$

- EC_M Monthly final energy consumption(kWh/m²)
- EC_A Annual final energy consumption(kWh/m²)
- A Cooling and Heating EC_M (kWh/m²)
- B Cooling and Heating EC_A (kWh/m²)
- C Heating EC_A (kWh/m²)
- D Cooling EC_A (kWh/m²)

In this method, as a first step in separating energy performance, the amount of the base-load must be estimated in the total energy consumption. The base-load generally appeared in April-May and September-October every year. However, the base-load of each year is not the same, because the variables, exception made for temperature, influenced the base-load. Therefore, it is necessary to calculate the representative base-load of the building.

To calculate the representative base-load, two months were selected that showed the lowest energy consumption each year from 2013 to 2015. The use of the selected six energy consumptions set up the cases as shown in Table 1, and examined the cooling and heating energy regression models for each case.

Table 1 – Base-load calculation cases

Definition of cases	
A	Selects the smallest value among the six energy consumptions as the representative base load.
B	Selects the second smallest value among the six energy consumptions as the representative base load.
C	Selects the third smallest value among the six energy consumptions as the representative base load.
D	Selects the fourth smallest value among the six energy consumptions as the representative base load.
E	Selects the fifth smallest value among the six energy consumptions as the representative base load.
F	Selects the largest value among the six energy consumptions as the representative base load.

As a result, the number of buildings with high abnormal data and R² was examined and outlined in Table 2.

Table 2 – Analysis the results of regression of base-load cases

CASE	Case A	Case B	Case C	Case D	Case E	Case F	
Error case①	1,653	924	419	178	165	216	
Error case②	66	85	101	102	111	179	
Total	1,719 (44%)	1,009 (26%)	520 (13%)	280 (7%)	276 (7%)	395 (10%)	
Heating regression	R ² < 0.2	2 0 %	27 1 %	55 1 %	105 3 %	97 2 %	88 2 %
	R ² < 0.3	4 0 %	11 0 %	50 1 %	62 2 %	66 2 %	76 2 %
	R ² < 0.4	10 0 %	26 1 %	48 1 %	84 2 %	82 2 %	105 3 %
	R ² < 0.5	8 0 %	25 1 %	69 2 %	99 3 %	123 3 %	107 3 %
	R ² < 0.6	33 1 %	64 2 %	105 3 %	144 4 %	152 4 %	159 4 %
	R ² < 0.7	65 2 %	147 4 %	191 5 %	230 6 %	224 6 %	259 7 %
	R ² < 0.8	170 4 %	284 7 %	406 10 %	431 11 %	458 12 %	448 11 %
	R ² ≥ 0.8	1894 49 %	2312 59 %	2461 63 %	2470 63 %	2427 62 %	2268 58 %
Total	2,186 (56%)	2,896 (74%)	3,385 (87%)	3,625 (93%)	3,629 (93%)	3,510 (90%)	
Cooling regression	R ² < 0.2	8 0 %	48 1 %	165 4 %	277 7 %	349 9 %	359 9 %
	R ² < 0.3	18 0 %	43 1 %	114 3 %	164 4 %	174 4 %	175 4 %
	R ² < 0.4	29 1 %	100 3 %	155 4 %	192 5 %	188 5 %	202 5 %
	R ² < 0.5	58 1 %	118 3 %	198 5 %	223 6 %	244 6 %	242 6 %
	R ² < 0.6	116 3 %	216 6 %	278 7 %	319 8 %	305 8 %	309 8 %
	R ² < 0.7	214 5 %	340 9 %	407 10 %	402 10 %	424 11 %	421 11 %
	R ² < 0.8	443 11 %	625 16 %	635 16 %	668 17 %	703 18 %	690 18 %
	R ² ≥ 0.8	1300 33 %	1406 36 %	1433 37 %	1380 35 %	1242 32 %	1112 28 %
Total	2,186	2,896	3,385	3,625	3,629	3,510	

If the heating start temperature was higher than the cooling start temperature or the cooling and heating start temperatures did not correspond to the temperature category of the domestic climate, they were deemed abnormal data and removed. Next, the R² values of the cooling and heating regression equations of office buildings for which the abnormal data had been removed, were examined.

2.2 Analysis of Building and Energy Performance Information

Next, the building information was investigated and analysed. The building information and characteristics are outlined in Table 3.

Table 3 – The building information of office buildings

Variable type	Variable	Group classification criteria		Frequency	
Discrete variable	Region	-		16	
	Structure	-		9	
	Roof type	-		4	
Continuous variable	Gross area (m ²)	1	0~25%	3000 ~ 3968 m ²	4
		2	25~50%	3968~5334 m ²	
		3	50~75%	5334~9483 m ²	
		4	75~100%	More than 9483 m ²	
	Floor area (m ²)	1	0~25%	Less than 3004 m ²	4
		2	25~50%	3004~4047 m ²	
		3	50~75%	4047~6623 m ²	
		4	75~100%	More than 6623m ²	
	Period (years)	1	0~25%	Less than 14years	4
		2	25~50%	14~21years	
		3	50~75%	21~26years	
		4	75~100%	More than 26year	
	Ratio of the floors (Aboveground)	1	0~25%	Less than 0.75	4
		2	25~50%	0.75~0.8	
		3	50~75%	0.8~0.83	
		4	75~100%	More than 0.83	
Building height (m)	1	0~25%	Less than 17m	4	
	2	25~50%	17~27m		
	3	50~75%	27~40m		
	4	75~100%	More than 40m		

Most of this information affects energy performance, but it was difficult or impossible to regard these items as energy conservation measures (ECM). Furthermore, when the building information was a nominal variable, the number of office buildings was greatly different by group. This implies that there is a high possibility of error in the statistical results. Thus, selected the building information corresponding to a continuous variable as peer groups, it was divided according to the quartiles. The quartiles of a ranked set of data values are the three points that divide the data set into four equal groups, each group comprising a quarter of the data.

The first quartile (Q1) is defined as the middle number between the smallest number and the median of the data set. The second quartile (Q2) is the median of the data. The third quartile (Q3) is the middle value between the median and the highest value of the data set.

However, classifying all building data into peer groups may result in a large number of inefficient

groups, or derive the insignificant statistical benchmarks. Thus, we analysed the building information to verify the building information that can classify meaningful peer groups. For the analysis methods, a statistical technique to test the quantitative differences of the data and a practical significance test to professionally review the possibility that such differences can occur practically were applied. Performing signification statistics test on a statistical technique can show whether the analysis result for a sample reached a statistical probability that can be regarded as an actual characteristic of the population. In general, the comparison of the representative values of the group tests the difference, and if the significance probability (p) is lower than the specified significance level, the difference can be declared statistically significant. However, even if statistically significant results are obtained, expert review is required regarding the cause(s) of differences in performance.

Therefore, the Kruskal-Wallis statistical method was applied to analyse the difference in energy performance according to building information. As a result, the gross area was found to generate significant differences in performance for all energy parameters, and the gross area was set as the classification criterion for peer groups.

2.3 Derivation of Benchmarks

Generally, statistical techniques are used to reflect the attributes of samples and to calculate them as the representative values of the samples. Examples of such statistical techniques include regression analysis and the representative value calculation methods. Regression analysis is a suitable method to calculate the benchmarks that reflects the characteristics of the individual buildings because it derives a value reflecting the characteristics of individual samples. However, as has already been shown, the current building data has limitations. Thus, in this study, we used the representative value calculation methods.

The representative value calculation methods include the median, mean, and mode calculation methods, with the appropriate method chosen ac-

Table 5 – Energy performance diagnostic indicators

Indicator	Range of cumulative percentages	
	b_1, b_4	Others
★★★	More than 90 %	Less than 10 %
★★☆	75 % ~ 90 %	10 % ~ 25 %
★★	50 % ~ 75 %	25 % ~ 50 %
★☆	25 % ~ 50 %	50 % ~ 75 %
★	10 % ~ 25 %	75 % ~ 90 %
☆	Less than 10 %	More than 90 %

Next, to examine the validity of the benchmarking model, the energy performance evaluation of the energy consumption of 3,625 office buildings was performed by using the benchmarks, and the results were analysed. This was performed with the following Equation:

$$\text{Energy Efficiency Ratio} = \frac{\text{Building energy use}}{\text{benchmark}}$$

The Energy Efficiency Ratio (EER) approaches 1 if the building has the same performance as the benchmark. On the other hand, as the energy efficiency increases or decreases, the EER of the building will deviate from 1. The accumulation of EER scores for individual buildings can be used to obtain the cumulative frequency of buildings according to the EER. If the building group that is closest to the benchmark is located at the center of the distribution, it can be said that the representative nature of the benchmark has been satisfied.

Table 6 shows the evaluation results of the energy performance of five parameters for 3,625 office buildings using the derived benchmark. For all the energy performance information, the EER was close to 1 when the cumulative distribution of data was 50 %. Furthermore, in the cases of cooling sensitivity, the corresponding EER score was much higher than the one for other energy performance data when the cumulative frequency distribution was 90 %. In other words, even though buildings with extremely high cooling sensitivity distorted the data distribution, as the benchmark using the median calculation method was derived, the EER scores of buildings with extreme performance data

were very high and the distribution of the building group corresponding to the score of 1 was concentrated in the median.

Table 6 – the EER evaluation results of the five parameters

Cumulative percentages (%)	Energy Efficiency Ratio (EER)				
	b_0	b_1	b_2	b_3	b_4
10 %	0.56	0.35	0.76	0.44	0.86
25 %	0.77	0.60	0.87	0.71	0.92
50 %	1.07	1.08	0.97	1.29	0.98
75 %	1.51	1.55	1.07	2.72	1.06
90 %	2.02	1.93	1.15	3.77	1.15

Fig. 2 shows the energy performance diagnosis result of a randomly selected building. The energy performance of the parameters is diagnosed using the energy performance diagnostic indicators in Table 5 and EER results. The energy performance of the parameters is diagnosed as the caution level if we judged that an energy performance improvement is necessary only in energy efficiency diagnosis indicators, or only in EER evaluation results. If both indicators and EER results indicate that energy efficiency is required, the diagnostic results are presented according to the indicators and EER result levels.

Cumulative percentages of gross area(m ²)	Star	Energy performance compare/diagnosis table							
		Base-load (kWh/m ²)	Heating Sensitivity	Heating Start T(°C)	Cooling Sensitivity	Cooling Start T(°C)	H+C	Heating	Cooling
Group 3	★★★	Less than 5.49	More than -0.30	Less than 11.38	Less than 0.25	More than 20.77	Less than 22.31	Less than 14.86	Less than 3.96
	★★☆	5.49 ~ 7.38	-0.30 ~ -0.49	11.38 ~ 12.71	0.25 ~ 0.42	20.77 ~ 19.36	22.31 ~ 23.52	14.86 ~ 25.50	3.96 ~ 7.96
	★★	7.38 ~ 10.30	-0.49 ~ -0.85	12.71 ~ 14.09	0.42 ~ 0.77	19.36 ~ 17.97	23.52 ~ 27.27	25.50 ~ 46.18	7.96 ~ 17.30
	★☆	10.30 ~ 14.50	-0.85 ~ -1.19	14.09 ~ 15.63	0.77 ~ 1.52	17.97 ~ 16.82	27.27 ~ 103.16	46.18 ~ 84.42	17.30 ~ 37.77
	★	14.50 ~ 18.56	-1.19 ~ -1.46	15.63 ~ 16.77	1.52 ~ 2.05	16.82 ~ 15.90	103.16 ~ 133.22	84.42 ~ 84.42	37.77 ~ 53.75
	☆	More than 18.56	Less than -1.46	More than 16.77	More than 2.05	Less than 15.90	More than 133.22	More than 84.42	More than 53.75
EER	Energy Efficiency Ratio = $\frac{\text{Building energy use}}{\text{benchmark}}$								
Gross area of your building (m ²)		7421.5							
Evaluation contents		Value	STAR	EER	Caution level Star rating is between ★★ and ★★★, but EER is greater than 1 or Star rating is between ☆ and ★☆, but EER is lower than 1				
Base-load (kWh/m ²)		15.59	★	1.62					
Annual heating and cooling energy consumption (kWh/m ²)		33.61	★★★	0.6					
Annual energy consumption(kWh/m ²)		20.94	★★★	0.5					
Heating	Sensitivity	-0.46	★★★	0.62	Improvement is recommended. ☆☆				
	Start T(°C)	12.81	★★	0.89					
Cooling	Annual energy consumption(kWh/m ²)	14.00	★★	1.22	Improvement is needed. ★				
	Sensitivity	0.66	★★	1.27					
		18.80	★★	1.02	Must be improved ! ☆				
Diagnostic results		Improvement of base-load is needed ! • Reduce equipment schedules • Eliminate any electric heating • Reduce lighting load • Reduce plug loads • Check fossil fuel baseload • Be careful about using cooling energy							

Fig. 2 – Diagnosis result using developed benchmarking model

4. Conclusion

In this study, we developed a benchmarking model that can provide benchmarks of existing office buildings to compare the energy performance of a building and to provide understandable information to building owners and operators at the early stage of office building retrofitting. The results of this study are summarized as follows.

- (1) To develop the benchmarking model, we analysed the DB of EPIIS. The information such as gross area, period, and height of the building, etc. was collected, but information related to energy performance such as window U-value, SHGC or envelope information was not collected.
- (2) In order to provide easy-to-understand energy performance information to energy consumers, the heating, cooling, and base loads were separated from the final energy consumption DB. To do this, it was necessary to collect monthly temperature information and to correct the monthly energy performance.
- (3) Since various kinds of building information were not built in EPIIS, we set up a peer-group based on gross area and benchmarks that were calculated by applying the method of the calculating median.
- (4) The results of this study can be used as the energy performance evaluation and diagnostic criteria for existing office buildings by providing useful energy performance information based on the actual energy consumption. However, to improve and manage the energy of buildings in the future, it is necessary to collect the related building information to improve energy such as the u-value of walls and windows, SHGC of windows, and equipments, etc.

Acknowledgements

This research was supported by Basic Science Research Program through the National Research Foundation of Korea (NRF) funded by the Ministry of Science, ICT & Future Planning (NO. 2014R1A2A2A01007405)

References

- Donnelly, M., J. Kummer, K. Drees. 2013. *LEAN Energy Analysis: Using Regression Analysis to Assess Building Energy Performance*. Washington, U.S.A.: Jonson Controls.
- Energy in Buildings and Communities Programme (EBC). 2013. *Total energy use in buildings (Annex 53): Analysis and evaluation methods*. Tokyo, Japan: Institute for Building Environment and Energy.
- Energy in Buildings and Communities Programme (EBC). 2013. *Statistical analysis and prediction methods (Annex 53): Separate Document Volume V*. Tokyo, Japan: Institute for Building Environment and Energy.
- Environmental Protection Agency (EPA). ENERGY STAR Portfolio manager(ESPM). "Technical Reference." <http://www.energystar.gov/>
- Kissock, J.K., J.S. Harberl, D.E. Claridge. 2002. *Development of a Toolkit for Calculating Linear, Change-point Linear and Multiple-Linear Inverse Building Energy Analysis Models: ASHRAE Research Project 1050-RP*. Tokyo, Japan: Institute for Building Environment and Energy; and Atlanta, U.S.A.: ASHRAE.
- National Institute of Standards and Technology. 2013. *e-Handbook of Statistical Methods*. <http://www.itl.nist.gov/div898/handbook/>
- Shengwei, W., T. Chengchu, X. Fu. 2012. "Quantitative energy performance assessment methods for existing buildings". *Energy and Buildings* 55: 873-888. doi:10.1016/j.enbuild.2012.08.037
- Si-Won, Y., K. Sun-Sook. 2014. "Improvement of operation rating method in building energy performance disclosure system". *Journal of the architectural institute of Korea planning and design* 30(12): 307-314. doi:10.5659/JAIK_PD.2014.30.12.307

Parametric Technical and Economic Analysis of Thermal Comfort and Productivity in Industrial Buildings

Mariantonietta Tarantini - Free University of Bozen-Bolzano - mariantonietta.tarantini@natec.unibz.it

Giovanni Pernigotto - Free University of Bozen-Bolzano - giovanni.pernigotto@unibz.it

Fabian Ochs – University of Innsbruck - fabian.ochs@uibk.ac.at

Andrea Gasparella - Free University of Bozen-Bolzano - andrea.gasparella@unibz.it

Abstract

Thermal comfort is an important aspect to occupants' well-being and productivity in a workplace. Indeed, as observed by some authors in the literature, a high thermal comfort can improve workers' productivity and progressively reduce the number of accidents as well as occupational diseases. This paper aims at investigating to what extent the level of thermal comfort in workplace influences productivity, estimated according to Roelofsen model (2001). In particular, the study analyses the economic benefits of investing in additional air-conditioning systems to improve thermal comfort conditions, considering the impact of insulation of the envelope, internal gains and climate.

1. Introduction

In workplaces, the indoor environment quality - IEQ has an impact not only on people's comfort, health and safety but also on their productivity (Haynes, 2008). Moreover, in industrialized countries, labour costs often exceed energy costs (Wood, 1989). Although higher productivity rates can be key factors for economic success, limited interest is generally given to indoor comfort conditions in productive buildings and the focus is only on energy aspects.

The literature reports several studies describing the relationship between occupants' comfort conditions, health and productivity in workplaces (Milton et al., 2000; Wyon et al., 2000). In a previous research (Tarantini et al., 2017), the authors focused on a specific IEQ aspect, i.e., thermal comfort, and reviewed the literature about its correlation with performance and productivity, observing that several researches re-

port losses due to thermal discomfort conditions. For example, Wyon and Wargocki (2005) underlined that some air temperature conditions can lower arousal and learning performance (Wargocki and Wyon, 2006), reduce manual dexterity and increase Sick Building Syndrome symptoms. Lan and Lian (2009) reported productivity loss when workers are in non-neutral comfort conditions, especially when feeling warm (Lan et al., 2011). DeRango (2003) observed that neutral thermal comfort conditions lead to a reduction of physical efforts and a growth of productivity. However, as observed by the authors (Tarantini et al., 2017), only a limited number of models are available for a quantitative assessment of productivity changes as a function of thermal comfort conditions. One example is Roelofsen model (2001).

This paper analyses the economic convenience of the adoption of HVAC solutions to ensure thermal comfort conditions in productive buildings. A small-size productive building of 1500 m³ was modelled with TRNSYS and a sample of 30 different configurations defined, from a full factorial combination of five European climates, two levels of internal gains and three different kinds of opaque components. The parametric set was simulated considering two scenarios - with or without sensible cooling system, and, for both, the productivity in each working hour was assessed by means of Roelofsen model (2001). Afterwards, the net present value, NPV, was calculated for each configuration without mechanical cooling, considering the installation cost of the sensible cooling system, and the running costs related to the energy and workforce.

2. Methods

2.1 Set of Configurations

A small productive building of 30 m x 10 m x 5 m, with façades oriented towards the main cardinal directions, was selected as the base case to build a parametric set of configurations and modelled with TRNSYS 17 (SEL, 2012) as a simplified mixed thermal zone. South and north façades have a window area of 4.32 m² and a door area of 14.4 m² each. East and west façades have, respectively, window areas of 34.56 and 26.4 m² and the latter includes also a door of 22 m².

Windows have a glazing thermal transmittance U_{gl} equal to 2.83 W m⁻² K⁻¹, a SHGC of 0.755, no shadings and a frame thermal transmittance U_{fr} equal to 3.2 W m⁻² K⁻¹, while doors have a thermal trans-

mittance of 1.4 W m⁻² K⁻¹. As summarized in Table 1, three different wall constructions (i.e., concrete wall, concrete wall with an external insulation and sandwich wall - respectively “concrete”, “ins_conc” and “sandwich” in the next Figures and Tables) were considered. Taking into account the different surfaces finishing, a solar absorbance of 0.3 was assumed for the two concrete walls and 0.6 for the sandwich wall. The three types of envelope were selected in order to cover a wide range of components, from the uninsulated ones, common in South Europe, to insulated and well-insulated ones, more frequent in North Europe. The typical weekday work schedule was assumed from 8:00 am to 5:00 pm, including the break hours, and no-work was programmed over the week-end. A total of 30 workers were considered.

Table 1 – Envelope details of the 3 kinds of opaque components, with materials properties according to the UNI EN ISO 10456 (UNI, 2008)

	Layer	Thickness [m]	Thermal Conductivity [W m ⁻¹ K ⁻¹]	Specific Heat Capacity [kJ kg ⁻¹ K ⁻¹]	Density [kg m ⁻³]
CONCRETE WALL (“concrete” in the Figures)					
Ground floor [U = 4.17 W m ⁻² K ⁻¹]	Concrete slab	0.08	1.15	1	1800
External wall [U = 2.91 W m ⁻² K ⁻¹]	Concrete block	0.20	1.15	1	1800
External roof [U = 0.44 W m ⁻² K ⁻¹]	Concrete block	0.10	1.15	1	1800
	Polystyrene	0.08	0.04	1.47	40
INSULATED CONCRETE WALL (“ins_conc” in the Figures)					
Ground floor [U = 4.17 W m ⁻² K ⁻¹]	Concrete slab	0.08	1.15	1	1800
External wall [U = 0.41 W m ⁻² K ⁻¹]	External plaster	0.03	0.43	1	1200
	Polystyrene	0.08	0.04	1.47	40
	Concrete block	0.20	1.15	1	1800
External roof [U = 0.44 W m ⁻² K ⁻¹]	Concrete block	0.10	1.15	1	1800
	Polystyrene	0.08	0.04	1.47	40
SANWICH WALL (“sandwich” in the Figures)					
Ground floor [U = 4.17 W m ⁻² K ⁻¹]	Concrete slab	0.08	1.15	1	1800
External wall [U = 0.11 W m ⁻² K ⁻¹]	Zinc corrugated sheet	0.002	30	0.460	7900
	Polystyrene	0.35	0.04	1.47	40
	Zinc corrugated sheet	0.002	30	0.460	7900
External roof [U = 0.32 W m ⁻² K ⁻¹]	Zinc corrugated sheet	0.002	30	0.460	7900
	Polystyrene	0.12	0.04	1.47	40
	Zinc corrugated sheet	0.002	30	0.460	7900

During occupancy hours, a natural ventilation rate of $30 \text{ m}^3 \text{ h}^{-1}$ per person was imposed in accordance with EN 13789 (CEN, 2007a). An infiltration rate of 0.07 vol h^{-1} was estimated in accordance with EN 15242 (CEN, 2007b) and UNI EN 12831 (UNI, 2006), considering a leakage rate at 50 Pa of $5 \text{ m}^3 \cdot \text{h}^{-1}$ per m^2 of façade and a shielding coefficient of 0.03. Two levels of internal sensible gains, i.e., $20 \text{ W} \cdot \text{m}^{-2}$ and $40 \text{ W} \cdot \text{m}^{-2}$ (respectively “_20” and “_40” in the next Figures and Tables), were considered as representative of different type of activity sectors according to DIN V 18599 1-10 (DIN, 2016), with a total of 6000 W or 12000 W, half convective and half radiative as suggested by EN ISO 13790 (CEN, 2008). In line with the ISO 7730 (ISO, 2005) metabolic rate of 1.6 met (i.e., light industry activity) and with ASHRAE Handbook of Fundamentals (2009), internal gains per occupant were set to 75 W of sensible heat, 43.5 W radiative and 31.5 W convective, and $158 \text{ g} \cdot \text{h}^{-1}$ of generated water vapour. Considering the presence of 30 occupants, the building was characterized by additional 2250 W of sensible gains. The analysis was performed considering five European climates: Berlin, Germany, Messina, Milan and Rome, Italy, and Vienna, Austria. TMY2 weather data were used as weather data source. A seasonal distinction, with summer lasting from June to September or from May to October, depending on the weather data of each location, was applied for the clothing factor, with 1 clo for winter and 0.5 clo for summer time according to ISO 9920 (ISO, 2007).

Every case was simulated with an ideal sensible heating system with an air temperature setpoint of $18 \text{ }^\circ\text{C}$ according to the Italian law, DPR 412 (President of the Italian Republic, 1993). The heating system starts running an hour before the set working timetable (i.e., 7:00 am) and turns off at the end of the working timetable (i.e., 5:00 pm). The set of 30 cases was modelled both with and without sensible cooling system. For those configurations with sensible cooling system, it was modelled as an ideal system with an air temperature setpoint of $26 \text{ }^\circ\text{C}$, operating during occupancy time. Heating and cooling systems are operative all year long, without a definition of heating and cooling seasons.

2.2 The Estimation of the Productivity Loss

As explained in the introduction, in this work Roelofsen model (2001) was used to calculate the productivity losses due to non-neutral thermal comfort conditions. The model was developed for office environments and, in the current research, was applied considering specific working tasks, such as assembly work, manufacturing machine programming and quality control, which are comparable to office tasks in terms of mental activities. The model estimates the percentage of hourly productivity loss as a function of Fanger’s Predicted Mean Vote, PMV, distinguishing thermal discomfort by cold and warm sensation (Fig. 1 and Table 2).

$$PL = b_0 + b_1 \cdot PMV + b_2 \cdot PMV^2 + b_3 \cdot PMV^3 + b_4 \cdot PMV^4 + b_5 \cdot PMV^5 + b_6 \cdot PMV^6 \quad (1)$$

Productivity loss was neglected in case of a slightly cold sensation, i.e., in a range of PMV between 0 and -0.5 (see Fig. 1). Moreover, Jin et al. (2012) suggested a limit of applicability for the Roelofsen model, equal to $-1.4 \leq PMV \leq +1.5$. In this study, the productivity losses found for $PMV = -1.4$ and for $PMV = +1.5$ were adopted also for smaller and larger PMV, respectively.

Table 2 – The values of the regression coefficients, $b_0 - b_6$, in Equation (1)

Regression coefficients	PMV < 0	PMV > 0
b_0	1.2802070	-0.15397397
b_1	15.9954510	3.88202970
b_2	31.5074020	25.17644700
b_3	11.7549370	-26.64136600
b_4	1.4737526	13.11012000
b_5	-	-3.12968540
b_6	-	0.29260920

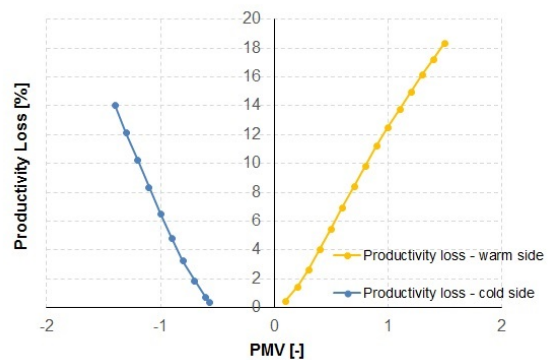


Fig. 1 – Productivity loss according to Roelofsen model (2001)

2.3 Economic Analysis

For each case not equipped with cooling, the Net Present Value, NPV, was calculated, according to the following assumptions:

- investment costs of a cooling system in the range of 11 200 EUR to 17 000 EUR, depending on the required capacity, sizing from 5 kW to 20 kW and selected to satisfy only sensible cooling; indeed, considering the significant air change rate per ventilation and infiltration, the impact of internal vapour generation was assumed limited.
- running electricity costs according to Eurostat data, respectively equal to 0.1979 EUR kWh_{el}⁻¹ (Austria), 0.2804 EUR kWh_{el}⁻¹ (Germany) and 0.3229 EUR kWh_{el}⁻¹ (Italy);
- labour hourly costs according to Eurostat data, respectively equal to 34.9 EUR h⁻¹ per worker (Austria), 37.1 EUR h⁻¹ per worker (Germany) and 28 EUR h⁻¹ per worker (Italy);
- real discount rate of 3 % and period of consideration of 20 years;
- seasonal Coefficient of Performance, sCOP, of the cooling system equal to 3.5, selected to comply with the minimum requirements by the Italian law (Italian Government, 2015).

Moreover, an economic sensitivity analysis was performed on the number of workers, accounting also for the scenarios with 20 and 40 workers in addition to the reference case with 30.

3. Results

3.1 Annual Energy Demand

The specific annual energy demand for heating and cooling were analysed for each configuration. Heating demand ranges from the minimum in Messina to the maximum in Berlin, respectively for the insulated cases with high internal gains (less than 1 kWh m⁻² a⁻¹) and for the uninsulated cases with low internal gains (more than 50 kWh m⁻² a⁻¹), as it can be seen in Fig. 2. On the contrary, the opposite is true for the cooling needs, with the largest demand in Messina for the case with sandwich walls and high internal gains (more than 30 kWh m⁻² a⁻¹) and almost null demand in Berlin and Vienna for the cases with concrete components and low internal gains (Fig. 3).

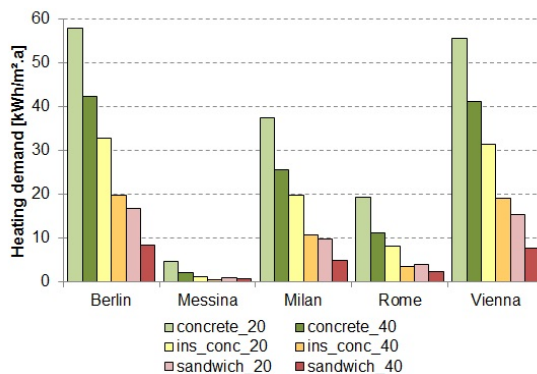


Fig. 2 – Comparison of the annual heating demand for the simulated configurations

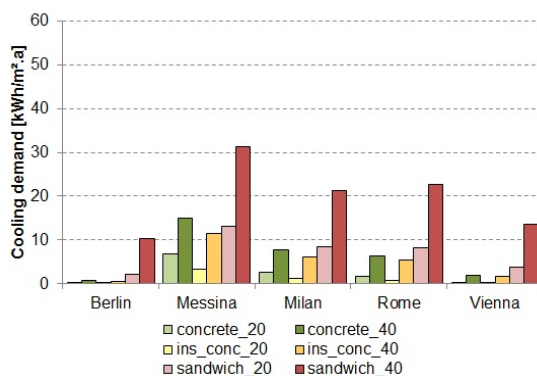


Fig. 3 – Comparison of the annual cooling demand for the simulated configurations with cooling system

3.2 Operative Temperature

The annual distribution of the hourly operative temperatures simulated during the working hours was represented by means of box and whisker charts. For each of the analysed cases, the upper lines represent the maximum, the lower lines the minimum, the points in the middle the medians and the rectangular boxes the range between the first and the third quartile of all the operative temperatures in the simulated working hours.

Focusing on the interquartile ranges of the distributions, it can be seen that the solutions with low internal gains show operative temperature values lower than the ones with high internal gain. The same is true for those cases with uninsulated components with respect to those with insulated or well-insulated envelope, and moving from colder to warmer climates. The result of the installation of a cooling system is clearly visible by comparing Figs 4 and 5. As it can be seen in the latter Figure, the cooling system is able to keep the maximum values of the operative temperature below 27 °C

during occupancy time, with the largest benefits registered for the city of Messina, especially for the solution with the sandwich wall and high internal gains.

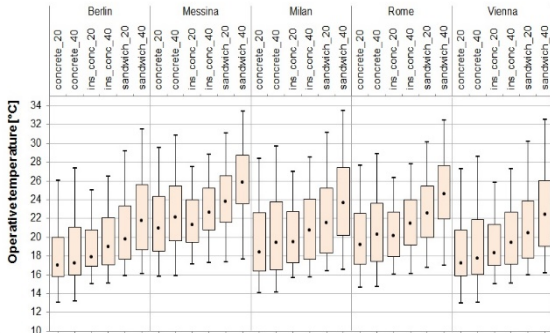


Fig. 4 – Distributions of hourly operative temperature for the cases without cooling system, during working hours

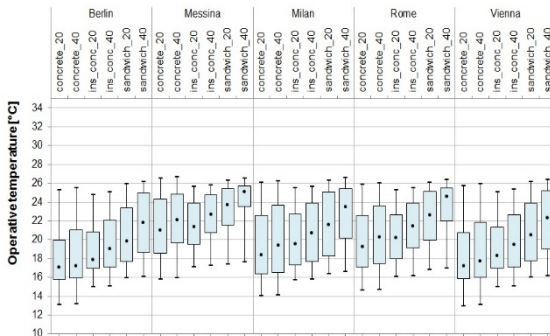


Fig. 5 – Distributions of hourly operative temperature for the cases with cooling system, during working hours

3.3 Annual Distributions of PMV and PPD

The PMV annual distributions were calculated setting a metabolic activity level of 1.6 met, a clothing insulation equal to 1 clo during the winter period and 0.5 clo during the summer, an air velocity of 0.05 m s^{-1} , and the operative temperatures generated by TRNSYS output and relative humidity values calculated balancing internal vapour generation, outdoors relative humidity and mass exchanges. As it can be seen in Figs 6 and 7, the cases with lower operative temperatures (e.g., with uninsulated envelope and low internal gains in colder climates) are characterized also by lower PMV. In all cities, the cases with uninsulated concrete walls and low internal gains are also those with PMV closest to neutrality, and, therefore, those with lowest productivity losses. With the use of a cooling system, the values of maximum and third quartiles and, to a lower

extent, of medians are lowered (Fig. 7), especially for Messina.

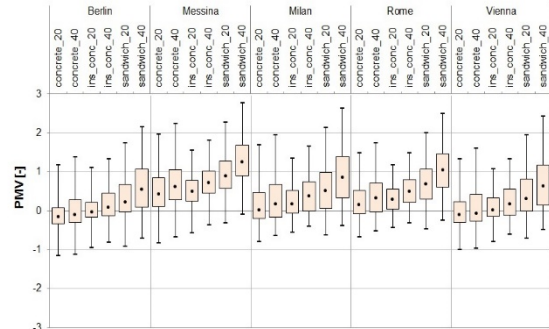


Fig. 6 – Distribution of hourly PMV for the cases without cooling system, during working hours

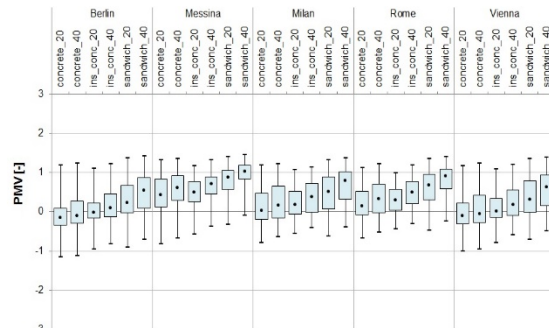


Fig. 7 – Distribution of hourly PMV for the cases with cooling system, during working hours

Figs 8 and 9 display the predicted percentage of dissatisfied, PPD, highlighting those cases with important fraction of time with PPD larger than 15 %, i.e., category C limit according to ISO 7730. In case of insulated envelope and high internal gain, the frequency of high PPD increases, especially for south Europe climates.

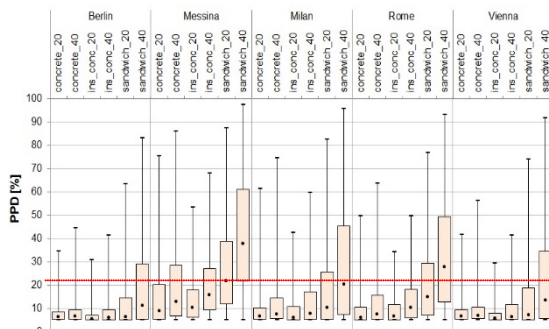


Fig. 8 – Distribution of hourly PPD for the cases without cooling system, during working hours. The red line indicates the limit of a category C environment (ISO 7730)

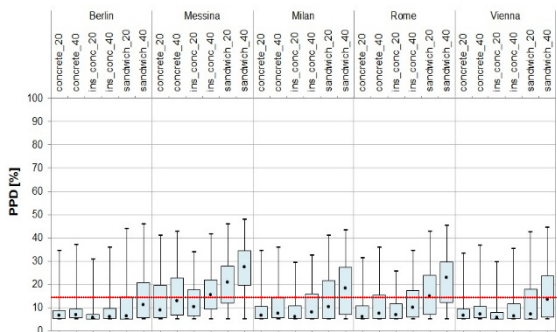


Fig. 9 – Distribution of hourly PPD for the cases with cooling system, during working hours. The red line indicates the limit of a category C environment (ISO 7730)

3.4 Annual and Seasonal Productivity Loss

The hourly productivity losses were calculated as a function of hourly PMV, according to Roelofsen model. As a result, the configurations characterized most frequently by lower PMV values, i.e., the cases with uninsulated envelope and low internal gains, have the lowest loss for while the opposite occurs with well-insulated components and high internal gains. As in Figs 10 and 11 and in Table 3, the cooling system can reduce the annual average of productivity loss, especially in Messina during the summer season.

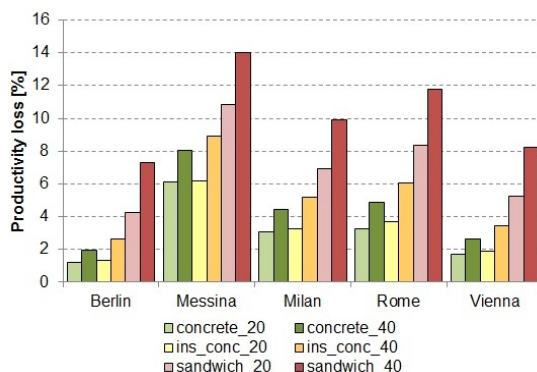


Fig. 10 – Annual average of productivity loss for the cases without cooling system

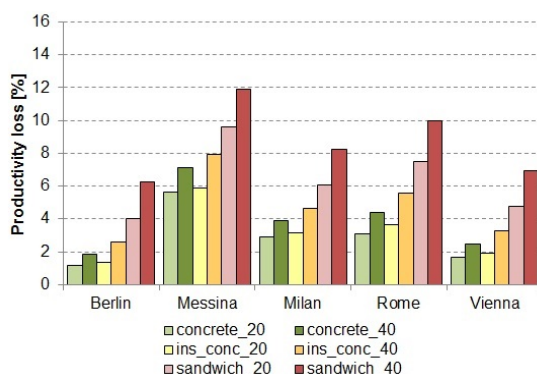


Fig. 11 – Annual average of productivity loss for the cases with cooling system

Table 3 – Seasonal average increase of productivity after the installation of a cooling system

	Berlin		Messina		Milan		Rome		Vienna	
	winter	summer	winter	summer	winter	summer	winter	summer	winter	summer
Concrete_20	-	-	-	1.1 %	-	0.6 %	-	0.4 %	-	0.1 %
Concrete_40	-	0.2 %	-	2.1 %	-	1.5 %	-	1.3 %	-	0.6 %
Ins_conc_20	-	-	-	0.7 %	-	0.3 %	-	0.2 %	-	-
Ins_conc_40	-	0.2 %	-	2.1 %	-	1.5 %	-	1.3 %	-	0.6 %
Sandwich_20	-	0.8 %	-	2.6 %	-	2.3 %	-	2.3 %	-	1.5 %
Sandwich_40	0.2 %	3.2 %	0.5 %	4 %	0.2 %	4.1 %	0.4 %	4.2 %	0.2 %	3.8 %

3.5 Economic Analysis

Fig. 12 shows the Net Present Value for the investments related to the installation of a sensible cooling system in the productive buildings. As costs are expressed as positive values, a negative NPV means economic benefit, with the discounted savings overbalancing the initial costs. The investment is always profitable, except for 4 configurations, i.e., for the cases with either uninsulated and insulated concrete walls and low internal gains in Berlin and Vienna,

for which the increase of productivity is null all over the year as seen in Table 3.

A sensitivity analysis was performed also on the number of workers, considering the economic convenience both in case of 20 and of 40 workers. As in Fig. 13, with fewer employees, the cases with concrete walls and low internal gains have null or positive NPV also in Milan and Rome. Moreover, in Berlin also those cases with high internal gains and concrete structures are no more convenient. As a

whole, for the other cases all absolute values of NPV are reduced when compared to the base case with 30 workers. On the contrary, the opposite occurs with 40 workers (Fig. 14).

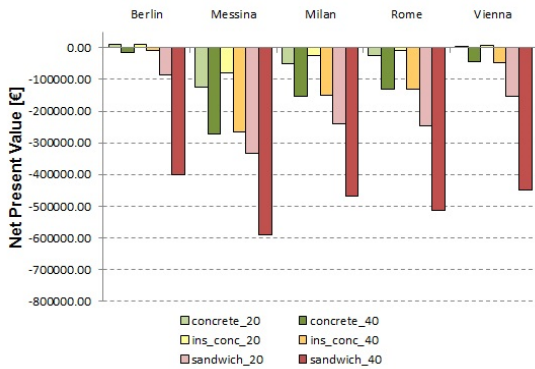


Fig. 12 – Net Present Values considering 30 workers

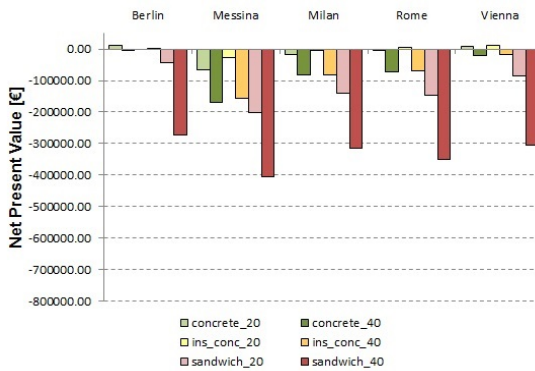


Fig. 13 – Net Present Values considering 20 workers

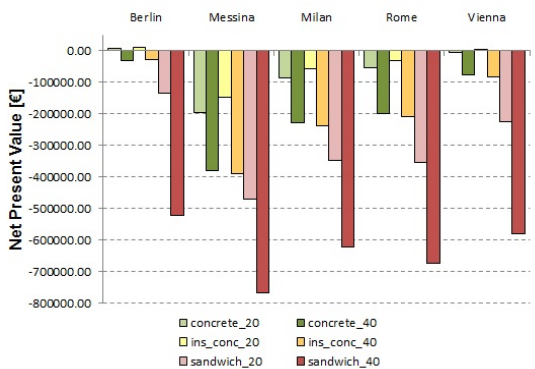


Fig. 14 – Net Present Values considering 40 workers

4. Discussions and Conclusions

This preliminary study focused on thermal comfort in productive buildings and potential improvement to productivity arising from the adoption of cooling systems, generally not present in such a kind of building. A parametric set of small-size productive

buildings was simulated with TRNSYS, considering different European climates, kind of envelopes, as well as internal gains. The economic benefit of the cooling system was assessed by contrasting the higher achievable productivity rate with the additional investment and running energy costs. We observed that:

- there is a high risk of thermal discomfort by warm sensation because of internal gains, which depends on the specific machineries and type of process;
- this risk can be increased further in case of insulated envelope and, in particular, for the Mediterranean climates;
- a cooling system can successfully reduce the thermal discomfort, increasing the productivity rate up to 4 % in the most critical configurations during the summer season;
- the improvement of the thermal comfort conditions in the workplace are economically convenient in most scenarios, with the exception of the configurations with uninsulated envelope and low internal gains in Berlin and Vienna;
- even a small improvement in average productivity (e.g. 1-2 %) is sufficient to pay off the additional costs for space cooling.

In conclusion, investments in HVAC systems for the improvement of workers’ thermal comfort conditions demonstrated to be an effective strategy to increase the productivity rate and gain competitive advantage. Further developments are expected to focus on actual case-studies, with the aim of assessing the limits of applicability of the Roelofsen correlation between productivity and thermal comfort to the different industrial activities as well as the influence of local comfort/discomfort on workers’ productivity.

Acknowledgements

This study has been funded by the project “Klimahouse and Energy Production” in the framework of the programmatic-financial agreement with the Autonomous Province of Bozen-Bolzano of Research Capacity Building.

References

- ASHRAE. 2009. *ASHRAE Handbook of Fundamentals*. Atlanta, U.S.A.: ASHRAE.
- CEN. 2007a. *EN ISO 13789:2007 Thermal performance of buildings - Transmission and ventilation heat transfer coefficients - Calculation method*. Brussels, Belgium: CEN.
- CEN. 2007b. *EN 15242: 2007 Ventilation for buildings Calculation methods for the determination of air-flow rates in buildings including infiltration*. Brussels, Belgium: CEN.
- CEN. 2008. *EN ISO 13790: 2008 Energy performance of buildings. Calculation of energy use for space heating and cooling*. Brussels, Belgium: CEN.
- DeRango, K. 2003. "Office Workers' Productivity Enhanced by Ergonomics". *Employment Research Newsletter* 10(3): 1-3. doi: 10.17848/1075-8445.10(1)-1.
- DIN. 2016. *DIN V 18599 1-10. 2016. Energy efficiency of buildings – calculation of the net, final and primary energy demand for heating, cooling, ventilation, domestic hot water and lighting*.
- Haynes, B. 2008. "The impact of office comfort on productivity". *Journal of Facilities Management* 6: 37–51. doi: 10.1108/14725960810847459.
- ISO. 2005. *ISO 7730: 2005, Ergonomics of the thermal environment – Analytical determination and interpretation of thermal comfort using calculation of the PMV and PPD indices and local thermal comfort criteria*. Geneva, Switzerland: ISO.
- ISO. 2007. *ISO 9920:2007 Ergonomics of the thermal environment—Estimation of thermal insulation and water vapour resistance of a clothing ensemble*. Geneva, Switzerland: ISO.
- Italian Government. 2015. "DECRETO 26 giugno 2015: Applicazione delle metodologie di calcolo delle prestazioni energetiche e definizione delle prescrizioni e dei requisiti minimi degli edifici". *Gazzetta Ufficiale* 162 of the 15th July 2015.
- Lan, L., Z. Lian. 2009. "Use of neurobehavioral tests to evaluate the effects of indoor environment quality on productivity". *Building and Environment* 44: 2208–2217. doi: 10.1016/j.buildenv.2009.02.001.
- Lan, L., P. Wargocki, D.P. Wyon, Z. Lian. 2011. "Effects of thermal discomfort in an office on perceived air quality, SBS symptoms, physiological responses, and human performance". *Indoor Air* 21: 376–390. doi: 10.1111/j.1600-0668.2011.00714.x.
- Jin, Q., M. Overend, P. Thompson. 2012. "Towards productivity indicators for performance-based façades design in commercial buildings". *Building and Environment* 57: 271-281. doi:10.1016/j.buildenv.2012.05.009.
- Milton, D.K., P.M. Glencross, M.D. Walters. 2000. "Risk of Sick Leave Associated with Outdoor Air Supply Rate, Humidification, and Occupant Complaints". *Indoor Air* 10: 212-221. doi: 10.1034/j.1600-0668.2000.010004212.x.
- President of the Italian Republic. 1993. "DPR 412/1993: Regolamento recante norme per la progettazione, l'installazione, l'esercizio e la manutenzione degli impianti termici degli edifici ai fini del contenimento dei consumi di energia". *Gazzetta Ufficiale Serie Generale* 242 of 14-10-1993 - *Suppl. Ordinario* 96.
- Roelofsen, P. 2001. "The design of the workplace as a strategy for productivity enhancement." In: *Proceedings of Clima 2000 Conference*. Naples, Italy.
- Solar Energy Laboratory. 2012. *TRNSYS 17. A transient system simulation program*, <http://sel.me.wisc.edu/trnsys>
- UNI. 2006. *UNI EN 12831:2006 Heating systems in buildings. Method for calculation of the design heat load*. Milan, Italy: UNI.
- UNI. 2008. *UNI EN ISO 10456: 2008 Building materials and products. Hygrothermal properties. Tabulated design values and procedures for determining declared and design thermal values*. Milan, Italy: UNI.
- Tarantini, M., G. Pernigotto, A. Gasparella. 2017. "A Co-Citation Analysis on Thermal Comfort and Productivity Aspects in Production and Office Buildings". *Buildings* 7(2): 36. doi:10.3390/buildings7020036.
- Wargocki, P., D.P. Wyon. 2006. "Effects of HVAC on student performance". *ASHRAE Journal* 48: 22–28.
- Wood, J.E. 1989. "Cost avoidance and productivity in owning and operating buildings". *Occupational Medicine* 4(4): 753–770.
- Wyon, D.P., K.W. Tham, B. Croxford, A. Young, T. Oreszeczyn. 2000. "The effects on health and self-estimated productivity of two experimental interventions which reduced airborne dust levels in office premises". In: *Proceedings of Healthy Buildings*. Espoo, Finland.
- Wyon, D.P., P. Wargocki. 2005. "Room temperature effects on office work". In: *Creating the Productive Workplace*, 2nd ed., London, UK: Taylor and Francis.

Building Simulation applications (BSA) 2017 was the third IBPSA-Italy conference on building performance simulation to take place at the Free University of Bozen-Bolzano, from 8th to 10th February 2017. The main topics dealt with were the impact of micro-climate conditions on building performance, detailed modelling of physical phenomena and building system components, optimization techniques for high performance buildings, energy retrofit and advanced HVAC controls, integrated performance analysis, and visual and thermal comfort assessment.

The principal mission of the International Building Performance Simulation Association (IBPSA) is to promote and advance the practice of building performance simulation in order to improve the design, construction, operation and maintenance of new and existing buildings. IBPSA-Italy, the Italian affiliate, is a non-profit association, which includes researchers, developers and practitioners acting on the topic of building performance simulation. IBPSA-Italy was founded in January 2011 and has now more than 160 members including university professors, researchers, professionals, software developers and students.

bu,p

ISBN 978-88-6046-136-0



9 788860 461360